26TH CONGRESS
AND GENERAL
ASSEMBLY OF THE
INTERNATIONAL UNION OF
CRYSTALLOGRAPHY

22-29 August 2023

Melbourne Convention and Exhibition Centre

www.iucr2023.org

ORAL ABSTRACTS

Proudly hosted by

IUCr

SCANZ
Society of Crystallographers in Australia and New Zealand

Sponsors

MELBOURNE Convention Bureau

MELBOURNE Victoria Australia

TOURISM AUSTRALIA

DAY 2

Wednesday 23 August 2023

Keynote 1
Room 203/4
9.00am – 9.50am

Keynote–01 –230823

AlphaFold changes everything (and nothing)

Thomas C. Terwilliger[1,2], Dorothee Liebschner[3], Tristan I. Croll[4,6], Christopher J. Williams[5], Airlie J. McCoy[4], Billy K. Poon[3], Pavel V. Afonine[3], Robert D. Oeffner[4], Christopher J. Schlicksup[3], Claudia Millán[4,7], Jane S. Richardson[5], Randy J. Read[4], and Paul D. Adams[3,8]

[1]New Mexico Consortium, Los Alamos, New Mexico, USA; [2]Los Alamos National Laboratory, Los Alamos, NM, USA; [3]Lawrence Berkeley National Laboratory, Berkeley, CA, USA; [4]Cambridge Institute for Medical Research, University of Cambridge, The Keith Peters Building, Hills Road, Cambridge CB2 0XY, UK; [5]Duke University, Durham, North Carolina, USA; [6]Altos Labs, Cambridge, UK; [7]SciBite Ltd, BioData Innovation Centre, Wellcome Genome Campus, Hinxton, Cambridge CB10 1DR, UK; [8]University of California, Berkeley, Berkeley, CA, USA

tterwilliger@newmexicoconsortium.org

Keywords: AlphaFold, AI, protein structure, structure prediction, hypothesis

The ability to create an AlphaFold model for any protein sequence in a few minutes changes nearly every protein crystal structure determination into a molecular replacement problem and nearly every protein cryo-EM structure determination into a docking problem. Making this even more transformative is the ability to iteratively improve AlphaFold modeling by docking an AlphaFold model into density, rebuilding it, and using the rebuilt model as a template for further AlphaFold model generation (Fig. 1) [1,2]. These features of AlphaFold make structure determination by crystallography and cryo-EM easier and more powerful than ever before.

Despite jumpstarting structure determination, AlphaFold does not fundamentally change the importance of the experiment [3], because protein conformations depend on conditions and the presence of other macromolecules and small molecules, and because even high-confidence parts of AlphaFold predictions can contain errors.

Anyone can carry out AlphaFold predictions and improvement of these predictions using X-ray or cryo-EM data easily using Phenix [4] and free cloud-based Google Colab notebooks.

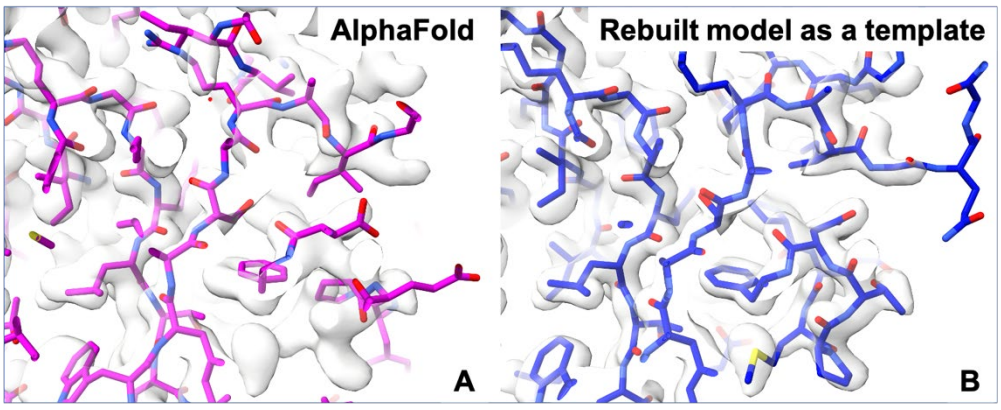

Figure 1. AlphaFold prediction using implicit experimental information for PDB entry 7oa7. A. AlphaFold prediction made without the use of templates (sequence and multiple sequence alignment only). B. Template-based AlphaFold prediction made using a model rebuilt based on experimental data. Models in A and B are superimposed on experimental electron density map without further adjustment (no coordinate refinement was carried out).

[1] Terwilliger, T. C. et al. Improved AlphaFold modeling with implicit experimental information. Nature Methods, (2022).

[2] Terwilliger, T. C. et al. Accelerating crystal structure determination with iterative AlphaFold prediction. bioRxiv, 2022.2011.2018.517112, (2022).

[3] Terwilliger, T. C. et al. AlphaFold predictions: great hypotheses but no match for experiment. bioRxiv 2022.11.21.517405; doi: https://doi.org/10.1101/2022.11.21.517405.

[4] Liebschner, D. et al. Macromolecular structure determination using X-rays, neutrons and electrons: recent developments in Phenix. Acta Crystallogr D Struct Biol 75, 861–877 (2019).

Keynote 2
Room 210/11
9.00am – 9.50am

Keynote–02 –230823

Chromic soft crystals based on photofunctional metal complexes

M. Kato

Department of Applied Chemistry for Environment, School of Biological and Environmental Sciences, Kwansei Gakuin University, Sanda, Hyogo 669-1330, Japan
katom@kwansei.ac.jp

Keywords: Platinum(II) complex, Soft crystal, Assembly-induced luminescence,

Various chromic phenomena such as thermochromism, photochromism, mechanochromism, and vapochromism have fascinated researchers for long time. Particularly, chromic crystalline materials are important to investigate the mechanisms structurally. Using organic and metal-complex crystals, interesting chromic materials that exhibit color and luminescence changes in response to various stimuli such as light, heat, and vapor have been developed. However, the studies that link chromic phenomena with structural dynamics were limited. To challenge the subjects, our group has focused on such chromic crystalline materials as soft crystals [1]. In this presentation, I focus on the recent progress in our studies on photo- and multi-functional metal complexes that exhibit remarkable color and luminescence changes [2-8].

Self-assembled systems of Pt(II) complexes bearing aromatic ligands have attracted much attention because of their assembly-induced luminescence based on the Pt···Pt interaction. They are also expected to be sensitive to the environmental conditions such as temperature, pressure, and vapor. We have succeeded in the constructions of a series of Pt(II)-NHC complexes (NHC = N-heterocyclic carbenes) that exhibit intense red-blue luminescence based on the assembled structures [4]. In addition, vapochromic luminescence changes based on the reversible single-crystal-to-single-crystal transformation were achieved for a weakly stacked system (Figure 1) [5]. Using weak intermolecular interactions, we have further developed a new type of stacked systems of Pt(II) complexes that exhibit assembly-induced luminescence.

Meanwhile, our group also focused on anionic Pt(II) complexes to control the molecular assembly using counter cations [6-7]. Here, the control of luminescence properties of anionic cyclometalated Pt(II) complexes by the cations will be also discussed. For example, thermo- and mechano-triggered luminescence ON-OFF switching of the luminescence has been achieved by using a Pt(II) complex ionic liquid with a phosphonium cation [7]. The characteristic properties are derived from the phase transition between highly luminescent crystal state and non-luminescent super-cooled state.

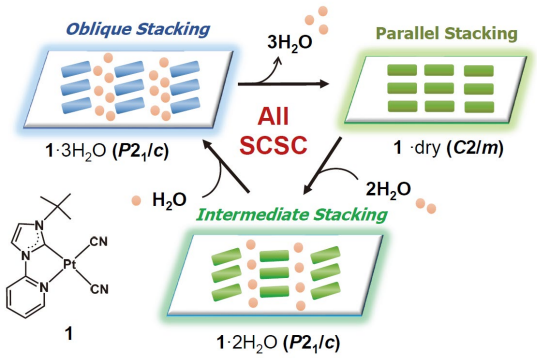

Figure 1. Reversible SCSC transformations of a vapochromic luminescent Pt-NHC complex [5].

[1] Kato, M., Ito, H., Hasegawa, M. & Ishii, K. (2019). *Chem. Eur. J.*, **25**, 5105.

[2] Kato, M.; Yoshida, M.; Sun, Y. & Kobayashi, (2022). *J. Photochem. Photobiol. C*, **51**, 100477.

[3] Kar, P., Yoshida, M., Shigeta, Y., Usui, A., Kobayashi, A., Minamidate, T., Matsunaga N. & Kato, M. (2017). *Angew. Chem. Int. Ed*., **56**, 2345.

[4] Saito, D., Ogawa, T., Yoshida, M., Takayama, J., Hiura, S., Murayama, A., Kobayashi, A. & Kato, M. (2020). *Angew. Chem. Int. Ed*., **59**, 18723.

[5] Saito, D., Galica, T., Nishibori, E., Yoshida, M., Kobayashi, A. & Kato, M. (2022). *Chem. Eur. J.*, e202200703.

[6] Yoshida M. & Kato, M. (2020) *Coord. Chem. Rev.*, **408**, 213194.

[7] Ogawa, T., Yoshida, M., Ohara, H., Kobayashi, A. & Kato, M. (2015). *Chem. Commun*., **51**, 13377.

[8] Yoshida, M.; Sääsk, V.; Saito, D.; Yoshimura, N.; Takayama, J.; Hiura, S.; Murayama, A.; Põhako-Esko, K.; Kobayashi, A. & Kato, M. (2022). *Adv. Opt. Mater.,* **10**, 2102614.

Keynote 3
Room 212/13
9.00am – 9.50am

Keynote–03 –230823

Laboratory X-ray Powder Diffraction in the Research of Painted Artworks

S. Švarcová[1], P. Bezdička[1], J. Hradilová[2], D. Hradil[1,2]

[1]Institute of Inorganic Chemistry of the Czech Academy of Sciences, ALMA Laboratory, Husinec 1001, 250 68 Husinec-Řež, Czech Republic, [2]Academy of Fine Arts in Prague, ALMA Laboratory, U Akademie 4, 170 22 Praha 7, Czech Republic

svarcova@iic.cas.cz

Keywords: XRPD, Paintings, Origin, Degradation

Materials in painted artworks (i.e., panel, easel and miniature paintings, wall paintings, polychromed sculptures and other objects decorated by paint layers) represent an extensive set of inorganic and organic phases, which are often present in complicated mixtures and exhibit characteristics reflecting either their geological genesis (mineral pigments), manufacturing technology (artificial pigments) or diverse biological nature (binders or dyes). The resulting painting technique, i.e., the artists' choice of the painting materials and the way of their application, is influenced both by local availability of materials [1] as well as by iconographic convention, period style, workshop/artists' preferences or regional tradition [2]. To complicate the issue, painting materials tend to change in time. Besides acceptable patina caused by gradual and natural aging of materials, severe degradation can occur, resulting in undesired changes of appearance or endangered stability of artworks [3]. Therefore, the main motivations for material investigation of paintings are i) to describe their painting technique, ii) to identify characteristics suitable for origin/provenance determination and dating of both materials and paintings and iii) to recognise degradation products with the aim to understand the processes of deterioration [1-4]. However, the analyses are often made challenging by the heterogeneous nature and minute size of micro-samples or, in some cases, even by the impossibility of sampling due to preciousness, fragility or small dimensions of the artwork [5]. Nevertheless, laboratory X-ray powder (micro-)diffraction represents a very powerful tool in material investigation of paintings [6] and its efficiency and importance will be illustrated on numerous examples.

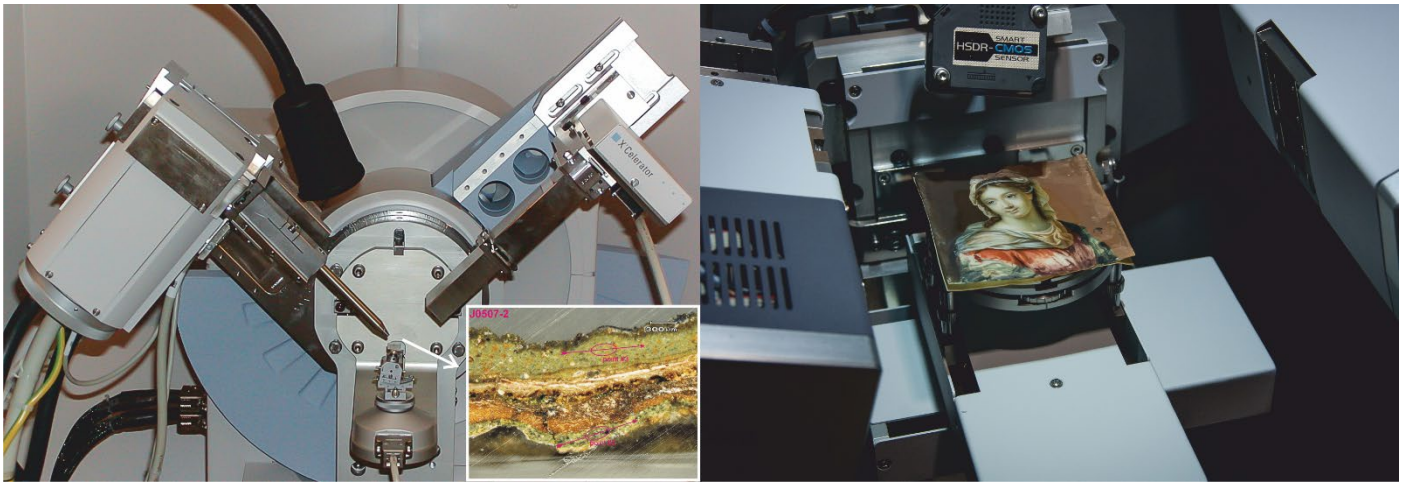

Figure 1. Analytical challenge: analysis of heterogenous micro-sample (left) and delicate miniature painting with prohibited sampling (right) using laboratory XRPD in micro- (left) and conventional (right) set-up.

[1] Hradil, D., Hradilová, J., Bezdička, P., (2020). *Minerals* **10**, 255.

[2] Hradil, D., Hradilová, J., Bezdička, P., Švarcová, S., (2008). *X-ray Spect.* **37**, 376.

[3] Kotulanová, E., Bezdička, P., Hradil D., Hradilová, J., Švarcová, S., et al, (2009). *J. Cult. Her.***10**, 367.

[4] Švarcová, S., Kočí, E., Bezdička, P., Garrappa, S., Kobera, L., et al., (2020). *Dalton Trans*. **49**, 5044

[5] Hradilová, J., Hradil, D., Pech M., Bezdička, P., Neděla, V., et al., (2020). *Microchem. J.* **153**, 104371

[6] Švarcová, S., Kočí, E., Bezdička, P., Hradil, D., Hradilová, J., (2010). *Anal. Bioanal. Chem.* **398**, 1061

The special acknowledgement is addressed to all present and former members of the ALMA Laboratory as well as owners of artworks and numerous co-workers from the field of restoration, conservation and art history, who have contributed to deepening the knowledge of materials in paintings. The work was supported by the Czech Academy of Sciences within the frame of research programme Strategy AV21 No. 23 - City as a Laboratory of Change; Historical Heritage and Place for Safe and Quality Life and by the Czech Science Foundation, project No. 22-17966S.

Keynote 4
Room 203/4
10.20am – 11.10am

Keynote–04 –230823

Flow-induced structural transitions and instability formation in self-assembled micelles revealed by flow-small angle neutron scattering

Patrick J. McCauley 1, Satish Kumar 1, Michelle A. Calabrese 1

Department of Chemical Engineering and Materials Science, University of Minnesota Twin Cities, 421 Washington Avenue SE, Minneapolis, Minnesota, 55455 USA

mcalab@umn.edu

Keywords: rheo-SANS 1, micelle 2, self-assembly 3

Spatially-resolved flow-small angle neutron scattering (flow-SANS) methods paired with time-resolved data processing algorithms are employed to link flow-induced structural transitions and instability formation to measured rheology in surfactant and polymeric wormlike micelles (WLMs) [1-3]. The shear-induced alignment of the micelles is spatially and temporally characterized under shear startup flows by flow-SANS in the flow-gradient planes; results are verified by rheo-particle tracking velocimetry (rheo-PTV). Newly developed, advanced methods of time-resolved data analysis improve the temporal resolution of the SANS experiments by orders of magnitude [1]. By employing SANS during flow startup, we gain insight into how flow-induced structures and WLM flow instabilities like shear banding form and evolve, which differs for surfactant vs. polymeric WLMs (Fig. 1) [2, 3]. Local segmental orientation and alignment in the flow-gradient plane is found to be a complex function of the amphiphile type (surfactant vs. polymer), radial position, and deformation rate. Advances in time-resolved measurements upon shear startup allow both previously observed and new mechanisms of shear band formation to be identified in these solutions. This research quantitatively links micellar flow-induced microstructure and instability formation to the measured nonlinear shear rheology of WLM solutions, aiding in the formulation of WLMs for specific applications, as well as providing data necessary for critically testing modern, microstructure-based constitutive equations.

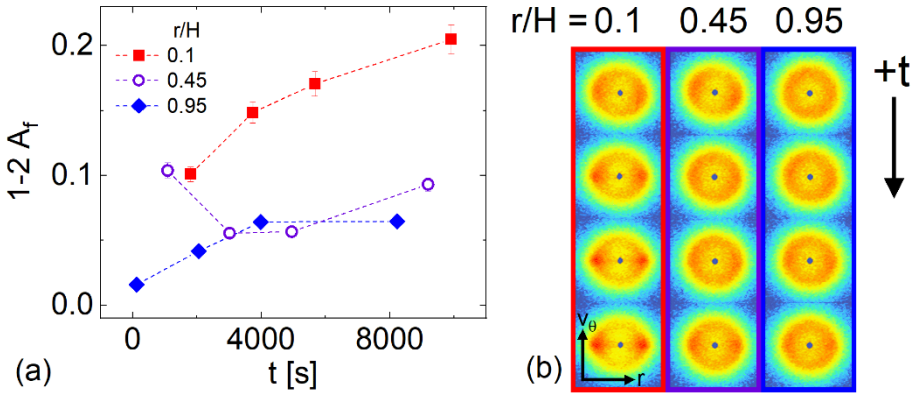

Figure 1. Time- and spatially-dependent alignment factor (a) and corresponding 2D scattering patterns (b) for a polymeric wormlike micelle (WLM) solution during shear startup. Unlike in surfactant WLMs which exhibit a decrease in alignment and scattering anisotropy in time following shear startup, for polymer WLMs, the alignment (a) and degree of anisotropy in the 2D patterns (b) increase in time.

[1] Calabrese, M. A., Wagner, N. J. & Rogers, S. A. (2016). *Soft Matter,* **12**, 2301.

[2] Calabrese, M. A. (2017). *Developing structure-property relationships in branched wormlike micelles via advanced rheological and neutron scattering techniques.* University of Delaware.

[3] McCauley, P. J., Huang, C., Porcar, L., Kumar, S. & Calabrese, M. A. (2023). *J. Rheol.*, **67**, 661.

Keynote 5
Room 210/11
10.20am – 11.10am

Keynote–05 –230823

Finding the atoms that matter in functional materials

J. Etheridge1,2,3, W. Li2, W. Chao2, B. Esser2, T. Petersen1,3

1. Monash Centre for Electron Microscopy, Monash University, VIC 3800, Australia, 2. Dept of Materials Science and Engineering, Monash University, VIC 3800, Australia, 3. School of Physics and Astronomy

joanne.etheridge@monash.edu

Keywords: electron microscopy, nanoparticle, perovskite

It can be small departures from perfect periodicity that give a material its distinctive and useful properties. When these departures occur at the level of individual atoms, they can be particularly challenging to detect and measure, making it difficult to correlate structure with properties.

In modern transmission electron microscopes, electron wavefields can be focussed to form a probe smaller than an atom, providing a powerful tool with which to probe tiny volumes of matter. Furthermore, this probe can be stepped across the material and, every few picometres, the distribution of scattered electrons can be recorded generating a wealth of information about atomic-scale volumes of a specimen. By tuning the incident probe and harvesting selected parts of the scattered signal, specific structural, chemical and/or electronic information can be obtained.

This talk will give an overview of these methods. It will illustrate them with applications to a range of problems in functional materials, such as crystal growth and shape control in metal nanoparticles; structure-property relationships in photoactive, ion-conducting, magneto-resistive and ferroelectric perovskites; surface plasmon polaritons in metallic nanostructures; and bonding in semiconducting heterostructures.

This work was supported by Australian Research (ARC) Grants DP200103070, DP220103800 and FL220100202. The authors acknowledge the use of the instruments and scientific and technical assistance of A/Prof Matthew Weyland at the Monash Centre for Electron Microscopy, a Node of Microscopy Australia, and used equipment funded by ARC Grants LE170100118 and LE0454166.

Keynote 6
Room 212/13
10.20am – 11.10am

Keynote–06 –230823

X-ray crystallography of solid-liquid interfaces

E. Vlieg

Radboud University, Institute for Molecules and Materials, Nijmegen, The Netherlands

e.vlieg@science.ru.nl

Keywords: interface structure, crystal growth, liquid ordering

A full understanding of crystal growth requires knowledge of interfacial processes at the atomic length and time scales. No single method can provide this, but a combination of tools should be able to [1]. Finding consistency among the unsurpassed structural accuracy of X-ray diffraction, the local structure information from modern microscopy tools and the results from molecular dynamics computer simulations is a route to achieve reliable knowledge. This route starts at well-behaved, smooth interfaces and eventually leads to the local structure and dynamics at steps and kinks.

The focus of this presentation will be on the current capabilities of X-ray diffraction to reveal the structure of solid-liquid interfaces. Like in many types of diffraction, also here area detectors have improved the method enormously. A structure determination of an interface requires the intensity from a synchrotron radiation source, hard X-rays to penetrate the liquid, and the analysis of crystal truncation rods. In general, the crystal part of the interface is straightforward to determine because it is (typically) well-ordered, but the liquid part has much less order and 'crystallography' becomes very challenging. The GaN-Ga interface, Figure 1, shows this characteristic behaviour, where the liquid rapidly loses order away from the crystal surface [2]. If possible, it is therefore useful to use supplementary methods and in the case of the calcite-water interface, the results of X-ray diffraction were combined with Molecular Dynamics simulations [3]. When using the best available potentials, or computationally expensive DFT simulations, a very consistent picture of this interface emerges. In the calcite-water case, the liquid order does *not* decay slowly away from the interface, but is found to be restricted to only two monolayers of water.

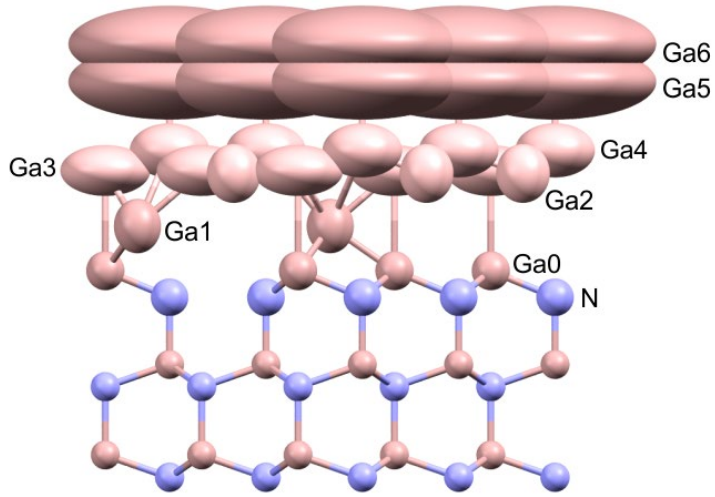

Figure 1. A side view of the GaN(0001)-Ga interface, showing the order in the liquid layers in contact with the crystal as well as the Ga vacancies in the top crystal layer.

[1] E. Vlieg, J. Cryst. Growth (2022) **597**, 126850.
[2] A.E.F. de Jong, V. Vonk, M. Bockowski, I. Grzegory, V. Honkimäki, E. Vlieg, Phys. Rev. Lett. (2020) **124**, 086101.
[3] S.J.T. Brugman, P. Raiteri, P. Accordini, F. Megens, J.D. Gale and E. Vlieg, J. Phys. Chem. C. (2020) **124,** 18564.

A013 Rapid Response Toward Biomedical Threats

Room 208

1.10pm – 3.30pm

A013-01-230823

Structural basis for enhanced cytoplasmic aggregation of familial ALS-associated SFPQ mutants

J. Widagdo[1], S. Udagedara[2], N. Bhembre[1], J.Z.A. Tan[1], L. Neureiter[1], J. Huang[2], V. Anggono[1], M. Lee[2]

[1]*Clem Jones Centre for Ageing Dementia Research, Queensland Brain Institute, The University of Queensland, Brisbane, Queensland 4072, Australia*

[2]*Department of Biochemistry and Chemistry, La Trobe Institute for Molecular Science, La Trobe University, Melbourne, Victoria 3086, Australia*

mihwa.lee@latrobe.edu.au

Keywords: amyotrophic lateral sclerosis, protein aggregation, RNA-binding protein

Splicing factor proline- and glutamine-rich (SFPQ) is a nuclear RNA-binding protein that is involved in a wide range of physiological processes including neuronal development and homeostasis. However, the mislocalization and cytoplasmic aggregation of SFPQ are associated with the pathophysiology of amyotrophic lateral sclerosis (ALS). We have previously reported that zinc mediates SFPQ polymerization and promotes the formation of cytoplasmic aggregates in neurons. Here we characterize two familial ALS (fALS)-associated SFPQ variants, which cause amino acid substitutions in the proximity of the SFPQ zinc-coordinating centre (N533H and L534I). Both mutants display increased zinc-binding affinities, which can be explained by the presence of a second zinc-binding site revealed by the 1.83 Å crystal structure of the human SFPQ L534I mutant. Overexpression of these fALS-associated mutants significantly increases the number of SFPQ cytoplasmic aggregates in primary neurons. Although they do not affect the density of dendritic spines, the presence of SFPQ cytoplasmic aggregates causes a marked reduction in the levels of the GluA1, but not the GluA2 subunit of AMPA-type glutamate receptors on the neuronal surface. Taken together, our data demonstrate that fALS-associated mutations enhance the propensity of SFPQ to bind zinc and form aggregates, leading to the dysregulation of AMPA receptor subunit composition, which may contribute to neuronal dysfunction in ALS.

A013-02-230823

Identification and structural analysis of a novel two-component toxin complex reveals the assembly of membrane pores regulated by proteolytic activation

B.A. Johnstone[1,2], J.C. Evans[3], S.L. Lawrence[4], C.J. Morton[1], H.G Brown[5], M.P. Christie[1,2], R.K. Tweten[3] and M.W. Parker[1,2,4]

[1]Department of Biochemistry and Pharmacology, Bio21 Molecular Science and Biotechnology Institute, University of Melbourne, Parkville, VIC, 3010, Australia. [2]ARC Centre for Cryo-electron Microscopy of Membrane Proteins, Bio21 Molecular Science and Biotechnology Institute, University of Melbourne, Parkville, Victoria, Australia. [3]Department of Microbiology and Immunology, University of Oklahoma, Health Sciences Center, Oklahoma City, OK 73104, USA. [4]Structural Biology Laboratory, St. Vincent's Institute of Medical Research, Fitzroy, VIC 3065, Australia. [4]Ian Holmes Imaging Centre, Bio21 Molecular Science & Biotechnology Institute, University of Melbourne, Parkville, Victoria, Australia
bronte.johnstone@unimelb.edu.au

Keywords: pore-forming protein, bacterial toxin, membrane protein

Cholesterol-dependent cytolysins (CDCs) are bacterial pore-forming toxins that are secreted as soluble monomers and oligomerise into large circular pre-pores on the surface of cholesterol -rich membranes. Various structural changes and transitions results in insertion of β-hairpins into the lipid bilayer, forming a large β-barrel pore that results in cell lysis [1]. We have identified a newly discovered toxin superfamily of more than 200 members that is distantly related to the well characterised CDCs, designated as the "CDC-like" (CDCL) protein family [2]. Many of these CDCLs exist as homologous pairs. We have identified a novel CDCL pair, referred to as EaCDCL long (EaCDCL-L) and EaCDCL short (EaCDCL-S), that originates from the species *Elizabethkingia anophelis,* a commensal bacterium of the *Anopheles* mosquito. We have used X-ray crystallography to reveal the monomeric structures of EaCDCL-L and EaCDCL-S, which both reveal similarities alongside distinct differences compared with the characteristic CDC domains. In the presence of lipids, EaCDCL-L and EaCDCL-S show pore-forming activity – a process we have discovered is dependent on the presence of both protein partners, but also prior proteolytic activation of both EaCDCL-L and EaCDCL-S. Biochemical analysis, X-ray crystallography and small-angle X-ray scattering (SAXS) reveal the role of proteolytic cleavage in cleaving the respective "activation loop". Analysis of the pore species by electron microscopy reveals a large circular oligomeric complex reminiscent of CDC pore complexes, although smaller in diameter. To investigate the structural changes between monomeric and pore states we obtained the cryo-EM structure of the EaCDCL-L/EaCDCL-S pore complex on the surface of liposomes. The inserted b-barrel structure obtained reveals substantial insight into the dramatic conformational changes occurring, which is further supported by cross-linking mass spectrometry data. In summary, we have shown that the ALY toxins share some structural resemblance to CDCs, but in contrast form a two-component pore complex that is regulated by a unique proteolytic cleavage mechanism. CDCL proteins are present in a wide range of bacterial species and are suspected to play key roles in microbial survival and human disease. Our work on ALY provides the first functional and structural insights into the pore-forming mechanism for this fascinating family of proteins.

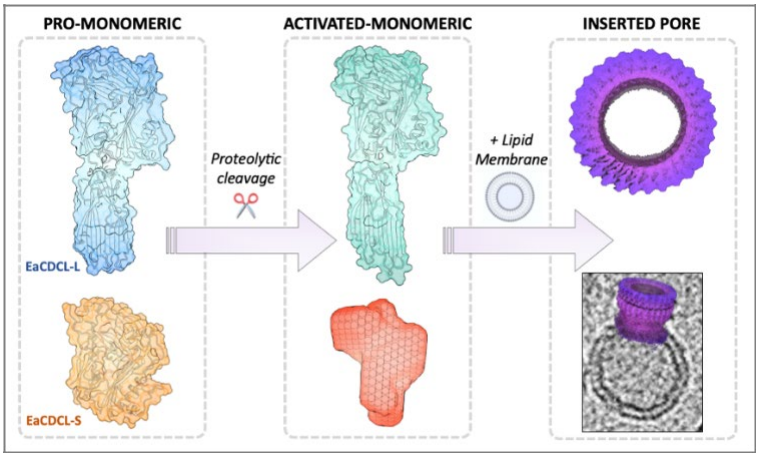

Figure 1. The pore-forming mechanism of EaCDCLs.

Pore formation is associated with substantial conformational changes, progressing from the pro-form of EaCDCL-L and EaCDCL-S to the proteolytically-cleaved activated forms and finally to the bicomponent b-barrel membrane pore.

1 Johnstone, B.A, Joseph, R., Christie, M.P., Morton, C.J., McGuiness, C., Walsh, J.C. Böcking, T., Tweten, R.K., Parker, M.W. (2022) *IUBMB Life*. https://doi.org/10.1002/iub.2661
2 Evans, J.C*, Johnstone, B.A.*, Lawrence, S.L., Morton, C.J., Christie, M.P., Parker, M.W., Tweten, R.K. (2020) *mBio*, 11: e02351-20

A013-03-230823

A story of SARS-CoV-2 RNA capping

Zihe Rao

Tsinghua University, Beijing, China

The coronavirus family has many pathogens that cause severe human diseases, including SARS, MERS and COVID-19.

Starting from the SARS outbreak in 2003, our group has been dedicated to understanding coronavirus Replication-Transcription Complexes (RTCs). During the early part of the COVID-19 outbreak, we rapidly initiated a structural study of SARS-CoV-2 RTCs, aiming to dissect the key mechanisms for SARS-CoV-2 in human cells and provide structural information to discover potent antivirals. With great efforts from our laboratory and outside collaborations, we successfully determined the structure of the central RTC (C-RTC) composed by nsp12 (RNA-dependent RNA polymerase, RdRp) with cofactors nsp7 and nsp8[1], providing the first picture to visualize this key antiviral target. We also elucidated the mechanism of C-RTC catalysis and how remdesivir (RDV) inhibits the synthesis of RNA. This was achieved by determining the structure of C-RTC in complex with the template-product duplex RNA and the active form of RDV[2]. Subsequently, we presented the structure of the elongation RTC (E-RTC), showing how nsp13 (helicase) unwinds the highly-ordered structure in genome to yield the functional template for RNA synthesis in C-RTC[3]. After that, we discovered a key intermediate state of RTC leading towards mRNA capping [Cap(-1)'-RTC], demonstrating the nsp12 NiRAN is indeed the key enzyme to catalyze the second capping action and how it presents nsp9 as an "adaptor" for the further recruitment of capping enzymes into RTC[4]. In a following study, we assembled Cap(0)-RTC by Cap(-1)'-RTC and nsp10/nsp14, showing how the co-transcriptional capping and an *in trans* backtracking mechanism for proofreading concert in one RTC[5]. In our most recent work, we discovered a previously unknown protein modification - RNAylation on nsp9, and demonstrated nsp12 NiRAN utilizes the RNAylated nsp9 and GTP as substrates to synthesize the GpppA cap core, reasoning a novel RNA capping pathway[6]. We also showed that the nucleotide analogue inhibitors (NAIs) can be linked to nsp9 by NiRAN and thus block the occurrence of RNAylation and GpppA formation, furthering the understanding of the mechanism of action of NAIs. An 'induce-and-lock' mechanism is proposed to design new inhibitors against SARS-CoV-2 RNA capping. These works not only provides a basis to understand SARS-CoV-2 proliferates in the host cells through a structural biology lens, but also sheds new light for antiviral development against rapidly emerging SARS-CoV-2 variants.

1 Gao, Y. *et al.* Structure of the RNA-dependent RNA polymerase from COVID-19 virus. *Science* **368**, 779-782, doi:10.1126/science.abb7498 (2020).

2 Wang, Q. *et al.* Structural Basis for RNA Replication by the SARS-CoV-2 Polymerase. *Cell* **182**, 417-428.e413, doi:10.1016/j.cell.2020.05.034 (2020).

3 Yan, L. *et al.* Architecture of a SARS-CoV-2 mini replication and transcription complex. *Nat Commun* **11**, 5874, doi:10.1038/s41467-020-19770-1 (2020).

4 Yan, L. *et al.* Cryo-EM Structure of an Extended SARS-CoV-2 Replication and Transcription Complex Reveals an Intermediate State in Cap Synthesis. *Cell* **184**, 184-193 e110, doi:10.1016/j.cell.2020.11.016 (2021).

5 Yan, L. *et al.* Coupling of N7-methyltransferase and 3'-5' exoribonuclease with SARS-CoV-2 polymerase reveals mechanisms for capping and proofreading. *Cell* **184**, 3474-3485 e3411, doi:10.1016/j.cell.2021.05.033 (2021).

6 Yan, L. *et al.* A mechanism for SARS-CoV-2 RNA capping and its inhibition by nucleotide analogue inhibitors. *Cell*, doi:10.1016/j.cell.2022.09.037 (2022).

A013-04-230823

The structural biology of complex IV biogenesis

M. J. Maher

School of Chemistry and Bio21 Institute, The University of Melbourne, Australia.

Megan.maher@unimelb.edu.au

Keywords: mitochondria, complex IV, copper, heme

The mitochondrial oxidative phosphorylation (OXPHOS) system generates the bulk of cellular ATP, fuelling the energy demands of most eukaryotes. Five multi-subunit protein complexes in the mitochondrial inner membrane, termed complexes I to V, comprise the OXPHOS system.

Complex IV is the last complex of the electron transport chain, transferring electrons from cytochrome *c* to molecular oxygen, and in the process, pumping four protons across the inner membrane. In humans, this complex is composed of 14 subunits with the three mtDNA encoded subunits (COX1-3) forming the catalytic core of the enzyme. Assembly of complex IV requires the participation of a host of cysteine-rich proteins of the mitochondrial intermembrane space (IMS), which take part in a tightly choreographed series of intermolecular interactions for complex IV assembly. However, the identities of all proteins involved, their respective roles and the sequence of their participation in complex IV biogenesis are not known.

Crucially, disruptions in this pathway lead to defects in complex IV assembly, inhibition of oxidative phosphorylation and, in humans, manifests in mitochondrial disease. This presentation will describe our recent work on the characterisation of assembly factors in this pathway, including COA7 [1], COA6 [2,3] and COA5 which reveal the roles of these proteins in complex IV assembly. This research explains the molecular mechanisms of pathogeneses that occur because of identified patient mutations.

[1] Formosa L. E., Maghool S., Sharpe A. J., Reljic B., Muellner-Wong L., Stroud D. A., Ryan M. T., Maher M. J. 'Mitochondrial COA7 is a heme binding protein with disulfide reductase activity, which acts in the early stages of complex IV assembly'. (2022) **PNAS**, 119, e2110357119.

[2] Maghool S., Ryan M. T. and **Maher M. J.** 'What role does COA6 play in cytochrome c oxidase biogenesis: a metallochaperone or thiol oxidoreductase, or both?' (2020) **Int. J. Mol. Sci.**, 21, 6983.

[3] Maghool S., Cooray D. N. G., Stroud D. A., Aragão D., Ryan M. T., **Maher M. J.** 'Structural and functional characterization of the mitochondrial complex IV assembly factor Coa6.' (2019) **Life science alliance**, 2, e201900458.

A013-05-230823

Targeting Multiple proteins that Scavenge, transport, and metabolize Neu5Ac in Gram -ve bacteria.

Parveen Goyal[1], KanagaVijayan Dhanabalan[2], VinothKumar Kutti[3], Ramaswamy Subramanian[1,2]. *Institute for Stem Cell Science and Regenerative Medicine, Bangalore, India. Department of Biological Sciences, Purdue University, USA and National Center for Biological Sciences – TIFR, Bangalore, India. subram68@purdue.edu*

Keywords: Sialic Acid, Gram -ve bacteria, ABC-transporter, TRAP-transporter.

Sialic Acids are nine-carbon sugars. While they form a large class of sugars implicated in various functions, N-glycolylneuraminic acid (Neu5Gc) is the most common among mammals. However, humans synthesize N-acetylneuraminic acid (Neu5Ac) – which has an additional hydroxyl group at the N-5 position. Sialic acids are usually the outermost sugars in most glycoconjugates and play a significant role in cell-cell communication. The presence of Neu5Ac as the outermost sugar signals the human immune system that they are self. Several bacterial species (mostly Gram -ve bacteria) that cause diseases in the oral cavity, brain, intestine, and respiratory tract have been experimentally examined to contain genes to catabolize sialic acids scavenged from their hosts[1]. Pathogens like *Haemophilus influenzae* and *Fusobacterium nucleatum* will not only use sialic acid as a carbon source but have enzymes that will add it as the outermost sugar of their Lipooligosaccharide, helping them evade the human immune system, multiply and cause mortality.

Over the last decade, we have determined the structures of all the proteins involved in scavenging, transport, and catabolism of Neu5Ac into F-6-P and enzymes involved in adding the Neu5Ac as the outermost sugar to the Lipopolysaccharide. We have published earlier the structure of the periplasmic sialic acid binding proteins from several Gram -ve bacteria, including *H. influenzae* and *H. ducreyi* [2,3]. We also reported the structures of the enzyme NanA the first enzyme in the conversion of Neu5Ac into F-6-P, and CMP-Sialic acid synthase, the enzyme that produces the activated sugar for the glycosyl transferase to add sialic acid to Lipooligosaccharide [4,5].

The transport of the Neu5Ac from the periplasm to the cytoplasm is carried out by three types of transporters (SSS type transporter, ATP cassette transporter, and TRAP transporter). In 2018, we published the SSS–type transporter [6]. There are two publications (one where the presenter here is a co-author) of TRAP transporters recently. However, neither has substrate-bound. Building on these studies, we have determined the structure of the TRAP transporter from *F. nucleatum* with and without bound sialic acid and the ATP-dependent transporter from *H. ducreyi*. The details of these structures will be presented.

All of these proteins bind to Neu5Ac. We hope to present the two new structures of the Neu5Ac transporters and a comparison of the binding pocket of all these proteins bound to Neu5Ac. Our hope was to design molecules that would bind to all these Neu5Ac bind sites – which will not only be effective but also prevent the quick development of antimicrobial resistance. Our work demonstrates the interesting challenges faced in designing drug molecules where the binding pocket of the same substrate displays various modes of interactions across these pathogenic bacterial species.

1 Haines-Menges BL, Whitaker WB, Lubin JB, Boyd EF. Host Sialic Acids: A delicacy for the pathogen with discerning taste.

2 Microbiol Spectr. 2015;3: 10.1128/microbiolspec.MBP-0005–2014. doi:10.1128/microbiolspec.MBP-0005-2014

3 Gangi Setty T, Cho C, Govindappa S, Apicella MA, Ramaswamy S. Bacterial periplasmic sialic acid-binding proteins exhibit a conserved binding site. Acta Cryst D. 2014;70: 1801–1811. doi:10.1107/S139900471400830X

4 Setty TG, Mowers JC, Hobbs AG, Maiya SP, Syed S, Munson RS, et al. Molecular characterization of the interaction of sialic acid with the periplasmic binding protein from Haemophilus ducreyi. Journal of Biological Chemistry. 2018;293: 20073–20084. doi:10.1074/jbc.RA118.005151

5 Manjunath L, Guntupalli SR, Currie MJ, North RA, Dobson RCJ, Nayak V, et al. Crystal structures and kinetic analyses of *N*-acetylmannosamine-6-phosphate 2-epimerases from *Fusobacterium nucleatum* and *Vibrio cholerae*. Acta Crystallographica Section F Structural Biology Communications. 2018;74: 431–440. doi:10.1107/S2053230X18008543

6 Bose S, Purkait D, Joseph D, Nayak V, Subramanian R. Structural and functional characterization of CMP-N-acetylneuraminate synthetase from Vibrio cholerae. Acta Crystallographica Section D: Structural Biology. 2019;75: 564–577. doi:10.1107/S2059798319006831

7 Wahlgren WY, Dunevall E, North RA, Paz A, Scalise M, Bisignano P, et al. Substrate-bound outward-open structure of a Na+-coupled sialic acid symporter reveals a new Na+site. Nature Communications. 2018;9: 1753. doi:10.1038/s41467-018-04045-7

A013-06-230823

Structural biology response to biomedical threats

W. Minor

Department of Molecular physiology and Biological Physic, University of Virginia, Charlottesville, VA 22903, USA

Keywords: Covid-19, coronavirus, Zika,,Ebola, virusMED

Structural information is the quintessential prerequisite for structural-guided drug discovery[1]. However, accurate structural information is only a piece of information necessary to understand the big picture of medical disorders[2]. To provide a rapid response to emerging biomedical challenges and threats like COVID-19, we need to analyze medical data in the context of other in-vitro and in-vivo experimental results[3,4]. This approach may revolutionize drug discovery, albeit only when these data are combined and analyzed with effective data management framework like Advanced Information System proposed in 2017[4]. The recently published virusMED system is a blueprint for Advanced Information Systems[5,6].

[1] Zheng H, Hou J, Zimmerman MD, Wlodawer A, Minor W (2014) The future of crystallography in drug discovery. Expert Opin. Drug Discov. 9:125–37.

[2] Zheng H, Handing KBB, Zimmerman MDD, Shabalin IGG, Almo SCC, Minor W (2015) X-ray crystallography over the past decade for novel drug discovery - where are we heading next? Expert Opin Drug Discov 10:975–989.

[3] Grabowski M, Macnar JM, Cymborowski M, Cooper DR, Shabalin IG, Gilski M, Brzezinski D, Kowiel M, Dauter Z, Rupp B, et al. (2021) Rapid response to emerging biomedical challenges and threats. IUCrJ 8:395–407.

[4] Zheng H, Porebski PJ, Grabowski M, Cooper DR, Minor W (2017) Databases, Repositories, and Other Data Resources in Structural Biology. Methods Mol. Biol. 1607:643–665.

[5] Coulibaly F (2021) VirusMED: Your travel guide to the virus world. IUCrJ 8:857–859.

[6]. Zhang H, Chen P, Ma H, Woinska M, Liu D, Cooper DR, Peng G, Peng Y, Deng L, Minor W, et al. (2021) VirusMED: An atlas of hotspots of viral proteins. IUCrJ 8:931–942.

A020 Modern Statistical Tools and Computational Methods in Structure Determination

Room 209

1.10pm – 3.30pm

A020-02-230823

A global Ramachandran score identifies protein structures with unlikely stereochemistry

O. V. Sobolev1, P. V. Afonine1, N. W. Moriarty1, M. L. Hekkelman2,3, R. P. Joosten2,3, A. Perrakis2,3, P. D. Adams1,4

Molecular Biosciences and Integrated Bioimaging Division, Lawrence Berkeley National Laboratory, Berkeley, CA 94720, USA, Division of Biochemistry, The Netherlands Cancer Institute, Plesmanlaan 121, 1066 CX Amsterdam, the Netherlands, Oncode Institute, Amsterdam, the Netherlands, Department of Bioengineering, University of California, Berkeley, CA 94720, USA osobolev@lbl.gov

Keywords: Ramachandran plot, validation, Rama-Z

Ramachandran plots report the distribution of the (φ, ψ) torsion angles of the protein backbone and are one of the best quality metrics of experimental structure models. Typically, validation software reports the number of residues belonging to “outlier”, “allowed” and “favored” regions. While “zero outliers” is considered the “gold standard”, it can be misleading if deviations from expected distributions, even within the favored region, are not considered.

At low resolution it is often necessary to use additional information such as internal molecular symmetry, homologous structure models, information about secondary structure and rotameric states of protein amino-acid side chains. Clearly, the well-defined distribution of protein main-chain φ and ψ angles in Ramachandran space is yet another source of information that can guide model building and refinement. Ramachandran restraints can prevent deterioration of backbone conformation during low-resolution refinement, thereby helping to obtain chemically meaningful models. Many software packages provide an option to use Ramachandran restraints.

While helpful for refinement, actively using the Ramachandran plot as a source of restraints reduces its merit as an independent validation metric. The refined model may then appear to have desirable Ramachandran statistics in terms of expected fractions of residues belonging to favored/allowed/outlier regions, while the distribution of (φ, ψ) itself is improbable: this may not be obvious to an untrained eye.

We therefore turned our attention to the Ramachandran Z-score (Rama-Z), a quality metric introduced three decades ago, but underutilized [1].

We re-implemented Rama-Z in CCTBX using modern high quality models from top8000 database used to derive Ramachandran plot contours in MolProbity. Increased number of high quality models allowed us to use smaller grid size. We advocate that Rama-Z is well suited to assess backbone geometry and highlight unusual distributions of (φ, ψ) angles on Ramachandran plot that otherwise can be unnoticed. The metric does not depend on experimental data (X-ray or Cryo-EM) used to derive atomic model.

One of the limitations of the Rama-Z score is that it is not very suited for small structures with few residues. This is mostly caused by the nature of the metric that relies on normalization against a control set of structure models. Normalization is not well suited to small sample sizes, i.e. few available residues. To estimate the reliability of the Rama-Z score for a particular model we use the Jackknife method to estimate RMSD.

The method is implemented and available in open-source CCTBX (mmtbx.rama_z) library as well as in Phenix as command line tool phenix.rama_z and also in various validation reports generated by Phenix. The tortoize implementation is available in PDB-REDO and will become available in the CCP4 and CCP-EM suites in the near future.

We suggest new cutoffs for Rama-Z validation being |Rama-Z| > 3 is for improbable backbone geometry, 2 < |Rama-Z| < 3 for unlikely yet possible, |Rama-Z| < 2 is for normal backbone geometry. Particular Rama-Z scores should be reported along with its reliability.

We argue for a greater acceptance of this metric by the community. PDB-REDO has been reporting Rama-Z score since its inception. More discussion of this metric is published recently [2].

1 Hooft, R. W. W., Sander, C. & Vriend, G. (1997). *Bioinformatics*. **13**, 425–430.

2 Sobolev, O. V., Afonine, P. V., Moriarty, N. W., Hekkelman, M. L., Joosten, R. P., Perrakis, A., Adams, P. D. (2020). *Structure*. **28**. 1249-1258.

This work was supported by the NIH (Project P01 GM063210), the Phenix Industrial Consortium and by the Netherlands Organization for Scientific Research (NWO; Vidi grant 723.013.003).

A020-03-230823

Direct Phase Determination in Protein Crystallography using Iterative Projection Algorithms

R.L. Kingston[1], M.J. Barnett[1], R.P. Millane[2]

[1]School of Biological Sciences, University of Auckland, Auckland, New Zealand. [2]Computational Imaging Group, Department of Electrical and Computer Engineering, University of Canterbury, Christchurch, New Zealand.

Email: rl.kingston@auckland.ac.nz

Keywords: *ab initio* phasing, non-convex optimization problems, difference map algorithm

The problem of phase determination in protein crystallography can be treated as a constraint satisfaction problem, in which an image is sought that is consistent with both the diffraction data, and generic constraints on the density function in the crystal. If the constraints on the density are sufficiently powerful, then the solution to the phase problem will be unique. However, it may be non-trivial to locate the solution, as the associated optimization problem is highly non-convex.

In a typical protein crystal more than 50% of the volume is occupied by solvent. This provides a powerful image constraint, as the density in the solvent region is effectively featureless. We recently showed that the *solvent flatness constraint* is powerful enough to overcome the phase problem in protein crystallography [1]. Using *iterative projection algorithms*, with good global convergence properties, it is possible to locate the correct solution without *any* initial phase information. A correct image can be routinely formed direct from the diffraction data when the solvent fraction of protein crystals exceeds ~0.7. A practical phase determination procedure was developed [2] which breaks the problem down into two stages; initial approximation of the molecular envelope at low resolution, followed by subsequent phase determination using all of the data (Fig. 1). The procedure works at the modest resolutions typical of protein crystallography (1.9–3.5 Å), and the resultant maps are free of model bias.

The challenge now is to extend the reach of this approach. About 4.5% of protein crystals are expected to have solvent fraction greater than 0.7, but 19% will have solvent fraction greater than 0.6, and 52% will have solvent fraction greater than 0.5 [3]. Hence even a small lowering of the threshold solvent content for applicability of the method would bring many more structures within scope. We will describe how the reach of our procedure has been extended, both through further development of the computational approach, and the incorporation of additional constraints on the image.

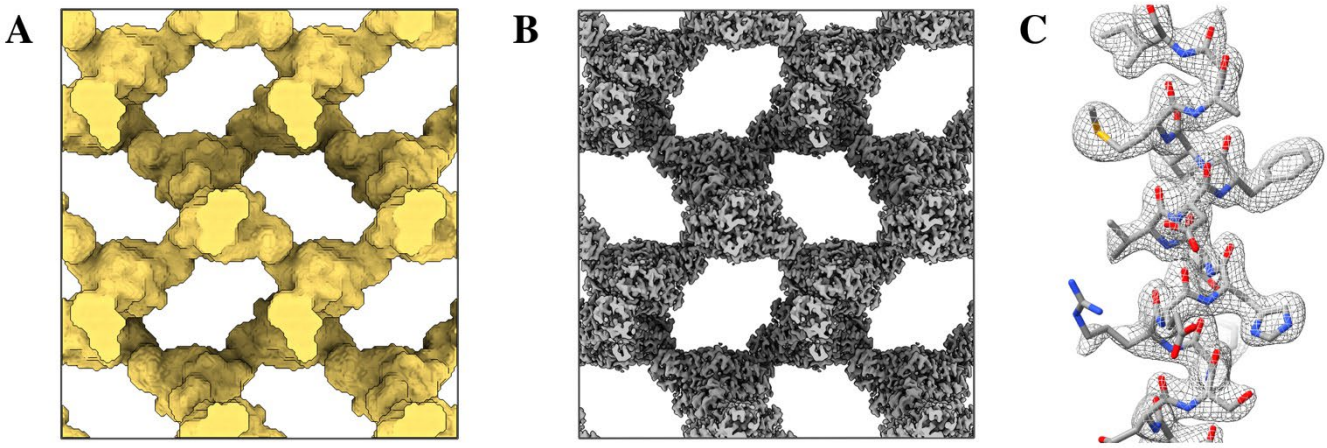

Figure 1. Direct phase determination for a test case (PDB ID 2rha, solvent fraction 0.8, resolution 2.1Å). (A) The consensus molecular envelope. (B) An overview of the reconstructed density function. (C) Detail of the reconstructed density together with the deposited atomic model.

[1] Kingston R.L. & Millane R.P. (2022). *IUCrJ*. **9**, 648–65.
[2] Program IPA: Iterative Projection Algorithms for protein crystallography. https://github.com/rlkingston/IPA
[3] Weichenberger, C. X. & Rupp, B. (2014). *Acta Cryst.* D**70**, 1579–1588.

We gratefully acknowledge financial support from the Royal Society of New Zealand Marsden fund.

A020-04-230823

Phasing Neural Network: Ab-initio determination of crystal structures at 2 Å resolution

Anders S. Larsen, Toms Rekis and Anders Ø. Madsen

Department of Pharmacy, University of Copenhagen. Unviersitetsparken 2, Copenhagen, Denmark.

Keywords: Ab-initio phasing, Machine learning, Neural network

For a crystal structure to be solved from the diffraction data, it is necessary to obtain the complex structure factors, F_H, of the measured reflections. Their squared moduli, $|F_H|^2$, are proportional to the measured intensities, but the phase angles needed to reconstruct the complete complex numbers cannot be determined experimentally. Since the exact solution to this phase problem is not known, several methods to overcome this crucial step in crystal structure determination have been developed over time. For example, direct methods or the charge flipping algorithm can be used for most organic, inorganic, and metal-organic structures. Nevertheless, these methods fail if, for example, the available data resolution is not sufficiently high, the completeness of the data is low, or if the number of atoms in the asymmetric unit is very high - as is the case for macromolecular crystals and some framework structures.

Here we demonstrate how the phase problem can be solved using a neural network. The network has been trained on millions of fictive structures containing metal atoms and/or molecular fragments. At the time of writing the neural network has only been trained on structures in the centrosymmetric space group $P2_1/c$.

A validation set consisted of thousands of structures retrieved from the Cambridge Structural Database for which the structure factor amplitudes, |FH|, were generated at several resolution limits and fed into the trained network to output phases. The phases could be retrieved with a striking accuracy leading to correct structure solutions for over 99% of the validation set entries. Furthermore, the phase accuracy was also high if the resolution limit was chosen to be low, i.e. dmin = 2 Å. Several dozens of experimentally measured diffraction data sets were also used for validation. Our results indicate that deep learning can be used to obtain electron density maps of structures for which only a limited resolution data can be obtained, and which are problematic to solve using currently available methods.

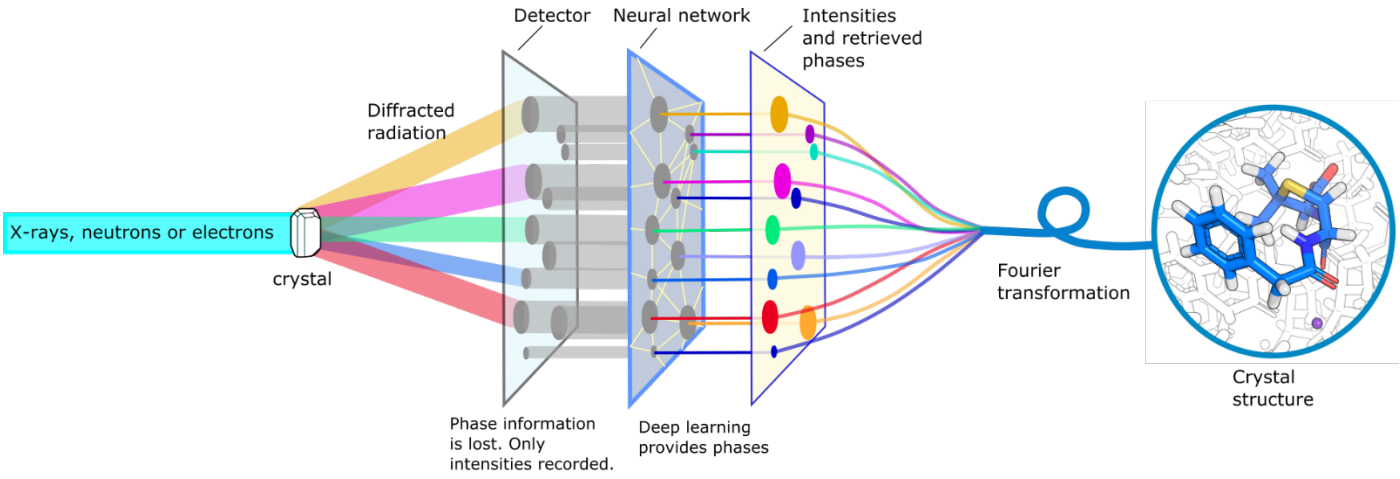

Figure 1. The neural network has been trained to provide ab-initio phases. This allows structure determination at 2 Å resolution.

A020-05-230823

Robust and efficient likelihood-based docking of models into cryo-EM reconstructions

Randy J Read[1], Claudia Millán[1,2], Airlie J McCoy[1] and Thomas C Terwilliger[3,4]

[1]Cambridge Institute for Medical Research, University of Cambridge, The Keith Peters Building, Hills Road, Cambridge CB2 0XY, UK; [2]SciBite Ltd, BioData Innovation Centre, Wellcome Genome Campus, Hinxton, Cambridge CB10 1DR, UK; [3]New Mexico Consortium, Los Alamos, NM 87544, USA; [4]Los Alamos National Laboratory, Los Alamos, NM 87545, USA

Email: rjr27@cam.ac.uk

Keywords: cryo-EM, likelihood, docking

Fast, reliable docking of models into cryo-EM maps requires understanding of the errors in the maps and the models. Likelihood-based approaches to errors have proven to be powerful and adaptable in experimental structural biology, finding applications in both crystallography and cryo-EM. Indeed, previous crystallographic work on the errors in structural models is directly applicable to likelihood targets in cryo-EM.

In this work, we have derived likelihood targets in Fourier space to characterise, based on the comparison of half-maps, the direction and resolution-dependent variation in the strength of signal and noise in the data. Because the signal depends on local features, the signal and noise are preferably analysed in local regions of the cryo-EM reconstruction.

The signal and error parameters deduced from the comparison of half-maps are then used, in likelihood targets, to measure the agreement with docked atomic models. The likelihood-based rotation function used in crystallography in *Phaser* [1] can be employed to establish plausible orientations in a docking search. A phased likelihood translation function then yields scores for the placement and rigid-body refinement of oriented models.

For crystallographic molecular replacement, we have previously shown that expected log-likelihood-gain (eLLG) scores can be predicted from the anticipated quality of the model and the quality and completeness of the data, then used to inform the search strategy [2]. We show here that similar eLLG scores can be computed, in advance of the search calculation, for docking models into cryo-EM reconstructions. These scores are used to devise optimal strategies for choices of the resolution of data and the size of search volumes.

Tests demonstrate that the new procedure is fast, robust and effective at placing models into cryo-EM maps. Fig. 1 shows an example in which one chain from the crystal structure of the membrane domain of *E. coli* respiratory complex 1 (PDB entry 3rko [3]) can be docked correctly into the cryo-EM reconstruction of the whole complex (PDB entry 7nyu, EMDB entry 12654 [4]), in a region where the local resolution is about 11 Å.

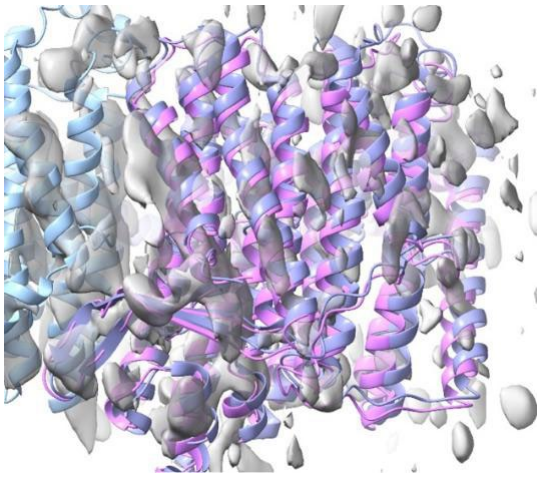

Figure 1. Chain L of 3rko (X-ray structure) docked into poorly-ordered cryo-EM density. The docked model is shown in magenta, with chains L and M of the deposited structure (7nyu) in dark and light blue respectively.

1 McCoy AJ, Grosse-Kunstleve RW, Adams PD, Winn MD, Storoni LC and Read RJ. *J. Appl. Cryst.* **40**: 658-674 (2007). PMC2483472
2 Oeffner RD, Afonine P, Millán C, Sammito M, Usón I, Read RJ and McCoy AJ. *Acta Cryst.* **D74**: 245-255 (2018). PMC5892874

3 Efremov RG and Sazanov LA. *Nature* **476**: 414-420 (2011).
4 Kolata P and Efremov RG. *Elife* **10**: e68710 (2021).

This research was supported by the Wellcome Trust (grant 209407/Z/17/Z to RJR) and the National Institutes of Health USA (grant GM063210 to TCT and RJR).

A020-06-230823

CCP-EM 2.0: Software tools for efficient, accurate, and reproducible management and automation of cryoEM processing from images to structures

T. Burnley, M. Iadanza1, A. Joseph1, C. Palmer1, M.Winn1

Scientific Computing Department, STFC, Rutherford Appleton Laboratory, Fermi Ave, Harwell, Didcot OX11 0QX

tom.burnley@stfc.ac.uk

Keywords: cryo-electron microscopy, methods, computation

The multiple steps necessary to generate accurate atomic models from raw cryoEM micrographs can be accomplished using a large variety of methods and software packages and it is incumbent on researchers to track and accurately report methods used to generate their structures. Unfortunately, both the level of detail and accuracy on the methods used to generate the over 18,000 records in the EMDB and almost 10,000 EM-derived atomic models in the PDB are inconsistent.

Here we present CCP-EM 2.0 a software package to streamline cryoEM data processing and metadata management. CCP-EM 2.0 is built on the CCP-EM Pipeliner and Doppio modules. Pipeliner is a unified framework for all steps of data processing that tracks details of the processing workflow. Doppio provides a user-friendly graphical interface to the Pipeliner, allowing users to visualize the workflow of their project, launch processing tasks, and manage the structure of the project.

The CCP-EM Pipeliner includes software tools contributed by >10 collaborating groups. These include: Buccaneer, DockEM, FlexEM, LAFTER, LocScale, Modelangelo, Relion, Refmac, LocScale, Model Validation and TEMPy and cover all aspects of processing cryoEM data, from raw micrographs through a validated atomic model, and supports seamless integration of other programs through a plug-in system. The software generates both metadata reports and archives from entire projects or subsections of a project. Reports present complete data about the processing methods and results in a standardized format with defined data schema to streamline integration into downstream applications. Archives preserve entire project workflows, allowing projects to be transferred and reproduced.

Methods sections in publications rarely have the level of detail necessary to completely recreate a processing workflow limiting data reproducibility and use for training ML algorithms. Even the more extensive processing data recorded in databases such as the PDB and EMDB do not contain full running parameters for every processing step. These resources are additionally limited by dependency on users accurately recording and transcribing every step in complex workflows. CCP-EM 2.0 provides a suite of tools for end-to-end data management which will reduce barriers to users depositing complete and accurate processing information with their published structures which will be a valuable resource to researchers and software developers alike.

Alongside presenting the Pipeliner and the Doppio an overview of the current tools in the CCP-EM suite will be given alongside new developments.

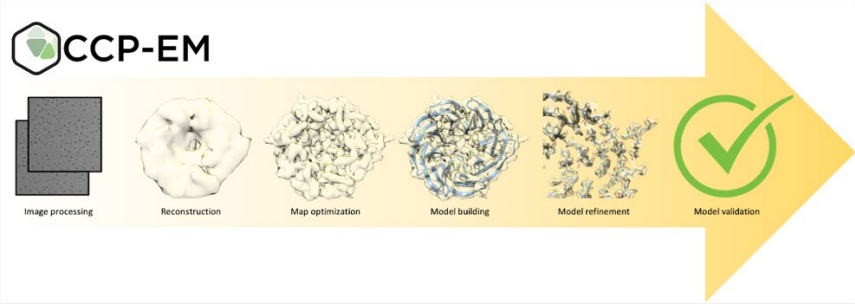

Figure 1. From images to validated structures in the CCP-EM 2.0 software suite.

A036 Combining Electron and X-ray Crystallography for Structure Characterization
Room 217
1.10pm – 3.30pm

A036-01-230823

3D electron diffraction of pure sulfur: challenges and achievements

Sepideh Rahimi, Joke Hadermann

EMAT, Department of Physics, University of Antwerp, Antwerpen 2020, Belgium

Sepideh.rahimi@uantwerpen.be

Keywords: Sulfur, 3DED, In-situ electron microscopy

As the cathode material in Lithium-sulfur batteries (LSBs), sulfur is known to give a high specific capacity (1675 mAh/g) [1]. The transformation of the sulfur structure during cycling is an interesting aspect. In LSBs, the limitation is the shuttling effect where the polysulfides that are produced during the oxidation reaction of sulfur with lithium, dissolve in the electrolyte [2]. As a consequence, sulfur will deposit on the lithium anode. It is important to know the crystal structure of the deposited species so they could be confined in the first place at the cathode [3].

So far a few forms of polysulfides have been studied with X-ray crystallography using high-quality datasets but no electron microscopy study [4-7]. This is due to sulfur sublimation in high vacuum conditions of TEM which has been proved theoretically and experimentally [9]. Also, during experiments in this work, it was revealed that sulfur is highly sensitive to the electron beam thus conventional TEM studies are not applicable to this element.

Nowadays, thanks to the progress in *in-situ* facilities developed for TEM [10], sulfur can be kept isolated from the vacuum by a gas or liquid cell. Therefore, it is potentially possible to study the crystal structure of polysulfides either in the stable phase (conventional powders in a gas cell) or during a reaction for less stable phases (intermediate species in a liquid nanoreactor).

In this work, for the first time, the crystal structure of the sulfur S_8 phase has been studied under a protected atmosphere with 3D electron diffraction (3DED) and the structure has been solved successfully. Due to the geometry of the *in-situ* cells, there is a limitation in the tilt range for data acquisition, leading to less coverage of reciprocal space. So determining the cell parameters is a challenge in the first step. However, comparison with XRD results helped in the cell parameters determination, complemented by electron diffraction data for symmetry and space group determination. In addition, merging several datasets from different particles added more completeness to the imported data for solving the structure

1) Shi, K., Lin, Y., Li, J., Xiong, Z., Liao, J., Liu, Q. (2022) *Ind. Eng. Chem. Res.*, **61(6)**, 2502–2510.

2) Huang, J. Q., Zhang, Q., Peng, H. J., Liu, X. Y., Qian, W. Z., Wei, F. (2014) *Energy Environ. Sci.*, **7**, 347-353.

3) Han, F., Yue, J., Fan, X., Gao, T., Luo, C., Ma, Z., Suo, L., Wang, C., (2016) *Nano Lett.* , 16(7), 4521–4527.

4) Pawley, G.S. & Rinaldi, R.P. (1972) *Acta Crystallographica B*, **28**, 3605-3609.

5) Templeton, L. K., Templeton, D., H., Zalkin, A. (1976) *Inorg. Chem.*, **15(8)**, 1999–2001.

6) Steudel, R., Bergemann, K., Buschmann, J., Luger, P. (1996) *Inorg. Chem,* **35**, 2184-2188.

7) Gromilov, S.A., Piryazev, D.A., Egorov, N.B., Akimov, D.V. (2016) *J. Str. Chem.,* **57(8)**, 1663-1666.

8) Ferreira, A. G. M. & Lobo, L.Q. (2010) *J. Chem. Ther.*, **43(2)**, 95-104.

9) Ronan O, Downing C and Nicolosi V. (2022) *Open Res Europe*, **2**:1.

10) Karakulina, O. M., Demortière, A., Dachraoui, W., Abakumov, A. M., Hadermann, J. (2018) *Nano Lett.*, **18(10)**, 6286–6291.

A036-02-230823

Correlation between 2- and 3-dimensional crystallographic lattices for epitaxial analysis

J. Simbrunner[1], J. Domke[2], O.T. Hofmann[3], T. Fritz[2], R. Forker[2], R. Resel[3]

[1]Division of Neuroradiology, Vascular and Interventional Radiology, Medical University Graz, Austria, [2] Institute of Solid State Physics, Friedrich Schiller University Jena, Germany, [3]Institute of Solid State Physics, Graz University of Technology, Austria

josef.simbrunner@medunigraz.at

Keywords: GIXD, LEED, crystallographic lattice, surface unit cell

While the crystalline properties of an epitaxially grown thin film can be studied in three dimensions by X-ray methods like grazing incidence X-ray diffraction (GIXD), the first monolayer is only accessible by surface sensitive methods that allow the determination of a two-dimensional lattice like low-energy electron diffraction (LEED). GIXD measurements with sample rotation on epitaxially grown film (with thicknesses from 10 to 30 nm) are compared with distortion-corrected LEED experiments of molecular monolayers: PTCDA, 6,13-pentacenequinone (P2O), 1,2;8,9-dibenzopentacene (trans-DBPen) and dicyanovinylquaterthiophene (DCV4T-Et2) grown by physical vapour deposition on Ag(111) and Cu(111) single crystals. For these molecular crystals, which exhibit different crystallographic lattices and crystal orientations as well as epitaxial properties, the geometric parameters of the three-dimensional lattice are compared with the corresponding geometry of the first monolayer. The theoretical basis has been derived which provides a mathematical relationship between the six lattice parameters of the three-dimensional case with the three parameters obtained for the surface unit cell, together with their orientation to the single crystalline substrate [1]. In two dimensions, the positive and negative orientations of the contact planes, i.e., the planes with the Miller indices (uvw) and -(uvw), correspond to surface unit cells with mirror symmetry about an axis along the lattice vector a. In each case, unit cells with 60° symmetry were observed. Thus, rotational and mirror symmetries coexist. An excellent correlation could be achieved between the predicted and the experimentally obtained two-dimensional unit cell parameters [2].

A comparison of the monolayer lattice from LEED investigations with the surface unit cells of multilayer lattices determined by rotated GIXD experiments reveals a correlation between the first monolayer and the epitaxial growth of three-dimensional crystals together with lattice distortions and re-alignment of molecules. The selected examples showed three possible scenarios of crystal growth on top of an ordered monolayer: (1) In PTCDA/Ag(111) and P2O/Ag(111) the growth of a single polymorph was obtained with congruent two-dimensional lattices in the monolayer and multilayer. (2) In DCV4T-Et2/Ag(111) three different polymorphs with various cell parameters, orientations and azimuthal alignments were observed in the multilayer. Whereas their threedimensional lattices differ significantly, their surface unit cells converge to a single unit cell in the monolayer. (3) In transDBPen/Cu(111) strong lattice distortion and distinct molecular re-alignments from the monolayer to epitaxially grown crystals were observed (see Fig. 1). In this work, a combined experimental approach of GIXD and LEED is introduced which can be used to investigate the effect of the epitaxial monolayer on the evolution of molecular crystals with epitaxial order grown on top.

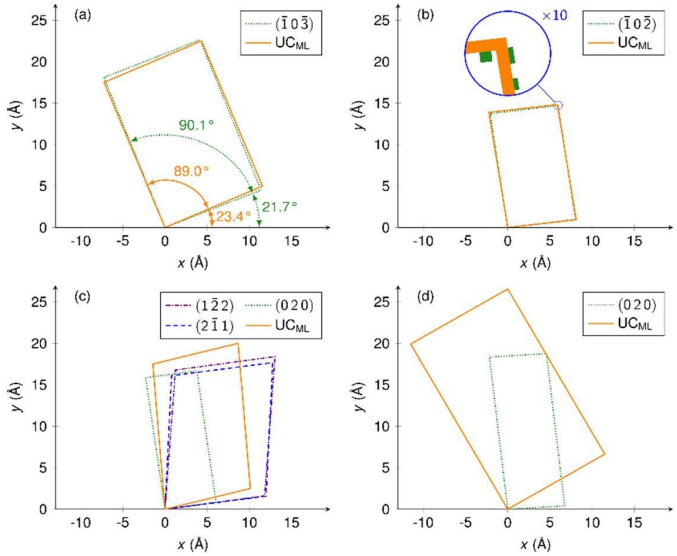

Figure 1. Real-space visualization of the results (a) PTCDA/Ag(111), (b) P2O/Ag(111), (c) DCV4T-Et2/Ag(111), and (d) transDBPen/Cu(111). Broken lines depict the surface unit cells extracted from the GIXD measurements, where (uvw) indicate the contact planes of the epitaxially oriented crystals. Solid lines show the surface unit cells of the monolayer (UC_{ML}) in contact with the substrate, as measured with LEED.

[1] Simbrunner, J., Domke, J., Resel, R., Forker, R. & Fritz, T. (2022). Acta Cryst. A78, 262
[2] Simbrunner, J., Domke, J., Sojka, F., Jeindl, A., Otto, F., Gruenewald, M., Hofmann, O. T., Fritz, T., Resel, R. & Forker, R. (2022). Acta Cryst. A78, 272

A036-03-230823

Complementary use of electron and X-ray microcrystallography to reveal quantum structural information of organic molecules

K. Takaba1, S. Maki-Yonekura1, I. Inoue1, K. Tono1,2, M. Yabashi1,2, K. Yonekura1,3

RIKEN SPring-8 Center, Sayo, Hyogo, 679-5148, Japan, JASRI, Sayo,Hyogo, 679-5198, Japan, IMRAM, Tohoku University, Sendai, Miyagi, 980-8577, Japan

takaba@spring8.or.jp

Keywords: Serial XFEL crystallography, 3D ED, atomic charge, hydrogen polarity

Structure determination of micro- to nano-meter sized crystals has been greatly enhanced over the past decade with diffraction using synchrotron X-rays or electron microscopy. The scattering phenomena through these beam sources are intrinsically different and should be reflected in structure modelling and interpretations. Though quantum insights into the crystal structures have been limited to some easily grown or less complex samples, they are hoped that such a microcrystallographic approach will extend to more general targets, including organic molecules. To realize this concept, we must perform both crystallographic analysis in carefully but practically designed experimental setups to obtain as accurate atomic or sub-atomic structures as possible. Moreover, the description on the features of the available density maps must also be improved to maximize the information extracted.

We have recently improved 3D electron diffraction, so called *3D ED* or *microED*, of organic compound microcrystals using a JEOL electron microscope [1, 2], and also shown that a serial X-ray crystallography, *SX* or *SFX*, with femtosecond XFEL pulses at SACLA in Japan was applicable to such microcrystalline samples [3]. In these processes, we not only investigated the advantages and disadvantages of both methods, but also evaluated the obtained structures quantitatively. In the most ideal sample so far, Rhodamine-6g crystals, the sensitivity to atomic charges was evaluated to be better for electrons than for X-rays, while X-rays yielded atomic positions more precisely than electrons. Hydrogen atoms were distinctively visualized in the electron density and Coulomb potential maps obtained with XFEL and electron beams, respectively, and systematic differences as in Fig. 1 should indicate the polarity reflecting the chemical environments around. Such quantum information will effectively estimate the inter- and intra-molecular non-covalent interactions more quantitatively and indispensable to the more direct comparison with computational chemistry. We here discuss these complementary crystallographic approaches and the challenges for further development.

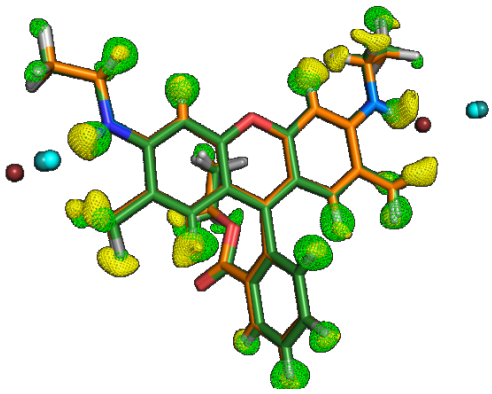

Figure 1. Structures of rhodamine-6g and the electron density (green) and Coulomb potential (yellow) maps for hydrogen atoms, obtained from SX and 3D ED, respectively.

[1] Takaba, K., Maki-Yonekura, S., Yonekura, K. (2020). *J. Struct. Biol.*, **211**, 107549.

[2] Takaba, K., Maki-Yonekura, S., Inoue, S., Hasegawa, T., Yonekura, K. (2021). *Front. Mol. Biosci.*, **7**, 612226.

[3] Takaba, K., Maki-Yonekura, S., Inoue, I., Tono, K., Hamaguchi, T., Kawakami, K., Naitow, H., Ishikawa, T., Yabashi, M., Yonekura, K. (2021). preprinted in *ChemRxiv* and to be published.

We thank Tasuku Hamaguchi, Keisuke Kawakami, and Hisashi Naitow for their supports on the SX data collection.

A036-04-230823

In-depth characterization of ultrasmall nanoparticles by combined X-ray techniques

O. Prymak[1], O. Wetzel[1], N. Wolff[1], K. Loza[1], M. Heggen[2], C. Weidenthaler[3], C.L.P. Oliveira[4], M. Epple[1]

[1]Inorganic Chemistry and Center for Nanointegration Duisburg-Essen (CeNIDE), University of Duisburg-Essen, Universitätsstr. 5-7, 45117 Essen, Germany, [2]Ernst Ruska-Centre for Microscopy and Spectroscopy with Electrons, Forschungszentrum Jülich GmbH, 52425 Jülich, Germany, [3]Max-Planck-Institut für Kohlenforschung, Kaiser-Wilhelm-Platz 1, 45470 Mülheim an der Ruhr, Germany, [4]Institute of Physics, University of São Paulo, Rua do Matão 1371, 05508-090 São Paulo, Brazil

oleg.prymak@uni-due.de

Keywords: Ultrasmall nanoparticles, metal oxides, diffraction

Ultrasmall nanoparticles (usNPs) of noble metals are of high interest in materials science, e.g. in catalysis, photonics and biomedicine, due to their high specific surface area. The synthesis of very small sized particles (1-2 nm) and especially their structural characterization is very challenging and requires complex diffraction, spectroscopic and microscopic techniques using X-ray beam. In this work usNPs of coin (Ag, Au) and platinum (Ru, Rh, Pd, Os, Ir, Pt) metals were wet-chemically prepared by reduction with $NaBH_4$ and colloidally stabilized with glutathione (GSH). Their monodispersity (possible agglomeration), chemical composition (potential oxidation) and crystallinity (twinning) had to be studied, because their further surface functionalization and applicability in different scientific fields would be strongly affected by this. Thus, after colloid-chemical characterization with disc centrifugal sedimentation (DCS), usNPs were investigated by high-resolution transmission electron microscopy (HRTEM), X-ray powder (PXRD) and electron (ED) diffraction, small-angle X-ray scattering (SAXS), X-ray photoelectron spectroscopy (XPS). It turned out that all prepared usNPs were spherical and monodisperse with an average diameter up to 2.0 nm and possessed a good crystallinity, typically twinned in structure. Despite the extremely broad diffraction peaks caused by the ultrasmall particle size, a challenging quantitative analysis by Rietveld refinement provided important information about the partial oxidation state and the unit cell contraction in usNPs. These results significantly differed from a comparable study of nanoparticles of the same metals, which were larger in size (>5 nm). Additionally to the chemical composition of usNPs as elucidated by PXRD, the oxidation state of the nanoparticles was studied by XPS and supported by ED and HRTEM (Fig. 1). Due to the strong scattering contrast of usNPs (compared to the organic shell), SAXS data mainly provided information about the size and dispersion state of the nanoparticles, including the identification of small aggregates.

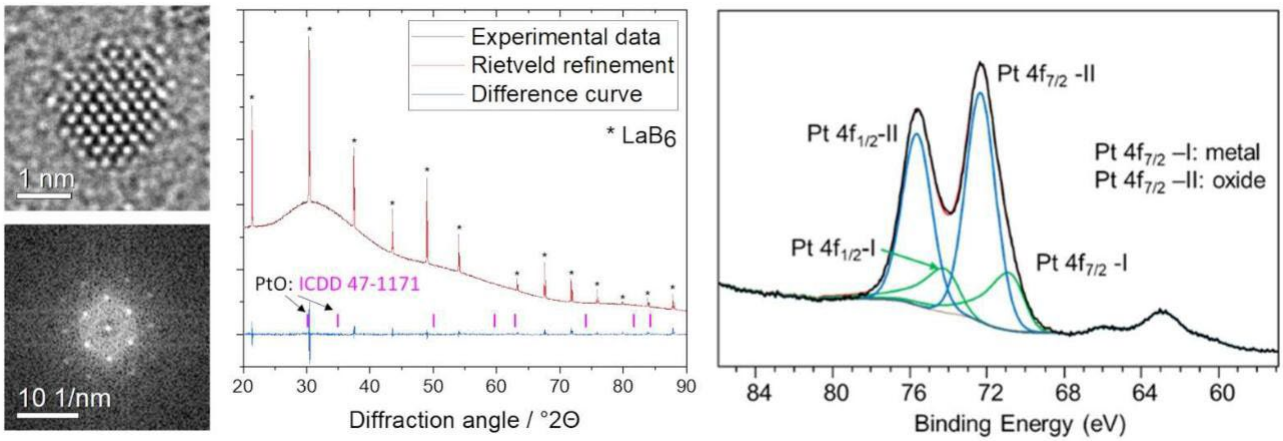

Figure 1. Representative HRTEM and ED images (left), PXRD with Rietveld refinement (center), and XPS (right) analysis of partially oxidized platinum usNP.

A036-05-230823

Quantitative comparison between the diffuse scattering from single-crystal X-ray and single-crystal electron diffraction

Romy Poppe[1], Nikolaj Roth[2], Reinhard B. Neder[3], Lukáš Palatinus[4], Bo B. Iversen[2], Joke Hadermann[1]

[1]*University of Antwerp, Department of Physics, Groenenborgerlaan 171, B-2020 Antwerp, Belgium*

[2]*University of Oxford, Inorganic Chemistry Laboratory, South Parks Road, Oxford OX1 3QR, United Kingdom*

[3]*Friedrich-Alexander-Universität Erlangen-Nürnberg, Kirstallographie und Strukturphysik, Staudtstraße 3, 91058 Erlangen, Germany*

[4]*Czech Academy of Sciences, Department of Structure Analysis, Na Slovance 2, 182 21 Prague, Czech Republic*

[5]*Aarhus University, Department of Chemistry, Langelandsgade 140, 8000 Aarhus, Denmark*

romy.poppe@uantwerpen.be

Keywords: 3D electron diffraction, diffuse scattering, 3D-ΔPDF

In contrast to perfectly periodic crystals, materials with short-range order produce diffraction patterns that contain both Bragg reflections and diffuse scattering.

Our study shows, for the first time, a quantitative comparison between single-crystal electron and single-crystal X-ray diffraction, both for the Bragg reflections and the diffuse scattering. Single-crystal electron diffraction allows the study of nanometre-sized crystals, which are too small to be studied with single-crystal X-ray diffraction.

Three-dimensional electron diffraction (3D ED) and synchrotron X-ray diffraction data were acquired on single crystals of the thermoelectric Nb0.83CoSb. The average structure (occupancies and atomic positions) was refined from the Bragg reflections, whereas the local structure (the vacancy distribution) was refined from the diffuse scattering.

The occupancies and atomic positions were refined from both synchrotron X-ray diffraction and 3D ED.
A model of the short-range order in Nb0.83CoSb was created by assuming that nearest and next-nearest neighbour vacancies avoid each other. The correlations between the first and next-nearest neighbour vacancies were refined using an evolutionary refinement algorithm in DISCUS. A good agreementΔ was achieved between the simulated and the experimental intensityΔdistribution of the diffuse scattering (Fig. 1). The 3D- PDF of the simulated 3D diffuse scattering also agrees well with the 3D- PDF of the experimental 3D diffuse scattering.

Both the average and the local structure could thus successfully be refined from our 3D ED and synchrotron X-ray diffraction data. Small differences between the experimental and the simulated diffuse scattering will be discussed, together with the advantages and disadvantages of both methods.

We will also show that the model of the short-range order in Nb0.83CoSb can easily be applied to determine the short-range order parameters in other materials with similar diffuse scattering, such as the lithium-ion battery cathode material LiNi0.5Sn0.3Co0.2O2.

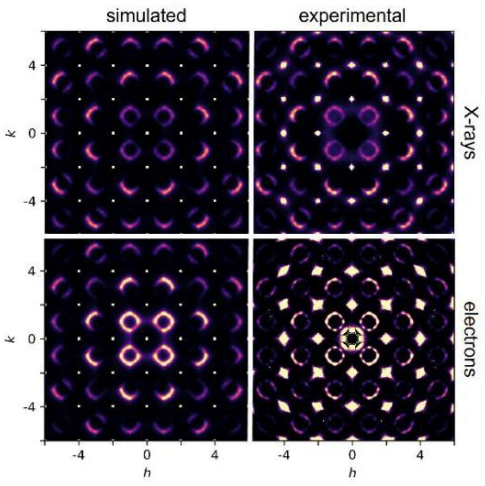

Figure 1. Comparison between the diffuse scattering from single-crystal X-ray and single-crystal electron diffraction.

This research was funded by the Research Foundation Flanders (FWO) (grant No. G035619N).

A036-06-230823

X-ray and electron microscopy techniques as material science structural characterization tools

K. Balzuweit[a,b], P.R.G. Brandão[c], N.G.S. Almeida[d], C.G. de Faria,[d,e], P.R. Cetlin[d], M.T.P. Aguilar[e]

[a]Physics Dept., ICEX, Universidade Federal de Minas Gerais, Belo Horizonte, MG, Brazil
[b]Centro de Microscopia da UFMG, Belo Horizonte, MG, Brazil
[c]Dept. of Mining Eng.,Engineering School, UFMG, Belo Horizonte, MG, Brazil
[d] Dept.Mechanical Eng., Engineering School, UFMG, Belo Horizonte, MG, Brazil
[e]University Center Newton de Paiva, Belo Horizonte, MG, Brazil
[f]. Dept.of Construction and Materials, Engineering School, UFMG, Belo Horizonte, MG, Brazil
karlaweit@gmail.com, karla@fisica.ufmg

Keywords: x-ray diffraction, electron microscopy, crystallography

X-ray and electron microscopy techniques have always been used in the study of materials in a very broad way, from life sciences to materials science. The variety of techniques, equipment and new developments in the last years are fundamental from the synthesis of new materials up to understanding the very atomic organization in almost every area. Knowledge of the techniques itself and their limitations are key for a successful and efficient research. The combination of several techniques together with some simple steps and smart design of the experiments adds to the success of the results, especially in addressing complex problems.

X-ray powder diffraction is one of the most basic techniques which enables gathering information from simple phase identification unto crystalline structure determination. A smart combination of techniques allows for example the study of large volumes of mineral materials to address the huge environmental problems caused by the mining processes and allow for a more sustainable process by characterizing the ore tailings and enables the use of the tailings in other industrial processes [1]. Combining x-ray diffraction (XRD) and Mineral Liberation Analysis (MLA) also helps in increasing the efficiency of the mining process.

Texture analysis which is broadly used both in the study of minerals as of metals, but not only, can be addressed either/or via XRD, electron backscattered diffraction (EBSD) [2] or the ASTAR precession technique [3], depending on the material, expected result and facility access.

Powder diffraction and electron crystallography are getting more complementary over the last decades [4], especially in the crystallographic structure determination which is already established for decades in XRD and responsible for millions of solved structures [5], but now with the advances in electron diffraction, can help in the solution of heterogeneous, nanometric scale materials and beam sensitive materials [6].

The development of portable equipment which is allowing the study of cultural heritage objects in museums and cultural heritage sites, using in between others, macro XRD [7] to study the microstructure of paintings helps studying the characteristics of the paintings for provenance studies and degradations processes opens huge possibilities in several areas.
Some of those aforementioned cases and techniques will be discussed in a more detailed way in the presentation.

[1] Carmignano, O.R., Vieira, S.S., Teixeira, A.P.C., Lameiras, F.S., Brandão, P.R.G., Lago, R.M., Journal Of the Brazilian Chemistry Society, vol. 32, No.10, 1895-1911 (2021).

[2] de Faria, C.G., Almeida, N.G.S., Balzuweit, K., Aguilar, M.T.P., Cetlin, P.R., Materials Letters 290, 129462 (2021).

[3] Rauch, E.F., Véron, M., Acta Cryst., B75, 505-511 (2019).

[4] Kolb, U., Shankland, K., Meshi, L., Avilov, A., David, W.I.F., Uniting Electron Crystallography and Powder Diffraction, NATO Science for Peace and Security Series B: Physics and Biophysics (2012).

[5] https://www.iucr.org/resources/data/databases

[6] Gemmi, M, Mugnaioli, E., Gorelik, T.E., Kolb, U., Palatinus, L., Boullay, P., Hovmöller, S., Abrahams, J.P., ACS Cent. Sci. 5, 1315-1329 (2019)

[7] Simoen, J., De Meyer S., Vanmeert F., Keyser N. de, Avranovich E., Snickt G.V. der, Van Loon A., Keune Katrien, Janssens K., HeritageScience 7, 1-12 (2019).

Acknowlegments: Centro de Microscopia da UFMG; FAPEMIG; CNPq; FINEP; CAPES, colleagues and collaborators.

A040 Crystal Structure of Functional Materials
Room 207
1.10pm – 3.30pm

A040-01-230823

In situ 3DED in gas and liquid environments for following structural evolutions during reactions

D. Vandemeulebroucke1, Amirhossein Hajizadeh1, M. Batuk1, J. Hadermann1

EMAT, University of Antwerp, Groenenborgerlaan 171, B-2020 Belgium

Joke.hadermann@uantwerpen.be

Keywords: 3DED, in situ, redox

Many functional materials are applied in the form of nanosized particles. To follow their structural evolution during reactions, *in situ* X ray powder diffraction or *in situ* neutron powder diffraction can miss out on details due to this small particle size. In such cases, *in situ* 3DED (three dimensional electron diffraction) would allow to gather single crystal type information on the structural changes. However, currently there are still many open questions on how the results from *in situ* 3DED relate to *ex situ* results and results from bulk experiments. Using closed cell environmental holders (gas, liquid, electrochemistry), combined with heating and cooling holders, we have studied their structural evolutions during redox reactions during heating in O_2 and H_2 versus vacuum of a range of perovskite based materials and have systematically related the resulting reduced structures to those obtained by other techniques.

For $Sr_2Fe_2O_5$ (*Pcmb*), investigated for solid oxide fuel cells, chemical looping and heterogeneous catalysis, *in situ* XRD and *in situ* NPD in gas environments only observed transformations between brownmillerite and perovskite type (*Pm-3m*) structures, while *in situ* 3DED allowed to also observe an intermediate *Cmmm* phase known from *ex situ* and electrochemistry experiments before reaching the perovskite type phase. *In situ* 3DED also showed the manifestation of nanotwins upon oxidation. After reducing the oxidized phase again in hydrogen at 700°C, the ordering of the tetrahedral chains between planes was lost but the order within planes remained. Cooling instead the oxidized phase in oxygen resulted in an intergrowth of brownmillerite and perovskite. [1] The reduction of the Ruddlesden-Popper structure $La_{0.5}Sr_{1.5}MnO_4$, also a candidate for solid oxide fuel cell cathodes, resulted in the creation of a perovskite layer at the surface which was not noticed before in bulk in situ experiments involving redox reactions in gas. Parallel *ex situ* reductions showed also faint superstructure reflections in the 3DED datasets pointing towards a surface reconstruction with ordered oxygen vacancies, which could not be detected in the in situ 3DED experiments. Differences in surface layers are important as they are the most active parts in catalytic reactions. Sr_2MnO_4 could not be reduced using an *in situ* reaction with H_2 into the supercell with oxygen-vacancy order from literature, while this did succeed during parallel *ex situ* reduction experiments as well as during *in situ* heating in vacuum.

$CaMnO_3$, a material for chemical looping applications, was successfully reduced using *in situ* reduction both by heating in hydrogen gas as well as by heating in vacuum, achieving not only the well characterized $CaMnO_{2.5}$ phase, but also the intermediate $CaMnO_{2.75}$, which was thus far not solved and had contradicting models in literature. Using the results from the *in situ* 3DED experiments, the $CaMnO_{2.75}$ was solved in a *Pmmm* space group. These results were then compared to *in situ* 3DED results on the evolution of the Fe and Sr doped compounds which show better chemical looping properties.

In situ 3DED in gas environments has thus already given new, complementary information to what was observed with *in situ* XRD and *in situ* NPD for each perovskite based material we have studied so far. We therefore believe that in future studies *in situ* 3DED will unlock a vast amount of new information on functional materials in general.

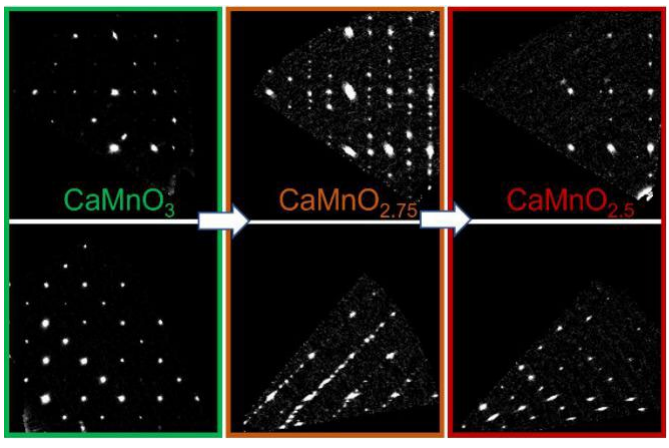

Figure 1. [110] (top) and [001] (bottom) sections (indexed in parent perovskite cell parameters) from in situ 3DED data sets taken during vacuum heating of CaMnO3, from left to right, at room temperature, 350°C and 650°C.

[1] Maria Batuk et al., ChemRXiv, doi: 10.26434/chemrxiv-2022-gn3fm

Financial support is acknowledged from FWO I003218N, University of Antwerp BOF TOP 38689 and the European Commission NanED Grant number 956099.

Permissible walls between ferroelastic domains of monoclinic symmetry

I. Biran, S. Gorfman

Department of Materials Science and Engineering, Tel Aviv University, Tel Aviv, Israel

gorfman@tauex.tau.ac.il

Keywords: ferroelectric perovskites, polarization rotation, functional materials

The concept of monoclinic ferroelectric phases plays an important role for the description of the crystal structures of functional perovskite oxides. The evidence of such phases was for the first time reported by Noheda et al. [1] and supported by the splitting of Bragg peaks in high-resolution powder diffraction patterns. Monoclinic ferroelectric phases are invoked to explain the unusual physical properties, e.g., the enhancement of giant piezoelectric effect in $PbZr_{1-x}Ti_xO_3$. The notion of "monoclinic ferroelectrics" revolutionized the view on ferroelectricity by suggesting that spontaneous polarization can be rotated, rather than inverted / extended only. The true nature of the monoclinic phases is still debated: it is not yet clear if such phases is genuine / long range ordered or, alternatively, "mimicked" by tetragonal of rhombohedral nanodomains. Regardless of what the true character is, the concept remains useful for the description of various phenomena in ferroelectrics and shape memory alloys. Unfortunately, the understanding of the crystallographic structures of monoclinic phases and the microstructures of monoclinic domain is impaired by the complexity of the subject.

The aim of this work is to describe the orientation and properties of permissible walls between monoclinic domains of ferroelectric perovskite oxides. The term permissible (coined by Fousek and Janovec [2]) denotes a domain wall, which connect two domains without any lattice mismatch. For example, tetragonal domains are permitted to connect along six different domain walls (with the Miller indices {110}), rhombohedral domains are "permitted" to connect along twelve different orientations (with the Miller indices {110} and {100}). Using the formalism developed in [3], we demonstrate that monoclinic domains (Figure 1) are permitted to connect along 84 types of domain walls. We show that 36 of these walls are the so-called prominent domain walls (P-walls) which have fixed crystallographic orientation. In contrast to P-walls, S-walls change their orientation if the corresponding lattice parameters change too. We predict the rotation angle of the walls for the reasonable change of the lattice parameters and calculate the angles between polarization directions. The results of this work are useful for the understanding of physical properties of functional materials, associated with the formation of rich domain microstructures.

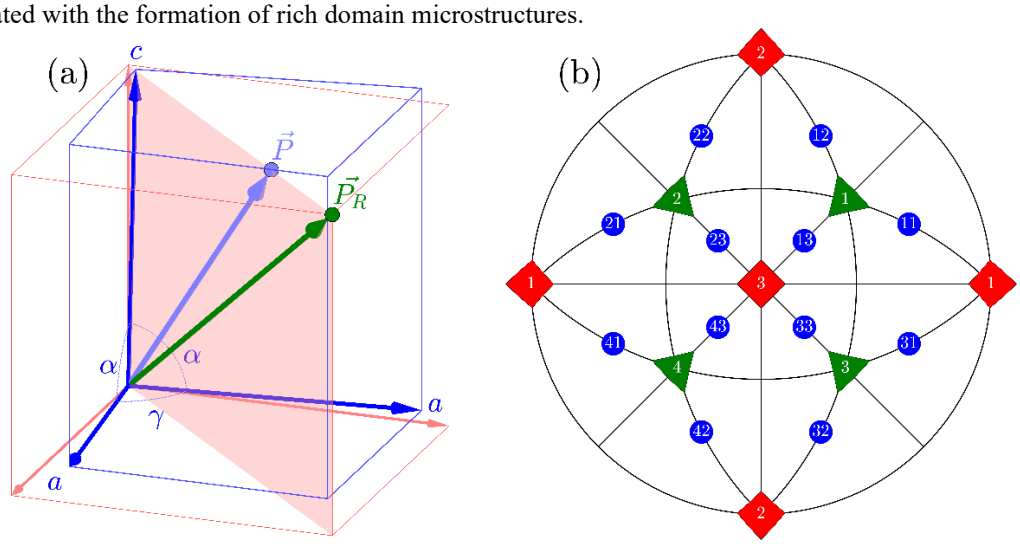

Figure 1. The schematic view of the distortion of the monoclinic unit cell and the directions of spontaneous polarization. (a) free lattice parameters, describing the distortion of the unit cell, associated with the polarization rotation. (b) spontaneous polarization directions for 3 tetragonal (red), 4 rhombohedral (green) and 12 monoclinic (blue) domains.

[1] Noheda, B., Cox, D.E., Shirane, G., Gonzalo, J.A., Cross, L.E. & Park, S.-E. (1999). *Appl. Phys. Lett.*, **74**, 2059.

[2] Fousek J., Janovec, V., (1969). *J. Appl. Phys.* **40**, 135

[2] Gorfman, S., Spirito, D., Zhang, N., Detlefs, C. & Zhang, N. (2022). *Acta Crystallogr. A.* **78**, 158.

The authors acknowledge the funding for this research was provided by: Israel Science Foundation [grant No. 1561/18]; United States-Israel Binational Science Foundation (grant No. 2018161); Israel Science Foundation + National Natural Science Foundation of China (grant ISF No. 3455/21)

A040-03-230823

Interfacial segregation and structure of precipitates in aluminium alloys

L. Bourgeois1,2, Z. Zhang2,3,4, S. Su2, N.V. Medhekar2

Monash Centre for Electron Microscopy, Monash University, Victoria 3800, Australia Department of Materials Science & Engineering, Monash University, Victoria 3800, Australia Electron Microscopy for Materials Research (EMAT), University of Antwerp, Groenenborgerlaan 171, 2020 Antwerp, Belgium Department of Materials, University of Oxford, 16 Parks Road, Oxford OX1 3PH, United Kingdom

laure.bourgeois@monash.edu

Keywords: Interfaces, scanning transmission electron microscopy, aluminium alloys

Solid-state precipitates are key components in high-strength aluminium alloys used in a multitude of structural applications, from packaging and construction to automobiles and aerospace. Precipitates that are most effective at blocking dislocations and hence strengthening an alloy are usually metastable phases with high aspect ratios and one or two dimensions at the nanoscale or even sub-nanoscale [1]. Interfacial structure therefore constitutes a critical part of the structure of such precipitates. An understanding of interfacial segregation and structure is important not only for developing models of precipitate nucleation and growth, but also when addressing the issue of recycling aluminium [2]. Yet it is only in the last 10-15 years that such structures have been experimentally characterised at the atomic scale, thanks mainly to high-resolution scanning transmission electron microscopy (STEM).

Here we present experiments and simulations of interfacial structures and solute segregation behaviour of precipitates in several model binary and ternary aluminium alloys, some of which form the basis of important engineering alloys. STEM experiments reveal that even in seemingly simple and well-known binary alloys, precipitates can possess complex interfacial structures or unexpected phases [3-5]. Density-functional theory calculations enable a partial understanding of the experimental observations. For example, the calculated solute defect energy can provide an indication as to whether this solute will segregate at coherent interfaces [3, 4, 6]. However, there exists as yet no predictive model for complex interfacial structures. This will be discussed, as well as the challenge remaining in using atomistic observations and calculations to predict thermodynamic behaviour, such as precipitates nucleation and growth.

1 Polmear, I. J., St John, D., Nie, J. F. & Ma, Q. (2017). *Light Alloys. Metallurgy of the Light Metals*. 5th Edition, Butterworth-Heinemann.
2 Raabe, D. et al. (2022). *Prog. Mater. Sci.* **128**, 100947.
3 Bourgeois, L., Dwyer, C., Weyland, M., Nie, J. F. & Muddle, B. C. (2011). *Acta Mater.* **59**, 7043.
4 Zhang, Z., Rosalie, J. M, Medhekar, N. V. & Bourgeois, L. (2019). *Acta Mater.* **59**, 7043.
5 Bourgeois, L., Zhang, Y., Zhang, Z., Chen, Y. & Medhekar, N. V. (2020). *Nature Comm.* **11**, 1248.
6 Su, S., Bourgeois, L. & Medhekar, N.V., submitted.

The authors acknowledge the use of the instruments and scientific and technical assistance at the Monash Centre for Electron Microscopy, a Node of Microscopy Australia. Computational work was undertaken with the assistance of resources and services from the National Computational Infrastructure (NCI), Pawsey Supercomputing Centre, and from the MonARCH HPC cluster. This work was funded by the Australian Research Council (DP150100558 & DP210101451).

A040-04-230823

Precession Electron Diffraction Tomography for Structural Analysis of Nanoparticles: A study of minimal size and associated dynamical effects

E.Cordero Oyonarte[1], L.Rebecchi[2,3], D.G. Calatayud[4], V.Pralong[1], I.Kriegel[2], L.Palatinus[5], P.Boullay[1]

1. Normandie Université, ENSICAEN, UNICAEN, CNRS, CRISMAT, Caen France ; 2. Functional Nanosystems, IIT, Genova, Italy ; 3. Dipartimento di Chimica e Chimica Industriale, Universita di Genova, Genova, Italy. 4. Instituto de Ceramica y Vidrio, CSIC, Madrid, Spain. 5. Department of Structure Analysis, Institute of Physics of the Czech Academy of Sciences, Prague, Czech Republic

Keywords :3D Electron Diffraction, Precession Electron Diffraction, nanoparticles.

The resolution and applicability of traditional techniques like X-ray and neutron crystallography for single crystal structure solution of a wide range of materials is limited by the size of the sample. 3D electron diffraction has emerged as a promising alternative for smaller specimens [1]. The shorter wavelength of electrons, at approximately 2 pm, results in a stronger interaction with matter, while the electron beam can be focused to an extremely fine probe size, at approximately 1 nm. While previous studies have estimated the minimum size of nanoparticles that can be analyzed by electron diffraction [2], there has been a dearth of experimental data demonstrating the feasibility of both kinematical and dynamical approaches for crystal structure solution and refinement. The present project aims to fill this gap by providing experimental data using Precession Electron Diffraction Tomography (PEDT) [3,4] for different materials with nanoparticle sizes [5] down to 10 nm (Fig. 1).

Our findings highlight the various challenges encountered during data acquisition and subsequent data processing. For smallest nanoparticles, the R-values appear sometimes to be quite similar when comparing the results obtained from kinematical and dynamical refinements (see ITO results in Fig. 1). We will see this does not mean that we have reached the size limit, where the dynamic effect ceases to exist, but that the reason lies in the way the 3D Electron Diffraction data is processes. This study demonstrates first that it is possible to accurately refine the structure of individual nanoparticles down to 10 nm and second that dynamic scattering effects are still present even for such small crystals.

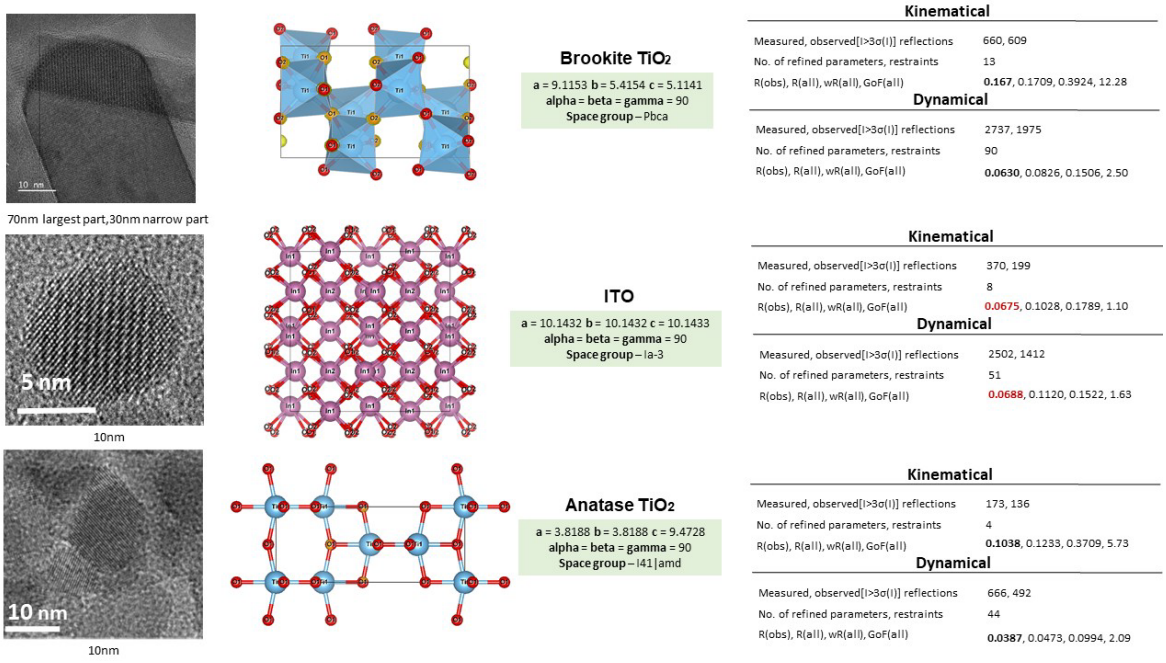

Figure 1. Brookite TiO2, ITO and Anatase TiO2, structure solution, cell parameters and Refinement results

These results are obtained withing the framework of European project NanED (Electron Nanocrystallography – H2020-MSCA-ITN GA956099.

[1] Hongyi, X. (2021). Elsevier Inc.
[2] Kolb, U., Gorelik, T., Kubel, C., Otten, M.T., Hubert, D. (2007). Ultramicroscopy, **107**, 507-513
[3] Corrêa, C.A., Klementová, M., Palatinus, L. (2015). Acta Physica Polonica A. **128**, 651-653
[4] Gemmi, M., Mugnaioli, E., Gorelik, TE., Kolb, U., Palatinus, L., Boullay, P., Hovmoller, S., Abrahams, JP. (2019). ACS Central Science. **5**, 1315-1329
[5] Libo, W., Zhang, J., Watanabe, W. (2011). Advanced Drug Delivery Reviews. **63**, 456-469

A040-06-230823

Quantifying short-range order — a case study using CoCrNi medium entropy

Mengwei He, Will Davids, Andrew Breen, Simon P. Ringer*

Australian Centre for Microscopy and Microanalysis, and School of Aerospace, Mechanical and Mechatronic Engineering, The University of Sydney, Sydney, NSW 2006, Australia

Corresponding author email: simon.ringer@sydney.edu.au

Keywords: High entropy alloy; short range ordering; atomic clustering; atom probe tomography; microscopy.

Medium and high entropy alloys (M/HEAs) are an emerging class of materials that can exhibit outstanding combinations of strength and ductility [1]. As such, their high potential for challenging engineering applications has attracted much attention. Computational simulations have suggested the presence of short-range order (SRO) in CoCrNi alloys, and recent experimental evidence that supports this is beginning to emerge [2].

Unfortunately, the difficulty in quantifying the SRO under different heat treatment conditions has generated much debate on the atomic preferencing, and the implications of SRO on mechanical properties [3, 4]. Using atom probe tomography (Figure 1), we put forward a novel approach to quantify SRO. We also demonstrate the method with a case study of the CoCrNi alloy and use this to monitor SRO changes induced by heat treatments.

In the study, we provided a comparison of quantitative analysis of SRO in simulated APT data with intentionally introduced degree of randomness and ordering. The sensitivity of the SRO quantification procedure to the APT detection efficiency and varying extent of spatial resolution are evaluated to establish a go/no-go boundary of the approach. Afterwards, we applied the method in the experimental APT results generated from [110] oriented grains of as homogenizing and annealed CoCrNi M/HEAs and compared the ordering behaviours in the alloys. These species-specific SRO measurements enable the generation of computational simulations of atomic neighbourhood models that are equivalent to the experiment and can contribute to the further understanding and design of M/HEAs and other materials systems where SRO may occur.

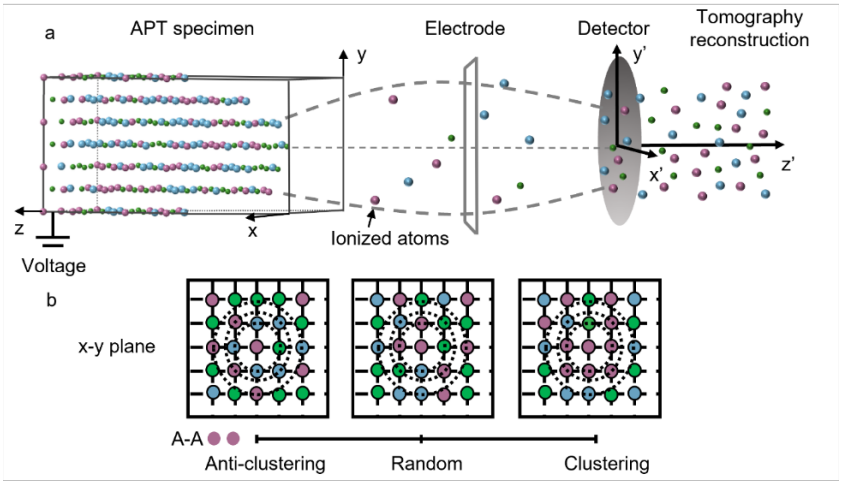

Figure 1. (a) A schematic graph of atom probe tomography (APT). (b) A 2D schematic of anti-clustering, random and clustering SRO behaviours (refer to the purple atom pairs).

[1] George, E. P., Raabe, D. & Ritchie, R. O. (2019). *Nat. Rev. Mater.* **4**, 515-534.

[2] Wu, Y., Zhang, F., Yuan, X., Huang, H., Wen, X., Wang, Y., Zhang, M., Wu, H., Liu, X., Wang, H., Jiang, S. & Lu, Z. (2021). *J Mater. Sci. Technol.* **62**, 214-220.

[3] Inoue, K., Yoshida, S. & Tsuji, N. (2021). *Phys. Rev. Mater.* **5**, 085007.

[4] Zhang, R., Zhao, S., Ding, J., Chong, Y., Jia, T., Ophus, C., Asta, M., Ritchie, R. O. & Minor, A. M. (2020). *Nature* **581**, 283-287.

A055 Diffuse Scattering Analysis of Short Range Crystal and Magnetic Order
Room 220
1.10pm – 3.30pm

A055-01-230823

Interaction space modelling for ultra-fast diffuse scattering phase diagram calculations

E. M. Schmidt[1,2] & Arkadiy Simonov[3]

[1]Crystallography & Geomaterials Research, Faculty of Geosciences, University of Bremen, Bremen, Germany [2] MARUM-Center for Marine Environmental Sciences, University of Bremen, Bremen, Germany
[3]Department of Materials, ETH Zürich, Zürich, Switzerland
Ella.schmidt@unibremen.de

Keywords: diffuse scattering, disorder analysis, materials modelling

Advances in neutron, X-ray and electron diffraction setups have made the routine collection of single crystal diffuse scattering data possible. However, the interpretation of single crystal diffuse scattering is still regarded as a complex problem, where the determination of meaningful descriptors that describe the disorder causing the diffuse scattering is a challenge. Increased computation power and advanced algorithms now enable the refinement of full three-dimensional diffuse scattering data sets using direct or reverse Monte Carlo simulations, 3D-DPDFs or our recently introduced interaction space modelling approach [1].

In this approach we utilize a simple interaction Hamiltonian and apply a mean filed approximation to calculate the expected diffuse scattering without the need to generate large supercells. The parametrization of the disorder model in terms of only a few terms in the interaction Hamiltonian makes this approach not only efficient in terms of parameters but also fast for the calculation of the diffuse scattering. Hence, a big parameter space can be probed with little computational effort.

Here, we use this approach for the ultra-fast calculation of diffuse scattering phase diagrams: These diagrams show for a crystalline configuration with a certain flexibility the expected diffuse scattering in terms of several parameters such as temperature, composition and nearest neighbour interactions. We apply this to simulate the phase diagrams of oxyfluorides [2], disordered rocksalt structures [2], half Heussler systems [3] and Prussian blue analogues [4] (see Figure 1) and compare our results with disorder models reported in literature. We demonstrate that by applying this simple and easy calculation approach, the diffuse scattering for many systems cannot just be predicted accurately but also the interaction parameters can be refined, as long as the disorder sill lies within the stability regime of the mean field approximation.

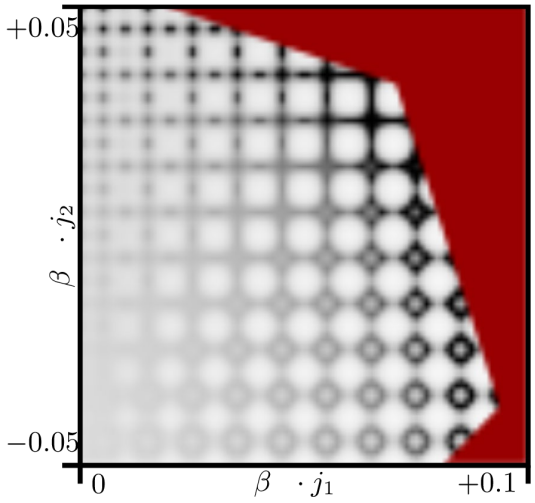

Figure 1: *hk*0-layer of single crystal diffuse scattering from Prussian blue analogues as a function of interaction parameters b j_1 (drive for local electroneutrality) and b j_2 (drive for local centro-symmetry). For comparison see the phase diagram based on Monte Carlo simulations in [4], red part indicates the boundary of the mean-field stability regime [1].

[1] Schmidt, E.M. *et al.* (2022) *IUCrJ* **9**(1), 21-30.
[2] Withers, R. (2015) *IUCrJ* **2**(1), 74-84.
[3] Roth, N. (2020) *IUCrJ* **7**(4), 673-680.
[4] Simonov, A. *et al.* (2020) *Nature* **578**, 256–260.

A055-02-230823

Magnetic Structure and Highly Unusual In-field Behaviour of D-type Erbium Disilicate

4 Islam[1], M. Ciomaga Hatnean[1,2], N. d'Ambrumenil[1], P. Manuel[3], F. Orlandi[3], D. Khyalyavin[3], J. Olivier[4], G. Balakrishnan[1], O. A. Petrenko[1]

[1]Department of Physics, University of Warwick, Coventry, CV4 7AL, UK, [2]Laboratory for Multiscale materials eXperiments, Paul Scherrer Institute, 5232 Villigen PSI, Switzerland; Materials Discovery Laboratory, Department of Materials, ETH Zurich, 8093 Zurich, Switzerland, [3]ISIS Neutron and Muon Source, STFC Rutherford Appleton Laboratory, Didcot, OX11 0QX, UK, [4]Institut Laue Langevin, CS 20156, 38042 Grenoble, France

manisha.islam@warwick.ac.uk

Keywords: Magnetic diffuse scattering, inelastic neutron scattering, magnetic frustration

Despite their promising optical properties, little is known of the polymorphic rare-earth disilicates (RE2Si2O7) due to their complex structural phase diagram. The magnetic rare-earth ions within the majority of the disilicates are arranged in a distorted honeycomb structure, giving potential for fundamental magnetism interest.

For the monoclinic D-type Er2Si2O7, initial predictions of a magnetic order below 1.8 K with a proposed q = 0 four-sublattice antiferromagnetic arrangement of the magnetic moments [1] have been recently confirmed via powder neutron diffraction measurements [2]. The highly anisotropic magnetisation curves were understood by the use of simple Monte-Carlo simulations however, the presence of a magnetic plateau at 1/3 of the magnetic saturation, disagreed with the theoretical model [1]. Here, both polycrystalline and single crystals of D-type Er2Si2O7 have been synthesised [3] and investigated using powder and single crystal neutron scattering techniques as well as magnetisation measurements.

Our $H \parallel a$ single crystal magnetisation measurements reveal a plateau at 1/3 of magnetic saturation, accompanied by a significant increase of the magnetic unit cell. Fig. 1 illustrates the dramatic change in the single crystal neutron diffraction patterns when the narrow plateau stabilisation is reached. Magnetic diffuse features along the k and l directions suggest shorter-range magnetic correlations on the plateau along b^* and c^*.

The magnetic non-integer peaks indexed as (0, k+1/2, l+1/2), (0, k+1/3, l) and (0, k+2/3, l), where k and l are integers during the plateau imply a change in the size of the unit cell. This change from the confirmed zero-field four-sublattice structure to the larger unit cell accommodates for the surprising 1/3 plateau. We also report that our magnetic excitations in the ordered state, observed via inelastic neutron scattering, suggest an almost ideal Ising system. The dispersionless low-energy excitations low temperature spectrum also demonstrates Ising-like behaviour in lower and higher fields and significantly softens on the magnetisation plateau.

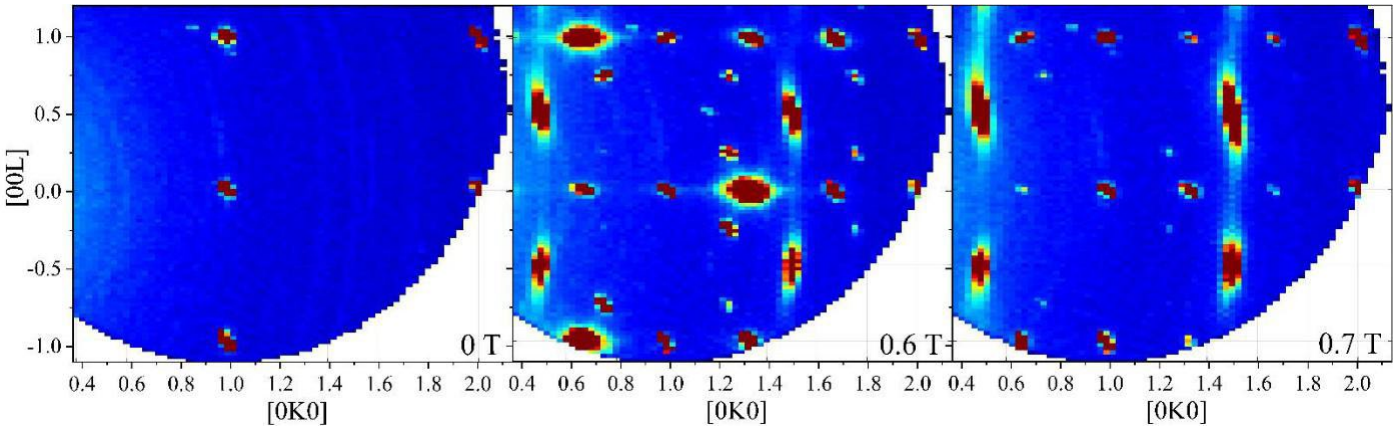

Figure 1. Intensity maps of single crystal in-field neutron diffraction of Er2Si2O7 measured on IN5 at ILL, with $H \parallel a$. Magnetic q=0 peaks are observed at zero-field until the magnetisation plateau region is reached. The plateau then stabilises at 0.6 T, accompanied by additional magnetic peaks with fractional, non-integer indices. Remnants of the diffuse scattering remain above the plateau region as seen in 0.7 T, until saturation. Some of these non-integer peaks are not resolution limited, suggesting shorter-range magnetic correlations.

1 M. J. M. Leask, P. R. Tapster, et al., J. Phys. C Solid State **19**, 1173 (1986).
2 G. Hester, T. N. DeLazzer, et al. Phys. Condens. Mat. **33**, 405801 (2021).
3 M. Ciomaga Hatnean, O. Petrenko, et al. Cryst. Growth. Des. **20**, 6636-6648 (2020).

A055-03-230823

Frustrated magnetism, orbital molecules and magnetocaloric properties unravelled by neutron magnetic diffuse scattering

P. Manuel

ISIS Pulsed Neutron and Muon Source, STFC Rutherford Appleton Laboratory, Harwell Science and Innovation Campus, Chilton, Oxfordshire, OX11 0QX, United Kingdom

pascal.manuel@stfc.ac.uk

Keywords: diffuse scattering, magnetism, neutron diffraction

For decades, Neutron scattering has been able to provide a detailed and quantitative microscopic understanding of magnetic structures and excitations and remains the technique of choice for studying magnetism. The increase in complexity of the type of magnetic structures studied has been matched with the progress in neutron instrumentation which has allowed researchers to engineer and fine tune the properties of a whole variety of quantum materials. As well as revealing detailed information on long range ordered magnetic structures, neutron scattering can also be used to extract short range magnetic correlations through the analysis of the diffuse scattering. In this talk, I will review some recent examples of such diffuse scattering data collected on both powder and single crystal samples on the cold neutron diffractometer WISH at the second target station at the ISIS pulsed neutron and muon source, UK. The examples will be chosen in the field of frustrated magnetism, orbital molecules and magnetocalorics. Finally, I will also mention some new opportunities for such studies with planned new instrumentation at ISIS.

References

[1] Nature Communications 10 5475
[2] J. Mater, Chem. C 7, 13111-13119
[3] https://www.isis.stfc.ac.uk/SiteAssets/WISH-II%20Project_UserMeeting3.pdf

A055-04-230823

Hidden structural transition upon dehydration of Prussian Blue analogues (PBAs)

Yevheniia Kholina, Arkadiy Simonov

ETH Zürich, Switzerland, Department of Materials, Laboratory for Multifunctional Ferroic Materials

yevheniia.kholina@mat.ethz.ch

Keywords: local structure, diffuse scattering, Prussian Blue analogues, dehydration

Prussian blue analogues (PBAs) are a diverse family of transition metal cyanide materials with chemical formula $M[M'(CN)_6]_{1-x}\square_y \cdot nH_2O$, which we abbreviate here as M[M'] (M and M'=transition metal ions, □=vacancy). These materials are known for their highly connected porous network, enabled by structural vacancies of M'(CN)6 with sufficiently large channels to transport or store small molecules and ions. Currently these systems are actively investigated for application as hydrogen storage media, humidity sensors, and alkali ion sieves.

One step which is often overlooked in the research is drying. PBAs are typically grown from water solutions and water has to be removed by heating the sample either in vacuum or in dry atmosphere. Since drying doesn't change the average structure, it is generally assumed that this step doesn't alter the porous network of PBAs. We demonstrate that dehydration step in fact causes a hidden structural transition that involves irreversible rearrangements of vacancies. Such rearrangements modify the pore-network characteristic, like fraction of accessible volume and conductance of matter through the channels. We collect diffuse scattering from Mn[Co] single crystals and use 3D-ΔPDF analysis to characterize their local structure and monitor any structural changes upon water removal. We also demonstrate that same material dehydrated at slightly different conditions shows different performance, drawing a link between a local structure and materials properties.

A055-05-230823

Truchet-tile structure of a topologically aperiodic metal–organic framework

E. G. Meekel[1], E. M. Schmidt[1,2], L. J. Cameron[3], A. D. Dharma[3], H. J. Windsor[3], S. G. Duyker[3,4], A. Minelli[1], T. Pope[5], G. Orazio Lepore[6], B. Slater[5], C. J. Kepert[3], A. L. Goodwin[1]

[1]Inorganic Chemistry Laboratory, University of Oxford, Oxford OX1 3QR, U.K., [2]Fachbereich Geowissenschaften, Universität Bremen, D-28359 Bremen, Germany, [3]School of Chemistry, University of Sydney, NSW 2006, Australia, [4]Sydney Analytical, Core Research Facilities, University of Sydney, NSW 2006, Australia, [5]Department of Chemistry, University College London, London WC1H 0AJ, U.K., [6]Earth Sciences Department, University of Florence, Florence 50121, Italy

andrew.goodwin@chem.ox.ac.uk

Keywords: Metal–organic frameworks, aperiodic structures, diffuse scattering

When tiles decorated to lower their symmetry are joined together, they can form aperiodic and labyrinthine patterns. Such Truchet tilings offer an efficient mechanism of visual data storage related to that used in barcodes and QR codes. In this contribution, we show that the crystalline metal–organic framework $[OZn_4][1,3\text{-benzenedicarboxylate}]_3$ (TRUMOF-1) is an atomic-scale realization of a complex three- dimensional Truchet tiling [1]. Its crystal structure consists of a periodically-arranged assembly of identical zinc-containing clusters connected uniformly in a well-defined but disordered fashion to give a topologically aperiodic microporous network. Both single-crystal diffuse scattering and 3D-ΔPDF measurements are sensitive to the particular kind of topological aperiodicity present in TRUMOF-1. We suggest that this unusual structure emerges as a consequence of geometric frustration in the chemical building units from which it is assembled.

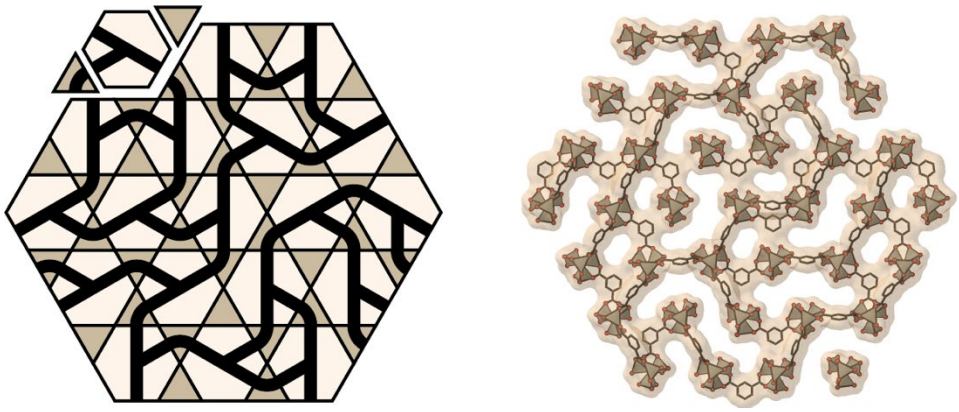

Figure 1. (Left) Truchet tiling consisting of patterned hexagons and triangles; (right) representative layer of TRUMOF-1 structure showing the coexistence of a periodic arrangement of Zn-containing clusters and aperiodic channels.

[1] Meekel, E. G., Schmidt. E. M., Cameron, L. J., Dharma, A. D., Windsor, H. J., Duyker, S. G., Minelli, A., Pope, T., Orazio Lepore, G., Slater, B., Kepert, C. J. & Goodwin, A. L. (in press). *Science.*

A055-06-230823

Polarised neutrons for magnetic pair distribution function analysis: methods and applications

Benjamin A. Frandsen[1]

Department of Physics and Astronomy, Brigham Young University, Provo, Utah 84602, U.S.A.

benfrandsen@byu.edu

Keywords: magnetic pair distribution function, short-range magnetic correlations, polarized neutrons

Magnetic pair distribution function (mPDF) analysis is a promising method of studying local magnetic correlations. The mPDF approach involves Fourier transforming magnetic scattering data to yield the pairwise magnetic correlation function in real space, which, in some cases, can enable more intuitive interpretation and reliable modelling of the data compared to reciprocal-space approaches. To date, most applications of mPDF analysis have used data obtained from unpolarised neutrons. These efforts have been largely successful, but limitations exist in regard to the real-space resolution of the measured mPDF data and the ability to detect weak signals when unpolarised neutrons are used. Here, we present the first mPDF data obtained from polarised neutrons and introduce a data-processing algorithm that significantly improves upon previous limitations using unpolarised neutrons [1]. We apply this approach to the antiferromagnetic semiconductor MnTe below and above the Neel temperature (see Fig. 1), highlighting the ability to probe both long-range and short-range magnetic correlations with mPDF analysis and revealing nontrivial anisotropic correlations in the paramagnetic state. We conclude with a discussion of the promising outlook of mPDF analysis using polarised neutrons and the potential value of this approach for studying a variety of other magnetic materials, such as geometrically frustrated magnets and multiferroics.

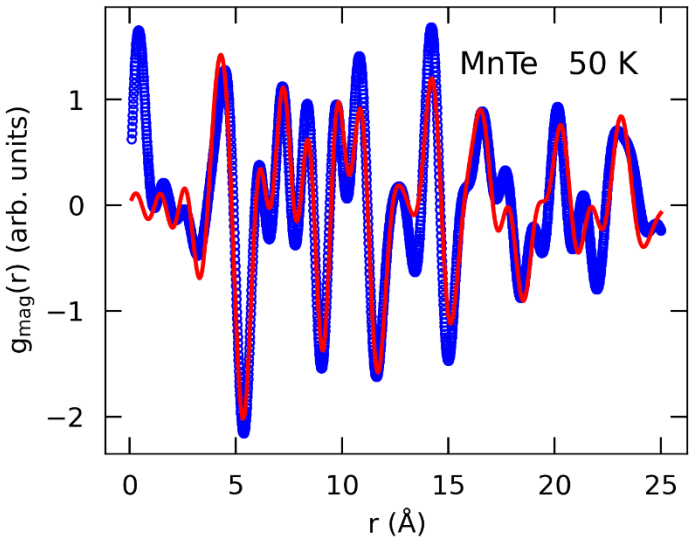

Figure 1. High-resolution magnetic pair distribution function data (blue curve) for MnTe at 50 K obtained from polarised neutron scattering data, together with a fit (red curve) using the known antiferromagnetic structure of MnTe.

[1] Frandsen, B. A., Baral, R.., Winn, B. & Garlea, V. O. (2022). *J. Appl. Phys.*, **132**, 223909.

This work was supported by the U.S. Department of Energy, Office of Science, Office of Basic Energy Sciences through award No. DE-SC0021134.

A076 In-situ Studies of Materials Synthesis and Crystal Growth

Room 212/13

1.10pm – 3.30pm

A076-01-230823

Phase Evolution During Solid-State Synthesis of Disordered Rocksalt Cathodes

K.H. Stone1, Y. Liu1, D. Sokaras1, W. Chueh1, J.L. Nelson Weker1,

SSRL, SLAC National Accelerator Laboratory, Menlo Park, California 94025 USA

khstone@slac.stanford.edu

Keywords: Synthesis, Rietveld Refinement, In-situ Diffraction

Cation-disordered rocksalt (DRX) materials have recently garnered attention for their potential as cathodes in lithium-ion batteries. These materials are lithium transition metal oxides which assume a rocksalt type structure with a disordering of the lithium and one or more transition metals on the cation sublattice. The disordering results in several desirable properties such as good lithium transport and small volume changes with cycling. Unlike layered transition metal oxides that are inherently unstable when significant lithium is removed, limiting practical compositions to combinations of cobalt, nickel, and manganese, DRX cathodes can also be synthesized with widely available transition metals to avoid expensive or critical materials.[1] Additional fluorine substitution for oxygen can increase stability for higher lithium content and improve long term capacity retention during cycling.[2,3] Solid-state synthesis, where solid precursors are mixed together, sometimes through ball-milling, then heated either in air or inert gas to high temperatures (typically ~1000˚C), has been one of the chief methods for fabricating disordered or partially disordered cathod e materials. For solid-state synthesis, the reaction can go through multiple intermediates before the reaction is completed. These intermediates are not always known and could be desirable end products in themselves, however, without *in situ* methods, only the endpoints of the synthesis can be studied. X-ray diffraction is a powerful approach for tracking crystalline structures *in situ* during solid state synthesis.

At the Stanford Synchrotron Radiation Lightsource (SSRL), we have used *in situ* X-ray diffraction to study the solid-state synthesis of disordered rocksalt cathode materials. After careful preparation of the precursor mixture, it is possible to monitor the reaction as the sample is heated to and held at the reaction temperature. From this data it is possible to monitor the phase evolution of the precursors and the formation of the disordered rocksalt product. This *in situ* data provides important mechanistic insight into the formation reaction of the disordered rocksalt material and allows for easy determination of the impact of changes to the precursor materials or the annealing process. In combination with detailed structural characterization of the product *ex situ*, we accurately determine the final product composition, level of order/disorder, and performance as a cathode material for lithium-ion batteries.

1 Cava, R. J., Murphy, D. W., Zahurak, S., Santoro, A. & Roth, R. S. (1984) *J. Solid State Chem.* **53**, 64-75.
2 Clément, R. J., Lun, Z. & Ceder, G. (2020) *Energy and Environmental Science* **13**, 345–373.
3 Li, H., Fong, R., Woo, M., Ahmed, H., Seo, D.-H., Malik, R. & Lee, J. (2022) *Joule* **6**, 53–91 (2022)

A076-02-230823

Go with the flow: in-situ X-ray diffraction during segmented flow crystallisation

E. Galtry[1,2], D. Allan[2], M. Warren[2], S. Day[2], and K. Robertson[1]

5 Faculty of Engineering, University of Nottingham, Nottingham, UK, NG7 2RD, 2: Diamond Light Source, Harwell Science and Innovation Campus, Fermi Ave, Didcot, UK, OX11 0DE

elizabeth.galtry@nottingham.ac.uk

Keywords: flow crystallisation, polymorphism, morphology

In-situ X-ray diffraction of crystallisation enables the monitoring of crystal nucleation and growth, probing the polymorphic form and transformations during the crystallisation process; this facilitates the understanding and potential optimisation of crystallisation processes. The KRAIC (kinetically regulated automated input crystalliser) uses segmented flow for highly reproducible crystallisation environments with minimal interaction with reactor surfaces during crystallisation due to the tri-segmented regime, shown below in Fig. 1.[1] This work presents the developments of in-situ powder X-ray diffraction (PXRD) and single crystal X-ray diffraction (SCXRD) KRAIC systems to probe crystallisation.

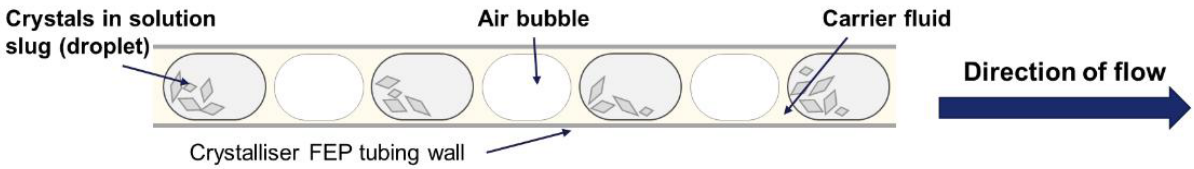

Figure 1. Diagram of segmented flow regime used in the KRAIC series of crystallisers. Diagram shows crystal-solution slugs separated by air bubbles and coated in a carrier fluid to remove crystal build-up from the tubing walls.

This work features the development of the temperature-cycling segmented flow system, the KRAIC-T (for temperature cycling), in collaboration with beamline I11 for high resolution PXRD at Diamond Light Source, the UK's national synchrotron. Temperature-cycling during crystallisation is a technique used to control key crystal properties such as crystal size distribution, morphology, and polymorphism. Building on the success of the KRAIC-D (for diffraction), a segmented flow cooling crystalliser coupled with in-situ PXRD [2], the KRAIC-T uses in-situ PXRD to study the effect of variable temperature on crystallisation or slurrying of polymorphic systems; recently studying the effect of temperature-cycling on the solution-mediated phase transitions during slurrying of a model small molecule system, ortho-aminobenzoic acid (oABA) during beamtime on I11, shown below in Fig. 2a. Developments to the data collection methodology of the KRAIC-T allowed for increased data acquisition times improving the efficiency of data collection and resultant diffraction data quality

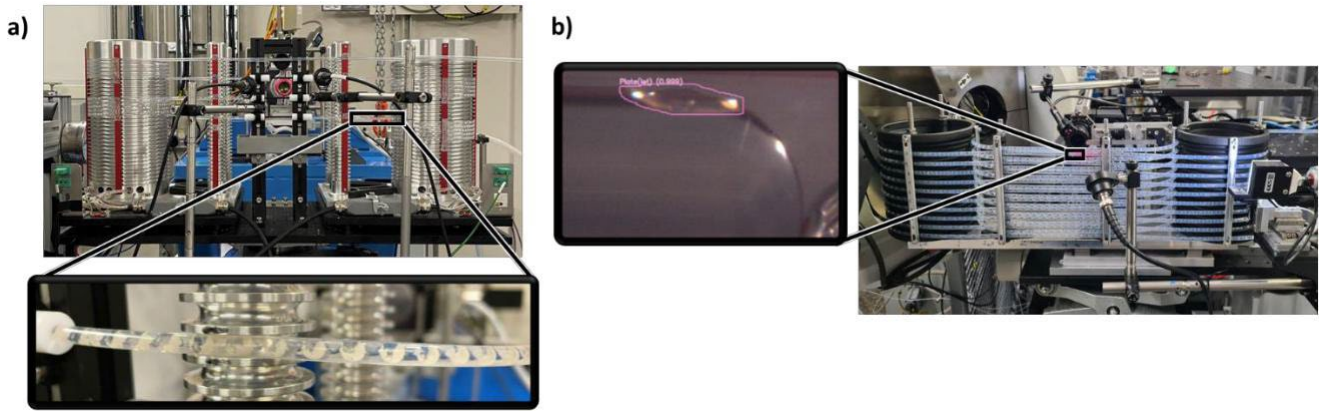

Figure 2. a) the KRAIC-T on I11, highlighting oABA in segmented flow slurrying, b) the KRAIC-S on I19, highlighting a single paracetamol crystal in a slug with image analysis identifying platelet morphology.

Also featured in this work is the KRAIC-S (for single crystal), developed in collaboration with beamline I19 for small molecule SCXRD at Diamond Light Source. Through a novel slug-triggering shuttle analysis module, the KRAIC-S collects SCXRD data from singly-crystallising paracetamol for a prolonged period of time, enabling structural refinement of crystals in flow. Recent upgrades to the KRAIC-S system now facilitates SCXRD analysis at successive points along the crystalliser to monitor crystal growth, with current work focusing on implementing SCXRD coupled with automated image analysis for morphology recognition in flow, shown above in Fig 2b.

1 Robertson, K., Flandrin, P.-B., Klapwijk, A. R., & Wilson C. C. (2016). *Cryst.Growth Des.,* **16**, 4759−4764.
2 Levenstein, M., Wayment, L., Scott, C., Lunt, R., Flandrin, P.-B., Day, S., Tang, C., Wilson, C. C., Meldrum, F., Kapur, N., & Robertson, K. (2020), *Anal.Chem.*, **92**, 7754−7761.

A076-03-230823

In situ X-ray diffraction study of nanopowders Spark Plasma Sintering under very high pressure

Sylvie Le Floch1, Thomas Gaudisson1, Sandrine Cottrino2, Vittoria Pischedda1, Yann Le Godec3

1 ILM, Univ. Claude Bernard Lyon 1, UMR CNRS 5306, 10 rue Ada Byron, 69622, Villeurbanne 2 MATEIS, INSA-Université Lyon1 - CNRS, UMR 5510, INSA de Lyon, 69621 Villeurbanne 3 IMPMC, Sorbonne Université, UPMC, UMR CNRS 75090, 4, Place Jussieu, 75005 Paris sylvie.le-floch@univ-lyon1.fr

Keywords: *In situ* X-ray diffraction, High-pressure spark plasma sintering, Grain growth

SPS (Spark Plasma Sintering) is a pressure sintering technique that uses pulsed current heating. The very high heating and cooling rates allow a fast consolidation of the powders with limited grain growth. Nanostructuring allows modulating the mechanical, thermal or optical properties of materials. Therefore, SPS is widely used in the search for materials with remarkable properties. However, SPS has its limitations and one of the ways of improvement is the application of very high pressures during sintering. Increasing the pressure significantly lowers the densification temperature of the powders [1, 2]. SPS at very high pressures is therefore a promising process for the elaboration of bulk nanostructured materials, and, for the sintering of temperature unstable materials and materials that are difficult to sinter without the addition of a binder. Commercially available SPS devices are limited to 150 MPa. Modified devices can reach 1 GPa. But these pressures are insufficient to sinter some materials under their thermodynamic stability conditions (e.g. diamond, c-BN). We have pushed the limit to 10 GPa, by adapting a pulsed electric current heating to a high pressure synthesis equipment of PE type (Paris-Edinburgh press) [2, 3]. Our SPS-PE device is portable and suitable for *in situ* measurements on large facilities (synchrotron, neutron source) for the study of material transformation kinetics during the sintering process as a function of temperature, pressure and applied current characteristics. This type of real-time analysis (Fig.

1) is not possible on any other SPS device. We will present the results of sintering studies conducted on different oxide nanopowders and on nanodiamond.

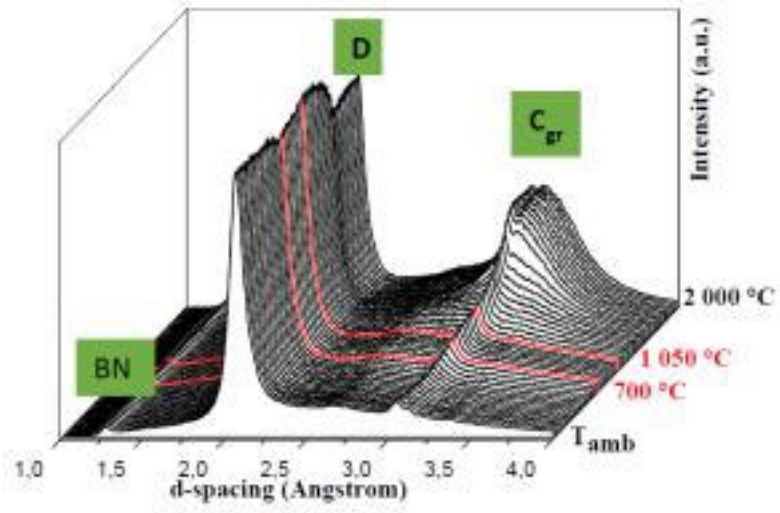

Figure 1. *In situ* X-ray diffraction monitoring of a diamond nanopowder (5 nm) sintering under 5 GPa (D, diamond; C_{gr}, graphite; BN, hexagonal boron nitride). The heating rate is 500°C/min. The acquisition rate of 10 diffractograms per second on the PSICHE beamline (synchrotron Soleil, France) allows to follow the grain growth in real time and to detect any graphitisation.

1) A. Verchère, S. Cottrino, G. Fantozzi, S. Mishra, T. Gaudisson, N. Blanchard, S. Pailhès, S. Daniele and S. Le Floch, Ceramics, 4, (2020) 507.
2) S Cottrino, T. Gaudisson, S. Pailhès, E. Archina Ferrara, S. Mishra, S. Daniele, M. Mézouar, A. Largeteau, Y. Le Godec, S.Le Floch, Journal of the European Ceramic Society (2022), doi.org/10.1016/j.jeurceramsoc.2022.11.037
3) Y. Le Godec, S. Le Floch, S. Pailhès and J.-M. Combes, US11247267B2, 2022.

A076-04-230823

In situ synchrotron X-ray powder diffraction of mechanochemically induced self-sustaining reactions

Hidetaka Kasai, Yanyan Zheng and Eiji Nishibori

University of Tsukuba, 305-8571 Tsukuba, Japan

kasai.hidetaka.fw@u.tsukuba.ac.jp

Keywords: mechanochemically induced self-sustaining reaction, ball milling, in situ synchrotron X-ray diffraction

A mechanically induc
ed self-sustaining reaction (MSR) is a combustion-like reaction ignited by a mechanical force [1]. MSRs have been observed in various highly exothermic powder mixtures. Once a MSR starts, it proceeds without external energy. This makes it difficult to extract powder at a certain reaction time during a MSR. It requires in situ observation to reveal the MSR process. So far, in situ observations have been reported for temperature of a milling container, pressure in the container and a macroscopic view of powder using a transparent container to reveal the MSR process [1-3]. The MSR process has not yet fully understood due to the lack of knowledge of time evolution of reactants and products.

We applied in situ synchrotron X-ray powder diffraction to monitoring MSR and non-MSR processes in mechanochemical reduction of AgCl with metals [4]. The in situ diffraction technique for mechanochemical reactions by ball milling was first developed by Friščić and coworkers [5]. We measured in situ diffraction data during ball milling with 2 s per frame using our in situ apparatus [6] and a flat panel detector at SPring-8 BL02B2. The wavelength of incident X-ray was 0.7 Å. The temperature of milling jar was also monitored using thermography. We performed Rietveld refinements with our developed multi-distance method [6] for the in situ data with a time resolution of 60 s or less by summing the frames.

We successfully observed time dependence of relative amounts for the reactants and products during milling. For both of MSR and non-MSR, the amount of Ag increased with time after the activation time. In addition of consumption by the reactions, the amount of AgCl increased in the observation area by increasing its fine particles by size reduction, and the amount of metals decreased by spreading. For the MSRs using Al and Zn, we observed a drastic increase of amounts for Ag. The ignition and deceleration of MSRs were identified by the jar temperature. The onset of the drastic amount changes was consistent with the abrupt increase of jar temperature, i.e. the ignition of MSR. In the case of Al, we observed growth of Ag for 6 minutes with the kinetics induced by the MSR for 2 minutes.

The growth kinetics was described with the Kolmogorov-Johnson-Mehl-Avrami (KJMA) model. In the both of MSR and non-MSR, the kinetic exponent n was estimated as 2, indicating the same growth mechanism. We observed the rate constant ln(k) of - 10 for MSR and -14 for non-MSR. This indicates a faster contact formation [7] for MSR than non-MSR, supporting the contribution of local melting in the MSR [4].

1) Takacs, L. (2002). Prog. Mater. Sci. 47, 355.
2) Deidda, C., Delogu, F. & Cocco, G. (2004). J. Mater. Sci. 39, 5315.
3) Pauls, J. M., Shkodich, N. F. & Mukasyan, A. S. (2019). J. Phys. Chem. C 123, 11273.
4) Takacs, L. (2007). J. Therm. Anal. Cal. 90, 81.
5) Friščić, T. et al. (2013). Nat. Chem. 5, 66.
6) Zheng, Y., Kasai, H., Kobayashi, S., Kawaguchi, S. & Nishibori, E. submitted.
7) Michalchuk, A. A. L. et al. (2017). Adv. Sci. 4, 1700132.

This work was supported by JSPS KAKENHI (Grants No. JP19KK0132, JP20H04656 and JP21H05235). The synchrotron experiments were performed at SPring-8 BL02B2 with the approval of the Japan Synchrotron Radiation Research Institute (JASRI) (Proposal No. 2022A1754, 2022A1231 and 2022B1683).

A076-05-230823

In-situ studies of synthesis of oxy-fluorides and fluorides using solid-state fluorine sources

Y. Inaguma[1], T. Katsumata[2], S. Kobayashi[3], S. Kawaguchi[3]

[1]*Gakushuin University, Tokyo Japan,* [2]*Tokai University, Hiratsuka, Japan,* [3]*JASRI, Hyogo, Japan*

Email of communicating yoshiyuki.inaguma@gakushuin.ac.jp

Keywords: In-situ X-ray diffraction, oxy-fluoride, fluoride, synthesis, solid-state fluorine source

Fluorine-containing solid-state inorganic materials, fluorides and oxy-fluorides, exhibit excellent chemical and physical properties attributable to high electronegativity of fluorine and different metal-anion bonds, M-O and M-F[1,2]. However, the number of the reported fluorine-containing compounds is much less than that of reported oxide. This is related to the difficulty of synthesis of fluorine-containing compounds compared to oxides because most of fluorides used as raw materials are unstable at ambient atmosphere and we sometimes have to use hazard HF and molecular F_2. To facilitate the exploration of fluorine-containing compounds, we need to provide new synthetic concepts and develop facile synthetic routes. Further, elucidation of reaction process would lead developments of novel compounds. In this symposium, we will present our in-situ studies of synthesis of oxy-fluorides and fluorides. One is synthesis of novel silver-containing oxy-fluorides such as a perovskite-type $AgTiO_2F$(ATOF)[3] using an approach adopting the hard and soft acids and bases (HSAB) principle[4]. Another is synthesis of complex fluorides, Li_2MF_6 (M: transition metal) using fluorine source of CuF_2 [5]. In-situ synchrotron X-ray diffraction (SXRD) experiments were conducted at the BL02B2 beamline at SPring-8.

Fig. 1 shows the evolution of SXRD patterns for formation of ATOF. The mixture of AgF and TiO_2 was then packed into a Ni tube, which was sealed in a SiO_2 glass capillary. ATOF was not formed by a direct reaction between AgF and TiO_2 but formed via Ag_3TiOF_5 and Ag_2O as intermediated compounds. The formation of Ag_2O is consistent with the HSAB principle[4].

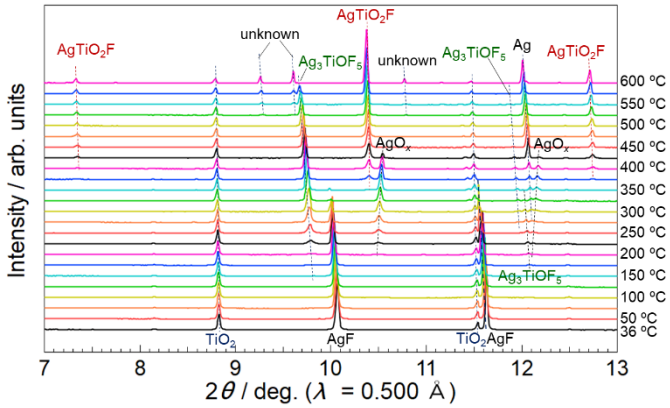

Figure 1. In-situ X-ray diffraction patterns for formation of $AgTiO_2F$.

Further, we tried to synthesize Li_2MF_6 (M = Ti, V, Zr, Nb, Mo) via a reaction between LiF, M and solid-state fluorine source of CuF_2 under ambient pressure and high pressure. In the experiments, known trirutile-type Li_2MoF_6 and novel Li_2ZrF_6-type Li_2MoF_6 were obtained under ambient pressure and high pressure of 3 GPa, respectively[5]. In both cases, the total reaction proceeds according to eq. (1), and CuF_2 then works as oxidizing reagent as well as fluorine source.

$$2\ LiF + Mo + 3\ CuF_2 \rightarrow Li_2MoF_6 + 3\ Cu. \quad (1)$$

We elucidated the reaction behaviour of trirutile-type Li_2MoF_6 via a combination of XRD and differential scanning calorimetry experiments under ambient pressure. Details will be presented in the symposium.

[1] Leblanc, M.; Maisonneuve, V.; Tressaud, A., *Chem. Rev.* (2015). **115**, 1191.

[2] Kageyama, H. et al., *Nat. Commun.* (2018). **9**, 772.

[3] Inaguma, Y.; Sugimoto, K.; Ueda, K. (2020). *Dalton Trans.*, **49**, 6957

[4] Pearson, R. *J. Am. Chem. Soc.* (1963). **85**, 3533; Pearson, R. *J. Chem. Educ.* (1987) **64**, 561.

[5] Inaguma, Y.; Oyanagi, M.; Ueda, K. (2022). *Inorg. Chem.*, **61,** 1728.

The SXRD experiment was conducted with the approval of JASRI (proposal nos. 2020A1393, 2021B1409, 2022B1586, 2022B1812, and 2023A1546). This work was supported by a Japan Society for the Promotion of Science (JSPS) KAKENHI grant (no. 19K22235), a Grant-in-Aid for Scientific Research on the Innovative Area "Mixed anion" from JSPS (no. JP16H06439).

A076-06-230823

Mechanistic Understanding of Ceramic Cold Sintering with In Situ Synchrotron-based High-Energy X-Ray Scattering and Diffraction

Fan Zhang[1], Russell A. Maier[1], Igor Levin[1], Andrew J. Allen[1], Jun-Sang Park[2], Peter Kenesei[2], Ivan Kuzmenko[2], Pete Jemian[2], and Jan Ilavsky[2]

1. *Materials Measurement Science Division, National Institute of Standards and Technology, Gaithersburg, Maryland, MD 20899, USA*
2. *X-ray Science Division, Advanced Photon Source Argonne National Laboratory, Argonne, IL 60559, USA*

fan.zhang@nist.gov

Keywords: ceramics processing, cold sintering, in situ, high-energy X-ray scattering

Ceramic cold sintering processing represents a novel and environmentally friendly sintering technology capable of producing fully dense ceramic parts under a uniaxial compression typically lower than 500 MPa and at low temperatures less than 500 °C [1]. A mechanistic understanding of cold sintering processing is lacking, hindering its technology development and commercial maturation [2].

To meet this challenge, we developed an integrative in situ monitoring methodology consisting of simultaneous measurements of macroscopic temperature, pressure, volumetric shrinkage, microstructure, and atomic structure, utilizing synchrotron-based high-energy small-angle X-ray scattering and X-ray diffraction techniques. Using ZnO, the most widely studied materials system for ceramic cold sintering [3,4], as a model system, we investigated the phase transition and grain growth mechanism of cold sintering. We demonstrated that cold sintering could occur at unusually low pressure (50 MPa), circumventing the hydrothermal condition previously considered necessary for cold sintering.

We comprehensively characterized the morphological, structural, and interfacial evolution under an isothermal and isobaric condition. Our results revealed three distinct stages. The first stage, associated with heating ZnO to a target temperature, sees a significant volumetric shrinkage and creates the surface contact necessary for sintering. The intermediate stage features the most structural and morphological changes. We observed a kinetic evolution of two nanocrystalline phases and the ZnO, accompanied by systematic changes in the surface area, pore volume, and interfacial roughness. The final stage features a continued evolution of nanocrystalline phases and a reduction of the surface roughness, with a clear presence of residual nanocrystalline phases in the final cold sintered ZnO.

Our results unveil the structural transformation kinetics of cold sintering of ZnO at an unprecedented level and provide previously unattainable data for model validation. Our methodology, extended to other cold-sintering systems, will enable a comprehensive understanding of the transient structural transformations necessary for producing cold-sintered materials with desired mechanical and functional properties.

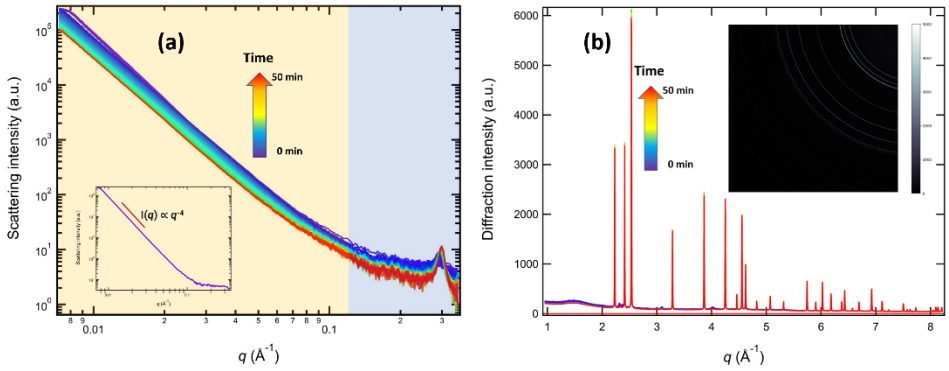

Figure 1: (a) in situ SAXS and (b) XRD data revealing the phase and microstructural transforamtion during ceramics cold sintering.

This research used resources of the Advanced Photon Source, a U.S. Department of Energy (DOE) Office of Science user facility operated for the DOE Office of Science by Argonne National Laboratory under Contract No. DE-AC02-06CH11357.

[1] A. Galotta and V. M. Sglavo, Journal of the European Ceramic Society **41**, 1 (2021).
[2] S. Grasso, M. Biesuz, L. Zoli *et al.*, Advances in Applied Ceramics **119**, 115 (2020).
[3] S. Funahashi, J. Guo, H. Guo *et al.*, Journal of the American Ceramic Society **100**, 546 (2017).
[4] J. Gonzalez-Julian, K. Neuhaus, M. Bernemann *et al.*, Acta materialia **144**, 116 (2018).

A093 Nucleation and Crystal Growth

Room 219
1.10pm – 3.30pm

A093-01-230823

Crystallising natural products via encapsulated nanodroplet crystallisation protocols.

Alexandra Longcake[1], Lina Mardiana[1], Nicholas H. Oberlies[2], Michael J. Hall[1]* and Michael R. Probert[1]*

[1]Department of Chemistry, School of Natural and Environmental Sciences, Newcastle University, Newcastle upon Tyne, NE1 7RU, United Kingdom. [2]Department of Chemistry and Biochemistry, The University of North Carolina, Greensboro, North Carolina 27402, United States.

alexandra.longcake@newcastle.ac.uk

Keywords: high-throughput crystallisation, oil encapsulation, natural products, polymorph

Natural products (molecules made by bacteria, fungi, plants and animals) are a rich source of inspiration for the development of new medicines. Natural products and their derivatives have been used to treat a host of diseases and conditions, such as pain management (aspirin and morphine), cancer (paclitaxel and doxorubicin), heart disease (captopril and enalapril) and infection (penicillin and tetracycline).[1, 2] In fact, more than 50 % of small molecule drugs developed in the United States between 1981-2014 were derived from natural products or semisynthetic derivatives.[2] However, absolute structure determination of new bioactive molecules – an essential step in the development of a clinical drug – remains a time-consuming practical impediment. Therefore, methods to increase the speed at which the 3D molecular structure of an unknown natural product can be solved must be developed in order to alleviate this "bottleneck" in the discovery process of clinical compounds.

Herein, we report the successful deployment of a new crystallisation approach to rapidly access crystals of complex organic molecules that are otherwise challenging to crystallise (including natural products). Using encapsulated nanodroplet crystallisation (ENaCt) protocols, a significant number of natural products have been obtained as single crystals and structurally characterised by single crystal X-ray diffraction (Figure 1).[3] The 3D structures of these molecules have been unambiguously confirmed by single crystal X-ray diffraction analysis, both at Newcastle University and through collaboration with the UK National Crystallography Service and Diamond Light Source (the UK's national synchrotron science facility). The first results of this highly successful proof of concept project are soon to be published, thus allowing other groups to apply our approaches to related problems, particularly in cases were traditional solution phase characterisation techniques yield ambiguous results which require further verification.

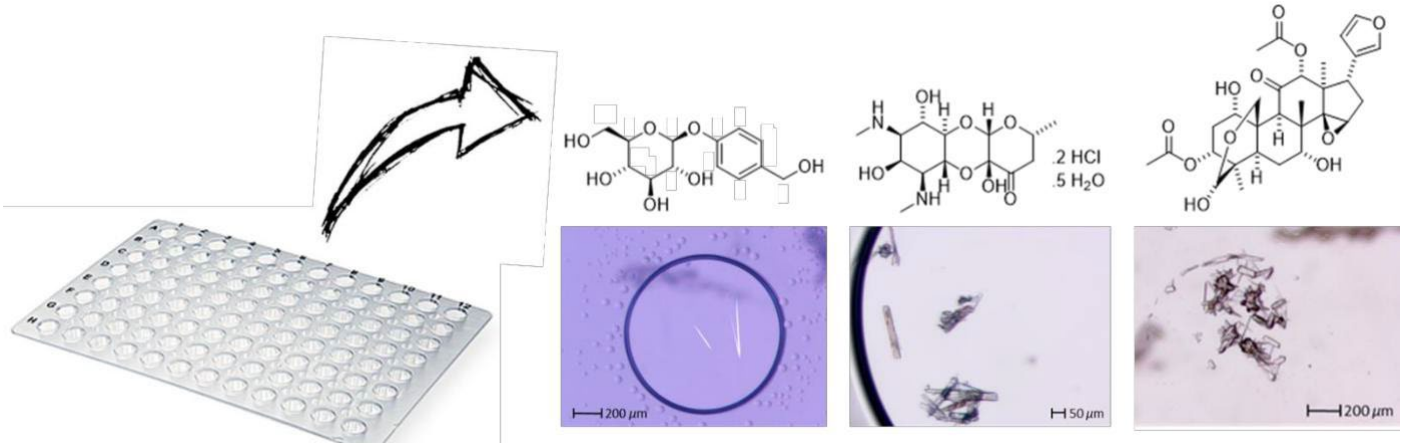

Figure 1. Examples of compounds crystallised using ENaCt protocols.

1 A. G. Atanasov, S. B. Zotchev, V. M. Dirsch, the International Natural Product Sciences Taskforce and C. T. Supuran, *Nat. Rev. Drug Discov.,* 2021, **20**, 200-216.

2 F. Li, Y. Wang, D. Li, Y. Chen and Q. P. Dou, *Expert Opin. Drug Discov.*, 2019, **14**, 417-420.

3 A. R. Tyler, R. Ragbirsingh, C. J. McMonagle, P. G. Waddell, S. E. Heaps, J. W. Steed, P. Thaw, M. J. Hall and M. R. Probert, *Chem*, 2020, **6**, 1755-1765.

A093-02-230823

Chaperone compounds for co-crystallization of small molecules

Tim Berking[1], Tobias Stuerzer[2], Wolfgang Frey[1], Clemens Richert[1], Martin Adam[2], Prathapa Jagannatha[3]

[1]Universität Stuttgart, Institut für Organische Chemie, Stuttgart, Germany; [2]Bruker AXS GmbH, Karlsruhe, Germany; [3]Bruker India Scientific Pvt. Ltd, Sahakara Nagar 4, Bangaluru -560 092 India
Martin.adam@bruker.com

Keywords: co-crystallization, absolute structure, chaperone

Modern instrumentation and processing techniques enable high-quality 3D structure analysis – including absolute structure determination – often in less than an hour, i.e. faster and more comprehensively than many spectroscopic methods can achieve. However, many small or highly flexible organic molecules remain intractable to current crystallization methods, including the crystal-sponge method[1]. A new chaperone-aided crystallization method[2] based on Tetraaryladamantane ethers (Fig 1) has delivered high quality co-crystals in a fair number of cases, allowing for the structure determination of analytes, including their stereochemistry. The adamantane chaperone approach works well for analytes that are liquid at room temperature and adds an important tool to the toolbox for both synthetic organic chemists and crystallographers, facilitating the investigation of small molecules, such as new natural products, synthetic intermediates, pharmaceutically active ingredients, or fragrances.

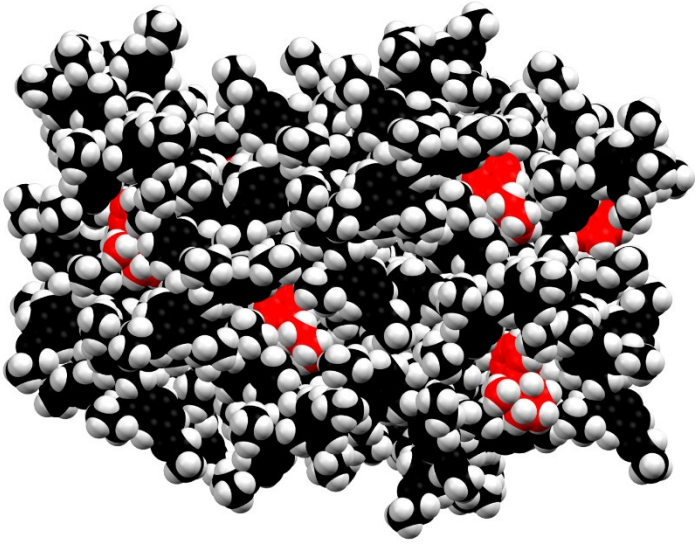

Figure 1. Extended triptycyl group: RTrp*

Figure 1. Tetraaryladamantane ethers easily form co-crystals with a large number of organic compounds difficult to crystallize by other methods (here nicotine/1,3,5,7-tetrakis(2,4-diethoxyphenyl)adamantane (TEO) co-crystals are shown.)

The chaperone-aided crystallization method is easy to apply and crystals suitable for the determination of absolute configuration are typically obtained within minutes or hours. With modern X-ray instrumentation the method can provide very fast access to the full 3D structure of an important class of organic analytes.

Salient features include:

- Structures in hours or days rather than weeks
- Small quantities of analyte required
- No solvent screening required

Three chaperone compounds are being made available, helping to obtain suitable crystals with ordered analyte in the unit cell, allowing for determination of relative or absolute configuration.

We will discuss the method and demonstrate rapid crystal growth for examples, such as the two enantiomers of limonene.

[1] Inokuma, Y.; Yoshioka, S.; Ariyoshi, J.; Arai, T.; Hitora, Y.; Takada, K.; Matsunaga, S.; Rissanen, K.; Fujita, M. *Nature* **2013**, *495*, 461-466.
[2] Krupp, F.; Frey, W.; Richert, C. *Angew. Chem. Int. Ed.* **2020**, 59, 15875–15879.

The authors would like to acknowledge the EPSRC, the UK National Crystallography Service and Diamond Light Source.

A093-04-230823

Effects of introducing various alkyl chains at the bridgehead position of extended triptycyl groups and their application for highly reactive species

Y. Wakasa, M. Minoura

Department of Chemistry, College of Science, Rikkyo University,

3-34-1, Nishi-Ikebukuro, Toshima-ku, Tokyo 171-8501, Japan

minoura@rikkyo.ac.jp

Keywords: Crystal engineering, Main group element, Germylene

In the structural chemistry of main group element compounds containing reactive chemical bonds, crystal growth is an essential part for the characterization the bonding nature as well as the crystal structure determination. The solubility and crystallinity of the target compounds are key factors in molecular design. We have designed and synthesized of an extended triptycyl group, Trp*, which have been used for kinetic stabilization of highly reactive species. It has superior steric protection and large reaction space around reaction center, however, compounds with bulky substituents, such as Trp*, have low solubility and poor crystallinity in some cases. In fact, the synthetic studies of Trp*-substituted germanium compounds initially yielded only crystals that were too small to be analyzed structurally by X-ray diffraction.

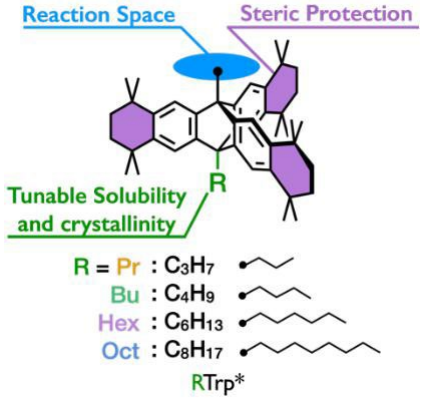

Germylenes (R_2Ge:), divalent species of germanium, are the germanium analogue of carbene and show high reactivity due to their unique electronic state. The isolation of monomeric germylenes has been achieved by the kinetic stabilization with bulky substituents around the Ge [1]. We have succeeded the isolation of the first dialkylgermylene (Trp^*_2Ge:) as a thermally stable compound [2]. However, some derivatives of Trp^*_2Ge: had low solubility and crystallinity, making characterization difficult. To improve these problems of Trp* compounds, we focused on the concept of crystal engineering, in which intermolecular interactions are intentionally controlled to design and synthesize solid-state structures with desired properties. [3, 4].

We report here, the synthesis of RTrp* groups having alkyl chains (R= Pr, Bu, Hex, Oct) at the bridge head position of Trp*. (Fig. 1) and applied them to the synthesis of dialkylgermylenes ($RTrp^*_2Ge$:) in the expectation of improving those crystallinities by intermolecular interactions with the packing forces in the solid states.

The isolated $RTrp^*_2Ge$: showed better solubility and crystallinity than the corresponding Trp^*_2Ge:. Especially, $HexTrp^*_2$ Ge: showed characteristic change in the packing structure to form suitable single crystals for X-ray analysis (Fig. 2). The details of synthesis and structure of $RTrp^*_2Ge$:, and packing structures in the solid state will be discussed.

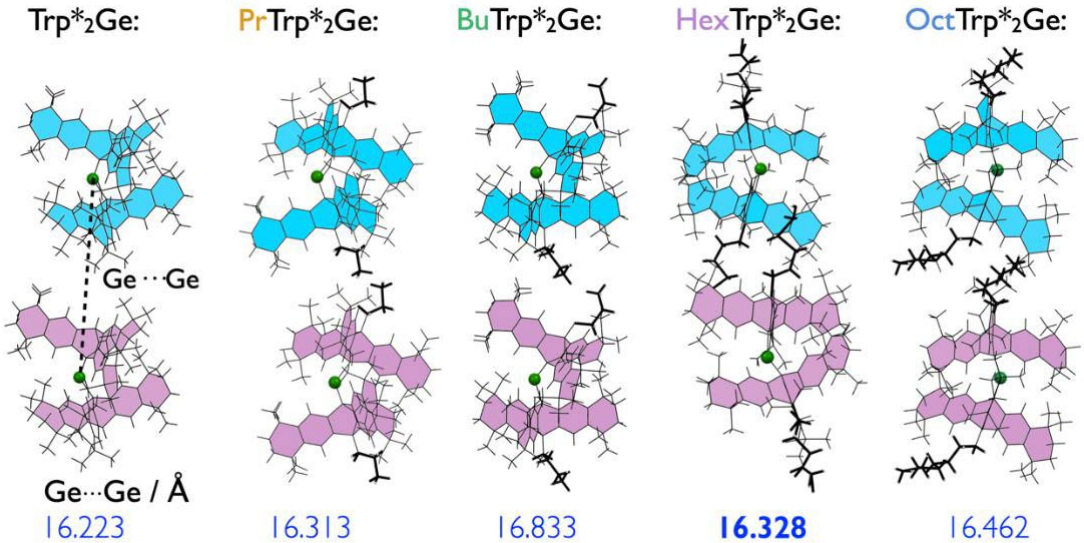

Figure 2. Packing structure of RTrp*$_2$Ge:

1 Tokitoh,N. & Okazaki, R. (2000). *Coord. Chem. Rev.*, **210**, 251.

2 Suzuki, F., Nishino, R., Yukimoto, M., Sugamata, K. & Minoura, M. (2020). *Bull. Chem. Soc. Jpn.*, **93**, 249.

3 Braga, D., Desiraju, G. R., Miller, J. S., Orpen, A. G. & Price, S. L. (2002). *Cryst. Eng. Commun.,* **4**, 500.

4 Desiraju, G. R. (2013). *J. Am. Chem. Soc.*, **135**, 9952.

A093-05-230823

High-throughput nanoscale co-crystallisation of organic molecules

4 Metherall[1], M. Probert[1], M. Hall[1], J. McCabe[2], P. Corner[2].

[1]Chemistry - School of Natural and Environmental Sciences, Newcastle University, Newcastle, UK, [2]Early Product Development, Pharmaceutical Sciences, R&D, AstraZeneca, Macclesfield, UK. j.metherall@newcastle.ac.uk

Keywords: High-throughput, Nanodroplet, Co-crystallisation

Modern material characterisation at atomic structural resolution is heavily dependent on the availability of single, high-quality crystals for analysis by Single Crystal X-ray Diffraction (SCXRD). Success in growing single crystals strongly correlates to the total volume of crystallisation space explored, posing an experimental problem due to the number of variables that need to be examined (e.g., solvent, temperature, concentration and additives). Growing single crystals of a co-crystal, which contain two or more chemically inequivalent, non-solvent molecules, is an even bigger experimental challenge as it involves finding successful conditions to crystallise multiple components at the same time. Co-crystallisation is very important, especially in the area of pharmaceuticals, as a co-crystal can have enhanced physical properties compared to the active pharmaceutical ingredient on its own.

Approaches to searching crystallisation space have undergone a 'step-change' in recent years with new techniques [1-3] becoming available via the use of technological advancements in liquid handling [4]. High-throughput Encapsulated Nanodroplet Crystallisation (ENaCt), allows rapid exploration of crystallisation space, with multiple experimental conditions screened in parallel whilst using low overall quantities of analyte [1, 5-7].

Until now, ENaCt has not been applied to the problem of co-crystallisation despite the technique being particularly suited to this challenge. Using a liquid-handling robot (SPT Labtech Mosquito®) [4], parallel screening of co-crystallisation conditions was undertaken (Fig. 1), with each experiment using a few nanolitres of analyte, reducing the overall material demand. Following exploration of different experimental ENaCt screening methods, several known and new pharmaceutically relevant co-crystals have been grown and analysed via SCXRD.

Our results clearly demonstrate that high-throughput crystallisation screening methods can be employed to obtain high quality co-crystals, suitable for SCXRD, in short timeframes with low overall sample requirements. We anticipate that our co-crystallisation techniques will be of great use in the pharmaceutical industry for the development of new and improved medicines.

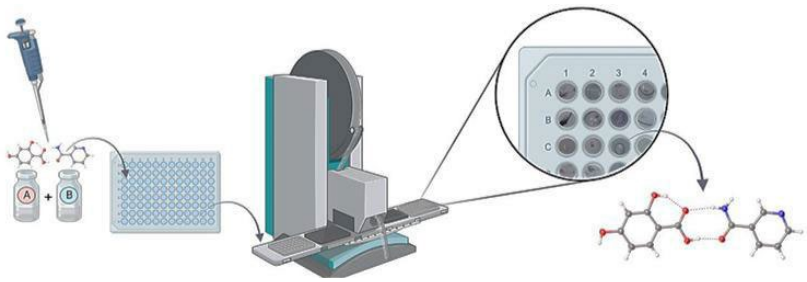

Figure 1. The ENaCt methodology for co-crystal screening experiments.

1 Tyler, A. R., Ragbirsingh, R., McMonagle, C. J., Waddell, P. G., Heaps, S. E., Steed, J. W., Thaw, P., Hall, M. J. & Probert, M. R. (2020). *Chem*, **6**, 1755-1765.

2 Barbor, M., Nievergelt, P. P., Čejka, J., Zvoníček, V. & Spingler, B. (2019). *IUCrJ*, **6**, 145-151.

3 Hoshino, M., Khutia, A., Xing, H., Inokuma, Y. & Fujita, M. (2016). *IUCrJ*, **3**, 139-151.

4 SPT Labtech Mosquito®, https://www.sptlabtech.com/company.

5 Al Subeh, Z. Y., Waldbusser, A. L., Raja, H. A., Pearce, C. J., Ho, K. L., Hall, M. J., Probert, M. R., Oberlies, N. H. & Hematian, S. (2022). *J. Org. Chem*., **5**, 2697-2710.

6 Zhu, J., Moreno, I., Quinn, P., Yufit., D. S., Song, L., Young, C. M., Duan, Z., Tyler, A. R., Waddell, P. G., Hall, M. J., Probert, M. R., Smith, A. D. & O'Donoghue, A. C. (2022). *J. Org. Chem*., **6**, 4241-4253.

7 Cooper, M. S., Zhang, L., Ibrahim, M., Zhang, K., Sun, X., Roske, J., Gohl, M., Bronstrup, M., Cowell, J. K., Sauerhering, L., Becker, S., Vangeel, L., Jochmans, D., Neyts, J., Rox, K., Marsh, G. P., Maple, H. J. & Hilgenfeld, R. (2022). *J. Med. Chem*., doi:10.1021/acs.jmedchem.2c01131.

A093-06-230823

Diffraction studies of meteorites at the Australian Synchrotron

H. E. A. Brand[1], N. R. Stephen[2], A. D. Langendam[1], E. C. Campbell[1] and A. G. Tomkins[3]

1. ANSTO, Australian Synchrotron, 800 Blackburn Rd., Clayton, VIC 3168, Australia, 2. Plymouth Electron Microscopy Centre, University of Plymouth, Drake Circus, Plymouth, PL4 8AA, United Kingdom, 3. School of Earth, Atmosphere and Environment, Monash University, Melbourne, VIC 3800, Australia;

helenb@ansto.gov.au

Keywords: Mineralogy, Meteorites, powder diffraction

Meteorites are windows on the solar system. They provide invaluable insights into the composition and geological processes which formed and continue to shape the solar system. Most of the investigations into these planetary materials typically use microscopic and spectroscopic techniques. However, there is much to be learned using scattering techniques to investigate the bulk properties and mineralogy of these materials.

In this contribution we will summarise projects undertaken across beamlines at the Australian synchrotron. Topics discussed will include:

Thermal properties of meteorites and terrestrial analogues with a view to ISRU
Planetary analogue simulants are materials, terrestrial in origin and usually mixtures of minerals, which are designed to be spectrally and compositionally identical to the materials we observe on other planets. Both ESA and NASA produce and curate simulant materials for various planetary bodies. In coming years, there are a number of sample return missions scheduled and interest in benchmarking simulant materials and their properties relative to "real" extra-terrestrial samples is growing. This is especially timely in relation to In Situ Resource Utilisation (ISRU) requirements as human space flight programs such as Artemis begin in earnest. Most analogues are made of pristine materials and although they may be chemically similar to the rocks they emulate, mineralogically they can be very different. In this study, we compare the thermal properties of a range of meteorites to their curated analogue materials.

Using powder diffraction to classify micrometeorites
Micrometeorites are samples of extraterrestrial dust that continually fall to the surface of the Earth. They hold records of the early solar system as well as the state of the Earth's atmosphere when they passed through it. Handling these tiny samples, sometimes as small as 10 micron, can be difficult. Sectioning means that you can only see a 2-dimentional section that is unlikely to be fully representative of the mineralogy. Powder diffraction offers a pathway to obtain a bulk mineralogy analysis of individual micrometeorites, which is not possible by other approaches. Here we will discuss the best way to screen and classify micrometeorites using lessons learnt from other crystallographic disciplines and develop a sample holder that allows entire populations to be screened using powder diffraction before being easily transferred for other studies such as microscopy.

Development of simultaneous microdiffraction and fluorescence mapping of meteorite mineral phases on the X-ray Fluorescence microscopy beamline
Being able to spatially determine mineralogical changes across a sample are key to understanding the process that shaped the rock. At the Australian synchrotron we are developing a new technique to conduct simultaneous microdiffraction analysis and fluorescence mapping. The meteorites chosen for this exploratory experiment demonstrate how we can use the XFM beamline to map mineralogy and to investigate texture in texturally complex but mineralogically simple natural samples.

A112 X-ray Imaging and Spectroscopy in Life Sciences

Room 216

1.10pm – 3.30pm

A0112-02-230823

Complex Atomic Fine Structure - New Technology at Advanced Synchrotrons

C.Q. Tran[1,2], T. Kirk[1,2], P. di Pasquale[1,2], M.H. Dao[1,2], C.M. Kewish[1,3], D. Paterson[3], M.J. de Jonge[3], A. Kirby[3], S. Mudie[3], and C.T. Chantler[4]

1 Department of Mathematical and Physical Sciences, La Trobe University, Bundoora, Victoria 3086 Australia, [2] La Trobe Institute for Molecular Science, La Trobe University, Bundoora, Victoria 3086 Australia,

3 Australian Nuclear Science and Technology Organisation, Australian Synchrotron, Clayton, Victoria 3168, Australia. [4] School of Physics, The University of Melbourne, Parkville, Victoria 3010, Australia

Email of communicating cq.tran@latrobe.edu.au

Keywords: X-ray Absorption Fine Structure, Complex Atomic Fine Structure, X-ray Phase Imaging, X-ray Spectroscopy.

X-ray Absorption Fine Structure (XAFS) has been a powerful tool for probing chemical and electronic structures of a wide range of materials. Routinely used at all synchrotron facilities around the world, XAFS-related techniques involve fitting the measured absorption/fluorescence versus energy spectra to extract three-dimensional structural information of the samples under investigation. However, the use of a two-dimensional observation to interpret a three-dimensional structure leads to inevitable problems, unavoidable simplifications and approximations, and to difficulties in the interpretation of results. In this presentation, we describe and demonstrate a new technique which combines X-ray holographic phase imaging and spectroscopy for simultaneously extracting the amplitude and the phase components of the Complex Atomic Fine Structure (CAFS) using the K-edges of copper and iron as an example. The results provide evidence that there is new information in the phase domain of CAFS which promises exciting opportunities for developing current XAFS techniques in a new dimension.

A0112-03-230823

Characterisation of LPMO Intermediates using XAS and Rapid Freeze Quenching

A.J. Telfer[1,2], P.H. Walton[1], S. Diaz-Moreno[2]

[1]*University of York, YO10 5NB, UK*

[2]*Diamond Light Source Ltd., OX11 ODE, UK*

abbey.telfer@diamond.ac.uk

Keywords: HERFD, LPMO, copper, metalloenzyme, radical

Lytic Polysaccharide Monooxygenases (LPMOs) are a family of naturally occurring copper-containing enzymes which have the ability to be able to perform the oxidative saccharification of cellulose. Cellulose is the most abundant natural polymer on Earth and is therefore an ideal potential feedstock for the production of second-generation biofuels [1]. Understanding of the LPMO catalytic mechanism is fundamental in developing biofuels as an attractive source of renewable energy.

Stopped-flow spectrophotometry has shown that the catalytic mechanism of LPMOs includes the formation of short-lived intermediate species when reacted with an oxidant. The development of anaerobic rapid freeze quenching techniques for the preparation of XAS samples has led to the characterisation by HERFD-XANES of a copper histidyl-radical species which forms and decays on a millisecond timescale. On the decay of the histidyl-radical intermediate, a more stable tyrosyl intermediate is formed (Figure 1). It is suggested that the formation and decay of these intermediates is part of a repair mechanism which mitigates oxidative damage in tandem with the elusive catalytic reaction mechanism of LPMOs, allowing for more efficient turnover [2]. This mechanism could be significant in a number of metal-histidine oxygenase complexes.

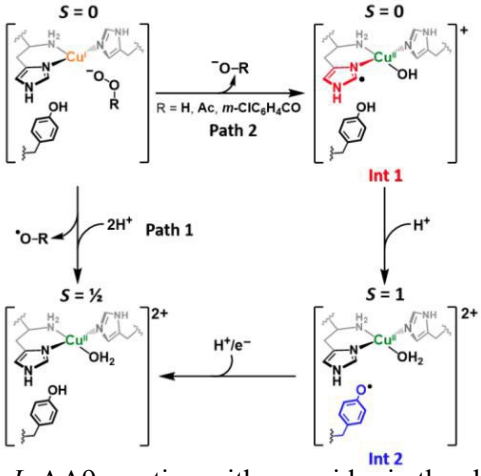

Figure 1: Reaction pathways of Cu(I)-*Ls*AA9 reacting with peroxides in the absence of substrate [2].

The preparation of freeze quenched LPMO samples and XAS data collection has many challenges including the rate of photoreduction of copper(II) species, the anaerobic conditions and fast rate of decay of LPMO radical intermediates. The insights we can gain from the combination of anaerobic rapid freeze quenching and XAS in the study of LPMOs have profound applications in the production of biofuels as well as in oxygenase and copper chemistry.

1) L. Lo Leggio *et al*., *Nat. Commun.*, 2015, **6**, 5961.
2) J. Zhao *et al*., *Research Square*, 2022. [Preprint]. DOI: 10.21203/rs.3.rs-1350705/v1

A112-05-230823

XAS database of reagents frequently used in structural biology

J. Sławek1, A. Klonecka1,2, G. Gazdowicz1, A. Maximenko1, M. Kozak1,3

1. SOLARIS National Synchrotron Radiation Centre, Jagiellonian University, Czerwone Maki 98, 30-392 Kraków, Poland; 2. Faculty of Physics, Astronomy and Applied Computer Science, Jagiellonian University, Łojasiewicza 11, Kraków, Poland; 3. Faculty of Physics, Adam Mickiewicz University, Uniwersytetu Poznańskiego 2, Poznań, Poland.

joanna.slawek@uj.edu.pl

Keywords: XANES, sulphur, XAS database

XAS (X-ray absorption spectroscopy), including XANES (X-ray absorption near-edge structure) and EXAFS (extended Xray absorption fine structure) is a powerful method to study biological systems and biologically relevant compounds [1]. For proteins, it allows to investigate the metal binding sites, providing structural information about coordination, geometry of neighboring atoms and chemical nature of the interactions [2]. As a contrary to the crystallography, it doesn't require the long-range order, so the protein-metal interaction can be characterized in physiological or close to physiological conditions. XAS can be also used to investigate biologically relevant nonmetals such as sulfur. Due to the strong shifts in XAS signal with the change of the oxidation state of sulfur, XAS is a useful method to track the catalytic processes or study the radiation damage. Sulphur is also present in many chemicals used for the protein production and purification, so XAS measurements can be used to assess the sample quality and purity.

Here in this study, we present the measurement possibilities of ASTRA beamline in biological research. ASTRA is one of the newest beamlines at SOLARIS NSRC (Krakow, Poland), that entered the commissioning mode in 2022 [4]. As the introduction to studies of protein and protein complexes, the library of XANES spectra was created. Spectra were recorded for biologically relevant sulfur-containing chemicals and can be used to predict the oxidation state of element of interest in measured material or to determine the percentage of the substance of interest in the measured sample (Fig. 1). The main idea of creating such database of substances containing sulphur and used in structural biology, biochemistry or biophysics is to collect them in repeatable conditions at the same beamline, place their XAS spectra in one place, so that they can be used by users in the future. The series of measurements currently carried out are the first stage of creating the aforementioned XAS database, which will be successively expanded.

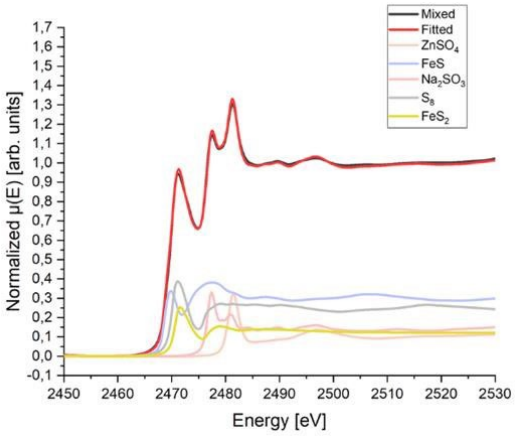

Figure 1. *Sulfur K-edge XANES spectra of selected sulfur-containing compounds and their fitted spectra and mixture.*

[1] Hummer, A. A., Rompel, A. (2013). *Advances in Protein Chemistry and Structural Biology,* edited by C. Z. Christov, pp. 257305.
[2] Jano, Y., Yachandra (2009). *Photosynth. Res, **102**, 241.* [3] Hackett, M. S., Smith, S. E., Paterson, P. G., Nichol, H., Pickering I. J., George, G. N. (2012) ACS Chem. Neurosci., **3**, 3.
[4] Hormes, J., Klysubun, W., Gottert, J. Lichtenberg, H., Maximenko, A., Morris, K., Nita, P., Prange, A., Szade, J., Wagner, L., Zając, M. (2021), *Nucl. Instrum. Methods Phys. Res B,* **489**, 76

A0112-06-230823

Compton microscopy with multilayer Laue lenses

S.Bajt[1,2], H.N. Chapman[1,2,3], T. Li[2], H. Fleckenstein[1], M. Prasciolu[1], J. L. Dresselhaus[2], N. Ivanov[1], O. Yefanov[1], W. Zhang[1], D. Pennicard[4], P. Villanueva-Perez[5], O. Gutowski[4], A.-C. Dippel[4]

1. Center for Free-Electron Laser Science CFEL, Deutsches Elektronen Synchrotron DESY, Hamburg, Germany;

2. Centre for Ultrafast Imaging, Universität Hamburg, Hamburg, Germany;

3. Department of Physics, Universität Hamburg, Hamburg, Germany;

4. Deutsches Elektronen Synchrotron DESY, Hamburg, Germany;

5. Synchrotron Radiation Research and NanoLund, Lund University, Lund, Sweden.

sasa.bajt@desy.de

Keywords: Microscopy, imaging, Compton scattering

High resolution X-ray imaging of biological samples is usually limited by radiation damage. One way to overcome this limitation is to work at higher photon energies, where the dominant interaction with matter occurs through inelastic or Compton scattering. We calculated that the signal per dose for imaging biological samples is maximized at about 60 keV [1]. X-ray optics for such high energies were until recently limited to reflective mirrors and refractive compound lenses. However, wedged multilayer Laue lenses (MLLs) [3] offer high efficiency and very high resolution of a few nanometers and only limited by the effective source size and the bandwidth. With our own developed MLLs [4] we performed proof-of-principle experiments and demonstrated scanning Compton X-ray microscopy on biological objects at PETRA III synchrotron [2]. Recently, we optimized this method and obtained low dose images of several dried biological objects. We calibrated the scattering signals using well defined silicon objects, which enabled us to collect quantitative images of the projected densities of the biological objects. Compton microscopy in combination with diffraction-limited X-ray sources and large solid angle detectors have great potential for imaging of un-sectioned and unlabeled cells with lower dose than previously achievable.

1) Villanueva-Perez, P., Bajt, S., and Chapman, H. N. Optica 5, 450 (2018).
2) Villanueva-Perez, P., Fleckenstein, H., Prasciolu, M., Murray, K. T., Domaracký, M., Gregorič, K., Marian, V., Gelisio, L., Kuhn, M., Hannappel, J., Yefanov, O., Ivanov, N., Sarraou, I., Pennicard, D., Becker, J., von Zimmermann, M., Gutowski, O., Dippel, A.-C., Chapman, H. N., and Bajt, S. Opt Lett 46, 1920 (2021).
3) Prasciolu, M., Leontowich, A. F. G., Krzywinski, J., Andrejczuk, A., Chapman, H. N., and Bajt, S**.** Opt Mat Express 5, 748 (2015).
4) Bajt, S., Prasciolu, M., Fleckenstein, H., Domaracký, M., Chapman, H. N., Morgan, A. J., Yefanov, O., Messerschmidt, M., Du, Y., Murray, K. T., Mariani, V., Kuhn, M., Aplin, S., Pande, K., Villanueva-Perez, P., Stachnik, K., Chen, J. P., Andrejczuk, A., Meents, A., Burkhardt, A., Pennicard, D., Huang, X., Yan, H., Nazaretski, E., Chu, Y. S., and Hamm, C. E. Light: Sci Appl 7, 17162 (2018).

A007 Structural Biology in the Fight Against Infectious Diseases

Room 203/4

4.00pm - 6.30pm

A007-01-230823

Structural biology of bacterial pathogenesis: insights into the function and inhibition of bacterial virulence proteins

J. Paxman[1], L. Hor[1], A. Pilapitiya[1], K. Clarke[1], M. Schembri[2], B. Heras[1]

[1]Department of Biochemistry and Chemistry, La Trobe Institute for Molecular Science, La Trobe University, Melbourne, Vic 3086, Australia

[2]Australian Infectious Diseases Research Centre, School of Chemistry and Molecular Biosciences, The University of Queensland, Brisbane QLD 4072, Australia

b.heras@latrobe.edu.au

Keywords: Bacterial infection, Autotransporters, Antimicrobials

Antimicrobial Resistance is a global threat that requires urgent solutions. Our research focuses on investigating virulence proteins, the molecular weaponry bacteria deploy to cause disease. Combining X-ray crystallography with molecular and biochemical studies, we dissect the mechanism of action of key bacterial virulence factors. We then apply the gained knowledge for developing antimicrobials that "disarm rather than kill bacteria", a novel approach that promises to reduce resistance development.

Central to bacterial virulence potential are autotransporters, the largest group of secreted and surface proteins in Gram-negative bacteria [1-2]. Autotransporters allow bacteria to aggregate, adhere to human cells, and form biofilms, all key facilitators of pathogenesis. We recently constructed a much-needed update to autotransporter phylogeny through combining extensive sequence and published experimental data, to reveal new important functional relationships and divisions within this diverse protein family [2]. This phylogeny has revealed significant knowledge gaps within new and existing groups that we are addressing. For example, using our multidisciplinary approach, we have comprehensively characterised different autotransporter adhesins including Ag43, TibA and UpaB from *Escherichia coli* pathotypes [3-5]. We have shown that heat-to-tail associations between autotransporter proteins in adjacent cells leads to bacterial clumping. Our data to date demonstrates that this is a universally conserved mechanism for autotransporter mediated aggregation and biofilm formation. We have also elucidated the structure-function characterisation of EspC, an autotransporter cytotoxin from enteropathogenic *E. coli*. Most critically, we have determined the structure and mechanism of a subtilase autotransporter from *Serratia marcescens*, the first member from this large relatively unknown group of autotransporters. Finally, we are using these findings to develop specific autotransporter inhibitors such as our recently patented biofilm blocker [6].

[1] Vo, J. L., Martinez Ortiz, G. C., Subedi, P., Keerthikumar, S., Mathivanan, S., Paxman, J. J. & Heras, B. (2017) Proteomics **17**

[2] Clarke, K. R., Hor, L., Pilapitiya, A., Luirink, J., Paxman, J. J., and Heras, B. (2022) Front Immunol **13**, 921272

[3] Heras, B., Totsika, M., Peters, K. M., Paxman, J. J., Gee, C. L., Jarrott, R. J., Perugini, M. A., Whitten, A. E. & Schembri, M. A. (2014). Proc Natl Acad Sci U S A **111**, 457-462

[4] Paxman, J. J., Lo, A. W., Sullivan, M. J., Panjikar, S., Kuiper, M., Whitten, A. E., Wang, G., Luan, C. H., Moriel, D. G., Tan, L., Peters, K. M., Phan, M. D., Gee, C. L., Ulett, G. C., Schembri, M. A. & Heras, B. (2019) Nat Commun **10**, 1967.

[5] Vo, J. L., Ortiz, G. C. M., Totsika, M., Lo, A. W., Hancock, S. J., Whitten, A. E., Hor, L., Peters, K. M., Ageorges, V., Caccia, N., Desvaux, M., Schembri, M. A., Paxman, J. J. & Heras, B. (2022) NPJ Biofilms Microbiomes 8, 20[1

[6] Heras B, Paxman J.J., Lo, A. Schembri, M.A. (2019) (PCT/AU2019/050893).

A007-02-230823

Structural basis of T cell recognition of SARS-CoV-2 variants

Stephanie Gras

Department of Biochemistry and Chemistry, La Trobe Institute for Molecular Sciences (LIMS), La Trobe University

s.gras@latrobe.edu.au

Keywords: COVID-19, SARS-CoV-2, T cell, epitope presentation

The current COVID-19 vaccination roll out is now seeing the call for a 4th shot of the vaccine for our population, and it is anticipated that more booster doses will be proposed to the population. Despite the vaccine efficacy, a lot of question remain, to whether infection and vaccination provide a similar or comparable response beyond the level of neutralising Antibody, and how long is the protection from the vaccines.

As other viruses, SARS-CoV-2 replicates in an imperfect way that lead to mutations and generation of new viruses that are a potential danger for the efficacy of our currents vaccines. While the Antibody response wane with time, T cells have the advantage to hold immune memory that allow them to remember the antigens and act faster upon re-infection or due to vaccination.

We have used X-ray crystallography and biophysical methods to analysis in great details the T cell response to Spike-derived peptides that bind to one of the most frequent HLA molecule in human population. Our work show that specific T cells, via their high affinity T cell receptors are able to “see” mutations of the Spike-derived peptide and avoid viral escape by recognising new strains. We solved the structures of the peptide and its variants with and without the T cell receptor to show how the receptor could adapt its flexible loops to accommodate the mutations and still recognise the peptides. The structures help understand why some T cells are better than other, and should be targeted specifically by vaccines. Our work highlight the importance of additional booster dose of the vaccine, as the T cell response against the mutated peptides was stronger with additional booster shot of the vaccine.

Overall our work help better understand the ability of T cells to recognise Spike-derived peptides as well as their variants, offering strong protection against emerging new viral strains of SARS-CoV-2.

A007-03-230823

Structural basis of immune recognition of SARS-CoV-2 and variants: Implications for pan-coronavirus vaccines and therapeutics

Ian A. Wilson[1]

[1]*Department of Integrative Structural and Computational Biology, The Scripps Research Institute, La Jolla, CA*
wilson@scripps.edu

The continuous evolution of SARS-CoV-2, the etiological agent of COVID-19, has resulted in the accumulation of mutations that either increase its transmissibility or aid in immune escape. Identification and characterization of neutralizing antibodies targeting highly conserved sites are critical to combat SARS-CoV-2 variants and other related sarbecoviruses. We have determined crystal structures of over 50 antibodies to the SARS-CoV-2 receptor binding domain (RBD), other CoV RBDs, and S2 peptides by x-ray crystallography. We have also analyzed their binding and assessed their potency and breadth in neutralization assays with collaborators. These structures have helped delineate the landscape of the antibody immune response to SARS-CoV-2 and led to identification of vulnerable sites (neutralizing epitopes) on SARS-CoV-2 and mechanisms of antibody neutralization. Recurring motifs and binding modes are commonly used by these antibodies and certain antibody germline genes are preferentially used to target particular epitopes. We have also analyzed the structural effects of mutations in the variants of concern from alpha to omicron to explain why certain classes of antibodies are differentially affected by mutations. In summary, we have identified which sites (epitopes) on the SARS-CoV-2 spike protein can be targeted by antibodies with greater breadth and potency. This structural information can aid in design of pan-coronavirus vaccines and antibody therapeutics.

A007-03-230823

Fragment screening as a tool for the search of human dihydroorotate dehydrogenase inhibitors

Nonato, M. C.[1,2], Purificação, A. D.[1,2]; Godoi, B. F.[1,2]; Santos, T.[1,2]; Emery, F. S.[1,2];

[1]School of Pharmaceutical Sciences, University of São Paulo and [2]Center for Research Advancement in Fragments and Targets

Avenida do café S/N Ribeirão Preto, S.P. Brazil 14040-903

cristy@fcfrp.usp.br

Keywords: dihydroorotate dehydrogenase, fragment screening, COVID-19

Our work aims at contributing to the development of an innovative therapy against COVID-19 based on the selective inhibition of the human enzyme dihydroorotate dehydrogenase (HsDHODH). HsDHODH takes part of the *de novo* pyrimidine biosynthetic pathway [1]. The fact that the virus relies on the host cell biochemical machinery to provide nucleosides for its viral replication cycle DHODH a potential target for the development of broad spectrum antivirals. Our objectives envolve fragment synthesis, evaluation and characterization of DHODH fragment-based inhibitors as a strategy for the development of innovative treatment for viral diseases such as COVID-19. Inhibiton assays against HsDHODH were carried out using 2,6-dichloroindophenol (DCIP) as the final electron acceptor. Co-crystallization assays were performed using vapour diffusion methods. Inhibitors were evaluated regarding their citotoxicity and antiviral properties in Calu-3 cells. At 10 uM, 8 non-citotoxic nanomolar inhibitors were found to inhibit 100% of viral replication.

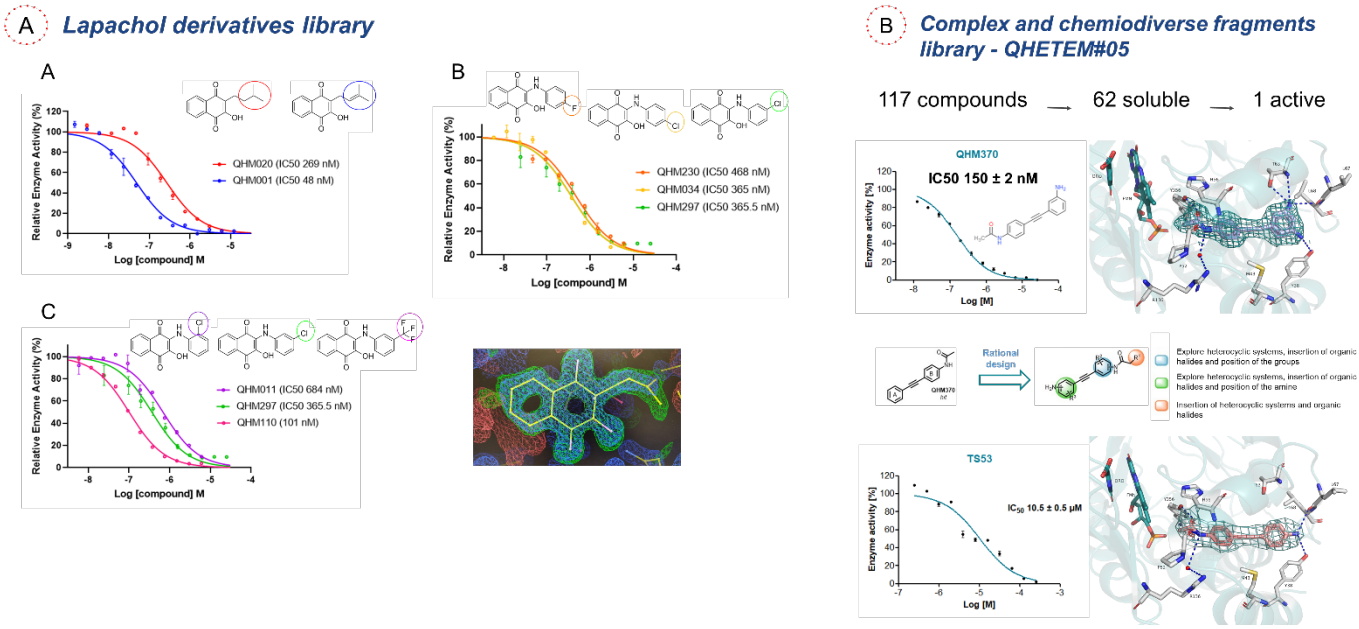

Figure 1. Screening and characterization of human DHODH inhibitors. Different libraries have been tested and potent inhibitors have been identified and characterized by inhibition assays and X-ray crystallography.

The search for new inhibitors for the HsDHODH enzyme is an important strategy in the fight against SARS-CoV-2, responsible for the COVID-19 pandemic with devastating consequences. In this scenario, the fragment screening (FS) is a great tool that can be exploited. In our work, we approched FS by screening different libraries and mapping the molecular basis of ligand interaction by X-ray crystallography. Our results show promising hits tools can be used for the discovery of new inhibitors for the HsDHODH.

[1] Reis RAG, Calil FA, Feliciano PR, Pinheiro MP, Nonato MC. (2017) Arch Biochem Biophys. **632**:175-191.

Acknowledgements: We would like to thank Fundação de Amparo à Pesquisa do Estado de São Paulo (FAPESP), Coordenação de Aperfeiçoamento de Pessoal de Nível Superior Conselho Nacional (CAPES) and Instruct-ERIC for funding. We also thank Manacá beamline at Sirius- Brazil and HZB Fragment Screening Facility for data collection.

A007-05-230822

Discovery of inhibitors targeting viral proteases from SARS-CoV-2

Haitao Yang

Shanghai Institute for Advanced Immunochemical Studies and School of Life Science and Technology, ShanghaiTech University, Shanghai, China.

yanght@shanghaitech.edu.cn

Keywords: SARS-CoV-2, main protease, papain-like protease, drug discovery

A new coronavirus (SARS-CoV-2) has been identified as the etiologic agent for the COVID-19 outbreak. Currently, effective treatment options remain very limited for this disease; therefore, there is an urgent need to identify new anti-COVID-19 agents. The main protease (M^{pro}) and papain-like protease (PLpro) play pivotal roles in viral replication and transcription, making them attractive drug target for CoVs [1].

We initiated a program of combined structure-assisted drug design, virtual drug screening and high-throughput screening to identify new drug leads that target the SARS-CoV-2 M^{pro} [2, 3]. We assayed over 10,000 compounds including approved drugs, drug candidates in clinical trials, and other pharmacologically active compounds as inhibitors of M^{pro}. Six of these inhibit M^{pro} with IC_{50} values ranging from 0.67 to 21.4 μM. We determined the crystal structures of SARS-CoV-2 M^{pro} in complex with an antineoplastic drug carmofur [4] and a preclinical compound N3 (Fig. 1), respectively, to elucidate their inhibitory mechanisms. Both ebselen and disulfiram have been approved by FDA to enter phase II clinical trials. Additionally, we carried out drug screening against SARS-CoV-2 PLpro and identified that YM155, an anticancer drug candidate in clinical trials, has the most potent antiviral activity with an EC50 value of 170 nM [5]. We determined the crystal structures of PLpro and its complex with YM155, revealing a unique binding mode. YM155 simultaneously targets three "hot" spots on PLpro, including the substrate-binding pocket, the interferon stimulating gene product 15 (ISG15) binding site and zinc finger motif.

Our results demonstrate the efficacy of this screening strategy, which can lead to the rapid discovery of drug leads with clinical potential in response to new infectious diseases where no specific drugs or vaccines are available.

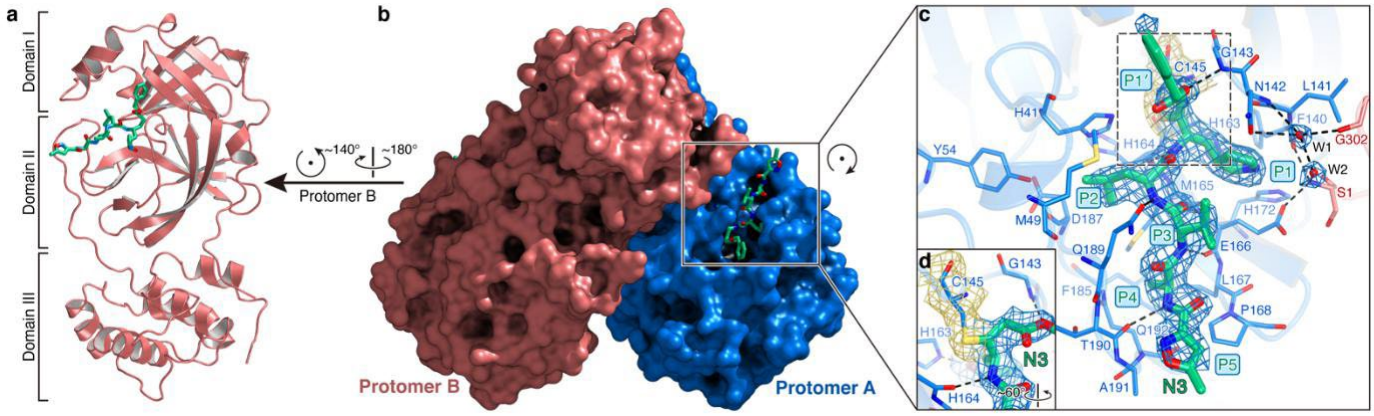

Figure 1. The architecture of functional dimer of M^{pro} with a Michael acceptor inhibitor N3 binding in its catalytic pocket.

1 Lu, L., Su, S., Yang, H., and Jiang, S. (2021). *Cell* **184**, 1604-1620.
2 Jin, Z., Du, X., Xu, Y., Deng, Y., Liu, M., Zhao, Y., Zhang, B., Li, X., Zhang, L., Peng, C., et al. (2020). *Nature* **582**, 289-293.
3 Dai, W., Zhang, B., Jiang, X.-M., Su, H., Li, J., Zhao, Y., Xie, X., Jin, Z., Peng, J., Liu, F., et al. (2020). *Science* **368**, 1331-1335.

4 Jin, Z., Zhao, Y., Sun, Y., Zhang, B., Wang, H., Wu, Y., Zhu, Y., Zhu, C., Hu, T., Du, X., et al. (2020). *Nature Structural & Molecular Biology* **27**, 529-532.
5 Zhao, Y., Du, X., Duan, Y., Pan, X., Sun, Y., You, T., Han, L., Jin, Z., Shang, W., Yu, J., et al. (2021). *Protein Cell* **12**, 877-888.

A007-06-230823

Structural studies of SARS-CoV-2 proteins and their complexes

Andrzej Joachimiak[1,2,3], Jerzy Osipiuk[1,2], Mateusz Wilamowski[1,3], Natalia Maltseva[1,2], Christine Tesar[1,2], Changsoo Chang[1,2], Michael Endres[1,2], Lucy Stols[1,2], Kemin Tan[1,2], Karolina Michalska[1,2] and Youngchang Kim[1,2]

[1]Center for Structural Genomics of Infectious Diseases, Consortium for Advanced Science and Engineering, University of Chicago, Chicago, IL 60667, USA, [2]Structural Biology Center, X-ray Science Division, Argonne National Laboratory, Argonne, IL 60439, USA, [3]Department of Biochemistry and Molecular Biology, University of Chicago, Chicago, IL, 60367, USA

The coronavirus SARS-CoV-2 is an agent causing COVID-19 disease and world-wide pandemic affecting hundreds of millions. Although this virus is similar to both, human and animal SARS- and MERS-CoVs, their infectivity and virulence are different and therefore the detailed information about SARS-CoV-2 proteins structures and functions is urgently needed to support development of effective therapeutics. We applied the high-throughput protein production and structure determination pipeline at the Center for Structural Biology of Infectious Diseases and Structural Biology Center to produce SARS-CoV-2 proteins and determine high resolution crystals structures. We focused on nonstructural proteins (Nsps) expressed as polyproteins 1a and 1ab that are processed and assemble into a large membrane-bound replicase-transcriptase complex and exhibit multiple enzymatic and binding activities. Thus far, we have determined 84 structures for 10 CoV-2 proteins and their complexes. These structures include Nsp3 ADP-ribose phosphatase domain (ADRP, also known as macrodomain) and PLpro papain-like protease, Nsp5 main protease Mpro, Nsp7/Nsp8 primase complex, Nsp9 RNA-binding protein, Nsp10/Nsp16 a 2'-O-ribose methyltransferase complex and Nsp15 a uridylate-specific endoribonuclease. We compare these structures with previously reported homologs from SARS and MERS coronaviruses and point to similarities and differences. We also determined structures of complexes with ligands and inhibitors, including FDA approved drugs. We deposit all structures to the Protein Data Bank and release the coordinates to scientific community prior publication. We also share all reagents and protocols. These structures provide a basis for structure-based drug development.

A027 Teaching Crystallographic Symmetry for Materials Science

Room 212/13

4.00pm - 6.30pm

A027-01-230823

Teaching symmetry: an overview of molecular structure across chemistry

Inbal Tuvi-Arad

Department of Natural Sciences, The Open University of Israel, Raanana, Israel

inbaltu@openu.ac.il

Keywords: Symmetry, Chirality, Educational Technology, Molecular Visualization, Structure

Symmetry is an eye-catching phenomenon that expresses the beauty and mystery of nature. In chemistry, it is a fundamental concept, frequently perceived as a driving force that controls the shape of molecular structure and directly influence their physical and chemical properties. Symmetry considerations influence the interaction of light and matter and can predict the course of chemical reactions. For students, visualization of symmetry at the molecular level can be an eye opening experience that promotes the development of visual-spatial abilities and high order thinking skills. In the undergraduate chemistry curriculum symmetry is discussed in various courses such as spectroscopy, quantum chemistry, inorganic chemistry and solid state. Dedicating a special course to symmetry is a less common approach. However, it encounters a unique opportunity for students to see the big picture and explore molecular structure across chemistry. Recently we developed such as course that discusses symmetry related topics from various fields including group theory, spectroscopy, stereochemistry, biochemistry and more. Advance educational technology was incorporated for interactive molecular visualization, working with open molecular databases and quantifying distortion levels of structures with near symmetry. In this talk, pedagogical considerations in determining the curriculum of this course will be discussed in details.

A027-02-230823

Animations, videos and 3D models for teaching space group symmetry

L. Bucio, R. Moreno-Tovar, E. Hernández-Juárez, S. Pérez-Arévalo

Laboratorio de Cristalofísica y Materiales Naturales, Instituto de Física, Universidad Nacional Autónoma de México. Circuito de la Investigación Científica s/n, Ciudad Universitaria, Coyoacán, 04510 Mexico City, Mexico

bucio@fisica.unam.mx

Keywords: Animations, Videos, 3D Models

In this contribution, we will present a series of animations, videos and three-dimensional models that were developed, filmed or built, in order to teach the symmetry properties of crystals. These resources have been designed for graduate students taking a basic crystallography course, coming from different chemistry, physics and engineering careers at the National Autonomous University of Mexico and some other universities in Mexico. In particular, the COVID-19 epidemic had the effect of accelerating the generation of the aforementioned didactic material. This has been of great benefit to both students and teaching activities at our university. An example of gif-like animation is illustrated in Fig. 1a. It illustrates the action of the Seitz operator on the asymmetric unit of the lupeol crystal structure. The animation appears frozen just at the moment when the Seitz operator $\{2|t_{10½}\}$ is applied to the asymmetric unit and, at the same time, the corresponding position, represented according to the conventions of the International Tables of Crystallography Vol. A [1], is simultaneously depicted. The way in which the Seitz operators are applied to fill the three-dimensional space reaches a macroscopic version that can be clearly attested by filmed videos of crystals growing. Fig. 1b shows a screenshot of our video of the growth of chromium alum crystals. The grown crystals represent a great opportunity to learn geometrical crystallography! (Fig. 1c). We have constructed three-dimensional models to illustrate the way in which space is filled by applying the Seitz operators to the asymmetric unit, according to certain types of very illustrative crystal structures. We have tried to show the role of the generators of the space group, and the other symmetry operations; as well as various curiosities about the forms of packing. Figs. 1d-1e are photos of three-dimensional models we constructed of the ice crystal structure.

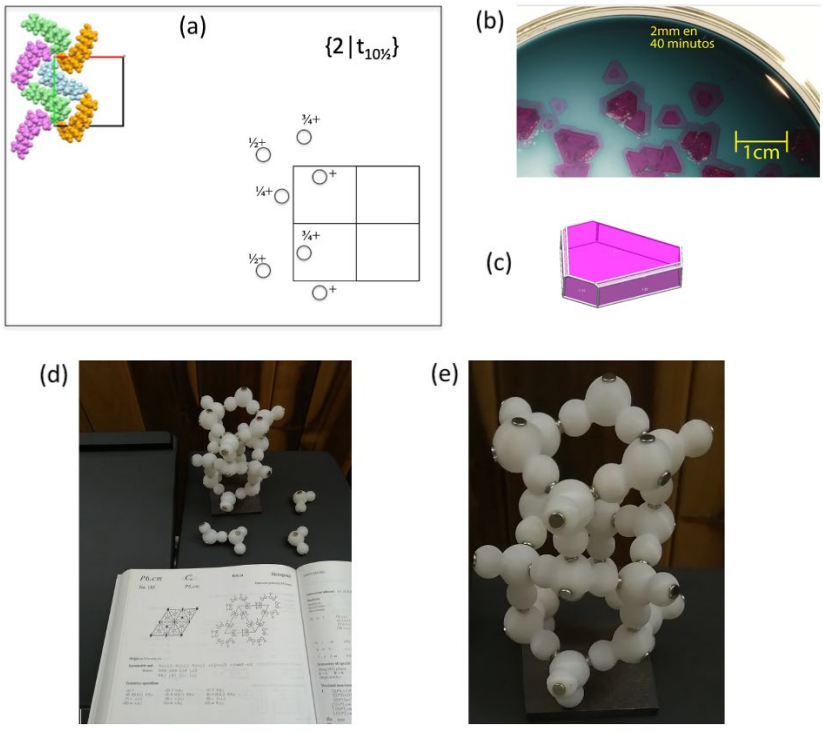

Figure 1. (a) Screenshoot of a gif animation; (b) Screenshot of a video of chromium alum crystals growing; (c) Geometrical representation of the external morphology of the chromium alum crystals; (d-e) 3D model for ice crystals.

[1] *International Tables for Crystallography*, Volume A, Space-group symmetry (2016). 6th edition. Edited by Mois I. Aroyo. Wiley. Pp. xxi + 873.

A027-03-230823

In situ 3DED in gas and liquid environments for following structural evolutions during reactions

D. Vandemeulebroucke1, Amirhossein Hajizadeh1, M. Batuk1, J. Hadermann1

EMAT, University of Antwerp, Groenenborgerlaan 171, B-2020 Belgium

Joke.hadermann@uantwerpen.be

Keywords: 3DED, in situ, redox

Many functional materials are applied in the form of nanosized particles. To follow their structural evolution during reactions, *in situ* X ray powder diffraction or *in situ* neutron powder diffraction can miss out on details due to this small particle size. In such cases, *in situ* 3DED (three dimensional electron diffraction) would allow to gather single crystal type information on the structural changes. However, currently there are still many open questions on how the results from *in situ* 3DED relate to *ex situ* results and results from bulk experiments. Using closed cell environmental holders (gas, liquid, electrochemistry), combined with heating and cooling holders, we have studied their structural evolutions during redox reactions during heating in O_2 and H_2 versus vacuum of a range of perovskite based materials and have systematically related the resulting reduced structures to those obtained by other techniques.

For $Sr_2Fe_2O_5$ (*Pcmb*), investigated for solid oxide fuel cells, chemical looping and heterogeneous catalysis, *in situ* XRD and *in situ* NPD in gas environments only observed transformations between brownmillerite and perovskite type (*Pm-3m*) structures, while *in situ* 3DED allowed to also observe an intermediate *Cmmm* phase known from *ex situ* and electrochemistry experiments before reaching the perovskite type phase. *In situ* 3DED also showed the manifestation of nanotwins upon oxidation. After reducing the oxidized phase again in hydrogen at 700°C, the ordering of the tetrahedral chains between planes was lost but the order within planes remained. Cooling instead the oxidized phase in oxygen resulted in an intergrowth of brownmillerite and perovskite. [1] The reduction of the Ruddlesden-Popper structure $La_{0.5}Sr_{1.5}MnO_4$, also a candidate for solid oxide fuel cell cathodes, resulted in the creation of a perovskite layer at the surface which was not noticed before in bulk in situ experiments involving redox reactions in gas. Parallel *ex situ* reductions showed also faint superstructure reflections in the 3DED datasets pointing towards a surface reconstruction with ordered oxygen vacancies, which could not be detected in the in situ 3DED experiments. Differences in surface layers are important as they are the most active parts in catalytic reactions. Sr_2MnO_4 could not be reduced using an *in situ* reaction with H_2 into the supercell with oxygen-vacancy order from literature, while this did succeed during parallel *ex situ* reduction experiments as well as during *in situ* heating in vacuum.

$CaMnO_3$, a material for chemical looping applications, was successfully reduced using *in situ* reduction both by heating in hydrogen gas as well as by heating in vacuum, achieving not only the well characterized $CaMnO_{2.5}$ phase, but also the intermediate $CaMnO_{2.75}$, which was thus far not solved and had contradicting models in literature. Using the results from the *in situ* 3DED experiments, the $CaMnO_{2.75}$ was solved in a *Pmmm* space group. These results were then compared to *in situ* 3DED results on the evolution of the Fe and Sr doped compounds which show better chemical looping properties.

In situ 3DED in gas environments has thus already given new, complementary information to what was observed with *in situ* XRD and *in situ* NPD for each perovskite based material we have studied so far. We therefore believe that in future studies *in situ* 3DED will unlock a vast amount of new information on functional materials in general.

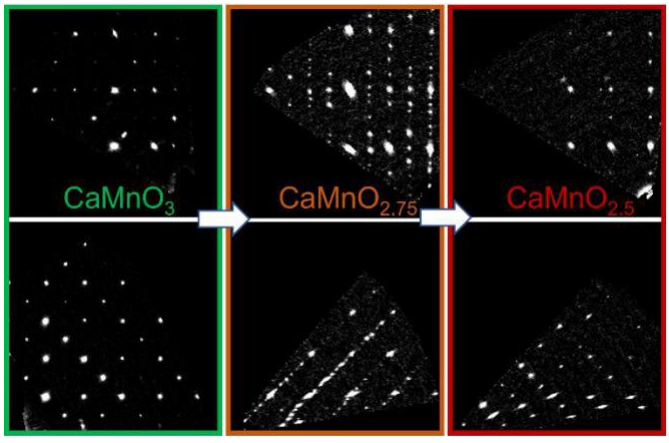

Figure 1. [110] (top) and [001] (bottom) sections (indexed in parent perovskite cell parameters) from in situ 3DED data sets taken during vacuum heating of $CaMnO_3$, from left to right, at room temperature, 350°C and 650°C.

[1] Maria Batuk et al., ChemRXiv, doi: 10.26434/chemrxiv-2022-gn3fm

Financial support is acknowledged from FWO I003218N, University of Antwerp BOF TOP 38689 and the European Commission NanED Grant number 956099.

A027-04-230823

Exploring and learning from symmetry in the CSD

I. Gimondi, S. C. Ward

The Cambridge Crystallographic Data Centre - Cambridge (United Kingdom)

igimondi@ccdc.cam.ac.uk

Keywords: Symmetry, CSD, Education

Symmetry is all around us: from flowers, snowflakes, honeycombs in the natural world to human-made tiles and buildings. Even though we are surrounded by many incredible examples, symmetry is a complex concept to teach and learn, especially as we delve into the realm of crystallography. This topic cannot be overlooked though: in crystallography symmetry operations are central in describing the arrangement of molecules in the structure, which in turn determines its properties. In this talk we will focus on how resources and materials from the Cambridge Crystallographic Data Centre (CCDC) can support how you can learn about symmetry using the Cambridge Structural Database (CSD) and the wider CSD Portfolio of software.

With over 1.2 million organic and metal-organic small molecule crystal structures, the CSD has a wealth of information on space groups and combinations of symmetry operations, that makes it a precious resource for teaching and learning about symmetry in chemistry and crystallography.

First, we will introduce the CSD Teaching Subset, a collection of over 750 structures selected by the CCDC in collaboration with educators in the community, that is free for download and use in education. In particular, we will focus on structures that have been selected to demonstrate and exemplify symmetry operations, both in molecules and in crystal structures.

As the topic of symmetry strongly benefits from the possibility to visualise symmetry elements and operations in three dimensions, we will next present Mercury, the CCDC's visualization software. The free version of Mercury enables educators and students to visualise molecules and crystal structures in 3D with features for analysis specifically dedicated to the study of symmetry. We will present these features and show how educators can learn more about using Mercury in education.

Alongside these resources and tools, the CCDC and our collaborators have curated materials in different formats designed to learn symmetry, including teaching modules and popular videos. The CCDC also provides a platform for educators from the community to share their resources and tools to each symmetry, which are shared in the Database of Educational Crystallographic Online Resources (DECOR), available on our website. We will select and highlight some of these resources.

A050 Complex Structures of Minerals and Inorganic Materials

Room 210/11

4.00pm - 6.30pm

A050-01-230823

Exploratory syntheses and crystal chemistry of new complex multinary chalcogenides

Jai Prakash

Department of Chemistry, Indian Institute of Technology Hyderabad, Sangareddy, Medak District, India

Email: jaiprakash@chy.iith.ac.in

Keywords: New structure types, Molten-flux method, Mixed atomic sites, Single crystal X-ray diffraction

The structural aspects of metal chalcogenides have been actively studied for a long time, mainly by solid-state chemists and mineralogists, owing to their rich crystal chemistry. In the last few decades, the study of structure-property relationships of these chalcogenides has become one of the thrust areas of research in the field of materials sciences. These chalcogenides are important for diverse technological applications such as thermoelectric materials, data storage, photovoltaics, magnetism, charge and spin density wave, superconductivity, etc. In recent years, complex metal chalcogenides, especially tellurides, have been explored for their promising thermoelectric properties. We have been actively working on the exploratory syntheses and characterization of new semiconducting mixed metal ternary and quaternary chalcogenides. Our efforts have led to the discovery of various multinary chalcogenides with unprecedented structure types in the last few years. The single crystals X-ray diffraction studies determined these phases' crystal structures at room temperature. The crystal structures of these compounds are anisotropic in nature (Fig. 1). The structural aspects of these new compounds, namely AkScMQ_3 (Ak = Sr and Ba; Q = S, Se, and Te) [1], $Ba_{2-\delta}Ln_{1-x}Mn_2Q_5$ (Ln = lanthanides) [2], $Ba_4Ge_2Sb_2Te_{10}$ [3], and Ba_4FeAgS_6 [4] will be presented in detail along with their relationship with other known structures of metal chalcogenides. The transition metals (or main group metalloids), lanthanides, and chalcogen atoms in these structures form anionic frameworks. The alkaline-earth metal cations mainly act as electron donors and are stuffed in the open spaces of these anionic frameworks. Optical absorption and temperature-dependent resistivity studies show that these compounds are narrow bandgap semiconductors, which could be promising for future thermoelectric (*TE*) applications. Understanding the structural relationship among these structure types is vital for discovering and designing new compounds with desired physical properties.

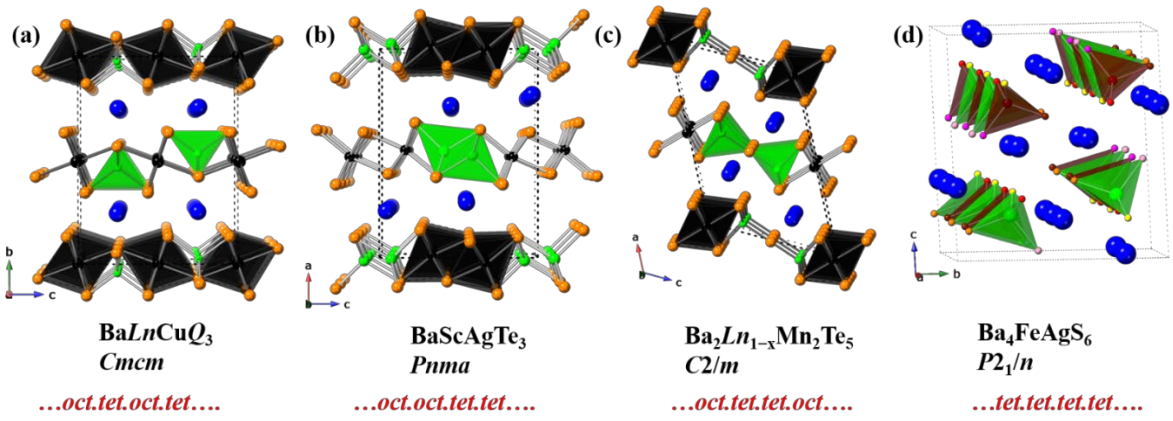

Figure 1. The unit cell structures of (a) BaLnCuQ_3, (b) BaScAgTe$_3$, (c) $Ba_2Ln_{1-x}Mn_2Te_5$, and (d) Ba_4FeAgS_6.

[1] Ishtiyak, M., Subhendu, J., Karthikeyan, R., Ramesh, M., Tripathy, B., Malladi, S. K., Niranjan, M. K. & Prakash, J. (2021). *Inorg. Chem. Front.,* **8**, 4086.
[2] Panigrahi, G., Subhendu, J., Ishtiyak, M., Narayanswamy, S., Bhattacharjee, P. P., Ramanujachary, K. V., Niranjan, M. K. & Prakash, J. (2021). *Dalton Trans.*, **50**, 6688.
[3] Subhendu, J., Panigrahi, G., Ishtiyak, M., Narayanswamy, S., Bhattacharjee, P. P., Niranjan, M. K. & Prakash, J. (2022). *Inorg. Chem.,* **61**, 968.
[4] Panigrahi, G., Jana, S., Yadav, S., Ramanujachary, K. V., Niranjan, M. K., & Prakash, J. (2022). *Dalton Trans.*, in print.

JP thanks DST-SERB, the Government of India (GOI) for the financial support (Grant numbers: CRG/2021/0003641 & ECR/2017/0822), and IIT Hyderabad for research facilities.

A050-02-230823

Unravelling the components of diffuse scattering using deep learning

Chloe A. Fuller[1] and Lucas S. P. Rudden[2]

[1]Swiss-Norwegian Beamlines, ESRF, Grenoble, France, [2]Institute of Bioengineering, EPFL, Lausanne, Switzerland chloe.fuller@esrf.fr

Keywords: Deep learning, Single crystal diffuse scattering, Local structure

To elucidate structure-property relationships in functional materials, it is crucial to understand both the average and the local structure, as many properties are underpinned by disorder and short-range structural correlations. Local structure information is contained within the diffuse scattering between the Bragg peaks and is typically very challenging to model. Recent advances have shown that factorising the diffuse scattering into its constituent parts (the squared difference in molecular form factor of the disordered part of the structure (MFF) multiplied by the short-range order (SRO), as in equation 1) can accelerate modelling and allow for the direct extraction of quantitative correlation parameters[1].

$$I(\vec{h}) = \Delta MFF \times SRO = |\langle F(\vec{h})\rangle - \langle F(\vec{h})\rangle|^2 \left(1 + \sum \cos(2\pi \vec{h}\vec{v})\right) \quad (1)$$

However, the factorisation is intractable to perform with numerical methods without any prior structural knowledge because a large proportion of the dataset may be 0 (or close to it). This can be compounded by incomplete data or experimental artefacts in the planes of interest. Machine learning, specifically deep learning, is ideally suited to such a task given its success and versatility when applied to analogous image processing applications[2]. Here we present an adapted pix2pix Generative Adversarial Network (GAN)[3] with self-attention (Fig. 1a), trained on a dataset of 140000 planes of simulated diffuse scattering from a diverse range of molecular fragment pairs, unit cells and short-range correlations. The network accurately reproduces the two components on 14000 unseen simulated examples (see Fig. 1b), even when data completeness is low, demonstrating the generalisability of the network.

This new approach could simplify the modelling of diffuse scattering in single crystals, without needing prior knowledge of the system, leading to improved structural understanding on significantly reduced timescale. Our method, to the best of our knowledge, provides the first application of deep learning methods to diffuse scattering modelling and lays the foundation towards separating other complex scattering components e.g. thermal and substitutional diffuse, or perhaps Bragg from diffuse scattering.

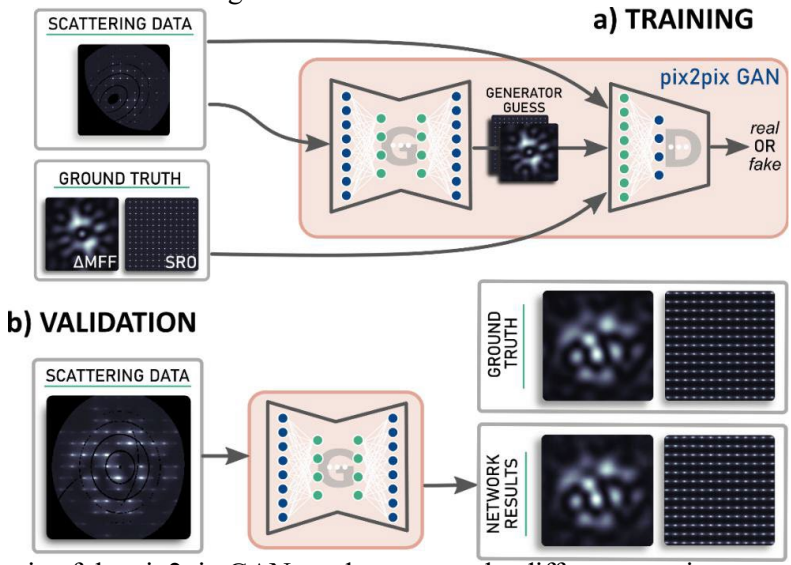

Figure 1. a) Schematic of the pix2pix GAN used to extract the diffuse scattering components and b) a representative example output generated from unseen simulated scattering data, compared to the ground truth.

1 E. Schmidt and R. Neder, *Acta Cryst.* (2017), **A73**, 231-237
2 K. Choudhary, B. DeCost, C. Chen, A. Jain, F. Tavazza, R. Cohn, C. Woo Park, *et. al., npj Comput. Mater.* (2022), **8**, 59.
3 P. Isola, J.-Y. Zhu, T. Zhou, A. A. Efros, *Computing Research Respository,* (2018)

A050-03-230823

In situ neutron low-temperature pair distribution function (PDF) analysis and molecular dynamics simulations of CH_4 and CO_2 hydrates

Bernadette R. Cladek[1]*, S. Michelle Everett[1], Marshall T. McDonnell[2], Matthew G. Tucker[1], David J. Keffer[3], Claudia J. Rawn[3]

Neutron Scattering Division, Oak Ridge National Laboratory[1], Oak Ridge, Tennessee, [2]Computer Science and Mathematics Division, Oak Ridge National Laboratory[2], Oak Ridge, Tennessee, Department of Materials Science and Engineering, University of Tennessee, Knoxville, Tennessee[3]

Keywords: Neutron scattering, molecular dynamics, gas hydrates

Natural gas hydrates (NGH) form on the ocean floor and in sub-surface permafrost deposits in high-pressure, low temperature environments. Research on these deposits is driven by their potential as an energy source. Naturally occurring CH4 hydrates primarily crystallize in the sI clathrate structure. The lattice is composed of hydrogen bonded water cages (the host), each of which occlude one gas molecule (the guest). Though the sI framework can host other molecules, this research focuses on CH4-CO2 hydrates to support current explorations in which CH4 may be harvested from hydrate deposits via exchange with CO2. CO2 replacement in the hydrate structure is energetically preferred, facilitating CO2 byproduct sequestration while providing CH4 as a fuel source. Equilibrium models predict that a mixed hydrate solid solution in which CO2 replaces some CH4 is stable at higher temperature and lower pressure compared to pure CH4 hydrate, and thermodynamic stability increases as the CO2 fraction increases. The impact of varying the type of guest molecules and mixed guest systems is a relevant topic to explore due to concerns about the stability of NGH under changing environmental conditions. A detailed understanding of the guest-host interactions in gas hydrates is necessary for the advancement of emerging technologies and processes which will utilize NGH deposits. The gas hydrate crystal has a high degree of disorder at all temperatures due to the motion of the occluded gas molecules and their interactions with the H2O lattice. Molecular dynamics (MD) simulations show that this disorder is not described by long-range crystallographic models. *In situ* neutron total scattering experiments and pair distribution function (PDF) analysis are used to characterize the short-range order in CH4-CO2 hydrates. Extraction of detailed information from PDF data of complex systems requires methods such as MD simulations combined with Reverse Monte Carlo (RMC) fitting. MD models of CH4-CO2 hydrates demonstrate the benefit of neutron PDF experiments by providing simulated PDFs, visualization of molecular motion, and analysis of thermodynamic interaction energies throughout the CH4-CO2 guest composition while providing large-box structural models for PDF data analysis. Variable temperature neutron PDF data of CH4, CO2, and mixed CH4-CO2 hydrate were collected on the NOMAD beamline at the Spallation Neutron Source (SNS), Oak Ridge National Laboratory. RMCProfile was used to fit the data to large-box models produced with MD simulations. PDF experiments performed *in situ* provide structural characterization, while the variable temperature measurements lead to inferred dynamics. This analysis shows that when CH4 and CO2 co-occupy the hydrate, the host is more strongly distorted than in either pure CH4 or pure CO2 hydrates, but this becomes less defined with increasing temperature. The presence of CO2 in mixed hydrate increases the stability range and creates a barrier for CH4 to completely leave the structure.

This research used resources at the Spallation Neutron Source (SNS), a US Department of Energy (DOE) Office of Science User Facility operated by Oak Ridge National Laboratory (ORNL). BRC has been partially supported by the Center for Materials Processing, a Tennessee Higher Education Commission (THEC) Center of Excellence located at the University of Tennessee, Knoxville, a University of Tennessee Chancellor's Fellowship, and the Office of Science Graduate Student Research (SCGSR) program. The SCGSR program is administered by the Oak Ridge Institute for Science and Education for DOE. Research at SNS was sponsored bythe DOE Office of Basic Energy Sciences. The ICE-MAN software suite used for this work was funded by the ORNL Laboratory Directed Research and Development program.

A050-04-230823

Ordering phenomena in rare-earth oxoborates $RCa_4O(BO_3)_3$ (R = Er, Y, Dy, Gd, Sm, Nd, La)

M. Münchhalfen, J. Schreuer

Ruhr-Universität Bochum, Institute for Geology, Mineralogy and Geophysics,

Universitätsstr. 150, Bochum, 44801, Germany

marie.muenchhalfen@rub.de

Keywords: Thermal expansion**,** non-convergent cation ordering, bond valence model, *RCOB*, Order/disorder effects

Monoclinic (space group *Cm*) rare-earth oxoborates $RX_2Z_2O(BO_3)_3$ have been studied for about 20 years because of their promising non-linear optical properties. More recently, these crystal species also gathered interest regarding their potential use for high-temperature piezoelectric sensing applications, since they combine a high melting point at around 1770 K with no reported phase transitions, high piezoelectric sensitivity and low electric resistivity [1]. Numerous cations can be substituted on the *R*-, *X*-and *Z*-site, which allows the electromechanical properties to be adjusted within certain limits. However, depending on composition and temperature more or less pronounced cation disorder has been observed.

To determine the cause of the disorder and its effect on the electromechanical behavior, the cation ordering in $RCa_4O(BO_3)_3$ crystals with R = Er, Y, Dy, Gd, Sm, Nd, La grown from melt using the Czochralski method was investigated on annealed and quenched samples. Additionally, the coefficients of thermal expansion, of piezoelectric stress tensor and the elastic stiffnesses were measured between 100 K and 1373 K using dilatometry and resonant ultrasound spectroscopy, respectively.

Reproducible anomalies in thermal expansion, characterized by an excess strain at high temperatures, occur at different temperatures depending on the type of the R_{3+} cation. Single- crystal diffraction experiments indicate that non-convergent cation ordering processes involving exchange of Ca_{2+} and R_{3+} on all independent cation positions play an essential role. The driving force of the ordering processes is a combination of the specific arrangement of the cation sites in parallel polyhedral chains along [001] and the size mismatch between the divalent cation (here Ca_{2+}) and the trivalent rare earth cation. Resulting internal stresses are minimized by the disorder. The onset temperatures of the anomalies in the thermal expansion are directly related to these processes [3].

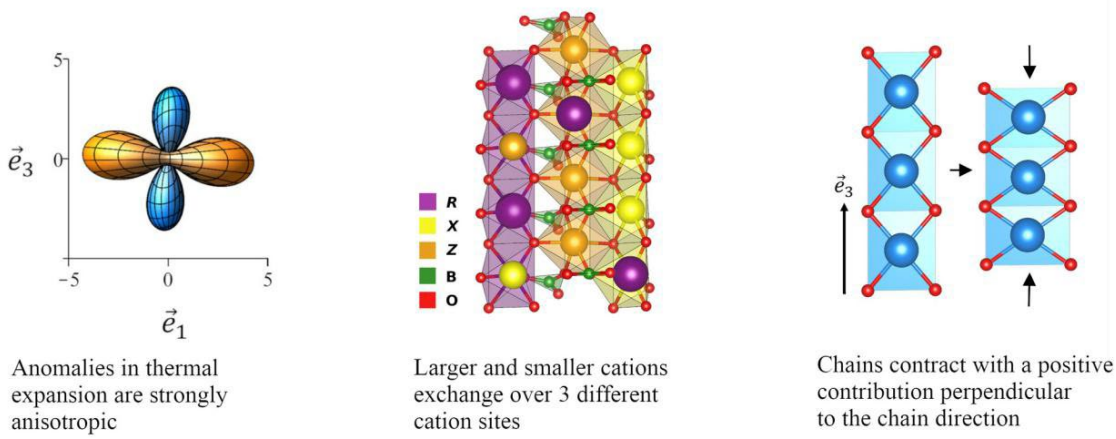

Figure 1. Correlation between anisotropy of thermal expansion (left), cation disorder (middle) and resulting relaxation along the polyhedral chains in the structure (right).

1 Yu, F., Hou, S., Zhao, X., Zhang, S. (2014) *IEEE Trans. Ultrason., Ferroelect., Freq. Control*, **61**, 8.
2 Zhang, S., Yu, F. (2011) *J. Am. Ceram. Soc.,* **94**, 3153-3170.
3 Münchhalfen, M., Schreuer, J., Reuther, C., Stöcker, H. (2022) *Materialia,* **26**, 2589-1529.

The authors gratefully acknowledge the financial support of the DFG for projects SCHR 761/4-1, GO 677/11-1 and ME 1433/14-1 within PAK 921.

A050-05-230823

Structure analysis of superionic thermoelectric Ag_8SnSe_6 with combining Bragg and Diffuse scattering

Seiya Takahashi1, Hidetaka Kasai1, Lei Miao2, Eiji Nishibori1

Department of Physics, Faculty of Pure and Applied Sciences, University of Tsukuba, School of Material Science and Engineering, Guilin University of Electronic Technology.

Email of communicating s2230061@s.tsukuba.ac.jp

Keywords: Diffuse Scattering, Superionic Conductor, Phonon-Liquid Electron-Crystal, Synchrotron Powder X-ray Diffractions

The concept of "Phonon-Liquid Electron-Crystal (PLEC)" has attracted attention as a design guideline for the high-performance thermoelectric materials [1]. Materials in this concept have a structure with crystalline part favourable for the high electrical conduction and the liquid-like part favourable for the low thermal conduction. Argyrodite compounds which is expressed by $A_{12-n}{}^{+}B^{n+}Q_6{}^{2-}$($A^+$= Li^+, Ag^+, Cu^+; Bn^+ = Ga^{3+}, Al^{3+}, Si^{4+}, Ge^{4+}, Sn^{4+}, P^{5+}, As^{5+}; Q^{2-} = S^{2-}, Se^{2-}, Te^{2-}) belong to PLEC. Ag is considered to behave like a liquid in the high-temperature phase [2].

The purpose of this study is to reveal the structure of Ag_8SnSe_6 which related to the low thermal conductivity. Synchrotron X-ray powder diffraction experiments with an Imaging plate (IP) as a detector were performed at BL02B2 SPring-8. A wide dynamic range of IP enables us to simultaneously measure both strong Bragg and weak diffuse scatterings in one dataset. Bragg and diffuse scatterings were analysed to reveal an accurate structure of Ag_8SnSe_6.

We found a profile of the diffuse scattering of Ag_8SnSe_6 changes with the phase transition. The change was reproduced to the multiple cycle of phase transitions. The profile of the diffuse scattering in the high-temperature phase was similar to the scattering from a liquid. Multiple anomalous diffraction data using 0.498 Å, 0.488 Å, and 0.487 Å wavelengths which were close to an absorption edge of Ag were measured to investigate the contribution of Ag atoms in the profile of the diffuse scattering. The diffuse scattering intensities proportionally changed over the entire diffraction angle by changing wavelength. The fact indicates that the diffuse scattering in the high-temperature phase is mainly from the scattering by the liquid-like Ag.

We also found that the diffuse scattering from the liquid-like Ag is not only in the high-temperature phase but also in the low-temperature phase. The existence of the liquid-like Ag in the low-temperature phase is inconsistent with the Ag-localized structural model of the previous studies [3]. The diffuse scattering intensities in the low temperature phase were increased with increasing temperature.

We constructed the structure model for the low temperature phase by the combination of the Ag-localized and the Ag-disordered structures for the Rietveld refinement. The reliability factors based on the weighted profiles *Rwp* improved from 1.83 % to 1.74 % by using the structure model with the Ag-disordered part. These facts confirm that the existence of the liquid-like Ag in the low temperature phase.

[1] Liu, H.; Shi, X.; Xu, F.; Zhang, L.; Zhang, W.; Chen, L.; Li, Q.; Uher, C.; Day, T.; Snyder, G. J., *Nat. Mater*., 2012, 11, 422.

[2] Yang, C.; Luo, Y., Li X., Cui J., *RSC Adv*., **2021**, 11, 3732-3739.

[3] Gulay, L. D.; Olekseyuk, I. D.; Parasyuk, O. V., *J. Alloys Compd*., **2002**, 339, 113.

Dr. Kawaguchi Shogo and Dr. Kobayashi Shintaro, Beam Line Scientists at BL02B2, provided generous support for remote synchrotron radiation experiments. This work was supported by JSPS KAKENHI (Grants No. JP19KK0132, JP20H04656 and JP21H05235). The synchrotron experiments were performed at SPring-8 BL02B2 with the approval of the Japan Synchrotron Radiation Research Institute (JASRI) (Proposal No. 2021A0068, 2021B1630 and 2021B1775).

A050-06-230823

Incommensurate local structural modulations in the uranium oxide system α-U_3O_8 studied at the diffuse x-ray scattering station ID28-II - ESRF

D. A. Chaney[1], A. Bosak[1], E. Lawrence Bright[1], L. Harding[2], R. Springell[2], G. H. Lander[3]

[1]European Synchrotron Radiation Facility, Grenoble, France, [2]University of Bristol, Bristol, UK, [3]Institute for Transuranium Elements, Joint Research Centre, Karlsruhe, Germany

daniel.chaney@esrf.fr

Keywords: Diffuse x-ray scattering, Local structural modulation, Synchrotron Source

Started in 2015 and now largely complete the 150M€ extremely brilliant source upgrade has elevated the European Synchrotron to the most brilliant synchrotron source in the world. At the ID28 beamline we operate two separate instruments: a meV resolution inelastic x-ray scattering (IXS) spectrometer [1] and more recently also a diffuse x-ray scattering diffractometer [2] designed to go beyond the limits of classical crystallography and study the extremely low intensity diffuse signal which exists in between the Bragg peaks and is characteristic of correlated deviations away from perfect periodicity. The diffuse scattering instrument has been designed to deliver maximum flux ($\sim 10^{12}$ ph/s) with minimal background to routinely capture low intensity diffuse signal and allow large regions of reciprocal space to be explored for almost all sample types and environmental conditions. Further, the beamline is optimized for small samples, $0.1 - 10^{-6}$ mm^3, and is ideally suited to experiments normally impossible to perform at neutron sources. Providing single crystals can be obtained diffuse scattering studies maintain a number of distinct advantages over total scattering techniques due to the preservation of $\boldsymbol{q}$-dependant information. The diffuse and Bragg signals are well separated in reciprocal space so can be treated independently and information on dimensionality, directionality and lengthscale of correlations is directly accessible. The formation of long-range structural modulations such as charge density wave states can also be studied and coupled use of the IXS instrument allows energy resolved studies to directly investigate the dynamic or static origin of any diffuse signal.

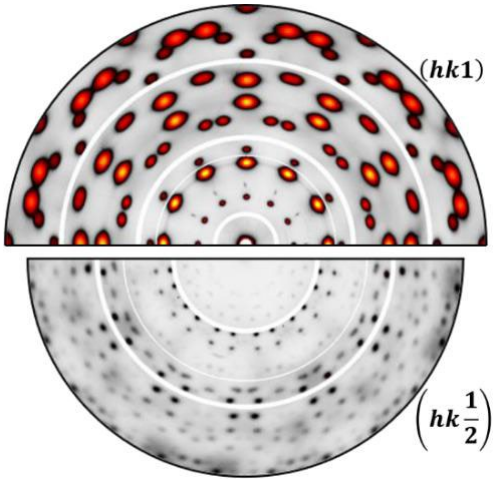

Figure 1. Reconstructed reciprocal space planes (a) the (h 1) "Bragg" plane and (b) the (h $^1/_2$) "diffuse" plane containing the diffuse satellite reflections corresponding to a doubled ***c*** parameter with further modulations of ***a*** and ***b***.

The capabilities of the beamline as well as the complementary nature of the two techniques will be highlighted via a recent study of the uranium oxide system α-U3O8. It is well known that below approximately 573 K α-U3O8 exhibits an orthorhombic structure (C2mm) with two distinct uranium sites. Both absorption spectroscopy [3] and x-ray photoemission spectroscopy [4] studies agree that the uranium valence is U(VI) for the U1 site, i.e. 5*f*0, and U(V), i.e. 5*f*1 for the U2 site. However, the system transitions to a pseudohexagonal structure (P-62m) above this temperature losing its distinct uranium sites. This creates a contradiction between structural and charge order in system for which two possible solutions have been proposed, either the presence of a local superstructure or rapid valance fluctuations [5]. Through extensive grazing incidence diffuse x-ray scattering studies on an 80 nm epitaxial thin film we provide conclusive evidence for the former. As shown in Fig. 1 we have discovered a complex pattern of diffuse superstructure reflections that lie in the (h ^{1}2) plane and indisputably indicate incommensurate local structural modulations are present at room temperature. The diffuse reflections persist almost unchanged through the transition thus alleviating the apparent contradiction between local structural and charge order previously identified.

1 Krisch, M. & Sette, F. (2017). *Crystallography Reports* **62**, 1-12.

2 Girard, A., Nguyen-Thanh, T., Souliou, S. M., Stekiel, M., Morgenroth, W., Paolasini, L., Minelli, A., Gambetti, D., Winklera, B. & Bosak, A. (2019). *Journal of Synchrotron Radiation* **26**, 272-279.

3 Kvashnina, K. O., Butorin, S. M., Martin, P. & Glatzel, P. (2013). *Phys. Rev. Lett.* **111**, 253002.

4 Enriquez, E., Wang, G., Sharma, Y., Sarpkaya, I., Wang, Q., Chen, D., Winner, N., Guo, X., Dunwoody, J., White, J., Nelson, A., Xu, H., Dowden, P., Batista, E., Htoon, H., Yang, P., Jia, Q., & Chen, A. (2020). *ACS Appl. Mater. Interfaces* **12**, 35232.

5 Miskowiec, A., Spano, T., Hunt, R., Shields, A. E., Niedziela, J. L. & Finkeldei, S. (2020). *Phys. Rev. Materials* **4**, 093610.

A062 Geometrically-frustrated Magnetism
Room 220
4.00pm - 6.30pm

A062-03-230823

Understanding Spin Textures in Frustrated Magnets

J. A. M. Paddison[1], H. Zhang[2], B. Rai[3], J. Yan[1], A. F. May[1], M. B. Stone[1], S. Calder[1], M. D. Frontzek[1], D. A. Dahlbom[2], K. M. Barros[4], S. Do[1], S. Gao[1], M. J. Cliffe[5], C. Batista[2], A. D. Christianson[1]

[1]Oak Ridge National Laboratory, Oak Ridge, TN 37830, USA, [2]University of Tennessee, Knoxville, TN 37996, USA, [3]Savannah River National Laboratory, Aiken, SC 29808, USA, [4]Los Alamos National Laboratory, Los Alamos, NM 87545, USA, [5]University of Nottingham, Nottingham NG7 2RD, United Kingdom

paddisonja@ornl.gov

Keywords: Frustrated magnetism, topological magnetism, neutron scattering

Magnetic frustration can suppress conventional magnetic ordering and stabilize unconventional magnetic states. These states can include spin liquids, in which conventional long-range magnetic order is absent. Alternatively, frustration may promote complex long-range magnetic order with novel properties. For example, materials with noncoplanar magnetic structures can show unusual physical properties driven by their nontrivial topology [1].

Both spin liquids and complex magnetic orders present exciting challenges for crystallographic analysis. On the one hand, the absence of magnetic Bragg scattering in spin liquids means that analysis of diffuse magnetic scattering is crucial. On the other hand, Bragg intensities alone may contain insufficient information to solve non-coplanar magnetic states. In particular, such states are often multi-wavevector (multi-**q**) structures, which are challenging to solve because their magnetic Bragg diffraction patterns are usually identical to single-**q** structures in the presence of domain or powder averaging [2].

In this talk, I will discuss how information obtained from diffuse, inelastic, and Bragg scattering can be combined to determine spin textures in frustrated magnets, and to identify the magnetic interactions that stabilize these states. I will focus on two classes of frustrated magnetic materials. First, I show that the insulating double perovskites Ba_2YRuO_6 and Ba_2LuRuO_6 [3,4] host a non-coplanar triple-**q** structure on the face-centred cubic lattice. Our study employs inelastic neutron-scattering experiments to measure the spin-wave excitations in powder samples of these materials. By refining the magnetic structure and magnetic interactions simultaneously against our inelastic neutron-scattering data, we show that a triple-**q** structure yields the best agreement with experiment, and this state is stabilized by non-Heisenberg interactions in the Hamiltonian, namely biquadratic interactions [5]. Second, I discuss the intermetallic Gd_2PdSi_3, in which Gd^{3+} ions occupy a triangular lattice. This centrosymmetric material hosts a multi-**q** skyrmion spin texture under small applied magnetic fields [6]. I show how the magnetic diffuse scattering measured above its magnetic ordering temperature can identify the magnetic interactions that stabilize the skyrmion phase, establishing a space of magnetic interactions that can promote skyrmion formation [7].

I conclude by discussing the outlook for refinement of magnetic models in interaction space, and introduce a computer program that can be used to refine interaction models against magnetic diffuse scattering data [8].

[1] Tokura, Y., Kanazawa, N., (2021). *Chem. Rev.* **121**, 2857.
[2] Kouvel, J., Kasper, J., (1963). *J. Phys. Chem. Solids* **54**, 529.
[3] Battle, P., Jones, C., (1989). *J. Solid State Chem.* **78**, 108.
[4] Nilsen, G. J., Thompson, C. M., Ehlers, G., Marjerrison, C. A., Greedan, J. E. (2015). *Phys. Rev. B.* **91**, 054415.
[5] Paddison, J. A. M., Zhang, H., Yan, J., Cliffe, M. J., Do, S., Gao, S., Stone, M. B., Dahlbom, D., Barros, K., Batista, C. D., Christianson, A. D.. *arXiv 2301.11395* (2023).
[6] Kurumaji, T., Nakajima, T., Hirschberger, M., Kikkawa, A., Yamasaki, Y., Saayama, H., Nakao, H., Taguchi, Y., Arima, T., Tokura, Y., *Science* **365,** 914 (2019).
[7] Paddison, J. A. M., Rai, B. K., May, A. F., Calder, S., Stone, M. B., Frontzek, M. D., Christianson, A. D., *Phys. Rev. Lett.* **129**, 137202 (2022).
[8] Paddison, J. A. M., *arXiv 2210.09016* (2022).

This work was supported by the U.S. Department of Energy, Office of Science, Basic Energy Sciences, Materials Sciences and Engineering Division. It used resources at the Spallation Neutron Source, a DOE Office of Science User Facility operated by the Oak Ridge National Laboratory.

A062-04-230823

Structural, magnetic, and spectroscopic studies of the frustrated S = 1 kagome magnet $ND_4Ni_{2.5}V_2O_7(OD)_2.D_2O$

Eamonn T. Connolly[1], Jean-Chistophe Orain [2], Madeleine Georgopoulou[3,6], David Boldrin[4], Jacques Ollivier[3], Simutis Gediminas[2], Fabrice Bert[5], Björn Fåk[3], Andrew S. Wills

[1] *Physical Sciences, Diamond Light Source, Didcot, United Kingdom*

[2] *Paul Scherrer Institute, Villigen, Switzerland*

[3] *Spectroscopy Group, Institut Laue-Langevin, Grenoble, France*

[4] *Physics Department, University of Glasgow, Glasgow, United Kingdom*

[5] *Physique des Solides, Université Paris-Saclay, Paris, France*

[6] *Chemistry Department, University College London, London, United Kingdom*

eamonn.connolly@diamond.ac.uk

Keywords: frustrated magnetism, kagome, neutron spectroscopy, powder diffraction

Isometric 2-dimensional kagome antiferromagnets (KAFM) are probably the best candidate materials for studies of exotic ground states because conventional magnetic order is suppressed through the maximal geometric frustration of the lattice. For small-spin kagome magnets, quantum fluctuations couple with this frustration to form exotic electronic states, such as the quantum spin-liquid state observed in S = 1/2 KAFM material herbertsmithite ($ZnCu_3(OH)_6Cl_2$) [1]. Less well studied are the S = 1 KAFM systems, where the role played by the bosonic nature of the spin is debated and a range of unconventional ground states are predicted, from spin nematic phases to the valence bond solid [2, 3].

The novel material $ND_4Ni_{2.5}V_2O_7(OD)_2.D_2O$ was synthesised to further explore and characterise the ground state of the S = 1 KAFM systems. $ND_4Ni_{2.5}V_2O_7(OD)_2.D_2O$ is a model S = 1 KAFM due to its highly 2-dimensional isometric kagome lattice of S = 1 Ni^{2+} ions (Figure 1a) [4]. Geometric frustration in this system is observed through the antiferromagnetic mean field (θ_W = -32 K) and absence of magnetic order down to T = 280 mK in muSR analysis. Diffuse magnetic scattering is observed through inelastic neutron scattering (INS) and provides insight into the nature of the disordered ground state (Figure 1b). Moreover, the build-up of strong magnetic corelations is observed in bulk magnetometry data which coincides with the formation of super structure peaks in low-temperature synchrotron powder X-ray diffraction (SPXD) studies. These combined studies provide insight into the nature of the ground state corelations in $ND_4Ni_{2.5}V_2O_7(OD)_2.D_2O$ which enrich understanding of the S = 1 phase space and the role of bosonic spins in frustrated kagome magnets.

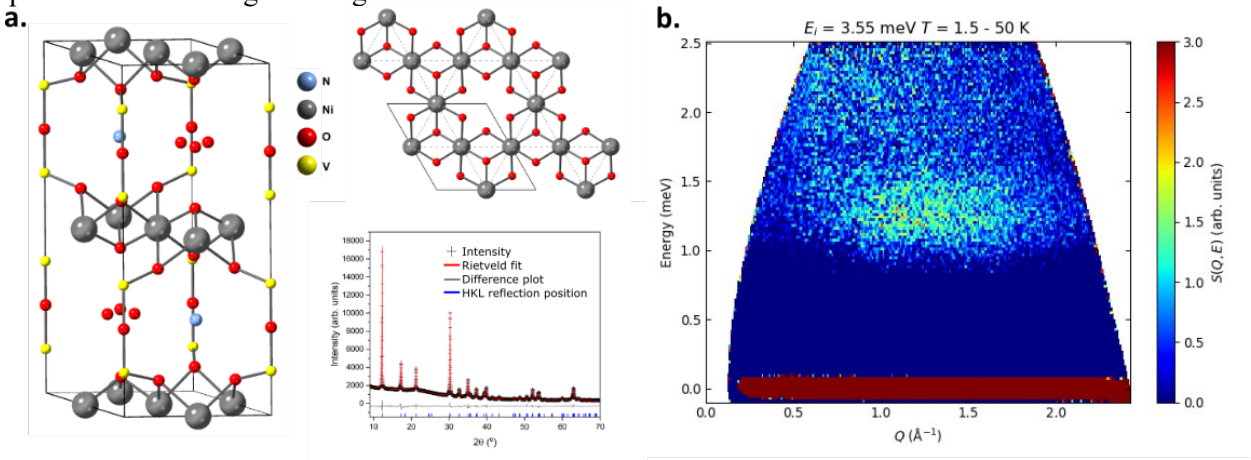

Figure 1: a. Crystal structure and kagome lattice of $ND_4Ni_{2.5}V_2O_7(OD)_2.D_2O$ refined from SPXD data **b. L**ow-energy diffuse magnetic excitation from disordered ground state of $ND_4Ni_{2.5}V_2O_7(OD)_2.D_2O$ in the INS spectrum

[1] Han, T. H., Helton, J. S., Chu, S., Nocera, D. G., Rodriguez-Rivera, J. A., Broholm, C. & Lee, Y. S. (2012). *Nature*, **492**, 406.
[2] Xu, C. & Moore, J. E. (2007). *Phys. Rev. B,* **76**, 104427.
[3] Changlani, H. J. & Läuchli, A. M. (2015). *Phys. Rev. B*, **91**, 100407.
[4] Connolly, E., Reeves, P., Boldrin, D. & Wills, A. S. (2018). *J. Phys.: Condens. Matter*, **30**, 025801.

A062-05-230823

Structure and magnetism of doped-$SrCu_2(BO_3)_2$

M. Dragomir[1,2], L. Šibav[1,2], G. King[3], Z. Jagličić[4,5], D. Arčon[1,6]

[1]Jožef Stefan Institute, Jamova cesta 39, 1000 Ljubljana Slovenia, [2] Jožef Stefan International Postgraduate School, Jamova cesta 39, 1000 Ljubljana, Slovenia, [3]Canadian Light Source, 44 Innovation Blvd, Saskatoon, SK S7N 2V3, Canada, [4]Institute of Mathematics, Physics and Mechanics, Jadranska cesta 19, 1000 Ljubljana, Slovenia, [5]Faculty of Civil and Geodetical Engineering, University of Ljubljana, Jamova cesta 2, 1000 Ljubljana, Slovenia, [6]Faculty of Mathematics and Physics, University of Ljubljana, Jadranska ulica 19, 1000, Slovenia

mirela.dragomir@ijs.si

Keywords: frustrated magnetism, crystal growth, doped- $SrCu_2(BO_3)_2$

The geometrically frustrated $SrCu_2(BO_3)_2$ is the experimental realization of the Shastry-Sutherland model with interesting magnetic plateaux and dynamic properties [1, 2]. $SrCu_2(BO_3)_2$ crystallises in the tetragonal $I\bar{4}2m$ space group, where magnetic $Cu_2(BO_3)_2^{2-}$ layers alternate with nonmagnetic Sr^{2+} ions along the crystallographic *c*-axis [3]. The $S = 1/2$ of Cu^{2+} ions form orthogonal dimers in a 2D network of interacting spins - Figure 1. This arrangement leads to spin frustration and very localised magnon excitations with a spin gap of 34 K. Consequently, $SrCu_2(BO_3)_2$ exhibits rich physics under applied magnetic field and/or pressure [4]

A strong interplay between the crystal structure and magnetic properties is also expected, as unique ground states such as quantum spin liquid states or superconductivity are predicted when the system is doped. However, the chemical doping of SCBO has not been sufficiently explored [5].

In this contribution, the effects of both A- and B- doping on the structural and magnetic properties of SrCu2(BO3)2 will be presented [6]. Various A-site and B-site doped SrCu2(BO3)2 samples were synthesised in polycrystalline form by the solid-state method, while single crystals of selected compositions were grown by a newly developed flux method - Figure 1. A combination of techniques including synchrotron powder diffraction, magnetic susceptibility, electron paramagnetic resonance, and differential scanning calorimetry were employed to investigate the changes in the structural and magnetic properties as a function of doping type and concentration. Moreover, some of these properties were also investigated under GPa pressure in diamond anvil cells.

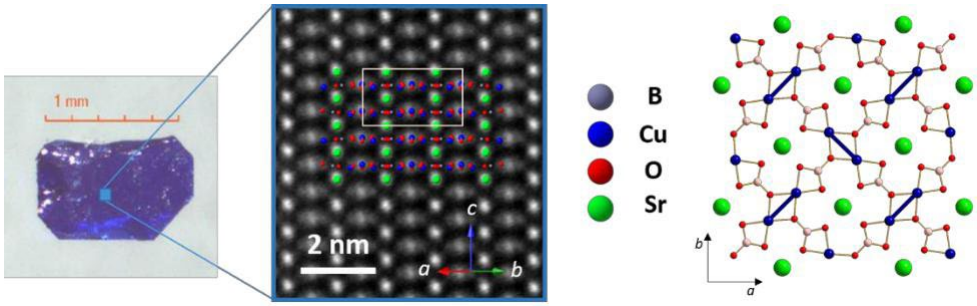

Figure 1. Optical micrograph of undoped, plate -like $SrCu_2(BO_3)_2$ single crystal (left) alongside with the atomic resolution image of the crystal viewed along [110] (center). The $S = 1/2$ Cu^{2+} ions form orthogonal spin dimers within 2D planes (right).

1 Shastry, B. S., Kumar, B. (2002). *Prog. Theor. Phys.*, **145**, 1.
2 Nojiri, H., Kageyama, H., Onizuka, K., Ueda Y & Motokawa, M. (1999). *J. Phys. Soc. Jpn.*, **68**, 2906.
3 Smith, R.W. & Keszler, D. A. (1991). *J. Solid State Chem.*, **93**, 430.
4 Haravifard, S., Graf, D., Feiguin A. E. *et al.* (2016). *Nat. Commun.*, **7,** 11956.
5 Shi, Z., Steinhardt, W., Graf, D. *et al.* (2019). *Nat. Commun.*, **10**, 2439.
6 Dragomir, M. *et al* (2022). *Manuscript in preparation*.

The authors would like to acknowledge dr. Mojca Otoničar for the TEM image.

A062-06-230823

Geometrical frustration in natural minerals linarite and atacamite

K.C. Rule[1]

1 Australian Nuclear Science and Technology Organisation, Lucas Heights NSW 2234 Australia.

Email of communicating: kirrily@ansto.gov.au

Keywords: Frustrated quantum magnets, Inelastic neutron scattering, Exotic phase diagrams

Geometric frustration pertains to a degenerate magnetic ground state that evolves in a system with competing magnetic interactions. Often described in terms of Ising spins on a triangular lattice with antiferromagnetic nearest neighbour interactions, it is clear that the geometrical constraints inhibit simple, long-range-ordered spin configurations to form due to magnetic frustration. In fact, due to imposed magnetic conditions including anisotropy, geometrically frustrated magnets cannot simultaneously satisfy nearest neighbour interactions. Interest in frustrated lattices has burgeoned over recent years due to the exotic magnetic phases that these systems can host – from spin-liquid, spin-nematic and spin-ice phases, to monopole physics, to "order-by-disorder" and multipolar phases.

However, geometric frustration doesn't only exist on triangular-based lattices – but can also exist on square lattices and even in 1D spin-chains where next nearest neighbour interactions play a significant role. In this talk I will discuss recent dynamic neutron scattering results from two highly frustrated natural minerals, linarite [1, 2] and atacamite [3], detailing how quantum effects, coupled with competing magnetic interactions can lead to rich and exotic phase diagrams.

1 K.C. Rule et al., Physical Review B 95, 024430 (2017)
2 L. Heinze et al., Physical Review B 106, 144409 (2022).
3 L. Heinze et al., Physical Review Letters 126, 207201 (2021)

A090 Biomolecular SAS and Integrative methods: Standards and Validation
Room 208
4.00pm - 6.30pm

A090-01-230823

Structural plasticity of the coiled-coil interactions in SFPQ

Heidar J. Koning[1], Jia Y. Lai[1], Andrew C. Marshall[1], Gavin J. Knott[3,4], Timothy M. Ryan[5], Archa H. Fox[7], Andrew Whitten [6], Mihwa Lee * [2], Charles S. Bond* [1]

[1] School of Molecular Sciences, University of Western Australia, 35 Stirling Highway, Crawley, Western Australia 6009, Australia [2] Department of Biochemistry and Genetics, La Trobe Institute for Molecular Science, La Trobe University, Melbourne, Victoria 3086, Australia [3]Department of Molecular and Cell Biology, University of California, Berkeley, CA 94720, USA. [4]Monash Biomedicine Discovery Institute, Department of Biochemistry & Molecular Biology, Monash University, Victoria 3800, Australia.[5] Australian Synchrotron, 800 Blackburn Road, Clayton, VIC 3168, Australia [6] ANSTO New Illawarra Rd, Lucas Heights NSW 2234 [7] School of Human Sciences, University of Western Australia, Crawley, Western Australia, 6009. To whom correspondence should be addressed. Tel: +61 8 64884406; Fax: +61 8 64887330; Email: Charles.Bond@uwa.edu.au

Keywords: paraspeckles, coiled coils

The proteins SFPQ (splicing Factor Proline/Glutamine rich) and NONO (Non-POU domain-containing octamer-binding protein), are mammalian members of the Drosophila Behaviour/Human Splicing (*DBHS*) protein family, which share 76% sequence identity in their conserved 320 amino acid DBHS domain [1, 2]. SFPQ and NONO are involved in all steps of post-transcriptional regulation [1] and are primarily located in *paraspeckles* in mammals: liquid phase-separated, ribonucleoprotein sub-nuclear bodies templated by NEAT1 long non-coding RNA [3]. A combination of structure and low-complexity regions provide polyvalent interaction interfaces which facilitate homo- and heterodimerisation, polymerisation, interaction with oligonucleotide, mRNA, long non-coding RNA, and liquid phase-separation. The strength and competition of these interaction modes defines their ability to dissociate from paraspeckles to fulfil functional roles throughout the nucleus or the cytoplasm. The imbalanced nucleocytoplasmic distribution of SFPQ has been shown to be an important factor in the neurodegenerative diseases ALS, FTLD and AD likely due to the disruption of the protein's essential nuclear functions [4,5]. We have defined and dissected the coiled-coil interactions which promote the polymerisation of DBHS proteins, via a crystal structure of an SFPQ/NONO heterodimer which reveals a flexible coiled-coil interaction interface which differs from previous studies [2]. We support this through extensive solution small-angle X-ray scattering experiments using a panel of SFPQ/NONO heterodimer variants which are capable of tetramerising to varying extents, ranging from null (quadruple coiled-coil mutant), through equilibrium (truncated proteins), to constitutive tetramerization (using an R542C mutation which mimics the pathological drosophila nonAdiss allele [6]). We demonstrate that coiled-coil interactions in addition to the previously-described canonical coiled-coil interface also play a role in determining the affinity for DBHS proteins which each other. The detail of these interactions and their relative strengths may be of significance to DBHS target recognition and protein oligomerisation *in vivo*, and ultimately disease pathology.

[1] Knott, G. J., Bond, C. S. & Fox, A. H. The DBHS proteins SFPQ, NONO and PSPC1: a multipurpose molecular scaffold. *Nucleic Acids Res* **44**, 3989–4004 (2016).

[2] Lee, M. *et al.* The structure of human SFPQ reveals a coiled-coil mediated polymer essential for functional aggregation in gene regulation. *Nucleic Acids Res* **43**, 3826–3840 (2015).

[3] Fox, A. H., Nakagawa, S., Hirose, T. & Bond, C. S. Paraspeckles: Where Long Noncoding RNA Meets Phase Separation. *Trends in Biochemical Sciences* **43**, 124–135 (2018).

[4] Huang, J. *et al.* Structural basis of the zinc-induced cytoplasmic aggregation of the RNA-binding protein SFPQ. *Nucleic Acids Res* **48**, 3356–3365 (2020).

[5] Lim, Y. W., James, D., Huang, J. & Lee, M. The Emerging Role of the RNA-Binding Protein SFPQ in Neuronal Function and Neurodegeneration. *Int J Mol Sci* **21**, 7151 (2020).

[6] Rendahl, K. G., Gaukhshteyn, N., Wheeler, D. A., Fry, T. A. & Hall, J. C. Defects in courtship and vision caused by amino acid substitutions in a putative RNA-binding protein encoded by the no-on-transient A (nonA) gene of Drosophila. *J Neurosci* **16**, 1511–1522 (1996)

A090-02-230823

New small angle scattering reference standard and application to biosaxs

R. Joseph Kline, Angela Folz, William Guthrie, and Andras Vladar

National Institute of Standards and Technology, Gaithersburg, MD, USA

joe.kline@nist.gov

Keywords: small angle X-ray scattering, calibration, reference standard

The National Institute of Standards and Technology (NIST) has developed a new standard reference material (SRM 3605) for use as a calibration standard for small angle X-ray scattering (SAXS). The standard is 100 nm pitch line grating superimposed on a 1 µm two-dimensional grid. The standard has 100 nm tall tungsten lines on a free-standing silicon nitride membrane. The silicon nitride minimizes sample absorption for SAXS and allows the standard to be used for energies from 200 eV to over 30 keV. The tungsten-air scattering contrast is quite large and produces very strong scattering. Over 12 orders of diffraction are observable in 60 s on the NIST laboratory SAXS system. Figure 1 shows the structure and an example scattering pattern from a synchrotron SAXS beamline. We have fabricated a wafer full of the reference samples and are currently finalizing the certification. The uncertainty goal for the ≈100 nm pitch is ±0.05 nm. We plan to have the SRM ready for shipping this summer.

We will report on comparison studies between different beamlines and laboratory instruments with a focus on application to biosaxs measurements.

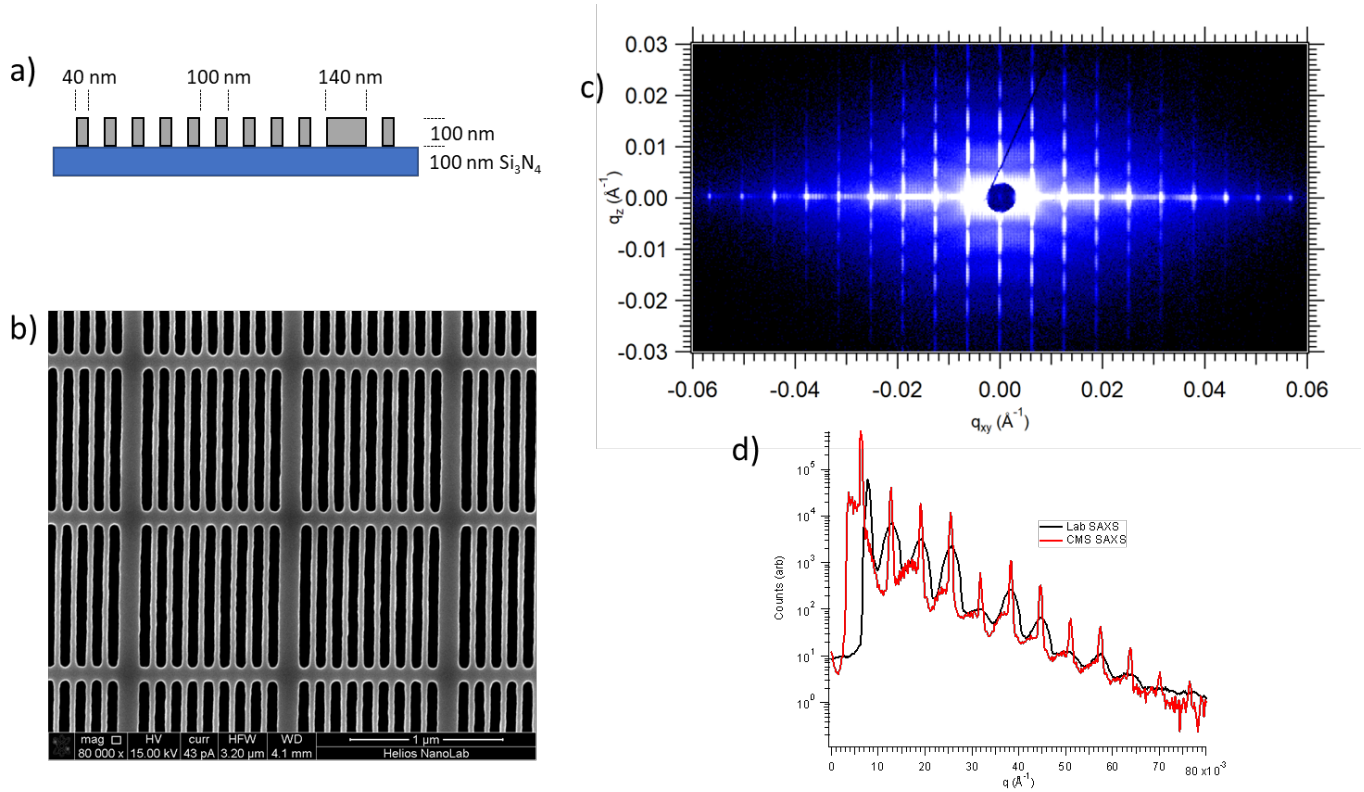

Figure 1. a) Schematic of SRM 3605, b) scanning electron microscope image of structure, c) synchrotron SAXS image of SRM 3605 prototype, d) comparison one-dimensional line cuts from synchrotron and lab SAXS systems.

We thank Ruipeng Li for providing synchrotron measurements on prototype test structures.

A090-03-230823

Biomolecular small-angle scattering: data reproducibility, benchmarking predictive methods, and best practice reporting

Jill Trewhella

School of Life & Environmental Sciences, U. Sydney, NSW, 2006, Australia, and Dept. of Chemistry, U. Utah, UT 84112, U.S.A.

jill.trewhella@sydney.edu.au

Keywords: small angle scattering, SAXS, SANS, structural biology

In 2019, a round robin study was initiated aimed at providing a quantitative assessment of the reproducibility of biomolecular SAS data and consensus profiles. Five proteins (RNaseA, lysozyme, xylanase, urate oxidase and xylose isomerase) were measured on twelve Small-Angle X-ray Scattering (SAXS) and four Small-Angle Neutron Scattering (SANS) instruments [1]. From these data, the solvent-subtracted protein scattering profiles were shown to be reproducible, with the caveat that an additive constant adjustment was required to account for small errors in solvent subtraction. Further, the major features of the obtained consensus SAXS data over the q-measurement range 0 – 1 $Å^{-1}$ are consistent with theoretical prediction, but with residual differences that can now be accounted for. The inherently lower statistical precision for SANS limited the reliably measured q-range to < 0.5 $Å^{-1}$, but within the limits of experimental uncertainty the major features of the consensus SANS data are also consistent with prediction for all five proteins measured in H_2O and in D_2O. Thus, a foundation set of consensus SAS profiles has been obtained for benchmarking scattering profile prediction from atomic coordinates. Additionally, two sets of SAXS data measured at different facilities to q > 2.2 $Å^{-1}$ showed good mutual agreement, affirming that this region has interpretable features for structural modelling. SAS measurements with in-line SEC proved generally superior for eliminating sample heterogeneity, but with unavoidable sample dilution during column elution, while batch SAS data collected at higher concentrations and for longer times provided superior statistical precision. Careful merging of data measured using in-line SEC- and batch-modes, or low- and high-concentration data from batch measurements, was successful in eliminating small amounts of aggregate or interparticle interference from the SAS data while providing improved statistical precision overall for the benchmarking data set.

Data for the round robin study were assessed and analyzed using all the criteria and tools described in the 2017 publication guidelines for reporting biomolecular SAS data and 3D modelling [2] that were established through a consultive process spanning more than a decade and a half [3]. In 2022, the IUCr journal editors mandated deposition of SAS data used in biomolecular structure solution to a public archive [4], and notes for authors specify adherence to the 2017 reporting guidelines. The accompanying standard table templates therefore were reviewed and updated to include standard descriptions for proteins, glycosylated proteins, DNA and RNA, with some reorganization of data to improve readability and interpretation. A specialized template was also developed for reporting SAS-contrast variation (SAS-cv) data and models that includes the additional reporting required for these more complex experiments (Trewhella, Whitten & Jeffries accepted for publication *Acta Cryst. D*, Dec 2022). This framework of best practice reporting standards for the field has helped to position biomolecular SAS to achieve its full potential at the frontier of integrative structural biology, as evidenced by the fact that the prototype archiving system for structural models obtained using integrative modeling, PDB-Dev [5], includes validation reports for contributing SAS data with links to the SAS Biological Data Bank (SASBDB), which now has > 3000 experimental SAS profiles and > 4000 associated models [6,7].

This presentation will focus on the findings of the round robin study and work done since their publication utilizing the consensus profiles and briefly review the rationale for the updates to the template tables for biomolecular SAS and 3D modelling.

[1] Trewhella, J., Vachette, P., Bierma, J., Blanchet, C., Brookes, E., Chakravarthy, S., Chatzimagas, L., Cleveland, T. E. t., Cowieson, N., Crossett, B., Duff, A. P., Franke, D., Gabel, F., Gillilan, R. E., Graewert, M., Grishaev, A., Guss, J. M., Hammel, M., Hopkins, J., Huang, Q., Hub, J. S., Hura, G. L., Irving, T. C., Jeffries, C. M., Jeong, C., Kirby, N., Krueger, S., Martel, A., Matsui, T., Li, N., Perez, J., Porcar, L., Prange, T., Rajkovic, I., Rocco, M., Rosenberg, D. J., Ryan, T. M., Seifert, S., Sekiguchi, H., Svergun, D., Teixeira, S., Thureau, A., Weiss, T. M., Whitten, A. E., Wood, K. & Zuo, X. (2022). *Acta Cryst. D* **78**, 1315-1336

[2] Trewhella, J., Duff, A. P., Durand, D., Gabel, F., Guss, J. M., Hendrickson, W. A., Hura, G. L., Jacques, D. A., Kirby, N. M., Kwan, A. H., Perez, J., Pollack, L., Ryan, T. M., Sali, A., Schneidman-Duhovny, D., Schwede, T.,

Svergun, D. I., Sugiyama, M., Tainer, J. A., Vachette, P., Westbrook, J. & Whitten, A. E. (2017). *Acta Cryst. D* **73**, 710-728.
[3] Trewhella, J. (2022 in press) *Methods in Enzymology* **678**, 1-22
[4] Baker, E. N., Bond, C. S., Garman, E. F., Newman, J., Read, R. J. & van Raaij, M. J. (2022). IUCrJ 9, 1-2.
[5] Burley, S. K., Kurisu, G., Markley, J. L., Nakamura, H., Velankar, S., Berman, H. M., Sali, A., Schwede, T. & Trewhella, J. (2017). *Structure* **25**, 1317-1318.
[6] Valentini, E., Kikhney, A. G., Previtali, G., Jeffries, C. M. & Svergun, D. I. (2015). *Nucleic Acids Res.* **43**, D357-363.
[7] Kikhney, A. G., Borges, C. R., Molodenskiy, D. S., Jeffries, C. M. & Svergun, D. I. (2020). *Protein Science* **29**, 66-75.

A090-04-230823

Biomolecular small-angle neutron scattering data reproducibility and consensus curves

A. E. Whitten[1], A. Martel[2], S. Kruegar[3], S. Teixeira[3], K. Wood[1]

[1]Australian Nuclear Science and Technology Organisation, New Illawarra Rd, Lucas Heights, NSW 2234, Australia, [2]Institut Laue-Langevin, 71 avenue des Martyrs, CS 20156, 38000 Grenoble, France, [3]National Institute of Standards and Technology,

100 Bureau Drive, Gaithersburg, MD 20899, U.S.A

andrew.whitten@ansto.gov.au

Keywords: Small-angle neutron scattering, protein structure, deuterium exchange

A recent international effort [1], involved the collection of both small-angle X-ray scattering (SAXS) and small-angle neutron scattering (SANS) data from five different proteins (ribonuclease A, lysozyme, xylanase, urate oxidase and xylose isomerase). The original aim of this project was to generate experimental scattering data from a well set of well characterised proteins to provide a benchmark for the calculation of small-angle scattering profiles from atomic resolution biomolecular structures. The measurements also represented an opportunity to test the reproducibility of biomolecular scattering data across a large number of different instruments, collecting in different modes (i.e. in a batch configuration, or in a size-exclusion chromatography (SEC) configuration).

While small-angle X-ray scattering beamlines at synchrotrons have progressed such that scattering measurements on very dilute solutions can be made with extraordinary precision within a few seconds, neutron scattering still present a number of challenges. From a sample preparation aspect, samples for neutron scattering are at higher concentrations due to the relatively low flux of neutron sources and the high levels of incoherent scattering from ^{1}H that adds to the noise. Further, the effect of deuterium in the solvent can affect interactions between molecules in solution. Another issue is that SEC-SANS is currently only available at one facility globally, while a batch configuration is the dominant collection method used. Averaging data across different facilities is also potentially difficult, as while synchrotron SAXS beamlines can be reasonably approximated as point sources, the q-resolution at neutron sources is variable. Finally, the number of software packages available to compute neutron scattering profiles at arbitrary solvent deuterium levels (and including the effect of the solvent layer) is much smaller than that available for X-ray scattering.

These complicating factors will be discussed in context of the aims of the benchmarking project.

1 Trewhella, J., Vachette, P., Bierma, J., Blanchet, C., Brookes, E., Chakravarthy, S., Chatzimagas, L., Cleveland, T. E., IV, Cowieson, N., Crossett, B., Duff, A. P., Franke, D., Gabel, F., Gillilan, R. E., Graewert, M., Grishaev, A., Guss, J. M., Hammel, M., Hopkins, J., Huang, Q., Hub, J. S., Hura, G. L., Irving, T. C., Jeffries, C. M., Jeong, C., Kirby, N., Krueger, S., Martel, A., Matsui, T., Li, N., Perez, J., Porcar, L., Prange, T., Rajkovic, I., Rocco, M., Rosenberg, D. J., Ryan, T. M., Seifert, S., Sekiguchi, H., Svergun, D., Teixeira, S., Thureau, A., Weiss, T. M., Whitten, A. E., Wood, K. & Zuo, X. (2022). *Acta Crystallogr.* **D78**, 1315.

A090-05-230823

Solution structure of Type I tropocollagen revealed by small- and wide-Angle X-ray scattering, chromatographic-based optical methods, and molecular dynamics simulation

Ying-Jen Shiu,[1] Bradley W. Mansel,[1] Kuei-Fen Liao,[1] Ting-Wei Hsu,[1] Je-Wei Chang,[1] Orion Shih,[1] Yi-Qi Yeh,[1] Chen-An Wang,[1] and U-Ser Jeng[1,2*]

1 National Synchrotron Radiation Research Center, Hsinchu Science Park, Hsinchu 30076, Taiwan; 2 Department of Chemical Engineering, National Tsing Hua University, Hsinchu 30013, Taiwan

Keywords: Type I tropocollagen, SAXS-WAXS, molecular dynamics simulation, optical probes

Tropocollagen molecules, comprising triple helical polypeptide strands, can pack into collagen microfibrils and bundles as supporting matrixes of vertebrate tissues. Despite highly organized collagen structures in various forms such as bones, tendons, and dermis are well studied, the solution structure of single tropocollagen molecules, however, remains elusive. In this study, the global and local structural features of type I tropocollagen in solution are revealed using simultaneous small- and wile-angle X-ray scattering (SAXS-WAXS). Complementary information is also revealed from multi-angle laser light scattering and dynamic light scattering, coupled with size-exclusion-column (SEC) and UV-vis absorption and refractive of index spectrometers. The results reveal a shape factor $S = Rg/Rh \sim 2.3$, with the extracted radius of gyration Rg (50 nm) to hydrodynamic radius Rh (22 nm), revealing significantly flexible conformation, compared to the needle-like crystalline form of $S = 10.9$. Consistently, the local structure can be described by a worm-like-chain model, with a persistence length much shorter (a few tens of nm) than the contour length (ca. 300 nm) for the solution tropocollagen. Furthermore, integrated with molecular dynamics (MD) simulation, the WAXS result reveal several characteristic distances of 2.8, 5.2, and 4.1 Å , assigned respectively for the intra- and inter chain distances and the hydration water associated distance. A molecular model is proposed to describe the local structure of tropocollagen in solution observed. From which model, edge-on and flat-on orientated water molecules through hydrogen-bonding with specific amino acids of the triple helical polypeptide strands are identified. *Acknowledgements: we thank the TPS 13A beamline team for the assistance of the SWAXS measurements.*

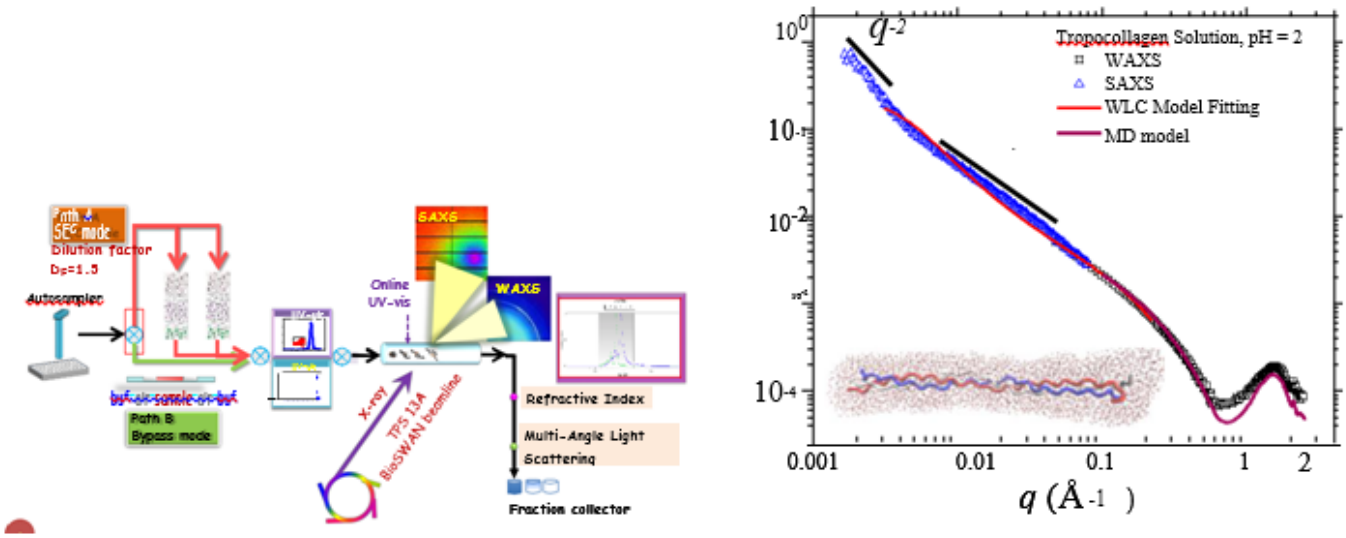

Figure 1. (Left) Schematic of the simultaneous SAXS-WAXS instrument at the 13A BioSWAXS beamline of Taiwan Photon Source. (Right) SWAXS data and the fitting results of integrated worm-like-chain (WLC) model and MD simulation.

1 Shih, O., Liao, K.-F. Yeh, Y.-Q., Su, C.-J. Wang, C.- A., Chang, J.-W., Wu, W.-R., Liang, C.-C., Lin, C.-Y., Lee, T.-H., Chang, C.-H., Chiang, L.-C., Chang, C.-F. Liu, D.-G., Lee, M.-H., Liu , C.-Y., Hsu, T.-W., Mansel, B., Ho, M .-C., Shu, C.-Y. Lee, F., Yen, E., Lin, T.-C., Jeng, U-S., *J. Appl. Crystallogr.* 2022, **55**, 340-352.
2 Liu, D.-G., Chang, C.-H., Chiang, L.-C., Lee, M.-H., Chang, C.-F., Lin, C.-Y., Liang, C.-C., Lee, T.-H., Lin, S.-W., Liu, C.-Y., Hwang, C.-S., Huang, J.-C., Kuan, C.-K., Wang, H.-S., Liu, Y.-C., Tseng, F.-H. Chuang, J.-Y., W.-R. Liao, Li, H.-C., Su, C.-J., Liao, K.-F., Yeh, Y.-Q., Shih, O., Wu, W.-R., Wang, C.-A., Jeng, U-S. *J. Synchrotron Rad.* 2021, **28**, 1954–1965.

A090-06-230823

PDB-Dev: A prototype system for archiving integrative structures

Brinda Vallat[1,2], Benjamin Webb[3], Arthur Zalevsky[3], Serban Voinea[4], Hongsuda Tangmunarunkit[4], Monica Sekharan[1], John D. Westbrook[1,2], Carl Kesselman[4], Stephen K. Burley[1,2,5,6], Helen M. Berman[1,6], Andrej Sali[3]

[1]*RCSB Protein Data Bank and Institute for Quantitative Biomedicine, Rutgers, The State University of New Jersey, Piscataway, NJ 08854, USA*

[2]*Cancer Institute of New Jersey, Rutgers, The State University of New Jersey, New Brunswick, NJ 08901, USA*

[3]*Department of Bioengineering and Therapeutic Sciences, the Quantitative Biosciences Institute (QBI), and the Department of Pharmaceutical Chemistry, University of California, San Francisco, San Francisco, CA 94157, USA*

[4]*Information Sciences Institute, Viterbi School of Engineering, University of Southern California, Los Angeles, California, USA*

[5]*Research Collaboratory for Structural Bioinformatics Protein Data Bank, San Diego Supercomputer Center, University of California, La Jolla, CA 92093, USA*

[6]*Department of Chemistry and Chemical Biology, Rutgers, The State University of New Jersey, Piscataway, NJ 08854, USA*

brinda.vallat@rcsb.org

Keywords: PDB-Dev, IHM-dictionary, PDBx/mmCIF, data standards, integrative modeling

Structures of many complex biological assemblies are increasingly determined using integrative approaches, in which data from multiple experimental methods are combined. Based on recommendations from the worldwide Protein Data Bank (wwPDB) integrative/hybrid methods task force, a standalone prototype system, called PDB-Dev, has been built for archiving integrative structures and making them publicly available [1]. Data standards and software tools have been developed for collecting, curating, validating, visualizing, archiving, and disseminating integrative structures that span diverse spatiotemporal scales and conformational states. Mechanisms have been created to validate integrative structures based on the experimental data underpinning the structure. Building upon the foundational framework, PDB-Dev has been further expanded to handle large dynamic macromolecular ensembles and integrative structures that combine experimental restraints with initial structural models computed by deep learning algorithms. Data standards and supporting tools have been extended to capture information regarding conformational dynamics and related kinetic data derived from biophysical methods. Following the FAIR (Findable, Accessible, Interoperable and Reusable) principles, PDB-Dev ensures that the results of integrative structure determination are freely accessible to everyone. Work is in progress to merge the PDB-Dev structures and supporting software tools with the PDB archive so that integrative structures can be disseminated widely through the PDB.

1 Vallat, B., Webb, B., Fayazi, M., Voinea, S., Tangmunarunkit, H., Ganesan, S.J., Lawson, C.L., Westbrook, J.D., Kesselman, C., Sali, A. & Berman, H.M. (2021). *Acta Crystallogr D Struct Biol.,* **77 (Pt 12)**, 1486-1496.

Development of PDB-Dev has been funded by NSF awards DBI-2112966, DBI-2112967, DBI-2112968, DBI-1756248, DBI-1756250, and DBI-1519158.

A104 Structural databases in materials development

Room 219

4.00pm - 6.30pm

A104-01-230823

Effect of the synthons O —H (Sec. Alcohol) - - -O=C (ketone) and Csp^2—H (furan) - - - OOC (acetate) in the supramolecular packings of two bioactive molecules

Kenfack T. P.[1], Tontsa T. A[2], Nangmo K. P.[3], Kenfack T. S.[1], Mkounga P.[2], Nkengfack E. A.[2], Tonlé K. I.[1]

[1]Chemistry Department, Faculty of Science, University of Dschang, 67, Dschang, Cameroon, [2]Organic Chemistry Department, Faculty of Science, University of Yaoundé I, 812, Yaoundé, Cameroon, [3]Institute of Medical Research and Medicinal Plants Studies, 6163, Yaoundé, Cameroon

Email of communicating: patrice.kenfack@univ-dschang.org, pakenfack@gmail.com

Keywords: Crystal engineering, Vilasinin, Gedunin, Cambridge Structural Database

Crystal engineering aims to successfully control the assembly of molecules or ions in the solid state through the use of non-covalent interactions to produce materials with desired and interesting properties [1, 2]. In this process, understanding these interactions in the context of the crystal packing of molecular entities is primordial and the information obtained is explored in the construction of functional materials. Particularly in the pharmaceutical sector, for example, this understanding is useful for the enhancement of the efficiency of bioactive molecules. Natural products (NP) extracted from biological sources are of particular interest for this purpose. The crystal structures of two bioactive molecules of the vilasinin and gedunin classes of limonoids, rubescin D (**1**) and monadelphin A (**2**) are reported. **1** crystallizes in the P21 space group and its molecular structure consists of three six-membered rings (A, C, and D) and three five-membered rings (B, E, and F). Many synthons found in the crystal packing of **1** are in agreement with the expectations derived from molecules sharing the same moieties. However, the O—H (Sec. alcohol)
1- -O=C (ketone) synthon which has a low occurrence value (2.9 %) contributes a lot to its layered packing while the Csp^2— H (furan) - - - O=C (ketone) and O—H (Sec. alcohol)- - -OC2(epoxide) synthons usually found in these compounds (occurrence of 20.6 and 17.6% respectively) are missing. The packing of **1** is close to that of Ceramicine B (**3**) [3] but is completely different from that of TS3 (**4**) [4] (See Figure 1) suggesting that the absence of the epoxide group in **3** would have favored the Csp^2— H (furan) - - OH (Sec. alcohol) synthon and that the missing hydroxyl group in **4,** a strong hydrogen bond donor, would have favored the involvement of water molecules in its crystal packing. The molecular structure of **2** consists of four six-membered fused rings (A, B, C, and D) and one five-membered ring (E); they have twist-boat (A and C rings), chair (B ring), screw-boat (D ring) and planar (E ring) conformations. This molecule crystallizes in the P212121 space group with the contribution of many synthons usually found in compounds having the same moieties. But the synthons O—H (Sec. alcohol) - - OOC (acetate) and O—H (Sec. alcohol) - - - O=C(ketone) (occurrence of 16.7% in these compounds) are missing. However, the Csp^2— H (furan) - - OOC (acetate) synthon non-observed in these compounds greatly contributes to the layered packing of **2**.

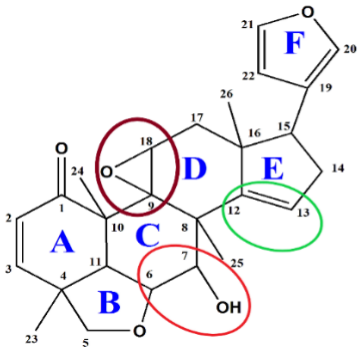

(**1**)

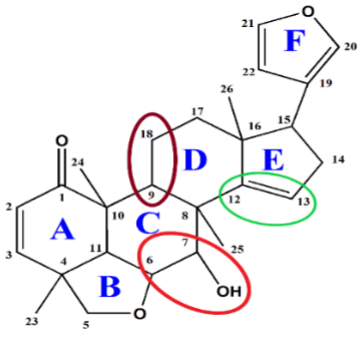

(**3**)

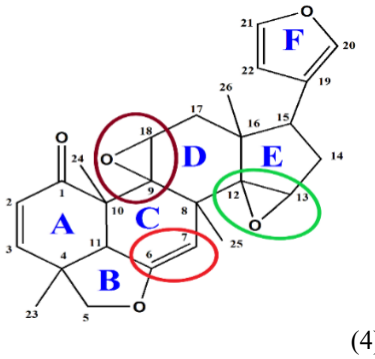

(4)

Figure 1 Diagrams showing the molecular structures of rubescin D (**1**), ceramicine B (**3**) and TS3 (**4**). The differences between these structures are circled in red, green and brown

1 Braga, D., Grepioni, F., Maini, L. & d'Agostino, S. (2017). *IUCrJ.* **4**, 369–379.

2 Fashapoyeh, A. M., Shahrabi, M. M. & Eshtiagh-Hosseini, H. (2017). *Nanochem Res*. 2, 71-85.

3 Galek, P. T. A., Chisholm, J. A., Pidcock, E. & Wood, P. A. (2014). Acta Cryst. B70, 91–105.

4 Tsobnang, K. P., Tontsa, T. A., Mkounga, P., Nkengfack, E. A. & Kenfack, T. I. (2018). Acta Cryst. E74, 1083–1086.

The Authors thank the IUCr and Cambridge Crystallographic Data Centre (CCDC) for the promotion of Crystallography and structural Chemistry in Cameroon via the IUCr Africa initiative and the FAIRE program respectively.

A104-02-230823

Statistical analysis of coordination environments of metals in organic and organometallic crystals

O. V. Grineva

Chemistry Department of Moscow M. V. Lomonosov State University, Moscow, 119991, Russia, ovg@chem.phys.msu.ru

Keywords: Cambridge Structural Database, coordination number, coordination polyhedron

The use of crystallographic databases makes it possible to obtain generalized information about the crystal structure of various classes of chemical compounds. When describing the structure of substances containing metal atoms, the analysis of the coordination environment of these atoms is essential. For crystals of inorganic compounds, the coordination environment of a wide range of metal elements in oxides was considered [1], but for substances containing organic molecules or fragments of molecules, such a general study could not be found.

In this work, coordination environments of metal elements based on the CSD data (version 5.43 with 3 updates) were analyzed. Several subsets were formed, including taking into account the number of different structural residues in the unit cell (NRes) and the types of bonds (any, only with nonmetal atoms, only with metal atoms, etc.) that form the coordination environment of metals. On Fig. 1 denotes the metal elements for which there are data in the CSD related to some of the subsets considered.

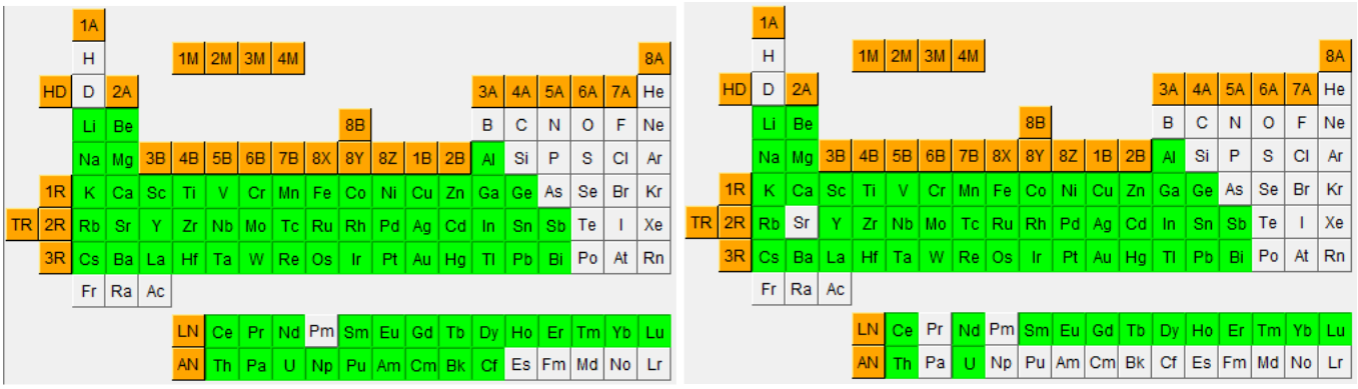

Figure 1. Metal elements occurring in the subsets with NRes > 1 and any type of bonds (left) or having at least one metal-to-metal bond (right).

It turned out, in particular, that the maximum coordination number is 20. Examples of molecules with such coordination are shown in Fig. 2.

Figure 2. Examples of molecules having coordination number for metal equal to 20.

1 Waroquiers, D., Gonze, X., Rignanese, G.-M., Welker-Nieuwoudt, C., Rosowski, F., Göbel, M., Schenk, S., Degelmann, P., André, R., Glaum, R. & Hautier, G. (2017). *Chem. Mater.* **29**, 8346.

A104-03-230823

Materials development using powder diffraction techniques and the Powder Diffraction File™

T. Blanton1, S. Kabekkodu1, J. Blanton1, V. Bosnic1

International Centre for Diffraction Data, Newtown Square, PA, USA

tblanton@icdd.com

Keywords: database, powder XRD, materials characterization

Powder X-ray diffraction (XRD) has historically been the analytical technique of choice for phase identification of crystalline materials. Today, advances in radiation sources, optics and detectors, allow scientists to use XRD to probe beyond phase identification and extend studies to investigate material microstructure as well as nanostructure properties. Whether the material of interest being studied is crystalline or amorphous, randomly or preferentially oriented, inorganic or organic, powder or solid, there are many diffraction methods available that can be used to analyze a sample and provide help in understanding how material processing affects material properties. In addition to improvements in diffraction instrumentation, new developments in the ICDD Powder Diffraction File (PDF®) databases have produced an array of solid-state analysis tools resulting from a combination of single crystal and powder diffraction data. Advanced features include: atomic coordinates for Rietveld refinement techniques; amorphous and nano material references; digital simulation tools for evaluating X-ray, synchrotron, electron and neutron diffraction data as well as crystallite size and analysis of two-dimensional diffraction data.

Diffraction methods and the Powder Diffraction File together create a synergy between data collection and data analysis that has been proven to assist scientists in finding a more complete and correct answer to their materials characterization questions. The origins of the PDF will lead to a review of current capabilities of databases and software, resulting in solutions for materials analyses.

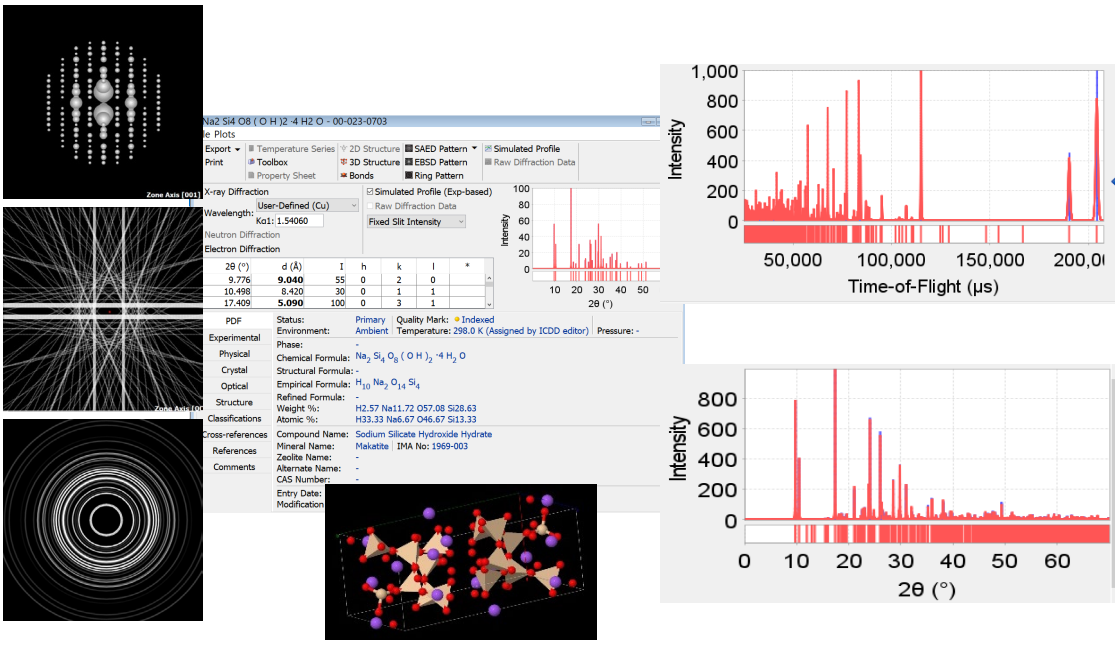

Figure 1. PDF entry and corresponding X-ray, electron and neutron diffraction data for $Na_2Si_4O_8(OH)_2 \bullet 4H_2O$, Makatite

The work is a part of researches on the theme No. 121031300090-2.

A104-04-230823

The Crystal Isometry Principle justifies a new data standard for all periodic crystals

Andrew I Cooper, Daniel E Widdowson, Matthew J Bright, Vitaliy A Kurlin

Materials Innovation Factory, University of Liverpool, United Kingdom, vitaliy.kurlin@gmail.com

Keywords: Crystal Isometry Principle, periodic crystals, data standard, materials genome, structural invariants, crystal descriptors

Conventional crystal representations by unit cells and motifs in a typical Crystallographic Information File (CIF) are unreliable for comparing real structures because any reduced cell can discontinuously change (even by volume) under almost any perturbation.

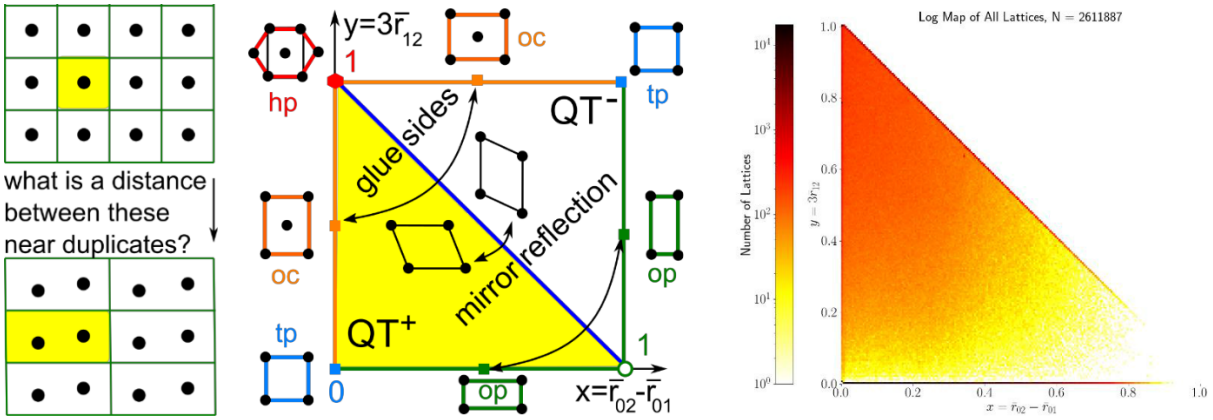

Figure 1. **Left**: all reduced cells are discontinuous under perturbations. **Middle**: a continuous map of 2D lattices showing singular Bravais classes as low-dimensional subspaces. **Right**: the log-scale heat map of 2D lattices from all periodic crystals in the CSD.

Since crystal structures are determined in a rigid form, there is no practical sense to distinguish crystals up to rigid motion, which is a composition of translations and rotations in the ambient 3-dimensional space. On the other hand, geometrically close but not rigidly equivalent structures can have different properties. Hence it is important to distinguish crystals that are not related by rigid motion or (slightly more general) isometry including mirror reflections, which can be easily detected by a sign of orientation.

The traditional classification by symmetries is weaker and produces only 230 space groups, which are insufficient to distinguish more than 1.2 million structures in the Cambridge Structural Database (CSD) [1]. All periodic crystals in the CSD were recently distinguished by hierarchical invariant descriptors [2-3] that are so fast that more than 200 billion pairwise comparisons were finished within two days on a modest desktop computer. This huge experiment detected five pairs of geometric duplicates that have all geometric data identical to the last decimal place but one atom was replaced with a different one, for example Cd with Mn in the pair HIFCAB vs JEPLIA, which seems physically impossible. As a result, five journals are investigating the data integrity.

The much more important conclusion is **the Crystal Isometry Principle** [1-2] saying that all periodic crystals live in a common **Crystal Isometry Space** (CRISP) continuously parameterized by complete invariants. Conventional crystal representations were used in the past like passport photos to represent a human. Our passports move toward biometric data. A DNA code is practically complete and unambiguous for identifying people with 100% certainty. The complete invariants are geographic-style coordinates [4] providing the *new data standard* to identify any periodic crystal without any restriction by chemical composition or symmetry.

CRISP shows *all known crystals* as visible stars in the continuous crystal universe and includes *all not yet discovered crystals*. Hence a map of CRISP should guide any further exploration without wasting time and resources on generating of hypothetical crystals that can be concentrated around the same minima of energy. The first maps of CRISP for 2D lattices were visualized [4-5] for more than *2.6 million lattices from real crystals* in the CSD. The CRISP establishes a new area of Continuous Crystallography that studies all periodic crystals in a common space in the same way as Mendeleev's table covers all known chemical elements.

1 Ward. S., Sadiq G. Introduction to the CSD–a wealth of knowledge gained from a million structures. CrystEngComm. 2020;22(43):7143-4.

2 Widdowson, D., et al. Average Minimum Distances of periodic point sets. *MATCH Comm. Math. Comp. Chem*, v.87(3), p.529-559, 2022.
3 Widdowson, D., Kurlin, V. Resolving the data ambiguity for periodic crystals. *Adv. Neural Information Processing Systems*, v.35 (2022).
4 Kurlin, V. Mathematics of 2-dimensional lattices. *Foundations of Computational Mathematics* (2023), http://arxiv.org/abs/2201.05150.
5 Bright, M., Cooper, A., Kurlin, V. Geographic-style maps for 2-dimensional lattices. *Acta Cryst. A* (2023), http://arxiv.org/abs/2109.10885.

A104-06-230823

From crystal to tablet – linking structure to function through compression studies

J. Gasol Cardona1 2, M. R. Ward1 2, D. Comboni3, M. Hanfland3, R. Scatena4, D. R. Allan4, A. A. Moldovan5, A. G. P. Maloney5, I. D. H. Oswald1 2

1. Strathclyde Institute of Pharmacy and Biomedical Sciences (SIPBS), University of Strathclyde, Glasgow, United Kingdom,

2. EPSRC Future Manufacturing Research Hub for Continuous Manufacturing and Advanced Crystallisation (CMAC), University of Strathclyde, Glasgow, United Kingdom,

3. ID15B beamline, European Synchrotron Radiation Facility (ESRF), Grenoble, France,

4. I19 beamline, Diamond Light Source (DLS), Harwell Science and Innovation Campus, Didcot, United Kingdom,

5. Cambridge Crystallographic Data Centre (CCDC), Cambridge, United Kingdom

julia.gasol-cardona@strath.ac.uk

Keywords: Solid-state pharmaceuticals, slip planes, dual pressure-range analysis

Pharmaceutical tablets are the most widely used oral solid dosage form worldwide. They have a convenient design that favours high patient compliance, display good stability to atmospheric conditions, and can be manufactured at a large scale with the correct formulation. [1] During the tablet manufacturing process, the pharmaceutical powder blend is subjected to applied pressure at various stages of the production line, usually up to 0.3 GPa. Key properties of the crystalline components in the formulation (mechanical properties, solid state properties, chemical stability) directly impact the behaviour the components exhibit during processing, and define the quality and nature of the final product.

Currently, the relationship between the structural characteristics of crystalline pharmaceuticals and their behaviour under pressure is not well understood. In our study, we begin to investigate this relationship between structure and function by exploring alternative strategies to analyse and understand the compressibility observed in high-pressure crystallographic datasets. Active slip planes are reported to be responsible for plastic deformation in organic pharmaceutical crystals. [2] Additionally, their presence is shown to correlate with superior tabletability. [2] To investigate the potential impact of slip planes during the compression of systems of pharmaceutical relevance, we present a new approach to mapping molecular movement upon compression, and tracking the movement against slip planes predicted using the CSD-Particle tool (Cambridge Structural Database). [2]

We illustrate the outcome of this approach on a study of the racemic and chiral crystal structure of an active pharmaceutical ingredient used as an antibiotic: ofloxacin and levofloxacin. The difference in chirality between both crystals give rise to differing solid state landscapes [3][4], making them exciting candidates to examine under pressure. X-ray diffraction data has been collected on ofloxacin, levofloxacin hemihydrate and levofloxacin anhydrous under moderate pressures using a medium pressure sapphire capillary pressure cell on beamline I19 at Diamond Light Source ($\leq$ 0.12 GPa) [5], and at high pressures using standard diamond anvil cells in-house and on beamline ID15B at the European Synchrotron Radiation Facility ($\leq$ 7 GPa). We present data on the compressibility of these systems at tabletting pressures and beyond in an effort to determine the impact of chirality on their structural behaviour under pressure, and relate these to our present understanding of slip planes.

[1] Advankar A., Kapoor D., Maheshwari R., Raval N., Tambe V., Tekade R. K. & Todke P. (2019) *Drug Delivery Systems*. Amsterdam: Elsevier.
[2] Bryant M. J., Maloney A. G. P. & Skyes R. A (2018), *CrystEngComm*, **19**, 2698.
[3] Mahapatra S., Venugopala K. N. & Row T. N. G. (2010), *Cryst. Growth Des.*, **10**, 1866.
[4] Wei N., Jia L. N., Shang Z. R., Gong J. B., Wu S. G., Wang J. K. & Tang W. W. (2019), *CrystEngComm*, **21**, 6196.
[5] McMonagle C. J., Allan D. R., Warren M. R., Kamenev K. V., Turnere G. F. & Moggach S. A. (2020), *J. Appl. Cryst.*, **53,** 1519.

A111 In vivo crystallography and synchrotron radiation

Room 217

4.00pm - 6.30pm

A111-01-230823

Structural biology of bacterial insecticides using in vivo grown crystals and nanoSFX.

A. Williamson[1], M. Galchenkova[2], R. Bean[3], H. Best[1], A. Munke[2], K. Dörner[3], R. Schubert[3], J. Bielecki[3], A. Henkel[2], O. Yefanov[2], P.J. Rizkallah[4], H.N. Chapman[2,5,6], N. Crickmore[7], C. Berry[1], D. Oberthür[2]

[1]School of Biosciences, Cardiff University, UK; [2]Center for Free Electron Laser Science CFEL, Deutsches Elektronen-Synchrotron DESY, Notkestr. 85, 22607 Hamburg, Germany; [3]European XFEL GmbH, Schenefeld, Germany; [4]School of Medicine, Cardiff University, UK: [5]Centre for Ultrafast Imaging, Universität Hamburg, Hamburg, Germany; [6]Department of Physics, Universität Hamburg, Hamburg, Germany; [7]School of Life Sciences, University of Sussex, Brighton, UK. dominik.oberthuer@desy.de

Keywords: serial crystallography, in vivo crystals, alphafold

Bacillus thuringiensis (Bt) is a gram positive, spore-forming bacterium that produces a range of toxins that are active against invertebrate targets. Toxin profiles vary from one isolate to another and individual toxins may show toxicity to different orders of insects, nematodes and protozoa. In some cases, activity against cancerous human cells has also been demonstrated. Any individual toxin will show a relatively narrow target range, owing to the receptor-mediated mechanism of action. Bt products represent the largest and most important part of the commercial bioinsecticide market with over 40 years of worldwide use in crop protection and control of insect vectors of disease. In addition, Bt toxins are a major resource for use in the production of insect resistant, transgenic plants. The toxins produced by Bt are deposited as natural protein crystals when the host bacterium sporulates. Their occurrence as native nanocrystals and lack of structural homologues prevented many structure determination efforts to understand their mode of action. Serial femtosecond crystallography (SFX) offers the potential to overcome the significant hurdles of production and analysis of *in vitro* crystallization by direct analysis of natural, *in vivo* grown crystals, as initially demonstrated by our determination of the structure of non-recrystallized granulovirus protein using the X ray free-electron laser LCLS [1]. In the field of pesticidal proteins, SFX has previously been applied by others to solve the structures of the Cyt1Aa and Cry11 toxins from *B. thuringiensis*, and the Tpp1Aa2/Tpp2Aa2 toxin from *L. sphaericus* [2-4]. We used MHz serial femtosecond crystallography [5] at a nano-focused X-ray free electron laser (nanoSFX), which allowed rapid and high-quality data collection to determine the Tpp49Aa1 structure at 1.62 Å resolution from native nanocrystals [6], the first new protein structure to be obtained at the European XFEL (EuXFEL). In two beamtimes we additionally solved the structures of five other pesticidal proteins, for which previously no experimental structures where known. Two of these structures where determined *de novo*, using models generated by Alphafold as templates. Furthermore, we could analyse the response of three proteins to pH-shifts by mix-and-diffuse SFX, mimicking the pH environment within the target gut during toxin solubilization.

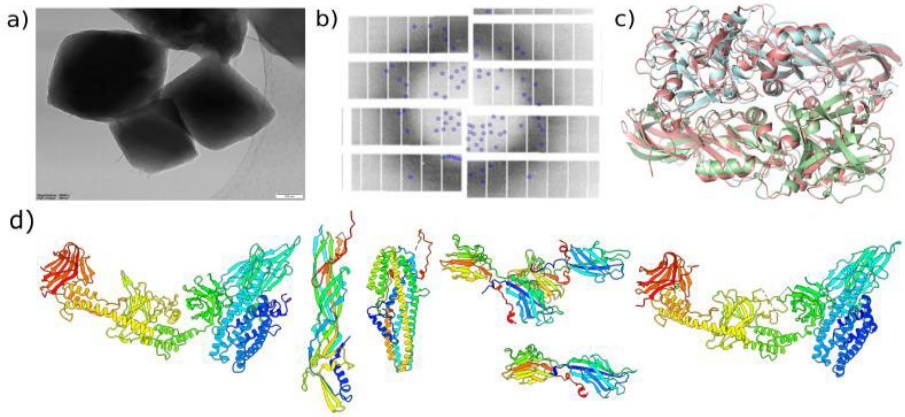

Figure 1. a) negative stain TEM image of Tpp49 crystals at 50000x magnification (scale bar = 100nm) b) diffraction pattern as recorded with AGIPD at SPB (EuXFEL). c) model of the homo dimer of Tpp49 (chain A light blue, chain B light green) built based on the collected data and aligned with the *Lysinibacillus sphaericus* BinAB hetero dimer (rose). d) new insecticide structures based on data from our recent beamtimes.

1 Gati, C., Oberthuer, D., Yefanov, O., et al. (2017). *Proc Natl Acad Sci U S A*. **114**, 2247–2252.
2 Tetreau, G., Banneville, A.-S., Andreeva, E. A., et al. (2020). *Nat Commun*. **11**, 1153.
3 Tetreau, G., Sawaya, M. R., De Zitter, E., et al. (2022). *Nat Commun*. **13**, 4376.

4 Colletier, J. P., Sawaya, M. R., Gingery, et al. (2016). *Nature*. **539**, 43–47.
5 Wiedorn, M. O., Oberthuer, D., Bean, R., et al. (2018). *Nat Commun.* **9**, 4025.
6 Williamson, L. J., Galchenkova, M., Best, H. L., et al. (2022). *bioRxiv* 2022.01.14.476343.

A111-02-230823

Protein crystallography using 500 nm-sized crystals

K. Hirata[1], S. Abe[2], M. Kojima[2], T. Ueno[2], H. Matsuura[1], Y. Kawano[1], M. Yamamoto[1]

[1]RIKEN SPring-8 Center, 1-1-1, Koto, Sayo-cho, Sayo-gun, Hyogo, JAPAN,

Email of communicating kunio.hirata@riken.jp

Keywords: macromolecular crystallography, micro crystal

Proteins are involved in all biological activities. For example, to develop a drug that inhibits a specific disease, it is essential to identify the protein that causes the disease and elucidate its structure. X-ray crystallography is widely used to elucidate the three-dimensional structure of proteins, which requires highly purified, high-quality protein single crystals. However, it generally takes several months to synthesize the target protein, purify it, and crystallize it to obtain crystals of sufficient size and quality for high-resolution structure analysis, even using the latest technology and equipment. In this research, a cell-free protein synthesis method, in which DNA or mRNA, etc. carrying genetic information of target proteins are added to extracts taken from cells to synthesize proteins, and "polyhedra," referred to as PH, in which crystals are formed autonomously in cells, are combined to directly synthesize proteins without going through the complicated "purification" and "crystallization" processes. Success in cell-free protein crystallization to obtain protein crystals directly without complicated "purification" and "crystallization" processes. Compared to conventional protein synthesis using living cells, the process has been greatly simplified, and the time required has been dramatically shortened to less than 24 hours. Furthermore, although the obtained crystals are as tiny as several hundred nano-meters (nm), they are of high quality, and a 1.8 Å resolution structure was successfully obtained by automated measurement using the beamline BL32XU dedicated to microcrystal structure analysis at SPring-8, a large synchrotron radiation facility.

In the presentation, we will describe the details of the crystals used for this structural analysis, the details of the beam focused to 1 micron, and discuss the crystal sizes that can be determined by X-rays.

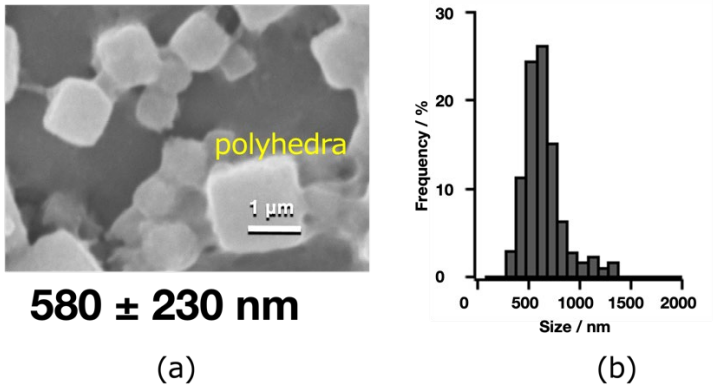

Figure 1. (a) SEM image of PH crystals crystallized with this method, and (b) crystal size distribution of PH crystals in this study

[1] “Cell-free Protein Crystallization for Naonocrystal Structure Determination” S. Abe, J. Tanaka, M. Kojima, S. Kanamaru, K. Hirata, K. Yamashita, A. Kobayashi and T. Ueno DOI: 10.1038/s41598-022-19681-9

A111-03-230823

Time-resolved fs crystallography: Unravelling the dynamics of biomolecules

Petra Fromme[1] (see references for co-authors)

Biodesign Center for Applied Structural Discovery and School of Molecular Sciences, Arizona State University, Tempe, Arizona, 85287 USA

Email: pfromme@asu.edu

Keywords: X-Ray Free electron Lasers, Serial femtosecond Crystallography, protein dynamics

New avenues for structural discovery of the function and dynamics of biomolecules have been opened by X-ray Free Electron Lasers (XFELs) by Serial Femtosecond Crystallography (SFX). SFX provides a novel concept for structure determination, where X-ray diffraction "snapshots" are collected from a fully hydrated stream of nanocrystals, using femtosecond pulses from high energy X-ray free-electron lasers (XFELs) [1-4]. The XFEL pulses are so strong that they destroy any solid material, but a femtosecond is so short (1 fs =10 -15s) that X-ray damage is diminished and diffraction from the crystals is observed before destruction takes effect [3]. Structural Biology with X-ray Free electron lasers allows for data collection at near physiological conditions at room temperature [5-13] thereby opening new avenues for the study of light-driven systems in pump probe experiments [7-12] as well as the study of medical important proteins that could enhance structure-based drug design with SFX studies [5,13]. The talk will give an overview of XFEL studies on medical important proteins, including the XFEL studies on the SARS-CoV2 protein NendoU that hides the virus from the immune system [14]. The talk will also report on our most recent time-resolved studies on light-driven systems including Photosystem I and II and give an overview of the development of compact X-ray Free electron Lasers and their future impact for Structural Biology.

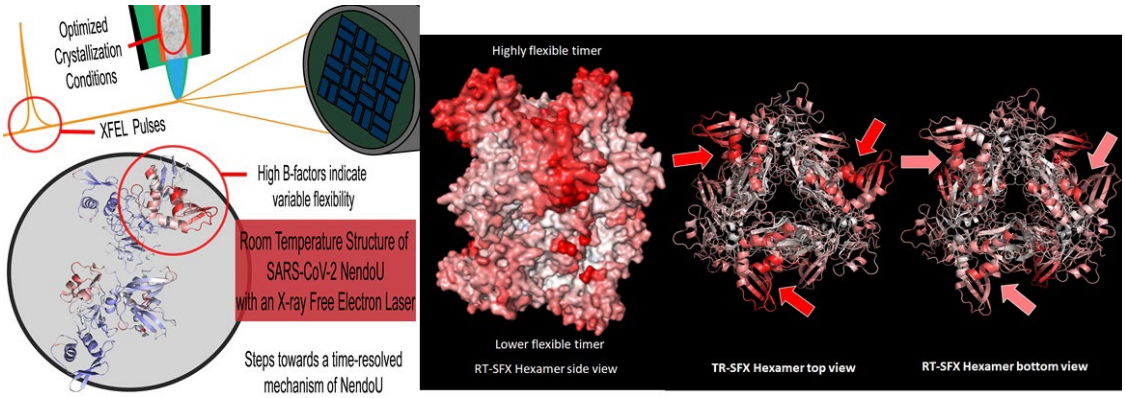

Figure 1. First room temperature structure of the SARS-CoV2 protein NendoU determined by SFX [14].

[1] Chapman,HN et al 2011, Nature, 470, 73-77 ;
[2] Fromme P and Spence JC, 2011 Curr Opin Struct Biol 2011, 21: 509-516;
[3] Barty A et al. 2012, Nature Photonics 6, 35–40
[4] Boutet S et al. 2012, Science, 337: 362-364
[5] Liu W et al. 2013, Science 342: 1521-1524
[6] Aquila,A et al. 2012, Optics Express, 20 (3), 2706-16
[7] Kupitz C et al. 2014, Nature 513, 261-5
[8] Suga M et al. 2017, Nature 543, 131-135
[9] Ibrahim M et al. 2020, PNAS 117 (23), 12624-12635
[10] Li H et al. (2021), IUCrJ 8 (3) 431-443
[11] Gisriel C et al. 2019, Nature Communications 10(1), 5021
[12] Pandey S et al. (2020), Nature Methods, 17(1), pp.73-78
[13] Pandey S et al. (2021), IUCrJ 8(Pt 6): 878-895
[14] Jernigan R et al (2023) Structure, 31, Issue 2: pp 138-151.e5

This work is supported by the National Science Foundation BIOXFEL STC (NSF-1231306) and NSF RAPID IIBR 2031343 grant, the National Institute of General Medical Sciences grant R01 GM095583 and the Biodesign Institute at Arizona State University

A111-04-230823

Finding and diffracting protein crystals in living insect cells.

JM. Lahey-Rudolph123, L. Redecke12

Institute of Biochemistry, University of Lübeck, Ratzeburger Allee 160, 23562 Lübeck, Germany, DESY, Notkestraße 61, Hamburg, Germany,
Current: Technical University of Applied Sciences/ TH Lübeck, Mönkhofer Weg 231, 23562 Lübeck.
Mia.Lahey-Rudolph@th-luebeck.de

Keywords: *in cellulo*, native ligands, SFX

Protein crystals in living cells have been observed in all domains of life and surprisingly often. This crystallization approach can grow millions of micron-sized high quality protein crystals in the crowded environment of the cell in a short time. [1] We have established a streamlined process towards a systematic use of *in cellulo* crystallization in insect cells for structural biology [2-4].

The gene of interest is cloned into baculovirus transfer vectors. The associated recombinant baculoviruses are generated to infect insect cells. Crystal formation can be detected a few days after infection within the cell culture by a growing arsenal of detection methods including a very sensitive approach combining SAXS and X-ray powder detection that we have developed [5]. If intracellular crystallization was successful, protein crystals can be extracted from the cell and diffraction data of the *in cellulo*-grown crystals are collected using serial crystallography approaches using either XFELs or third generation synchrotron sources, depending on the average crystal diffraction volume. [3,4,6,7] The arsenal of potentially binding cofactors within the cell is almost unlimited, therefore high affinity binding ligands may be found and identified in high-resolution electron density maps [4,6]. This approach can be a valid alternative to elaborate soaking experiments and approach physiological conditions.

Today, *in cellulo* crystallization is still a method used by a minority of crystallographers. This is due to major bottlenecks: The fraction of crystal containing cells in a batch varies between over 80 % and less than 1 %. This mainly depends on the recombinant protein sequence. Furthermore, cell lysis and crystal purification out of the cellular debris, always accompanied by necessary changes of environmental conditions, can reduce crystal integrity [1,2].

This contribution presents one solution to these two limitations: optimization of data collection strategies for this special kind of membrane-surrounded sample. We have established and fine-tuned techniques for serial diffraction data collection from *in cellulo* grown crystals *directly within* the living insect cells. The presented approaches avoid crystal purification and transfer of the living, crystal-containing cells for diffraction data collection [4,5,7].

Much of the underlying molecular biology of this fascinating phenomenon intracellular protein crystallization remains to be discovered. Our results pave the way to a more efficient use of crystal containing insect cells as suitable targets for serial diffraction data collection at synchrotrons and XFELs.

[1] Schönherr, R. Lahey-Rudolph, JM. and Redecke, L., (2018). *Biol. Chem*., **399** (7), 751–772.
[2] Schönherr*, R., Klinge*, M., Rudolph, J.M., Fita, K., Rehders, D., Lübber, F., Schneegans, S., Majoul, I.V., Duszenko, M., Betzel, C., Brandariz-Nunez, A., Martinez-Costas, J., Duden, R., Redecke, L. (2015), *Struct. Dyn*, **2**.
[3] Redecke, L. *et al*. (2013). *Science*, **339**, 227-231.
[4] Schönherr*, R., Boger*, J., Lahey-Rudolph*, JM. (…), Redecke, L. (2022) to be submitted.
[5] Lahey-Rudolph, JM., Schönherr, R., Jeffries, C.M., Blanchet, C.E., Boger, J., Ferreira Ramos, A.S., Riekehr, W.M., Triandafillidis, D.-P., Valmas, A., Margiolaki, I, Svergun, D., Redecke, L. (2020) *JAC*, **53**, 1168-1180.
[6] Nass*, K., Redecke*, L., (…), Lahey-Rudolph, J.M., (…) Chapman, H.N., Betzel, C. (2020), *Nat. Commun*. **11**, 620.
[7] Lahey-Rudolph, JM. *et al*. (2021) *IUCrJ*, **8**, 665-677.

This work was partly supported by the German Federal Ministry for Education and Research (BMBF; grant 05K18FLA). M. Lahey-Rudolph acknowledges a PhD scholarship from the Joachim Herz Foundati

A111-05-230823

Intracellular protein crystallization – pushing the limits

Redecke12

Institute of Biochemistry, University of Lübeck, Ratzeburger Allee 160, 23562 Lübeck, Germany,
Deutsches Elektronen Synchrotron (DESY), Notkestraße 85, 22607 Hamburg, Germany
redecke@biochem.uni-luebeck.de

Keywords: *in cellulo*, cell fusion, serial crystallography

Crystallization of proteins in living cells is an emerging field complementing conventional methods of protein crystallization [1]. Our established workflow, denoted as '*InCellCryst* pipeline', includes the process of recombinant protein crystallization after gene expression using a baculovirus vector system and subsequent crystal formation and diffraction in insect cells. As a screening parameter for suitable crystallization conditions we use the specific environment within the different compartments of the cell. This approach enables an easy production of homogenous microcrystals highly required and well-suited for serial diffraction experiments at XFELs and synchrotron sources [2-4], without the need for purification of the target protein. The identification of natively bound ligands in the native cellular environment is unique [3] and cannot be replaced by upcoming AI-based structure prediction algorithms.

However, some bottlenecks still limit the application of this fascinating approach: (*i*) Depending on the target protein the fraction of crystal containing cells within a culture varies between more than 90 % and less than 1 %; (*ii*) despite the high-throughput SAXS/XRPD technique recently established by our group [5], particularly the detection of tiny, sub-micrometre crystals is still a challenge within living cells; (*iii*) cell lysis and crystal isolation out of the cellular debris to increase the crystal concentration can reduce crystal integrity, due to the change in the environmental conditions [2,3]; and (*iv*) some intracellular protein crystals diffract synchrotron radiation only to low resolution.

Diffraction signals in higher resolution shells can be intensified by either increasing the brilliance of radiation, e.g., by applying XFEL pulses or by enlarging the diffractive volume of the crystal. However, access to XFELs is still difficult to obtain for most scientists. Thus, optimizing crystal dimensions within the cells appears to be a more promising approach. In intracellular crystallization the crystal volume is controlled by the size of the cell, however not limited to the cell diameter, since crystals can stick out of the cells without affecting the cellular integrity [6]. To overcome this frequently observed barrier, we developed a protocol for cell fusion using polyethylene glycol, resulting in the formation of syncytia combining up to 50 cells, sometimes even more. After infection using recombinant baculoviruses encoding different model proteins, crystals were formed in the syncytia, characterized by approximately five-fold increased volumes compared to crystals of the same proteins formed in single insect cells. Serial diffraction of the crystal-containing syncytia at a synchrotron beamline allowed protein structure elucidation at resolutions improved by approximately 0.5 A.

Overcoming this bottleneck of *in cellulo* crystallization will enable other protein structures to be solved by exceeding the resolution limit of a protein crystal in the future, expanding the application of the intracellular protein crystallization approach.

[1] Schönherr, R. Lahey-Rudolph, JM. and Redecke, L., (2018), *Biol. Chem*. **399**, 751–772.
[2] Redecke, L. *et al.* (2013), *Science* **339**, 227-231.

[3] Nass, K., Redecke, L. *et al*., (2020), *Nat. Commun*. **11**, 620.

[4] Lahey-Rudolph, JM. *et al*. (2021), *IUCrJ* **8**, 665-677.
[5] Lahey-Rudolph, JM., *et al.* (2020), *J. Appl. Cryst.* **53**, 1168-1180.
[6] Schönherr, R. *et al*. (2015), *Struct. Dyn*. **2**, 041712.

A111-06-230823

Cell-free and in-cell protein crystallization for high-throughput screening of structure determination

B.Abe1, M. Kojima1 J. Tanaka[1], K. Hirata[2], and T. Ueno[1]

[1] *School of Life Science and Technology, Tokyo Institute of Technology, Nagatsuta-cho 4259, Yokohama, 226-8501, Japan*

[2] *SR Life Science Instrumentation Unit, RIKEN/SPring-8 Center, 1-1-1, Kouto, Sayo-cho, Hyogo, 679-5148, Japan*

tueno@bio.titech.ac.jp

Keywords: Cell-free protein synthesis, in-cell protein crystallization, nanocrystal

In-cell protein crystallization (ICPC) has recently been investigated with the aim of structural biology because it does not require protein purification and crystallization processes. However, it is still challenging to obtain high-quality crystals of various proteins for structural analysis because the crystals are formed accidentally in living cells. It is difficult to control the size and quality of the crystals. We achieved the cell-free protein crystallization (CFPC) method to overcome these problems, direct protein crystallization using cell-free protein synthesis.

First, CFPC was validated by crystalizing polyhedra proteins, synthesized in insect cells by the infection of cytoplasmic polyhedrosis virus. Polyhedrin monomer expressed using cell-free protein synthesis at a reaction scale of 200μL could form nanocrystals spontaneously within six hours. We determined the structure at a high resolution of 1.8 Å using the obtained nanocrystals. We achieved dramatic reaction scale-down and crystallization time-reduction compared to ICPC and in vitro crystallization.

This technology provides a new methodology for protein crystallization and structural analysis. It will lead to breakthroughs in structural biology, such as high-throughput screening for crystallization and structure determination of foreign proteins and peptides that are difficult to crystallize. Therefore, it is of broad interest to chemists and biologists and is expected to contribute to developing new research areas of structural biology, crystal engineering, and supramolecular chemistry.

1 M. Kojima, S. Abe, T. Furuta, D. P. Tran, K. Hirata, K. Yamashita, Y. Hishikawa, A. Kitao, and T. Ueno (2022) *Biomaterials Sci.,* **11**, 1350.

2 S. Abe, J. Tanaka, M. Kojma, S. Kanamaru, K. Hirata, K. Yamashita, A. Kobayashi, and T. Ueno (2022) *Sci. Rep.***, 12**, 16031.

3 M. Kojima, S. Abe, T. Ueno (2022) *Biomaterials Sci.***, 10**, 354.

A118 Raw Diffraction Data Reuse: Warts and All
Room 216
4.00pm - 6.30pm

A118-01-230823

Situations where small molecule raw data should be made available

S.J. Coles

School of Chemistry, Faculty of Engineering and Physical Sciences, University of Southampton, Southampton, SO17 1BJ, UK. S.J.Coles@soton.ac.uk

Keywords: Raw Data, Chemical Crystallography, Structural Chemistry

It is now de-facto best practice to deposit structure factors when publishing and making small molecule crystal structures available. This means that the small molecule crystallography community now caters very well for the *validation* of 'routine structures' as part of the publication process. The clear benefits that we are now seeing arise from this approach are that journal articles are better evidenced and the crystallographic databases contain even better quality records. Increasing personal experience of the need/desire to assess structures in different ways not necessarily supported by the model published by the original authors illustrates the value of providing structure factors in promoting the appropriate *reuse* of crystal structures. Work that makes use of collections of structures from databases generally involves a lot of 'data massaging' depending on the goal of the research, e.g re-refinement with more modern software approaches to improve accuracy or without restraints/constraints to explore geometry. A very compelling recent scenario is that one can now perform Quantum Crystallographic aspherical atom refinements with the original data made available on publication to greatly improve the structure and extract chemical or bonding information that wasn't possible at the time.

This fundamental change in the way we communicate our results has greatly enhanced validation and reuse of crystal structures, however this is generally only the case if all aspects of a raw image are fully and/or properly accounted for and the model is correct or appropriate. So, our community can clearly take more steps to better support *reanalysis* and *reinterpretation* of the data collected in single crystal diffraction experiments.

It follows that in some cases raw data may no longer be required. If it can be conclusively shown, preferably by a trusted, automated and enduring mechanism, that all diffraction events are accounted for by the integration and processing stages of the analysis, that nothing further could be obtained from the raw data, then arguably there is no need to retain them. This would obviate the management and financial burdens of curation of a considerable proportion of the raw data generated.

However, there are a significant proportion of cases of results arising from raw data where thorough evidence and justification may be necessary or where it is highly likely that a better analysis may be performed in the future because of method and software innovations. Moreover, there are increasing pressures from bodies e.g. funders to make the data relating to research outputs Findable, Accessible, Interoperable and Reusable (FAIR) and it may be important to keep raw data for these reasons. This talk will present a range of small molecule crystallography cases where raw data publication would be key e.g. in underpinning advanced or dynamic crystallographic experiments, validating claims and quality, evidencing pathological samples and diffraction, supporting future development and to crowd source solutions. These cases are based on the outcomes of a significant community survey [1] on raw data management practices and workshop discussions [2]. There are a number of different approaches that could be implemented to address these cases and these will be outlined as well as showcasing the recent introduction of a new category of article in IUCrData – Raw Data Letters [3].

1 Coles, S.J., Sarjeant, A. (2018). *IUCr Newsletter*, volume 26, number 2; Coles, S.J., Sarjeant, A. (2020). *IUCr Newsletter*, volume 28, number 1.

2 When should small molecule crystallographers publish raw diffraction data (2021). Twenty-Fifth Congress and General Assembly of the International Union of Crystallography, https://www.iucr.org/resources/data/commdat/prague-workshop-cx.
3 Kroon-Batenburg, L. M. J., Helliwell, J. R. & Hester, J. R. (2022). IUCrData 7.

A118-02-230823

Compression and data reduction in serial crystallography

Galchenkova[1], A. Tolstikova[2], D. Oberthuer[1], J. Sprenger[1], W. Brehm[1], T. A. White[2], A. Barty[2], H.N. Chapman[1], O.M. Yefanov[1]

Center for Free-Electron Laser Science, Deutsches Elektronen-Synchrotron DESY, Notkestr. 85, 22607 Hamburg, Germany; 2. Deutsches Elektronen-Synchrotron, Notkestrasse 85, Hamburg 22607, Germany

oleksandr.yefanov@cfel.de

Keywords: serial crystallography, compression, data reduction

Protein crystallography is one of the most successful methods for biological structure determination. This technique requires many diffraction snapshots to get 3D structural information of the studied protein. Even more patterns are needed for studying fast protein dynamics that can be achieved using serial crystallography (SX). Fortunately, new X-ray facilities such as 4th generation synchrotrons and Free Electron Lasers (FELs) combined with newly developed X-ray detectors opened a way to carry out these experiments at a rate of more than 1000 images per second. The drawback of this increase in acquisition rate is the volume of collected data - up to 2 PB of data per experiment could be easily obtained. Therefore, new data reduction strategies have to be developed and deployed. Lossless data reduction methods will not change the data, but usually fail to achieve a high compression ratio. On the other hand, lossy compression methods can significantly reduce the amount of data, but they require careful evaluation of the resulting data quality.

We have tested different approaches for both lossless and lossy compression applied to SX data, proposed some new ways for lossy compression and demonstrated appropriate methods for data quality assessment. By checking the resulting statistics of compressed data (like CC*/Rsplit, Rfree/Rwork) we have demonstrated that the volume of the measured data can be greatly reduced (10-100 times!) while the quality of the resulting data was kept almost constant. In addition, we tested lossy compression methods on the SAD dataset (thaumatin collected at 4.57 keV, measured at the SwissFEL) and demonstrated that even such very sensitive data can be successfully compressed. It allowed us to determine the limit of application for all considered lossy compressions. Some of the proposed compression strategies, tested on SX and MX datasets, can be used for other types of experiments, even with different sources (for example electron and neutron diffraction).

Authors are thankful to K.Nass and D.Ozerov for sharing the SAD, to V. Mariani for useful comments. Taking into account the practical impact of this work, starting from 2020 the authors shared the ideas described in this paper with the data scientists at eXFEL, LCLS, SwissFEL, ESRF, APS, Petra III as well as at different conferences and workshops to demonstrate the ways of data compression and quality checks for the SX data.

A118-03-230823

The raw, the cooked and the medium-rare: unmerged diffraction data as a rich source of opportunities for data re-use and improvements in methods and results

G. Bricogne, C. Flensburg, R.H. Fogh, P.A. Keller, I.J. Tickle, C. Vonrhein

Global Phasing Limited, Sheraton House, Castle Park, Cambridge CB3 0AX.

gb10@globalphasing.com

Keywords: Raw diffraction data, Unmerged diffraction data, Scaling and merging methods

Deposition into the PDB of experimental diffraction data, in the form of merged intensities or of "structure factor[amplitude]s", to accompany atomic models determined and/or refined from them, was made mandatory in 2008. This brought benefits that went well beyond the intended purpose of making the deposited models verifiable and correctable, in the form of an unanticipated "virtuous circle" whereby deposited data fuelled improvements in refinement software that in turn enabled improvements to be made in the initially deposited models, from the same data. The need to manage the outcome of this continuous improvement process led to the introduction of a versioning mechanism into the archiving of atomic models by the PDB in 2017.

The creators of the Electron Density Server had already noted in 2004 that "*perhaps we should consider deposition of unmerged intensities or even raw diffraction images in the future*" [1], without however anticipating the potential for a similar auto-catalytic cycle of simultaneous improvements in data reduction methods and in final structural results that could follow. This potential was later articulated in e.g. [2] in the following terms: "*those [merged] deposited X-ray data are only the best summary of sets of diffraction images according to the data-reduction programs and practices available at the time they were processed. Just like refinement software, those programs and practices are subject to continuing developments and improvements, especially in view of the current interest and efforts towards better understanding radiation damage during data collection and in taking it into account in the subsequent processing steps*."

Strong general support for the idea of archiving raw diffraction images, together with the recognition that this task was beyond the remit and resources of the PDB, has led over the past decade to the emergence of a delocalised infrastructure (whereby raw data storage and curation takes place at synchrotrons and other dedicated repositories while the PDB provides a capability to annotate entries with a DOI that points to the raw data storage location) that is a major topic in this Microsymposium.

Our own interest has been to document the scientific case for depositing and archiving suitably annotated *unmerged* diffraction data into the PDB, a goal achievable with modest storage requirements while already creating a *standardised* resource capable of feeding improvements in scaling and merging methods resulting in better refined models than those originally deposited. This goal is the focus of the current activities of the Subgroup on Data Collection and Processing of the PDBx/mmCIF Working Group of the wwPDB, in which we participate, to expand the mmCIF dictionary to support such extended deposition and archiving.

Crucially, unmerged data collected by the rotation method can preserve instrumental metadata about the image number and the detector position at which each diffraction spot was located and integrated, providing a broader decision-making scope over the way it is incorporated into the scaling and merging process. This opens a wide range of possibilities for improving any initially performed

scaling/merging steps and for extraction of further data. We will present examples touching upon the following areas:

1. production of full validated data quality metrics that are often incomplete or inconsistent in deposited merged data;
2. detection of problematic images and image ranges, and remediation by their selective exclusion from scaling/merging;
3. anisotropic diffraction limit analysis (or re-analysis) with STARANISO, if not already performed;
4. extraction of previously unexploited anomalous signal and computation of anomalous difference Fourier maps;
5. "reflection auditing" by tracing outliers detected at the refinement stage back to their unmerged contributors in terms of specific image numbers and detector positions, thus diagnosing ice rings, poor beamstop masks, angular overlaps, etc. ;
6. detection of radiation damage via F_{early} - F_{late} maps; adapting parametrisation to patterns of structural radiation damage.

We are grateful to the PDBx/mmCIF Subgroup on Data Collection and Processing, especially Aaron Brewster, Ezra Peisach, Stephen Burley and David Waterman, for a stimulating collaboration that provided a context for presenting these investigations.

[1] Kleywegt, G.J., Harris, M.R., Zou, J.-Y., Taylor, T.C., Wählby, A. & Jones, T.A. (2004). *Acta Cryst.* **D**60, 2240.
[2] Joosten, R.P., Womack, T., Vriend, G. & Bricogne, G. (2009). *Acta Cryst.* **D**65, 176.

A118-04-230823

imgCIF as a solution for automated processing of raw crystallographic data

J. R. Hester

ANSTO, Locked Bag 2001, NSW 2232, Australia

jxh@ansto.gov.au

Keywords: raw data, FAIR, interoperability

Laboratories and large-scale facilities currently produce a torrent of raw crystallographic data from a variety of bespoke and off-the-shelf instruments. Ideally, arbitrary raw data sets from these instruments could be automatically processed without time-consuming user intervention to determine the appropriate format and instrument setup. Unfortunately, the plethora of experimental geometries and data formats, the lack of a predictable link between DOI and the raw data URL, and the unwieldiness of working with non-local data sets all lead to serious challenges in creating such a hands-off machine-interoperable data ecosystem.

The imgCIF format [1], which was originally envisioned as an archival container for raw data, has been expanded and repurposed to improve automatic interoperability. An imgCIF file may now refer to raw data frames located externally to the imgCIF file, while precisely specifying the geometry of the instrument for each data frame, thus allowing automated raw data processing via an imgCIF file with no manual intervention. This approach relies for its effectiveness on previous work on crystallographic raw data standards: in particular, widespread storage of raw data in either the Crystallographic Binary Format (CBF) [2] or HDF5 [3,4] standards alleviates most issues associated with correctly converting streams of bytes into images, with the imgCIF file then relating the image pixels to laboratory coordinates. The "CheckCIF for raw data" work developed under the auspices of IUCr Journals [5] is a simple example of the automated computation on raw data enabled by such imgCIF files. The current approach is not inherently limited to single-crystal X-ray data from flat detectors, and so, for example, can be used to describe raw powder diffraction data from curved or flat area-detector instruments from both X-ray and neutron sources with no further changes to the imgCIF standard.

A number of limitations are evident for this imgCIF-based approach to raw data. The need to use pointers to data frames that, unlike DOIs, are not guaranteed to be stable over time makes imgCIF files containing raw data pointers somewhat fragile for archival purposes. In addition, the range of raw data frame formats that are defined as accessible via an imgCIF file is currently restricted to that large subset of current files for which support is easy to implement due to simplicity, the availability of cross-platform libraries, or well-specified standards: CBF, HDF5, and SMV. Other raw formats should be converted to one of these formats (typically CBF) when depositing. The utility of this approach is also limited by the recognition of imgCIF files by common data analysis software, and availability of tools to produce imgCIF files; work to create such tools is ongoing [6].

[1] Bernstein, H. J (2006) *International Tables for Crystallography*, Volume G, edited by S. R. Hall and B. McMahon, pp 199-205

[2] Bernstein, H. and Hammersley, A. P. (2006) *International Tables for Crystallography*, Volume G, edited by S. R. Hall and B. McMahon, pp 37-43

[3] The HDF Group (1997-2022) *Hierarchical Data Format, version 5.* https://www.hdfgroup.org/HDF5

[4] Könnecke, M., *et al* (2015) *J. Appl. Cryst.* **48**, 301-305.

[5] Kroon-Batenburg, L. M. J., Helliwell, J. R. & Hester, J. R. (2022). *IUCrData* **7**, x220821

[6] https://github.com/COMCIFS/instrument-geometry-info/tree/main/Tools

The author acknowledges the imgCIF mailing list and the IUCr Journals raw data working group for feedback on this work.

A118-05-230823

Raw Data, metadata and the experimental narrative: Reuse of time-of-flight neutron diffraction data.

M. Guthrie

Oak Ridge National Laboratory, Oak Ridge, TN 37830

Guthriem@ornl.gov

Keywords: Neutron, Time-of-Flight, Data

Modern Time-Of-Flight (TOF) neutron diffractometers, consist of wide angular banks of highly pixilated detectors. The TOF of arriving neutrons, which are emitted in precisely controlled pulses, is proportional to energy and, thus, each pixel resolves energy by precisely recording the arrival time of detected neutrons. At the Spallation Neutron Source at Oak Ridge National Laboratory (ORNL), the resulting raw data sets are recorded in "event mode", consisting of lists containing pixel id, TOF and the absolute time of the generating pulse for every neutron detection event. In parallel to the neutron events, raw data sets also contain a complete set of metadata including both experimentally logged process values and a full mathematical description of the instrument. The data are stored according to the nexus standard [ref]. The ORNL Neutron facilities follow a principle of hosting and persists all raw data, which are owned by the experimental team and can be made openly accessible at their request.

However, in order that the raw data to be compatible with FAIR principles, they must be linked with calibration data and the calibration parameters derived from these. Of equal importance is standardized data-reduction procedures and persistence of the parameters these use. The latter is particularly pertinent for TOF diffraction for two main reasons. Firstly, the data set contains simultaneous measurement of volumes of reciprocal space that can be integrated and reintegrated via various schemes (often exchanging counting statistics for diffraction resolution and range). Secondly, wavelength-dependent attenuation corrections can be complicated and use algorithms that continue to evolve with time. Thus, details of the entire reduction workflow must also be captured both for provenance and to allow future re-processing with algorithms that may improve over time.

A last, critical component of the data generation is something that may be called the "experimental narrative". This is e flow of reactive decision making and responsive, real-time adjustment or optimization of the instrumentation that forms the context of otherwise adjacent datasets in the catalogue. Often, by nature of experimental science, where the answers are not known a priori, the extraction of analytic conclusions – by human or machine actors – is impossible without this accompanying information. In this presentation, I will highlight some approaches that are employed in the ORNL Neutron Facilities and discuss some opportunities for future improvements of these.

A118-06-230823

80 Years of the Powder Diffraction File™ (PDF®): A Database Perspective

S. Kabekkodu and T. Blanton

International Centre for Diffraction Data 12 Campus Blvd, Newtown Square, PA19073, USA
Kabekkodu@icdd.com

Keywords: Crystallographic database, Powder Diffraction, Raw Data Archival, Phase Identification,

Crystallographic databases play a vital role in materials research, influencing materials development and providing a reference for materials characterization. Design, data curation, and data management are all critical factors in developing a successful and useful database.
The International Centre for Diffraction Data (ICDD®) Powder Diffraction File (PDF) is a powerful database for materials characterization that has been used extensively by the scientific community. Starting with 1000 entries on printed cards in 1941, the database has grown to contain over 1 million unique material data sets. The Powder Diffraction File has a wealth of information that a materials scientist can take advantage of for materials identification, characterization, computation and design. The Powder Diffraction File in Relational Database (RDB) format contains extensive chemical, physical, bibliographic and crystallographic data including atomic coordinates enabling characterization and computational analysis.

Proper database structure, data validations and phase-type classifications are crucial in making any database useful and reliable. While using a database, it is important to know the quality of the crystal structure, diffraction pattern data and any data field of interest found in the database. With the varying quality of published data in the literature, the PDF database editorial review processes require rigorous data evaluation methods to define data based on its quality.

This presentation will focus on various aspects of data archival, curation and classifications. The current progress and challenges in archiving raw powder patterns for the future reusability will be covered in detail.

DAY 3

Thursday 24 August 2023

Keynote 7

Room 203/204

9.00am – 9.50am

Keynote-07-240823

Structural and biochemical studies of different forms of bacterial-type L-asparaginases, enzymes used as anti-leukemia drugs

Alexander Wlodawer, Jacek Lubkowski

Center for Structural Biology, Center for Cancer Research, National Cancer Institute, Frederick, MD 21702, USA
wlodawer@nih.gov

Keywords: cancer drugs, enzyme mechanism, quaternary structure

Anticancer activity of L-asparaginase (ASNase) has been known for well over half a century [1] and an enzyme produced by *Escherichia coli* (named EcAII) has been a major component in treatment of acute childhood lymphoblastic leukemia (ALL) for over 40 years. It was later joined by ErA from *D. dadantii*. These therapies, however, are often associated with serious side effects. It is not yet certain whether the significant glutaminolytic activity, observed for many ASNases, is responsible for some of the side effects, or conversely whether a possible requirement for such an activity is needed for a successful therapeutic outcome.

Based on their structural features, bacterial-type ASNases can be broadly classified into four subgroups, type I and II, each homologous to their respective enzymes in *E. coli*, extremophilic ASNases (i.e. the enzyme from *H. pylori*), and short-chain asparaginases, like ASNase from *R. rubrum* [2,3]. Enzymes from the first three categories contain a polypeptide chain consisting of over 300 amino acids organized in two topological domains, sometimes accompanied by an additional domain, and form homotetramers assembled of two "tight" dimers. These enzymes, often called bacterial-type ASNases, have been also identified in archaea or eukarya. Very poorly characterized short-chain ASNases contain polypeptides forming only a single topological domain corresponding to the N-terminal fragment of more typical ASNases, but the functional form of these enzymes is also a tetramer [3]. Although over 110 structural models of ASNases have been deposited in the Protein Data Bank during the last 30 years [2], an agreement on the enzymatic mechanism of these enzymes has been slow to be reached. Based on results of multipronged studies of type I and II ASNases, we were able to show unequivocally that substrate hydrolysis follows the doubledisplacement (ping-pong) mechanism, with a specific Thr residue being the primary nucleophile [4]. All ASNases share common active sites that are quite distinct compared to their counterparts in other hydrolases. Residues from both protomers forming a tight dimer contribute to the active site pocket. A motif of three residues, Asp-Lys-Thr, reminiscent of the 'catalytic triad' in serine proteases, is present in all bacterial-type ASNases. The threonine residue from this motif, however, does not act as the primary nucleophile. That role is played by another threonine side chain, placed on the opposite side of the substrate molecule and not directly accompanied by a general base. Activation of this threonine is provided by a distant motif of two carboxylate groups (a proton sink) that is formed only after binding of a substrate molecule. The process is mediated by a series of well-positioned hydroxyl groups, contributed primarily by water molecules. Also, the 'oxyanion hole', a motif observed in all hydrolases and responsible for stabilization of an anionic tetrahedral intermediate, is unique in L-asparaginases, as it incorporates an invariant water molecule.

We have shown that type I ASNase may be active in a dimeric form [5]. Similar determination is currently not possible for type II ASNases as these enzymes exist exclusively as tetramers even at low nanomolar concentrations. The molecular basis of other important properties of these enzymes, such as their substrate specificity, are still being evaluated. Results of structural and mechanistic studies of L-asparaginases are being utilized in efforts to improve the clinical properties of this important anticancer drug.

[1] Broome, J. D. (1961). *Nature* **191**, 1114.
[2] Lubkowski, J. & Wlodawer, A. (2021). *FEBS J.*, **288**, 5786.
[3] Dobryakova N. V., Zhdanov D. D., Sokolov N. N., Aleksandrova S. S., Pokrovskaya, M. V. & Kudryashova, E. V. (2022) *Pharmaceuticals* **15**, 406.
[4] Lubkowski, J., Vanegas, J., Chan, W.-K., Lorenzi, P. L., Weinstein, J. N., Sukharev, S., Fushman, D., Rempe, S., Anishkin, A. & Wlodawer, A. (2021) *Biochemistry* **59**, 1927.
[5] Strzelczyk, P., Zhang, D., Alexandratos, J., Piszczek, G. Wlodawer, A. & Lubkowski, J. (2022) *FEBS J.*, doi: 10.1111/febs.16635

This project was funded by the Intramural Research Program of the NIH, National Cancer Institute.

Keynote 8
Room 210/211
9.00am – 9.50am

Keynote–08 –240823

Exploring energy landscapes of molecular crystals for functional materials discovery

G. M. Day

School of Chemistry, University of Southampton, Southampton, United Kingdom

Email of communicating g.m.day@soton.ac.uk

Keywords: crystal structure prediction, computational chemistry, Keyword 3

This lecture explores the application of crystal structure prediction (CSP) methods to the inverse design of molecular materials with targeted properties. There has been impressive recent progress in computational methods for predicting crystal structures from first principles, making use of efficient methods for exploring energy landscapes coupled with accurate evaluations of the relative energies of computer-generated crystal structures. For a property of interest that is dependent on how molecules are arranged in their crystal structure, how do we make the best use of CSP to identify the most promising molecules to deliver the desired property? Our goal is to build a computational framework that integrates structure prediction, property prediction and methods to explore the chemical space of possible molecules [1]. We are also developing how these computational methods will interact with automation in the materials chemistry lab, where promising molecules are screened to realise interesting predicted structures [2]. Example studies will be used to illustrate the challenges of developing this computational framework, including the automation of large-scale CSP, ranking of molecules based on predicted energy-structure-function (ESF) maps [3] and developing advanced methods for identifying the most likely observable crystal structures from computed crystal structure landscapes [4].

[1] Cheng, C. Y. & Day, G. M. (2020), *Chemical Science*, **11**, 4922.

[2] Cui, P., McMahon, D. P., Spackman, P. R., Alston, B. M., Little, M. A., Day, G. M. and Cooper, A. I. (2019), *Chemical Science*, **10**, 9988.

[3] Pulido, A., Chen, L., Kaczorowski, T., Holden, D., Little, M. A., Chong, S. Y., Slater, B. J., McMahon, D. P., Bonillo, B., Stackhouse, C., Stephenson, A., Kane, C. M., Clowes, R., Hasell, T., Cooper, A. I. and Day, G. M. (2017), *Nature*, **543**, 657

[4] Yang, S. & Day, G. M. (2022), *Communications Chemistry*, **5**, 86.

Keynote 9
Room 212/213
9.00am – 9.50am

Keynote–09 –240823

Topological textures in frustrated magnetic materials

O. Zaharko

Laboratory for Neutron Scattering and Imaging, Paul Scherrer Institut, Villigen PSI Switzerland

oksana.zaharko@psi.ch

Keywords: magnetic order, nontrivial topology, frustration

The concept of topology applied to solid state physics and chemistry gives new perspectives for connecting symmetry, electronic structure and physical properties of materials. The discovery of magnetic skyrmions, topologically protected quasiparticle-like swirls of spins, stimulated the vast amount of ongoing work on skyrmion-hosting crystals, the most well-known being: chiral (MnSi, Cu_2OSeO_3), polar (GaV_4S_8, $VOSe_2O_5$, CeAlGe) and centrosymmetric (Gd_2PdSi_3, $SrFeO_3$) materials. Theoretical developments have identified the antisymmetric exchange, magnetic anisotropy, mediation by itinerant electrons and geometrical frustration as the dominant factors promoting such topologically nontrivial magnetic states. The progress in the field allows us to understand the stability and emergent properties of these states paving a way for future new technology using skyrmions as magnetic information carriers.

Since a number of excellent reviews are available [1-3], I shall focus on my own perspective of the field and highlight our findings in the spinel $MnSc_2S_4$. This this system magnetic frustration and magnetic anisotropy give rise to an exotic multi-k fractional antiferromagnetic skyrmion crystal, which we revealed for the first time using neutron scattering experiments and Monte-Carlo modelling [4-6].

[1] Batista, Ch. D., Lin, S.-Z. & Hayami, S. (2016). *Rep. Prog. Phys.* **79**, 084504.

[2] Tokura, Y. & Kanazawa, N. (2021). *Chemical Reviews*, **121**, 2857.

[3] Hayami, S. & Motome, Y. (2021). *J. Phys.: Condens. Matter*, **33**, 443001.

[4] Rosales, H. D., Gómez Albarracìn, F. A., Guratinder, K., Tsurkan, V., Prodan, L., Ressouche, E., & Zaharko, O. (2022). *Phys. Rev. B*, **105**, 224402.

[5] Gao, S., Rosales, H. D., Gómez Albarracìn, F. A., Tsurkan, V., Guratinder, K., Fennell T., Steffens, P., Boehm, M., Cermak, P., Schneidewind, A., Ressouche , E., Cabra, D. C., Rüegg, Ch. & Zaharko, O. (2020). *Nature*, **586**, 37.

[6] Gao, S., Zaharko, O., Tsurkan, V., Su, Y., White, J. S., Tucker, G. S., Roessli, B., Bourdarot, F., Sibille, R., Chernyshov, D., Fennell T., Loidl, A. & Rüegg, Ch. (2018). *Nature Physics*, **13**, 157.

I thank all my collaborators for their participation in the presented work. This work was supported by the Swiss National Science Foundation, the Deutsche Forschungsgemeinschaft, CONICET and SECyT.

Keynote 10
Room 203/204
10.20am – 11.10am

Keynote–10 –240823

Exploring chemical function in structurally disordered systems

Daniel T Bowron

ISIS Neutron and Muon Source, UKRI-STFC Rutherford Appleton Laboratory, Chilton, Didcot, OX11 0QX

daniel.bowron@stfc.ac.uk

Keywords: Neutron scattering, X-ray spectroscopy, Liquids and complex systems

Over the past decade, the inexorable trends in the exploitation of structurally disordered systems for chemical synthesis and action, have highlighted an increasing need for analytical methods that can provide a holistic view of atomic and molecular structure. Atomistic models driven for consistency with diffraction data [1] have proven to be a powerful window into this world, and particularly when enhanced via reference to complementary information drawn from other experimental probes such as X-ray absorption spectroscopy or small angle scattering. In this presentation I will outline the basis of these methods and illustrate their application to questions in chemical science on length scales ranging from the atomic and molecular, to the chemically engineered nanoscale. Examples will include investigations of chemical speciation and interactions [2], nanoparticle growth and templating [3], and molecular adsorption [4], as well as addressing questions such as "How much disorder is too much disorder?" or "What kind of influence can a support matrix have on chemical or physico-chemical outcomes?". The presentation will conclude with a few thoughts and remarks on the new directions these techniques are taking, and the challenges that are driving their evolution.

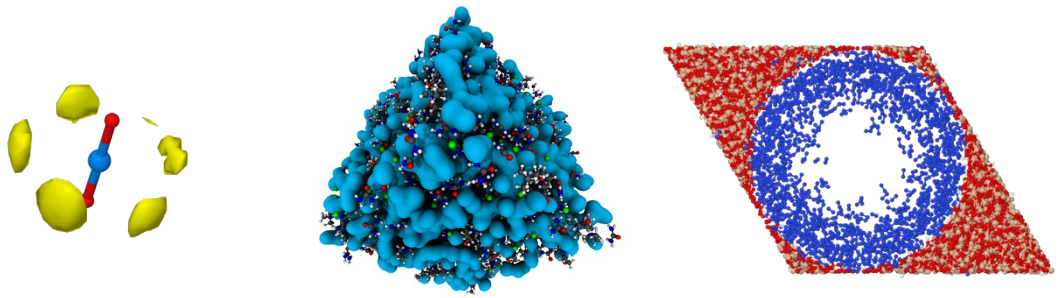

Figure 1. Examples of structurally disordered systems characterised by refinement against diffraction data, from left to right (i) the structure of the UO_2^{2+} aqua-ion [2], (ii) the structure of a hydrated deep eutectic solvent [3], and (iii) the structure of liquid nitrogen confined with MCM-41 silica [4].

[1] *Experimentally consistent atomistic modelling of bulk and local structure in liquids and disordered materials by empirical potential structure refinement.* Daniel T. Bowron, *Pure Appl. Chem.* **80** 1211 (2008)

[2] *Insights into the solution structure of the hydrated uranyl ion from neutron scattering and EXAFS experiments.* Samuel J. Edwards, Daniel T. Bowron and Robert J. Baker, *Dalton Trans.* **51**, 13631 (2022)

[3] *Structural evolution of iron forming iron-oxide in a deep eutectic-solvothermal reaction*. Oliver S. Hammond, Ria S. Atri, Daniel T. Bowron, Liliana de Campo, Sofia Diaz-Moreno, Luke L. Keenan, James Doutch, Salvador Eslava and Karen J. Edler, *Nanoscale* **13** 1723 (2021)

[4] *Adsorption of simple gases into the porous glass MCM-41*. Alan K. Soper and Daniel T. Bowron, *J. Chem. Phys.* **154** 184503 (2021)

Keynote 11
Room 210/211
9.00am – 9.50am

Keynote–11 –240823

Persistence of atoms in molecules: from wavefunctions to open quantum systems to electron densities

A. Martín Pendás.

Dept. Química Física y Analítca. Universidad de Oviedo. Spain

ampendas@uniovi.es

Keywords: Quantum Crystallography, Quantum Chemical Topology, Chemical Bonding

Chemists understand nature in terms of atoms that interact with each other to form aggregates, be them isolated molecules or extended solids. Basic to chemical taxonomy is the concept of atomic transferability: atoms or slightly larger functional groups are found to maintain their individuality upon interaction with other moieties, endowing them with specific properties and characteristic reactivities. Since general quantum mechanical states are intrinsically non-separable, recovering the atom-in-the-molecule (AIM) from basic theory is not easy. In Quantum Chemical Topology (QCT) [1], arguably one of the most successful approaches to this problem to date, the electron density scalar field is used to induce a topology in R^3 that results in an atomic partition of real space. These AIMs are accessible both from theory and experiment [2], and have contributed to obtain a wealth of chemically relevant information over the years [3].

However, in the absence of an exact density functional, the one-electron density scalar is just a shadow of the full N-electron underlying reality. Access to the energy, for instance, requires the two-particle density [4], and other relevant chemical objects depend on further-order reduced density matrices. A first proposal to unveil to what extent an atom-in-a-molecule persists as a full N-electron object comes from considering AIMs as open quantum subsystems [5]. This approach has already demonstrated how important understanding the non-constancy of the electron number in an AIM is. New evidence of the persistence of the full electronic structure of atoms in molecules is also accumulating from the study of the 3N dimensional global and local maxima of the square of the wavefunction [6]. This lecture will provide a tour showing how the final computed or measured electron densities emerge from the N-electron behavior by examining a set of selected examples and problems.

[1] Bader, R. F. W. (1990). *Atoms in Molecules: A Quantum Theory.* Oxford: Clarendon Press.

[2] Koritsansky, T. S. & Coppens, P. (2001). Chem. Rev. **101**, 1583.

[3] Gatti, C. & Macchi, P. (2010). *Modern Charge Density Analyses*. Berlin: Springer.

[4] Martín Pendás, A., Blanco, M. A. & Francisco, E. (2005). *J. Chem. Theory Comput*. **1**, 1096.

[5] Martín Pendás, A. & Francisco, E. (2019). *J. Chem. Theory Comput*. **15**, 1097.

[6] Menéndez-Herrero, M., Munárriz, J., Franciso, E. & Martín Pendás, A. (2022). *J. Chem. Phys.* **156**, 164103

Keynote 12
Room 212/213
9.00am – 9.50am

A001 and A002 Crystallographic Approaches to Study Cultural Heritage and Artists Materials and their Spontaneous Degradation

Room 204

1.10pm - 3.30pm

A001/A002-01-240823

Combining microscopic and macroscopic X-ray fluorescence and X-ray powder diffraction mapping for highly specific imaging of degradation phenomena in historical paintings

K. Janssens,[+,*] F. Vanmeert,[+] St. De Meyer,[+] E. Avranovich Clerici[+] and K. Keune[*]

[+] *Dept. of Physics, University of Antwerp, Groenenborgerlaan 171, B-2020 Antwerp, Belgium;*

** Rijksmuseum Amsterdam, Museumstraat 1, The Netherlands*

koen.janssens@uantwerpen.be

Keywords: Cultural Heritage, paintings degradation, X-ray powder diffraction

Cultural heritage (CH) artefacts such as paintings, stained glass windows and (illuminated) manuscripts are examples of complex macroscopic objects consisting of a multitude of different materials, in close proximity to or in intimate contact with one another. Given sufficient time and a number of external stimuli (such as impinging UV and visual light, variable relative levels of humidity or of reactive volatile species from the ambient atmosphere) these react with one another and form secondary products. When such spontaneous chemical reactions negatively influence the mechanical properties of the artefact (or part thereof) at the macro-level or significantly change one of its relevant properties (color, surface texture, …), they become noticeable. Understanding the mechanisms and principal factors that trigger or determine the speed of these alteration reactions is very relevant for both preventive and corrective art conservation.

To gain such insights, employing a combination of analytical methods that allow to extract information on the chemical constituents of the degraded surface of CH artefacts at different length scales and with relevant chemical specificity, has been proved to be very effective. Preferably (but not all) such methods are non-invasive, i.e. do not cause damage to the CH artefacts being studied. At the macro-scale, i.e., the length scale of the CH artefacts in their totality (cm to m), various forms of hyperspectral imaging can be used. Macroscopic X-ray fluorescence (MA-XRF) and diffraction (MA-XRPD) are non-invasive imaging methods with intermediate to high chemical specificity that are very suitable for examining the surface of CH artefacts, either to obtain information on the original materials used to construct the artefacts or on any surface alteration that took place during the artefact's history. MA-XRF and MA-XRPD scanners can be constructed using X-ray tube sources.

Large scale particle accelerators such as synchrotron facilities are able to generate X-ray beams of sub-micrometer dimensions. With these, it is possible to study heritage materials at the nanometer to micrometer level. Methods such as (sub)microscopic X-ray fluorescence, X-ray absorption spectroscopy and X-ray diffraction, either used sequentially or simultaneously, allow to study minute samples of CH artefacts, complementing the information obtained by macro-level investigations and allowing to formulate hypotheses on the manufacturing technology the artefacts and/or degradation mechanisms that have modified their surface.

As a first example of the combined use of micro- and macro-level chemical imaging methods, (a) the study of metal-based inks used to write Egyptian papyri. Red and black inks inscribed on 12 ancient Egyptian papyrus fragments belonging to the Papyrus Carlsberg Collection (Copenhagen), deriving from the Tebtunis temple library in Fayum, Egypt were analyzed using synchrotron-based 2D elemental and phase mapping. From the XRF maps, information can be extracted on the ingredients used to prepare the inks while XRD allowed to identify the secondary Pb compounds that formed in situ.

As a second example, the degradation of the pigments present on the ceiling of Upper Basilica of St. Francis in Assisi, Italy will be discussed. Part of these 13th century frescos, painted by Cimabue, Giotto and their studios, collapsed during an earthquake in 1997, making unique sample materials available for analysis. More specifically, the use of micro- and macrolevel XRF and XRPD will be discussed to study the degradation/blackening of pigments such as lead white, vermilion and azurite. As common triggering factor for the alteration over a period of ca 700 years, the presence of oxidizing Cl-compounds is strongly suspected.

A third example involves the use of micro- and macro-level XRF and XRPD for the study of the pigments and their degradation behavior in Rembrandt's masterpiece 'The Nightwatch', a large oil on canvas from the 17th C owned by the City of Amsterdam that is part of the collection of the Rijksmuseum. Especially the MA-XPRD maps of the white (lead-rich) areas of the paint reveals information on the manner in which Rembrandt intentionally altered the rheological properties of the paint by adding specific chemical agents to it.

The authors would like to acknowledge the help and assistance obtained from the scientific staff of the various synchrotron facilities that were employed in the above research: ESRF (beamline ID13 and ID21), PETRA-III (beamline P06) and SOLEIL (PUMA Beamline).

A001/A002-02-240823

New robotic tools for multimodal, non-destructive analysis and characterization of 2D and 3D objects.

M. Kotrly1, J. Uher2, I. Turkova1

Institute of Criminalistics, Praha, Czech Republic,
Radalytica a.s., Praha, Czech Republic

marek.kotrly@pcr.cz

Keywords: forensic analysis, robotic multimodal and non-destructive analysis, material characterization

The forensic field has until now been missing more versatile equipment for non-destructive characterization, analysis and inspection of 2D and 3D objects. Also, the need for increasingly frequent analysis of art forgeries, where non-destructive analysis is required, at least in the first step, is calling for a multimodal solution. A prototype device for robotic analysis, imaging and mapping of 3D objects is being developed and tested to be used in these areas. The system´s principle is integration of imaging and analytical technologies onto six-axis robotic arms which allow wide flexibility range concerning the sample size or shape. The system allows non-destructive examination of wide spectrum of samples with complicated curvatures. The new generation of X-ray imaging detectors provides a high picture quality with a spatial resolution level in the micrometre range in 2D or 3D imaging. The basic version of the robotic scanner allows transmission X-ray imaging and mapping of the individual photons with high sensitivity and resolution detectors. These detectors are the result of an intensive international cooperation led by the CERN laboratory in Geneva. The particular used type of imaging detectors allows to measure X-ray wave lengths [1]. From the changes in the X-rays spectrum after it has gone through the sample, it is possible to presume the elemental composition of the examined object. The key parts of the scanner are two robotic stations. One robot carries an X-ray tube whose emission spot size range is 8 – 40 μm, and the operating voltage range is 10 – 130 kV, and the other one holds a photon-counting imaging detector of the Widepix MPX3 family [2]. Robots can move and rotate freely about the sample in a precisely synchronized movement. It provides almost absolute flexibility of viewing angles. The very high sensitivity, spatial resolution, and dynamic range of the used detectors enable us to push the X-ray image quality to its physical limits. System is equipped with accurate geometrical calibrations that allow positioning both robots precisely yet arbitrarily. Therefore, the robots can be moved to different locations during on-site inspections. Differences in spectrum changes then reflect in the resultant image in the form of false colours. Another extension modality is XRD phase mapping which exploits properties the Timepix3 spectral imaging detector which records the position and energy of every detected photon as well as the time of detection. Regarding these properties, a monochromator can be left out from the XRD device [3]. The construction fundamentally simplifies the XRD device and allows integration with robots. The robotic scanner further allows scanning and mapping of crystallographic properties of the whole examined object on surface. This information is further combined with the XRF elemental mapping of the whole object. There exist many possibilities how to combine the XRF data with transmission maps and X-ray imaging data – a robotic scanner measures all analytical modalities in a common reference system. The system is supplemented with other modalities which allow to obtain more analytical data – VNIR, SWIR and the UV modules. The use of this information is very wide. The individual image layers can be switched on and arbitrarily combined with the obtained maps.

The system will provide a huge amount of data, using Artificial Intelligence (AI) for exact and error-free evaluation of big data is being prepared. Exact data evaluation, anomaly detection and match design are becoming beyond the capabilities of the operator/expert (e.g. to detect tiny differences between the original and the suspect trace). The application of customised AI software for real-time processing of datasets and anomaly finding in the form of new technological approaches is planned.

1 Ghita M., Uher J., Boháčová J., Kadeřábek R. (2022): Arbitrary Path CT by Multi-Robot Imaging Platform (RadalyX). *11th Conference on Industrial Computed Tomography, Wels, Austria.*
2 ADVAPIXTPX3: Datasheet [online], *https://advacam.com/wp-content/uploads/2022/03/APXT3M-Xxx201030-AdvaPIX-TPX3-Datasheet-2020-11-11.pdf*
3 The X-ray diffraction (XRD) with Timepix3 detector and polychromatic beam. Hawkeye: Spectral imaging [online], *https://hawkeyesi.com/news/the-x-ray-diffraction-xrd-with-timepix3-detector-and-polychromatic-beam/*

This work has been supported by the project of the Ministry of the Interior of the Czech Republic: Advanced robotic multimodal system for non-destructive forensic material analysis (VB01000046).

A001/A002-03-24-08-23

The tin content of lead inclusions in ancient tin-bronze artefacts: A time-dependent process?

G. Artioli[1], A. Fontanari[1], M. Etter[2], H. Jeppesen[2], S. Shilstein[3], S. Shalev[3]

[1]Geosciences, UNIPD, Padova, Italy, [2]DESY, FS-PETRA-D, Hamburg, Germany, [3]Weizmann Institute of Science, Rehovot, Israel
E-mail: gilberto.artioli@unipd.it

Keywords: Archaeometallurgy, Sn-bronze, Pb inclusions, Synchrotron, XRD

Lead was a common alloying element in the production of bronze artefacts in antiquity, especially large statues, to impart fluidity to the casting process [1]. As lead is not forming a solid solution with pure Cu or with the Sn-Cu alloy phases, it is normally observed in recent and ancient bronze artefacts as globular particles in interstitial positions among the Sn-bronze crystals (normally the α-phase) in the matrix [2-3], as the last crystallizing phase (at 326 °C) during the cooling process of the Cu-Sn-Pb ternary melt.

Recently, Shilstein et al. [4] suggested that Pb inclusions in leaded tin-bronze actually contain a measurable amount of Sn, and that the time dependence of the incorporation of Sn in the lead inclusions could actually be a viable parameter to detect modern materials. The process implies that Pb inclusions in recent Sn-bronze artefacts are actually a metastable solid solution of Pb-Sn containing about 3 % atomic Sn, whereas in ancient artefacts unmixing processes and diffusion of Sn from the micro- and nano-inclusions of Pb to the matrix occur, so that the Pb inclusions contain a substantially lower amount of Sn.

The possibility of reliably assessing the Sn content in the lead inclusions relies on the accurate measurement of the lattice parameter of the phase in the Pb-Sn solid solution, since for low Sn values it follows closely Vegard's law [5], as shown in Fig. 1. Here, the literature on the subject is critically reviewed, and several new data on modern and ancient samples are discussed in order to verify the applicability of the method to the detection of modern artwork. The issues involved include the time dependence of the Sn diffusion process, the role played by the Sn content in the starting ternary melt, the limits of accuracy and precision of the lattice parameter measurements, and the potential effect of re-activation of the Sn diffusion by thermal heating.

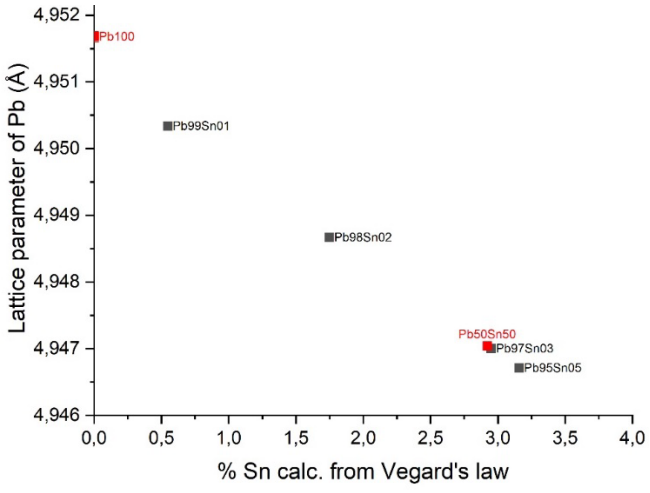

Figure 1. Linear dependence of the lattice parameters of the Pb-Sn solid solution phases in the low-Sn region.

[1] Ruusila, V., Nyysso, T., Kallio, M., Vuorinen, P., Lehtovaara, A., Valtonen, K., Kuokkala, V.T. (2013). *The effect of microstructure and lead content on the tribological properties of bearing alloys,* J. Engineering Tribology, **227**, 878
[2] Scott, D.A. (1992). *Metallography and microstructure in ancient and historic metals.* Los Angeles: Getty publications.
[3] Scott, D.A. (2002). *Copper and bronze in art: corrosion, colorants, conservation.* Los Angeles: Getty publications.
[4] Shilstein, S., Berner, A., Feldman, Y., Shalev, S., Rosenberg, Yu. (2019). *Distinguishability between ancient and modern leaded tin bronzes by the composition of their lead inclusions,* STAR: Science & Technology of Archaeological Research, **5**, 29
[5] Fecht, H.J., Perepezko, J.H. (1989). *Metastable Phase Equilibria in the Lead-Tin Alloy System: Part I. Experimental*, Metallurgical Transactions A, **20**, 785

The Jomon Pottery from Fukushima 5000 years ago

T. Kamiyama1, K. Kobayashi2, M. Kasai3, D. S. Adipranoto4, T. Ishigaki4, E. Sakagami5, T. Shinmen5, S. Ninomiya5

A. China Spallation Neutron Source, Institute of High Energy Physics, CAS, Dongguan, 523803, China 2 Faculty of Letters, Chuo University, Hachioji, Tokyo, 192-0393, Japan
Research Institute of Cultual Properties, Teikyo University, Fuefuki, Yamanashi, 406-0032, Japan
1 Frontier Research Center for Applied Atomic Sciences, Ibaraki University, Tokai, Ibaraki 319-1106, Japan
Tokyo Gakugei University, Koganei, Tokyo, 184-8501
kamiyama@ihep.ac.cn

Keywords: Jomon pottery, neutron diffraction, Cord-marked earthenware

Cord-marked earthenware potteries are commonly seen in the early stage of the settled-lifestyle cultures in the world. In Japan, the potteries are called Jomon potteries, and the era is called Jomon era. The Jomon era is characterized by the fact that the society was maintained over 10,000, while other world began agriculture, created a disparity between upper and lower status and formed nations in the period. The styles of the Jomon potteries changed in the long period; some of them known with flames-shaped ornamentation have received high artistic recognition, and have been stimulating modern artists. Why did the Jomon era last so long? How have societies changed and people and materials exchanged over the past 10,000 years, and how has technology and art developed? We will challenge such questions using crystallographic techniques.

Figure 1
A Jomon pottery with flames-shaped ornamentation (photo by Kamiyama on 2008).

Jomon pottery is produced by open burning. Therefore, the uniformity of the sample is poor, and X-ray diffraction is less reliable, even with repeated measurements. On the other hand, since neutron diffraction has a large penetrating power, the volume to be measured at one time is large and the reproducibility is found to be high. Therefore, it is expected to obtain much reliable information for the possible place of production, firing temperature, burial conditions and the state of preservation. On the other hand, earthenware is a heterogeneous mixture of various minerals, so analysis is not easy.

In our study, we accumulated over hundreds of neutron data as well as fluorescent X-ray analysis, mineralogical analysis by microscopy, and neutron diffraction of standard rocks. Quantitative analysis of mineral crystals in pottery was performed by comparing with neutron diffraction patterns.

Among the pottery materials measured so far, we report the preliminary results of the middle Jomon (5,000 years ago) pottery fragments obtained during excavations at the Ide Uenohara site in Naraha-cho, Fukushima conducted between from 2006 and 2007 by Kobayashi *et al*. This area has been inaccessible since the 2011 earthquake and the Fukushima Daiichi nuclear power plant accident. The plagioclase in the KEK93 pottery fragment is close to that in granodiorite (different from andesite, basalt and gabbro). The Abukuma Mountains area is presumed to be a strong candidate for raw material production.

The pottery firing temperature was estimated by high-temperature neutron diffraction as well as preliminary X-ray measurements; high-temperature neutron experiments showed a change at about 600°, suggesting that the pottery was fired at a lower temperature than previously expected.

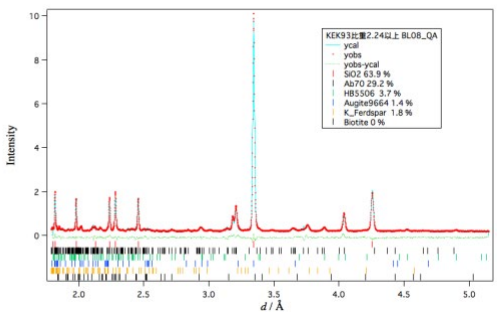

Figure 2
(left) Neutron diffraction experiment on pottery fragments. (right) Neutron diffraction pattern of a powdered sample with a density larger than 2.24.

A001/A002-05-240823

Teaching crystallography through beauty of symmetries of Algerian old buildings, carpets and jewels.

Pr N. Benali-Cherif

Algerian Academy of Sciences and Technologies (AAST), Algiers, 16000-Algeria.

& President of University of Jijel, cité Oued Aissa, BP 98 Jijel, 18000 Algeria.

benalicherif@hotmail.com

Keywords: Symmetries, crystallography, Algerian heritage

Symmetries are present in the cultural heritage of all regions of Algeria, this largest country in the African continent. We meet in the *Aures* region (south-east of Algeria) women with symmetrical tattoos, wearing silver jewellery of a fine and beautiful symmetry and weaving the wonderful Babar carpets, made of sheep's wool: the most beautiful carpets of Algeria [1].

In the north of the country, the *Kabylie* region contains treasures of pottery, coloured dresses and Ait Yenni's jewellery in sterling silver where symmetry is omnipresent. The Sahara, north, west, east and major cities of Algeria like Algiers, Constantine and Oran are adorned by symmetrical designs like that observed in crystals and their atomic stacking.

This Algerian heritage has crossed the centuries, transmitted without the slightest wrinkle from generation to generation, embellished and enriched at times and sometimes destroyed by the passage of the Romans, Arabic, Turkish and French occupations and civilizations.

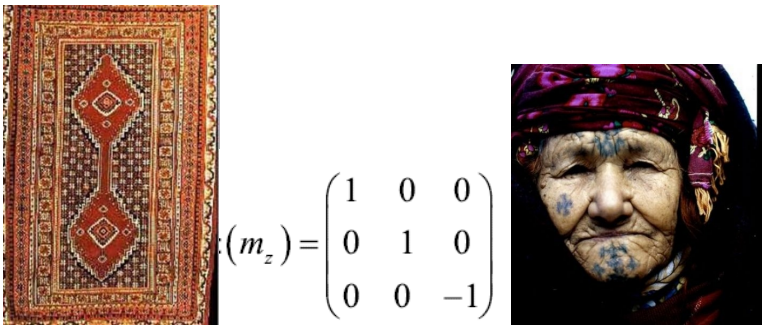

Fig1. Very symmetrical carpet and crystallography, by an old illeterate woman

We use this cultural and artistic heritage to make it easier for beginning students to learn and understand the geometrical operations of rotation-reflection-translation and enable them to 'see' and manipulate different elements of symmetry encountered in crystallography.

[1] Benali-Cherif N.,*Beauty of symmetries in carpet of Babar (Khenchela-Algeria),* (2009). ActaCryst. **A65**, s 193

[2] Aboufadil, A., *La cristallographie dans l'art ornemental Marocain*, Doctorat thesis, Cadi Ayyad University, Morocco (2016).

A001/A002-05-240823

Metallurgy in Antiquity: a new insight with neutrons

F. Salvemini

Australia's Nuclear Science and Technology Organisation, New Illawarra Rd, Lucas Heights NSW 2234, Australia

Keywords: Archaeometallurgy, Neutron Techniques, Non-invasive analysis

This paper demonstrates how a non-invasive analytical protocol based on neutron techniques has enabled to shed new light on the diverse technological knowledge acquired within different multi-dimensional cultural contests in the past.

Metallurgy particularly has played a substantial role in the rise of modern civilisation. The techniques of metal working developed in antiquity encompass an understanding or intuition of the properties of materials. The most advanced manufacturing processes can be rediscovered, when the traditional knowledge has faded, by investigating the artefacts that produced: arms and armours, votive items, numismatics objects, etc.

The value of such material documents transmitted to us by our ancestors is incommensurable. Therefore, when examining such samples, their integrity must be preserved so to be pass to future generations, thus prompting the need for a non-invasive analytical protocol. On the other hand, due to the manifold nature of objects of cultural heritage significance, their study requires a trans-disciplinary and multi-technique approach.

Neutron techniques have become a well-established analytical means for the non-invasive investigation of ancient artefacts. The fundamental properties of the neutron — no electric charge, deep penetration power into matter, and interaction with the nucleus of an atom rather than with the diffuse electron cloud —make this sub-atomic particle the ideal probe to characterize compositional and micro-structural properties of the balk of a variety of materials, especially metals.

The most relevant cross-disciplinary studies conducted at the Australian Nuclear Science and Technology Organisation (ANSTO) and undertaken in collaboration with Australian research institutions, universities, and international stakeholders will be showcased.

A017a Enzyme Mechanisms and Regulation

Room 203

1.10pm - 3.30pm

A017a-01-240823

Structural and mechanistic insights in RiPP biosynthesis by a radical SAM enzyme

X. Kubiak1, I. Polsinelli1, L.M.G. Chavas3, C.D Fyfe1, A. Guillot1, L. Fradale1, C. Brewee1, S. Grimaldi4, G. Gerbaud4, A. Thureau2, P. Legrand2, O. Berteau1* & A. Benjdia1

1 Micalis Institute, ChemSyBio, INRAE, AgroParisTech, Université Paris-Saclay, 78350 Jouy-en-Josas, France, 2 Synchrotron SOLEIL, HelioBio group, L'Orme des Merisiers, 91190 Gif sur-Yvette, France, 3 Nagoya University, Nagoya 464-8603, Japan, 4 Aix Marseille Univ, CNRS, BIP, IM2B, IMM, Marseille, France.

Email of communicating Alhosna.Benjdia@inrae.fr

Keywords: radical SAM enzyme, natural product, RiPP

Ribosomally-synthesized and post-translationally modified peptides (RiPPs) form one of the major families of natural products. They have attracted considerable interest because of their involvement in the homeostasis of the human microbiota and their potential to develop innovative antibiotics. In the last decade, radical *S*-adenosyl-L-methionine (SAM) enzymes have been shown to be major biocatalysts installing novel and unprecedented post-translational modifications in RiPPs. However, the mechanisms underpinning this biochemical process are poorly understood and the structural basis remains unknown [1].

Thanks to the development of a novel approach, we succeeded after more than a decade of investigation, in obtaining the first atomic-resolution crystal structures of a radical SAM RiPP-modifying enzyme in complex with its substrate properly positioned in the active site.

Collectively, by combining X-ray crystallography, EPR spectroscopy, SEC-SAXS and biochemical analyses, our study reveals how radical SAM enzymes install post-translational modifications in RiPPs and support a unique enzyme mechanism [2]. Our study also proposes novel approaches to investigate RiPP-modifying enzymes and brings unique perspectives on how radical SAM enzymes interact with RiPPs and catalyze unprecedented post-translational modifications in natural products and antibiotics.

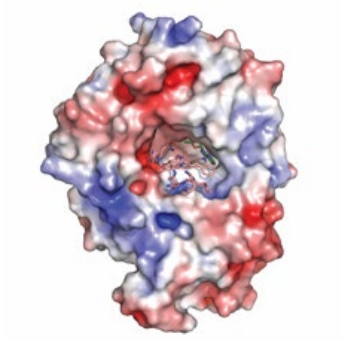

Figure 1. Structure of a radical SAM enzyme in complex with its RiPP substrate.

[1] Benjdia, A. & Berteau, O. (2021) Front Chem **9**, 678068, doi:10.3389/fchem.2021.678068.

[2] Kubiak, X., Polsinelli, I., Chavas, L.M.G., Fyfe, C.D , Guillot, A. , Fradale, L. , Brewee, C. , Grimaldi, S., Gerbaud, G., Thureau, A., Legrand, P. , Berteau O. & Benjdia A. *submitted*

Acknowledgements: This work was supported by the European Research Council (ERC consolidator grant 617053) and ANR (ANR-20-CE44-0005).

A017a-02-240823

Structural studies of voltage sensing phosphatase

Hirotaka Narita[1], Makoto Matsuda[1], Yumiko Hara[1], Eiki Yamashita[1], Yasushi Okamura[2], Atsushi Nakagawa[1]

[1]Institute for Protein Research, Osaka University, 3-2 Yamadaoka, Suita, Osaka 565-0871 Japan, [2]Graduate School of Medicine, Osaka University, 2-2 Yamadaoka, Suita, Osaka 565-0871 Japan

atsushi@protein.osaka-u.ac.jp

Keywords: Membrane protein, Voltage-sensor, Phosphatase

Voltage Sensing Phosphatase (VSP) was initially identified in the ascidian, *Ciona intestinalis*, by systematic genomic survey and has been found to be conserved in the various animal phyla [1, 2]. VSP is a membrane bound enzyme which dephosphorylates phosphatidyl inositol phosphates and its activity is regulated by membrane potential changes. VSP is consisted of two distinct regions; a voltage sensor domain (VSD) and a cytosolic catalytic region (CCR), which is consisted with phosphatase domain (PD) and C2 domain, and these two regions are connected by VSD-PD liner. A voltage sensor domain is embedded in a cell membrane and is consisted of four–helix bundle of which the 4th transmembrane helix (S4) of VSD senses membrane potential with several positively charged residues on the S4 as voltage sensing ion channels, such as voltage–dependent potassium channels (Kv), voltage–dependent sodium channels (Nav) and so on. CCR shares sequence and structural similarities with a tumor suppressor gene product, phosphatase and tensin homolog deleted on chromosome 10 (PTEN). PTEN is a tumor suppressor gene product and its orthologs have been identified in various organisms, such as mammals, birds, reptiles, fish, insects and plants [3]. It is known that its mutations of this gene cause development of many cancers [4]. Despite of high sequence identity between cytoplasmic catalytic region of VSP and PTEN, these enzymes show different substrate specificities; PTEN dephosphorylates phosphatidylinositol 3,4,5–trisphosphate [PtdIns(3,4,5)P3], but VSP dephosphorylates PtdIns(3,4,5)P3 and phosphatidylinositol

4,5-bisphosphate [PtdIns(4,5)P2] [5]. Since PTEN is one of the major proteins of which mutation(s) cause high risks of cancers in human, many atomic structures, including wild–type and mutants, have been determined. However, structure of the complex of PTEN and its substrate (or substrate analogue) have not been reported yet. Atomic structures of the complexes of various substrates of VSP may give useful information on the substrate recognition of these enzymes.

Various mutants of the CCR of *C. intestinalis* have also been determined and regulation mechanism has been discussed [6, 7]. However, the coupling mechanism of membrane potential and enzymatic activity is still unclear, since no structural information of the interaction of these two regions have been known. In addition, atomic structures of VSDs from *C. intestinalis* in various states have been determined using several mutants which stabilized various activation states, and activation mechanism has been proposed based on these structures [8].

We have succeeded to solve the atomic structures of VSP, which contains both VSD and CCR. It suggested the molecular mechanism of membrane voltage-enzymatic activity coupling and substrate recognition.

1 Murata, Y., Iwasaki, H., Sasaki, M., Inaba, K. & Okamura, Y. (2005). *Nature*, **435**, 1239.
2 Okamura, Y., Kawanabe, A. & Kawai, T. (2018). *Physiol. Rev.*, **98**, 2097.
3 Worby, C. A. & Dixon, J. E. (2014). *Annu. Rev. Biochem.*, **83**, 641.
4 Maehama, T. & Dixon, J. E. (2011). *Trends Cell Biol.*, **9**, 125.
5 Iwasaki, H., Murata, Y., Kim, Y., Hossain, M. I., Worby, C. A., Dixon, J. E., McCormack, T., Sasaki, T. & Okamura, Y. (2008). *Proc. Natl. Acad. Sci. USA,* **105**, 7970.
6 Liu, L., Kohout, S. C., Xu, Q., Muller, S., Kimberlin, C. R., Isacoff, E. Y. & Minor, D. L., Jr. (2012). *Nat. Struct. Mol. Biol.*, **19**, 633.
7 Matsuda, M., Takeshita, K., Kurokawa, T., Sakata, S., Suzuki, M., Yamashita, E., Okamura, Y. & Nakagawa, A. (2011). *J. Biol. Chem.*, **286**, 23368.
8 Li, Q., Wanderling, S., Paduch, M., Medovoy, D., Singharoy, A., McGreevy, R., Villalba-Galea, C. A., Hulse, R. E., Roux, B., Schulten, K., Kossiakoff, A. & Perozo, E. (2014). *Nat. Struct. Mol. Biol.*, **21**, 244.

A017a-03-240823

Conformational changes of the HisZG complex revealed by SAXS and SANS with contrast variation

E. J. Parker[1], E. K. Livingstone[2], F. De Pol[1], G. Mittelstädt[1], A. E. Whitten[3], A. P. Duff[3], N. Cowieson[4]

[1]Ferrier Institute, Victoria University of Wellington, Lower Hutt 5010, New Zealand, Institute for Molecular Bioscience, University of Queensland, St Lucia QLD 4072, [2]Australia, Australian Nuclear Science and Technology Organisation, New Illawarra Rd, Lucas Heights, NSW 2234, Australia, [4]Diamond Light Source, Harwell Science & Innovation Campus, Didcot Oxfordshire OX11 0DE, United Kingdom

emily.parker@vuw.ac.nz

Keywords: Small-angle scattering, allosteric regulation, low-resolution structure

Adenosine triphosphate phophoribosyltranferase (ATP-PRT) is an enzyme involved in the first step of histidine biosynthesis in bacteria, archaea, and plants [1]. Both the long ($HisG_L$) and short ($HisG_S$) forms of ATP-PRT are encoded by the *hisG* gene. $HisG_L$ is composed of a catalytic domain, and a regulatory domain, and assembles into a homo-hexamer. HisGS lacks the regulatory domain and assembles into a hetero-octomer with a histidyl-tRNA synthetase paralogue (HisZ).

Allosteric regulation is a mechanism employed by many biosynthetic enzymes [2-3]. $HisG_L$ is one such enzyme, where histidine triggers the regulatory domain to inhibit further biosynthesis. For the shorter form, the interaction of HisZ with $HisG_S$ not only confers allosteric regulation by histidine, but it also enhances catalytic activity of $HisG_S$ [4]. However, the mechanism is not well understood [5-6] and it is something we are attempting to understand in more detail. Here we reveal using small- angle X-ray and small-angle neutron scattering with contrast variation, that catalysis is inhibited by a significant conformation change that occurs upon histidine binding.

We will describe these conformational states in detail, and the structural details of the allosteric inhibition mechanism.

[1] Alifano, P., Fani, R., Lio, P., Lazcano, A., Bazzicalupo, M., Carlomagno, M. S. & Bruni, C. B. (1996) *Microbiol. Rev.*, **60**, 44.
[2] Perica, T., Marsh, J. A., Sousa, F. L., Natan, E., Colwell, L. J., Ahnert, S. E. & Teichmann, S. A. (2012). *Biochem. Soc. Trans.,* **40**, 475.
[3] Motlagh, H. N., Wrabl, J. O., Li, J. & Hilser, V. J. (2014)., *Nature,*
[4] Livingstone, E. K., Mittelstaedt, G., Given, F. M. & Parker, E. J. (2016). *FEBS Lett.,* **590**, 2603.
[5] Sissler, M., Delorme, C., Bond, J., Ehrlich, S. D., Renault, P. & Francklyn, C. (1999). *Proc. Natl. Acad. Sci. U. S. A.,* **96**, 8985.
[6] Bovee, M. L., Champagne, K. S., Demeler, B. & Francklyn, C. S. (2002) *Biochemistry*, **41**, 11838.

A017a-04-240823

Acetohydroxyacid Synthase: Structure, Function, Regulation and Inhibition

Luke W Guddat[1]

School of Chemistry and Molecular Biosciences, The University of Queensland, Brisbane, 4072, Australia

Keywords: branched chain amino acid metabolism, allostery, antifungal

Acetohydroxyacid synthase is the first enzyme in the branched chain amino acid biosynthesis pathway. It has been the target for herbicides since the 1980s. In total, 58 AHAS inhibitors have been developed into commercial products [1]. This enzyme is only found in plants, bacteria and fungi but not in humans, making it an attractive target not only for herbicide development but also for the discovery of novel antibacterial and antifungal agents [1]. Recently, we have used X-ray crystallography and cryo-EM to solve the first structures of fungal and plant AHAS that include both the regulatory and catalytic subunits [2]. As a result, we can explain for the first time the mechanism of allostery and feedback inhibition for this enzyme. We have also investigated the enzyme as a target for the development of new drugs to treat *Candida albicans* infection. We have shown that mice infected with *C. albicans* recover after treatment with a known plant AHAS inhibitor chlorimuronethyl [3]. Furthermore, we have shown that AHAS inhibitors prevent the growth of *C. albicans*, *Candida glabrata*, *Candida parapsilosis*, *Candida auris* and *C. neoformans* in cell susceptibility assays with IC_{50} values as low as 4 nM. In addition, we have determined crystal structures of these compounds in complex with *Candida albicans* AHAS to explain how they bind to the target and to allow for rational structure-based drug discovery. Progress towards the development of AHAS inhibitors as antibacterial and antifungal drugs will be discussed.

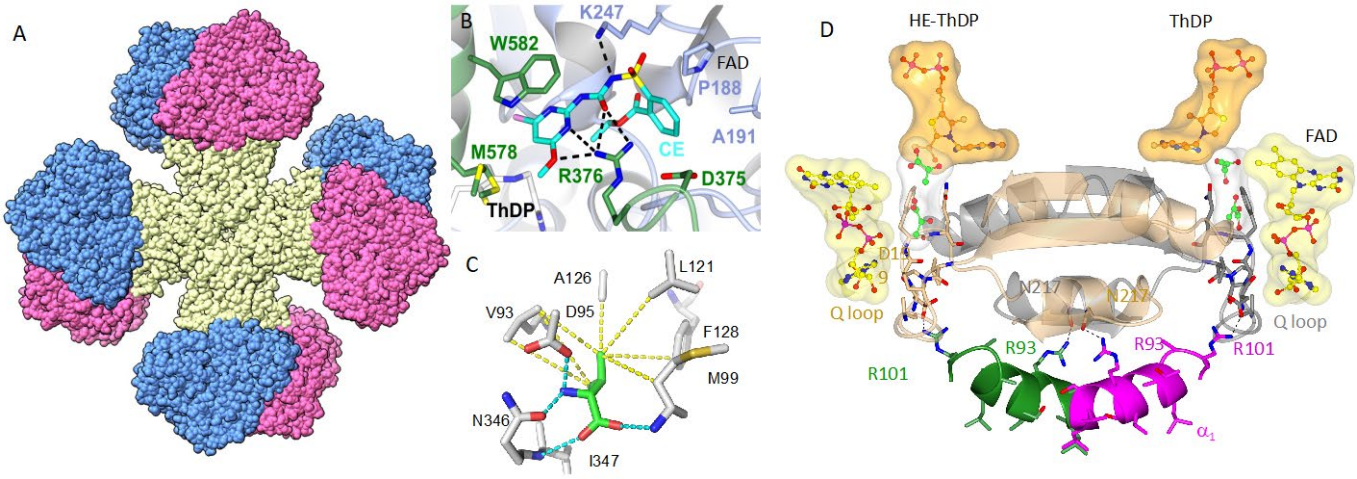

Figure 1. A. Cryo-EM structure of *A.thaliana* AHAS B. The binding of chlorimuronethyl to *C. albicans* AHAS. **C.** The binding of valine to the regulatory subunit of AHAS. **D.** The mechanism for allosteric activation and inhibition of the catalytic subunit by the regulatory subunit of AHAS and by valine.

[1] Garcia, M.D., Nouwens, A., Lonhienne, T.G., Guddat, L.W. (2017) Proc Natl Acad Sci, **114**, E1091-E1100
[2] Lonhienne, T., Low Y. S, Garcia, M., Croll, T., Gao. Y, Wang Q., Brillault, L., Williams, C.M., Fraser, J.A., McGeary, R. P., West, N, Landsberg, M.J., Rao, Z., Schenk, G., Guddat, L.W. (2020) *Nature*, 34, 317-321.
[3] Garcia, M.D., Chua, S.M., Low Y.S, Lee, Y.T., Agnew-Francis, K., Wang J.G., Nouwens A., Lonhienne, T, Williams, C.W., Fraser, J.A., Guddat, L.W. (2019) **115** *Proc Natl Acad Sci* E9649-E9658

A017a-05-240823

Solvent effects of protic ionic liquids on protein structures

Q. Han[1], C. Darmanin[2], T. Ryan[3], C. Drummond[1], T. Greaves[1]

[1]School of Science, RMIT University, Melbourne, Victoria 3000, Australia
[2]La Trobe Institute for Molecular Sciences, La Trobe University, Victoria 3086, Australia
[3] SAXS/WAXS beamline of the Australian synchrotron, ANSTO, Clayton, Victoria 3168, Australia

tamar.greaves@rmit.edu.au

Keywords: SAXS, ionic liquids, protein crystallography

The design of solvents and buffers for use with many biomolecules is currently both very complex and limited in what is available. Currently buffered aqueous salt solutions are used as solvents for proteins, but these do not sufficiently control protein solubility and stability, which adversely affects protein activity, folding-unfolding transitions, aggregation and crystallisation. Therefore, there is a need for new solvents which can control protein and biomolecule solubility and stability.

Protic ionic liquids (PILs) are cost efficient "designer" solvents which can be tailored to have properties suitable for a broad range of applications.[1] These are liquid salts which are typically liquid at room temperature and miscible with water. Certain aqueous PIL solutions have beneficial properties, including stabilising biomolecules, suppressing aggregation and enhancing protein crystal growth. However, there is a lack of understanding about the interactions present, which prevents solvent design for specific protein applications.

Here, I will discuss our ongoing work into designing PIL solvents for proteins, including protein structural changes, activity and identifying specific ionic interactions of PILs, cations and anions, with the protein surface.[2] This also includes developing and adapting characterisation methods for use with proteins in PIL solutions.[3] Recently, we have combined results from Solution SAXS and Protein Crystallography, using the Australian Synchrotron SAXS/WAXS and MX2 beamlines, to obtain a deeper understanding of ionic liquid-protein interactions.[4] In these studies we have used model proteins, with a focus on hen egg white lysozyme.

Specifically, we have identified conformational changes of the protein in solution due to changes in the ionic liquid chemical structure and/or concentrations. We have also identified the ion-binding sites of the ionic liquid solvated cations and anions. From these results we have clearly shown that the anion has significantly more interactions with the protein, and preferentially binds to positively charged and aromatic side chains, whereas few of the cations were identified in the solvation layer. Crystallographic studies using the MX2 beamline on lysozyme crystals grown in the presence of PILs provided insight into which ions are present at the surface and the key amino acids ionically bonded to the PILs which is important for protein stability. These findings will contribute towards being able to produce designer solvents for specific biomolecule applications.

[1] Greaves, T. L., Drummond, C. J. (2008) *Chem. Rev.,* **108**, 206.
[2] Han, Q., Brown, S., Drummond, C. J. (2022) Greaves, T. L., *J. Colloid Interface Sci.,* **608**, 1173.
[3] Han, Q., Binns, J., Zhai, J., Guo, X., Ryan, T. M., Drummond, C. J., Greaves, T. L. (2022) *J. Mol. Liq.,* **15**, 2430.
[4] Han, Q., Smith, K. M., Darmanin, C., Ryan, T. M., Drummond, C. J., Greaves, T. L. (2021) *J. Colloid Interface Sci.,* **585**, 433.

A017a-06-240823

Allosteric transitions in Mycobacterial ribonucleotide reductases revealed by X-ray crystallography and Cryo-Electron Microscopy

Shekhar Mande[1], Lumbini Yadav[2], Vinoth Kumar Kutti[3], Janesh Kumar[4]

1.Savitribai Phule Pune University, Pune, 2. National Centre for Cell Science-Pune, 3. National Centre for Biological Sciences-Bangalore, 4. Centre for Cellular & Molecular Biology, Hyderabad

Keywords: Ribonucleotide reductase, Allostery

Ribonucleotide reductases (RNR) catalyze the reduction of ribonucleotides to deoxyribonucleotides through abstraction of 2' hydroxyl group, and are known to be essential for survival in all organisms. These follow a unique radical transfer mechanism, in which a Tyr-radical formed in one subunit is transferred to another, at a distance of more than 30Å. The initiation of radical formation in the Class Ib RNR of Mycobacteria is in the NrdF subunit at its di-manganese site. Allostery plays an important role, both in association of NrdF and NrdE subunits for facilitation of free radical transfer, and during catalysis within the NrdE dimer. We have been able to map such allosteric transitions through Cryo-electron microscopy structures of NrdE dimer, NrdE: NrdF binary complex and NrdE: NrdF: NrdI ternary complex. Apart from these, X-ray crystallographic structures of NrdI, and those of NrdF:NrdI complexes determined by us have also yielded useful insights into the radical transfer mechanism. 3D variability analysis revealed major allosteric changes. These in the NrdE dimer are mediated at the interface of the homodimer, and are characterized by sliding movement of α-helices and differences in atomic interactions near the active sites in the two monomers. Similarly, changes are seen prominently at the interface of NrdE and NrdF binary complex in the Cryo-EM structures. Thus, we have been able to map allosteric movements of different subunits in the important ribonucleotide reductase enzyme complexes by combination of the two structural techniques.

This work was supported by DST-NPDF (PDF/2015/000961) and DBT-Centre of Excellence Grant (BT/PR15450/COE/34/46/2016). National Cryo-EM Facility, NCBS Bangalore, Daouda Traore from ESRF CMO1 beamline for Cryo-EM data collection and ESRF ID 23 for NrdI reduced, Raghurama P Hegde XRD2 beamline - Elettra Sincrotrone Trieste for X-ray fluorescence scan, Diamond Light Source UK.

A021 Computing in Fragment Screening

Room 212

1.10pm - 3.30pm

Fully automated data collection and data management at the Swiss Light Source

K. Smith[1], E. Panepucci[1], S. Aumonier[1], D. Eris[1], C.Y. Huang[1], D. Eris[1], D. Buntschu[1], N. Meier[1], W. Glettig[1], K. McAuley[1], M. Sharpe[1], M. Wang[1], J. Wojdyla[1]

[1]Paul Scherrer Institute (PSI), 5232 Villigen, Switzerland

Kate.smith@psi.ch

Keywords: automation, crystallography, data acquisition, databases, fragment screening

With the advent of fragment screening and increased industrial demands for beamtime, synchrotrons have had to adapt their services to provide reliable high throughput systematic data collections. The Swiss Light Source (SLS) has recently upgraded their data acquisition hardware and software to meet automation needs at the macromolecular crystallography (MX) beamlines [1, 2, 3]. Unattended data collection at the SLS is best suited for single crystals from well characterized crystallization systems, such as crystals from high-throughput screening or fragment-based drug discovery pipelines. The recent development of the SLS MX Fast Fragment and Compound Screening (FFCS) platform [4, 5] has produced large quantities of fragment-soaked crystals for a number of academic and industrial targets, which were successfully measured with the smart digital user (SDU).

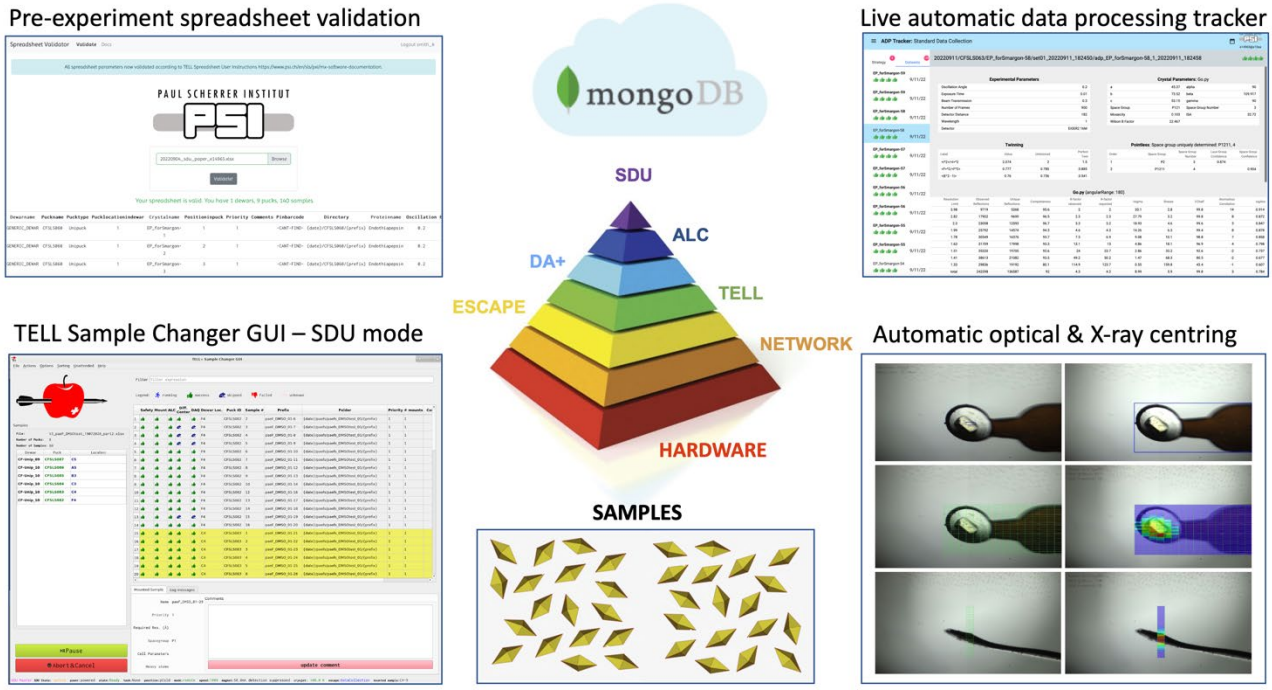

Figure 1: Graphical representation of core components of the SDU pipeline used at PSI macromolecular crystallography beamlines for single crystal experiments and FFCS campaigns.

I will first present the development of SDU, automatic loop centring (ALC) and the expansion of our software microservice framework [6]. The SDU is a sophisticated communications and decision-making software which performs systematic, fully automated data collection at all three MX beamlines with a maximum throughput of 25 samples per hour. I will also present the migration of our mongo database (MXDB) to the cloud and how this is central to our current and future samples management, data acquisition, automation and data processing pipeline strategies. The current external webpage allows users to validate excel sample spreadsheets prior to their experiment, in the future this will be modernized to provide users with extensive sample management capabilities, including logistics, data acquisition, data processing and post-experiment analysis.

[1] Wojdyla et al. (2018). J. Synchrotron Rad. 25(1), 293-303
[2] Basu et al. (2019). J Synchrotron Rad. 26(1), 244-52
[3] Martiel et al. (2020. J Synchrotron Rad. 27(3), 860-863
[4] Kaminski et al., (2022). *Acta Cryst D.,* 78(3), 328-36
[5] Sharpe et al., (2021). *Nihon Kessho Gakkaishi*, 63(3), 232-235
[6] Smith et al., (2022). *Manuscript submitted for review.*

Making the most of crystal polymorphism in fragment-based lead discovery

Alessandro T. Caputo[1], Roberta Ibba[2,3], James D. Cornu[2,4], Benoit Darlot[2], Mario Hensen[2], Colette B. Lipp[2], Gabriele Marcianò[2], Snežana Vasiljević[2], Nicole Zitzmann[2], Pietro Roversi[5,6]

1 Commonwealth Scientific and Industrial Research Organisation, Clayton, VIC, Australia,

2 Biochemistry Department, University of Oxford, Oxford, United Kingdom,

3 Department of Medicine, Surgery and Pharmacy, University of Sassari, Sassari, Italy,

4 Wellcome Trust Centre for Cell Biology, University of Edinburgh, Scotland, United Kingdom,

5 IBBA-CNR Unit of Milano, Institute of Agricultural Biology and Biotechnology, Milano, Italy,

6 Department of Molecular and Cell Biology, Leicester Institute of Structural and Chemical Biology, University of Leicester, Leicester, United Kingdom

Email of alex.caputo@csiro.au

Keywords: UGGT, crystal polymorphism, fragment-based lead discovery

Polymorphism in protein crystals is a regular occurrence and can lead to ambiguities in assignment of point-group symmetry and cell parameters. In fragment screening using X-ray crystallography, many datasets are collected and processed through automated pipelines that involve minimal user intervention. In presence of crystals belonging to different polymorphs, crystal lattice parameters and symmetry can be incorrectly assigned and hamper the subsequent analysis. We describe here a semi-automated procedure for assigning each fragment screen dataset to one of a set of known polymorphs. The protocol is implemented in a series of scripts called CoALLA (crystal polymorph and ligand likelihood-based assignment) [1]. Each dataset is processed and the structure refined in each of the known polymorphs; the polymorph with the lowest refinement R_{free} is then chosen as the most likely one (Fig. 1). Using examples from fragment screens and subsequent hit-to-lead elaboration across a variety of target classes, we illustrate the use of CoALLA to automatically assign polymorphs to large set of fragment screening X-ray diffraction data. The CoALLA protocol can be used for routine assessment of polymorphism in fragment-based lead discovery by X-ray diffraction.

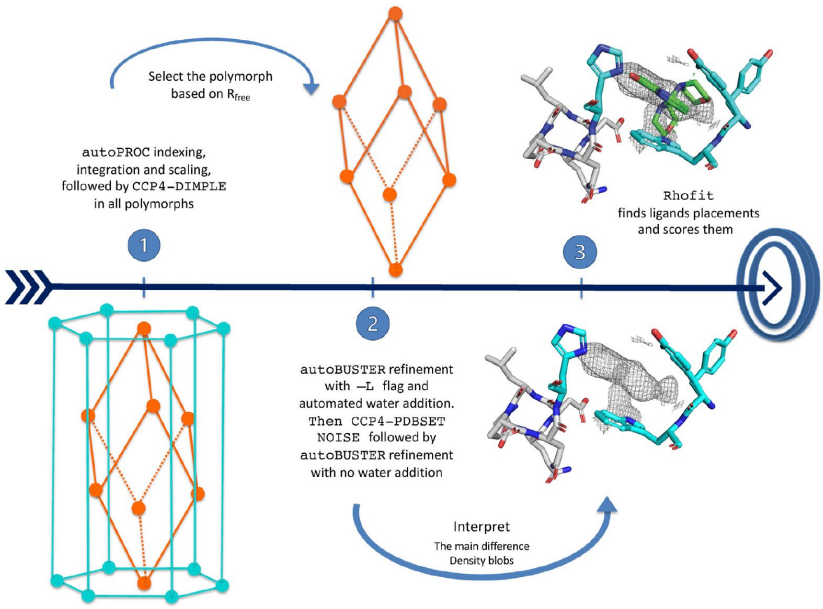

Figure 1. Overview of the CoALLA decision flow

[1] Caputo, A. T., Ibba, R., Cornu, J. D. L., Darlot, B., Hensen, M., Lipp, C. B., Marcianò, G., Vasiljević, S., Zitzmann, N. & Roversi, P. (2022). Frontiers Mol Biosci 9, 960248.

The SLS FFCS Pipeline: HTP Crystallographic Screening for Fragment-Based Drug Discovery

M. Sharpe *on behalf of the MX group*

Swiss Light Source, Paul Scherrer Institute, 5232 Villigen PSI, Switzerland

may.sharpe@psi.ch

Keywords: Fragment-based drug discovery, automation, software

In recent years, fragment-based drug discovery (FBDD) has revolutionized the development of potent lead compounds against protein targets. This “start small, elaborate efficiently” approach promises to address many deficiencies of traditional medicinal chemistry. It has been used successfully by industry and academics, delivering several drugs to the clinic, and many more to late-stage clinical trials. Probably the most useful and informative technique for FBDD is X-ray crystallography, employed most effectively as a primary screen to detect the binding of fragment hits to protein target sites, while simultaneously elucidating binding poise and identifying possibilities for fragment development.

In recent years, technological advances at macromolecular crystallography beamlines in terms of instrumentation, beam intensity, and robotics have enabled the development of dedicated platforms at synchrotron sources for FBDD using X-ray crystallography.
In this presentation I will talk about the development of the Fast Fragment and Compound Screening (FFCS) platform at the Swiss Light Source (SLS), an integrated next-generation pipeline for crystal soaking, handling, and data collection, which allows crystallography-based screening of protein crystals against hundreds of fragments and compounds[1,2].

[1] Kaminski, J. W., Vera, L., Stegmann, D., Vering, J., Eris, D., Smith, K. M. L., Huang, C.-Y., Meier, N., Steuber, J., Wang, M., Fritz, G., Wojdyla, J. A. & Sharpe, M. E. (2022). *Acta Cryst*. D**78**, 328-336.

[2] Wojdyla, J. A. & Sharpe, M. E. (2021). Nihon Kessho Gakkaishi **63**, 232-235

A021-04-240823

Automated collection and screening capabilities at the Australian Synchrotron MX beamlines)

R. M. Williamson[1], A. Riboldi-Tunnicliffe[1], S. A. Boer[1], S. J. Harrop[1], Y. Khandokar[1], C. Szeto[1], R. J. Young[1], S. Panjikar[1]

ANSTO Australian Synchrotron, 800 Blackburn Road, Clayton, VIC 3158, Australia

rachelw@ansto.org.au

Keywords: automation, fragment screening, synchrotron

Fragment screening using synchrotron macromolecular crystallography is one of the most common approaches for identifying binding sites and binding mechanisms of small organic drug molecules to protein targets and is a well-established approach to initial lead identification and drug discovery. ANSTO's Australian Synchrotron houses the two most powerful and advanced instruments in the field of protein crystallography in Australia, with the Macromolecular (MX1) and Microfocus (MX2) Crystallography Beamlines (soon to be joined by MX3) being the cornerstone of structure-based ligand design for local and international researchers. However, even when using synchrotron beamlines for data collection, the time consuming nature of acquiring and processing the data and analysing the structures of the 100's to 1000's of models involved in a fragment screening campaign results in primary screening remaining outside the repertoire of most laboratories. Recognising the need for such a national capability, the MX Beamlines are developing on-site fragment screening capabilities at the Australian Synchrotron.

Developments in our automation capabilities include: automated sample centering and initial screening for diffraction, automated data acquisition (including mounting, crystal location, centering, data collection). A processing and refinement pipeline, utilising code developed at the Australia Synchrotron, has been used to solve structures and identify ligands in over 100 datasets in less than 30 min, indicating the throughput possible with our modular framework.

A021-05-240823

Towards comprehensive analysis of large crystallographic fragment screening campaigns

T. Krojer

MAX IV Laboratory, Lund University, PO Box 118, S-221 00 Lund, Sweden

tobias.krojer@maxiv.lu.se

Keywords: FragMAXapp, fragment screening, batch processing

The throughput of macromolecular X-ray crystallography experiments has surged over the last decade. Increases in the availability of high-intensity X-ray beams, fast detectors, and high levels of automation have permitted this extraordinary improvement in productivity. These advancements have allowed for the establishment of the *FragMAX* facility [1] and several other specialized centres for crystal-based fragment screening, which enable preparation and collection of hundreds of single-crystal diffraction datasets per day. In addition, crystal structure determination has become significantly easier due to the availability of user-friendly software packages, which support users with different levels of experience from data processing to model building and structure refinement. However, simultaneous analysis of numerous related crystal structures, such as those present in fragment screening or structure-based drug design programs, remains a formidable problem because all major software suites adhere to the prevalent idea of "*one project equals one structure*". Moreover, fragment screening generates an abundance of meta-data that must be tracked for subsequent analysis and PDB deposition, but such functionality is currently not integrated in the available software packages.

FragMAXapp is a new web application developed at *MAX IV Laboratory* to overcome this issue by facilitating the parallel processing of hundreds of datasets from crystallographic screening campaigns [2]. It provides an intuitive user interface for data processing and analysis. This presentation will cover the implementation of *FragMAXapp*, present its various features, and highlight recent advancements. It will also outline potential future developments because there is an unmet need for more generic systems that can also support newer approaches such as (time-resolved) serial crystallographic studies. In addition to processing, a full platform must allow for annotation, data mining, graphical representation of protein-ligand data, and model quality. Such advancements will be essential if we are to realize the full potential of the enormous throughput of modern synchrotron beamlines and allow structural biologists to devote their valuable time to structure analysis rather than data management and processing. Expansion of existing and creation of new tools will not be simple but will greatly boost protein crystallographers' output.

[1] Lima, G. M. A., Talibov, V. O., Jagudin, E., Sele, C., Nyblom, M., Knecht, W., Logan, D. T., Sjögren, T., & Mueller, U. (2020). *Acta Cryst. D*, **76**, 771.
[2] Lima, G. M. A., Talibov, V. O., Jagudin, E., Benz, L. S., Marullo, C., Barthel, T., Wollenhaupt, J., Weiss, M. S. & Mueller, U. (2021). *Acta Cryst. D*, **77**, 799.

A028 Insights from 3D Diffraction Microstructural Imaging of in-situ Deformation of Engineering Alloys

Room 213

1.10pm - 3.30pm

A028-01-240823

Benchmarking discrete dislocation dynamics simulations with dark field x-ray microscopy movies

Felix Frankus [a], Henning Friis Poulsen [b], Anter El-Azab [c], Grethe Winther [a]

[a] *Department of Civil and Mechanical Engineering, Technical University of Denmark, 2800 Kgs. Lyngby, Denmark.*
[b] *Department of Physics, Technical University of Denmark, 2800 Kgs. Lyngby, Denmark.*
[c] *School of Materials Engineering, Purdue University, West Lafayette, IN 47907, USA.*
Email of communicating fefra@dtu.dk

Keywords: Materials Simulation, Diffraction Imaging, Dislocations

In many engineering applications of metals, their plastic properties play an essential role. They influence fundamental parameters such as the formability, and strength. Plastic properties are governed by the hierarchical interplay of structures along various length-scales, such as grains, sub-grains, and dislocations. Dislocations are line defects in the crystalline lattice imposing elastic distortion. During plastic deformation dislocations multiply and self-organise into patterns.

Discrete dislocation dynamics offer a framework to numerically investigate the mutual interaction between dislocations through their surrounding stress fields. However, there is still a lack of 3D experimental data as input for and validation of the simulations.

Recently, dark field x-ray microscopy (DFXM) has enabled time resolved visualization of dislocation structures with single dislocation resolution of in-situ deformed aluminium tensile samples.

The talk will focus on how to import such 3D DFXM movies of dislocation motion into discrete dislocation dynamics simulations, aiming at understanding the mechanics of the initial self-organisation of dislocations and their patterning.

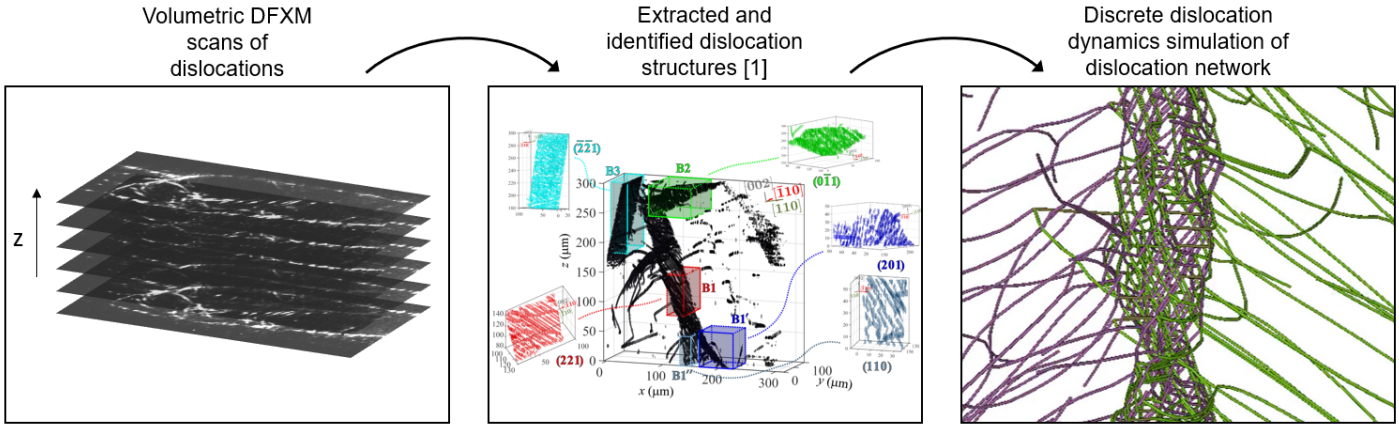

Figure 1. Processing pipeline for extraction of single dislocations from DFXM images and representation of their configuration in discrete dislocation dynamics simulations.

[1] Yildirim, Can, et al. "Extensive 3d mapping of dislocation structures in bulk aluminum." arXiv preprint arXiv:2208.14284 (2022).

A028-02-240823

3D movies of self-organisation of individual dislocations during plastic deformation

Borgi[1], G. Winther[2], H. F. Poulsen[1]

B Technical University of Denmark, Department of Physics, Denmark,

Technical University of Denmark, Department of Civil and Mechanical Engineering, Denmark

Email of communicating: borgi@dtu.dk

Keywords: XRD, self-organization, non-destructive, 3D mapping, plastic deformation, dislocations

The mechanical and many physical properties of metals are governed by defects, known as dislocations. TEM can display these line defects in thin films but cannot probe the structural dynamics and the local stress field in a representative way, as this requires studies of bulk specimens. As a result, it has until recently been impossible to visualize the self-organisation of dislocations taking place during plastic deformation.

In this talk I present the first in situ 3D experimental movies of the initial patterning of dislocations in a pristine sample during deformation using Dark-Field X-ray Microscopy, DFXM [1]. The angular sensitivity of DFXM is 10^{-3} degrees, allowing the dislocations to be in Bragg condition, while the rest of the crystal lattice is not, giving rise to contrast. Using a tensile rig, individual defects are identified deep within a mm-sized single crystal of aluminium and tracked as function of external load at beamline ID06 at ESRF. As an example, Figure 1a is a snapshot of an ensemble of dislocations within a 2D slice of the sample.

Next, I present forward simulations of DFXM images based on either geometrical optics or wavefront propagation. As an example, Figure 1b displays a DFXM image of a 2D slice of an aluminium single crystal, with a large domain exhibiting a few randomly dispersed dislocations. Comparing experimental data and simulations is used to guide the modelling, e.g. to identify dislocation types. The forward simulations tools also allow to interface data directly to discrete dislocation dynamics (DDD) [2]. Depending on progress with analysis I will report on the physical mechanisms underlying the self-organization observed and discuss current limitations.

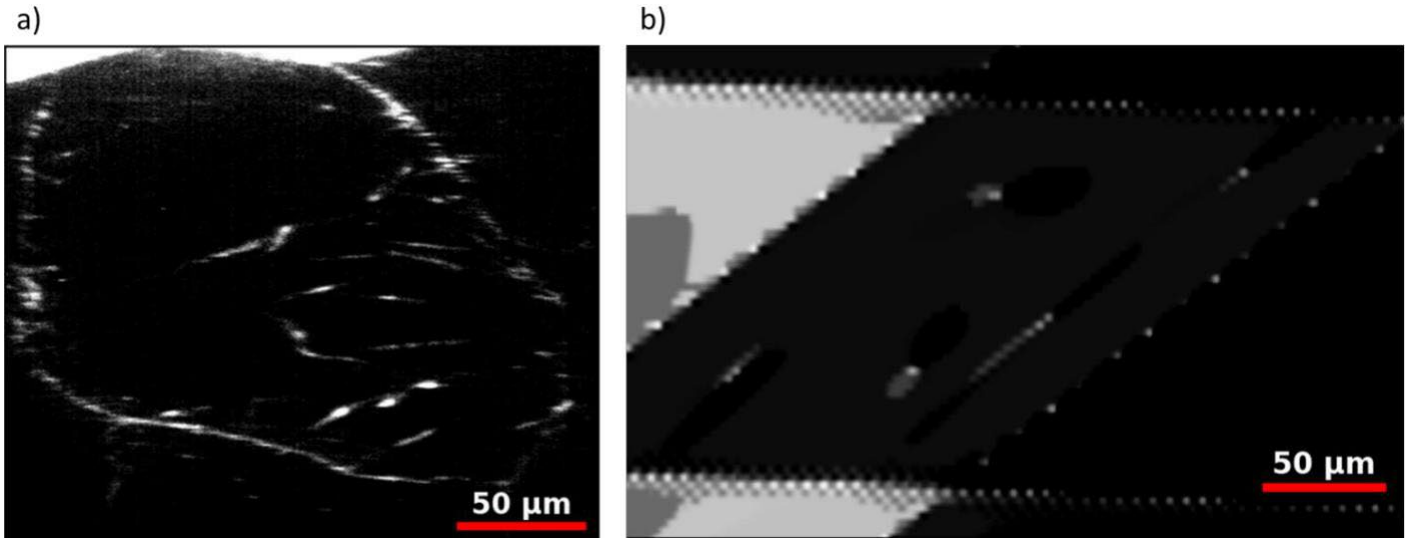

Figure 1. 2D images of a layer in a single crystal aluminium (111 reflection). (a) Experimental DFXM image of domain with clear individual dislocations, in a weak beam configuration. (b) Simulated DFXM image, displaying the contrast of 5 random edge dislocations within a domain.

[1] Yildirim, C., Poulsen, H.F., Winther, G., Detlefs, C., Huang, P. H. & Dresselhaus-Marais, L. E. (2022). *arXiv:2208.14284*

[2] Po, G., Mohamed, M. S., Crosby, T., Erel, C., El-Azab, A. & Ghoniem, N. (2014). *TMS.* **66**, 2108-2120.

A028-03-240823

Neutron/ X-ray diffraction study of crystalline texture and residual stresses of directional solidified Al-Si alloys at different cooling rates

E. R. Ibañez1, P. R. Alonso2, A. E. Ares1

1. Materials Institute of Misiones, IMAM. Posadas, Misiones. Argentina. 2. National Commission of Atomic Energy, CNEA. Buenos Aires, Argentina.

aares@fceqyn.unam.edu.ar

Keywords: Al-Si alloys, Directional solidification, Texture

Aluminum-Silicon (Al-Si) alloys are characterized by being versatile, economical, and attractive in a wide range of uses and applications; because they have good mechanical properties and good corrosion resistance, in addition to high performance and versatility when they are subjected to forming and machining processes to obtain parts with complex geometries [1].

In general, the solidification of metallic alloys is expected that the structure obtained in solidification is completely columnar, or completely equiaxial. However, under certain solidification circumstances (different cooling rates and thermal gradients), there is a zone where both columnar (Col.) and equiaxial (Eq.) grains are simultaneously present; this zone where both types of grains coexist is called the columnar-to-equiaxed transition zone (CET) [2, 3].

In this type of solidification, there are cooling differences at different distances from the cooling zone. The cooling rate decreases as we move away from the base of the specimen, on the other hand, different temperature gradients are also generated along the specimen resulting in different types of grains and sizes. These can cause the presence of residual stresses, crystallographic textures thus generating elastic, and plastic anisotropy that are characteristic of the solidification process.

Although no studies of these stresses were carried out, it is considered that they can be macroscopic or intergranular and will depend on the crystallographic texture that the material adopts in the solidification process and can generate defects in its subsequent handling such as deformation, for example. The texture and stresses that develop during the manufacturing process affect both the quality of the process and the properties of the final product.

[1] Moustafa, M.A., Samuel F.H., Doty H.W., Valtierra S. (2002). *Int. J. Cast Metals Res.* **14**, 235.

[2] Ares A.E., Triveño Ríos C., Caram R., Schvezov C. E.. (2002). *Light Metals 2002*, edited by W. Schneider, pp. 793-799. United States of America: The Minerals, Metals and Materials Society.

[3] I. L Ferreira, A.L.Moreira, J.A. Aviz et al. (2018) Journal of Manufacturing Processes. **35**, 634.

A028-04-240823

A three-dimensional X-ray diffraction study of intergranular stress relationships in a BCC ferritic steel

J. A. D. Ball[1,3], A. Kareer[2], O. V. Magdysyuk[1], S. Michalik[1], T. Connolley[1], *D. M. Collins[3]

Diamond Light Source Ltd., Harwell Science and Innovation Campus, Didcot, OX11 0DE, United Kingdom
Department of Materials, University of Oxford, Parks Road, Oxford, OX1 3PH, United Kingdom
School of Metallurgy and Materials, University of Birmingham, Edgbaston, Birmingham, B15 2TT, United Kingdom

**D.M.Collins@bham.ac.uk*

Keywords: 3DXRD, Diffraction, EBSD, Texture, Grain-resolved stress, Grain neighbourhood

To fully understand the response of a polycrystalline material to deformation, it is necessary to study the factors that govern the onset of plastic deformation for individual grains. Computational studies of cubic systems [1] have linked the development of grain stress-states to the immediate neighbourhood of a grain in addition to the macroscopic crystal orientation. This has been verified experimentally in hexagonal close-packed systems [2] and for a limited number of grains in cubic systems [3, 4]. For the first time at Diamond Light Source, three-dimensional X-ray diffraction (3DXRD) has been used *in-situ* to determine centre-of-mass positions, orientations, and Type II stress tensors of grains in a single-phase low carbon ferritic steel sample (Fig. 1a) under uniaxial tension. Residual elastic stresses, per grain, are widely distributed with no load applied (Fig. 1b). During subsequent loading, the stress development of individual grains broadly follow the macroscopic stress-strain trend, however, there are several examples of outliners and evidence of significant variation of intergranular stress magnitudes among the polycrystal (Fig. 1c).

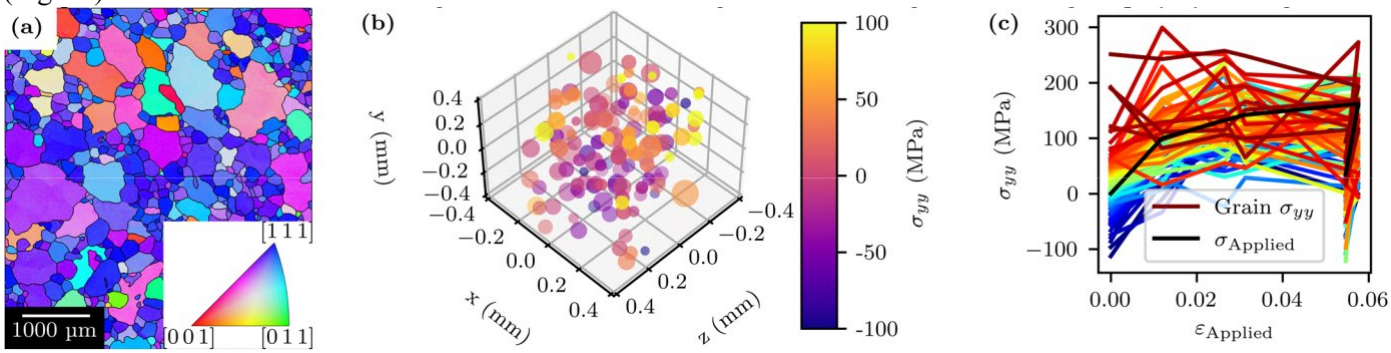

Figure 1. (a): EBSD IPF-Z map of the undeformed sample; (b): 3DXRD grain centre-of-mass positions map, coloured by lab-frame *y*-axis stress, scaled by grain volume; (c): 3DXRD grain stress-strain response, coloured by initial *y*-axis stress plus the macroscopic stress-strain curve (black).

A grain neighbourhood effect is observed: the Schmid factor of serial adjoining grains (neighbours in the tensile direction) influences the stress state of a grain of interest (Fig. 2a), whereas parallel neighbours (those adjoining in the transverse direction) are much less influential (Fig. 2b). This phenomenon is strongest at low plastic strains only (Fig. 2a-b), with the effect diminishing as plasticity builds (Fig. 2c-d). The influence of initial residual stresses becomes less evident, and grains rotate to eliminate any orientation dependent load shedding. The ability of the BCC ferrite to exhaust such neighbourhood interactions is considered to be a crucial factor to explain the high ductility possessed by these materials.

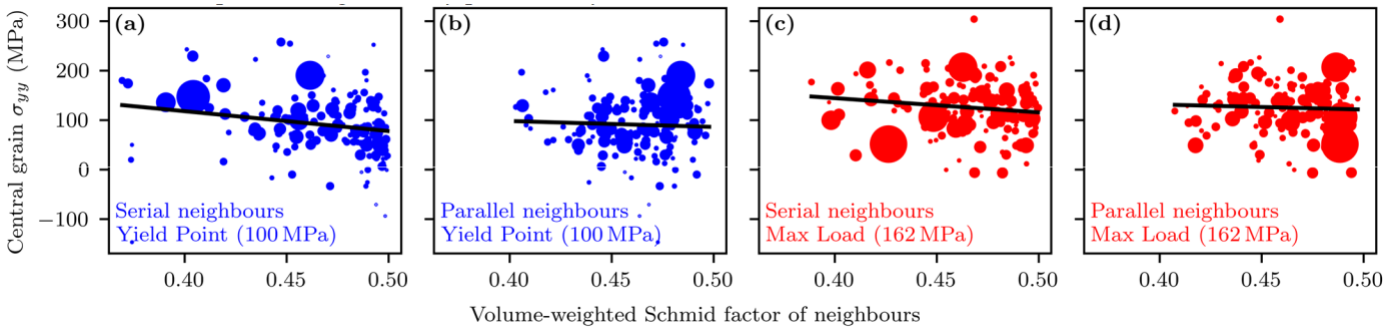

Figure 2. Grain axial stress vs mean Schmid factor of serial (a, c) and parallel (b, d) neighbours at yield point (blue, a-b) and max load (red, c-d).

1 Bretin, R., Levesque, M. & Bocher, P. (2019). *Int. J. Solids Struct.*, **176-177**, 36–48.
2 Abdolvand, H., Wright, J. & Wilkinson, A. J. (2018). *Nat. Commun.*, **9**, 1–11.
3 El Hachi, Y., Berveiller, S., Piotrowski, B., Wright, J., Ludwig, W. & Malard, B. (2022). *Acta Mater.*, **235**, 118107.

4 Jimenez-Melero, E., van Dijk, N. H., Zhao, L., Sietsma, J., Offerman, S. E., Wright, J., van der Zwaag, S. (2009). *Acta Mater.*, **57**, 533-543.

J. Ball would like to thank the Diamond Light Source [NT26376] and the University of Birmingham for jointly funding his PhD program, and Younes El-Hachi and Jon Wright for their assistance with the bootstrap method of grain parameter error determination. A. Kareer is funded by the Engineering and Physical Sciences Research Council [EP/R030537/1].

A028-06-240623

Image-guided diffraction at Diamond Light Source: the DIAD beamline

A. Leonardi[1], H. Deyhle[2], A. James[1], J. Le Houx[1], C. Reinhard[3], M. Drakopoulos[4], and S. Ahmed[1]

1. Diamond Light Source Ltd., Rutherford Appleton Laboratory, Harwell Science Campus, Didcot, Oxfordshire OX11 0QX, United Kingdom, 2. University of Basel, Biomaterials Science Center, Allschwil, Hegenheimermattweg 167B/C, 4123, Switzerland 3. The University of Manchester at Harwell, Diamond Light Source, Harwell Science Campus, Didcot, Oxfordshire OX11 0DE, United Kingdom, 4. Brookhaven National Laboratory, National Synchrotron Light Source II, Upton NY, Bldg. 741, P.O. Box 5000, 11973-5000, United States

alberto.leonardi@diamond.ac.uk

Keywords: Synchrotron; full field micro-tomography; micro-diffraction; time-resolved studies, phase identification, strain

Understanding the interaction between microstructure, strain and phase is crucial in science areas such as energy storage, carbon sequestration and bio-medical engineering. However, scientists and researchers find it challenging to quantify these properties as it requires multiple instruments, which are usually separated by space and time. The Dual Imaging And Diffraction (DIAD) beamline at Diamond Light Source (DLS) has been designed to address this challenge. DIAD enables its users to visualise internal structures (in 2- and 3D) as well as identify and measure compositional/phase and strain changes. DIAD enables in-situ and in-operando experiments that require spatially correlated information. The DIAD beamline provides two independent beams combined at one sample position allowing "quasi-simultaneous" X-ray Computed Tomography (XCT) and X-ray Powder Diffraction (XRD). The key functionality of the beamline is its ability to perform "image-guided diffraction" or "diffraction-guided imaging". A setup in which the micron-sized diffraction beam can be scanned over the complete area of the imaging field-of-view without moving the specimen. This "moving beam" setup enables the collection of location-specific information about the phase composition and/or strains at any given position within the image/tomography field of view. The innovative capabilities offered by the DIAD beamline instrument are shown *via* a selection of outstanding studies about battery materials, biomaterials, catalysis, and geophysics.

1 Reinhard, C., Drakopoulos, M., Ahmed, S. I., Deyhle, H., James, A., Charlesworth, C. M., Burt, M., Sutter, J., Alexander, S., Garland, P., Yates, T., Marshall, R., Edmund, B. K., Pueyos, W. A., Bradnick, B., Nagni, M., Winter, A., D., Filik, J., Basham, M., Wadeson, N., King, O. N. F., Aslani, N., Denta, A. J., (2021). *J. Synchrotron Rad.*, **28**, 198

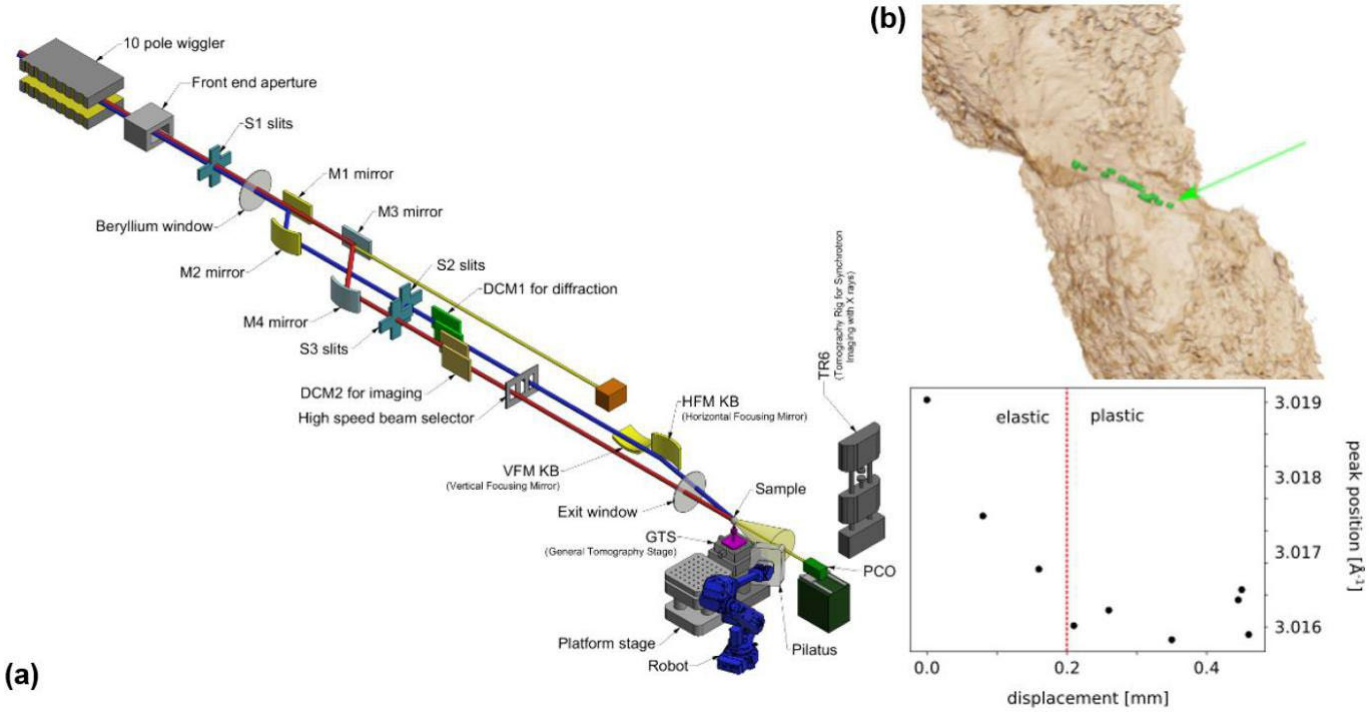

Figure 1. (a) DIAD beamline layout. (b) Early results from a deformation commissioning experiment.

A035 Multimodal approaches to interfaces, defects and thin films

Room 219

1.10pm - 3.30pm

A035-01-240823

Development of magnetic (Fe-Ga) multi-layered thin films for applications in magnetic sensor devices

A. Durniak[1], S. Foster[2], D. Bulla[2]

[2] European Spallation Source ERIC P.O. Box 176 SE - 221 00 Lund Sweden [2] DST Group, P.O. Box 1500 Edinburgh SA 5111 Australia celine.durniak@ess.eu

Keywords: magnetostrictive materials, thin films, Fe-Ga alloys

Fe-Ga alloys (Galfenol) have recently received intense interest due to their giant magnetostriction in low saturation magnetic fields, with possible applications in many industries. These include automotive, biomedical [1], defence and aerospace. In addition, the emergence of compact cavity-based strain sensors has seen a renewal of interest in magnetostrictive thin films [2]. While the influence of the composition of Fe-Ga on its magnetostriction is well-studied for the bulk material [3], for thin films, the final crystallographic structures and the potential additional induced stresses are still new topics of research [4] with many points still to be understood.

Here we report on different experimental characterisation techniques for magnetostrictive Fe-Ga thin films deposited on geometrically distinct substrates (flat wafers and optical fibres) which were either lying at the bottom of the deposition chamber or continuously rotated below the sputtering target. Our objective is to study the effects of thin film layouts on the magnetic and crystallographic properties of the samples. The crystal structures were characterised using Scanning Electron Microscope (SEM) (Fig. 1a, b), Energy Dispersive x-ray Spectroscopy, Electron Backscattering Diffraction, and X-ray diffraction (XRD) (lab Fig. 1c and synchrotron). Investigations of the magnetic properties used a Vibrating Sample Magnetometer (VSM) to obtain magnetic hysteresis loops, enabling first order reversal curve (FORC) analysis (Fig. 1d).

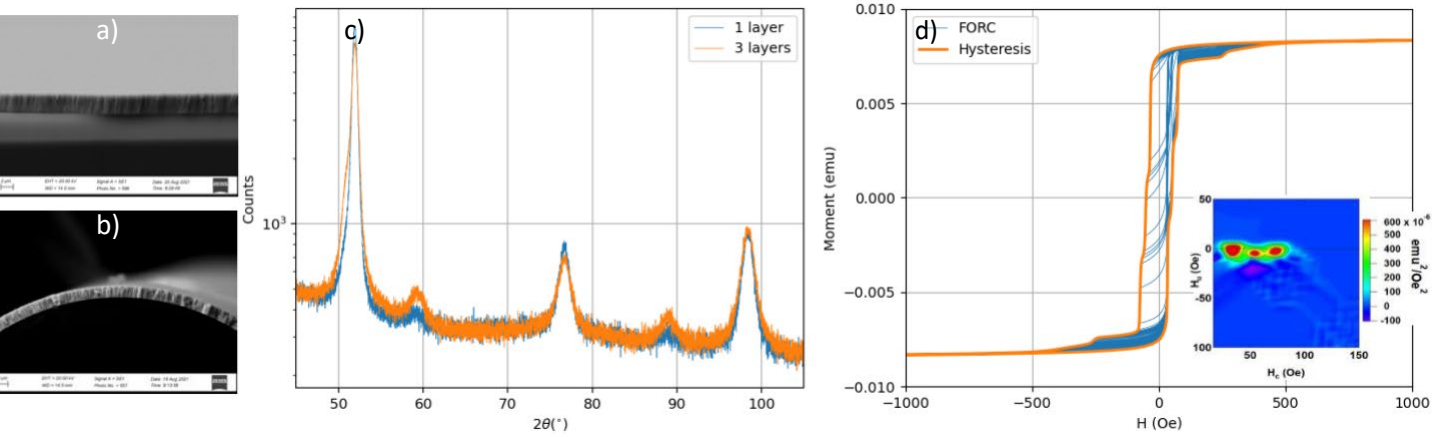

Figure 1. *SEM image of film deposited on a) Si wafer, and b) optical fibre sensor. c) Lab XRD spectra (Co K at grazing incidence angle of 3) of samples with 1 layer (blue curve) or 3 layers of Cu-GaFe (orange curve) deposited on Si wafer. Both samples have a total average thickness of 310 nm. d) VSM hysteresis and FORC curves for the 3 layers film. The corresponding FORC diagram is shown in the inset.*

[1] Gao et al., *Bioactive Materials* **8**, 177 (2022)

[2] Foster et al., 40th Australian Conference on Optical Fibre Technology, Adelaide Australia 30 Nov-3 Dec, 96342F (2015); Li et al., *Appl. Photonics* **3**, 120806 (2018)

[3] Lograsso and Summers, *Materials Science and Engineering A* **416**, 240 (2006)

[4] Legall et al., *Phys. Rev. Appl.* **15**, 044028 (2021)

Facilities and funding supported by Australian Department of Defence including Next Generation Technologies Fund (NGTF). Part of this research was undertaken on the Powder Diffraction beamline at the Australian Synchrotron, ANSTO.

A035-02-240823

Formation and stability of Anti-Phase boundaries (APBs) in Al-Fe B2

Louisa Meshi[1], Guy Hillel[1], Itzhak Edry[2], Ekaterina Galaeva[1], David Fuks[1], Malki Pinkas[2]

[1]Department of Materials Engineering, Ben-Gurion University of the Negev, P.O.B 653, Beer-Sheva 8410501, Israel; [2]NRCN, P.O.B. 9001, Beer-Sheva, 841900, Israel

louisa@bgu.ac.il

Keywords: structural defects, APBs, TEM, *in-situ* TEM, B2 structure.

In recent decades, there is a renewal of interest in the B2 (ordered Body Centered Cubic (BCC)) phase, due to its important role in the new class of metallic alloys called "high entropy alloys" (HEAs). AlCoCrFeNi system, as one of the most studied HEA systems, exhibits microstructure of BCC particles embedded in the B2 matrix. The main disadvantage of this and related alloys is their relatively poor ductility. Since B2 is the matrix – improving its ductility may be the first step towards commercialization of the AlCoCrFeNi-based HEAs. It was suggested that B2 ductility may be improved by increasing the density of anti-phase boundaries (APBs) [1]. Since, in [2], it was reported that APBs are formed in the B2 matrix of the AlCoCrFeNi alloy – evaluation of the APBs formation mechanisms in B2 phase and their stability was stated as the goal of this research. To reach this goal, binary model system was chosen. Following theoretical calculations [3], FeAl B2 was suggested as most promising model system, since the energy of formation of the APBs in this system was the lowest out of the three possible binary B2 phases existing in the AlCoCrFeNi system. In the literature, formation mechanisms and evaluation of stability of the APBs were studied almost solely for the ordered Face Centered Cubic (FCC)-based structures. APBs were classified into two types, based on their morphology and the way they are formed [4]: thermal (appearing due to order/disorder transformation) and shear (through dislocation dissociation). In B2 structures, some researchers stated that formation of APBs in the ordered Fe-Al system without the addition of alloying elements is impossible [5, for example]. While in [6, for example], APBs were observed experimentally in Fe_xAl_{1-x} B2 at x>0.68, regardless the fact that order-disorder transformation starts at and above x=0.55. Current research focuses on the binary Fe-Al B2 system aiming at understanding APBs' formation and stability.

A series of Fe_xAl_{1-x} (x = 0.5÷0.73) alloys were cast, homogenized, and investigated using Transmission Electron Microscopy (TEM). Classical TEM methods of 2 beam conditions (2bc) and trace analysis were used for characterization of structural defects. All studied Fe_xAl_{1-x} alloys possessed dislocations with <100> or <111> Burgers vectors, indicating varying partial disorder. Moreover, since <111> type dislocations bound APBs in B2 structure, it may be possible that these dislocations can dissociate into ½<111> superpartials if the energy of the APBs is low enough, and, in turn, form APB between them. However, up to x=0.68 - no APBs were formed in studied alloys. At Fe content above 68 at. %, alongside APBs, small DO_3 domains were detected, see image of the Fe-70 at. % alloy (for example) in Fig. 1. Despite various heat treatment and subsequent quenching - DO_3 domains were impossible to prevent from forming, therefore an *in-situ* TEM heating experiment was performed. Above critical temperature, DO_3 domains disappeared and APBs in B2 phase remained and even grew. It was found that formation of the stable APBs in the Fe-Al B2 phase requires specific state of disorder (above critical value). These experimental findings were supported by Density Functional Theory calculations which pointed on a decrease of the APBs energy in the partially disordered Fe-Al B2 phases with increasing the Fe content.

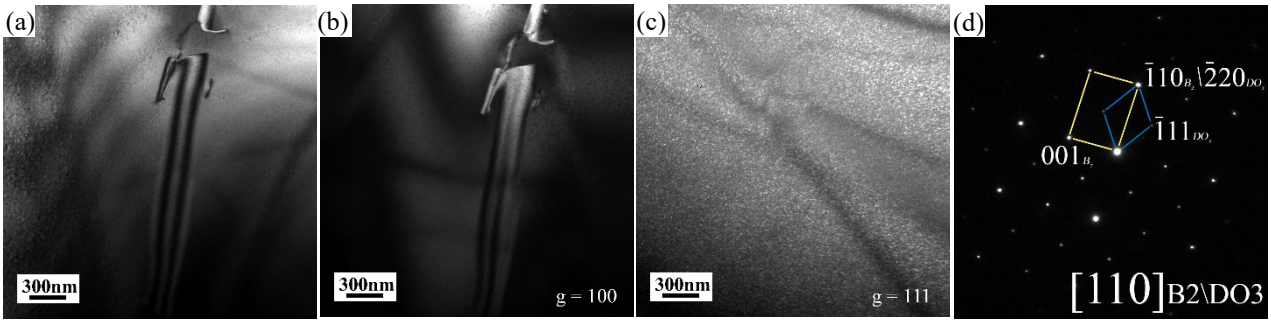

Figure 1. Fe_7Al_3 alloy: (a) Bright-field image of the APBs in the B2; (b) APB illuminated in g=100 (2bc); (c) Same area as (a-b), DO_3 domains illuminated in g=111 (2bc); (d) electron diffraction pattern indexed in terms of B2 and DO_3 phases.

[1] Inoue A., et al (1983) *Metallurgical Transactions A*. **14(7)**, 1367.

[2] Linden Y., et al (2017) *Scripta Mater.* **139**, 49.
[3] Vidal D., et al. (2022) *Intermetallics*, **141** 107434.
[4] Rong TS., et al. (2001) *Intermetallics*, **9**(6) 499.
[5] Khachaturyan A.G. (1973) *Soviet Physics Jetp*. **36**(4) 753.
[6] Prakash U., et al. (1991) *Philosophical Magazine A*. **64**(4) 797.

A035-03-240823

Defects and Thin-films Analysis using Four-Dimensional Scanning Transmission Electron Microscopy

Jian-Min Zuo1, Saran Pidaparthy1, Haoyang Ni1, Hanyu Hou1, Robert Busch1, Kaijun Yin1, Daniel D. P. Abraham2

1. *University of Illinois at Urbana-Champaign, Materials Science and Engineering, Illinois, United States of America*
2. *Argonne National Laboratory, Chemical Sciences and Engineering Division, Lemont, Illinois, United States of America*

jianzuo@illinois.edu

Keywords: Electron crystallography, diffraction imaging, defects and thin-films

The study of order and disorder is a fundamental theme in crystallography and its applications in materials science and condense matter physics. Examples include doping of semiconductors, advanced alloys with complex compositions, nanocrystalline and amorphous materials for energy and environmental technologies. These materials feature minute, significant and strong departures from perfect crystallinity, and their crystallographic analysis is a challenge. Transmission electron microscopy (TEM) has played a predominant role in the discovery of disorder within order or order within disorder, from atomic resolution imaging of crystal defects and fluctuation analysis of short- and medium-range ordering in amorphous solids. However, large gaps remain in our ability for the interrogation of significantly and strongly disordered materials. Here we introduce the concept of cepstral STEM (scanning TEM) for filling these gaps [1-5]. The basic idea is to collect large amounts of nanodiffraction patterns using scanning electron nanodiffraction (SEND) and Fourier transform the logarithmic intensities into cepstral patterns to detect the harmonics captured by diffraction and use the quefrency signals for imaging and structural analysis (Fig. 1). This talk will detail this method and demonstrate its effectiveness through applications to defect analysis in semiconductors, structure determination of high entropy alloys and analysis of silicon anode in lithium batteries.

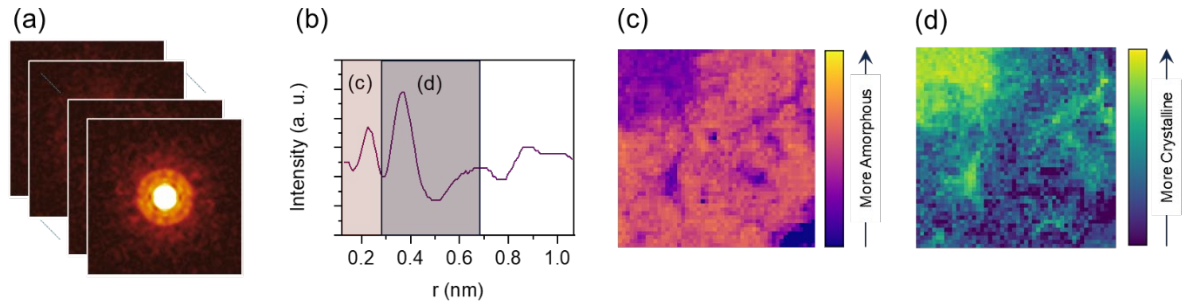

Figure 1. Cepstral STEM for imaging silicon anode. (a) Starting cepstrum stack computed from SEND dataset with (b) corresponding radial cepstrum profile. Image reconstruction of (c) amorphous material and (d) crystalline material.

[1] Shao, Y.-T., Yuan, R., Hsiao, H.-W., Yang, Q., Hu, Y., Zuo, J.-M. (2021), Ultramicroscopy, 113252.
[2] Pidaparthy, S., Ni, H., Hou, H., Abraham, D. P. & Zuo, J.-M. (2022), Microscopy and Microanalysis 28, 450-452, (2022).
[2] Pidaparthy, S., Ni, H., Hou, H., Abraham, D. P., Zuo, J. M. (2022), Ultramicroscopy, Submitted
[3] Hsiao, H.-W., Feng, R., Ni, H., An, K., Poplawsky, J. D., Liaw, P. K. & Zuo, J.-M. (2022), Nature Communications 13, 6651.
[4] Chen, W., Zhan, X., Yuan, R., Pidaparthy, S., Yong, A. X. B., An, H., Tang, Z., Yin, K., Patra, A., Jeong, H., Zhang, C., Ta, K., Riedel, Z. W., Stephens, R. M., Shoemaker, D. P., Yang, H., Gewirth, A. A., Braun, P. V., Ertekin, E., Zuo, J.-M. & Chen, Q. (2022), Nature Materials, doi:10.1038/s41563-022-01381-4.
[5] Zuo, J. M., Yuan, R. L., Shao, Y. T., Hsiao, H. W., Pidaparthy, S., Hu, Y., Yang, Q. & Zhang, J. (2022), Microscopy 71, i116-i131.

Work supported by DMR-2226495 from the Metals and Metallic Nanostructures Program (MMN) within the Division of Materials Research, National Science Foundation.

A035-04-240823

GISANS Study The Structure Evolution in P(S-b-MMA)/dPS Blend Films

Chun-Ming Wu[1] *, Ting-Wei Hsu[1], Ya-Sen Sun[2].

1. National Synchrotron Radiation Research Center, Hsinchu 30076, Taiwan.

2. Department of Chemical Engineering, National Cheng Kung University, Tainan City 701, Taiwan

wu.cm@nsrrc.org.tw

Keywords: GISANS, perforated layers, deuterated polystyrene

The distributions of dPS (deuterated polystyrene) in PLs (perforated layers)// [1-3] can be probed by grazing-incidence small-angle neutron scattering (GISANS). In this work, by adjusting the composition (ϕPS+dPS = 63.8 vol%) of the total PS/dPS component and annealing temperature (230 and 270 °C), P(S-b-MMA)/dPS blend films mainly form perforated layers with parallel orientation (hereafter PLs //). Where basically follow up our previous studied segmental distributions of polymer chains in blend films of a weakly-segregated polystyrene-block-poly(methyl methacrylate) [P(S-b-MMA)] and dPS [4]. The GISAXS/GISANS results offer evidence that dPS chains are preferentially located at the free surface and within the PS layers for blend films that were annealed at 230 °C. Upon annealing at 270 °C, dPS chains distribute within PS layers and perforated PMMA layers. Nevertheless, dPS chains still retain a surface preference for thin films. In contrast, such surface segregation of dPS chains is prohibited for thick films when annealed at 270 °C.

[1] Hong, J. W.; Chang, J. H.; Chang, I. C. Y.; Sun, Y. S. (2021),Phase Behavior in Thin Films of Weakly Segregated Block Copolymer/
Homopolymer Blends. Soft Matter, 17, 9189 − 9197.
[2] Tanaka, H.; Hasegawa, H.; Hashimoto, T. (1991),Ordered Structure in Mixtures of a Block Copolymer and Homopolymers. 1. Solubilization of Low Molecular Weight Homopolymers. Macromolecules, 24, 240 − 251.
[3] Wang, H. F.; Yu, L. H.; Wang, X. B.; Ho, R. M. A (2014), Facile Method to Fabricate Double Gyroid as a Polymer Template for Nanohybrids. Macromolecule, 47, 7993 − 8001.
[4] Hong, J. W., Chang, J. H., Chang, Iris C.Y., Sun, Y. S. (2021), Influence of Osmotic Pressure on Nanostructures in Thin Films of a Weakly-Segregated Block Copolymer and Its Blends with a Homopolymer, *Polymers, 13, 2480.*

Financial support from the Ministry of Science and Technology (grant numbers MOST107-2221-E-008-034-MY3, MOST 108-2739-M-213-001, and MOST 110-2221-E-008-001-MY3) is gratefully acknowledged.

A035-05-240823

Picometre structural changes and the effect of interfaces in LCMO/PCMO superlattices identified using STEM

Wei Chao1, Biying Ye2, Yinyan Zhu2, Espen Drath Bøjesen3, Timothy Petersen4, Changlin Zheng2, Jian Shen2 and Joanne Etheridge1,4

Department of Materials Science and Engineering, Monash University, Clayton, VIC 3800, Australia,

Department of Physics, Fudan University, Songhu Road 2005, Shanghai 200438, China,

Interdisciplinary Nanoscience Centre, Aarhus University, Gustav Wieds Vej 14 8000, Danmark,

Monash Centre for Electron Microscopy, Monash University, Clayton, VIC 3800, Australia.

Email of communicating joanne.etheridge@monash.edu

Keywords: perovskite structures, A-site displacements, superlattices, interfaces

Colossal magnetoresistance (CMR) materials, mainly manganites with perovskite structures, have drawn great attention due to the significant changes in electrical resistivity upon exposure to an external magnetic field. Praseodymium (Pr)-doped lanthanum calcium manganite (LPCMO) is a typical CMR system and the CMR properties are extremely sensitive to the designed thin film structures. In a previous study, growing a superlattice structure with alternating two-unit-cell thick lanthanum calcium manganite (LCMO) and one-unit-cell thick praseodymium calcium manganite (PCMO) layers has been shown to reduce the scale of the phase separation and to increase the phase transition temperature structure by 100°C compared with random Pr-doped thin film without a LCMO/PCMO layered structure [1]. A non-linear relationship of ferromagnetism of the thin films with the periodicity (changing n values in superlattice $LCMO_{2n}PCMO_n$) while maintaining the same composition has also been reported [2].

To study the role of interfaces in affecting the properties of superlattices in the LPCMO system, we perform an atomic-scale microstructure investigation of these thin films with aberration-corrected Scanning Transmission Electron Microscopy (STEM). The recorded atomic resolution STEM images are further analysed using a modified Atomap package [3]. By mapping the A-site displacements across the LCMO and PCMO layers, both of which have a perovskite structure of Pnma space group, we directly observe the coupling of LCMO and PCMO layers in the superlattices. An oscillation between large displacements in PCMO and small displacements in LCMO is displayed. We also find that in the superlattice with a small periodicity which can be regarded as an interface-dominated structure, for example, n = 4 (8 layers of LCMO alternated with 4 layers of PCMO), the value of the A-site displacement in LCMO is reduced compared with bulk LCMO. As n increases, the displacements in LCMO increase. While correlating linearly with the Mn-O-Mn bond angle, this change in A-site displacements gives hints to the charge transfer rate of the material at low temperatures. Our observations suggest structurally that by generating LCMO/PCMO interfaces in superlattices, the charge transfer in LCMO layers becomes more energetically favourable compared to that in bulk LCMO. The effect of interfaces can be tuned by layer thickness and layer periodicities.

These measurements of picometer-scale atomic shifts and structural changes allow us to visualize the effect of interfaces directly, providing new insights as to how to engineer the CMR properties by controlling the density of interfaces and width of layers in LPCMO thin film heterostructures.

[1] Zhu, Y., et al., Nature Communications, 2016. 7(1), 11260.

[2] Zhu, Y., et al., Physical Review B, 2020. 102(23), 235107.

[3] Nord, M., et al., Advanced Structural and Chemical Imaging, 2017. 3(1), 9.

The authors acknowledge the use of the instruments and scientific and technical assistance at the Monash Centre for Electron Microscopy, a Node of Microscopy Australia. This research used equipment funded by Australian Research Council grant LE045416, LE0882821 and was supported by ARC Discovery Project grant DP200103070.

A035-06-240823

Probing defects and disorders in nanoporous materials by electron crystallography

Xiaodong Zou

Department of Materials and Environmental Chemistry, Stockholm University, Sweden

xzou@immk.su.se

Keywords: Electron crystallography, 3D ED, nanoporous materials

Nanoporous materials including zeolites and metal-organic frameworks (MOFs) have well-defined pores and channels in molecular dimensions. They have a wide range of applications from adsorption, separation to catalysis. The properties of a nanoporous material depend both on its crystal structure and on the defects and disorders in the crystal. It is therefore important to elucidate the periodic atomic structure as well as the defects. Point defects caused by vacancies or incorporation of additional atoms and extended defects (1 D and 2 D) appear frequently in nanoporous materials [1]. They often impact the performance of the materials. High-resolution (scanning) transmission electron microscopy (HRTEM/HRSTEM) has unique advantages in observing defects and disorders [2]. However, it is very challenging to obtain high atomic resolution images from porous materials because of electron beam damage. Three-dimensional electron diffraction (3D ED) requires, on the other hand, two orders of magnitude lower electron dose than HRTEM/HRSTEM, which is more useful for studying beam-sensitive samples [3-4]. 3D ED has been shown to be powerful for determination of atomic structures from nano- and micron-sized crystals that are too small to be studied by single crystal X-ray diffraction [5]. In this talk, I will give several examples on how various imaging and 3D ED techniques can be used for *ab initio* structure determination of novel nanoporous materials, and for studying defects and crystal intergrowth. Using HRTEM imaging, it was possible to observe atomic surfaces and crystal interfaces in zeolites [6-7], as well as missing linkers/clusters in MOFs. Using 3D ED, we can identify missing clusters (0 D), chain disorders (1 D) and layer stacking faults (2 D) [8-9]. With the sub-Ångström resolution of 3D ED data, it was possible to resolve and refine disordered atomic sites that are only 0.4 Å apart, from which the nature of the disorders in zeolites could be elucidated. Finally I will show how 3D ED can be used to visualize the structural transformation of a series of zeolites obtained by defect engineering.

[1] Sholl, D.S. & Lively R.P. (2015). *J. Phys. Chem. Lett.* **6**, 3437-3444.
[2] Willhammar, T. & Zou, X. (2013). *Z. Kristallogr.* **228**, 11-27.
[3] Wan, W., Sun, J., Su, J., Hovmöller, S. & Zou, X. (2013). *J. App. Crystallogr***. 46**, 1863-1873.
[4] Cichocka, M.O., Jonas Ångström, J., Wang, B., Zou, X. & Smeets, S. (2018). *J. Appl. Cryst.*, **51***,* 1652-1661.
[5] Zhehao Huang, Z., Willhammar, T. & Zou, X. (2021). *Chem. Sci*. **12**, 1206-1219.
[6] Smeets, S.; Xie, D.; Baerlocher, C.; McCusker, L. B.; Wan, W.;Zou, X.; Zones, S. I. (2014). *Angew. Chem. Int. Ed.*, **53**, 10398-10402.
[7] Willhammar, T., Sun, J., Wan, W., Oleynikov, P., Zhang, D., Zou, X., Moliner, M., Gonzalez, J., Martínez, C. & Rey, F. (2012). *Nat. Chem.* **4**, 188−194.
[8] Jo, D., Zhao, J., Cho, J., Lee, J.H., Liu, Y., Liu, C.-J., Zou, X. & Hong, S.B. (2020). *Angew. Chem. Int. Ed.* **59**, 17691–17696.
[9] Kapaca, E., Jiang, J., Cho, J., Jose L. Jorda, J.L., Diaz-Cabañas, M.J., Zou, X., Corma, A. & Willhammar, T. (2021) *J. Am. Chem. Soc.,* **143**, 8713–8719.

I would like to thank the former and current group members who contributed to the method developments and the work presented here, and collaborators who provided interesting and challenging samples. The work has been supported by Swedish Research Council (VR), the Knut and Alice Wallenberg Foundation (KAW) and the EU H2020 MSCA-ITN NanED project.

A042 Quantum Materials

Room 220

1.10pm - 3.30pm

A042-01-240823

Studying the spin-liquid behaviour in $A_2RE_3Sb_3O_{14}$ and derivatives

Pragati M. Pherwani, S.D Kaushik

UGC-DAE-Consortium for Scientific Research Mumbai centre

Email id: pherwanipm@barc.gov.in, sdkaushik@csr.res.in

Keywords: Spin liquids, Kagome lattice, Neutron diffraction

Kagome structures are structures exhibiting frustrated magnetism due to their triangular geometry. A three-dimensional analogue of the Kagome lattice is the pyrochlore lattice (represented as $A_2B_2O_7$) which is constructed from corner sharing tetrahedra. Pyrochlore lattices (space group Fd-3m) containing A and B type of cations (magnetic, non-magnetic ions) that are stacked alternatively as A_3B and B_3A layers [1]. By selective doping of nonmagnetic ions, two-dimensional Kagome lattice can be isolated from the pyrochlore lattice. In the Tripod Kagome Lattice (TKL) compound, spins remain entangled and do not order in the zero-temperature limit [2]. Therefore, the kagome compounds are potential candidates for quantum spin liquid.

We aim to scrutinize the structural and physical properties of $A_2R_3Sb_3O_{14}$ (A = Mg,Zn,Co,Ca ; R = Ho,Pr). The scope of the study includes magnetic and transport properties along with crystal structure and magnetic structure of these compounds. We have prepared $Mg_2Ho_3Sb_3O_{14}$, $Zn_2Ho_3Sb_3O_{14}$, $Co_2Ho_3Sb_3O_{14}$, $Ca_2Pr_3Sb_3O_{14}$ compounds by solid-state reaction method and the XRD study shows that the majority phase is $Mg_2Ho_3Sb_3O_{14}$, (Mg-Ho) with some impurity phase. The neutron diffraction study confirms formation of Zn-Ho in single phase whereas Co-Ho and Ca-Pr are still under study. Magnetization study for Zn-Ho has been carried out by employing Physical Properties Measuring Systems (PPMS) with a magnetic field of 1000 Oe in the temperature range of 3K to 300K. No magnetic ordering was observed down to 3K The temperature-dependent neutron diffraction by employing a powder neutron diffractometer (PD-3) is underway. Analysis of temperature-dependent neutron diffraction will lead us to understanding of magnetism involved. Through this systematic study, we also intend to explore the quantum spin liquid state in these compounds.

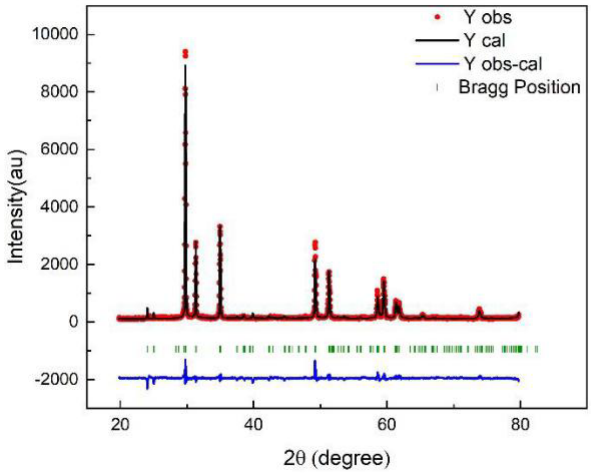

Fig1: Reitveld refinement profile for $Zn_2Ho_3Sb_3O_{14}$

1 Zhao-Feng Ding, Yan-Xing Yang, Jian Zhang, Cheng Tan, Zi-Hao Zhu, Gang Chen, and Lei Shu

2 Z. L. Dun, J. Trinh, M. Lee, E. S. Choi, K. Li, Y. F. Hu, Y. X. Wang, N. Blanc, A. P. Ramirez, and H. D. Zhou PHYSICAL REVIEW B 95, 104439 (2017)

A042-02-240823

Contrasting magnetic and multiferroic properties in the isostructural polar magnets Lu*M*WO$_6$ (*M* = Fe and Cr)

S. Mishra[1], P. Yanda[1], F. Orlandi[2], P. Manuel[2], H. J. Koo[3], M. H. Whagnbo[3,4], A. Sundaresan[1]

[1]*School Advanced Materials, Chemistry and Physics of Materials Unit,*
Jawaharlal Nehru Centre for Advanced Scientific Research, Jakkur P.O., Bangalore 560064 India,
[2]*ISIS Facility, Rutherford Appleton Laboratory, Didcot OX11 0QX, United Kingdom,*
[3]*Department of Chemistry and Research Institute for Basic Sciences, Kyung Hee University, Seoul 02447, Republic of Korea,*
[4]*Department of Chemistry, North Carolina State University, Raleigh, North Carolina*

sundaresan@jncasr.ac.in

Keywords: Aeschynites, polar magnetic oxides, multiferroic, noncollinear and collinear commensurate spin structure

The compounds, LuFeWO$_6$ and LuCrWO$_6$, prepared under high pressure, and high-temperature crystallize in a polar orthorhombic aeschynite-type mineral structure (space group *Pna*2$_1$) with the ordered Fe^{3+}/Cr^{3+} and W^{6+} ions. Magnetization measurements reveal the antiferromagnetic ordering of Fe^{3+} spins at T_N = 11.8 K and the Cr^{3+} spins at T_N = 19.2 K, respectively. Analysis of neutron diffraction data at 1.5 K reveals an unusual noncollinear magnetic structure in LuFeWO$_6$ with **k** = (0, ½, ½), and a collinear magnetic structure with **k** = (0, 0, 0) for LuCrWO$_6$. The absence of switchable polarization indicates that both compounds are pyroelectric in the paramagnetic state. A dielectric anomaly and a change in polarization (ΔP) occur at T_N in LuFeWO6, demonstrating magnetoelectric coupling. On the other hand, no additional polarization occurs at T_N in LuCrWO$_6$; hence, this compound remains multiferroic without significant magnetoelectric coupling. In my talk, I will discuss the contrasting magnetic and magnetoelectric behavior of these compounds.

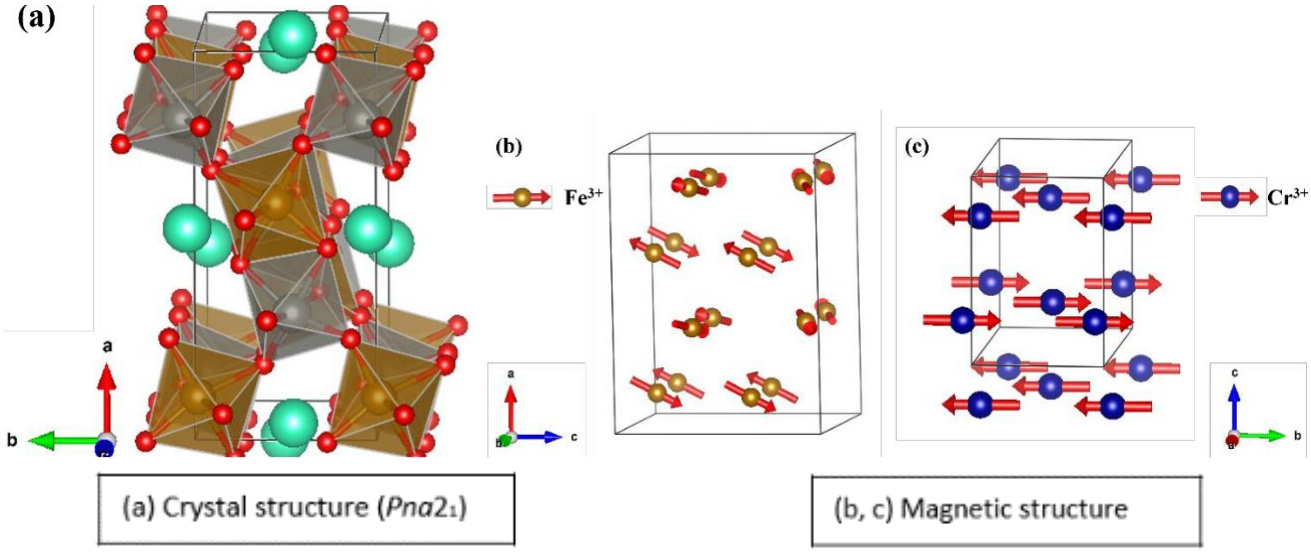

Figure 1. (a) The ordered aeschynite-type crystal structure of Lu*M*WO6 (*M* = Fe and Cr). Lutetium (Turquoise), Transition metal (Brown), Tungsten (Grey), and Oxygen (Red). (b and c) Noncollinear magnetic structure in LuFeWO6 and collinear in LuCrWO6.

1 S. Mishra, P. Yanda, F. Orlandi, P. Manuel, H. J. Koo, M. H. Whangbo, and A. Sundaresan (Submitted for publication)

A042-03-240823

Bulk crystal growth of materials with possible novel quantum states with *R*MX structure-type

B. Pomjakushina[1]

[3] *Laboratory for Multiscale Materials Experiments, Paul Scherrer Institut, 5232 Villigen PSI, Switzerland*
ekaterina.pomjakushina@psi.ch

Keywords: floating zone, flux-growth, Weyl semimetals

In ternary intermetallic systems *R*MX structure-type class of materials, where *R* being a rare earth metal, M a transition metal and a main group element, the hybridization between the localized f-electrons of rare-earth elements, and the itinerant conduction d-electrons supplied by surrounding atoms, leads to very extraordinary physical phenomena. First discovered in 1992, *R*AlGe (*R* – rare earth metal) was reported initially to crystallize in the so-called $ThSi_2$ structure-type with a centrosymmetric space group I41/amd (No. 141) [1]. Later on, it has been realized instead that *R*AlGe crystallizes in the LaPtSi-type structure,[2,3] with a body-centered space group I41md (No. 109).

From recent first principle theoretical calculations, it has been predicted that the members of the *R*AlGe (*R* = Pr, Ce) system, which crystallize in the LaPtSi-type structure, are new magnetic Weyl semimetals[4]. This system offers remarkable tunability, since the number and location of Weyl nodes may be controlled by choice of the rare-earth metal, and the types of broken symmetry, via the Al/Ge content. In addition, in the presence of combined broken symmetries, the system offers a rich phase diagram that may be explored via self-doping or chemical substitution. Therefore, to enable a broad range of experimental studies on this class of material, there is a clear interest in establishing the details for the growth of sizable (mm^3) single crystals and their basic physical characterization.

Recently we have reported on the crystal growth by floating zone and a flux-growth techniques and basic characterization of *R*AlGe family (*R* = Ce, Pr) .[5] We investigated the macroscopic and microscopic physical properties of the solid solution of $Ce_{1-x}Pr_xAlGe$ [6] and reported the discovery of topological magnetism in the candidate magnetic Weyl semimetal CeAlGe.[7] In my talk I will show the difficulties of crystal growth of this family of compounds and related materials and compare their properties depending on different crystal growth methods.

[3] S. Dhar, S. Pattalwar, R. Vijayaraghavan (1992). *Journal of Magnetism and Magnetic Materials*, **104-107**, 1303.
[4] S. Dhar and S. Pattalwar **(1996).** *Journal of Magnetism and Magnetic Materials*, **152**, 22.
[5] E. Gladyshevskii N. Nakonechna, K. Cenzual, R. Gladyshevskii, J.-L. Jorda (2000). *Journal of Alloys and Compounds,* **296**, 265.
[6] Guoqing Chang, Bahadur Singh, Su-Yang Xu, et al. **(2018).** *Physical Review B*, **97**, 04114.
[7] P. Puphal, C. Mielke, N. Kumar, Y. Soh, T. Shang, M. Medarde, J. S. White, E. Pomjakushina (2019). *Physical Review Materials,* **3**, 024204.
[8] Pascal Puphal, Sarah Krebber, Emmanuelle Suard, Robert Cubitt, Chennan Wang, Tian Shang, Victor Ukleev, Jonathan S. White, and Ekaterina Pomjakushina (2020). *Physical Review B,* **101**, 214416.
[9] Pascal Puphal, Vladimir Pomjakushin, Naoya Kanazawa, Victor Ukleev, Dariusz J. Gawryluk, Junzhang Ma, Muntaser Naamneh, Nicholas C. Plumb, Lukas Keller, Robert Cubitt, Ekaterina Pomjakushina, Jonathan S. White (2020). *Physical Review Letters,* **101**, 214416.

A042-04-240823

Growth and magnetic properties of M_2TiO_4 (M=Mn, Fe and Co) single crystals

Dharmalingam Prabhakaran[1]

[1]*Department Of Physics, University of Oxford, Oxford OX14 1XR, United Kingdom*

E-mail: d.prabhakaran@physics.ox.ac.uk

Keywords: Crystal growth, inverse spinel, frustrated magnet

The spinels AB2O4, are a common class of cubic compounds ($Fd3^{"}m$), with a frustrated corner sharing tetrahedral network of B-site atoms [1]. The cubic phase has mixed occupancies and adopts the so called inverse spinel structure, meaning that the cations take the positions B[AB]O4, rather than the 'normal' distribution in A[B2]O4 [2]. The normal and ordered-inverse spinel structures are also known to undergo characteristic structural changes as a function of temperature, which are a consequence of the A and B cations exchanging their lattice sites [3].

In normal spinel, what happens is a continuous increase in disorder, also known as nonconvergent disordering, which preserves the overall cubic ($Fd3^{"}m$) symmetry. In the case of the M2TiO4 (M=Mn, Fe, Co and Zn) system, it has been assumed that the electronic state of Ti in M2TiO4 is Ti^{4+}, similar to M2SnO4 where Sn^{4+} is more stable. However, recently we have observed that the electronic state of Ti in M_2TiO_4 is not diamagnetic Ti^{4+} but primarily magnetic Ti^{3+} resulting in the configuration $[M^{2+}][M^{3+}Ti^{3+}]O4$. It is a ferrimagnetic compound that undergoes a compensating magnetic transition depending on the transition metals; Mn= 48K, Fe= 58K, and Co=28K respectively. In the case of Mn2TiO4, two different structures have been reported; cubic (*Fd-3 m*) when Mn^{2+} and Ti^{4+} occupy B sites randomly, and tetragonal (*P4322*) when Mn^{2+} and $Ti^{4+}$are ordered on B sites [5].

In this talk, I will present some of the growth challenges and how to control the valency state of M2TiO4 (Mn, Fe and Co) and Co2SnO4 single crystals. The crystal structural of the synthesised powder and single crystals and magnetic anisotropy of these family of materials will be discussed.

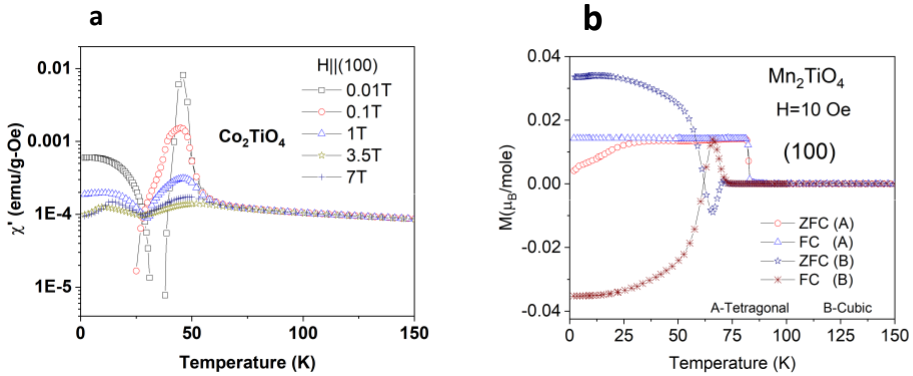

Fig. (a). Temperature dependence of magnetisation measured along (100) direction of cubic Co2TiO4 and (b) Mn2TiO4 tetragonal (A) and cubic (B) crystals

[1] W.H. Bragg, Nature 95 561 (1915)

[2] S.K. Banerjee, et al Phys. Letters **20**, 455 (1966).

[3] Vladan Stevanovic, et al. J. Am. Chem. Soc. **133**, 11649 (2011).

[4] S. Nayak, S. et al. Phys. Rev. **92**, 214434 (2015).

[5] Q. Liu, et al. J Magn. Magn. Materials 546 (2022) 168864.

Acknowledgments: I would like to acknowledge U.K. Engineering Physical Science Research Council (EPSRC grant no. EP/T028637/1) and Oxford-ShanghaiTech collaboration project for their financial support.

A042-05-230823

Topological nodal lines in bulk and monolayer $W_2O_3I_4$

Taikang Chen[1ξ], Yu Zhu [1ξ], Chang Liu[1], Yongchang Li [1], Guangsheng Song[2], Xiangjian Meng[4], Xiaoshuang Chen[4], Heng Gao[1,2,3,4*], and Wei Ren[1,5‡]

Department of Physics, Shanghai Key Laboratory of High Temperature Superconductors, International Centre of Quantum and Molecular Structures, Shanghai University, Shanghai 200444, China
Key Laboratory of Green Fabrication and Surface Technology of Advanced Metal Materials (Anhui University of Technology), Ministry of Education, Maanshan 243002, China
State Key Laboratory of Surface Physics and Department of Physics, Fudan University, Shanghai 200433, China
State Key Laboratory of Infrared Physics, Shanghai Institute of Technical Physics, Chinese Academy of Sciences, 200083, Shanghai, China
Zhejiang Laboratory, Hangzhou 311100, China

Email of communicating renwei@shu.edu.cn

Keywords: Topological nodal line, external field modulation, spin-orbit coupling

Recently, a new phase of tungsten oxyhalide $W_2O_3I_4$ has been synthesized in experiment [1]. Surprisingly this material has never been studied by theoretical prediction, nor has its specific electronic structure been discussed. By means of first-principles calculations, we study the topological nontrivial electronic structures and lattice dynamics of bulk and monolayer $W_2O_3I_4$ [2]. We find that both of them are nodal line semimetals in the absence of spin-orbit coupling (SOC). Moreover, $W_2O_3I_4$ bulk and monolayer exhibit excellent mechanical and thermal stability. By studying the external field modulation of topological nodal lines without SOC effect in monolayer $W_2O_3I_4$, we find that the nodal lines are extremely robust against the biaxial strain but destroyed under vertical electric field due to the breaking of horizonal mirror symmetry.

[1] M. Löber, M. Ströbele, C. P. Romao, and H.-J. Meyer, Dalton Transactions **50**, 6789 (2021).
[2] T. Chen, Y. Zhu, C. Liu, Y. Li, G. Song, X. Meng, X. Chen, H. Gao and W. Ren, Phys. Rev. B **107**, 205411 (2023).

A042-06-240823

Coherent magnetic excitations in the Kondo semimetal $CeFe_2Al_{10}$

D. T. Adroja,[1, 2], Zhihui Luo[3], Dao-Xin Yao[3], Peter S. Riseborough[4], Y. Muro[5], H. C.Walker[1], Yijie Zeng[6], T. Takabatake[7], J.-M. Mignot[8], K. A. McEwen[9] and A. T. Boothroyd[1]

[1]*ISIS Neutron and Muon Source, STFC-Rutherford-Appleton Laboratory, Harwell Campus, Oxfordshire, OX11 0QX, UK*

[2]*Highly Correlated Electron Group, Physics Department, University of Johannesburg, P.O. Box 524, Auckland Park 2006, South Africa*

[3]*State Key Laboratory of Optoelectronic Materials and Technologies, School of Physics, Sun Yat-Sen University, Guangzhou 510275, China*

[4]*Department of Physics, Temple University, Barton Hall, 1900N. 13th Street, Philadelphia, PA 19122, USA*

[5]*Faculty of Engineering, Toyama Prefectural University, Imizu 939-0398, Japan*

[6]*Hangzhou Dianzi University, Hangzhou 310018, China*

[7]*Graduate School of Advanced Science and Engineering, Hiroshima University, Higashi-Hiroshima, 739-8530, Japan*

[8]*Laboratoire Léon Brillouin, CEA-CNRS, CEA/Saclay, 91191 Gif sur Yvette, France*

[9]*Department of Physics and Astronomy, University College London, Gower Street, London WC1E 6BT*

[10]*Department of Physics, Clarendon Laboratory, Oxford University, Oxford OX1 3PU, United Kingdom*

Email: debashibhai.adroja@stfc.ac.uk

Keywords: Magnetic excitations, Kondo insulator, Neutron scattering study

Recently the orthorhombic compound CeT_2Al_{10} (T=Fe, Ru and Os) have attracted considerable interest in the condensed matter physics due to unusual physical properties [1-3]. The Ru- and Os-based systems exhibit an antiferromagnetic (AFM) ordering with relatively high Néel temperatures of T_N = 27 and 28.5 K and reduced ordered state Ce magnetic moments of 0.3–0.4 μ_B aligned along the CEF hard axis (c-axis) [1, 2]. On the other hand, $CeFe_2Al_{10}$ compound, however, shows no magnetic ordering down to 80 mK and exhibits Kondo insulating ground state [3]. We have used time-of-flight inelastic neutron scattering to map the low energy magnetic excitation spectrum of the Kondo insulator $CeFe_2Al_{10}$ throughout the Brillouin zone, and to measure its temperature dependence. Our inelastic neutron scattering (INS) spectra reveal an 8 meV spin gap along all high symmetry directions, and a maximum energy of ~20 meV at 5 K. The excitations exhibit both excitonic (in the ab-plane) and spin-wave-like (along the c-axis) characteristics. A crossover from a coherent to an incoherent magnetic response occurs as the temperature is raised to 100 K. We present the theoretical calculations to understand the ground state property and observed magnetic excitations. Our calculations with density functional theory combined with dynamical mean-field theory down to 10 K verify a Fermi liquid semimetallic ground state with strong mixing of Ce 4f and Fe 3d states, suggesting a particle–hole scenario for the magnetic excitations and strong suppression of the effective magnetic coupling. We have used a four-band Anderson lattice model, which reproduces the salient features of the magnetic excitation spectrum. The results show that the magnetic excitation spectrum of correlated ground state of heavy fermion systems can be explained using the Anderson lattice model.

2 Kato, H., Kobayashi, R., Takesaka, T., Nishioka, T., Matsumura, M., Kaneko, K., and Metoki, N., (2011) . *J. Phys. Soc. Japan* **80**, 073701.

3 Khalyavin, D.D, Hillier, A.D., Adroja, D.T., Strydom, A.M., Manuel, P, Chapon, L.C., Peratheepan, P., Knight, K., Deen, P., Ritter, C., Muro, Y., and Takabatake, T., (2010). Phys. Rev. B **82**, 100405

4 see for review, Adroja, D.T., Muro, Y., Takabatake, T., Le, M., Walker, H., McEwen, K., and Boothroyd, A.T., (2016). Solid State Phenomena, **257**, 11.

5 Adroja, D.T., Luo, Z., Yao, D.-X,, Riseborough, P.S., Muro, Y., Walker, H. C., Zeng Y., Takabatake, T., Mignot, J.-M., McEwen, K. A., and Boothroyd, A. T., (2022). Manuscript in preparation

A077 Phase Transitions
Room 211
1.10pm - 3.30pm

A077-01-240823

Synergistic hydration-distortion mechanism in 6H-$Ba_4Ta_2O_9.½H_2O$

C.D. Ling[1], F.P. Marlton[1], A. J. Brown[1], M. Sale[1], W. Lewis[1], I. Luck[1], M.L. Wood[1], A. Maljuk[2], B. Büchner[2], R.A. Mole[3]

[1]The University of Sydney, Sydney 2006, Australia; [2]IFW-Dresden, Helmholtzstraße 20, 01069 Dresden, Germany; [3]ANSTO, New Illawarra Road, Lucas Heights 2234, Australia

chris.ling@sydney.edu.au

Keywords: Perovskite, phase transition, ionic conduction

Lattice hydration plays a critical role in proton conduction, which is a critical materials property for energy technologies including solid-oxide fuel cells. It also plays an important role in the Earth sciences, where even at ppm levels, the pressure- and temperature-dependencies of hydration processes mean that they affect the total amount of water available on Earth and the rheological properties of the lithosphere (plate tectonics, earthquakes etc.). In this presentation we report the discovery of a synergistic hydration-distortion mechanism in the hexagonal perovskite 6H-$Ba_4Ta_2O_9$, whereby the presence of very large Ba^{2+} cations in octahedral interstitial sites (perovskite-type *B* sites) forces the adjacent vacant octahedral interstitial sites to also expand, allowing them to hydrate. This destabilises the structure so that it distorts on cooling in a way that cannot be explained by conventional symmetry lowering. The mechanism is distinct from conventional hydration of metal oxides via hydroxylation of oxide vacancies or layered intercalation, and to the best of our knowledge is unique among close-packed ionic compounds at ambient pressure.

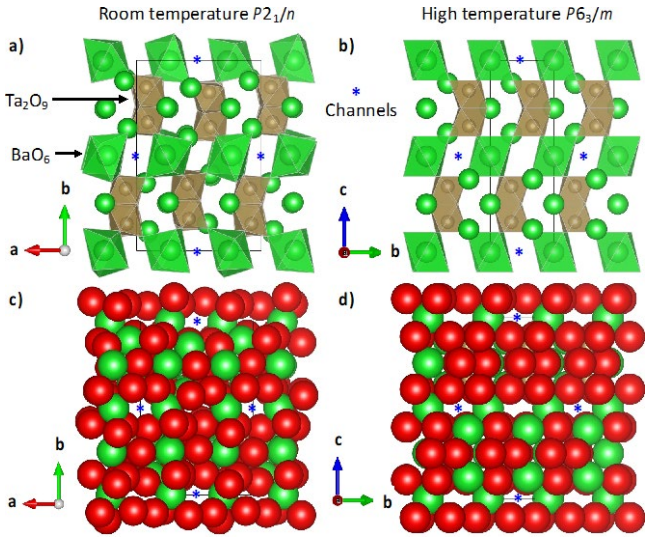

Figure 1. Polyhedral representations of the a) room-temperature and b) high-temperature structures of 6H-$Ba_4Ta_2O_9$. The same structures are shown in c) and d) respectively, in close-packed representations. Ba and Ta atoms and their corresponding octahedra are green and brown, respectively; O atoms are red. Blue asterisks (*) mark the location of the interstitial site channels that selectively hydrate and expand on cooling, driving an unusual symmetry lowering pathway.

A077-02-240823

In situ high-temperature 3D-reciprocal space mapping as a new way to study solid state phase transition

R. Guinebretière[1], D.P. Fowan[1], E. Thune[1], R.R.P. Purushottam Raj Purohit[2], S. Arnaud[3], G. Chahine[4], N. Blanc[3], O. Castelnau[5]

[1]Université de Limoges, IRCER, UMR CNRS 7315, 12 rue Atlantis, Limoges 87068, France
[2]Université Grenoble Alpes, CEA, IRIG, MEM, CNRS, 17 avenue des Martyrs, Grenoble, 38000, France
[3]Université Grenoble Alpes, CNRS, Institut Néel UPR CNRS 2940, 38000 Grenoble, France.
4 Université Grenoble Alpes, SIMaP, Grenoble INP, CNRS, 38000 Grenoble, France
[5]Laboratoire PIMM, UMR CNRS 8006, ENSAM, CNAM, 151 Bd de l'Hôpital, 75013 Paris, France
rene.guinebretiere@unilim.fr

Keywords: 3D-reciprocal space mapping, Phase transitions, in situ at high temperature

Solid-state phase transitions (SPT) are fundamental processes that are driving a large part of the effective physical properties of single crystals as well as polycrystalline materials. In addition to the structural evolutions that can be described by space group transitions, SPTs are often associated with transformations that occur at the mesoscale and generate structural defects such as dislocations, twinning, stacking faults, strain fields, etc. Such defects can be detected and quantitatively studied in the reciprocal space through high-resolution x-ray diffraction experiments. Originally developed to study defects in epitaxial layers, the Reciprocal Space Mapping (RSM) method has been extended to cover everything from imperfect single crystals to complex polycrystals. Over the past decade, the widespread use of 2D solid-state detectors at synchrotron radiation sources has promoted the development of 3D-RSM on timescale that enables to follow the sample evolutions as a function of external stimuli. In the case of polycrystals, it has been shown that this approach allows to select the crystals of interest in reciprocal space from all the crystals constituting the probed volume. We have recently shown that this method can be used even at very high temperature (over 1000 °C) [1, 2]. We will show during the conference that high temperature 3D-RSM can be extended to in situ observation of solid-state phase transition allowing to evidence the formation of crystallographic variants and twins.

The potential of this approach will be illustrated by the in situ study of two successive phase transitions in pure zirconia dense polycrystal. Under atmospheric pressure, pure zirconia solidifies into a cubic crystal structure (c) (space group Fm3m). Upon cooling it transforms first to tetragonal (t) (space group P42/nmc) and then to monoclinic (m) (space group P21/c). We will show that the method allows following the temperature induced splitting of an initially unique Reciprocal Lattice Node (RLN) into 24 RLNs generated by the loss of symmetry axis through two successive phase transitions. Moreover, since the SPT occurs under huge stresses [3], the RLNs are embedded in a large, 3-dimensional, diffuse scattering signal that is very clearly evidenced (see Fig. 2). The crystallographic interpretation of RLN splitting and the diffuse scattering signal associated with the phase transitions in pure zirconia polycrystal will be discussed during the talk according to [2] and another article that we published in October 2022 [4].

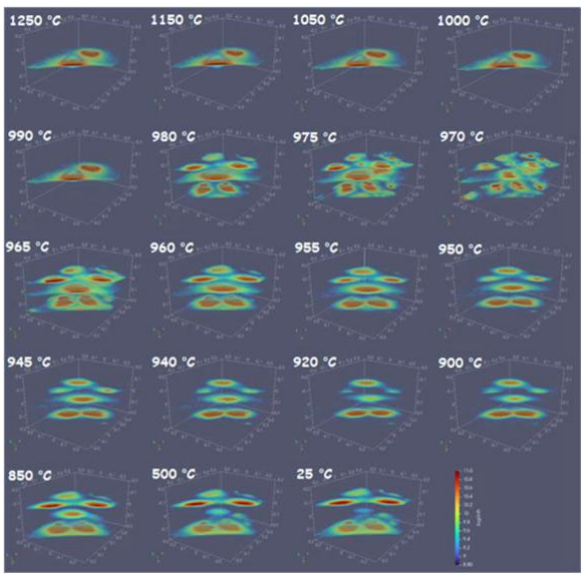

Figures 1. in situ high-temperature observation of the splitting of the tetragonal 111 RLN during the tetragonal to monoclinic phase transition in pure zirconia.

1 Guinebretière, R., Arnaud, S., Blanc, N., Boudet, N., Thune, E., Babonneau, D., Castelnau, O. (2020) J. Appl. Cryst. 53, 650-661.
2 Guinebretière, R., Ors, T., Michel, V., Thune, E., Huger, M., Arnaud, S., Blanc, N., Boudet, N., Castelnau, O. (2022) Phys. Rev. Mater. 6, 013602.
3 Ors, T., Gouraud, F., Michel, V., Huger, M., Gey, N., Micha, J.S., Castelnau, O., Guinebretière, R. (2021) Mater. Sci. Eng. A 806, 140817.

4 Purushottam Raj Purohit, R.R.P., Fowan, D.P., Thune, E., Arnaud, S., Chahine, G., Blanc, N., Castelnau, O., Guinebretière, R. (2022) Appl. Phys. Lett. 121, 191901.

A077-03-240823

Crystal structure evolution in mercury containing quadruple perovskites

W.-T. Chen [1,2] , E.-P. Liu [1,3] , C.-W. Wang [3] , M. Senn [4]

[1] Center for Condensed Matter Sciences and Center of Atomic Initiative for New Materials, National Taiwan University,
[2] Taiwan Consortium of Emergent Crystalline Materials, National Science and Technology Council, Taipei City, Taiwan,
[3] Department of Physics, National Taiwan University, Taipei City, Taiwan,
[4] National Synchrotron Radiation Research Center, Hsinchu City, Taiwan,
[5] Department of Chemistry, University of Warwick, Coventry, United Kingdoms
weitinchen@ntu.edu.tw

Keywords: charge ordering, high pressure synthesis, quadruple perovskite

AMn$_7$O$_{12}$ manganite belongs $AA'_3B_4O_{12}$ quadruple perovskite family, where $Mn^{A'}$ Mn^B cations occupy square-planar and heavily tilted octahedral sites, respectively. Novel quadruple perovskite AMn$_7$O$_{12}$ (A = Hg, HMO) was prepared by high pressure high temperature (HPHT) synthesis techniques and exhibit multiferroic property at low temperature. [1] In addition to the charge ordering phase transition from cubic to rhombohedral phases observed at its analogue cousin CaMn$_7$O$_{12}$, HMO experiences a further symmetry-lowering phase transition to *Pnn*2 orthorhombic phase close to room temperature ~260 K. It was revealed from symmetry element analysis that the improper ferroelectric polarization in HMO originates from the lattice instabilities directly linked to charge and orbital degrees of freedom. On the other hand, AMn$_7$O$_{12}$ solid solution (A = $La_{1-x}Ca_x$ and $Na_{1-x}Ca_x$) series were also realized by HPHT techniques. [2] Detailed crystallographic study revealed the evolution of tetragonality and the transformation of orbital ordering distortion modes in the solid solution. An alternating ordered-insulating and disordered-conducting electron stripes arrangement was observed at particular doping region, showing a new state of matter. From these studies, it was demonstrated that while the A'-site is rather robust, the charge and orbital ordering and their intrinsic coupling are very sensitive to the A cation oxidation state and consequently B cation valence. In this report, the rhombohedral to orthorhombic phase transition observed in HMO is further investigated with chemical pressure, electron- and hole-doping, and the crystal structure evolution of HMO pristine material are discussed.

[1] Chen, W.-T., Wang, C.-W., Wu, H.-C., Chou, F.-C., Yang, H.-D., Simonov, A. & Senn, M. S. (2018). *Phys. Rev. B*, **97**, 144102.

[2] Chen, W.-T., Wang, C.-W., Cheng, C.-C., Chuang, Y.-C., Simonov, A., Bristowe, N. C. & Senn, M. S. (2021). *Nat. Commun.*, **12**, 6319

Acknowledgements: This work was supported by National Science and Technology Council (Taiwan) with Grant Nos. 108-2112-M-002-025-MY3 and 111-2124-M-002-020, and National Synchrotron Radiation Research Center for the synchrotron XRD beamtimes and NPD supports.

A077-04-240823

Crystal polymorphs and multiple pathways of phase transitions in ionic liquids

H. Abe

National Defense Academy, Yokosuka 239-8686, Japan

ab@nda.ac.jp

Keywords: Keyword Crystal polymorph, Multiple pathways, Ionic liquids

Ionic liquids consist simply of a cation and an anion. The representative cation is 1-alkyl-3-methylimidazolium, $[Cnmim]^+$, where n reveals the alkyl chain length. Even in the simple molecular system, complicated phase transitions were observed at low temperature (LT) and high pressure (HP) [1-5]. The complicated phase behaviours were caused by a competition between molecular conformational polymorph and packing polymorph.

At LT, simultaneous X-ray diffraction and differential scanning calorimetry measurements were carried out using a vertical goniometer (SmartLab Rigaku Co.). A one-dimensional detector (D/teX, Rigaku Co.) was integrated into the diffractometer for rapid scanning. The X-ray incident wavelength was Cu Kα (λ = 0.1542 nm). HP X-ray diffraction experiments were performed using a Mao-Bell type diamond anvil cell (DAC) in the BL-18C of the Photon Factory (KEK in Japan). In a glovebox with dry flowing helium, the sample and ruby balls were loaded into DAC. A microbeam with a diameter of 35 m was obtained using double collimators. Two-dimensional (2D) diffraction patterns were obtained using an imaging plate system (BAS2500, Fuji-Film Co., Japan). Subsequently, the 2D data were converted into 1D intensity data to minimize the preferred orientation on the Debye rings. To eliminate air scattering, a vacuum chamber was used. The incident wavelength (0.08293 nm) was calibrated by using a standard CeO2 polycrystalline.

Figure 1 reveals the complicate phase behaviours of 1-butyl-3-methylimidazolium perfluorobutanesulfonate, [C4mim][PFBS]. Both cation and anion have conformational degrees of freedom (Fig. 1) [3]. The crystal structures of [C4mim][PFBS] are characterized by the long lattice constants, which are derived from the lattice modulations. At LT and HP, different kinds of crystal polymorphs were distinguished by X-ray diffraction. Particularly under HP, the HP crystal polymorph was irreversible upon compression and decompression. The hybrid layered structure, which is different from the liquid crystal-like layered structure, was formed. Moreover, gauche conformers both of cation and anion were preferred for the high packing efficiency. The HP-crystal polymorph based on the cationic and anionic conformational varieties supports a concept of the crystal energy landscape [6].

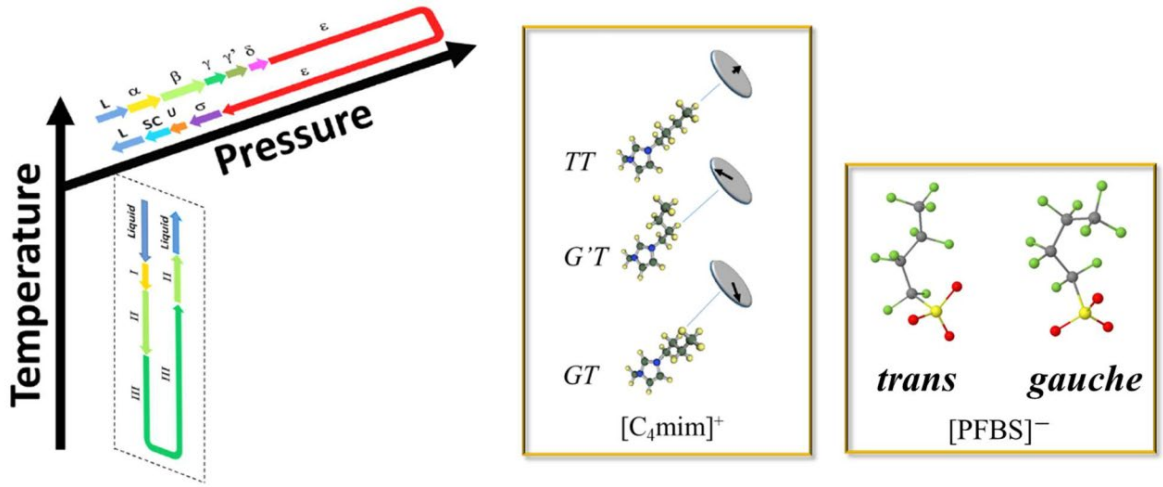

Figure 1. Schematic crystal polymorphs of [C4mim][PFBS] at LT and HP and their molecular conformers.

1 Koyama, Y., Shimono, S., Abe, H. & Matsuishi, K. (2020) J. Mol. Liq., 317, 113908.
2 Abe, H., Koyama, Y., Kishimura, H. & Matsuishi, K. (2020) J. Mol. Liq., 318, 113959.
3 Koyama, Y., Shimono, S., Kishimura, H., Takekiyo, T., Yoshimura, Y., Abe, H. & Matsuishi, K. (2021) J. Mol. Liq., 335, 116415.
4 Abe, H. & Kishimura, H. (2022) J. Mol. Liq., 352, 118695.
5 Abe, H., Koyama, Y., Shimono, S., Kishimura, H. & Matsuishi, K. (2022) Chem. Phys. 557, 111479.
6 Price, S. L. (2008) Phys. Chem. Chem. Phys., 10, 1996.

A077-05-240823

A combined neutron and DFT study of the pressure-induced structural transition in Zabuyelite (Li_2CO_3)

C.J. Ridley

ISIS Neutron and Muon Source, Rutherford Appleton Laboratories, Didcot OX11 0QX, United Kingdom

christopher.ridley@stfc.ac.uk

Keywords: lithium, high-pressure, neutron diffraction

Zabuyelite, Li_2CO_3, is one of the largest global sources of lithium, used as a precursor in the synthesis of lithium-ion battery cathode materials, the supply of which is increasingly stressed with a growing demand for battery technology. This is a field where the use of high-pressure has yet to be fully investigated; it can, for example, be used to stabilise the synthesis of unusually doped cathode materials which can then be recovered to ambient conditions [1], or be used to control particle size, or alter synthesis efficiency for existing materials. In addition, Zabuyelite has been demonstrated to be effective as a solvent-catalyst for diamond growth, a process of understated industrial importance [2]. Despite this, there is relatively little known about the crystallography of Li_2CO_3 at high-pressure, beyond the existence of a hexagonal phase at elevated pressures [3].

I present a full structural analysis of Zabuyelite as a function of applied pressure, as measured using neutron powder diffraction with a large volume press (from the PEARL instrument at the ISIS Neutron and Muon Source), supported with Raman spectroscopy measurements, and density functional theory (DFT) analysis. The carbonate was found to show unusual high-pressure behaviour, differing to that reported in the literature from X-ray measurements, showing negative linear compressibility, leading to a distortive first-order phase-transition to a hexagonal structure above ~8 GPa, with a change to octahedral Li^+ coordination.

1 Stoyanova, R., Zhecheva, E., Alcántara, R., Tirado, J-L., Bromiley, G., Bromiley, F. & Ballaran, T. B. (2002). Journal of Materials Chemistry **12**, 2501-2506.

2 Pal'yanov Yu. N., Sokol, A. G., Borzdov, Yu. M., Khokhryakov, A. F., Shatsky, A. F. & Sobolev, N. V. (1999). Diamond and Related Materials **8**, 1118-1124.

3 Grzechnik, A., Bouvier, P. & Farina L. (2003). Journal of Solid State Chemistry **173**, 13-19.

A077-06-240823

Structural and magnetic phase transitions in oxides and mixed-anion materials

E. E. McCabe

Department of Physics, Durham University, Durham DH1 3LE, U.K.

emma.mccabe@durham.ac.uk

Keywords: powder diffraction, magnetism, non-centrosymmetric

The properties of functional materials are determined in large part by their crystal structures (and symmetries), and so powder diffraction is a key technique for their characterisation. However, diffraction data alone, or data collected at a single point in the phase diagram, don't always allow a complete understanding of a material's properties. Exploring how structure and properties change in response to stimuli (e.g. temperature, applied magnetic field) and the nature of phase transitions can give a better understanding of the origins of functionalities including magnetic, dielectric and electronic properties.

This presentation focuses on structural and magnetic phase transitions (and transitions in which these are coupled) in transition metal oxides and mixed-anion materials including perovskite-related phases,[1] corundum-derived systems[2, 3] and layered oxychalcogenides.[4] The presentation the additional insight gained from neutron and x-ray powder diffraction experiments carried out as a function of temperature or applied magnetic field, and the importance of complementary techniques.

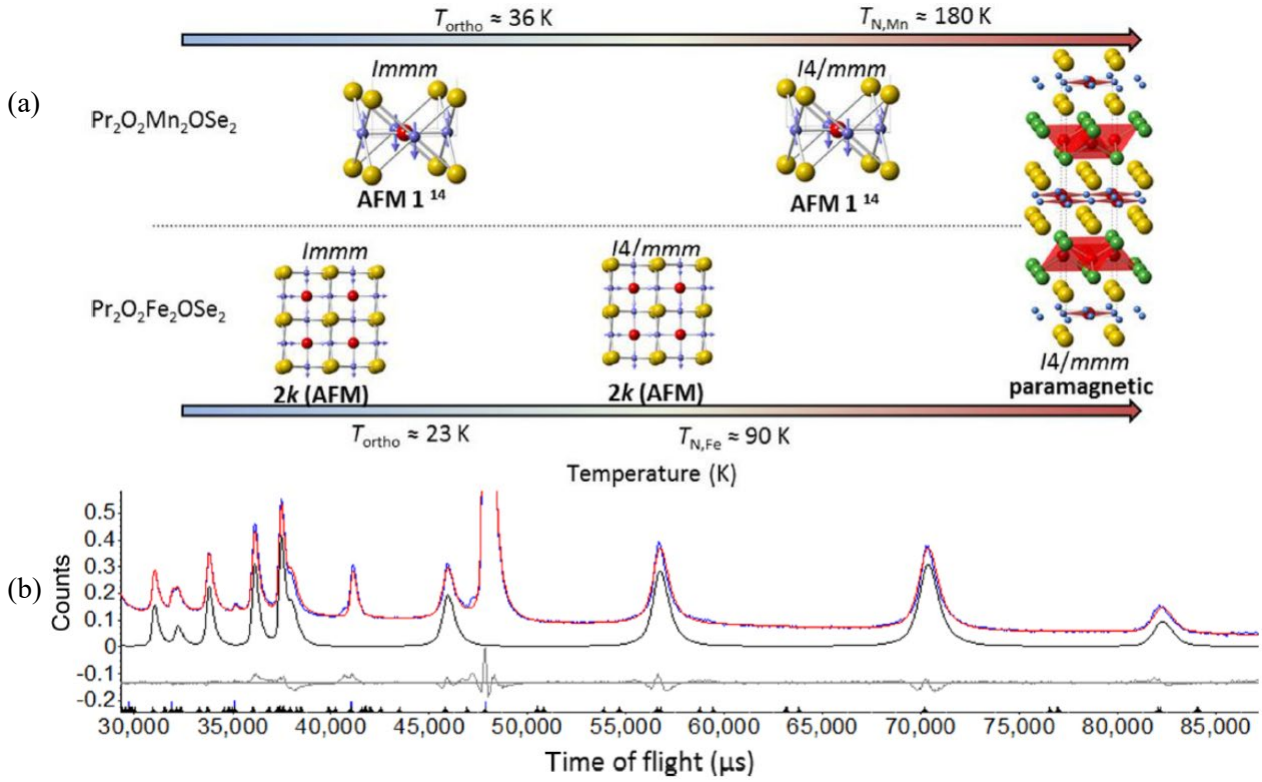

Figure 1. (a) Schematic illustrating phase transitions of $Pr_2O_2M_2OSe_2$ (in zero field) with temperature; (b) the higher *d*-spacing region Rietveld refinement profiles of NPD data (1.5 K, *M* = Fe) emphasizing magnetic reflections (black line).

1 V. A. Cascos, J. Roberts-Watts, C. Skingle, I. Levin, W. Zhang, P. S. Halasyamani, M. C. Stennett, N. C. Hyatt, E. Bousquet and E. E. McCabe, *Chemistry of Materials*, 2020, **32**, 8700-8712.

2 C. E. Frank, E. E. McCabe, F. Orlandi, P. Manuel, X. Tan, Z. Deng, C. Jin, M. Croft, T. Emge, S. Yu, H. Wang, V. Gopalan, S. Lapidus, M. Wu, M.-R. Li, J. Gross, P. Burger, A. Mielewczyk-Gryń, T. Klimczuk, W. Xie, D. Walker and M. Greenblatt, *Chemistry of Materials*, 2022, **34**, 5020-5029.

3 M.-R. Li, E. E. McCabe, P. W. Stephens, M. Croft, L. Collins, S. V. Kalinin, Z. Deng, M. Retuerto, A. Sen Gupta, H. Padmanabhan, V. Gopalan, C. P. Grams, J. Hemberger, F. Orlandi, P. Manuel, W.-M. Li, C.-Q. Jin, D. Walker and M. Greenblatt, *Nature Communications*, 2017, **8**, 2037.

4 R. Oogarah, C. Stockdale, C. Stock, J. S. O. Evans, A. S. Wills, J. W. Taylor, E. E. McCabe, *Phys. Rev. B*, 2017, **95**, 174441.

A077-07-240823

Revised phase diagram of low-Ti $PbZr_{1-x}Ti_xO_3$: strange modulations and diffuse scattering

A. Bosak[1], D. Chernyshov[2], S. Vakhrushev[3], I. Leontiev[4], N. Leontiev[4]

[1]*European Synchrotron Radiation Facility, Grenoble, France*

[2]*Swiss-Norwegian Beamlines at ESRF, 38043 Grenoble, France*

[3]*Laboratory of Neutron Research, The Ioffe Physical-Technical Institute, Saint-Petersburg, Russia*

[4]*Faculty of Physics, Southern Federal University, Rostov-on-Don, Russia*

bossak@esrf.fr

Keywords: PZT, diffraction, phase diagram

Lead zirconate-titanate (PZT) system likely is the most explored among ferroics, but multiple controversies still exist concerning the phase diagram. That is due to the fact that some regions are underexplored as they are less attractive for the application, but also because the most of studies are made on polycrystalline samples. The polycrystallinity can obscure and/or wash out significant features, hide phase transitions and displace the phase equilibria.

In this work we studied a set of PZT single crystals with Ti content up to ~6% by x-ray diffraction, establishing the new version of phase diagram (Figure 1). New diffraction station at ID28 ESRF beamline [1] was an indispensable tool for such a task, providing high momentum resolution together with high flux density and wide range of accessible temperatures.

Five phases were identified: O = orthorhombic phase *Pbnm*, as for pure $PbZrO_3$
R1 = low-temperature phase with superstructure spots in R points – rhombohedral or monoclinic
ICM = incommensurate monoclinic phase – superstructure spots in M points and (1/2±δ 1/2±δ ±δ) points, where d is of the order of 0.01 r.l.u. or less, monotonically changing with temperature.
R2 = high-temperature rhombohedral phase – no superstructure spots, diffuse intensity in M points
C = primitive cubic phase

Rather surprising feature is very large extent of field of incommensurate phase, identified as monoclinic. Symmetry of the phases and nature of transitions between them are discussed.

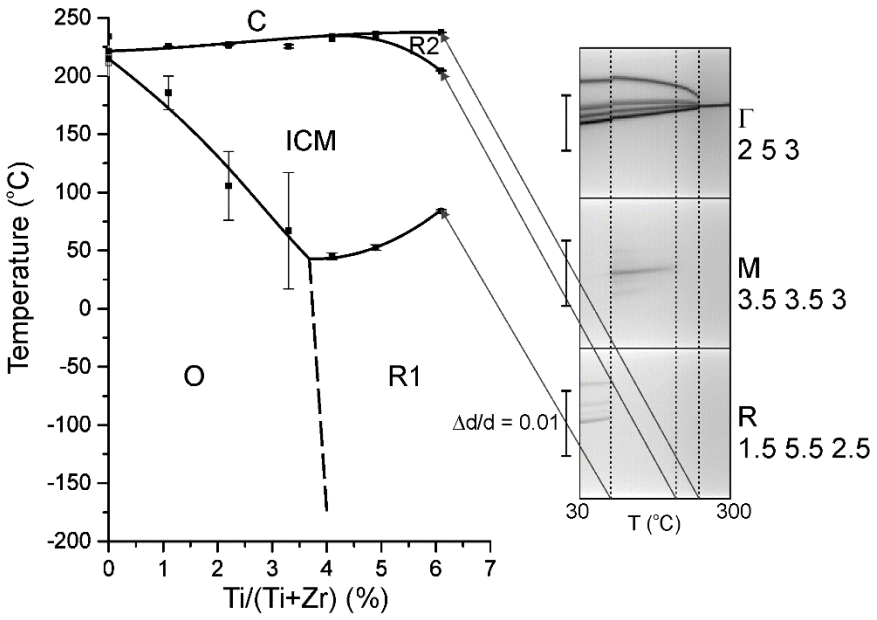

Figure 1. Phase diagram of $PbZr_{1-x}Ti_xO_3$ for x≤0.061. Solid symbols correspond to the average between cooling and heating transition temperatures, error bars denote the hysteresis. Insets represent the dependence of peak splitting from temperature.

[1] Girard A. *et al.* (2019). *Journal of Synchrotron Radiation*, **26**, 272.

A098 Postsynthetic modification of crystals

Room 210

1.10pm - 3.30pm

A098-01-240823

TAAC and TEAC, two topochemical reactions for synthesizing crystalline polymers

Kana M. Sureshan

School of Chemistry, IISER Thiruvananthapuram, Maruthamala, Thiruvananthapuram, Kerala-695551, India

kms@iisertvm.ac.in

Keywords: click chemistry, polymer, topochemical reactions, crystal engineering, topochemical polymerization

The properties of solid materials are decided by their molecular packing. Order imparts special properties to materials and polymers are no exception. However the polymer products formed in traditional solution-phase polymer synthesis are usually amorphous in nature. Topochemical reactions, the reaction between pre-organized reacting motifs in the crystal lattice, are attractive as they do not require solvents, catalysts and other special reaction conditions for the reaction and provide products in crystalline form.[1-2] We have employed thermal Topochemical Azide–Alkyne Cycloaddition (TAAC) reaction to synthesize various biopolymer mimics in crystalline form.[3] We have exploited hydrogen bonding for the pre-organization of monomers molecules in an arrangement suitable for their topochemical polymerization reaction. Lattice controlled polymerization reaction of such pre-organized monomers gave various biopolymer mimics.[4-8] Recently, we have developed Topochemical Ene-Azide Cycloaddition (TEAC) reaction for the synthesis triazoline linked polymers.[9] This novel methodology offers regiospecific and stereospecific synthesis of triazolines in the crystal and their facile denitrogenation to aziridines.[10] In this talk, the design and execution of such topochemical syntheses will be discussed.

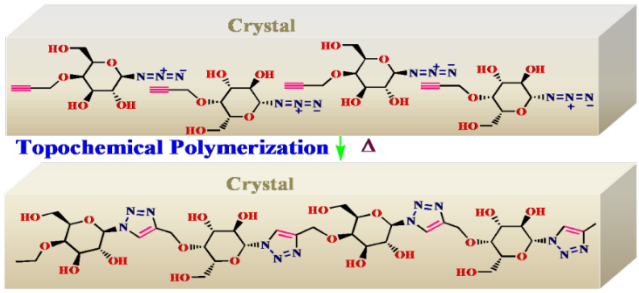

Figure 1. Schematic representation of TAAC polymerization

References

[1] Ravi, A., Hassan, S. Z., Bhandary, S. & Sureshan, K. M. (2022). *Angew. Chem. Int. Ed.*, **61**, e202200954

[1] Kuntrapakam, H., Ravi, A., Raju, C. & Sureshan, K. M. (2021). *Chem. Sci*., **12**, 5361-5380.

[2] Kuntrapakam, H., Ravi, A., Raju, C., Rai, R., Pathan, J. R. & Sureshan, K. M. (2021). *Chem. Soc. Rev*., **50**, 4062-4099.

[3] Kuntrapakam, H. & Sureshan, K. M. (2019). *Acc. Chem. Res*., **52**, 3149.

[4] Kuntrapakam, H., Raju, C., Bhandari, S. & Sureshan, K. M. (2022). *Angew. Chem. Int. Ed*., **61**, e202210733

[5] Raju, C., Kunnikuruvan, S. & Sureshan, K. M. (2022). *Angew. Chem. Int. Ed.,* **61**, e202210453

[6] Ravi, A., Hassan, S. Z., Bhandary, S. & Sureshan, K. M. (2022). *Angew. Chem. Int. Ed*., **61**, e202200954

[7] Rai, R. & Sureshan, K. M. (2022). *Angew. Chem. Int. Ed*., **61**, e202111623

[8] Athiyarath, V., Madhusudhanan, M. C., Kunnikuruvan, S. & Sureshan, K. M. (2022). *Angew. Chem. Int. Ed*., **61**, e202113129

[9] Khazeber, R. & Sureshan, K. M. (2021). *Angew. Chem. Int. Ed*., **60**, 24875-24881.

[10] Khazeber, R. & Sureshan, K. M. (2022). *Proc. Natl. Acad. Sci. U.S.A*., **119**, e2205320119

A098-02-240823

Post-synthetic transformation of metal-organic frameworks revealing secondary coordination sites for incorporation of catalytic metal centres

Pavel M. Usov[1], Terumasa Shimada[1], Misaki Aimoto[1], Yuki Wada[1], Takaya Matsumoto[1, 2] and Masaki Kawano[1]

[1]Department of Chemistry, School of Science, Tokyo Institute of Technology, 2-12-1 Ookayama, Meguro-ku, Tokyo 152-8550, Japan, [2]Central Technical Research Laboratory, ENEOS Corporation, 8 Chidoricho, Naka-ku, Yokohama, Kanagawa 231-0815, Japan

usov.p.aa@m.titech.ac.jp

Keywords: Metal-organic framework, Catalysis, X-ray absorption spectroscopy

Metal-organic frameworks (MOFs) are a class of porous materials composed of metal ions and organic linkers that have been extensively studied as platforms for the development of heterogeneous catalysts [1]. Due to their chemical tunability and highly ordered structures, MOFs offer unique advantages over other solid supports. Catalytic centres can be incorporated directly into the organic linkers, which allows to achieve very high density of active sites while maintaining pore access. However, when metal complexes are introduced using this strategy, their coordination can interfere with the formation of the framework backbone. To overcome this limitation, post-synthetic metal insertion is an attractive method since it separates MOF crystallisation and catalytic centre incorporation into two distinct steps [2].

In the present report, a novel organic linker featuring a five-membered ring core was developed and employed for the synthesis of Zr and Hf based frameworks [3]. The central motif acts as a protecting group and can undergo a ring-opening reaction to reveal a secondary coordination site, which could not be introduced into the framework by direct synthesis (Fig. 1). Uniquely, this modification induces a pivot motion through the centre of the linker causing buckling of the entire MOF structure. An Ir complex was inserted into the deprotected coordination sites, creating catalytically active frameworks (Fig. 1). The structural changes accompanying the post-synthetic ring opening of the linker and subsequent Ir incorporation were investigated using X-ray absorption spectroscopy (XAS) and X-ray total scattering techniques, uncovering rich structural dynamics. In addition, the resultant catalytic MOF displayed promising activity towards high-value chemical reactions.

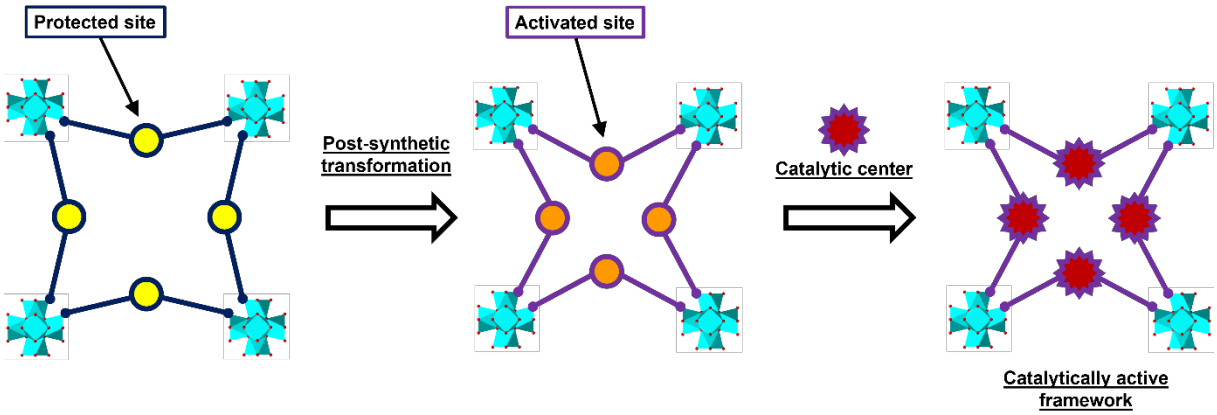

Figure 1. Post-synthetic deprotection of secondary coordination sites followed by insertion of catalytic metal centres to generate catalytically active MOF.

[1] Wang, C., An, B. & Lin, W. (2019). *ACS Catal.*, **9**, 130.
[2] Mandal, S., Natarajan, S., Mani, P. & Pankajakshan, A. (2021). *Adv. Funct. Mater.*, **31**, 2006291.
[3] Bai, Y., Dou, Y., Xie, L-H., Rutledge, W., Li, J-R. & Zhou, H-C. (2016). *Chem. Soc. Rev.*, **45**, 2327.

A098-03-240823

Metal-Organic and Covalent-Organic Frameworks (MOFs and COFs): from Single Crystals to Novel Functional Materials

N. B. Shustova, K. C. Park

Department of Chemistry and Biochemistry, University of South Carolina, 631 Sumter Street, Columbia, South Carolina 29208, United States

shustova@sc.edu

Keywords: MOFs, COFs, PSM

The development of novel materials with enhanced performance is a continuous process mainly driven by everyday demands. Optoelectronics is an excellent example of a field where constantly growing societal demands in energy consumption have forced material evolution to speed up. Metal-organic or covalent-organic frameworks (MOFs and COFs), crystalline porous materials consisting of organic and inorganic building blocks, have been evaluated as promising candidates for a variety of renewable energy applications.[1,2] The self-assembled nature of MOFs provides a very powerful tool for arranging hundreds of organic compounds with high structural organization and, therefore, provides an opportunity to utilize MOFs as light-harvesting mimics of the natural photosystem. At the same time, MOF crystallinity allows one to determine the precise distances and angles between self-assembled organic linkers and, therefore, study and model short- and long-range energy transfer processes. Furthermore, MOFs can be used as a "three-in-one" platform, which integrates the three aspects of artificial photosynthesis: photon absorption, generation of charge-separated excited states, and charge transfer to a reaction center into a single material to enhance, for instance, sensing efficiency or be applied as a photocatalyst. MOFs also offer a high degree of synthetic tunability, which could help to adjust optical, electrical, and sometimes even mechanical properties through postsynthetic modification (Figure 1). Thus, MOFs have ideal properties for the development of new systems with improved functionalities. To highlight this concept in my presentation, I will summarize the recent advancements achieved in my group focusing on postsynthetic modification for understanding of MOF photophysics with an emphasis on energy transfer processes[1]. We also applied the acquired fundamental principles toward mapping of changes in material properties, which could provide a pathway for monitoring material aging or structural deterioration. I will also discuss our progress in understanding the tunability of electronic structure for bimetallic frameworks as well as recent developments towards utilizing MOF modularity and porosity for novel wasteforms [2].

The authors acknowledge support from the NSF Award (DMR-2103722), SC EPSCoR GEAR grant, and Center for Hierarchical Wasteform Materials (CHWM), under grant DE-SC0016574.

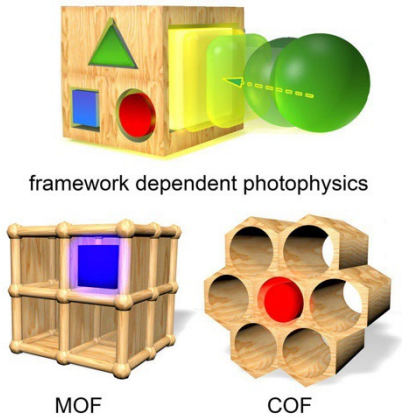

Figure 1. Postsynthetic modification of MOFs and COFs for tailoring material optoelectronic properties.

[1] Thaggard, G. C.; Haimerl, J.; Park, K. C.; Lim, J.; Fischer, R.; Maldeni Kankanamalage, B. K. P.; Yarbrough, B. J.; Wilson, G. R.; Shustova, N. B. (2022). *J. Am. Chem. Soc.* **144**, 23249.

[2] Park, K. C.; Martin, C. R.; Leith, G. A.; Thaggard, G. C.; Wilson, G. R.; Yarbrough, B. J.; Maldeni Kankanamalage, B. K. P.; Kittikhunnatham, P.; Mathur, A.; Jatoi, I.; Manzi, M. A.; Lim, J.; Lehman-Andino, I.; Hernandez-Jimenez, A.; Amoroso, J. W.; DiPrete, D. P.; Liu, Y.; Schaeperkoetter, J.; Misture, S. T.; Phillpot, S. R.; Hu, S.; Li, Y.; Leydier, A.; Proust, V.; Grandjean, A.; Smith, M. D.; Shustova, N. B. (2022). *J. Am. Chem. Soc.* **144**, 4457.

A098-04-240823

Multi-facetted dynamic behaviour of a flexible metal-organic framework through post-synthetic modification

M. Roseveare[1], G. Donval[2], D. J. Ashworth[3], R. Smith[1], A. Dettori[1], E. J. Carrington[1], O. Parry[1], S. F. Dodsworths[1,4], M. R. Warren[4], S. P. Thompson[4], I. D. H. Oswald[3], A. J. Fletcher[3], T. Düren[2], L. Brammer[1]

[4] The University of Sheffield, Sheffield, UK, [2] University of Bath, Bath, UK, [3] Strathclyde University, Glasgow, UK. [4] Diamond Light Source, Didcot, UK.

Email: tom.roseveare@sheffield.ac.uk

Keywords: Metal-Organic Framework, Post-synthetic modification, Structural dynamics

Metal-organic frameworks (MOFs) are constructed from inorganic coordination nodes and multi-topic organic linkers to form a regular repeating network. These polymeric materials possess large solvent -filled voids, which are often retained upon solvent removal, making MOFs attractive for applications involving adsorption and release of small molecules (e.g. gas separation). In recent years, however, it has been shown that a growing number of these materials undergo dynamical structural changes upon removal or inclusion of guest molecules. Such dynamic behaviour is often enabled by flexibility of ligands or coordination geometry and can result from a response to a variety of stimuli, such as temperature, pressure and guest content. To fully understand and harness the dynamic behaviour a combination of diffraction, other physical measurements and computational techniques are required.

In recent years we have extensively explored one such flexible MOF material, SHF-61,[1] which comprises indium metal nodes connected with aminoterephthlate linkers into a doubly interpenetrated anionic diamondoid framework, the charge being balanced by mobile cations within the pores. Initial studies demonstrated a continuous solvent -dependent *two-dimensional* breathing behaviour (pore-width changes).[1] Subsequent post-synthetic modification of the organic linker to convert amino groups to amides (SHF-62) unlocked a *three-dimensional* flexible response upon solvent (pore-width and pore-length changes).[2] Most recently we have identified a third means of framework modification through replacement of the mobile cation within the pores of the framework. This has allowed evaluation of the effect of cation size and intermolecular interactions on the dynamic range of the material and has highlighted the key role of the cation in the dynamic response of this family of MOF materials.

This presentation will demonstrate that through three means of post-synthetic modification (solvent exchange, ligand modification and cation replacement, Figure 1) it has been possible to develop comprehensive picture of the large-amplitude continuous dynamic behaviour in the framework SHF-61 and its related family of MOFs. All materials have been characterised extensively by SCXRD and PXRD methods, including *in situ* diffraction studies during pore-solvent removal and gas adsorption, using both laboratory data and synchrotron data from Diamond Light Source. The diffraction studies are complemented by a variety of othe r characterisation methods and mechanistic understanding is enhanced by adsorption studies and computational modelling.

The ability to apply three different post-synthetic modification methods presents a unique opportunity to not only control the flexibility but also potentially tailor the guest inclusion properties and applications of this versatile material.

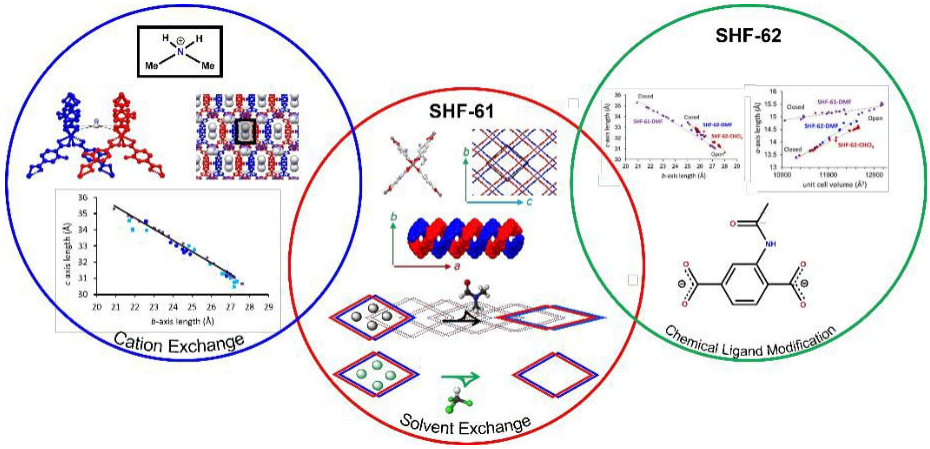

Figure 1. Overview of the three modifications for SHF-61

[5] Carrington E.J., McAnally C. A., Fletcher A. J.,Thompson S. P.,Warren M., Brammer L. (2017). *Nat. Chem.,* **9**, 882-889.
[6] Carrington E. J., Dodsworth S. F., van Meurs S., Warren M. R., Brammer L. (2021). *Angew. Chem. Int. Ed.,* **60**, 17920-17924.

Acknowledgements: We are grateful for support from EPRSC (grants EP/T034068/1, EP/T034130/1, EP/T034114/1) and for

A098-05-240823

Access to polymorphs of polymers via topochemical reactions

Kana M. Sureshan

School of Chemistry, IISER Thiruvananthapuram, Maruthamala, Thiruvananthapuram, Kerala-695551, India

kms@iisertvm.ac.in

Keywords: polymorph, polymer, topochemical reactions, crystal engineering, TAAC

Solids exhibit different properties by adopting different packing, an ideal case being different forms of carbon viz. diamond and graphite. Polymorphism originates from different packing of a compound leading to different crystal forms and there by exhibiting very different properties [1]. Polymorphism has been widely exploited to tune the properties of small molecules. Polymorphism is expected to make huge impact in the area of polymers, as different polymorphs of a particular polymer can have different properties. However, due to the difficulty in crystallising polymers, accessing polymorphs of polymers is an unresolved challenge. However, topochemical polymerization [2-3] is promising as different reactive polymorphs of a monomer can yield different polymorphs of a polymer. By adopting topochemical polymerization of different polymorphs of monomers we have achieved the synthesis of different polymorphs of polymers [4-6]. In this talk, I will try to demonstrate the promising future of the marriage of polymorphism and topochemistry in obtaining polymorphs of polymers.

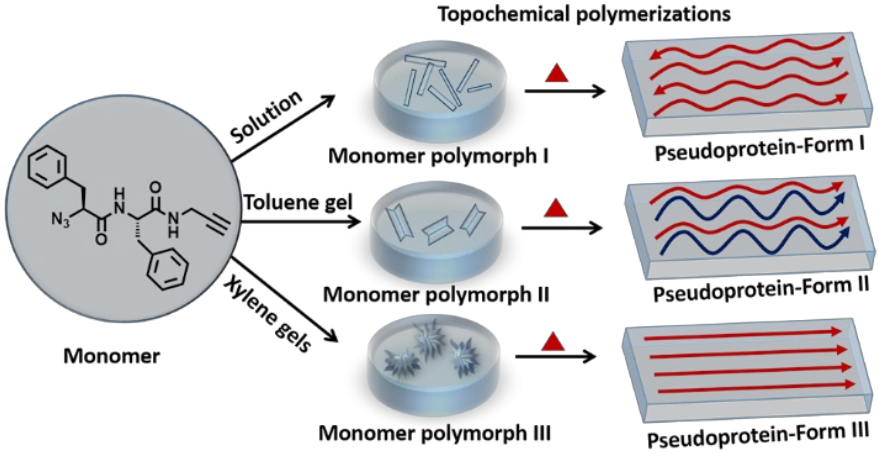

Figure 1. Three polymorphs of a polymer via TAAC polymerization of polymorphs of a dipeptide monomer

[1] Bernstein, J. *Polymorphism in Molecular Crystals*, Oxford University Press, New York, 2002.
[2] Kuntrapakam, H., Ravi, A., Raju, C., Pathan, J. R., Rai, R. & Sureshan, K. M. (2021). *Chem. Soc. Rev.,* **50**, 4062.
[3] Kuntrapakam, H., Ravi, A., Raju, C. & Sureshan, K. M. (2021). *Chem. Sci.,* **12**, 5361.
[4] Mohanrao, R., Hema, K. & Sureshan, K. M. (2020). *Nat. Commun*., **11**, Article No. 865.
[5] Ravi, A., Hassan, S. Z., Bhandary, S. & Sureshan, K. M. (2022). *Angew. Chem. Int. Ed.*, **61**, e202200954
[6] Rai, R. & Sureshan, K. M. (2022). *Angew. Chem. Int. Ed*., **61**, e202111623

A098-06-240823

Post-Synthetic Modification of Crystalline Materials

Jinjin Liu, Yao Chen, Zhenjie Zhang*

College of Chemistry, Nankai University

zhangzhenjie@nankai.edu.cn

Keywords: Post-Synthetic Modification; Crystalline; Framework Materials

The application of crystalline materials in various emerging fields has received increasing attention, but crystalline materials also have some limitations, such as poor processability. The post-modification of crystalline materials provides a new way to solve these limitations and bottlenecks, not only bringing new properties to the material itself but also affording new materials, which are difficult to be obtained through one-step methods. Our research on the post-modification of crystalline materials can be divided into two parts. One of them is the post-modification of the interior of the crystalline materials. For example, we synthesized new anthracene derivatives dimers that were photoresponsive to visible light with interesting bending behaviors owing to their [4+4] photodimerization within crystals[1]. Moreover, we employed a coordination-driven self-assembly strategy to secure the appropriate head-to-tail alignment of anthracene moieties and obtained large-sized Pt-based linear polymer crystals through a [4+4] cycloaddition of anthracene in a single-crystal to single-crystal fashion[2]. Another example, freestanding membranes (PEG-COF-42) could occur the configurational change of acylhydrazone (i.e., E ↔ Z isomerization) accompanied by an excited-state intramolecular proton transfer (ESIPT) process under UV light but good reversibility upon blue light or heating, which behaved as a fast mechanical response (e.g., bending) [3]. The other is the post-assembly of crystalline materials and other materials. We constructed MOPs-cored crosslinking networks by hierarchical post-assembling, named hypercrosslinked MOPs, and successfully prepared a series of new hybrid membranes. The membranes maintained the characteristics of the polymer matrix (flexibility, processability, etc.) and obtained many attractive properties, such as significantly improving the mechanical properties, offering selective separation performance of gas/liquid phase, self-healing, shape memory properties, and so on[4, 5]. The post-modification of crystalline materials has enriched the methods available to create new materials and broadened the scope of advanced materials.

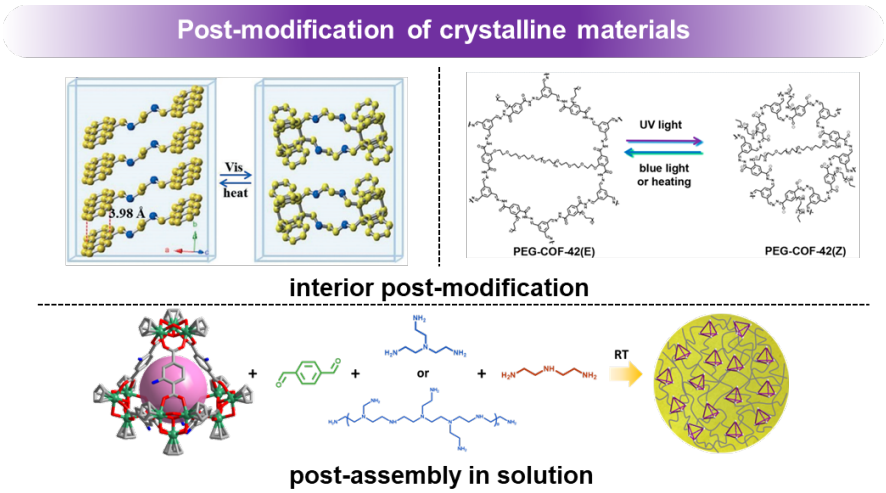

Figure 1. This is a figure caption (Heading 6 style, Times New Roman 9 pt).

[1] Yu, Q., Yang, X., Chen, Y., Yu, K., Gao, J., Liu, Z., Cheng, P., Zhang, Z., Aguila, B. & Ma, S. (2018). *Angew. Chem. Int. Ed.* **57**, 10192.
[2] Yu, Q., Li, M., Gao, J., Xu, P., Chen, Q., Xing, D., Yan, J., Zaworotko, Michael J., Xu, J., Chen, Y., Cheng, P. & Zhang, Z. (2019). *Angew. Chem. Int. Ed.* **58**, 18634.
[3] Guo, X., Mao, T., Wang, Z., Cheng, P., Chen, Y., Ma, S. & Zhang, Z. (2020). *ACS Cent. Sci.* **6**, 787.
[4] Liu, J., Duan, W., Song, J., Guo, X., Wang, Z., Shi, X., Liang, J., Wang, J., Cheng, P., Chen, Y., Zaworotko, Michael J. & Zhang, Z. (2019). *J. Am. Chem. Soc.* **141**, 12064.
[5] Liu, J., Li, J., Qiao, S., Wang, Z., Zhang, P., Fan, X., Cheng, P., Li, Y.-S., Chen, Y. & Zhang, Z. (2022). *Angew. Chem. Int. Ed.* **61**, e202212253.

A017b Enzyme Mechanisms and Regulation

Room 203

4.00pm - 6.30pm

A017b-01-240823

Visualizing the gas channel of a monofunctional carbon monoxide dehydrogenase

Alison Biester[1], Sébastien Dementin[2], Catherine L. Drennan[1,3,4,5]

[1] Dept. of Chemistry, Massachusetts Institute of Technology, Cambridge, MA 02139, United States, [2] CNRS, Aix-Marseille Université, Laboratoire de Bioénergétique et Ingénierie des Protéines, Institut de Microbiologie de la Méditerranée, 13009 Marseille, France, [3] Dept. of Biology, Massachusetts Institute of Technology, Cambridge, MA 02139, United States, [4] Howard Hughes Medical Institute, Massachusetts Institute of Technology, Cambridge, MA 02139, United States, [5] Canadian Institute for Advanced Research, Bio-inspired Solar Energy Program, Toronto, ON M5G 1M1 Canada abiester@mit.edu

Keywords: CO-dehydrogenase, Carbon monoxide, Crystallography, Xenon, Gas channels, Tunnels

Carbon monoxide dehydrogenase (CODH) plays an important role in the processing of the one-carbon gases carbon monoxide and carbon dioxide. In CODH enzymes, these gases are channeled to and from the Ni-Fe-S active sites using hydrophobic cavities. In this work, we investigate these gas channels in a monofunctional CODH from *Desulfovibrio vulgaris*, which is unusual among CODHs for its oxygen-tolerance. By pressurizing *D. vulgaris* CODH protein crystals with xenon and solving the structure to 2.10 Å resolution, we identify 12 xenon sites per CODH monomer, thereby elucidating hydrophobic gas channels. We find that *D. vulgaris* CODH has one gas channel that has not been experimentally validated previously in a CODH, and a second channel that is shared with *Moorella thermoacetica* carbon monoxide dehydrogenase/acetyl-CoA synthase (CODH/ACS). This experimental visualization of *D. vulgaris* CODH gas channels lays groundwork for further exploration of factors contributing to oxygen-tolerance in this CODH, as well as study of channels in other CODHs.

A017b-02-240823

Location and identification of light element co-factors by long-wavelength macromolecular crystallography

A. Wagner, R. Duman, C. Orr, K. el Omari, V. Mykhaylyk

Diamond Light Source, Harwell Science & Innovation Campus, Didcot OX11 0DE, United Kingdom, Research Complex at Harwell, Rutherford Appleton Laboratory, Didcot OX11 0FA

armin.wagner@diamond.ac.uk

Keywords: ion identification, long-wavelength crystallography, structural biology

Interpretation of electron densities from X-ray diffraction experiments is not always easy and sometimes it is very difficult to distinguish ions bound to a macromolecule from water molecules. In particular for only partially occupied sites or at medium or low resolution this becomes a challenge. Anomalous contrast is an elegant way to overcome this issue by using the wavelength dependency of the anomalous contribution f" to the structure factor. Across an elemental absorption edge f" changes drastically, hence the interpretation of two phased anomalous difference Fourier maps, one measured below and a second above the absorption edge, allows to unambiguously assign the element to a given site of interest [1].

Macromolecular crystallography (MX) beamlines at synchrotron light sources are typically optimised for wavelengths around 1 Å, allowing experiments with wavelengths longer than 2 Å only in exceptional cases. For longer wavelengths air absorption and scattering become a limiting factor, compromising the data quality significantly. Helium sample environments are available at some beamlines, but the maximum achievable resolution is typically limited by a flat detector. Beamline I23 at Diamond Light Source is the only fully dedicated long-wavelength MX beamline covering a unique wavelength range from 1.1 Å to 5.9 Å. It is operated in a vacuum environment, has a semi cylindrical detector for diffraction angles up to 2 = 100° and a multi-axis goniometer enabling collection of complete anomalous data sets of high multiplicity even from triclinic space groups [2].

The extended wavelength range available covers the absorption edges of several lighter elements of high biological relevance. Phosphorus is not only an important part of the phosphate backbone of both RNA and DNA, it is also present in many co-enzymes and phosphorylation is a key step in cell regulation. Sulfur is present in the two amino acids cysteine and methionine and in many drug molecules, e.g. beta lactams. Cl^-, K^+ and Ca^{2+} are important co-factors and their concentration gradients are used in various transport and regulatory processes. Long-wavelength MX allows the determination of the exact position of these elements to understand these fundamental biological mechanisms in further detail.

Anomalous contrast from lighter elements has supported already a variety of structural studies of enzymes / ribozymes. Data collected above and below the potassium K-absorption edge (λ = 3.436 Å) revealed the importance of K^+ cations for the function of the 70S ribosome from *Thermus thermophilus* [3]. Small anions like chloride allow to metabolically control the function of the phosphoenolpyruvate carboxykinase (PEPCK). Experiments around the chloride absorption edge (λ = 4.393 Å) for crystals exposed to different concentrations of KCl revealed how chloride binding in the active site affects the enzyme activity [4].

1 Handing, K. B., Niedzialkowska, E., Shabalin, I. G., Kuhn, M. L., Zheng, H. & Minor, W. (2018). *Nat. Protocols.* **13**, 1062.
2 Wagner, A., Duman, R., Henderson, K. & Mykhaylyk, V. (2016). Acta Crystallogr., **D72**, 430.
3 Rozov, A., Khusainov, I., El Omari, K., Duman, R., Mykhaylyk, V., Yusupov, M., Westhof, E., Wagner, A. & Yusupova, G. (2019). *Nat. Commun.*, **10**, 2519.
4 Barwell, S., Duman, R., Wagner, A. & Holyoak, T. (2022). *Biochem. Biophys. Res. Commun.*, **637**, 218

A017b-03-240823

Mechanisms of substrate recognition and N^6-methyladenosine demethylation revealed by crystal structures of ALKBH5–RNA complexes

Wei Shen Aik[1], Simranjeet Kaur[1], Nok Yin Tam[1], Michael A. McDonough[2], Christopher J. Schofield[2]

Department of Chemistry, Hong Kong Baptist University, Kowloon Tong, Hong Kong SAR, China. 2) The Department of Chemistry and the Ineos Oxford Institute for Antimicrobial Research, Chemistry Research Laboratory, University of Oxford, 12 Mansfield Road, Oxford, OX1 3TA, UK.

aikweishen@hkbu.edu.hk

Keywords: N^6-methyladenosine (m^6A), RNA demethylase, 2OG Oxygenase, ALKBH5

AlkB homologue 5 (ALKBH5) is a ferrous iron and 2-oxoglutarate dependent oxygenase that demethylates RNA N^6-methyladenosine (m^6A), a post-transcriptional RNA modification with an emerging set of regulatory roles. Along with the fat mass and obesity-associated protein (FTO), ALKBH5 is one of only two identified human m^6A RNA oxidizing enzymes and is a potential target for cancer treatment. Unlike FTO, ALKBH5 efficiently catalyzes fragmentation of its proposed nascent hemiaminal intermediate to give formaldehyde and a demethylated nucleoside. A detailed analysis of the molecular mechanisms used by ALKBH5 for substrate recognition and m^6A demethylation is lacking. We report three crystal structures of ALKBH5 in complex with an m^6A-ssRNA 8-mer substrate and supporting biochemical analyses [1]. Strikingly, the single-stranded RNA substrate binds to the active site of ALKBH5 in a 5'-3' orientation that is opposite to single-stranded or double-stranded DNA substrates observed for other AlkB subfamily members, including single-stranded DNA bound to FTO. The combined structural and biochemical results provide insight into the preference of ALKBH5 for substrates containing a (A/G)m^6AC consensus sequence motif. The results support a mechanism involving formation of an m^6A hemiaminal intermediate, followed by efficient ALKBH5 catalyzed demethylation, enabled by a proton shuttle network involving Lys132 and Tyr139.

[1] Kaur, S., Tam, N. Y., McDonough, M. A., Schofield, C. J., Aik, W. S. (2022). *Nuc. Acids. Res.* **50**, 4148.

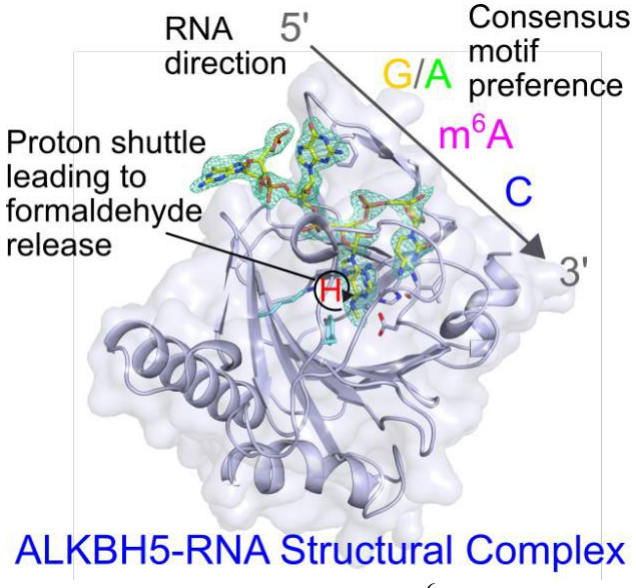

Figure 1. Crystallographic analyses of ALKBH5 bound to a single-stranded m^6A-containing RNA substrate reveal details of ALKBH5-substrate interactions and how ALKBH5, unlike the other m^6A oxygenase FTO, can catalyze rapid m^6A demethylation.

W.S.A. thanks the Research Grants Council of Hong Kong (Early Career Scheme 2019/20 [22301719]) and Hong Kong Baptist University for funding (Tier 2 Start-Up Grant [RC-SGT2/18-19/SCI/003]). C.J.S. thanks the Biotechnology and Biological Research Council, the Wellcome Trust [106244/Z/14/Z], and Cancer Research UK for funding. We thank the Diamond Light Source and staff for the allocation of beam time and support, Judy Tsz-Shan Lum for technical support on MALDI-TOF MS, and Yuen Kit Cheng and Chi Sing Lee for helpful discussion.

A017b-04-240823

Poly-γ-glutamylation of biomolecules

G. Bashiri[1,2], E. Bulloch[1,2], W. Bramley[1], M. Davidson[3], S. Stuteley[1], P. Young[1,2], P. Harris[1,2], M. Naqvi[1], M. Middleditch[1], M. Schmitz[4], W.-C. Chang[3], E. Baker[1,2], C. Squire[1,2]

[1]School of Biological Sciences, The University of Auckland, Private Bag 92019, Auckland, New Zealand.
[2]Maurice Wilkins Centre for Molecular Biodiscovery, The University of Auckland, Private Bag 92019, Auckland, New Zealand.
[3]Department of Chemistry, North Carolina State University, NC 27695-8204, USA.
[4]School of Chemical Sciences, The University of Auckland, Private Bag 92019, Auckland 1142, New Zealand.

Email of communicating author c.squire@auckland.ac.nz

Keywords: poly-γ-glutamylation, processive enzyme mechanism, substrate "bulging"

Poly-γ-glutamate tails regulate the binding and biological activity of archaeal, bacterial, and eukaryotic cofactors, and in particular the folates and coenzyme F_{420} [1]. Despite many decades of interest and scientific research, the mechanism through which such long poly-γ-glutamate chains are generated is almost entirely unknown. We now show definitively that both folylpolyglutamate synthase and γ-glutamyl ligase, two non-homologous enzymes, poly-γ-glutamylate folates and F_{420} respectively by extending the growing γ-glutamyl chain from its terminus. This confirms a long-held but unproven hypothesis. Our crystal structure "snapshots" of an archaeal γ-glutamyl ligase (CofE), an enzyme that adds just two L-glutamates to F_{420} [2], follow this molecular machine in action. A complex active site involving manganese and sodium cations and a GTP molecule, provides the scaffold for substrate binding, activation by phosphoryl transfer, and ligation of L-glutamate. We also see two glutamyl binding sites, one a cryptic pocket and putative high-affinity site revealed only on substrate binding, and the second showing promiscuous binding of either the glutamyl or phospholactate moieties of F_{420} substrates. The key part of the mechanistic puzzle is revealed in the "bulged" conformation of F_{420}-2 (F_{420} with two glutamyl residues in its tail) that projects the growing glutamyl chain into solvent while retaining specific binding of both the core chromophore and the terminal glutamyl residue of the substrate. The cofactor is, in essence, held at both ends tightly with the middle section free to move. The crystal structures of CofE and modelling of its *M. tuberculosis* homolog FbiB, which can produce much longer-chain species (up to 14 or more Glu added) [3], afford a tantalising hypothesis of how long negatively charged chains may be stabilised within positively charged surface grooves.

Our "bulging" substrate model of processive poly-γ-glutamylation by terminal extension, irrespective of the final length of the polyglutamate chain, is arguably ubiquitous, and suggests convergent evolution in diverse species from archaea to humans. Could the same key features of our *poly-γ-glutamylation-with-a-bulge* model apply to other biopolymerization reactions that require substrate specificity?

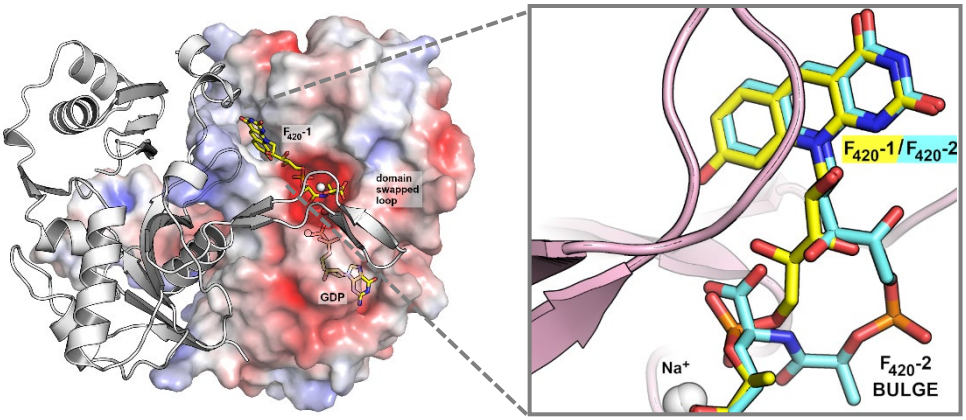

Figure 1. *Archaeoglobus fulgidus* γ-glutamyl ligase (*Af*-CofE) and inset zoom of F_{420} substrate bulging .

[1] Janke, C., Rogowski, K. & and van Dijk, J. (2008). *EMBO Rep*, **9**, 636.
[2] Li, H., Graupner, M., Xu, H. & White, R.H. (2003). *Biochemistry*, **42**, 9771.
[3] Nocek, B., Evdokimova, E., Proudfoot, M., Kudritska, M., Grochowski, L.L., White, R.H., Savchenko, A., Yakunin, A.F., Edwards, A. & Joachimiak, A. (2007). *J Mol Biol*, **372**, 456.
[4] Bashiri, G., Rehan, A. M., Sreebhavan, S., Baker, H. M., Baker, E. N. & Squire, C. J. (2016). *J Biol Chem*, **291**, 6882.

A017b-05-240823

Crystal structure of a MarR family protein from the psychrophilic bacterium *Paenisporosarcina* sp. TG-14 in complex with a lipid-like molecule

Jisub Hwang,[a,b‡] Hackwon Do,[a] and Jun Hyuck Lee[a,b*]

[a]*Research Unit of Cryogenic Novel Material, Korea Polar Research Institute, Incheon 21990, Republic of Korea,* [b]*Department of Polar Sciences, University of Science and Technology, Incheon 21990, Republic of Korea*

Email of communicating author hjsub9696@kopri.re.kr

Keywords: MarR family protein, Transcription regulator, lipid-like effector

MarR family proteins regulate the transcription of multiple antibiotic-resistance genes and are widely found in bacteria and archaea [1, 2]. Recently, a new MarR family gene was identified by genome analysis of the psychrophilic bacterium *Paenisporosarcina* sp. TG-14, which was isolated from sediment-laden basal ice in Antarctica [3]. In this study, the crystal structure of the MarR protein from *Paenisporosarcina* sp. TG-14 (*Pa* MarR) was determined at 1.6 Å resolution. In the crystal structure, a novel lipid-type compound (palmitic acid) was found in a deep cavity, which was assumed to be an effector-binding site (Fig. 1) . Comparative structural analysis of homologous MarR family proteins from a mesophile and a hyperthermophile showed that the DNA-binding domain of *Pa*MarR exhibited relatively high mobility, with a disordered region between the β1 and β2 strands [4]. In addition, structural comparison with other homologous complex structures suggests that this structure constitutes a conformer transformed by palmitic acid. Biochemical analysis also demonstrated that *Pa*MarR binds to cognate DNA, where *Pa*MarR is known to recognize two putative binding sites depending on its molar concentration, indicating that *Pa*MarR binds to its cognate DNA in a stoichiometric manner. The present study provides structural information on the cold-adaptive MarR protein with an aliphatic compound as its putative effector, extending the scope of MarR family protein research [5].

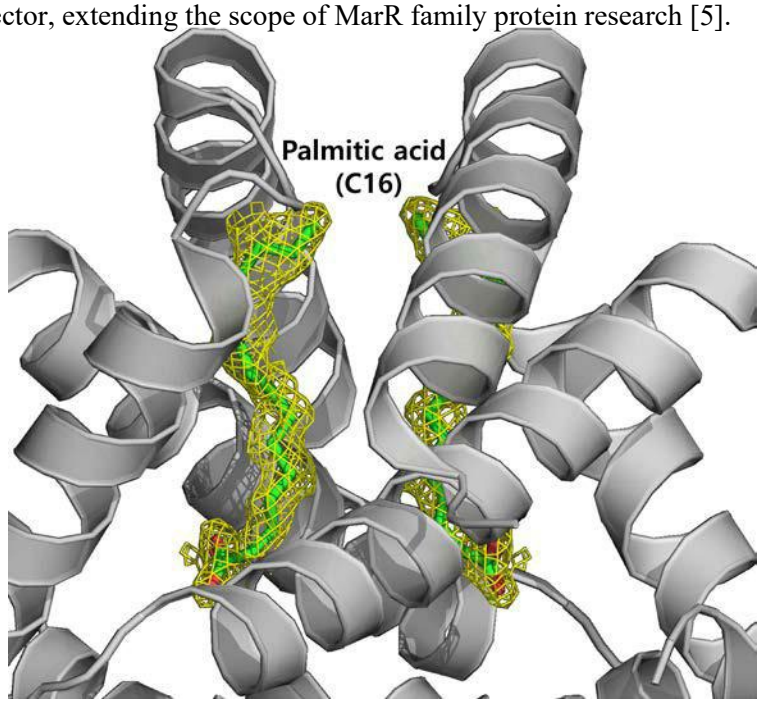

Figure 1. A novel lipid-type effector bound in *Pa*MarR

1 Grove A. (2013). *Curr Biol.* 23(4), R142–R143.
2 Gupta, A., Pande, A., Sabrin, A., Thapa, S. S., Gioe, B. W., & Grove, A. (2018). *Microbiol Mol Biol Rev.* 83(1), e00039-18.
3 Koh, H. Y., Lee, S. G., Lee, J. H., Doyle, S., Christner, B. C., & Kim, H. J. (2012). *J Bacteriol*. 194(23), 6656-6657
4 Kumarevel, T., Tanaka, T., Umehara, T., & Yokoyama, S. (2009). *Nucleic Acids Res*. 37(14), 4723-4735.
5 Hwang, J., Park, S.-H., Lee, C. W., Do, H., Shin, S. C., Kim, H.-W., Lee, S. G., Park, H. H., Kwon, S. & Lee, J. H. (2021). *IUCrJ.* 8, 842-852.

A017b-06-240823

Spectroscopically validated multiple structures from one crystal (MSOX) and Damage Free atomic structures using XFEL for copper Nitrite Reductases

Samuel L. Rose[1], Svetlana V. Antonyuk[1], Robert R. Eady[1], Felix Ferroni[2], Takehiko Tosha[3], Masaki Yamamoto[3], Samuel Horrell[4], Robin Owen[4] and S. Samar Hasnain[1*]

Molecular Biophysics Group, Life Sciences Building, Institute of Systems, Molecular and Integrative Biology, Faculty of Health and Life Sciences, University of Liverpool, L69 7ZB, UK; [2] CONICET-CCT SANTA FE, Departamento de Física-FBCB-UNL, Ciudad Universitaria. Paraje El Pozo. Ruta Nac. 168 Km472, Argentina; [3]RIKEN SPring-8 Center, 1-1-1 Kouto, Sayo, Hyogo, 679-5148, Japan; [4]Diamond Light Source, Harwell Science & Innovation Campus, Didcot, Oxfordshire, OX11 0DE

Many enzymes utilize redox-coupled centres for performing catalysis where the centres are used to control and regulate the transfer of electrons required for catalysis, whose untimely delivery can lead to a state incapable of binding the substrate i.e. a dead-end enzyme. Copper nitrite reductases (CuNiRs), which catalyse the reduction of nitrite to nitric oxide (NO), have proved to be a good model system for studying these complex processes including proton-coupled electron transfer and their orchestration for substrate binding/utilisation [1].

X-rays used to collect crystallographic data can in itself result in changes in the redox states of transition metals utilised by many biological systems including metalloproteins. This disadvantage has been harnessed to drive a complex chemical reaction requiring the delivery of an electron to the active site and recording the structural changes accompanying catalysis providing a 'real-time' structural movie of an enzymatic chemical reaction, a dream of enzymologist for decades. By coupling MSOX technique with single-crystal and solution optical spectroscopy, we show that the electron transfer between the T1Cu and T2Cu redox centres is heavily gated and show a structural movie capturing the bond-breakage, product formation and its release from the catalytic centre for CuNiRs from two organism [2].

Structures **f**ree from **r**adiation-**i**nduced **c**hemistry (FRIC structures) for proteins containing redox centres have become possible using single shot femtosecond pulses from X-ray Free Electron Lasers [3]. We have used high energy X-rays from SACLA to obtain atomic/sub-atomic resolution structures of three different nitrite reductases in a variety of functional states including substrate and product bound species alongside single crystal optical spectra. These spectroscopically validated very high resolution FRIC structures with unrestrained SHELXL refinement are providing unprecedented level of details including protonation states of key residues in the catalytic pocket. These new results will be reported at the Congress.

These recent developments would be reviewed with wider applicability in mind.

1 *New horizons in structure-function studies of copper nitrite reductase (2022) R. R. Eady & S. S. Hasnain,* ***Coordination Chemistry Reviews,*** *460. doi:10.1016/j.ccr.2022.214463*

2 *An unprecedented insight into the catalytic mechanism of copper nitrite reductase from atomic-resolution and damage-free structures (2021) S. L. Rose, S.V. Antonyuk, D. Sasaki, K. Yamashita, K. Hirata, Go Ueno, H. Ago, R. R. Eady, T. Tosha, M. Yamamoto, S. S. Hasnain* ***Science Adv.*** *7 eabd8523*

3 Single crystal spectroscopy and multiple structures from one crystal (MSOX) define catalysis in copper nitrite reductases. (2022*) S. L. Rose, S. Baba, H. Okumura, S. V. Antonyuk, D. Sasaki, T. M. Hedison, M. Shanmugam, D. J. Heyes, N. S. Scrutton, T. Kumasaka, T. Tosha, R. R. Eady, M. Yamamoto & S. S. Hasnain* ***Proc. of the National Academy of Sciences, 119****(30):e2205664119.*

A049 Crystallography of Solid-state Ionic Conductors

Room 204

4.00pm - 6.30pm

A049-01-240823

Evaluation of the crystallization of 75Li2S·25P2S5 binary system by RMC modeling using the laboratory diffractometer

5 Yoshimoto[1], Y. Shiramata[1], T. Kimura[2], C. Hotehama[2], A. Sakuda[2], A. Hayashi[2], K. Omote[1]

Rigaku Corporation, 3-9-12 Matsubara-cho, Akishima, Tokyo, Japan,
B. Graduate School of Engineering, Osaka Metropolitan University, 1-1, Gakuen-cho, Naka-ku, Sakai, Osaka, Japan m-yosimo@rigaku.co.jp

Keywords: sulfide solid electrolyte, total scattering measurement, reverse Monte-Carlo modeling

The solid-electrolytes (SEs) are a key component in all-solid-state Li-ion batteries (LIBs). The sulfide SEs are the promising candidates for all-solid-state LIBs in its property; intermediate Young's moduli, high Li-ion conductivity, and the stability of electrochemical reaction. It is well known that a 75Li2S·25P2S5 (mol%) glass, which is one of the most famous sulfide SEs, shows the phase transition from glass to crystal around T = 473 K. However, there are few studies on the local structural changes during crystallization process due to the lack of a unified local structural analysis method applicable to both glassy and crystalline states. Recently, we have developed a method to evaluate the local structural changes during the phase transition by using X-ray total scattering profiles combined with a reverse Monte-Carlo (RMC) modeling [1].

Figure 1 shows the experimental and RMC results for both the glassy and crystalline states. We have successfully constructed structural models consistent with the experimental total scattering profiles. The angular histograms of S-(P)-S and S-(S)-S respectively had peaks at S-(P)-S = 109.5 and S-(S)-S = 60°and the results indicated that the PS4 clusters remain the tetrahedral structure over the wide range from glass to crystal. We also calculated the average spatial distribution maps of P and S atoms. Figure 2 shows the experimentally obtained Gobs(r) and the average spatial distribution maps of S and P atoms of the PS4 cluster. S atom has a wider distribution between the corner of PS4 tetrahedra at the higher temperature of the glassy state and then to be narrow distribution due to the crystallization. The S-Li correlation at r = 2.5 Å shown in Gobs(r) show little change at any temperature, indicating that the motion of Li-ion is followed to the libration of PS4 clusters. The trend is in good agreement with the Li-ion conductivity obtained in the previous study [2]. The RMC results suggest that the PS4 cluster motion plays an important role in the Li-ion migration in 75Li2S·25P2S5 (mol%) glass and crystals. We will also discuss about local structure changes during the crystallization process.

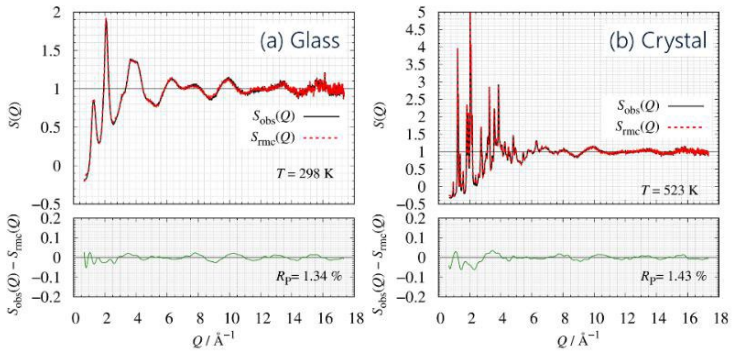

Figure 1. Observed (black solid line) and calculated (red broken line) structure factor, corresponding residual curve (green solid line) of 75Li2S·25P2S5. (a) glass and (b) crystal

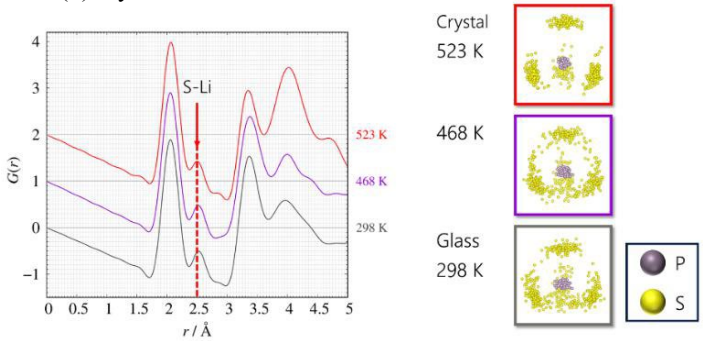

Figure 2. Experimentally obtained G(r) and spatial distribution of P (purple) and S (yellow) atom of each state.

1 M. Yoshimoto and K. Omote, (2023) *Appl. Phys. Express*, **16**, 015005.

2 S. Shiotani, K. Ohara, H. Tsukasaki, S. Mori, R. Kanno, (2017) *Sci. Rep.* **7** 6972.

A049-02-240823

Fluoride-ion conductors for future solid state battery applications

C. Hull[1] and H.Y. Playford[1]

[6] *The ISIS Facility, STFC Rutherford Appleton Laboratory, Chilton, Didcot, Oxfordshire, OX11 0QX, U.K.*

stephen.hull@stfc.ac.uk

Keywords: fluoride-ion conduction, neutron powder diffraction, solid state batteries

The vast majority of rechargeable batteries currently used for mobile electronics and vehicle applications are lithium-ion, exploiting their impressive energy densities and relatively high voltage. However, concerns around the safety, high cost and geopolitical distribution of the raw materials, coupled with the degradation of Li^+-ion cells on repeated recharging, has motivated studies of other battery chemistries. Na^+-ion cells are at the most advanced stage of development, driven by the high earth abundance of sodium, but the limited intercalation of Na^+ into graphite requires the development of new anodes. Multivalent mobile cations such as Mg^{2+} and Al^{3+} potentially offer increased energy densities, but are hampered by large structural changes associated with the insertion/removal of these highly charged species into/from the electrodes.

Until recently, batteries based on mobile anions (rather than cations) have been largely ignored, despite reports of high mobility of F^- ions within solids dating back to Michael Faraday's studies of the 'fluoride of lead', β-PbF_2, in 1838 [1]. A major challenge for cells based on fluorine chemistry is the lack of a suitable liquid electrolyte, as most candidates contain HF^-_2 ions with a small voltage stability window and/or react with atmospheric moisture to form HF. However, a significant advance occurred in 2011, with reports of viable cells using solid electrolytes such as $BaSnF_4$ [2], which has recently attracted the interest of car companies including Honda and Toyota (see, for example, [3]). However, these batteries have a major drawback, needing to be operated at elevated temperatures (typically 80-150ºC) to achieve sufficiently high F^--ion conductivity within the solid electrolyte [4].

This presentation will focus on the structure-property relationships within a number of F^--ion conductors, including a discussion of our current understanding of the archetypal compound β-PbF_2. This will be followed by a more detailed presentation of a number of ternary derivatives of PbF_2, such as $KPbF_3$ [5], $PbSnF_4$ [6], $CsSn_2F_5$ [7] and β-$KSbF_4$ [8]. Information on the crystal structure, including the nature of the dynamic F^- disorder, has been provided by neutron powder diffraction studies, exploiting the sensitivity of the technique to the locations of the anions in the presence of heavier cations. Finally, the factors that promote extensive F^-disorder within such solid phases will be considered, including the influence of crystal structure on the preferred anion diffusion mechanisms and the role of electron lone-pairs associated with cations such as Pb^{2+} and Sn^{2+} in promoting high F^- mobility.

[1] Faraday, M. (1838). *Phil. Trans. R. Soc. Lond.*, 90.
[2] Reddy, M.A. & Fichtner, M. (2011). *J. Mater. Chem.*, **21**, 17059-17062.
[3] https://www.electrive.com/2020/08/14/toyota-developing-flouride-ion-battery-with-1000-km-range/
[4] Nowroozi, M.A., Mohammed, I., Molaiyan, P., Wissel, K., Munnangi, A.R. & Clemens, O. (2021). *J. Mater. Chem. A*, **9**, 5980-6012.
[5] Hull, S., Berastegui, P., Eriksson, S.G. & Gardner, N.J.G. (1998). *J. Phys.: Condens. Matter,* **10**, 8429–8446.
[6] Castiglione, M., Madden, P.A., Berastegui, P & Hull, S. (2005). *J. Phys.: Condens. Matter*, **17**, 845–861.
[7] Berastegui, P., Hull, S. & Eriksson, S.G. (2010). *J. Solid State Chem.*, **183**, 373–378.
[8] Kawahara, K., Ishikawa, R., Nakayama, K., Shibata, N. & Ikuhara, Y. (2021). *J. Power Sources*, **483**, 229173.

A049-03-240823

Effects of Mo^{6+} doping on ionic conductivity and the fergusonite–scheelite phase transition in $LaNbO_4$

J. Auckett[1,2], L. Lopez-Odriozola[1], S. Clark[3], I. Evans[1]

[1]Department of Chemistry, Durham University, Durham, United Kingdom [2]Australian Synchrotron, Australian Nuclear Science and Technology Organisation, Clayton, Australia [3]Department of Physics, Durham University, Durham, United Kingdom josiea@ansto.gov.au

Keywords: scheelite, ferroelastic phase transition, oxide-ionic conductor

Solid oxide fuel cells (SOFCs) offer a technological alternative to petroleum combustion engines for small vehicles and stationary electricity generation, but their commercialization has been hindered by a lack of high-performance oxide-ionic conducting solids to act as cathodes and electrolytes at desirable operating temperatures (400–650 °C). Many classes of ceramic materials have been investigated as potential SOFC electrolytes, including several mixed-metal oxides with the scheelite structure type, such as LaNbO4. We observe that doping LaNbO4 with Mo^{6+} (LaNb1-xMoxO4+0.5x, x = 0–0.2) enhances its total conductivity by two orders of magnitude at 600 °C, with $\sigma = 7.0 \times 10^{-3}$ S cm^{-1} at 800 °C measured for x = 0.16. The effects of local defects on oxide-ionic conductivity in LaNb1-xMoxO4+0.5x are illustrated and rationalized using bond valence energy landscape analysis, which reveals facile oxide ion migration pathways in the vicinity of interstitial oxide ions.

The presence of a symmetry-breaking tetragonal-to-monoclinic phase transition in LaNbO4 is known to have implications for both oxide-ionic conductive and ferroelastic properties. Mo^{6+} doping is found to suppress the transition. Symmetry distortion mode refinement-based analysis, applied to this phase transition for the first time in any scheelite material, demonstrates that the $\Gamma 2^+$ displacive mode of the Nb atoms is the most significant structural distortion leading to the transition in undoped LaNbO4. Our X-ray diffraction data and ab initio lattice dynamics calculations show that this transition exhibits first-order characteristics [1].

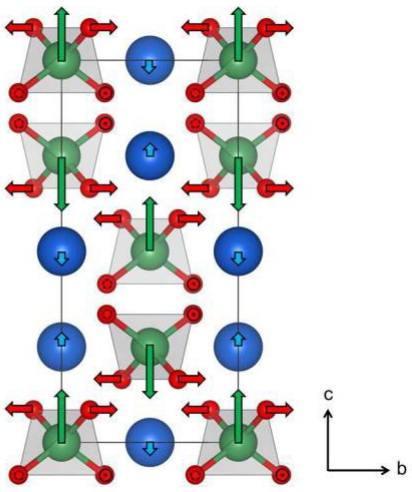

Figure 1. Representation of atomic displacements in the fergusonite–scheelite phase transition in LaNbO4.

[1] Auckett, J. E., Lopez-Odriozola, L., Clark, S. J. & Evans, I. R. (2021). J. Mater. Chem. A 9, 4091.

A049-04-240823

Local structures in BIMEVOX oxide ion conductors

Yajun Yue[1], Ping Miao[1], Isaac Abrahams[2]

1. *China Spallation Neutron Source, 1 Zhongziyuan Road, Dalang, Dongguan ,Guangdong 523000, China*
2. *Department of Chemistry, Queen Mary University of London, Mile End Road London, E1 4NS, U.K.*

yueyj@ihep.ac.cn

Keywords: local structure, total scattering, solid electrolyte

Despite concern over their stability in reducing atmospheres, the use of bismuth oxide based solid electrolytes in solid oxide fuel cells has recently been demonstrated as feasible [1]. The best low temperature oxide ion conductors known are the BIMEVOX ($Bi_2Me^{l}_{x}V^{1-}_{x}O_{5.5-(5-l)x/2-\delta}$, Me = dopants, l = valency) family of solid electrolytes based on substitution of V and or Bi in $Bi_4V_2O_{11-\delta}$ [2]. A huge variety of cations have been successfully used as substituents to stabilize the disordered γ-phase to low temperature, most notably divalent cations such as Cu^{2+} (x = 0.10) with conductivity of ca. 10^{-3} S cm^{-1} at 237 °C [2]. The high conductivity is affected by local structures, including preferred coordination, atom distribution and defect ordering. However, details of local structure are difficult to access and have rarely been reported.

In past, examination of local structure in BIMEVOXes relies mostly on careful analysis for the average structure using neutron/X-ray diffraction and Rietveld refinement [3,4]. The development of total scattering methods in recent years has afforded the opportunity of re-examining the local structure of the BIMEVOXes and the parent compound $Bi_4V_2O_{11-\delta}$ in ways that were not previously possible, to yield a better understanding of the structure-conductivity relationship in these important systems. We have recently reported the local structure analysis for tetravalent- and trivalent-substitution BIMEVOX (ME = Ge, Ga) systems, and found special vacancy deficiency ordering in the former case [5, 6]. Therefore, in the current work, we focus on $Bi_2V_{0.9}Cu_{0.1}O_{5.35}$ and its parent compound $Bi_4V_2O_{11-\delta}$, using neutron total scattering technique plus the Reverse Monte Carlo (RMC) simulation methods, to detect their local structure and possible structure-property relationships. New findings in this type of complicated oxide ion conductors will be presented on the conference.

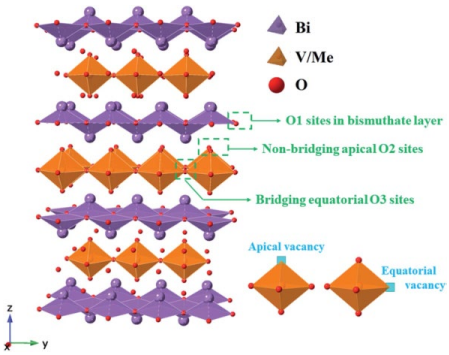

Fig. 1 Ideal structure of γ-BIMEVOX and positions of apical and equatorial vacancies .

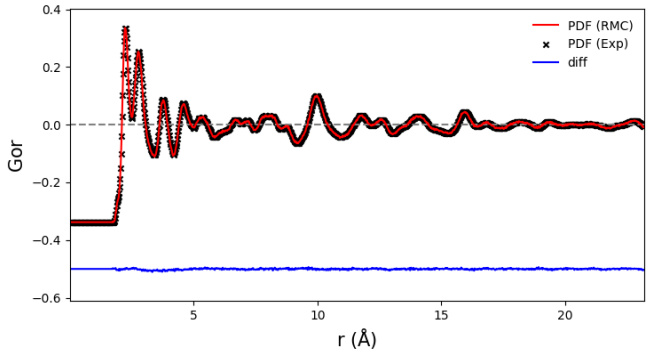

Fig. 2 Fitted pair distribution function of $Bi_2V_{0.9}Cu_{0.1}O_{5.35}$ using RMC calculation.

[1] E.D. Wachsman, K.T. Lee, *Science* 334 (2011) 935-939.
[2] F. Abraham, J. C. Boivin, G. Mairesse, G. Nowogrocki, *Solid State Ionics*, 40/41 (1990) 934-937.
[3] I. Abrahams, J.A.G. Nelstrop, F. Krok, W. Bogusz, *Solid State Ionics*, 110 (1998) 95-101.
[4] F. Krok, I. Abrahams, D. Bangobango, W. Bogusz, J.A.G. Nelstrop, *Solid State Ionics*, 111(1998) 37-43.
[5] Y.J. Yue, A. Dzięgielewska, S. Hull, F. Krok, R.M. Whiteley, H. Toms, M. Malys, M. Zhang, H.X. Yan, I. Abrahams, *J. Mater. Chem. A* 10 (2022) 3793-3807.
[6] Y.J. Yue, A. Dzięgielewska, F. Krok, R.M. Whiteley, H. Toms, M. Malys, H.X. Yan, and Isaac Abrahams, *J. Phys. Chem. C* 126 (2022) 2108–2120.

A049-05-240823

When is size mismatch good? The anomalous behaviour of scandium in titanate-based proton conductors

P.F. Henry[1,2], W.A. Slawinski[3]

[1]ISIS pulsed neutron & muon source, Rutherford Appleton Laboratory, Didcot, OX11 0QX, UK, [2]Department of Chemistry - Ångström Laboratory, Box 538, SE-751 21 Uppsala, Sweden, [3]University of Warsaw, Faculty of Chemistry, UW Pasteura 1, 02-093 Warsaw, Poland

paul.henry@stfc.ac.uk

Keywords: neutron diffraction, proton conductor, total scattering

The search for new and improved solid-state ionic conductors (SSICs) is one of the most active fields in materials chemistry, driven by their key role in application-based technologies. Seemingly paradoxical SSIC chemical and structural requirements bring challenges, requiring long-range order for mechanically stable frameworks, together with short-range disorder to allow ion migration. SSIC rational design and optimisation depend on detailed understanding of atomic-scale architectures that permit resolution of this paradox

In Sc-doped barium titanates (designated BTSx, where x = Sc doping % for Ti), the proton conduction properties are driven both by the structure type adopted and the Sc doping level. [1] At low doping levels, <BTS33, thematerial is hexagonal (*P6₃/mmc*) with relatively poor hydration and proton conduction properties. Above BTS33, the material becomes a simple cubic perovskite (*Pm3m*), despite the large size mismatch between Sc^{3+} and Ti^{4+}. Further, higher Sc doping levels yield significantly improved proton conduction properties and availability of oxygen ion vacancies to initial hydration, such that all can be hydrated. The volume change on hydration is also suppressed by higher Sc doping, [2] all features required for potential application and future rational design of new materials.

Here, we present the results of neutron average structure and total scattering local structure for three doping levels in the series, BTS20, BTS50 and BTS70, as well as *in situ* dehydration study insight into the effects of defect association as a function of Sc doping. [2-3] Fig. 1 shows an overview of the big-box modelling results from dehydrated BTS50, which illustrate the origin of the high oxygen vacancy availability.

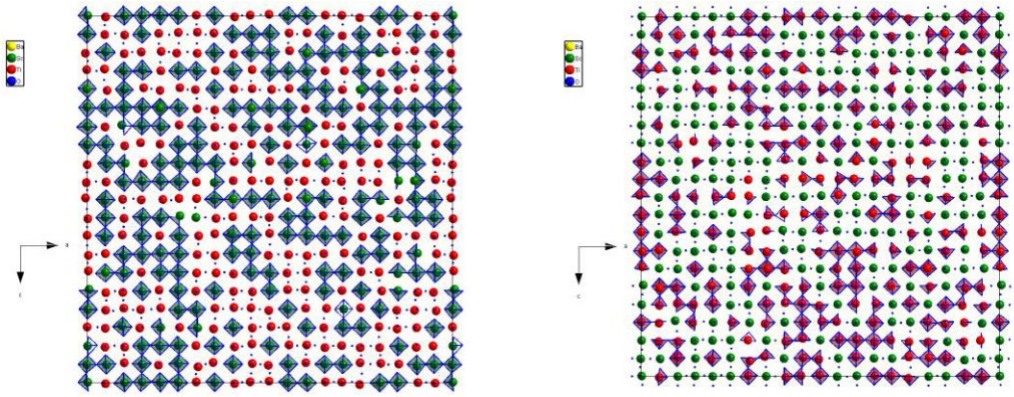

Figure 1. (left) Scandium and (right) titanium coordination polyhedra in BTS50.

1 N. Torino, P.F. Henry, C.S. Knee, T.S. Bjorheim, S.M.H. Rahman, E. Suard, C. Giacobbe, S.G. Eriksson. *Dalton Trans.* 2017, **46(26)**, 8387-8398. DOI:10.1039/c7dt01559c.

2 N. Torino, P.F. Henry, C.S. Knee, S.K. Callear, R.I. Smith, S.M.H. Rahman, S.G. Eriksson. *Solid State Ionics* 2018, **324**, 233-240. DOI:10.1016/j.ssi.2018.07.010.

3 A. Perrichon, N. Torino, E.J. Granhed, Y.C. Lin, S.F. Parker, M. Jiminez-Ruiz, M. Karlsson, P.F. Henry. *J. Phys. Chem. C* 2020, **124(16)**, 8643-8651. DOI: 10.1021/acs.jpcc.0c01705.

A049-06-240823

Structural Science of New Ionic Conductors

K. Fujii, M. Yashima

Department of Chemistry, School of Science, Tokyo Institute of Technology, 2-12-1-W4-17, O-okayama, Meguro-ku, Tokyo 152-8551, Japan

kfujii@cms.titech.ac.jp

Keywords: Ionic conductor, Ceramic material, Neutron diffraction

Ionic conductors have attracted considerable attention because of their potential applications such as fuel cells, batteries, and gas sensors. Ionic conductivity is strongly dependent on the crystal structure, and it is important to explore new structure family of ionic conductors, and investigate the mechanism of ionic conductors through structure analysis. Our group reported a number of new oxide-ion conductors and proton conductors, which were discovered by several different strategies (Fig. 1). The crystal structures of these ionic conductors were investigated by (synchrotron) X-ray and neutron diffraction techniques, and we investigate ion conduction paths and origins of high (or sometimes low) conductivity. In this presentation, the details of our researches on new ionic conductors will be shown.

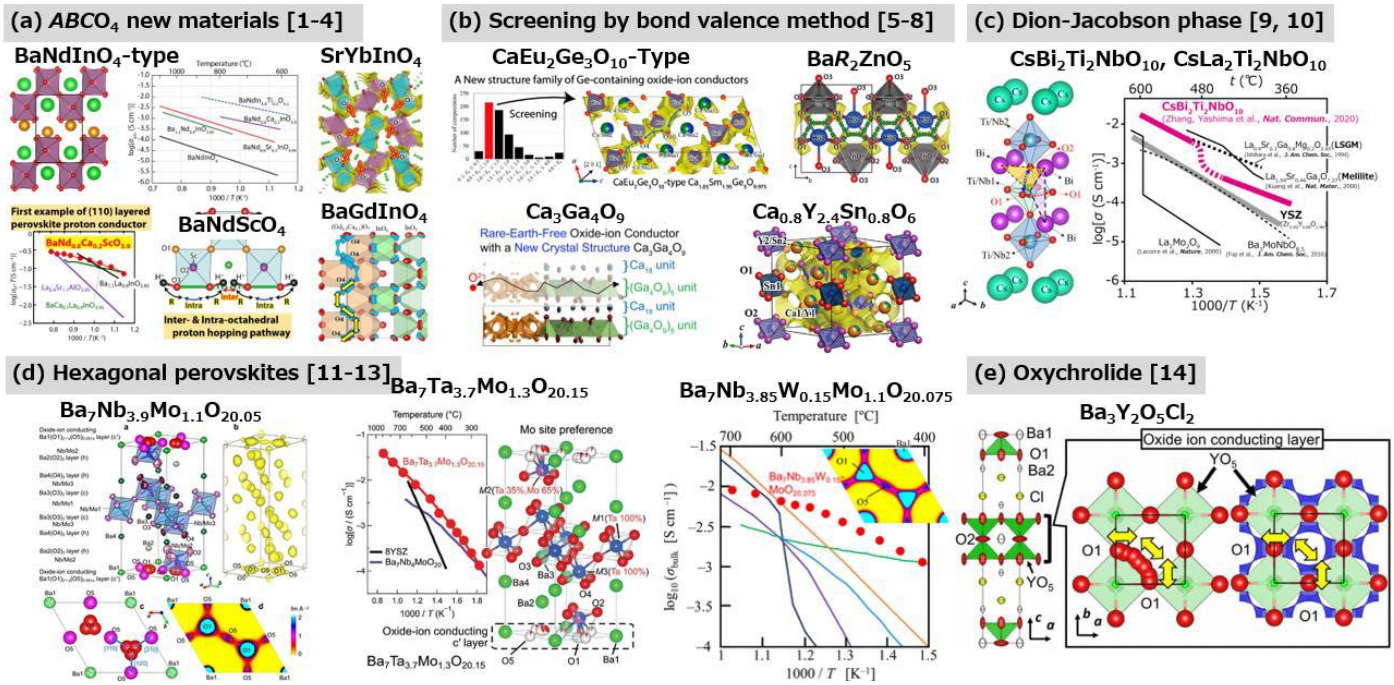

Figure 1. Ionic conductors reported by our group.

1 Fujii, K., Esaki, Y., Omoto, K., Yashima, M, Hoshikawa, A. & Ishigaki, T. (2014). *Chem. Mater.* **26**, 2488.
2 Fujimoto, A., Yashima, M., Fujii, K. & Hester, J. R. (2017). *J. Phys. Chem. C*, **121**, 21272.
3 Yaguchi, H., Fujii, K. & Yashima, M. (2020). *J. Mater. Chem. A*, **8**, 8638.
4 Shiraiwa, M., Kido, T., Fujii, K. & Yashima, M. (2021). *J. Mater. Chem. A*, **9**, 8607.
5 Inoue, R., Fujii, K., Shiraiwa, M., Niwa, E. & Yashima, M., (2018). *Dalton Trans.*, **47**, 7515.
6 Nakamura, K., Fujii, K., Niwa, E. & Yashima, M., (2018). *J. Ceram. Soc. JPN*, **126**, 292.
7 Yasui, Y., Niwa, E., Matsui, M., Fujii, K. & Yashima, M., (2019). *Inorg. Chem.*, **58**, 9460.
8 Matsui, M., Fujii, K., Shiraiwa, M. & Yashima, M., (2022). *Inorg. Chem.*, **61**, 12327.
9 Zhang, W., Fujii, K., Niwa, E., Hagihala, M., Kamiyama, T. & Yashima, M., (2020). *Nat. Commun.*, **11**, 1224.
10 Zhang, W., Fujii, K., Ishiyama, T., Kandabashi, H. & Yashima, M. (2020). *J. Mater. Chem. A*, **8**, 25085.
11 Yashima, M., Tsujiguchi, T., Sakuda, Y., Yasui, Y., Zhou, Y., Fujii, K., Torii, S., Kamiyama, T. & Skinner, S. J. (2021). *Nat. Commun.*, **12**, 1.
12 Murakami, T., Shibata, T., Yasui, Y., Fujii, K., Hester, J. R. & Yashima, M., (2021). *Small*, **18**, 2106785.
13 Suzuki, Y., Murakami, T., Fujii, K., Hester, J. R., Yasui, Y. & Yashima, M., (2022). *Inorg. Chem.*, **61**, 7537.
14 Yaguchi, H., Fujii, K., Tsuchiya, Y., Ogino, H., Tsujimoto, Y. & Yashima, M., (2022). *ACS Appl. Energy Mater.*, **5**, 295.

A056 Magnetic Order in Aperiodic Systems
Room 212
4.00pm - 6.30pm

A056-01-240823

Crystal and magnetic structure of CrAs as function of temperature and pressure

K. Friese[1,2], A. Eich[1,2], Y. Su[3], M. Hanfland[4], T. Wolf[5], V. Petricek[6], A. Grzechnik[2,3]

[1]*Jülich Centre for Neutron Science, Forschungszentrum Jülich GmbH, 52428 Jülich, Germany*

[2]*Institute for Crystallography, RWTH Aachen University, Jägerstr. 15-17, 52066 Aachen, Germany*

[3]*Jülich Centre for Neutron Science at Heinz Maier-Leibnitz Zentrum(MLZ), Forschungszentrum Jülich GmbH, Lichtenbergstr. 1, 85747Garching, Germany*

[4]*European Synchrotron Radiation Facility, 38000 Grenoble, France*

[5]*Institute for Quantum Materials and Technologies, Karlsruhe Institute of Technology, 76021 Karlsruhe, Germany*

[6]*Institute of Physics, Czech Academy of Sciences, Prague 8, 18221, Czech Republic*

k.friese@fz-juelich.de

Keywords: CrAs, extreme conditions, magnetic structure

Chromium arsenide, CrAs (space group *Pnma* at ambient conditions), is considered a model system in which superconductivity and helimagnetism coexist. The superconductivity is induced by pressure and forms a dome-like phase region with a maximum T_C of 2.2 K at about 1 GPa. The superconductivity occurs in the vicinity of an antiferromagnetically ordered phase of CrAs. We investigated the crystal structure of CrAs using synchrotron X-ray single crystal diffraction in dependence of temperature (30– 400 K) and on pressure increase (0–9.46 GPa) [1]. The isosymmetrical magnetostructural phase transition at $T_N \approx 270$ K induces a change in the microstructure by twinning due to a crossing of the orthohexagonal setting of the unit-cell parameter ratio c/b. Within the crystal structure, one particular Cr–Cr distance exhibits an anomalous behavior in that it is nearly unaffected by temperature and pressure in the paramagnetic phase, which is stable above 270 K and at high pressures. The distinct behavior of this shortest Cr–Cr distance might be of importance for the superconducting properties of CrAs.

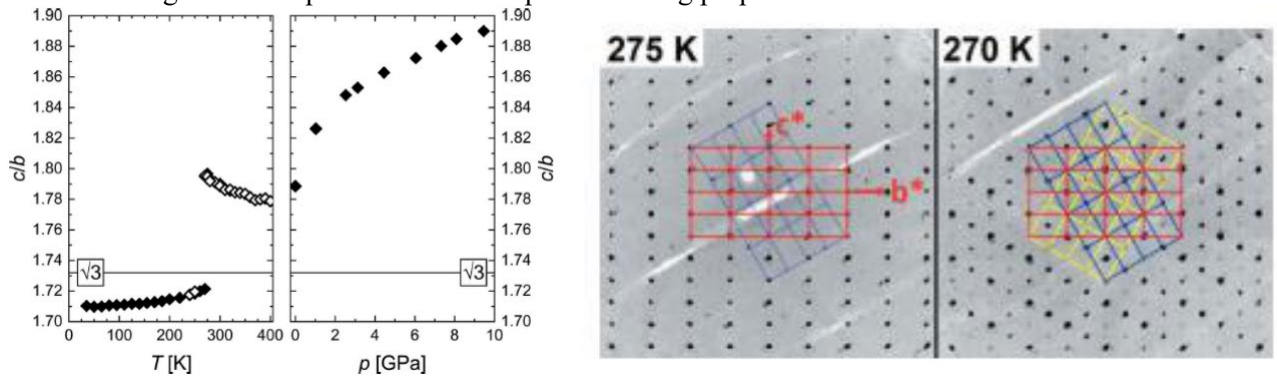

Figure 1. *c/b* ratio of CrAs as a function of temperature and pressure(left). The phase transition at ≈270 K induces a change in the microstructure that is clearly visible in the reconstructions of reciprocal space (right)

The magnetic structure of CrAs is incommensurate and described as a double helix in the literature. This model was first proposed on the basis of neutron powder diffraction data and assuming an analogous magnetic structure as the one observed for MnP [2]. Since the model was in reasonable agreement with the powder diffraction data, it was henceforth considered to be correct for CrAs. We have re-investigated the magnetic structure of CrAs for the first time by means of neutron high-pressure single-crystal diffraction in clamp cells. The results clearly show that the established model of the magnetic structure of CrAs is not in accordance with the measured intensities and can be discarded. While our data do not allow an unambiguous identification of one singular model, we identify four candidate models based on a stringent use of group theoretical considerations and the subsequent refinement using magnetic superspace groups with the program Jana2006 [3]. Details of these models will be presented. Recently, we performed synchrotron diffraction studies under simultaneous variation of temperature and pressure at various LT and HP conditions on beamline ID15B at the ESRF and were able to determine the crystal structure at 10 K and 0.8 GPa very close to the stability field of the superconducting phase. Preliminary results show that the structure at these conditions is still orthorhombic and that the observed twinning persists.

1 Eich, A. Grzechnik, A., Paulmann, C., Müller, T., Su, Y., Wolf, T., Friese, K. (2021), Acta Crystallogr. **B77**, 594.
2 Watanabe, H., Kazama, N., Yamaguchi, Y. & Ohashi, M. (1969), *J. Appl. Phys*. **40**,1128.
3 Petříček, V., Dušek, M., Palatinus, L. (2014), Z. Kristallogr. **229**, 345.

Acknowledgments: This work was supported by the BMBF under project No.05K19PA2.

A056-03-240824

Magnetic properties investigation of the Au-Ga-Tb 1/1 approximant crystals with single ferromagnetic and successive ferromagnetic/antiferromagnetic transitions

Farid Labib[1], Kazuhiro Nawa[2], Shintaro Suzuki[1], Asuka Ishikawa[3], Takenori Fujii[4], Ryuji Tamura[1] and Taku J. Sato[2]

[1] *Department of Material Science and Technology, Tokyo University of Science, Tokyo 125-8585, Japan*
[2] *Institute of Multidisciplinary Research for Advanced Materials (IMRAM), Tohoku University, Sendai 980-8577, Japan*
[3] *Research Institute of Science and Technology, Tokyo University of Science, Tokyo 125-8585, Japan*
[4] *Cryogenic Research Center, The University of Tokyo, Bunkyo, Tokyo 113-0032, Japan Labib.farid@rs.tus.ac.jp*

Keywords: Approximant crystal, Long-range order, Magnetic structure, Neutron diffraction

Quasicrystals are aperiodically ordered intermetallic compounds that generate non-periodic array of sharp Bragg reflections with 5fold rotational symmetry in their diffraction patterns [1]. In the Tsai-type cubic approximant crystals (ACs), which are cubic counterparts of the quasicrystals, long-range magnetic orders are established and their occurrence have been shown to follow systematic compositional dependence behavior, as seen in Fig. 1, where antiferromagnetic (AFM) and ferromagnetic (FM) orders are established at lower and intermediate electron concentrations (expressed as *e/a*), respectively. The spin configuration in the AFM phase (based on recent neutron diffraction experiments on the AFM $Au_{72}Al_{14}Tb_{14}$ [2] and $Au_{65}Ga_{21}Tb_{14}$ 1/1 ACs [3]) is of a noncoplanar type on the icosahedral clusters whirling around the [111] axes, with the spin directions being primarily fixed by the local anisotropy. In the FM state (based on the neutron diffraction experiments on $Au_{70}Si_{17}Tb_{13}$ [4] and Au-Si-*RE* (*RE* = Tb, Ho) [5] 1/1 ACs), noncoplanar whirling spin configuration on the icosahedron clusters are reported giving rise to the intensity of some crystallographically-allowed reflections (the strongest one being 200) for the BCC lattice in the low-2θ region of the neutron diffraction pattern.

In the present study, magnetic properties of the Tsai-type $Au_{64}Ga_{22}Tb_{14}$ and $Au_{60}Ga_{26}Tb_{14}$ 1/1 ACs whose *e/a* equal to 1.72 and 1.80 (as shown in Fig. 1) are examined via dc magnetic susceptibility and the powder neutron diffraction (PND) measurements. The former evidenced successive long-range magnetic transitions of antiferromagnetic (AFM) and ferromagnetic (FM) types at $T = 9.9$ and 11.2 K (based on the specific heat capacity measurements), respectively, while the latter exhibited a single FM transition at $T = 15.5$ K. The magnetic structure refinement of the powder neutron diffraction data (under some restraints) on the latter sample (see Fig. 2) suggests noncoplanar ferromagnetic order with the orientations of the moments being 87 degrees canted away from the pseudo 5f-axis. In the former sample, on the other hand, the coexistence of AFM order with identical magnetic structure to that of $Au_{72}Al_{14}Tb_{14}$ 1/1 AC [2] and FM order with almost the same magnetic structure to that of the latter sample is noticed at $T = 10$ K. Overall, the findings of the present work supports the idea that both the noncoplanar AFM and FM orders are induced by the same origin: the uniaxial anisotropy and competing magnetic interactions.

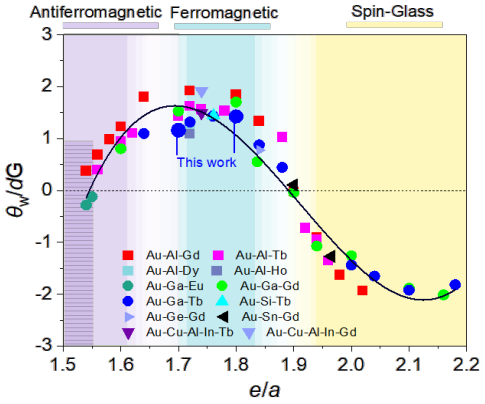

Figure 1 Variation of normalized Weiss temperature, Θ_w/dG and the magnetic ground states versus the electron-per-atom (e/a) ratio spanning from 1.5 and 2.2.

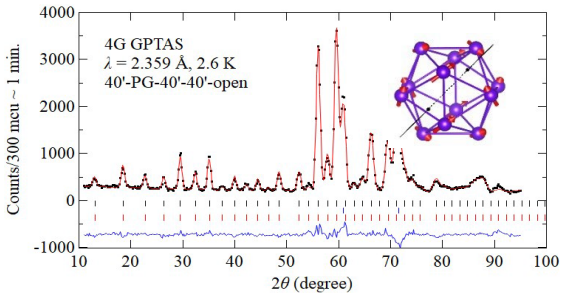

Figure 2. Variation of Rietveld refinementof $Au_{60}Ga_{26}Tb_{14}$ 1/1 AC under some restraints. Inset shows the magnetic structure obtained from the refinement. Observed intensities, calculated intensities, and their difference are represented by black dots, red and blue curves, respectively.

[1] D. Shechtman *et al.* Phys. Rev. Lett. **53**, 1951 (1984).
[2] T. J. Sato *et al.* Phys. Rev. B **100**, 054417 (2019).
[3] K. Nawa, *et al.* ArXiv:2204.00868 1 (2022).
[4] T. Hiroto *et al.* J. Phys. Condens. Matter **32**, 415802 (2020).
[5] G. H. Gebresenbut et al. Phys. Rev. B **106**, 1 (2022).

A056-02-240823

Search for new Eu-based magnetic quasicrystal approximants

S. Suzuki1, R. Takeuchi1, T. Abe1, Y. Shimozaki1, A. Ishikawa2, T. Fujii3 and R. Tamura1

[1]Department of Materials Science and Technology, Faculty of Advanced Engineering, Tokyo University of Science, Tokyo 125-8585, Japan, [2]Reserch Institute for Science and Technology, Tokyo University of Science, Chiba 278-8510, Japan, [3]Cryogenic Research Center, University of Tokyo, Tokyo, 113-0032, Japan

s_suzuki@rs.tus.ac.jp

Keywords: Quasicrystal approximants, Magnetism

Recently, magnetic ordering, i.e., ferromagnetism, in quasiperiodic lattice was observed for the first time in Au-Ga-(Ga,Tb) Tsai-type quasicrystals [1]. These compounds were discovered based on the correlation among the valence electron concentration per atom (*e/a*), the paramagnetic Curie temperature ($_p$) and the magnetic ground state [2], which was established through extensive magnetic studies on Gd and Tb based quasicrystal approximants (AC). To search for an antiferromagnetic quasicrystal as a next new long-range magnetic ordering in quasiperiodic system, further knowledge on this correlation in a variety of rare-earth systems is highly favorable. Recently, one example of antiferromagnetism in 2/1 AC was discovered in the Au-Ga-Eu system [3]. Therefore, it is of interest to investigate the correlation among *e/a*, $_p$ and the magnetic ground state also for Eu-based Tsai-type ACs in order to understand the condition of antiferromagnetism in Eu-based systems.

In this presentation, we report on the magnetism of the Au-Si-Eu AC. Magnetization and specific heat measurements revealed that this compound shows magnetic ordering as the ground state and hysteresis between zero field cooling (ZFC) and field cooling (FC) (Fig. 1). The *e/a*-$_p$ relation shows a completely different behavior compared to Gd and Tb based ACs. We will discuss this relationship with respect to recent calculations [4,5].

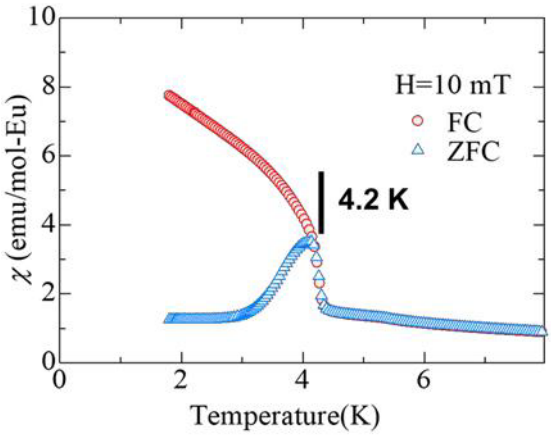

Figure 1. The temperature dependence of the magnetic susceptibility of the Au-Si-Eu 1/1 AC

1 R. Tamura, *et al.,* J. Am. Chem. Soc. **143**, 19938 (2021).
2 S. Suzuki, *et al.,* Mater. Trans. **62**, 298 (2021).
3 S. Yoshida, *et al.,* Phys. Rev. B **100**, 18 (2019).
4 H. Miyazaki *et al.,* Phys. Rev. Mater. **4**, 022417 (2020).
5 S. Suzuki, *et al.,* Mater. Trans. **62**, 367 (2021).

A056-04-240823

Nuclear and Magnetic Structure of $Ba_{1-p}Cr_2Se_{4-p}$ an aperiodic ferrimagnetic semiconductor

J. B. Claridge[1], K. Routeledge[2], J. Alaria[2], O. Pérez[3], D. Pelloquin[3].

1 Department of Chemistry, University of Liverpool, Crown Street, Liverpool, L69 7ZD, U. K. 2 Department of Physics, University of Liverpool, Oxford Street, Liverpool, L69 7ZE, U. K. 3 CRISMAT, ENSICAEN, 6 boulevard du Maréchal Juin, F-14050 CAEN Cedex 4 France
Email of communicating j.b.claridge@liv.ac.uk

Keywords: Aperiodic, Ferrimagnet, Magnetic Structure

The family of compounds $A_{1-p}Cr_2X_{4-p}$ (A: Ba, Sr, Eu, Sn, Pb; X: S, Se)[1]. They established these compounds as a class of isotypic chromium sulphides and selenides. The structure is described as intergrowth of three different structural subsystems, including a host framework and two different chains that lie within, sharing a common hexagonal basal (**a-b**) plane but have different **c** axes.

The framework consists of CrX_6 octahedra, containing strips of edge sharing octahedra (Figure 1(a)) similar to those in rutile interconnected by face sharing octahedra. These form a framework which contain channels/tunnels centred on the threefold and sixfold axes (*3/m* and *6/m*). The chains that occupy the triangular tunnels consist of A_3X units, whereas the chains that occupy the hexagonal tunnels consist of $A_6Cr_2X_6$ units.

We have re-examined the Barium selenide previously reported to be a commensurate superstructure, by X-ray single crystal and neutron powder diffraction. Single crystal measurements show that the first two subsystems are well ordered and described in super space group *P6/m(00α)s0* whilst the third subsystem is highly disordered giving rise to strong diffuse scattering (Figure 1 (b)).

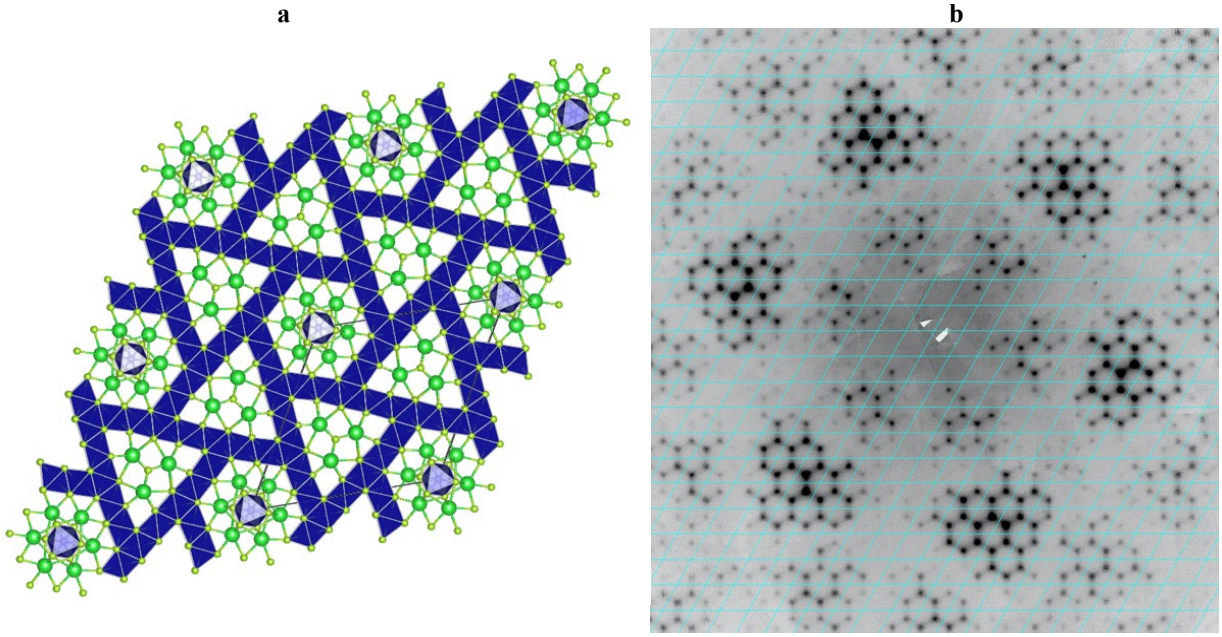

Figure 1. (a) Projection of average structure along c. (b) Diffuse scattering in hk0.6 plane

Bellow 120 K the structure orders ferrimagnetically and refinement of the neutron powder diffraction at 10 K gives the best fit for magnetic structures which break inversion symmetry. These agree well with the measured moments and indicate that the material is multiferroic at low temperatures.

[1] Brouwer, R. & Jellinek, F. *J. Chem. Soc., Chem. Comm.,* **1977**, 879.
Acknowledgements: This work is supported from JSPS KAKENHI Grant Numbers JP19H05817 and JP19H05818.

A056-05-240823

Heavy fermion behaviour in Pr-based quasicrystalline approximants

Y. Muro1, T. Namiki2, T. Kuwai2, A. Ishikawa3, S. Suzuki3, R. Tamura3

Center for Liberal Arts and Sciences, Toyama Prefectural University, Imizu 939-0398, Japan Graduate School of Science and Engineering, University of Toyama, Toyama 930-8555, Japan Department of Materials Science and Technology, Tokyo University of Science, Tokyo 125-8585, Japan ymuro@pu-toyama.ac.jp

Keywords: Pr-based quasicrystalline approximants, heavy fermion, single crystal, crystalline electric field

A combination between strongly correlated electron systems (SCES) and quasicrystals is one of fascinating research fields in the condensed matter physics. The first exciting discovery is the non-Fermi liquid behaviour in Au-Al-Yb quasicrystal [1]. The heavy fermion behaviour, that is one of principal theme in SCES, is also found in Ag-In -Ce and Au-Al-Ce systems [2, 3]. In Ce-, Yb- or U-based materials, heavy fermion behaviours are attributable to the Kondo effect between localized rare-earth 4 *f* electrons and conduction electrons. For some Pr-based heavy fermion systems, on the other hand, two routes are studied. The one is the correlation between the electric quadrupolar moment in the non-Kramers Γ3 doublet of Pr 4*f* electrons and conduction electrons another route is the inelastic scattering of conduction electrons by the angular momentum associated with the crystalline electric field levels which is called excitonic mass enhancement [5]. The latter mechanism is discussed in the large Sommerfeld coefficient γ in a skutterudite PrOs4Sb12 ($\gamma \sim 350$ mJ/mol K^2) [6] and PrRh2B2C ($\gamma \sim 250$ mJ/mol K) [7]. In this presentation, we report the magnetic and transport properties of new Pr-based quasicrystalline approximants Au-X-Pr (X = Si and Ge) by the magnetic susceptibility, electrical resistivity and specific heat measurements.

In this study, we succeeded to grow single crystals of Au-X-Pr by the flux method. Both compounds crystallize in Tsai-type 1/1 cubic approximant. The lattice parameter $a = 15.00$ Å for X = Si and $a = 14.85$ Å for X = Ge were determined by the least-square refinement of powder X-ray diffraction patterns. The SEM/EDX study reveals the nominal compositions Au71Si15Pr14 and Au63Ge23Pr14.

Figure 1 shows the temperature dependence of inverse magnetic susceptibility *H/M* of Au- X-Pr. Both compounds obey the Curie-Weiss behaviour down to 20 K. The estimated effective moments μeff = 3.44 μB for X = Si and 3.51 μB for X = Ge are close to the theoretical value 3.58 μB for free Pr^{3+} ion. Figure 2 shows the specific heat of Au-Si-Pr below 20 K. No phase transitions down to 0.5 K indicate the singlet ground state of Pr 4*f* electrons. As shown in the inset, a large value of $\gamma \sim 250$ mJ/mol-Pr K suggests that Au-Si-Pr is a non-magnetic heavy fermion system. This enhancement of γ should result from the excitonic mass enhancement because no signs of Kondo effect are observed in the electrical resistivity.

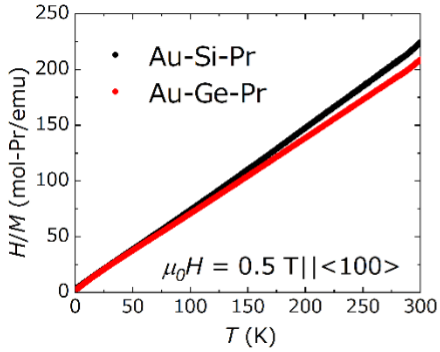

Fig. 1. Temperature dependence of inverse magnetic susceptibility of Au-X-Pr 1/1 approximants.

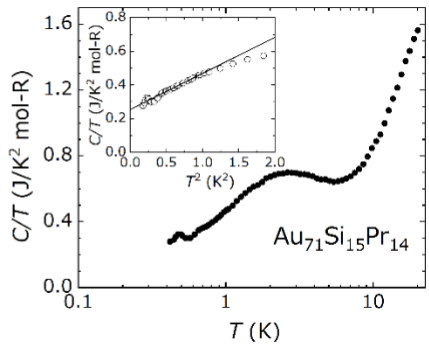

Fig. 2. Specific heat of Au-Si-Pr. The inset shows the *C/T* versus T^2 plot below 1.5 K. A solid line represents the result of linear fitting below 1 K.

1 Deguchi, K. *et al.* (2012). *Nat. Mater.*, **11**, 1013.
2 Imura, K. *et al*. (2017). *J. Phys. Soc. Jpn.*, **86**, 093702.
3 Muro, Y. *et al.* (2021). *Materials Transactions*, **62**, 321.
4 Cox, D. L. (1987), *Phys. Rev. Lett.*, **59**, 1240.
5 White, H. M. & Fulde, P. (1981), *Phys. Rev. Lett.*, **47**, 1540.
6 Goremychkin, E. A. *et al*. (2004), *Phys. Rev. Lett.*, **93**, 157003.
7 Anand, V. K. *et al.* (2009), *Phys. Rev. B* **79**, 113107.

This work was supported by JSPS KAKENHI Grant Number JP19H05818.

A056-06-240823

Long-range magnetic order in the quasicrystals and approximants

T. J. Sato

Institute of Multidisciplinary Research for Advanced Materials, Tohoku University
taku@tohoku.ac.jp

Keywords: Magnetic Structure, Quasicrystal, Approximant

Existence or absence of a long-range magnetic order in quasiperiodic spin systems has been one of the central controversies in quasicrystal research since its discovery in 1982 [1]. Historically, magnetic quasicrystals found in early stage all show spin-glass-like behaviour, suggesting that long-range order is somehow prohibited in quasiperiodic materials. On the other hand, more and more magnetic long-range order has been found in quasicrystal "approximants", in which local atomic (and consequently magnetic) clusters, being identical to those in quasicrystals, form spatially periodic network. Representative examples of such magnetic approximants are Cd6*RE* [2], Au-Si-Tb [3], and Au-Al-Tb [4], just to note a few. We have studied magnetic structures in the ordered phase of those approximants, and found intriguing non-collinear non-coplanar arrangement of spins, named "whirling spin order". Representative magnetic structure, found in the Au-Al-Tb 1/1 approximant, is shown in Fig. 1.
Systematic study on the magnetic order in the approximants further suggests that the condition for the establishment of the long-range order is indeed related to electron density [5]. Encouraged by this inspiring idea, Tamura *et al.* designed a new quasicrystalline phase in Au-Ga-*RE* (*RE* = Gd and Tb) alloy system [6]. Bulk magnetic characterization combined with neutron diffraction clearly shows formation of ferromagnetic order in the Au-Ga-Gd and Au-Ga-Tb quasicrystals, the first confirmation of the long-range magnetic order in quasicrystals. We have recently extended the higher dimensional crystallography to magnetic structure analysis. Using an irreducible representation table for the six-dimensional Pm-3-5 space group, higher-dimensional magnetic representation method has been developed, and implemented in the home-made powder Rietveld analysis code. Preliminary Rietveld fitting has been tried to the data obtained in the Au-Ga-Tb magnetic quasicrystal. In this talk, present status of the development of the analysis method will be presented, along with various magnetic structures found in the approximants.

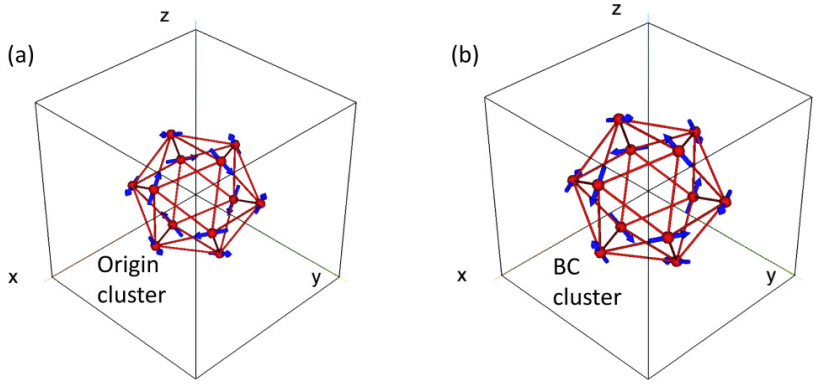

Figure 1. Spin arrangement in the ordered phase in the Au-Al-Tb 1/1 approximant. (a) the spin arrangement in the icosahedral cluster at the origin, and (b) at the body-centre position.

[1] Shechtman, D., Blech, I., Gratias, D. & Cahn, J. W. (1984). *Phys. Rev. Lett*. **53**, 1951.
[2] Tamura, R., Muro, Y., Hiroto, T., Nishimoto, K. & Takabatake, T. (2010). *Phys. Rev. B* **82**, 220201R.
[3] Sato, T. J., Ishikawa, A., Sakurai, A., Hattori, M., Avdeev, M. & Tamura, R. (2019). *Phys. Rev. B* **100**, 054417.
[4] Hiroto, T., Sato, T. J., Cao, H., Hawai, T., Yokoo, T., Itoh, S. & Tamura, R. (2020). *J. Phys.: Condens. Matter* **32**, 415802.
[5] Ishikawa, A., Hiroto, T., Tokiwa, K., Fujii, T., & Tamura, R. (2016). *Phys. Rev. B* **93**, 024416.
[6] Tamura, R., Ishikawa, A., Suzuki, S., Kotajima, T., Tanaka, Y., Seki, T., Shibata, N., Yamada, T., Fujii, T., Wang, C.-W., Avdeev, M., Nawa, K., Okuyama, D. & Sato, T. J. (2021). *J. Am. Chem. Soc*. **143**, 19938.

Acknowledgements: This work has been performed under the collaboration with many researchers including A. Ishikawa, S. Suzuki, T. Kotajima, Y. Tanaka, T. Seki, N. Shibata, T. Yamada, T. Fujii, C. -W. Wang, M. Avdeev, K. Nawa, D. Okuyama, T. Hiroto, H. Cao, T. Hawai, T. Yokoo, S. Itoh, K. Takagi and Y. G. So.. The author thanks late professor A. P. Tsai for his continuous support during this study. This work is partly supported by JSPS KAKENHI (JP22H00101, JP19KK0069, JP19K21839, and 19H05824).

A063 Crystal Structure Prediction
Room 213
4.00pm - 6.30pm

A063-01-240823

A seventh blind test of crystal structure prediction methods

Lily M. Hunnisett1, Jonas Nyman1, Nicholas Francia1, Ghazala Sadiq1, Isaac Sugden1, Susan Reutzel-Edens1, Jason Cole1

The Cambridge Crystallographic Data Centre, 12 Union Road, Cambridge, CB2 1EZ, UK

lhunnisett@ccdc.cam.ac.uk

Keywords: Crystal structure prediction, polymorphism

Since 1999 the Crystal Structure Prediction (CSP) blind tests, a community initiative currently coordinated by the Cambridge Crystallographic Data Centre (CCDC), have provided state-of-the-art CSP methods with an opportunity to validate and benchmark methodologies against unpublished data, with subsequent publications capturing the developments made over the years and providing readers with an overview of the methodologies available and in-development [1-6]. The 7th test saw participation from 129 researchers belonging to 28 groups from both academia and industry across 14 countries worldwide.

This talk explores the challenges that CSP currently faces as demonstrated by results and analysis of the 7th test including crystal structure similarity comparison, the value and treatment of disorder, and overprediction, indicating urgent paths for future CSP research.

1 J. P. M. Lommerse et al., (2000) *Acta Cryst.* B**56**, 697-714
2 W. D. S. Motherwell et al., (2002) *Acta Cryst.* B**58**, 647-661
3 G. M. Day et al., (2005) *Acta Cryst.* B**61**, 511-527
4 G. M. Day et al., (2009) *Acta Cryst.* B**65**, 107-125
5 D. A. Bardwell et al., (2011) *Acta Cryst.* B**67**, 535-551
6 A. M. Reilly et al., (2016) *Acta Cryst.* B**72**, 439-459

The authors wish to thank the scientists providing experimental data to this initiative including crystallographers and solid-form scientists, in addition to the computational researchers who participated in the test.

A063-02-240823

Ab initio design and crystal structure prediction of metal-organic frameworks

M. Arhangelskis[1],' Y. Xu[1], J. M. Marrett[2], H. M. Titi[2], J. P. Darby[3], M. Ferguson[4], A. J. Morris[5], T. Friščić[4]

[1]Faculty of Chemistry, University of Warsaw, Poland, [2]Department of Chemistry, McGill University, Montreal, Canada, [3]Department of engineering, University of Cambridge, UK, [4]School of Chemistry, University of Birmingham, UK, [4]School of Metallurgy and Material, University of Birmingham, UK

m.arhangelskis@uw.edu.pl

Keywords: metal-organic frameworks, *ab initio* design, molecular dynamics

Metal-organic frameworks (MOFs)[1,2] are crystalline microporous materials, constructed of transition metal nodes connected by organic linkers. In terms of functionality, MOFs are renowned for the diversity in applications: gas storage and separation, water purification, catalysis, light harvesting, energetic materials and fuels. What is the reason for such diversity? Evidently, the number of organic molecules that can act as MOF linkers is large. This, multiplied by the number of possible nodes, and further considering that each combination of nodes and linkers can produce multiple polymorphs, leads to a truly vast structural and topological space that MOF chemists have to navigate when screening for a material with specific functional properties.

In our group we develop methods for the computational design of MOFs, on the basis of our latest method for *ab initio* crystal structure prediction (CSP) of MOFs. Our approach is based on *ab initio* random structure search (AIRSS)[3] method for structure generation, combined with the Wyckoff alignment of molecules (WAM)[4] procedure for the determination of crystallographic symmetry of the randomly-generated structures. WAM analyses the point group symmetry of individual MOF building blocks and determines which space group symmetries are consistent with the molecular symmetry of the individual MOF components.

In this presentation the details of AIRSS+WAM method will be explained, highlighting the differences between CSP of MOFs and molecular crystals, and present examples of successful application of our method for the prediction of MOF structures subsequently found in the experimental synthesis, with the most notable example of copper(II)-based zeolitic imidazolate frameworks with rapid ignition (hypergolic) behaviour with the potential to be used as rocket propellants.[5] These materials are the first examples of MOFs designed truly *ab initio*, with the synthesis inspired by the computational prediction of structures and properties.

Conventional CSP procedure defines the likelihood of formation for a particular MOF polymorph based on its energy ranking within the complete set of the predicted structures. This, entirely thermodynamic, analysis does not take into consideration the effects of the reaction environment on the outcome of MOF synthesis. Specifically, the thermodynamic effects of solvent inclusion inside the voids of the porous structures are not taken into account, which leads to an artificial overestimation of the stability of the non-porous polymorphs over the lower-density structures capable of incorporating solvent molecules inside their pores. With the aid of molecular dynamics (MD) simulations, we will demonstrate how solvent inclusion leads to a qualitative change of the calculated crystal energy landscape and explains the existence of highly porous structures, which would be deemed metastable in the absence of solvent guests.

The presented developments for MOF CSP pose promise for the future, where experimental MOF screening will be supported by computational structure and property prediction, presenting opportunities for faster, target-driven synthesis of structures with predicted performance, with a reduced number of necessary experimental trials.

1 Eddaoudi, M., Moler, D. B., Li, H., Chen, B., Reineke, T. M., O'Keeffe, M. & Yaghi, O. M. (2001). *Acc. Chem. Res.* **34**, 319–330.
2 Hoskins, B. F. & Robson, R. (1989). *J. Am. Chem. Soc.* **111**, 5962–5964.
3 Pickard, C. J. & Needs, R. J. (2011). *J. Phys. Condens. Matter.* **23**, 053201.
4 Darby, J. P., Arhangelskis, M., Katsenis, A. D., Marrett, J. M., Friščić, T. & Morris, A. J. (2020). *Chem. Mater.* **32**, 5835–5844.
5 Xu, Y., Marrett, J. M., Titi, H. M., Darby, J. P., Morris, A. J., Friščić, T. & Arhangelskis, M. (2022). *ChemRxiv*.

A063-03-240823

Improving molecular crystal stability rankings via multimer embedding

J. Hoja, A. List, A. D. Boese

Institute of Chemistry, University of Graz, Heinrichstr. 28, 8010 Graz, Austria

johannes.hoja@uni-graz.at

Keywords: molecular crystals, embedding methods, density functional theory, free energies

As the final step, molecular crystal structure predictions regularly require highly accurate relative stabilities at a certain temperature, since polymorphs often differ only by very few kJ/mol in their Gibbs free energies [1]. However, high-level electronic structure calculations are often prohibitively expensive for relevant molecular crystals. One way of circumventing such expensive periodic calculations is the usage of embedding methods. The periodic result of a high-level method can for instance be approximated by a subtractive embedding scheme, in which a fully periodic calculation is only performed utilizing a less expensive lower-level method and then monomer energies, dimer interaction energies, etc. are replaced by those of the high-level method [2]. Furthermore, vibrational contributions are typically calculated within the harmonic approximation, while the thermal expansion can be approximated by using the quasi-harmonic approximation [3, 4]. However, a proper anharmonic description of coupled vibrational/phonon modes within molecular crystals remains challenging for electronic structure methods due to its computational complexity.

Herein, we present a multimer embedding approach containing up to trimer interactions for energies, structures, and vibrational properties of molecular crystals [5] intended for the final re-ranking stage of a molecular crystal structure prediction. This allows the inclusion of sophisticated electronic structure methods at reduced computational cost, thereby extending the applicability to larger systems or more structures. We demonstrate the high accuracy of this approach for the X23 benchmark set of molecular crystals by approximating a periodic hybrid density functional (PBE0+MBD) by embedding multimers into less expensive PBE+MBD calculations. We show that trimer interactions are crucial for accurate lattice energies and cell volumes, while harmonic vibrational properties can already be captured at the dimer level. In addition, we also discuss the application of this methodology to stability rankings of target systems from recent molecular crystal structure prediction blind tests. Finally, we introduce another multimer embedding approach incorporating anharmonic effects via second-order vibrational perturbation theory calculations of monomers and dimers.

1 Hoja, J., Ko, H. Y., Neumann, M. A., Car, R., DiStasio Jr., R.A. & Tkatchenko, A. (2019). *Sci. Adv.* **5**, eaau3338.
2 Boese, A. D. & Sauer, J. (2017). *Cryst. Growth Des.* **17**, 1636.
3 Hoja, J., Reilly, A. M. & Tkatchenko, A. (2016). *WIREs Comput. Mol. Sci.* **7**, 1294.
4 Dolgonos, G. A., Hoja, J. & Boese, A. D. (2019). *Phys. Chem. Chem. Phys.* **21**, 24333.
5 Hoja, J., List, A. & Boese, A. D. (2022). *arXiv preprint* arXiv:2209.02687.

A063-04-240823

The four stacking modes of experimental and predicted Lapachol polymorphs.

N. Di Benedetto1, Brad C. Ayers2, Mario A. Macías3, Grame P. Day2, Miguel A. Martínez-Cabrera4, L. Suescun1

Cryssmat-Lab/DETEMA, Facultad de Química, Universidad de la República, Casilla 1157, Montevideo, Uruguay,
School of Chemistry, University of Southampton, Southampton, SO17 1BJ, United Kingdom,
Departamento de Química, Facultad de Ciencias, Universidad de los Andes, Carrera 1 # 18A – 12, Bogotá, Colombia,
Facultad de Ciencias Exactas y Naturales, Universidad de Asunción, Asunción, Paraguay.

leopoldo@fq.edu.uy

Keywords: Lapachol, Polymporphism, Structure prediction

Lapachol (2-hydroxy-3-(3-methyl-2-butenyl)-1,4-naphthoquinone) is a pigment extracted from the bark of *Handroanthus heptaphyllus* (Vell.) Mattos commonly known as pink trumpet tree or lapacho. The group of 1,4-naphthoquinones and its derivatives has always attracted a lot of attention since these compounds exhibit a wide range of biological and pharmacological effects. In particular, lapachol has demonstrated properties as an antitumor, anticarcinoma, antiviral, bactericidal, fungicidal and antimalarial agent, among others. Two lapachol polymorphs were described by Larsen et al. (1992) [1] with triclinic $P\bar{1}$ (LAPA I: a=5.960(1), b=9.569(2), c=10.679(2) Å, α=96.82(2), β=98.32(2) and γ=90.32(2) ˚) and monoclinic $P2_1/c$ (LAPA II: a=6.035(1), b=9.427(2), c=20.918(5) Å and β=98.27(2) ˚) crystal structures at 105K.

During the course of an investigation of lapachol complexes we accidentally found a new polymorph, also monoclinic $P2_1/c$ (LAPA III: a= 9.5943(19), b= 6.0173(10), c= 21.566(2) Å, α= 90, β=96.815(2), γ= 90 ˚) with the unit cell closely related to that of LAPA I and LAPA II. The three structures show identical lapachol dimeric layers (formed by centrosymmetric lapachol dimers) that define the constant a~6.0, b~9.6 Å and g≈90 ˚ unit cell parameters, with exact overlap of lapachol conformations among crystal structures. These layers stack through van der Waals interactions in three different ways defining the three observed crystal structures. In LAPA I consecutive layers are just related by translation along c. In LAPA II and LAPA III consecutive layers are related by a 2_1 screw axis along a and b axes respectively.

The rigid behaviour of lapachol molecule in the three experimental crystal structures led us to examine the energy landscape of lapachol crystals, in order to test if the new lapachol polymorph could have been predicted and whether other molecular conformations are able to produce low energy crystal structures. The structure prediction algorithm [2] found the three observed crystal structures among the four lowest energy predicted structure, and additionally a fourth crystal structure with similar energy to that of LAPA III showing the same dimeric layers of lapachol with consecutive layers related by a 2_1 axis along the normal to the invariant a-b plane (LAPA IV, monoclinic $P2_1/n$: a=9.078, b=21.611, c=6.350 Å, α= 90, β=89.7, γ= 90˚).

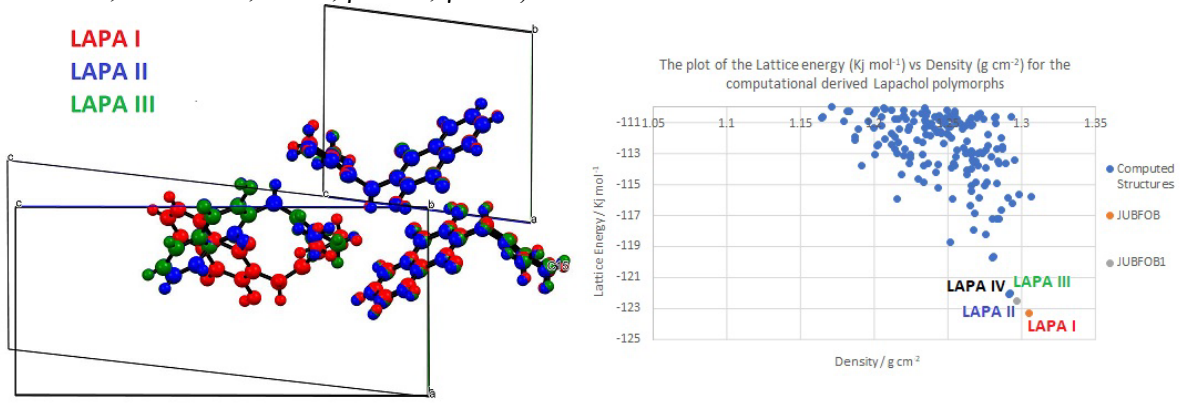

Figure 1. Left: Overlay of experimental lapachol crystal structures & unit cells. Molecules of one layer fit perfectly while the next layer shows a change in orientation in II and III. Right: Plot of lattice energy vs density for predicted crystal structures.

We will present the structural analysis of the four lapachol polymorphs emphasizing on the similarities and difference and inform of the results of the on-going search of the missing polymorph in the lab.

[1] Larsen, I.K., Andersen, L.A. & Pedersen, B.F. (1992). *Acta Cryst.* C**48**, 2009-2013.

[2] Case, D. H., Campbell, J. E., Bygrave, P. J. & Day, G.P. (2016) *J. Chem. Theory Comput.* 12(2), 910-924.

A063-05-240823

Stability of sulfur molecules and insights into sulfur allotropy

Maria Fedyaeva[1,2], Sergey V. Lepeshkin [2, 3, 4] and Artem R. Oganov[3]

1 Moscow State University, Leninskie Gory, Moscow 119991, Russia, 2 Vernadsky Institute of Geochemistry and Analytical Chemistry, Russian Academy of Sciences, Kosygina, 19, Moscow, 119991, Russia, 3 Skolkovo Institute of Science and Technology, Bolshoy Boulevard 30, bld. 1, Moscow 121205, Russia, 4 Lebedev Physical Institute, Russian Academy of Sciences, 53 Leninskii prosp., 119991 Moscow, Russia
Email of communicating: femaal.femaal3@yandex.ru

Keywords: Sulfur, Allotropy, Stability

Elemental sulfur occurs in more allotropic forms than any other element in the periodic table except, perhaps, carbon [1]. In nature, elemental sulfur occurs in over 30 allotropes, including both native forms and inclusions in minerals and biological systems. Due to the importance of sulfur in natural processes, we applied the evolutionary algorithm USPEX [2, 3, 4] and *ab initio* calculations to determine the structures (Fig. 1) of sulfur molecules (S_n, where n = 2-21). We examined the stability of the molecules using several criteria, including the second derivative of energy with respect to composition ($\Delta_2 E$), fragmentation energy (E_{frag}), and HOMO-LUMO energy levels. Based on these data, we identified the most stable ("magic") clusters, which are expected to be the most prevalent. In our work we have shown that “magic” molecules play a special role in the structural chemistry and geochemistry of sulfur. All low-pressure crystalline sulfur allotropes have molecular crystal structures. As it is easier to grow the crystal from the most abundant molecules, nearly all known sulfur allotropes are made of “magic” molecules (such as S_8, S_{12}, S_6 and others) [5]. This rule can also be applied to other molecular crystals, because individual molecules in them are weakly bound to each other,

Taking into account vibrational and entropic effects, we have calculated the proposed stability measures at different temperatures. The obtained values (G_{at}, $\Delta^2 G$ and G_{frag}) can be used for predicting which molecules will be the most abundant at different temperatures. Typically, $\Delta_2 E$ (or $\Delta_2 G$ at finite temperatures) is a quantitative measure of stability, which allows us to predict the ease of formation of molecules and corresponding molecular crystals. For example, the S_8 molecule has the highest value of $\Delta_2 E$ and forms the most common allotrope of sulfur (orthorhombic α-S), which eventually transforms into this form at room temperature. Another well- known molecule, S_7, has a negative $\Delta_2 G$ at temperatures around 300 K, but thermal effects make the S_7 molecule magic above 900 K, explaining its relatively high abundance. The temperature dependence of these stability indicators explains the wide range of facts about sulfur crystal allotropes, gas-phase molecules, and so on.

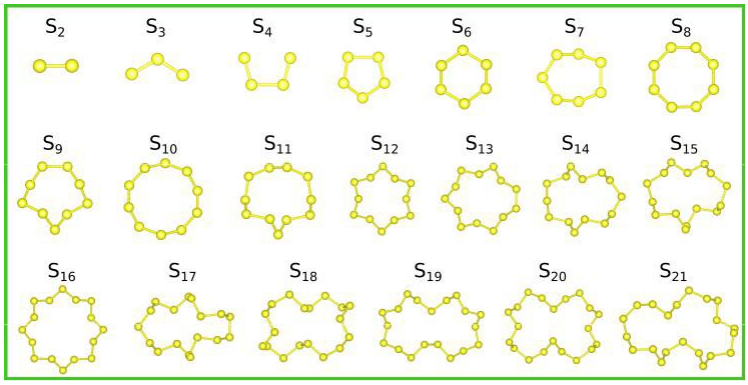

Figure 1. Lowest-energy structures of sulfur molecules S_n (n = 2 – 21).

1 Earnshaw, A. and Greenwood, N.N., 1997. *Chemistry of the Elements* (Vol. 60). Oxford: Butterworth-Heinemann.
2 Oganov, Artem R., and Colin W. Glass. 2006. “Crystal Structure Prediction Using Ab Initio Evolutionary Techniques: Principles and Applications.” *The Journal of Chemical Physics* 124 (24): 244704.
3 Oganov, Artem R., Andriy O. Lyakhov, and Mario Valle. 2011. “How Evolutionary Crystal Structure Prediction Works--and Why.” *Accounts of Chemical Research* 44 (3): 227–37.
4 Lyakhov, A.O. et al. (2013) ‘New developments in evolutionary structure prediction algorithm USPEX’, *Computer physics communications*, 184(4), pp. 1172–1182.
5 Steudel, R. and Eckert, B., 2003. Solid sulfur allotropes. Elemental sulfur and sulfur-rich compounds I, pp.1-80.

A063-06-240823

The potential energy wonderland

Dr Jack Yang

Materials and Manufacturing Futures Institute, School of Material Science and Engineering, University of New South Wales, Kensington, NSW 2052, Australia

jianliang.yang1@unsw.edu.au

Keywords: Potential energy surface, organic semiconductors, inorganic perovskites, machine learning

The concept of potential energy surface (PES) is fundamentally important in material science. The preferred three-dimensional arrangements of atoms for a given material are those that can maximally minimise its potential energy. Access to this structural information is a prerequisite for determining their corresponding physical and chemical properties using computational approach, which is a key step towards property-driven material designs, the Holy Grails of material science. In this talk, I will discuss our research in mapping the chemistry-structure-energy-property relationships for both the crystalline organic and inorganic materials, through sampling the PES at both the global and local minimum level. Specific examples include (a) the optimisation of the functionalisation patterns in planar acene molecules to achieve high charge mobilities via enhancing the π stackings in their crystalline phases [1], and (b) how the material chemistries affect the room temperature dynamical stabilities of inorganic cubic perovskites [2], which are fundamentally determined by the topology of the local minimum that can be measured in terms of the vibrational anharmonicities. Special focus will be devoted to exemplify how unsupervised atomistic machine learning techniques[3] can be utilised to generate intriguing insights on the structure-property relationships embedded in the data generated from these high-throughput studies, which are non-trivial to be rationalised and can be easily overlooked using only the human intuition.

[1] F. Musil, S. De, J. Yang, J.E. Campbell, G.M. Day, M. Ceriotti, *Chem. Sci*., **9**, 1289 (2018); J. Yang, S. De, J.E. Campbell, S. Li, M. Ceriotti, G.M. Day, *Chem. Mater.*, **30**, 4361 (2018); J. Yang, N. Li, S. Li, *CrystEngComm*, **21**, 6137 (2019).

[2] J. Yang, *J. Mater. Chem. C,* **8**, 16815 (2020); J. Yang, S. Li, *Mater. Horiz.*, **9**, 1896 (2022); J. Yang, J. Fan, S. Li, *Chem. Mater.*, **34**, 9072 (2022).

[3] S. De, A.P. Bartok, G. Csanyi, M. Ceriotti, *PCCP*, **18**, 13754 (2016).

A080 Industrial and Engineering Powder Diffraction

Room 211

4.00pm - 6.30pm

A080-01-240823

Characterization of polymers used in pharmaceutical and biomedical applications

T. Blanton1, M. Rost1, D. Bohnenberger1

International Centre for Diffraction Data, Newtown Square, PA, USA

tblanton@icdd.com

Keywords: pharmaceutical, phase identification, polymer

Polymers show a range of order from amorphous to semi-crystalline. Traditional organic analytical techniques, such as infrared spectroscopy (IR), differential scanning calorimetry (DSC), thermal gravimetric analysis (TGA), and nuclear magnetic resonance (NMR), are typically used for polymer analysis. Though X-ray diffraction (XRD) is not commonly used as the primary technique for polymer characterization, XRD does provide unique information about a polymer particularly when assessing crystallinity and crystallite size. In medical applications, polymers are often used as excipients in pharmaceuticals, and the base material for delivery devices used in biomedical applications.

ICDD has been adding polymer diffraction data to the Powder Diffraction File (PDF®) with the focus on adding raw data diffraction patterns (1D and 2D) as part of the PDF entry. The inclusion of the raw data diffraction pattern is important in correctly identifying the polymer contribution to a composite material diffraction pattern. A traditional d-spacing/intensity stick pattern or simulated diffraction pattern is not capable of accounting for the full-pattern diffraction profile of polymers since all polymers have some amorphous component. This polymer project focuses on industrially important polymers with an added emphasis on polymers used in medical and biomedical applications. New entries resulting from this project will be presented along with phase identification analysis results for pharmaceutical formulations including an interesting finding for a change in the polymers used in the formulation of opioid based oxycodone pain medication.

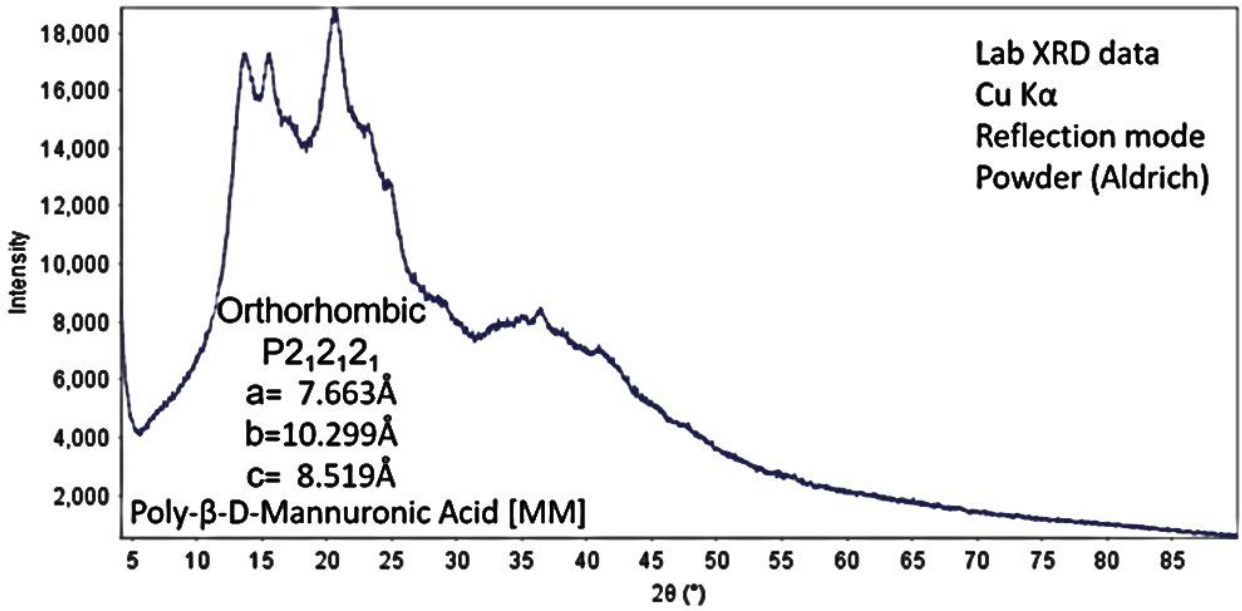

Figure 1. X-ray diffraction pattern (Cu Kα radiation) for alginic acid, poly-β-D-mannuronic acid [MM] type, used as a drug delivery excipient.

A080-02-240823

Combined use of X-ray diffraction and microtomography for accurate cement hydration studies

M.A.G. Aranda*, A. Cuesta, S. Shirani, A.G. De la Torre, I. Santacruz, A. Morales-Cantero, I. Koufany, C. Redondo-Soto, I.R. Salcedo and L. León-Reina

Universidad de Málaga, 29071-Málaga, Spain,

g_aranda@uma.es

Keywords: In situ studies, degree of hydration, accuracy, Rietveld analysis, segmentation, pozzolanic reaction

Accuracy in early age Portland cement (PC) hydration analyses is not straightforward as multimineral material has an inherent variability and different techniques are subject to different experimental errors and diverse approximations in the calculations.

Here, an innovative *in situ* PC hydration investigation is reported. The PC conforms to CEM I 42.5R according to EN 197-1. The paste was prepared with a water-to-cement mass ratio of 0.50, at 25±2 ºC, without admixture(s) and loaded and sealed in a thick glass capillary, □**=2.0 mm**, *to have excellent powder averaging* for the X-ray powder diffraction and microtomographic analyses. The data were taken on a D8 ADVANCE (Bruker) diffractometer using strictly monochromatic MoKα_1 radiation (λ=0.7093 Å) and on a SKYSCAN 2214 (Bruker) scanner using a source of LaB_6. Data were taken not simultaneously but sequentially.

On the one hand, from diffraction, we quantitatively followed the dissolution of the cement phases and the crystallization of portlandite and ettringite. The amount of C-S-H gel has been indirectly determined from the known-chemical reactions (mass balance calculations.). See top row of Fig. 1 for inspecting the quality of the resulting Rietveld plots. Hence, time and phase-dependent degree of hydration (DoH) were obtained. On the other hand, from □CT, the dissolution of the anhydrous cement phases (whitish particles) and the crystallization/precipitation of hydrates (darkish regions) can be followed. See bottom row of Fig. 1 for observing these processes. In these conditions, (i) $Ca(OH)_2$ carbonation is avoided, (ii) experimental errors are minimised because the use of rotating capillary (like water microbleeding in flat-sample geometry), and chiefly the results from two techniques are combined which improves the accuracy and it allows to detect errors.

This is a (required) first step in our long-term endeavour of using the combination of □CT and LXRPD, for determining the DoH of amorphous materials in PC blends with supplementary cementitious materials (SCMs). Our final goal is to be able to directly measure the DoH of amorphous components of SCMs as well as the $Ca(OH)_2$ consumption by the pozzolanic set of reactions.

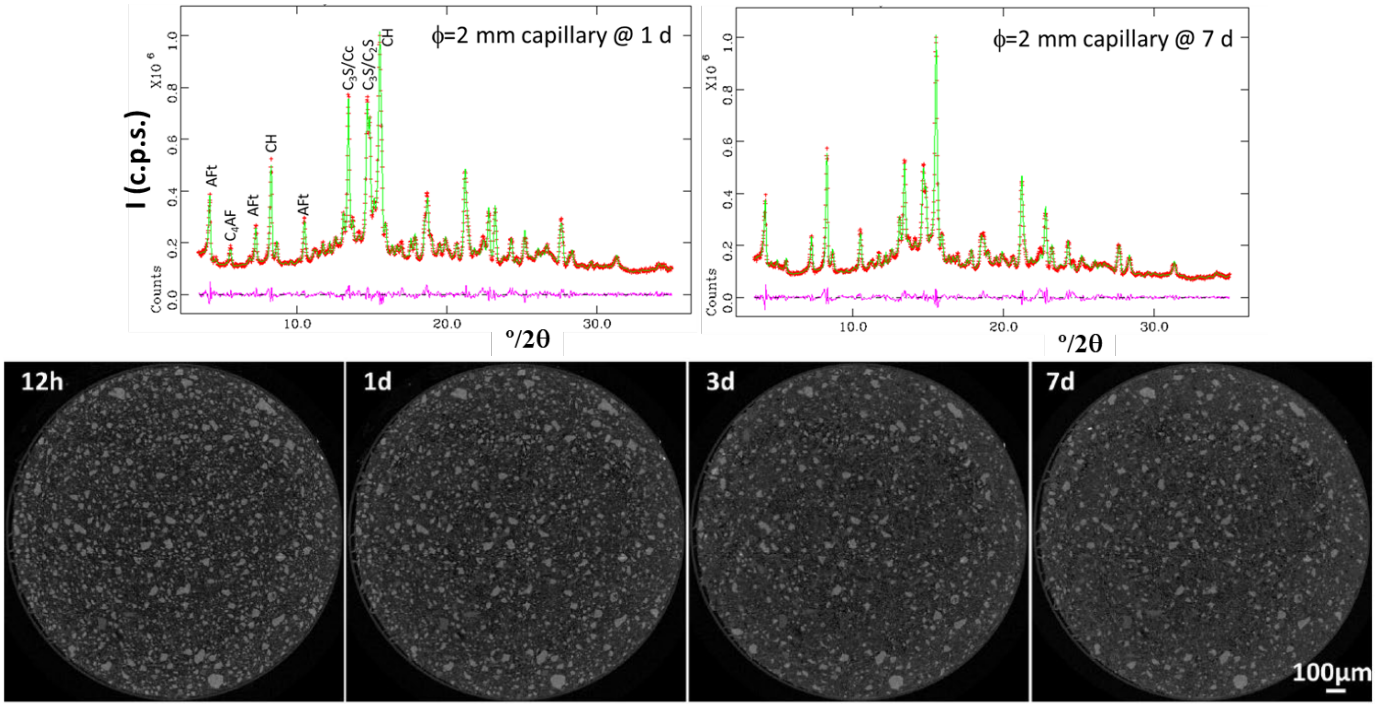

Figure 1. Combined diffraction and tomographic study in the same capillary, ϕ=2.0 mm, where a PC 42.5R paste is hydrating. Top row: Selected Rietveld plots (λ=0.7093 Å) at 1 day (left) and 7 days (right). Key diffraction peaks are labelled. The decrease in the intensities for alite (C_3S) and the increase for portlandite (CH) peaks is evident. Bottom row: Selected orthoslices showing the cement hydration evolution with time. The whitish particles are the anhydrous Cement Particles and the grey regions are the Hydrated Products. Porosity develops as blackish regions

More technical and scientific details will be presented at the meeting.

Financial support from PID2019-104378RJ-I00 research grant, which is co-funded by FEDER, is gratefully acknowledged.

A080-03-240823

Crystal structures of large-volume commercial pharmaceuticals

J. A. Kaduk1, T. M. Ens1, N. C. Boaz1, A. V. Dosen2, S. Gates-Rector2, T. N. Blanton2

North Central College, Naperville IL USA, ICDD, Newtown Square PA USA

kaduk@polycrystallography.com

Keywords: pharmaceutical, powder diffraction, density functional theory

As part of a continuing project, the room-temperature crystal structures of seven commercial pharmaceutical APIs have been solved and refined using synchrotron X-ray powder diffraction data (11-BM at APS), and optimized using density functional techniques. *Meglumine diatrizoate* (C7H17NO5)(C11H8I3N2O4) crystallizes in space group *P21* (#4) with a = 10.74697(4), b = 6.49364(2), c = 18.52774(7) Å, β = 90.2263(3), V = 1292.985(5) Å^3, and Z = 2. *Encorafenib* C22H27ClFN7O4S crystallizes in space group *P21* (#4) with a = 16.17355(25), b = 9.52338(11), c = 17.12368(19) Å, β = 89.9928(22), V = 2637.49(4) Å^3, and Z =4 *Omadacycline dihydrate* C29H40N4O7(H2O)2 crystallizes in space group *R3* (#146) with a = 24.34435(8), c = 14.55213(5) Å, V = 7468.849(29) Å^3, and Z = 9. *Nicarbazin* (C12H10N4O5)(C6H8N2O) crystallizes in space group *P-1* (#2) with a = 6.90659(8), b =70794(4), c = 13.5040(7) Å, α = 115.5709(11), β = 102.3658(6), γ = 91.9270(4)°, V = 982.466(5) Å^3, and Z = 2. *Oxfendazole* C15H13N3O3S crystallizes in space group *P21/c* (#14) with a = 18.87326(26), b = 10.40333(5), c = 7.25089(5) Å, β = 91.4688(10)° V = 1423.206(10) Å^3, and Z = 4. *Butenafine hydrochloride* C23H28NCl crystallizes in space group *P21* (#4) with a = 13.94807(5), b = 9.10722(2), c = 16.46676(6) Å, β = 93.9663(5)°, V = 2086.733(8) Å^3, and Z = 4. *Besifloxacin hydrochloride* C19H22ClFN3O3Cl crystallizes in space group *P1* (#1) with a = 5.36596(8), b = 10.3234(4), c = 17.9673(14) Å, α = 98.122(5), β = 92.9395(9), γ = 96.1135(3)°, V = 977.483(13) Å^3, and Z = 2. Other new structures may be presented as they become available.

Use of the Advanced Photon Source at Argonne National Laboratory was supported by the U. S. Department of Energy, Office of Science, Office of Basic Energy Sciences, under Contract No. DE-AC02-06CH1135

A080-04-240823

Effect of mono- and divalent extra-framework cations on the structure and the internal surface area of chabazite zeolites

Huan V. Doan[1], Ka Ming Leung[2], Asel Sartbaeva[3] and Valeska P. Ting[1]

[1]*Department of Mechanical Engineering, University of Bristol, Bristol BS8 1TR, UK.*

[2]*Inorganic Chemistry Lab, South Parks Road, University of Oxford, Oxford OX1 3QR, UK.*

[3]*Department of Chemistry, University of Bath, Bath BA2 7AY, UK.*

huan.v.doan@bath.edu

Keywords: chabazite, structural chemistry, NMR, PXRD, gas sorption, simulation

Chabazite (CHA), one of the most common zeolite framework types, has been studied extensively in selective gas sorption. This is due to the remarkable capacity of this zeolite to accommodate cations within the unique CHA framework. Here, we report a systematic study on a series of chabazite zeolites exchanged by divergent extra-framework cations with valence and atomic radius differences. The results showed that chabazite (KNa-CHA) was synthesised successfully from zeolite Y, and six chabazite zeolites including K-CHA, Cs-CHA, Ca-CHA, Ba-CHA, Sr-CHA and Zn-CHA were prepared from the parent chabazite by ion exchange. These samples were examined by numerous techniques and it was found that the difference in valence and size between extra-framework cations exerts a significant effect on the abundance of these cations positioned in the framework, resulting in differing nitrogen sorption ability measured in the synthesised chabazite zeolites. These findings will help to understand the molecular sieve of the zeolite countercation which is a promising mechanism to selectively sequester and separate gases.

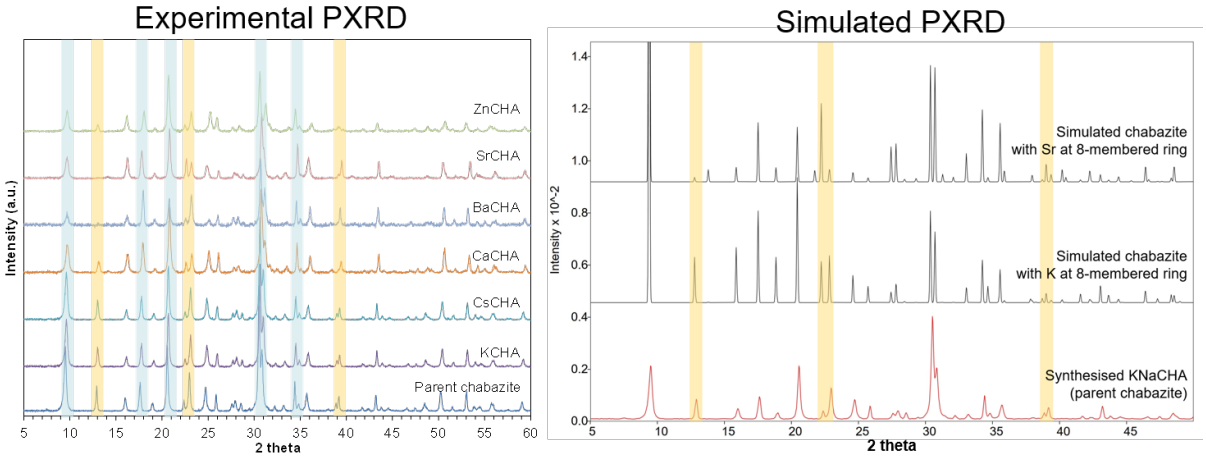

Figure 1. Left: PXRD of parent chabazite and ion-exchanged CHA zeolites compared to simulated chabazite. Key peaks that remained the same are highlighted in light blue. Key peaks that changed or disappeared are highlighted in light orange. PXRD spectra are offset in intensity, for clarity. Right: PXRD patterns of simulated K-CHA and simulated Sr-CHA (K and Sr positioned at the eight-membered ring) in comparison to the PXRD pattern of synthesised KNa-CHA.

References:

[1] J. W. Physick, D. J. Wales, S. H. R. Owens, J. Shang, P. A. Webley, T. J. Mays and V. P. Ting, *Chem. Eng. J.*, 2016, **288**, 161–168.

[2] F. N. Ridha and P. A. Webley, *Sep. Purif. Technol.*, 2009, **67**, 336–343.

[3] J. Shang, G. Li, R. Singh, P. Xiao, J. Z. Liu and P. A. Webley, *J. Phys. Chem. C*, 2013, **117**, 12841–12847.

A080-05-240823

Solving energy sector industry problems using *in situ* neutron powder diffraction

V.K. Peterson[1,2]

1. *Australian Centre for Neutron Scattering, Australian Nuclear Science and Technology Organisation, New Illawarra Road, Lucas Heights, NSW, Australia, 2. Institute for Superconductivity and Electronic Materials, University of Wollongong, Squires Way, North Wollongong, NSW, Australia*
vanessa.peterson@ansto.gov.au

Keywords: Neutron powder diffraction, Energy, *In situ*

Creating a global energy system that is both environmentally and economically sustainable is one of the largest challenges facing scientific and engineering communities today. This challenge is multifaceted and spans many industries, including the mining industry that supplies raw materials for energy technology and infrastructure, the existing and emerging chemical industries underpinning the production of active materials for energy devices, the nuclear industry where safety in accident conditions is a concern, and to the emerging hydrogen industry which requires the rapid development of materials and technologies.

To advance the sector as a whole, it is necessary to understand the reactions and processes taking place at the atomic level in the materials at the heart of working devices, as well as in the manufacturing and synthesis of those materials. This is a difficult area in which to gain understanding, given the complexity and composition of the materials and the operating environment and processing conditions being probed. Here, advanced materials characterisation tools such as neutron powder diffraction excel, and where robust application of *in situ* methods can quantitatively and accurately capture representative phase and crystal structure changes to answer complex materials questions.

This talk will give examples of real time *in situ* neutron powder diffraction applied to non-equilibrium systems to understand processes and reactions relevant to the energy sector. Crystallographic investigations of ore processing in the production of critical minerals for the existing battery industry, of electrode material formation targeting high energy density for the emerging battery industry, of corrosion processes in nuclear fuels to drive the development of accident tolerant fuels, and of hydrogen storage mechanisms in materials to inform the engineering of storage systems that balance performance with operational cost. Details of experimental set ups and sample environments enabling these insights will also be presented.

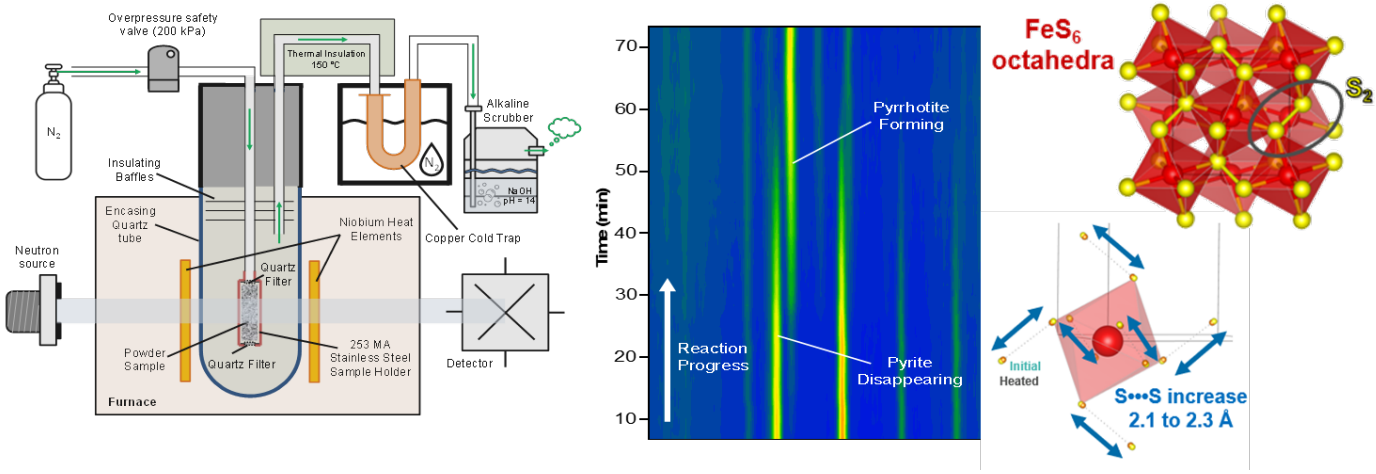

Figure 1. Left: Schematic of the in beam setup for studying the industrial high temperature processing of pyrite ore to produce battery ready sulfur and cobalt. Centre: *In situ* neutron powder diffraction data with intensity in colour from red (highest) to blue (lowest). Right: Derived structural information for the process.

[1] Menon, A. S., Ulusoy, S., Ojwang, D. O., Riekehr, L., Didier, C., Peterson, V. K., Salazar-Alvarez, G., Svedlindh, P., Edstrom, K., Pay Gòmez, C., & Brant W.R. (2021). *ACS Appl. Energy Mater.* **4,** 1924.
[2] Liu, J., Gasparrini, C., White, J. T., Johnson, K., Lopes, D. A., Peterson, V. K., Studer, A., Griffiths, G. J., Lumpkin, G. R., Wenman, M. R., Burr, P. A., Sooby, E. S., & Obbard, E. G. (2023). *J. Nucl. Mater.* **575,** 154215.

A084 Structural chemistry (r)evolution by quantum crystallography

Room 219

4.00pm - 6.30pm

A084-01-240823

Experimental electronic structure of transition metal complexes

J. Kožíšek

Faculty of Chemical and Food Technology STU in Bratislava

jozef.kozisek@stuba.sk

Keywords: quantum crystallography, experimental electronic structure, coordination compounds

Despite the fact that in transition metal complexes the ratio of the core to valence electrons is not favorable for the study of the experimental electronic structure, when the crystals are of good quality and the experiment is carried out with high redundancy, important results can be obtained. The distribution of valence electrons is a robust property, so the main features are easily recognized. The classical coordination bond was found in Cu-Cu and Cr-Cr dinuclear acetate complexes. Metal-metal interactions are discussed [1]. The titanium(IV) coordination compound with peroxo anion is a possible model structure of the reaction center for the theoretical study of hemoglobin. We have shown that the O—O bonding electron density is significantly shifted towards the central titanium atom. The O-O bond in the peroxide complex is weakened and, therefore, could be susceptible to a nucleophilic addition reaction [2]. The study of Ni(II) and Ni(III) complexes with the same ligand (3,6-dichlorobenzene-1,2-dithiolate) shows similar and typical square-planar coordination. In the experimental results, we see two combined effects. One effect is that the positive charge on the central atom is always lower than the formal oxidation state, and the other is that one part of electron density is shifted from the central atom to the non-innocent ligand. Thus, the non-innocent ligand can adapt to the requirements of the central atom [3]. In nitrosyl a μ_3-Oxido Trinuclear Diiron(III)−Ruthenium(II) complex we have studied whether such a complex can release NO photolytically [4].

We will discuss also tetrahedral Cu(I) and pseudo-octahedral Cu(II) complexes with biphenyldiimino dithioether as the blue copper protein model structures (Fig.1). The electronic structures of the Mn(II) and Cu(II) complexes with diclofenac are also studied. The real challenge is a compound with the Cr-Cr distance of 1.8077(7) Å [5]. Is there a sufficient electron density for one σ, two π and two σ bonds? We will find the answer in a joint project with Prof. Dietmar Stalke from Göttingen.

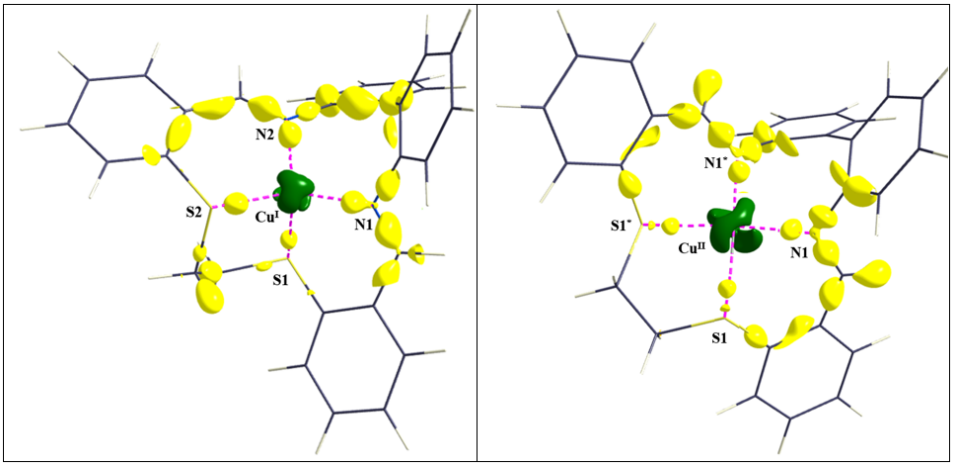

Figure 1. Three-dimensional plot (Hübschle & Dittrich, 2011) of the static electron deformation density at the isosurface value of 0.3 e Å^{-3}
(or 0.6 e Å^{-3} for Cu^{I} and Cu^{II}, respectively) around left) Cu^{I}; right) Cu^{II} atom in the distance of 5.3 Å.

[1] Herich, P., Bucinsky, L., Breza, M., Gall, M., Fronc, M., Petricek, V. & Kozisek, J. (2018). *Acta. Cryst.* **B74**, 681.
[2] Koziskova, J.A., Breza, M., Valko, M., Herich, P., Bucinsky, L. & Kozisek, J. (2021). *IUCrJ* **8**, 295.
[3] Koziskova, J.A., Chen, Y.S., Grass, S.Y., Chuang, Y.C., Hsu, I.J., Wang, Y., Lutz, M., Volkov, A., Herich, P., Venosova, B., Jelemenska, I., Bucinsky, L., Breza, M. & Kozisek, J. (2021). *Acta. Cryst.* **B77**, 919.
[4] Stepanenko, I., Mizetskyi, P., Orlowska, E., Bucinsky, L., Zalibera, M., Venosova, B., Clemancey, M., Blondin, G., Rapta, P., Novitchi, G., Schrader, W., Schaniel, D., Chen, Y.S., Lutz, M., Kozisek, J., Telser, J. & Arion V.B. (2022). *Inorg. Chem.* 2022, **61**, 950.
[5] Wolf, R., Ni, C., Nguyen, T., Brynda, M., Long, G.J., Sutton, A.D., Fischer, R.C. Fettinger, J.C., Hellman, M., Pu, L.H. & Power, P.P. (2007). *Inorg. Chem.* **46**, 11277.

This study was financially supported by Research and Development Agency of the Slovak Republic (the contracts No. APVV-19-0087 and No. APVV-20-0213), and Scientific Grant Agency of the Slovak Republic (VEGA Project 1/0139/20).

A084-02-240823

Structural chemistry of organo-chalcogen compounds: Quantum crystallographic insights into exotic bonds and supramolecular interactions

Ashi Singh, Kiran Avinash, Aditya Kumar Prajapati, Sajesh P. Thomas

Department of Chemistry, Indian Institute of Technology Delhi, Hauz Khas, New Delhi, India, 110016.

sajesh@iitd.ac.in

Keywords: Quantum crystallography, chalcogen bonds, thiols

Structural analyses of organo-chalcogen compounds reveal exciting features of bonding as well as supramolecular interactions. We present some recent applications of quantum crystallography [1-2] (QCr) in probing the nature and strength of some of the chalcogen-containing bonds in relation to the reactivity and solid-state properties of these compounds. The relevance of QCr in establishing the accurate structures of pharmaceutically relevant thiols and their intermolecular interactions will be demonstrated. The analyses based on the *experimental X-ray wavefunctions* from QCr reveal some intriguing features of intramolecular bonds involving chalcogens that have implications in their chemistry. We revisit the bond cleavage mechanism in the organoselenium anti-oxidant ebselen and its derivatives previously established by us [3], but now in terms of bond order parameters obtained from X-ray wavefunctions. In addition, the role of chalcogen bonding interactions involving Se and Te atoms in the band structure of solids will also be examined in relation to the optical properties and energy bandgaps of some chalcogenide crystals[4]. In a nutshell, the discussion will include quantitative characterization of intermolecular interactions such as chalcogen bonding (such as Se…O, Se…Se, Te…Te and Te…π etc.), weak thiol hydrogen bonds[5] such as S–H…O and S–H…S and intramolecular bonds such as the thiol S-H bond, quasi-ionic Se–N bond, and the putative Se–Se or Te–Te *'charge shift bonds'*.

[1] Grabowsky, S., Genoni, A., Thomas, S.P., Jayatilaka, D. (2020). *The Advent of Quantum Crystallography: Form and Structure Factors from Quantum Mechanics for Advanced Structure Refinement and Wavefunction Fitting.* In: Mingos, D., Raithby, P.R. (eds) *Structure and Bonding,* vol 186. Springer.
[2] Thomas, S. P., Dikundwar, A. G., Sarkar, S., Pavan, M. S., Pal, R., Hathwar, V. R., Guru Row, T. N. (2022), *Molecules*, **27**, 3690
[3] Thomas, S. P.; Satheeshkumar, K.; Mugesh, G.; Guru Row, T. N. (2015), *Chem. - Eur. J.,* **21**, 6793
[4] Thomas, S. P., Thomas, R., Grønbech, T. B. E., Bondesgaard, M., Mamakhel, A. H., Birkedal, V., Iversen, B. B. (2021), *J. Phys. Chem. Lett.* **12,** 3059.
[5] Thomas, S. P.; Sathishkumar, R.; Guru Row, T. N. (2015), *Chem. Commun.,* **51**, 14255.

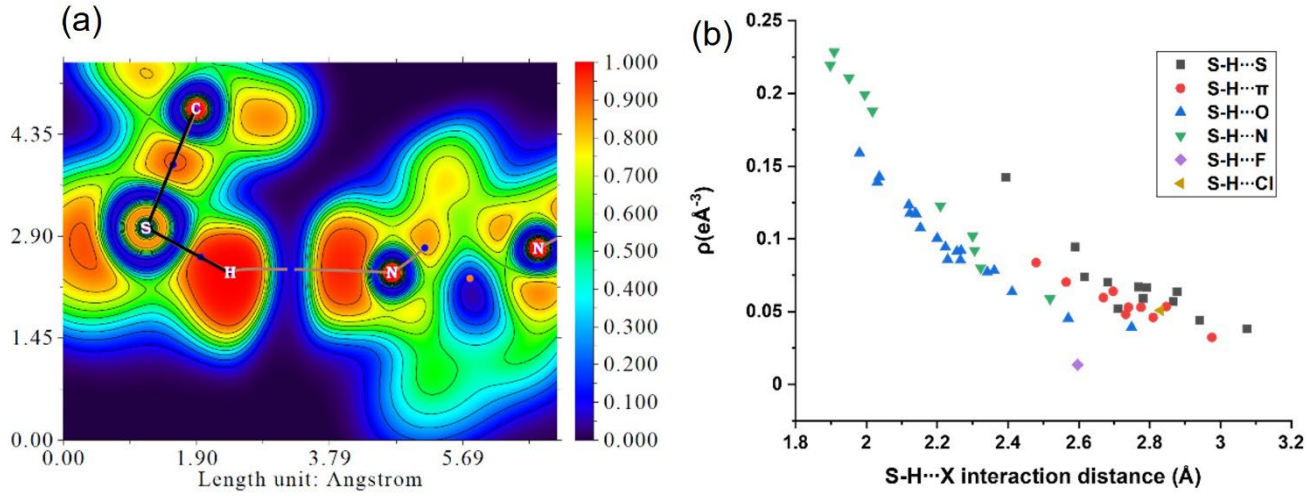

Figure 1. a) Electron localization function (ELF) plots of S-H···N interactions (contours at 0.1 step sizes) with bond paths and bond critical points (BCP). b) Plot of electron density ρ(eÅ-3) at the bond critical points (BCP) vs interaction distance (Å) of types of S-H···X (X = S, π, O, N, F, Cl) interaction for N = 53 data points.

A084-03-240823

Visualizing intrinsic property of functional materials using synchrotron radiation by quantum crystallography

K. Sugimoto[1]

Kindai University, 3-4-1 Kowakae, Higashi-osaka, Osaka 577-8502 Japan

Email: sugimoto@chem.kindai.ac.jp

Keywords: Quantum crystallography, Intrinsic property, Electrostatic potential, Synchrotron radiation

The intrinsic property of functional materials can be described mainly by the behavior of electrons and intermolecular interactions. We have been developing a single-crystal structural analysis beamline BL02B1 at SPring-8 in Japan to directly visualize the intrinsic property of functional materials. By introducing a hybrid-type pixel detector using CdTe as a device, we are promoting research that also includes dynamical quantum crystallography through highly efficient measurements. For direct visualization of electron orbitals, we focus on a dinuclear cobalt complex [$Co_2(\mu\text{-}OH_2)(O_2CCMe_3)_4(HO_2CCMe_3)_4$], which is constructed by using pivarate as a bridging ligand. This study aimed to visualize the correlation between the electron density distribution of Co^{2+} d orbitals and magnetism based on quantum crystallography using synchrotron radiation. The deformation density map of the dinuclear cobalt complex tells us the quantization axes of the d orbitals of each Co^{2+}, estimated from the electron density distribution of the deformation model, are found to agree with the magnetic behavior. In another study, the valence electrons on the d orbitals of volvosite ($Cu_3V_2O_7(OH)_2 \bullet 2H_2O$) that consist of Kagome lattice layers of $CuO_4(OH)_2$ and pillars of V_2O_7, were elucidated by quantum crystallography using synchrotron radiation single crystal X-ray diffraction experiments. The $dx^2\text{-}y^2$ orbital flipping phenomenon occupied by d^9 electrons in the 3d orbital was successfully visualized directly. In these studies, we demonstrated direct visualization of orbitals occupied by valence electrons by precise structural analysis using synchrotron radiation. It is expected to play an important role in elucidating the correlation between the structure and function of materials in the future. For electrostatic potential estimated from quantum crystallography, we focused to clarify the key points of crystal stability and solubility by analyzing the electrostatic potentials inside the co-crystal and to construct a design and synthesis method based on this understanding. Co-crystals, which are constructed by electrostatic interactions between two or more organic molecules, are attracting attention as a new drug discovery technology because one molecule has a pharmaceutical efficacy, and the stability and solubility can be controlled by the other constituent molecule. Co-crystals are constructed by supramolecular synthons with weak electrostatic interactions such as hydrogen bonding. For these co-crystals, direct visualization of electrostatic potentials experimentally using synchrotron radiation makes it possible to relate the electrostatic field to the crystallization conditions. Furthermore, we visualize molecular functions by clarifying the correlation between the co-crystal and stability and solubility based on differences in the electrostatic field of the co-crystals. This research will enable the design of molecular functions of pharmaceutical functional co-crystals required from the viewpoint of structural science. In our presentation, we will discuss visualizing the intrinsic property of functional materials using synchrotron radiation by quantum crystallography.

A084-04-240823

QuantumBox: The future of crystallography

H. Puschmann[1], P. N. Ruth[1], S. Coles[2]

[1]Durham University, Chemistry Department, Durham, UK, [2]University of Southampton, School of Chemistry, Southampton, UK
horst.puschmann@durham.ac.uk

Keywords: quantum crystallography, small-molecule crystallography, community project

QuantumBox is a collaborative community project which brings together all the tools that are required to perform modern small-molecule crystallographic analyses accessibly, reliably and with ease.

Interoperability: The data management system underlying QuantumBox ensures that many 'standard' crystallographic packages can operate securely on the same data. This covers the entire crystallographic workflow including data integration, primary structure solution and refinement as well as cutting-edge modern refinement techniques and extending into charge density analysis and properties calculations.

Beyond IAM: In going beyond the **I**ndependent **A**tom **M**odel, QuantumBox opens the world of quantum crystallography to 'routine' structure analyses. Modern experimental diffraction data contains so much more information than was conceivable in the past – and together with equally unprecedented cheap and accessible computing power, crystal structures can be so much more than those based on techniques that were developed many decades ago.

Resilience: Inherent to QuantumBox is a desire to protect contributing software as well as resulting structures from falling into oblivion as time goes by. By linking their crystallographic software to QuantumBox, authors can ensure that their contribution to the field of crystallography will endure. Equally, when authoring a crystal structure of any kind through QuantumBox, a full version history is maintained so that every step along the analysis can be repeated using the correct version of the various software that was used during creation.

Reusability: QuantumBox evolves by constantly increasing the number of reusable functions which are available for use by all participating existing software – or from which entirely new crystallographic software can be built. This is achieved by contributing the Quantum Crystallographic Toolbox (*qctbx*) to the well-established *cctbx* [1] project.

Organisation: The project has been funded for three years (starting in September 2022) and is led by the University of Southampton and Durham University. This publicly funded project is open source and free to use for everyone. Anyone with an interest in contributing their software – be it a large and complex software system or a single function is welcome to join QuantumBox. Professional research software engineers will work with contributors to ensure that the integration will be carried out sustainably and with maximum effect. QuantumBox has been endorsed and has the full support of the relevant European and IUCr commissions in quantum crystallography. The governing body of the project, together with the crystallographic expertise available in Southampton and Durham ensures that this really will be the future of crystallography.

For the latest information regarding QuantumBox, please refer to our website at: https://qubox.org/

1 https://cci.lbl.gov/docs/cctbx/

We wish to acknowledge the EPSRC for funding this project under the heading ***Software for research communities*** *– it is great to see that the need for such an important project has been funded as* ***EP/W02958/1*** *and* ***EP/W03011X/***

A084-05-240823

Understanding electronic structure and reactivity of halogen bonded cocrystals- synergy of experiment and theory

A. Kumar,[1] A. Tripathi,[1] D. Trzybiński,[1] K. Leko,[2] V. Nemec,[2] N. Bregovic,[2] D. Cinčić,[2] F. Topić,[3] K. Lisac,[4] T. Friščić,[5] M. Arhangelskis[1]*

[1] Faculty of Chemistry, University of Warsaw, Poland, [2] Department of Chemistry, University of Zagreb, Croatia, [3] Department of Chemistry, McGill University, Canada, [4] Ruđer Bošković Institute, Croatia, [5] School of Chemistry, University of Birmingham, UK

Email: l.kumar@uw.edu.pl

Keywords: halogen bonding, experimental charge density, periodic DFT

A halogen bond (XB) is a supramolecular interaction that involves a region of positive electrostatic potential(σ hole) [1] on the halogen donor atom and a nucleophilic acceptor atom or functional group. The use of XB therefore provides an opportunity to utilize heavy elements, such as bromine and iodine, which are not readily amenable to forming hydrogen bonds, in the construction of multicomponent solids, particularly cocrystals. The use of XB in crystal engineering enables materials with unprecedented supramolecular architectures. [2,3] These unusual supramolecular architectures find their way in diverse functional applications, including liquid crystals, [4] organic catalysis, [5] and room temperature pphosphorescent materials.[6]

Design of halogen-bonded cocrystals with desired properties relies on good understanding of the energies controlling the halogen bond formation. [7] This is where computational chemistry, particularly periodic density-functional theory (DFT) calculations provide an excellent account for the overall lattice stability of halogen-bonded crystals, and thermodynamics of their solid-state transformations.

In this presentation, I will describe the diverse experimental techniques that we use in combination with periodic DFT calculations to obtain the most comprehensive understanding of the halogen-bonded materials. This includes mechanochemical synthesis for rapid and quantitative interconversions between different halogen-bonded cocrystals, high resolution single crystal X-ray diffraction (XRD) measurements for the experimental determination of electron density distribution, as well as dissolution calorimetry for the experimental determination of lattice stability.

I will demonstrate how charge density analysis of cocrystals containing unusual halogen bonds to heavy pnictogen atoms (P, As, Sb) [3] can be determined using high resolution SC-XRD measurements and analysed using Bader's "atoms in molecules" AIM theory, for convenient comparison with the theoretical charge density distributions computed by different DFT functionals. These comparisons can be used to determine which functionals provide the most accurate description of the electronic structure of the halogen-bonded cocrystals.

Finally, I will present a series of mechanochemical reactions dedicated to the interconversion of halogen-bonded cocrystals via exchange of donor or acceptor components. These reactions were inspired by the theoretical predictions of reaction thermodynamics and further validated by experimental dissolution calorimetry measurements. The periodic DFT calculations are shown as an excellent predictor for the occurrence of the reaction under experimental conditions, while the simultaneous use of dissolution calorimetry to verify the accuracy of periodic DFT calculations presents the first such benchmark of periodic DFT calculations for halogen bonded materials.

This work demonstrates the benefits of the simultaneous use of experimental and computational techniques to study halogen-bonded materials: experimental studies help us improve the accuracy of periodic DFT calculations, while periodic DFT calculations allow us to predict the stability of halogen-bonded cocrystals and inspire mechanochemical reactions.

References

[1] Politzer, P., Murray, J. S. & Clark, T. (2013). *Phys. Chem. Chem. Phys.* **15**, 11178–11189.
[2] Catalano, L., Germann, L. S., Julien, P. A., Arhangelskis, M., Halasz, I., Užarević, K., Etter, M., Dinnebier, R. E., Ursini, M., Cametti, M., Martí-Rujas, J., Friščić, T., Metrangolo, P., Resnati, G. & Terraneo, G. (2021). *Chem*. **7**, 146–154.

[3] Lisac, K., Topić, F., Arhangelskis, M., Cepić, S., Julien, P. A., Nickels, C. W., Morris, A. J., Friščić, T. & Cinčić, D. (2019). *Nat. Commun.* **10**,61.
[4] Nguyen, H. L., Horton, P. N., Hursthouse, M. B., Legon, A. C. & Bruce, D. W. (2004). *J. Am. Chem. Soc.* **126**, 16–17.
[5] Parisini, E., Metrangolo, P., Pilati, T., Resnati, G. & Terraneo, G. (2011). *Chem. Soc. Rev.* **40**, 2267–2278.
[6] Kniep, F., Jungbauer, S. H., Zhang, Q., Walter, S. M., Schindler, S., Schnapperelle, I., Herdtweck, E. & Huber, S. M. (2013). *Angew. Chemie Int. Ed.* **52**, 7028–7032.
[7] Wang, W., Zhang, Y. & Jin, W. J. (2020). *Coord. Chem. Rev.* **404**, 213107.

A084-06-240823

Hydrogen atom restraints and disorder treatment in Hirshfeld atom refinement of polypeptides

L. A. Malaspina[1], R. Sankolli[1], F. Kleemiss[1,2], E. Wieduwilt[3], A. Genoni[4], S. Grabowsky[1]

[1]Department of Chemistry, Biochemistry and Pharmaceutical Sciences - University of Bern, Freiestrasse 3, 3012 Bern, Switzerland
[2]Universität Regensburg, Universitätsstraße 31, 93053 Regensburg, Germany
[3]Department of Physics, Chemistry and Pharmacy, University of Southern Denmark, Campusvej 55, 5230 Odense M, Denmark
[4]Laboratory of Theoretical Physics and Chemistry, CNRS & University of Lorraine, 1 Boulevard Arago, 57078 Metz, France

lorraine.malaspina@unibe.ch

Keywords: Quantum Crystallography, Software, Method development

Hydrogen atoms play an essential role in protein structures, functions, stabilities as well as protein-ligand interactions. For example, their locations in intermolecular interactions involving peptide groups and water molecules are decisive for the energetics and mechanisms of proton-transfer reactions. More specifically, biologically important proton-transfer and proton-shuttle mechanisms very often involve water molecules as mediators [1-3]. However, in crystals, larger biomolecules are usually disordered which complicates X-ray structure determination especially for hydrogen atom refinement and also lowers the attainable maximum resolution and data quality. Therefore, we will here present new developments in quantum crystallography how to treat disordered (poly-)peptides with a focus on hydrogen atoms.

In general, the use of more advanced models for structure refinement that include a non-spherical description for atoms in molecules, such as Hirshfeld Atom Refinement (HAR) [4,5], significantly improves hydrogen atom localization and the determination of accurate X-H bond lengths. Moreover, it gives access to protonation states and to chemically meaningful electron density overall. However, the computational costs for performing such refinements in large biological systems prevent the widespread use of HAR in protein crystallography. The HAR-ELMO approach [6], as originally implemented in the lamaGOET software [7], uses extremely localized molecular orbitals (ELMOs) [8] in a database-like transfer of fragment-localized orbitals, allowing the reconstruction of molecular wavefunctions for large systems almost instantaneously and therefore expanding the applicability-range of HAR. Although it is easily applicable, in its original implementation this method is limited by the presence of disorder.

Therefore, we expanded the approach and now we offer it via the NoSpherA2 [9] routine implemented in the Olex2 software, where the HAR-ELMO procedure can be performed even with disorder models. In addition, the NoSpherA2-Olex2 implementation allows the use of restraints for hydrogen atoms in HAR, which has not been possible before. In this presentation, we will show the examples of HAR for triaspartic acid which includes dynamic disorder involving water molecules and HAR-ELMO for the following three cases: a co-crystal of L-Asparagine and L-aspartic acid, where, in addition of being monohydrated, the co-crystal is described through a case of substitutional disorder; a tetrapeptide containing disorder about symmetry equivalent positions; and a cyclolinopeptide which presents an extra challenge on the wavefunction transfer due to the cyclic character of the structure.

[1] Garczarek, F. & Gerwert, K. (2006). *Nature*, **439**, 109–112.
[2] Kandori, H., Yamazaki, Y., Sasaki, J., Needleman, R., Lanyi, J. K. & Maeda, A. (1995). *J. Am. Chem. Soc.* **117**, 2118–2119.
[3] Freier, E., Wolf, S. & Gerwert, K. (2011). *Proc. Natl. Acad. Sci. USA*, **108**, 11435–11439.
[4] Jayatilaka, D. & Dittrich, B. (2008). *Acta Cryst. A*, **64**, 383-393.
[5] Capelli, S. C., Bürgi, H., Dittrich, B., Grabowsky, S. & Jayatilaka, D. (2014). *IUCrJ.* **1**, 361–379.
[6] Malaspina, L. A., Wieduwilt, E. K., Bergmann, J., Kleemiss, F., Meyer, B., Ruiz-López, M. F., Pal, R., Hupf, E., Beckmann, J., Piltz, R. O., Edwards, A. J., Grabowsky, S. & Genoni, A. (2019). *J. Phys. Chem. Lett.* **10(22)**, 6973-6982.
[7] Malaspina, L. A., Genoni, A., & Grabowsky, S. (2021). *J. Appl. Cryst.* **54(3)**, 987-995.
[8] Meyer, B., Guillot, B., Ruiz-Lopez, M. F., & Genoni, A. (2016). *J. Chem. Theory Comput.* **12(3)**, 1052-1067.
[9] Kleemiss, F., Dolomanov, O. V., Bodensteiner, M., Peyerimhoff, N., Midgley, L., Bourhis, L. J., Genoni, A., Malaspina, L.A., Jayatilaka, D., Spencer, J. L., White, F., Grundkötter-Stock, B., Steinhauer, S., Lentz, D., Puschmann, H., & Grabowsky, S. (2021) *Chem. Sci.* **12(5)**, 1675-1692.

A091 Advanced Characterization of Additive Manufacturing using Synchrotron and Neutron Scattering Methods

Room 220

4.00pm - 6.30pm

A091-01-240823

Time-resolved synchrotron PXRD of additive manufacturing process using a hybrid-photon-counting EIGER2 CdTe detector

T. Donath[1], B. Zhang[2]

[1]DECTRIS Ltd, Taefernweg 1, 5405 Baden, Switzerland, [2]Institute of High Energy Physics, Chinese Academy of Sciences, 19B Yuquan Road, Beijing, Beijing, 100049, People's Republic of China
tilman.donath@dectris.com

Keywords: X-ray powder diffraction, additive manufacturing, time-resolved, hybrid photon counting

Monitoring of melting and solidification dynamics during additive manufacturing often requires elaborate experimental setups that feature high temporal resolution and a relatively wide 2θ coverage. This can be achieved by combining high energy X-rays at a synchrotron source with a wide detector. In order to capture the dynamics of melting and solidification of Ti alloys, the BL3W1 beamline of the Beijing Synchrotron Radiation Facility (P.R.o.C) used an EIGER2 X CdTe 1M-W hybrid photon counting (HPC) detector [1], with quantum efficiency of about 68% at the employed photon energy of 51.2 keV. In particular, the Lines-ROI feature of the detector was adjusted to read out 2'068 × 256 pixels in 8-bit mode, with an effective time resolution of approximately 110 µs (8-bit mode) at a frame rate of 9 kHz. This unambiguously resolved the fast phase transportations (α→β→α) during the additive manufacturing process (see Figure).

The novel Lines-ROI readout implemented in several EIGER2 detectors [2] is a feature that allows increasing the frame rate and adjust the time resolution to the phase transformation dynamics. It achieves frame rates beyond what is possible in full-frame readout (2.25 kHz in 16-bit and 4.5 kHz in 8-bit readout), continuously and deadtime-free up to 98 kHz frame rate by reducing the readout area to a selectable number of central pixel lines. This brings advanced performance and flexibility to time-resolved scattering experiments, especially for the characterization of irreversible processes such as additive manufacturing. In the presented case, frame rate >20 kHz of the EIGER2 CdTe 1M-W detector could not be exploited due to the limited X-ray flux. However, the current proof-of-principle experiment highlights the potential of EIGER2 detectors in the coming 4th generation synchrotron facilities, especially in time-resolved experiments, carried out at high X-ray energies.

An outlook is given on the PILATUS4 CdTe detector currently under development, a high-energy HPC detector with large active area suitable to cover large solid angle for maximizing the integrated diffraction, while offering even higher frame rates than the EIGER2 detector series.

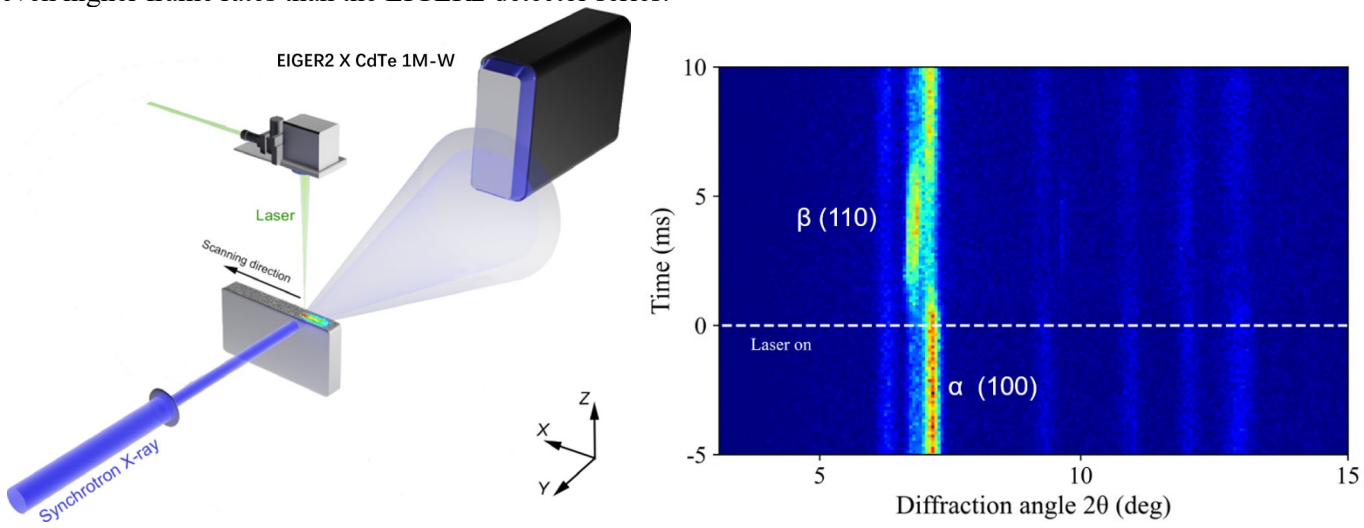

Figure 1. Capturing the fast melting and solidification dynamics of Ti alloys during additive manufacturing. *Left*: Schematic rendering of the in-situ additive manufacturing setup implemented at BL3W1 of Beijing Synchrotron Radiation Facility. *Right*: The 9 kHz time-resolved diffraction patterns of Ti alloy during a laser melting of 1 ms with laser on at $\tau = 0$ ms.

[1] Brönnimann, C. & Trüb, P. (2016). *Hybrid Pixel Photon Counting X-Ray Detectors for Synchrotron Radiation* in *Synchrotron Light Sources and Free-Electron Lasers*, edited by E. J. Jaeschke *et al*. pp. 995–1027. Cham: Springer International Publishing.
[2] Donath, T. *et al., submitted to Journal of Synchrotron Radiation*

A091-03-240823

Next generation USAXS-SAXS-WAXS instrument for hierarchical structures characterization

J. Ilavsky

Advanced Photon Source, Argonne National Laboratory, Lemont., IL, USA

Ilavsky@aps.anl.gov

Keywords: Ultra-small-angle scattering, Hierarchical microstructure, Diffraction

Additive manufacturing methods result in complex, hierarchical, microstructures where the final engineering properties are governed by features from angstroms (phase composition) to multiple microns (grains, grain boundaries, and voids) – and everything in between. Understanding of these complex hierarchical structures often requires combination of the most advanced synchrotron and neutron methods. These often include imaging, tomography, diffraction, and scattering techniques and nearly always require multiple devices and sometimes even multiple facilities. Both X-rays and neutrons have their distinct advantages and disadvantages, and their proper selection is critical for successful research. Main synchrotron benefits are wavelength tunability, high flux, and, for dynamical measurements, coherence; with the new generation synchrotrons, coming online now, offering new generation capabilities.

APS USAXS-SAXS-WAXS instrument [1] has been available to user community since 1998 and during this time its users published over 650 journal publications and theses. While this instrument has yet to find serious synchrotron based following, multiple commercial devices are currently available and provide similar capabilities, albeit at much longer data collection times and only fixed (generally lower) X-ray energies. APS upgrade, planned for 2023/2024, will result, among others, in major increase in brightness and reduction in X-ray divergence, providing opportunity to modify the design APS USAXS-SAXS-WAXS instrument. This will result in major performance improvements in the future. The new device was procured as part of APS upgrade and commissioned at current APS in October 2022. It was tested and shown to achieve the planned performance targets – for example we were able to extend the low Q range to below 3e-5 [1/A] with possibility to reduce this low Q range even lower in the future. X-ray energy range is now 12 – 27 keV, with option to extend it even further in the future, depending on beamline capabilities. This device therefore allows study of materials (such as metal alloys) that are hard to perform using commercial USAXS lab source devices or other synchrotron instruments. In combination with improved SAXS and diffraction (WAXS) capabilities, this new generation USAXS-SAXS-WAXS now offers *up to 6 decades of scatter size characterization in about 4 minutes*. After APS-U (Fall 2024) this new generation USAXS-SAXS-WAXS instrument will take advantage of higher X-ray flux and reduced divergence, which will reduce data collection times to 90 seconds or less. Faster data collection is critical for in-situ time-resolved studies (such as annealing) needed for understanding of post-processing of additively manufactured components. Longer term upgrade is addition of X-ray imaging and tomography, USAXS imaging, and potentially other methods which will extend the measured size range from tens of microns to millimeters.

Overall, this new generation USAXS will offer world-unique facility with combined capabilities of USANS instrument for low-q range, SAXS instrument for medium Qs, and powder diffraction device on high-q/WAXS, with penetration capabilities comparable with neutrons for many materials but with much shorter times. *It will be one-stop-shop where users will be able to fully characterize all length scales of their complex structures, at one instrument, in reasonably short times*. This new instrument was already tested and utilized by general user community before shutdown of current APS, albeit with lower flux, and will become available again after APS-U restart and commissioning. This presentation will discuss design of the new device, results obtained during commissioning, and planned capabilities in the future.

[1] Ilavsky, J., Zhang, F., Andrews, R.N., Kuzmenko, I., Jemian, P.R., Levine, L.E., & Allen, A.J. (2018). *J. Appl. Cryst.* ***51***, 867.

This research used resources of the Advanced Photon Source, a U.S. Department of Energy (DOE) Office of Science user facility at Argonne National Laboratory and is based on research supported by the U.S. DOE Office of Science-Basic Energy Sciences, under Contract No. DE-AC02-06CH11357.

A091-04-240823

In-situ XRD and PDF investigation of battery fluorides materials $MF_3.3H_2O$ (M = Fe, Cr) in controlled atmosphere: accessing new phases with controlled chemistry

O. Narygina[1], G. Nénert[2], K. Forsberg[3], C. V. Colin[4]

7 *Malvern Panalytical, Chipping Norton, Australia, (2) Malvern Panalytical, Almelo, The Netherlands, (3) Royal Institute of Technology, Stockhlom, Sweden, (4) Université Grenoble Alpes, Grenoble, France.*

olga.narygina@malvernpanalytical.com

Keywords: *In-situ* reactions, battery electrodes, fluorides

Iron fluoride (FeF3.nH2O) shows high capacity as cathode material for lithium-ion batteries combined to low toxicity and low cost. The water content of iron fluoride has been shown to be of prime importance in the performances of the cathode. So far, the various synthesis routes do not allow for a precise water content control, especially on the low amount regime which is the most interesting range of composition [1]. In addition, CrF3 has been shown to significantly increase the conductivity of LiF film [2]. Consequently, it is of interest to look for the *in-situ* formation of the various MF3-x(OH)x.nH2O phases (M = Cr, Fe).

In this contribution, we report on the *in-situ* formation of MF3-x(OH)x.nH2O (M = Fe, Cr) phases using self-generated atmosphere. Traditionally, the heating MF3.3H2O in open air results in the full oxidation and decomposition of the fluorides giving rise to nano-based oxides. Here, we make use of self-generated atmosphere to control the precise crystal chemistry of those phases upon heating preventing full oxidation at mild temperatures while stabilizing new phases relevant for battery applications.

Some of the results, related to FeF3-x(OH)x.nH2O *in situ* heating, are presented in Figure 1. Precise control of the water content of the FeF3-x(OH)x.nH2O could be reached with n ranging from 1/3 to 0. Within the composition range formation of at least 10 new pure phases is documented. Furthermore, we experimentally demonstrated the previously assumed stabilising role of water in the formation of the FeF3.1/3H2O phase, phase which is relevant for battery application [1]. In addition, the controlled *in-situ* decomposition of CrF3.3H2O led to the formation of a new CrF3-x(OH)x pyrochlore which was characterized structurally and magnetically. This work demonstrates the added value of *in-situ* experiment using self-generated atmosphere for synthetising new phases.

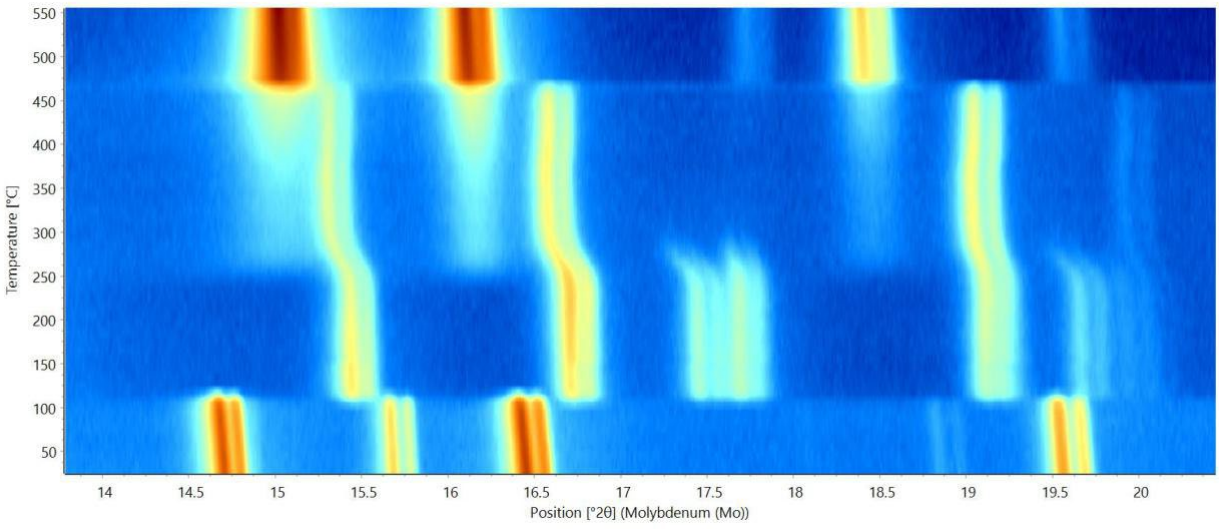

Figure 1. Isoline plot of the *in-situ* diffraction upon heating of $FeF_3.3H_2O$ illustrating the various stable phases obtained using self-generated atmosphere.

Kim et al., (2010). *Adv. Mater.* **22**, 5260; Ma et al., (2012), *Energy Environ. Sci.*, **5**, 8538

Tetsu, O., (1984). *Materials Research Bulletin*, **19**, 451.

A091-05-240823

Precipitation behaviour of additively manufactured 15-5 precipitation hardened steel

Koppoju Suresh[1], G. Janaki Ram[1], Baswanta S Patil[1], M. Tarun Babu[1], T. Gururaj[1], M. Ramakrishna[1]

[1]*International Advanced Research Centre for Powder Metallurgy and New Materials (ARCI), Balapur PO, Hyderabad 500 005, India*

Email : sureshkoppoju@arci.res.in

Keywords: Additive manufacturing, 15-5 PH steels, SAXS

Additive manufacturing (AM) technology has gained popularity in recent times due to flexibility in producing complex geometries with advanced rapid prototyping machines. Laser-based Powder Bed Fusion (L-PBF) is a metal AM process that can be used to build metallic components layer by layer by moving a focused laser beam in a particular pattern along each metal powder layer. The mechanical properties of laser-based additive manufactured parts are reported to be comparable to or better than their conventional counterparts. In the L-PBF process, fine-grained structures are formed due to the high cooling rates of the molten pool, which results in considerably good tensile strength. Among the precipitation hardening steels, 15-5 PH steels are one of the main classes of materials with good potential for production using the additive manufacturing process of PBF-LB, with a broad range of applications in the automotive, shipping, medical and aerospace sectors.

In the present study, we aimed to investigate the precipitation behaviour of additively manufactured 15-5 PH steel builds with aging at 480°C for durations from10 min. to 4 h. Since AM process involves non-equilibrium solidification, microstructural inhomogeneity is expected. Hence these builds were subjected to solutionisation at 1045°C for 1h and aged, and the precipitation was studied. Conventional wrought 15-5 PH steel was also investigated along with these builds as a benchmark for performance. Hardness of solutionised aged builds and wrought alloy is very similar, about 460±3.4 HV, in 4 hrs aged condition, whereas the builds directly aged for 4 hrs possessed hardness of nearly 30 HV lower of around 433±6.2 HV (Fig. 1(a)). Small angle X-ray scattering, transmission electron microscopy and atom probe tomography were applied to investigate precipitation behaviour, especially for Cu precipitate size and its size distribution, number density, and volume fraction in these AM builds and wrought 15-5 PH steel. It was found that the lower hardness in directly aged AM builds (AMAB4h) is due to the lower volume fraction of the Cu precipitates whereas wrought (WS4h) and solutioninsed and aged AM builds (AMBS4h) possess similar volume fraction and size of Cu precipitates (Fig. 1(b)). Correlation between the precipitation hardening and mechanical behaviour will be presented.

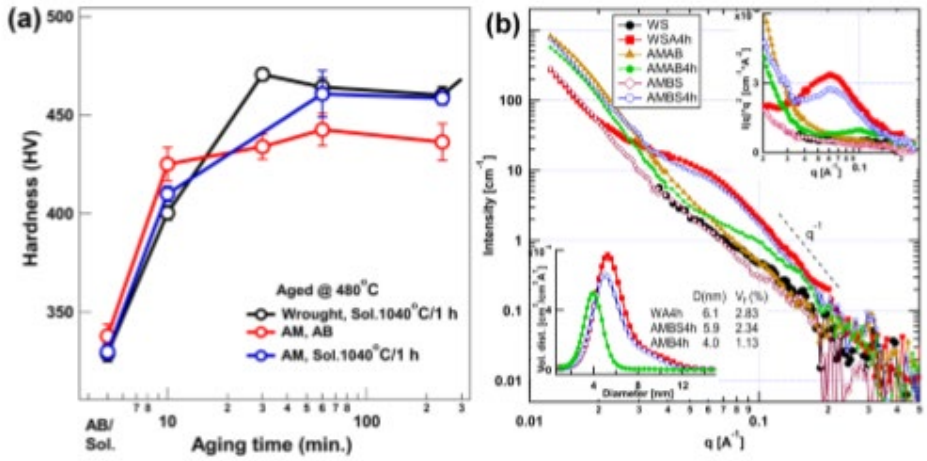

Fig. 1(a): Hardness with aging, and (b) SAXS intensity of the selected samples of the 15-5 PH steels. Inset to figure 1(b), (top): Kratky plots showing presence of Cu precipitates upon aging at 480 ºC for 4h, and inset at the bottom: size distribution of Cu precipitates.

A091-06-240823

NSF's ChemMatCARS Advanced Crystallography Capabilities after the Upgrade

NSF's ChemMatCARS is a national user facility located in Chicago, IL, USA, which specializes in frontier research in chemistry and materials science using synchrotron X-rays at the Advanced Photon Source (APS) at Argonne National Laboratory(ANL). Operated by The University of Chicago, NSf's ChemMatCARS offers a unique high-brilliance X-ray resource that facilitates research in advanced small-molecule crystallography, liquid surface and interface scattering, and anomalous small-angle X-ray scattering. For more information on the current capabilities of Advanced Crystallography at NSF's ChemMatCARS, please visit our website at https://chemmatcars.uchicago.edu/scientific-program/advanced-crystallography/.

As part of the APS upgrade project (APS-U) dark period, NSF's ChemMatCARS is also building a canted beamline that will expand its advanced crystallography capabilities. The new techniques developed as part of this initiative include resonant diffraction, which can utilize lower X-ray energies down to roughly 3.5 keV, providing access to the entire series of 3d and 4d transition metals, as well as small molecule serial crystallography. A poster will be presented that showcases these new techniques, and the facility will be seeking users who are interested in getting involved in the commissioning process as well as those who want to utilize these techniques once they are fully developed.

A097 Neutron Diffraction for Chemical Crystallography
Room 210
4.00pm - 6.30pm

A097-01-240823

Single-crystal neutron structure analyses of molecular crystals at SENJU

Ohhara[1], R. Kiyanagi[1], A. Nakao[2], K. Munakata[2], Y. Ishikawa[2], K.Moriyama[2], I. Tamura[1], K. Kaneko[1]

[1]J-PARC Center, Japan Atomic Energy Agency, Tokai, Ibaraki 319-1195, Japan, [2]Neutron Science and Technology Center,
CROSS, Tokai, Ibaraki 319-1106, Japan
Email of communicating takashi.ohhara@j-parc.jp

Keywords: SENJU, Single-crystal neutron diffraction, Molecular crystal

SENJU at J-PARC is a time-of-flight (TOF) single-crystal neutron diffractometer designed for precise crystal and magnetic structure analyses under multiple extreme environments, such as low-temperature, high-pressure and high-magnetic field, as well as for taking diffraction intensities of small single crystals with a volume of less than 1.0 mm^3 down to 0.1 mm^3 [1]. Recently, we added four area detectors to SENJU in the obliquely downward direction of the sample position. The additional detectors can cover the blind region in the reciprocal space when measuring a low-symmetry sample and improve the measurement efficiency of low-symmetric molecular crystals. While the primary target materials of SENJU are inorganic crystals such as oxides or alloys, numerous structural studies of molecular crystals have been performed, and many scientific results have been achieved. In this presentation, we show the current situations of diffraction measurements of molecular crystals at SENJU, *e.g.,* crystal sizes and sample environments, with some actual research conducted at SENJU.

In the usual measurement procedure of SENJU, a sample crystal is mounted on/in a sample environment device such as a closed-cycle cryostat or a furnace and put in a vacuum sample chamber. In the case of a solvent-containing sample crystal, the sample is coated by grease or enclosed in a quartz-glass capillary.

The sample crystal sizes and measurement times in the research of a photo-functional salt-cocrystal continuum [2] are typical at the current SENJU. Two sample crystals were 0.23 mm^3 and 0.8 mm^3 in size, respectively, and the measurement times were 2.5 and 3 days, respectively, including the time for temperature change. The accelerator power during the measurement was 500 kW.

For crystals with a volume greater than 1.0 mm^3, it is realistic to complete the diffraction measurement at SENJU within one day for one temperature condition [3]. In such cases, experiments can be performed using a mail-in program called Fast Track Proposal, which is open anytime.

Magnetic structure analysis of molecular crystal can be a realistic target since low-temperature diffraction measurement of less than 10 K is available, almost routine, at SENJU. The magnetic structure analysis of a coordination polymer of cobalt [4] is our first example of magnetic structure analysis of molecular crystal. Although the sample size was larger than the usual structure analysis, we expect that the available crystal size will become smaller according to the increase of the accelerator power (800 kW in Nov. 2022).

1 Ohhara, T., Kiyanagi, R., Oikawa, K., Kawasaki, T., Tamura, I., Nakao, A., Hanashima, T., Munakata, K., Moyoshi, T., Kuroda, T., Kimura, H., Sakakura, T., Lee, C-. H., Takahashi, M., Ohshima, K., Kiyotani, T., Noda, Y. & Arai, M. (2016). *J. Appl. Cryst.,* **49,** 120.
2 Yano, Y., Ono, T., Ohhara, T. & Hisaeda, Y. (2021). *Chem. Eur. J.,* **27,** 17802.

3 Terasawa, Y., Ohhara, T., Sato, S., Yoshida, S. & Asahi, T. (2022). *Acta Cryst. Sect. E,* **78,** 306.
4 Nakane, T., Yoneyama, S., Kodama, T., Kikuchi, K., Nakao, A., Ohhara, T., Higashinaka, R., Matsuda, T. D., Aoki, Y. & Fujita, W. (2019). *Dalton Trans.,* **48,** 333.

A097-02-240823

Structure determination of high-pressure phases of hydrogen-bonding crystals by the combination of in-situ single-crystal x-ray diffraction and neutron diffraction

K. Yamashita[12], K.Komatsu[1], H.Kagi[1]

[1]GCRC,UTokyo, Japan, [1]UIBK, Austria

Keishiro.Yamashita@uibk.ac.at

Keywords: High pressure, single crystal, neutron diffraction

The physicochemical properties of materials are strongly correlated with the atomic arrangements. Depending on the pressure and temperature conditions, materials can form various structures, especially hydrogen-bonding crystals as seen in the case of water ice. Moreover, multi-component systems like saline solution can change the compositions of the crystalline forms, or in other words, salt hydrates can form from solution instead of phase segregation into anhydrous salt and pure water ice. The phase complexity is a result of the fragile balance among various contributions such as the hydrogen bonds and electrostatic interactions around the ionic species. Ionic species can affect the bonding natures of water molecules in a similar way to pressure in their vicinity (*e.g.* [1]), but their actual contribution and behaviours are yet to be investigated. Despite the ubiquity and simplicity of the components, thermodynamically stable crystalline phases in salt-water systems are not fully clarified even for simple inorganic salts under pressure.

In these years, we performed *in-situ* diffraction experiments to determine and elucidate the hydrogen-bonding structures of high-pressure phases of water ice and salt hydrates, mainly of $MgCl_2$ and NaCl, with some technical improvements. The structure analyses have proceeded mainly in two stages: i) single-crystal x-ray diffraction to derive structure models without hydrogen atoms, ii) neutron diffraction to determine the hydrogen-bond structures. Single-crystal diffraction is a strong technique to derive structure information, such as cell parameters, symmetry, and chemical compositions from scratch with little ambiguity. On the other hand, there are still some technical challenges for *in-situ* single-crystal diffraction experiments, such as obtaining single-crystalline samples in the high-pressure vessel without unwanted co-existing crystals, the limited pT conditions around the liquid-solid phase boundary, and requiring accurate diffraction intensities with a wide coverage of reciprocal spaces. The appropriate scheme needs to be optimised for the cases by trial and error mostly affirmed using a lab source x-ray diffractometer. Once the initial structure model is derived, powder diffraction can be applied for further analyses such as pressure/temperature-dependent structure changes. Neutron diffraction is the definitive technique to determine the hydrogen-bonding structures, but the small contrast in scattering length among elements makes the initial phase determinations of unknown structures difficult. Then, the structure models without hydrogen atoms derived from the single-crystal x-ray diffraction are used as the initial structure. In most cases, the structure analysis can be accomplished for powder samples using well-established instruments such as the MITO system [2] but the developed diamond anvil cells [3] are also used for single-crystalline samples with complicated structures. The obtained neutron data can clarify the distortion of hydrogen-bond networks [4], atomic distributions displaced from average positions [5], and hydrogen disorder in the network. Here, we present the applications to determine the structures of specific high-pressure phases of hydrogen-bonding crystals from scratch.

1 Suzuki, Y. & Mishima, O. (2013). *J. Chem. Phys.* **138**, 084507.

2 Komatsu, K., Moriyama, M., Koizumi, T., Nakayama, K., Kagi, H., Abe, J. & Harjo, S. (2013). *High Press. Res.* **33**, 208–213.
3 Yamashita, K., Komatsu, K., Ohhara, T., Munakata, K., Irifune, T., Shinmei, T., Sugiyama, K., Kawamata, T. & Kagi, H. (2022). *High Press. Res.* **42**, 121–135.
4 Yamashita, K., Komatsu, K., Hattori, T., Machida, S. & Kagi, H. (2019). *Acta Cryst. C***75**, 1605–1612.
5 Yamashita, K., Komatsu, K., Klotz, S., Fabelo, O., Fernández-Díaz, M. T., Abe, J., Machida, S., Hattori, T., Irifune, T., Shinmei, T., Sugiyama, K., Kawamata, T. & Kagi, H. (2022). *Proc. Natl. Acad. Sci.* **119**, 1–6.

We thank Dr. Hattori, Dr. Machida, Prof. Klotz, Dr. Fernández-díaz, Dr. Fabelo, Dr. Ohhara, and Dr. Munakata for their support on the neutron diffraction experiments. We are also grateful to Prof. Irifune, Dr. Shinmei, Prof. Sugiyama, and Prof. Kawamata for their contributions to the development of the diamond anvil cells for single-crystal neutron diffraction.

A097-03-240823

Engineering Chiral Frameworks for Separations

D.R. Turner

School of Chemistry, Monash University, Clayton, VIC 3800, Australia

david.turner@monash.edu

Keywords: coordination polymers, chirality, crystal engineering

Chiral coordination polymers have potential applications as solid phases in enantioselective separations. One major pitfall is that the ligands used must themselves be enantiopure and, ideally, not cost-prohibitive to synthesize.

Our approach has been to use naphthalenediimides (NDIs) and related, shorter diimide species, that are appended by amino acids at the imide positions, thus being accessible as an enantiopure product in a one-step reaction from a dianhydride precursor. We have found that chiral ligands containing this NDI core reliably form a metallomacrocyclic motif as part of coordination polymers (Figure 1, left) [1]. Furthermore, the window within these macrocycles is the ideal size to accommodate an aromatic guest, including catenation with other macrocycles and formation of rotaxanes using linear co-ligands. We have successfully translated these motifs from the solid-state into solution [2]. These macrocycles are very sensitive to the amino acid substituent and achiral analogues have been shown not to form the motif due to inherently different steric demands of the imide functionality [3]. As such, they have proven useful from a crystal engineering perspective. With a smaller, rigid diimide, for example, we have recently reported a chiral framework capable of selective uptake of a particular enantiomer of 1-phenylehtanol which has been shown crystallographically (Figure 1, right) [4]. The use of different core groups, either smaller, more flexible or bent, lead to radically different materials, typically discrete complexes including lantern-type cages and polyhedral [5].

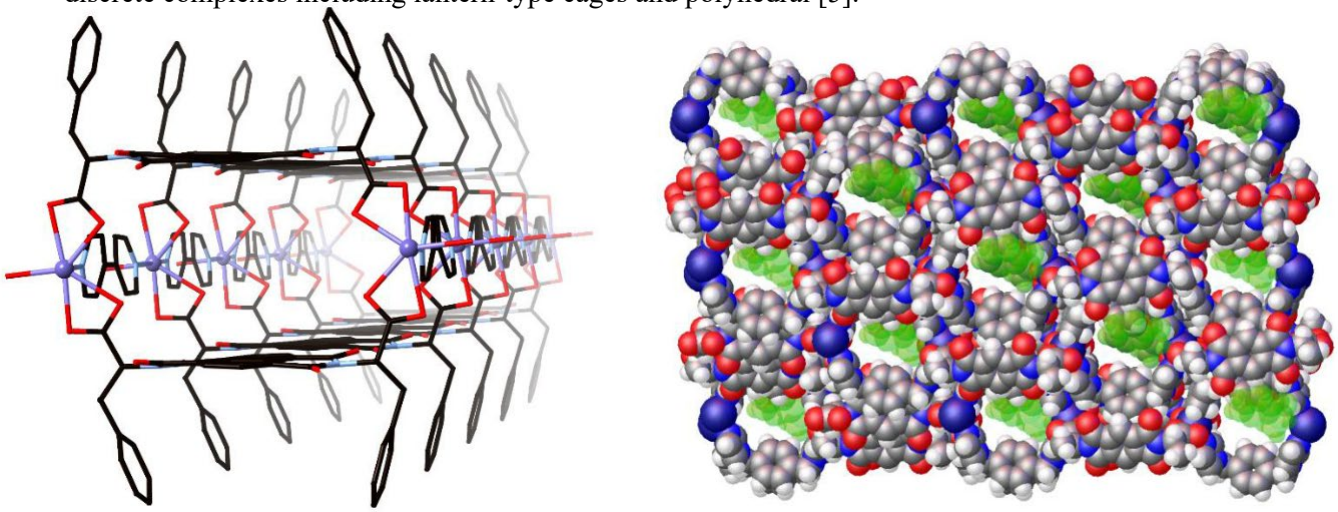

Figure 1. (Left) Naphthalenediimides appended with amino acids reproducibly form macrocyclic motifs within coordination polymers, due to conformational preferences of the ligand, which are conducive to crystal engineering of interlocked networks. (Right) A framework containing a shorter, chiral diimide ligand has been shown to selectively host one enantiomer of 1-phenylethanol using crystallography.

1 Boer, S.A. & Turner, D.R. (2016). *Cryst.Growth Des.* **16**, 6294.
2 Boer, S.A., Cox, R., Beards, M.J., Wang, H., Donald, W.A., Bell, T.D.M. & Turner, D.R.. (2019). *Chem. Commun.*, **55**, 663.
3 Kyratzis, N., Cao, W., Izgorodina, E.I. & Turner, D.R. (2018). *CrystEngComm,* **20**, 4115.
4 Cao, W., Missen, O.P. & Turner, D.R. (2022). *Inorg. Chem. Front.*, **9**, 709.
5 Boer, S.A. & Turner, D.R. (2015). *Chem. Commun.*, **51**, 17375.

A097-04-240823

What contribution does neutron single-crystal diffraction make to chemical crystallography? KOALA, COBRA and LAUEG yielded structures published for maximum impact for chemistry and crystallography

A.J. Edwards

Australian Centre for Neutron Diffraction (ACNS), ANSTO, New Illawarra Rd, Lucas Heights, NSW, 2232 Australia Alison.Edwards@ansto.gov.au

Keywords: Neutron, Single-crystal, Chemical Crystallography

From inception, KOALA was intended to be used for chemical crystallography in addition to the well established range of physics-based applications then typical at neutron facilities. An open consultation across the potential user community had revealed significant demand for a single-crystal instrument suitable for chemical crystallography applications and the advantages of a Laue image plate system were apparent with an instrument based on VIVALDI at the ILLwas commissioned. The chemistry community has provided significant demand for instrument time across a broad range of studies from the occasional (once every 3-5 year) "unprecedented" one-off structure for which neutrons are the key through to systematic studies with variations of counter-ion, temperature or pressure or indeed combinations of these parameters. Deep insights into chemistry have been obtained across the full range of studies undertaken.

Critical to the success of KOALA in the chemical crystallography realm have been the implementation of a COBRA™ cryostream to facilitate data accumulation from air, moisture and temperature sensitive compounds, and the development of the data reduction interface LAUEG [1-2]. These improvements have made feasible the completion of optimised neutron single-crystal diffraction studies in a timeframe which sees them available for publication when the chemistry which has prompted the structure determination is published. It is notable that KOALA has produced a high proportion of the neutron single-crystal studies reported in the Cambridge data base across its years of operation (with many more to come). The impact factor of the journals in which the chemical crystallography papers from KOALA have appeared has significantly exceeded the initial ambition for the instrument and today we regularly submit manuscripts reporting structures from KOALA to Tier One general science journals such as Nature and Science where they are well received with papers appearing in Nature, Nature Chemistry and Nature Communications with many of the remaining papers appearing in premiere journals, notably J.A.C.S. and Angewandte Chemie.

It is important to understand that there is a significant range in the crystallographic "quality" of the structures which can be derived with the optimal exploitation of the data available for any given crystal being critical to the contribution which the neutron structure determination can make to the overall scientific findings. The "routine" approach to structure determination is often inadequate to the scientific task and a more nuanced approach to extracting valid scientific content from the hard won data will yield important chemical insights. On occasion, low resolution data only are obtainable but in many instances these data are precisely those that speak to the question at issue.

At the time this abstract is being written, installation of the replacement instrument for KOALA is in progress. We have optimised aspects of the instrument which could be improved and importantly, the successful approach of standardization of components applied to all of the other instruments at ACNS is being implemented for the replacement.

This talk will survey published results from KOALA (highlighting in particular the non-standard methodologies which have yielded our greatest successes) and draw comparisons with other instruments, setting out the successes, opportunities and challenges we have in exploiting the facilities available to us at the major central science facilities. The successes in chemical crystallography at this neutron facility have been underpinned by the fundamental crystallographic education of the instrument scientists. How to transmit this knowledge to potential successors and capitalise on the existing learning is an important aspect of the manner of operation of our instrumentation.

[1] Piltz, R. O., Accurate data processing for neutron Laue diffractometers, J. Appl. Cryst. 2018, 51, 635-645.
[2} Piltz, R.O., LaueG software for displaying and processing neutron Laue images, J. Appl. Cryst. 2018, 51, 963-965.

A097-05-240823

Is H/D isotopic replacement always neutral to crystal structures?

Silvia C. Capelli[a], Dominic Fortes[a], Carlo Gatti[b]

ISIS Neutron and Muon Source, Rutherford Appleton Laboratory, Harwell Science Campus, Chilton. Didcot, OX11 0QX, United Kingdom
CNR-ISTM Istituto di Scienze e Tecnologie Molecolari, via Golgi 19, Milano I-20133, Italy.

Keywords: neutron diffraction, isotopic replacement, intermolecular interactions

H/D isotopic substitution is a very useful tool in neutron diffraction, used to minimise the incoherent scattering contribution of hydrogen atoms to the diffraction pattern and therefore optimise the signal to noise ratio. Up to now, isotopic substitution has been used, especially in protein crystallography, under the assumption that it will have little or no effect on the crystallographic structure or the macroscopic properties of the material. Recent experimental data lead us to question such assumptions: structural phase transitions that appear at low temperature only for the deuterated species or variations of physical properties for the different isotopomers are evidence of deviations from the expected "neutrality" of isotope substitution. In order to understand and potentially develop a way to predict when H/D isotopic replacement is "non-neutral", especially in molecular crystals, a multi-technique study combining neutron scattering and QM calculations has been undertaken on urea as a test case.

A097-06-240823

Prediction and control of modulation in molecular materials

Amber L. Thompson*[1], Nicholas P. Funnell[2], A. Dominic Fortes[2] and Kirsten E. Christensen[1]

Chemical Crystallography, Chemistry Research Laboratory Department of Chemistry, Oxford, UK;
ISIS Neutron and Muon Facility, Rutherford Appleton Laboratory, Harwell Science and Innovation Campus, Chilton, UK

amber.thompson@chem.ox.ac.uk

Keywords: Modulated Phases; Neutron Diffraction; Barluenga's Reagent

IPy2BF4 (where Py = pyridine) also known as *Barluenga's Reagent* (Figure 1), is widely used in organic synthesis for iodinating and oxidising due to the positively charged iodine atom which is readily available for nucleophilic attack [1-4]. In the solid crystalline state, it has also been shown to exhibit a temperature induced phase transition [4,5]. On close examination, this was found to proceed via a short-lived modulated phase the existence of which has been rationalised using the *Ratchet Model* (Figure 2).

Substituting iodine with bromine or silver, $BF4^-$ with other singly charged counter-ions, and pyridine with substituted pyridines has, in some case, demonstrated the presence of more phase transitions [5,6]. This gives a prototypical set of compounds that can be used to test theories in an effort to try to understand, and ultimately, control modulation in this class of molecular compound. While attempting to rationalise the behaviour across the series, we predicted the presence of modulation induced by pressure in IPy2ClO4. On studying this further, more unexpected phases were discovered giving a more complex phase diagram which we have characterised with laboratory X-ray instrumentation and high-resolution neutron powder diffraction, using HRPD at the ISIS Spallation Neutron Source.

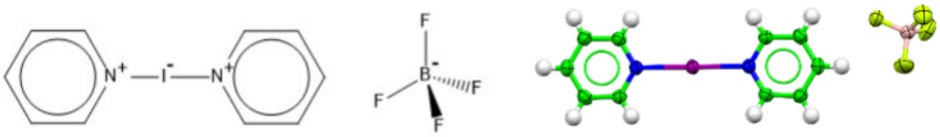

Figure 1. Scheme of Barluanga's Reagent with a displacement ellipsoid plot showing one formula unit.

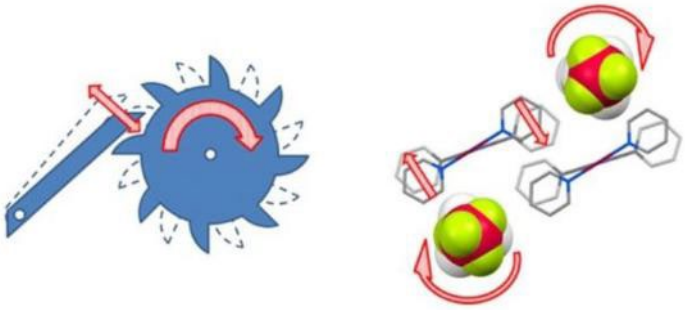

Figure 2. Schematic of the Ratchet Model [5] showing a gear and pawl on the left: as the tetrahedral anion tumbles (shown right), it affects the orientation of its neighbouring cation, which in turn affects the orientation of its own nearest neighbours.

[1] Barluenga, J., González, J. M., Campos, P. J. & Asensio, G. (1985). *Angew. Chem. Int. Ed.* **24**, 319–320.
[2] Barluenga, J., González-Bobes, F., Murguía, M. C., Ananthoju, S. R. & González J. M. (2004). *Chem. Eur. J.* **10**, 4206–4213.
[3] Barluenga, J. (1999). *Pure App. Chem.* **71**, 431–436.
[4] Chalker, J. M., Thompson, A. L. & Davis, B. G. (2010). *Org. Synth.* **87**, 288–298.

[5] Kim, Y., Mckinley, E.J., Christensen, K.E., Rees, N.H. & Thompson, A.L. (2014). *Cryst. Growth Des.* **14**, 6294–6301.
[6] Morgan, L.C.F., Kim, Y., Blandy, J.N., Murray, C.A., Christensen, K.E. & Thompson, A.L. (2018). *Chem. Comm.* **54**, 9849–9852.

DAY 4

Friday
25 August 2023

Keynote 13
Room 203/204
9.00am – 9.50am

Keynote–13 –250823

The macromolecular machine that opens up double-stranded DNA for gene transcription: from structures to functions

Ye F, Gao F, Liu X, Glyde R, Buck M and Zhang X

Imperial College London, South Kensington, London SW7 2AZ, UK

Xiaodong.zhang@imperial.ac.uk

Keywords: Transcription initiation, RNA polymerase, AAA+ ATPase

Our genetic information is stored in DNA which must be accessed for the essential processes of duplicating DNA (replication), converting to RNA (transcription) and damage repair. Gene transcription is carried out by the multi-subunit RNA polymerase (RNAP), which is conserved from bacteria to human. RNAP utilises a single DNA strand as a template to synthesize mRNA. Transcription initiation is the process that converts the double-stranded DNA to a transcription bubble, with one strand delivered to the RNAP active centre ready for mRNA synthesis. Transcription initiation is a highly dynamic process and has thus been difficult to be studied structurally. We use a specialised form of bacterial RNAP, which requires activators belonging to the large ATPases associated with diverse cellular activities (AAA+) family. Using structural techniques including X-ray crystallography and cryo electron microscopy, we have captured a series of structures representing different functional intermediates during initiation, unravelling the structural basis and molecular mechanisms for this fundamental process. Our studies reveal a remarkable macromolecular machine that undergoes large dynamic conformational transformations to manipulate DNA, leading to DNA opening, transcription bubble formation and eventually productive transcription. I will discuss our findings and explain how DNA is opened up, stabilised and delivered into the active centre for transcription and how this special form of bacterial RNAP adapts distinct mechanisms in this process. I will also discuss how various protein structures/features have been utilised in this process and the mechanisms of the remarkable multitasking AAA+ activators in manipulating both proteins and DNA.

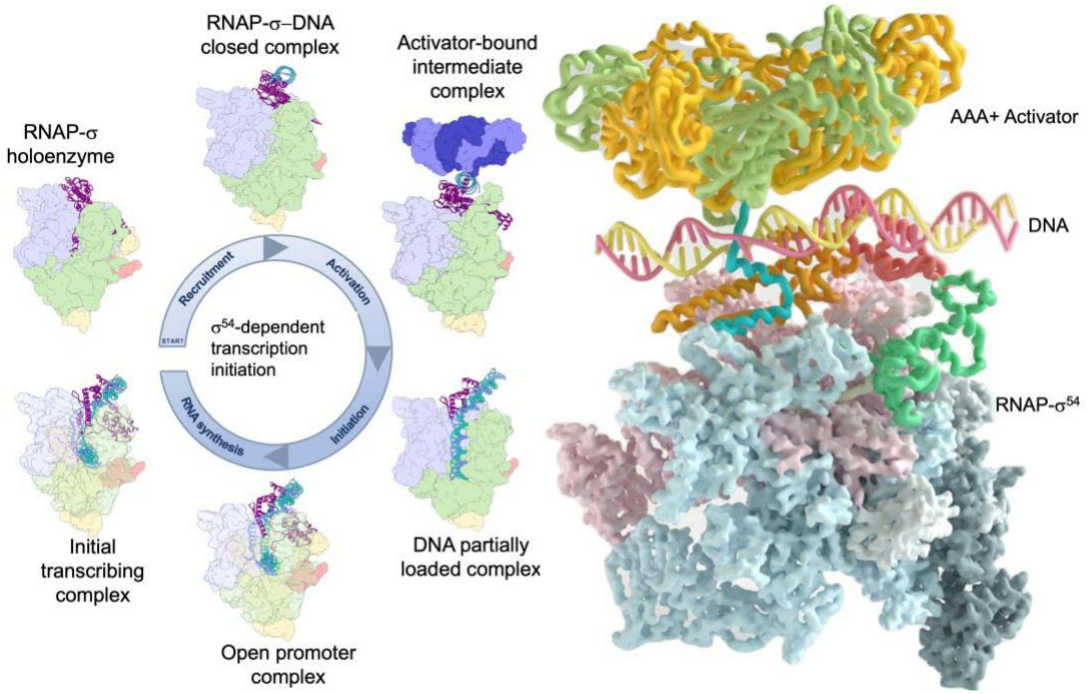

Figure 1. **Left**: Major structural snapshots captured along the transcription initiation process. **Right,** in activator-bound intermediate complex, a peptide is threaded in-between DNA strands and captured by the AAA+ hexameric activator, initiating the transcription bubble formation.

1 Ye F, Gao F, Liu X, Buck M and **Zhang X** (2022). "Mechanisms of DNA opening revealed in AAA+ transcription complex structure". ***Science Advances, in press***.

2 Gao F, Danson AE, Ye F, Jovanovic M, Buck M, **Zhang X**. (2020). "Bacterial Enhancer Binding Proteins – AAA+ Proteins in Transcription Activation. ***Biomolecules.*** 10(3):351

3 Danson A, Jovanovic M, Buck M, **Zhang X** (2019). "Mechanisms of s54-dependent Transcription Initiation and Regulation". ***Journal of Molecular Biology***. 431(20):3960-3974

4 Glyde R, Ye F, Jovanovic M, Kotta-Loizou I, Buck M and **Zhang X** (2018). "Structures of Bacterial RNA Polymerase Complexes Reveal the Mechanism of DNA Loading and Transcription Initiation". ***Mol Cell***. 70(6):1111-1120.

5 Glyde R, Ye F, Darbari VC, Zhang N, Buck M and **Zhang X** (2017). "Structures of RNA Polymerase Closed and Intermediate Complexes Reveal Mechanisms of DNA Opening and Transcription Initiation". ***Mol Cell.*** 67(1):106-116

Keynote 14
Room 210/211
9.00am – 9.50am

Keynote–14 –250823

Crystal Adaptronics: Intersectional and Collective Properties and Effects of Dynamic Molecular Crystals

P. Naumov

Smart Materials Lab, New York University Abu Dhabi, United Arab Emirates; Center for Smart Engineering Materials, New York University Abu Dhabi, United Arab Emirates; Molecular Design Institute, New York University, NY, USA

pance.naumov@nyu.edu

Keywords: molecular crystals, dynamic properties, smart materials

The anticipated shift in focal point of interest of solid- state chemists, crystal engineers and crystallographers from structure to properties to function of organic solids parallels the need to apply our accumulated understanding of the intricacies of crystal structure to explaining the related properties, with the ultimate goal of harnessing that knowledge in applications that require soft, light-weight, and/or biocompatible organic solids. In these developments, the adaptive molecular single crystals warrant a particular attention as a new class of materials for light, flexible, and environmentally benign devices, primarily memories, capacitors, sensors, and actuators. Some of the outstanding requirements for application of these dynamic materials as high-efficiency energy storage devices are strongly induced polarization, high switching field, and narrow hysteresis in reversible dynamic processes. However, having been studied almost exclusively by crystallographers, molecular crystals still lack the appropriate investigations that reliably evaluate their reproducibility, scalability, and actuating performance, and some important drawbacks have diverted the interest of engineers from these materials. United under the umbrella term *crystal adaptronics*, the recent research efforts aim to realistically assess the appositeness of dynamic crystals for applications that require fast, reversible and continuous operation over prolonged periods of time [1-13]. With the aim to highlight the most recent developments in the research of adaptive molecular crystals, this lecture discusses their assets and pitfalls. Using machine learning for the first time, we identify inherent features and structure-function relationships that fundamentally impact the mechanical response of dynamic molecular crystals. Our approach factors in different crystal properties in tandem and deciphers their intersectional and combined effects on the dynamic performance. It also provides some hints on the likely future developments that capitalize on the untapped, sequestered potential for applications of this distinct materials class.

[1] Mahmoud Halabi, J., Al-Handawi, M. B., Ceballos, R., Naumov, P. (2023) *J. Am. Chem. Soc*. doi: 10.1021/jacs.3c02184
[2] Awad, W. M., Davies, D. W., Kitagawa, D., Mahmoud Halabi, J., Al-Handawi, M. B., Tahir, I., Tong, F., Campillo-Alvarado, G., Shtukenberg, A. G., Alkhidir, T., Hagiwara, Y., Almehairbi, M., Lan, L., Hasebe, S., Prasad Karothu, D., Mohamed, S., Koshima, H., Kobatake, S., Diao, Y., Chandrasekar, R., Zhang, H., Sun, C. C., Bardeen, C., Al-Kaysi, R. O., Kahr, B., Naumov, P. (2023) *Chem. Soc. Rev.* **52**, 3098.
[3] Karothu, D. P., Mahmoud Halabi, J., Ahmed, E., Ferreira, R., Spackman, P. R., Spackman, M. A., Naumov, P. (2022) *Angew. Chem. Int. Ed.* **61**, e202113988.
[4] Spackman, P. R., Grosjean, A., Thomas, S. P., Karothu, D. P., Naumov, P., Spackman, M. A. (2022) *Angew. Chem. Int. Ed.* **134**, e202110716.
[5] Mahmoud Halabi, J., Ahmed, E., Sofela, S., Naumov, P. (2021) *Proc. Nat. Acad. Sci. USA* **118**, e2020604118.
[6] Naumov, P., Karothu, D. P., Ahmed, E., Catalano, L., Commins, P., Mahmoud Halabi, J., Al-Handawi, M. B., Li, L. (2020) *J. Am. Chem. Soc.* **142**, 13256.
[7] Commins, P., Al-Handawi, M. B., Karothu, D. P., Raj, G., Naumov, P. (2020) *Chem. Sci*. **11**, 2606.
[8] Karothu, D. P., Mahmoud Halabi, J., Li, L., Colin-Molina, A., Rodríguez-Molina, B., Naumov, P. (2020) *Adv. Mater.* **32**, 1906216.
[9] Ahmed, E., Karothu, D. P., Warren, M., Naumov, P. (2019) *Nat. Commun.* **10**, 3723.
[10] Li, L., Commins, P., Al-Handawi, M. B., Karothu, D. P., Mahmoud Halabi, J., Schramm, S., Weston, J., Rezgui, R., Naumov, P. (2019) *Chem. Sci.* **10**, 7327.
[11] Ahmed, E., Karothu, D. P., Naumov, P. (2018) *Angew. Chem. Int. Ed.* **57**, 8837.
[12] Commins, P., Tilahun D. I., Karothu, D. P., Panda, M. K., Naumov, P. (2016) *Chem. Commun.* **52**, 13941.
[13] Naumov, P., Chizhik, S., Panda, M. K., Nath, N. K., Boldyreva, E. (2015) *Chem. Rev.* **115**, 12440.

Keynote 15
Room 212/213
9.00am – 9.50am

Keynote–15 –250823

Crystal chemistry and crystallography of thermoelectric materials for energy conversion applications

Winnie Wong-Ng

National Institute of Standards and Technology, Gaithersburg, MD 20899, United States of America

winnie.wong-ng@nist.gov

Keywords: thermoelectric materials, crystallography, properties, SRMs

The growing demand for energy, especially "green" energy, has become one of the more urgent global concerns over the past few decades, resulting in a large increase of relevant research activities. Advances in energy conversion materials, technologies and applications are some of the key areas that can have a significant impact on the worldwide economy and on civilization in general. Energy conversion technologies include thermoelectric (TE) devices, solar cells, fuel cells, batteries, and others. For TE materials, in addition to conventional semiconductors, oxide materials have also been discovered as suitable candidates, particularly due to their stability at high temperatures (Fig 1). In this talk, the background information on TE materials, including the current efforts on the structural characterization, pertinent phase diagrams [1], and property measurements will be discussed. The conversion efficiency of TE materials is characterized by the dimensionless figure-of-merit, *ZT*, which is defined as $S^2\sigma T/\kappa$, where *S* is the Seebeck coefficient, σ is the electrical conductivity, κ is the thermal conductivity, and *T* is the absolute temperature. Optimization of *ZT*, however has been a difficult task due to the inter-dependence of the above properties. Examples of recent research on improving the *ZT* values will be highlighted [2]. The high-throughput combinatorial process is one of the state-of-the-art approaches for discovery of new materials and for improving material properties; current efforts in high throughput research on TE materials will be summarized [3]. Standard reference materials (SRMs™) are critical for interlaboratory data comparison, and so efforts at NIST on the development and distribution of Seebeck coefficient SRMs [4] will also be discussed.

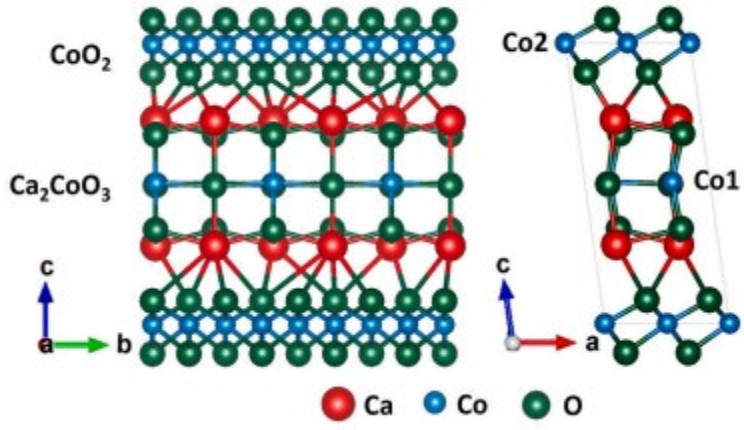

Figure 1. The unit cell structure of $Ca_3Co_4O_{9+\delta}$ showing the alternating subsystems of electrically conductive CoO_2 sheets and insulating rock-salt-type Ca_2CoO_3 layers.

[1] Wong-Ng, W., Laws, W., Huang, Q., Hou, J., Lapidus, S.H., Ribaud, L., Kaduk,J.A. (2020). *Solid State Sci.,* **107**, 106348, 1-9.
[2] Romo-De-La-Cruz, C.-O., Chen, Y., Liang, L., Paredes-Navia, S.A., Wong-Ng, W., Song, X. (2023). *Ren. & Sust. Energy Rev.* **175**, 113186.
[3] Wong-Ng, W., Yan, Y., Otani, M., Martin, J., Talley, K.R., Barron, S., Carroll, D.L., Hewitt, C., Joress, H., Thomas, E.L. Green, M.L. and Tang, X.F. (2015). *J. Electronic Mater*. **44** (6), 1688.
[4] Martin, J., Lu, Z. Q., Wong-Ng, W., Krylyuk, S., Wang, D., and Ren, Z. (2021). J. Mater. Res. **36**, 3339.

Keynote 16
Room 203/204
10.20am – 11.10am

Keynote–16 –250823

Europe’s Photon and Neutron Open Science Clouds for Raw and Processed Data: Aims and Achievements to Date

Dr Andy Gotz (France)

European Synchrotron Radiation Facility (ESRF).

The Photon and Neutron Open Science Cloud (PaNOSC) and the European Open Science Cloud Photon and Neutron Data Services (ExPaNDS) are two European Community financed projects comprised of 8 synchrotrons, 2 FELs, 3 laser and 4 neutron central facilities, which have been established in Europe to facilitate Open Science, an enhanced science methodology. Through such a coordination there can be (i) an increased fraction of published research by release of raw data to the public after a 3 year embargo period (ii) in cases of an agreed cooperation between specific research communities where measurements are now outpacing the capabilities of individual teams to analyse the raw data (iii) for more conventional ‘single research team’ science publication can be underpinned by a single digital object identifier (DOI) to the appropriate dataset held in the facility data archive, without need for raw dataset transfer to the home university. The implementation of data archiving is facilitated by great increases in tape storage capabilities. There are 30 case studies that document the opportunities of these projects including open science and reproducibility of science. Crystallography, diffraction and scattering experiments certainly yield big data flows at the relevant ESRF EBS beamlines with Xray imaging, EM and SSX beamlines reach massive data flow levels. All these benefits must be balanced with carbon footprint of such a data archive in today's world. The carbon footprint of archiving petabytes of data is a balancing act between the financial cost, the impact on the environment and the value of the data compared to the cost of redoing the experiment. The example of the ESRF data archive which is based on "cold storage" (*i.e.* tape storage) will be used to illustrate how the different costs can be calculated and compared.

Keynote 17
Room 210/211
10.20am – 11.10am

Keynote–17 –250823

Quantum crystallography for accurate structure determination and chemical bonding analysis

S. Grabowsky

University of Bern, Department of Chemistry, Biochemistry and Pharmaceutical Sciences, Freiestrasse 3, 3012 Bern, Switzerland
simon.grabowsky@unibe.ch

Keywords: quantum crystallography, electron density, Hirshfeld atom refinement

The methods and techniques of experimental electron-density research have a long and successful history, but only recently they have been rejuvenated under the umbrella term *quantum crystallography* when wavefunction-based refinement techniques emerged as realistic alternatives to more established multipole and maximum-entropy methods [1,2]. In my lecture, I will only focus on such wavefunction-based techniques. They can be categorized as follows:

i) Accurate structure determination methods that utilize quantum-mechanical wavefunctions to improve the results of least-squares refinements, specifically *Hirshfeld atom refinement (HAR)* [3].

ii) Experimentally fitted wavefunctions for chemical bonding analysis, specifically *X-ray constrained wavefunction (XCW) fitting* [4].

For HAR, I will outline to which extent we can obtain more information and more accurate information, and at what speed such information can be generated with modern X-ray diffractometers and modern software. I will give an overview over the software available today (such as NoSpherA2, lamaGOET with Tonto, Discamb) and the underlying approximations for treating the crystalline environment (such as ELMO embedding, periodic boundaries). I will exemplify the gain in the obtained information contents for fundamental and ubiquitous compounds such as the *YLID* test crystal and biomolecular structures (e.g., drugs such as ibuprofen). Finally, I will allude to the remaining challenges and problems, for example related to CIF and raw data standards.

For chemical bonding analysis with XCW fitting, the first question to discuss is the problem of significance and reproducibility as the information left in the structure factors after non-spherical structure refinement is barely above the noise level. Can we obtain physical effects such as electron correlation and polarization by the neighbours in the crystal field experimentally via XCW fitting? In this context, I will allude to unsolved experimental problems such as the treatment of anomalous dispersion, absorption, and radiation damage in small-molecule crystallography. However, I will finally present two studies where we believe that XCW fitted wavefunctions contribute to a better understanding of fundamental chemical questions: hypervalency of period-3 elements and bond-order/bond-length relationships in (conjugated) olefins.

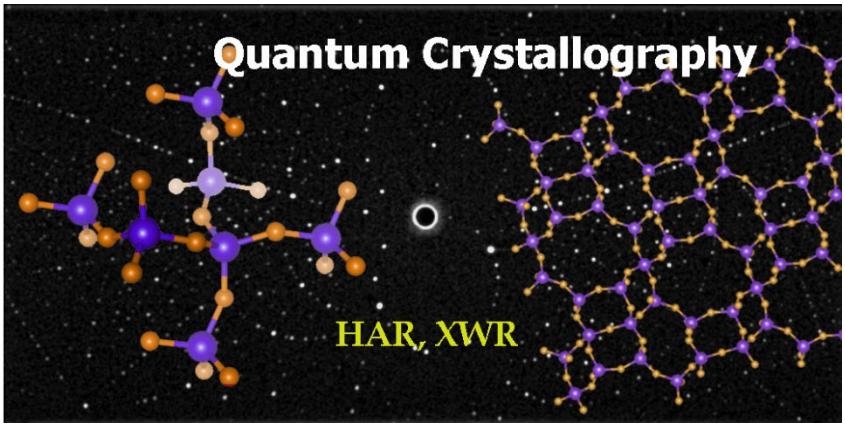

Figure 1. Quantum crystallography combines X-ray diffraction experiments and wavefunction calculations for more accurate structure determination and experimental chemical bonding analysis.

[1] Grabowsky, S., Genoni, A. & Bürgi, H.-B. (2017). *Chem. Sci.* **8**, 4159.

[2] Grabowsky, S., Genoni, A., Thomas, S. P. & Jayatilaka, D. (2020). The advent of quantum crystallography: form and structure factors from quantum mechanics for advanced structure refinement and wavefunction fitting, in: Mingos, D. M. P. & Raithby, P. R. (Eds.), 21st Century Challenges in Chemical Crystallography II., Structure and Bonding, Springer, vol. 186, pp. 64–144.
[3] Capelli, S. C., Bürgi, H.-B., Dittrich, B., Grabowsky, S. & Jayatilaka, D. (2014). *IUCrJ* **1**, 361.
[4] Davidson, M. L., Grabowsky, S. & Jayatilaka, D. (2022). *Acta Cryst. B* **78**, 312.
I thank all my former and present co-workers in Perth, Bremen, and Bern for their dedicated and excellent work.

Keynote 18
Room 212/213
10.20am – 11.10am

Keynote–18 –250823

Understanding quantum materials by X-ray techniques under high pressure

Ricardo dos Reis

Brazilian Synchrotron Light Laboratory (LNLS), Brazilian Center for Research in Energy and Materials (CNPEM), 13083-970, Campinas, Sao Paulo, Brazil

The research exploring the limits of thermodynamic parameters, such as pressure, temperature, and magnetic field, is a rapidly growing and fascinating discipline of science and technology that uncovers many truths and facts about nature that are not possible to observe in ambient conditions. In this talk, we will discuss how we can use synchrotron techniques, including x-ray absorption, diffraction, and scattering, together with external pressure (hydrostatic and uniaxial), low temperature, and high magnetic fields to continuously and cleanly tune quantum correlations, and drive materials through the critical region where the state of matter changes, and inherently quantum effects dominate. We will focus on materials that are on the verge of a phase instability with distinct crystalline structures and electronic behavior that display nontrivial topology. We will also present the first results of the Extreme condition Methods of Analysis beamline (EMA) at the Brazilian light source, which was specifically designed to overcome the challenges of obtaining high-quality experimental data under extreme thermodynamic conditions. The EMA provides both ~0.5x1 μm² and ~100x100 nm² focused beam sizes with well-defined Gaussian beam shape, enabling us to carry out X-ray absorption (XAS), X-ray diffraction (XRD), coherent diffraction imaging (CDI), and X-ray Raman experiments at extreme pressures with good spatial selectivity and to avoid pressure gradients. The talk will highlight the findings of our current research using several synchrotron techniques to investigate quantum materials.

A019 Structural Immunology

Room 203

1.10pm – 3:30pm

A019-01-250823

Cigarette smoking suppress T cell immunity in MR1 dependent mechanism

Wael Awad[1], Weijun Xu[2], Lauren Howson[1], Xin Yi Lim[3], Jemma Mayall[4], David Fairlie[2], Philip Hansbro[4], Alexandra Corbett[3], Jamie Rossjohn[1]

[1]Infection and Immunity Program and Department of Biochemistry and Molecular Biology, Biomedicine Discovery Institute, Monash University, Melbourne, Australia. [2]Institute for Molecular Bioscience, The University of Queensland, Brisbane, Australia. [3]Department of Microbiology and Immunology, Peter Doherty Institute for Infection and Immunity, University of Melbourne, Melbourne, Australia. [4] Centre for Inflammation, Centenary Institute, and University of Technology Sydney, Faculty of Science, Sydney, Australia

Email of communicating author: Wael.awad@Monash.edu

Keywords: MAIT, T cell receptors, MR1, antigen presentation, cigarette smoking, immunity

Cigarette smoking is a worldwide epidemic and is linked to numerous diseases. While cigarette smoke (CS) compromises the immune system, relatively little is known about its effect on T cell functions. CS is a complex mixture of products resulting from the combustion of tobacco and other components of the cigarettes. The MHC I-related molecule MR1 presents small molecule metabolites [1] to a diverse population of αβ and γδ MR1-restricted T cells including Mucosal-Associated Invariant T (MAIT) cells [2, 3]. MAIT cells are an innate-like T cell population that are highly abundant in a number of tissues, including the lung and is emerging as a major player in antimicrobial immunity, autoimmunity and cancers [4].

Using cellular, biochemical, and structural approaches, we identified components of cigarette smoke that could bind MR1, impact MR1 cell surface expression, and modulate T cell mediated immunity. These included nicotinaldehyde, phenylpropanoid, and benzaldehyde-related scaffolds. The high-resolution crystal structures of four ternary MAIT T cell receptor (TCR)-MR1-CS complexes showed that these MR1-binding CS based ligands reside within the A` pocket of MR1.Furthermore, we found that cigarette smoke extract (CSE) modulated T cell activation and effector functions *ex-vivo* in MR1 dependent manner. CS exposure increases lung MAIT cells in uninfected mice but dysregulates their responses to influenza A virus infection. Thus, cigarette smoking may impair the function of T cells in humans via interactions between cigarette smoke components and MR1, with potential implications in their response to respiratory infection or disease.

1) **Awad, W.[#],** Ler, G.J.M.[#], et al. (2020) *Nature Immunology* 21, 400-411.
2) Souter M., **Awad, W**., et al. (2022). *JEM*, 219 (9): e20210828.
3) Salio, M.[#], **Awad, W.[#],** et al. (2020). *PNAS*: 202003136.
4) Howson, L.J., **Awad, W**., et al. (2020). Science Immunology 5(49): eabc9492

A019-02-250823

Structural basis of biased T cell recognition of immune-dominant epitope of sars-cov-2 spike protein

Priyanka Chaurasia[1], Thi H.O Nguyen[2], Louise C. Rowntree[2], Jennifer A. Juno[2], Adam K. Wheatley[2], Stephen J. Kent[2], Katherine Kedzierska[2], Jamie Rossjohn[1] and Jan Petersen[1]

1 *Biomedicine Discovery Institute, Monash University, Clayton, Department of Microbiology and Immunology,*

2 *Peter Doherty Institute for Infection and Immunity, University of Melbourne.*

Email of communicating author priyanka.chaurasia@monash.edu

Keywords: COVID-19, Spike epitope, T cell recognition

SARS-CoV-2, responsible for the ongoing worldwide COVID-19 pandemic, has caused over 670 million infections to date. CD8+ T cells are crucial in establishing adaptive immunity against SARS-CoV-2 infection. Several CD8+ T cell epitopes with different human leukocyte antigen (HLA) restrictions have been identified, but the molecular basis underlying T cell receptor (TCR) recognition for SARS CoV-2 epitopes is relatively recent to establish long-term T cell-based vaccine development. In individuals carrying common HLA A*201 allomorph, the spike protein-derived epitope $S^{269–277}$ is the most immuno-dominant epitope [1]. We characterised four TCRs from $S^{269–277}$ responsive CD8+ T cells based on biased TRAV12 gene usage, named NR1A, NR1C, NR1D and NR2F. These TCRs show high affinity towards HLA-$A2^{S269–277}$ complex. We determine the crystal structure of NR1C-HLA-$A2^{S269–277}$ ternary complex, showing S269-277 epitope recognition dominated by TRAV12-1 germline-encoded residues in CDR3α and CDR3β loop region (Figure 1A). Surface Plasmon Resonance and tetramer studies suggested that TRAV12 TCRs poorly cross-react with $S^{269–277}$ variants and epitopes from other closely related coronaviruses (Figure 1B). In summary, the study defined the molecular mechanism behind biased CD8+ T cell recognition of immuno-dominant HLA-$A2^{S269–277}$ epitope and provided a scaffold for understanding cross-reactivity and potential viral escape in the HLA-$A2^{S269–277}$ restricted T cell response [2].

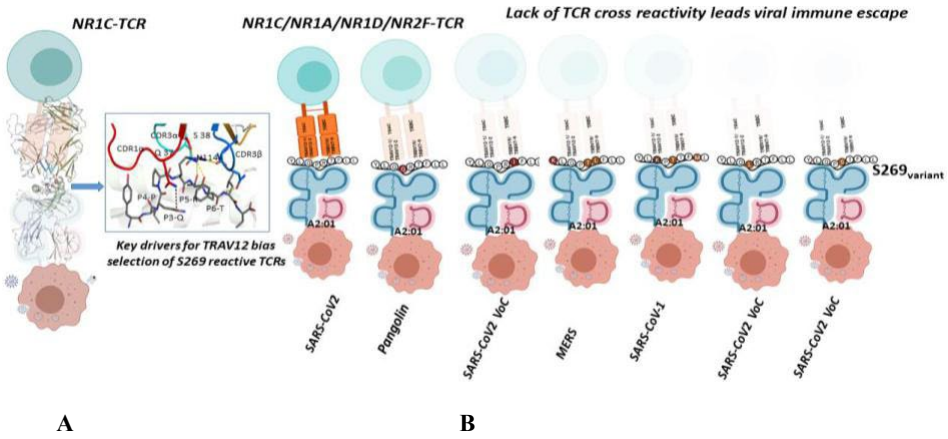

A **B**

Figure 1. A- Represents the overall docking of S269 reactive TCR on HLA A201 presenting S269 epitope (residues involved in peptide interaction in inset). B- Representative model for viral escape in SARS CoV-2 infection.

1 Habel, J., Nguyen, T.H.O., Sandt,C., Juno, J., Chaurasia, P., Wragg, K., Koutsakos, M., Hensena, L., Jia, X., Chua, B.Y., Zhang, W., Tana, H., Flanagan, K., Doolani , D., Torresia, J., Chenj, W., Wakim, L., Chengk, A., Doherty, P., Petersen, J., Rossjohn, J., Wheatley, A.K., Kent, S.J., Rowntree, L.C & Kedzierska, K. (2020). Suboptimal SARS-CoV-2−specific CD8+ T cell response associated with the prominent HLA-A*02:01 phenotype. *Proc. Natl. Acad. Sci. U. S. A.* **117**: pp-24384-24391.

2 Chaurasia, P., Nguyen, T.H.O., Rowntree, L.C., Juno, J., Wheatley, A., Stephen, J.K., Toressi, J., Cheng, A.K., Kedzierska, K., Rossjohn, J., & Petersen, J., (2021), A structural basis underpinning biased T cell receptor recognition of an immune-dominant HLA-A2 restricted epitope from the SARS-CoV-2 spike protein. *J. Bio. chem.* **297** pp.1-10.

A019-03-250823

T cell receptor recognition of unusual antigens

Jamie Rossjohn

Biomedicine Discovery Institute, Monash University

Jamie.rossjohn@monash.edu

Keywords: T cell receptor, metabolites, lipids

Alpha-beta T cell antigen receptors (abTCRs) recognise peptides, lipids and small molecule metabolites presented by MHC, CD1 and MR1 molecules, respectively. While there is considerable variation in the modes of recognition of abTCRs towards their Ag presenting molecules, they nevertheless invariable bind 'end-to-end' – presumably due to signaling constraints. While gamma-delta (gd) TCRs can recognise a more diverse range of ligands, they can also recognise MHC-I like molecules. However, the constraints of gdTCR docking modalities upon MHC-I like molecules appears to be completely different to that of abTCRs. These observations shall be discussed.

A019-04-250823

Structural mechanism of peptide exchange of MHC-I complexes in antigen presentation

J. Jiang, K. Natarajan and D.H. Margulies

Molecular Biology Section, Laboratory of Immune System Biology, National Institute of Allergy and Infectious Diseases, NIH, Bethesda, MD 20892

jiangji@niaid.nih.gov

Keywords: Antigen presentation, Peptide exchange, PLC, MHC-I/tapasin, MHC-I/TAPBPR

MHC-I (Major Histocompatibility Complex class I) molecules loaded with peptides for cell surface expression are critical for adaptive immunity. Tapasin, a component of the Peptide Loading Complex (PLC), serves as an MHC-I chaperone and facilitates peptide loading onto MHC-I in the endoplasmic reticulum (ER). Although the structure of TAPBPR (a homolog of tapasin) complexed with MHC-I was reported **[1]**, the detailed mechanism of peptide loading by tapasin remains unclear. We recently reported the crystal structure of a complex of tapasin with the MHC-I molecule, HLA-B*44:05, and with each of two anti-tapasin antibodies **[2]**. The model of tapasin/HLA-B*44:05 compared with that of unliganded HLA-B*44:05 reveals dramatic changes that reflect both chaperone and catalytic activities. The extended N-terminal domain of tapasin cradles the MHC-I molecule through contacts with the a1 and a2 domains, with additional interactions between tapasin's membrane proximal IgC domain and the MHC-I a3 domain and β2-microglobulin (β2m) subunit.The tapasin-stabilized peptide-receptive state of HLA-B*44:05 is characterized by distortion of the peptide binding groove and destabilization of the β2m interaction, leading to the release of peptide. Movements of the membrane-proximal Ig-like domains of tapasin, HLA-B*44:05, and β2m accompany the transition to a peptide-receptive state. Together this ensemble of tapasin structures provides insights into a distinct mechanism of tapasin-mediated peptide exchange. We compare this tapasin/HLA-B*44:05 structure with our previously determined structure of TAPBPR/H2-D^d. Although the general dispositions of tapasin and TAPBPR are the same in their complexes with MHC-I, the structural details of their interactions differ. Thus, the two MHC-I dedicated chaperones, tapasin and TAPBPR, despite acting at distinct stages of the MHC-I loading pathway, show broadly conserved binding modes and mechanisms of peptide loading in antigen presentation (**Fig. 1**). Mutational studies of several critical regions of tapasin that contact the MHC-I molecule lend additional insight into the dynamic details of tapasin's dual function as both a stabilizing chaperone and a peptide editor.

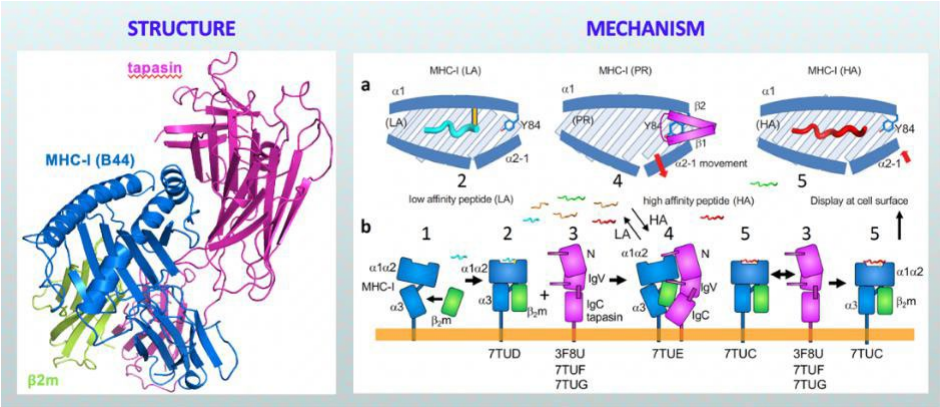

Figure 1. Structural mechanism of peptide exchange as illustrated from structure to mechanism

1 Jiang J., Natarajan, K., Boyd, L., Morozov, G.I., Mage, M. & Margulies, D.H. (2017). ***Science* 358**, 1064.
2 Jiang J., Taylor D.K., Kim E.J., Boyd L., Ahmad J., Mage M., Truong H.V., Woodward C.H., Sgourakis N.G., Cresswell P., Margulies, D.H. & Natarajan, K. (2022). ***Nature Communications***, **13**, 5470.

Acknowledgements: *X-ray diffraction data were collected at SER-CAT/APS. These studies were supported by the Intramural Research Program of the NIAID, NIH.*

A019-05-250823

Structural insights into immunoglobulin M

Junyu Xiao

State Key Laboratory of Protein and Plant Gene Research, School of Life Sciences, Peking University, Beijing, China
Email of communicating junyuxiao@pku.edu.cn

Keywords: Immunoglobulin M, J-chain, pIgR, FcμR

Immunoglobulin M (IgM) plays a pivotal role in both humoral and mucosal immunity. Its assembly and transport depend on the joining chain (J-chain) and the polymeric immunoglobulin receptor (pIgR), but the underlying molecular mechanisms of these processes are unclear. We have determined a cryo-electron microscopy structure of the Fc region of human IgM in complex with the J-chain and pIgR ectodomain. The IgM-Fc pentamer is formed asymmetrically, resembling a hexagon with a missing triangle. The tailpieces of IgM-Fc pack into an amyloid-like structure to stabilize the pentamer. The J-chain caps the tailpiece assembly and bridges the interaction between IgM-Fc and pIgR, which undergoes a large conformational change to engage the IgM–J complex.
We have also investigated the recognition of IgM by its specific receptor FcμR, and delineated the structural basis of the FcμR-IgM interaction by crystallography and cryo-electron microscopy. Together, these results provide a structural basis for the function of IgM.

[1] Li, Y., Wang, G., Li, N., Wang, Y., Zhu, Q., Chu, H., Wu, W., Tan, Y., Yu, F., Su, X.D., Gao, N., Xiao, J. (2020). *Science* 367:1014-1017.
[2] Li, Y., Shen, H., Zhang, R., Ji, C., Wang, Y., Su, C., Xiao, J. (2022). *PREPRINT (Version 1) available at Research Square*.

A019-06-250823

Structural biology of nucleic acid sensing Toll-like receptors

T. Shimizu

Graduate School of Pharmaceutical Sciences, The University of Tokyo, Tokyo 113-0033, Japan)
Email of communicating shimizu@mol.f.u-tokyo.ac.jp

Keywords: innate immunity, Toll-like receptor, nucleic acid

Toll-like receptors (TLRs) are pattern-recognition receptors of the innate immune system that are activated when conserved molecular signatures on microbial or host molecules (pathogen- and danger-associated molecular patterns (PAMPs and DAMPs, respectively)) are detected. TLRs are classified into two groups: cell surface TLR1, 2, 4, 5, and 6 recognize bacterial cell surface components, while endosomal TLR3, 7, 8, and 9 recognize microbial or viral nucleic acids. As nucleic acids from viruses, bacteria, and even humans share common chemical and structural features, their recognition must be strictly regulated spatiotemporally. Endosomal compartmentalization, achieved by segregating nucleic acid sensing TLRs from self-derived materials, is thought to be a safeguard mechanism for avoiding unwanted immune responses due to self-derived nucleic acids. UNC93B1, a membrane protein with 12 TM helices, is essential for trafficking nucleic acid sensing TLRs from the endoplasmic reticulum (ER) to the endosome. We demonstrated that cryo-EM structures of full-length endosomal Toll-like receptors TLR3 and TLR7 in complex with UNC93B1 [1]. Binding of UNC93B1 prevent active TLR dimer formation by steric hindrance. Furthermore, structural work revealed the various factors such as juxtamembrane regions and transmembrane region define the UNC93B1-dependency of TLRs. TLR3 recognizes double-stranded (ds) RNA. Previous studies demonstrated that dsRNA-induced receptor activation of TLR3 is indeed length-dependent, with the minimal size for efficient activation of ca. 40-50 bp, which confirmed well by the findings of the structural study. They also demonstrated that the interaction of TLR3 with dsRNA is highly dependent on dsRNA length and expression levels. Cryo-EM analyses of TLR3-dsRNA complex demonstrated that TLR3 dimers laterally cluster along dsRNA, promoting further multimerization and efficient signal transduction [2].

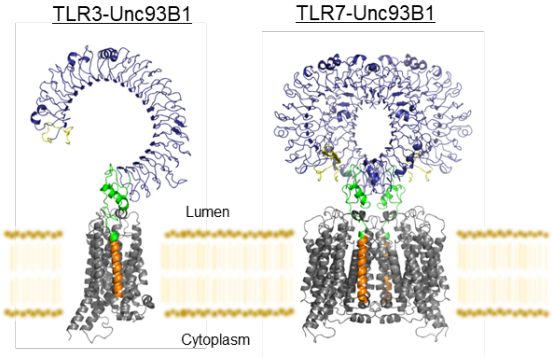

Figure 1. The structures of TLR3-Unc93B1 and TLR7-Unc93B1.

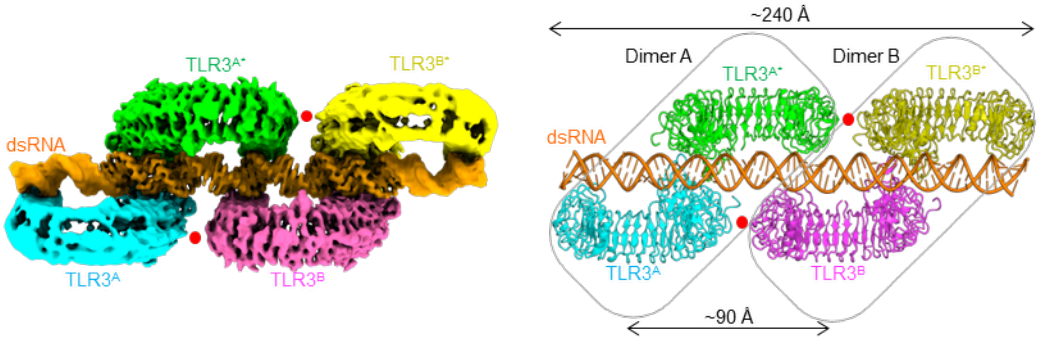

Figure 2. The structure of TLR3-dsRNA

[1] Ishida, H, Asami J, Zhang Z, Nishizawa T, Shigematsu H, Umeharu Ohto and Shimizu T (2021) *Nature Struc Mol Biol.* **28**, 173-180
[2] Sakaniwa K, Fujimura A, Shibata T, Shigematsu H, Ekimoto T, Yamamoto M, Ikeguchi M, Miyake K, Ohto U, Shimizu T (2023) *Nature Commun.* **14**(1):164

A025 Diffraction Science in Virtual/Remote Settings – Remote Access to Instrumentations

Room 204

1.10pm – 3:30pm

A025-01-250823

I04 – a versatile variable and microfocus macromolecular crystallography beamline at Diamond Light Source enabling new data collection protocols

R. Flaig[1], P. Romano[1], M. Mazzorana[1], D. Aragao[1]

Diamond Light Source, Harwell Science and Innovation Campus, Didcot OX11 0DE, UnitedKingdom
ralf.flaig@diamond.ac.uk

Keywords: data collection protocols, data quality, microfocus beamline

The macromolecular crystallography beamline I04 at Diamond [1] is a versatile variable and microfocus beamline aiming to provide the best quality diffraction data from crystals of macromolecules mainly at cryo temperatures. Beam delivery is achieved through the combination of a double crystal monochromator (DCM) with a F-switch which houses compound refractive lenses (CRL) that can be brought individually into the beam path. Both devices were designed inhouse and this combination allows variable focus of a very stable beam from the microfocus regime (8 µm x 5 µm (h x v)) to larger beam sizes (up to 110 µm x 100 µm) over the whole energy range of 6-18 keV. Beam delivery within 3% RMS of the beam size is achieved by making use of a dedicated feedback system using X-ray beam position monitors (XBPMs). In June 2022 the original U23 insertion device has been replaced with a cryocooled permanent magnet undulator (CPMU) and this has resulted in a significant flux increase which has opened up new opportunities, including faster data collection and the ability to address more challenging data collections, in particular for microcrystallography. Related to the insertion device upgrade we are carefully monitoring any heat load effects on the optics and are further characterising the performance of our F-switch device with the aim to optimise beam delivery.

The combination of the stable beamline optics with the SmarGon multi-axis goniometer and Eiger2 XE 16M detector provides a versatile yet very stable setup that allows to optimise the experiment based on sample properties and the scientific aim as well as providing new scientific capability. The beamline can be used in interactive or remote mode making full use of the tools available to tackle even the most challenging samples in the microfocus regime. More recently we have added functionality which allows to run a dose-driven data collection rather than providing an exposure time. For experimenters it is very difficult to understand the I04 beam properties given the recent insertion device upgrade and the possibility to focus the beam to various beam sizes and this can easily lead to too low or too high exposure times for a given sample. The dose -based approach is taking away the decision about the correct exposure time and rather tries to direct towards the experimental aim and if implemented on other beamlines will also allow an easier comparison of data sets. The current implementation is based on assuming a crystalline sample with standard composition, but further developments are ongoing to include more sample-based information. The dose-driven data collection is also used in our unattended data collection (UDC) mode where we offer fully automated data collection protocols depending on the scientific aim and data collection requirements based on user input to the ISpyB/Synchweb interface. We intend to provide this combination of crystallographic expertise system and dose-aware data collection also via the graphical user interface. Multi-sweep, multi-orientation data collection protocols are routinely used with the multi-axis SmarGon goniometer resulting in high multiplicity high quality data sets [2].

We are constantly developing and improving our tools for beamline quality and speed monitoring, and this allows us to easily diagnose any changes in performance after a hardware or software configuration change. Furthermore, we are looking into providing additional tools and ancillary techniques that would provide additional sample information while keeping a streamlined user experience. An outlook will also be given about plans to improve beam delivery further.

1 https://www.diamond.ac.uk/Instruments/Mx/I04.html
2 Winter, G. *et al.* (2019). *Acta Cryst.*, **D75**, 242-261.
Acknowledgement: Beamline development would not be possible without the contributions of the various teams in the MX Group as well as engineering and support teams a Diamond. Their contributions are greatly acknowledged.

A025-02-250823

In-tray screening at the Australian Synchrotron's MX3 beamline

E. Campbell[1], G. Barrow[1], N. Cain[1], S. Chen[1], H. Cherukuvada[1], D. Eriksson[1], F. Hernandez Vivanco[1], R. Khemaram[1], J. Oldfield[1], J. Quinton[1], T. Caradoc-Davies*[1]

[1]ANSTO Australian Synchrotron, 800 Blackburn Road, Clayton, VIC, Australia, 3168

**thomasc@ansto.gov.au*

Keywords: synchrotron, beamline, data collection, screening, optimisation, software

Too often, we see beautiful crystals at X-ray beamlines fail to diffract. Where targets of interest can be generated rapidly and X-ray data can be collected *via* high throughput pipelines, obtaining structural data is often bottlenecked by optimisation of crystallisation conditions. Early X-ray diffraction screening of crystalline material can direct researchers' efforts towards the most promising conditions, guiding optimisation and minimising wasted synchrotron time.

As part of development of the new MX3 beamline at the Australian Synchrotron, we are establishing a highly automated crystallisation tray screening program. By combining MX3's tray-compatible robot and goniometer, automated sample centring and unattended data collection, and a user-friendly interface, we aim to build the world's easiest-to-access tray screening program, making screening available to synchrotron users and non-users alike.

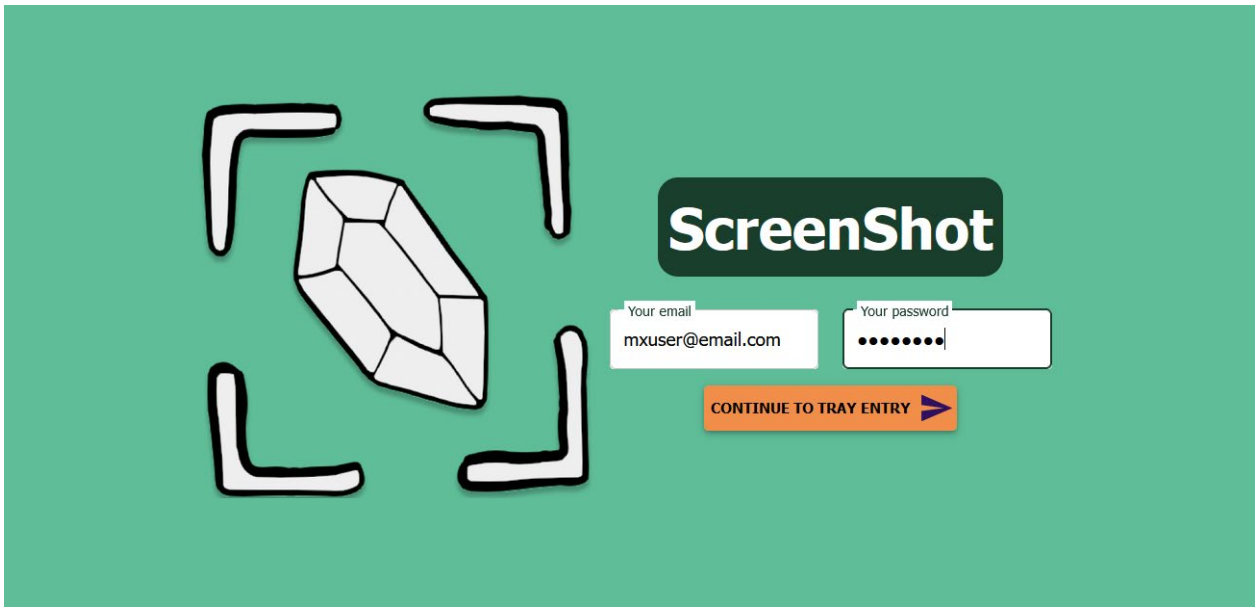

Figure 1. The home page of ScreenShot, the user interface for tray submission to MX3's tray screening program

A025-03-250823

The need for a ground up approach for remote access to instrumentation and data in diffraction science.

Alun W. Ashton

Division for Scientific Computing, Theory and Data, Paul Scherrer Institut, 5232 Villigen PSI, Switzerland
Alun.Ashton@psi.ch

Keywords: remote access, data, experiment control

While commercial or community “free to use” remote desktop solutions can provide a remote facility user with a local environment to the instrument, the challenging aspect to safely control the experiment in a multiuser environment while addressing the growing concern of scientific data security and cybersecurity threats remains. There is also an additional expectation for accessible resources for computational analysis and associated data storage at the source of the data far beyond the initial allocation of time at the facility. While factors such as pandemics and environmental concerns has undoubtedly accelerated the demand for remote resources, the increased complexity and volumes of measured data have also been a major driving force that predate the most recent environmental factors.

The recent and upcoming upgrades to synchrotron facilities in Europe and wider afield offer an opportunity to revisit the operation mode of these facilities to address these factors from the ground up. The imminent upgrade of the Swiss Light Source (SLS2.0) [1] at the Paul Scherrer Institut (PSI) is no exception and within the financial constraints of an upgrade program, a holistic approach to the full digital lifecycle of future experiments and data is being prepared. This talk will cover the current status of the remote access to facilities at PSI and how we are leveraging Swiss national resources, our place at the heart of Europe and collaborations from around the world to deliver the best possible solution to the future community of the facility.

[1] https://www.psi.ch/en/sls2-0

A025-04-250623

Science during a pandemic – remote access to neutron diffractometers

M. Kirkham1, R. Benson1, R. Crompton2, M. Everett1, L. Grace1, P. Parker2, H. Skorpenske1, J. Thomson1, K. Vodopivec1, J. Werner3, A. White3

1Neutron Sciences Directorate, 2Information Technology Services Division, 3Environment, Safety, Health and Quality Directorate, Oak Ridge National Laboratory, Oak Ridge, Tennessee, 37831 USA

kirkhammj@ornl.gov

Keywords: neutron diffraction, remote experiment, facility access, instrumentation

The neutron sources at Oak Ridge National Laboratory (ORNL), namely the High Flux Isotope Reactor (HFIR) and the Spallation Neutron Source (SNS), have for many years attracted scientists from all over the world to perform neutron scattering research. That ground to a halt in 2020 when the global pandemic restricted the ability of researchers to travel to the facility. Though SNS soon restarted in a limited way to conduct coronavirus-related research, a more structured approach was needed to return to full operation. Therefore, the Neutron Sciences Directorate instituted a Remote Experiment Task Force to implement remote access to instruments at both neutron sources. Remote experiments are distinguished from already-existing mail-in programs primarily by allowing users to remotely control the instruments, and such access was eventually implemented across almost all instruments and experimental setups. Additionally, automation and communication tools were developed to improve workflows. These developments allowed the neutron sources to maintain high levels of productivity even with restricted on-site access by users. The availability of remote experiments has many benefits, including increased accessibility to neutrons for those whose ability to travel is restricted due to financial, family, health or other limitations. However, remote experiments also have drawbacks that must be considered, such as difficulty training new users remotely and increased workload on instrument staff to handle all the hands-on tasks for the experiment. That said, the benefits outweigh the drawbacks and remote experiments will continue to be part of the landscape of neutron scattering at ORNL going forward, even as pandemic travel restrictions are lifted.

Many hands at ORNL contributed to this work, including Ke An, YQ Cheng, Clarina Dela Cruz, Jaime Fernandez-Baca, Garrett. Granroth, Christina Hoffman, Bradley Horn, Rob Knudson, James Kohl, Bhargavi Krishna, Mark Lumsden, Kelly Mahoney, Gergely Nagy, Naresh Osti, Daniel Pajerowski, Jeff Patton, Shuo Qian, Toni Sawyer and Wei Tan. This research used resources at the High Flux Isotope Reactor and the Spallation Neutron Source, DOE Office of Science User Facilities operated by the Oak Ridge National Laboratory.

A025-05-250823

The Canadian Macromolecular Crystallography Facility: upgrades and performance improvements

M. Fodje, K. Mundboth, K. Janzen, J. Gorin, S. Colville, D. Lang, P. Grochulski

Canadian Macromolecular Crystallography Facility, Canadian Light Source, 44 Innovation Boulevard, Saskatoon, SK S7N 2V3, Canada.

michel.fodje@lightsource.ca

Keywords: Macromolecular crystallography, beamline, double multi-layer monochromator

The Canadian Macromolecular Crystallography Facility (CMCF) consists of two beamlines (CMCF-ID and CMCF-BM). The facility has been an invaluable resource for the Canadian crystallographic community since 2006, with more than 95% of access to the facility by remote access, suiting the vast expanse of Canadian geography.

We recently completed upgrades on both beamlines to increase throughput and flux to support the next generation of more demanding experiments. At CMCF-BM, this included an enhanced monochromator, automounter software upgrades and a faster detector. At CMCF-ID, the upgrade involved the replacement of almost every component, including the undulator, optical components, and detector.

These upgrades have resulted in drastic improvements in flux, throughput, and the availability of micro-beam capabilities. Equipped with state-of-the-art software for sample management and data collection, the facility is poised to be the destination of choice for Canadian Synchrotron macromolecular crystallography experiments.

Funding for this research was provided by: Canada Foundation for Innovation; Natural Sciences and Engineering Research Council of Canada; National Research Council Canada; Canadian Institutes of Health Research; Government of Saskatchewan; University of Saskatchewan.

A025-06-250823

Remote Access X-ray Spectroscopy at the Stanford Synchrotron Radiation Lightsource

Ritimukta Sarangi, Oliver Mueller, Matthew Latimer, Martin George, Allyson Aranda

Hard X-ray Spectroscopy and Structural Molecular Biology Group, Stanford Synchrotron Radiation Lightsource, SLAC National Accelerator Laboratory, Menlo Park, CA-94025

Stanford Synchrotron Radiation Lightsource (SSRL) operates seven full time and one shared (~50%) beamlines (BLs) for x-ray spectroscopy (XAS). These BLs that serve an energy range of 2-35 keV and serve a diverse range of scientific problems from a broad range of U.S.-based and international scientific communities. The XAS beam line operations is centrally managed, with spectroscopy staff working in a group supporting all beam lines, which enables uniform application, operational consistency and high efficiency. This central management has led to the development of uniform hardware and software systems across beamline facilities providing users the same interface and routines for measurement. The SSRL spectroscopy staff have developed a browser agnostic web-based data collection system that allows for remote measurements from any smart device. This system called the WebXAS is currently integrated with a variety of detectors and enables remote measurements in transmission (ion chambers) and fluorescence modes (silicon drift diodes and 30- and 100-element Ge detector systems). Data queuing modules have been developed that allows users to import prepopulated multi-sample measurement routines allowing for uninterrupted measurement on a plurality of samples and spots. Other features in WebXAS, either already developed or in development, include automated edge changes and beamline optimizations, a motorized foil changer, automated region file generators, preliminary data reduction and analysis, automated routines to evaluate data channels from multi-element detector systems, automated optimized gas delivery into ion-chambers, implementation of robotic arm for Lytle filter selection and a simulation mode for training new users. An update on the status and future vision of WebXAS data collector at SSRL will be presented.

SSRL operations are funded by the Department of Energy, Office of Basic Energy Sciences. The SSRL Structural Molecular Biology program is supported by the National Institutes of Health, National Center for Research Resources, Biomedical Technology Program, and Department of Energy, Office of Biological and Environmental Research.

A039 New Approaches to the Crystal Structure of Pharmaceutics and Macromolecules
Room 211
1.10pm – 3:30pm

A039-01-250823

Determining membrane protein structures using microcrystal electron diffraction

M.W. Martynowycz[1], A. Shiriaeva[1], M.T.B. Clabbers[1], W.J. Nicolas[2], S.J. Weaver[1], J. Hattne[2], T. Gonen[1,2]

[1]Department of Biological Chemistry, University of California, Los Angeles CA USA 90095
[2]Howard Hughes Medical Institute, University of California, Los Angeles CA USA 90095

mikewm@g.ucla.edu

Keywords: CryoEM, MicroED, Membrane Proteins, Ion-beam milling

Membrane proteins, such as G protein-coupled receptors (GPCRs) are important membrane proteins in the human body, but their structures can be difficult to determine using traditional X-ray crystallography [1]. This is because they often require crystallization in lipidic cubic phase (LCP), which can be challenging due to the small size of many membrane protein crystals and the difficulty in extracting them from the viscous LCP [2]. X-ray free electron lasers (XFEL) have been used as an alternative approach, but this requires many crystals, is costly, and data processing is difficult. Single particle cryogenic electron microscopy (cryoEM) is another approach but is often impossible for small GPCRs prior to the binding of a signalling partner. Microcrystal electron diffraction (MicroED) is a cryoEM method that can determine structures using nanocrystals, which is ideally suited for small membrane protein samples, such as GPCRs [3]. However, the use of this method has been limited due to the challenges associated with preparing LCP embedded samples for MicroED experiments.

Thinning biological specimens using a focused ion-beam has become a standard method to prepare samples for cryo-tomography (cryoET) and macromolecular MicroED experiments. Here, we detail the recent advances in plasma focused ion-beam milling, correlative light and electron microscopy (CLEM) and using direct electron detectors in electron counting mode to determine membrane protein structures for tiny crystals embedded in dense media. These approaches have successfully led to the determination of multiple membrane proteins, such as the human A2A adenosine receptor (**Figure 1**) [4-6]. We highlight these results and discuss the future possibilities of the methods.

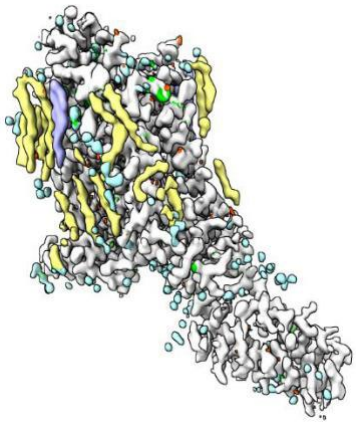

Figure 1. The structure of the human A_{2A} adenosine receptor determined by MicroED to 2Å resolution.

1 Rosenbaum, Daniel M., Søren GF Rasmussen, and Brian K. Kobilka. "The structure and function of G-protein-coupled receptors." Nature 459.7245 (2009): 356-363.
2 Landau, Ehud M., and Jürg P. Rosenbusch. "Lipidic cubic phases: a novel concept for the crystallization of membrane proteins." Proceedings of the National Academy of Sciences 93.25 (1996): 14532-14535.
3 Nannenga, Brent L., and Tamir Gonen. "The cryo-EM method microcrystal electron diffraction (MicroED)." Nature methods 16.5 (2019): 369-379.
4 Martynowycz, Michael W., et al. "MicroED structure of the human adenosine receptor determined from a single nanocrystal in LCP." Proceedings of the National Academy of Sciences 118.36 (2021): e2106041118.
5 Martynowycz, Michael W., et al. "Ab initio phasing macromolecular structures using electron-counted MicroED data." Nature Methods 19.6 (2022): 724-729.
6 Martynowycz, Michael W., et al. "A robust approach for MicroED sample preparation of lipidic cubic phase embedded membrane protein crystals." Nature Communications 14.1 (2023): 1086.

A039-02-250823

Probing charge states of metal ion cofactors in protein crystals by microED

Laura Pacoste[1], Gerhard Hofer[1], Rohit Kumar[2], Hugo Lebrette[3], Thomas Thersleff[1], Cheng Cho Lee[4], Hongyi Xu[1], Martin Högbom[2], Xiaodong Zou[1]

[1]Department of Materials and Environmental Chemistry, Stockholm University, Stockholm,
[2]Department of Biochemistry and Biophysics, Stockholm University, Stockholm
[3]Laboratoire de Microbiologie et Génétique Moléculaires, Center for Integrative Biology, CNRS, UPS, Toulouse, France
[4]Umeå Centre for Electron Microscopy, Chemical Biological Center, Umeå University, Umeå

Keywords: IUCR; Abstracts; 3DED; MicroED; charge-state

Knowing the charge states of various catalytic intermediates in 3D protein structures is crucial for understanding the functions and chemical processes in biological systems. Microcrystal electron diffraction (MicroED) is an attractive alternative to X-ray diffraction for studying protein structures from microcrystals [1-3] and has shown potential for determining charge states of atoms in crystalline species [4]. However, more insight is needed in how different charge states are reflected in the electron diffraction data and if this difference is within the accuracy of the experiment. Furthermore, it is of fundamental importance to understand at what critical dose a charged species becomes reduced by the electron beam.

In this study, the R2 protein of class I ribonucleotide reductase (R2a) containing a diiron center ($Fe^{III}Fe^{III}$) [5] has been used as a model protein to simulate electron diffraction data. Experimentally, two different strategies were explored for preparing R2a crystals. These include cryo-FIB milling and optimization of microcrystal growth. The later method produced ideal plate-like crystals for MicroED data collection up to 2 Å resolution. The crystal structure could be determined to 2.0 Å resolution, which shows to be similar to the $Fe^{III}Fe^{III}$ R2a structure determined by synchrotron X-ray diffraction [6]. Furthermore, R2a protein crystals containing reduced diiron center ($Fe^{II}Fe^{II}$) were produced. These crystals were also studied by MicroED and a structure of 2.4 Å resolution could be obtained. Structure analysis is currently being carried out.

Meanwhile, in order to estimate the electron doses that can be applied without reducing the metal centres, we are currently investigate the influence of electron dose on the charged species by electron energy loss spectroscopy (EELS). We expect that these studies will provide critical insight into the feasibility of utilizing MicroED for probing charge states of species.

[1] Shi, D., Nannenga, B.L., Iadanza, M.G., Gonen, T., (2013). *eLife* **2**, e01345.
[2] Xu, H., Lebrette, H., Clabbers, M.T.B., Zhao, J., Griese, J.J., Zou, X., Högbom, M., (2019). *Sci. Adv.* **5**, eaax4621.
[3] Clabbers, M.T.B., Holmes, S., Muusse, T.W., Vajjhala, P.R., Thygesen, S.J., Malde, A.K., Hunter, .J.B., Croll, T.I., Flueckiger, L., Nanson, J.D., Rahaman, Md.H., Aquila, A., Hunter, M.S., Liang, M., Yoon, .H., Zhao, J.. Zatsepin, N.A., Abbey, B., Sierecki, E., Gambin, Y., Stacey, .J., Darmanin, C., Kobe, B.,Xu, H., Ve, T., (2021). *Nat. Commun*. **12**, 2578.
[4] Yonekura, K., Kato, K., Ogasawara, M., Tomita, M., Toyoshima, C., (2015). *Proc. Natl. Acad. Sci.* **112**,3368–3373.
[5] Srinivas, V., Banerjee, R., Lebrette, H., Jones, J.C., Aurelius, O., Kim, I.-S., Pham, C.C., Gul, S., Sutherlin, K.D., Bhowmick, A., John, J., Bozkurt, E., Fransson, T., Aller, P., Butryn, A., Bogacz, I., Simon, P., Keable, S., Britz, A., Tono, K., Kim, K.S., Park, S.-Y., Lee, S.J., Park, J., Alonso-Mori, R., Fuller, F.D., Batyuk, A., Brewster, A.S., Bergmann, U., Sauter, N.K., Orville, A.M., Yachandra, V.K., Yano, J., Lipscomb, J.D., Kern, J., Högbom, M., (2020). *J. Am. Chem. Soc*. **142**, 14249–14266.
[6] Högbom, M., Galander, M., Andersson, M., Kolberg, M., Hofbauer, W., Lassmann, G., Nordlund, P., Lendzian, F., (2003). *Proc. Natl. Acad. ci.* **100,** 3209–3214.

A039-03-250823

Direct electron detection, phasing and hydrogens

Max T.B. Clabbers[1], Michael W. Martynowycz[1], Johan Hattne[2], Tamir Gonen[1,2,3]

[1]Department of Biological Chemistry, University of California, Los Angeles CA 90095, [2]Howard Hughes Medical Institute, University of California, Los Angeles CA 90095, [3]Department of Physiology, University of California, Los Angeles CA 90095
clabbers@ucla.edu

Keywords: MicroED, hydrogens, direct electron detectors

Microcrystal electron diffraction (MicroED) uses electron cryo-microscopy (cryo-EM) for protein structure determination of crystalline samples too small for conventional X-ray crystallography [1]. Electrons interact with the electrostatic potential of the crystal, which means that scattered electrons carry information about the charged state of atoms *and* provide relatively stronger contrast for localizing hydrogen atoms. Identification of individual hydrogen atoms typically requires atomic resolution data and has thus far remained elusive for macromolecular MicroED. Here, we present the structure of triclinic hen egg-white lysozyme at 0.87 Å resolution using electron counting data collection on a direct electron detector at a significantly reduced exposure [2]. The low exposure ensures that the counts remain within the linear range of the camera, and reduces any negative effects of radiation damage to the structural integrity of the protein and the ability to localize hydrogen atoms. To enhance the signal at low exposure conditions we used focused ion-beam (FIB) milling to produce thin crystalline lamellae of an optimal thickness [3], combined with a slow rotation rate to systematically cover reciprocal space [2]. The structure was determined *ab initio* by placing an idealized helical fragment of three residues, followed by density modification and automated model building. Using the subatomic resolution data, we identified over a third of all possible hydrogen atoms in our structure from strong difference peaks, enabling direct visualization of hydrogen bonding interactions and the charged states of residues [4]. Furthermore, we find that the hydrogen bond lengths are more accurately described by the inter-nuclei distances than the centers of mass of the corresponding electron clouds. These results indicate a substantial improvement in MicroED data quality using electron counting, providing accurate intensities for phasing and visualizing hydrogen atoms and hydrogen-bond interactions in macromolecules.

[1] Nannenga, B. L., Shi, D., Leslie, A. G. W. & Gonen, T. (2014). *Nat. Methods* **11**, 927–930
[2] Martynowycz, M. W., Clabbers, M. T. B., Hattne, J. & Gonen, T. (2022). *Nat. Methods* **19**, 724–729
[3] Clabbers, M. T. B., Martynowycz, M. W., Hattne, J. & Gonen, T. (2022). *J. Struct. Biol. X* **6**, 100078
[4] Martynowycz, M. W., Clabbers, M. T. B., Unge, J., Hattne, J. & Gonen, T. (2021). *PNAS* **118**, e2108884118

A039-04-250823

Prospects and problems with absolute structure determination using electron diffraction

P. Klar[1], P. Brazda[3], Y. Krysiak[2], L. Palatinus[3]

[1]Faculty of Geosciences, University of Bremen, Germany, [2]Institute of Inorganic Chemistry, Leibniz University Hannover, Germany, [3]Institute of Physics, Czech Academy of Sciences, Prague, Czechia paul.klar@uni-bremen.de

Keywords: electron crystallography, 3D electron diffraction, dynamical refinement

The *de facto* standard method for absolute structure determination is based on the analysis of Bijvoet differences $|F_{\mathbf{h}}|-|F_{-\mathbf{h}}|$ caused by resonant scattering in single crystal X-ray diffraction experiments. In 3D electron diffraction (3D ED) [1], the each individual reflection is sensitive to the absolute structure because of dynamical diffraction effects, namely multiple scattering [2]. This has been used to determine the absolute structure of chiral inorganic and chiral organic compounds [3,4]. Here, we report on the recent progress on absolute structure determination from 3D ED data [5]. Routine and problematic cases are discussed.

We determine the absolute structure by performing two refinements, one for each enantiomorph. After convergence, the dynamical refinements are compared in terms of 1) refinement statistics (*R* factors) and 2) a *z*-score. The latter expresses the confidence level at which we may reject the statement that the better fit is the result of random variations of the intensities. *z* is calculated as $(2k-N)/\mathrm{sqrt}(N)$, where *N* is the total number of reflections and *k* is the number of reflections that better fit to one of the enantiomorph. We here investigate the dependence of the *z*-score on the data set resolution and the deviation of the structure from centrosymmetry determined by the program superflip based on the evaluation of phase differences (Fig. 1).

With this approach the absolute structures from about one hundred individual data sets were determined. In several inorganic examples the dependence of modelled intensities on the absolute structure is so strong that its determination cannot be considered optional (z-score > 15σ) because the wrong enantiomorph compromises the refinement statistics and model accuracy. For one pseudo-centrosymmetric compound (space group *P*1, inversion center deviation factor = 27.4), the *z*-score of individual data sets ranges between -0.2σ and 5.0σ (average 2.6σ). The only compound for which an unambiguous assignment of the handedness was not achieved (z-scores close to 0σ) is the case of biogenic hemozoin (*P*1, inversion center deviation factor = 1.4) [6].

This work quantifies the reliability of the absolute structure assignment via dynamical refinement against electron diffraction data. Despite the relatively high *R* factors encountered in electron crystallography, a reliable determination was achieved in all but one case because the strong dependence of diffracted intensities on the absolute structure. We expect that ongoing methodological improvements (e.g. considering inelastic scattering) will enable to tackle also the problematic cases in the future.

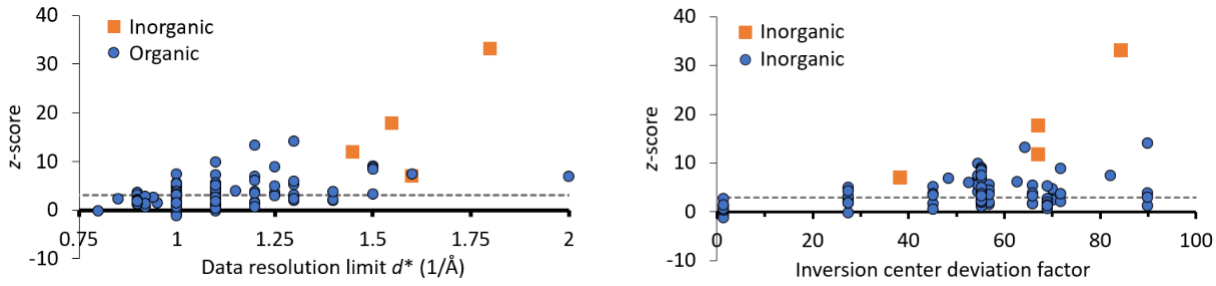

Figure 1. Reliability (z-score) of absolute structure determination as function of diffraction data resolution limit (left) and deviation from centrosymmetry (right). The latter is based on the evaluation of phase differences (higher factor means stronger deviation). Dashed lines mark the 3σ level.

1 Gemmi, M., Mugnaioli, E., Gorelik, T., Kolb, U., *et al.* (2019). *ACS Cent. Sci.* **5**, 1315−1329.

2 Spence, J.C.H., Zuo, J.M., O'Keeffe, M., Marthinsen, K., Hoier, R. (1994). *Acta. Cryst*. **A50**, 647−650.
3 Ma, Y., Oleynikov, P., Terasaki, O. (2017) *Nat. Mat.*. **16**, 755–759.
4 Brázda, P., Palatinus, L., Babor, M. (2019). *Science*. **364**, 667−669.
5 Klar, P.B., Krysiak, Y., Xu, H., Steciuk, G., *et al*. (2023). *Nat. Chem.* (accepted)
6 Klar, P.B., Waterman, D., Gruene, T., *et al*. (2023). *bioRxiv*. 507960 (preprint)

Financial support by GAČR project EXPRO, grant No. 21-05926X is gratefully acknowledged.

A039-05-250823

Structure determination of TLR2 TIR domain induced MyD88 TIR domain higher-order assembly revealed by microcrystal electron diffraction (MicroED)

Y. Li[1], J. D. Nanson[1], L. C. Pacoste[2], H. Xu[2], B. Kobe[1]

[1]School of Chemistry and Molecular Biosciences, The University of Queensland, Brisbane, Queensland, Australia, [2]Department of Materials and Environmental Chemistry, Stockholm University, Stockholm, Sweden

yan.li9@uq.net.au

Keywords: TIR domain, Macromolecular structure, MicroED, Structure comparison

Microcrystal electron diffraction (MicroED) is considered an ideal structure determination method for crystals too small or too complex for X-ray diffraction. High resolution structure is determined by continuous-rotation data collection in MicroED [1]. TIR (Toll/interleukin-1 receptor/resistance protein) domains are cytoplasmic domains widely found in both eukaryotic and prokaryotic proteins. Eukaryotic TIR domains signal via TIR: TIR interactions, either self-association or interaction with other TIR domains.

[2] In mammals, TIR domains are found in Toll-like receptors (TLRs) and cytoplasmic adaptor proteins, such as MyD88 (myeloid differentiation primary response gene 88) and MAL (MyD88 adaptor-like protein). These proteins are involved in pro-inflammatory signalling. Previous work revealed that adaptor MAL TIR domains nucleate the assembly of MyD88 TIR domain into crystalline arrays *in vitro* [2]. A MicroED structure of the MyD88 TIR domain assembly was solved with data completeness of 73.7% at 3.0 Å resolution, revealing a two-stranded higher-order assembly arrangement of TIR domains [3].

Here, we observed receptor TLR2 TIR domain also induces formation of crystalline higher-order assemblies of MyD88 TIR domain in vitro. By optimizing experimental procedures, we were able to reveal MicroED structure of the TLR2 induced MyD88 TIR microcrystals at a higher resolution (2.8 Å) and higher completeness (90%) comparing to the previous MAL induced MyD88 TIR assemblies. MAL TIR induced MyD88 TIR higher-order assemblies suggests a molecular templating mechanism for nucleation and assembly [1]. A similar nucleation mechanism was confirmed using a novel dynamic experiment to capture the crystal growth process. To summarize, both assemblies share high similarities in micro-ED structures, and reveal conformational changes at several key regions for signal transduction (e.g., BB loop, CD loop) compared to the X-ray structures of monomeric proteins.

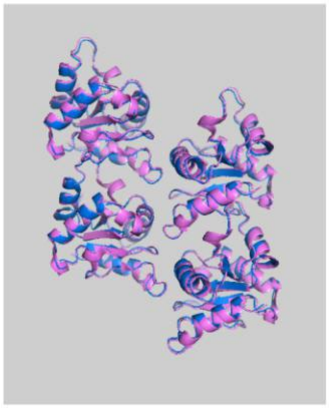

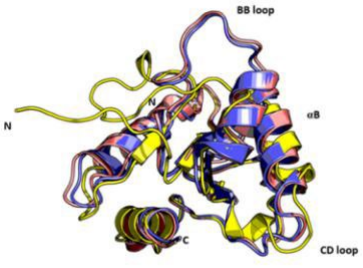

Figure 1. (a) Structure comparisons between MAL TIR (Pink) and TLR2 TIR (Blue) induced MyD88 higher-order assemblies, respectively. (b) Structure comparisons between MyD88 higher-order assemblies and monomeric X-ray structure (Yellow; PDB: 4EO7).

1 Shi, D., Nannenga, B. L., Iadanza, M. G., & Gonen, T. (2013). Three-dimensional electron crystallography of protein microcrystals. elife, 2, e01345.
2 Ve, T., Vajjhala, P. R., Hedger, A., Croll, T., DiMaio, F., Horsefield, S., ... & Kobe, B. (2017). Structural basis of TIR-domain-assembly formation in MAL-and MyD88-dependent TLR4 signaling. Nature structural & molecular biology, 24(9), 743-751.
3 Clabbers, M. T., Holmes, S., Muusse, T. W., Vajjhala, P. R., Thygesen, S. J., Malde, A. K., ... & Ve, T. (2021). MyD88 TIR domain higher-order assembly interactions revealed by microcrystal electron diffraction and serial femtosecond crystallography. Nature communications, 12(1), 1-14.

A039-06-250823

High-throughput and high-resolution 3D ED structure analysis through AI-based data collection and hybrid approach.

S. Maki-Yonekura1, K. Takaba1, K. Kawakami1, K. Yonekura1,2

RIKEN, SPring-8 center, Sayo, Hyogo 679-5148, Japan, Tohoku University, IMRAM, Sendai 980-8577, Japan

makis@spring8.or.jp

Keywords: 3DED, Serial XFEL crystallography, AI

Electron crystallography, one of the main methods of cryo-EM, is used to determine the detailed structure of samples from their tiny three-dimensional crystals. Since structures with spatial resolution beyond 1 Å can be obtained from various samples in aqueous solution, organic solvents, and powders, this technique called 3D ED or microED is being used not only in the life sciences but also in drug discovery, material sciences, and a wide range of other fields. We have been involved in the development of this technology, and it is now possible to complete the automatic processing and high-throughput structure determination [1] from large numbers of diffraction data collected by AI control of the electron microscope operation [2]. Our recent results include a new double helix structure built by self-assembly of nanographene [3], thin crystals of an organic semiconductor [4], and fibrous crystals of polypeptides related to a neurological disease, amyotrophic lateral sclerosis (ALS) [5]. However, 3D ED has limitations in rotation angles and /or sample thickness, which sometimes hamper structure determination by this technique alone. We have overcome these difficulties by introducing serial XFEL crystallography [6]. XFEL had been used for protein crystals so far, as the correct indexing of diffraction spots needs many diffraction spots per frame. We have shown that the XFEL patterns from small organic compounds are able to be efficiently processed with lattice parameters obtained by 3D ED. This strategy has worked well for various samples including novel compounds for drug discovery and organic semiconductors.

Our cryo-EM system also performs well for high-resolution single-particle cryo-EM, which allowed us to obtain signals of most hydrogen atoms and charges in a test protein [7]. Signals from hydrogen atoms are weak both with X-rays and electrons, but their properties can now be studied by 3D ED, XFEL crystallography, and single-particle cryo-EM. In this microsymposium, I will present and compare our recent results obtained by these methods. Topics also cover advanced applications including AI data collection, dynamical refinement, hydrogen properties, and charge analysis.

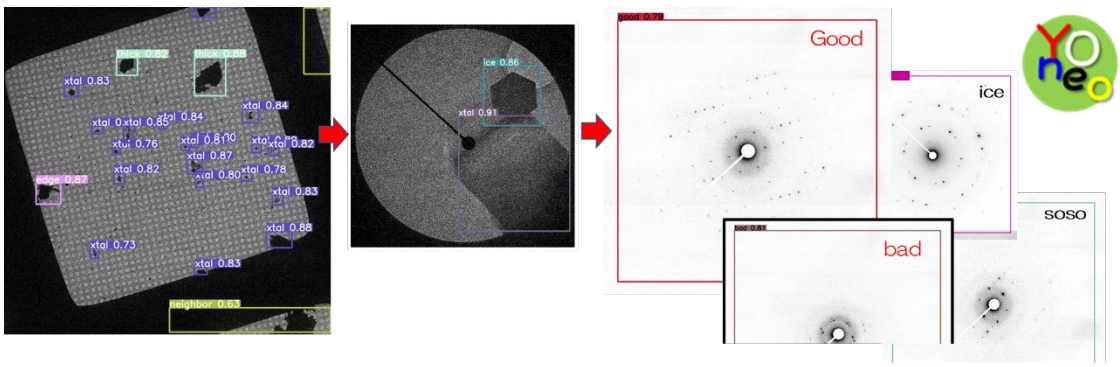

Figure 1. AI-based cryo-ED data collection using the yoneoLocr program suite.

[1] Takaba, K., Maki-Yonekura, S., Inoue, S., Hasegawa, T., Yonekura, K. (2021). *Front. Mol. Biosci*. **7**, 612226.
[2] Yonekura, K., Maki-Yonekura, S., Naitow, H., Hamaguchi, T., Takaba, K. (2021). *Commun Biol*. **4**, 1044.
[3] Kato, K., Takaba, K., Maki-Yonekura, S. *et al.* (2021). *J. Am. Chem. Soc.* **143**, 5465-5469.
[4] Inoue, S. *et al.* (2022). *Chem. Mater.* **34**, 72-83.
[5] Sekiyama, N., Takaba, K., Maki-Yonekura, S. *et al.* (2022). *PNAS*. **119**, e2122523.
[6] Takaba, K., Maki-Yonekura, *et al*. (2023). *Nat. Chem*. **15**, 491-497.
[7] Maki-Yonekura, S., Kawakami, K. *et al*. (2023). Preprint in *BioRxiv*.

We thank Inoue, I., Tono, K., and Yabashi, M. for their support of the XFEL experiments.

A046 Diffraction Studies in Dynamic Compression Experiments

Room 213

1.10pm – 3:30pm

A046-02-250823

Dynamic compression of bismuth at the European XFEL results from Exp. 3076

E.F. O'Bannon III[1], C.M. Pepin[2], and co-proposers from Exp. 3076

[1]Physics Division, Physical and Life Sciences Directorate, Lawrence Livermore National Laboratory. Livermore, California 94550, USA, [2]CEA, DAM, DIF, F-91297 Arpajon, France

obannon2@llnl.gov

Keywords: Bismuth, dynamic diamond anvil cell, EU-XFEL

Bismuth (Bi) has a rich phase diagram at relatively low pressures and temperatures with a variety of crystal structures accessible below 10 GPa. At ambient temperature, Bi undergoes the following sequence of structural phase transitions, Bi-I (hR2) transforms to Bi-II (mC4) at ~2.55 GPa. Bi-II transforms to the complex host-guest incommensurate structure at ~2.7 GPa and above ~8 GPa (depending on the reference) Bi-III transforms to Bi-V a high symmetry bcc phase [1]. The high-pressure behavior of Bi has been extensively studied using a variety of high-pressure techniques and diagnostics. Static DAC techniques combined with x-ray diffraction [1,2,3], dynamic diamond anvil cell (dDAC) with x-ray diffraction [4,5], and dynamic laser ramp and shock compression with x-ray diffraction and /or VISAR [6,7,8, 9, 10].

Early shock compression studies found that the phase transition pressures were consistent with the phase transition pressures reported from static compression studies [11-13]. However, these studies did not utilize techniques which yielded crystal structure information. Structural determination under dynamic compression has been carried out recently using time resolved X-ray diffraction techniques at XFELs and synchrotrons where significant deviations from the equilibrium phase diagram were observed [6,7,9]. Interestingly incommensurate Bi-III was not observed in any of these experiments on compression, and instead Bi-V was observed alongside an unidentified metastable phase Bi-M at pressures as low as 3 GPa [6,7]. Additionally, the observation of Bi-V at lower pressures in shock experiments when compared to static compression experiments is surprising, since kinetic hinderance typically results in over-driving of the phase transition boundary [8].

To resolve these discrepancies, we carried out a series of dDAC experiments at the High Energy Density (HED) instrument at the European X-ray free electron laser (EU-XFEL) facility. A ~15 µm beam size at 18 keV was used. We utilized the long pulse trains where we collected data for 550 µs with a time resolution of ~1.78 µs. This mode allowed us to collect diffraction data across the entire compression ramp of the dDAC. A new triggering scheme was also developed which allowed us to collect diffraction data on the hold and decompression parts of the ramp.

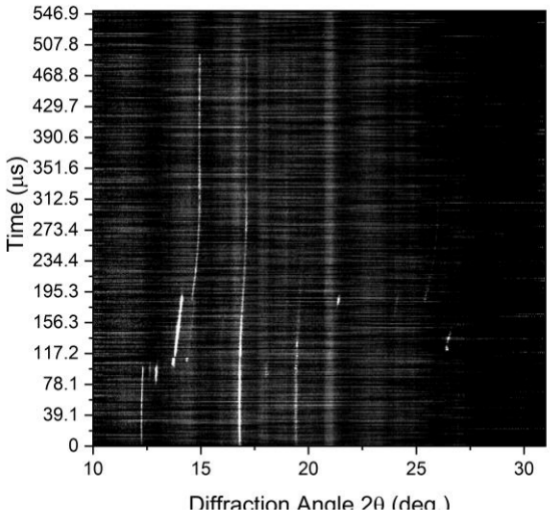

Before each ramp we carried out dry runs to assess heating of the sample and reduced the X-ray fluence until minimal heating was observed. In all the runs we observe the phase transition sequence that has been established from static compression experiments Figure 1. Hence, we do not skip Bi-III in these runs and our preliminary analysis suggests that the Bi-III stability field may be shrinking at these compression rates. Notably, the compression rates we achieved in these runs are much slower than those reported in [6]. Experiments carried out during Exp. 3076 demonstrated that the long pulse trains can be used to cover the entire compression part of the dDAC ramp, and that structural information can be obtained at these extreme compression rates with unparalleled time resolution.

1 O. Degtyareva, M. I. McMahon, and R. J. Nelmes, High Pressure Research 24, 319 (2004).
2 Y. Akahama, H. Kawamura, and A. K. Singh, Journal of Applied Physics 92, 5892 (2002).
3 W. Klement, G. C. Kennedy, and A. Jayaraman, Physical Review 131, 632 (1963).
4 R. J. Husband, et al., Scientific Reports 11, 14859 (2021).
5 D.-L. Yang, et al., Chinese Physics B 28, 036201, 036201 (2019).
6 M. G. Gorman et al., Scientific Reports 8, 16927 (2018).
7 C. M. Pepin, et al., Physical Review B 100, 060101 (2019).
8 R. F. Smith, et al., Physical Review Letters **101**, 065701 (2008).

9 J. B. Hu *et al.*, Applied Physics Letters **103**, 161904, 161904 (2013).
10 M. G. Gorman *et al.*, Applied Physics Letters **114**, 120601 (2019).
11 J. P. Romain, Journal of Applied Physics **45**, 135 (1974).
12 D. B. Larson, Journal of Applied Physics **38**, 1541 (1967).
13 Z. Rosenberg, Journal of Applied Physics **56**, 3328 (1984).

We acknowledge European XFEL in Schenefeld, Germany, for provision of X-ray free-electron laser beamtime at Scientific Instrument HED (High Energy Density Science) and would like to thank the staff for their assistance. The authors are indebted to the HIBEF user consortium for the provision of instrumentation and staff that enabled this experiment. We acknowledge DESY (Hamburg, Germany), a member of the Helmholtz Association HGF, for the provision of experimental facilities. Parts of this research were carried out at PETRA III (beamline P02.2).

A046-03-250823

Hidden pathways of crystallization on H2O at room temperature

G. W. Lee1,2, Y.-H. Lee1, Y.J. Kim1,3*, M. Kim1, Y.C. Cho1

1.Frontier in Extreme Physics, Korea Research Institute of Standards and Science, Daejon, South Korea

2.Applied Measurement Science, University of Science and Technology, Daejon, South Korea

3.Lawrence Livermore National Laboratory, Livermore, CA, USA

gwlee@kriss.re.kr

**current affiliation: LLNL*

Keywords: Crystallization pathways, Supercompressed water, Dynamic diamond anvil cell

Stable phases often form through metastable intermediate phases, which is called Ostwald's step rule. Water has shown abundant phases including metastable phases across various pressure and temperature ranges. Therefore, there exist multiple pathways of phase transition between the phases. In particular, such multiple pathways have been reported at low temperature where kinetic effect becomes dominant, such as recent reports with the observations of low and high density liquid (LDL, and HDL) and low and high density non-crystalline phases (LDN and HDN) by compressing ice Ic and Ih [1], and the discovery of a ice I_h-IX'-XVI'-VIII' pathway during a slow compression[2] and an ice VI- XVβ-XV pathway with proton ordering [3]. However, we expect such phenomena may not be often possible at high temperature, since the kinetics of phase transition is too fast and thermodynamics governs the transition. Due to this reason, we anticipate that the pathways of phase transition may be simple and quite directly occur. Here, we present hidden multiple pathways in water freezing and ice melting at room temperature under highly supecompressed situation. Such a deep metastable condition yields fast transition between the phases which should take more efficient ways for the transition via the metastable phases. Using the dynamic diamond anvil cell (dDAC) in Korea Research Institute of Standards and Science (KRISS), we reveal the hidden freezing and melting pathways of the supercompressed water and ice. We will discuss the mechanism of multiple pathways in solidification of supercompressed water by structural similarity between the phases.

[1] Chuanlong Lin, et.al., Phys. Rev. Lett. 121, 225703, 2018
[2] Chuanlong Lin, et.al., PNAS 115, 2010, 2018
[3] Chris A. Tulk, et.al., Nature 569, 542, 2020

Portions of this work were performed under the auspices of the U.S. Department of Energy by Lawrence Livermore National Laboratory under contract DE-AC52-07NA27344.

A046-04-250823

In situ X-ray diffraction study of shock and release dynamics of SiO_2

K. Appel[1], M. O. Schoelmerich[1,2], A. E. Gleason[3], S. Tracy[4], M. Harmand[5], C. A. Bolme[6], E. Cunningham[3], E. Galtier[3], Y. Inubushi[7,8], K. Katagiri[9], K.Miyanishi[7], B. Nagler[3], N. Ozaki[9], T. R. Preston[1], R. Redmer[10], R. F. Smith[2], T. Tobase[11], T. Togashi[7,8], Y. Umeda[12], L. Wollenweber[1], T. Yabuuchi[7,8], U. Zastrau[1], and T. Tschentscher[1]

1European XFEL Hamburg, Holzkoppel 4, 22869 Schenefeld, Germany, 2Lawrence Livermore National Laboratory, USA, 3SLAC National Accelerator Laboratory, USA, 4Earth and Planets Laboratory, Carnegie Institution of Washington, USA, 5Institute of Mineralogy, Materials Physics and Cosmochemistry, Sorbonne Universités, Paris, 75005, France, 6Los Alamos National Laboratory, USA, 7Physics Institute, RIKEN SPring-8 Center, Sayo-cho, Sayo-gun, Hyogo, 679-5148, Japan, 8Japan Synchrotron Radiation Research Institute, Sayo-cho, Sayo-gun, Hyogo, 679-5198, Japan, 9Osaka University, Suita, Osaka, 565-0871, Japan, 10Rostock University, Germany, 11Center for High-Pressure Science and Technology Advanced Research (HPSTAR), Shanghai, 201203, China 12Institute for Integrated Radiation and Nuclear Science, Kyoto University, Japan.
karen.appel@xfel.eu

Keywords: SiO_2 modifications, dynamic compression, XFEL

SiO_2 and its high-pressure polymorphs are important constituents in geo- and material science, widely investigated due to its role as a major building block in planetary mantles [1]. The high pressure and high temperature (PT) response of SiO_2 at very high PT is essential for understanding planet formation processes and determines evolutionary models of rocky planets and exoplanets from initial solidification to late cooling. With the accessibility of new high P techniques, properties of SiO_2 modifications at high PT conditions have been extensively investigated in static diamond anvil cell experiments and with dynamic compression experiments at different strain rates using either dynamic DACs or gas gun or optical laser induced dynamic compression techniques. Results on equilibrium phase transitions and melting of silica are in stark contrast to results from dynamic compression experiments. Recent experiments using dynamic compression of fused silica and quartz have shown a high-pressure phase transformation to stishovite [2,3] or a respective competing intermediate metastable silica phase [4] at higher pressures compared to static work [5,6].

In this study, we have investigated in situ the structural transformation of α-quartz, fused silica and α-cristobalite on their respective Hugoniot with the use of laser induced shock compression techniques coupled with highly brilliant and coherent femtosecond X-ray pulses that allow to obtain structural snapshots during compression and release. Structural properties were studied with X-ray diffraction and small angle X-ray scattering. We have performed time delay scans over a range of -2 to 200 ns around shock breakout covering states at maximum compression (up to 94 GPa) and subsequent pressure release. Our study reveals that α-quartz and fused silica transform to crystalline stishovite and at higher pressures to a metastable crystalline high-pressure phase whereas cristobalite obtains an amorphous structure during shock transit. At late X-ray probe time delays of up to 200 ns, we furthermore observe a recrystallisation from initially crystalline material (α-quartz and α- cristobalite) but not from vitreous fused silica, which indicates a remaining short-range order within the melt, from which strong coalescence growth can be assumed. Our findings have been backed by density functional theory and molecular dynamics simulations to access phase stabilities during dynamic loading.

1 Duffy, T. N., Madhusudhan, N. and Lee, K. K. M. (2015). *Treatise on Geophysics.* **2**, 149.
2 Gleason, A. E., Bolme, C. A., Lee, H. J., Nagler, B., Galtier, E., Kraus, R., Sandberg, R. et al. (2017). *Nat. Commun*. **8**, 1481.
3 Tracy, S. J., Turneaure, S. J. and Duffy, T. S. (2018). *Phys. Rev. Lett.* **120**, 135702.
4 Tracy, S. J., Turneaure, S. J. and Duffy, T. S. (2020). *Sci. Adv*. **6**, 3913.
5 Dmitriev, V., Toledano, P., Torgashev, V. and Salje, E. (1998). *Phys. Rev.* B **58**, 11911.
6 V. Prakapenka, V., Shen, G., Dubrovinsky, L., Rivers, M. and Sutton, S. (2004). *J. Phys. Chem. Sol.* **65**, 1537.

We acknowledge the LCLS, USA and the SACLA, Japan for granting beamtime under proposal LS84 in 2018 and proposal 2019A8072 in 2019. We would like to thank the European XFEL for supporting and hosting the project. We wish to acknowledge the Deutsche Forschungsgemeinschaft (DFG) for the funding support via the Research Unit FOR 2440 Matter under Planetary Interior Conditions and DFG project AP262/2-1.

A046-05-250823

Negative linear compressibility and tuneable phase transition sequence in selenium and selected high entropy oxides under high pressure conditions *via* compressional rate control

Lisa Luhongwang Liu[1,2], Arthur Haozhe Liu[3]

1. *University of Illinois at Urbana Champaign, IL, 61801, USA*
2. *SHARPS, Shanghai, 201203, China*
3. *HPSTAR, Beijing, 100094, China*

Haozhe.liu@hpstar.ac.cn, lisaliu@illinois.edu

Keywords: High pressure, Negative linear compressibility, Phase transitions

The behaviour of crystalline materials under high pressure extreme conditions attracted great deal of interest. Unusual behaviour, such as various types of negative linear compressibility (NLC) were reported but not fully understood. NLC is a rare phenomenon where a crystal expands along one direction under hydrostatic compression. In this presentation, several selected systems were *in situ* studied in diamond anvil cell (DAC) under high pressure using synchrotron x-ray diffraction at over 100 GPa conditions. For example, in selenium case, the two types of NLC mechanism were found at various pressure regions, i. e. at around 10 GPa, and around 120 GPa, respectively, in this same elemental sample [1, 2]. By adjusting the compressional rate, from relatively slow at about 0.5 GPa/s to relatively fast at over 200 GPa/s in dynamic DAC, the modified or even disappearance of NLC behaviour and tuneable phase transition sequences were discovered in selenium and selected high entropy oxides, which reveal the kinetic effect of the compressional rate on the NLC and phase boundaries under strong compression.

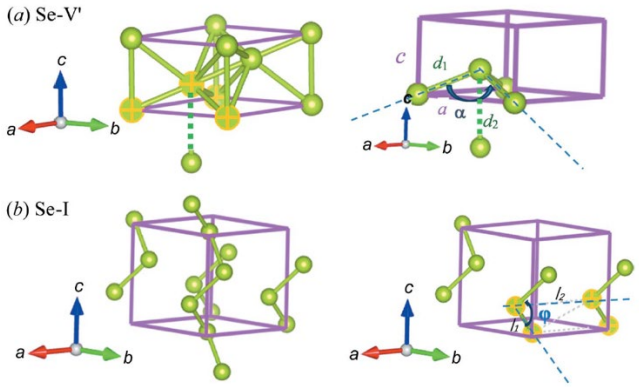

Figure 1. Schematism of geometrical interpretation of negative linear compressibility in the structures of phase (a) Se-V'; (b) Se-I at around 120 GPa and 10 GPa, respectively.

[1] Shuhua Yuan, Luhong Wang, Sheng-cai Zhu, Fuyang Liu, Dongzhou Zhang, Vitali B. Prakapenka, Sergey Tkachev, Haozhe Liu, Negative linear compressibility in Se at ultra-high pressure above 120 GPa, (2022). *IUCrJ*, **9**, 253.
[2] Kamil F. Dziubek, Negative linear compressibility at extreme pressure, (2022). *IUCrJ*, **9**, 165.

This work was supported by the Natural Science Foundation of China. Portions of this work were performed at GeoSoilEnviroCARS (The University of Chicago, Sector 13) and HPCAT (Sector 16), Advanced Photon Source (APS), Argonne National Laboratory. GeoSoilEnviroCARS is supported by the National Science Foundation – Earth Sciences (EAR – 1634415) and Department of Energy- GeoSciences (DE-FG02-94ER14466). HPCAT operations are supported by DOE-NNSA's Office of Experimental Sciences. This research used resources of the Advanced Photon Source, a U.S. Department of Energy (DOE) Office of Science User Facility operated for the DOE Office of Science by Argonne National Laboratory under Contract No. DE-AC02-06CH11357.

A046-06-250823

Probing off-Hugoniot states in laser-driven, shock-ramp experiments

A.L. Coleman[1], R.F. Smith[1], T. Lockard[1], K. Alidoost[1], K. R. Maskaly[1], D.C. Swift[1], J.M. McNaney[1]

[1]*Lawrence Livermore National Laboratory, Livermore, California 94500, USA*

coleman55@llnl.gov

Keywords: Dynamic-Compression, Extreme-Conditions, High-Pressure

Dynamic compression is one of the most potent techniques for exploring materials at extreme conditions. High-pressure, high-temperature states can be accessed using shock compression to a point on a Hugoniot curve, while high-pressure, lower-temperature conditions can be reached using ramp -compression on a quasi-isentrope. Both techniques have been used at the National Ignition Facility (NIF) to access material states in the terapascal regime [1,2] and the implementation of x-ray diffraction diagnostics in such experiments has yielded structural information on materials at conditions previously inaccessible to the high-pressure community.

As we strive to define more complete phase diagrams and to better characterize materials in high-pressure regimes, we must look to techniques outside of shock, and ramp compression to access thermodynamic compression paths between the Hugoniot and quasi-isentrope. With high precision laser pulse shaping at facilities such as NIF and the Omega-EP laser, and state of the art target synthesis techniques, combined shock and ramp compression can now be employed to tailor the region of phase space accessible under dynamic compression. This talk presents the challenges and successes of shock-ramp experimental implementation on various materials at high-energy laser facilities such as NIF and Omega-EP. These techniques are combined with in situ nano-second x-ray diffraction, which serves as a structural probe to identify phase boundaries at extreme conditions.

This work was performed under the auspices of the U.S. Department of Energy by Lawrence Livermore National Laboratory under Contract DE-AC52-07NA27344

1 Lazicki, A., McGonegle, D., Rygg, J.R., *et. al,* (2021) Nature, **589**, 532
2 Smith, R.F., Eggert, J.H., Jeanloz, R. *et. al,* (2014) Nature, **511**, 330

A053-01-250823

Topological magnetic structures in MnGe: Neutron diffraction and symmetry analysis

Pomjakushin[1], I. Plokhikh[2], J. S. White[1], Y. Fujishiro[3], N. Kanazawa[4], Y. Tokura[5], and E. Pomjakushina[2]

[1]Laboratory for Neutron Scattering and Imaging (LNS), Paul Scherrer Institut (PSI), CH-5232 Villigen Switzerland, [2]Laboratory for Multiscale Materials Experiments (LMX), Paul Scherrer Institut, CH-5232 Villigen PSI, Switzerland, [3]RIKEN Center for Emergent Matter Science (CEMS), Wako, Saitama 351-0198, Japan, [4]Department of Applied Physics, The University of Tokyo, Bunkyo-ku, Tokyo 113-8656, Japan, [5]Department of Applied Physics, The University of Tokyo, Bunkyo-ku, Tokyo 113-8656, Japan and RIKEN Center for Emergent Matter Science (CEMS), Wako, Saitama 351-0198, Japan

vladimir.pomjakushin@psi.ch

Keywords: Magnetic SuperSpace Group MSSG, isotropy subgroup, magCIF, magnetic structure, neutron diffraction

From new neutron powder diffraction experiments on the chiral cubic (*P213*) magnet manganese germanide (MnGe), we analyze all of the possible crystal symmetry-allowed magnetic superstructures that are determined successfully from the data [1]. The incommensurate propagation vectors *k* of the magnetic structure are found to be aligned with the [100] cubic axes, and correspond to a magnetic periodicity of about 30 Å at 1.8 K. Several maximal crystallographic symmetry magnetic structures are found to fit the data equally well and are presented. These include topologically nontrivial magnetic hedgehog and "skyrmion" structures in multi-k cubic or orthorhombic 3+3 (No.198.3.206.1.m10.2, 19.3.95.4.m26.4) and orthorhombic 3+2 (No. 19.2.29.2.m26.3) dimensional magnetic superspace groups (MSSG) respectively, with either potentially responsible for topological Hall effect (THE). The presence of orthorhombic distortions in the space group *P212121* (No. 19) caused by the transition to the magnetically ordered state does not favor the cubic magnetic hedgehog structure, and leave both orthorhombic hedgehog and skyrmion models as equal candidates for the magnetic structures. We also report on a new combined mechanochemical and solid-state chemical route to synthesize MnGe at ambient pressures and moderate temperatures, and compare with samples obtained by the traditional high pressure synthesis.

The magnetic structures in MnGe are compared with topological magnetism in the candidate magnetic Weyl semimetal CeAlGe [2], where the topological properties of a phase stable at intermediate magnetic fields parallel to the *c* axis are suggested by observation of the THE as well. CeAlGe has polar tetragonal *I41md* crystal symmetry with the magnetic structure based on two propagation vectors along [100] and [010] axes in tetragonal plane with periodicity about 70 Å. The multi-*k* structure is realised in maximal symmetry 3+2 dimensional tetragonal MSSG (No. 109.2.67.4.m240.2).

Both 3+2 structures in MnGe and CeAlGe host lattices of magnetic particle-like objects called (anti)merons $Q=\pm 1/2$ with half-integer topological numbers. Calculations show that in the external magnetic fields perpendicular to the propagation plane the total charge per magnetic cell abruptly changes from $Q=0$ to skyrmion-like charge $|Q|=1$ in accordance with is the experimental observation of the THE.

1 V. Pomjakushin, I. Plokhikh, J. S. White, Y. Fujishiro, N. Kanazawa, Y. Tokura, and E. Pomjakushina, Phys. Rev. B **107**, 024410 (2023)

2 P. Puphal, V. Pomjakushin, N. Kanazawa, V. Ukleev, D. J. Gawryluk, J. Ma, M. Naamneh, N. C. Plumb, L. Keller, R. Cubitt, E. Pomjakushina, and J. S. White, Phys. Rev. Lett. **124**, 017202 (2020)

A053-02-250823

New incommensurate magnetic phases in the multiferroic compound $MnCr_2O_4$.

Pardo Sainz[1,7], A Toshima[2], G. André[3], J Basbús[4], G. Cuello[5], T. Honda[6], T Otomo[6], K Inoue[2], Y Kousaka[7,2], J Campo[1,*]

[1]Aragón Nanoscience and Materials Institute (CSIC-University of Zaragoza), [2]Chirality Research Center and Institute for Advanced Materials Research (Hiroshima University), [3]Laboratoire Leon Brillouin, [4]Centro Atómico de Bariloche, [5]Institut Laue Langevin, [6]Institute of Materials Structure Science, Tsukuba, [7]Osaka Metropolitan University,

**email javier.campo@csic.es*

Keywords: incommensurate phases, magnetic symmetry, magnetic superspace groups

Nowadays, chromium-based normal spinel oxides ACr_2O_4 are one of the most studied materials in the condensed matter community due to the interplay between its magnetic, electric and structural properties [1,2]. In particular, for $MnCr_2O4$, the ground state magnetic structure is still controversial because the magnetic structures reported by different groups and investigated by independent techniques are inconsistent [1-3].

The magnetic structure of this compound was reinvestigated by magnetization, specific heat and neutron diffraction experiments at different temperatures. The results revealed that a new magnetic phase, not previously reported, is developed below 18 K. The magnetic phases present in this sample were: ferrimagnetic order below T_C = 45 K; conical spin order with propagation vector K_{S1}= (0.62(1), 0.62(1), 0) below T_{S1} = 20 K; and conical spin order with propagation vector K_{S2}=(0.660(3), 0.600(1), 0.200(1)) below T_{S2} =18K.

Using the super-space group formalism, the symmetry of the nuclear and magnetic structures is determined (see figure 1). Through simple theoretical calculations, we derive the directions along which the electric polarization lies for each magnetic phase.

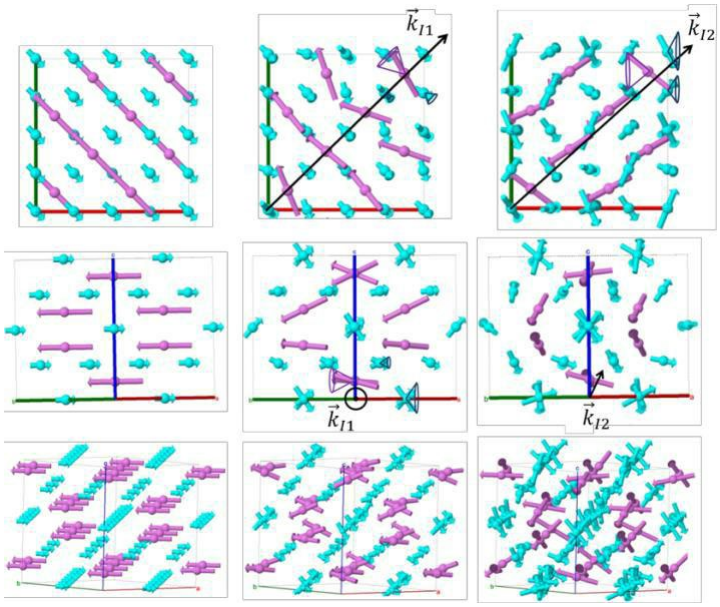

Figure 1. Scheme of the magnetic structures for each of the 2 different phases

1 K. Dey et al., Journal of Magnetism and Magnetic Materials 435, 15 (2017).
2 K. Tomiyasu et al., Phys. Rev. B 70, 214434 (2004).
3 J. M. Hastings and L. M. Corliss, Phys. Rev. 126, 556 (1962).

A053-03-250823

The unified (UNI) system of magnetic space-group symbols

Branton J Campbell[1], Harold T Stokes[1], J. Manuel Perez-Mato[2], Juan Rodríguez-Carvajal[3]

[1]Physics & Astronomy, Brigham Young University, Provo, Utah, 84602, USA. [2]Facultad de Ciencia y Tecnología, Univ. del País Vasco, Apdo. 644, Bilbao, 48080, Spain. [3]Diffraction Group, Institut Max Von Laue - Paul Langevin (ILL), 71 Avenue des Martyrs, CS 20156, Grenoble, 38042, France

branton_campbell@byu.edu

Keywords: magnetic space group, symmetry, UNI

The symbol used to represent a crystallographic symmetry group plays an important role in our understanding of the group elements and their restrictions on physical properties. In recent decades, the two commonly used symbols (with accompanying numbers and settings) for representing the 1651 three-dimensional magnetic space groups (MSGs) were those of Belov-Neronova-Smirnova (BNS) and of Opechowski-Guccione (OG). Both of these symbols present challenges of interpretation to novice and expert users alike, which can inhibit understanding and lead to errors in published magnetic structures.

To address these challenges going forward, we introduce a new unified (UNI) MSG symbol [1], which combines a modified BNS symbol with essential information from the OG symbol. The UNI symbol is easier to interpret correctly than previous MSG symbols, at the expense of some compactness. The UNI MSG symbol (1) is true to the spirit of the Hermann-Mauguin symbols and settings used in the International Tables for Crystallography, (2) clearly conveys the magnetic point group (MPG) of the MSG, (3) explicitly communicates the translational part of the time-reversal generator of each type-4 MSG, (4) separates the time-reversal from other generators for clarity, (5) distinguishes each type-1 MSG from the corresponding non-magnetic space group, and (6) and reveals the conventional lattice centering of both the MSG itself and the underlying non-magnetic family space group (FSG).

[1] Branton J. Campbell, Harold T Stokes, J. Manuel Perez-Mato, and Juan Rodríguez-Carvajal, *Acta Cryst.* **A** 78, 99-106 (2022).

A053-04-250823

MAGNDATA, the database of magnetic structures in the Bilbao crystallographic server, reaches 2,000 entries

J.M. Perez-Mato[1], E. S. Tasci[2], G. Madariaga[3], L. Elcoro[3], G. de la Flor[4], M. I. Aroyo[3], J. Gabirondo-Lopez[3]

[1]Facultad de Ciencia y Tecnología, Universidad del País Vasco, UPV/EHU, Apdo. 644, 48080 Bilbao, Spain. [2]Department of Physics Engineering, Hacettepe University, Ankara 06800, Turkey. [3]Departamento de Física, Universidad del País Vasco UPV/EHU, Leioa, Spain. [4]Institute of Applied Geosciences, Karlsruhe Institute of Technology, Karlsruhe, Germany.

jm.perezmato@gmail.com

Keywords: Magnetic structures, Database, Magnetic symmetry, Bilbao Crystallographic Server

Back in 2014, we started to collect published magnetic structures and made them available in the Bilbao Crystallographic Server (BCS) within the program named MAGNDATA. Based on the thesis work of Samuel V. Gallego, this program accumulated by 2016 about 400 magnetic structures, all described under a standardized methodology using either magnetic space groups (MSGs) or magnetic superspace groups (MSSGs) depending on the structure being commensurate or incommensurate [1,2]. The build-up of this incipient database of magnetic structures was possible thanks to the design of the magCIF file format, which under the auspices of the *Commission on Magnetic Structures* of the *IUCr* was being developed at this time by a team headed by Branton J. Campbell. This extension of the CIF (Crystal Information Framework) dictionary, formally approved by the IUCr in 2016, is a natural generalization of the CIF format for non-magnetic structures. It uses in a standardized way, analogous to that employed in ordinary crystallography, the symmetry constraints of the magnetic group to produce a simple and unambiguous description of the magnetic structure. The listing of the magnetic moments (and their modulations in the case of incommensurate structures), together with the atomic positions, is then restricted to an asymmetric unit under the relevant magnetic group. The magCIF format was rapidly implemented in most of the available computer tools for the analysis, visualization and determination of magnetic structures, allowing a direct communication among all these programs. In particular, during a visit in Bilbao, Robert M. Hanson, made the program Jmol fully compatible with magCIF files, both commensurate and incommensurate, and through his collaboration Jmol became the basic visualization tool of MAGNDATA. Also Koichi Momma kindly accepted our request and implemented the magCIF format in his program VESTA (for the moment only of commensurate structures), and VESTA came to be a very important help both for generating and checking new entries, and as an additional visualization tool in the database.

Since 2016, new entries are being steadily introduced. In June 2020 the collection had more than 1,000 magnetic structures, and by the time of this congress, it will have surpassed 2,000. Considering that the number of published magnetic structures with enough information may be several thousands and every year some hundred new ones are published, the database is still far from being complete, but its size is already very significant and allows massive searches and analyses (see for instance [3,4]). One must however emphasize that MAGNDATA does not make any validation check. Therefore *the presence of a magnetic structure in the database is no guarantee of its correctness*. In fact, it is not uncommon to find conflicting models of the same structure. In order to introduce a new structure the fundamental step is the construction of an appropriate magCIF file. This implies to interpret and translate the information of the original paper into the mentioned standardized description. In many cases this requires to identify for the first time the magnetic symmetry group of the proposed structure. This is usually done using the tools available in the magnetic section of the BCS or, specially in the case of incommensurate structures, in the ISOTROPY webpage [5]. Although the situation is improving, often the information provided in the article, specially in the case of incommensurate structures, is unfortunately incomplete or ambiguous, and these structures have been necesssarily discarded.

In the long term MAGNDATA can only be kept updated, if the authors actively participate and directly submit their new published structures to the database in the form of magCIF files. This can be easily done following the instructions available in the webpage of the program. We hope that through the generalized use of this new direct submission option, MAGNDATA will consolidate as a freely available and very useful research tool in the field.

[1] Gallego, S.V. , Perez-Mato, J. M., Elcoro, L., Tasci, E. R., Hanson, R. M., Momma, K., Aroyo, M. I. & Madariaga, G. (2016). *J. Appl. Cryst.* **49**, 1750

1 Gallego, S.V. , Perez-Mato, J. M., Elcoro, L., Tasci, E. R., Hanson, R. M., Aroyo, M. I. & Madariaga, G. (2016). *J. Appl. Cryst.* **49**, 1941

2 Xu, Y., Elcoro, L., Song, Z-D., Wieder, B.J., Vergniory, M.G., Regnault, N., Chen, Y., Felser C. & Bernevig, B.A. (2020) Nature, 586, 702

3 Zhang, H. (2021) Electronic Structure **3**, 033001

4 Stokes, H.T., Hatch, D.M. & Campbell, B.J., ISOTROPY Software Suite, iso.byu.edu.

A053-05-250823

Antiferromagnetic domains distribution carried by stoichiometry

A. Mandziak [1]*, C. Granados-Miralles[2], A. Berja[2] A. Quesada[2] , J. E. Prieto[3], M. Foerster[4], L. Aballe[4] , M. A. Nino4, J. de la Figuera[3] and P. Nita[5]

[1]National Synchrotron Radiation Centre SOLARIS, Jagiellonian University, 30392 Cracow, Poland
[2]Instituto de Cerámica y Vidrio (CSIC), Madrid 28049, Spain
[3]Instituto de Química Física "Rocasolano", Madrid, 28006, Spain
[4]Alba Synchrotron Light Facility, CELLS, Barcelona E-08290, Spain
[5]Faculty of Physics, Astronomy and Applied Computer Science, Jagiellonian University, 30348 Cracow, Poland

Email: anna.mandziak@uj.edu.pl

Antiferromagnets are (AFM) promising materials for future spintronic applications owing to their advantageous properties: They are magnetically ordered, but neighboring magnetic moments point in opposite directions, which results in zero net magnetization. This means antiferromagnets produce no stray fields and are insensitive to external magnetic field perturbations. Furthermore, they show intrinsic high frequency dynamics (in THz regime), exhibit considerable spin–orbit and magneto-transport effects. Over the past decade, it has been realized that antiferromagnets have more to offer than just being utilized as a components in exchange bias applications. In a wide variety of AFM materials, transition metal oxides (e.g. NiO or CoO) play an important role due to their properties. These properties are especially evident in systems of reduced dimensionality, as pointed out by a number of studies [1, 2]. However, in thin film growth, as necessary for devices, the quality is often disappointing, dictated by the defect density.

Here we demonstrate a route for preparing high quality ultrathin antiferromagnetic oxide films on a metallic substrate. Mixed nickel-cobalt oxides have been grown on Ru(0001) by high temperature oxygen-assisted molecular beam epitaxy. A comprehensive characterization is performed combining LEEM and LEED for structural characterization and PEEM (PhotoEmission Electron Microscopy) with synchrotron radiation for chemical and magnetic analysis via X-ray Absorption Spectroscopy and X-ray Magnetic Linear Dichroism (XAS-PEEM and XMLD-PEEM, respectively).

Depending on the chosen stochiometry the growth leads to the formation of high quality 2D islands of different compositions. The high crystalline and morphological quality of prepared films result in optimized properties with respect to films grown by other methods, such as magnetic domains, larger by several orders of magnitude. By means of vectorial magnetometry, the spin axis orientation was determined with nanometer spatial resolution, and found to depend on the Ni:Co ratio.

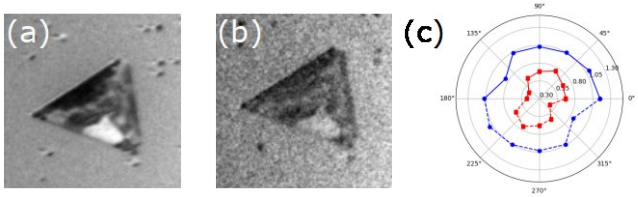

Figure 1. XMLD PEEM images obtained at (a) Co and (b) Ni edge. (c) Polar plots with the experimental L_2 ratio extracted from single domain area for Co (red) and Ni (blue).

Acknowledgements: This research was funded by the SciMat Priority Research Area budget under the program "Excellence Initative - Research University" at the Jagiellonian University in Kraków - Grant No. 75.1920.2021

[1] D. Alders et al. *Temperature and thickness dependence of magnetic moments in NiO epitaxial films*. Phys. Rev. B, 1998. doi:10.1103/PhysRevB.57.11623.
[2] S. D. Peacor and T. Hibma. *Reflection high-energy electron diffraction study of the growth of NiO and CoO thin films by molecular beam epitaxy*. Surf. Sci., 1994. doi:10.1016/0039-6028(94)91283-1.

A053-06-250823

Implementation strategy of magnetic space group in spglib

A. Togo[1,2], K. Shinohara[3], I. Tanaka[2,3]

1. *Research and Services Division of Materials Data and Integrated System, National Institute for Materials Science, 2. Center for Elements Strategy Initiative for Structural Materials, Kyoto University, 3. Department of Materials Science and Engineering,*

Kyoto University

togo.atsushi@nims.go.jp

Keywords: Magnetic space group, Software development

In computer simulation of solids, e.g., first-principles calculation and phonon calculation, use of crystal symmetry is essential to efficiently compute physical quantities and to improve the numerical accuracy. Therefore, detailed application of crystal symmetry information must be implemented everywhere in the calculation code. Usually, in those codes, geometry of the input crystal structure is given without space group information, e.g., basis vectors and point coordinates and types of atoms are only given. Then, space group information is searched on the fly in those codes. We have been developing a crystal symmetry search software library, spglib [1], which is distributed under a permissive free software license. Using spglib, each of those simulation codes is unnecessary to implement its own symmetry search routine. Spglib searches symmetry operations in matrix representation. From the symmetry operations, space group type is identified by matching to the datasets of space group types. Since the input crystal structure may have different orientation and origin from those expected by the datasets, the identification requires transformation of the symmetry operations, which is not a trivial task. In the implementation of the space group type identification, we followed the algorithm reported by Grosse-Kunstleve [2] and used the datasets provided by Seto [3]. Symmetrization of a given distorted crystal structure is another important feature of spglib.

Recently, spglib was extended to support magnetic space group (MSG) [4]. In our talk, algorithms for determining magnetic symmetry operations of magnetic crystal structures, identifying magnetic space group types by matching to the MSG datasets [5], and symmetrizing the magnetic crystal structures using the MSGs will be presented. The determination of magnetic symmetry operations is implemented with minimal modifications from the existing code written for space group. MSG types are identified by combining space group type identification and the use of affine normalizers. Point coordinates and magnetic moments of the magnetic crystal structures are symmetrized by projection operators for the MSGs. Fig. 1 shows an illustration of group-subgroup relationship among MSG related groups. (***A***, ***X***, ***T***, ***M***) represents basis vectors, point coordinates of atoms, atomic types, and magnetic moments, respectively. *S, F, D, M* are the space group, family space group, maximal space subgroup, and MSG, respectively. MSG and MSG type are determined as follows. (1) *S* is determined ignoring ***M***. (2) *M* is searched using information of *S* with considering ***M***. (3) *F* and *D* are constructed from *M*. (1), (2), (3) are performed in the matrix representation. To identify MSG type, obtained symmetry operations of *M* are transformed to match the dataset of an MSG type. Therefore, the identification reduces to the problem of finding the transformation, for which *F* and *D* are used systematically. Depending on construction types (I, II, III, IV) and crystal families, different identification algorithms are used. To tolerate distortion of ***M*** is important for practical use, however, it is one of the most difficult parts to implement.

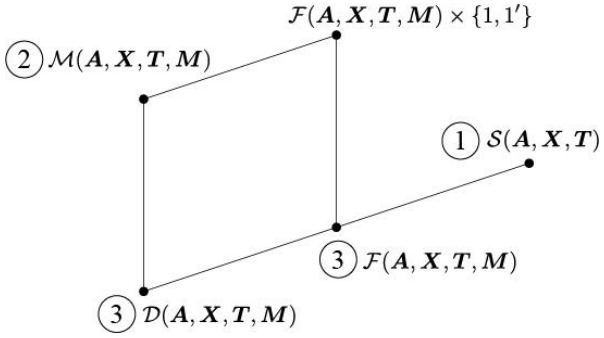

Figure 1. Group-subgroup relationships of MSG related groups [4]

[1] Spglib software project, https://spglib.github.io/spglib, https://github.com/spglib/spglib.
[2] Grosse-Kunstleve, R. W. (1999). Acta Cryst. A, 55(2-2):383–395.
[3] https://yseto.net/
[4] Shinohara, K., Togo, A. & Tanaka, I. (2022). arxiv.2211.15008
[5] González-Platas, J., Katcho, N. A. & Rodríguez-Carvajal, J. (2021). J. Appl. Crystallogr. 54(1), 338–342

This work was supported by MEXT Japan through ESISM (Elements Strategy Initiative for Structural Materials) of Kyoto University, JSPS KAKENHI Grant Number JP21K04632 and JSPS Research Fellows Grant Number 21J10712.

A075 Total Scattering Studies of Disordered Materials

Room 212

1.10pm – 3:30pm

A075-01-250823

Structural complexity in amorphous calcium carbonate

T. C. Nicholas[1], A. E. Stones[2], A. Patel[1], F. M. Michel[3], R. J. Reeder[4], V. L. Deringer[1], A. L. Goodwin[1]

[1]Inorganic Chemistry Laboratory, Department of Chemistry, University of Oxford, Oxford, UK [2]Physical and Theoretical Chemistry Laboratory, Department of Chemistry, University of Oxford, UK [3]Department of Geosciences, Virginia Tech, Blacksburg VA, USA [4]Department of Geosciences, Stony Brook University, Stony Brook NY, USA

thomas.nicholas@chem.ox.ac.uk

Keywords: amorphous modelling, effective pair potential, geometric frustration

Amorphous calcium carbonate (ACC) is an important metastable precursor for marine organism biomineralisation processes. However, the origin of the metastability of ACC is currently not well understood. Here, we use hybrid reverse Monte Carlo (HRMC) to generate atomistic models of ACC, driven by *both* experimental total scattering measurements [1] *and* interatomic potentials [2].

Using a recently-developed algorithm [3], we inverted the Ca—Ca pair correlation function from our HRMC model to obtain the effective Ca—Ca interaction potential. The form of this interaction resembles a Lennard-Jones—Gaussian (LJG) potential, characterised by two competing length scales [4]. This competition is known to frustrate crystallisation. The parameterisation of the LJG potential for ACC highlights the origin of geometric frustration in this system; namely, two distinct carbonate-bridging motifs (Fig. 1).

Simulations driven by this effective Ca—Ca potential recover the two dominant characteristics of the ACC structure model: a heterogeneous structure, and a resilience to crystallisation. We therefore attribute both features to the geometric frustration encoded in the effective interactions between calcium ions.

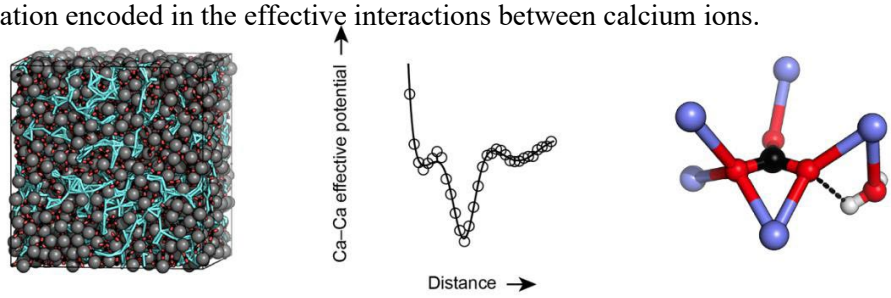

Figure 1. *Left*: representation of ACC structure model obtained using HRMC. *Middle*: schematic representation of the effective Ca—Ca interaction potential obtained by inverting the high quality Ca—Ca pair correlation function derived from our model.

Right: representative carbonate coordination environment. Note the two possible Ca—CO_3—Ca motifs: pairs of Ca atoms with a common oxygen donor, and those connected across the carbonate molecule (e.g. Ca—O—C—O—Ca pathway).

1 Michel, F. M., MacDonald, J., Feng, J., Phillips, B. L., Ehm, L., Tarabrella, C., Parise, J. B. & Reeder, R. J. (2008). *Chem. Mater.* **20**, 4720—4728.
2 Raiteri, P., Gale, J. D., Quigley, D. & Rodger, P. M. (2010). *J. Phys. Chem. C* **114**, 5997—6010.
3 Stones, A. E., Dullens, R. P. A. & Aarts, D. G. A. L. (2019). *Phys. Rev. Lett.* **123**, 098002.
4 Dshemuchadse, J., Damasceno, P. F., Phillips, C. L., Engel, M. & Glotzer, S. C. (2021). *Proc. Natl. Acad. Sci. U.S.A.* **118**, e2024034118.

A075-02-250823

Machine learning assisted reverse Monte Carlo modeling for neutron total scattering data

Y. P. Zhang[1], P. Cuillier[2], M. G. Tucker[1]

[1]Neutron Scattering Division, Oak Ridge National Laboratory, 1 Bethel Valley Rd. Tn, 37830. [2]Materials Science and Engineering, Ohio State University, 122 Hitchcock Hall, 2070 Neil Avenue, Columbus, OH 43210.

Keywords: Reverse Monte Carlo, Machine Learning, LAMMPS

In the area of atomic-level structure modelling, there are two well-known parallel problems. The theory driven modelling usually cannot fully account for the disorder of practical system and therefore may fail to reproduce the complete picture of structure model as observed experimentally. The data driven approach tries to derive the structural model from the experimental data in a reverse manner (i.e., data to model) and therefore naturally is able to catch features observed experimentally. But quite often it lacks the accurate coverage of energetic landscape from the theoretical perspective. In this contribution, we aim at bringing in a novel approach combining the theoretical and experimental considerations. To realize this, the LAMMPS module for energy calculation is implemented into the reverse Monte Carlo routine (here, the RMCProfile package was used) for modelling total scattering data. Through such a combined approach, atomic positions would be adjusted according to the agreement with experimental scattering data and the energy landscape simultaneously. Specifically concerning the energy calculation, the Gaussian processing-based machine learning routine for potential field construction is employed here. Such an approach, at the same time providing density functional theory level of accuracy, guarantees a reasonably short computational time which is required for the metropolis algorithm for structure modelling. The LAMMPS implemented RMCProfile package for conducting the combined modelling is generally applicable to utilize neutron and X-ray total scattering data, X-ray absorption spectroscopy data, electron scattering data, etc. for structure modelling to provide insights into structure-property link of general condensed matter systems.

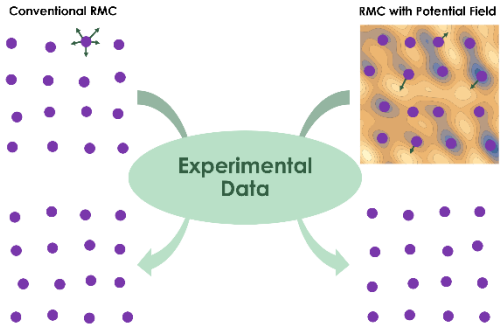

Figure 1. RMC+LAMMPS for driving atomic configuration.

[1] Vandermause, J., Torrisi, S. B., Batzner, S., Xie, Y., Sun, L. X., Kolpak, A. M. & Kozinsky, B. (2020). *Npj Comput. Mater.*, **6**, 20.
[2] Zhang, Y., Eremenko, M., Krayzman, V., Tucker, M. G., Levin, I. (2020). *J. Appl. Cryst.*, **53**, 1509-1518.
[3] Tucker, M. G., Keen, D. A., Dove, M. T., Goodwin, A. L., Hui, Q. (2007), *J. Phys. Condens. Matter*, **19**, 335218.

A075-03-250823

"Polar Nano-Regions" originated from local displacive correlations in relaxor-ferroelectrics

N. Zhang, Z. Wang, Z. An, F. Li, Z.-G. Ye

Electronic Materials Research Laboratory, Key Laboratory of the Ministry of Education & International Center for Dielectric Research, School of Electronic and Information Engineering, Xi'an Jiaotong University, Xi'an 710049, China; Department of Chemistry and 4D LABS, Simon Fraser University, 8888 University Drive, Burnaby, British Columbia V5A 1S6, Canada

nzhang1@xjtu.edu.cn

Keywords: Pair Distribution Function, Relaxors, Polar-nano regions

Relaxor-ferroelectric is a family of functional perovskites possessing complex locally disordered structures. The existence of the so-called "polar-nano regions" (PNRs), in which the local polarizations have different orientations with the matrix, is believed to be responsible for the dielectric relaxation behaviour and high piezoelectricity. With increasing temperatures, the PNRs change in size and dynamic frequency of polarization. However, because of the small size of the PNRs, direct observation is still lacking, which makes many theories about PNRs under extensive debate.

In this work, we performed neutron atomic pair distribution function (PDF) analysis to study the local-structural features of several relaxor-ferroelectric materials at low temperatures. The PDF profile reveals a much stronger correlation of atomic displacements in the very-short-*r* range compared with the classical ferroelectrics [1][2]. Different from the traditional view of relaxor materials, our structural modeling results suggest that the key factor differentiating the structures in the short- and medium-*r* ranges is the displacement correlation rather than the structural symmetry. In different systems with different average structures, the local symmetry varies, but the variation of the strength of correlation between the nano-regions and the matrix persists. Therefore, we conclude that the characteristics of the PNRs, including their formation and sizes, are governed by the displacive correlation [3]. The temperature-dependent correlation change also reflects the macroscopic dielectric properties [4]. This finding provides a better understanding of the unique disordering structural characteristics of relaxor-$PbTiO_3$ materials.

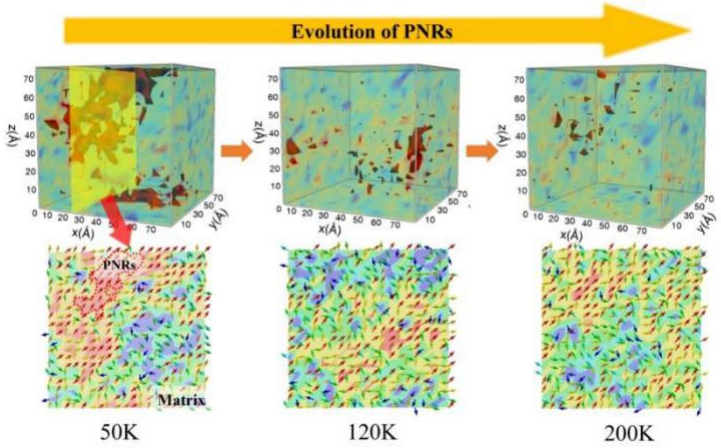

Figure 1. Correlation change as a function of temperature in $0.72Pb(Mg_{1/3}Nb_{2/3})O_3$–$0.28PbTiO_3$ [3].

[1] Zhang, N., Yokota, H., Glazer, A. M., Ren, Z., Keen, D. A., Keeble, D. S., Thomas, P. A. & Ye, Z.-G. (2014) *Nat. Commun.***5,** 5231.
[2] Zhang, N., Yokota, H., Glazer, A. M., Keen, D. A., Gorfman, S., Thomas, P. A., Ren, W. & Ye, Z.-G. (2018). *IUCrJ.*, **5**, 73-81.
[3] Wang, Z., An, Z., Zhuang, J., Li, F., Ren, W., Ye, Z.-G. & Zhang, N. (2022). *J. Mater. Chem. C* **10**, 16731-16738.
[4] Li, F., Zhang, S., Yang, T., Xu, Z., Zhang, N., Liu, G., Wang, J., Cheng, Z., Ye, Z.-G., Luo, J., Shrout, T. R. & Chen, L.-Q. (2016) *Nat. Commun.* **7**, 13807.

A075-04-250823

PDF characterization of fine effects in supported Pd and Pt nanoparticles catalysts during activation in liquid phase

Bonavia[1,2], A. Ricchebuono[2], E. Vottero[2], R. Pellegrini[3], A. Piovano[4], E. Groppo[2], D. Ferri[5], S. Checchia[1]

1, ID15A European Synchrotron Radiation Facility, Grenoble, France; 2, Department of Chemistry, NIS and INSTM, University of Turin, Turin, Italy; 3, Chimet SpA – Catalysts Division, Viciomaggio Arezzo, Italy; 4, Institut Laue-Langevin, Grenoble, France; 5, Paul Scherrer Institute, Villigen, Switzerland

Corresponding author: daniele.bonavia@esrf.fr

Keywords: Nanoparticles, PDF, time-resolved, liquid environment

Pd and Pt heterogeneous catalysts are widely used in hydrogenation reactions for the synthesis of fine and bulk chemicals, which are often conducted in liquid phase. Since the active phases are commonly deposited in their oxidised form on the support, building on previous works [1-2] we sought to study how the catalyst activation procedure affects the reducibility of the oxide phase, as well as the properties of the supported nanoparticles and how these correlate with the catalyst behaviour during hydrogenation. We carried out experiments in liquid phase at various temperatures, at different nature and concentrations of the reducing agent, and in three solvents to isolate the kinetics and dynamics of the reduction of the oxide phases (PdO, PtO) and the formation of metallic (Pd, Pt) and hydride (PdH, PtH) phases.

At the ESRF beamline ID15A we used High-Energy X-Ray Diffraction (HE-XRD) and Pair Distribution Function Analysis (PDF) to quantify hydride, metallic, and oxide phases in both average and local structure, and thus separate long-range from short-range structural effects overcoming the complications of investigating a heterogeneous catalyst in a liquid environment through total scattering: parasitic signals, competing side reactions and thermodynamic limitations involving the solvent.

In the case of Pd nanoparticles (size ~ 2.4 nm) PDF was used to follow the consumption of PdO upon reduction, the subsequent formation of metallic Pd and the nucleation of a bulk Pd hydride phase with a time resolution of 1s. Analysing the ΔPDF on this timescale (Fig.1A) allowed us to determine the kinetics of formation of metallic Pd and Pd hydrides. By testing various reducing agents at different concentration in three different solvents we observed different kinetics, suggesting a different extent of reducing ability. Fast-scanning XAS measurements performed on X10DA at SLS independently confirmed the reliability of the PDF data timescale. FT-EXAFS and MCR analysis confirmed what PDF highlighted in the first place: the formation of PdH does not start until all of the PdO has been reduced to Pd (Fig.1B).

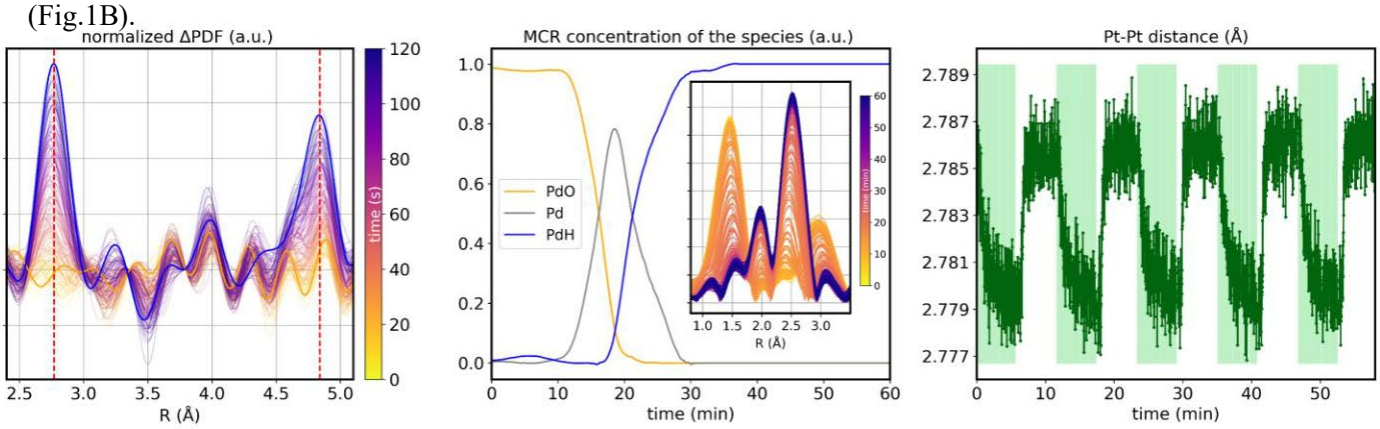

Figure 1. (A) fast acquisition ΔPDF of the reduction of PdO in HCOONa (10mM in H2O), Pd-Pd distances in red; (B) MCR concentrations of quick-XAS data collected in the same conditions, time-resolved FT-EXAFS data in the inset; (C) reversible evolution of Pt-Pt distance during a M.E. experiment with Ar (light green) and H_2 (white) in cyclohexane

As to Pt nanoparticles, deposited clusters only consist of 55 atoms (size ~ 1.4 nm) dramatically reducing the scattering contribution with respect to the Pd case. Modulated Excitation – Phase Sensitive Detection [3] proved necessary to isolate the contribution of the metal in the reciprocal space, allowing to observe just the fraction of atoms that respond to the repeated pulsing of solutions. Modulated Excitation-PDF on fully hydrogenated Pt nanoparticles with cycles of Ar- and H2-saturated solvent was able to detect the reversible reconstruction of the NPs due to the formation of surface hydrides detached from the support. This subtle effect was theorized via DFT simulations [4] and never structurally observed before to our knowledge, thus requiring a very sensitive method to directly detect it. Both these

cases show how PDF can be successfully used to investigate fine structural effects in metal nanoparticles under actual working conditions in a liquid environment, which make it challenging for total scattering experiments.

1 Groppo, E., Agostini, G., Piovano, A., Muddada, N., Leofanti, G., Pellegrini, R., Longo, A. & Lamberti, C. (2012). *J. Catal.,* **287**, 44
2 Fovanna, T., Alxneit, I., Clark, A., Checchia, S., Di Michiel, M., Nachtegaal, M. & Ferri, D. (2021). *J. Phys. Chem. C,* **125**, 16473.
3 Chiarello, G. & Ferri, D. (2015). *Phys. Chem. Chem. Phys*., **17**, 10579-10591
4 Mager-Maury, C., Bonnard, G., Chizallet, C., Sautet, P. & Raybaud, P. (2011). *ChemCatChem,* **3**, 200-207

A075-05-250823

Hidden structural transition upon dehydration of Prussian Blue analogues (PBAs)

Yevheniia Kholina, Arkadiy Simonov

ETH Zürich, Switzerland, Department of Materials, Laboratory for Multifunctional Ferroic Materials

yevheniia.kholina@mat.ethz.ch

Keywords: local structure, diffuse scattering, Prussian Blue analogues, dehydration

Prussian blue analogues (PBAs) are a diverse family of transition metal cyanide materials with chemical formula $M[M'(CN)_6]_{1-x}\square_y \cdot nH_2O$, which we abbreviate here as M[M'] (M and M'=transition metal ions, □=vacancy). These materials are known for their highly connected porous network, enabled by structural vacancies of M'(CN)6 with sufficiently large channels to transport or store small molecules and ions. Currently these systems are actively investigated for application as hydrogen storage media, humidity sensors, and alkali ion sieves.

One step which is often overlooked in the research is drying. PBAs are typically grown from water solutions and water has to be removed by heating the sample either in vacuum or in dry atmosphere. Since drying doesn't change the average structure, it is generally assumed that this step doesn't alter the porous network of PBAs. We demonstrate that dehydration step in fact causes a hidden structural transition that involves irreversible rearrangements of vacancies. Such rearrangements modify the pore-network characteristic, like fraction of accessible volume and conductance of matter through the channels. We collect diffuse scattering from Mn[Co] single crystals and use 3D-ΔPDF analysis to characterize their local structure and monitor any structural changes upon water removal. We also demonstrate that same material dehydrated at slightly different conditions shows different performance, drawing a link between a local structure and materials properties.

A075-06-250823

Uncovering disorder in scheelite structured oxides through local-scale analysis

Frederick P. Marlton[1], Bryce G. Mullens[2], Matilde Saura-Múzquiz[3], Philip A. Chater[4], Alicia María Manjón-Sanz[5], Joerg C. Neuefeind[5], Michelle Everett[5], Helen E. A. Brand[6], Subrata Mondal[7], Ganapathy Vaitheeswaran[7], and Brendan J. Kennedy[2]

[1]School of Mathematical and Physical Sciences, Faculty of Science, University of Technology Sydney, Sydney, New South Wales2007, Australia; [2]School of Chemistry, University of Sydney, Sydney, New South Wales 2006, Australia; [3]Departamento de física de Materiales, Facultad de CC. Físicas, Universidad Complutense de Madrid, 28040 Madrid, Spain; 4Diamond Light Source, Didcot, Oxfordshire OX11 0DE, U.K.; 5Neutron Scattering Division, Oak Ridge National Laboratory, Oak Ridge, Tennessee 37831, United States; 6Australian Synchrotron, Australian Nuclear Science and Technology Organisation, Clayton Victoria 3168, Australia; 7School of Physics, University of Hyderabad, Hyderabad 500046 Telangana, India

frederick.marlton@uts.edu.au

Keywords: Materials Science, Structure property relationships, Local structure

Oxides exhibiting the scheelite-type structure are an important class of functional materials with notable applications in photocatalysis, luminescence, and ionic conductivity. Like all materials, understanding their atomic structure is fundamental to engineering their physical properties. This presentation covers the unique phase transitions and local-scale features in scheelite oxides TlReO4[1] and RbReO4[2].

TlReO4 is a rare example of a non-magnetic material exhibiting a re-entrant phase transition and emphanitic behavior in the long range structure. Here, we describe the role of the Tl^+ $6s^2$ lone pair electrons in these unusual phase transitions and illustrate its tunability by chemical doping, which has broad implications for functional materials containing lone pair bearing cations. First principles density functional calculations clearly show the contribution of the Tl^+ $6s^2$ in the valence band region. Local structure analysis, via neutron total scattering, revealed that changes in the long-range structure of TlReO4 occur due to changes in the correlation length of the Tl^+ lone pairs. This has a significant effect on the anion interactions, with long-range ordered lone pairs creating a more densely packed structure. This resulted in a trade-off between anionic repulsions and lone pair correlations that lead to symmetry lowering upon heating in the long-range structure, whereby lattice expansion was necessary for the Tl^+ lone pairs to become highly correlated. Similarly, introducing lattice expansion through chemical pressure allowed long-range lone pair correlations to occur over a wider temperature range, demonstrating a method for tuning the energy landscape of lone pair containing functional materials.

The scheelite-type oxide RbReO4 exhibits a rare long-range phase transition from *I*41/*a* to *I*41/*amd* upon heating. Additionally, in the long-range *I*41/*a* model, the Re−O tetrahedral distance undergoes significant contraction upon warming. Recent studies of other scheelite oxides have attributed this apparent contraction to incoherent local-scale tetrahedral rotations. In this study, we use X-ray pair distribution function analysis to show that RbReO4 undergoes a unique symmetry-lowering process on the local scale, which involves incoherent tetrahedral displacements. The rare *I*41/*a* to *I*41/*amd* long-range phase transition was found to occur via a change from static to dynamic disorder on the local scale, which is due to the combination of the size of the A-site cation and lattice expansion. This demonstrates how careful manipulation of the ionic radius of the A-site in the scheelite structure can be used to induce local-scale disorder, which has valuable implications for tailoring the physical properties of related materials.

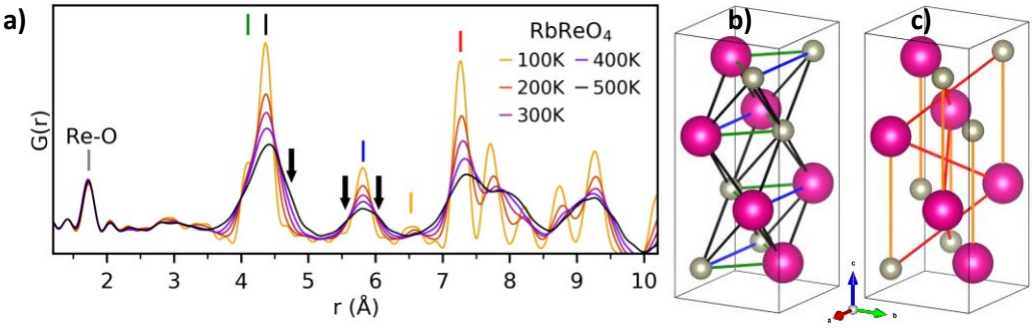

Figure 1. a) Variable temperature X-ray PDF data of $RbReO_4$ at 100, 200, 300, 400 and 500 K. Vertical markers correspond to some of the nearest atom-atom pairs in the $I4_1/a$ structure at 100 K. The color of cation-cation pairs marked in the structures in b) and c) correspond to the color of the markers in a). In b,c) the Rb, Re are represented by fuschia and mink colored spheres, respectively, while the oxygen atoms have been omitted. Black arrows in a) indicate extra features in the PDF at 400 and 500 K that are not described by the $I4_1/a$ model.

1 Saura-Múzquiz, M., et al., *Journal of the American Chemical Society* **2022,** *144* (34), 15612-15621.
2 Marlton, F. P., et al., *Inorganic Chemistry* **2022,** *61* (38), 15130-15137.

A102 Landscapes, Hills and Valleys: A World of Crystal Forms
Room 210
1.10pm – 3:30pm

A102-01-250823

Dapsone cocrystals through experiment and theory: polymorphism, hydrate formation and different stoichiometric ratios rationalised

Doris E. Braun

Institute of Pharmacy, University of Innsbruck, Innrain 52c, 6020 Innsbruck, Austria

e-mail: doris.braun@uibk.ac.at

Keywords: cocrystal, crystal structure prediction, thermodynamic stability

Controlling the physical properties of solid forms for Active Pharmaceutical Ingredients (APIs) through cocrystallisation is an important step in drug product development [1]. However, it is difficult to know *a priori* which coformers will form cocrystals with a given compound. Furthermore, cocrystals may exist with different coformer ratios, can exhibit different packing arrangements with the same composition (polymorphism) and may also incorporate a solvent (solvates) or water (hydrates). Several computational [2,3] and experimental methods [4] have been developed to estimate cocrystallisation and the synthesis of cocrystals, although with little consistency in the application of the proposed experimental protocols. Thus, the current state-of-the-art cocrystal discovery remains a time-consuming process.

The cocrystal solid form landscapes of dapsone with five coformers (2,2'-bipyridine, 4,4'-bipyridine, caffeine, ε-caprolactame and caffeine) were systematically elucidated, using cutting-edge experimental and computational approaches. The computationally generated (co)crystal energy landscapes had the experimental forms (API, coformers and cocrystals) as lowest energy structures. Both, the experimental and computational screen, reproduced the literature known cocrystal forms [5,6,7] and lead to novel multicomponent solid-state forms. For dapsone/2,2'-bipyridine the first cocrystals were found. Cocrystal polymorphism was confirmed for the combinations of dapsone with 2,2'-bipyridine, ε-caprolactam and flavone. Furthermore, the dapsone/flavone system was found to form a non-stoichiometric hydrate in molar ratios ranging from 1:1:0 to 1:1:0.66 (dapsone:flavone:water).

Finally, for dapsone/4,4'-bipyridine and dapsone/caffeine different cocrystal stoichiometries were rationalized. The experimental structures of the novel cocrystals were solved form PXRD data. Solution calorimetry and lattice energy calculations unravelled the thermodynamic driving force for cocrystal formation. The obtained materials were thoroughly characterised with advanced analytical techniques (thermal analysis, isothermal calorimetry, X-ray diffraction, spectroscopy, moisture sorption, solubility) in order to understand the dapsone cocrystal forms.

This study demonstrates the importance of applying complimentary computational and analytical techniques for understanding cocrystal formation, cocrystal stability and the correlation between structural features and pharmaceutical applicability.

[1] Kavanagh, O. N., Croker, D. M., Walker, G. M. & Zaworotko, M. J. (2019). *Drug Discov. Today* **24**, 796-804.
[2] Kumar, A. & Nanda, A. (2021). *Journal of Drug Delivery Science and Technology* **63**, 102527.
[3] Sugden, I. J., Braun, D. E., Bowskill, D. H., Adjiman, C. S. & Pantelides, C. C. (2022). Crystal Growth & Design 22, 451-4527
[4] Rodrigues, M., Baptista, B., Lopes, J. A. & Sarraguca, M. C. (2018). *International Journal of Pharmaceutics* **547**, 404-420.
[5] He, H., Jiang, L., Zhang, Q., Huang, Y., Wang, J.-R. & Mei, X. (2015). *CrystEngComm* **17**, 6566-6574.
[6] Jiang, L., Huang, Y., Zhang, Q., He, H., Xu, Y. & Mei, X. (2014). *Crystal Growth & Design* **14**, 4562-4573.
[7] Martins, I., Martins, M., Fernandes, A., Andre, V. & Duarte, M. T. (2013). CrystEngComm **15**, 8173-8179.

A102-02-250823

Mechanoresponsive luminescence switching by polymorphs and doped crystals of donor–acceptor-type benzothiadiazoles

Suguru Ito,[1] Sayaka Nagai,[1] Ryohei Yoshida,[1] Takashi Ubukata,[1] Takashi Tachikawa[2]

[1]*Department of Chemistry and Life Science, Graduate School of Engineering Science, Yokohama National University, 79-5 Tokiwadai, Hodogaya-ku, Yokohama 240-8501, Japan*
[2]*Department of Chemistry, Graduate School of Science and Molecular Photoscience Research Center, Kobe University, 1-1 Rokkodai-cho, Nada-ku, Kobe 657-8501, Japan*

suguru-ito@ynu.ac.jp

Keywords: Energy transfer, Luminescent chromism, Phase transition

Over the past decade, a growing number of luminescent organic crystals have been developed through appropriate molecular design strategies to overcome the problem of concentration quenching. The development of stimuli-responsive crystals capable of switching luminescence properties is an important target in the field of luminescent organic crystals. Since mechanical stimulation is the ubiquitous external stimulus, particular attention has been paid to mechanochromic luminescence (MCL) of organic crystals. In order to elucidate the relationship between the crystal structure and the mechanoresponsive properties of luminescent organic crystals, an increasing number of polymorphic and multicomponent organic crystals have emerged in recent years [1].

Recently, we have reported the versatile MCL properties of donor–acceptor (D–A) type benzothiadiazole derivatives [2,3]. These derivatives are composed of an electron-rich heteroaromatic ring and an electron-deficient benzothiadiazole ring. Given that the emission wavelength of D–A molecules is sensitive to the polarity of the surrounding environment, crystalline D–A compounds often change their emission colors when the crystal structure collapses in response to mechanical stimulation.

Reported here is a thienyl-substituted benzothiadiazole derivative **1** as a new donor–acceptor-type MCL dye [4]. Both bicolor and tricolor MCL have been realized by the three polymorphic crystals of **1** (Figure 1a). The emission colour of these polymorphic crystals should be determined by the dihedral angle between benzothiadiazole and thiophene rings as well as the packing mode. Both crystal a and b formed isolated dimers, whereas extended intermolecular stacks were observed for crystal g.

The control over the mechanoresponsive luminescence of crystalline 4-(2-thienyl)-2,1,3-benzothiadiazole (**2**) has also been achieved by doping a trace amount of 4,7-di(2-thienyl)-2,1,3-benzothiadiazole (**3**) [5]. Most remarkably, the mechanoresponsive shift in the maximum emission wavelength has been extended from 10 nm to 69 nm by preparing the doped mixed crystals **2**·**3** (Figure 1b). The larger shift in the emission band of the doped mixed crystals **2**·**3** compared with the single-component crystals of **2** should be attributed to the mechano-induced on–off switching of the Förster resonance energy transfer from **2** to **3**.

Figure 1. (a) Multi-color mechanochromic luminescence of three polymorphic crystals of **1**. (b) Extension of the mechanoresponsive luminescence shift of **2** by doping with **3**.

1 Ito, S. (2022). *CrystEngComm* **24**, 1112.
2 Ito, S., Taguchi, T., Yamada, T., Ubukata, T., Yamaguchi, Y., & Asami, M. (2017). *RSC Adv.* **7**, 16953.
3 Nagai, S., Yamashita, M., Tachikawa, T., Ubukata, T., Asami, M. & Ito, S. (2019). *J. Mater. Chem. C* **7**, 4988.
4 Ito, S., Nagai, S., Ubukata, T. & Tachikawa, T. (2021). *CrystEngComm* **23**, 5899.
5 Yoshida, R., Tachikawa, T. & Ito, S. (2022). *Chem. Commun.* **58**, 6781.

This work was partly supported by JSPS KAKENHI Grant Numbers JP20K05645, JP18H04508, JP20H04665, and JP20H04673 and JST, PRESTO Grant Number JPMJPR21A3, Japan. Part of this work was carried out by the joint research program Numbers R02019 and R03007 of Molecular Photoscience Research Center, Kobe University.

A102-03-250823

Sublimation as a route to new crystal forms

Delia A. Haynes

Department of Chemistry & Polymer Science, Stellenbosch University, P. Bag X1, Matieland, Stellenbosch, 7602, Republic of South Africa.

dhaynes@sun.ac.za

Keywords: sublimation, co-crystals, salts, hydrates, polymorphism

Sublimation is an under-explored technique for the crystallisation of multi-component crystals [1]. We have recently explored the use of sublimation to produce crystals of organic salts and co- crystals, including hydrates [2 -4]. We have also explored competition between hydrogen bonding and halogen bonding when crystals are grown from the gas phase [5]. Sublimation can result in the isolation of crystal forms that are difficult to prepare from solution.

Changes in sublimation conditions can lead to isolation of one crystal form in preference to another, for example appropriate conditions can favour crystallisation of a salt or a co-crystal of the same components. A systematic study of the effect of various sublimation conditions on crystal form has been carried out. Variables such as pressure, temperature and size of the sublimation vessel can impact the outcome of a sublimation crystallisation. Additives, such as solvents, gases or other small molecules, can have a significant effect on the product that is preferentially crystallised from a sublimation experiment. Our results in this regard will be presented, and compared to results obtained from solution and mechanochemistry.

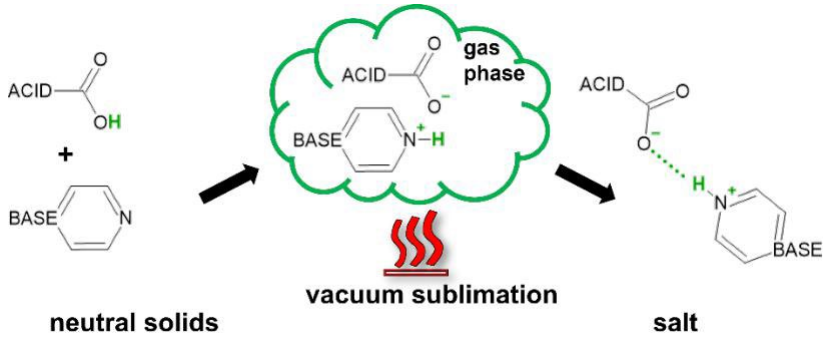

Figure 1. Organic salts can be crystallised from the gas phase.

1 McArdle, P. & Erxleben, A. (2021). *CrystEngComm*, **23**, 5965-5975.
2 Carstens, T.; Haynes, D. A. & Smith, V. J. (2020). *Cryst. Growth Des.*, **20**, 1139-1149.
3 Lombard, J.; le Roex, T. & Haynes, D. A. (2020). *Cryst. Growth Des.*, **20**, 7840-7849.
4 Lombard, J.; Smith, V. J.; le Roex, T. & Haynes, D. A. (2020). *CrystEngComm*, **22**, 7826-7831.
5 Lombard, J.; le Roex, T. & Haynes, D. A. (2020). *Cryst. Growth Des.*, **20**, 7384-7391.

A102-04-250823

Unusual crystal forms to motif prediction from quasiracemic materials

Kraig A. Wheeler, Katelyn N. Koch, Emily K. Needham, Diana R. Schepens and Aaron J. Teo

Whitworth University, Spokane, WA 99251 USA

kraigwheeler@whitworth.edu

Keywords: Quasiracemates, Molecular Topology, Approximate Symmetry

Understanding the underlying structural features responsible for the construction of various crystal landscapes is of ongoing interest. Focused investigations in this area often probe fundamental molecule-molecule contacts that ultimately hold importance to the design and application of functional materials. These collective efforts have shown that noncovalent interactions can be robust and directional (*e.g.,* hydrogen and halogen bonds), influence crystal alignment [1, 2], form with conditional exceptions [3], and reliably contribute to crystal stabilization [4, 5]. Chemical features that produce less manageable motifs *via* ill-defined or weak contacts are relatively underexamined but no less critical to the overall molecular recognition process. The three-dimensional molecular shape of molecular crystal components is one such feature. While generally recognized as an essential contributor to molecular assembly, the systematic use of topological features as design elements to explore crystal landscapes remains an area relatively unexplored. The lack of direct attention to molecular shape likely relates to the intractable nature of this structural attribute. Currently, no suitable set of parameters or methods for determining the effects of molecular shape on crystal forms exists. Developing chemical systems and methods that examine molecular topology is crucial for understanding the molecular recognition process.

Quasiracemic materials – materials formed from pairing near enantiomers (*e.g., S*-X and *R* -X') – offer an attractive entry point to molecular-shape derived molecular assemblies [6]. Unlike conventional studies that probe interaction-derived molecular assemblies, the complementary shapes of the quasiracemic components (quasienantiomers) serve as the primary driving force for crystal alignment. Inspecting the extant database of quasiracemic crystal structures reveals several notable structural themes. These structures are often constructed from pairs of sterically similar quasienantiomers with motifs that mimic the inversion symmetry found in the related *S*-X/*R*-X or *S*-X'/*R*-X' racemates. This investigation explores homologous families of quasiracemic materials that produce unexpected crystal landscapes and cocrystallization successes from pairs of structurally diverse quasienantiomers. Systematically examining these cocrystal systems using a suite of methods (crystallography, hot stage thermomicroscopy, shape matching, and lattice energy determinations) provides insight into the role molecular shape plays in the molecular recognition process of these quasiracemic materials.

1 Grabowski, S. J. (2021) *Understanding hydrogen bonds: theoretical and experimental views*; Theoretical and computational chemistry; Royal Society of Chemistry: Cambridge, England.
2 Liu, G., Wei, S. -H. & Zhang, C. (2020). *Cryst. Growth Des.,* **20**, 7065.
3 Liao, W. -Q., Tang, Y. -Y., Li, P. -F., You, Y. -M. & Xiong, R. -G. (2018). *J. Am. Chem. Soc.*, **140**, 3975.
4 Gavezzotti, A. (2021). *Isr. J. Chem.*, **61**, 498.
5 Spackman, M. A. (2015). *Cryst. Growth Des.*, **15**, 5624.
6 Fredga, A. (1973). *Bul. Soc. Chim. Fr.*, **1**, 173.

This work was generously supported by the US National Science Foundation (DMR1904651 and CHE1827313) and a Hugh Johnston Interdisciplinary Research Grant from Whitworth University.

A102-05-250823

Encapsulated nanodroplet crystallisation: Expanding solution-phase crystallisation methodologies for statistically directed polymorph screening.

J. Weatherston, M. Probert, M. Hall

School of Natural and Environmental Sciences, Newcastle University, Newcastle upon Tyne, NE1 8QB.

J.Weatherston@newcastle.ac.uk

Keywords: High-throughput, Crystallisation, Polymorphism

Polymorphism is a solid-state phenomenon where a chemical species may adopt different conformational or packing arrangements, therefore allowing for the formation of more than one distinct crystal structure. As a result of these different packing arrangements, crystal polymorphs can exhibit varying physical and chemical properties. These properties such as solubility, hardness, colour, and melting point can all be important in the design of the compound.[1]

In the pharmaceutical and crystal engineering fields, a thorough understanding of the polymorphic landscape of a chemical species is critical to reliably select and grow crystal forms with suitable properties for their intended functionality. For example, the bioavailability of an active pharmaceutical ingredient can be drastically altered by the crystal form in which it is formulated.[2]
Whilst computational crystal structure prediction can be used to highlight likely crystal forms of a given chemical species,[1] manual crystallisation screens remain the only way to effectively assess the impact of polymorphism on a compound. The techniques classically applied to grow high-quality single crystals are often time-consuming and require significant quantities of the sample compound. In the pharmaceutical industry, this often leaves crystal form screening to a later stage of drug development when large quantities of material are available for such experiments. This has led to significant demand for rapid small-scale crystallisation techniques that would permit crystal form screening at a much earlier stage of drug development.[3]

Herein, we describe how encapsulated nanodroplet crystallisation (ENaCt) can be applied to rapidly probe areas of the polymorphic landscape that are inaccessible to other solution-phase crystallisation experiments. Furthermore, the statistical power of such small-scale high-throughput experiments can be harnessed to gain selectivity of the polymorphic outcome of complex highly stochastic crystallisation systems. Using the current most polymorphic organic compound, Methyl-2-[(2-nitrophenyl)amino]-3-thiophenecarbonitrile (ROY) as a test system, ENaCt polymorph screening revealed the 14th observed polymorph ‘O22’ as well as forms previously undocumented from solution-phase crystallisation.[4-6]

1 A. J. Cruz-Cabeza, N. Feeder and R. J. Davey, *Commun Chem*., (2020). **3**, 1-4.
2 E. H. Lee, *Asian Journal of Pharmaceutical Sciences*., (2014). **9**, 163-175
3 A. R. Tyler, R. Ragbirsingh, C. J. McMonagle, P. G. Waddell, S. E Heaps, J. W. Steed, P. Thaw, M. J. Hall, and M. R. Probert, *Chem*, (2020). **6**, 1851-1853.
4 S. Chen, I. A. Guzei, and L. Yu, *J. Am. Chem. Soc*., (2005). **127**, 9881–9885.
5 X. Li X. Ou, H. Rong, S. Huang, J. Nyman, L. Yu and M. Lu, *Cryst. Growth Des*., (2020). **20**, 7093– 7097.
6 A. Levesque, T. Maris, and J. D. Wuest, *J. Am. Chem. Soc*., (2020). **142**, 11873– 11883.

A102-06-250823

Orienteering' through the crystal engineering landscape

D.-K. Bučar

Department of Chemistry, University College London, 20 Gordon Street, London WC1H 0AJ, United Kingdom d.bucar@ucl.ac.uk

Keywords: crystal engineering, molecular crystals, crystal form screening

In this contribution, we highlight some of the challenges encountered during the discovery of crystal forms in the high-energy regions of crystal structure landscapes, the pursuit of putative crystal forms, and the retrieval of crystal forms that seem to have 'disappeared' in our laboratories. We discuss the feasibility and use of crystal structure prediction methods in these pursuits. We also report the use of real-time and *in situ* X-ray diffraction monitoring of thermal and mechanochemical cocrystallisation reactions (using a modified differential scanning calorimeter [1] and an adapted ball mill [2]) in crystal form screens.

Examples from various research activities in our group (namely, the study of supramolecular synthons in multi-component molecular crystals, the development of pharmaceutical oral solid dosage form with specific properties and the development of porous molecular crystals) will be used to critically assess a range of concepts and ideas that form the basis of contemporary crystal engineering research, with the intention of continuing a community-wide conversation about the current state of the art [3, 4].

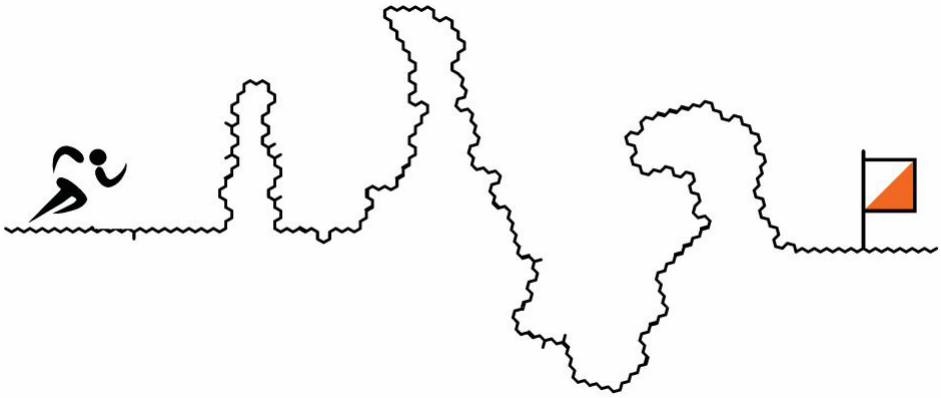

Figure 1. 'Orienteering' through the crystal engineering landscape.

1 Clout A., Buanz, A. B. M., Prior, T. J., Reinhard, C., Wu, Y., O'Hare, D., Williams, G. R., & Gaisford S. (2016) *Analytical Chemistry* **88**, 10111.
2 Friščić, T., Halasz, I., Beldon, P. J., Belenguer, A. M., Adams, F., Kimber, S. A. J., Honkimäki, V. & Dinnebier, R. E. (2013) *Nat. Chem*. **5**, 66.
3 Bučar, D.-K. (2017) *Cryst. Growth Des.* **17**, 2913.
4 Corpinot, M. K. & Bučar, D.-K. (2019) *Cryst. Growth Des.* **19**, 1426.

A109 Data-Driven Science: Current Status and Outlook

Room 220

1.10pm – 3:30pm

A109-01-250823

Microsecond time-resolved serial crystallography data pipeline for Swiss Light Source 2.0

B. C. Leonarski[1], G. Assmann[1], K. Smith[1], A. Mozzanica[1], H.-C. Stadler[1], P. Gasparotto[1], L. Barba[1,2], B. Béjar[1,2], H. Mendonça[3], F. Dworkowski[1], M. Janousch[1], M. Burian[4], M. Wang[1]

[1]Paul Scherrer Institute (PSI), 5232 Villigen, Switzerland [2]Swiss Data Science Center (SDSC), 1015 Lausanne, Switzerland [3]Swiss National Supercomputing Centre (CSCS), 6900 Lugano, Switzerland [4]DECTRIS AG, 5405 Baden-Dättwil, Switzerland

filip.leonarski@psi.ch

Keywords: X-ray data analysis, data acquisition, X-ray detectors, FPGA, GPU, FAIR data

The years to come for macromolecular crystallography at the Swiss Light Source (SLS) are bright. The SLS will undergo a major upgrade in years 2023-2025 that will increase X-ray brilliance by more than an order of magnitude. This, paired with beamline improvements and developments in charge-integrating X-ray detector technology [1], opens new opportunities for time-resolved synchrotron serial crystallography [2]. The new source will allow for 10 microsecond measurements, while the current source limits time resolution to the millisecond range. However, handling many GBs of X-ray images per second is a big data challenge

1 that must be overcome in order to make collecting and processing diffraction images at rates up to 10 kHz feasible in the future (see Fig. 1). In this presentation, I will highlight a few aspects of the development at the PSI to handle big data in the future.

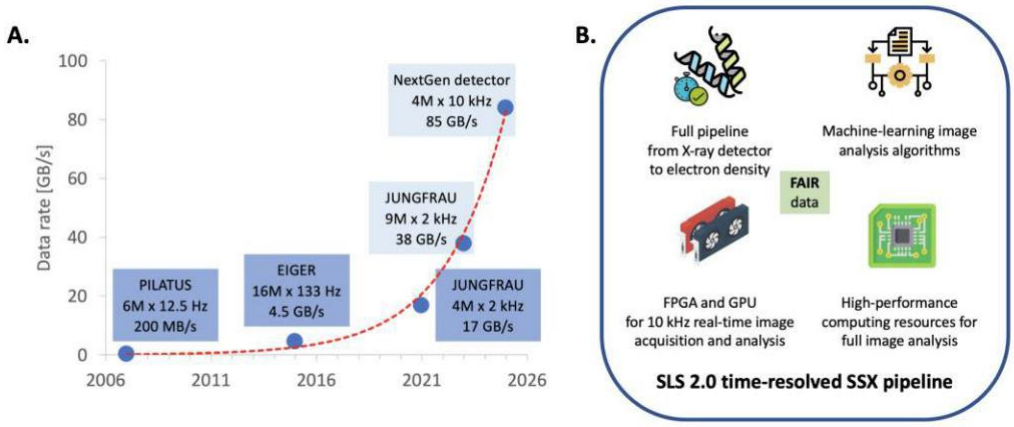

Figure 1: A. Data rates of detectors used at PSI macromolecular crystallography beamlines and planned for the future [4].

B. Graphical presentation of main features of the new SLS 2.0 pipeline for the time-resolved serial synchrotron crystallography.

I will first present Jungfraujoch, a detector read-out system with FPGAs and GPUs capable of handling 30 GB/s data rates within a single server. The system can run real-time image analysis to provide fast experimental feedback, including spot finding and radial integration. After the Jungfraujoch system writes images to the facility file system, the next step is an automated data analysis pipeline currently under development. The pipeline is designed to produce electron density maps and to inform the experiment team during beamtime about the progress.

1will present PSI and SDSC efforts in improving spot-finding and indexing algorithms using modern machine-learning frameworks optimized to run efficiently on distributed CPUs and GPUs. I will also give an outlook for operating our image processing pipeline at the high-performance computing cluster Alps, allowing online data processing with massive data rates.

2

I will show how the FAIR principles will be applied to the data that will be written by the pipeline. The images, metadata, and analysis results produced by the pipeline are written according to community standards [5]. All collected datasets are ingested into the SciCat data catalogue, saved on tapes for long-term storage, and accessed according to the PSI Data Policy.

Finally, I will present a collaboration with DECTRIS to include hardware-accelerated real-time data acquisition and analysis features in the DECTRIS Next Generation Detector Control Unit, allowing more facilities to use these features.

[1] F. Leonarski et al. (2018). *Nat. Methods*, **15**, 799–804.
[2] T. Weinert et al. (2019). *Science*, **365**, 61-65.
[3] F. Leonarski et al. (2020). *Struct. Dyn.*, **7**, 014305.
[4] F. Leonarski et al. (2022). *J. Synchrotron Rad.*, **30**, 227-234.
[5] H. Bernstein et al. (2020). *IUCrJ*, **7**, 784-792.

F.L. acknowledges support for part of this work by the Open Research Data Program of the ETH Board.
P.G., L.B., B.B., H.M. acknowledge Swiss Data Science Center for funding RED-ML project under grant no. C19-03.

A109-02-250823

Current status of SACLA Data Center and outlook of SPring-8 Data Center

Y. Joti[1,2], T. Hatsui[2]

[1]Japan Synchrotron Radiation Research Institute, 1-1-1 Kouto, Sayo-cho, Sayo-gun, Hyogo 679-5198, [2]RIKEN SPring-8 Center, 1-1-1 Kouto, Sayo-cho, Sayo-gun, Hyogo 679-5148, JAPAN
joti@spring8.or.jp

Keywords: X-ray data science, data center, big data analysis

The rapid development in synchrotron radiation science has increased the amount of raw data collected during each experiment. As an example of data processing at SACLA, we consider an experimental scheme for serial femtosecond crystallography (SFX), in which single-shot diffraction patterns from micrometer-sized crystals are recorded for every XFEL shot. When we run an SFX experiment with a maximum repetition rate of 60 Hz at SACLA, we obtain ~1.6-terabyte (TB) diffraction data (216,000 diffraction patterns) per hour, which corresponds to a high data throughput of 4 gigabits per second (Gbps). Furthermore, the data throughput reaches 6 Gbps when we utilize an arrival-timing monitor [1] for a pump-probe SFX experiment with a repetition rate of 60 Hz. For these XFEL experiments, all data from the detectors with the beam parameters should be reliably stored and properly analyzed. To meet these requirements, we have developed SACLA Data Center, which is designed for reliable shot-to-shot data recording with a data throughput up to 6 Gbps and big data analysis [2,3]. To increase user flexibility and efficiency for the big data analysis, user application program interfaces (APIs) have been developed so that user programs such could directly access data in the data center. Using these APIs we have developed a data processing pipeline for SFX at SACLA [4].

Recently, the frame rates of high-speed X-ray imaging detectors for synchrotron radiation experiment are improved to be over 10 kframes/s. Among these detectors, CITIUS is one of the first detectors. The raw data rate will reach 10 Tbps when the system is composed to form 20 Mpixels (30 x 30 cm^2) operating at 17 kfps. Annual data generation will reach several exabytes. Together with the other detectors equipped with high-end machine vision image sensors, the overall data generation will demand a new scheme of the data infrastructure. At SPring -8, we are proposing SPring-8 Data Center Initiative, where key elements consist of the on-the-fly data processing/compression, I/O intensive online analysis during the experiment for the feedback, post-experiment data analysis by using the on-site data center and HPCI supercomputers [5] such as Fugaku with a performance of ~ 400 petaflops.

In this report, we introduce current status of SACLA Data Center and outlook of SPring-8 Data Center.

1 Nakajima, K., Joti, Y., Katayama, T., Owada, S., Togashi, T., Abe, T., Kameshima, T., Okada, K., Sugimoto, T., Yamaga, M., Hatsui T. & Yabashi, M.(2018). *J. Synchrotron Rad.*, **25**, 592.
2 Joti, Y., Kameshima, T., Yamaga, M., Sugimoto, T., Okada, K., Abe, T., Furukawa, Y., Ohata, T., Tanaka, R., Hatsui, T. & Yabashi, M. (2015). *J. Synchrotron Rad.* **22**, 571.
3 Joti, Y., Nakajima, K., Kameshima, T., Yamaga, M., Abe, T., Okada, K., Sugimoto, T., Hatsui T. & Yabashi, M. (2017). *Synchrotron Rad. News*, **30**, 16.
4 Nakane, T., Joti, Y., Tono, K., Yabashi, M., Nango, E., Iwata, S., Ishitani R. & Nureki, O. (2016). *J. Appl. Cryst.*, **49**, 1035.
5 https://www.hpci-office.jp/en

A109-03-250823

Automatic data analysis at ESRF MX beamlines

Max Nanao

nanao@esrf.fr

Keywords: MX, phasing

Dramatic improvements in MX synchrotron beamline hardware and software have transformed the once leisurely activity of data collection into a struggle just to keep up. Automatic data processing provides valuable user feedback to the user and enables efficient use of beam time. At the ESRF, automatic data reduction has been available to users since 2009, and has since then undergone significant changes and improvements. I will provide an overview of the ESRF automatic data processing architecture, including initial data reduction as well as downstream services such as molecular replacement and anomalous phasing.

A109-04-250823

Integrated Structural Analysis Platform for Life Science and Drug Discovery Research in Japan by AMED/BINDS phase II Project

Masaki Yamamoto, *on behalf of the AMED/BINDS phase II Structural Analysis Unit*

Life Science Research Infrastructure Group, RIKEN SPring-8 Center, 1-1-1 Kouto, Sayo, Hyogo, 679-5148, Japan

yamamoto@riken.jp

Keywords: Integrated Structural Analysis Platform, Macromolecular Crystallography, Cryo-Electron Microscopy

Accurate three-dimensional structural information of proteins is indispensable for modern life science research and drug discovery research, which are approaching biological functions at the atomic and molecular levels. “Research Support Project for Life Science and Drug Discovery (Basis for Supporting Innovative Drug Discovery and Life Science Research (BINDS Phase II))” from AMED since 2022 is promoting further advancement of various cutting-edge structural analysis technologies, mainly using synchrotron radiation and Cryo-Electron Microscopy (cryo-EM), which have been developed in the previous BINDS Phase I project (FY 2016-2021) and will support a wide range of life science researchers using these analysis technologies to promote drug discovery research and life science research in Japan.

We will provide support for structural analysis for biological macromolecules by combining various structural analysis techniques; X-ray crystallography, including micro-focus beamlines and fully automated data collection systems at SPring -8 and KEK/PF, neutron crystallography at J-PARC, time-resolved crystallography at the X-ray free electron laser SACLA, single particle analysis and tomography using cryo-EMs, in-situ measurement of solution samples using synchrotron small-angle X-ray and neutron scattering (BioSAXS and BioSANS) and NMRs.

Furthermore, we will build an "Integrated Structural Analysis Platform" that combines complementary experimental structural information in various time spaces obtained from state-of-the-art structural analysis techniques and the vast amount of structure-related information accumulated in PDBj with the help of computational science toward the understanding of function from structure. This will lead to innovative analysis to meet the demand for advanced structural information, such as elucidating structure dynamics and functional manifestation mechanisms and promote life science research, such as drug discovery.

The presentation will introduce the AMED/BINDS Phase II Integrated Structural Analysis Platform and discuss the efforts and use of the platform for analytical methods for biomacromolecules in various spatiotemporal hierarchies.

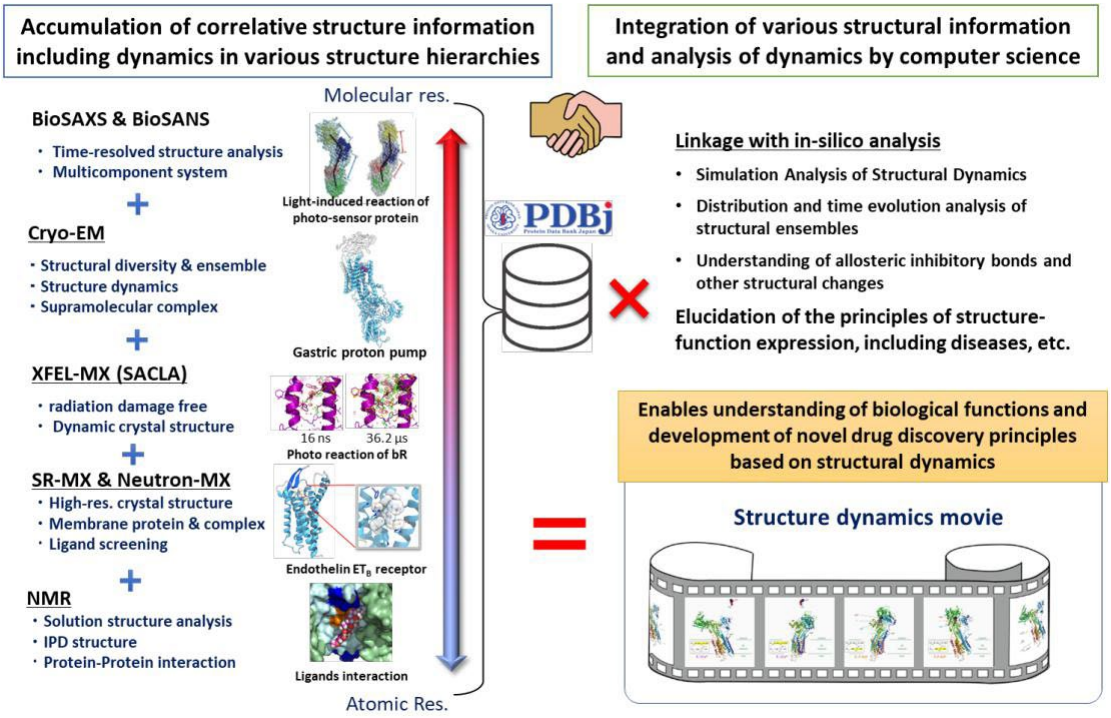

Figure 1. Concept of Integrated Structural Analysis Platform

A109-05-250823

Advanced detector and data pipeline design to fully utilize experiments at next-generation synchrotron sources

S. Brandstetter[1], S. Grimm[1], F. Leonarski[2], M. Burian[1]

[1]DECTRIS AG, 5405 Baden-Dättwil, Switzerland, [2]Paul Scherrer Institute (PSI), 5232 Villigen, Switzerland

stefan.brandstetter@dectris.com

Keywords: X-ray data management, data acquisition, X-ray detectors, Hybrid photon counting

Advancing scientific discoveries requires a deep understanding of dynamic processes. The brilliance of next-generation synchrotron sources combined with hybrid photon counting (HPC) X-ray detectors enables to study fast reactions in greater detail. HPC detectors provide noise-free detection [1], making them a vital component for cutting-edge synchrotron research. For example, the EIGER2 detectors combine all advantages of previous HPC detector generations while offering count rates of more than 10^7 photons per pixel per second, and kilohertz frame rates.

To efficiently manage the large amount of data generated by advanced detectors, several approaches can be employed. One common strategy is the implementation of lossless compression methods, as is typical for most hybrid photon counting (HPC) detectors. Bitshuffle LZ4 compression [2] has emerged as a favorable solution, striking a balance between computational efficiency and compression ratio. Another effective approach is to compress the data directly on the photon-detecting chip. Floating-point counter encoding is a method, which significantly reduces the number of bits required to read out from the pixel counters, and minimizes the amount of data to be transferred. And, when appropriately designed, the recorded values can be smaller or comparable in magnitude to the Poisson limit. These methods offer efficient solutions for data management of HPC detectors.

However, the amount of data produced by these experiments is still immense and requires sophisticated data services to store, process, and analyze the information. A tailored detector read-out system utilizing the full potential of GPUs and FPGAs can handle data rates of 30 GB s^{-1} within a single server [3]. For larger data rates more elaborated services are essential to exploit the data generated by these experiments. Such services can include data management, data processing, data visualization, and data analysis tools, among others. Data services also allow researchers to access and analyze data remotely facilitating easy and efficient collaboration.

In this talk, we will explore examples of using current HPC detector designs and their limitations. Additionally, we will present examples of prototype detectors and data pipelines that employ advanced designs to efficiently handle large volumes of data. Through these examples, we will highlight various options for future design concepts that can effectively harness the full potential of next-generation synchrotron sources.

[1] Förster, A., et al. (2019) Philos. Trans. R. Soc. Math. Phys. Eng. Sci. 377, 20180241.
[2] Masuia, K., et al. (2015) Astronomy and Computing, 12, 181
[3] Leonarski, F., et al. (2023) J. Synchrotron Rad. 30, 227

A109-06-250823

Linking scientific instruments and computation: Patterns, technologies, experiences

Ian Foster

The University of Chicago, Chicago, Illinois, USA & Argonne National Laboratory, Lemont, Illinois, USA
foster@uchicago.edu

Keywords: Automation, big data, synchrotron light sources, high-performance computing

Powerful detectors at modern experimental facilities routinely collect data at multiple GB/s. Online analysis methods are needed to enable the collection of only interesting subsets of such massive data streams, such as by explicitly discarding some data elements or by directing instruments to relevant areas of experimental space. Such online analyses require methods for configuring and running high-performance distributed computing pipelines—what we call here *flows*—linking instruments, data center computers (e.g., for analysis, simulation, AI model training), edge computing (for analysis), data stores, data catalogs, high-speed networks, and other resources.

I review common patterns associated with such flows, describe methods for instantiating those patterns, and present experiences with the application of these methods to the processing of data from a range of light source beamlines, each of which engages HPC resources for data inversion, machine learning model training, or other purposes. I also discuss implications of these methods for operators and users of scientific facilities. More details on this work are provided in a recent article [1].

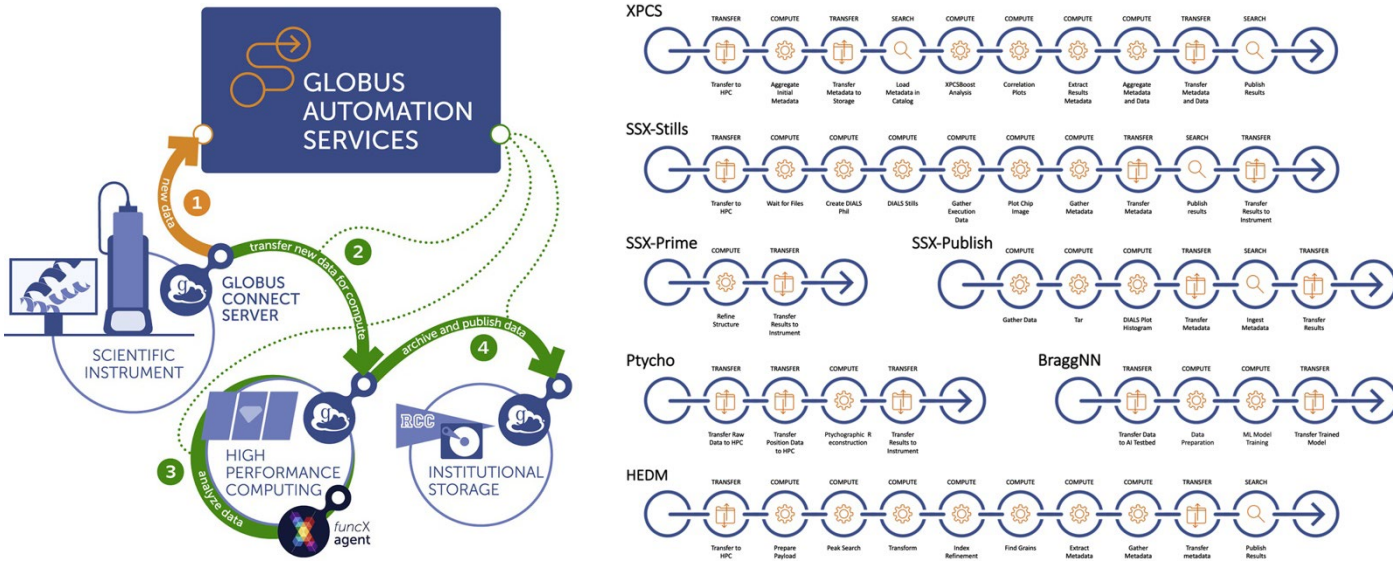

Figure 1. *Left*: Cloud-hosted Globus automation services are used in this work for reliable and secure orchestration of flows, often triggered by data availability, and linking various resources including, as shown here, scientific instruments, high-performance computers, and storage systems. Globus and funcX agents provide access to storage and compute resources, respectively.

Right: Example flows used at Advanced Photon Source (APS), Argonne Leadership Computing Facility (ALCF), and Stanford Synchrotron Radiation Lightsource (SSRL) for x-ray photon correlation spectroscopy (XPCS), serial synchrotron crystallography (SSX-Stills, SSX-Prime, SSX-Publish [2]), ptychography (Ptycho), high energy diffraction microscopy (BraggNN [3], HEDM).

[1] R. Vescovi et al. *Patterns* 3, no. 10 (2022): 100606. doi: 10.1016/j.patter.2022.100606
[2] D. Sherrell et al. *Journal of Synchrotron Radiation* 29, no. 5 (2022): 1141-1151. doi: 10.1107/S1600577522007895
[3] Z. Liu, et al. *IUCrJ* 9, no. 1 (2022): 104-113. doi: 10.1107/S2052252521011258

This work was supported in part by the US Department of Energy under contract DE-AC02-06CH11357, including by the Office of Advanced Scientific Computing Research's Braid project; by NSF grants OAC-1835890 and OAC-2004894; and by award 70NANB14H012 from the US Department of Commerce, National Institute of Standards and Technology, as part of the Center for Hierarchical Material Design (CHiMaD). We are grateful to staff at the APS, ALCF, University of Chicago Globus group, and SSRL for assistance with this work.

A012 Integrative Methods Applied to Structural Biology in memoriam of Prof Raimond Ravelli

Room 203

4.00pm – 6:30pm

A012-01-250823

A PPR protein-based FRET sensor for RNA

Charles S. Bond[1], Brady Johnston[1], Jason Schmidberger[1], Nicholas Marzano[2], Mark Agostino[3], Bishnu Paudel[2], Ian Small[1], Antoine van Oijen[2]

1- School of Molecular Sciences, The University of Western Australia, Crawley, WA, Australia
2- Molecular Horizons, University of Wollongong, Wollongong, NSW, Australia
3- Curtin University, Bentley, WA, Australia

Charles.Bond@uwa.edu.au

Keywords: RNA-binding proteins, Helical disorder, single-molecule FRET

Pentratricopeptide repeat (PPR) proteins are modular single-stranded RNA-binding proteins. They consist of an alpha-solenoid structure composed of repeating 35 amino acid alpha hairpins, which form an extensive superhelix. Modification of just two amino acids per repeat, according to a derived code, can alter the specificity of a protein to a different target RNA sequence. Studies of wild-type, and consensus PPR proteins demonstrate a conformational change on RNA binding. For example, our crystallographic studies of idealised consensus ("designer") PPR proteins in the presence and absence of RNA show that they have a superhelical structure of 9, or 10 repeats per superhelical turn in the presence or absence of RNA. Helical averaging of molecules in the superhelix in both crystal structures produced challenges for refinement, but ultimately produced molecular models that effectively represent infinitely long proteins binding to infinitely long RNA (Figure 1). The conformational change on RNA binding results in a contraction of the superhelical pitch from 85 Å to 43 Å, a change that is compatible with the Foerster distance of commonly used FRET fluorophores. We thus built a protein-based RNA FRET sensor by introducing two cysteine residues at appropriate spacing in the structure, and chemically labelling them with Cy3 and Alexafluor647 fluorophores. Having established a plate-based FRET ssRNA-binding assay which yields comparable dissociation constant to alternative methods, we then built a biotinylated version of the protein which can be immobilised suitably for single molecule FRET measurements. In these experiments we explore the conformational repertoire of populations of individual PPR proteins in the presence of variant RNA sequences thus providing insights into the mechanism and kinetics of RNA-binding by this class of biotechnologically useful proteins.

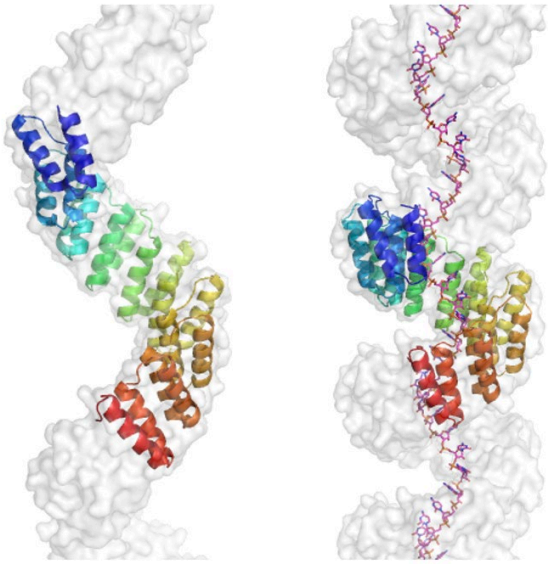

Figure 1. Crystal structures of apo- and RNA-bound designer PPR proteins demonstrate suitability for design of a FRET-based RNA sensor

A012-02-250823

NP³: an integrated platform for natural product-based drug discovery centred on X-ray protein crystallography

Daniela B B Trivella[1*], Joane K. Rustiguel[1], Cristina F. Bazzano[1,2], Rafael de Felicio[1], Luiz G. Alves[1], Raphael Meneghello[1], Marcos G. Cunha[1], Guilherme Telles[2], Andrey Z. Nascimento[1], Ana C. M. Zeri[1]

1 Brazilian Center for Research in Energy and Materials (CNPEM), Campinas-SP, Brazil; [2] University of Campinas, Campinas-SP, Brazil

Email of communicating: daniela.trivella@lnbio.cnpem.br

Keywords: high throughput protein crystallography, drug discovery, natural products, deep learning

Natural products (NP) provide new chemical scaffolds for drug discovery and can probe novel enzyme binding sites and inhibition mechanisms [1]. However, the identification of bioactive natural products and their enzyme binding mechanisms is challenging, sample and time-consuming [2]. We have developed an integrated approach to overcome these gaps, based on high throughput screening, high throughput X-ray protein crystallography, massive mass spectrometry analyses and customized software. This approach is named the NP³ platform (Fig. 1).

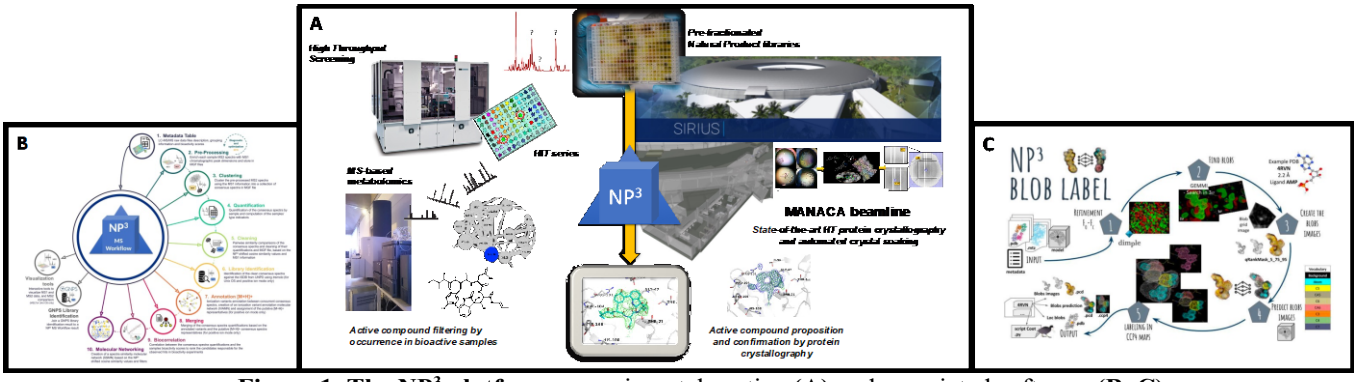

Figure 1. The NP³ platform: experimental routine **(A)** and associated software **(B, C)**.

The NP³ platform starts with the HT screening of pre-fractionated NP libraries, finding bioactive NP samples, which represent mixtures of unknown natural substances. These active samples are then subjected to HT protein crystallography, aiming to capture the bioactive NPs using the crystal itself as the bait. This is done by directly soaking the bioactive NP sample into the protein crystals, following X-ray diffraction data collection, processing and extraction of the residual electron density. The latter, in turn represents the captured NP ligand revealing the active natural product binding site, its mechanism of interaction with the protein, and providing initial clues on its chemical structure. LC-MS/MS-based metabolomics is then employed for filtering candidate *m/z* (compounds) in the unknown mixture. Using an iterative process of crystal electron density and MS/MS spectra interpretation, it is possible to reveal the chemical identity of the bioactive natural product. The experimental data is integrated and mined, using designed computer algorithms for identifying bioactive natural products and their enzyme binding sites, in the very early stages of natural product-based drug discovery. Two software were developed, the *NP³ MS Workflow* (**Fig. 1B**), a software for mass spectrometry data treatment, bioactive NP ranking and chemical structure annotation (available at https://github.com/danielatrivella/NP3_MS_Workflow); and the *NP³ Blob Label* (**Fig. 2C**), a *deep learning application* for unknown ligand segmentation to ligand building in X-ray protein crystallography.

This iterative approach proved successful even when using low resolution protein crystals and active natural products present in trace amounts in complex chemical samples. The process can be performed in miniaturized scales, in which each step is compatible with high throughput techniques. The NP³ platform is empowering natural product drug discovery, as it will be exemplified by target-based drug discovery projects currently running in our pipeline.

1. Bruder, M.; Polo, G.; Trivella, D.B.B. Natural allosteric modulators and their biological targets: Molecular signatures and mechanisms. *Nat. Prod. Rep.* **2020**, *37*.
2. Beutler, J.A. Natural products as a foundation for drug discovery. *Curr. Protoc. Pharmacol.* **2009**, 1–30.

Acknowledgement: Serrrapilheira Institute (Serra-1709-19681/Instituto Serrapilheira)

A012-03-250823

Time-resolved structural studies for nanoparticle systems and their early event dynamics in biological environments: system investigations for nanomedical applications

N. Iranpour Anaraki[1,2,3], L. Krupnik[1,2,3], J. Avaro[1], P. Wick[2], A. Neels[1,3]

[1]*Swiss Federal Laboratories for Materials Science and Technology, Center for X -Ray Analytics, St. Gallen, Switzerland,* [2]*Swiss Federal Laboratories for Materials Science and Technology, Laboratory for Particles-Biology Interactions, St. Gallen, Switzerland,* [3]*University of Fribourg, Department of Chemistry, Fribourg, Switzerland*

antonia.neels@empa.ch

Keywords: NP self-assembly, NP colloidal stability, microfluidics SAXS, nanomedecine

Nanoparticle (NP) systems in nanomedical applications are becoming increasingly important. However, after transferring NPs to a biological environment, the inter-particle interaction and their interactions with the media are complex and not yet fully understood. Different parameters such as ionic strength, pH conditions, and biomolecules such as proteins initiate alterations in NPs structure and influence their colloidal stability. Here, we focused on detailed investigations of NPs interactions and their structural changes in early events in biological environments, as it can be found in body fluids. Our lab developed a characterization method based on small-angle X-ray scattering (SAXS) for in-situ, label-free and dynamic studies on early events of NPs interactions after exposure to a biological environment. A microfluidic mixing device is used with benchtop SAXS instruments and synchrotron facilities. Silica [1] and gold [2,3] NP systems are investigated for their colloidal stability. The developed SAXS method allows studying the mechanisms of NPs agglomeration and self-assembly processes, bringing new light to the essential requirement for a better understanding of NPs – body interactions (Fig. 1).

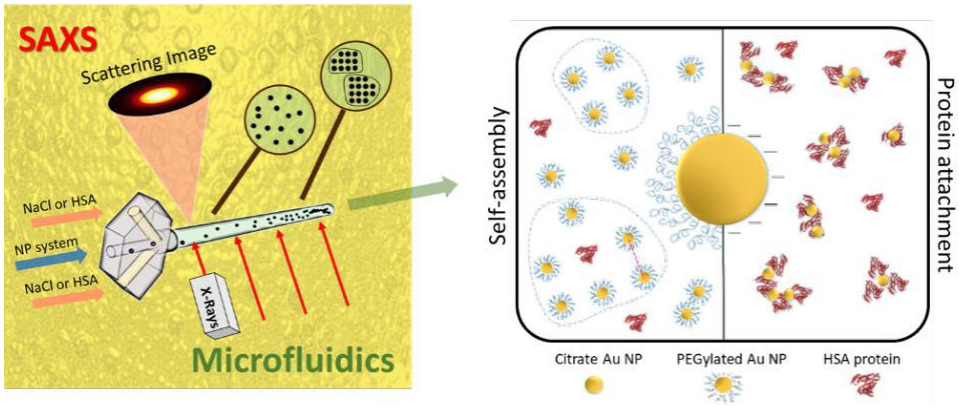

Figure 1: left: Scheme of the micro-fluidics SAXS setup for the in-situ investigation of early events in NPs interactions in a biological environment [1,3]; right: two different stabilization mechanisms for gold NPs in biological environments containing human serum albumin (HSA) [2].

We present a generic approach to analyze nanoparticle systems and their respective transformations in a biological environment. Our studies will be extended to holistic investigations for local drug administration systems investigating the dynamics of nanoparticle release and uptake. The combination of a microfluidic approach for synchrotron-based dynamics (early structural changes) with lab-based static small-angle X-ray scattering (SAXS) measurements (longer time scale for product reliability investigations) allows qualifying nanoparticle (NP) systems for their use in nanomedical applications.

1 Iranpour A., N., Sadeghpour, A., Iranshahi, K., Ong Khac, Q., Cendrowska, U., Toncelli, C., Dommann, A., Wick, P., Neels, A. (2020) A new approach for time-resolved and dynamic investigations on nanoparticles agglomeration, *Nanoresearch* **13**, 2847-2856, doi.org/10.1007/s12274-020-2940-4.

2 Iranpour A., N, Liebi, M., Ong, Q., Blanchet, C., Maurya, A. K., Stellacci, F., Salentinig, S., Wick, P., Neels, A. (2022) In-situ Investigations on Gold Nanoparticles Stabilization Mechanisms in Biological Environments Containing HSA, *Adv. Funct. Materials*, **32**, 2110253, 1-14, doi.org/10.1002/adfm.202110253.

3 Iranpour A., N, Liebi, M., Iranshahi, K., Blanchet, C., Wick, P., Neels, A. (2022) Time-Resolved Study on Self-Assembling Behavior of PEGylated Gold Nanoparticles in the Presence of Human Serum Albumin: A System for Nanomedical Applications, *ACS Appl. Nano Materials*, doi.org/10.1021/acsanm.2c04628.

A012-04-250823

Structural evolution of TIR-domain signalosomes in mammalian, plant and bacterial immunity characterized by integrative structural biology

Bostjan Kobe[1], Jeffrey D. Nanson[1], Mohammad K. Manik[1], Sulin Li[1], Weixi Gu[1], Mengqi Pan[1], Yan Li[1], Timothy W. Muusse[1], Parimala R Vajjhala[1], Katryn J. Stacey[1], Susannah Holmes[2], Connie Darmanin[2], Max T. B. Clabbers[3], Hongyi Xu[3], Yun Shi[4], Thomas Ve[4]

[1]University of Queensland, Brisbane, Queensland, Australia; [2]La Trobe University, Melbourne, Victoria, Australia; [3]Stockholm University, Stockholm, Sweden; [4]Institute for Glycomics, Griffith University, Southport, Queensland, Australia
b.kobe@uq.edu.au

Keywords: TIR domain, Toll-like receptor, plant NLR

TIR (Toll/interleukin-1 receptor) domains are widely distributed in animals, plants and bacteria, and function through self-association and homotypic interactions with other TIR domains [1]. Across phyla, these domains feature in proteins with immune functions - TLRs (Toll-like receptors), IL-1Rs (interleukin-1 receptors) and their adaptor proteins in animals; NLRs (nucleotide-binding, leucine-rich repeat receptors) in plants; and antiphage defence proteins in bacteria. Although long assumed to only have protein interaction functions, the TIR domains across kingdoms also feature self-association-dependent enzymatic activities, namely cleavage of nucleotides such as NAD^+ [2,3]. We used an integrated structural biology approach to characterize the signalosomes formed by different TIR domains. We reconstituted large assemblies of the TLR/adaptor TIR domains (not known to have enzymatic activities); the structures of the filamentous assemblies of the TIR domains of TLR adaptor MAL [4], TRAM and the TLR4:MAL complex (unpublished) were determined by cryo-electron microscopy (cryoEM) helical reconstruction, and the structures of crystalline arrays of MyD88 were determined by micro-electron diffraction and serial femtosecond crystallography [5]. We further stabilized the active assemblies of enzyme TIR domains from the mammalian protein SARM1 (involved in axon degeneration; octameric complexes) [6] and the bacterial protein AbTir from *Acinetobacter baumanii* [3] (filamentous assemblies) with NAD^+ mimics and determined their structures using single-particle cryoEM and helical reconstruction, respectively. We found that all these TIR domain assemblies feature a head-to-tail arrangement of TIR molecules, with the enzyme active site located in the interface between two molecules, explaining the requirement for self-association in enzyme activity. However, such head-to-tail row of molecules in stabilized by another row associating in an antiparallel fashion in enzyme assemblies such as those from SARM1 and plant NLRs, and in a parallel fashion in both scaffold assemblies (in TLR adaptors) and bacterial enzyme assemblies (Fig. 1). In all cases, we validated the observed interactions by structure-guided mutagenesis and functional assays (e.g. [7]). The products of enzymatic reactions have downstream signalling functions in immune pathways or their suppression. Our studies will form the foundation of applications ranging from the treatment of inflammatory disorders and bacterial infections in humans to the prevention of plant diseases.

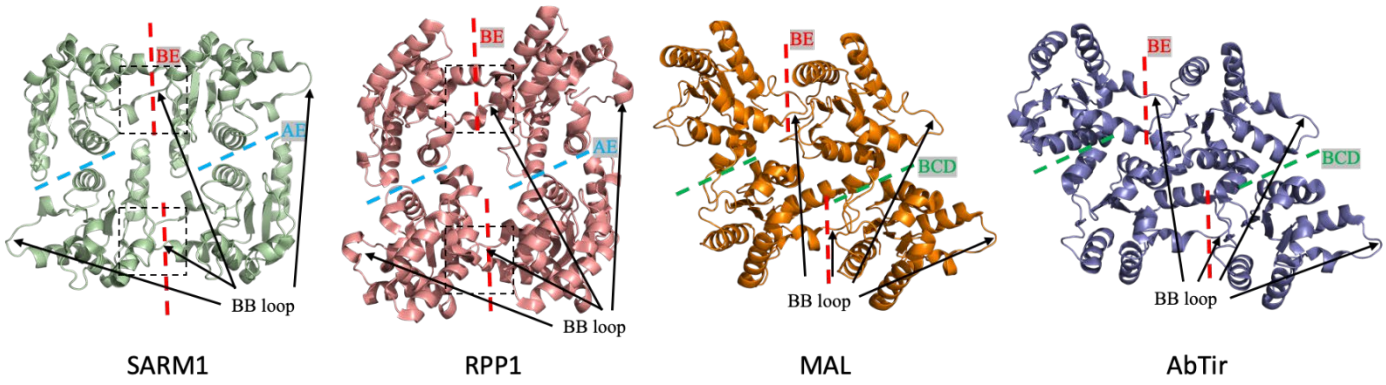

Figure 1. Structures of filamentous TIR-domain assemblies (four TIR domains are shown in each case, but the assemblies are open-ended from left to right of the page).

[1] Nimma et al & Kobe (2021) Front Immunol 12, 784484
[2] Horsefield et al & Kobe (2019) Science 365, 793
[3] Manik et al & Kobe (2022) Science, eadc8969
[4] Ve et al & Kobe (2017) Nat Struct Mol Biol 24, 743
[5] Clabbers et al & Ve (2021) Nat Commun 12, 2578
[6] Shi et al & Ve (2022) Mol Cell 82, 1643
[7] Muusse et al. & Stacey (2022) J Biol Chem, 102666

A012-05-250823

Understanding the conformational landscape of a protein complex from cryo-EM and mass-spectrometry data

R. Vuillemot 1,2, S. Valimehr 1, A. Sethi 1,3, M Kazemi 1, S. Jonic 2, I. Rouiller 1

1 Dpt Biochemistry & Pharmacology, Bio21 Institute, The University of Melbourne, Victoria, Australia.
2 IMPMC-UMR 7590 CNRS, Sorbonne Université, Muséum National d'Histoire Naturelle, Paris, France.
3 The Australian Synchrotron, Clayton, Victoria 3168, Australia
Email of communicating: isabelle.rouiller@unimelb.edu.au

Keywords: Cryo-EM, HDX-MS, XL-MS, AAA ATPase, Conformation

Detecting and characterizing the range of conformations that a protein complex adopts is essential to understand its functional molecular mechanism and its regulation. Through discrete-state classification methods, single particle cryo-EM enables to determine the structure of intermediate conformations. However, these methods assume countable number of conformations and produce three-dimensional density maps where dynamic regions of the protein complexes and regions that undergo continuous conformational changes are poorly defined or even not visible due to averaging artifacts. This is a common problem for many protein complexes, and it is particularly notorious for one of the most abundant protein in cell, the AAA ATPase, where six large protein domains are either averaged out or poorly defined in the EM maps [1, 2].

Using a novel approach based on a 3D-to-2D fitting method, called Molecular Dynamics for Single Particle Analysis of Continuous Conformational hEterogeneity or MDSPACE [3], we have analyzed the range of conformations adopted by these domains in the wild-type p97 protein and in a protein that contains a mutation (amino acid substitution) associated with the development of neurological diseases [2, 4]. Here, we will introduce the image analysis method [3], present the results from this analysis with dynamic results (Fig. 1) and compare them with results obtained using cross-linking and Hydrogen Deuterium Exchange mass spectrometry (XL-MS and HDX-MS).

Our study shows excellent agreement between these different methods and demonstrates that mass-spectroscopy and cryo-EM could complement each other in the study of the molecular and dynamic mechanisms of protein complexes.

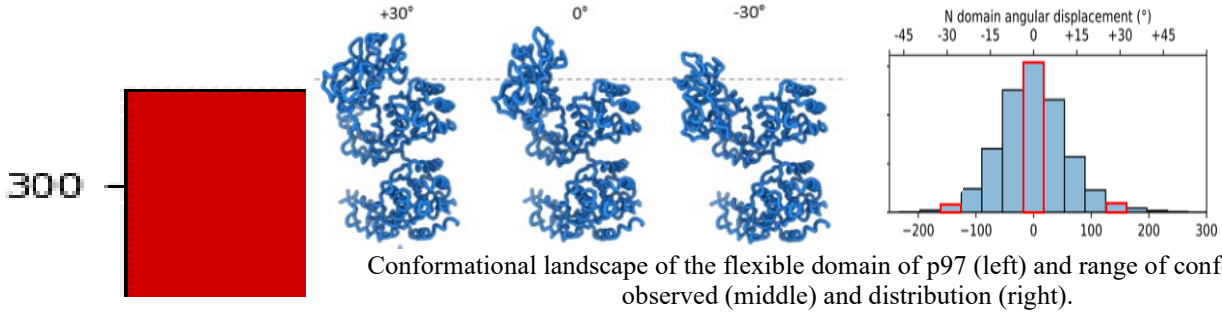

Figure 1. Conformational landscape of the flexible domain of p97 (left) and range of conformations observed (middle) and distribution (right).

Acknowledgement: The University of Melbourne start-up fund (to IR), The Bio21 Research Platform (Ian Holmes Imaging Center, Melbourne Mass Spectrometry and Proteomics, High Performance Computing), The French National Research Agency - ANR (ANR-19-CE11-0008 to SJ, BK, FT, and IR), the cooperation between the CNRS and the University of Melbourne (The Melbourne-CNRS Network, PRC 2889 to SJ and IR, CNRS 80 Prime to SJ, joint PhD scholarship to RV), Australian Research Council Centre for Cryo-Electron Microscopy of Membrane Proteins (CCeMMP).

[1] Rouiller, I., et al., *Conformational changes of the multifunction p97 AAA ATPase during its ATPase cycle.* Nat Struct Biol, 2002. **9**(12): p. 950-7.

[2] Mountassif, D., et al., *Cryo-EM of the pathogenic VCP variant R155P reveals long-range conformational changes in the D2 ATPase ring.* Biochem Biophys Res Commun, 2015.

[3] Vuillemot, R., et al., *MDSPACE: Extracting Continuous Conformational Landscapes from Cryo-EM Single Particle Datasets Using 3D-to-2D Flexible Fitting based on Molecular Dynamics Simulation.* J Mol Biol, 2023: p. 167951.

[4] Halawani, D., et al., *Hereditary inclusion body myopathy-linked p97/VCP mutations in the NH2 domain and the D1 ring modulate p97/VCP ATPase activity and D2 ring conformation.* Mol Cell Biol, 2009. **29**(16): p. 4484-94.

A012-06-250823

Crystallogenesis and structural research on human transferrin as a potential drug transporter

Camila Campos-Escamilla[1], Dritan Siliqi[2], Abel Moreno[1]

[1]Instituto de Química, Universidad Nacional Autónoma de México, Ciudad de México, CP 04510, Mexico City, México.
[2]Institute of Crystallography (IC), National Research Council (CNR), Via Amendola 122/O, 70126, Bari, Italy
Email: carcamo@unam.mx

Keywords: Transferrin, SAXS, X-ray crystallography

The present work explores the proposal of using an endogenous transport molecule, human transferrin, to perform a highly specific transport of ligands with anti-cancer activity, thanks to its receptor-mediated transcytosis mechanism [1]. Human transferrin is a ~80 kDa bilobular protein that transits the bloodstream to transport iron from its absorption sites to the different cells in the organism, through the coordination of the metal with 4 amino acids located in the interdomain region in each lobe [2-3]. This work is focused, therefore, on the nucleation, crystal growth, and 3D characterization of this protein, by means of two structural resolution techniques that use synchrotron radiation, small angle X-ray scattering (SAXS) and X-ray protein crystallography, to find potential ligand binding sites. To accomplish this, we have studied the conformational changes of transferrin at different pH conditions of physiological relevance, as well as the interaction with ruthenium-center coordination compounds developed as anti-cancer prodrugs [4]. The current advances have shown the co-existence of three main conformations [5], as well as a possible interaction with one of said metallic complexes on the surface of one of transferrin's domains.

Figure 1. SAXS-based pseudo-atomic modelling using MultiFoXS for holo-transferrin at pH 5.5. Multi-state models at different pH values were obtained after sampling over 10,000 conformations using PDB 2HAV (chain A) structure as a starting model. Three conformations were observed in the following proportions: closed, 13% (A); partially open, 57% (B); open, 30% (C).

[1] Kawabata, H. (2019). Transferrin and transferrin receptors update. Free Radical Biology and Medicine, 133, 46-54
[2] Fernandes, M.A., Hanck-Silva, G., Baveloni, F. G., Oshiro Junior, J.A., de Lima, F. T., Eloy, J.O., &Chorilli. M. (2020). A Review of properties, Delivery Systems and Analytical Methods for the Characterization of Monomeric Glycoprotein Transferrin. Critical Reviews in Analytical Chemistry, 1-12.
[3] Yang, N., Zhang, H., Wang, M., Hao, Q., & Sun, H. (2012). Iron and bismuth bound human serum transferrin reveals a partially-opened conformation in the N-lobe. Scientific reports, 2(1), 999.
[4] Scalambra, F., Serrano-Ruiz, M., Nahim-Granados, S., & Romerosa, A. (2016). Ruthenium Complexes Containing 2,2'-Bipyridine and 1,3,5-Triaza-7-phosphaadamantane. European Journal of Inorganic Chemistry, 10, 1528-1540.
[5] Campos-Escamilla, C., Siliqi, D., Gonzalez-Ramirez, L. A., Lopez-Sanchez, C., Gavira, J. A., & Moreno, A. (2021). X-ray Characterization of Conformational Changes of Human Apo- and Holo-Transferrin. International Journal of Molecular Sciences, 22, 13392.

One of the authors (C. C-E.) is a doctoral student from the Programa de Doctorado en Ciencias Biomédicas, Universidad Nacional Autónoma de México (UNAM) and has received scholarship with CVU 856528 from the Consejo Nacional de Ciencia y Tecnología (CONACyT). One of the authors (D.S) acknowledges SAXS data collection at B29 of ESRF (Grenoble, France) through Italian BAG MX2363 and Francesco Baldassarre (IC-CNR, Bari, Italy) for the sample preparations. This project was supported by the grant DGAPA-PAPIIT project No. 207922. Use of the Stanford Synchrotron Radiation Lightsource, SLAC National Accelerator Laboratory, is supported by the U.S. Department of Energy, Office of Science, Office of Basic Energy Sciences under Contract No. DE-AC02-76SF00515. The SSRL Structural Molecular Biology Program is supported by the DOE Office of Biological and Environmental Research and by the National Institutes of Health, National Institute of General Medical Sciences (P30GM133894). Use of the NSLS-II beamline from Brookhaven National Laboratory is supported by the U.S. Department of Energy under contract No. DE-SC0012704.

A032 Mapping atomic scale structure using electron diffraction and imaging
Room 211
4.30pm – 6:30pm

A032-01-250823

Crystal structure and charge density analysis at interfaces and domain boundaries using convergent-beam electron diffraction

D. Morikawa[1*], Y. Noguchi[2], K. Tsuda[3]

Institute of Multidisciplinary Research for Advanced Materials, Tohoku University, Sendai 980-8577, Japan,
[2] Faculty of Advanced Science and Technology, Kumamoto University, Kumamoto 860-8555, Japan,

Frontier Research Institute for Interdisciplinary Sciences, Tohoku University, Sendai 980-8578, Japan
[*] daisuke.morikawa.e5@tohoku.ac.jp

Keywords: convergent-beam electron diffraction, twin boundary, polar domain boundary

Convergent-beam electron diffraction is one of the powerful tools for the analysis of local structures using electron nano-probes. We have so far developed a crystal structure and electrostatic potential analysis method by quantitatively comparing the experimental CBED patterns and the simulated ones. The method was successfully applied to several materials with bulk form [1-4]. CBED patterns can be used for the analysis of non-centrosymmetric structures because of the dynamical scattering effect. Those advantages of the CBED technique, such as local structure analysis by the electron nano-probe with transmission electron microscopy and analysis of non-centrosymmetric structures, are useful for the analysis of interfaces and domain boundaries.

Recently, we reported a CBED analysis of a specific polar structure observed at the twin boundary of $CaTiO_3$ [5], which has a centrosymmetric structure in the bulk form. Figure 1(a) shows a TEM image with a so-called 90° twin boundary and (b) shows a

schematic structure. The CBED patterns were recorded across the boundary by scanning the electron probe (STEM-CBED) with a 0.2 nm step and 40×3 positions. (d)-(f) are CBED patterns obtained at the probe positions 1, 5, and 9, respectively. The twin boundary is located at position 5. CBED patterns from (d) and (f) have the same symmetry as those in the bulk form, with these symmetries being ***2mm*** which means two-fold rotational symmetry and two kinds of mirror symmetry. The 90° rotation between [1] and (f) corresponds to the twin structure. It is noteworthy here that the CBED pattern just at the twin boundary shows a single mirror symmetry and the position of the mirror is parallel to the boundary, which is not the same as the bulk form. Quantitative analysis of the CBED pattern obtained at the twin boundary suggests that polar structure is realized. The electrostatic potential and electron density will be discussed from the refinement of crystal structure factors with a superstructure including the twin.

The analysis of interface and domain boundary using CBED can be one of the powerful tools to understand the crystal structure and charge density distribution in a local specimen area. The CBED analysis is also applied to the polar domain boundary of ferroelectric materials. The domain width and features of the twin boundary and polar domain boundary show different tendencies and the details will be discussed.

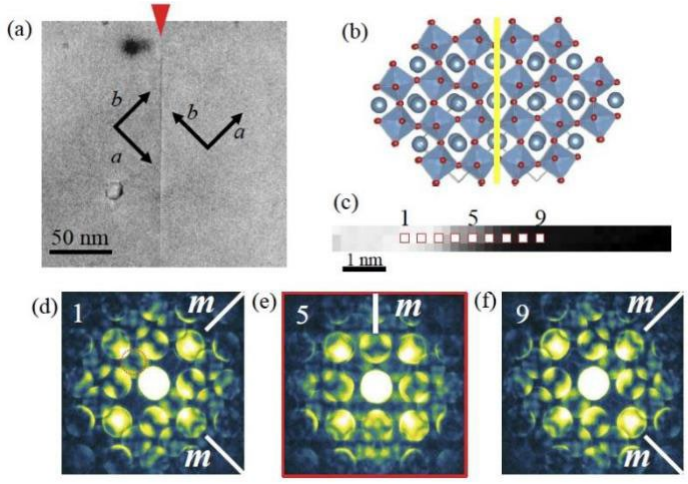

Figure 1. (a) Transmission electron microscopy image of a twin boundary in CaTiO3. (b) Schematic picture of a twin boundary.

(c) Reconstructed scanning transmission electron microscopy image formed by summing the intensities at the position indicated by the red circle in (d). (d)-(f) CBED patterns obtained for the positions shown in (c) 1, 5, 9, respectively [5].

[1] Tsuda, K., & Tanaka, M. (1999). *Acta Cryst.*, A**55**, 939.
[2] Tsuda, K., Ogata, Y., Takagi, K., Hashimoto, T., & Tanaka, M. (2002). *Acta Cryst.*, A**58**, 514.

[3] Ogata, Y., Tsuda, K., & Tanaka, M. (2008). *Acta Cryst.*, A**64**, 587.

[4] Aryal, B., Morikawa, D., Tsuda, K., & Terauchi, M. (2021). *Acta Cryst.*, A**77**, 289.

[5] Morikawa, D., & Tsuda, K. (2021). *Appl. Phys. Lett.,* **118**, 092901.

The authors thank Professor Masami Terauchi for the fruitful discussions and Mr. M. Ageishi of Tohoku University for the support during the experiments. This work was partially supported by JSPS KAKENHI Grant Nos. JP18H03674, JP18K18931, JP19K14623, 20H05176, and JP22H04495, the Research Program of "Dynamic Alliance for Open Innovation Bridging Human, Environment and Materials" in "Network Joint Research Center for Materials and Devices.", The Murata Science Foundation, The Mitsubishi Foundation, and JST PRESTO JPMJPR22AB, Japan.

A032-02-250823

Designing better 4D Scanning Transmission Electron Microscopy Experiments

B. D. Esser, J. Etheridge

Monash Centre for Electron Microscopy, Monash University, VIC 3800, Australia.
Bryan.Esser@monash.edu

Keywords: 4D Scanning Transmission Electron Microscopy

Modern scanning transmission electron microscopes (STEMs) come with a variety of advanced hardware that make atomic resolution imaging routine. From fast and highly sensitive detectors to higher-order aberration correction and purpose-built facilities, high spatial and energy resolution imaging and spectroscopy are standard practice in materials characterization. As these tools have become more pervasive, the types of experiments and amount of data we can collect in a single session have grown significantly. One of the most important hardware improvements of the last few years has been the development of high-speed direct electron detectors capable of capturing diffraction patterns $I(k_x, k_y)$ as a function of probe position (r_x, r_y), yielding a 4-dimensional (4D-STEM) dataset, Figure 1a. [1-5] These spatially resolved diffraction patterns can be used to generate a virtually unlimited number of images by making use of various scattering regimes and more advanced post-processing, such as centre-of-mass imaging, electron ptychography, strain mapping, and virtual dark field, to name a few. [6]

State-of-the-art 4D-STEM detectors typically compromise on number of pixels (10^4 to 10^7 pixels), frame rate (10^2 to $>10^5$), and dynamic range (10s to $>10^6$ electrons), depending on the intended use cases. Detectors can also be mounted in various locations within the microscope column, including behind an energy filter, adding additional functionality, Figure 1b. In this talk we demonstrate the capabilities of 4D-STEM on the world-first double spherical aberration corrected Thermo Scientific Spectre φ. The instrument is equipped with a monochromated source capable of fast high tension switching from 30-300 kV in the same session, as well as an EMPAD and pre- and post-energy filter Gatan K3 cameras, all capable of collecting 4D-STEM data. The ability to quickly change the wavelength of the incident electron beam whilst maintaining high spatial resolution opens the door for novel scattering experiments on a wide range of materials. We will present our most recent 4D-STEM studies making the most of this class-leading instrument and its range of detectors, as well as integrate simulated data as a guide for future experiments.

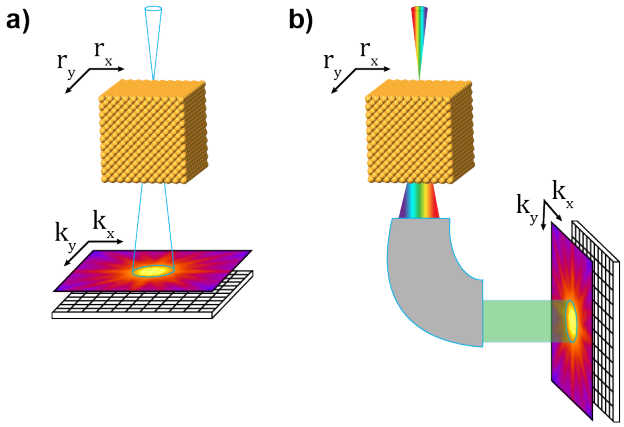

Figure 1: 4D-STEM detectors can be used to collect diffraction patterns as a function of probe position. (a) Standard and (b) energy filtered mounting positions allow more flexible experimental setups.

[1] M.W. Tate *et al.*, *Microscopy and Microanalysis* **22** (2016) 237–249.
[2] P. Pelz *et al.*, *Microscopy and Microanalysis* **27** (2021) 188–189.
[3] H. Ryll *et al.*, *Journal of Instrumentation* **11** (2016) P04006.
[4] I. MacLaren *et al.*, *Microscopy and Microanalysis* **26** (2020) 653–666.
[5] G.W. Paterson *et al.*, *Microscopy and Microanalysis* **26** (2020) 944–963.
[6] C. Ophus, *Microscopy and Microanalysis* **25** (2019) 563–582.

This work was supported by Australian Research Council (ARC) grant DP160104679 and used a Titan3 80-300 FEG-TEM funded by ARC LE0454166 and the Spectra Phi FEG-TEM funded by ARC LE170100118 in the Monash Centre for Electron Microscopy.

A032-03-250823

Using 4D-STEM to measure the nanoscale structure of materials in 2D and 3D

C Ophus[1], PM Pelz[2], HA Sternlict[1], BH Savitzky[1], A Rakowski[1], A Bruefach[3], S Ribet[1], MS Scott[1,3]

[1]NCEM, Molecular Foundry, Lawrence Berkeley National Laboratory, 1 Cyclotron Road, Berkeley, USA,
[2]Department of Materials Science and Engineering, Friedrich-Alexander-Universität, Cauerstraße 3, Erlangen, Germany
[3]Materials Science and Engineering, University of California Berkeley, 110 Sproul Hall Berkeley, USA,

cophus@gmail.com

Keywords: 4D scanning transmission electron microscopy, analysis software, diffraction

Characterizing the morphology of beam-sensitive hard and soft matter with scanning transmission electron microscopy (STEM) is challenging because these materials are often weakly scattering, and can be easily damaged by the electron dose required to resolve atomic-scale features. One of the most dose-efficient methods to study these materials is to record images of the diffracted STEM probe as a function of probe position. The resulting datasets consist of two real space and two diffraction space measurements, generating a four-dimensional array known as a 4D-STEM dataset [1]. High-speed direct electron detectors can now record thousands or even millions of diffraction patterns per experiment. To analyse this large amount of data, we have developed the py4DSTEM toolkit [2]. One of the most common 4D-STEM applications is to measure the orientation of Bragg diffracted peaks from crystalline samples using a nearly parallel electron beam, as shown in Fig. 1(a). By measuring the peak positions, we can reconstruct the morphology of beam sensitive samples [3]. Fig. 1(b) shows how the chemistry of a hierarchically ordered polymer and its chemical model can be directly connected to the resulting morphology [4]. We can also simulate diffraction patterns from crystalline materials, to measure the 3D orientation of crystalline grains through the incorporation of prior knowledge [5]. We can also boost the resolution of a 4D-STEM measurement by increasing the convergence angle until the probe size is sub-atomic, as shown in Fig. 1(c). By recording diffraction patterns of many overlapping atomic-scale probes, we can use the computational imaging method of ptychography to reconstruct the phase of the sample. Fig 1(c) also demonstrates how ptychographic measurements recorded at many sample tilts allows us to solve the structure of complex materials in 3D, for the example of a ZrTe nanowire inside a double-walled carbon nanotube (Dw-CNT) [6]. In this talk, I will describe these experiments in detail with a focus on the data analysis pipelines, and the importance of open source analysis codes and datasets.

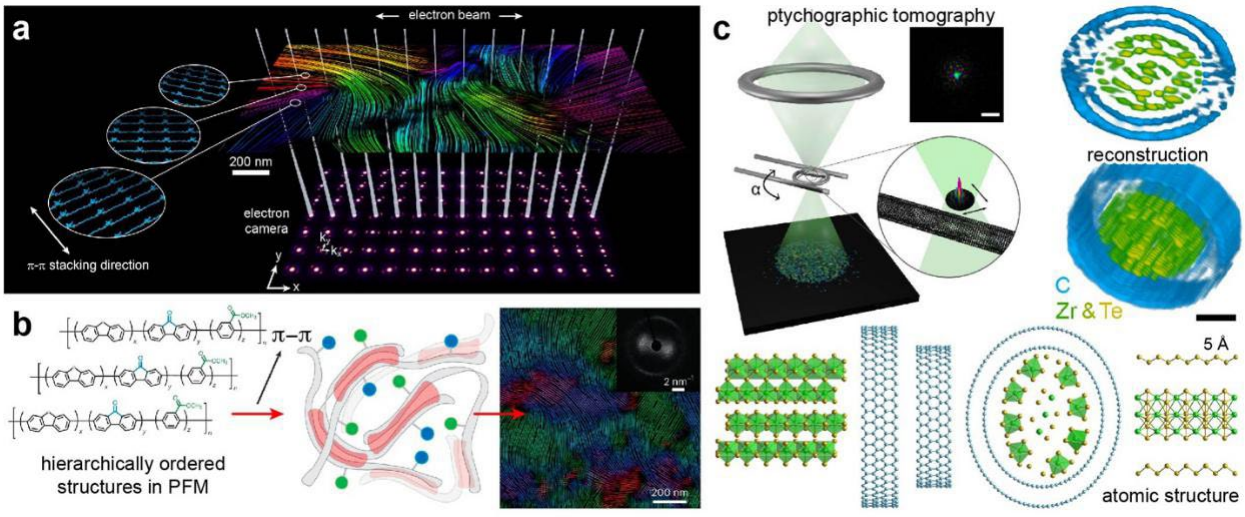

Figure 1. **(a)** 4D-STEM experimental geometry, with reconstructed sample, adapted from [3]. **(b)** Orientation mapping of a polymer, adapted from [4]. **(c)** Ptychographic 3D tomography measurement of ZrTe nanowire in DW-CNT, adapted from [6].

1 C Ophus, Microscopy and Microanalysis 25, 563 (2019).
2 B Savitzky, SE Zeltmann, LA Hughes, et al., Microscopy and Microanalysis 27, 712 (2021).

3 K Bustillo, SE Zeltmann, M Chen, et al., Accounts of Chemical Research 54, 2543 (2021).
4 T Zhu, H Sternlicht, H Yang, et al., Nature Energy (2023).
5 C Ophus, SE Zeltmann, A Bruefach, et al., Microscopy and Microanalysis 28, 390 (2022).
6 PM Pelz, S Griffin, S Stonemeyer, et al., arXiv preprint arXiv:2206.08958 (2022).

A032-04-250823

Revealing atomic structure and composition in ultrahigh energy storage density ferroelectric thin-films using (scanning) transmission electron microscopy

S. L. Y. Chang1,2, D. Stroppa3, R. Webster1, Yunlong Sun2, Danyang Wang2

Electron Microscope Unit, Mark Wainwright Analytical Centre, University of New South Wales, Sydney, NSW 2052, Australia.
School of Materials Science and Engineering, University of New South Wales, Sydney, NSW 2052, Australia
Dectris Ltd., Taefernweg 1, 5405 Baden-Daetteil, Switzerland

shery.chang@unsw.edu.au

Keywords: Ferroelectrics, Scanning transmission electron microscopy, 4D STEM

Ferroelectric thin film material is positioned to be a strong candidate for nano/microelectronics component with ultra-high energy storage density with low electric field [1]. One of the key strategies to achieve such high energy storage density is by creating a secondary phase nanostructure around the morphotropic phase boundary. Here we show detailed characterisation of (Bi, Na)TiO_3 (BNBT) and $BiFeO_3$ (BFO) thin films grown on $SrTiO_3$ single crystal substrate. The nanostructures in the thin films as well as their electronic structures and composition variations were characterised using a range of (S)TEM techniques including high angular dark field (HAADF-STEM), and 4D STEM, as well as Negative Cs phase contrast TEM imaging (NCIS). In addition electron energy loss spectroscopy (EELS) was used to probe the composition and the electronic structure across the nanostructured domains. These techniques were performed on the newly installed double aberration corrected JEOL GrandARM300F2 (S)TEM instrument at UNSW.

We found that there is Bi segregation forming strips of half unit cell wide β-Bi_2O_3 layers. Such composition is confirmed by the atomic resolution EELS maps, showing no presence of Ti within the β-Bi_2O_3 bright strips. The effect of the β-Bi_2O_3 layers is to laterally displace the lattice above the defect by half a unit cell, resulting a morphotropic anti-phase domain boundary. In addition, the Bi_2O_3 segregation layer gives about 22% longer c-axis for the 3 unit cell around the defect. Such large expansion of c-axis is attributed to the presence of the super-tetragonal phase (super-T) [2-3]. The electronic structures of Ti and O sites adjacent to the β-Bi_2O_3 , measured using EELS Ti L edge and O K edge, is consistent with the lattice distortions, measured from NCIS HRTEM and 4D STEM. Such complex nanostructures with multiple structure phases con-existent forming nanodomains is found to be the key for the ultra-high performance of such ferroelectric thin films.

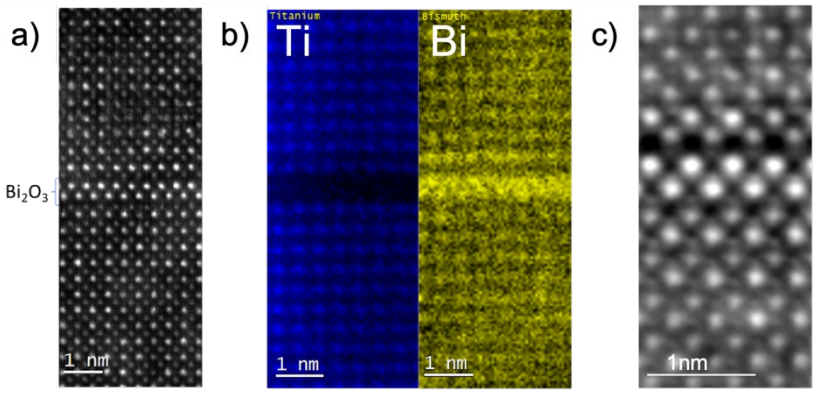

Figure 1. *a) HAADF-STEM image showing the structure of the Bi segregation into half unit cell of* β-Bi_2O_3. *b) Atomic resolution EELS map of Ti L edge and Bi M edge elemental maps from the same region shown in a), and c) the integrated differential phase contrast image derived from the 4D-STEM dataset showing the oxygen sites.*

[1] Pan, H.; Lan, S.; Xu, S.; Zhang, Q.; Yao, H.; Liu, Y.; Meng, F.; Guo, E.-J.; Gu, L.; Yi, D. (2021) *Science* **2021,** *374* (6563), 100-104.
[2] Sun, Y., Zhang, L., Huang, Q., Jin, L., Chang, S. L. Y., Wang, Y., Zhang, P., Liao, X., Li, S., Zhang, S., Wnag, D. (2022) Adv. Sci., 2203926.

The authors acknowledge the facilities and the scientific and technical assistance of Microscopy Australia at the Electron Microscope Unit (EMU) within the Mark Wainwright Analytical Centre (MWAC) at UNSW Sydney. SLYC acknowledge the funding support from Australian Research Council (DP220102790). Acquisition of 4D STEM data using the Dectris ARINA detector in collaboration with Dectris is gratefully acknowledged.

A032-05-250823

The L-phase precipitates in Al-Mg-Si-Cu alloys

R. Holmestad[1], C.D. Marioara[2], E. Thronsen[2], S. Wenner[2], S.J. Andersen[2]

[1]Norwegian University of Science and Technology, Department of Physics, Høgskoleringen 5, 7491 Trondheim, Norway [2]SINTEF Industry, Materials and Nanotechnology, 7492 Trondheim, Norway randi.holmestad@ntnu.no

Keywords: aluminium alloys, HAADF-STEM, SPED

Age-hardenable aluminium alloys like Al-Mg-Si-Cu, Al-Mg-Zn and Al-Cu are important structural materials for construction and automotive applications due to properties like high strength/weight ratio and good formability, often combined with good corrosion resistance. One overall objective in our research is to improve the understanding of the fundamental physics taking place at the atomic scale in these alloys – which decides nucleation, phase stabilization and precipitation [1]. The size, density and crystal structure of the hardening precipitates are given by the alloy composition and the thermo-mechanical history of the material and will to a large extent decide the material's properties. In Al-Mg-Si alloys the main hardening precipitates are β'' needles [2]. In Mg-richer alloys with small additions of Cu, the β''-phase is often replaced by fine lath-shaped, Cu-containing *L*-phase precipitates.

The *L*-phase structure is disordered, often containing sub-units of the periodic Q′ and *C* phases, ordered on an inherently projected hexagonal *Si-network* [1], which aligns with ⟨100⟩Al. All the precipitate structures in the Al-Mg-Si system are based on this network. *L* has high coherence, less strain and strong bonding with the Al matrix and therefore shows a larger resistance toward dissolution and growth [3]. The high thermal stability is supported by *in-situ* TEM experiments, which indicate that all *L*-phase precipitates form at an early stage and remain after long thermal exposure [4]. In addition to being promoted by increased Cu levels, the formation of *L*-phase precipitates is triggered by increased Mg/Si ratios, likely due to a stabilising effect of Cu enriched interfaces [5]. Due to its disordered nature, the composition of the *L*-phase is varying. An average composition can be estimated by determining the atomic species in each atomic column from aberration-corrected high-angle annular dark-field scanning transmission electron microscopy (HAADF-STEM) images. For heavily deformed alloys, the *L*-phase nucleates both as discrete precipitates on dislocation lines and homogeneously in the undistorted regions of the Al matrix [6]. The incorporation of Cu in precipitates may also make the alloy less prone to intergranular corrosion [7].

This presentation will demonstrate how HAADF-STEM can be used to study precipitate phases like *L* in aluminium alloys. In combination with the scanning precession electron diffraction (SPED) technique utilizing effective machine learning approaches and digital post-processing [5,6] this is a very useful methodology to get comprehensive information about precipitate morphology and phase compositions, as well as crystallite orientations, also in deformed materials.

1 Andersen, S.J., Marioara, C.D., Friis, J. et al. (2018) *Adv. in Physics: X*, **3**,1.
2 Zandbergen, H.W., Andersen, S.J. & Jansen, J. (1997) *Science* **277**,1221.
3 Marioara, C.D., Andersen, S.J., Røyset, J. et al. (2014) *Metall Mater Trans A* **45**, 2938.
4 Sunde, J.K., Wenner, S. & Holmestad, R. (2020) *Journ. of Microscopy* **279,** 143.
5 Sunde, J.K., Marioara, C.D. & Holmestad, R. (2020) *Mat. Char.* **160**, 110087.
6 Thronsen, E., Marioara, C.D, Sunde, J.K. et al. (2020) *Materials & Design* **186**,108203.
7 Marioara, C.D., Lervik, A., Grønvold, J. et al. (2018) *Metall Mater Trans A* **49**, 5146.

This work is supported by the Research Council of Norway and Norwegian light metal industry through several projects and the NORTEM infrastructure at the TEM Gemini Centre in Trondheim (NFR 197405).

A032-06-250823

Resolving exotic superstructure ordering in emerging materials using advanced STEM

C. Xu[1], Y. Zhu[1]

[1]*Department of Applied Physics, The Hong Kong Polytechnic University, Hung Hom, Kowloon, Hong Kong SAR, China*
Email of communicating: yezhu@polyu.edu.hk

Keywords: Structural modulation, Octahedral tilting, Polarization mapping

Novel functional materials are usually characterized by emerging ordering beyond the conventional unit-cell level. Examples include artificial superlattices, self-assembled nanostructures, ferroic domain structures, and charge-density waves. Such complex ordering, even though occurring collectively, commonly suffers nanoscale fluctuations that destroy the long-range periodicity that is required for conventional diffraction-based structure analysis, posing a formidable challenge for accurate structure determination. On the other hand, the maturation of aberration-corrected TEM/STEM presents an alternative real-space approach to probe the local complex ordering, through directly imaging the atomic structure with picometer precision. In this talk, I will give several examples demonstrating the power of advanced STEM on resolving the complex atomic ordering in perovskite oxides and 2D materials: i) By developing an imaging condition optimized for oxygen contrast, we can image sensitively the octahedral structure in perovskite oxides with picometer precision. It further enabled us to reveal an extraordinary 2D ordered octahedral tilting in the solid electrolyte $Li_{0.5-3x}Nd_{0.5+x}TiO_3$ (Fig. 1a and 1b), and to demonstrate its dependence on the competition between Li content and lattice strain.[1] ii) Through atomic displacement mapping based on high-resolution imaging, and electric polarization mapping based on 4D-STEM, we made the first experimental discovery of 2D antiferroelectricity in vdW In_2Se_3 (Fig. 1c), and resolved the true nature of its superstructure that had been under debate for over four decades.[2] We also demonstrated the 2D ferroelasticity coupled with this antiferroelectricity through the spontaneous lattice strain.[3] iii) Lastly, iDPC technique in STEM allowed us to unravel the exotic polar textures associated to the modulated octahedral tilting in complex perovskites. The characterization strategy and capability in our work demonstrate a powerful tool to probe the structure-property interplay in emerging functional materials at the atomic scale.

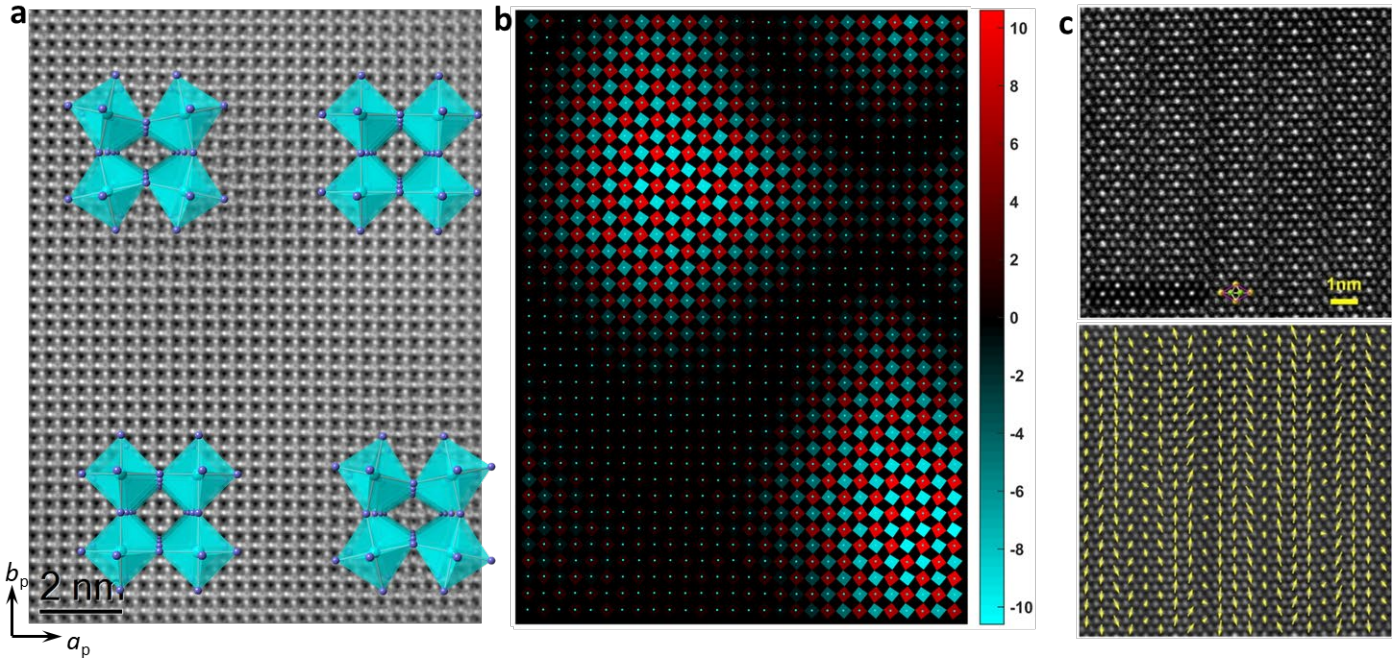

Figure 1. (a) Oxygen-sensitive STEM image and (b) the associated octahedral-tilt map, showing modulated octahedral tilt in on $Li_{0.5-3x}Nd_{0.5+x}TiO_3$. (c) ADF-STEM image on vdW In_2Se_3 and the associated polarization map, showing unusual 2D antiferroelectricity.[2]

[1] Zhu, Y.*, Withers, R. L., Bourgeois, L., Dwyer, C. & Etheridge, J.* (2015). *Nat. Mater.* **14**, 1142.
[2] Xu, C., Chen, Y., Cai, X., Meingast, A., Guo, X., Wang, F., Lin, Z., Lo, T. W., Maunders, C., Lazar, S., Wang, N., Lei, D., Chai, Y., Zhai, T., Luo, X. & Zhu, Y.* (2020). *Phys. Rev. Lett.* **125**, 047601.
[3] Xu, C., Mao, J., Guo, X., Yan, S., Chen, Y., Lo, T. W., Chen, C., Lei, D., Luo, X., Hao, J., Zheng, C. & Zhu, Y.* (2021). *Nat. Commun.* **12**, 3665.

Y. Z. thanks the financial support from the Research Grants Council of Hong Kong (N_PolyU531/18, C5029-18E) and the Hong Kong Polytechnic University grant (1-ZVRP).

A060 In memoriam of Igor Dzyaloshinskii and Sergey V. Maleyev: Antisymmetric Exchange, Magnetic Chirality, from Helimagnets to Topological Spin Textures

Room 219
4.00pm – 6:30pm

A060-01-250823

Toroidal transitions and chirality of Dzyaloshinskii-Moriya interactions

Huibo Cao[1*], Sang-Wook Cheong[2]

[1]Oak Ridge National Laboratory
[2]Rutgers University

caoh @ornl.gov

Keywords: Toroidal moment, Chirality, Local Magnetic Susceptibility

A toroidal dipole moment appears independent of the electric and magnetic dipole moment in the multipole expansion of electrodynamics. It arises naturally from vortex-like arrangements of spins. A toroidal order breaks various combinations of global symmetries, such as time and space inversion. Observing and controlling spontaneous long-range orders of toroidal moments are promising for spintronics but remain challenging. We have reported that a vortex-like spin configuration with a staggered arrangement of toroidal moments, a ferritoroidal state, was realized in a chiral triangular-lattice magnet $BaCoSiO_4$[1]. Upon applying a magnetic field, we observed multi-stair toroidal transitions correlating directly with metamagnetic transitions. A first-principles microscopic Hamiltonian has been established to explain both the formation of toroidal states and the metamagnetic toroidal transition as a combined effect of the magnetic frustration and the Dzyaloshinskii-Moriya (DM) interactions allowed by the crystallographic chirality in $BaCoSiO_4$. To confirm the chirality of DM interactions, we have measured polarized neutron diffraction, which will be introduced in this focused microsymposium in memoriam of Igor Dzyaloshinskii and Sergey V. Maleyev.

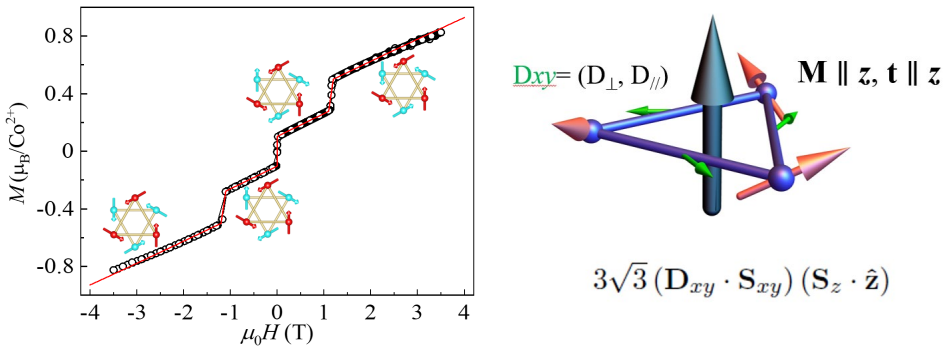

Figure 1. Magnetic vortex switch under field and illustration of DM vectors with spins

[1] Ding L., Xu X., Jeschke H.O., Bai X., Feng E., Alemayehu A.S., Kim J.W., Huang F., Zhang Q., Ding X., Harrison N., Zapf V.S., Khomskii D., Mazin I.I., Cheong S.W., Cao H.B., (2021). *Nature Communications*, **12**, 5339.

The work at Oak Ridge National Laboratory (ORNL) was supported by the US Department of Energy (DOE), Office of Science, Office of Basic Energy Sciences, Early Career Research Program Award KC0402020, under Contract No. DE-AC05-00OR22725. This research used resources at the High Flux Isotope Reactor, the DOE Office of Science User Facility operated by ORNL. The work at Rutgers University was supported by the DOE under Grant No. DOE: DEFG02-07ER46382.

A060-02-250823

Chiral spin liquid ground state in $YBaCo_3FeO_7$

W. Schweika[1,2], M. Valldor[3], J. D. Reim[2,4], U. Rößler[5]

[1]European Spallation Source ERIC, Lund, Sweden, [2]Forschungszentrum Jülich, Germany; [3]Centre for Materials Science and Nanotechnology, Department of Chemistry, University of Oslo, Norway; [4]Institute of Multidisciplinary Research for Advanced Materials, Tohoku University, Sendai, Japan; [5]Leibniz-Institut für Festkörper- und Werkstoffforschung IFW Dresden, Germany

werner.schweika@ess.eu

Keywords: chirality, antisymmetric exchange, polarised neutrons,

A chiral spin liquid state is discovered in the highly frustrated, noncentrosymmetric swedenborgite compound $YBaCo_3FeO_7$, a layered kagome system of hexagonal symmetry. This state remains stable down to very low temperatures, despite of very strong antiferromagnetic super-exchange and its existence can be traced back to the underlying antisymmetric exchange in the system arising from broken symmetry along the exchange paths. It is shown within a fundamental theoretical analysis based on a classical mechanism that this chiral spin liquid state is a possible ground state of the system.[1]

The scattering experiments with polarized neutron were performed at the DNS at MLZ Munich. We measured the diffuse scattering in the (hk0) plane of a single domain crystal at low temperature, in spin-flip mode and with polarization reversal along the scattering vector **Q**. In an extension to the conventional XYZ method and analysis [2], the related intensity difference yields the chiral scattering, which shows a characteristic antisymmetry, see Figure 1 (left). A model description is found by the Fourier transform of the vector chirality $\mathbf{C} = \mathbf{S} \times \mathbf{S}'$ in terms of cycloidal spin correlations. These cycloidal spin correlations emanate from trigonal sites with threefold rotational symmetry around the polar *c*-axis and spread out into the adjacent kagome layers forming a solitonic, lump-like structure. An approximate picture of the spin lump pattern is displayed in Figure 1 (right).

The present scenario displays similarities to the avoided phase transition in coupled gauge and matter fields for subnuclear particles. Chiral properties are invisible to conventional neutron scattering, but show up in the antisymmetric scattering of polarized neutrons. There are many frustrated spin systems with a non-centrosymmetric structure, where the lack of long-range order may originate from a similar, yet hidden, chirality.

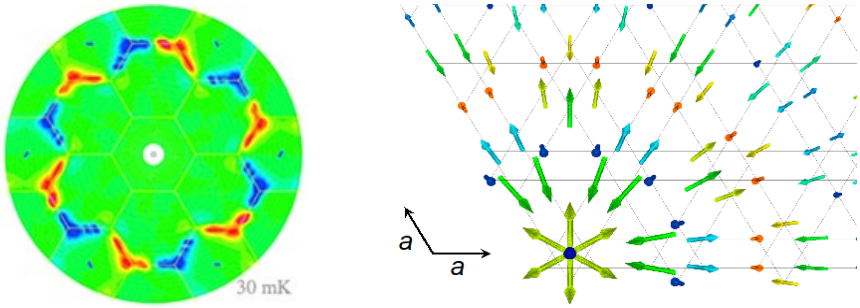

Figure 1. Chiral state in a $YBaCo_3FeO_7$ single crystal at very low temperatures. (left) Antisymmetric chiral scattering in the (hk0) plane and (right) a sketch of the chiral lump motif, a cylindrical wave composed of three cycloids, which emanate from a trigonal site between adjacent kagome layers.

[1] W. Schweika, M. Valldor, J. D. Reim, and U. K. Rößler, Chiral Spin Liquid Ground State in $YBaCo_3FeO_7$. (2022). *Phys. Rev. X* **12**, 021029.

DOI: https://doi.org/10.1103/PhysRevX.12.021029

[2] W. Schweika (2010), J. Phys. Conf. Ser. **211**, 012026.

A060-03-250823

Generalized Dzyaloshinskii-Moriya Interaction and Chirality-Induced Phenomena in Chiral Crystals

J. Kishine

The Open Univ. Japan

kishine@ouj.ac.jp

Keywords: Dzyaloshinskii Moriya Interaction, Lifshitz invariant, Chiral crystals, Chiral Soliton Lattice, Chirality-induced spin selectivity, Chiral phonon

I will review recent advances on the studies on magnetic[1], electronic[2], spintronic[3], and phononic[4,5] properties of chiral crystals, with a focus on the connection between Dzyaloshinskii Moriya interaction (DMI) and chirality in materials[1]. Importantly, a microscopic DMI is elevated to a macroscopic Lifshitz invariant (LI) in chiral crystals, where mirror-reflection and inversion symmetry are globally broken. As a consequence, chiral crystals exhibit nontrivial physical responses over a macroscopic scale. Indeed, in chiral magnetism, a chiral spin soliton lattice (CSL), which is one of the prominent outcomes arising from the DMI and LI as envisioned by Dzyaloshinskii in 1960s, appears in monoaxial chiral magnetic crystals and exhibits a variety of nontrivial physical properties characterized by coherent and topological nature of the CSL[1]. Furthermore, a giant spin polarization emerges over a macroscopic scale in a wide range of chiral materials from organic molecules to inorganic crystals[6]. The first-order spatial dispersion like the LI also appears in elastic or phonon degrees of freedom in chiral crystals. These examples show how a time-even pseudo scalar (electric toroidal monopole term in the language of multipole), which corresponds to a generalized concept of the DMI and LI, is realized in chiral media. The full content of this presentation will be presented as a review article [6] in the special volume of Journal of Physical Society of Japan, titled “Dzyaloshinskii-Moriya Interactions: physics of inversion symmetry breaking.”

[1] Kishine, J. & Ovchinnikov. (2015). *Solid State Physics* **66**, 1.

[2] Kishine, J., Kusunose H. &Yamamoto, H.M. (2022). *Isr. J. Chem.* **62**, e202200049.

[3] Kato, A., Yamamoto H.M. & Kishine, J. (2022). *Phys. Rev.* **B105**, 195117.

[4] Kishine, J., Ovchinnikov, A. S. & Tereshchenko A. A.(2020). *Phys. Rev. Lett.***125**, 245302.

[5] Ishito, K., Togawa, Y., Kishine, J., & Takuya Satoh et al. (2023). *Nature Physics* **19**, 35–39.

[6] Togawa, Y., Ovchinnikov, A.S. & Kishine, J. (2023). *J. Phys. Soc. Jpn. to appear in Special Topics Dzyaloshinskii-Moriya Interactions: physics of inversion symmetry breaking.*

This presentation is mainly based on collaboration with Y. Togawa, A.S. Ovchinnikov, H.Y. Yamamoto and H. Kusunose. This work was supported by JSPS KAKENHI Grants No. 21H01032 and JSPS Bilateral Joint Research Projects (JSPS-RFBR).

A060-04-250823

Emergent helical texture of electric dipoles

E. Khalyavin1, F. Orlandi1, P. Manuel1, R.D. Johnson2, P.G. Radaelli3, A.A. Belik4

2 ISIS Facility, Rutherford Appleton Laboratory, Harwell Oxford, Didcot OX11 0QX, United Kingdom, 2 Department of Physics and Astronomy, University College London, London, WC1E 6BT, United Kingdom, 3 Department of Physics, University of

Oxford, Clarendon Laboratory, Parks, Road, Oxford, OX1 3PU, United Kingdom, 4 Research Center for Functional Materials, National Institute for Materials Science (NIMS), 1-1 Namiki, Tsukuba, Ibaraki 305-0044, Japan

dmitry.khalyavin@stfc.ac.uk

Keywords: Chirality, Dipole order, Electric DMI

Materials with ordered magnetic or electric dipole moments have many important technological applications. Historically, ordering of magnetic dipoles was discovered first for simple ferro and antiferromagnets and then similar orderings of electric dipoles were suggested by analogy with magnetism, and then realised as ferroelectrics and antiferroelectrics. Later, exotic magnetic structures beyond the collinear paradigm have been revealed with the prototype example of incommensurate helical order in metallic Ho. This gives rise to a natural question, how far can the analogy between ordering of magnetic and electric dipoles go and is there an electric-dipole counterpart to the most complex magnetic structures found to date? In the present work, nearly sixty years after the discovery of a spin-helix in Ho, we report the first observation of an analogous helical ordering of electric dipoles. In perovskite $BiMn_7O_{12}$, hole-doping stabilizes a chiral crystal structure, where lone pair electrons of Bi^{3+}, and related atomic displacements, are ordered into an incommensurate structural helix (Fig. 1). The helical phase is preceded by a high-temperature, non-chiral, modulated state. This behaviour represents a full structural analogue to prototypical magnetic multiferroics in which non-polar collinear spin-density-waves are followed by a polar phase with rotating spins. Similar to this magnetic phenomenon, the helical structure of $BiMn_7O_{12}$ couples to a macroscopic electrical polarization, which opens a unique opportunity to control chiral structural domains and their associated optical activity with an applied electric field. Phenomenological term describing the coupling to the macroscopic polarization is identical to the cases of magnetic dipole texture, implying a possible existence of antisymmetric Dzyaloshinskii-Moria interaction between electric dipoles.

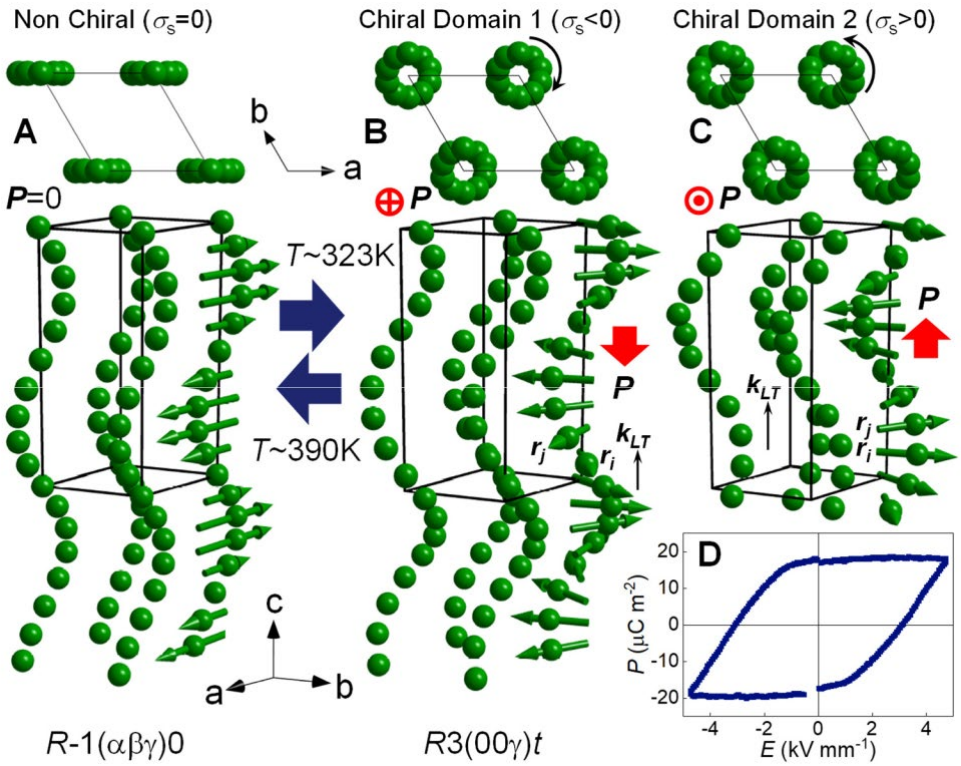

Figure 1. Schematic representation of the displacements of Bi in the high temperature non-chiral (A) and low-temperature chiral (B and C) modulated phases of $BiCu_{0.1}Mn_{6.9}O_{12}$. The black lines indicate an approximately commensurate supercell. The displacement directions are shown by arrows whose length is proportional to the magnitude of the displacement. In the chiral phase, two domains with opposite chirality, and hence opposite direction of the weak macroscopic polarization ***P***, are shown. (D) P-E loop measured for ceramic sample at T = 77 K, demonstrating switching between the domains of opposite polarity.

A060-05-250823

Complex magnetic structures in EuPtAs

6 Xie1234, P. J. Bereciartua Perez4, X. Y. Zheng3, M. Smidman3, T. Takabatake35, P. Miao12, and H. Q. Yuan3*, S. Francoual4*

[1]*Institute of High Energy Physics, Chinese Academy of Sciences, Beijing 100049, P. R. China;*
[2]*Spallation Neutron Source Science Center, Dongguan 523803, P. R. China;*
[3]*Center for Correlated Matter and Department of Physics, Zhejiang University, Hangzhou, 310027, China*
[4]*Deutsches Elektronen-Synchrotron (DESY), Notkestraße 85, 22607 Hamburg, Germany*
[5]*Department of Quantum Matter, AdSM, Hiroshima University, Higashi-Hiroshima 739-8530, Japan*

hqyuan@zju.edu.cn ; sonia.francoual@desy.de

Keywords: noncentrosymmetric, topological spin texture, Dzyaloshinskii–Moriya interaction

Magnetic systems lacking inversion symmetry (noncentrosymmetric, NC) and with significant spin-orbit coupling can exhibit the antisymmetric Dzyaloshinskii-Moriya (DM) interaction between magnetic moments, in addition to the Heisenberg-typed exchange interactions, which can give rise to a number of complex non-collinear magnetic ground states[1], such as helical magnetic structures. Furthermore, in some systems such as MnSi, the competition of these two interactions may lead to a topological-nontrivial magnetic skyrmion phase under applied magnetic fields [2]. More recently, a similar field-temperature phase diagram has been reported in EuPtSi, in which there is also a magnetic skyrmion phase [3] showing characteristics different to that in MnSi. Such observations have stimulated the search for skyrmion-like topological spin textures (TST) in rare-earth based compounds [4]. For example, neutron diffraction and Hall effect measurements on CeAlGe have revealed a field-induced Meron phase where there is a double-k magnetic ground state with a topological charge Q = 1/2 [5], while isostructural NdAlSi exhibits a chiral spin texture driven by topological Weyl fermions [6].

We have recently characterized the physical properties and phase diagrams of EuPtAs with the NC polar structure, which is isostructural to CeAlGe [7]. Using the x-ray resonant magnetic scattering (XRMS) technique, we have studied the magnetic structures in different phases. Our results suggest that EuPtAs exhibits incommensurate magnetic structure below T_N followed by a lock-in transition at T_M. Together with the neutron diffraction measurements, our studies indicate noncollinear magnetic structures in EuPtAs at zero field, while the evidences for potential TST under magnetic fields have also been observed.

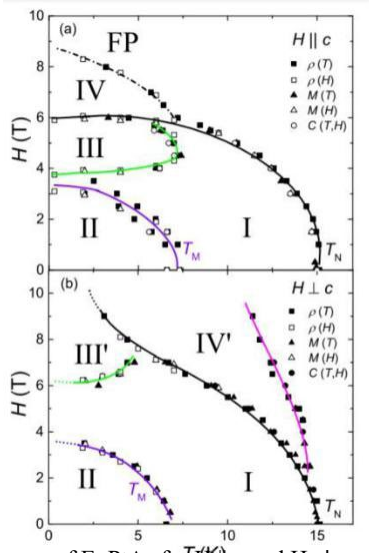

Fig. 1. Field-temperature phase diagrams of EuPtAs for H ∥ c and H ⊥ c, where the different magnetic phases are labeled

1 *I. Dzyaloshinsky, J. Phys. Chem. Solids. 4 241–255 (1958); T. Moriya, Phys. Rev. 120 91–98 (1960).*
2 *S. Mühlbauer et al., Science 323, 915 (2009).*
3 *C. Tabata, et al., J. Phys. Soc. Jpn. 88, 013702 (2019);*
4 *T. Kurumaji, et al., Science 365, 914 (2019); Nat. Commun. 10, 5831 (2019).*
5 *P. Puphal et al., Phys. Rev. Lett. 124, 017202 (2020);*
6 *J. Gaudet et al. Nat. Mater. 10. 1038 (2021);*
7 *G. Wenski and A. Mewis, Z. Anorg. Allg. Chem. 543, 49 (1986).*

A060-06-250823

Topological magnetic structures in MnGe: Neutron diffraction and symmetry analysis

Pomjakushin[1], I. Plokhikh[2], J. S. White[1], Y. Fujishiro[3], N. Kanazawa[4], Y. Tokura[5], and E. Pomjakushina[2]

[1]Laboratory for Neutron Scattering and Imaging (LNS), Paul Scherrer Institut (PSI), CH-5232 Villigen Switzerland, [2]Laboratory for Multiscale Materials Experiments (LMX), Paul Scherrer Institut, CH-5232 Villigen PSI, Switzerland, [3]RIKEN Center for Emergent Matter Science (CEMS), Wako, Saitama 351-0198, Japan, [4]Department of Applied Physics, The University of Tokyo, Bunkyo-ku, Tokyo 113-8656, Japan, [5]Department of Applied Physics, The University of Tokyo, Bunkyo-ku, Tokyo 113-8656, Japan and RIKEN Center for Emergent Matter Science (CEMS), Wako, Saitama 351-0198, Japan

vladimir.pomjakushin@psi.ch

Keywords: Magnetic SuperSpace Group MSSG, isotropy subgroup, magCIF, magnetic structure, neutron diffraction

From new neutron powder diffraction experiments on the chiral cubic ($P2_13$) magnet manganese germanide (MnGe), we analyze all of the possible crystal symmetry-allowed magnetic superstructures that are determined successfully from the data [1]. The incommensurate propagation vectors k of the magnetic structure are found to be aligned with the [100] cubic axes, and correspond to a magnetic periodicity of about 30 Å at 1.8 K. Several maximal crystallographic symmetry magnetic structures are found to fit the data equally well and are presented. These include topologically nontrivial magnetic hedgehog and "skyrmion" structures in multi-k cubic or orthorhombic 3+3 (No.198.3.206.1.m10.2, 19.3.95.4.m26.4) and orthorhombic 3+2 (No. 19.2.29.2.m26.3) dimensional magnetic superspace groups (MSSG) respectively, with either potentially responsible for topological Hall effect (THE). The presence of orthorhombic distortions in the space group $P2_12_12_1$ (No. 19) caused by the transition to the magnetically ordered state does not favor the cubic magnetic hedgehog structure, and leave both orthorhombic hedgehog and skyrmion models as equal candidates for the magnetic structures. We also report on a new combined mechanochemical and solid-state chemical route to synthesize MnGe at ambient pressures and moderate temperatures, and compare with samples obtained by the traditional high pressure synthesis.

The magnetic structures in MnGe are compared with topological magnetism in the candidate magnetic Weyl semimetal

CeAlGe [2], where the topological properties of a phase stable at intermediate magnetic fields parallel to the c axis are suggested by observation of the THE as well. CeAlGe has polar tetragonal $I4_1md$ crystal symmetry with the magnetic structure based on two propagation vectors along [100] and [010] axes in tetragonal plane with periodicity about 70 Å. The multi-k structure is realised in maximal symmetry 3+2 dimensional tetragonal MSSG (No. 109.2.67.4.m240.2).

Both 3+2 structures in MnGe and CeAlGe host lattices of magnetic particle-like objects called (anti)merons $Q=\pm 1/2$ with half-integer topological numbers. Calculations show that in the external magnetic fields perpendicular to the propagation plane the total charge per magnetic cell abruptly changes from $Q=0$ to skyrmion-like charge $|Q|=1$ in accordance with is the experimental observation of the THE.

1 V. Pomjakushin, I. Plokhikh, J. S. White, Y. Fujishiro, N. Kanazawa, Y. Tokura, and E. Pomjakushina, Phys. Rev. B **107**, 024410 (2023)

2 P. Puphal, V. Pomjakushin, N. Kanazawa, V. Ukleev, D. J. Gawryluk, J. Ma, M. Naamneh, N. C. Plumb, L. Keller, R. Cubitt, E. Pomjakushina, and J. S. White, Phys. Rev. Lett. **124**, 017202 (2020)

A067-01-250823

Information-theoretic classifications and quantifications of the symmetries and pseudo-symmetries in two-dimensional experimental data from crystals and quasicrystals

P. Moeck

Department of Physics, Portland State University, Portland/OR, USA
pmoeck@pdx.edu

Keywords: Symmetry, Pseudo-Symmetry, Information Theory

Recently developed information-theory-based methods enable *objective* classifications and quantifications of the crystallographic [1-5] and non-crystallographic [6] symmetries in noisy experimental data that are deemed to be translation periodic or quasi-periodic in two dimensions (2D). These classifications are objective because they are based solely on the experimental data via the fulfillment or violation of numerical inequalities that are based on pair-wise ratios of geometric Akaike Information Criterion (G-AIC) values for non-disjoint geometric models of the data. Because the models are in minimal supergroup to maximal subgroup relationships with each other as far as their symmetries are concerned, an a priori estimate of the noise level in the experimental study is not required. Confidence level can be assigned for the selection of a geometric model that features the symmetry of a minimal supergroup over a non-disjoint model that features a maximal subgroup. G-AIC values are in essence geometric bias corrected sums of squared residuals of the difference between the experimental data and geometric models of that data. The type of microscope or diffraction apparatus that has been used for the recording of the experimental data is immaterial for the application of the new methods. Pseudo-symmetries [7] can reliably be distinguished from genuine symmetries [1], even in the presence of large amounts of generalized noise [2].

Generalized noise includes all effects of (unavoidably) imperfect recordings of experimental data, all kinds of rounding effects and numerical approximations by any kinds of data processing algorithms, and all structural defects in crystalline and quasi-crystalline real-world material samples. When there are many noise sources and the effects of none of these sources dominate, the resulting generalized noise is approximately Gaussian distributed (by generalizations of the central limit theorem of statistics [6]). Such an approximate distribution is the precondition for the application of G-AIC framework [8]. After an information theoretic symmetry classification has been made, one obtains a good a posteriori estimate of the noise level of the experimental study as a byproduct [1].

Conditional symmetry model probabilities, i.e. so called geometric Akaike weights, within model sets [2, 3] can also be calculated on the basis of the G-AIC values of the individual geometric models of the experimental data. These weights represent the probability that a certain geometric model of the experimental data is the Kullback-Leibler best model in the selected model set. The mathematical feature that probabilities need to be multiplied when one wants to obtain joint probabilities aids the distinction between genuine symmetries and pseudo-symmetries in experimental data [3] on a quantitative basis.

The prevailing common practice in materials science is, by stark contrast, to make crystallographic symmetry classifications on the basis of *subjective* judgments whenever an unknown crystalline or quasicrystalline sample is involved. Those classifications are bound to be misleading or false on occasions, especially when the images or diffraction patterns feature a comparatively large amount of generalized noise, metric specializations [7], and/or pseudo-symmetries.

Note that the information-theoretic methods deliver only probabilistic crystallographic or non-crystallographic symmetry classifications as it is fundamentally unsound to assign abstract mathematical concepts such as a single 2D Bravais lattice type, a crystallographic or non-crystallographic projected Laue class, a point symmetry group, or a plane symmetry group with 100 % certainty to a real-world image or diffraction pattern from a crystal or quasicrystal. The new methods quantify deviations from symmetries, which can be interpreted as providing “error-bars” on symmetry measurements.

Experimental atomic-resolution transmission electron microscope images (both in parallel illumination and the scanning probe mode) as well as scanning tunneling microscope images serve as examples for the demonstration of the image-based symmetry classification and quantification methods. Experimental selected-area electron diffraction spot patterns and precession electron diffraction patterns serve as examples for the demonstration of the diffraction-pattern based counterparts [4, 5] of these methods.

[1] Moeck, P. (2022). *Acta Cryst. A* **78**, 172, doi: 10.1107/S2053273322000845.

[2] Dempsey, A. & Moeck, P. (2020). *arXiv:* 2009.08539.

[3] Moeck, P. (2018). *Symmetry* **10**, 133, doi: 10.3390/sym10050133.

[4] Moeck, P., von Koch, L. (2022). *arXiv:* 2201.04789.

[5] Moeck, P., von Koch, L. (2022). *arXiv:* 2202.00220.

[6] Moeck, P. (2021). *Proc. IEEE 21st Intern. Conf. Nanotechnology*, doi: 10.1109/NANO51122.2021.9514320.

[7] Moeck, P. & DeStefano, P. (2018). *Adv. Struct. Chem. Imag.* **4**, 5, doi: 10.1186/s40679-018-0051-z.

[8] Kanatani, K. (1998). *Intern. J. Computer Vision* **26**, 171, doi: 0.1023/A:1007948927139.

A067-02-250823

Exploiting the role of growth induced interfacial layer in highly strained epitaxial YIG thin-films by high-resolution XRD.

S. Satapathy[1, 2], H. K. Singh[1, 2], R. P. Pant[1], K. K. Maurya[1, 2*]

[1] *CSIR- National Physical Laboratory, Dr. K.S. Krishnan Marg, New Delhi-110012, India,*
[2] *Academy of Scientific and Innovative Research (AcSIR), Ghaziabad-201002, India*

Email: subhashree10887@nplindia.org

Keywords: Gadolinium Iron Garnet (GdIG), Rocking curve (RC), high-resolution reciprocal space mapping (RSM), X-ray reflectivity (XRR).

Oxide-based stable systems, where the interface promotes anti-ferromagnetic exchange coupling, are of great economic and technological interest for spintronics world [1]. Several researchers believe that the interfacial layer is detrimental for magnetic behaviour of the parent film as it develops a net magnetization opposite to the parent layer, thereby decreasing the net moment. However, in some cases these kind of coupling plays a vital role, i.e., using this cost effective stable synthetically coupled antiferromagnets in pure spin current generation to manipulate its propagation direction [2]. In this work, we have structurally established a comparative analysis of RF sputtered $Y_3Fe_5O_{12}$ (YIG) thin films grown on $Gd_3Ga_5O_{12}$ (GGG) under different working gas pressure ($Ar+O_2$). Before proceeding for any device fabrication process a complete knowledge on the crystal symmetry of the matter and its optimization is crucial. Here using a high-resolution x-ray diffractometer (HRXRD), we have performed several measurements such as 2θ-ω (Fig.1, Left), RC, XRR (Fig.1, Right), RSM. Which independently showed us the contribution of interfacial layer ($Gd_3Fe_5O_{12}$, GIG) in building structural crystallinity. A high-quality strained film was grown by varying pressure in the range of 10-30 mT, and all other parameters remaining constant (power:75W, substrate and annealing temperature:800◦C).

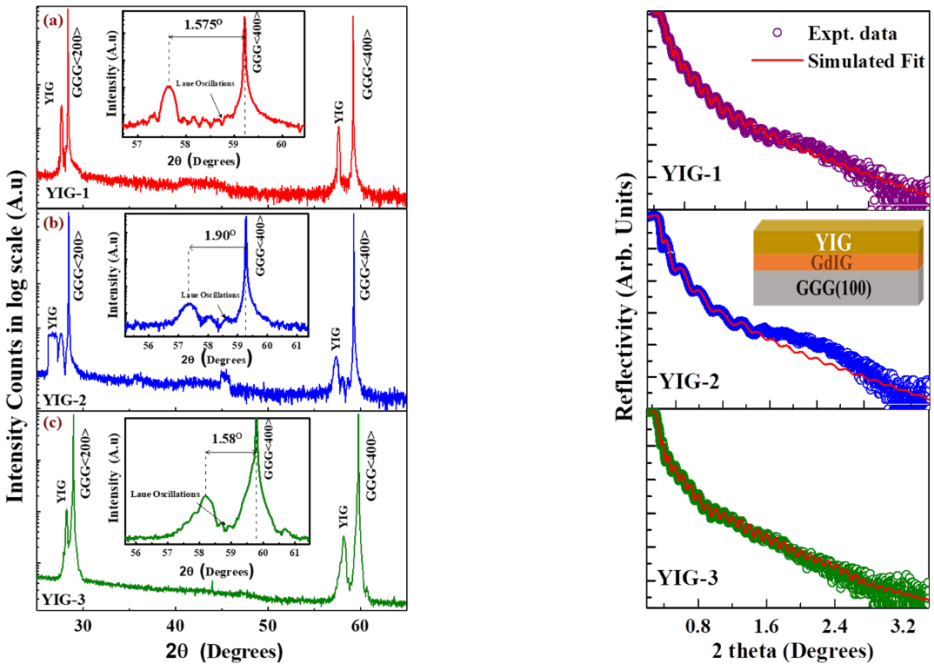

Figure 1. (Left) 2theta-omega scan diffractogram of YIG/GGG (100) with all the planes of (h00) family. The inset diagram shows the enlarged view of (400) plane, (Right) XRR measurements on YIG/GGG (100) showing GdIG layer involved in simulation.

The 2θ-ω scan showed an increase in crystallinity and compressive bi-axial stress with decreasing pressure (best for YIG-1), The XRR measurement revealed the exact thickness of the films to be 45.14 nm, 43.42 nm, and 41.86 nm for YIG-3, YIG-2 and YIG-1 respectively, along with the interfacial GIG layer calculated to be 1.04 nm, 2.1 nm, 3.07 nm. High resolution reciprocal space mapping study (RSM) and ϕ scan was performed on symmetric as well as asymmetric plane to verify the stress, strain and relaxation on deposited films. Further atomic force microscopy (AFM) and optical spectroscopic techniques such as Raman and Photo luminescence was used to detect the structural quality of the films. YIG is an important member of oxide family, meeting all the conditions for commercialization, we hope this study will add a vital value to crystallography data set of this material while depositing epitaxial films from different application perspective. This study is further supported by some advanced experiments such as ferromagnetic resonance (FMR) and terahertz spectroscopy (TRUS) techniques which will be discussed in detail at conference.

[1] J.M. Gomez-Perez, S. Vélez, L. Mckenzie-Sell, M. Amado, J. Herrero-Martín, J. López-López, S. Blanco-Canosa, L.E. Hueso, A. Chuvilin, J.W.A. Robinson, F. Casanova. (2018). *Phy. Rev. App.* **10**.
[2] R. Kumar, S.N. Sarangi, D. Samal, Z. Hossain. (2021. *Phy. Rev. B*. **103**.

A067-03-250823

Crystallography and crystal chemistry of NaSICONs

M. Avdeev

Australian Nuclear Science and Technology Organisation, New Illawarra Road, Lucas Heights, New South Wales 2234, Australia.
School of Chemistry, The University of Sydney, Sydney 2006, Australia

max@ansto.gov.au

Keywords: NaSICON, structure type, symmetry-adapted distortion modes.

A very large number of compositions $A_xM_2(TO_4)_3$ crystallize in the NaSICON crystal structure type built of corner-sharing octahedra [MO_6] and tetrahedra [TO_4]. The voids in the framework can be either empty or filled with A cations (Figure 1). Such topology enables very rich crystal chemistry and remarkable flexibility, similar to that of the perovskite family. The NaSICON structure accommodates hundreds of M and T cation combinations, which leads to a wide range of physical properties. As a result, NaSICON-type materials find applications in very different areas, from nuclear waste immobilization to A-conducting solid electrolytes. Depending on composition and temperature, many NaSICONs also undergo displacive and order-disorder phase transitions.

The previous attempts to rationalize crystal chemistry of the NaSICON structure type had limited success, since the structure has eight internal degrees of freedom and thus no simple 'tolerance factor' could be established. In this talk, I will demonstrate that the R-3c structure with undistorted [MO_6] octahedra and [TO_4] tetrahedra can be used as a common reference point for any NaSICON-type material. More than 300 NaSICON-type oxides present in the Inorganic Crystal Structure Database were quantitatively analysed and it is shown that distortion from the ideal structure is primarily driven by the size mismatch between the A cations and $M_2(TO_4)_3$ framework, that can be used to optimize the geometry of the structure to control properties, such as A-ionic conductivity or thermal expansion. [1]

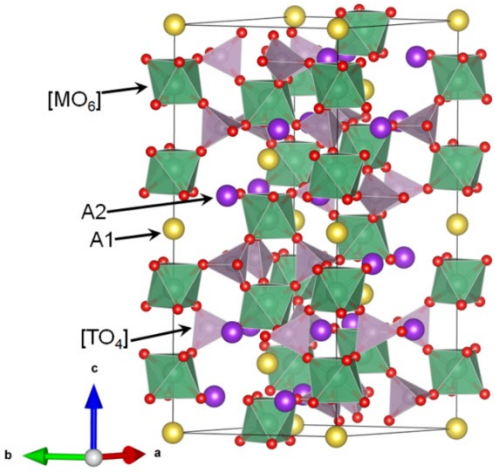

Figure 1. General view of the $A_xM_2(TO_4)_3$ structure with M in [MO_6] octahedra and T in [TO_4] tetrahedra. The A1 and A2 labels indicate two inequivalent A sites with multiplicities 6 and 18, respectively

[1] Avdeev, M., (2021). *Chem. Mater.* **33**, 7620.

A067-04-250823

An algebraic search for large-angle rigid unit modes

Bryce T Eggers[1], Harold T Stokes[1], Branton J Campbell[1]

[1]Physics & Astronomy, Brigham Young University, Provo, Utah, 84602, USA.

branton_campbell@byu.edu

Keywords: rigid unit mode (RUM), irreducible representation, algebraic

Rigid Unit Modes (RUMs), which involve cooperative patterns of polyhedral or molecular rotations and translations, influence a wide variety of important material properties. Recent work provided an algebraic approach to systematically and exhaustively predicting the small-angle RUMs for a given crystal structure, which are classified by irreducible representations of the parent symmetry group of the unrotated structures [1-3]. When some small-angle RUMs are extended to large angles, their rigid units become substantially distorted, indicating that they are not large-angle RUMs. Because large-angle RUMs are also important to many crystalline materials, an algorithm capable of predicting or identifying large-angle RUMs would be very desirable. We report on such an algorithm and its implementation.

[1] Campbell *et al*., Acta Cryst. A 74, 408-424 (2018).
[2] Campbell *et al*., J. Appl. Cryst. 54, 1664-1675 (2021).
[3] Campbell *et al*., J. Appl. Cryst. 54, 1847-1856 (2021).

A067-05-250823

Origin of enhanced dielectric and piezoelectric properties in Li and Ta co-substituted $K_{0.5}Na_{0.5}NbO_3$ ceramics

Satyaranjan Sahoo1, Dhiren K. Pradhan2,3, Anupam Mishra4, Md. Mijanur Rahaman5, Ashok Kumar6,7 ,Reji Thomas8,9, Dillip K. Pradhan1*

1Department of Physics and Astronomy, NIT Rourkela, Rourkela, Odisha 769008, India
2Department of Materials Science and Engineering, University of Tennessee, Knoxville, Tennessee 37996, USA
3Center for Nanophase Materials Sciences, Oak Ridge National Laboratory, Oak Ridge, Tennessee 37831, USA
4Department of Materials Engineering, Indian Institute of Science, Bangalore, 560012, India
5Departmental of Materials Science and Engineering, University of Rajshahi, Rajshahi 6205, Bangladesh
6CSIR-National Physical Laboratory, Dr. K. S. Krishnan Marg, New Delhi 110012, India
7Academy of Scientific and Innovative Research (AcSIR), Ghaziabad 201002, India
8Division of Research and Development, Lovely Professional University, Jalandhar-Delhi G.T. Road, Phagwara, Punjab 144411, India
9School of Chemical Engineering and Physical Sciences, Lovely Professional University, Jalandhar-Delhi G.T. Road, Phagwara, Punjab 144411, India

dillippradhan@nitrkl.ac.in

Keywords: X-ray Diffraction, Structural Phase Transitions, Piezoelectric Properties

Ferroelectric ceramic oxides have been widely used in various devices such as non-volatile random access memory, sensors, actuators, transducers and high energy density capacitors, due to its excellent dielectric, ferroelectric and piezoelectric properties

Potassium sodium niobate ($K_{0.5}Na_{0.5}NbO_3$, KNN) based ceramics and its solid solutions are considered as one of the promising lead free ferroelectric materials. Unfortunately, due to the evaporation of the volatile potassium (K) and sodium (Na), the synthesis of stoichiometric KNN is difficult [1,2]. At the same time the piezoelectric properties of KNN based ferroelectrics need to be enhanced for the device applications. It has been reported that addition of Li^+ at the K/Na site in KNN improves densification, lowers the T_{O-T} (orthorhombic to tetragonal phase transition temperature), and raises the T_C (Curie temperature) [1, 3]. On the other hand, Ta^{5+} substitution at the Nb^{5+} site in KNN lowers both T_{O-T} and T_C and enhances the piezoelectric properties [1, 3]. So in the present study, Li and Ta co-substituted KNN ceramics are considered. In view of this, we have prepared
$(K_{0.48}Na_{0.48}\ Li_{0.04})(Nb_{1-x}Ta_x)O_3$ (x=0 to 0.40) ceramic using conventional solid state reaction route and investigated the compositional driven structural phase transitions using X-ray diffraction and Raman spectroscopic techniques. Rietveld

refinement analysis of X-ray diffraction patterns indicate a compositional induced structural phase transition from orthorhombic (Amm2) phase ($x<0.10$) to tetragonal (P4mm) phase ($x>0.20$) through the coexistence of both orthorhombic and tetragonal (Amm2+P4mm) phases for $0.10\leq x\leq 0.20$. This compositional driven phase transitions is well correlated with the Raman spectroscopic analysis. FESEM micrograph shows a highly dense microstructure with inhomogeneous distribution of grains and the gain size decreases with increase in Ta content. The temperature-dependent dielectric properties of the ceramic were measured to further study the ferroelectric phase transitions behaviour. Based on the RT XRD, Raman spectroscopic analysis and temperature dependent dielectric properties, a phase diagram has been constructed. For the ceramic with x=0.20, we have obtained maximum piezoelectric coefficient (d_{33}=159pC/N) and dielectric constant (ε_r=556) at RT which can be explained due to the coexistence of O+T phases around the MPB (morphotropic phase boundary). The in-depth analysis of the crystal structure and its relationship to the improvement of physical properties will be discussed.

1 Wu, J., Xiao, D., & Zhu, J. (2015). Chem. Rev. ***115****, 2559.*
2 Xu, K., Li, J., Lv, X., Wu, J., Zhang, X., Xiao, D., & Zhu, J., (2016). Adv. Mater. ***28****, 8519.*
3 Hollenstein, E., Davis, M., Damjanovic, D., & Setter, N. (2005). Appl. Phys. Lett. ***87****, 182905.*

A067-06-250823

Topological Characterization of Nonmagnetic One-dimensional Crystals – Elementary Band Representations for Line Groups -

A. Milošević, S. Dmitrović, T. Vuković, M. Damnjanović

Faculty of Physics, University of Belgrade, Studentski trg 12, 11001 Belgrade, Serbia

ivag@rcub.bg.ac.rs

Keywords: Line groups, Elementary band representations, Electronic band topology

Line groups (LGs) [1] describe symmetry of quasi one-dimensional (quasi-1D) systems with either translational or helical periodicity. As for 1D periodic systems there is no crystallographic restriction on the order of the rotational axis there are infinitely many LGs (gathered into 13 LG families), among which are 75 rod groups, with the order q of the principle axis of rotation of the isogonal group taking crystallographic values $q = 1, 2, 3, 4, 6$, or $q = 1, 2, 3$ for the groups with roto-reflections (pertaining to the LG families 2, 9 and 10). Conceptually, LGs describe wider class of symmetries than the rod groups. While the latter describe only translationally periodical objects, LGs include also the symmetries of incommensurate periodical structures, with helical periodicity only. Indeed, just the incommensurability is one of new features related to quasi-1D strucutres.

Topological quantum chemistry [2], highlighting the link between the topology and local chemical bonding, relates the symmetry, in terms of elementary band representations (EBRs), with combinatorial graph theory, giving universal description of electronic band structure topology of short-range entangled matter.

Here, derived are complete sets of nonequivalent (physical) EBRs, for quasi-1D systems with either translational or helical periodicity. Apart from the system configuration symmetry described by LGs, considered are also the additional symmetries: time-reversal (grey-LGs), the symmetry originating from spin degree of freedom (double-LGs and double-grey-LGs) [3,4]. The results obtained are complete and exhaustive, thus enabling thorough algorithmic search for topological compounds across 1D matter. Hence, the task of characterization of nonmagnetic quasi-1D topological crystals by means of the theory of topological quantum chemistry can be realized. The results obtained are illustrated on several examples: a chiral carbon nanotube, and Su-Schrieffer–Heeger and topological mirror chain models.

1 Damnjanović M. & Milošević I. (2010) *Line Groups in Physics*, Springer, Berlin Heidelberg
2 Bradlyn B., Elcoro L., Cano J., Vergniory M. G., Wang Z., Felser C., Aroyo M. I. & Bernevig B.A. (2017) *Nature,* **547**, 298
3 Milošević I., Dmitrović S., Vuković T., Dimić A. & Damnjanović M. (2020) *J. Phys. A: Math. Theor.* **53**, 455204
4 Dmitrović S., Vuković T., Milošević I. & Damnjanović M. (2022) *J. Phys. A: Math. Theor.* **55**, 385201

A081 Advances in Quantum Crystallography
Room 212
4.00pm – 6:30pm

A081-01-250823

A periodic calculation for a periodic system: Using projector augmented wave densities as basis for Hirshfeld Atom refinement.

Paul Niklas Ruth

Durham University, Chemistry Department, Durham, UK

panikruth@gmail.com

Keywords: Hirshfeld atom refinement, hydrogen atom positions, periodic calculations

In 1993 Peter Blöchl proposed the projector augmented wave method [1] , which combines the convergence properties of pseudo-potential based methods with the benefits of projector based methods. Of major interest in this context is the availability of the all-electron density. I want to present the applicability of this method as a basis for the calculating the atomic form factors in Hirshfeld atom refinement.

Having been originally proposed in 2008, Hirshfeld atom refinement [2-3] uses atomic densities derived by Hirshfeld partitioning [4]. So far the calculation has so far mainly conducted using densities from non-periodic calculations. After one initial non-iterative publication by Wall [5], the potential of projector augmented waves remained largely unexplored.

I want to remedy this fact, as the periodic calculation yields hydrogen bond distances with superior agreement to X-H distances derived from neutron diffraction [6]. While the computation time is higher than neglection of the crystal environment or a classical description in the form of charges surrounding the calculated molecules, it is still significantly faster than describing even one shell of surrounding molecules fully quantum mechanically. This can clearly be seen with the comparison of different refinements of the L-Alanin molecule presented in Figure 1.

In addition to refinement results I want to introduce a software which interested viewers can use to apply the method to their own crstallographic structures.

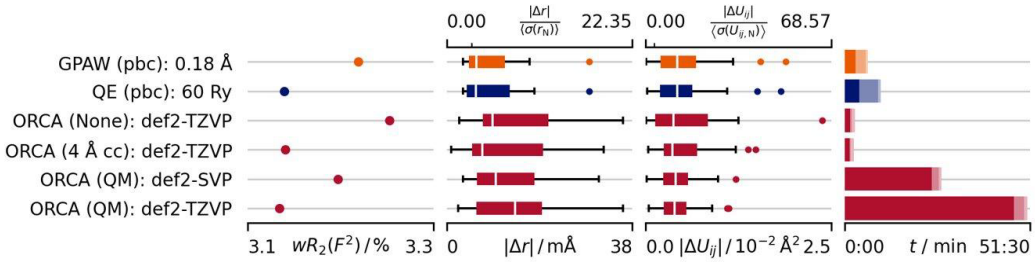

Figure 1. Results of the Hirshfeld atom Refinement of already published X-ray diffracion data [7] of the L-Alanin molecule using the PBE functional. Naming of the individual rows is composed of the the quantum mechanical software used for the calculation of the density. Following in the brackets is the approximation of the crystal environment where: pbc: periodic boundary conditions using PAW; None: no description of the crystal environment. 4 Å cc: 4 Å of cluster charges and QM: Cluster of molecules, which were calculated using a full quantum mechanical calculation. Finally the last entry denominates the basis, where GPAW uses a real-space grid spacing and Quantum Espresso uses a plane wave basis with the given energy cut-off and ORCA uses the given basis set. Agreement to neutron values [8] is given as box-whisker plot.

[1] Blöchl, P. E. (1994). *Phys. Rev. B*, **50**, 17953–17979.
[2] Jayatilaka, D. & Dittrich, B. (2008). *Acta Cryst.* A**64**, 383–393.
[3] Capelli, S. C., Bürgi, H.-B., Dittrich, B., Grabowsky, S. & Jayatilaka, D. (2014). *IUCrJ*, **1**, 361–379.
[4] Hirshfeld, F. L. (1971). *Acta Cryst.* B**27**, 769–781
[5] Wall, M. E. (2016). *IUCrJ*, **3**, 237–246.
[6] Ruth, P.N., Herbst-Irmer, R., Stalke, D., (2022). *IUCrJ* **9**, 286–297
[7] Destro, R., Marsh, R. E. & Bianchi, R. (1988). *J. Phys. Chem.* **92**, 966–973.
[8] Malaspina, L. A., Wieduwilt, E. K., Bergmann, J., Kleemiss, F., Meyer, B., Ruiz-López, M. F., Pal, R., Hupf, E., Beckmann, J., Piltz, R. O., Edwards, A. J., Grabowsky, S. & Genoni, A. (2019). *J. Phys. Chem. Lett.* **10**, 6973–6982.

A081-02-250823

HAR_NoMoRe – the future of a quantum crystallography refinement?

Helena Butkiewicz1, Anders Ø. Madsen2, Michał Chodkiewicz1, Anna A. Hoser1

Faculty of Chemistry, University of Warsaw, Pasteura 1, 02-093 Warsaw, Poland; Department of Pharmacy, University of Copenhagen, Universitetsparken 2, Copenhagen, Denmark)

h.butkiewicz@o2.pl

Keywords: lattice dynamics, phonons, Hirshfeld Atom Refinement, thermodynamic properties

Ever since the first diffraction pattern for a single crystal was recorded, X-ray diffraction (XRD) has been developed into a widely used, powerful, and indispensable characterization method for structural analysis. Now, the theory and experiments are in a mature state, XRD diffractometers have new, strong X-ray sources and modern hybrid pixel detectors, enabling the collection of the diffraction patterns with accuracy and precision about which no one dreamed a few years ago. It requires state of the art models to extract all information present in collected experimental results as the intensity of the diffracted beam depends on both: electron density and thermal motion. Whereas much work was done with the electron density modelling (e.g. Hansen-Coppens multipole model [1], Hirshfeld atom refinement (HAR)[2, 3]), thermal motion treatment remains the same as it was a century ago. Therefore, we have developed a new method, in which instead of routine atomic displacement parameters (ADPs) refinement against single-crystal X-ray diffraction data, we refine frequencies from periodic *ab-initio* calculations4. We called such refinement Normal Mode Refinement (*NoMoRe*).

Herein we will present for the first time a new model that join those two worlds: the best description of the charge density model (HAR) and the best model to describe thermal motion (*NoMoRe*), Fig. 1. We will present how model works for exemplary compounds: urea, alanine, xylitol, naphthalene, glycine polymorphs.

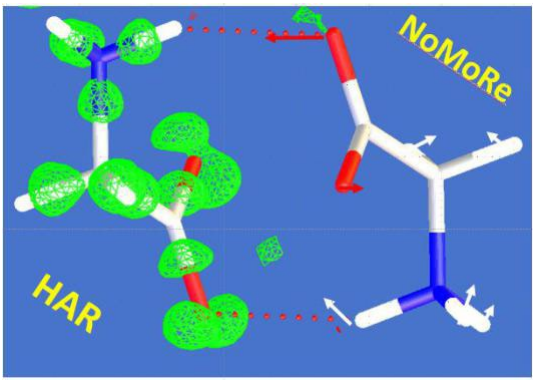

Figure 1. Schematic visualization of combination of HAR with NoMoRe.

1 Hansen, N. K.; Coppens, P. (1978). *Acta Crystallographica Section A*, **34**, 909-921.
2 Jayatilaka, D.; Dittrich, B. (2008) *Acta Cryst*., **A64**, 383-393.
3 Capelli, S. C.; Burgi, H.-B.; Dittrich, B.; Grabowsky, S.; Jayatilaka, D. (2014) *IUCrJ 2014*, **1**, 361-379.
4 Hoser, A. A.; Madsen, A. Ø. (2016) *Acta Crystallographica Section A*, **72**, 206-214.

A081-03-250823

Gas Phase X-Ray Scattering – A Path To Pair Correlation Functions And Electron Densities

A081-04-250823

Iterative quantum crystallographic refinement based on theoretical multipole atoms derived from solid-state calculations using a Gaussian basis set

Patzer[1], N. Nöthling[1], R. Goddard[1], C. W. Lehmann[1]

[1]*Max-Planck-Institut für Kohlenforschung, Kaiser-Wilhelm-Platz 1, 45470 Mülheim an der Ruhr, Germany patzer@kofo.mpg.de*

Keywords: *quantum crystallography, intermolecular interactions, methodology*

A python based code has been developed, which performs a Quantum Crystallographic (QCr) refinement using a solid-state single point calculation with the program code CRYSTAL17. [1] The *ReCrystal* software, similar to the programs for applying Hirshfeld atomic refinement (HAR, e.g., tonto or NoSpherA2/OLEX2 interface), requires a Gaussian basis set, a DFT functional, and the number of CPUs for refinement of the crystal structure. [2-3] Additionally, the *Pack-Monkhorst* and *Gilat* shrinking factors must be specified, which define a grid in the first Brillouin zone. After *k*-point sampling, structure factors are calculated directly from the density. Multipole parameters are subsequently generated from these structure factors and used for least-square refinement. Hirshfeld partitioning of the calculated density was not performed in the present analysis. The results of this approach are comparable to those from HAR (performed with NoSpherA2/ORCA 5.0.3). Whether periodic boundary conditions actually lead to a better result in a QCr refinement has to be clarified. In 2016, *Wall* elegantly demonstrated for the first time the use of a periodic wave function in refinement with HAR. [4] In addition, *Dietmar Stalke's* group presented a plane wave based method for Hirshfeld atom refinement (PAW-HAR) in 2022 and could show the benefit of the periodic charge density model. [5] To evaluate the results, primarily the experimentally determined residual electron density was considered. Crystallographic R-factors are less suitable as a benchmark at this point, as significant differences can almost not be detected. Especially in molecular crystals, like urea or oxalic acid dihydrate, where hydrogen bonding motives can be found, periodic boundary conditions can contribute to an improved description of the residual bond electron density (see Figure 1). Evidence has already been provided that the theoretical multipole model atom is also suitable for determining accurate nuclear coordinates of hydrogen atoms. [6] *ReCrystal* represents an iterative extension of the transferable multipole approach. A particular advantage is that *ReCrystal* is not connected to specific databases. Another aspect is that theoretical multipole parameters can serve as a starting point for multipole refinement. This is important because multipole parameters can account for effects that are not due to bond electron density. The major concern is overinterpretation of the results, since crystals are not ideal objects as we think of them. Rather, crystals are imperfect systems with dislocations, vacancies, and interstitial atoms that affect the diffraction pattern.

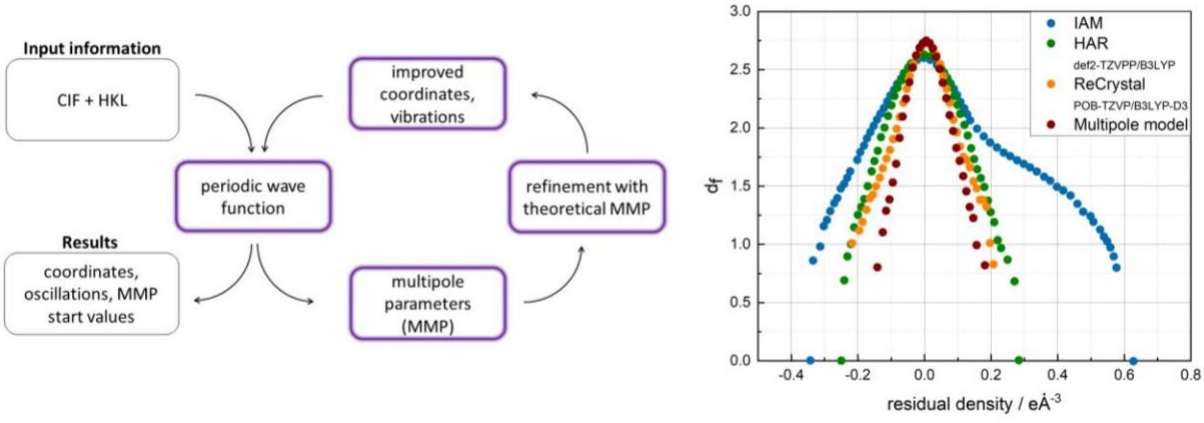

Figure 1. Left: Flowchart of the quantum crystallographic refinement based on a periodic wave function; right: Residual density vs. fractal dimension [7] for oxalic acid dihydrate; the independent atom model (IAM) is compared with NoSpherA2/ORCA5, the new in-house program *ReCrystal* and the Hansen-Coppens-multipole model (resolution 0.45 Å).

1 Dovesi, R., et al., (2018). *WIREs Comput. Mol. Sci.* **8**, 1360.
2 Jayatilaka, D. & Dittrich, B., (2008). *Acta Cryst. Section A* **64(3)**, 383-393.
3 Kleemiss, F., et al., (2021). *Chem. Sci.* **12**, 1675-1692.
4 Wall, M. E., (2016). *IUCrJ* **3**, 237-246.
5 Ruth, P. N., Herbst-Irmer, R. & Stalke, D., (2022). *IUCrJ* **9**, 286–297.
6 Jha, K. K., Gruza, B., Kumar, P., Chodkiewicz, M. L. & Dominiak, P. M., (2020). *Acta Cryst. Section B* **76 (3)**, 296-306.
7 Meindl, K. & Henn, J., (2008). *Acta Cryst. Section A* **64(3)**, 404-418.
8 Grabowsky, S., Genoni, A. & Bürgi, H.-B., (2017). *Chem. Sc.* **8(6)**, 4159-4176.
9 Dittrich, B., Koritsánszky, T. & Luger, P., (2004). *Angewandte Chemie Int. Edition* **43(20)**, 2718-2721.

A081-05-250823

Transition metal hydrides - can quantum crystallography provide accurate positions and thermal motions of hydrogen atoms?

M. Woińska, S. Pawlędzio, A. A. Hoser, M. L. Chodkiewicz, K. Woźniak

Biological and Chemical Research Centre, Chemistry Department, University of Warsaw, Żwirki i Wigury 101, 02-089
Warszawa, Poland

magdalena.woinska@uw.edu.pl

Keywords: transition metal hydrides, Hirshfeld Atom Refinement, atomic thermal motions

Transition metal (TM) bound hydrides play the key role in processes of catalysis, energy conversion and search for hydrogen storage materials or superconductors. Establishing the structure of these compounds with X-ray diffraction is crucial for many areas of research. However, it is impeded by the problematic aspects of determining hydrogen position with X-rays, which are particularly exacerbated if the hydrogen atom is bonded to a TM atom. Moreover, it is difficult to collect high-quality, let alone high-resolution X-ray data for such compounds, and even more difficult to obtain neutron data which could be the source of reliable information about hydrogen positions. TM hydride complexes are also a computationally demanding group of compounds, which makes them a challenge for theoretical computations which are inherent in quantum crystallography.

Hirshfeld Atom Refinement (HAR) is a method belonging to the realm of quantum crystallography which has been proven to locate hydrogen atoms bonded to light elements based on standard resolution X-ray data with accuracy and precision very close to the one of neutron experiments [1]. In certain cases, HAR has been reported to improve significantly positions of hydrogen atoms in TM-H bonds [1, 2], as compared to the Independent Atom Model (IAM). The presented study is based on 10 X-ray structures of crystals of TM hydride complexes with hydrogen atoms bonded to heavy elements from period IV (Fe, Ni), V (Nb, Ru, Rh, Sb) and VI (Os) for which also the corresponding neutron structure is available. The main goal was to evaluate the capabilities of HAR in terms of establishing positions of hydrogen atoms (especially in TM-H bonds) and their thermal motions. To this end, HAR for the selected structures was performed in various versions in order to check how the results vary with factors such as: including interactions with the crystal environment, taking into account relativistic effects, changing the DFT functional used for wave function calculations (B3LYP, PBE, M06-2X) and selection of the basis set. Moreover, the 10 compounds were ordered according to the quality of the X-ray and the neutron data and the quality of the refinement performed for each of the structures. This allowed to observe that HAR, in general resulted in TM-H bond lengths in very good agreement with the neutron values for structures from the top of the ranking, whereas the performance of HAR was hindered by decreasing quality of the data sets.

In order to address the problem of treatment of hydrogen thermal motions in HAR and its influence on the positions of hydrogen in TM hydride complexes, advanced tools enabling estimation of H ADPs such as SHADE3 or Normal Mode Refinement (NoMoRe) [3] were applied together with HAR. The ADPs obtained in the course of SHADE3, NoMoRe, HAR and the neutron ADPs (Fig. 1) will be compared and their influence on hydrogen positions and refinement statistics will be discussed. Additionally, a high-resolution X-ray structure of a complex containing a Cr-H-Cr bond with neutron data collected at a similar temperature [4] will be used to investigate the effects of data resolution on H position and H ADPs estimated with HAR.

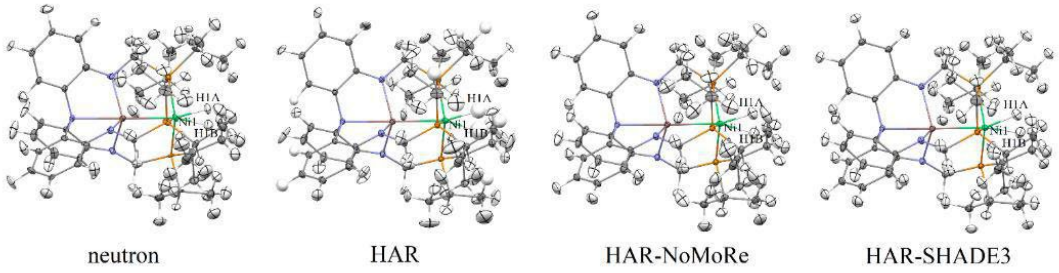

Figure 1. Crystal structures of the nickle hydride complex obtained with various experimental and refinement techniques.

1 Woińska, M., Grabowsky, S., Dominiak, P. M., Woźniak, K. & Jayatilaka, D. (2016). *Sci. Adv.* **2**, e1600192.
2 M. Woińska, M. L. Chodkiewicz, K. Woźniak, *Chem. Commun.,* **2021**, 57, 3652-3655.
3 A. A. Hoser, A. Ø. Madsen, *Acta Cryst.*, **2016**, A72, 206–214; A. A. Hoser, A. Ø. Madsen, *Acta Cryst.*, **2017**, A73, 102–114.
4 P. Macchi, D. Donghi, A. Sironi, *J. Am. Chem. Soc.,* **2005**, 127, 47, 16494–16504.

Acknowledgements*: We are grateful for the financial support from the Polish National Science Centre (NCN) under Opus grant DEC-2018/31/B/ST4/02142. Wroclaw Centre for Networking and Supercomputing of Wroclaw University of Technology and the PL-Grid infrastructure are gratefully acknowledged for providing computational facilities.*

A081-06-250823

Do functionals affect HAR refinement and other topological descriptors?

Julia Contreras-García[1], Paulina Dominiak[2], Bruno Landeros[3]

CNRS, UMR 7616, Laboratoire de Chimie Th´eorique, Paris, France
Biological and Chemical Research Centre, University of Warsaw, Poland
UNAM, Instituto de Química,Ciudad Universitaria, Ciudad de México, 04510

julia.contreras_garcia@sorbonne-universite.fr

Keywords: DFT, topology, HAR

The effect of mixing different amounts of Hartree-Fock (HF) exchange with hybrid density functionals applied to Hirshfeld atom refinement of urea and oxalic acid dihydrate will be explored. The results show that changing the amount of HF exchange, no matter the level of theory, has an impact almost exclusively on the H atom refinement parameters. Contrary to pure quantum mechanical calculations, the best match with respect to neutron diffraction values are not necessarily found with intermediate exact exchange mixtures. While the non-hydrogen covalent bond distances are insensitive to the combination of method or basis set employed, the X-H bond distances always increase proportionally to the HF exchange. This outcome is opposite to what is normally observed from geometry optimizations. Additionally, the thermal ellipsoids tend to shrink with larger HF exchange, specially for those H atoms involved in strong hydrogen bonding.

The present work [1] highlights that common assumptions in quantum computations do not always hold for HAR. One could have anticipated that increasing the basis set, mixing certain amount of HF exchange, or using correlated methods as MP2 would have improved the modelled ρ(r) needed for HAR. Nevertheless, none of those trends were invariably observed for the selected systems. While the lowest R1 values weere obtained for HF exchange mixtures of around 25%, such a correlation was not found for the better description of X-H distances or the ADPs of H atoms. Some required very high values of HF exchange, while other needed none. Thus, the development of density functionals useful for HAR, where the only important property is ρ(r) and the energy has no direct role, may take a different direction to that employed for quantum chemical calculations.

Effects of progressively including weight of experimental densities we will also show the effect of correlation.

1 Bruno Landeros-Rivera, Julia Contreras-García, Paulina M. Dominiak, David I. Ramírez-Palma, Fernando Cortés-Guzmán (submitted)

A088 Lipid Self-assembly and the Design of Lipidic Materials
Room 213
4.00pm – 6:30pm

A088-01-250823

How ionic liquid composition and structure affect micelle morphology

J. B. Marlow[1,2], K. Wood[1], R. Atkin[3], G. G. Warr[2]

[1] Australian Nuclear Science and Technology Organisation, Lucas Heights, NSW 2234, Australia
[2] School of Chemistry and Sydney Nano Institute, The University of Sydney, Sydney, NSW 2006, Australia,
[3] School of Molecular Sciences, The University of Western Australia, Perth, WA 6009, Australia
marlowj@ansto.gov.au / joshua.marlow@sydney.edu.au

Keywords: Ionic Liquids, Surfactants, RheoSANS

A common method of making viscoelastic, wormlike micelles in water is to combine a cationic surfactant with a salt featuring a strongly bonding or hydrotropic counterion, such as sodium salicylate. Despite the pre-existing high ionic strength, however, this strategy has proven ineffective when employing ionic liquids (ILs) as the self-assembly solvent.

In this work, micelle structures of a series of alkyltrimethylammonium and alkylpyridinium salicylate surfactants by small-angle neutron scattering (SANS) in the protic ionic liquids ethylammonium nitrate (EAN), ethanolammonium nitrate (EtAN), ethanolammonium formate (EtAF), and their mixtures and dilutions with water. Results reveal a variety of micellar systems, including wormlike micelles, in a host of ionic liquid and mixed solvents. This is exemplified in Fig. 1, where compositions of two different ionic liquids, each with unique physicochemical properties, support different self-assembled structures in mixtures of IL and water.

This work reveals the conditions under which wormlike micelles form and elucidates how solvent structural features such as ionic strength, H-bond connectivity, and the inherent liquid nanostructure of an ionic liquid affect micelle morphology and, thanks to the application of *in situ* deformation with rheoSANS, the viscoelastic properties of wormlike micellar systems. In turn, learning about these subtleties provides a greater understanding of how amphiphilic self-assembly occurs in neoteric solvents, allowing for more directed design of such systems for a variety of applications.

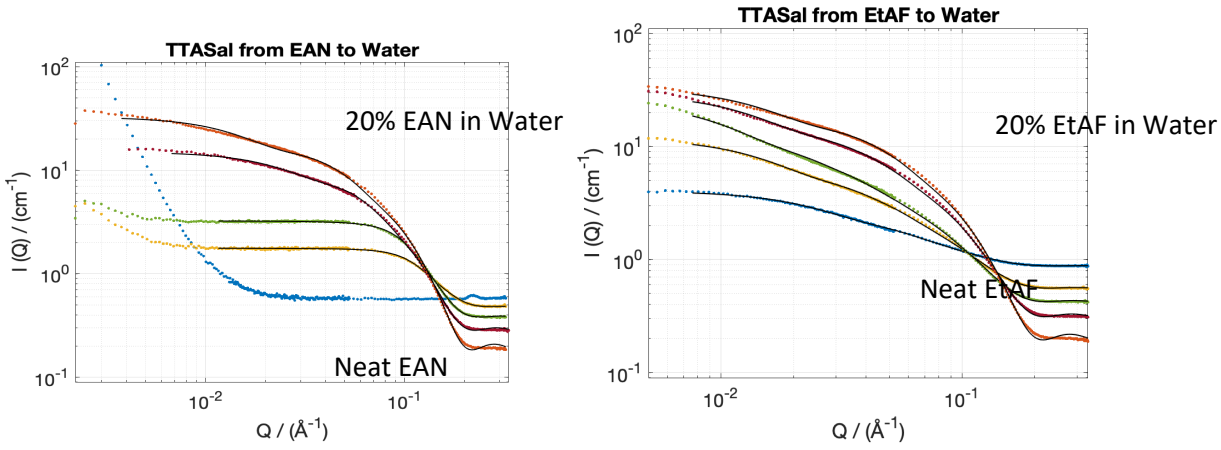

Figure 1. SANS spectra for 5% w/w tetradecyltrimethylammonium salicylate (TTASal) in mixtures of ethylammonium nitrate (EAN, left) and ethanolammonium formate (EtAF, right) with water. The blue line (highest background at high values of Q) represents neat IL, and subsequent spectra represent solvents with 80%, 60%, 40%, and 20% ionic liquid in water. Black lines represent preliminary fits.

A088-02-250823

Human antimicrobial peptide inactivates enveloped viruses

S. Watts1, E. Hanni2, S. Salentinig2

1 School of Chemical and Biomedical Engineering, Nanyang Technological University, 70 Nanyang Drive, Singapore, 637457, Singapore, 2 University of Fribourg, Chemin du musée 9, 1700 Fribourg, Switzerland cs-samuel.watts@ntu.edu.sg

Keywords: enveloped virus, antimicrobial peptide, small angle X-ray scattering

Enveloped viruses are responsible for numerous diseases, including influenza and Covid. Wide range antiviral therapies that inactivate viruses through non-specific interactions are mostly non-existent. The cathelicidin LL-37 is an antimicrobial peptide part of the human innate immune system and a promising antiviral therapeutic.[1] LL-37 interacts with lipid structures and modify the lipid colloidal structures. Its antibacterial activity has been linked to the reorganisation of the bacterial membrane's lipid structure.[2] However, the mechanism of interaction that inactivates viruses needs to be better understood.

Here, LL-37's antiviral mechanism is studied by investigating the enveloped virus' function-structure modifications upon interaction with LL-37. The bacteriophage Phi6 is used as surrogate for pathogenic enveloped virus. The particle's size and morphology are investigated with multi-angle dynamic light scattering. Whereas the particle's nanostructure is studied by the combination of small angle X-ray scattering and model independent data fitting. Infectivity assays allowed to correlate the resolved structures with the viral biological function. LL-37 is found to actively integrate into the lipid envelope, leading to lipid packing modifications. Eventually, the lipid envelopes peels off the nucleocapsid, inactivating the virus by separating the genomic material from the host cell recognition function, as depicted in Figure 1. Understanding the structural effect antimicrobial peptides on viral self-assembled lipid structures will allow to guide the design of peptide-based antiviral drugs and therapies.

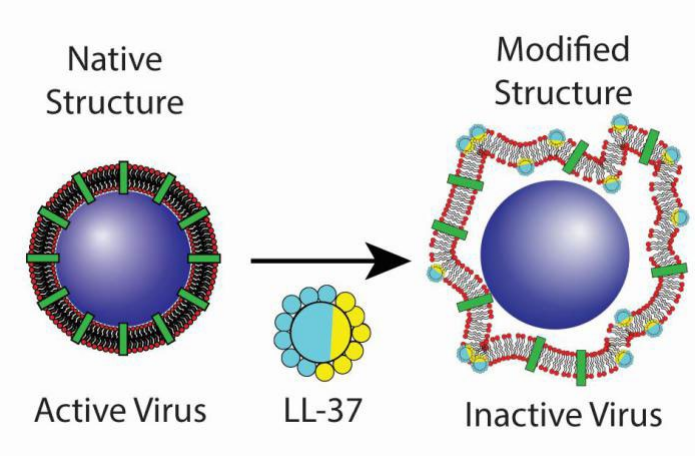

Figure 1. Antiviral mechanism of human antimicrobial peptide LL-37. The peptide integrates the lipid envelope modifying the packing and curvature which leads to inactivation.

1 Dürr, U. H. N., Sudheendra, U. S., Ramamoorthy, A.,(2006) *Biochimica et Biophysica Acta (BBA) - Biomembranes* **1758**, 1408.

2 Freire, R.V.M., Pillco-Valencia, Y., Da Hora, G.C.A., Ramstedt, M., Sandblad, L., Soares, T.A., Salentinig, S., (2021). *J Colloid Interface Sci*. **596**, 352

A088-03-250823

Hydrocarbon-Fluorocarbon Patterns in the Membranes of Star-Polyphile Mesophases

Liliana de Campo[1], Minoo Moghaddam[2], Trond Varslot[3], Toen Castle[4], Rainer Mittelbach[3], Stuart Ramsden[3], Nigel Kirby[5], and Stephen Hyde[3]

[1]ANSTO, Lucas Heights, Australia, [2]Nanomed Pty, Sydney, Australia, [3]ANU, Canberra, Australia
[4]Latrobe University, Bendigo, Australia, [5]Australian Synchrotron, Melbourne, Australia, [5]Sydney University, Sydney, Australia,
liliana.decampo@ansto.gov.au

Keywords: SAXS, SANS, lipid mesophases, lipid de-mixing, small angle crystallograph

Star-polyphiles are generalizations of lipids or surfactants [1]: they are small molecules consisting of 3 mutually immiscible chains attached to a common center: a hydrocarbon, a fluorocarbon and a water soluble oligo-ethylene glycol chain [2,3]. When brought in contact with water, these self-assemble into mesophases, most of which structurally resemble those found in lipids like monoolein, including lamellar, hexagonal, micellar and bicontinuous cubic mesophases. However, the hydrophobic membrane is split into separate hydrocarbon and fluorocarbon domains [4], which significantly increases structural complexity and hierarchical ordering can occur.
Here we give an overview on possible and experimentally determined mesophase geometries, focusing on their experimental investigation by SAXS and SANS in combination with scattering simulations of model structures.

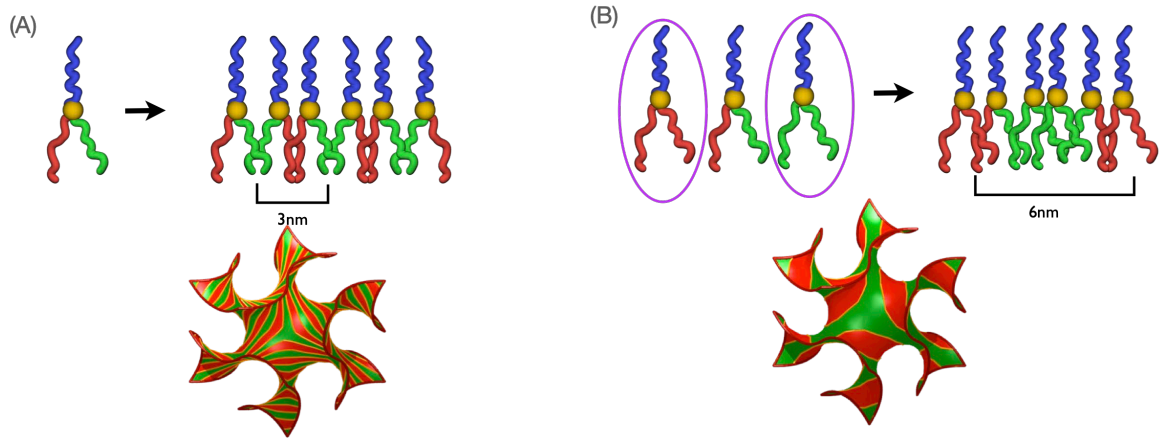

Figure 1. Gyroid mesophase based on star-polyphiles with de-mixed hydrocarbon-fluorocarbon domains schematically drawn in the form of stripes. In a binary star-polyphile/water system the demixed domain widths are limited by the geometry of the molecules (A). De-mixed domain widths can be enlarged by replacing part of the star-polyphile with the corresponding double-chain molecules (B)

[1] Hyde, S. T., De Campo, L., & Oguey, C. (2009). *Soft Matter, 5*(14), 2782-2794.
[2] de Campo, L., Moghaddam, M. J., Varslot, T., Kirby, N., Mittelbach, R., Sawkins, T., & Hyde, S. T. (2015). *Chemistry of Materials, 27*(3), 857-866.
[3] de Campo, L., Castle, T., & Hyde, S. T. (2017). *Interface Focus, 7*(4), 20160130.
[4] de Campo, L., Varslot, T., Moghaddam, M. J., Kirkensgaard, J. J., Mortensen, K., & Hyde, S. T. (2011). *Physical Chemistry Chemical Physics, 13*(8), 3139-3152.

A088-04-250823

Interactions of biliary micelles with polar lipids and digestion products from milk

Andrew J. Clulow[1,2], Patrick Tai[3,4], Malinda Salim[2], Thomas Eason[2], Susanne Seibt[1], Timothy M. Ryan[1], David W. Everett[3,5] and Ben J. Boyd[2,6]

[1]Australian Synchrotron, ANSTO, 800 Blackburn Road, Clayton, VIC 3168, Australia; [2]Monash Institute of Pharmaceutical Sciences, 381 Royal Parade, Parkville, VIC 3052, Australia; 3Riddet Institute, Palmerston North, New Zealand; 4School of Food and Advanced Technology, Massey University, Palmerston North, New Zealand; 5AgResearch, Palmerston North, New Zealand; 6Department of Pharmacy, University of Copenhagen, Universitetsparken 2, 2100 Copenhagen, Denmark

Corresponding author email: clulowa@ansto.gov.au

Keywords: Milk, lipid self-assembly, lipid digestion, bile

Milk or milk-like emulsions are our sole source of nutrition for the first six months of life and milk lipids carry fat-soluble nutrients through the gut as well as providing most of the energy we consume from milk. The digestion and absorption of milk lipids and entrained nutrients is therefore crucial for infant survival and growth. Triglycerides make up 98% of milk lipids, with the remainder comprising polar lipids including sphingomyelins.[1, 2] Bile salts and phospholipids in the intestinal fluids combine to form a colloidal sink into which the poorly-soluble lipid digestion products can partition and be absorbed at the intestinal walls.[3] This work describes small angle X-ray scattering (SAXS) studies into how the structures of biliary micelles change when they absorb milk polar lipids and triglyceride digestion products under intestinal conditions (**Figure 1**).

Firstly, mixtures of fatty acids and monoglycerides were prepared that mimic the digestion products of human and bovine milk.[4] Structural changes occurring when biliary micelles were mixed with these milk-mimicking digestion product mixtures were found to be dictated primarily by the type of lipid chains present, with a secondary effect observed on varying the pH between 6.3 and 7.7 to simulate passage down the intestinal tract.

In a second study, the solubilisation of milk sphingomyelin-based vesicles by bile was investigated. It was found that incorporation of increasing amounts of cholesterol led to the formation of multilamellar vesicles that were increasingly stabilised against absorption into the biliary micelles. This was observed through both retention of diffraction features from the multilamellar vesicles and commensurately reduced increases in the radii of gyration of the biliary micelles upon mixing with vesicle dispersions of higher cholesterol content.

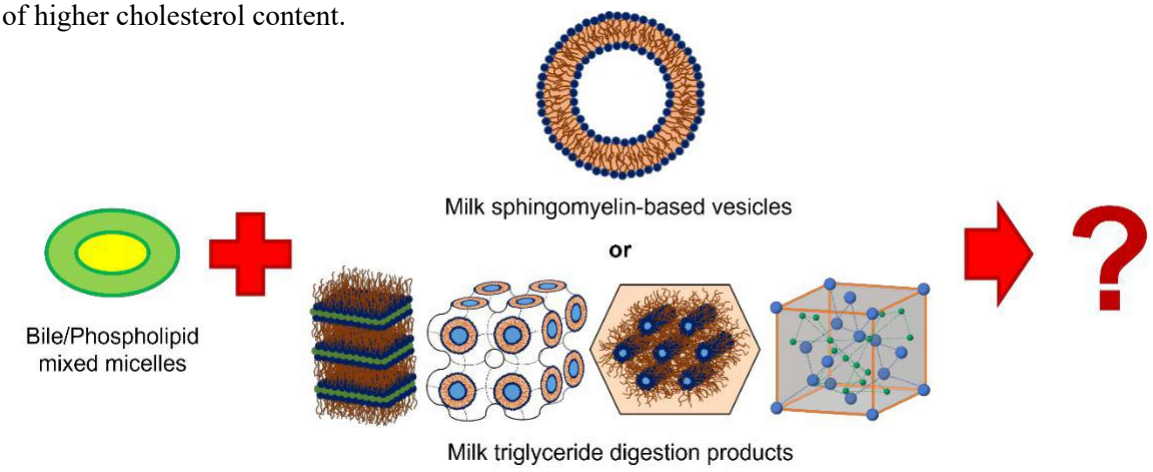

Figure 1 Bile salt/phospholipid mixed micelles self-assemble with milk polar lipids and triglyceride digestion products to form a variety of structures based on the lipid composition

1 Jensen, R. G.; Bitman, J.; Carlson, S. E.; Couch, S. C.; Hamosh, M.; Newburg, D. S., Chapter 6 - Milk Lipids: A. Human Milk Lipids. In *Handbook of Milk Composition*, Academic Press: San Diego, **1995**; pp 495-542.
2 Jensen, R. G.; Newburg, D. S., Chapter 6 - Milk Lipids: B. Bovine Milk Lipids. In *Handbook of Milk Composition*, Academic Press: San Diego, **1995**; pp 543-575.
3 Carey, M. C.; Small, D. M., (1972) *Arch. Internal Med.* ***130***, (4), 506-527.
4 Clulow, A. J.; Salim, M.; Hawley, A.; Boyd, B. J., (2021) *Food Hydrocolloids* ***110***, 106126.

A088-05-250823

The effect of surfactants on the in vitro behaviour of suppositories: spontaneous structure formation effects solubility

Wye-Khay Fong[1]*, Emma Ruth Lucille Brisson[1], Olivier Laczka[2], Quach Truong[2], and Livia Salvati Manni1,3,4*

[1]Department of Chemistry, School of Environmental and Life Science, University of Newcastle, Callaghan NSW, 2308;
[2]Noxopharm, Chatswood NSW, 2067; Schools of [3]Chemistry and [4]Medicine, University of Sydney, Camperdown NSW, 2006.

Khay.fong@newcastle.edu.au

Keywords: emulsion, structure, drug delivery, synchrotron

INTRODUCTION: Many drugs have a limited bioavailability when delivered via oral administration. Rectal drug delivery allows for the absorption of drugs by bypassing some major metabolic hurdles [1]. Little is understood about how drug uptake is influenced by the surfactants in the suppository formulation; thus, fundamental research into the effect that formulation components of suppositories have on the bioavailability of drugs delivered rectally is required. Surfactants have played a role in aiding the adhesion of suppository formulations to the rectal wall in a hope to increase drug uptake, but no systematic study into their structure-property relationships pertaining to drug bioavailability has been performed. Insights from a colloid and interface science perspective can elucidate a mechanism of action that is easily controlled through formulation modifications.

METHODS: One hydrophilic (acetaminophen) and two hydrophobic drugs (indomethacin and idronoxil) were formulated into a

hard fat suppository using surfactants with a range of HLB values: Tween 80 (HLB 15), TPGS (13.2), Kolliphor EL (12.7) and Myrj S8 (10.8). Each formulation was then introduced into a simulated rectal environment by mixing the drug formulations in simulated rectal fluid [2] at physiological temperature (37 °C). Drug partitioning was measured using UV-Vis spectrophotometry. Synchrotron small angle X-ray scattering (sSAXS) and cryogenic scanning electron microscopy (cryoSEM) were used to characterise the spontaneous formation of hydrated amphiphilic nanostructures of the suppository formulations.

RESULTS AND DISCUSSION: The spontaneous formation of amphiphilic structures upon the hydration of suppositories in simulated rectal conditions was observed to investigate the influence of structure in these two-phase systems on the solubility of hydrophilic and hydrophobic drugs. The spontaneous emulsification or micellisation was observed to be dictated by the properties a range of non-ionic surfactants. Time resolved structural analysis revealed that the more hydrophilic surfactants, those with a higher HLB, were more likely to promote the formation of micelles whereas the more hydrophobic surfactants (low HLB) emulsify the formulation on hydration. As the bioavailability of drugs are closely linked to their solubility, the impact of these structure of the hydrophilic partitioning experiments. It was found that the non-ionic surfactants had no significant impact on the solubility of the hydrophilic drug, acetaminophen. On the other hand, the solubility of the poorly water soluble drugs, were significantly enhanced through emulsification and the maintenance of the lamellar structure within the lipid droplets.

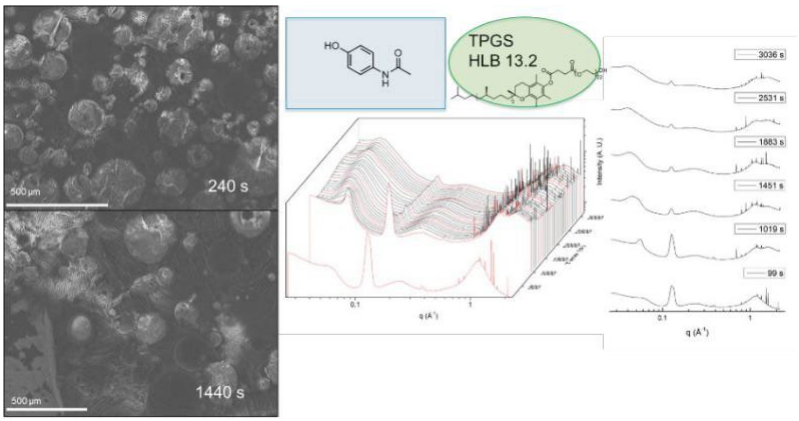

Figure 1. Time resolved structural analysis of the formation of structures during the hydration of suppositories (acetaminophen and TPGS) in simulated rectal fluid. Upon hydration, sSAXS indicate the spontaneous formation of micelles which gradually incorporated increasing amounts of oil over time. The resulting emulsion shown in the cryoSEM images appear very inhomogeneous. This process was repeated for all mixtures.

Through fundamental physicochemical studies, understanding the relationship between formulation, structure formation and solubility will allow for the better design and formulation of lipidic delivery systems for pharmaceutical treatments.

1 S. Hua, Physiological and Pharmaceutical Considerations for Rectal Drug Formulations, Front. Pharmacol. 10 (2019) 1–16.

2 M. Vertzoni, A. Diakidou, M. Chatzilias, E. Söderlind, B. Abrahamsson, J.B. Dressman, C. Reppas, Biorelevant Media to Simulate Fluids in the Ascending Colon of Humans and Their Usefulness in Predicting Intracolonic Drug Solubility, Pharm. Res. 27 (2010) 2187–2196.

A088-06-250823

Photoinduced bidirectional switching in phospholipid membranes

C. Hövelmann[1,3,4], Jonas E. Warias[1], R. P. Giri[1], J. Kuhn[1], K. Hansen[1], Lukas Petersdorf[1], Nicolas Hayen[1], P. Jordt[1], A. Sartori[1], C. Shen[3], F. Reise[2], O. M. Magnussen[1], T. K. Lindhorst[2], B. M.Murphy[1,4]

[1]Institute of Experimental and Applied Physics, Kiel University, Leibnizstr. 19, D-24118 Kiel, Germany, [2]Otto Diels Institute of Organic Chemistry, Kiel University, Otto-Hahn-Platz 3-4, D-24118 Kiel, Germany, [3]Deutsches Elektronen-Synchrotron DESY, Notkestraße 85, D-22607 Hamburg, Germany, [4]Ruprecht Haensel Laboratory, Kiel University, D-24118 Kiel, Germany

hoevelmann@physik.uni-kiel.de

Keywords: lipid monolayer, **X**-ray scattering, structure determination, bidirectional switch, glycolipids

The role of the lipid environment within a biomembrane is of fundamental interest to understand intercellular and cell-cell interaction. The lipid molecules define not only the cell structure and geometry but also influence the functionality and self-assembly of membrane proteins and channels.[1,2] Dynamic switching behaviour of the membrane associated proteins and channels regulates the transportation of ions and metabolites of immense cellular importance through the lipid membrane into the cell. However, the in-depth molecular mechanisms involved in the switching are poorly understood. Thus, molecular switches in biomembranes are currently under intense investigation owing to their diverse applications in biosensor engineering and drug delivery. To understand the interaction between lipid and functional molecules, we investigate photoswitchable glycoconjugates embedded in a 1,2-dipalmitoyl-phosphatidylcholine (DPPC) model systems in the form of Langmuir films and vesicles. Here, the structure of photoswitchable glycoconjugates change reversibly between their *trans*- and *cis*-conformation by illumination with visible and UV light[1] inducing a reversible change in the molecular arrangement within the surrounding membrane[4]. The resulting structural changes, their evolution and time scales are characterised with multiple measurement techniques including absorption spectroscopy, surface pressure-area isotherm, X-ray reflectivity, grazing incident X-ray diffraction and also X-ray and neutron small angle scattering. Studies performed on mixed monolayers and vesicles with varying glycoconjugates identify an additional phase transition, which unexpectedly represents a crossover point. The surface pressure and monolayer thickness change in opposite directions above and below the phase transition indicate that the photoswitchable glycoconjugates change orientation within the monolayer. Therefore, photoswitchable glycoconjugates can act as a bidirectional switch in DPPC monolayers.

In addition, as this work is part of a pilot project within the DAPHNE4NFDI consortium[5], the best practice for scientific data handling to ensure that our data is findable, accessible, interoperable and re-usable (FAIR), will be discussed.

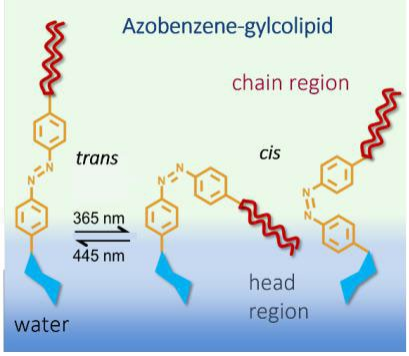

Figure 1. Schematic showing the conformational modification in the glycoconjugate azobenzene-glycolipid induced by UV and visible light.

1 Reise, F., Warias, J. E., Chatterjee, K., Krekiehn, N. R., Magnussen, O., Murphy, B. M., Lindhorst, T. K. (2018). *Chemistry – A European Journal* **24**, 17497-17505.

2 Laganowsky, A., Reading, E., Allison, T. M., Ulmschneider, M. B., Degiacomi, M. T., Baldwin, A. J., Robinson C. V. (2014). *Nature* **510**, 172.

3 Phillips, R., Ursell, T., Wiggins, P., Sens, P. (2009). *Nature* **459**, 379.

4 Warias, J. E., Reise, F., Hövelmann, S. C., Giri, R. P., Röhrl, M., Kuhn, J., Jacobsen, M., Chatterjee, Arnold, T., Shen, C., Festersen, S., Sartori, A., Jordt, P., Magnussen, O., Lindhorst, T. K., Murphy, B. M. *submitted*.

5 DAPHNE4NFDI is a National Research Data Infrastructure consortium funded by the German German Research Foundation (DFG). https://www.daphne4nfdi.de/

A088-07-250823

SAXS determination of the conformational information of VPPase embedded in a phospholipid nanodisc environment

Orion Shih[1], Yi-Qi Yeh[1], Kuei-Fen Liao[1], Chun-Jen Su[1], Kun-Mou Li[2], Chieh-Chin Li[3], Yuh-Ju Sun[2], Yun-Wei Chiang[3], and U-Ser Jeng[1,4,*]

[1]National Synchrotron Radiation Research Center, Hsinchu 30076, Taiwan
[2]Department of Life Science and Institute of Bioinformatics and Structural Biology, College of Life Science, National Tsing Hua University, Hsinchu 30013, Taiwan
[3]Department of Chemistry, National Tsing Hua University, Hsinchu 30013, Taiwan
[4]Department of Chemical Engineering, National Tsing Hua University, Hsinchu 30013, Taiwan
E-mail: shih.orion@nsrrc.org.tw

Keywords: SAXS, nanodisc, membrane protein

Vigna radiata H+-PPase (VPPase) is a proton pump that hydrolyzes pyrophosphate (PPi) to drive proton transportation across cellular membranes against the electrochemical gradient [1]. These enzymes are found in plants and various unicellular organisms and are essential for survival under different stress conditions [2]. However, the detailed mechanisms underlying the translocation reactions and structural changes between other conformational states of VPPase (ligand-free or PPi-binding) are still unclear. In this report, high-performance-liquid-chromatography, small-angle X-ray scattering (SAXS), UV−Vis absorption, differential refractive index (RI) detections, and modified core-shell bicelle model fitting are integrated to probe the structural information of VPPase-incorporated POPC nanodiscs (Fig. 1). The results indicate that VPPase is stable in the POPC nanodiscs, and the length of VPPase slightly thickens when changing from resting state (R-state, ligand-free) to initiated state (I-state, PPi-binding). This integrated analysis scheme can be applied to other membrane protein/detergents/lipids complexes and provides a new approach to membrane protein studies.

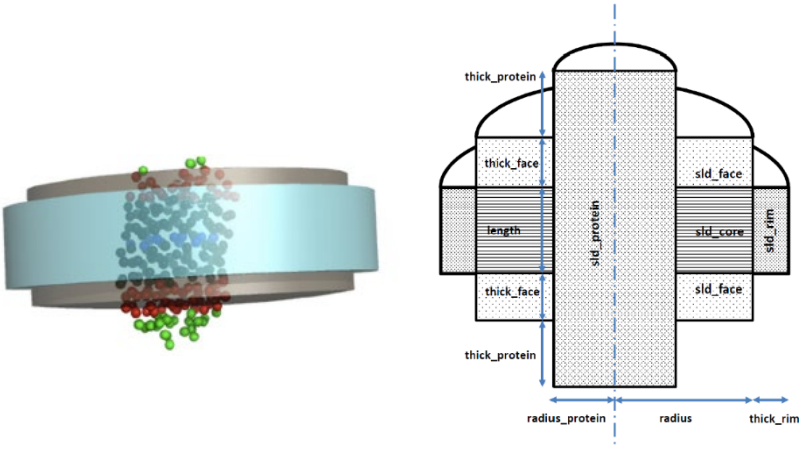

Figure 1. (left) Schematic diagram showing VPPase loaded in a nanodisc, and (right) the simulation model for this complex.

[1] Luoto, H. H., Baykov, A. A., Lahti, R. & Malinen, A. M. (2013) *Proc. Natl Acad. Sci. USA* **110**, 1255–1260.
[2] Maeshima, M. (2000) *Biochim. Biophys. Acta* **1465**, 37–51.

A094 Crystal Engineering Applications to Pharmaceuticals
Room 210
4.00pm – 6:30pm

A094-01-250823

Pre-nucleation aggregation of caffeine-benzoic acid as a prediction of co-crystal formation

Yichun Shen[a], Aurora J. Cruz-Cabeza[b], Katharina Edkins[a]

[a] School of Health Sciences, University of Manchester, Manchester M13 9PT, UK,
[b] Department of Chemistry, Durham University, South Road, Durham D1 3LE, UK Email of communicating:

yichun.shen@manchester.ac.uk

Keywords: NMR, Pharmaceutical, Solvent influence

Pharmaceutical co-crystals have been researched for decades as a promising alternative formulation of some drugs because of their improved physicochemical properties.[1] Most studies focus on experimental co-crystal screening such as mechanochemical methods, slurry conversion, and evaporation but they are trial-and-error based processes and the co-crystals which are harder to nucleate may be missed easily during the screening.[2] Computational prediction is an alternative method; however, most of the used algorithms are based on the thermodynamically driven formation of the final co-crystal form without taking into account whether they can be obtained *via* solution co-crystallisation.[3] There has been hardly any work done towards fast, efficient and reliable prediction of experimental co-crystal formation from solution. To increase the efficiency of co-crystallisation screening, it is important to investigate the pre-nucleation aggregation in solution, where small and thermodynamically stable molecular clusters form *prior* to nucleation.[4]

Here, we study the caffeine (CAF)-benzoic acid (BA) co-crystal system, due to its reported difficulty to crystallise spontaneously making the presence of hetero-nuclear seeds necessary for nucleation.[5] In our work, CAF-BA co-crystal has been prepared using both ball mill and solution co-crystallisation method without heteronuclear seeding for the first time. The formation of CAFBA co-crystal can be predicted using nuclear magnetic resonance (NMR) spectroscopy for the used solvents acetonitrile, acetone, and methanol. The large apparent binding constant and apparent Gibbs free binding energy calculated between CAF and BA in acetonitrile indicates strong heteromeric interactions, coinciding with the result from the solid state where the co-crystal is easy to crystallise. Although we did not obtain the co-crystal from acetone and methanol in the initial experiments, the NMR results show strong interactions between the two solutes in these solvents indicating the possibility of the co-crystal formation. This result was further corroborated by the ternary phase diagrams of these systems. Contrary to acetone and methanol, weak interactions between CAF and BA in dimethyl sulfoxide (DMSO) suggests DMSO is an unsuitable solvent in the formation of the co-crystal. The result supports the hypothesis that there is a link between pre-nucleation aggregates and the final co-crystal formation, and NMR spectroscopy is a promising, easy and timesaving technique to predict co-crystal formation and screen for suitable solvents.

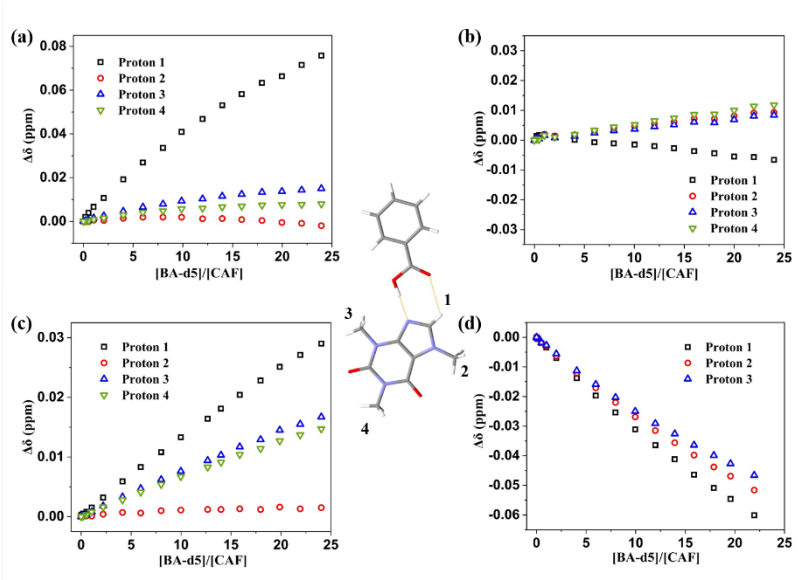

Figure 1. ^{1}H NMR proton positions of CAF protons 1-4 in CAF-BA-d5 titration as function of BA-d5 concentration in ace-tonitrile-d3 (a), DMSO-d6 (b), acetone-d6 (c), and methanol-d4 (d).

[1] R. Shaikh, R. Singh, G. M. Walker and D. M. Croker, *Trends in Pharmacological Sciences*, 2018, **39**, 1033-1048.

[2] K. Fucke, S. A. Myz, T. P. Shakhtshneider, E. V. Boldyreva and U. J. Griesser, *New Journal of Chemistry*, 2012, **36**, 1969-1977.

[3] M. Ro drigues, B. Baptista, J. A. Lopes and M. C. Sarraguca, *International Journal of Pharmaceutics*, 2018, **547**, 404-420.

[4] H. Fu, X. Gao, X. Zhang and L. Ling, *Crystal Growth & Design*, 2021, DOI: 10.1021/acs.cgd.1c01084.

[5] D. K. Bucar, G. M. Day, I. Halasz, G. G. Z. Zhang, J. R. G. Sander, D. G. Reid, L. R. MacGillivray, M. J. Duer and W. Jones, *Chemical Science*, 2013, **4**, 4417-4425.

A094-02-250823

Rajni Miglani Bhardwaj

Research & Development, AbbVie Inc., 1 N Waukegan Road, North Chicago, Illinois 60064, United States; *rajni.bhardwaj@abbvie.com*

Keywords: Paritaprevir, structure property relationship, solid form complexity, beyond rule of 5 drug, experimental soldi from screening, computational tools

There has been significant increased interest in the discovery and development of orally available beyond rule of 5 (bRo5) drugs in the pursuit of less druggable high value targets specially to meet unmet medical needs. bRo5 molecules are generally good fit for large, flexible, groove, flat, or featureless binding sites characteristics of "difficult to-drug" targets. An existence of significant number of orally bioavailable drugs and clinical candidates in this space points to the opportunities in bRo5 space [1-3]. However, these opportunities come with challenges including poor in vitro-in vivo correlation, higher synthetic complexity, purification complexities, prolific solvate formation, higher tendency to form non-stochiometric solid forms, requirement of enabling solid form/formulation due to poor solubility and permeability. In this presentation, we will be discussing challenges associated with solid form screening and selection of bRo5 molecules. Case study of a bRo5 drug i.e. Paritaprevir, will be presented where experimental and computational approaches were used in conjunction to underpin the link between the structural features and derived solid state properties. In addition, we will also be discussing the chameleonicity of bRo5 molecules, where they can hide/expose their polarity depending on the environment and its implications by detailing the conformational journey from gas phase-solid state-formulation-receptor ligand complex explored by computational methods [4-6].

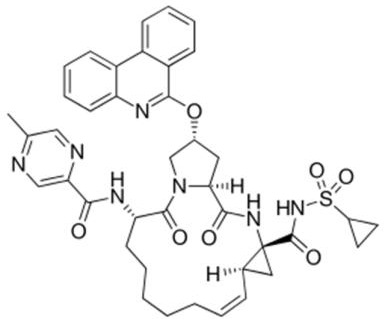

$C_{40}H_{43}N_7O_7S$

MolecularWeight:765.9g/mol

Figure 1. Chemical Structure of Paritaprevir

1 DeGoey, D., Chen, H., Cox, P., Wendth, M., (2018), J. Med. Chem., 61, 2636.
2 Kihlberg, J., (2014), Chemistry & Biology, 21, 1115
3 Pike A, et.al, (2020), Drug Discovery Today, 25, 1793
4 Sheikh, A.Y., Mattei, A., Miglani Bhardwaj, R., Hong, R.H., (2021). *J. Am. Chem. Soc.*, **143**, 17479.
5 Hong, R.H., Mattei, A., Miglani Bhardwaj, R., Sheikh, A.Y., (2022). *Cryst. Growth Des.,* **22,** 726.
6 Miglani Bhardwaj, R., Ho. R., Gui, Y., Sheikh, A.Y., (2022). *Cryst. Growth Des.* **22,** 4250.

A094-03-250823

Sodium Salt Hydrate Crystals of Nonsteroidal Anti-inflammatory Drugs: Structure and Solid-State Dehydration Transition Relationship

H. Oyama, H. Uekusa

Department of Chemistry, School of Science, Tokyo Institute of Technology, Tokyo, Japan

Email: uekusa@chem.titech.ac.jp

Keywords: NSAIDs, Hydrate crystal, Dehydration

Many active pharmaceutical ingredient (API) crystals have solubility problems, so sodium salt formation is frequently used to improve insolubility, and the widely used nonsteroidal anti-inflammatory drugs (NSAIDs) are no exception. Sodium salts are known to form hydrate crystals because the sodium cation draws water into the lattice. On the other hand, hydrate crystals are subject to dehydration and hydration transition depending on the environmental conditions (temperature and humidity) during manufacturing and storage, which poses a significant problem in assuring the stability of pharmaceutical crystals. Therefore, it is essential to investigate the crystal structure of sodium salt hydrate crystals (most commonly used Multi-Component Crystal) and elucidate the correlation with dehydration/hydration behaviour.

We have studied the dehydration-hydration transition of many pharmaceutical hydrate crystals [1-4]. In particular, we have shown the mechanism of solid phase dehydration transition of Sodium Diclofenac hydrate, in which dehydration proceeds with partial retention of the crystal structure of the hydrate [5]. This research clarified the relationship between the crystal structure and dehydration transition behaviour of the propionic NSAIDs sodium salt hydrate crystals of Loxoprofen, Flurbiprofen, Ibuprofen, Ketoprofen, Fenoprofen (Fig.1 left).

Interestingly, in all crystals, the sodium salts of NSAIDs formed a dihydrate and crystallized in a similar layered structure despite differences in molecular structure. A characteristic hydrophilic linear channel structure was present in the crystal structure, consisting of a water molecule (1), Sodium cation, and carboxylate oxygen atoms, which were hydration water channels with a water molecule (2) encapsulated in the centre (Fig.1 centre).

A single-crystal-to-single-crystal dehydration transition was observed when single hydrate crystals were placed under low humidity. A similar layered structure of anhydrous crystals was again observed, but the dehydration closed the hydration water channels, and this change in crystal structure was accompanied by compression of the hydrophobic layer. Thermal analysis revealed a positive correlation between the dehydration temperature and the length of the hydration water channels, indicating a dehydration mechanism whereby water molecules desorb through the channels, and a transition occurs (Fig.1 right). Furthermore, kinetic analysis of the solid phase reaction model supported this dehydration transition mechanism.

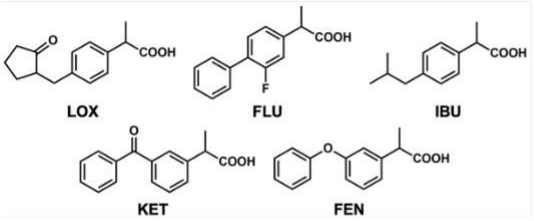

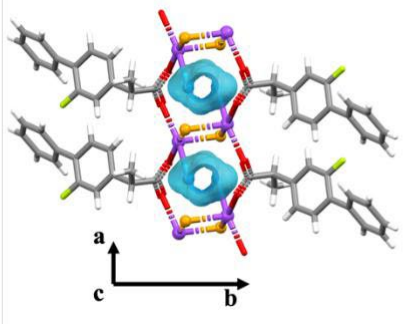

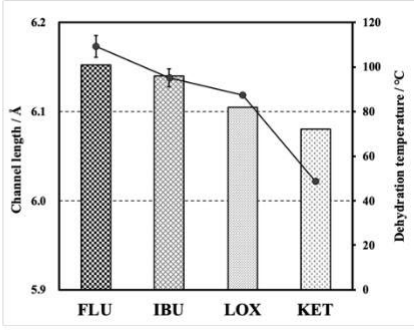

Figure 1. NSAIDs, hydration water channel, and channel-temperature relationship.

1 Fujii, K., Uekusa, H., Itoda, N., Hasegawa, G., Yoneochi, E., Terada, K., Pan, Z. & Harris, K.D.M. (2010). *J. Phys. Chem. C*, **114**, 580.
2 Fujii, K., Uekusa, H., Itoda, N., Yoneochi, E. & Terada, K. (2012). *Crystal Growth & Des.*, **12**, 6165.
3 Fujii, K., Aoki, M. & Uekusa, H. (2013). *Crystal Growth & Des.*, **13**, 2060.
4 Sakon, A., Sekine a. & Uekusa H. (2016). *Crystal Growth & Des.*, **16**, 4635.
5 Oyama, H., Miyamoto, T., Sekine, A., Nugrahani, I. & Uekusa, H. (2021). *Crystals*, **11**, 412.

A094-04-250823

Polymorphism of ribavirin at high pressure

Tiwari[1,2], N. Giordano[1], H.P. Liermann[1], S. Parsons[2]

Deutsches Elektronen-Synchrotron DESY, Notkestr. 85, 22607 Hamburg, Germany
School of Chemistry and Centre for Science at Extreme Conditions, The University of Edinburgh, King's Buildings, West Mains Road, Edinburgh, UK, EH9 3JJ
bhaskar.tiwari@desy.de

Keywords: APIs, High-pressure, Polymorphism

Thorough characterisation of polymorphism in active pharmaceuticals ingredients (APIs) is vital in the development of solid forms used in patient therapy. Different polymorphic forms may have varying physicochemical properties such as solubility and compressibility, which may affect the overall bioavailability or tabletability of a drug [1]. Structural modifications in the API solid form may be engineered by co-crystal formation *e.g.* salts, hydrates, and solvates [2] but another, less conventional route is by the application of externally applied force, which modifies the underlying crystal packing without chemical interference [3]. The drive to minimise volume at high pressure transforms the thermodynamic landscape, making pressure an extremely attractive method to explore polymorphism, intermolecular interactions, and phase transitions in the APIs under conditions which are completely unexplored by traditional solvent screens. The pressures need not be very high, work in this area is almost exclusively carried out below 10 GPa (~100 000 atm).

Ribavirin ($C_8H_{12}N_4O_5$), is a synthetic nucleoside analogue that has been used as a broad-spectrum antiviral in the treatment of hepatitis-C, Lassa fever, and respiratory syncytial virus. Only two ambient conditions polymorphs are reported in the literature, 'V1', and the marketed 'V2' form [4]. Both forms crystallise in the $P2_12_12_1$ space group and are best described as conformational polymorphs. Single crystals of the V2 form were studied to 10 GPa by single crystal X-ray diffraction in a diamond anvil cell (Fig.1b) using synchrotron radiation ($\lambda \approx 0.2900$ Å) on beamline P02.2 at PETRA III, DESY. The ribofuranosyl ring and triazole moieties present in ribavirin show an unprecedented degree of torsional flexibility as pressure is increased, leading to the formation of three new conformational polymorphs containing five different conformers. The V2 form undergoes a transition to a short-lived intermediate phase, V3, at 5.4 GPa, which manifests as a tripling of the unit cell with three different conformers present in the asymmetric unit ($P2_12_12_1$, Z = 12, Z' = 3). V3 transforms into V4 ($P2_12_12_1$, Z = 4, Z' = 1) at 6.0 GPa with similar cell parameters to V2 and is akin to a re-entrant phase transition but the five-membered ribofuranosyl ring changes from an envelope to a twist conformation. Finally, V5 ($P2_12_12_1$, Z = 4, Z' = 1) forms at 7.2 GPa and manifests as a rotation about the hydroxymethyl group of the ribofuranosyl ring. Above 7 GPa, ribavirin can exist either as V4 or V5. The phase pathway may occur sequentially from V3 to V4 to V5, or directly transition from V3 to the V5 form. On decompression, V4 and V5 revert back to the ambient pressure, V2 phase.

(a)

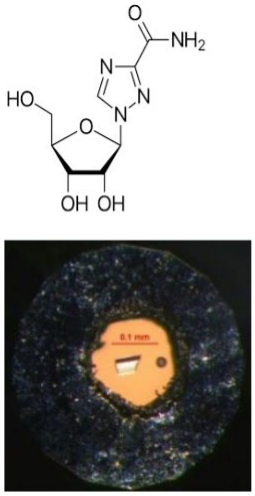

(c)

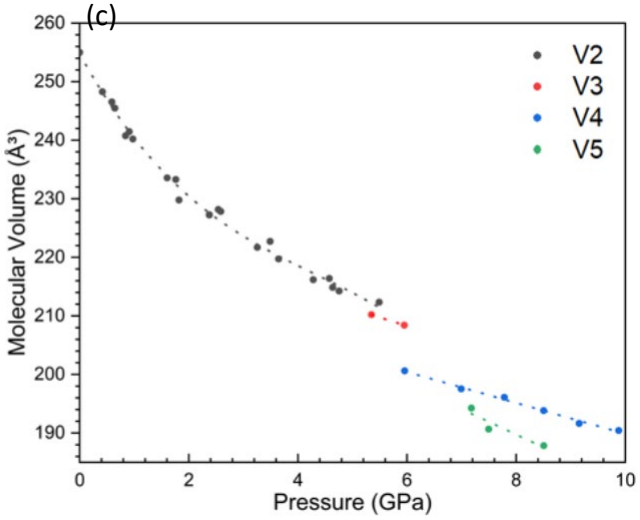

Figure 1 (a) chemical structure of ribavirin. (b) a single crystal of ribavirin loaded in a diamond anvil cell at 1.8 GPa alongside a ruby sphere for pressure determination and (c)molecular volume of ribavirin as a function of pressure.

[1] Christopher E. Marjo, Mohan Bhadbhade, James M. Hook, and Anne M. Rich *Molecular Pharmaceutics* **2011** *8* (6), 2454-2464
[2] E. Grothe, H. Meekes, E. Vlieg, H. J. ter Horst and R. de Gelder *Crystal Growth & Design* **2016** *16* (8), 3237-3243
[3] Francesca P. A. Fabbiani, David R. Allan, William I. F. David, Alistair J. Davidson, Alistair R. Lennie, Simon Parsons, Colin R. Pulham, and John E. Warren *Crystal Growth & Design* **2007** *7* (6), 1115-1124
[4] Prusiner, P. & Sundaralingam, M. Acta Cryst. B **1976** 32, 419-426

A094-06-250823

Intermolecular compatibility to drive solid form development

Amy A. Sarjeant[1], Bhupinder Sandhu[2], Scott Savage[3]

[1]Drug Product Development, Bristol Myers Squibb, 1 Squibb Dr. New Brunswick, NJ 08903 USA. [2]Pharmaceutical Candidate Optimization, Bristol Myers Squibb, 10300 Campus point Dr, San Diego, CA, 92130 USA. [3]Chemical Process Development, Bristol Myers Squibb, 1 Squibb Dr. New Brunswick, NJ 08903 USA.

amy.sarjeant@bms.com

Keywords: Crystal Engineering, Hydrogen bonding, Pharmaceuticals

Recent investigations into improving the long-term stability of inherently unstable drug candidates have focused on co-crystal formation as a potential solution [1,2]. Nitroxyl (HNO) has been an Active Pharmaceutical Ingredient (API) of interest for two decades in the treatment of congestive heart failure. More recently, Phase II clinical trials were enabled by a class of HNO prodrugs that had challenging stability above frozen conditions. In order to identify a commercially viable/stable HNO donor, a series of amino acid co-formers was analyzed as potential co-crystallization agents. Ultimately, L-proline was chosen as the most promising co-former. A systematic study of both the neat pro-drugs and their L-proline cocrystals underscores the importance of hydrogen bonding in forming a stable crystalline form. This talk will focus on the various techniques used to analyze the crystalline forms of these compounds and provide an understanding of the various stabilizing intermolecular interactions which drive cocrystal stability.

[1] Duggirala, N. K.; Perry, M. L.; Almarsson, Ö.; Zaworotko, M. J. Pharmaceutical Cocrystals: Along the Path to Improved Medicines. *Chem. Commun.* **2016**, *52* (4), 640–655. https://doi.org/10.1039/c5cc08216a.

[2] Karimi-Jafari, M.; Padrela, L.; Walker, G. M.; Croker, D. M. Creating Cocrystals: A Review of Pharmaceutical Cocrystal Preparation Routes and Applications. *Cryst. Growth Des.* **2018**, *18* (10), 6370–6387. https://doi.org/10.1021/acs.cgd.8b00933.

A116 Dynamical processes and transient structures underlying energy
conversion: x-ray spectroscopies from fs to μs
Room 220
4.00pm – 6:30pm

A116-01-250823

Capabilities of XEOL and TR-XEOL of TPS 23A X-ray nanoprobe via hybrid bunch mode

Bi-Hsuan Lin1*, Yu-Hao Wu1, Shang-Wei Ke1, Chien-Yu Lee1, Bo-Yi Chen1, Gung-Chian Yin1 and Mau-Tsu Tang1

National Synchrotron Radiation Research Center, Hsinchu, 30076, Taiwan

Email of communicating bihsuan@nsrrc.org.tw

Keywords: XEOL, TR-XEOL, X-ray nanoprobe

X-ray excited optical luminescence (XEOL) and Time-resolved XEOL (TR-XEOL) were developed successfully for the 23A X-ray nanoprobe beamline located at the Taiwan Photon Source (TPS). The advantages of the TR-XEOL include (i) a nano-focused X-ray beam (<60 nm) with excellent spatial resolution and (ii) a streak camera that can simultaneously record the XEOL spectrum and decay lifetime.[1] Especially, using an x-ray nanobeam operating in the hybrid bunch mode will provide not only a sufficiently high peak power density but also high-quality temporal domain (~ 200 ns) measurements for studying the luminescence dynamics of materials. The peculiar emission behavior has been observed in nonpolar a-plane MgZnO/ZnO multiple quantum wells (MQWs): the emission intensity increases more than 10 times after X-ray irradiation.[2] In addition, the X-ray fluorescence (XRF) of TPS 23A also can provide the visualization methods for the characterization of valence states in phosphor materials, such as Eu-doped $BaAl_2O_4$. XRF mapping not only gives information on the elemental distributions but also clearly reveals the valence state distributions of the Eu^{2+} and Eu^{3+} ions.[3]

We anticipate that X-ray nanoprobes will open new avenues with significant characterization ability for unravelling the emission mechanisms of light-emitting materials.

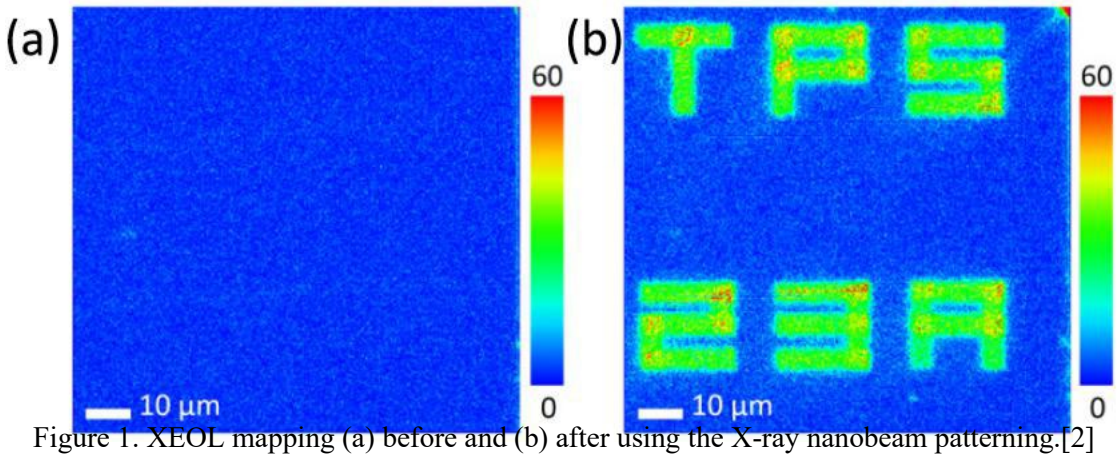

Figure 1. XEOL mapping (a) before and (b) after using the X-ray nanobeam patterning.[2]

1 Bi-Hsuan Lin, Yu-Hao Wu, Xiao-Yun Li, Hsu-Cheng Hsu, Yu-Cheng Chiu, Chien-Yu Lee, Bo-Yi Chen, Gung-Chian Yin, Shao-Chin Tseng, Shih-Hung Chang, Mau-Tsu Tang and Wen-Feng Hsieh,(2020). *Journal of Synchrotron Radiation*, **27**, 217.

2 Bi-Hsuan Lin, Yu-Hao Wu, Tai-Sing Wu, Yung-Chi Wu, Xiao-Yun Li, Wei-Rein Liu, Mau-Tsu Tang, and Wen-Feng Hsieh (2019). *Applied Physics Letters*, **115**, 171903.

3 Yu-Hao Wu, Yung-Yang Lin, Jeng-Lung Chen, Shih-Yu Fu, Shu-Chi Huang, Chien-yu Lee, Bo-Yi Chen, Gung-Chian Yin, E-Wen Huang, Mau-Tsu Tang and Bi-Hsuan Lin (2022). *Journal of Synchrotron Radiation* , **29**, 456.

A116-02-250823

Dynamical processes and transient structures underlying energy conversion: x-ray spectroscopies from fs to μs
Ultrafast optical spectroscopy of molecules using quantum light

Zhedong Zhang

Department of Physics, City University of Hong Kong, Hong Kong

Keywords: X-ray spectroscopy, quantum, light

Quantum states of the light, e.g., single photons, entanglement and squeezing, open up a new avenue for spectroscopy by utilizing the quantum optical fields as novel control knobs and through the variation of photon statistics. With the advancements of quantum optical technology and X-ray source technology, imaging and controlling the electron and vibrational motions of molecules can be achieved, towards unprecedented resolution and precision, not accessible by the classical light pulses [1]. Two key issues emerge at nanoscale: quantum states of photons and strong matter-light interaction. The underlying physics is still an open issue for molecules and spectroscopy.

In this talk, I will present an overview of our recent work on multidimensional spectroscopic probes for ultrafast dynamics of molecular polaritons. Several spectroscopic signals will be covered: multidimensional coherent probe, photon-coincidence counting, and Raman spectra with quantum optical fields [2,3,4]. Microscopic models for molecular polaritons using density matrix will be incorporated for a unified understanding of the spectroscopic signals.

A116-03-250823

Probing ultrafast structural and electronic dynamics in chemical and materials research using X-ray free electron lasers

C.J. Milne

European XFEL GmbH, Holzkoppel 4, 22869 Schenefeld, Germany

christopher.milne@xfel.eu

Keywords: XFEL, ultrafast dynamics, X-ray spectroscopy, X-ray scattering

X-ray spectroscopy and scattering allow a unique combination of electronic and structural information to be obtained from a variety of different types of samples in many different forms (solid, liquid, gas). The extension of these methods into the time domain has allowed measurement of dynamic processes, for example the tracking the photoinduced charge carriers in a functional material [1,2] or following the photocycle in a light activated protein [3,4]. In recent years X-rays have started to become routinely used to measure light-activated processes using a pump-probe scheme, where the sample is photoexcited with light and then probed after a variable time delay using an X-ray pulse. These methods can measure dynamics over a broad range of timescales, allowing them to probe everything from protein dynamics to ultrafast electronic spin-state changes in molecular systems. With the recent development of X-ray free electron lasers (XFELs) [5], time-resolved X-ray techniques have moved into the ultrafast regime, where the timescales of electron and nuclear motion can be accessed using the femtosecond X-ray pulses available from these facilities [6].

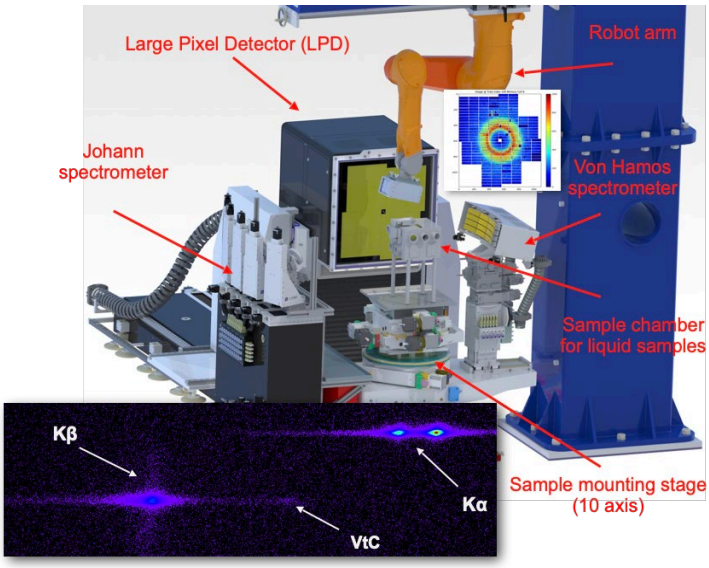

Figure 1. Layout of the FXE instrument for ultrafast X-ray measurements with some typical X-ray measurements displayed

This talk will present an overview of how X-ray techniques are being used at XFELs and the type of information the measurements can provide. The talk will introduce the European XFEL [7], a brand-new, high-repetition rate XFEL facility located in northern Germany, and its' Femtosecond X-ray Experiments (FXE) instrument [8,9] which is focussed on measuring ultrafast dynamics in the condensed phase. Finally the lecture will present some examples of the types of measurements XFELs can perform and the scientific questions that can be answered using ultrafast X-ray techniques.

[1] Penfold, T. J. *et al.* (2018). *Nat. Comm.* **9**, 478.

[2] Rittmann-Frank, M. H. *et al.* (2014). *Angew. Chem. Int. Ed.* **53**, 5858–5862.
[3] Bacellar, C. *et al*. (2020). *P Natl Acad Sci Usa* **117**, 21914–21920.
[4] Kinschel, D. *et al*. (2020). *Nat. Comm.* **11**, 4145.
[5] Barletta, W. A. *et al*. (2010). *Nuclear Inst. and Methods in Physics Research, A* **618**, 69–96.
[6] Seddon, E. A. *et al*. (2017). *Rep. Prog. Phys.* **80**, 115901.
[7] Decking, W. *et al*. (2020). *Nat Photonics* **14**, 391–397.
[8] Khakhulin, D. *et al.* (2020). *Appl. Sci.* **10**, 995.
[9] Galler, A. *et al.* (2019). *Journal of Synchrotron Radiation* **26**, 1–16.

A116-04-25082023

Hybrid structure analysis: precise structure determination of electrocatalysts by the combination of X-ray diffraction and absorption

K. Adachi1, A. Li2, S. Kong2, R. Nakamura2, D. Hashizume1

1 RIKEN Center for Emergent Matter Science (CEMS), 2-1 Hirosawa, Wako, Saitama 351-0198, Japan, 2 RIKEN Center for Sustainable Resource Science (CSRS), 2-1 Hirosawa, Wako, Saitama 351-0198, Japan

kiyohiro.adachi@riken.jp

Keywords: PXRD, XAFS, Electrocatalyst

The structure parameters such as bond length, bond angle, and occupancy of each atomic site greatly affect the performance of the activity of solid catalysts and the physical properties of electronic and magnetic materials. Precise structure analysis including accurate estimation of these parameters by powder X-ray diffraction (PXRD) is very important in the development of materials. Generally, occupancy is highly correlated with atomic displacement parameters, making it difficult to determine accurate values by PXRD, especially, in the case that atoms with close atomic numbers share the same site. Here, we will present a precise structure analysis of an electrocatalyst, spinels Co_3O_4 and Co_2MnO_4, by "hybrid structure analysis" combining the advantages of both PXRD and X-ray absorption fine structure (XAFS).

We chose Co_3O_4 as an example to prove the concept of "hybrid structure analysis." The structure parameters were shared between PXRD and XAFS, and refined alternately and iteratively to afford a more reliable result. Both of calculated PXRD pattern and FT-EXAFS spectrum matched the experimental ones well. We successfully obtained the final structure parameters including occupancies through the hybrid structure analysis, indicating the effectiveness of this method.

This method was further applied to a real material as an electrocatalyst, Co_2MnO_4. It is one of the most stable electrocatalysts for oxygen evolution reactions of water electrolysis among non-noble catalysts [1]. It was difficult to determine the distribution and occupancy of metals only by PXRD data due to their close atomic numbers of Co and Mn. The hybrid structure analysis enabled the elucidation of the accurate occupancy of each atom in Co_2MnO_4 before and after the electrolysis, showing that the metal at the tetrahedral A site was easier to leach than at the octahedral B site. The result was consistent with that of the DFT calculations, clarifying the stabilization mechanism of this catalysis.

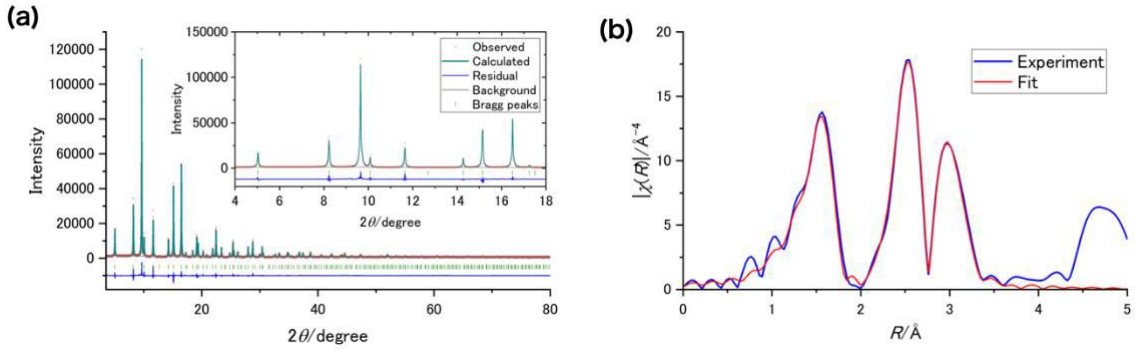

Figure 1. The results of the hybrid structure analysis of Co_3O_4. (a) Rietveld analysis and (b) EXAFS fitting at the final step.

[1] Li, A., Kong, S., Guo, C., Ooka, H., Adachi, K., Hashizume, D., Han, H., Xiao, J. & Nakamura, R. (2022) *Nat. Catal.* **5**, 109.

The synchrotron radiation experiments were performed at the BL14B2 (XAFS) and BL44B2 (SR-PXRD) of SPring-8 with the approval of the Japan Synchrotron Radiation Research Institute (JASRI) (proposal no. 2021B1856 and 2021B1892) and RIKEN (proposal no. 20210064), respectively. We thank K. Kato (RIKEN) and K. Shigeta (Nippon Gijutsu Center Co. Ltd) for their help in the SR-PXRD experiments at the BL44B2, and H. Ofuchi (JASRI) for his great support for the XAFS experiments. We also thank G. Takahashi (Rigaku) for the XRF measurements. KA is grateful to K. Muraoka for the fruitful discussion on XAFS and mathematical topics. respectively.

A116-06-250823

Dynamical processes and transient structures underlying energy conversion: x-ray spectroscopies from fs to μs
Excited state trajectories in photoactive transition metal complexes probed by ultrafast laser and x-ray spectroscopies and scattering

Lin X. Chen

Chemical Science and Engineering Division, Argonne National Laboratory, Lemont, Illinois 60439 USA, Department of Chemistry, Northwestern University, Evanston, Illinois 60208, USA

Keywords: Transition metal complex, excited state trajectory, X-ray spectroscopy and scattering

Many photochemical events start from initial light-matter interactions that cause atomic and electronic displacements in the excited states away from the energy minima of their potential energy surfaces. When certain photochemical events, such as bond breaking, intersystem crossing and electron/energy transfer taking place within the periods of key vibrational modes, the excited state energies are determined by the trajectories defined by the actual nuclear movements that may lead to different reaction pathways and outcome. Examples will be given in the work of tracking excited state pathways for transition metal complexes on the time scales from femtosecond to a few picoseconds, such as excited state Cu(I) and Pt(II) dimer complexes. Using fs broadband transient spectroscopy and fs X-ray solution scattering, coherent vibrational wavepacket motions can be examined.

From the time evolution of key vibrational modes in the Pt dimer complexes, particularly the Pt-Pt stretching mode, we mapped out excited state trajectories on potential energy surfaces of Pt-dimer complexes for light conversion, including coherent nuclear motions. These studies were carried out in a series of model platinum dimer complexes in solution and their electron donor acceptor complexes, featuring rich photochemistry and a set of intricate excited state potential energy surfaces on time scale previously unattainable.

For the time evolution of the structural dynamics of Cu(I) complex, the experimental results revealed the Jahn-Teller distortion that transforms the symmetry of the molecule from the D_{2d} in the ground state to D_2 in the triplet metal-to-ligand-charge-transfer (MLCT) state along the two key cooperative coordinates, the Cu-N distances and the angle between the two phenanthroline ligand planes. The detailed structural trajectories have been reproduced by quantum mechanical calculations to map out the actual excited state nuclear motions from the Frank-Condon structure to an intermediate triplet state and finally the triplet MLCT state.

DAY 5

Saturday 26 August 2023

Keynote 19

Room 203/204

9.00am - 9.50am

Keynote-019-260823

Driving Knowledge Discovery at RCSB.org: A one-stop-shop for exploration of experimentally determined PDB structures and Computed Structure Models

Stephen K. Burley

Research Collaboratory for Structural Bioinformatics Protein Data Bank, Institute for Quantitative Biomedicine, and Department of Chemistry and Chemical Biology, Rutgers, The State University of New Jersey, Piscataway, NJ 08854, USA; Rutgers Cancer Institute of New Jersey, New Brunswick, NJ 08901, USA; Research Collaboratory for Structural Bioinformatics Protein Data Bank, San Diego Supercomputer Center, University of California San Diego, La Jolla, CA 92093, USA

Stephen.Burley@RCSB.org

Keywords: Protein Data Bank, PDB, Open Access, RCSB Protein Data Bank, RCSB PDB, Worldwide Protein Data Bank, wwPDB, experimental structural biology, computational structural biology, computed structure models, protein structure prediction

The Research Collaboratory for Structural Bioinformatics Protein Data Bank (RCSB PDB), founding member of the Worldwide Protein Data Bank (wwPDB), is the United States data center for the PDB archive. As wwPDB-designated Archive Keeper, RCSB PDB is also responsible for PDB data security and updates releasing hundreds of new structures weekly. Every year, RCSB PDB serves >10,000 depositors of three-dimensional (3D) biostructures, supporting macromolecular crystallographers, electron microscopists, and nuclear magnetic resonance spectroscopists studying macromolecular structure and function on all six permanently inhabited continents. RCSB PDB delivers data to many millions of data consumers based in virtually every United Nations-recognized country, territory, *etc*. at no charge and with no limitations on usage.

This Keynote Lecture will describe how RCSB PDB (i) efficiently delivers services to many millions of users worldwide; (ii) works with wwPDB partners to process, validate, and biocurate >16,000 new depositions annually; (iii) enables exploration and visualization of public domain 3D biostructure data integrated with ~ 50 trusted external data resources through its research-focused web portal RCSB.org; and (iv) supports training, outreach, and education through its PDB101.RCSB.org web portal.

RCSB.org is a one-stop-shop for open access to >200,000 experimentally determined PDB structures of biological macromolecules alongside >1,000,000 incorporated Computed Structure Models (CSMs) of proteins predicted using artificial intelligence/machine learning methods. It is a "living data resource." Every PDB structure and CSM is integrated weekly with related functional annotations from trusted external biodata resources, providing up-to-date information for the entire corpus of 3D biostructure data. Within RCSB.org, PDB structures and CSMs are clearly identified as to their provenance (Fig. 1) and reliability. Both are fully searchable and can be analyzed and visualized using the full complement of RCSB.org capabilities, which will be exemplified with case studies drawn from fundamental biology, biomedicine, bioengineering/biotechnology, and energy sciences.

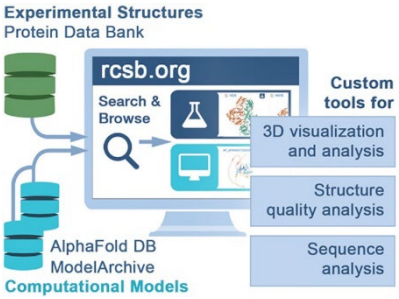

Figure 1. RCSB.org delivers PDB structures (identified with an Erlenmeyer flask icon on dark blue) and Computed Structure Models (computer screen icon on cyan) that can all be searched, analyzed, visualized, and explored using custom tools and features. Image from *Nucleic Acids Research* (2022) gkac1077, https://doi.org/10.1093/nar/gkac1077.

RCSB PDB thanks the more than 60,000 structural biologists worldwide who have deposited structures to the PDB, and the many millions of researchers, educators, and students around the globe who consume PDB data. We thank the RCSB PDB and wwPDB Advisory Committees for valuable advice. We acknowledge contributions to the success of the PDB made by past members of RCSB PDB and our Worldwide Protein Data Bank partners (PDBe, PDBj, PDBc, EMDB, and BMRB). Funding from NSF (DBI-1832184; PI: S.K. Burley), DOE (DE-SC0019749; PI: S.K. Burley), and NIH (R01GM133198; PI: S.K. Burley) for RCSB PDB Core Operations is gratefully acknowledged.

Keynote 20

Room 210/211
9.00am - 9.50am

Keynote-020-260823

The importance of being weak: how weak interactions trigger solid state dynamics

C. Tedesco, G. Pierri, R. Schettini, F. De Riccardis, I. Izzo

Dipartimento di Chimica e Biologia "A. Zambelli", University of Salerno, via Giovanni Paolo II 132, I-84084 Fisciano (Italy)

ctedesco@unisa.it

Keywords: peptoids, single-crystal to single-crystal transformation, weak interactions

Peptoids are *N*-substituted polyglycines with useful biological activities and interesting chemical properties both in solution and in the solid state [1]. In this contribution we will show how the lack of the amide proton prevents the formation of NH···CO hydrogen bonds and makes peptoids the ideal platform for evidencing the influence of weak intramolecular and intermolecular interactions, as CH···OC and CO···OC interactions, in stabilizing molecular conformations, triggering conformation polymorphism and phase transitions, and ultimately determine the dynamic behaviour in the solid state.

Our group reported on how inter-annular CH···OC hydrogen bonds can provide face-to-face or side-by-side arrangement of the macrocycles mimicking secondary structure in proteins [1]. Then, by combining in-situ powder and single crystal X-ray diffraction, thermal analyses, hot-stage optical microscopy we evidenced how environmental changes (such as temperature, humidity, gas pressure, etc.) may trigger the dynamic behaviour of cyclic peptoids in the solid state [2].

Thus, we established the solvatomorphic behaviour of a cyclic hexapeptoid decorated with four propargyl and two methoxyethyl side chains, which led to the discovery of two pure crystalline forms and four solvates [2,3]. Interestingly, the methanol solvate and the hydrate form result in a stable porous molecular framework, which adsorbs gases as propyne or carbon dioxide, but not methane [4], while the acetonitrile solvate undergoes a reversible single crystal to single crystal transformation at 40 °C, where two propargyl side chains move by 113° and form an unprecedented "CH-π zipper", which may be unzipped by exposure to guest vapours [2]. By conformational energy and lattice energy calculations we demonstrated the role of intermolecular CH···OC backbone-to-backbone interactions in tightening the peptoid porous framework and the role of CH···OC and CH-π host-guest interactions in the re-opening [5].

More recently, we highlighted the role of intramolecular backbone-to-backbone CO···CO interactions and CH···OC hydrogen bonds in the stabilization of enantiomorphic right- and left-handed polyproline type I helices in cyclic dodecapeptoids (**Fig. 1**) [6].

Finally, peptoids as peptidomimetics allowed us to appreciate that CH···OC interactions in peptoids replace NH···OC interactions in peptides and similarly produce secondary, tertiary and quaternary structures.

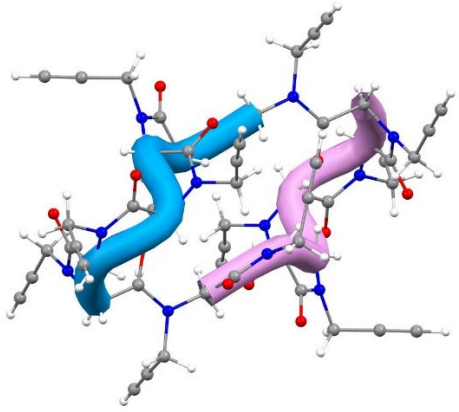

Figure 1. Right- and left-handed polyproline type I helices in a cyclic dodecapeptoid decorated with propargyl side chains.

[1] Tedesco, C., Erra, L., Izzo, I., De Riccardis, F. (2014). *CrystEngComm*, **16**, 3667.
[2] Meli, A., Macedi, E., De Riccardis, F., Smith, V. J., Barbour, L. J., Izzo, I., Tedesco, C. (2016). *Angew. Chem., Int. Ed.*, **55**, 4679.
[3] Macedi, E., Meli, A., De Riccardis, F., Rossi, P., Smith, V. J., Barbour, L. J., Izzo, I., Tedesco, C. (2017). *CrystEngComm*, **19**, 4704.
[4] Pierri, G., Landi, A., Macedi, E., Izzo, I., De Riccardis, F., Dinnebier R. E., Tedesco, C. (2020). *Chem. Eur. J.,* **26**, 14320.
[5] Pierri, G., Corno, M., Macedi, E., Voccia, M., Tedesco, C. (2021). *Cryst. Growth Des.,* **21**, 897.
[6] Pierri, G., Schettini, R., Summa, F. F., De Riccardis, F., Monaco, G., Izzo, I., Tedesco, C. (2022). *Chem. Comm.*, **58**, 5253.

The authors acknowledge the University of Salerno (FARB funding) and European Union (7FP 2007-2013 REA grant agreement N. PIRSESGA-2012-319011) for financial support.

Keynote 21

Room 212/213
9.00am - 9.50am

Keynote-021-260823

Competitive structural and electronic states under pressure: Quantum and Classical Effects in Dense Matter

S. Deemyad

Dept. of Physics & Astronomy, University of Utah, Salt Lake City, UT, USA

deemyad@physics.utah.edu

Keywords: High pressure, Quantum effect, Phase transitions, Superconductivity

Application of high pressure has profound effects on both structural and electronic stabilities of a material. Restricting the volume of a material, through application of pressure, changes the dominance of interactions within the material, and exposes unnatural states of matter not found in our predominantly adiabatic universe. High pressure studies are particularly important in understanding the electronic quantum states caused by electron-phonon interactions such as conventional superconductivity and charge density waves (CDW). In the vicinity of such instabilities, new states of matter often appear which may compete or co-exist. Exploring materials near phase instabilities provides access to rich physics and opportunity to discover exotic new states of matter.

While quantum fluctuations in electronic states are always relevant, it is also possible to observe quantum effects in lattice of very light elements. In light dense matter, the lattice remains far from static even at zero temperature and fascinating states of matter, such as a fluid ground state, may emerge due to the lattice quantum effects.
In this talk I will review some of the major goals of research in high pressure physics in exploring competitive states of materials at extreme conditions. I will present three distinct examples of our studies on pressure-induced classical and quantum effects in structural and electronic transitions in materials: 1) the coexistence of vitreous and crystalline phases of H_2O at ambient temperature [1], 2) the interplay between the CDW and superconducting states in 2D material $BaSbTe_{2.1}S_{0.9}$ under pressure and 3) the nuclear quantum effects in competitive structures of lithium isotopes [2],[3].

[1] Shargh, A. K., A. Picard, R. Hrubiak, D. Zhang, R. J. Hemley, S. Deemyad, N. Abdolrahim, and S. Saffarian. *Proceedings of the National Academy of Sciences* 119, no. 27 (2022)
[2] Elatresh, S. F.; Cai, W.; Ashcroft, N. W.; Hoffmann, R.; Deemyad, S.; Bonev, S. *Proceedings of the National Academy of Sciences* 114, no 2 (2017)
[3] Ackland, G. J.; Dunuwille, M.; Martinez-Canales, M.; Loa, I.; Zhang, R.; Sinogeikin, S.; Cai, W.; Deemyad, S *Science*, 356 (6344) (2017)

Collaboration with M. Kanatizdis group at Northwestern University is acknowledged in studying the pressure effects on electronic and structural properties of $BaSbTe_{2.1}S_{0.9}$

Keynote 22

Room 203/204

10.20am - 11.10am

Keynote-022-260823

Advancing Materials Characterization using Neutron Diffraction at ORNL's Spallation Neutron Source (SNS, the High Flux Isotope Reactor (HFIR) and the future Second Target Station (STS)

Clarina dela Cruz

Powder Diffraction Group, Neutron Sciences Directorate, Oak Ridge National Laboratory

Oak Ridge, Tennessee, USA 37831

delacruzcr@ornl.gov

Keywords: neutron diffraction, spallation neutron source, high flux isotope reactor

Oak Ridge National Laboratory's Neutron Sciences Directorate operates two neutron scattering Scientific User Facilities, the High Flux Isotope Reactor (HFIR) and the Spallation Neutron Source (SNS), for the US Department of Energy, Office of Science. We are committed to enabling high impact research in a broad array of scientific fields, by delivering a powerful array of world class neutron instrumentation and associated technologies for our users worldwide. This is aligned with our vision where important "human" problems are answered by advances in materials science, in which the unique strengths of neutron scattering play an essential role. In this talk I will give several examples of work done using our suite of neutron diffractometers that work in concert to deliver new capabilities to study quantum material, chemistry, energy materials and materials science and engineering- materials research that will push forward the forefront of energy relevant technologies of the future. Further demonstrating how neutron scattering is a versatile technique that increasingly serves the materials science community to solve problems ranging from the new superconductors to porous metal-organic-frameworks for hydrogen storage or carbon capture as well as new battery materials with earth abundant compositions. I will also talk about the 3-source strategy as we prepare for the Proton Proper Upgrade (PPU) at SNS and ensuing plans for the Second Target Station.

Figure 1. Future of Neutron Scattering at Oak Ridge National Laboratory: Three World Leading Neutron Scattering Facilities for Breakthrough Materials Science

[1] Calder S., An K., Boehler R., dela Cruz C., Frontzek M., Guthrie M., Haberl B., Huq A., Kimber S.A., Liu J., Molaison J.J., Neuefeind J., Page K., dos Santos A.M., Taddei K.M., Tulk C.A., Tucker M.G., "A suite-level review of the neutron powder diffraction instruments at Oak Ridge National Laboratory", Review of Scientific Instruments, 89, 9, 092701 (2018).
[2] Coates L., Cao H.B., Chakoumakos B.C., Frontzek M., Hoffmann C., Kovalevsky A., Liu Y., Meilleur F., dos Santos A.M., Myles D.A., Wang X.P., Ye F., "A suite-level review of the neutron single-crystal diffraction instruments at Oak Ridge National Laboratory", Review of Scientific Instruments, 89, 9, 092802 (2018).

Keynote 24

Room 212/213
10.20am - 11.10am

Keynote-024-260823

Teaching crystallographic symmetry

M. I. Aroyo

Department of Physics, University of the Basque country (UPV/EHU), Bilbao, Spain

mois.aroyo@ehu.es

Keywords: crystallographic symmetry, *Symmetry Database*, *Bilbao Crystallographic Server*

The knowledge of crystallographic symmetry is essential for the correct description and understanding of the physical and chemical properties of materials. During the years a variety of printed and online tools for visualizing and analyzing crystallographic symmetry are being developed. In this talk I will focus on the teaching potential of the sixth edition of Volume A of *International Tables for Crystallography* (*IT*A) [1], and the new sixth edition of the *Teaching Edition* (*TE*) [2]. The presentation will be illustrated with brief explanations and examples of the online databases and computer tools of the *Symmetry Database* [3] and the *Bilbao Crystallographic Server* [4].

*IT*A and *TE* treat in detail the symmetries of two- and three-dimensional space groups and point groups in direct space. Based on the matrix formalism, the two volumes offer a homogeneous text of educational and teaching nature for the different kinds of symmetry information found in the tables, and provide a unified and coherent introduction to the three 'symmetry' volumes of *International Tables for Crystallography*: the basic crystallographic data of plane and space groups in Volume A, the symmetry relations between space groups treated in Volume A1 (*IT*A1) [5], and the subperiodic group data of Volume E. The *Symmetry Database* is included in the online edition of *International Tables for Crystallography* (https://symmdb.iucr.org/), while the *Bilbao Crystallographic Server* (www.cryst.ehu.es) is a website that can be used free of charge from any computer with a web browser via Internet. Both web sources grant access to the space- and point-groups crystallographic databases along with more complex programs to facilitate the better understanding of fundamental crystallographic concepts, and the in-depth study of symmetry relations between space groups and their applications in crystal-structure relationships, phase transitions and domain-structure analysis. The online crystallographic databases expand and complement the symmetry information provided in the print editions of *IT*A and *IT*A1. Interactive programs permit not only the visualization of symmetry elements of crystallographic point and space groups but also the teaching of essential symmetry concepts. The *Symmetry Database* is available to all subscribers to the online version of *International Tables for Crystallography*. A *Teaching Edition* of the *Symmetry Database*, which can be used to obtain and explore the data for a selected set of space groups is also available online. The presentation of *IT*A and *TE*, and of the databases and tools offered by the *Symmetry Database* and the *Bilbao Crystallographic Server* will be accompanied by case studies illustrating the didactic capacity of the volumes and the efficiency of the online tools in teaching of crystallographic symmetry.

[1] *International Tables for Crystallography* (2016). Volume A, *Space-Group Symmetry*, 6th ed., edited by M. I. Aroyo. Chichester: Wiley.
[2] *International Tables for Crystallography* (2021), *Teaching Edition*: *Crystallographic Symmetry*, 6th ed. edited by M.I. Aroyo,. Chichester: John Wiley & Sons, Ltd.
[3] Kroumova, E., de la Flor, G., Ashcroft, N. & Aroyo, M. I. Acta Cryst A77 (2021), C668.
[4] Aroyo, M. I., Perez-Mato, J. M., Capillas, C., Kroumova, E., Ivantschev, S., Madariaga, G., Kirov, A. & Wondratschek H. (2006). *Z. Kristallogr.* **221**, 15-27.
[5] *International Tables for Crystallography* (2010). Volume A1, *Symmetry Relations between Space Groups*, 2nd ed. edited by H. Wondratschek & U. Müller, 2nd ed. Chichester: John Wiley & Sons.

A016a Structure-based Drug Design
Room 203/204
1.10pm - 3.30pm

A016a-01-260823

269 fragment hits reveal putative protein-protein interaction sites and reproduce binding modes

T. Barthel[1], J. Wollenhaupt[1], G. M. A. Lima[2], M. C. Wahl[3], M. S. Weiss[1]

[1]Helmholtz-Zentrum Berlin, Macromolecular Crystallography, Albert-Einstein-Str. 15, 12489 Berlin, Germany, [2]MAX IV Laboratory, BioMAX, Fotongatan 2, 224 84 Lund, Sweden, [3]Freie Universität Berlin, Institute of Chemistry and Biochemistry, Laboratory of Structural Biochemistry, Takustraße 6, 14195 Berlin, Germany

tatjana.barthel@helmholtz-berlin.de

Keywords: Crystallographic fragment screening, protein-protein interactions, spliceosome

Protein-protein interactions (PPIs) are essential in all biological processes. Misregulation of PPIs can result in diseases. Therefore, they are an attractive target for drug discovery efforts. To find starting points for PPI modulator development, fragment screening is a popular approach. The identification of fragments can be achieved via crystallographic fragment screening (CFS) [1], bearing the advantage of revealing the binding site of the fragments and their binding poses in the process.

Here, the spliceosomal protein-protein complex of the Prp8^{RNaseH} domain and Aar2 has been chosen as the target. Aar2 is Prp8's shuttling factor and relocates Prp8 into the nucleus [2], however little is known about other PPIs involving Aar2. Prp8 is the well-studied master regulator of the spliceosome and acts as a PPI -hub during the splicing process with several known binding partners interacting with the RNaseH domain. Thus, the identification of fragments bound to these proteins could be used to develop several PPI modulators. In this campaign, the F2X-Universal Library was screened against the Prp8^{RNaseH}-Aar2 complex [3] and the data was analysed semi-automatically via FragMAXapp [4]. The screening resulted in 269 hits out of 1013 screened compounds (27% hit rate) [5]. Thus, a multitude of starting points are available for further compound optimization. Additionally, several fragments binding at the same site have congruent structural features engaging in similar interactions with the protein, thus reproducing and confirming binding modes. Furthermore, the fragments cluster in nine distinct binding sites. Three of these binding sites overlap with known PPI sites. Therefore, it can be hypothesised that the remaining six binding sites potentially identify unknown PPI sites. The presented CFS campaign offers a variety of information to kick off further investigations and proves the advantage of performing an about 1000 fragments large crystallographic screening.

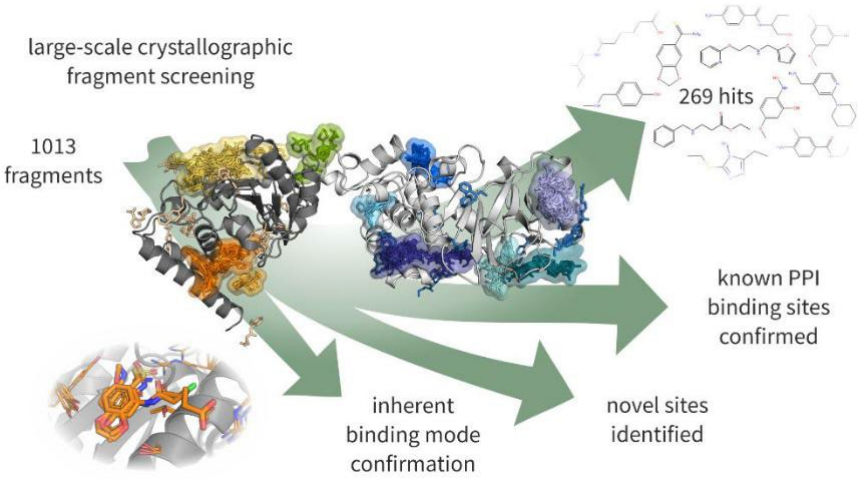

Figure 1. The multiple benefits of performing a large-scale crystallographic fragment screening are shown based on the screen of the F2X-Universal Library against the protein-protein complex of the Prp8^{RNaseH} domain and Aar2.

[1] Wollenhaupt, J., Barthel, T., Lima, G. M. A., Metz, A., Wallacher, D., Jagudin, E., Huschmann, F. U., Hauß, T., Feiler, C. G., Gerlach, M., Hellmig, M., Förster, R., Steffien, M., Heine, A., Klebe, G., Mueller, U. & Weiss, M. S. (2021). *J. Vis. Exp.* 2021, 1– 19

[2] Weber, G., Cristão, V. F., Santos, K. F., Jovin, S. M., Heroven, A. C., Holton, N., Lührmann, R., Beggs, J. D. & Wahl, M. C. (2013). *Genes Dev.* 27, 525–540.

[3] Wollenhaupt, J., Metz, A., Barthel, T., Lima, G. M. A., Heine, A., Mueller, U., Klebe, G. & Weiss, M. S. (2020). *Structure*. 28, 694-706.

[4] Lima, G. M. A., Talibov, V. O., Jagudin, E., Sele, C., Nyblom, M., Knecht, W., Logan, D. T., Sjögren, T. & Mueller, U. (2020). *Acta Crystallogr. Sect. D*. 76, 771–777.
Barthel, T., Wollenhaupt, J., Lima, G. M. A., Wahl, M. C., Weiss, M. S. (2022). *J. Med. Chem.* 65, 21, 14630

A016s-02-260823

Structural and functional studies on bitter taste receptors

Authors: Weixiu Xu[1,2], Lijie Wu[1], Shenhui Liu[1,2], Xiao Liu[1,2], Xiaoling Cao[1,2], Cui Zhou[1,2], Jinyi Zhang[1,2], You Fu[1,2], Yu Guo[1], Yiran Wu[1], Qiwen Tan[1], Ling Wang[1], Junlin Liu[1], Longquan Jiang[1,2], Zhongbo Fan[1,2], Yuan Pei[1], Jingyi Yu[4], Jianjun Cheng[1,2], Suwen Zhao[1,2], Xiaojiang Hao[3], Zhi-Jie Liu[1,2‡] and Tian Hua[1,2]

[1]iHuman Institute, ShanghaiTech University, Shanghai 201210, China
[2]School of Life Science and Technology, ShanghaiTech University, Shanghai 201210, China
[3]State Key Laboratory of Phytochemistry and Plant Resource in West China, Kunming Institute of Botany, Chinese Academy of Sciences, Kunming 650210, China
[4]School of Information Science and Technology, ShanghaiTech University, Shanghai 201210, China
[‡]Corresponding authors. Email: liuzhj@shanghaitech.edu.cn (Z.L.); huatian@shanghaitech.edu.cn (T.H.)

Keywords: G protein-coupled receptor, taste receptor, bitter taste receptor

The taste sensory system helps us to avoid ingestion of harmful substances. Taste perception is initiated by the physical interaction of tastants with the receptors located on the surface of taste receptor cells (TRCs) on the tongue and palate. In humans, tastants evoke five taste sensations: sweet, bitter, salty, sour and umami. Among the five taste modalities, ion channels transduce sour and salty signals, while bitter, sweet and umami tastes are mediated by G protein-coupled receptors (GPCRs). A distinct group of type 2 taste receptors (TAS2Rs) is responsible for bitter taste perception. TAS2Rs display low sequence identity (<20%) with other GPCRs and are classified as a separate class T GPCR subfamily. TAS2Rs recognize thousands of different bitter molecules. In humans, there are only ~25 TAS2Rs to cover this broad chemosensory space. Furthermore, the TAS2Rs are distributed, not only in the oral cavity, but also in extraoral tissues, including the upper and lower airways, gut, adipose tissue, brain, heart and immune cells. These ectopic bitter taste receptors are involved in a variety of physiological processes and are associated with different diseases. However, there are no bitter receptor structures solved so far. Here we report the cryo–electron microscopy structures of human TAS2R46 complexed with chimeric mini–G protein gustducin, in both strychnine-bound and apo forms. Several features of TAS2R46 are disclosed, including distinct receptor structures that compare with known GPCRs. This study provides a basis for further exploration of other bitter taste receptors and their therapeutic applications.

A016a-03-260823

Application of cryo-EM to understanding of peptide and small molecule binding to G protein-coupled receptors

P.M. Sexton[1,2], D. Wootten

[1]Drug Discovery Biology, and [2]ARC Centre for Cryo-electron Microscopy of Membrane Proteins, Monash Institute of Pharmaceutical Sciences, Monash University, Parkville 3052, Victoria, Australia.

Email: patrick.sexton@monash.edu

Keywords: cryo-electron microscopy, G protein-coupled receptor, drug discovery

G protein-coupled receptors (GPCRs) are the largest family of cell surface receptor proteins and critical targets for current and future therapeutics. Technological evolution in cryo-EM combined with continuing advances in biochemical approaches for the stabilisation of active-state complexes of GPCRs with different transducer proteins is now enabling structural interrogation of agonist binding, receptor activation and transducer engagement. Indeed, cryo-EM has become the predominant method for GPCR structure determination. Such cryo-EM enabled structures provide key insight into both peptide and small molecule drug action, while the breadth of application of cryo-EM for study of GPCRs has greatly expanded the number of independent receptors where structures have been determined. Moreover, cryo-EM can access conformational ensembles of GPCR complexes that are present during vitrification, which can provide a window into the dynamics of these complexes. Using exemplar receptors, I will discuss how we are using cryo-EM to provide novel insight into the structure and dynamics of drug-receptor complexes, including enhanced understanding of the molecular basis for distinct ligand pharmacology, how small molecules can potentially mimic peptide pharmacology (Fig. 1) and how small molecules and interacting proteins can modulate receptor engagement with endogenous ligands.

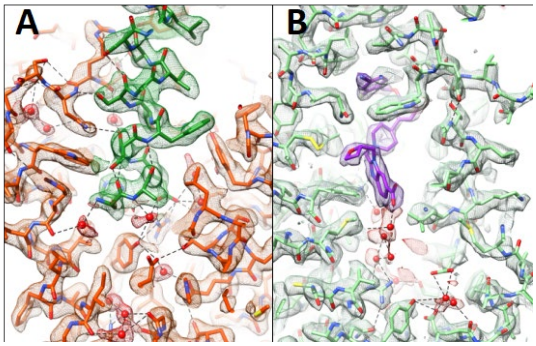

Figure 1. Activation of the glucagon-like peptide 1 (GLP-1) receptor by (**A**) the endogenous peptide ligand, GLP-1 (green map & model; orange receptor) or (**B**) the small molecule agonist PF-06882961 (purple map & model; light green receptor). Waters are coloured red. Hydrogen bonds are depicted as dashed lines (adapted from Zhang et al, 2020 [1]).

[1] Zhang, X., Belousoff, M.J., Zhao, P., Kooistra, A.J., Truong, T.T., Ang, S.Y., Underwood, C.R. Egebjerg, T., Šenel, P., Stewart, G.D., Liang, Y.L., Glukhova, A., Venugopal, H., Christopoulos, A., Furness, S.G.B., Miller, L.J., Reedtz-Runge, S., Langmead, C.J., Gloriam, D.E., Danev, R., Sexton, P.M., & Wootten, D. (2020). *Mol. Cell.*, **80**, 485-500.e7.

P.M.S is a scientific co-founder of Septerna Inc. and DACRA Therapeutics. D.W is an advisor for Septerna Inc. and a scientific co-founder of DACRA Therapeutics.

A016a-04-260823

The twisted link between a dual function glutamate transporter and Episodic Ataxia

R.M. Ryan

School of Medical Sciences, Faculty of Medicine and Health, University of Sydney

renae.ryan@sydney.edu.au

Keywords: glutamate transporter, chloride channel, cryo-EM

Glutamate is the predominant excitatory neurotransmitter in the mammalian central nervous system (CNS) [1]. Excitatory Amino Acid Transporters (EAATs) regulate extracellular glutamate by transporting it into cells, mostly glia, to terminate neurotransmission and to avoid neurotoxicity. EAATs also conduct chloride ions via a channel-like process that is thermodynamically uncoupled from transport. However, the molecular mechanisms that allow these dual-function transporters to carry out two seemingly contradictory roles, and the physiological role of Cl- conductance through EAATs, are unknown. I will describe the cryo-electron microscopy structure of a glutamate transporter homologue in an open-channel state, revealing an aqueous cavity that is formed during the transport cycle [2]. Using functional studies and molecular dynamics simulations, we show that this cavity is an aqueous-accessible chloride permeation pathway gated by two hydrophobic regions and is conserved across mammalian and archaeal glutamate transporters [3].

Mutations of human EAAT1 (hEAAT1) have been identified in patients with episodic ataxia type 6 (EA6). One mutation showed increased Cl^- channel activity and decreased glutamate transport, but the relative contributions of each function of hEAAT1 to mechanisms underlying the pathology of EA6 remain unclear. I will describe the characterisation of five additional EA6-related mutations on hEAAT1 function in Xenopus laevis oocytes, and on CNS function in a Drosophila melanogaster model of locomotor behaviour. Our results indicate that mutations with decreased hEAAT1 Cl- channel activity and functional glutamate transport can also contribute to the pathology of EA6, highlighting the importance of Cl- homeostasis in glial cells for proper CNS function [4]. Together, these results strongly support the idea that EA6 is primarily an ion channelopathy of CNS glia and provides a framework for the rational development of therapeutics that can differentially modulate substrate transport or channel properties for the treatment of neurological disorders caused by EAAT dysfunction, such as Episodic Ataxia.

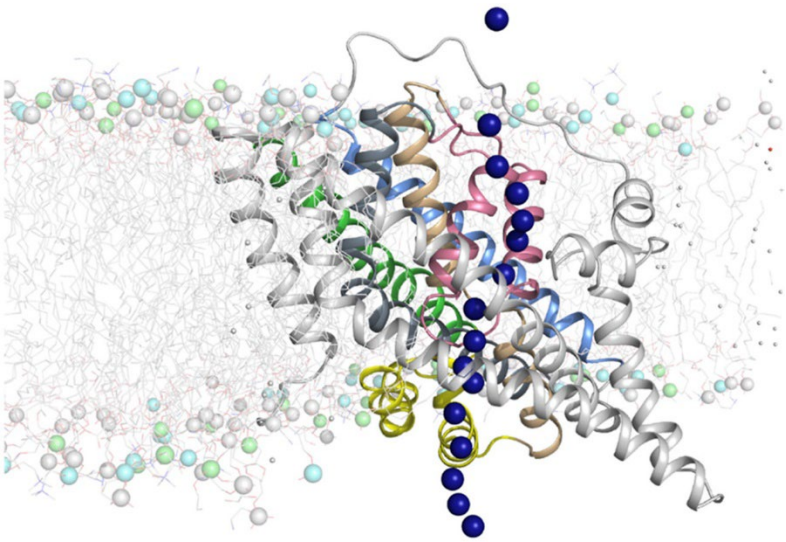

Figure 1. Chloride ions (blue balls) permeating the archaeal glutamate transporter, Glt_{Ph}.

[1] Vandenberg, R.J. & Ryan, R.M. (2013) *Physiological Reviews* **93**(4):1621-57.
[2] Chen, I., Pant, S., Wu, Q., Cater, R., Sobti, M., Vandenberg, R.J., Stewart, A.G., Tajkhorshid, E., Font, J., Ryan, R.M. (2021) *Nature*, **591**(7849):327-331.
[3] Pant, S., Wu, Q., Ryan, R.M. & Tajkhorshid, E. (2022) *ACS Chem Neuroscience* **13**(6):776-785.
[4] Wu Q, Akhter A, Pant S, Cho E, Zhu JX, Garner A, Ohyama T, Tajkhorshid E, van Meyel DJ, Ryan RM. (2022) *Journal of Clinical Investigation* **132**(7):e154891.

A024 New Software in Powder Diffraction
Room 207
1.10pm - 3.30pm

A024-01-260823

EasyDiffraction: Making diffraction data analysis and modelling easier

A. Sazonov, S. Ward, P. Rozyczko

European Spallation Source ERIC, Data Management and Software Center, P.O. Box 176, SE-221 00 Lund, Sweden

andrew.sazonov@ess.eu

Keywords: Diffraction, Analysis, Software

Diffraction is a key tool for structure analysis. However, currently available software for modelling and analysis of diffraction data may be, on the one hand, difficult for new users looking to apply diffraction to their field of expertise and, on the other hand, not flexible enough for domain experts.

EasyDiffraction (https://easydiffraction.org) is a new project aimed at lowering the barrier of entry to diffraction data analysis by providing a simple graphical interface (see Fig. 1) allowing for the calculation of powder diffraction patterns based on structural models and refinement of their parameters against experimental data. The software is distributed as an all-in-one package that includes all dependencies and can be installed with just a few clicks on different operating systems. For more complex problems and increased flexibility the Python library behind *EasyDiffraction* can be used through Jupyter notebooks and scripting.

EasyDiffraction relies on existing crystallographic libraries as calculation engines to cover the necessary functionality. This softwaee is still in beta and has only some basic features of the CrysFML (https://code.ill.fr/scientific-software/crysfml) and CrysPy (https://github.com/ikibalin/cryspy) libraries, such as support for one-dimensional constant wavelength and time-of-flight powder diffraction data. We are collaborating with the Institut Laue-Langevin (https://www.ill.eu) and Leon Brillouin Laboratory (https://www-llb.cea.fr/en) regarding the CrysFML and CrysPy, respectively. More functionality and support of other libraries will become available as the project matures.

EasyDiffraction evolved from the mock-up of the graphical interface for diffraction and has a strong focus on user experience and interaction. An intuitive and user-friendly interface of *EasyDiffraction* (see Fig. 1) can thus help improve the user experience in the field of diffraction and thereby make it easier to train users and students, as well as be better prepared for experiments. At the European Spallation Source (https://ess.eu), we plan to integrate *EasyDiffraction* into the full data processing workflow to increase experiment automation and make better use of beam time.

EasyDiffraction is built on the *EasyScience* framework (https://easyscience.software), a platform aimed at unifying data analysis and reduction software. In addition to diffraction, this framework has been successfully applied to reflectometry (https://easyreflectometry.org). Quasielastic neutron scattering and neutron imaging are also considered be targeted in the future.

EasyDiffraction is being developed free and open source (https://github.com/easyscience/EasyDiffraction) and we hope to attract interested people to jointly contribute to this project and help us, for the benefit of everyone, in making diffraction data analysis and modelling easier.

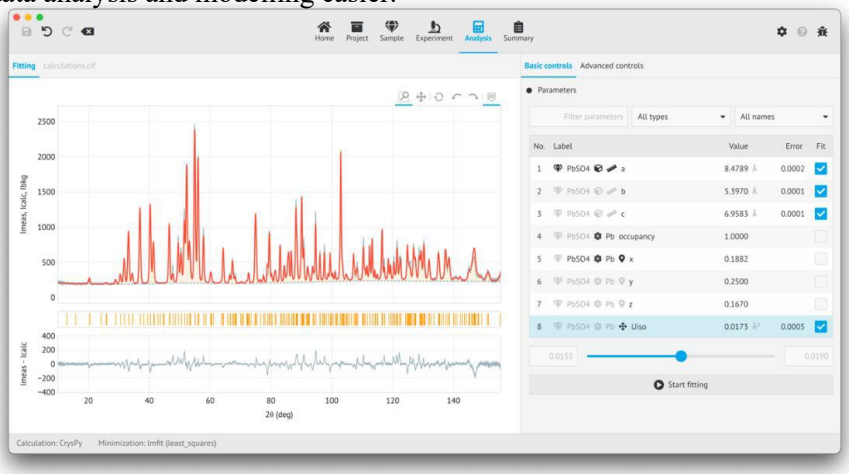

A024-02-260823

pdCIFplotter: A program for the visualisation of powder diffraction data in pdCIF format

Matthew R. Rowles

John de Laeter Centre, Curtin University, Perth, WA, Australia
rowlesmr@gmail.com

Keywords: CIF, powder diffraction, Python

The Crystallographic Information Framework (CIF) [1-2] is a text-based file format for the exchange and storage of crystallographic information. The core CIF dictionary was originally aimed at single-crystal data, but has since been extended to include a powder diffraction dictionary [3-4] – pdCIF – amongst others.

There are a variety of programs and libraries available for the creation, viewing, and editing of CIF files; however, there is a scarcity of end-user tools that work well with pdCIF, and as a result, the use of pdCIF is not as widespread is it should be. Powder diffraction software packages are often capable of outputting data and model results in pdCIF format, but are then unable to read in those same files. This lack of interoperability makes studying third-party data and models a difficult process without access to the original software and analysis files; *pdCIFplot* [5] was written to perform this task, but is no longer maintained. The IUCr have an online tool, *plotCIF* [6], which provides largely the same capability. Both are limited to showing a single diffraction pattern at a time.

To expand the available pdCIF software tools for the end-user, *pdCIFplotter* has been written to provide an easy-to-use interface for visualising powder data and models published in pdCIF format. In particular, support for the visualisation of multi-pattern datasets, such as *in situ* data, is provided through the provision of stack and surface plots. Examples of such visualisations are given.

pdCIFplotter is written in Python 3, and can run wherever a compatible runtime is available. The source code and Windows executable can be downloaded from various sources [7]. *TOPAS* [8] macros for the production of pdCIF files are also available [9].

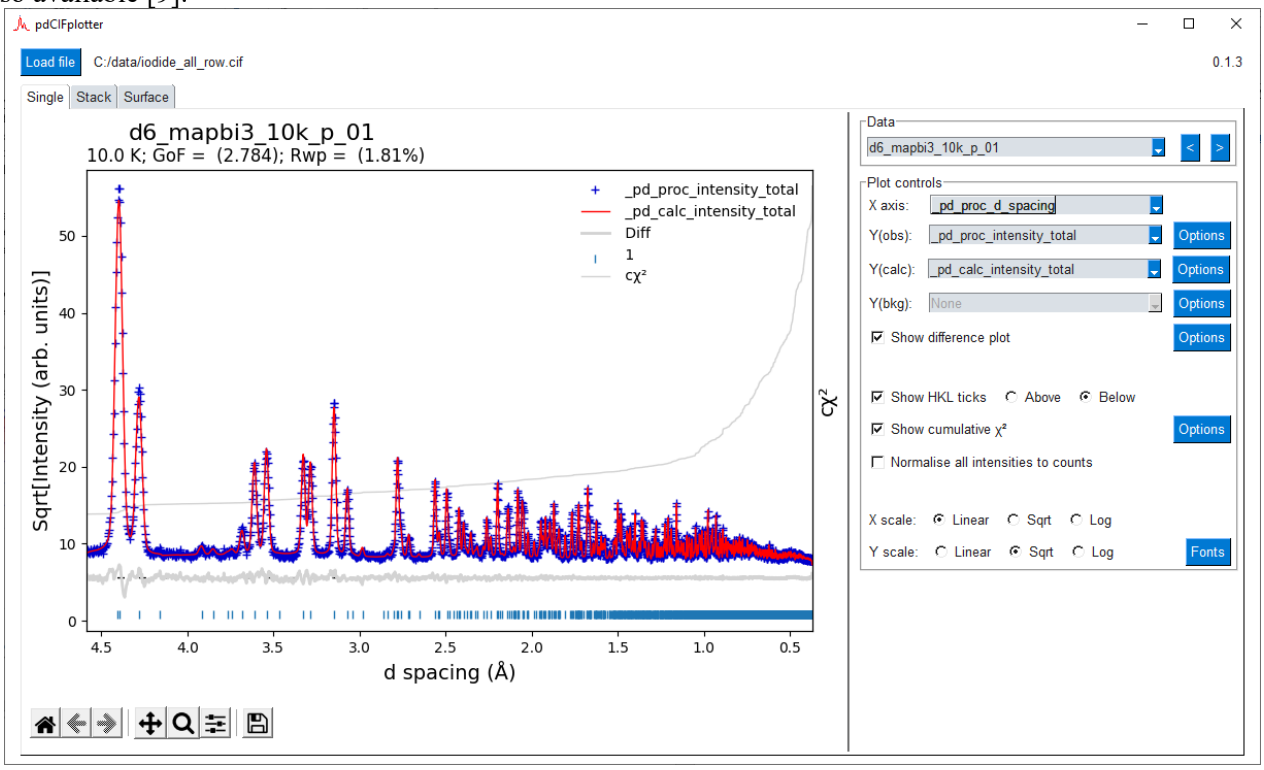

Figure 1. Screenshot of pdCIFplotter in use.

[1] Bernstein, H. J. et al. (2016). *J. Appl. Crystallogr.* **49**, 277-284.
[2] Hall, S. R., Allen, F. H. & Brown, I. D. (1991). *Acta Crystallogr. A* **47**, 655-685.
[3] Toby, B. H. (2006a). *International Tables for Crystallography Volume G,* edited by S. R. Hall & B. McMahon, pp. 117-130.
[4] Toby, B. H. (2006b). *International Tables for Crystallography Volume G,* edited by S. R. Hall & B. McMahon, pp. 258-269.
[5] Toby, B. H. (2003). *J. Appl. Crystallogr.* **36**, 1285-1287.
[6] IUCr (2021c). *plotCIF,* https://publcif.iucr.org/services/tools/pdcifplot.php.

[7] https://github.com/rowlesmr/pdCIFplotter; https://pypi.org/project/pdCIFplotter/; https://www.iucr.org/resources/commissions/powder-diffraction/projects/pdcif/pdcifplotter
[8] Coelho, A. A. (2018). *J. Appl. Crystallogr.* **51**, 210-218.
[9] Rowles, M.R. (2022) https://topas.awh.durham.ac.uk/doku.php?id=out_pdcif

A024-03-260823

Refining on 1000s of X-ray diffraction patterns simultaneously using TOPAS

A. A. Coelho[a*], A. Vamvakeros[b]

a) Coelho Software, 72 Cedar Street, Wynnum, Brisbane, Queensland 4178, Australia

b) Finden Limited, Merchant House, 5 East St Helens Street, Abingdon, OX14 5EG, United Kingdom

**AlanCoelho@bigpond.com*

Keywords: Rietveld, refinement, least squares, tomography

Non-linear least squares refinements comprising 10s of 1000s of X-ray diffraction patterns are being performed with 10s of 1000s of independent parameters constrained to sensible values across the diffraction patterns. Such refinements produce 3D maps of the specimen in disciplines such as X-ray Diffraction Computed Tomography (XRD-CT) [1]. The need for computational speed therefore is apparent. There are many aspects to performing such refinements; these include minimizing the use of computer memory; identifying and reducing degenerate calculations; utilizing threading across CPUs and the inclusion of vectorization where possible. In amongst these are the algorithms necessary to perform non-linear least squares on such large problems. This includes speeding up the solving of the matrix equation $\mathbf{A}\,\mathbf{x} = \mathbf{b}$ which scale by N^2 [2], rather than Newton methods which scale by N^3, and the use of sparse matrix methods.

For example, refining on 50,000 patterns comprising 1000,000 structures typically require each structure to have separate memory for hkls, lattice parameters, structure factors, peak buffers, calculated structure patterns and other Rietveld refinement style calculations. Without careful consideration of memory conservation memory usage could easily run into terabytes. As always, there's a trade-off between memory usage and the need to recalculate already calculated items. This presentation will give an overview of the techniques developed to overcome these difficulties as implemented in the computer program TOPAS [3].

[1] Vamvakeros, A., Coelho, A. A., Matras, D., Dong, H., Odarchenko, Y., Price, S. W. T., Butler, K. T., Gutowski, O., Dippel, A.-C., Zimmermann, M., Martens, I., Drnec, J., Beale, A. M. & Jacques, S. D. M. (2020). *J. Appl. Cryst.* **53**, 1531-1541.
[2] Coelho, A. A. (2005). *J. Appl. Cryst.* **38**, 455-461.
[3] Coelho, A. A. (2018). *J. Appl. Cryst.* **51**, 210-218.

A024-04-260823

Towards the formally validated crystallographic software

S. Gražulis[1,2], A. Merkys[1], A. Vaitkus[1], K. Petrauskas[2], L. Laibinis[2]

Institute of Biotechnology, Life Sciences Center, Vilnius University, Sauletekio 7, LT-10257 Vilnius, Lithuania

Institute of Computer Science, Faculty of Mathematics and Informatics, Vilnius University, Didlaukio 47, LT-08303 Vilnius, Lithuania

grazulis@ibt.lt

Keywords: crystallographic algorithms, formal verification, theorem proving

Digital computers have been used in crystallography since their very first applications for the purposes of pure science [1]. Software plays a crucial role in the determination, interpretation and analysis of crystal structures. As crystallographic models grow in size and complexity, so does the software that is needed to build and interpret them. Consequently, managing software "manually", i.e. by using currently available software development methods, becomes problematic. Unfortunate errors may creep unnoticed into the software code and yield incorrect interpretation of crystallographic data [2]. It is thus desirable to develop new approaches that would allow to catch more software errors early enough and provide additional software correctness guarantees.

We propose to use formal software verification methods to document required behaviour of crystallographic software and to prove formally, with the help of proof assistants [3] such as Isabelle/HOL [4], that the software code used for crystallographic computations is indeed compliant with the requirements. This approach is used for mission critical software such as avionics and has been recently advocated as method of improving software reliability [5].

As a proof of concept, we have applied this method [6] to prove the correctness of a well -known and widely used algorithm of space group reconstruction [7]. The algorithm was first formulated as a pseudocode, and then Isabelle/HOL theory was created to describe the required pre- and postconditions of the algorithm. It was then proven using the Isabelle proof assistant that these conditions are indeed satisfied, and executable code was derived manually from the same pseudocode [6]. Since software transformations from pseudocode to executable code are simpler than the correctness proofs themselves, such approach facilitates development of correctly working computer code.

To further automate the process of the development of reliable software, and to reduce the likelihood of human error, we are investigating the use of Ada/SPARK software development and verification system for the development of crystallographic software. The SPARK system can generate proof obligations from the annotated software code in a subset of the Ada programming language and forward them to various automatic theorem provers and proof assistants. At the same time, executable code can be generated from the same program source code using a high quality open source Ada compiler such as GNAT. Such approach could further improve reliability of crystallographic software and allow the community to build well documented, reliable and formally verified crystallographic software libraries.

[1] Shaffer, P. A., Schomaker, V. & Pauling, L. (1946). *The Journal of Chemical Physics*. **14**, 659–664.
[2] Chang, G. (2003). *J. Mol. Biol*. **330**, 419–430.
[3] Paulson, L. C. (1986). *J. Log. Program*. **3**, 237–258.
[4] Nipkow, T., Wenzel, M. & Paulson, L. C. (2002). *Isabelle/HOL: a Proof Assistant for Higher-Order Logic*. Berlin, Heidelberg: Springer-Verlag.
[5] Greengard, S. (2021). *Commun. ACM*. **64**, 13–15.
[6] Petrauskas, K., Merkys, A., Vaitkus, A., Laibinis, L. & Gražulis, S. (2022). *Journal of Applied Crystallography*. **55**, 515–525.
[7] Grosse-Kunstleve, R. W. (1999). *Acta Crystallographica, Section A: Foundations of Crystallography*. **55**, 383–395.
[8] Chapin, P. C. & McCormick, J. W. (2015). *Building High Integrity Applications with SPARK*. Cambridge University Press.

A024-05-260823

A semi-supervised deep-learning approach for automatic crystal structure classification

Satvik Lolla[1, 2], Haotong Liang[3], A. Gilad Kusne[2, 3, 4], Ichiro Takeuchi[3, 5], William Ratcliff[2, 3]

[1] Poolesville High School, Poolesville MD 20837 USA , [2] NIST Center for Neutron Research, NIST Gaithersburg MD 20899 USA, [3] Department of Materials Science and Engineering, University of Maryland College Park MD 20742 USA, [4] Materials Measurement Laboratory, NIST Gaithersburg MD 20889 USA, [5] Maryland Quantum Materials Center, College Park MD 20742
hliang16@umd.edu

Keywords: Generative Adversarial Network, Semi-supervised Learning, Neutron Powder Diffraction, Space Group Classification

The structural solution problem can be a daunting and time-consuming task. Especially in the presence of impurity phases, current methods, such as indexing, become more unstable. In this work, the novel approach of semi-supervised learning is applied towards the problem of identifying the Bravais lattice and the space group of *inorganic crystals*. The reported semi-supervised generative deep-learning model[1-3] can train on both labeled data, i.e. diffraction patterns with the associated crystal structure, and unlabeled data, i.e. diffraction patterns that lack this information. This *semi-supervised* scheme consists of a generator and discriminative models, which are bundled together into a *Generative Adversarial Network* as shown in Fig. 1. By training on the unlabeled diffraction patterns, the discriminator model gains the ability to extract useful features with regard to the diffraction patterns, which in principle, could be beneficial to performing downstream supervised tasks. This approach allows the models to take advantage of the troves of unlabeled data that current supervised learning approaches cannot, which should result in models that can more accurately generalize to real data. In this work, powder diffraction patterns are classified into all 14 Bravais lattices and 144 space groups (the number is limited due to sparse coverage in crystal structure databases), which covers more crystal classes than other studies. The reported models[4] also outperform current deep-learning approaches[5-7] for both space group and Bravais lattice classification using fewer training data.

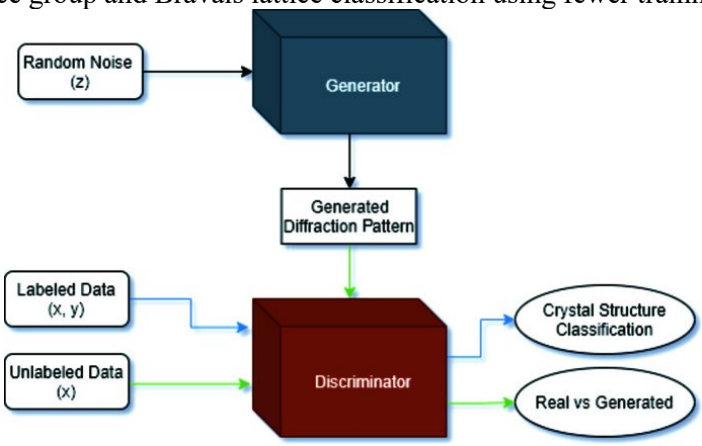

Figure 1. The architecture for the semi-supervised GAN.

[1] Odena, A. (2016). arXiv:1606.01583.
[2] Goodfellow, I., Pouget-Abadie, J., Mirza, M., Xu, B., Warde-Farley, D., Ozair, S., Courville, A. & Bengio, Y. (2020). Commun. ACM, **63**, 139–144.
[3] Salimans, T., Goodfellow, I., Zaremba, W., Cheung, V., Radford, A. & Chen, X. (2016). Adv. Neural Inf. Process. Syst. **29**, 2234–2242.
[4] Lolla, S., Liang, H., Kusne, A. G., Takeuchi, I., & Ratcliff, W. (2022). A semi-supervised deep-learning approach for automatic crystal structure classification. Journal of applied crystallography, **55**(Pt 4), 882–889. https://doi.org/10.1107/S1600576722006069
[5] Liu, C.-H., Tao, Y., Hsu, D., Du, Q. & Billinge, S. J. L. (2019). Acta Cryst. **A75**, 633–643.
[6] Ziletti, A., Kumar, D., Scheffler, M. & Ghiringhelli, L. M. (2018). Nat. Commun. **9**, 2775.
[7] Tiong, L. C. O., Kim, J., Han, S. S. & Kim, D. (2020). NPJ Comput. Mater. **6**, 196.

The authors are grateful to Austin McDannald and Hui Wu from NIST, and Brian Toby from Argonne National Laboratory. We acknowledge Stephan Rühl for the ICSD. The work at the University of Maryland was supported by NIST. Commercial disclaimer: Any mention of commercial products within this article is for information only; it does not imply recommendation or endorsement by NIST. Any acknowledgements authors wish to make should be included at the end of the abstract with no heading

A024-06-260823

A complete and easy to use PDF solution – HighScore(Plus) v.5.2

T.Degen[1], M.Sadki[1], E.Bron[1], M.Gateshki[1]

[1]*Malvern Panalytical B.V. Lelyweg 1, 7603EA Almelo, The Netherlands*
thomas.degen@malvernpanalytical.com

Keywords: PDF Fitting, PDF Analysis

This HighScore(Plus) [1] is a software package for qualitative and quantitative phase analysis of XRD powder data. Additionally, it contains crystallographic analysis, multivariate statistics like clustering [2], PCA/MMDS [3,4], PLSR [5], t-SNE [6], plus the option to calculate the PDF from X-ray powder diffraction data, based on the GudrunX [7] software by Alan Soper.

To complete the HighScore analytical toolchain, version 5.2 now adds the simulation and fitting of the PDF, for X-ray and neutron data. The chosen "small box" approach works straightforward and is transparent for the user, like the implemented quantitative Rietveld [8] analysis. The workflow is easy and automated as much as possible, a complete automation is possible by the Smart Batch feature of HighScore.

The simulation and fits are performed in the space group P1. Higher model symmetry is enforced by a set of linear constraints created automatically. For advanced use, the automatic constraints can be turned into manual constraints and then could be removed one by one by the user, to give more freedom to the model gradually.

In this presentation we explore the implementation in more detail, and we present a couple of interesting application examples.

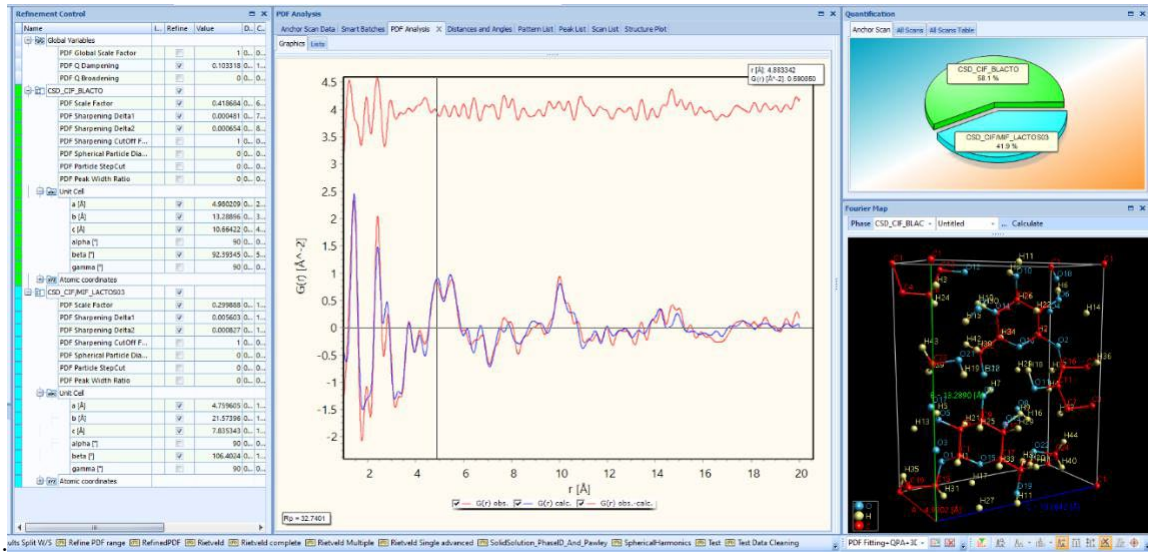

Figure 1. Multi-phase PDF fit including live QPA pie chart, as well as live structure plot.

[1] T. Degen, M. Sadki, E. Bron, U. König, G. Nénert, *The HighScore suite*, Powder Diffraction (2014), **29**, 13-18.
[2] G.N. Lance, W.T. Williams, *A general theory of classification sorting strategies 1.*, Hierarchical systems, Comp. J. (1966), **9**, 373–380.
[3] E.H. Malinowski and D.G. Howery (1980), *Factor Analysis in Chemistry*, John Wiley & Sons, New York.
[4] I. Borg, P. Groenen, *Modern Multidimensional Scaling: theory and applications (2nd ed.)*. New York: Springer-Verlag, (2005), 207–212.
[5] *S. de Jong*, SIMPLS: *An alternative approach to partial least squares regression, Chemometrics Intell. Lab. Syst.*, (1993), **18(3)**, 251-263.
[6] *L.J.P. van der Maaten and G.E. Hinton*, *Visualizing High-Dimensional Data Using t-SNE. Journal of Machine Learning Research* 2008, **9**, 2579-2605.
[7] A.K. Soper and E.R. Barney, *Extracting the pair distribution function (PDF) from white beam x-ray total scattering data*, J. Appl. Cryst. (2011), **44**, 714-726.
[8] H.M. Rietveld, *A profile refinement method for nuclear and magnetic structures*, J. Appl. Cryst. (1969), **2**, 65 – 71.

A024-07-260823

TOPAS macros for MEM analysis in RIETAN-FP & Dysnomia

Dr. Xiaodong (Tony) Wang[1], Dr. Maykel Manawan[2]

1 Central Analytical Research Facility, Queensland University of Technology, Australia tony.wang@qut.edu.au

2 PRMM, National Research and Innovation Agency, Indonesia maykeltem@gmail.com

Keywords: TOPAS, RIETAN, Dysnomia, MEM, Maximum Entropy Method

Two TOPAS macros have been composed to export .ins (instruction) and .int (measured diffraction data) files for RIETAN- FP and Dysnomia software to perform MEM (Maximum Entropy Method) analysis and generate 3D electron density map. MEM (Maximum Entropy Method) analysis [1,2] implemented in RIETAN-FP [3] & Dysnomia [4] software is often used to estimate 3D electron density map in unit cell. The termination effect (reflections not collected in high-Q region giving oscillations in real space) commonly seen in Fourier analysis is less obvious in MEM method, which provide more clear 3D electron density map, *e.g.* estimate ion transfer channels in solid electrolyte [5]. However, the RIETAN-FP .ins template file generated by VESTA [6] has more than 1000 lines (600+ non-comment lines), which makes it not as user-friendly as other software. TOPAS [7] is another flexible crystallographic optimization program which is famous for its openness to user-built macros on functionality expansions, wild convergence radius (tolerance to starting values far from true values), and user -friendliness (Rietveld .inp file in TOPAS is often less than 30 lines). These proposed TOPAS macros exports RIETAN-FP input .ins/.int files directly from Rietveld refinement in TOPAS, hopefully can facilitate researches [8] using both analyses platforms.

Each **figure** should have a caption placed below the figure. Number the figures and refer to them as Fig. 1 *etc*. The figure layout '*in line with text'* should be used.

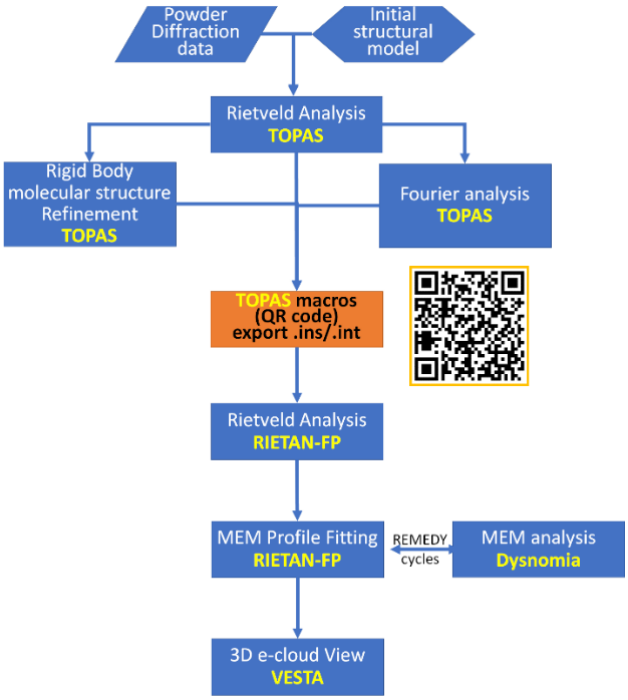

Figure 1. Analysis flow chart bridging TOPAS with RIETAN-VENUS integrated environment.

[1] Collins, D. M. (1982). *Nature* **298**, 49-51.
[2] Sakata, M. & Sato, M. (1990). *Acta Crystallogr. Section A* **46**, 263-270.
[3] Izumi, F. & Momma, K. (2007). *Solid State Phenomena* **130**, 15–20.
[4] Momma, K., Ikeda, T., Belik, A. A. & Izumi, F. (2013). *Powder Diffr.* **28**, 184-193.
[5] Manawan, M., Kartini, E. & Avdeev, M. (2021). *J. Appl. Crystallogr.* **54**, 1409-1415.
[6] Momma, K. & Izumi, F. (2011). *J. Appl. Crystallogr.* **44**, 1272-1276.
[7] Coelho, A. (2018). *J. Appl. Crystallogr.* **51**, 210-218.
[8] Ma, D., Yang, J., Manawan, M., Yang, C., Li, J., Liang, Y., Feng, T., Zhang, Y.-W. & Pan, J. H. (2022). *STAR Protocols* **3**, 101099.

A031 Advances in Electron Crystallography Methods for Solving Crystal Structures
Room 208
1.10pm - 3.30pm

A031-01-260823

A direct method for Fourier ptychography

L. Clark[1], D.M. Paganin[2], J. Zhao[3], E. Liberti[3], P.D. Nellist[4], A.I. Kirkand[3,4,5]

1. *School of Physics Engineering and Technology, University of York, York, YO10 5DD, UK,*
2. *School of Physics and Astronomy, Monash University, Clayton, VIC 3800, Australia,*
3. *Rosalind Franklin Institute, Harwell Research Campus, OX11 0FA, Didcot, Oxfordshire, UK,*
4. *Department of Materials, University of Oxford, Parks Road, OX1 3PH, Oxford, UK,*
5. *Electron Physical Sciences Imaging Centre, Diamond Light Source, Oxfordshire, OX11 0DE, UK.*

Laura.A.Clark@york.ac.uk

Keywords: Ptychography, phase contrast, direct methods

Recent years have seen huge progress made in atomic scale material characterisation as a result of ptychographic methods [1,2,3]. Ptychography describes a family of computational imaging techniques which allow diffraction patterns from multiple probe positions or images from multiple imaging conditions to be combined in such a way as to enable the reconstruction of the full complex exit wave of the specimen function [4] – the former approach describing conventional ptychography and the latter referring to Fourier ptychography. The development of non-iterative methods in conventional electron ptychography have enabled high-resolution phase contrast imaging at very low electron dose [5], while avoiding the convergence problems of the iterative ptychographic methods at low dose. In this presentation we show the development of a direct (non-iterative) method of Fourier ptychography. As such, it can be used in a conventional transmission electron microscope, or other scattering systems with an incident plane wave geometry. Our new method has a radiation-dose-distribution that is rather different to existing direct methods, and as such, is promising for enabling high-resolution characterisation of complex beam-sensitive materials. It can be used as a standalone method, or as a seeding technique for iterative methods.

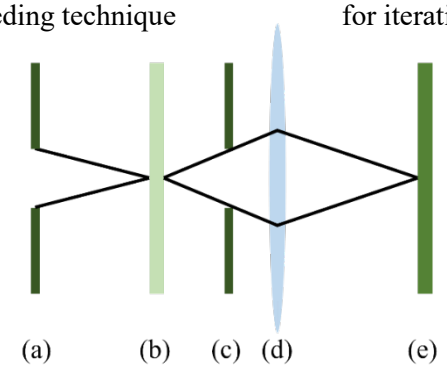

Figure 1. Underlying the derivation of this new method is the principle of reciprocity [6]. One can read the diagram left-right as a TEM: (a) condenser aperture, (b) specimen, (c) objective aperture, (d) objective lens, (e) detector; or right-left as a STEM: (e) source, (d) objective lens, (c) aperture, (b) specimen, (a) detector.

[1] Chen, Z., et al. (2021). *Science*, **372**(6544), 826-831.
[2] Ding, Z., et al. (2022). *Nature Communications*, **13**(1), 4787.
[3] Ophus, C. (2019). *Microscopy and Microanalysis*, **25**(3), 563-582.
[4] Rodenburg, J., & Maiden, A. (2019). Ptychography. Springer Handbook of Microscopy, 819-904.
[5] Chen, Z., et al. (2020). *Nature Communications*, **11**(1), 2994.
[6] Krause, F. F., & Rosenauer, A. (2017). *Micron*, **92**, 1-5.
LC acknowledges funding from a Royal Society University Research Fellowship (URF\R1\221270) and enhanced Royal Society funding (RF\ERE\221035).

A031-01-260823

3D-structure determination with MeV electron diffraction

A. Meents[1], V. Hennicke[1], M. Hachmann[2], A. Rodrigues[1], W. Brehm[1], P. Reinke[1], J. Meyer[1], S. Thekku Veedu[1], K. Bustos[1], L. Melo Costa[1], M. Galchenkova[1], O. Yefanov[1], M. Bartelmess[1], T. Pakendorf[1], H. Delsim Hashemi[2], S. Günther[1], H.N. Chapman[1], and K. Flöttmann[2]

[1] Center for Free Electron Laser Science (CFEL), DESY, Hamburg, Germany. [2] DESY, Hamburg, Germany.
alke.meents@desy.de

Keywords: electron diffraction, protein crystallography, time-resolved experiments

Electron diffraction is a promising and exciting alternative to structure determinations with X-rays. Electrons provide a 10^5 times higher interaction cross section accompanied by a 10^3 reduction of radiation damage effects compared to X-rays. Thus, electrons appear as superior probe in particular for the investigation of radiation sensitive biological samples such as proteins. Due to interaction with both electrons and protons, electron diffraction experiments further provide a much better visibility of hydrogen atoms, which play an important role in most enzyme reactions and are not directly visible in most X-ray diffraction experiments.

DESY is operating the low emittance **R**elativistic **E**lectron **G**un for **A**tomic **E**xploration (REGAE) providing electron pulses with energies between 2.5 and 6 MeV, a bunch charge of up to 100 fC and pulse duration down to 20 fs. In addition to the fs time resolution achievable with this machine in diffraction experiments, high-energy electron diffraction experiments have the advantage of using up to 1 µm thick samples for the experiments compared to 200 - 300 nm in case of conventional electron microscopes operating between 100 and 300 keV. The much longer focal lengths of the solenoids further allow the use of sophisticated sample environments, such as a setup for diffraction experiments of hydrated samples at room temperature.

In a first diffraction experiment at REGAE we have determined the 3D-structure of a 200 nm thick Mica sample. We collected a 120° rotation dataset with o0.01° increments at a frame rate of 50 Hz using an in-vacuum Jungfrau 1M detector. 25 single shot images were summed up per rotation increment (Fig 1, left). Data were processed with the XDS software package. Subsequent structure refinement with SHELXL resulted in a final R1-value of 16.7%. The resulting electron density maps show well resolved densities at the atom position with some elongation in direction of the crystallographic b-axis, which can be attributed to incomplete data caused by the missing wedge in this direction (Fig. 1, right). These first results highlight the potential of MeV electron diffraction for structure determination.

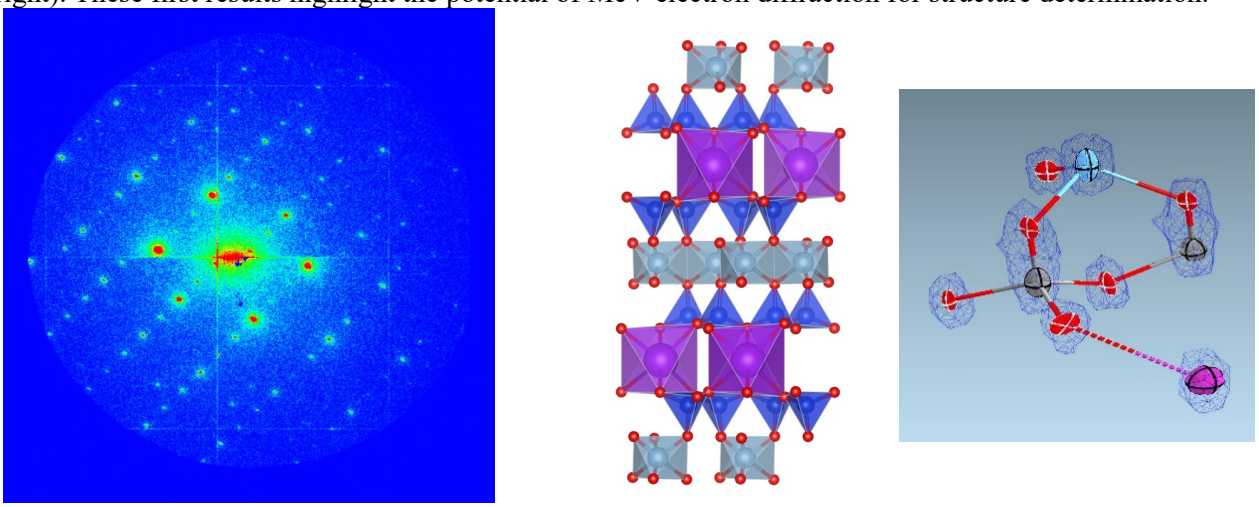

Figure 1: High-energy electron diffraction pattern of a 200 nm thick Mica sample recorded at REGAE with an energy of 3.3 MeV on a Jungfrau 1M detector (left) and the 3D-structure of the layer silicate Mica obtained with MeV electron diffraction data (center & right).

In future we aim at performing macromolecular diffraction experiments with nanocrystals at REGAE. A general challenge for accelerator-based electron diffraction experiments is bunch charging effects, which prevent compressing the electron bunches in both space and time whilst still maintaining a sufficient coherence length. In order to perform such experiments in future, we are currently implementing a bunch train mode, where the charge is spread over a few thousand micro-bunches separated by 0.3 ns and a total train duration of about 1.5 micro-seconds. With this unique

operation mode, we will be able to perform high-energy electron diffraction experiments at room temperature at REGAE with an electron beam size of 1 μm and a bunch charge of up to 100 fC providing ideal conditions for the exploration of macromolecular structures.

A031-03-260823

Quantification of 3D atomic structures and their dynamics from scanning transmission electron microscopy data

S. Van Aert1, A. De Backer1, E. Arslan Irmak1, Z. Zhang1, D.G. Sentürk1, T. Stoops1, L. Jones2, P.D. Nellist3, S. Bals1

1 EMAT and NANOlab Center of Excellence, University of Antwerp, Belgium; 2 CRANN & School of Physics, Trinity College Dublin, University of Dublin, Ireland; 3 Department of Materials, University of Oxford, United Kingdom

sandra.vanaert@uantwerpen.be

Keywords: Quantitative STEM, statistical parameter estimation, atom-counting, energy minimisation

Determining the atomic structure of nanomaterials in 2D and 3D is critical to understand their unique properties. Therefore, a thorough quantitative characterization by transmission electron microscopy is of great importance. Progress in the development of quantitative methods allows us to extract reliable structural and chemical information from experimental scanning transmission electron microscopy (STEM) images. In quantitative STEM, images are treated as datasets from which structure parameters are determined by comparison with image simulations, by using parameter estimation-based methods, and more recently by applying deep learning. This contribution aims to explain recent developments using current state-of-the-art experimental examples.

To overcome limitations related to conventional electron tomography, 3D characterization of beam-sensitive nanomaterials can be obtained from atom counts resulting from a single annular dark field (ADF) STEM image. For this purpose, the scattering cross-section (SCS), corresponding to the total intensity of electrons scattered by a single atomic column, has been shown to be successful. When combining image simulations and statistical parameter estimation, the number of atoms in an atomic column can be counted [1, 2]. This method has been extended to analyse time series of images using a hidden Markov model [3] and is very promising for revealing dynamic structural changes resulting during in situ experiments [4]. Moreover, progress has been made to extend atom-counting from homogeneous to heterogeneous materials by combining ADF STEM with energy dispersive X-ray spectroscopy [5]. This is facilitated by using a deep convolutional neural network and an atomic lensing model to efficiently compute SCSs of mixed atomic columns.

Next, atom counts can be used to create an initial atomic model which serves as an input for energy minimization to obtain a relaxed 3D reconstruction. A lot of effort has been put to improve the atom-counting/energy minimisation method. In order to avoid that purely computational energy minimisation approaches result in a close local minimum where the reconstructed structure may deviate from the experimental observation, the energy landscape can exhaustively be explored to find the local minimum corresponding to the experimentally observed structure. For this purpose, an iterative local minima search algorithm has been proposed which is followed by a molecular dynamics structural relaxation of candidate structures associated with each local minimum [6]. In this manner, it becomes possible to investigate the 3D atomic structure of supported nanoparticles, which may deviate from their ground state configuration. In parallel, a Bayesian genetic algorithm has been developed incorporating a priori information concerning the finite atom-counting precision and neighbour-mass relations [7]. Especially for incident electron doses below 10^4 $e^-Å^{-2}$, this method shows a clear benefit, especially to reconstruct surface atoms of nanoparticles. Finally, the information-richness and dose efficiency of 4D STEM will be explored.

[1] De Backer, A., van den Bos, K.H.W., Van den Broek, W., Sijbers, J. & Van Aert, S. (2016). *Ultramicroscopy* **171**, 104-116.
[2] De Backer, A., Bals, S. & Van Aert, S. (2023). *Ultramicroscopy* **247**, 113702.
[3] De wael, A., De Backer, A., Jones, L., Varambhia, A., Nellist, P.D. & Van Aert, S. (2020). *Physical Review Letters* **124**, 106105.
[4] Liu, P., Arslan Irmak, E., De Backer, A., De wael, A., Lobato, I., Béché, A., Van Aert, S. & Bals, S. (2021). *Nanoscale* **13**, 1770-1776.
[5] De Backer, A., Zhang, Z., Van den Bos, K.H.W., Bladt, E., Sánchez-Iglesias, A., Liz-Marzán, L.M., Nellist, P.D., Bals, S. & Van Aert, S. (2022). *Small Methods*, **6**, 2200875.
[6] Arslan Irmak, E., Liu, P., Bals, S. & Van Aert, S. (2021). *Small Methods* **5**, 2101150.
[7] De Backer, A., Van Aert, S., Faes, C., Arslan Irmak, E., Nellist, P.D. & Jones, L. (2022). *npj Computational Materials* **8**, 216.

This work was supported by the European Research Council (Grant 770887 PICOMETRICS to S. Van Aert and Grant 815128 REALNANO to S. Bals). This project has received funding from the European Union's Horizon 2020 innovation programme under grant agreement No 823717. The authors acknowledge financial support from the Research Foundation Flanders (FWO, Belgium).

A031-07-260823

Cryogenic Electron Ptychographic Single Particle Analysis (Cryo-EPty SPA)

Xudong Pei[1], Liqi Zhou[1], Chen Huang[2], Mark Boyce[3], Judy S. Kim[2,4], Emanuela Liberti[2] , Takeo Sasaki[5], Peijun Zhang[3,6], David I. Stuart[3], Angus I. Kirkland[2,4] and Peng Wang[7,*]

[1]College of Engineering and Applied Sciences, Nanjing University, Nanjing 210093, China.[2]The Rosalind Franklin Institute, Harwell Science and Innovation Campus, Didcot, OX11 0FA, UK. [3]Division of Structural Biology, Welcome Trust Centre for Human Genetics, University of Oxford, Oxford, OX3 7BN, UK. [4]Department of Materials, University of Oxford, Parks Road, Oxford OX1 3PH, UK. [5]JEOL Ltd., 3-1-2 Musashino, Akishima, Tokyo 196-8558 Japan. [6]Electron Bio-Imaging Centre, Diamond Light Source, Harwell Science and Innovation Campus, Didcot OX11 0DE, UK. [7]Department of Physics, University of Warwick,

Coventry CV4 7AL, UK.

peng.wang.3@warwick.ac.uk

Keywords: Cryo-EM, Ptychography, Diffractive Imaging, Single Particle Analysis

Cryo-electron microscopy (Cryo-EM) is an advanced technique for obtaining high-resolution, three-dimensional images of various biological samples in their natural, frozen-hydrated state. However, conventional cryo-EM images can be affected by low signal-to-noise ratios and low contrast due to the sensitivity of vitrified biological samples. To address these issues, cryo-EM single particle analysis typically records images at high defocus, but this method reduces the accuracy of high-frequency information. Our new technique utilizes cryo-electron ptychography (Cryo-EPty) [1], as depicted in Figure 1a, that is a variant of this method that uses scanning ptychographic diffractive imaging [2]. In Ptychography, the probe is scanned over the specimen in overlapping positions, using a defocused probe. As the full diffraction pattern is captured, this technique is highly efficient, especially when data is recorded using direct electron detectors that produce high signal-to-noise ratios at low electron doses [3]. This paper presents a new 3D SPA technique that is based on Cryo-EPty SPA and demonstrates its ability to restore 3D information from a single sample. The experimental Cryo-EPty SPA datasets (Figure 1b) [1] were used to reconstruct the ptychographic phase of rotavirus double-layered particles (DLPs) at a dose of 22.7 e/A^2. The particle-picking procedures developed for Cryo-EM SPA can be directly applied to this phase, producing a stack of particle phases that are coordinated by position, as shown in Figure 1b. A 3D density map of rotavirus DLPs (Figure 1c) was then reconstructed using 300 particles from this stack of phases. We believe that the combination of Cryo-EPty and SPA has the potential to produce high-resolution 3D reconstructions of biological samples [4].

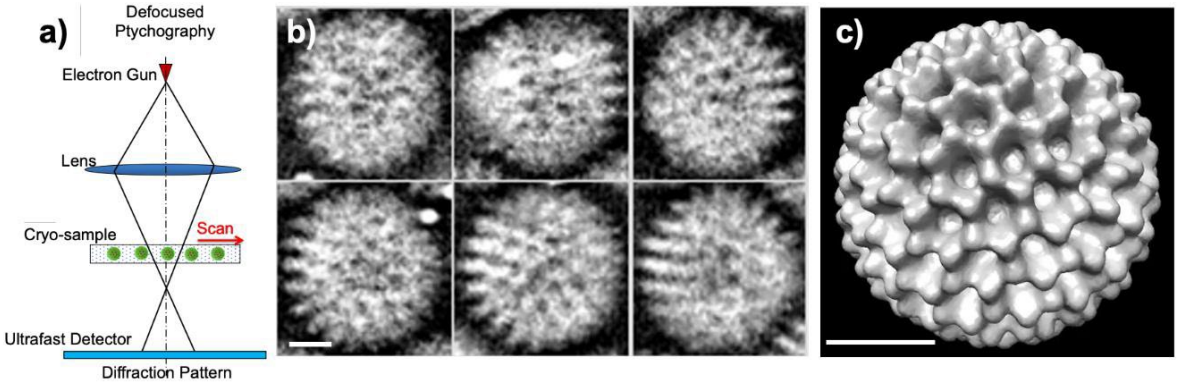

Figure 1. (a) Schematic optical configuration diagram of the workflow used for cryo-ptychography; (b) Many instances of the viral particles for single particle analysis can be extracted from reconstructed ptychographic phases, scale bars: 20 nm. (c) 3D map corresponding to the particle instances.

[1] Zhou, L., Song, J., Kim, J. S., Pei, X., Huang, C., Boyce, M., Mendonça, L., Clare, D., Siebert, A., Allen, C. S., Liberti, E., Stuart, D., Pan, X., Nellist, P. D., Zhang, P., Kirkland, A. I. & Wang, P. (2020). Nature Communications **11**, 2773.
[2] Rodenburg, J.M. (2008). Advances in Imaging and Electron Physics **150,** 87.
[3] Song, J., Allen, C. S., Gao, S., Huang, C., Sawada, H., Pan, X., Warner, J., Wang, P. & Kirkland, A. I. (2019). Scientific Reports **9**, 3919.
[4] The authors acknowledge funding from University of Warwick Research Development Fund (RDF) 2021-22 Science Development Award.

A031-05-260823

On the Cutting Edge of Electron Diffraction Quality

Hovestreydt[1], C. Jandl[1], J. Merkelbach[1], G. Steinfeld[1], D. Stam[1], P. Simoncic[1]

ELDICO Scientific AG, PARK INNOVAARE, 5234 Villigen-PSI, Switzerland
hovestreydt@eldico.ch

Keywords: electron diffraction, 3D ED, microED, pharmaceutics, polymorphism, accuracy

Electron diffraction (3D ED) has recently emerged as a powerful tool for structure determination on crystallites in the nanometer range, as it allows to bypass the common bottleneck of growing single crystals, big enough for x-ray diffraction. 3D-ED, using both the *continuous rotation* method and software as we know from X-ray crystallography, is gaining a lot of attention in all fields of research from organic and inorganic molecules, over polymorphism, geological sciences, natural products, biomolecules, material sciences to energy-storage materials and many others.

Here we showcase results from an ***ELECTRON DIFFRACTOMETER***, the first *entirely dedicated device for 3D ED*, on representative case studies dealing with challenging *organic compounds* to demonstrate the benefits over TEM-based MicroED experiments. Pioneers in the field of electron diffraction already agree that a dedicated device is of great advantage for all fields of nano-crystallography.

As a benchmark and to show the capabilities of a dedicated electron diffractometer, we recently performed 3D ED experiments on *metaxalone*, $C_{12}H_{15}NO_3$. Sold as Skelaxin, it is a muscle relaxant, but its exact mechanism of action is still not known. Metaxalone exhibits various *polymorphic* forms with substantial effects on e.g. solubility and bioavailability, one of which could only be obtained[1] as nanometer-sized needles and thus required electron diffraction for accurate structure elucidation.

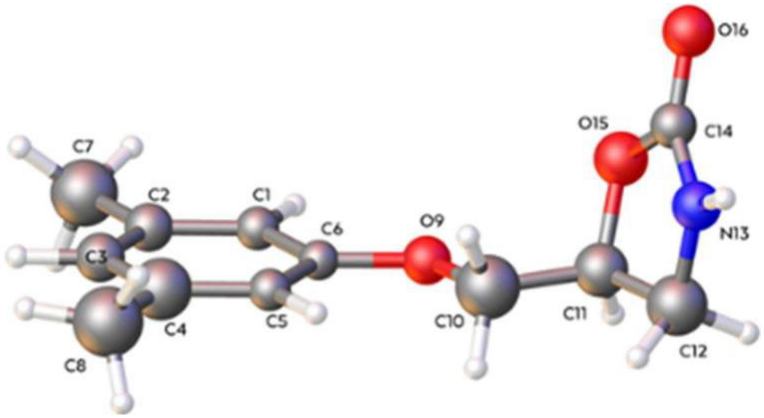

Figure 1. Metaxalone from nano-crystal.

The data quality obtained is clearly *superior* to previously reported[1], despite room-temperature data collection, indicating a higher performance of a dedicated diffractometer compared to equipment commonly used until today.

[1] Hamilton, V. et al. (2020). *Cryst. Growth Des.*, **20**, 4731–4739

A031-05-260823

Measureable order parameters from small-beam diffraction measurements on glasses

A.C.Y. Liu1,2

1 School of Physics and Astronomy, Monash University, Clayton, Victoria 3800, Australia, 2 Monash Centre for Electron Microscopy, Monash University, Clayton, Victoria, 3800, Australia amelia.liu@monash.edu

Keywords: glass, amorphous material, electron nanodiffraction, small-angle x-ray scattering, structural order

Traditionally, the science of crystallography has sought to solve structures exactly and uniquely in terms of the positions of all the atoms [1,2]. This foundational and underpinning methodology has driven much progress across many fields of science and engineering. In the case of amorphous materials and glasses, structure cannot currently be solved uniquely from diffracted intensities alone, providing significant roadblocks to further development and discovery [2].

Recent technological advances in beam definition to collect diffraction from small volumes, full-field counting detectors and automated data acquisition have made the collection of ensembles and arrays of small-beam, "speckle" diffraction patterns from disordered specimens a routine experiment. These patterns exhibit strong angular fluctuations in the diffracted intensity that vary from place-to-place, reflecting variations in the local order, and promising new ways to obtain interesting, statistical information about local structures in disordered materials [3,4]. While the interpretation of this information and the best analysis approach are ongoing challenges [2], there has been a lot of recent activity that has progressed the vision of early researchers [3,4].

In this presentation, I will discuss a framework for analyzing angular symmetries in small-beam diffraction patterns from hard-sphere colloidal and metallic glasses [5,6]. This approach associates, as far as possible, the magnitude of these angular intensity fluctuations with the bond orientational order (BOO) parameter measured from the arrangement of nearest-neighbours around a central particle. The BOO parameter is a good and general order parameter that has been extremely powerful for characterizing order in liquids and glasses, but requires particle positions to be known in three-dimensions [7]. Like the BOO parameter, the experimentally measureable order parameters from electron nanodiffraction may clarify the role of structure in disordered materials.

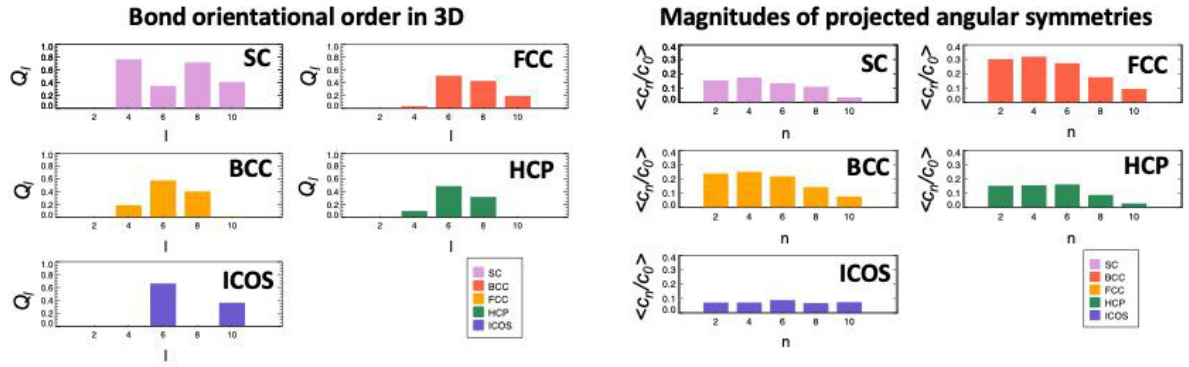

Figure 1. **A** Bond orientational order parameters (Q_l as a function of order, l) measured in three dimensions from atomic positions **B** Average projected angular symmetries measured from electron nanodiffraction patterns (normalized Fourier coefficients c_n/c_0 for each n-fold angular symmetry [5]). Unit polyhedra from the simple cubic (SC), face-centred cubic (FCC), body-centred cubic (BCC), hexagonal close-packed (HCP) and icosahedral (ICOS) structures are compared.

[1] Cartwright J H E and Mackay A L, *Phil. Trans. R. Soc. A*, (2012) 370, 2807-2822
[2] Bøjesen E D, Petersen T C, Martin A V, Weyland M and Liu A C Y, *J. Phys: Mater.*, (2020) **3**, 044002.
[3] Cowley J M, *Ultramicroscopy* (2002) **90** 197–206
[4] Howie A, McGill C A and Rodenburg J M, *J. de Phys. Colloque* (1985) 46-C9 59–62
[5] Liu A C Y, Tabor R F, Bourgeois L, de Jonge M D, Mudie S T and Petersen T C, *Phys. Rev. Lett.* (2016) **116** 205501
[6] Liu A C Y, Tabor R F, de Jonge M D, Mudie S T and Petersen T C, *Proc. Natl. Acad. Sci.*, (2017) **114** 10344–9
[7] Steinhardt P J, Nelson D R and Ronchetti M, *Phys. Rev. B* (1983) 28 784–805

The authors acknowledge the use of the instruments and scientific and technical assistance at the Monash Centre for Electron Microscopy, a Node of Microscopy Australia. This research used equipment funded by Australian Research Council grant LE045416. This research was undertaken on the SAXS/WAXS beamline at the Australian Synchrotron, Victoria, Australia. A.C.Y.L. acknowledges support from the Monash Centre for Electron Microscopy and the Australian Research Council (FT180100594). A. C. Y. L. thanks Timothy Petersen, Joanne Etheridge, Laure Bourgeois, Espen Bøjesen, Andrew Martin, Rico Tabor, Stephen Mudie, Peter Harrowell, and Alessio Zaccone for stimulating discussions and contributions to this work.

A045 Using High-pressure Diffraction to Design and Understand Functionality
Room 210/211
1.10pm - 3.30pm

A045-01-260823

High pressure behavior and metastable phases of SixGe1-x alloys

V. Pischedda[1], M. Gerin[1], S. Le Floch[1], S. Radescu[2], F. Alabarse[3], D. Amans[1], D. Machon[4]

[1]Institut Lumière Matière, UMR5306 Université Lyon 1-CNRS, 69622 Villeurbanne, France

[5] Departamento de Física, Universidad de La Laguna, Tenerife, Spain

[3] Elettra - Sincrotrone Trieste S.C.p.A., 34149 Basovizza, Trieste, Italy

[4]Laboratoire Nanotechnologies Nanosystèmes, CNRS UMI-3463-3IT, Univ. Sherbrooke, Sherbrooke, Canada

Email of communicating author: vittoria.pischedda@univ-lyon1.fr

Keywords: SiGe alloys, in-situ high pressure, phase transitions

Group IV elements, such as carbon, silicon and germanium are known to exhibit polymorphism under high pressure. Interestingly, some of these phases can be recovered when returning to ambient conditions, offering the access to new physical and mechanical properties.

Recently silicon and germanium alloys have gained new interest, especially in the energy applications. Recent research has shown that SixGe1-x is a potential thermoelectric material [1], an active anode material in lithium-ion battery cells [2–3] or extremely interesting for its luminescence properties [4].

High pressure techniques have proven to be a very efficient method of exploring new phases and properties in germanium and silicon, leading to the discovery of a large number of metastable phases with exotic properties. However, there is only a few experimental reports on the high-pressure behaviour of SixGe1−x alloys, mainly due to the difficulty to synthesize homogeneous SiGe alloys of good quality. In this study, we report the high pressure behaviour of different SiGe alloys studied using Paris-Edinburgh press and diamond anvil cells (DAC) coupled with in-situ characterization techniques such as Raman spectroscopy and X-ray diffraction. Upon compression, the stable SiGe diamond phase transforms into the β-metallic phase (Fig.1). Upon decompression, we observed the formation of new metastable structures named SiGe-r8 and SiGe-bc8. Experimental results are discussed in comparison with those reported in the literature and using DFT simulations. Understanding the transition pathway to metastable phases in SiGe alloys can be a key issue for future generations of semiconductors and energy-related technology.

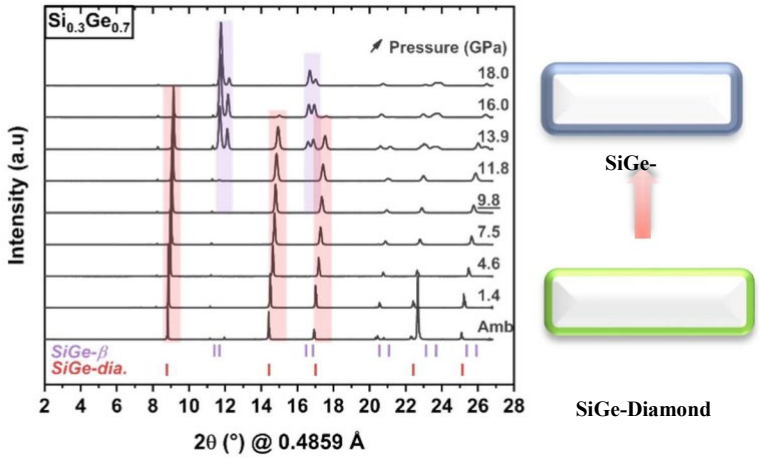

Figure 1. In-situ high pressure XRD patterns of $Si_{0.3}Ge_{0.7}$ collected at Elettra synchrotron using a DAC. Phase transition from the diamond to the metallic β structure starts at around 9.8 GPa.

[1] S. Bathula et al. (2012). Appl. Phys. Lett. 101, 213902.
[2] A. Desrues et al. (2019). Batter. Supercaps. 2, 970.
[3] M. Ge et al. (2015). Nanotechnology. 26, 255702.
[6] E. M. T. Fadaly et al. (2020) Nature, 580, 205.

A045-02-260823

High-pressure phase transitions in the Co(II) analogue of ZIF-8

I. Jones[1], G. Turner[1], S. Boer[2], S. Moggach[1]

[1]School of Molecular Sciences, The University of Western Australia, 35 Stirling Highway, Crawley, Perth, Western Australia, Australia 6009, [2]MX Beamlines, ANSTO Australian Synchrotron, 800 Blackburn Road, Clayton, Victoria, Australia 3168
isabelle.jones@uwa.edu.au

Keywords: X-Ray Crystallography, Zeolitic Imidazolate Frameworks, High-pressure Adsorption

The adsorption properties and structural behaviour of zeolitic imidazolate frameworks (ZIFs) rely upon the interplay of their organic ligands, metal centres and the guest molecules contained within their framework.[1–5] ZIF-8 and its isostructural derivatives with SOD-type topologies, composed of a single metallic centre connected by bi-dentate imidazolate (Im) linkers, are well known to alter their guest-mediated uptake behaviour upon metal or functional group substitution.[2, 3, 6, 7] Replacement of the metal ion can be particularly interesting as it not only impacts the pressure at which SOD-type ZIFs may undergo a "gate-opening" phase transition, whereby the Im linker rotates to allow greater access to the central pore, but may also have implications for catalysis by supplying more active centres.[6, 7] One of the most studied of the SOD-type ZIFs is ZIF-67, a Co-based isostructural equivalent to ZIF-8(Zn).[8–12] However, despite a wide variety of studies utilising ZIF-67 as a catalyst or adsorbent,[10, 12] few studies have examined the structural response of ZIF-67 under applied pressure,[9] and none in a penetrating medium at high pressure.

This study is the first to use high-pressure single crystal X-ray crystallography to probe structural transitions in ZIF-67 during compression in hydrostatic media of a methanol/ethanol mixture, MeOH:EtOH (4:1), and liquid nitrogen (LN2), with the aim of examining the relative compressibility of ZIF-67 against ZIF-8. The results demonstrated that ZIF-67, similarly to ZIF-8(Zn), displayed the prototypical transition to the "gate-opened" high-pressure phase in both mediums, characterised by a change in the angle between the average 2-methylimidazolate (mIm) plane and the [100] plane (denoted θ). Similarly to ZIF-8,[1, 4] ZIF-67 begins with θ of 64.5 to 66.9° in the ambient structures. On conversion to the high-pressure (ZIF-67-HP) phase, the mIm linker is rotated to θ =~89°. In MeOH:EtOH, this occurs at 1.57 GPa and is followed by both a sharp decrease in the unit cell volume (-3.75%) and contraction of the cell axes (-1.01%). In LN2, the transition is noticeable at the lowest measured pressure (0.43 GPa) and is associated with an immediate expansion of the unit cell (+1.2%), followed by continuous contraction by as much as 10.5% by 3.49 GPa. LN2 adsorption was modelled in 6 adsorption sites that fill progressively as pressure increases. Maximum LN2 adsorption site occupancies corresponded to the first observation of a noticeable and fully reversable colour transition in a ZIF crystal on compression, which was not found to occur in alcohol. Despite the presence of a Co^{2+} d^7 metal centre, the change in colour could not be linked to any local change in metal or ligand conformation that would suggest spin-crossover but is instead related to super filling of the structure by the N2. This work confirms and elucidates the nature of the guest-mediated gate-opening in both small alcohols and N2 of ZIF-67 at high pressures.

[1] Hobday, C. L., Woodall, C. H., Lennox, M. J., Frost, M., Kamenev, K., Düren, T., Morrison, C. A., & Moggach, S. A. (2018). *Nature Comm.*, **9 (1),** 1–9.
[2] Hobday, C. L., Bennett, T. D., Fairen-Jimenez, D., Graham, A. J., Morrison, C. A., Allan, D. R., Dü, T., & Moggach, S. A. (2017). *J. Am. Chem. Soc.*, **140, 1,** 382–387
[3] Fairen-Jimenez, D., A. Moggach, S., T. Wharmby, M., A. Wright, P., Parsons, S., & Düren, T (2011). *J. Am. Chem. Soc.*, **133 (23),** 8900–8902.
[4] Moggach, S. A., Bennett, T. D., & Cheetham, A. K. (2009). *Angew. Chem. Int. Ed.*, **48 (38),** 7087–7089.
[5] Bennett, T. D., Sotelo, J., Tan, J. C., & Moggach, S. A. (2015). *CrystEngComm*, **17 (2),** 286–289.
[6] López-Cabrelles, J., Romero, J., Abellán, G., Giménez-Marqués, M., Palomino, M., Valencia, S., Rey, F., & Mínguez Espallargas, G. (2019). *J. Am. Chem. Soc.*, **141 (17),** 7173–7180.
[7] Vitillo, J. G., Gagliardi, L. (2021). *Chem. Mater.*, **33,** 4465-4473.
[8] Banerjee, R., Phan, A., Wang, B., Knobler, C., Furukawa, H., O'Keeffe, M., & Yaghi, O. M. (2008). *Science*, **319 (5865),** 939–943.
[9] Vervoorts, P., Burger, S., Hemmer, K., & Kieslich, G. (2020). *Preprint.*
[10] Jadhav, H. S., Bandal, H. A., Ramakrishna, S., & Kim, H. (2022). *Adv. Mater.,* **34 (11),** 2107072.
[11] Andres-Garcia, E., Oar-Arteta, L., Gascon, J., & Kapteijn, F. (2019). *Chem. Eng. J.*, **360,** 10–14.
[12] Krokidas, P., Castier, M., Moncho, S., Sredojevic, D. N., Brothers, E. N., Kwon, H. T., Jeong, H.-K., Jong, ‖, Lee, S., & Economou, I. G., (2016) *J. Phys. Chem. C*, **120,** 8124.

A045-03-260823

Preservation of high-pressure materials in nanostructured diamond capsules

Z. Zeng1, J. Wen2, H. Lou1, T. Liang 1, X. Zhang1, L. Yang1, L. Tan1, B. Cheng1,3, X. Zuo4, W. Yang1, W. L. Mao5,6, H. Mao1, Q. Zeng1

1Center for High Pressure Science and Technology Advanced Research (HPSTAR), Shanghai, China; 2Center for Nanoscale Materials, Argonne National Laboratory, Argonne, Illinois, USA; 3Shanghai Institute of Laser Plasma, Shanghai, China; 4X-ray Science Division, Argonne National Laboratory, Lemont, Illinois, USA; 5Department of Geological Sciences, Stanford University, Stanford, CA, USA; 6Stanford Institute for Materials and Energy Sciences, SLAC National Accelerator Laboratory, Menlo Park, California, USA
Email: zengzd@hpstar.ac.cn

Keywords: diamond, high pressure, silicon

High pressure induces dramatic changes and novel phenomena in materials that are usually not preservable after pressure release. We proposed an approach to preserving high-pressure materials using *nanostructured diamond capsules* (NDCs)[1]. As a demonstration, we pressurized argon into enclosed nano-pores of glassy carbon precursors, then converted the glassy carbon into nanocrystalline diamond by heating, and eventually synthesized NDCs capable of permanently preserving high-pressure argon even after release back to ambient conditions (see Fig.1). With NDCs, various vacuum-based diagnostic probes, including electron microscopy, can be employed to characterize high-pressure argon directly. Synchrotron X-ray and high-resolution transmission electron microscopy-based diagnostic techniques show nm-sized argon crystals at ~22.0 GPa embedded in the nanocrystalline diamond matrix. Moreover, the preserved pressure of the argon sample inside NDCs can be readily tuned by controlling the NDCs synthesis pressure. To test the general applicability of the NDC process, we show high-pressure neon can also be trapped in NDCs as well. In principle, the NDC strategy can be applied to liquid and solid samples as well. Therefore, it could provide a unique approach to retaining high-pressure materials and their novel properties for ambient applications.

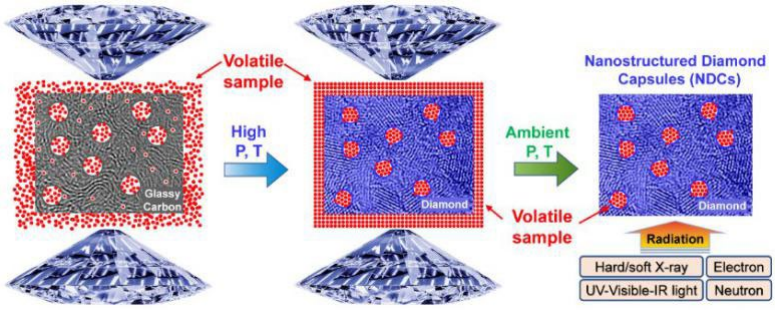

Figure 1. Schematic of the NDC synthesis process.

In addition, we will also introduce our recent work on measuring the mechanical properties of hexagonal silicon [2]. Hexagonal silicon (Si-IV) is a metastable silicon phase that can be synthesized through high-pressure treatment. It shows extraordinary optical properties and great potential for applications. However, its mechanical properties, critical for its applications, have not been experimentally studied yet. We investigated the mechanical properties of Si-IV by combining nanoindentation and in situ high-pressure synchrotron X-ray diffraction. The results suggest that the elastic moduli and hardness of Si-IV are close to those of the diamond cubic silicon. The similar mechanical properties of Si-IV and diamond cubic silicon are beneficial for integrating Si-IV into conventional Si-based devices using similar industrial processing and for its photovoltaic and optoelectronic applications.

[1] Zhidan Zeng, Jianguo Wen, Hongbo Lou, Xin Zhang, Liuxiang Yang, Lijie Tan, Benyuan Cheng, Xiaobing Zuo, Wenge Yang, Wendy L. Mao, Ho-kwang Mao, Qiaoshi Zeng (2022). *Nature*, **608**, 513.
[2] Tao Liang, Lianghua Xiong, Hongbo Lou, Fujun Lan, Junran Zhang, Ye Liu, Dongsheng Li, Qiaoshi Zeng, Zhidan Zeng (2022). *Scripta Materialia*, **220**, 114936.

A045-04-260823

Visible piezochromic response in a salicylideneaniline crystal under high pressure

B. Vatsha,[a*] M. Fernandes,[b] A. Lammerer,[b] G. R. Hearne[c]

[a]Research centre for synthesis and catalysis, Department of Chemical Sciences, University of Johannesburg, PO Box 524, Auckland Park 2006, South Africa.
[b]Molecular Sciences Institute, School of Chemistry, University of the Witwatersrand, Johannesburg 2050, South Africa.
[c]Department of Physics, University of Johannesburg, PO Box 524, Auckland Park 2006, South Africa.

bvatsha@uj.ac.za

Keywords: high pressure, crystallography, sensor crystals

Piezochromic materials respond to environmental stimuli by changing color or otherwise changing their appearance. The development of these promising materials for numerous applications, including pressure sensors, fluorescent switches, and optical devices, has been greatly sparked by this [1]. In order to understand how materials, react to other environmental stimuli, such as light and temperature, non-covalent interactions are constantly being investigated. One of the most extreme natural external stimuli is pressure, which has a substantial impact on how molecules interact and/or can break or establish new chemical bonds [2]. Herein, we describe a rapid mechanical reaction of 2,5-dichlorosalicylideneanilinebenzonitrile (**1**) that was further studied by single crystal X-ray diffraction (SCD) and ^{1}H and ^{13}C-NMR spectroscopy. Slow evaporation in acetonitrile produced single crystals of **1**, which were found to assemble in a monoclinic crystal system with space group $P2_1/n$. The single crystal was then loaded into a diamond anvil cell (DAC) for *in-situ* SCD analysis under various pressures (0 - 5.5 GPa). These findings, shown in Fig. 1, demonstrate how the color changes as pressure is increased. In-depth SCD analyses were performed to comprehend the pressurised crystal structures of **1**. The *a* and *b* axes of crystal **1** progressively shortened, along with a parallel contraction in the volume of the unit cell. The *b* axis response, however, was quite sluggish and much less change. These pressure-induced changes also involved shortening of the intermolecular interactions as determined by Hirshfeld surface analysis. The remarkable chemical stability established by *in-situ* SCD, the reversible color change, and compressibility all shed new insight on the possible sensor applications of crystal **1**.

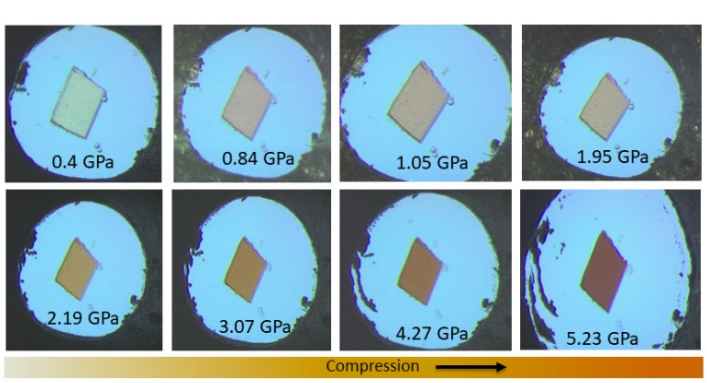

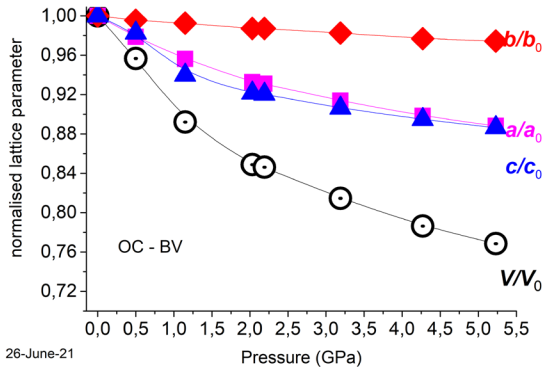

Figure 1. Digital images of crystal **1** (left) showing reversible color change under compression in the DAC at the pressure ranges of 0 – 5.23 GPa and (right) contraction of unit cell axes as pressure is increased.

[1] Andrzejewski, M., & Katrusiak, A. (2017). *J. Phys. Chem. Lett.*, **8**(1), 279.
[2] Collings, I. E., & Goodwin, A. L. (2019). *J. Appl. Phys.*, **126**(18), 181101.

A045-05-260823

Crystal and magnetic structures of $La_2O_3(Fe_{1-x}Mn_x)_2Se_2$ (x = 0, 0.5) under high pressure

K. Prokeš[1] and T. Hansen[2]

[1] Helmholtz Zentrum Berlin, Hahn-Meitner-Platz 1, D-14109 Berlin, Germany, [2] Institut Laue-Langevin, 71 avenue des Martyrs, CS 20156, 38042 GRENOBLE Cedex 9, France

Keywords: high pressure, antiferromagnetic structure, frustration

$La_2O_3(Fe_{1-x}Mn_x)_2Se_2$ (x=0, 0.5) tetragonal systems (space group I4/mmm that are not superconducting) are closely related to very intensively studied superconducting iron pnictides and chalcogenides. In the known iron pnictide and chalcogenide systems the Fe ion is tetrahedrally coordinated [1,2] and the environment is non-planar. The superconductivity in the latter systems appear either under pressure or via substitutions which alters the local Fe geometry. A large number of studies show that the highest superconducting phase transitions are achieved for X-Fe -X (X = pnictide/chalcogenide atom) bond angle that is close to the ideal value of 109.47 degrees. In $La_2O_3(Fe_{1-x}Mn_x)_2Se_2$, Fe has a planar Fe–O coordination with an additional non-planar Fe–Se bonding forming the iron oxyselenide layer as displayed in Fig. 1. $La_2O_3Fe_2Se_2$ is reported to be a Mott insulator and shows an AF magnetic order with a transition just below 90 K [3]. Magnetic order of $La_2O_3FeMnSe_2$ occurs around the same temperature.

It was hoped that a doping or an application of pressure could induce superconductivity. Doping did not lead to such a discovery. Pressure studies are, however, scarce in the literature. Consecutively, not much is known as how magnetic structures that are observed under ambient conditions develop under applied pressure. In fact, there is still some controversy regarding the ambient magnetic structure of x = 0 sample (propagation vector $q_{x=0}$ = (½ 0 ½)) that is reported to be either collinear (shown in Fig. 1 right panel) or non-collinear (2-k structure characterized by two propagation vectors $q_{x=0}$ = (½ 0 ½) and $q'_{x=0}$ = (0 ½ ½)) with Fe moments directed along two a-axis directions [5]. The x = 0.5 sample has the magnetic unit cell of the same size as the crystallographic unit cell.

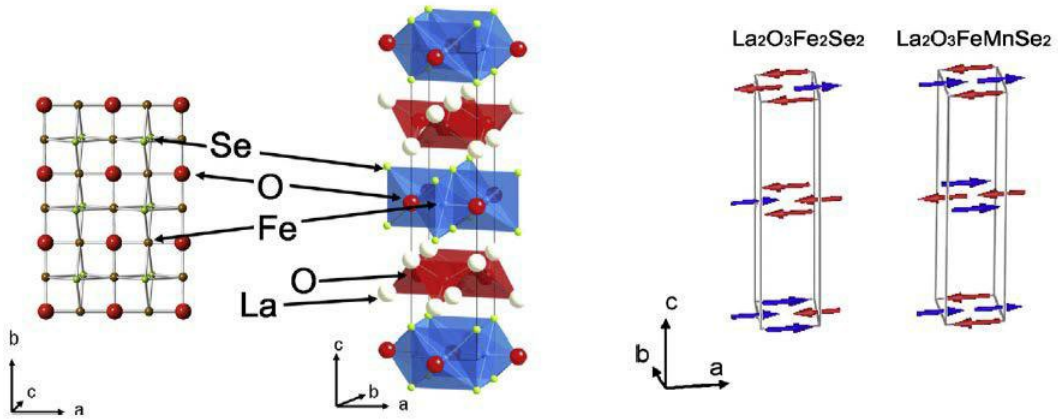

Figure 1. Left: Crystal structure of $La_2O_3Fe_2Se_2$. Right: Collinear antiferromagnetic structures $La_2O_3(Fe_{1-x}Mn_x)_2Se_2$ (x=0, 0.5) systems.

In this contribution we report the influence of high pressure up to 9 GPa on two oxyselenide $La_2O_3(Fe_{1-x}Mn_x)_2Se_2$ (x=0, 0.5) systems at low temperatures down to ~5 K using neutron powder diffraction. It appears that neither of the two system undergo a structural transition. However our results suggest that pressure influences strongly the lattice parameters and hence also atomic bonds. For instance, for the x = 0.5 sample, while the c axis parameter decreases at a rate of ~ -0.13 Å/GPa, the a axis parameter only at a rate of ~ -0.006 Å/GPa resulting to a reduced c/a ratio at high pressure. This, in turn, with the La and Se positional paremeters changing only marginally, leads to a modified atomic distances and bonding angles involving Fe/Mn. Notably, the Se-Fe/Mn and La-Fe/Mn distances decrease significantly, but the angle Fe/Mn-Se -Fe/Mn increases from 96.1 at ambient pressure [3] to 98.1 degrees at 7.8 GPa, still well below the ideal value of 109.47 degrees. However, we show that the application of pressure leads to a significant increase of the magnetic phase transition for both systems at a rate of ~ 2 K/GPa.

[1] Y. Kamihara et al., J. Am. Chem. Soc. **130**, (2008) 3296
[2] P.M. Aswathy et al., Superc. Sci. Technol. **23**, (2010) 073001
[3] D.G. Free et al., Phys. Rev. B **81**, (2010) 214433
[4] S. Landsgesell, et al. Acta Materialia **66**, (2014) 232

[5] E. E. McCabe, et al., Phys. Rev. B **89**, (2014) 100402(R)

A045-06-260823

Dual-cell, high-pressure studies of porous, flexible frameworks from 20 to 30,000 bar

D.J. Ashworth,[1] T.M. Roseveare,[2] E.J. Carrington,[2] C.J. McMonagle,[3] M.R. Warren,[4] A.J. Fletcher,[1] S.A. Moggach,[5] I.D.H. Oswald,[1] L. Brammer[2]

[1]University of Strathclyde, Glasgow, UK; [2]University of Sheffield, Sheffield, UK; [3]European Synchrotron Research Facility, Grenoble, France; [4]Diamond Light Source, Didcot, UK; [5]The University of Western Australia, Perth, Australia
david.ashworth@strathclyde.ac.uk

Keywords: metal-organic framework, high-pressure, structural dynamics

Metal-organic frameworks (MOFs) are at the heart of porous materials research, due predominantly to the framework pore spaces accessible after activation for molecular adsorption. Most research in this area has centred on rigid MOFs; we are still at the beginning, however, of understanding structure-property relationships of flexible framework materials. Increasing numbers of MOFs are being investigated in relation to their dynamic deformation under various external stimuli such as temperature or pressure [1], in order to map out structure-property relationships for utility in various applications including gas separations.

The SHF (Sheffield Framework) family of MOFs [2,3] are a series of two-fold interpenetrated diamondoid indium-based frameworks with aminoterephthalate-based organic linkers (Figure 1a,b). The parent SHF-61 MOF exhibits large-amplitude continuous 2D "breathing" with a *pseudo*-wine rack motion, as well as prominent host-guest chemistry which leads to gas separation capabilities [2]. Post-synthetic modification of the pendant amine groups to form acetamide yields the MOF SHF-62, which exhibits 3D breathing behaviour, where channel-length expansion/compression accompanies the dynamic deformation of channel cross-section [3]. Recently, the family has been extended through a series of cation-exchanges, whereby the parent dimethylammonium can be exchanged for larger cations, which has implications for the dynamic range of the materials. The large-amplitude dynamic motion observed upon removal/uptake of guest molecules raised questions around the structural response of these materials to other external stimuli, namely *pressure*.

In this work, we used a combination of different pressure cells to facilitate X-ray diffraction studies of SHF MOFs across multiple pressure ranges. A recently-developed sapphire capillary liquid-pressure cell [4] facilitated visualisation of the initial framework deformation at a mid-pressure range (20-1,500 bar), before higher pressure ranges were reached using the more commonly utilised diamond anvil cell (~0.1–3 GPa; 1,000–30,000 bar) (Figure 1c). Marked differences in framework behaviour were observed between using framework-penetrating and non-penetrating pressure-transmitting media (Figure 1d). This combination of pressure cells enables a uniquely detailed insight into the nuances of the dynamic response of these flexible frameworks across a wide pressure range.

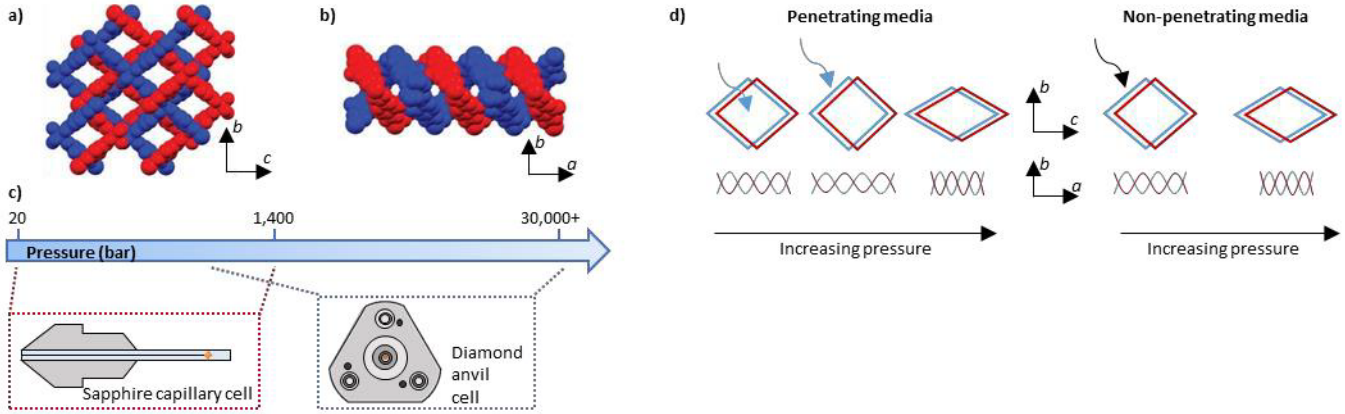

Figure 1. View down the a) *a*-axis and b) *c*-axis of the SHF-61 MOF; c) pressure ranges accessed with sapphire capillary and diamond anvil cells; d) schematic of framework deformations under from pressure.

[1] Vervoorts, P., Stebani, J., Mendez, A.S.J., Kieslich, G. (2021) *ACS Materials Lett.,***3**, 1635.
[2] Carrington, E.J., McAnally, C.A., Fletcher, A.J., Thompson, S.P., Warren, M.R., Brammer, L. (2017) *Nat. Chem.,* **9**, 882.
[3] Carrington, E.J., Dodsworth, S.F., van Meurs, S., Warren, M.R., Brammer, L. (2021) *Angew. Chem. Int. Ed.,* **60**, 17920.
[4] McMonagle, C.J., Allan, D.R., Warren, M.R., Kamenev, K.V., Turner, G.F., Moggach, S.A. (2020) *J. Appl. Cryst.,* **53**, 1519.

We acknowledge support from EPRSC (EP/T034068/1, EP/T034130/1, EP/T034114/1) and beamtime at Diamond Light Source.

A052 Year of Mineralogy
Room 216
1.10pm - 3.30pm

A052-01-260823

A historic perspective of the description of Gaylussite ($Na_2Ca(CO_3)_2 \cdot 5H_2O$) and synchrotron radiation study of a 200 year-old specimen from Mérida, Venezuela.

J.M. Delgado1, A. Dugarte-Dugarte1, G. Díaz de Delgado1, A. Fitch2, C. Dejoie2

1Laboratorio de Cristalografía-LNDRX, Facultad de Ciencias, Universidad de Los Andes, Mérida, Venezuela, 2ESRF, 71 Avenue des Martyrs, CS40220, 38043 Grenoble Cedex 9, France.

jmdq2000@gmail.com, migueld@ula.ve

Keywords: Gaylussite, carbonate minerals, Venezuela

The mineral gaylussite, $Na_2Ca(CO_3)_2 \cdot 5H_2O$, was first identified from samples obtained in 1823 by the French chemist Jean-Baptiste Boussingault and the Peruvian mining engineer and chemist Mariano de Rivero during an expedition to Colombia and Venezuela [1]. The mineral samples were collected from Laguna de Urao, a salt lake in Lagunillas, Mérida state, Venezuela. The German naturalist A. von Humboldt and the Venezuelan patriot, naturalist, and diplomat Manuel Palacio Fajardo had previously studied mineral samples from this site. The new mineral, the first discovered in Venezuelan territory, was name by Boussingault *gaylussite*, in honor of the eminent French chemist. The complex thermal and hydration/dehydration behavior of gaylussite has been the subject of different studies, aimed at understanding the chemical and crystallographic relationship with other naturally occurring carbonates. However, most of the studies have been carried out on synthetic gaylussite. There are conflicting reports on the formation of the intermediate hydrate *pirssonite*, $Na_2Ca(CO_3)_2 \cdot 2H_2O$, the low temperature (orthorhombic) and high temperature (hexagonal) anhydrates *nyerereite*, $Na_2Ca(CO_3)_2$.

The gaylussite specimen ENSMP 37496 (collected in 1823 by Boussingault) was an irregular cylinder-like grey fragment of 1.5x0.5 mm approximately. A white, powdery material easily disintegrated from the fragment upon handling. It was gently ground in an agate mortar and used to fill a 1.0 mm borosilicate capillary. High resolution X-ray powder diffraction patterns were collected at the ID22 beamline of ESRF. A Search/Match analysis using the PDF-4+ database [2] and a subsequent Rietveld analysis with TOPAS-Academic [3] indicated the presence of aragonite (29.2%), calcite (2.6%) and, surprisingly, sodium acetate trihydrate (67.9%). A small amount of quartz (0.3%) was also identified. These results prompted the examination of an inner section of the specimen which was carefully scrapped to eliminate material deposited on the surface. The analysis of this sample indicated a 46.5% of aragonite, 42.3% of $Na(CH_3COO) \cdot 3H_2O$, 0.3% of quartz, and 10.9% of gaylussite. It must be noted that calcium acetate efflorescence (as $Ca(CH_3COO)_2 \cdot H_2O$ or $Ca(CH_3COO)_2 \cdot 1/2H_2O$) has been extensively reported in calcareous museum objects stored for long periods of time [4,5] due to emission of acetic and formic acid from wood (particularly oak) cabinets [6]. However, $Na(CH_3COO) \cdot 3H_2O$ efflorescence has been reported mainly for glass objects. Upon heating at 650 °C, the Mérida sample shows decomposition to the high temperature phase of nyerereite, $Na_2Ca(CO_3)_2$, which is hexagonal. Upon cooling to ambient temperature, the low temperature orthorhombic form of nyerereite is obtained. For comparison, a study of specimen ENSMP 53763 from Lake Magadi (Kenya) indicated that this sample is almost pure gaylussite. No sodium or calcium acetate efflorescence is observed. The thermal decomposition was followed in situ by registering powder diffraction patterns every 10 °C from 20 to 650 °C. Pirssonite ($Na_2Ca(CO_3)_2 \cdot 2H_2O$) forms at approximately 120 °C, low-temperature nyerereite forms at 300 °C, and high-temperature nyerereite starts to form at around 430 °C. Above 450 °C only HT-nyerereite is present and, upon cooling, LT-nyerereite forms and remains at ambient temperature.

[1] Boussingault, J. B. (1826) *Ann. Chim. Phys.* **31**, 270-276.
[2] Gates-Rector, S. & Blanton, T. N. (2019) *Powder Diffr.* **34**, 352-360.
[3] Coelho, A. A. (2016) TOPAS-Academic version 6. Coelho Software, Brisbane, Australia.
[4] Byne, L. F. G. (1899) J. Conchol., **9**, 172–178.
[5] Tennent, N. H. & Baird, T. (1985) Stud. Conserv., **30**, 73–85.
[6] Gibson, L. T. & Watt, C. M. (2010) Corros. Sci., **52,** 172–178

We are grateful for the support of *LAAAMP* through a *FAST* Team award and to the STREAMLINE Insight Programme at ESRF. We also thank Dr. E. Gaillou and *Musée de Minéralogie MINES Paris* for providing the gaylussite specimens ENSMP 37496 (Venezuela) and ENSMP 53763 (Kenya) for this study.

A052-02-260823

Mineralogy2022 – a year to celebrate mineralogy

Razvan Caracas[1,2], Patrick Cordier[3,4]

Institut de Physique du Globe de Paris, Université Paris Cité, CNRS, 1 rue Jussieu Paris, France

[1] Center for Earth Evolution and Dynamics, Center for Planetary Habitability, University of Oslo, Oslo, Norway

Unité Matériaux et Transformations, Université de Lille, 59655 Villeneuve d'Ascq, France

4. Institut Universitaire de France, Paris, France

caracas@ipgp.fr

Keywords: Mineralogy, Haüy, International Year

The International Mineralogical Association declared 2022 the Year of Mineralogy. This marks a special year in the history of mineralogy: the bicentennial of the death of René Just Haüy (born 1743), who is a father of modern mineralogy and crystallography. 2022 is also 200 years after Haüy's Traité de minéralogie and Traité de cristallographie were published.

Mineralogy2022 was launched during the 23rd general meeting of the International Mineralogical Association, which was held in July 2022 in Lyon, France. With almost 500 participants, the meeting reunited again mineralogists from almost the entire world, Covid and the Ukrainian war restrictions taking a heavy toll on our participation.

Mineralogy is one of the oldest branches of science, it has played a key role in the deciphering of the structure of matter and in the development of science and technology. Ever since the stone age, humanity relied on mineralogy and geology to provide the raw materials for tools and technology. Mineralogy was always critical for identifying, characterizing, and extracting the minerals and elements necessary for our applications. With time history and mineralogy evolved hand in hand. Today, we cannot imagine living in a world devoid of high-end technology. Without a deep understanding of mineralogy, it would be close to impossible to obtain the raw materials needed for the technologies that are essential to our modern way of life. In recognition of the fundamental place of mineralogy in the basic sciences, Mineralogy2023 has been approved by UNESCO as part of the International Year of Basic Sciences for Sustainable Development (IYBSSD 2022)

Hence, Mineralogy2022 was a worldwide celebration of this discipline which has highlighted its importance in our everyday lives. While its official closure coincides with the IUCr 2023 meeting, we wish for its spirit to be long-lasting and over-reaching.

The major objectives of Mineralogy2022 were:

- to generate public interest for the science of matter and how it underpins most innovations and developments in our modern society;
- through the fascination of natural crystals to attract young people to science;
- to illustrate the universality of science;
- to intensify the emergence of mineralogical societies in developing countries where resources are exploited;
- to foster international collaboration between scientists worldwide, especially by building North–South networks and South-South collaborations;
- to promote education and research in mineralogy, crystallography and their links to other sciences;
- to increase public awareness of the importance of natural resources.

Here, we will try to outline a few major realizations of modern mineralogy, to present some of the latest mineralogical developments, and to bring in the attention of the general public some of the most remarkable on-going efforts related to the mineralogical sciences.

A052-03-260823

From fundamental discoveries to the impact of minerals on our daily lives: An essay to celebrate the International Year of Mineralogy

L. Bindi[1] & G. Cruciani[2]

[1]*Department of Earth Sciences, University of Florence, Via La Pira 4, I-50121 Florence, Italy* [2]*Department of Physics and Earth Sciences, University of Ferrara, Via Saragat 1, I-44122 Ferrara, Italy giuseppe.cruciani@unife.it*

Keywords: mineralogy, discoveries, crystallography

Minerals have played a critical role in shaping our planet and have been a source of inspiration for scientific and technological advancements since the beginning of time, from the formation of the Universe and Earth to the appearance of humans throughout history. The regular shapes of natural crystals sparked the first form of scientific curiosity, and René Just Haüy (1743-1822), a renowned mineralogist, marked a significant milestone in the field by laying the foundations of modern crystallography. In 2022, coinciding with the bicentenary of Haüy's death, the Year of Mineralogy presented an opportunity to compile some of the most important advances and fundamental discoveries of recent decades in one book [1]. The book encompasses a wide range of topics, including the discovery of fullerenes and quasicrystals in nature, minerals found in a near-Earth asteroid sample, and the advent of "mineral evolution" and mineral informatics. It also explores the structural and chemical complexity of minerals and the role of hydrogen as the principal agent of mineral diversity. Other areas of interest include the experimental discovery of mineral phases at high pressure and high temperature, the stability of hydrogen-bearing silicates under deep-Earth water conditions, and diamonds as windows into the Earth's interior. The mineralogy of planetary cores and the prediction of HP-HT Earth and planetary materials are also discussed. The impact of discoveries in mineralogy on human life is examined, discussing how mineralogy has revolutionized many areas of basic and applied science. The chapters offer compelling scientific adventures characterized by curiosity, persistence, intuition, and perseverance, driven by emotions. The book underscores the power of individuals, research groups, and the international scientific community in terms of comparison, sharing, and collaboration. Advances in mineralogy are intrinsically linked to the advancement of analytical techniques, including electron microscopy and the use of laser beams and large-scale radiation facilities for a wide range of spectroscopic and scattering methods. The book highlights mineralogy's unique attitude in building bridges with other disciplines, including physics, chemistry, material sciences, catalysis, metallurgy, archaeology, and biology.

This talk will provide an overview of the most significant discoveries and breakthroughs in mineral sciences, with a focus on minerals that have had a tangible impact on our everyday lives. Examples of mineralogy-related discoveries that have affected climate change, energy, industrial applications, health, and the environment will be discussed, along with mention of future opportunities in a sustainable changing world. An in-depth examination will be devoted to zeolites, both natural and synthetic, which are considered to be some of the most significant past, present, and future mineral discoveries.

[1] Luca Bindi and Giuseppe Cruciani Eds., Celebrating the International Year of Mineralogy: Progress and Landmark Discoveries of the Last Decades, Springer Mineralogy Series, eBook ISBN 978-3-031-28805-0, Hardcover ISBN 978-3-031-28804-3, Due: 03 June 2023, https://link.springer.com/book/9783031288043

A066 Subperiodic Symmetry Groups and their Applications
Room 217
1.10pm - 3.30pm

A066-01-260823

Perfect precise colorings of plane semiregular tilings

Manuel Joseph C. Loquias and Rovin B. Santos

University of the Philippines Diliman

rbsantos8@up.edu.ph

Keywords: semiregular tilings, hyperbolic tilings, perfect colorings, precise colorings

Aside from their aesthetic and mathematical appeal, symmetrically colored tilings have been studied because of their applications in crystallography and materials science. Of particular interest are perfect colorings of tilings, that is, colorings where every symmetry of the uncolored tiling sends all tiles of a given color to tiles of the same color [1, 2]. In addition, colorings of patterns in the hyperbolic plane have garnered attention because of their connection with quasicrystals and structural chemistry.

The term *precise coloring* was coined by Rigby in [3] to refer to a coloring of the regular triangular tiling (3^7) in the hyperbolic plane in which no two tiles of the same color share a common vertex.

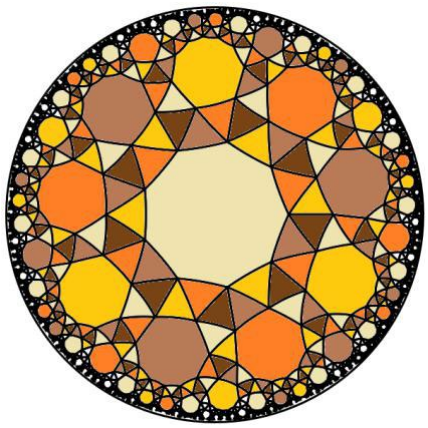

Figure 1. A perfect precise coloring of the tiling (3.3.3.3.9) using 5 colors.

This research is a continuation of work on identifying perfect precise colorings of planar tilings in [4, 5]. We demonstrate how to obtain perfect precise colorings with k colors of some families of plane semiregular k-valent tilings where $k \leq 6$. These colorings were generated using a combinatorial approach and are verified to be perfect through group-theoretic reasoning. Most of the Archimedean tilings considered by Crowe in [4] fall under the more general class of semiregular tilings examined in this work, and his findings become special cases of results in this paper.

[1] Frettlöh, D. (2001). Counting perfect colourings of plane regular tilings. *Z. Krist*. **223** (11-12).
[2] Junio, A. and Walo, M.L. (2019). Perfect colorings of patterns with multiple orbits. *Acta Crystallogr. Sect. A* **75** (6), 814-826.
[3] Rigby, J.F. (1997). Perfect precise colourings of triangular tilings, and hyperbolic patchwork. *Symmetry Cult. Sci.* **8**, 265-288.
[4] Crowe, D.W. (1999). Perfect precise colorings of Archimedean tessellations. *Vis. Math*. 1 (1) 9 HTML documents; approx.10.
[5] Santos, R. and Felix, R.P. (2011). Perfect precise colourings of plane regular tilings. *Z. Krist.* **226** (9) 726-730.

A066-02-260823

Layer groups associated with 2-way 2-fold fabrics

M. Tomenes* and M. L. A. N. De Las Peñas

Department of Mathematics, Ateneo de Manila University, Philippines

mark.tomenes@obf.ateneo.edu

Keywords: layer group, 2-way 2-fold fabric, symmetry group

The symmetry operations of an object in three-dimensional space form a *layer group* if it has translational symmetry only in two dimensions. In the literature, layer groups are often used to describe the symmetry groups of crystal structures [3].

Layer groups also describe the symmetry groups of woven fabrics [1]. Consider for example the *2-way 2-fold fabric* $\mathscr{F}$ shown in Figure 1a, where the strands have two directions: warp-horizontal and weft-vertical; and are at right angles to each other (2-way); with no more than two strands crossing each other (2-fold). The symmetries of $\mathscr{F}$ are marked with an oval (2-fold rotation), hollow circle (inversion), solid line (reflection) or arrows (2-fold rotation, 2-fold screw rotation or glide reflection) in Figure 1a. The side preserving symmetries of $\mathscr{F}$ are the 2-fold rotations with axes perpendicular to $\mathscr{F}$ and horizontal reflections, which send the front of
[6] to its front; whereas the side reversing symmetries are the inversions, 2-fold rotations with axes lying on $\mathscr{F}$, 2-fold screw rotations and glide reflections, which send the front of $\mathscr{F}$ to its back. This particular fabric has symmetry group the layer group in IUCr notation [2].

This study pertains to the characterization of the various layer groups that occur as symmetry groups of 2-way 2-fold fabrics via color symmetry theory. Here, the setting is such that a 2-way 2-fold fabric is represented by a *design*, which is a black and white coloring of a square tiling. A black colored tile means that the vertical strand passes over the horizontal strand and a white square means that the horizontal strand passes over the vertical strand. The three-dimensional symmetries of the fabric are arrived at by determining the color symmetries of its corresponding design. For instance, the design of $\mathscr{F}$ is shown in Figure 1b. The color symmetries that either interchange black or white or fix the colors constitute the two-dimensional crystallographic group 2 with lattice as shown. Each of the color symmetries correspond to the three dimensional elements of the layer group exhibited on the left.

In the talk we present all the color symmetry structures of the designs corresponding to two-way two-fold fabrics that have been derived, with their layer group structures.

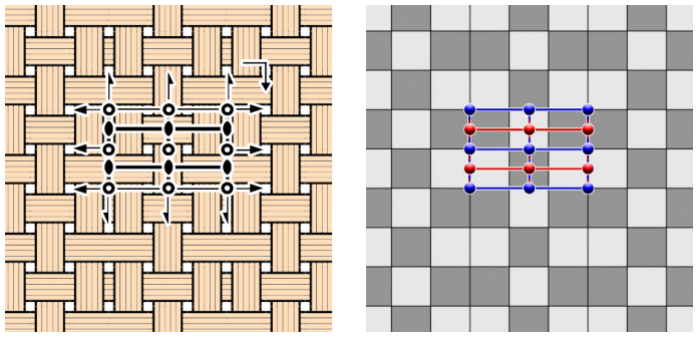

(a) (b)

Figure 1. (a) A 2-way 2-fold fabric with the lattice diagram of its symmetry group; and (b) its design with the lattice diagram of its color group.

[1] Hammond, C. (2015). *The Basics of Crystallography and Diffraction Fourth Edition*. Oxford: Oxford University Press.
[2] Kopský, V. & Litvin, D. B. (2002). *International Tables for Crystallography Volume E*. Dordrecht: Kluwer Academic Publishers.
[3] Müller, U. (2013). *Symmetry Relationships between Crystal Structures: Applications of Crystallographic Group Theory in Crystal Chemistry*. Oxford: Oxford University Press.

A066-03-260823

Topology Conservation Theorem, Quantum Instability and Violation of Subperiodic Symmetry of Complex Low-Dimensional Lattices

P. Avramov

Department of Chemistry, Kyungpook National University, Daegu, South Korea

Keywords: Topology Conservation Theorem, Quantum Instability, Violation of subperiodic symmetry

Topological and quantum instability and violation of subperiodic symmetry of complex low-dimensional crystals is studied using theoretical analysis and multilevel simulations. It is demonstrated that complex low-dimensional lattices are prone to structural deformations caused by linear periodic boundary conditions (PBC). To impose PBC mandatory limitations for complex low-dimensional lattices, the Topology Conservation Theorem (TCT) is formulated as: "To conserve the planar topology of one- or few-atomic layer one-unit-cell-thick low-dimensional crystals with small or zero stabilizing force constants acting in the perpendicular direction to the lattice plain, and to avoid uncompensated mechanical stress, the free-standing constituting fragments (unit cells) must perfectly fit planar low-dimensional space. Due to the leading contribution of the stretching force constants to the total energy, mechanical stress accumulated by small regular structural mismatch of planar structural units should be compensated by out-of-plane structural deformations coupled with either multiplication of translation periods or breakdown of periodicity in one or two dimensions."

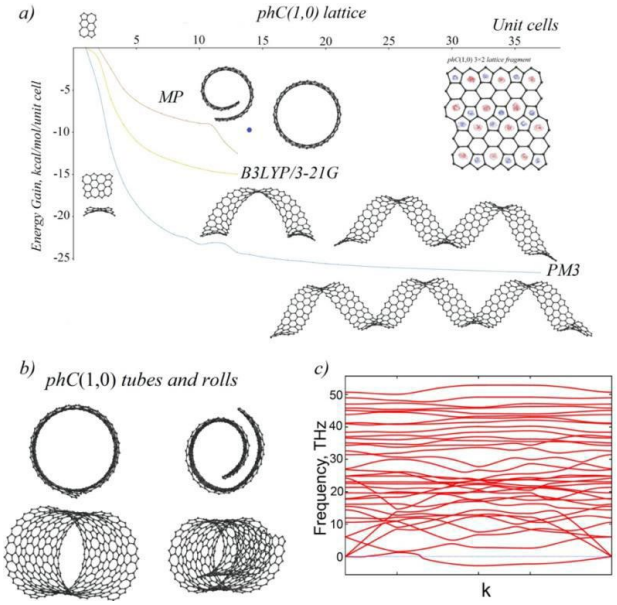

Figure 1. Violation of subperiodic symmetry of *phC(1,0)* lattice.

It is shown that the lack of perfect filling of planar low-dimensional crystalline space may cause the formation of i) Structure waves of either variable or constant wavelength; ii) Nanotubes or rolls; iii) Saddle structures; iv) Aperiodic ensembles of irregular asymmetric atomic clusters; v) Stabilization of 2D lattices by aromatic resonance, correlation effects, or van-der-Waals interactions. The effect of quantum instability of infinite structural waves is studied using quasiparticle approach. It is found that both perfect finite-sized and stabilized structural waves can exist. It is shown that for low-dimensional lattices prone to breakdown the translation invariance (TI), complete active space of normal coordinates cannot be reduced to a subspace of TI normal coordinates. As a result, constrained TI subspace structural minimization may artificially return a regular point at the potential energy surface as global/local minimum/maximum. It is proved that for such lattices, phonon dispersion cannot be used as solid and final proof of either their stability or metastability. It is shown that ab initio molecular dynamics (MD) PBC Nosé-Hoover thermostat algorithm constrains the linear dimensions of the periodic slabs preventing their thermostated equilibration. Based on rigorous TCT analysis, a flowchart algorithm for structural analysis of low-dimensional crystals is proposed and proved to be a powerful tool for theoretical design of advanced complex nanomaterials.

Study was supported by the National Research Foundation of the Republic of Korea funder the grant NRF 2021R1A2C1010455

A066-04-260823

Crystallography online by the Bilbao Crystallographic Server: new online programs for the analysis of the symmetry of low-dimensional materials

M. I. Aroyo[1], L. Elcoro[1,3], G. de la Flor[2], G. Madariaga[1,3]

[1]Departamento de Física, Universidad del País Vasco UPV/EHU, E-48080 Bilbao, (Spain), [2]Institute of Applied Geosciences, Karlsruhe Institute of Technology, Karlsruhe (Germany), [3]EHU Quantum Center, University of the Basque Country, UPV/EHU, E-48080 Bilbao, (Spain) Email: mois.aroyo@ehu.es

Keywords: Bilbao Crystallographic Server, subperiodic groups, scanning tables for layer and rod groups

Subperiodic crystallographic groups have gained significant relevance in recent years, due to the growing interest in the study of lower dimensionality compounds with potential technological applications, whose symmetry is given by the so-called *layer* and *rod groups*, three-dimensional groups in which the periodicity has been reduced to 2 and 1 dimensions, respectively. These groups are tabulated in the *International Tables of Crystallography,* Volume E: *Subperiodic groups* [1] (hereafter referred to as *IT*E). The *Bilbao Crystallographic Server* (www.cryst.ehu.es) [2-3] (hereafter referred to as BCS) gives *online* access to the crystallographic subperiodic groups databases, which includes information on generators and general positions (GENPOS), Wyckoff positions (WYCKPOS) and maximal subgroups (MAXSUB) for layer, rod and frieze groups. This database expands and complements the symmetry information provided in the print edition of *IT*E. The BCS also host the Brillouin-zone database (LKVEC) for layer groups [4].

The identification of the layer symmetry in a periodic section, defined by an arbitrary reciprocal vector perpendicular to it, requires the use of the so-called *scanning tables* [5]. To the best of our knowledge, there are not such tables to determine the so-called *penetration rod groups symmetries*. For this reason, the programs SECTIONS and RODS were recently developed in BCS in order to perform these types of calculations. The input of the programs only requires the space group number or a set of generators of the space group of the 3D structure, and the reciprocal direction normal to the layer or the direction of penetration (and a reference point in the unit cell). The program accepts as input a space group given in any arbitrary setting. The output includes the number and Hermann-Mauguin symbol of the layer (or rod) group as given in [1], as well as its general position, both in the basis chosen by the user and in the standard basis, along with the transformation matrix that relates both bases. Optionally, additional and more technical information related to the so-called *scanning group* is displayed to the user, thus retrieving the entire information contained in the scanning tables [5]. SECTIONS also allows the generation, restricted to certain normal vectors, of an inverse database to find which space groups, in their standard setting, are compatible with a certain layer symmetry, also in the standard setting. All these programs are available in the section of BCS dedicated to subperiodic groups (www.cryst.ehu.es/#subperiodictop).

[1] *International Tables for Crystallography*, Volume E: *Subperiodic groups*. Eds. V. Kopský and D. B. Litvin (2010). Dordrecht, Boston, London: Kluwer Academic Publishers.

[2] Aroyo, M. I., Perez-Mato, J.M., Capillas, C., Kroumova, E., Ivantschev, S., Madariaga, G., Kirov, A. and Wondratscheck H. (2006). *Z. Krist.* **221**, 15-27.

[3] Aroyo, M. I., Perez-Mato, J. M., Orobengoa, D., Tasci. E., de la Flor, G. and Kirov A. (2011). *Bulg. Chem. Commun.* **43**(2), 183-197.

[4] de la Flor, G., Souvignier, B., Madariaga, G. and Aroyo, M.I. (2021). *Acta Cryst*. A**77**, 559–571

[5] Kopský, V. and Litvin, D. B. (2010). *International Tables for Crystallography*, Volume E: *Subperiodic groups*. ch. 5.2, pp. 395-420. Dordrecht, Boston, London: Kluwer Academic Publishers.

A073 Transient Phenomena and in Operando Experiments and Modelling
Room 220
1.10pm - 3.30pm

A073-01-260823

In-situ mechanistic studies of two divergent synthesis routes forming the heteroanionic BiOCuSe

Laura C. Folkers[1], Mercouri G. Kanatzidis[2]

[1]*STOE & Cie GmbH, Darmstadt, Germany,*

[2]*Department of Chemistry, Northwestern University, Evanston, Illinois 60208, United States*

folkers@stoe.com

Keywords: Chemical reactions, Materials, Precursors

The homoleptic thermoelectric BiOCuSe crystallizes in the ZrCuSiAs structure type [1] featuring alternating insulating $[Bi2O2]^{2+}$ and conductive $[Cu2Se2]^{2-}$ layers. Since many synthesis protocols lead to the segregation of $[Bi2O2]^{2+}$ and $[Cu2Se2]^{2-}$, the reactions leading to alternating layers need to be understood to provide mechanistic insight. Therefore, two solid state reactions with different starting materials have been monitored by temperature resolved powder X-ray diffraction (PXRD). Syntheses either begin with the complex precursors Bi2O2Se and Cu2Se, or Bi2O3 and pure Bi, Cu and Se. While both reactions result in BiOCuSe, the complex precursor route has a 2.6% lower yield (96.3%) and forms the target phase at 10 K higher temperatures (713 K), than the elemental route (98.9% and 703 K, see Fig. 1).

The complex precursor synthesis progresses without any intermediates and with the advantage of having the same oxidation states as BiOCuSe and the $[Bi2O2]^{2+}$ building block already at hand. While the complex precursor synthesis must start with bond breaking, the synthesis from the elements can immediately begin with bond formation. However, one of the formed intermediates is CuSe which has different oxidation states (Se^{2-}, $Se2^{2-}$, $Cu^{+/2+}$) than BiOCuSe (Cu^{+}, Bi^{3+}, Se^{2-}). A temperature resolved control experiment shows that the synthesis of Cu2Se from pure elements also progresses via CuSe as intermediate, thus explaining its presence in the BiOCuSe reaction. The intermediates Bi2Se3, Bi3Se4, Cu2Se and Bi2O3 appear just before the target phase starts forming, indicating that not only CuSe, but also Bi3Se4 has to undergo a redox reaction to achieve the same oxidation states as in BiOCuSe.

Comparing the two reaction pathways (Fig. 1.) shows that the necessity to melt and recombine the precursors is disadvantageous even in relation to forming various intermediates and having to undergo a redox reaction before forming the target phase. Thus, temperature resolved PXRD teaches us that the reaction passing through fewer intermediates is not always the synthetically preferrable.

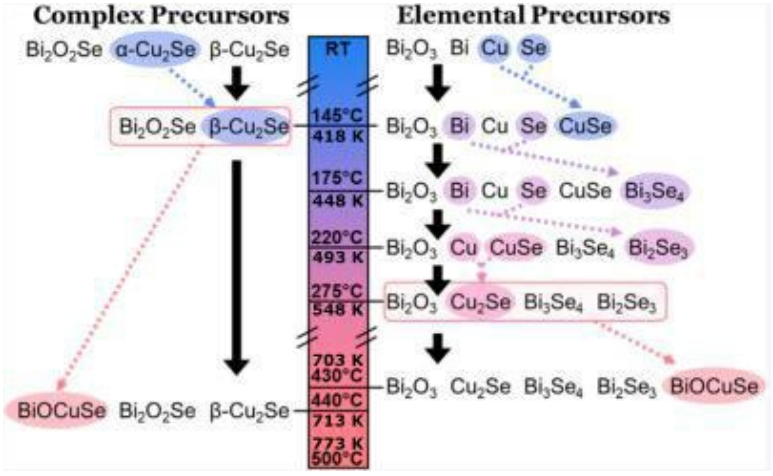

Figure 1:Comparison of the reaction pathways depending on the starting materials. Graphics from [2].

[1] R. Poettgen, D. Johrendt, *Z. Naturforsch., B: J. Chem. Sci.*, **2008**, *63*, 1135−1148.
[2] R. McClain, C. D. Malliakas, J. Shen, C. Wolverton, M. G. Kanatzidis, *J. Am. Chem. Soc.*, **2021**, *143*, 12090-12099.

A073-02-260823

Thermal evolution of electrochemically cycled materials

Junnan Liu[1], Henrik L. Andersen[2], Uttam Kumar[4], Neeraj Sharma[4]

[1.] *Yantai Research Institute & Graduate School, Harbin Engineering University, Yantai Shandong 265501 China*

[2.] *Department of Materials Physics, Complutense University of Madrid, 28040 Madrid, Spain*

[3.] *School of Chemistry, UNSW Sydney NSW 2052, Australia*

Email: neeraj.sharma@unsw.edu.au

Keywords: Batteries, Electrodes, Variable Temperature Diffraction

Lithium-ion batteries are ubiquitous in society in applications ranging from portable electronics to electric vehicles and grid-scale electricity storage. They rely on electrochemical reactions at the electrodes which result in changes in the crystal structure of the active electrode materials via lithium-ion insertion/extraction. This process also changes the composition of the electrodes. From a structural chemistry point-of-view the lithium-ion inserted/extracted compositions are “new” compositions that can be explored, and their phase diagrams mapped. In particular, our work has focused on the temperature dependent structural and phase evolution of the electrodes at various states of lithium-ion insertion/extraction. Similar work can be undertaken in sodium- and potassium-ion batteries and therefore phase space as a function of ion-type, ion insertion/extraction amount and temperature can be elucidated. This presentation will showcase studies of some conventional electrode materials and some more unusual electrodes that we have investigated, highlighting fascinating evolution.

A073-03-260823

In operando inelastic neutron scattering and pair distribution function analysis of water and carbon dioxide adsorption by calcium-based layered double hydroxide

M. Curria[1], C.E. White[1]

[1]*Department of Civil and Environment Engineering, and the Andlinger Center for Energy and the Environment, Princeton University, Princeton, New Jersey, United States*

whitece@princeton.edu

Keywords: inelastic neutron scattering, pair distribution function analysis, layered double hydroxide, gas adsorption, carbon dioxide capture

Layered double hydroxides (LDHs) have gained significant attention across various industries due to their enhanced specific surface area and catalytic activity. Among this family of materials, calcium-based LDH has emerged as a promising candidate for carbon capture applications due to a high density of basic adsorption sites. It is known that H_2O has a significant influence on the CO_2 capture capacity of the material, however, the fundamental mechanisms controlling this behaviour remain elusive. Here, in operando inelastic neutron scattering, in operando X-ray and neutron pair distribution function analysis, and molecular modelling are used to investigate (i) the H_2O adsorption-desorption behaviour of calcium-based LDH and (ii) the impact of adsorbed H_2O on the CO_2 capture mechanism, and (iii) thermal regeneration of the capture material (Fig. 1). Our results reveal that the exposure of calcium-LDH to H_2O and CO_2 can lead to changes in LDH interlayer spacing, coordination environment, and crystallinity. Moreover, by combining density functional theory normal mode analysis with inelastic neutron scattering data we uncover the mechanism by which adsorbed H_2O molecules affect adsorption of CO_2 molecules, and their subsequent molecular interactions with the Ca-based LDH.

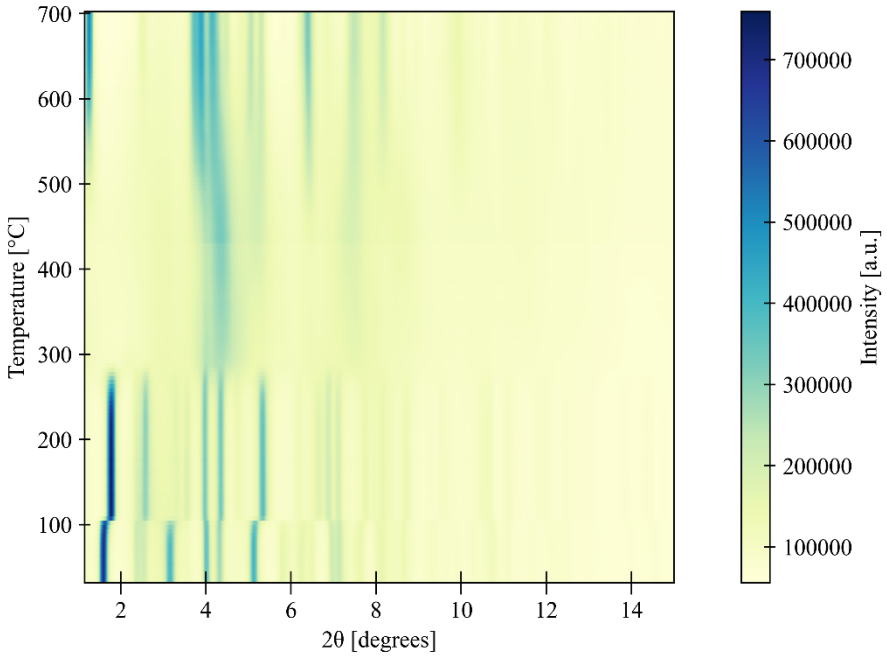

Figure 1. Synchrotron-based X-ray total scattering data of calcium-based layered double hydroxide exposed to elevated temperature (ambient to 700 °C).

A073-04-260823

Watching chemistry happen – dynamic studies on using external stimuli to induce transformation within crystals

M. Warren

Diamond Light Source Ltd., Harwell, Didcot. South Oxfordshire, OX11 0DE. UK.

mark.warren@diamond.ac.uk

Keywords: external-stimuli, light-induced, electric-field

The investigation of short-lived reaction intermediates and transient species upon activation in chemical species is of upmost importance to better understand the pathways in a reaction.

Linkage isomers are complexes that contain an ambidentate ligand that can bond to the metal centre through two or more donor atoms. The ambidentate ligand can be switched from one state to another in response to irradiation, and display a change in the bulk properties e.g. reflective index or colour change. Beamline i19 at Diamond Light Source, in collaboration with Hatcher group at the University of Cardiff have developed time-resolved techniques. Utilising the unique capabilities on the Tristan time-resolved detector (continuous nanosecond readout) to record and entire time series in a single experiment we can obtain structural snap shots of along the reaction pathway [1].

Ferroelectrics materials that have spontaneous polarisation which can be reversed by applying an electric field and have a wide range of potential applications, from memory storage to sensors. A family of hybrid perovskites [2,3] that has the advantage of both organic (low cost) and inorganic (high performance and electrical conductivity), have been shown to display impressive ferroelectric properties, rivalling that of the commonly used barium titanate, BTO. In collaboration with Yeung group at the University of Birmingham we have utilised the same time-resolved techniques to study the response of hybrid perovskites using Beamline i19 electric field cell [4] and Tristan time-resolved detector to better understand the materials' structural dynamics and domain relaxation.

[1] Hatcher, L. E., Warren, M. R., Skelton, J. M., Pallipurath, A. R., Saunders, L. K., Allan, D. R., Hathaway, P., Crevatin, G., Omar, D., Williams, B. H., Wilson, C. C.,Raithby, P. R, *Comm. Chem.*, (2022) **5**, 102
[2] W. Y. Zhang, Y. Y. Tang, P. F. Li, P. P. Shi, W. Q. Liao, D. W. Fu, H. Y. Ye, Y. Zhang & R. G. Xiong, J. Am. Chem. Soc., (2017), **139**, 10897–10902.
[3] H.-Y. Ye, Y.-Y. Tang, P.-F. Li, W.-Q. Liao, J.-X. Gao, X.-N. Hua, H. Cai, P.-P. Shi, Y.-M. You and R.- G. Xiong, *Science*, (2018), **361**, 151–155.
[4] Saunders, L. K., Yeung, H. H-M., Warren, M. R., Smith, P., Gurney, S., Dodsworth, S. F., Vitorica-Yrezabal, I. J., Wilcox, A., Hathaway, P. V., Preece, G., Roberts, P., Barnett, S. A., Allan, D. R. *J Appl Crystallogr*, (2021), **54**(Pt 5), 1349-1359

A073-05-260823

From total scattering to total understanding: Structure-functionality relationships in lone pair-containing scheelite-type oxides

B. Mullens,[1] F. Marlton,[1] M. Saura-Múzquiz,[2] and B. Kennedy[1]

1 School of Chemistry, the University of Sydney, F11, Sydney, NSW 2006, Australia 2 Department of Materials Physics, Universidad Complutense de Madrid, 28040 Madrid, Spain

bmul2806@uni.sydney.edu.au

Keywords: Total Scattering, Lone Pair, Photocatalysis, Scheelite, Disorder

The stereochemical activity of lone pair electrons play a central role in determining the structural and electronic properties of materials – from chemically simple compounds such as H_2O, to complex condensed phases with varied physicochemical properties. In particular, metal ions containing a s^2 lone pair – such as Tl(I), Pb(II), and Bi(III) – are responsible for a range of applications including photocatalysis, ionic conductors, and the storage of radioactive waste. The scheelite-type ABO_4 material has become a focus of engineering these lone pair interactions due to its ability to accommodate a large variety of combinations of atomic radii and charge. This has led to the emergence of $BiVO_4$ as a potential industry photocatalyst, doped-$PbWO_4$ as a promising ionic conductor for solid oxide fuel cells, and $TlTcO_4$ as a potential host matrix for highly mobile nuclear fission products. Paramount to the development of these technologies is a deep understanding of their structure-functionality relationships. In this work, we begin with anomalies that are present within the diffraction data of these materials and use total scattering techniques to fully understand the structural characteristics crucial to their performance.

$BiVO_4$ has been observed in the literature as a promising non-toxic photocatalyst – a material capable of splitting water into hydrogen and oxygen gas in the presence of sunlight. Key to the performance of this material is the Bi^{3+} $6s^2$ lone pair, where hybridization between the Bi(6*s*) and O(2 *p*) orbitals in the valence band are believed to be advantageous for the mobility of photogenerated charge carriers resulting in improved photocatalytic activity [1]. This hybridisation leads to appreciable distortion in the BiO_8 polyhedra because of ordering the 6 s^2 lone pair electrons. However, synchrotron X-ray and neutron diffraction measurements suggest the distortion is absent in the high-temperature tetragonal polymorph, demonstrating that ordering of the lone pair electrons is lost upon heating. Using neutron total scattering, results will be presented that monitor the evolution of the BiO_8 polyhedra, and whether any 'hidden' ordering of the lone pairs is present, to better understand these materials.

$PbWO_4$ has shown promising oxygen ionic conductivity properties for use in solid oxide fuel cells. In particular, lanthanoid-doped $PbWO_4$ displays remarkably high oxygen ionic conductivity [2]. However, the presence of Pb(II) make it non-ideal for industrial applications. Rietveld refinements of synchrotron X-ray and neutron diffraction data of $PbWO_4$ show a well-defined scheelite-type crystal structure. However, neutron total scattering data suggests multiple different Pb-O bonds are present, as expected from the presence of the $6s^2$ lone pair. This works suggests the necessity of understanding structure on different length scales to fully determine structure-functionality relationships in metal oxides.

Finally, $TlTcO_4$ has been proposed as a potential host matrix of Tc-containing by-products. However, $TlTcO_4$ exhibits several different phase transitions in the long-range structure, leading to complex chemical behaviour. Using neutron total scattering, we describe this behaviour in terms of the correlation length and ordering of the Tl(I) $6s^2$ lone pairs. Whilst the long-range average structure increases in symmetry upon heating, the local structure is best fitted with local distortions to the unit cell due to stereochemically-active Tl(I) lone pairs [3]. This work highlights the structural information that may be missed using traditional diffraction methods, and consequently, how total scattering can be used to provide a more wholistic structure-functionality relationship. This presents a possible method of tuning the energy landscape of lone pair-containing functional materials for various applications.

[1] D.J. Payne *et al.*; *Appl. Phys. Let.*, **2012**, *98* (21), 212100.
[2] H. Huang *et al.; J. Phys.: Condens. Matter*, **2003**, *15*, 5689.
[3] M. Saura-Múzquiz *et al.*; *J. Am. Chem. Soc.*, **2022**, *144* (34), 15612-15621.

A089a Coherent scattering methods using X-rays or electrons
Room 209
1.10pm - 3.30pm

A089a-01-260823

An experimental comparison between X-ray ptychography and holography for 3D imaging of biological tissues

A. Diaz[1], T. Thies[1], C. Bosch[2], M. Guizar-Sicairos[1,3], M. Holler[1], D. Karpov[4], E. Müller[1], A. Schaefer[2], P. Cloetens[4], A. Menzel[1], A. Pacureanu[4]

(1) Paul Scherrer Institute, Villigen PSI, Switzerland, (2) Francis Crick Institute, London, United Kingdom, (3) École Polytechnique Fédérale de Lausanne (EPFL), Lausanne, Switzerland, (4) ESRF, the European Synchrotron, Grenoble, France

ana.diaz@psi.ch

Keywords: X-ray ptychography, X-ray holotomography

Hard X-ray nano-tomography offers non-destructive visualization of biological tissue extending hundreds of micrometres in 3D, providing a valuable complementary tool for electron microscopy. X-ray ptychographic computed tomography (PXCT) [1] and X-ray nano-holotomography (XNH) [2] are two state-of-the-art approaches for hard X-ray nano-tomography: they both provide phase contrast with high spatial resolution, while the absence of optics between the sample and the detector favours a high dose efficiency. These features make the two techniques promising candidates for high-resolution imaging of biological tissues at 4th-generation synchrotron sources. Although both methods are already in use for imaging biological tissue [3,4], a systematic comparison between them for biological specimens is still lacking. Such a comparison is relevant as a basis for decisions regarding the design of instruments to be built in future upgraded synchrotron storage rings.
Here we present measurements at cryogenic temperature of a 100 □m-diameter stained, resin-embedded mouse brain tissue specimen performed first at 6.2 keV by near-field PXCT at the cSAXS beamline of the Swiss Light Source (SLS) and subsequently at 17 keV by XNH at the ID16A beamline of the ESRF, the European Synchrotron (see Figure 1). For this purpose, we make some compromises on the optimal performance of each instrument to accommodate the same specimen into the two cryogenic setups. In these conditions, we obtain similar imaging results with 3 times less dose with PXCT and 10 times shorter acquisition time with XNH. We further discuss the possibilities for improvement in both methods and the potential for their application to larger specimens at higher resolution compared to the about 100 nm that we achieve here.

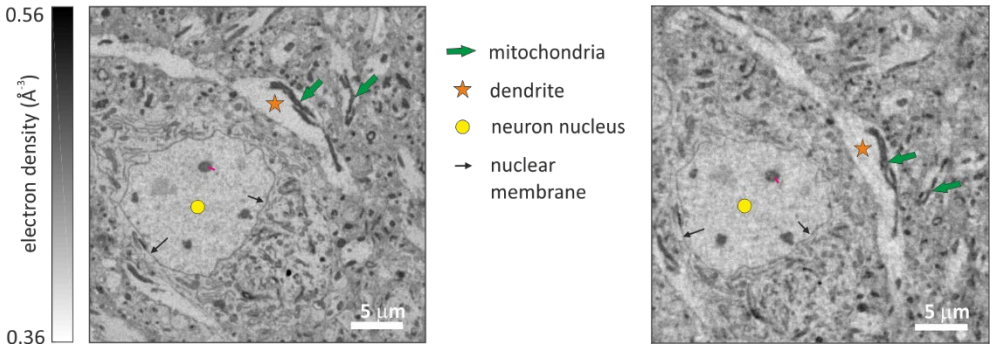

Figure 1. Virtual slices through 3D brain tissue images acquired by near-field PXCT (left) and XNH (right).

[1] Dierolf, M., Menzel, A., Thibault, P., Schneider, P., Kewish, C. M., Wepf, R., Bunk, O. & Pfeiffer, F. (2010). *Nature* **467**, 436.
[2] Villanova, J., Laurencin, J., Cloetens, P., Bleutet, P., Delette, G., Suhonen, H. & Usseglio-Viretta, F. (2013). *J. Power Sources*, **243**, 841.
[3] Tran, H. T., Tsai, E. H. R., Lewis, A. J., Moors, T., Bol, J. G. J. M., Rostmani, I., Diaz, A., Jonker, A. J., Guizar-Sicairos, M., Raabe, J., Stahlberg, H., van de Berg, W. D. J., Holler, M. & Shahmoradian, S. H. (2020). *Front. Neurosci.* **14**, 570019.
[4] Kuan, A. T., Phelps, J. S., Thomas, L. A., Nguyen, T. M., Han, J., Chen, C.-L., Azevedo, A. W., Tuthill, J. C., Funke, J., Cloetens, P., Pacureanu, A. & Lee, W.-C. A. (2020). *Nat. Neurosci*. **23**, 1637.

We acknowledge the Paul Scherrer Institute, Villigen, Switzerland, and the ESRF, the European Synchrotron, Grenoble, France, for provision of synchrotron radiation beamtime at beamlines cSAXS of the SLS (beamtime proposal 20200740) and ID16A, respectively.

A089a-02-260823

Three-dimensional structure determination via correlated scattering with an x-ray laser

T. B. Berberich[1,2], A. I. Lichtenstein[1,2], S. L. Molodtsov[1,3], R. P. Kurta[1]

1 European XFEL, Holzkoppel 4, 22869 Schenefeld, Germany, 2 I. Institute of Theoretical Physics, University of Hamburg, Notkestraße 9-11, 22607 Hamburg, Germany, 3 Institute of Experimental Physics, TU Bergakademie Freiberg, Leipziger Str.23, 09599 Freiberg, Germany

ruslan.kurta@xfel.eu

Keywords: Angular cross-correlation functions, rotational invariants, iterative phasing, structure determination

X-ray free electron lasers (XFELs) offer exciting possibilities for three-dimensional (3D) structure determination of biological materials. Ultrashort and ultrabright coherent x-ray pulses provided by an XFEL enable "diffraction before destruction" measurements of just individual bioparticles, such as viruses or macromolecules [1,2]. Such single-particle imaging (SPI) experiments allow, for instance, to study bioparticles for which crystals cannot be easily produced, and conventional crystallography approaches cannot be applied. At the same time, a limited resolution of the reconstructed biological objects demonstrated so far by SPI demands further theoretical and experimental efforts to establish biological imaging with an XFEL. Hence, alternative approaches for structure determination of non-crystalline particles with an XFEL are of great interest.

The fluctuation x-ray scattering (FXS) approach offers an alternative pathway for structural characterization with an XFEL [3,4]. In contrast to commonly used crystallography and imaging approaches, where the measured diffracted intensities are used to determine the structure of a bioparticle, the FXS approach relies on the detection of correlations in the scattered intensity fluctuations. The angular cross-correlation functions (CCFs) allow to access the rotational invariants, which can be employed for structure determination [5]. In this respect, the FXS approach represents a generalization of the small-angle x-ray scattering (SAXS) method, while the latter provides an access to the zero-order rotational invariant only [6]. The FXS measurements can be performed in the gas phase or liquid, from single- or multiple-particle samples, and require XFEL pulses that are shorter than rotational diffusion time of the particles.

Here we employ FXS to determine the 3D structure of nanoparticles in a liquid solution and aerosolized virus particles measured with an XFEL [6, 7]. We determine angular correlation maps, which comprise a complex fingerprint of the 3D structure of a particle, and can be used in model assisted structure determination. We also employ the multitiered iterative phase retrieval (MTIP) algorithm [5] for ab initio structure determination of particles from the rotation invariants (Fig. 1). Our results demonstrate the potential of FXS for the studies of the structure and dynamics of biological samples and nanoparticles with an XFEL.

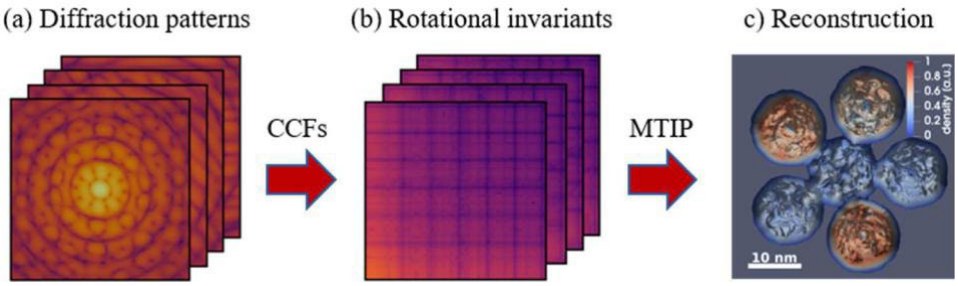

Figure 1. Illustration of the ab initio structure reconstruction workflow on the simulated data. Angular CCFs are averaged over the diffraction patterns (a) in order to extract the rotational invariants (b), which are used in the MTIP algorithm to recover the particle electron density distribution in 3D (c).

[1] Assalauova, D., et al. (2020). *IUCrJ.* **7**, 1102.
[2] Eckeberg, T., et al. (2022). *submitted*, doi: 10.1101/2022.03.09.483477
[3] Kam, Z. (1977). *Macromolecules* **10**, 927.
[4] Kurta, R. P., Altarelli, M. & Vartanyants, I. A. (2016). *Advances in Chemical Physics* **161**, 1.
[5] Donatelli, J. J., Zwart, P. H. & Sethian, J. A. (2015). *Proc. Nat. Acad. Sci.* **112**, 10286.
[6] Kurta, R.P., et al. (2017). *Phys. Rev. Lett.* **119**, 158102.
[7] Berberich, T., et al. *in preparation*.

A089A-03-260823

Structural evolution of nanoparticles under realistic conditions observed with Bragg coherent x-ray imaging

C. Atlan[1,2,3], C. Chatelier[1,2], M. Dupraz[1,2], E. Bellec[2], S. Labat[4], I. Martens[2], A. Viola[3], F. Maillard[3], E. Rabkin[5], S. J. Leake[2], M.-I. Richard[1,2]

[1]Univ. Grenoble Alpes, CEA Grenoble, IRIG, MEM, NRX, 17 avenue des Martyrs, F-38000 Grenoble, France.
[2]ESRF - The European Synchrotron, 71 Avenue des Martyrs, F-38000 Grenoble, France.
[3]Univ. Grenoble Alpes, Univ. Savoie Mont Blanc, CNRS, Grenoble INP, LEPMI, 38000 Grenoble, France.
[4]Aix Marseille Université, CNRS, Université de Toulon, IM2NP UMR 7334, 13397 Marseille, France
[5]Department of Materials Science and Engineering, Technion-Israel Institute of Technology, 3200003 Haifa, Israel.
mrichard@esrf.fr

Keywords: Coherent imaging, nanoparticles, catalysis

The advent of the new 4th generation x-ray light sources represents an unprecedented opportunity to conduct *in situ* and *operando* studies on the structure of nanoparticles in reactive liquid or gas environments.

In this talk, I will illustrate how Bragg coherent x-ray imaging [1] allows to image in three dimensions (3D) and at the nanoscale the strain and defect dynamics inside nanoparticles as well as their refaceting during catalytic reactions [2–4]. As an example, we successfully mapped the strain of a Pt nanoparticle in electrochemical environment (see Figure 1). Our results reveal that the strain is heterogeneously distributed between highly- and weakly-coordinated surface atoms, and propagates from the surface to the bulk of the Pt nanoparticle as (bi)sulphates anions adsorb on the surface [5].

We will also discuss the possibility to measure particles as small as 20 nm [6] and to enable high-resolution and high-energy imaging with Bragg coherent x-ray diffraction at 4th generation x-ray light sources. Finally, I will highlight the potential of machine learning to predict characteristic structural features in nanocrystals just from their 3D Bragg coherent diffraction patterns [7].

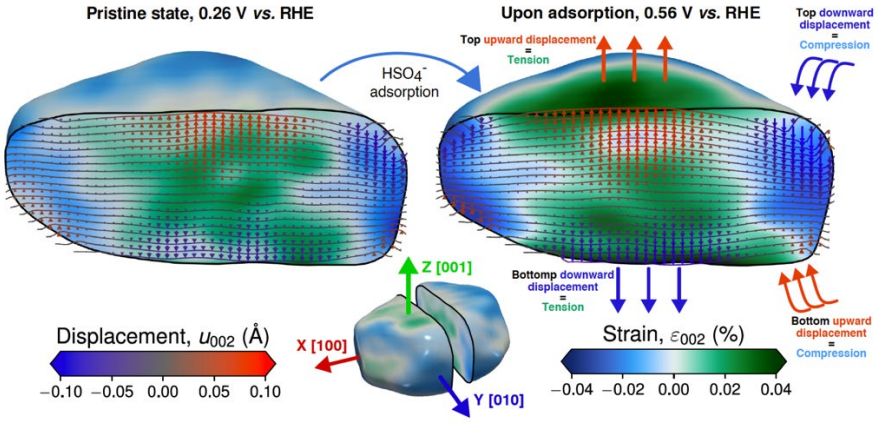

Figure 1. Evolution of the lattice displacement and strain of a Pt nanoparticle in its pristine state and under potential control (0.56 V *vs*. RHE) and in 0.05 M H_2SO_4.

We acknowledge funding from the European Research Council (ERC) under the European Union's Horizon 2020 research and innovation programme (grant agreement No. 818823).

[1] I. Robinson and R. Harder, *Coherent X-Ray Diffraction Imaging of Strain at the Nanoscale*, Nat. Mater. **8**, 291 (2009).
[2] J. Carnis, et al., *Facet-Dependent Strain Determination in Electrochemically Synthetized Platinum Model Catalytic Nanoparticles*, Small **17**, e2007702 (2021).
[3] J. Carnis et al., *Twin Boundary Migration in an Individual Platinum Nanocrystal during Catalytic CO Oxidation*, Nat. Commun. **12**, 5385 (2021).
[4] M. Dupraz et al., *Imaging the Facet Surface Strain State of Supported Multi-Faceted Pt Nanoparticles during Reaction*, Nat. Commun. **13**, 1 (2022).
[5] C. Atlan et al., *Imaging the strain evolution of a platinum nanoparticle under electrochemical control*, Nat. Mater. accepted (2023).
[6] M.-I. Richard et al., *Bragg Coherent Diffraction Imaging of Single 20 Nm Pt Particles at the ID01-EBS Beamline of ESRF*, J. Appl. Crystallogr. **55**, 621 (2022).
[7] B. Lim et al., *A Convolutional Neural Network for Defect Classification in Bragg Coherent X-Ray Diffraction*, Npj Comput. Mater. **7**, 1 (2021).

A089-04-260823

Serial diffractive imaging to visualize ultrafast dynamics in nanoscale systems

K. Ayyer[1,2]

Max Planck Institute for the Structure and Dynamics of Matter, Hamburg, Germany,
Center for Free-Electron Laser Science (CFEL), Hamburg, Germany
kartik.ayyer@mpsd.mpg.de

Keywords: XFELs, Diffractive Imaging, Ultrafast Dynamics

X-ray Free Electron Lasers (XFELs) provide a unique opportunity to categorize the structural variations in arbitrary ensembles of particles by diffractively imaging one particle at a time (serial imaging). The high peak brilliance allows one to obtain enough information from coherent diffraction patterns of single, aerosolized particles to not only determine their orientation, but also classify discrete and continuous structural heterogeneities. We demonstrate this with a proof-of-principle experiment on gold nanoparticles at the European XFEL, including by measuring X-ray induced melting of the particles [1,2]. Such an experiment also forms a template for exploring dynamics outside of the pump-probe paradigm, where the process is not precisely initiated by a pump pulse but rather through spontaneous fluctuations. We will also shortly discuss applications of the serial imaging method to hybrid perovskite quantum dots and the structural variability of viruses.

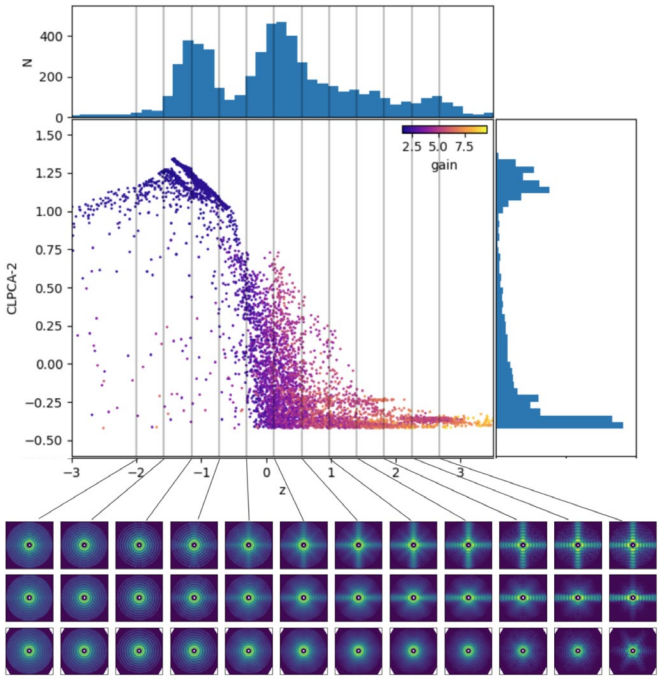

Figure 1. Reconstructed X-ray induced melting sequence of gold nanoparticles using deep learning. The input dataset consisted of around 1 million individual patterns of single nanoparticles in a random orientation and with an unknown degree of melting. Serial imaging enables the reconstruction (in three dimensions) of the structure as a function of the latent incident X-ray fluence.

[1] K Ayyer, PL Xavier, J Bielecki, Z Shen, BJ Daurer, *et al*, *Optica* **8**(1), 15-23 (2021)
[2] Y Zhuang, S Awel, A Barty, R Bean, J Bielecki, …, K Ayyer *IUCrJ* **9**(2) (2022)

A089a-05-260823

3D visualization of calcium carbonate morphology as a function of different additives using coherent X-ray diffraction imaging

D. Younas[1], I. U. Hageberg[1], Y. Chushkin[2], F. Zontone[2], S. Ucar[3], D. W. Breiby[1], B. Chattopadhyay[1]

[1] Department of Physics, Norwegian University of Science and Technology (NTNU), Høgskoleringen 5, Trondheim 7491, Norway,
[2]ESRF, The European Synchrotron, 71 Avenue des Martyrs, Grenoble 38000, France
[3]Department of Chemical Engineering, NTNU, Norway

Keywords: Coherent diffraction imaging, Calcium carbonate, 3D morphology

Calcium carbonate is an inorganic compound found abundantly in nature, most commonly as limestone in rocks and as a core component in biomineralization in organisms to form bones, shells, or pearls. CaCO3 occurs in three stable polymorphs named calcite, vaterite and aragonite - all of which can be precipitated in the laboratory under different reaction conditions, e.g., temperature, concentration [1]. Crystallization of any form of CaCO3 is greatly affected by additives which either inhibit or help crystalize different polymorphs or alter the growth and morphology of them. To investigate the effect of these additives, CaCO3 microparticles were prepared in the presence of Fetuin A, NaCl and polystyrene sulfonate in three separate experiments. Coherent diffraction imaging (CXDI) was performed on single particles isolated from each of the prepared samples. The experiments were performed at the ID10 beamline associated with the new low-emittance storage ring of ESRF [2]. 2D Wide-angle X-ray diffraction (WAXD) patterns were recorded simultaneously with the 3D CXDI datasets to identify the crystalline phase of preferred orientation of the crystallites constituting the CaCO3 microparticles. The phase retrieval [3] was performed with the PyNX software [4] developed at the ESRF and optimised for CXDI experiments.

The results from the CXDI reconstruction are shown in Fig. 1, with CaCO3 grown with Fetuin A, PSS and NaCl. Preliminary analyses of the data indicated that Fetuin A promotes the formation of calcite while PSS and NaCl give the polymorph of vaterite. In presence of supersaturated NaCl where the carbonate ions are in excess, agglomerates of vaterite nanoparticles are formed. In presence of PSS spherical vaterite particles are obtained. In this presentation, the variation of the internal structures of the three different CaCO3 morphologies will be discussed as well as the orientation of the crystallites present in the microparticles.

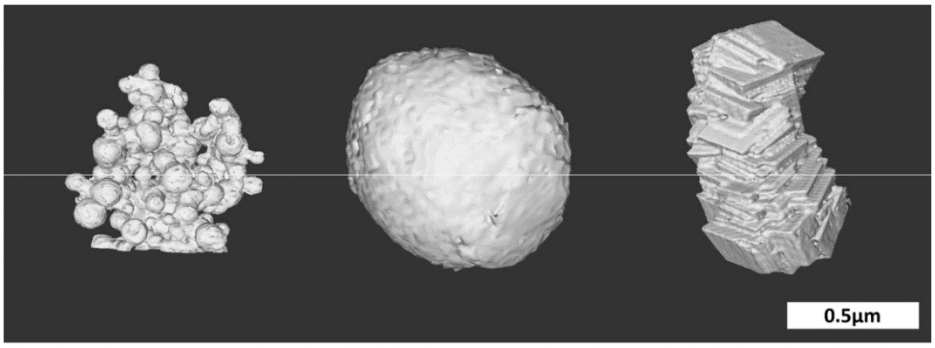

Figure 1. 3D external surface renderings of representative $CaCO_3$ microparticles prepared using a) sodium chloride, b) polystyrene sulfonate, and c) Fetuin A.

[1] Robinson I., Harder R., (2009). Nature Materials 8, 291.
[2] ESRF News. (2017). No. 77, December 2017.
[3] Miao, J., Charalambous, P., Kirz, J. & Sayre, D. (1999). Nature 400, 342.
[4] Favre-Nicolin V., Girard G., Leake S., Carnis J., Chushkin Y., Kieffer J., Paleo P. and Richard M.-I. (2020). J. Appl. Cryst. 53, 1404.

We thank the Research Council of Norway for funding through FRINATEK (No. 303252 and No. 275182) and ESRF for the beamtime allocated at the ID10 beamline.

A103 Mechanochemistry Meets Crystal Engineering
Room 219
1.10pm - 3.30pm

A103-01-260823

Automated analysis of mechanochemically-induced reaction with in situ X-ray diffraction

Y.Nakajima, T.Hawai, K.Ono

Osaka University, Osaka, Japan

yusaku_nakajima@ap.eng.osaka-u.ac.jp

Keywords: Mechanochemistry, Perovskite materials, Automated experiments

Mechanochemistry is attracted to the breakthrough of the materials fabrication [1]; however, the reaction mechanism needs to be clarified. Therefore, automated characterization is required to investigate the material structural change during the chemical reaction process to clarify the detailed reaction mechanism. In this paper, we developed an automated XRD characterization system, combining automated XRD measurement and Rietveld analysis to analyze mechanochemically-induced reactions. We investigated the mechanochemically-induced reaction process of the perovskite material CsPbX3, a promising material for next-generation solar cells.

The automated XRD system can perform fully automated XRD measurements with optimal measurement conditions. We used a previously developed automated analysis method (BBO-Rietveld) [3] for Rietveld analysis (Fig. 1 left).

We investigated the quantitative change of precursors, products, and by-products after a mechanochemically-induced process from CsBr and PbBr2 to CsPbX3. We performed the automated XRD experiment for 24 hours (Fig. 1 right). As a result, we found that the reaction process to CsPbX3 is not a single step, as reported previously, but also is composed of mechanochemically triggered spontaneous reactions.

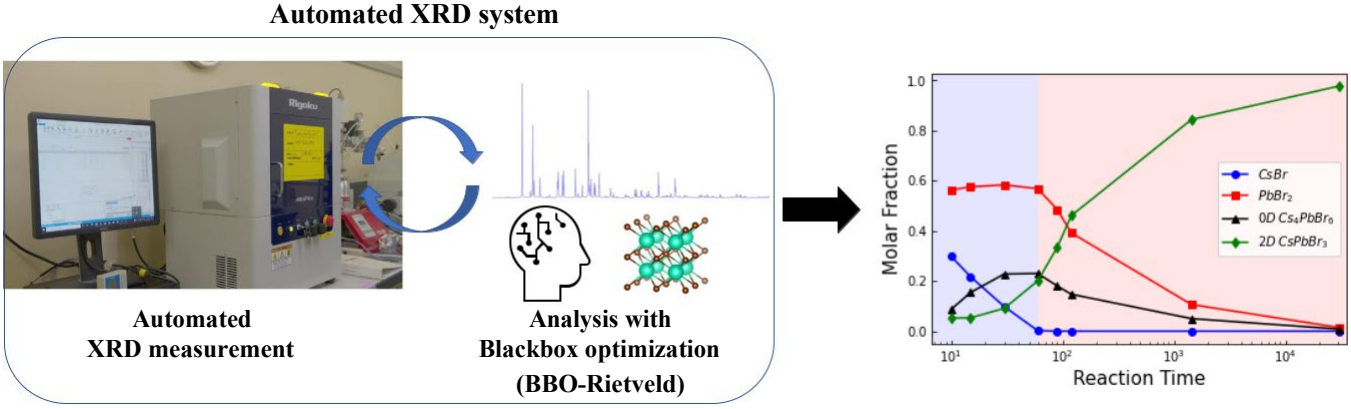

Figure 1. Schematic diagram of the automated XRD system and the results of the reaction process.

We found that the chemical reaction processes for CsPbBr3 are composed of two steps.

The first step (Fig. 1, blue area) is CsBr + PbBr2 → CsPbBr6; the chemical reaction proceeded until 1 hour after the mechanochemical reaction.

The second step (Fig. 1, red area) is CsPbBr6 + PbBr2 → CsPbBr3, which produces the final product.

In summary, we investigated the mechanochemical reaction mechanism for perovskite materials using the in situ automated XRD measurement and analysis system. This method helps understand the reaction path by characterizing mechanochemical reactions of various materials.

[1] F. Palazon, Y. El Ajjouri, and H. J. Bolink (2020). Adv. Energy Mater., 10, 13.
[2] P. Pal, S. Saha, A. Banik, A. Sarkar, and K. Biswas (2018). Chem. Eur. J., 24, 8.
[3] Y. Ozaki, Y. Suzuki, T. Hawai, K. Saito, M. Onishi, and K. Ono (2020). npj Comput Mater, 6,1.

This work was partly supported by the JST-Mirai Program (Grant Number JPMJMI21G2).

A103-02-260823

Computer vision for the evaluation of bending crystals deformation

Benjamin Hsieh[1], Arnaud Grosjean[1]

National Synchrotron Radiation Research Center (NSRRC), 101 Hsin-Ann Road, Hsinchu, 30076, Taiwan.

a.grosjean@nsrrc.org.tw

Keywords: computer vision, bending crystals, mechanical properties

Despite crystals being often perceived as hard and brittle, numerous examples exhibit appreciable deformation [1]. The mechanical properties of these crystals are intriguing and, therefore, developing methods to measure and quantify their deformation can prove helpful in studying their mechanical properties.

In perfect bending conditions, a beam (or needle shaped crystal) deflects with the fibers on one side compressing and those on the other, expanding, forming an arc. According to the Euler–Bernoulli beam theory [2], deformation (strain, ε) is given by z/ρ, where z is the distance from the neutral axis, and ρ is the radius. With this equation, the theoretical maximum deformation of a crystal can be evaluated once its thickness and radius of curvature are known. However, accurately measuring a crystal's thickness and curvature from a simple optical image can be challenging. Nevertheless, computer automation can make this process reasonably easy, reliable, and accurate.

Such an automated tool has been developed and Figure 1 shows the results of this computer tool to automatically evaluate the deformation of a bend crystal [3] from a simple optical microscope image. The obtained deformation is consistent with results from micro-focused single crystal X-ray diffraction mapping (μ-SCXRD) [3]. It is, therefore believed that this tool could prove useful for researcher interested in studying the mechanical properties of bend crystals. This tool will be made available at the TPS-15A synchrotron beamline of the NSRRC for users interested in performing μ-SCXRD.

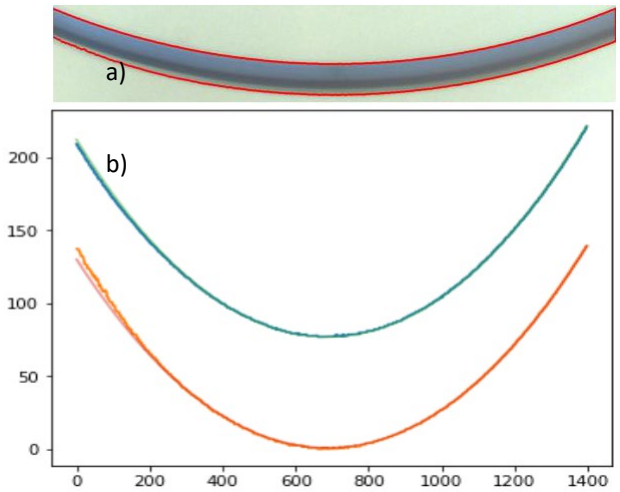

Figure 1. **a)** Crystal contours automatically obtained. **b)** Arc fitting of the contours to obtain thickness and curvature of the crystal (pixel unit)

[1] A. J. Thompson, A. Worthy, A. Grosjean, J. R. Price, J. C. McMurtrie, and J. K. Clegg, 'Determining the mechanisms of deformation in flexible crystals using micro-focus X-ray diffraction', *CrystEngComm*, p. 10.1039.D1CE00401H, 2021, doi: 10.1039/D1CE00401H.

[2] J. M. Gere and B. J. Goodno, *Mechanics of materials*, 8th ed. Stamford, CT: Cengage Learning, 2013.

[3] A. Worthy *et al.*, 'Atomic resolution of structural changes in elastic crystals of copper(II) acetylacetonate', *Nature Chemistry*, vol. 10, no. 1, Art. no. 1, Jan. 2018, doi: 10.1038/nchem.2848.

A103-04-260823

High-energy isochoric synthesis of elusive iodoplumbic acid

Szymon Sobczak,[1] Athena M. Fidelli,[2] Jean-Louis Do, [2] George P. Demopoulos,[3] Audrey Moores,[3] Tomislav Friščić,[3] Andrzej Katrusiak[1]

[1] Adam Mickiewicz University, Uniwersytetu Poznanskiego 8, 61-614 Poznań, Poland, [2] Department of Chemistry, McGill University, 801 Sherbrooke St. West, Montreal, QC, H3H 0B8 Canada; [3] Department of Materials Engineering, McGill University, 801 Sherbrooke St. West, Montreal, QC, H3A 0C5 Canada

szymon.sobczak@amu.edu.pl

Keywords: high-pressure chemistry, perovskites, high-pressure synthesis

The energy required to induce a chemical reaction can be provided to a reactant system through light, heat, or electric potential. It is however also possible to activate reactions using mechanical force. Mechanical energy, supplied by techniques like ball-milling, causes friction, stress, and strain and often results in breaking a crystal symmetry. This process can lead to the destabilization of the chemical bonds making compounds prone to react. It is important however that the mechanical energy can be as well supplied in a form of continuous and hydrostatic pressure on compression in a diamond anvil cell (DAC).

Here, we demonstrate the high-energy isochoric synthesis for obtaining two hydronium forms of the proposed but yet never demonstrated iodoplumbic acid $HPbI_3$ (Figure 1). The proposed $HPbI_3$ for many years was anticipated to be the simplest member of $APbI_3$ class of compounds (where A represents a cation counterbalancing the polyanionic sheet) and the progenitor of the wide class of hybrid as well as inorganic lead(II) perovskites [2]. Depending on the pressure range, the reaction of PbI_2 and aqueous concentrated hydriodic acid performed in a DAC and held between 0.11 and 1.20 GPa yielded in the synthesis of two hydrated hydronium salts with compositions $[H_3O][PbI_3] * nH_2O$ (n = 3, 4) in form of single crystals (Figure 1).[4] Both compounds are composed of polymeric one-dimensional PbI_3^- anions, which are so far the best match for the elusive $HPbI_3$. This high-energy synthesis from this same system above 2 GPa gave rise to the so far first known polymorph of β-PbI_2. Unlike the form α, crystallizing at standard conditions as yellow single crystals in the hexagonal $P6\text{-}3mc$ space group which structure is based on 2-dimensional sheets, phase β exhibits an unprecedented PbI_2 structure. The pink single crystals of monoclinic (space group $C2/m$) phase β are based on six- and seven-coordinated Pb^{2+} cations connected into a 3-dimensional structure (Figure 1).

This work highlights the potential of pressure-induced synthesis as a simple and straightforward means to discover new unprecedented materials, even from systems that have been extensively studied, over a long time.

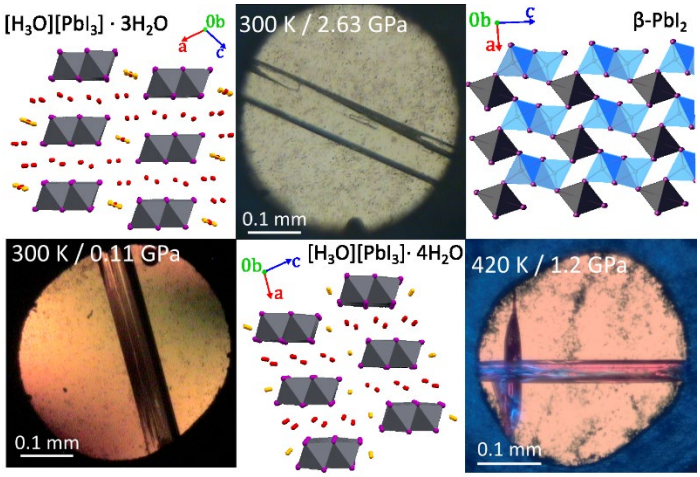

Figure 1. Two forms of hydrated iodoplumbic acid obtained in the reaction of PbI_2 with concentrated HI aqueous solution and new polymorph of PbI_2.

[1] James, S. L., Adams , C. J., Bolm, C., Braga, D., Collier, P., Friščić, T., Grepioni, F., Harris, K. D. M., Hyett, G., Jones, W., Krebs, A., Mack, J., Maini, L., Orpen, A. G., Parkin, I. P., Shearouse, W. C., Steed, J. W. & Waddell, D. C., *Chem. Soc. Rev.*, 2012, **41** , 413

[2] Euvrard, J., Yan, Y., Mitzi, D. B., *Nat. Rev. Mater.* **2021**, 6, 531–549

[3] Katrusiak, A. *Acta Crystallogr. Sect. B Struct. Sci. Cryst. Eng. Mater.* **2019**, *75*, 918–926.

[4] Sobczak, S.; Fidelli, A. M.; Do, J.-L.; Demopoulos, G. P.; Moores, A.; Friscic, T.; Katrusiak, A. 10.26434/chemrxiv.14369813

A103-05-260823

Investigation of σ-hole based chalcogen and halogen bonding in cocrystals

A. Hasija[1,2] L. Groslambert,[3] P. Pale,[3] E. Espinosa,[2] V. Mamane,[3] E. Aubert,[2] D. Chopra[1]

[1]*Indian Institute of Science Education and Research Bhopal, Bhopal By-Pass Road, Bhopal, Madhya Pradesh, India 462066*

[2]*Université de Lorraine, CNRS, CRM2, F-54000 Nancy, France*

[3]*LASYROC, UMR 7177, University of Strasbourg 1 Rue Blaise Pascal, 67000 Strasbourg (France)*

avantikah91@gmail.com

Keywords: Co-crystallization, Halogen bonding, Chalcogen bonding

Chalcogen/Halogen bonding is an attractive force between Lewis acid/electrophilic region of a chalcogen/halogen atom with a Lewis Base/nucleophile.[1,2] To investigate halogen bonding, synthesis of 5 stoichiomorphic co-crystals by combinations of triphenylphosphine sulphide (PS) with 1,3,5-triiodo-2,4,6-trifluorobenzene (I3F) and 1,4-diiodotetrafluorobenzene (IF) respectively, consisting of I···S halogen bonding interaction were synthesized.[3] These I-centred interactions have been investigated using the geometrical criteria and computational methods. The nature of short and directional I···S halogen bonds (shortest: **3.163Å**; most directional C-I···S, **179**°) in different stoichiomorphic cocrystals were investigated. The interaction energy is in the range of -16 to -32 kJ/mol, as established from DFT calculations. Topological analysis unequivocally establishes the presence of a (3, -1) bond critical point (Fig 1a.) and the NCI-RDG analysis establishes the attractive nature of the interaction. The elongation of the C-I bond length as a consequence of evident charge transfer from sulfur to iodine for I···S interaction is reflected via Natural Bonding Orbital. The atomic polarizability analysis establishes the mutual polarization of the iodine atom in the presence of the sulfur atom and vice-versa (Fig 1b).[4] On the other hand, the nature of chalcogen bonding (ChB) is investigated in *Tellurium based promising as-catalysts cations* and their synthesised cocrystals.[5] These tellurium based compounds are characterized using SCXRD, PXRD, ^{125}Te- NMR followed by analysis of different noncovalent interactions, primarily ChB, by utilizing several computational tools. Thus, a detailed experimental and computational analysis establishing the electronic characteristics of the chalcogen and halogen bonded cocrystals will be discussed in detail.

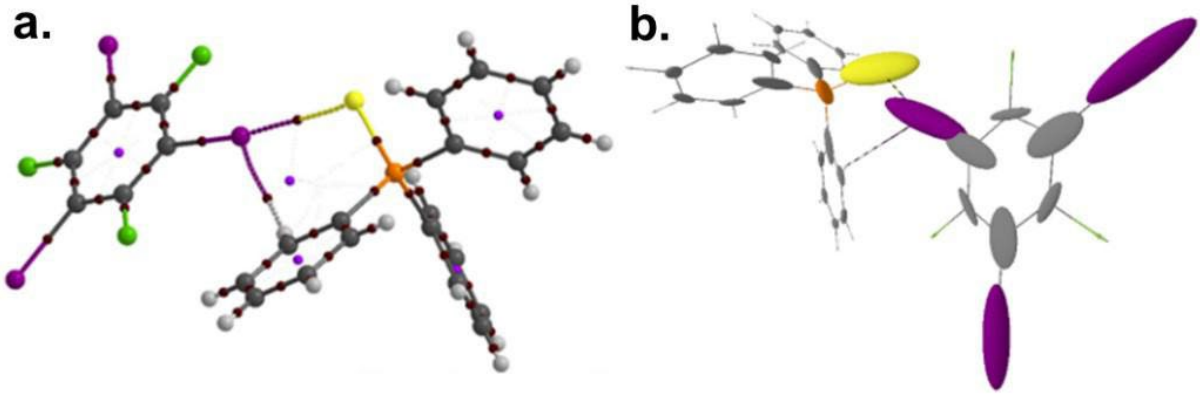

Figure 1.a. Bond critical point shown between I…S halogen bond; **b.** Mutual atomic polarizability between I and S computed through PolaBer.

[1] G. Cavallo, P. Metrangolo, R. Milani, T. Pilati, A. Priimagi, G. Resnati, G. Terraneo, (2016) *Chem. Rev.* **116**, 2478−2601.
[2] L. Vogel, P. Wonner, S. M. Huber (2019) *Angew. Chem. Int. Ed.* **58**, 7, 1880-1891.
[3] A. Hasija, D. Chopra (2020) *Cryst. Growth Des.* **20**, 10, 6272–6282.
[4] A. Krawczuk, D. Pérez, P. Macchi, (2014) *J. Appl. Crystallogr.* **47**, 1452.
[5] R. Weiss, E. Aubert, P. Pale, V. Mamane, (2021) *Angew. Chem. Int. Ed.* **60**, 19281.

A016b Structure-based Drug Design
Room 203/204
4.00pm - 6.30pm

A016b-01-260823

Developing MOZi, a chimeric MOF protein to aid structure-based drug design in MOZ

S.J. Hermans[1], M.C. Chung[1], J.B. Baell[2], M.W. Parker[1,3]

1. ACRF Rational Drug Discovery Centre, St Vincent's Institute of Medical Research, Fitzroy, Victoria, Australia.
2. Medicinal Chemistry Theme, Monash Institute of Pharmaceutical Sciences, Monash University, Parkville, Victoria, Australia.
3. Department of Biochemistry and Pharmacology, Bio21 Molecular Science and Biotechnology Institute, University of Melbourne, Parkville, Victoria, Australia
shermans@svi.edu.au

Keywords: MOZ, KAT6A, MOF, KAT6B, Acetyltransferase, Chimeric protein, Drug design

Obtaining the three-dimensional structure of a relevant protein target in complex with a compound of interest can assist in the development of more potent and selective compounds, a process known as structure-based drug design (SBDD). Where the structure of a target protein is unobtainable, through lack of successful crystallization conditions for example, crystallographers may need to be creative to determine useful structure-activity relationship (SAR) information.

MOZ (also known as KAT6A) belongs to the MYST family of histone acetyltransferases (HATs) and is a known oncogene causing acute myeloid leukaemia [1]. MOZ suppresses cellular senescence, and its inhibition may provide a therapeutic benefit in cancer [2]. An intensive drug discovery program has had recent successes in developing potent MOZ selective inhibitors capable of inducing cell cycle exit and cellular senescence without causing DNA damage [3-5].

A major limiting factor of these studies was the lack of successful crystallization conditions for MOZ in complex with compounds of interest. To overcome this challenge, a chimeric protein was developed using a close relative, MOF (also known as KAT6B). Based on the known HAT domain structures of MOZ and MOF in complex with the cofactor acetyl coenzyme A (Ace-CoA), this chimeric protein, dubbed MOZi in-house, contains the HAT domain of MOF with targeted mutations to the co-factor binding site so that it is structurally near identical to MOZ. The structure of MOZi in complex with Ace-CoA was used to validate this construct and crystals of MOZi in complex with compounds of interest were readily grown, diffracted to high resolution, and provided critically useful SAR information that aided in further MOZ drug development.

[1] Huang, F., Abmayr, S.M., Workman, J.L. (2016) *Mol Cell Biol*., **36**, 1900-1907.
[2] Sheikh, B., Phipson, B., El-Saafin, F. *et al.* (2015) *Oncogene*, **34**, 5807-5820.
[3] Baell, J.B., Leaver, D.J., Hermans, S.J. *et al*. (2018) *Nature*, **560**, 253–257.
[4] Priebbenow, D. L., Leaver, D. J., Nguyen, N. *et al*. (2020) *J. Med. Chem.*, **63**, 4655-4684.
[5] Wong, S. W., Vivash, L., Mudududdla, R. *et al*. (2021) *Eur J Med Chem.,* **226**:113822.

This research was undertaken in part using the MX2 beamline at the Australian Synchrotron, part of ANSTO, and made use of the Australian Cancer Research Foundation (ACRF) detector.

St. Vincent's Institute acknowledge the strong support from the Victorian Government and in particular the funding from the Operational Infrastructure Support Grant.

This work was funded by the Australian Government through NHMRC project grants, Research Fellowships, the NHMRC IRIISS and the Cancer Therapeutics Cooperative Research Centre.

A016B-02-260823

High-throughput screening at the PETRA III HiPhaX endstation

Guenther[1], P. Fischer[1], L. Gumprecht[1], J. Meyer[1], W. Ewert[1], P. Reinke[1], S. Falke[1], J. Lieske[1], S. Thekku Veedu[1], J. Wollenhaupt[2], M. S. Weiss[2], A. Meents[1]

[1] Center for Free-Electron Laser Science CFEL, Deutsches Elektronen-Synchrotron DESY, Notkestr. 85, 22607 Hamburg, Germany, 2 Helmholtz Zentrum Berlin, Macromolecular Crystallography, Albert-Einstein-Str. 15, 12489 Berlin, Germany
sebastian.guenther@desy.de

Keywords: Structure-based drug design, High-throughput, X-ray screening

The recent COVID pandemic exemplified the need for rapid response to newly emerging pathogens. Structure-based drug design has been instrumental in rapidly developing drugs against SARS-CoV-2. To identify lead molecules X-ray screening of fragment libraries and, more recently, also more complex compound libraries has become an increasingly successful approach as an alternative or complement to purely biochemical and biophysical high-throughput screening approaches [1]. While the structure offers extra information of an in-depth view of the binding-pose of identified ligands, there remain a few limitations hindering a higher throughput. Manual intervention is required for mounting crystals on sample holders and for subsequent data collection. To overcome these limitations, we are currently establishing a new instrument for macromolecular crystallography exclusively dedicated to high-throughput pharmaceutical X-ray screening. The goal of the project is to develop a fully automated endstation with the capability of determining more than 1000 protein structures per 24 hours. The beamline for *Hi*gh-throughput *Pha*rmaceutical *X*-ray screening (HiPhaX) operates at a fixed energy of 16 keV and will be equipped with an Eiger2 4M CdTe detector (Fig. 1A). Special care is taken to provide very low background scattering levels. We further aim at developing fully autonomous beamline operation, which does not require human intervention. To reach this goal we will implement fully automatic X-ray based crystal identification and centering and AI supported data collection and data analysis.

In addition to conventional cryo-crystallography with loop-mounted crystals and a storage dewar with space for more than 800 samples, the beamline is also capable of high-throughput screening at room temperature and provides a complete, highly automated workflow ranging from sample handling to data collection. For highest-throughput sample holders with multiple crystals will be supported. These holders are based on micro-patterned silicon chips [2] that provide space for multiple samples and can either be directly loaded with crystals or, for minimal manual intervention, crystals can be grown directly on the chips [3]. To reduce background scattering, excess liquid can be removed with an automated blotting station. Measurement-ready chips are then stored in a humidity-controlled chip hotel from which they can be mounted on the goniometer with a robotic arm. A temperature- and humidity-controlled sample chamber further guarantees well-defined measurement conditions.

I will present first results from several screening projects including a room-temperature fragment screen of the lassa and lacrosse virus cap-snatching endonucleases that represent drug-targets for pathogens with epidemic potential (Fig. 1B and C).

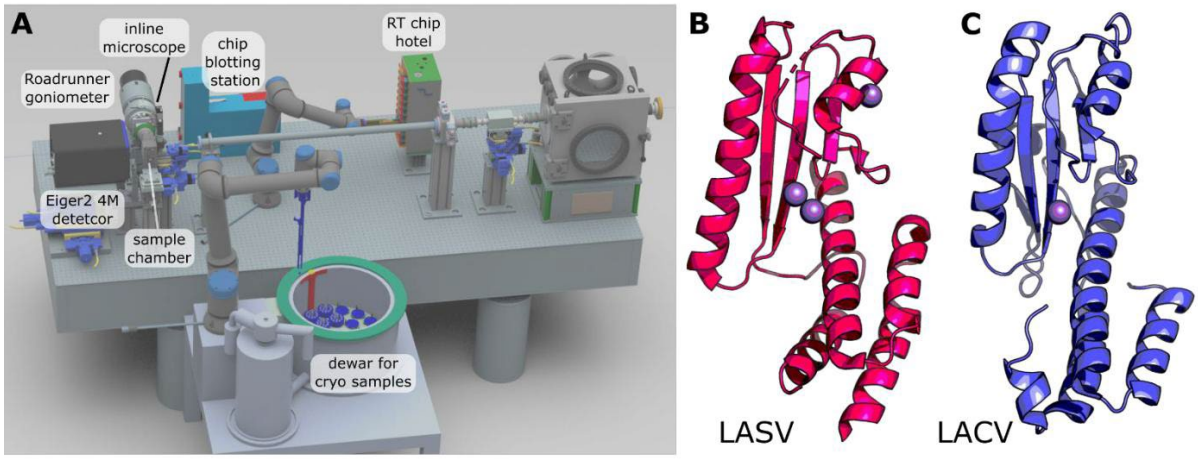

Figure 1. HiPhaX instrument at PETRA III for high throughput X-ray screening. A, schematic drawing of endstation including highly automated cryo and room-temperature data collection. B, Apo structures of Lassa (LASV) and, C, Lacrosse (LACV) virus cap-snatching endonucleases

Günther, S., et al. (2021). *Science*, **372**, 642.
Roedig, P., et al. (2015). *Sci Rep,* **5**, 10451.
Lieske, J., et al. (2019) *IUCrJ*, **6** (Pt 4), 714.

A016b-03-260823

High-throughput techniques enable structure guided drug discovery against the inflammatory target NLRP3

Andrew Thompson[1*], Tryfon Zarganis-Tzitzikas[1], Martin Lowe[2], Elena Fonfria[2], Emma Murphy[1], Frank von Delft[1], Paul Brennan[1]

[1]Centre for Medicines Discovery, Nuffield Department of Medicine, University of Oxford, Oxford OX1 3QU, UK
[2]Exscientia, The Schrödinger Building, Oxford Science Park, Oxford OX4 4GE, UK
**Current address: Chemical Biology Division, WEHI, Parkville 3052, VIC, AUS.*
Email: thompson.a@wehi.edu.au

Keywords: structure guided drug discovery, high-throughput, protein science, crystallography, NLRP3, neuroinflammation

The NLRP3 inflammasome is a key regulator of the pyroptosis response in the innate immune system. It is through this highly regulated signalling cascade that macrophages respond to danger and damage associated molecules. Consequently, NLRP3 mutants are associated with inflammatory diseases. Targeting NLRP3 with small molecule inhibitors is an attractive strategy for the treatment of cancer and neurodegenerative diseases such as Alzheimer's disease [1]. Currently, no NLRP3 inhibitors have reached the clinic, causing the hunt for alternate scaffolds to garner broad pharmaceutical investment.

Progress in the structural investigation of NLRP3 has been challenging due to its inherent instability and membrane association, impeding the development of structure-guided drug discovery pipelines that can consistently deliver high-resolution structural information. In recent years, several high impact structures of the various domains and binding partners of NLRP3 have revealed its biological mechanism [2]. Among these studies, it was confirmed that the NACHT nucleotide hydrolysis domain is the target for publicly available small molecule inhibitors, however the highest published resolution of this domain is 2.8Å [3], limiting structure-guided optimisation of inhibitors. In collaboration with the pharmaceutical company Exscientia, the Oxford Drug Discovery Institute aimed to improve upon this resolution by developing an in-house structure guided drug discovery pipeline.

Here, we describe the use of high-throughput cloning, expression, purification and crystallography techniques for the development of a structure-guided drug discovery pipeline against the NACHT domain of NLRP3 (Fig. 1). Broad and unbiased assessment of compounds and the N- and C-terminal boundaries for the NLRP3 NACHT domain constructs greatly influenced the crystallisation habit and the resulting resolution. Critically, the assessment of >450 crystals of NLRP3 was performed with the use of the semi-automated crystal harvesting robot: *Crystal Shifter (Oxford Lab Tech)* [4] in combination with unattended data collection and automated structure solution pipelines developed at Diamond Light Source. Using this approach, 8 high resolution structures of NLRP3 bound to lead molecules were solved (1.9-2.5Å), guiding medicinal chemistry outputs that are now patented. The use of formalised high-throughput processes was crucial to overcoming the technical challenges of working with an unstable protein. The techniques and mindset employed in this program are broadly applicable to many structure-guided drug discovery projects where higher throughput and resolution would be beneficial.

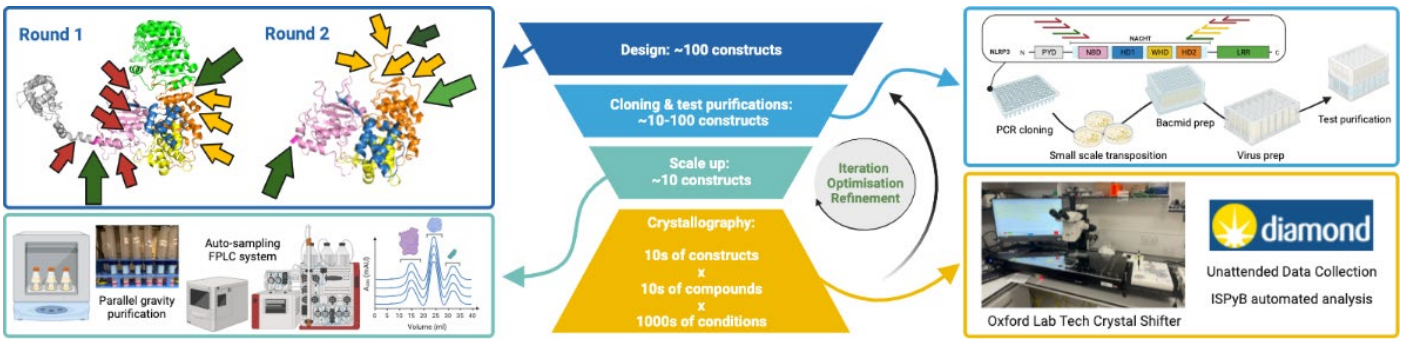

Figure 1. A workflow for the high-throughput development of a structure guided drug discovery pipeline. Construct design was performed to enumerate potentially soluble and crystallisable NLRP3 constructs. Through a combination of high-throughput PCR based cloning and gene synthesis, many proteins were expressed and purified at a small scale. Promising constructs were scaled up and purified in parallel. All observed crystals were harvested and sent for automated unattended data collection and analysis at Diamond Light Source. Critically, this process is iterative, with crystallography outputs guiding future construct design.

[1] Heneka, M. et al. (2013) *Nature* **493**, 674–678
[2] Le, X. *et al.* (2022) *Nature* **613**, 595-600

[3] Dekker, C, *et al.* (2021) *J Mol Biol* 3;433(24):167309
[2] Wright N.D., *et al.* (2021) *Acta Crystallogr D Struct Biol.* 77(Pt 1):62-74.

A016b-04-260823

PLK1 Inhibitor Co-complex Structures via the Surface Entropy Reduction Approach

R. C. Hillig

Nuvisan ICB GmbH, 13353 Berlin, Germany
roman.hillig@nuvisan.com

Keywords: Surface Entropy Reduction, small molecule inhibitor, cancer

Polo-like kinase 1 (PLK1) is a major regulator of cell division and therefore considered a drug target for cancer therapy. Crystallization of its kinase domain turned out to be exceptionally challenging. Previously, we published a crystallization approach using a PLK1-specific Designed Ankyrin Repeat Protein (DARPin) as crystallization facilitator [1]. Here, we report an alternative route where crystallization of PLK1 was successful after introduction of a double mutation designed following the concept of surface entropy reduction (SER) [2, 3, 4]. The resulting PLK1 crystal structures revealed that the successful double mutant not only reduced surface entropy but also enabled formation of a new crystal contact.

The new PLK1 crystal form presented here grows routinely and very robustly and allowed us to elucidate the molecular binding modes of a series of small molecule inhibitors, which will be presented and compared. The structures broaden the molecular understanding of PLK1 inhibition and will support future drug design for this important anti-cancer drug target.

[1] Bandeiras, T. M., Hillig, R. C., Matias, P. M., Eberspaecher, U., Fanghanel, J., Thomaz, M., Miranda, S., Crusius, K., Putter, V., Amstutz, P., Gulotti-Georgieva, M., Binz, H. K., Holz, C., Schmitz, A. A., Lang, C., Donner, P., Egner, U., Carrondo, M. A. & Muller-Tiemann, B. (2008). *Acta Crystallogr D Biol Crystallogr* **64**, 339.
[2] Derewenda, Z. S. (2004). *Structure* **12**, 529.
[3] Derewenda, Z. S. & Vekilov, P. G. (2006). *Acta Crystallogr D Biol Crystallogr* **62**, 116.
[4] Derewenda, Z. S. (2010). *Acta Crystallogr D Biol Crystallogr* **66**, 604.

A16B-05-260823

Utilizing Hydrogen Exchange Measurements to Drive Small Molecules into Cryptic Protein Binding Sites

Benjamin T Walters[1,2], Alexander Patapoff[2], Ping Wu[1], Weiru Wang[1], James Kiefer[1], Wayne Fairbrother[3]

Departments of Structural Biology[1], Biochemical and Cellular Pharmacology[2], and Early Discovery Biochemistry[3], Genentech, Inc., 1 DNA Way, South San Francisco, California. 94808, USA

walters.benjamin@gene.com

Keywords: hydrogen deuterium exchange (HDX), molecular dynamics, small molecule drug discovery

During the past several years, hydrogen deuterium exchange experiments (HDX) have become commonplace for studying protein dynamics and their interactions with other molecules. HDX experiments are highly sensitive to small changes in the folded state, which ultimately can reliably monitor both direct and allosteric effects resulting from ligand binding often with single amino acid resolution. When used in epitope- and binding-site mapping studies, these data can inform on mechanism of action, conformational changes that occur upon binding, and an overall picture of the binding site.

Over two decades ago, the first attempts were made to use the information from HDX to obtain atomistic models of structure and dynamics that agree with the data. These involved molecular dynamics simulations which initially used phenomenological expressions coupled with short MD trajectories [1] and later, physics-based calculations on msec length simulations [2], to reproduce HDX protection factors from MD with appreciable accuracy. This became a way to judge the accuracy of a particular simulation. Other groups have exploited HDX information to re-weight computational results, increasing agreement with X-ray crystallography or cryo-EM (see [3] for review), and HDX data were recently used to elucidate a degrader ternary complex and the mechanism behind subsequent degradation [4]. Despite this success, none of these approaches has unambiguously utilized HDX protection factors towards a generically reliable method to produce accurate small molecules bound to a cryptic pocket that did not exist in the structure used for computational analysis.

This study demonstrates a novel method employing data from HDX experiments to guide small molecules into cryptic pockets on a target protein within crystallographic resolution with a success rate greater than 85%. A cryptic pocket is a binding site that requires the ligand to exist. These pockets elude successful interrogation by computational techniques, such as virtual screening and present a considerable challenge for drug discovery. Within the context of a blinded test using an unbound X-ray structure of a kinase and five in-house compounds with solved X-ray structures the method will be described alongside critical aspects of the HDX experiments that enable this work.

Best, R.B. and M. Vendruscolo, *Structural Interpretation of Hydrogen Exchange Protection Factors in Proteins: Characterization of the Native State Fluctuations of CI2.* Structure, 2006. **14**(1): p. 97-106.

2Persson, F. and B. Halle, *How amide hydrogens exchange in native proteins.* Proc Natl Acad Sci U S A, 2015. **112**(33): p. 10383-8.

3Devaurs, D., D.A. Antunes, and A.J. Borysik, *Computational Modeling of Molecular Structures Guided by Hydrogen-Exchange Data.* Journal of the American Society for Mass Spectrometry, 2022. **33**(2): p. 215-237.

4Dixon, T., et al., *Predicting the structural basis of targeted protein degradation by integrating molecular dynamics simulations with structural mass spectrometry.* Nature Communications, 2022. **13**(1).

A016B-06-260823

Rapid hits, hotspots and hit-to-lead by crystallographic library screening: case studies in targeting proteins for novel drug discovery

Debanu Das, Ashley Deacon, Matthew Duncton

Accelero Biostructures, California, USA; XPose Therapeutics, California, USA

info@accelerobio.com, info@xposetx.com

Keywords: Fragment-based drug discovery, Structure-based drug discovery, therapeutics

Fragment-based drug discovery (FBDD) is widely used in the pharmaceutical industry to provide novel hits for developing new therapeutics. It allows a more efficient scanning of chemical space compared to high-throughput screening, which has important outcomes in early drug discovery.

Protein X-ray crystallography (PX) is the gold standard for experimentally defining exact binding of a ligand to asses directly target engagement. Absence of crystal structures of target-ligand complexes is a significant impediment to medicinal chemistry optimization of hits. Conventional crystallography is inefficient for screening a large fragment or scaffold library due to expense and effort. Complementary experimental techniques, such as SPR, NMR or TSA are often used to prescreen for ligands that bind, while crystallography is used in a second step to determine the exact binding of each ligand.

With foundational expertise in structural biology, structural genomics and PX, we have developed novel methods for hit generation in early drug discovery. Our platform for ultrahigh-throughput crystallography-based fragment and scaffold library screening accelerates hit generation and hit-to-lead development by directly providing 3D structures of target-bound ligands, potentially leading to ~5-7x reduction in early drug discovery effort while generating intellectual property in the form of identifying binding sites and protein-ligand interactions. This provides an unprecedented experimental route to high quality, high reliability and high value results simultaneously: identification and assessment of target engagement by ligand binding sites and poses; target ligandability; and differentiation of orthosteric and allosteric sites and binders. We will present results on various targets including scientifically validated drug targets that were previously undruggable, resulting in discovery and development of hits and leads in several weeks.

Elucidation of fragment-bound crystal structures reveals locations and poses of ligands and details of protein-ligand interactions, target ligandability, and differentiation of orthosteric and discovery of potential allosteric sites, allowing rapid assessment of synthetic tractability and intellectual property. This allows for fast hit-to-lead development by analog scoping, scaffold hopping and fragment growth, potentially leading to several fold reduction in early drug discovery effort.

We have discovered novel hits against APE1, from which we have developed novel functional inhibitors with IC50s ~250 nM to ~10 uM in *in vitro* biochemical assays with robust activity in cell-based assays. POLH (or POL Eta) is implicated in cisplatin resistant ovarian cancers. We have developed a POLH hit with IC50 ~220 uM in an *in vitro* assay. Our hits for APE1 and POLH represent the first crystal structures of these two DDR proteins bound to small molecule ligands. FEN1 is implicated in several cancers, for which we have identified a novel FEN1 inhibitor with KD ~170 nM.

We will present these results and discuss how we can facilitate new therapeutics development applying our approach to numerous proteins, with a special focus on novel targets that have rich DDR biology and scientific validation but lack clinical inhibitors ("undruggables"). We will also present how our APE1 inhibitors can be translated for related DDR endonucleases, APE2 and LINE1.

[1] Fragment- and structure-based drug discovery for developing therapeutic agents targeting the DNA Damage Response. Wilson DM 3rd, Deacon AM, Duncton MAJ, Pellicena P, Georgiadis MM, Yeh AP, Arvai AS, Moiani D, Tainer JA, Das D. Prog Biophys Mol Biol. 2021 Aug;163:130-142. doi: 10.1016/j.pbiomolbio.2020.10.005. Epub 2020 Oct 25

[2] Early Drug Discovery and Development of Novel Cancer Therapeutics Targeting DNA Polymerase Eta (POLH). Wilson DM, Duncton MAJ, Chang C, Lee Luo C, Georgiadis TM, Pellicena P, Deacon AM, Gao Y, Das D. *Front Oncol. 2021* Nov 19;11:778925. doi: 10.3389/fonc.2021.778925. eCollection 2021.

A038 Crystallography of Nanocrystalline Porous Materials
Room 208
4.00pm - 6.30pm

A038-01-260823

Effects of nanoscale confinement on hydrogen in porous carbons

Valeska P. Ting[1,2], Lui R. Terry [2], Stephane Rols [3], Mi Tian [4], Ivan da Silva [5]

[1]Australian National University, Australia, [2] University of Bristol, UK [3] Institut Laue-Langevin, France, [4] University of Exeter, UK [5] ISIS Neutron Source, UK

E-mail: v.ting@bristol.ac.uk

Keywords: hydrogen, nanopores, neutron scattering

High surface area nanoporous materials such as porous carbons, zeolites and metal-organic frameworks are exceptionally suited for applications in gas separation and storage. Their nanoscale structures can be tuned to allow exceptionally high densities of gas within their pores [1], which can lead to exciting possibilities for energy storage, both by physical adsorption of alternative fuel gases such as hydrogen and through emergence of unusual materials states via gas densification.

In bulk hydrogen, such dense phases typically only form at exceedingly low temperatures or extremely high (typically hundreds of GPa) pressures. However, confinement of H_2 within nanoporous materials has been shown to significantly manipulate the hydrogen phase diagram leading to preferential stabilization of unusual crystalline H_2 phases.

We used pressure and temperature-dependent neutron scattering to map out the phase diagram of H_2 when confined inside both meso- and microporous carbons, demonstrating stabilisation of crystalline hydrogen in microporous carbons, at temperatures far higher than would be possible in bulk H_2 [2]. Such nanoconfinement effects could potentially provide lower energy routes to the formation and study of more exotic non-equilibrium condensed phases of hydrogen that could be useful for a wide range of energy applications.

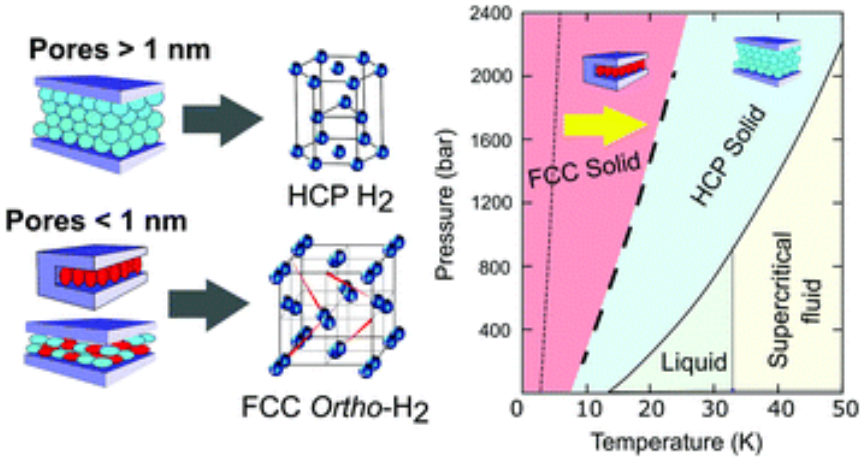

Figure 1. Confinement of hydrogen in nanoporous materials can lead to manipulation of the hydrogen phase diagram, as shown by neutron scattering studies under a range of pressures and temperatures [2]

[1] Ting, V. P, Ramirez-Cuesta, A. J., Bimbo, N., Sharpe, J. E., Noguera Diaz, A., Presser, V., Rudic, S. and Mays, T. J., Direct evidence for solid-like hydrogen in a nanoporous carbon hydrogen storage material at supercritical temperatures**.** *ACS Nano,* 2015, **9** (8), 8249–8254.

[2] Terry, L. R., Rolls, S., Tian, M., da Silva, I., Bending, S., Ting V.P., Manipulation of the crystalline phase diagram of hydrogen through nanoscale confinement effects in porous carbons, *Nanoscale,* 2022, **14,** 7250-7261

A038-02-260823

Low dose electron microscopy imaging for beam-sensitive metal-organic frameworks

Y. Zhou, O. Terasaki

School of Physical Science and Technology, ShanghaiTech University, Shanghai 201210, China

zhouyi@shanghaitech.edu.cn

Keywords: Low dose imaging, beam-sensitive materials, metal-organic frameworks

The proper structure characterization for nanocrystals of novel metal-organic frameworks (MOFs) can promote the development of new structures and design of new functions. High resolution electron microscopy imaging plays an important role in this aspect. However, due to the electron beam-sensitivity of MOFs, the high-resolution electron microscopy imaging for this kind of porous material systems meets great challenges. Herein, we showed several examples on our efforts for low dose electron microscopy imaging for MOF crystals, by which new MOF structures are confirmed and structure details such as pore arrangement and crystal edges are revealed.

In the case of a conjugated copper -catecholate framework (Cu-DBC) [1], because of the limited quality of three-dimensional electron diffraction (3D ED) data, only unit cell parameters and electron potential map are obtained. The structure model is built by fitting the potential map then. Nonetheless, this model needs to be further confirmed. By carefully controlling electron dose and apply proper image alignment procedure, clear pore arrangement with obvious crystal edges is observed along the *c* axis, which fits very well with the solved structure model. Meanwhile, high-resolution image perpendicular to the *c* axis reveals the alignment of different layers unambiguously. Based on the information of this image, 3D potential map could be reconstructed in which the linkage of the framework presented clearly (Fig. 1).

On the other hand, annular dark-field (ADF) imaging in scanning transmission electron microscopy (STEM) provides straightforward information of atom positions in the sample. Considering this advantage, we propose a universal strategy to improve electron utilization efficiency for high resolution and signal-to-noise ratio (SNR) in low-dose STEM imaging of beam sensitive MOF crystals [2]. By continuously adjusting convergence semi-angle α and collection angle β through lens control on commercial STEM, different optimal imaging conditions can be customized. Using this strategy, crystal edge features as well as metal cluster in MIL-101 MOF crystal are observed clearly under extremely low dose conditions with beam current as low as 0.20 pA.

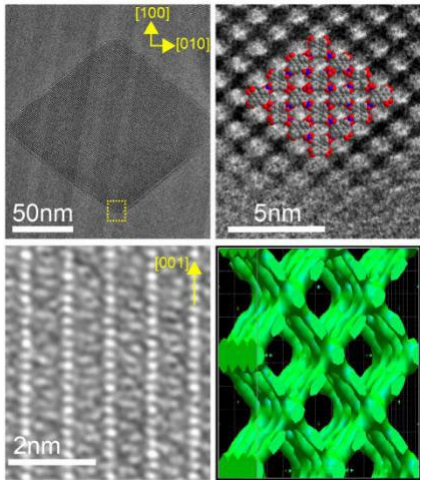

Figure 1. High resolution electron microscopy imaging of Cu-DBC MOF crystals

[1] Liu, J., Zhou, Y., Xie, Z., Li, Y., Liu, Y., Sun, J., Ma, Y., Terasaki. O. & Chen. L. (2020). *Angew. Chem. Int. Ed.*, **59**, 1081.
[2] Wang, L., Jiang, Y., Zhou, Y., Shi, R., Hosokawa, F., Terasaki, O. & Zhang, Q. (2022). *Part. Part. Syst. Charact.* DOI: 10.1002/ppsc.202200122.

A038-03-260823

Structure determination of natural-product-based MOFs by electron crystallography

E. Svensson Grape[1], A.J. Chacón[2], S. Rojas[2], Y. Pérez[2,3], M. Nero[1], M. Narongin-Fujikawa[4], C. Baresel[4], T. Willhammar[1], P. Horcajada[2], A.K. Inge[1]

[1]Department of Materials and Environmental Chemistry, Stockholm University, Sweden, [2]Advanced Porous Materials Unit, IMDEA Energy, Madrid, Spain, [3]Departamento de Biología y Geología, Física y Química Inorgánica, ESCET, Universidad Rey Juan Carlos, Madrid, Spain. [4]IVL Swedish Environmental Research Institute, Stockholm, Sweden.
andrew.inge@mmk.su.se

Keywords: electron diffraction, metal-organic frameworks, natural products

Research on metal-organic frameworks (MOFs) has gained much interest in recent decades, in part due to their unparalleled structural and chemical diversity within in the field of porous materials. When developing new MOF materials, structural characterization is essential in order to understand and exploit their physical and chemical properties. Most MOF structures are solved by single crystal X-ray diffraction. However, many of the more stable MOFs often tend to be synthesized as (sub)micrometer sized crystals that may be too small for this technique. With recent developments in single crystal electron diffraction techniques, structure determination from submicrometer sized crystals can often be quite straight forward, even for organic and metal-organic compounds.

Recently we have strived towards developing new MOFs that are relatively stable, inexpensive and easily synthesized from nontoxic metals combined with natural products i.e. organic molecules produced by living organisms. The most popular organic linkers used to synthesize MOFs are based on synthetic molecules functionalized with carboxylate groups, however we have been exploring the use of common plant-based phenolic molecules that are the building units of tannins i.e. natural polyphenols. We hypothesize that such MOFs could demonstrate chemical robustness while offering eco- and biocompatibility appealing for biomedical and environmental applications.

We reported the synthesis of the first MOF made from ellagic acid, a well-known edible antioxidant common in fruits, nuts, and tree bark[1]. This MOF, denoted SU-101, was synthesized in a simple and green procedure from entirely edible starting reagents stirred in water at room temperature. The MOF can be synthesized from ellagic acid sold as a dietary supplement and extracted from pomegranate peel or tree bark, which are waste materials from the food, pulp and paper industries. Although SU-101 demonstrated excellent chemical robustness for a MOF, its rather small pore size of 7 Å limited its application to the capture of small pollutant molecules such as CO_2, H_2S, SO_2.

More recently we have developed a second MOF from ellagic acid, denoted SU-102, with considerably larger 12 Å wide pores [2]. Due to the larger pore size, SU-102 could be applied to capture larger organic molecules, such as pharmaceutical pollutants found in real effluent from municipal wastewater treatment facilities. Both the structures of SU-101 and SU-102 were solved by electron diffraction (Fig. 1). Due to its high stability, sectioned crystals of SU-102 could also be imaged by scanning transmission electron microscopy (STEM).

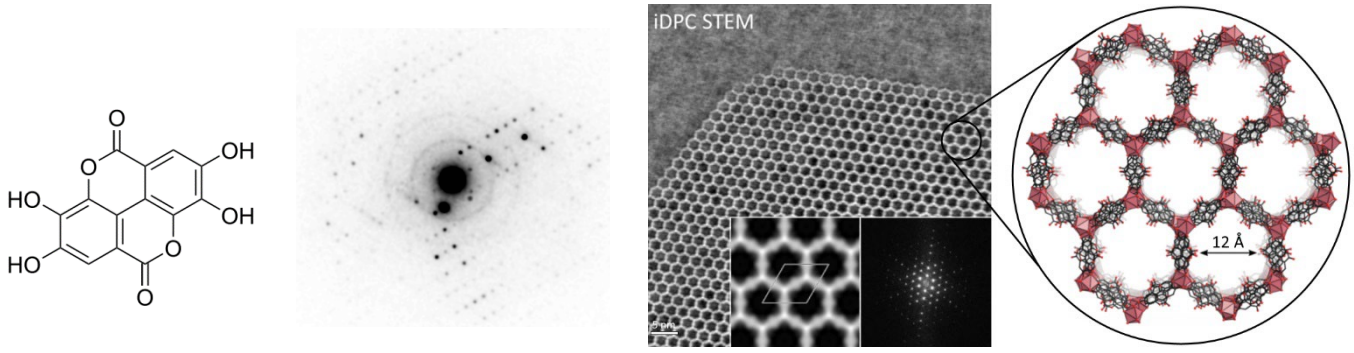

Figure 1. (far left) Ellagic acid. (left) A frame of electron diffraction data, (right) iDPC STEM image with lattice averaged image and its Fourier transform as inserts, and (far right) crystal structure of the MOF SU-102[2].

[1] Svensson Grape, E. et al. (2020). *J. Am. Chem. Soc.*, **142**, 16795.
[2] Svensson Grape, E. et al. (2022). *ChemRxiv*, DOI:10.26434/chemrxiv-2022-h3530.

AKI acknowledges the Swedish Foundation for Strategic Research (SSF) and the Knut and Alice Wallenberg Foundation (KAW).

A038-04-260823

Nano-crystalline sponge method enabled by 3D ED using a flexible Bi metal-organic framework

Sofiia Butonova, Jung Cho, Zhehao Huang, Xiaodong Zou

Stockholm University, Stockholm, Sweden

sofiia.butonova@mmk.su.se

Keywords: Crystalline Sponge Method, MOFs, 3D ED

The crystalline sponge method enables the determination of 3D structure of non-crystalline organic molecules through diffraction techniques by using well-ordered porous materials, such as metal-organic-frameworks (MOFs), to capture and transform the guests into a regularly ordered form. [1] This strategy obviates the need to crystallize a targeted compound in its liquid or gas phase and requires only a small amount of the sample to be analysed. However, the number of potential crystalline sponges is limited because porous materials are often nanocrystalline and unsuitable for single-crystal X-ray diffraction analysis. 3D electron diffraction (3D ED) overcomes the size limitation and allows for the determination of 3D structure from nano-sized powders, expanding the applicability of the crystalline sponge method. Herein, we demonstrate that 3D ED is a powerful method for characterising crystalline sponges by using a nanocrystalline Bi-MOF SU-100 [2] as the prototype sponge. SU-100 was chosen based on its ability to alter its unit cell accordingly to different guest molecules, and thus, the soaking progress could be easily tracked by powder X-ray diffraction. Attributable to the excellent chemical stability of SU-100, 7 molecules consisting of different interactions with the crystalline sponge were studied. The synthesis of SU-100 could be done in one hour, whereas the guest soaking could also be done in as little as an hour. By collecting 3D ED data under ultra-low electron dose (~0.0025 e-/Å·s) and cryogenic conditions, all guest species could be directly located at the atomic resolution.

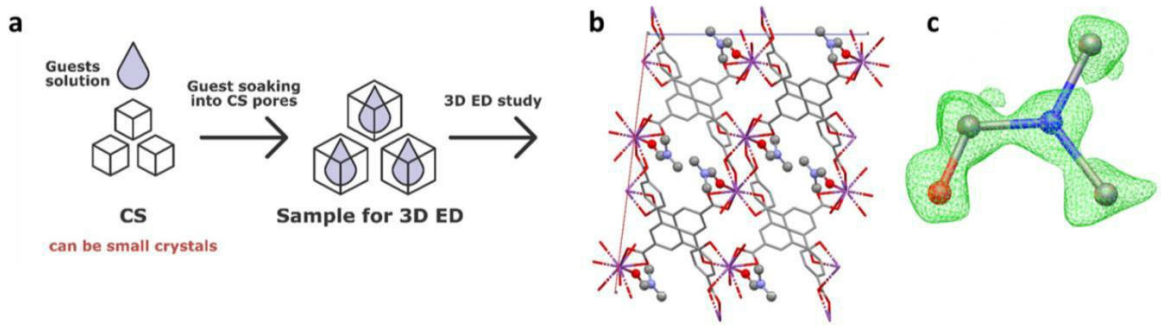

Figure 1. a. CS method based on flexible SU-100 by 3D ED. b, Framework structure of SU-100 comprising DMF, view along [010]. c, difference Fourier map (3σ) showing the electrostatic potential from the DMF molecule. The model of the DMF is superimposed.

[1] Inokuma, Y.; Yoshioka, S.; Ariyoshi, J.; Arai, T.; Hitora, Y.; Takada, K.; Matsunaga, S.; Rissanen, K.; Fujita, M. (2013), Nature, **495**, 461–466.

[2] Grape, E. S.; Xu, H.; Cheung, O.; Calmels, M.; Zhao, J.; Dejoie, C.; Proserpio, D. M.; Zou, X.; Inge, A. K. (2020), Cryst. Growth Des **20**, 320– 329.

A038-05-260823

Structure determination of nanocrystalline metal-organic frameworks by 3D electron diffraction

Jandl[1], J. Merkelbach[1], G. Steinfeld[1], G. Santiso-Quinones[1], D. Stam[1], P. Simoncic[1], E. Hovestreydt[1]

ELDICO Scientific AG, PARK INNOVAARE: deliveryLAB, 5234 Villigen, Switzerland

jandl@eldico.ch

Keywords: electron diffraction/3D ED/microED, MOFs

3D electron diffraction (3D ED, MicroED) is emerging as a powerful technique for the structural elucidation of challenging compounds as it bypasses the main limitation of growing crystals of suitable size for single-crystal X-ray diffraction. Applications range from natural products and pharmacology to geological sciences, advanced materials, nanotechnology, and many more.

Metal-Organic Frameworks (MOFs) are porous materials, which are commonly obtained from solvothermal synthesis and therefore cannot be recrystallised. Structure elucidation is thus limited to the as synthesised material. Being able to work with nanocrystalline powders makes 3D ED the ideal tool to tackle this problem and determine structures from crystals that are too small even for synchrotron facilities.

We show a range of examples including both nanocrystalline samples of known MOFs and new materials, all measured in continuous rotation mode on a dedicated electron diffractometer. High quality data also allow the study of molecular motion in the crystals and the identification of changes of the structures by solvent removal from the pores. The results illustrate the potential of this technique in the field of porous coordination networks and the benefits of dedicated instrumentation that has become available in recent years.

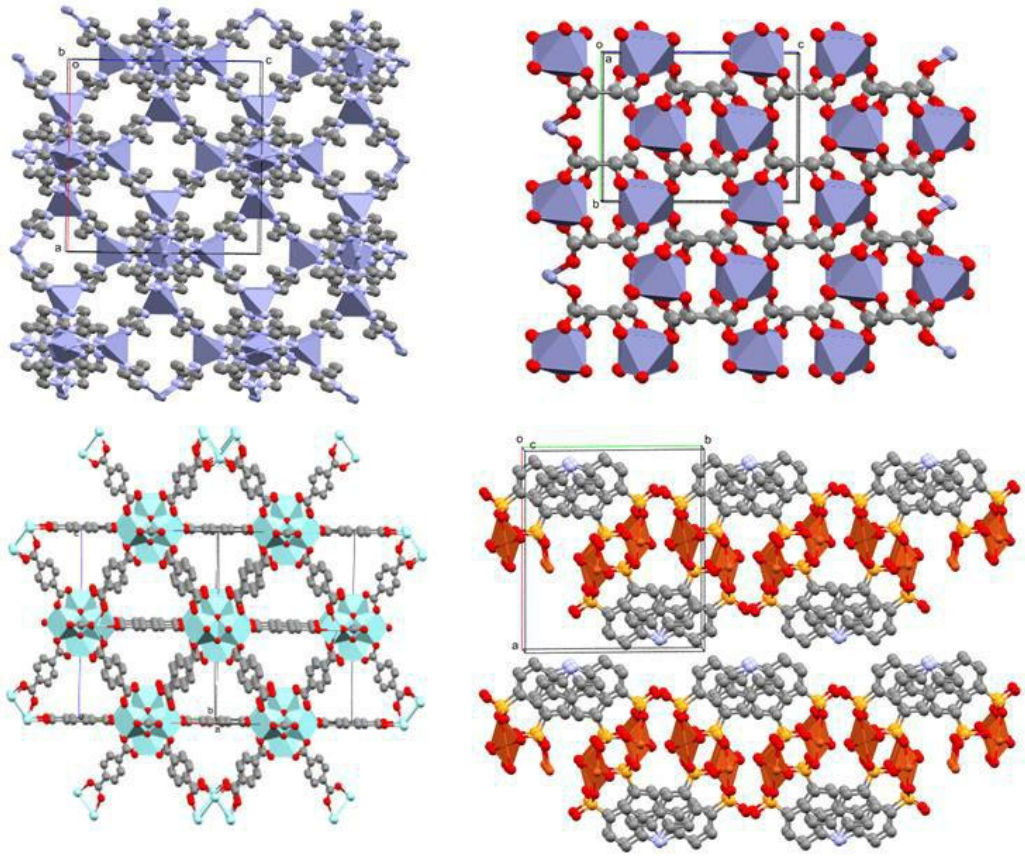

Figure 1. Packing diagrams of selected MOF structures determined by 3D ED: ZIF-8 (top left), UiO-66 (bottom left), Zn-tartrate (top right), CuDPC (bottom right, DPC = 3,6-diphosphonylcarbazole).

A038-06-260823

Transmission Electron Microscopy (TEM) methods for imaging beam sensitive crystals

Daliang Zhang

Multi-scale Porous Materials Center, Institute of Advanced Interdisciplinary Studies & School of Chemistry and Chemical Engineering, Chongqing University, Chongqing, China

Keywords: Low-dose TEM, Cryo-FIB, 4D-STEM

Imaging of electron beam sensitive materials is one of the most difficult applications in High-Resolution Transmission Electron Microscopy (HRTEM). The challenges include the preparation of TEM specimen without damaging the crystal structure, the alignment for crystal zone axes before high resolution TEM imaging, post-process of experimental images *etc*. We developed a suite of methods to acquire atomic-resolution TEM images by using Direct Electron Detection Camera (CCDC) [1-3], a new Cryo-FIB workflow for preparing TEM lamella of beam sensitive crystals[4]. The highest resolution observed in TEM images is about 0.14 nm from an HKUST MOF crystal. Structural dislocations, grain boundaries are observed by low dose HRTEM imaging with atomic resolution.

Recently, 4D scanning transmission electron microscopy (4D-STEM) and ptychography reconstruction presented strong potential in atomic resolution imaging of beam sensitive crystalline material, such like zeolites, Metal Organic Framework (MOF) structures. In contrast, the phase image constructed from 4D-STEM requiring a low electron dose rate and can be archive very high resolution for both weak and heavy atoms even with defocused or non-Cs-corrected electron beams. We have developed a new ray-path-reconstruction method to efficient image calculation, which also capable to depth estimation, refocusing, and 3D presentation et al.

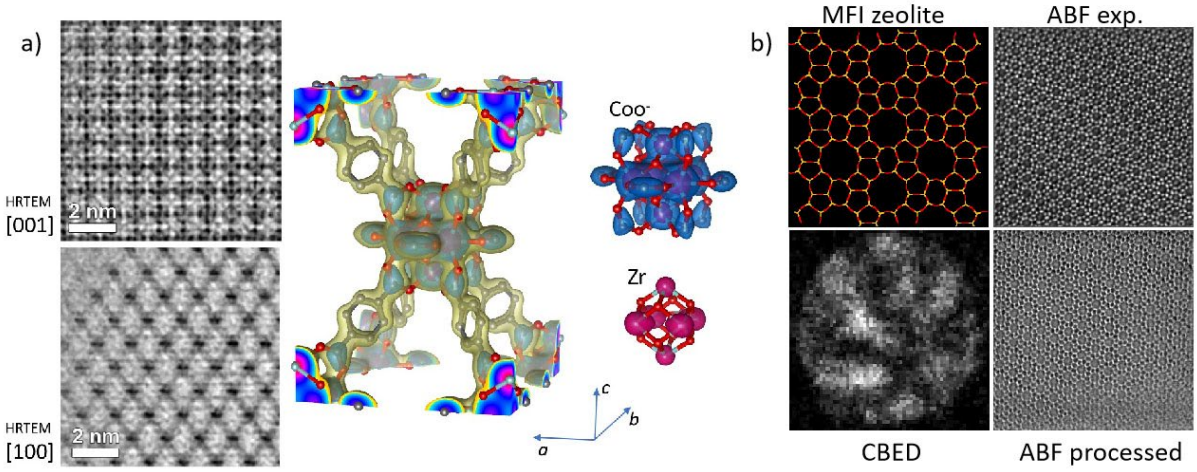

Figure 1. a) HRTEM imaging of defected MOF UiO-66 with 3D-reconstruction result of electron potential map; b) 4D-stem refocusing result of MFI zeolite along the [010] zone axis.

[1] Zhang D., Zhu Y., Liu L., Ying X., Hsiung C.-E., Sougrat R., Li K. & Han Y. (2018) *Science* **359**, 675
[2] Liu L., Chen Z., Wang J., Zhang D., Zhu Y., Ling S., Huang K., Belmabkhout Y., Adil K., Zhang Y., Slater B., Eddaoudi M. & Han Y. (2019) *Nature Chemistry* **11**, 622
[3] Li X., Wang J., Liu X., Liu L., Cha D., Zheng X., Yousef A., Song K., Zhu Y., Zhang D. & Han Y. (2019) *Journal of the American Chemical Society* **141**, 12021
[4] Zhou J., Wei N., Zhang D., Wang Y., Li J., Zheng X., Wang J., Alsalloum A., Liu L., Bakr O. & Han Y. (2022) *Journal of The American Chemical Society* **144**, 3182

A074 Methods for the Determination and Analysis of Magnetic Structures
Room 212/213
4.00pm - 6.30pm

A074-01-260823

A reverse Monte Carlo algorithm to simulate two-dimensional small-angle scattering intensities

L. C. Barnsley[1], N. Nandakumaran[2], A. Feoktystov[3], M. Dulle[4], L. Fruhner[4], M. Feygenson[5, 4]

[3] Australian Synchrotron, ANSTO, Clayon 3168, Australia, 2. Forschungszentrum Jülich GmbH, Jülich Centre for Neutron Science (JCNS-2) and Peter Grünberg Institut (PGI), JARA-FIT, 52425 Jülich, Germany, 3. Forschungszentrum Jülich GmbH, Jülich Centre for Neutron Science (JCNS) at Heinz Maier-Leibnitz Zentrum (MLZ), 85748 Garching, Germany, 4. Forschungszentrum Jülich GmbH, Jülich Centre for Neutron Science (JCNS-1), 52425 Jülich, Germany, 5. European Spallation Source ERIC, SE-22100, Lund, Sweden

Email of communicating author lester.barnsley@ansto.gov.au

Keywords: small-angle scattering; magnetic nanoparticles, reverse Monte Carlo simulations

Small-angle neutron scattering (SANS) and small-angle X-ray scattering (SAXS) are important, experimental techniques for studying the behaviour and properties of materials on the nanoscale. Small-angle scattering (SAS) has been used to investigate systems relevant to a range of scientific fields, including polymers [1], inorganic nanoparticles [2] and magnetic vortices [3]. While the technique is well-established for its versatility and compatibility with a range of sample environments for in-situ studies, analysis of experimentally acquired data is still challenging, particularly in light of the growing complexity of the studied systems.

Numerous out-of-the-box options exist for analysing structures measured by SAS, but many of these are underpinned by assumptions about the underlying interactions that are not always relevant for a given system. In this presentation, we describe a numerical algorithm based on reverse Monte Carlo simulations to model the intensity observed on a SAS detector as a function of the scattering vector [4]. The model simulates a two-dimensional detector image, accounting for magnetic scattering, instrument resolution, particle polydispersity and particle collisions, while making no further assumptions about the underlying particle interactions.

By simulating a 2-D image that can be potentially anisotropic, the algorithm is particularly useful for studying systems driven by anisotropic interactions. The final output of the algorithm is a relative particle distribution, allowing visualisation of particle structures that form over long-range length-scales (i.e., several hundred nanometres), along with an orientational distribution of magnetic moments. We show the effectiveness of the algorithm by modelling a SAS experimental dataset studying finite-length chains consisting of magnetic nanoparticles, which assembled in the presence of a strong magnetic field due to dipole interactions [5].

[1] Mortensen, K., *Advanced Functional Molecules and Polymers* **2**, 223 (2001).
[2] Mehdizadeh Taheri, S., Michaelis, M., Friedrich, T., Förster, B., Drechsler, M., Römer, F., Bösecke, P., Narayanan, T., Weber, B., Rehberg, I., Rosenfeldt, S. & Förster, S., *Proceedings of the National Academy of Sciences* **112**, 14484 (2015).
[3] Mühlbauer, S., Binz, B., Jonietz, F., Pfleiderer, C., Rosch, A., Neubauer, A., Georgii, R. & Böni, P., *Science* **323**, 915 (2009).
[4] Barnsley, L.C., Nandakumaran, N., Feoktystov, A., Dulle, M., Fruhner, L. & Feygenson, M., *Journal of Applied Crystallography* **55**, In press (2022).
[5] Nandakumaran, N., Barnsley, L., Feoktystov, A., Ivanov, S., Huber, D., Fruhner, L., Leffler, V., Ehlert, S., Kentzinger, E., Qdemat, A., Bhatnagar-Schöffmann, T., Rücker, U., Wharmby, M., Cervellino, A., Dunin-Borkowski, R., Brückel, T. & Feygenson, M. *Advanced Materials* **33**, 2008683 (2021).

A074-01-260823

Large magnetovolume effect in a cobaltite perovskite

Ping Miao[1,2], Zhijian Tan[1,2], Dong Zhang[1,2], Tan Zhenhong[1,2], Takashi Kamiyama[1,2]

[1]Institute of High Energy Physics, Chinese Academy of Sciences, [2]Spallation Neutron Source Science Center

Email of communicating miaoping@ihep.ac.cn

Keywords: negative thermal expansion, magnetovolume effect, neutron diffraction

Materials that show negative thermal expansion (NTE) have significant industrial merit because they can be used to fabricate composites whose dimensions remain invariant upon heating. In some materials, NTE is concomitant with the spontaneous magnetization due to the magnetovolume effect (MVE). Here we report a new class of MVE material; namely, an A-site ordered perovskite $PrBaCo_2O_{5.5+x}$ ($0 \leq x \leq 0.41$), in which strong NTE is induced by hole doping [1]. Through a comprehensive study with multiple probes, in particular neutron diffraction under variant temperatures, hydrostatic pressures and magnetic fields, we found the MVE originates from an magnetoelectric transition from an antiferromagnetic insulating large-volume (AFILV) phase to a ferromagnetic less-insulating small-volume (FLISV) phase (see Figure 1) [2, 3]. Based on the mechanism, we further modified the thermal expansion properties in the A-site disordered $La_{0.5}Ba_{0.5}CoO_{3-x}$, which crystallizes into a cubic structure and features the isotropic thermal expansion. Room-temperature zero thermal expansion has been finally achieved in this simple cubic perovskite, which holds high potential for practical applications [4, 5].

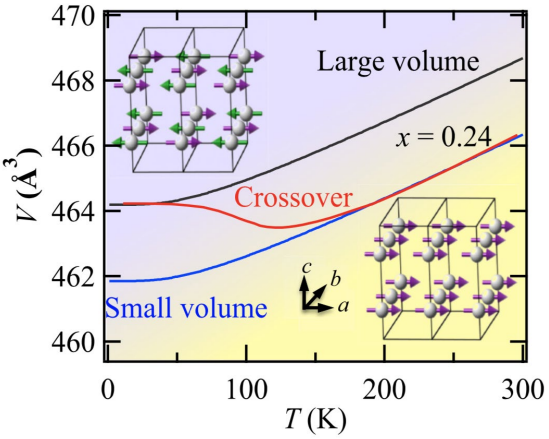

Figure 1. The magnetoelectric transition model for NTE of PrBaCo2O5.5+x (x = 0.24) [3].

[1] P. Miao, X. Lin, A. Koda, S. Lee, Y. Ishikawa, S. Torii1, M. Yonemura, T. Mochiku, H. Sagayama, S. Itoh, Y. Wang, R. Kadono and T. Kamiyama, (2017). *Adv. Mater.* **29**, 1605991

[2] Z. Tan, P. Miao, X. Lin, S. Lee, Y. Ishikawa, M. Hagihala, S. Torii, Y. Wang, M. Yonemura and T. Kamiyama, (2018). *Physica B*, **551**, 111

[3] P. Miao, Z. Tan, S. Lee, Y. Ishikawa, S. Torii, M. Yonemura, A. Koda, K. Komatsu, S. Machida, A. Sano-Furukawa, T. Hattori, X. Lin, K. Li, T. Mochiku, R. Kikuchi, C. Kawashima, H. Takahashi, Q. Huang, S. Itoh, R. Kadono, Y. Wang, F. Pan and T. Kamiyama, (2021). *Phys. Rev. B* **103**, 094302

[4] Z. Tan, P. Miao, Y. Ishikawa, M. Hagihala, S. Lee, S. Torii, M. Yonemura, T. Moyoshi and T. Kamiyama, (2018). *Atom Indonesia* **44**, 49

[5] Z. Tan, P. Miao*, Y. Ishikawa, M. Hagihala, S. Lee, S. Torii, M. Yonemura, T. Moyoshi and T. Kamiyama, (2020). *J. Phys. Chem. Lett.* **11**, 6785

A074-03-260823

Neutron scattering investigations of magnetism and competing interactions in 2D van der Waals layered materials

S. Calder[1], X. Bai[1,2], A. Haglund[3], Y. Liu[1], D. M. Pajerowski[1], H. Cao[1], T. Williams[1], A. I. Kolesnikov[1], G. E. Granroth[1], V. O. Garlea[1], F. Lechermann[4], A. F. May[1], D. Mandrus[3]

[1]Oak Ridge National Laboratory, Oak Ridge, TN 37831, USA. [2]Louisiana State University, Baton Rouge, LA, USA. [3]University of Tennessee, Knoxville, Tennessee 37996, USA. [4]Ruhr-Universität Bochum, D-44780 Bochum, Germany.
caldersa@ornl.gov

Keywords: Magnetism, neutron diffraction, inelastic neutron scattering, low dimensional, van der Waals

Reducing the dimensionality of a compound to topologically constrained layers can enhance quantum phenomena and drive novel behaviour. In this context two-dimensional (2D) layered materials, that can exist from the bulk down to single layers due to weak interlayer van der Waals (vdW) bonding, have undergone intense interest. A particular focus for quantum research is on the role of the magnetic spin in these 2D vdW materials on the emergent properties. Neutron scattering can provide unique insights into low dimensional materials through bulk powder and single crystal measurements that access the low dimensional behaviour in suitable chosen model materials. Here, a series of such materials will be explored and new insights provided on the magnetic structure, exchange interactions and further competing interactions through measurements and analysis with complementary neutron techniques.

Many 2D vdW materials undergo long range ordered magnetic transitions, however, the low dimensional nature leads to short range correlations developing that proceed the ordered phase. Neutron scattering can provide insights into both regimes. Detailed knowledge can be gained from symmetry analysis with magnetic space groups and irreducible representations for long range magnetic order. Measurements utilizing the pair distribution technique (PDF) can be applied to magnetism (mPDF) to reveal short range ordering. Competing interactions within ordered magnetic phases can also exist in 2D vdW materials that drive new or coexisting phases.

Neutron diffraction measurements on $CrPS_4$ [1], $MnPSe_3$ [2] and $Fe_{3-x}GeTe_2$ [3] will be presented to highlight the role of competing interactions from short-to-long range order and between different magnetic ground states within these 2D layered structures. The discussions will be complimented by inelastic neutron scattering measurements and half-polarized neutron powder diffraction (PNPD) to provide further details on the local magnetization and exchange interactions in low dimensional materials.

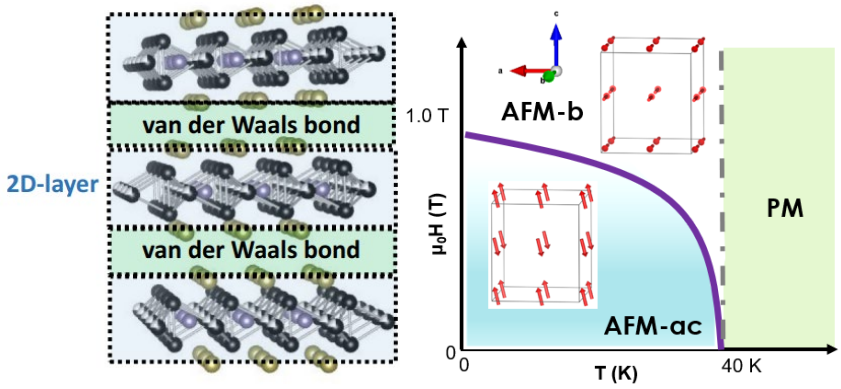

Figure 1. (Left) Crystal structure of the layered 2D van der Waals material $Fe_{3-x}GeTe_2$. (Right) Magnetic phase diagram in $CrPS_4$ determined with neutron diffraction.

[1] S. Calder, A. Haglund, Y. Liu, D. M. Pajerowski, H. B. Cao, T. J. Williams, O. V. Garlea, D. Mandrus, *Phys. Rev. B*, 102, 024408 (2020).
[2] S. Calder, A. Haglund, A. I. Kolesnikov, D. Mandrus, *Physical Review B*, 103, 024414 (2021).
[3] X. Bai, F. Lechermann, Y. Liu, Y. Cheng, A. I. Kolesnikov, F. Ye, T. J. Williams, S. Chi, T. Hong, G. E. Granroth, A. F. May, S. Calder, *Phys. Rev. B*, 106, L180409 (2022).

This research used resources at the High Flux Isotope Reactor and Spallation Neutron Source, a DOE Office of Science User Facility operated by the Oak Ridge National Laboratory.

A074-04-260823

Magnetic, electric and toroidal polarization modes describing the physical properties of crystals. $NdFeO_3$ case

P. Fabrykiewicz[1,2], R. Przeniosło[3], I. Sosnowska[3]

[1] *Institute of Crystallography, RWTH Aachen University, Germany*
[2] *Jülich Centre for Neutron Science (JCNS) at Heinz Maier-Leibnitz Zentrum (MLZ), Garching, Germany,*
[3] *Faculty of Physics, University of Warsaw, Poland*
Piotr.Fabrykiewicz@frm2.tum.de

Keywords: Symmetry, Magnetic ordering, Ferroelectric ordering, Toroidal ordering, Multiferroics, Orthoferrites, NdFeO3

We present [1] the answer to the question: *which groups allow to describe a given magnetic, electric and toroidal (anapole) polarization mode?* These three classifications are based on magnetic point groups used in two contexts: (i) the magnetic point group of the magnetic crystal class and (ii) the magnetic site symmetry point group of the Wyckoff position of interest. Magnetic, electric and toroidal modes are considered in restricted sense, i.e. as set-of-directions, disregarding the atomic positions. For magnetic, electric and toroidal orderings there are 64 modes: 3 pure ferro(magnetic/electric/toroidal) modes, 13 mixed ferro(magnetic/electric/toroidal) with antiferro(magnetic/electric/toroidal) modes, and 48 pure antiferro(magnetic/electric /toroidal) modes. The proposed classification of modes leads to useful observations: the electric and toroidal modes have many symmetry limitations similar to those already known for the magnetic modes [2, 3], e.g. continuous reorientations of the magnetic or electric or toroidal moments are possible only in triclinic or monoclinic symmetry. Similarly, antiferro(magnetic/electric/ toroidal) ordering with a weak perpendicular ferro(magnetic/electric/toroidal) component is possible only in monoclinic or orthorhombic symmetry.

To visualise the similarities of magnetic, electric and toroidal modes, we propose a new Rotation-Inversion (RI) notation [1] of magnetic point groups which does not prioritise or distinguish any of three generalised inversions: space inversion, -1, time inversion, 1', and both space-and-time inversion, -1'. Each operation O from a magnetic point group is a product O = RI of one proper rotation R = 1, 2, 3, 4 or 6 and one generalized inversion I = 1, -1, 1' or -1'. Proper rotations transform magnetic, electric and toroidal polarizations in the same way while inversions in different ways. Starting from the magnetic point group which describes a certain mode of the magnetic moment, we can obtain another magnetic point group which describes the same mode for electric polarization by a specific permutation of generalized inversions which changes -1 to 1' in RI decomposition of each operator of the magnetic point group as shown graphically in Fig. 1.

The general classifications of electric, magnetic and toroidal modes are presented for the case of NdFeO3. The predicted monoclinic NdFeO3 symmetry [1, 2] leads to a nontrivial Dirac multipoles motif which could be confirmed using neutron diffraction or resonant x-ray diffraction [4].

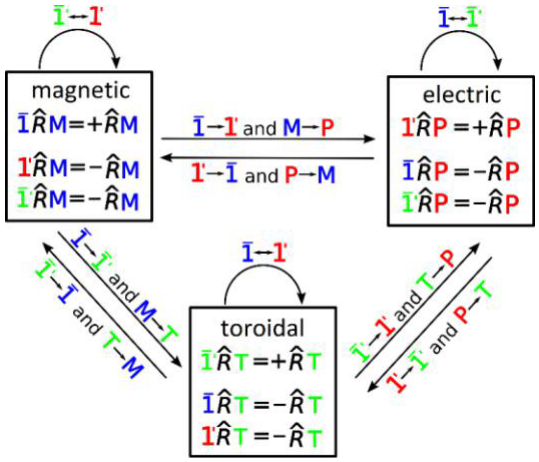

Figure 1. Schematic presentation of the action of permutations of generalised inversions -1, 1' and -1' on the magnetic moment, M, the electric polarization, P, and the toroidal polarization, T. Symbol R (with hat) represents the proper rotation.

[1] Fabrykiewicz P., Przeniosło R. & Sosnowska I. (2023). *Acta Cryst. A*, **79**, 80.
[2] Fabrykiewicz P., Przeniosło R. & Sosnowska I. (2021). *Acta Cryst. A*, **77**, 327.

[3] Przeniosło R., Fabrykiewicz P. & Sosnowska I. (2018). *Acta Cryst. A*, **74**, 705.
[4] Lovesey S. W. (2023). arXiv:2301.10189 [cond-mat.str-el].

A074-05-260823

The high pressure diffraction option on single crystals at MLZ: Development of an area detector prototype for HEiDi and other components

M. Meven[1,2], Andrzej Grzechnik[4], Andreas Eich[1,3], Muni Poli[1,2], Ralf Engels[3], Jianhui Xu[1,2], Robert Georgii[5], Yixi Su[2], Karen Friese[3]

[1]Institute of Crystallography, RWTH Aachen University, 52056 Aachen, Germany; [2]Jülich Centre for Neutron Science (JCNS) at Heinz Maier-Leibnitz Zentrum, Forschungszentrum Jülich GmbH, 85747 Garching, Germany; [3]JCNS-2/Peter Grünberg-Institute–4, Forschungszentrum Jülich GmbH, 52425 Jülich, Germany; [4]JCNS-4, Forschungszentrum Jülich GmbH, 52425 Jülich, Germany; [5]Research Neutron Source FRM II, Technische Universität München, 85748 Garching, Germany

martin.meven@frm2.tum.de

Keywords: neutron scattering, single crystal diffraction, high pressure

Numerous scientific topics in physics, chemistry, mineralogy and material sciences profit from single crystal neutron diffraction studies. For this purpose, the HEiDi single crystal diffractometer at the hot source of the MLZ's neutron source FRM II offers high neutron flux, high resolution and a large Q range making it an excellent tool to obtain detailed structural information.

In addition to temperature-dependent studies, pressure-dependent studies are becoming increasingly important, for example to better understand the behavior of functional materials such as magnetocalorics [1, 2]. In order to establish these capabilities at MLZ, within a BMBF funded project on HEiDi, its neutron optics were optimized for max. flux at short wavelengths (e. g. $\lambda = 0.87$ Å) and large signal-to-noise ratio for studies on small samples << 1 mm³ as well as diamond anvil cells up to 1 GPa and down to low temperatures [3]. Recently, within a second BMBF project, we have complemented these efforts by developing optimized clamp cell designs [4] for other instruments (POLI, DNS and MIRA). These cells are better suited for larger sample volumes and single-crystal neutron studies under an applied magnetic field. First tests of these cells show promising results [5].

In this context, we are also developing a position-sensitive area detector (PSD) in cooperation with JCNS. This prototype uses ^{6}Li glass for neutron-to-photon conversion and fifteen position-sensitive photomultipliers. This design offers high sensitivity at short wavelengths and a sensitive area of 23° x 13° (width x height) with a reasonable resolution, allowing rapid detection of weak signals and (e.g. incommensurate or magnetic) superstructure reflections, as well as faster and more efficient sample characterization and data collection.

In our conference contribution we report on the current status and details of our project, for example on pressure cells and PSD, and hope to be able to offer users at the MLZ high-pressure diffraction experiments on a regular base in the near future.

[1] A. Grzechnik et al. (2018); *J. Appl. Cryst.* **51**, 351-356.
[2] A. Eich et al. (2019); *Mater. Res. Express* **6**, 096118.
[3] A. Grzechnik et al. (2020); *J. Appl. Cryst.* **53**(1), 1 - 6.
[4] S. Klotz (2013); *Techniques in High Pressure Neutron Scattering. CRC Press*.
[5] Eich, A. et al. (2020); *High Press. Res.* **41**[1], 88–96 (2020).

We are grateful to the German Federal Ministry of Education and Research (BMBF) for financial support of the above projects (project no. 05K16PA3 and 05K19PA2).

A074-06-260823

Symmetry-dependent magnetic, electric, and optical properties in ferroic and multiferroic materials

Tsuyoshi Kimura

Department of Advanced Materials Science, University of Tokyo, Japan

tkimura@edu.k.u-tokyo.ac.jp

Keywords: Keyword multiferroics, magnetoelectric effect, ferroaxial materials

The symmetry breaking ascribed to the evolution of an order parameter is one of the most important concepts in materials physics. Representative examples are symmetry breakings in “ferroic” materials such as the symmetry breaking of time reversal in ferro-magnets and that of space inversion in ferro-electrics. Thus, one can find that this concept contributes to not only fundamental science but also materials’ functionalities available for device applications. Furthermore, recent research developments of “multiferroic” materials with broken time-reversal and space-inversion symmetries have triggered extensive studies on unconventional ferroic materials such as “ferro-toroidic” and “ferro-axial” materials.

The relationships among ferro-electric, ferro-magnetic, ferro-toroidal, and ferro-axial orders are schematically illustrated in Fig. 1. In the case of ferro-toroidal order whose order parameter is a toroidal moment, that is, the sum of the cross product of spin and its position vector. Most typically, the toroidal moment is generated by head-to-tail arrangement of magnetic dipoles, which breaks both the time-reversal and space-inversion symmetries. When we replace magnetic dipoles in toroidal moment with electric dipoles, ferro-axial moment is generated. In the ferro-axial order, a rotational electric-dipole arrangement breaking some mirror symmetry, the so-called ferro-axial moment, is an order parameter.

In this presentation, we show symmetry-dependent magnetic, electric, and optical phenomena characteristic of unconventional ferroic orders such ferro-toroidal, ferro-axial, and ferro-quadrupole orders. The phenomena include magnetoelectric effect, nonreciprocal optical responses, and electrogyration. Furthermore, in general, ferroic materials bear “domain” structures, that is, spatial distributions of order parameters. However, observations of domain structures in unconventional ferroic materials are not straightforward. Here, we also show ways to spatially visualize domain structures in such unconventional ferroic materials.

This work has been done in collaboration with K. Kimura, T. Hayashida, K. Arakawa, T. Oshima, R. Misawa, Y. Uemura, S. Matsuoka, T. Hasegawa, D. Morikawa, K. Tsuda, and S. Hirose, H. Morioka, F. Iga, and Y. Tanaka.

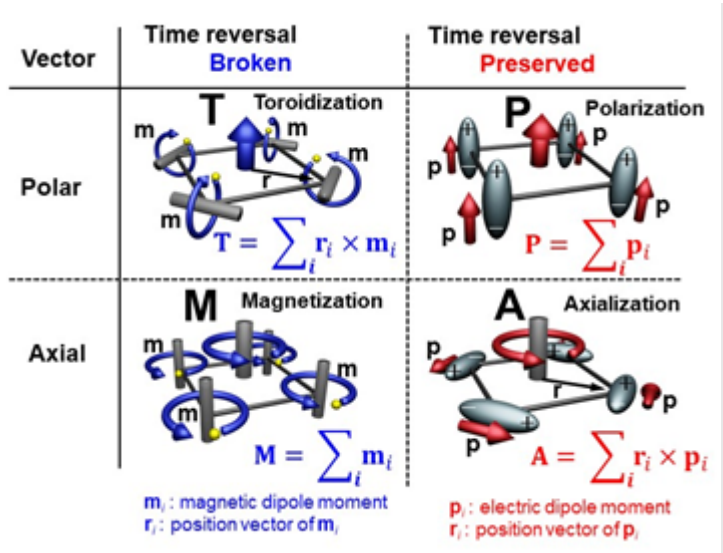

Fig. 1 Relationships among ferro-electric, ferro-magnetic, ferro-toroidal, and ferro-axial orders in terms of symmetry breakings.

A082 Materials Properties by Quantum Crystallography
Room 207
4.00pm - 6.30pm

A082-01-260823

Electronic structure crystallography: capture excited/distorted states of optical materials experimentally

Xiao-Ming Jiang, Guo-Cong Guo

Fujian Institute of Research on the Structure of Matter, Chinese Academy of Sciences, Fuzhou, Fujian 350002, P. R. China

xmjiang@fjirsm.ac.cn gcguo@fjirsm.ac.cn

Keywords: Excited state, Optical material, Electronic structure crystallography

Optical materials such as nonlinear optical and fluorescent materials have wide applications in industry and daily life, while the physical mechanisms of these materials are far from fully understood yet because they are closely related to the electronic structure of excited/distorted states, which can be hardly been revealed experimentally and even theoretically using first-principles calculations. Thanks to the fundamental works of Coppens [1], Massa [2], Jayatilaka [3], and many other scientists in the field of quantum crystallography, electronic structure of crystalline materials including subatomic/orbital resolved electron density (ED), density matrix, and wavefunction in real space and their topological characteristics can be obtained experimentally using high-quality X-ray/neutron/electron scattering. The majority of current works in quantum crystallography are focused on the ground states of materials, however, the emergence and development of photocrystallography give more opportunities for exploring excited states with steady-state and time-resolved techniques under external optical fields [4]. By using theoretical methods and in situ techniques in these two fields, we take typical nonlinear optical inorganics and fluorescent organics as examples to demonstrate the advantages of in situ electronic structure studies in characterizing the excited/distorted states of optical materials and revealing their structure-property relationships as well [5, 6]. Furthermore, except for electronic structure in the real (or position) space, energy levels and band structures in the momentum space also govern the optical performances of materials. Therefore, the full understanding of the function origin of optical materials, other spectroscopy methods such as angle-resolved photoelectron spectroscopy should be covered. Inspired by these ideas, the experimental extraction of the electronic structure of the ground and excited/distorted states in real and momentum/energy spaces can be termed electronic structure crystallography (Figure 1).

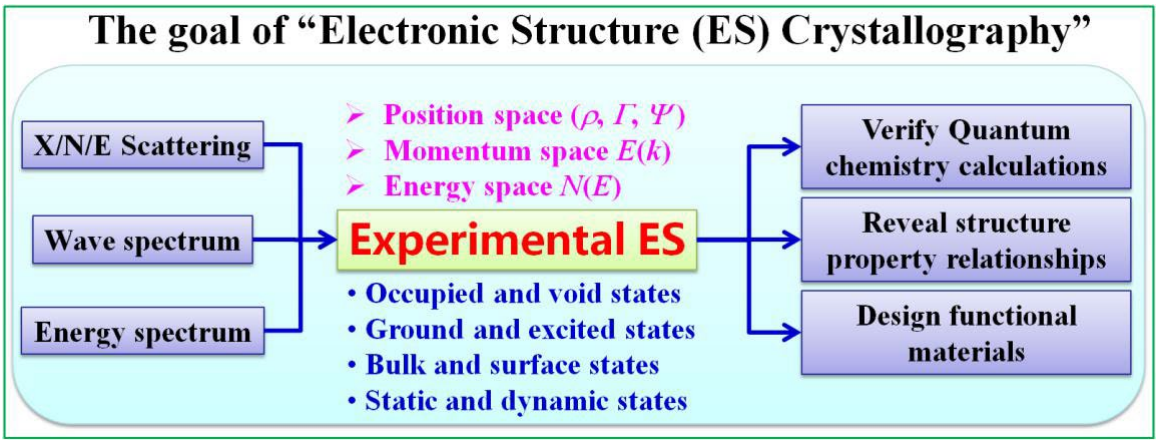

Figure 1. The goal of "electronic structure crystallography".

[1] Hansen, N. K., Coppens, P. (1978). Acta Cryst. A 34, 909-921.
[2] Huang, L., Massa L. and Karle, J. (1999). Int J Quantum Chem 73: 439–50.
[3] Jayatilaka, D., Grimwood, D. J. (2001). Acta Cryst. A 57, 76-86.
[4] Cole, J. M. (2008). Z. Kristallogr. 223, 363–369.
[5] Jiang, X.-M., Lin, S.-J., He, C., Liu, B.-W., Guo, G.-C. (2021). Angew. Chem. Int. Ed. 60, 11799-11803.
[6] Jiang, X.-M., Deng, S., Whangbo, M.-H., Guo, G.-C. (2022). Natl. Sci. Rev. 9, nwac017.

This work was supported by the National Natural Science Foundation of China (21827813, 21921001, 22175172), the Youth Innovation Promotion Association of Chinese Academy of Sciences (2020303), and the Natural Science Foundation of Fujian Provinces, China (2022L3090).

A082-02-260823

Evaluating the nature of arsenic-involving bonds and interactions related to piezoelectric properties using quantum crystallography and complementary bonding analysis

Yaser Balmohammadi,[1] Lorraine A. Malaspina,[1] Simon Grabowsky[1]

University of Bern, Department of Chemistry, Biochemistry and Pharmaceutical Sciences, Freiestrasse 3, 3012 Bern, Switzerland

simon.grabowsky@unibe.ch

Keywords: As-involving interactions, piezoelectricity, charge density

Elemental arsenic and its highly toxic compounds have many applications in medicine and materials science, but the nature of arsenic bonds and interactions is not clear yet. Some arsenic materials (e.g., gallium arsenate-$GaAsO_4$) exhibit the quartz crystal structure system as piezoelectric (i.e., a voltage is generated when the external stress is applied across that material [1]). The mainstay of piezoelectricity is the nature and geometric arrangement of the polar intra- and intermolecular interactions. To understand the relationship between piezoelectric properties and the bonding situation in arsenic materials, we need to understand first the behavior of arsenic in chemical interactions and bonds. To this end, we studied two different structure sets of arsenic compounds as model structures to compare with and evaluate the piezoelectric material ($GaAsO_4$). These model compounds have similar chemical bonds, intermolecular interactions, and environments to the piezoelectric material.

In the first study, to understand the nature of arsenic-involving intermolecular interactions and the effect of oxidation state on them, screening in the Cambridge Structural Database was performed. Then, 77 crystal structures were selected that include both oxidation states of arsenic (III/V) including arsenic interactions of the type As…X (X=As, O, N, Cl, I Br, S, Te) in the crystal packings.[2] In the second study, a series of arsenic compounds were synthesized or recrystallized to examine the As-O bond and As...O interactions which are the responsible bonds for piezoelectric properties in GaAsO4. The compounds are as follows: As3O6, As2O3, AsO4(NH4)3(H2O)3, HAsO4(NH4)2, H2AsO4(NH4), C6H8NAsO3, NH4Br.As2O3, H2O·As2O3, (C5H7N2) (C5H8N2) [AsO4]·H2O, C6H10N3O.AsH3O.AsH2O4, and GaAsO4 . Figure 1 shows a schematic representation of our study.

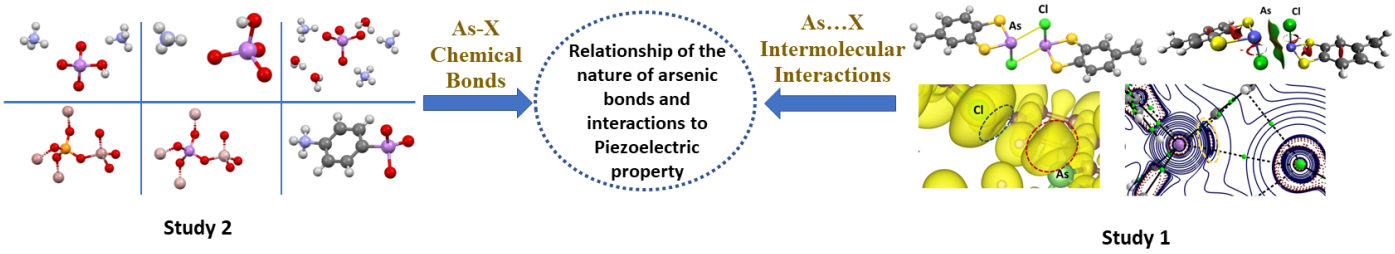

Figure 1. Schematic representation of both studies and the final aim. Some of the model structures of the second study (left) and evaluation of the nature of As-interactions (right)

For the first study, non-periodic and periodic DFT calculations were performed for all 77 structures. The properties and nature of arsenic-involving interactions were characterized by different bond descriptors derived from the electron density, electrostatic potential, and molecular orbitals (complementary bonding analysis [3]). Our results show that As(III) species act ambivalently in their interactions as Lewis acids or bases due to a lone pair, forming halogen, pnicogen, and chalcogen bonds, unlike As(V) which is only a Lewis acid. Besides the dualistic behavior of As(III), its intermolecular bonds are of significant strength, and this ability of As(III) should be employed by chemists to design novel materials, e.g. MOFs for removal of toxic As(III) compounds from freshwater.[2]

Next, high-resolution single-crystal X-ray diffraction data were collected with our Mo and Ag home-sources for study 2 and will be complemented by synchrotron experiments. A new periodic Hirshfeld atom refinement and the influence of an external electric field were introduced into tonto software. Non-periodic and periodic Hirshfeld atom refinements (HAR) along with x-ray constrained wave function fitting (XCW) were performed to obtain experimental wave functions. QTAIM results demonstrate that As-O bonds have a positive value of electron density Laplacian which shows them as a closed-shell interaction. Therefore, As-O bond is likely to be charge-separated not a hypervalent bond. Moreover, the As-O bonds will be characterized by complementary bonding analysis (molecular or periodic approach) to have more insight into this bond. Finally, the results of both studies as model compounds will be compared to the compounds GaAsO4 that exhibit piezoelectric properties. We will compare the bonding situation in GaAsO4 with and without an external electric field, and with the bonding in non-piezoelectric model compounds.

[1] Sezer, N., & Koç, M.; *Nano Energy*, **2021**, *80*, 105567.
[2] Balmohammadi, Y., & Grabowsky, S.; *Cryst. Growth Des*. **2023**, *23*, 2, 1033–1048
[3] Grabowsky, S. (Ed.). (**2021**). Complementary Bonding Analysis. Walter de Gruyter GmbH & Co KG.

MSA082-03-260823

Time resolved charge density study of diamond in non-thermal melting

E. Nishibori[1]

[1]*Department of Physics and Tsukuba Research Center for Energy Materials Science, University of Tsukuba, 1-1-1 Tennodai, Tsukuba 305-8571, Japan*

Keywords: X-ray Free Electron Laser, Diamond, Non-thermal melting

X-ray Free Electron Laser (XFEL) has established as a novel X-ray source for crystallography during past decade. XFEL was used for protein crystallography and various kinds of time-resolved diffraction studies. Highly intense femtosecond pulse of XFEL enable us to visualize a snapshot of materials showing their characteristic properties. Quantum crystallography as well as X-ray charge density studies of time-resolved XFEL data are highly required to reveal time-resolved electron distributions of materials.

Recently, ultrafast changes of electron density distribution in diamond after irradiation with an intense hard X-ray pulse have been visualized with X-ray pump–X-ray probe technique [1]. The charge density was derived from multipole modelling in the Hansen–Coppens formalism. Several special treatments for the analysis were required to reveal the time-resolved charge density distributions. Electron configuration of $1s^2$, $2s^2$, $2p^2$ was used in the analysis. We optimized κ and *O*2- parameters for five low order Bragg reflections, since κ and *O*2- parameters were mainly contributed the covalent bonding of diamond from our temperature dependence of charge density study [2].

Covalent bonds in diamond are broken and the electron distribution around each atom becomes isotropic within ~5 fs after the intensity maximum of the X-ray pump pulse. The 15 fs time delay observed between the bond breaking and atomic disordering. The present study shows an usefulness of quantum crystallographic study for XFEL crystallography.

[1] I. Inoue, Y. Deguchi, B. Ziaja, T. Osaka, M. M. Abdullah, Z. Jurek, N. Medvedev, V. Tkachenko, Y. Inubushi, H. Kasai, K. Tamasaku, T. Hara, E. Nishibori, M. Yabashi, *Phys. Rev. Lett.* **126** (2021) 117403.
[2] Y. Deguchi, E. Nishibori, *Acta. Crystallogr.* **B 74** (2018) 651-659.

A082-04-260823

Mechanical Flexibility in Molecular Crystals with Nitrile···nitrile Dipolar Interactions: Computational Prediction and Experimental Validation

Ashi Singh, Sajesh P Thomas

Department of Chemistry, Indian Institute of Technology Delhi

ashisingh.297@gmail.com

Keywords: *Quantum Crystallography*, *mechanical flexibility*, *energy framework, Hirshfeld atomic refinement*, *charge density modeling, electrostatic potential map, QTAIM analysis, C_{ij} tensor*

Crystal engineering [1] involves understanding intermolecular interactions involved in crystal packing to design and synthesize molecular materials of desired properties. We aim to employ *Quantum Crystallography* (QCr) [2,3] approaches along with other computational quantum chemistry tools to rationalize and predict *mechanical flexibility* in small molecular materials based on synthon and interaction anisotropy. In direction to this, we performed *energy framework*[4] analysis for a list of compounds restricted to nitrile···nitrile synthon and small molecular size to qualitatively analyze the anisotropy in intermolecular interaction. To add validation to our results, we did *Hirshfeld atomic refinement* (HAR) and *charge density modeling* to achieve deeper insights into interaction topology, studied electrostatic complementarity in the synthon region of interest in terms of the *electrostatic potential* mapped on hirshfeld surface[5], followed by *QTAIM analysis*[6] that enables topological studies of electron density in terms of bond descriptors in the interaction region. Further, we did C_{ij} *tensor* calculation to quantitatively analyze the elastic limit of such compounds and studied the effect of temperature variation on this elastic limit.

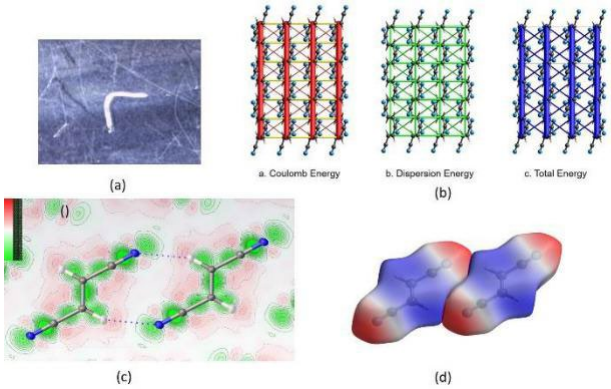

Figure 1. (a) Bend crystal, (b) Energy Frameworks, (c) Density deformation map and (d) ESP map plotted over hirshfeld surface

[1] G. R. Desiraju, "Crystal engineering: from molecule to crystal," *J Am Chem Soc*, vol. 135, no. 27, pp. 9952–9967, Jul. 2013, doi: 10.1021/JA403264C.

[2] S. Grabowsky, A. Genoni, and H. B. Bürgi, "Quantum crystallography," *Chem Sci*, vol. 8, no. 6, pp. 4159–4176, May 2017, doi: 10.1039/C6SC05504D.

[3] A. Genoni *et al.*, "Quantum Crystallography: Current Developments and Future Perspectives," *Chemistry*, vol. 24, no. 43, pp. 10881–10905, Aug. 2018, doi: 10.1002/CHEM.201705952.

[4] M. J. Turner, S. P. Thomas, M. W. Shi, D. Jayatilaka, and M. A. Spackman, "Energy frameworks: insights into interaction anisotropy and the mechanical properties of molecular crystals," *Chemical Communications*, vol. 51, no. 18, pp. 3735–3738, Feb. 2015, doi: 10.1039/C4CC09074H.

[5] M. A. Spackman, J. J. McKinnon, and D. Jayatilaka, "Electrostatic potentials mapped on Hirshfeld surfaces provide direct insight into intermolecular interactions in crystals," *CrystEngComm*, vol. 10, no. 4, pp. 377–388, Mar. 2008, doi: 10.1039/B715227B.

[6] C. Foroutan-Nejad, S. Shahbazian, and R. Marek, "Toward a Consistent Interpretation of the QTAIM: Tortuous Link between Chemical Bonds, Interactions, and Bond/Line Paths," *Chemistry – A European Journal*, vol. 20, no. 32, pp. 10140–10152, Aug. 2014, doi: 10.1002/CHEM.201402177.

A082-05-260823

Ternary [Cu(dipicolinate)(diimine)] complexes. Structural features vs. physiochemically relevant properties and cytotoxic activity.

N. Alvarez[1], A. Rocha[2], L. F. Mendes[3], A. A. Batista[2], J. Ellena[4], A. J. Costa-Fiho[3], G. Facchin[1]

[1]Facultad de Química, Universidad de la República, Montevideo, Uruguay, [2]Departamento de Química, Universidade Federal de São Carlos, São Carlos (SP), Brasil, [3]Faculdade de Filosofia, Ciências e Letras de Ribeirão Preto, Universidade de São Paulo, Ribeirão Preto (SP), Brasil, [4]Instituto de Física de São Carlos, Universidade de São Paulo, São Carlos (SP), Brasil
nalvarez@fq.edu.uy

Keywords: copper(II), antitumor activity, Hirshfeld surface analysis

In the search for new and more effective metallopharmaceuticals for cancer therapy our group focuses in the development of copper(II) complexes containing the $[Cu(diimine)]^{2+}$ pharmacophore coupled with an anionic co-ligand. For the last decade, [Cu(dipeptide)(phenanthroline)] have shown promising results where the cytotoxic activity is dependent on the phenanthroline moiety when comparing different complexes´ families and the dipeptide acts as a modulator within a family [1-4]. To broaden the scope the iminodiacetate anion was also studied as a co-ligand due to the stability of the complex species [5]. The mechanism of action may include DNA interaction, making it interesting to study the relationship between the intermolecular interactions observed in the crystal compared to the binding constant. For instance, in the case of [Cu(dipeptide)(neocuproine)] there is a direct relationship between C···C contacts percentage within the Hirshfeld surface and the spectrophotometrically determined DNA binding constant.

In this work, we explore dipicolinate as a co-ligand in the hope that its rigidity would give rise to a differentiated biological activity. Although most of the presented complexes have already been synthetized and characterized before, they were never tested for cytotoxic activity, neither their structure studied in-depth by means of quantum crystallography tools. The studied complexes include 2,2'-dipyridil-amine (bam), 2,2-bipyridine (bipy), 4,4-dimethyl-2,2-bipyridine (dmb), phenahtroline (phen), 4-methyl-phenanthroline (4met), 5-nitro-phenanthroline (5nitro), neocuproine (neo), bathophenthroline (batho), and 3,4,7,8-tetramethyl-phenanthroline (tetra). Coordination sphere presents a N3O equatorial plane donor scheme on octahedral environments, except for bam and neo where the equatorial donor scheme is N2O2 and the geometry is square pyramidal. Complexes were spectroscopically characterized in the solid state and in water and dimethyl sulfoxide solution, as well as thermogravimetric analysis. Hirshfeld surface analysis was conducted to determine relationships between type and propensity of intermolecular contacts with lipophilicity and DNA binding constant. Binding constants range between 1 and 15 $x10^3$ M^{-1} due to conformational changes in the DNA going from the B form to the C, A and Z form in presence of the complex. Cytotoxicity was assessed in MCF-7, MDA-MB-231, MCF-10A, A549 and MRC-5 cell lines with values that are lower or comparable with those observed for cisplatin in the same conditions.

[1]Iglesias, S.; et al; (2014), J. Inorg. Biochem., 139, 117.
[2]Iglesias, S.; et al; (2015) Structural Chemistry and Crystallography Communication, 1, 1.
[3]Alvarez, N; et al; (2020), J. Inorg. Biochem., 203, 110930.
[4]Alvarez, N.; et al; (2022) J. Biol. Inorg. Chem. 27, 431.
[5]Alvarez, N.; et al; (2018) Inorganica Chim. Acta 438, 61.

Authors would like to acknowledge CSIC (I+D grant to G. F.), PEDECIBA (Uruguay), FAPESP and CNPq (Brazil) for financial support.

A082-06-260823

Crystallography beyond structure

Bo Brummerstedt Iversen

Center for Integrated Materials Research, Department of Chemistry and iNANO, Aarhus University, Denmark

bo@chem.au.dk

Keywords: X-ray electron density, chemical bonding, 3D-□PDF, thermoelectrics, magnetism, MOFs

Crystallography is often only viewed as the science that finds the time and space averaged crystal structure of molecular crystals based on single crystal diffraction measurements. Historically, the average structure provides estimates of bond lengths and bond angles which are important insights for understanding of chemical systems. However, the standard independent atom model (IAM) used universally in crystal structure refinements neglects the very basis of chemistry since it does not contain any information about chemical interactions, which are then inferred based on the average structure. The obvious systematic error of the IAM leads to errors in the refined average structures such the underestimation of hydrogen bond length (X-ray data). Recent work has focus on improving the IAM by using aspherical scattering factors to improve the accuracy of the structure estimate, but the results of such refinements are still just the average nuclear positions.

X-rays scatter on the actual electron density distribution in the crystal, and for five decades accurate X-ray diffraction data for well-ordered crystals have been used to model crystal electron densities using the multipole model. In chemistry it is can be difficult from the average structure to identify the underlying chemical interactions that control the properties of materials, and analysis of the electron density represents a unique approach that provides insight beyond average structure. In the talk recent examples will be given. Furthermore, many crystals contain complex order, which gives rise to structured diffuse scattering. The field of correlated disorder attempts to decipher the true local structure of crystals based on analysis of diffuse scattering. However, as for the average structure of ordered crystals, the main chemical question is not just the structure, but the underlying chemical bonding origin that leads to the disorder. Ultimately, complex order must also be understood through chemical bonding.

A089b Coherent scattering methods using X-rays or electrons
Room 209
4.00pm - 6.30pm

A089B-01-260823

Reference-enhanced x-ray single particle imaging

Abhishek Mall[1*], and Kartik Ayyer[1,2]

Max Planck Institute for the Structure and Dynamics of Matter, 22761 Hamburg, Germany
Center for Free Electron Laser Science, 22761 Hamburg, Germany

** abhishek.mall@mpsd.mpg.de*

Keywords: X-ray Holography, Single Particle Imaging, Viruses, Proteins

High energy x-ray free electron laser (XFEL) sources facilitate the 3D structure determination of nanoscale biological entities such as viruses and cluster of proteins, from a large number of diffraction patterns. This technique of single particle imaging (SPI) enables collection of millions of patterns from copies of these objects in random orientations. However, the resolution of 3D structure is limited by relatively low signal due to background noise, total amount of patterns collected and heterogeneity of the target particle. We proposed two holographic-principle based experimental methodologies by attaching a strong scattering reference to target object for obtaining high-quality diffraction patterns, facilitating in gain of signal-to-noise by including scattering from a strongly scattering reference[1].

Here we conduct reference-SPI experiment by conjugating gold nanospheres (AuNP) with biological objects, in this case encapsulin proteins and MS2 phages, to capitalize on high scattering cross-section of AuNP enabling high collection rate. The composite system adds heterogeneity to the dataset, since the diffraction patterns vary not only in the orientation of the particles in the beam but also in the properties and relative position of the reference. To overcome the additional heterogeneity, we also develop a reconstruction algorithm [2] based on maximum likelihood estimation to recover the full 3D structure of a mostly reproducible object from a large number of patterns of composite structures consisting of the target object as well as a reference introduced by the attachment process, to obtain a high resolution (sub 2 nm) structure of the target particles.

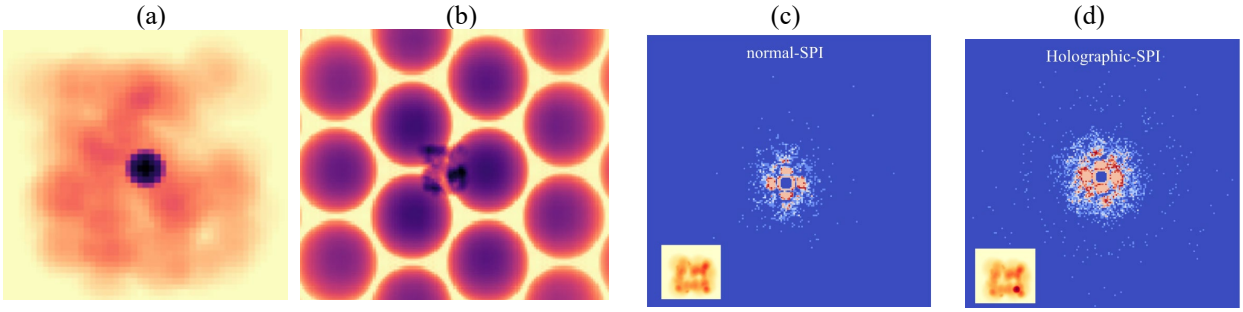

Fig. 1. Methodologies to attach a reference to a target object [1]. (a) random sphere cluster depicting biological like entities attached to spherical AuNP as reference used as the test object for illustration. (b) same cluster within a unit cell of 2d lattice. (c) Simulated diffraction pattern for a random object in a normal single-particle imaging (SPI) case with 4810 photons. (d) Diffraction pattern from the same particle with a small AuNP attached (10,000 photons). If background is present, structural information can be discerned at higher scattering angles in the holographic case [2].

[1] Kartik Ayyer, "Reference-enhanced x-ray single-particle imaging," Optica **7**, 593-601 (2020) .
[2] Mall, Abhishek, and Kartik Ayyer. "Holographic single particle imaging for weakly scattering, heterogeneous nanoscale objects." *arXiv preprint arXiv:2210.10611* (2022).

A089B-02-260823

Convergent beam X-ray crystallography and 3-D diffraction imaging using multilayer Laue lenses

Chufeng Li[1], Nikolay Ivanov[1], Mauro Prasciolu[1], Holger Fleckenstein[1], Martin Domaracky[1], J. Lukas Dresselhaus[2], Oleksandr Yefanov[1] , Wenhui Zhang[1], Margarita Zakharova[1], Alke Meents[1], Tjark Delmas[1], Ivan De Gennaro Aquino[1], Dominik Oberthuer[1], Janina Sprenger[1], Anastasios Pateras[1] , Alessandra Henkel[1], Aida Rahmani Mashhour[1], Johanna Hakanpää[2], Saša Bajt[1,2], and Henry N. Chapman[1,2,4]

Center for Free-Electron Laser Science CFEL, Deutsches Elektronen-Synchrotron DESY, Hamburg
The Hamburg Centre for Ultrafast Imaging, Hamburg
Deutsches Elektronen-Synchrotron DESY, Hamburg
Department of Physics, Universität Hamburg, Hamburg

chufeng.li@desy.de

Keywords: Convergent beam diffraction, multilayer Laue lens, microscopy

Highly-converging X-ray beams created by multilayer Laue lenses (MLLs) [1] bring new opportunities for X-ray crystallography and 3D diffraction microscopy. Our recent MLLs achieve a numerical aperture (NA) of ~ 0.02 at a photon energy of 17.5 keV (or 0.71 Å wavelength), meaning that beam converges onto the focus over an angular range of 40 mrad or 1.3º. When the crystal is placed downstream of the focus, there is a correlation between position in the beam and the angle of incidence of a ray. The crystal selects Bragg reflections from the supplied range of angles, at particular locations of the crystal (slices, in the case of a single crystal). In this configuration, the diffraction data provides a mix of crystallography and (tomographic) microscopy. We are particularly interested in developing convergent-beam diffraction as a way to obtain fully-integrated Bragg reflections in single exposures (to reduce the number of patterns required in serial crystallography at free-electron laser sources) and to obtain structure factors of high accuracy by observing and accounting for spatial variations in crystals, such as their shape, strain, or defect structure. Additionally, using the mapping between position and incidence angle, 3-D microscopic images of the diffraction efficiency of the crystal was obtained from the same data set. The simple experimental setup and data collection strategy offers advantages such as ample operational space and easy adjustment of the spatial resolution by changing the geometry. The convergent beam diffraction (CBD) scheme, with further development in progress is potentially applicable to multi-scale structural or dynamics studies for both material and life sciences.

References

[1] Bajt, S. *et al.* X-ray focusing with efficient high-NA multilayer Laue lenses. *Light Sci. Appl.* **7**, 17162–17162 (2018).

A089B-03-260823

Coherent X-ray diffraction with a convergent beam

H.N. Chapman[1,2,3], S. Bajt[1,2], C. Li[1], N. Ivanov[1], J.L. Dresselhaus[2], W. Zhang[1], M. Zakharova[1], Yefanov[1], A. Pateras[1], H. Fleckenstein[1], M. Prasciolu[1]

Center for Free-Electron Laser Science CFEL, Deutsches Elektronen Synchrotron DESY, Hamburg, Germany;
Centre for Ultrafast Imaging, Universität Hamburg, Hamburg, Germany;
Department of Physics, Universität Hamburg, Hamburg, Germany.

Henry.Chapman@desy.de

Keywords: Diffractive imaging, ptychography, crystallography

With the development of improved multilayer Laue lenses (MLLs) [1] and sensitive wavefront diagnostics [2,3], it is now possible to focus X-ray beams at synchrotron radiation facilities and X-ray free-electron lasers to spot sizes of 5 nm or less. These are diffractive optics made by layer deposition, in which the layer period varies inversely with distance from the optical axis and the layers are wedged [4] to ensure that the tilt of the layers satisfies the Bragg condition. In this way, an MLL is the physical embodiment of the Ewald sphere. The convergence angle of these lenses can exceed 0.03 rad for a wavelength of 0.7 nm (17 keV) This convergence is often greater than the angular separation of Bragg peaks in a macromolecular crystal, which is equivalent to saying that the focal spot is smaller than the unit cell of the crystal. This creates several interesting opportunities for the study of the structure of macromolecular crystals. When the crystal is placed in the focus, Bragg peaks may overlap and interfere [6], but extremely short exposure times are required to avoid radiation damage, requiring snapshot diffraction using XFEL pulses. Indexing and classification algorithms could then be used to generate a ptychographic dataset [7] that is a function of crystal orientation and the location of the focus relative to the unit cell. Damage can also be avoided by placing the crystal in the beam diverging from the focus, allowing topographic imaging of the crystals and Bragg lines that give fully-integrated reflections. This approach also has benefits for crystals with unit cell dimensions that are smaller than the focus size. It enables a simplified approach for multi-Bragg ptychography and the characterisation of strain and defects at high resolution. Experimental results and analysis of convergent-beam diffraction from protein and inorganic crystals will be presented.

Bajt, S., Prasciolu, M., Fleckenstein, H., Domaracký, M., Chapman, H. N., Morgan, A. J., Yefanov, O., Messerschmidt, M., Du, Y., Murray, K. T., Mariani, V., Kuhn, M., Aplin, S., Pande, K., Villanueva-Perez, P., Stachnik, K., Chen, J. P., Andrejczuk, A., Meents, A., Burkhardt, A., Pennicard, D., Huang, X., Yan, H., Nazaretski, E., Chu, Y. S., and Hamm, C. E. (2018). *Light: Sci. Appl.* **7**, 17162.
Morgan, A. J., Quiney, H. M., Bajt, S., and Chapman, H. N. (2020). *J. Appl. Cryst*. **53**, 760.
Ivanov, N., Dresselhaus, J. L., Carnis, J., Domaracky, M., Fleckenstein, H., Li, C., Li, T., Prasciolu, M., Yefanov, O., Zhang, W., Bajt, S., and Chapman, H. N. (2022). *Opt. Exp.* **30**, 25450.
Prasciolu, M., Leontowich, A. F. G., Krzywinski, J., Andrejczuk, A., Chapman, H. N., and Bajt, S. (2015). *Opt. Mater. Exp.* **5**, 748.
Dresselhaus, J. L., Fleckenstein, H., Domaracký, M., Prasciolu, M., Ivanov, N., Carnis, J., Murray, K. T., Morgan, A. J., Chapman, H. N., and Bajt, S. (2022). *Rev. Sci. Instrum.* **93**, 073704.
Spence, J. C. H., Zatsepin, N. A., and Li, C. (2014). *Phil. Trans. Roy. Soc. B* **369**, 20130325.
Kewish, C. M., Thibault, P., Bunk, O., and Pfeiffer, F. (2010). *New J. Phys.* **12**, 035005.

A089B-04-260823

Coherent diffraction imaging at the ESRF EBS - progress and challenges

Y. Chushkin, F. Zontone

ESRF –The European Synchrotron, 71, avenue des Martyrs, 38000 Grenoble, France

chushkin@esrf.fr

Keywords: CDI, high-resolution imaging

The last generation upgrades of synchrotron radiation storage rings such as the ESRF-ESB programme reduce the horizontal emittance of the electron beam offering intense X-ray beams with an unprecedented brilliance and degree of coherence [1]. Since the coherent flux is proportional to the brilliance, the up-to 100X increase in brilliance of ESRF-EBS strengthen the coherence based imaging techniques, in particular those based on coherent scattering such as Coherent Diffraction Imaging (CDI). CDI images isolated samples by numerically phasing a sufficiently oversampled Fourier space [2]. The resolution is determined by the largest scattering vector q where speckles are measured with sufficient signal-to-noise ratio (SNR).The expected benefits are mainly two-fold. Brighter X-ray beams coupled with larger detectors enable higher spatial resolution and sensitivity. For instance, for q^{-4} scattering samples, a 80 times increase of the scattering intensities translates into a three-fold gain in spatial resolution for the same SNR. At the same time, photon-counting two-dimensional detectors have to cope in size (q-range) and dynamic range (e.g.10^8 for 1□□m sample at 10nm resolution). In addition, brighter X-ray beams also mean faster data collection as increasing the coherent flux, e.g. by a factor of 60, can decrease the measurement time by up-to 20 times, opening the possibility for CDI to work in time-resolved mode for slow varying systems.

In this work we present the latest results of CDI obtained at the ESRF beamline ID10. As an example, Fig.1 shows that resolution is increased when the ESRF-EBS is used with a modern Eiger2 4M detector for a sample of 5□□m in size, boosted by a factor of ~4 when compared to the old synchrotron machine coupled with a MAXIPIX detector. Enhanced spatial and temporal resolution open the door for new applications of CDI. We also address the challenges related to handling and treatment of large data volumes and the radiation damage caused by intense beams.

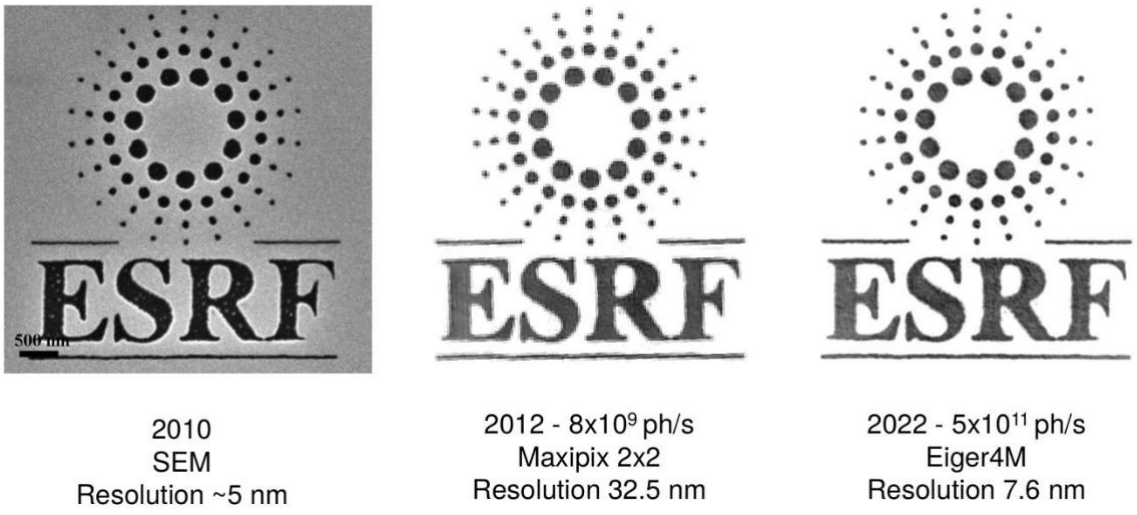

Figure 1. A test sample imaged with SEM and CDI before and after the EBS upgrade

[1] Raimondi, P. (2016). *Synchrotron Radiat. News,* **29**, 8.

[2] Miao, J., Charalambous, P., Kirz, J., & Sayre, D. (1999). *Nature*, **400**, 342.

The authors would like to acknowledge Vincent Favre-Nicolin and Jerome Kieffer for developing data analysis tools.

A089B-06-260823

Nanobeam electron diffraction studies of functional metal/semiconductor junctions

C. Cassidy[1*], A. Dhar[2], T. Unten[3], N. Kishi[3], B.C. Wolz[4], M. Labayen de Inza[4], T. Shintake[1]

Okinawa Institute of Science and Technology, 1919-1 Tancha, Onna-son, Okinawa 904-0495, Japan.
Stanford Linear Accelerator (SLAC), Menlo Park, CA 94025, USA.
ACRORAD Co. Ltd, 13-23 Suzaki, Uruma-shi, Okinawa 904-2234, Japan.
Siemens Healthcare GmbH, Diagnostic Imaging, Computed Tomography, Siemensstrasse 1, 91301 Forchheim, Germany.

**c.cassidy@oist.jp*

Keywords: electron diffraction, semiconductor, in operando

Nanobeam electron diffraction mapping is a technique for obtaining diffraction patterns in a rastered fashion from local regions of a thin specimen. This general approach is described by various names (e.g. 4D-STEM), which are based upon the same underlying concept. This approach enables high resolution mapping of orientation and strain in crystalline materials [1], and is thus highly useful for studies of semiconductor devices. Recently, nanobeam diffraction mapping has also been gaining interest for the mapping of electric fields within functional devices [2]. This is based upon the precise measurement and processing of slight displacements of the diffraction pattern caused by the electric (and magnetic) fields present in the specimen.

In this work, we present some preliminary nanobeam diffraction results obtained from functional metal/semiconductor interfaces. Our primary target system is an Al/CdTe Schottky junction (Fig. 1(a)), and we have also considered some other reference materials. We will firstly introduce results and specific challenges relating to sample preparation of these devices. Subsequently, we will introduce nanobeam diffraction mapping data acquired across the interface (examples in Fig. 1 (b-d)), and present the electric field measurements derived from those data. We also compare the results obtained from nanobeam diffraction against corresponding data obtained from off-axis electron holography measurements, as discussed conceptually in [3]. Finally, we will introduce preliminary results on the application of in situ electrical bias to the lamellae (Fig. 1(e)), towards the long term goal of visualizing and quantifying electrostatic field distributions under *in operando* conditions for these devices.

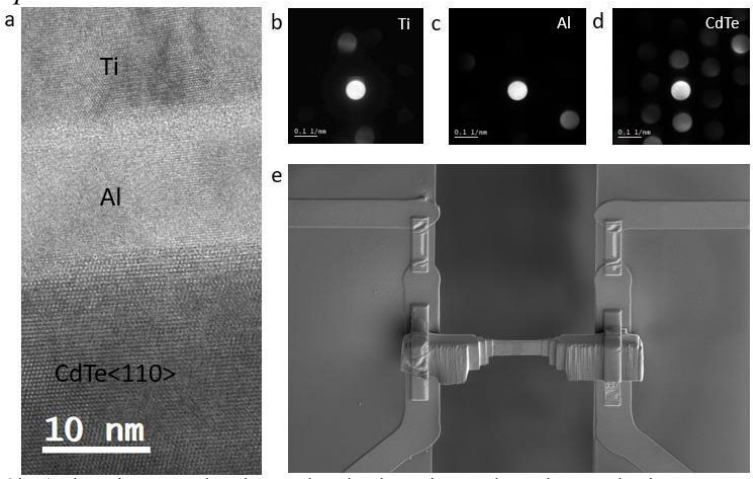

Figure 1. (a) TEM image (300kV) showing an Al-CdTe Schottky junction – the primary device type studied in this work. (b-d) local electron diffraction patterns, obtained using a probe of approximately 1nm diameter and 1.5mrad convergence angle, at 300kV. These are example diffraction patterns selected from larger pixelated maps of the interface region. (e) SEM image showing a prepared TEM lamella specimen, mounted to electrodes for application of in situ bias in the TEM. This example shows a Cu shunt specimen used for electrical functionality checks, and we have also prepared Al-CdTe devices in a similar fashion.

[1] V. B. Ozdol, C. Gammer, X.G. Jin, P. Ercius, C. Ophus, J. Ciston, A.M. Minor. (2015), *Applied Physics Letters* **106**, 253107.
[2] L. Bruas, V. Boureau, A.P. Conlan, S. Martinie, J.-L. Rouviere, D. Cooper (2020), *Journal of Applied Physics* **127**, 205701.
[3] F. Winkler, J. Bartel, R. Dunin-Borkowski, K. Mueller-Caspary (2020), *Ultramicroscopy* **210** 12926.

OIST acknowledges financial support and the provision of specimens by Acrorad Ltd and Siemens Healthineers, under the terms of a Collaborative Research Agreement (CRA).

A092 Scattering methods for Structural Elucidation in Food Systems
Room 216
4.00pm - 6.30pm

A092-01-260823\

Advanced Modelling of Lyotropic Liquid Crystals by Small Angle X-Ray Scattering

Cristiano L. P. Oliveira[1], Oscar R. Santos[2], Dennys Reis[1], Arnaldo G. Oliveira Filho[1] and Antonio M. Figueiredo Neto[1]

[1] Instituto de Física, Universidade de São Paulo, São Paulo-SP, Brazil, [2] Departamento de Física, Universidade Tecnológica Federal do Paraná, Campus Campo Mourão, Campo Mourão, Paraná, Brazil

crislpo@if.usp.br

Keywords: Small Angle X-Ray Scattering, oriented particles, nematic biaxial phase

The micelles of a lyotropic liquid crystal present long-distance orientational order sensitive to concentrations of amphiphilic molecules, alcohols, ions and to the temperature of the sample. Under specific combination of these parameters, a biaxial nematic phase may emerge between calamitic and discotic phases. Also, by the inclusion of small fractions of ferrofluids, the use of external magnetic fields can promote the orientation of the groups of micelles in the system [1,2]. Small-Angle X-ray scattering experiments is a very useful probe to investigate structural features on this system since it can be used directly in the solution system. However, since one has the micelles combined in different types of supramolecular arrangements, the analysis of the scattering data is not trivial, and demands the development of advanced modelling tools. In this work we present a recent model [3] very useful to investigate the micellar structure by the use of SAXS experiments. As will be shown, the micelles are modelled as core-shell ellipsoidal particles forming planar layers, which pills up as lamellar structures. From the fitting of the full scattering curve (**Figure 1**) one can obtains detailed structural parameters. This model was successfully applied for the investigation of the effect of chiral molecules in lyotropic cholesteric calamitic phases [3] but it is a very versatile approach and can be used in a number of systems composed by liquid crystals.

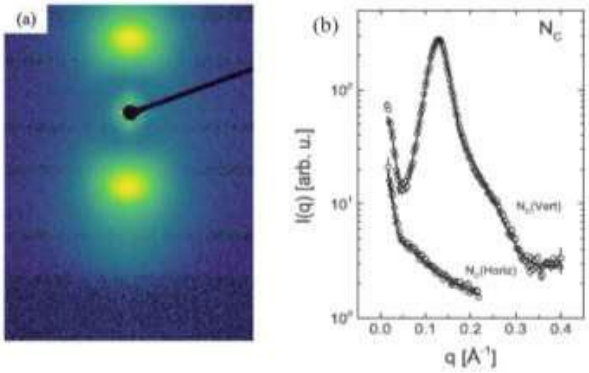

Figure 1. SAXS results. (a) 2D SAXS data for NC phase. (b) Vertical and horizontal cuts (symbols) with theoretical model fits (Solid lines).

[1] A. M. Figueiredo Neto, Y. Galerne, A. M. Levxelut, L. Liebert, J. Physique Lett. 46, 1985, L-455.
[2] E. Akpinar, K. Otluoglu, M. Turkmen, C. Cihan, D. Reis, A. M. Figueiredo Neto, Liquid Crystals 43 (11), 2016, 1693.
[3] O. R. Santos, D. Reis, A. G. Oliveira-Filho, C. L. P. Oliveira, and A. M. Figueiredo Neto, J. Mol. Liq., 2022, 349. 118097,

This work has been supported by FAPESP, CNPq and INCT-FCx..

A092-02-260823

Mixed Crystals of Linear Oleogelator Molecules: Existence Criteria

David Pink[1, 2], Erzsebet Papp-Szabo[2], Joseph Cooney[3, 4], Silvana Martini[4], Fernanda Peyronel[1*]

*[1]Department of Food Science, University of Guelph, Guelph, ON, Canada, [2]Department of Physics St. Francis Xavier University, Antigonish, NS, Canada, [3]Department of Physics Utah State University, 4415 Old Main Hill, Logan, UT, USA, [4]Department of Nutrition, Dietetics, and Food Sciences Utah State University, 8700 Old Main Hill, Logan, UT, USA. * = Presenter.*

Keywords: oleogels, lock in configuration, SAXS, USAXS

Oleogels comprise an oil as a solvent, preferably trapped by solid structures which are generally crystalline. Little is known about the defects (dislocations, disclinations, etc.) in the crystals. On question is whether the gelators used need to be in the form of essentially pure crystals or whether there is any advantage in utilising solid structures involving two or more gelators: can we create mixed crystals of pairs or triplets of gelators and is this advantageous to trapping oils and exhibiting the desired mechanical properties? To answer this, we need to specify the criteria for such mixed crystals to exist. Here we consider oleogelators which comprise unbranched long hydrocarbon chains such as Triacontane (TC), Stearic acid (SA), and Behenyl Lignocerate (BL).There are three different interactions for the three molecules studied here that will lead to a monolayer formation: (1) TC, an n-alkane hydrocarbon chain, interacts only via attractive $1/r^6$ dispersion energies [Parsegian, 200], (2) SA which forms hydrogen-bonded dimers at the carboxylic acid end [Garti et al., 1981; Goto & Asada, 1978]. (3) BL molecules possess an ester group in its center, which exhibits non-zero partial charges which cause a pair of adjacent molecules to be repelled.The Gibbs free energy changes, Δ , is defined to be, $\Delta = \Delta - \Delta$. Cooney et al [Cooney et al., 202]) showed that at = 30° the number of gauche excitations on a TC chain in a crystal comprising close-packed TC molecules is effectively zero. If we assume that hindered rotations of these rigid chains can be ignored, then there is only one chain state and the entropy change is $\Delta = 0$, so that free energy is determined by dispersion energies. In this work, we show "locked-in" configurations in accord with the calculation of Peyronel et al. (2023 to be submitted). These lock in configurations exhibit the lowest dispersion energies as shown in Fig.1 a, c, where red lines and arrows show surfaces and orientations, and the chains are shown terminated only for convenience. Cases b and c are close-packed but further apart. The tilt angles, , shown are 0 (a), and, approximately, 15° (b), 33° (c), and 43° (d). It was found that our models for TC and SA crystals predicted that the tilt angles for TC and SA dimers are ≈ 33°, with SAXS peaks at ≈ 0.195 $Å^{-1}$, and at ≈ 0.159 $Å^{-1}$ respectively, in acceptable agreement with the observations of = 0.181 $Å^{-1}$ and = 0.150 $Å^{-1}$

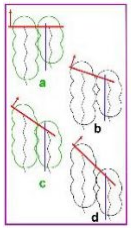

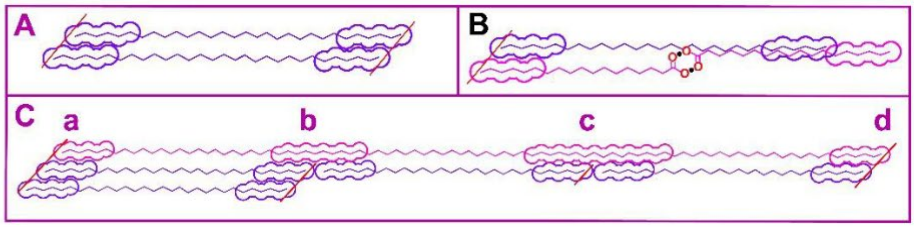

Fig.1. *Locked-in configurations (a, c)* ***Fig.2. A:*** *Two locked-in TC.* ***B:*** *TC and SA dimer.* ***C:*** *Locked-in TC and hypothetical chain* However, we found no SAXS evidence for the existence of crystals which comprised any two of TC, SA and BL. This was or with all three molecules (mixed crystals), and we asked ourselves why. Our answer is shown in Fig.2. There we see a pair of locked-in TC chains (A) with the surfaces shown as red lines and a tilt angle of ≈ 33°. If we try to create an analogous crystal from TC and SA molecules, however, and require that the left hand surface yields ≈ 33°, then the right hand surface will not yield a similar result (B), and it appears that a smooth surface is statistically-unikely to form. We can, however, form a mixed crystal from chains of different lengths as shown in (C), where the long red chain is locked into the first and third TC chains, but not into the central chain. It is clear that the positions of two long chains across a repeat distance boundary need not be spatially correlated as would have to be SA dimers in analogous positions.

Experimental measurements using ultra small angle X-ray scattering showed that the crystals arising in mixed systems are smaller than those in systems with only one kind of molecule and we ascribe this to the lower concentration of molecules of each kind. This is in accord with our observation that mixed crystals are not formed.

Cooney, J., Martini, S., Pink, D., & Peyronel, F. (2023). Triacontane and Behenyl Lingocerate Tilting in Crystals: Theory, Predictions and, Monte Carlo Simulations. *JAOCS to Be Submitted*.

Garti, N., Wellner, E., & Sarig, S. (1981). Effect of food emulsifiers on crystal structure and habit of stearic acid. *Journal of the American Oil Chemists' Society*, *58*(12), 1058–1060. http://resolver.scholarsportal.info/resolve/0003021x/v58i0012/1058_eofeocsahosa

Goto, M., & Asada, E. (1978). Goto 1978 The crystal structure of the B form of stearic acid. *Bulletin of the Chemical Society of Japan*, *51*(9), 2456– 2459.

Parsegian, V. A. (2005). *Van der Waals Forces. A Handbook for Biologists, Chemists, Engineers, and Physicists*. Cambridge University Press.

This work was supported by NSERC of Canada and Dr. Ilavsky and his group at APS, Argonne National Laboratory, USA

A092-03-260823

Unravelling the hierarchical structure of oleogels by small angle scattering

E.P. Gilbert

Australian Centre for Neutron Scattering, ANSTO, Lucas Heights, NSW 2234, Australia

elliot.gilbert@ansto.gov.au

Keywords: oleogel, SANS, SAXS

Limiting the consumption of saturated and trans fats has created the need for novel food ingredients to replace solid fats in food products without compromising sensory properties. One approach that has been pursued is the solidification of unsaturated liquid oils through the addition of oleogelators to yield soft solids (oleogels). Small-angle scattering provides structural information on the nanometre to micron length scale, particularly when combined with ultra-small-angle scattering; consequently, it represents a powerful tool to unravel the relationship between bulk behaviour and the underlying molecular and supramolecular structure from which such behaviour arises. This presentation will describe how small-angle scattering has been employed to understand the structure of oleogels with a particular focus on the application of neutron scattering [1-6].

[1] Cornet, S., de Campo, L., Martinez-Sanz, M., Scholten, E. & Gilbert, E.P. (2021) *Innovative Food Science and Emerging Technologies* **73** 102763.
[2] Nikiforidis, C.V, Gilbert, E.P. & Scholten, E. (2015) *RSC Advances* **5** 47466.
[3] Bot, A., Gilbert, E.P., Bouwman, W.G., Sawalha, H., den Adel, R., Garamus, V.M., Venema, P., van der Linden, E. & Flöter, E. (2012) *Faraday Discussions* **158** 223.
[4] Gilbert, E.P. (2022) *Food and Function* **13** 7123.
[5] Gilbert, E.P. (2019) *Current Opinion in Colloid & Interface Science* **42** 55.
[6] Gilbert, E.P. (in press), *Fat mimetics for food applications* edited by M. Cerqueira & L. Castro, John Wiley & Sons.

EPG acknowledges the contributions of all co-authors on the examples presented, particularly Arjen Bot from Unilever Research and Development who first introduced the author to these systems more than a decade ago.

A092-04-260823

Multiscale structures in fat

N. Arito Merino, E. Scholten

Wageningen University, Physics and Physical Chemistry of Foods, Bornse Weilanden, 6708 WG Wageningen, The Netherlands

elke.scholten@wur.nl

Keywords: Keyword 1, Keyword 2, Keyword 3

The properties of numerous food products, such as butter, chocolate and ice-cream, are greatly affected by the crystallization behavior of milk fats. When fat crystallizes, triacylglycerides (TAGs) form a 3-dimensional fractal network of colloidal polycrystalline particles. These TAGs can be arranged into different sub-cell structures (polymorphs) and form lamellae of different thickness. This arrangement of multiscale structures has a great impact on the functionality and sensory properties of countless products. In this presentation, we will discuss structures formed at small length scales using x-ray diffraction (WAXD). We developed a quantitative phase analysis (QPA) method [1], allowing us to quantify different structural polymorphs using calibration factors derived from pNMR measurements and solid fat content analysis. For different types of fat, we quantified the evolution of the polymorphic phases and produced phase transition diagrams during isothermal crystallization at different temperatures. We then linked these polymorphic structures to the structural organization of the network at different length scales using a variety of techniques: the molecular level (TAG composition by GC) and the sub-cell level (polymorphism by WAXD), to the lamellar stacking (by SAXS) and up to the morphology of their polycrystalline particles (by microscopy), as shown in Fig. 1 [2]. This way, we were able to link temperature-dependent structural changes in the crystal network to its rheological evolution. Using these techniques, we were also able to characterize how different variations in feed supplementation and differences in genetic variation for cows influences the crystallization process [3].

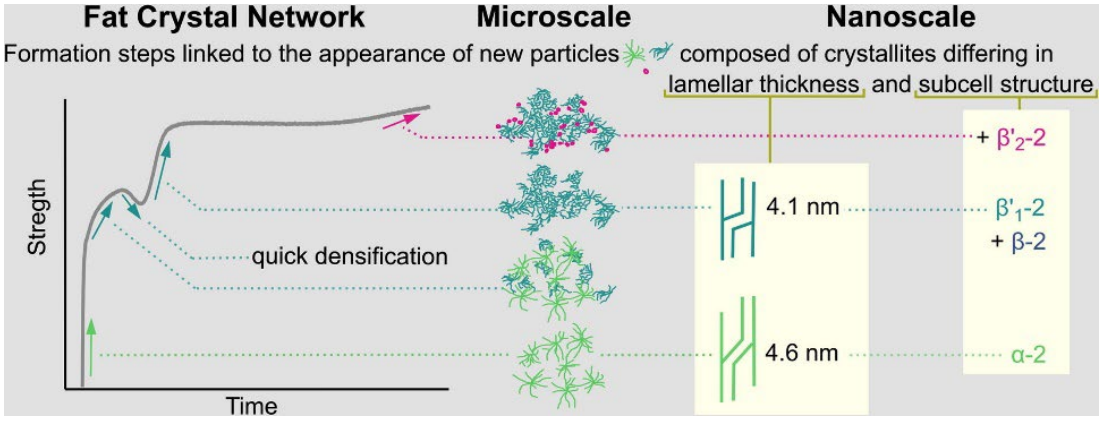

Figure 1. Rheological properties of fats related to small scale structures

.

References

[1] Arita-Merino, N., van Valenberg, H., Gilbert, E.P., Scholten., E. (2020). *Crystals Growth & Design.*, **20**, 5193.
[2] Arita-Merino, te Nijenhuis, L., van Valenberg, H., Scholten, E. (2022). *J. Colloid Int. Sci.* **607**, 1050.
[3] Arita-Merino, N., Yener, S., van Valenberg, H., Dijkstra, J., van Gastelen, S., Scholten, E., Tzompa-Sosa, D.A. (2023). *Food Chem.*, **407**, 135112.

A092-05-260823

Neutron scattering and neutron spectroscopy for insights into food emulsion interfaces

Theresia Heiden-Hecht, Henrich Frielinghaus, Olaf Holderer

Jülich Centre for Neutron Science (JCNS) at MLZ, Forschungszentrum Jülich GmbH, Garching, Germany

t.heiden-hecht@fz-juelich.de

Keywords: food emulsions, SANS, NSE

The stability of food emulsions depends -beside other effects- on a complex interplay between proteins, phospholipids, oil and water. Preparing milk-based and sustainable plant-based emulsions requires good knowledge in interfacial and emulsion stabilization mechanisms, affected by the emulsion composition. To understand these mechanisms in detail different length scales from interatomic to macroscopic distances need to be investigated.

Neutron scattering techniques provide insight into such emulsions on these length scales depending on the technique used. Combining structural information on molecular length scales from small angle x-ray and neutron scattering (SAXS and SANS) with time dependent neutron spin echo spectroscopy (NSE) allows to expand our understanding towards intermolecular interactions within the interface. These interactions are linked to the emulsion stability – the elastic properties of the protein or protein/phospholipid stabilized oil/water interface on molecular length scales. NSE provides in this combination the time dependent correlation function in reciprocal space, S(q,t), on molecular length scales and time scales in the nanosecond range relevant for thermally driven motion of mesoscopic systems such as the emulsion interfaces.

This presentation introduces the neutron and x-ray scattering techniques which broadens the classical characterization of food emulsions. Results from emulsions stabilized with -lactoglobulin as a representative milk protein, and different plant-based proteins, are presented and discussed. Contrast variation by deuteration of some components of the emulsions is applied to focus on the interfacial region, relying on the uniqueness of neutrons.

Connecting these emerging results with classical characterizations such as interfacial tension or viscoelasticity helps understanding the complex mechanisms of interfacial stability and may contribute to a knowledge driven development of sustainable food emulsions.

A092-06-260823

Application of synchrotron X-ray scattering to the understanding of the crystallization of complex mixtures of triglycerides, for a rational design of tailored confectionary products

Elena Simone[1], Holly Ewens[2], Michael Rappolt[2], Stephanie Marty-Terrade[3], Tom Rutherford[4], Francesca Giuffrida[3], Cynthia Marmet[3]

1 Department of Applied Science and Technology (DISAT), Politecnico di Torino, Torino, Italy
2 School of Food Science and Nutrition, Food Colloids and Bioprocessing Group, University of Leeds, Leeds, United Kingdom
3 Nestlé Research, Vers-chez-les-Blanc, Lausanne 26, 1000, Switzerland
4 Nestlé Product Technology Centre Confectionery, Haxby Road, York, YO31 8TA, United Kingdom

elena.simone@polito.it

Keywords: cocoa butter, crystallization, polymorphism, small angle X-ray scattering

Chocolate is a popular product and its supply is increasing, with sales in the UK estimated to be £6.7 billion in 2020, a £200 million increase from 2019. In recent years, confectionary companies have put increasing effort in developing novel recipes to improve the nutritional profile of chocolate and to counteract the increasing price of cocoa butter and address sustainability issues related to some chocolate ingredients. One of this these strategies is the use of cocoa butter equivalents (CBE), which are mixtures of triglycerides from multiple sources (e.g., sunflower oil, mango kernel, sal) that resemble cocoa butter in both physical and chemical properties. Despite being widely used, the crystallization behaviour of many CBEs is still poorly understood. The aim of this work was to develop a fundamental understanding, at the molecular level, of the crystallization behaviour of selected CBEs, and compare it with that of cocoa butter. In order to do so, chromatography was used to determine the composition of CBEs, in terms of fatty acids and triglycerides while the thermodynamic and kinetics of crystallization were studied using polarized microscopy, differential calorimetry and several, unique synchrotron X-ray scattering setups (the multi-capillary holder at Diamond Light Source in the United Kingdom, the combined DSC/SAXS at Elettra Sincrotrone Trieste in Italy and the combined SAXS/rheometry at ESRF in France). The combination of these techniques enabled the determination of crystal properties that affect the sensorial perception of chocolate: namely the type of crystals formed (e.g., polymorphism), their thermal stability and their size and shape distributions. Furthermore, the kinetics of crystallization as a function of CBE composition and the effect of shear were evaluated. The presented multi-technique investigation is the key for a rational design of new chocolate recipes and manufacturing processes.

A096 Progress and Application of Bond Valence Method
Room 217
4.00pm - 6.30pm

A096-01-260823

Discovery of a New Structural-Type Oxide-Ion Conductor by Screening

K. Matsuzaki, W. Zhang, K. Saito, K. Fujii, M. Yashima

Tokyo Institute of Technology

yashima@cms.titech.ac.jp

Keywords: oxide ion conductor, crystal structure, bond-valence-based energy calculation

Introduction Oxide-ion conductors have attracted much attention due to their wide applications such as oxygen gas sensors and solid oxide fuel cells (SOFCs). However, high oxide-ion conductivities are attained for the materials with limited crystal structures such as the fluorite-type and perovskite-type structures. Therefore, the exploration of a new structure family of oxide-ion conductors is challengeable and necessary for the development of the applications mentioned above. Many oxide-ion conductors containing cation species with d^{10} electronic configuration such as Ba2In2O5 and δ-Bi2O3 exhibit high oxide-ion conductivities. Herein, we focus on the compositions containing antimony (Sb) as an essential element. In this work, we report a new structure-type oxide-ion conductor Bi3GaSb2O11. The chemical composition Bi3GaSb2O11 was chosen by screening 402 Sb-containing materials through the bond-valence-based energy calculations.

Experiment We selected 402 Sb-containing oxides registered in the Inorganic Crystal Structure Database (ICSD) before the screening by the BV method. A program softBV was used to estimate the energy barrier for oxide-ion migration Eb based on the bond-valence-based energy. Bi3GaSb2O11 was synthesized by the solid-state-reaction method. Synchrotron X-ray powder diffraction data of Bi3GaSb2O11 were measured in air at 27-800 ºC on beamline BL02B2 at SPring-8. Neutron-diffraction (ND) data of Bi3GaSb2O11 were measured at 26-600 ºC by Time-Of-Flight (TOF) neutron diffractometer iMATERIA. The ND data were analyzed by the Rietveld method. Direct current (DC) electrical conductivity σDC of Bi3GaSb2O11 was measured by a four-probe method in flowing dry and wet air. The oxygen partial pressure P(O2) dependence of σDC was measured at constant temperature 916 °C in the P(O2) range from 8.1×10^{-1} to 5.5×10^{-2} atm controlled using nitrogen, oxygen and argon gas mixtures. Alternating current (AC) impedance spectra with Pt electrodes were recorded in the temperature range of 582 to 893 °C. Bond-valence-based energy landscapes (BVELs) for a test oxide ion were examined to investigate oxide-ion diffusion pathways in Bi3GaSb2O11.

Result & discussion Bi3GaSb2O11 composition was selected by screening 402 Sb-containing materials by the bond-valence-based-energy calculations. Bi3GaSb2O11 was synthesized by solid-state reactions and its electrical conductivity and crystal structure were investigated at high temperatures. No phase transitions were observed between 26 and 800 °C. The crystal structure of Bi3GaSb2O11 was successfully analyzed by the space group 3^{-} using Rietveld method and high-temperature neutron diffraction
data from 26 to 600 °C. In the refined structure, two (Ga1/3Sb2/3)O6 octahedra share their edges to form a (Ga2/3Sb4/3)O10 unit (**Fig.1**). Bi3GaSb2O11 exhibited a high bulk ionic conductivity of 6.2×10^{-3} S cm^{-1} at 893 °C with a low activation energy of 0.68(2) eV (**Fig. 2**). Oxide-ion conduction was strongly suggested by the oxygen partial pressure dependence of electrical conductivity, polarization measurements, wide band gap, and electrical conductivities in wet and dry atmospheres.

The bond-valence-based- energy calculations for the refined crystal structure at 600 °C indicated that oxide ions three-dimensionally migrate through thecurved paths along the edges and on the O–O–O faces of (Ga2/3Sb4/3)O10 unit in Bi3GaSb2O11 (**Fig. 3**).

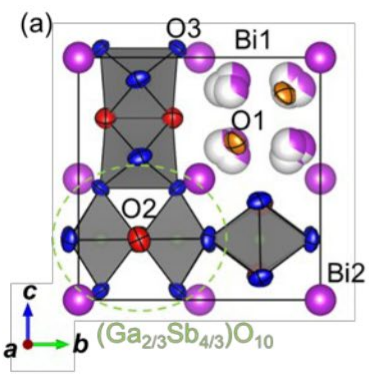

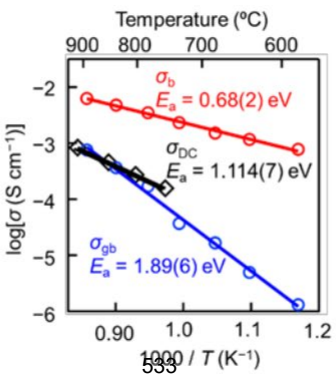

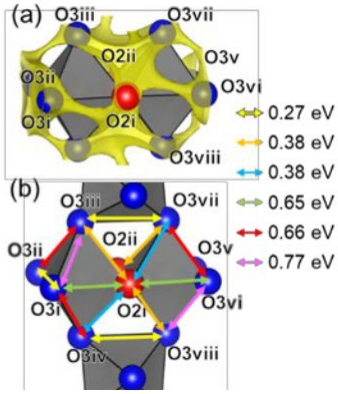

Figure 1 Crystal structure of $Bi_3GaSb_2O_{11}$ viewed along the *a* axis ($0.5 \le x \le 1$; $0 \le y \le 1$; $0 \le z \le 1$) refined using neutron diffraction data measured *in situ* at 600 °C.

Figure 2 Arrhenius plots of the DC electrical conductivity (black diamonds, σ_{DC}), bulk conductivity (red circles, σ_b), and grain-boundary conductivity (blue circles, σ_{gb}) of $Bi_3GaSb_2O_{11}$ in flowing dry air.

Figure 3 (a) Isosurfaces of the bond-valence-based energy for an oxide ion at 0.69 eV. (b) Lines with arrows denote possible diffusion pathways of the oxide ion.

A096-02-260823

Discovery of Novel Proton Conductors with 'Intrinsic Oxygen Vacancy'

Kei Saito, Kotaro Fujii, Masatomo Yashima*

Department of Chemistry, School of Science, Tokyo Institute of Technology, 2-12-1-W4-17, O-okayama, Meguro-ku, Tokyo 152-8551, Japan

** Corresponding author, E-mail: yashima@cms.titech.ac.jp*

Keywords: Novel proton conductor, Crystal structure analysis, Neutron diffraction

Proton conductors have a variety of applications such as proton ceramic fuel cells (PCFCs). In $AMO3-\delta$ perovskites (δ is the amount of oxygen deficiency), the aliovalent doping is a general strategy to increase the amount of 'extrinsic' oxygen deficiency δ, leading to higher oxide-ion and proton conductivities. However, the aliovalent doping might often be difficult and could lead to the phase instability and degradation in the use at high temperatures under different atmospheres. Recently, high oxide-ion and proton conductivities were reported in hexagonal perovskite-related oxides with intrinsically oxygen-deficient layers where a part of regular$AO3$ unit in $AMO3$ is replaced by the intrinsically oxygen deficient unit such as $AO2.5(V_{VO}^{\times})0.5$, $AO2(V_{VO}^{\times})$ and $AO(V_{VO}^{\times})2$. Here $V_{VO}^{\times}$ is the vacancy at the intrinsic oxygen vacant site VO through the Kröger-Vink notation and we call $V_{VO}^{\times}$ as 'intrinsic oxygen vacancy'. Here we report BaY1/3Ga2/3O2.5 as a new structural-type oxide-ion and proton conductor. Rietveld refinement of neutron-diffraction data indicated that BaY1/3Ga2/3O2.5 is a Ga/Y-cation- and $O/V_{VO}^{\times}$-anion-ordered perovskite-related oxide with the large amount of 'intrinsic oxygen vacancy' $V_{VO}^{\times}$ (16.7%), which was supported by bond-valance sums (BVSs) and *ab initio* DFT structural optimization (Fig. 1). Temperature and oxygen partial pressure dependencies of electrical conductivity of BaY1/3Ga2/3O2.5 in dry and wet atmospheres indicated that this compound exhibits high chemical and electrical stability and belongs to a new structure family of oxide-ion and proton conductors (Fig. 2).[1] Recently, we have discovered a new material with 'intrinsic oxygen vacancy', which exhibits high proton conductivity (Fig. 3). In our presentation, we would like to introduce the new material.

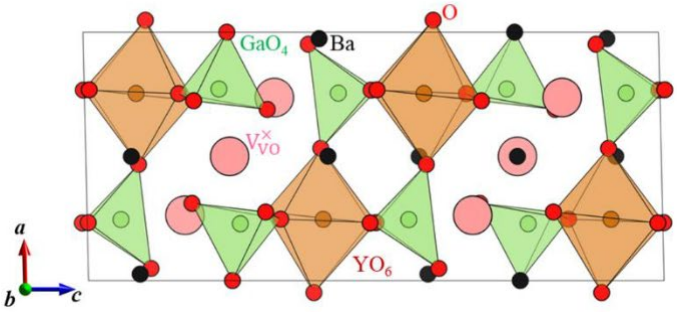

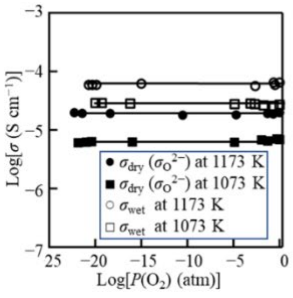

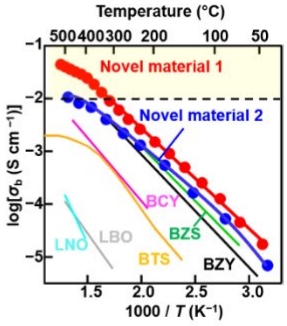

Figure 1. Refined crystal structure of BaY1/3Ga2/3O2.5 at 297 K, which shows both Y/Ga-cation- and $O/V_{VO}^{\times}$-anion-order. Closed black and red spheres denote the Ba and O atoms, respectively. Closed pink sphere stands for the 'intrinsic oxygen vacancy' $V_{VO}^{\times}$. Green tetrahedron and brown octahedron denote a GaO4 and a YO6, respectively.

Figure 2. Partial oxygen pressure $P(O2)$ dependence of electrical conductivity σ of BaY1/3Ga2/3O2.5 in dry air (σdry) and wet air (σwet) at 1073 K and 1173 K.

Figure 3. Arrhenius plots of bulk conductivity of novel perovskites and other proton conductors. In the yellow region, the proton conductivity exceeds 0.01 S cm^{-1}, which is required for the practical materials

A096-03-260823

Anhydrous superprotonic conductivity in a new zirconium acid phosphate: application of the BVSE method to proton conducting materials

S. Fop

University of Aberdeen, The Chemistry Department, Aberdeen, United Kingdom,

sacha.fop1@abdn.ac.uk

Keywords: proton conduction, bond-valence method, solid acid

Solid-state proton conductors (SSPCs) are ionic conductors in which the diffusion of H^+ ions is responsible for charge transfer. SSPCs with target proton conductivity of 10^{-2} S cm^{-1} at low temperatures (≤ 150 °C) are in demand for the development of fuel cells and other hydrogen-related technologies for portable and automotive applications [1]. However, at such low temperature, high relative humidity (RH > 90%) is required to attain sufficiently high proton conductivity. The requirement for active humidification forces the implementation of complex water management systems, thus imposing considerable limitations on the deployment of these technologies [2].

We have recently discovered a new zirconium solid acid triphosphate, $ZrH_5(PO_4)_3$ (ZP3), with record-high superprotonic conductivity of 0.5 – 3.1 x 10^{-2} S cm^{-1} in anhydrous conditions (RH << 1%). This value of anhydrous proton conductivity is unprecedent and comparable with benchmark polymer electrolytes and other proton conductors operating under high relative humidity [3]. Here, we report on the use of the bond-valence sum energy (BVSE) method for the characterization of the proton transport in this novel SSPC. We have successfully employed the BVSE method for the characterization of the proton and oxide ion diffusion in complex solid oxide ionic conductors [4], and we will first discuss these reports to show that this method can indeed be extended to systems other than Li-ion and alkali-metal conductors [5].

Our BVSE analysis on ZP3 revealed that equilibrium proton positions can be located around non-bridging oxygen atoms within disordered phosphate PO_4 units. Protons are bistable on two off-centre sites between two non-bridging oxygen atoms which compete as hydrogen bond donor and acceptor due to short –O2···O2– distance. Protons can diffuse on a 1-dimensional conduction pathway along the hydrogen bond network (Fig. 1a), following a Grotthus like mechanism composed by the rotation of a proton from position H1 to H2 (or vice versa) and hopping onto an adjacent oxygen atom (Fig. 1b). These hydrogen bond chains form an extended network running through the entire crystal structure and enabling long-range correlated proton motion (Fig. 1c).

These findings are of strong fundamental relevance as they evidence a conduction mechanism never seen before in a solid acid. In addition, the example of ZP3, suggests that the BVSE method could be successfully used to screen candidate materials containing native protonic defects, in search for innovative low temperature SSPCs.

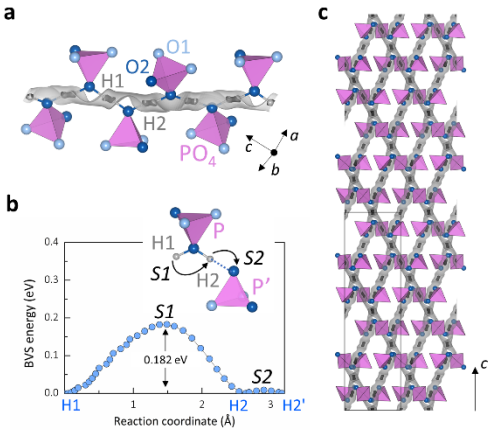

Figure 1. a) BVSE map for a test H^+ (isosurface levels are drawn at < 0.19 eV). b) BVSE barrier and schematic of the proton diffusion mechanism. c) Proton migration network within the ZP3 structure.

[1] Cano, Z. P., Banham, D., Ye, S., Hintennach, A., Lu, J., Fowler, M., Chen, Z., *Nature Energy* (2018), **3**, 279.
[2] Steele, B. C. & Heinzel, A., *Nature* (2001), **414**, 345-352; Boysen, D. A., Uda, T., Calum, R. I. C., Haile, S. M., *Science* (2004), **303**, 68.
[3] Fop, S., Vivani, R., Masci, S. Casciola, M., Donnadio, A. *Angew. Chem.*, under revision (preprint 10.26434/chemrxiv-2022-2h4g1).
[4] Wong, L. L.; Phuah, K. C., Dai, R., Chen, H., Chew, W. S., Adams, S., *Chem. Mater*. (2021), **33**, 625.
[5] Fop., S., McCombie, K., Smith, R. I., Mclaughlin, A. C., *Chem. Mater*. (2020), **32**, 4724; Fop., S., Dawson, J. A., Fortes, A. D., Ritter, C., Mclaughlin, A. C., *Chem. Mater*. (2021), **33**, 4651; Fop., S., Dawson, J. A., Tawse, D. N., Skellern, M. G., Skakle, J. M. S., Mclaughlin, A. C., *Chem. Mater*. (2022), **34**, 8190.

A096-04-260823

Experimental visualization of conduction pathways and direct observation of fast lithium-ion diffusion in superionic conductors using neutron scattering

K. Mori

Institute of Materials Structure Science, High Energy Accelerator Research Organization, 1-1 Oho, Ibaraki 305-0801, Japan

kmori@post.kek.jp

Keywords: Lithium-ion conductor, Neutron scattering, Reverse Monte Carlo modelling, Bond valence sum

Designing the next generation of lithium-ion batteries (LIBs) requires fundamental information that surprisingly often is still unknown – for example, details of how ions actually move through a working device. Li_2S–P_2S_5 superionic conductors have received a great deal of attention as a solid electrolyte for all-solid-state LIBs because of its extremely high ionic conductivity of 10^{-3} to 10^{-2} S/cm at room temperature [1,2]. The authors predict and visualize the conduction pathways of lithium ions in Li_2S–P_2S_5 glasses and $Li_7P_3S_{11}$ crystal, using reverse Monte Carlo (RMC) modelling [3] and the bond valence sum (BVS) approach [4] with neutron and synchrotron X-ray diffraction data (see Fig. 1(a)). The conduction pathways of lithium ions can be classified into two types: relatively "stable" regions and "metastable" regions for lithium-ion diffusion, respectively [5]. Moreover, the authors use quasi-elastic neutron scattering (QENS) to directly monitor the fast diffusion of lithium ions in $Li_7P_3S_{11}$ (see Fig. 1(b)). According to the jump diffusion model, the lithium ions migrate between stable regions within a jump length $< l > = 4.3$ Å along the conduction pathways [6]. This understanding is key to improved energy storage for applications ranging from vehicles to further smart grids.

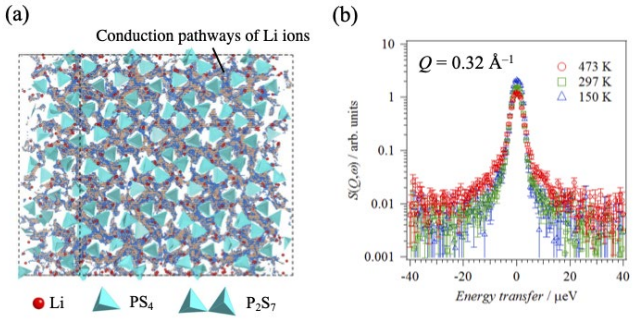

Figure 1. (a) Conduction pathways of Li ions in $Li_7P_3S_{11}$ superionic conductor at room temperature, predicted by RMC modelling and the BVS approach. (b) QENS spectra of $Li_7P_3S_{11}$ ($Q = 0.32$ Å^{-1}) collected at 150, 297, and 473 K.

[1] Mizuno, F., Hayashi, A., Tadanaga, K. & Tatsumisago, M. (2005). *Adv. Mater.*, **17**, 918.
[2] Seino, Y., Ota, T., Tadanaga, K., Hayashi, A. & Tatsumisago, M. (2014). *Energy Environ. Sci.*, **7**, 627.
[3] McGreevy, R. L. (2001). *J. Phys.: Condens. Matter*, **13**, R877.
[4] Adams, S. (2001). *Acta Cryst.*, **B57**, 278.
[5] Mori, K., Ichida, T., Iwase, K., Otomo, T., Kohara, S., Arai, H., Uchimoto, Y., Ogumi, Z., Onodera, Y. & Fukunaga., T. (2013). *Chem. Phys. Lett.*, **584**, 113.
[6] Mori, K., Enjuji, K., Murata, S., Shibata, K., Kawakita, Y., Yonemura, M., Onodera, Y. & Fukunaga., T. (2015). *Phys. Rev. Applied*, **4**, 054008.

A101 Organic-inorganic Hybrid Materials
Room 219
4.00pm - 6.30pm

A101-01-260823

Structural principles of polyoxometalate—silver ethynide hybrid materials

T. Ozeki

Department of Chemistry, College of Humanities and Sciences, Nihon University, 3-25-40 Sakurajosui, Setagaya-ku Tokyo, Japan ozeki.tomoji@nihon-u.ac.jp

Keywords: Polyoxometalate, Silver ethynide, Organic—inorganic hybrid cluster

Polyoxometalates are purely inorganic oxo-metal molecular anions that can be regarded as fragments of extended metal oxides. They can be hybridized with organic moieties using various methods. One promising synthetic approach for their organic hybrid compounds is to react them with silver(I) cations carrying various protecting organic ligands.

We have been successful in preparing polyoxometalate derivatives covered with silver(I) ions protected by *tert*-butylethynide, (CH3)3CC≡C–, ligands. Our synthetic strategy features site-selectively substituted polyoxometalates as the templates for the silver ethynide cluster formation. By substituting less positively charged Nb^{5+} for W^{6+}, surface electron density of the polyoxometalate increases in the vicinity of the Nb atoms, to which the positively charged Ag^{+} atoms prefer to attach. By this approach, we have been successful in prepared asymmetrical hybrid clusters where the polyoxometalate templates are partially covered by silver ethynide moieties, as shown in Fig. 1 [1, 2].

Characteristic structural features of [Ag 25{C≡CC(CH3)3}16(CH3CN)4(α-P2W15Nb3O62)] (Fig. 1 left) include the three pendant CH3CN ligands. They coordinate to Ag atoms that are not fully covered by the *tert*-butylethynide ligands. These acetonitrile ligands can be substituted with other ligands, successful results of which will also be presented.

On the other hand, all the Ag atoms in [Ag 42(CO 3){C≡CC(CH3)3}27(α- A- SiW9Nb3O40)2]$^{-}$ (Fig. 1 right) are fully covered by the *tert*-butylethynide ligands and there are no room for additional ligands to coordinate. Combined with the structural investigations of recently synthesized related compounds, structural principles that lead to these differences will be discussed.

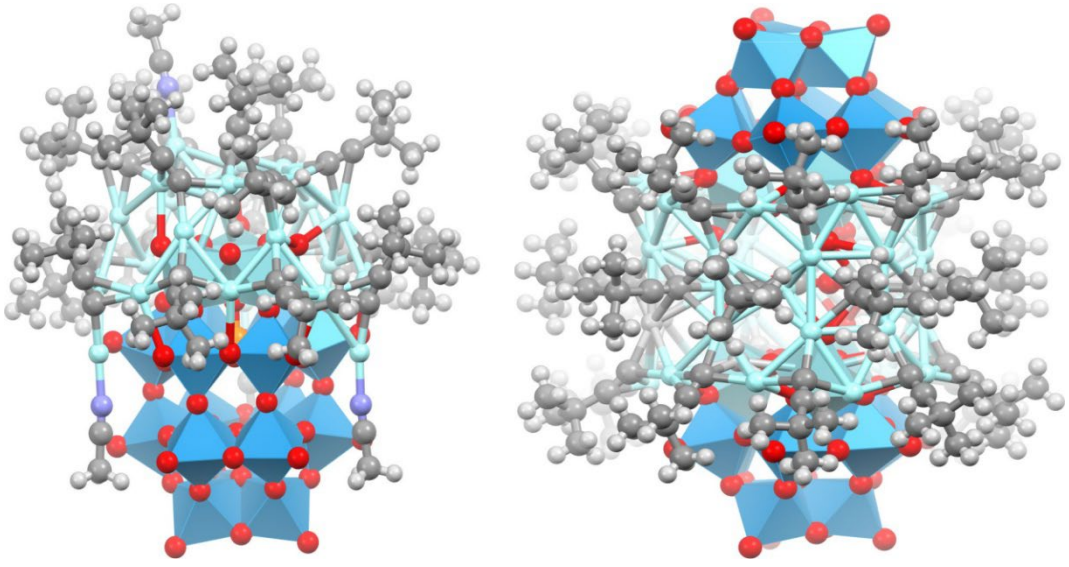

Figure 1. Structures of $[Ag_{25}\{C{\equiv}CC(CH_3)_3\}_{16}(CH_3CN)_4(\alpha\text{-}P_2W_{15}Nb_3O_{62})]$ (left) and $[Ag_{42}(CO_3)\{C{\equiv}CC(CH_3)_3\}_{27}(\alpha\text{-}A\text{-}SiW_9Nb_3O_{40})_2]^{-}$ (right). WO_6 and NbO_6 coordination spheres in the polyoxometalate moieties are displayed as the polyhedral representations, while other parts are shown in the ball-and-stick models.

[1] Kurasawa, M., Arisaka, F. & Ozeki, T. (2015). *Inorg. Chem.*, **54**, 1650.
[2] Tamari, S., Ono, K., Hashimoto, M. & Ozeki, T. (2015). *Dalton Trans.*, **44**, 19056.

This work was supported by JSPS KAKENHI grant 19K05510 and the JSPS Core-to-Core program (International Network in Polyoxometalate Science for Advanced Functional Energy Materials).

A101-02-260823

The development of metal-organic frameworks for oxygen separation that is both reversible and selective at room temperature

A. L. Sutton,[1] L. Melag[2], M. M. Sadiq,[1] K. Konstas,[1] M. R. Hill[1,2]

CSIRO, Private Bag 33, Clayton South MDC, VIC, 3169 Australia
Department of Chemical Engineering, Monash University, Clayton, VIC, 3168, Australia

ashley.sutton@csiro.au

Keywords: metal-organic framework (MOF), oxygen, separation

Oxygen is critical gas species for both medical and industry settings [1]. Currently, the mainstay for oxygen separation from air is cryogenic distillation. Unfortunately, this process is inefficient and energy intensive. Over the past decade, there have been significant efforts to generate materials that can separate oxygen from air at ambient temperatures. Metal-organic frameworks, which are hybrid inorganic-organic porous structures, have attracted significant attention in this area [2-4]. We report rationally designed metal-organic frameworks which can separate oxygen from air at room temperature across multiple sorption cycles.

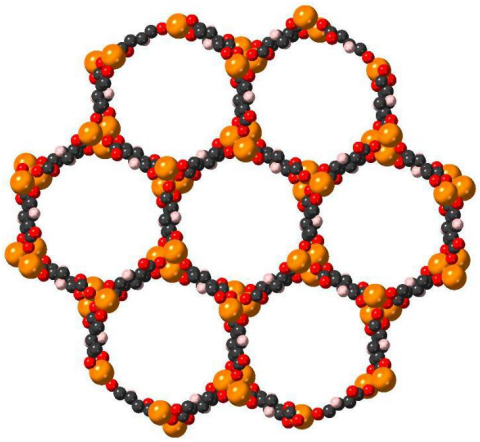

Figure 1. Illustration of a metal-organic framework which displays selectivity for capturing oxygen.

[1] Sutton A. L., Melag L., Sadiq M. M., Hill M. R. (2022). *Angew. Chem.* **61** (37), e2002208305
[2] Bloch E. D., Murray L. J., Queen W. L., Chavan S., Maximoff S. N, Bigi J. P., Krishna R., Peterson V. K., Grandjean F., Long G. J., Smit B., Bordiga S., Brown C. M., Long J. R. (2011) *J. Am. Chem. Soc.*, **131**, 14814.
[3] Xiao D. J., Gonzalez M. I., Darago L. E., Vogiatzis K. D., Haldoupis E., Garliardi L., Long J. R. (2016), *J. Am. Chem. Soc.*,**138**, 7161.
[4] Rosen, A. S., Mian M. R., Islamoglu T., Chen H., Farha O. K., Notestein J. M., Snurr R. Q. (2020), *J. Am. Chem. Soc.*, **142**,

A101-04-260823

Structure characterization and physical properties of some novel lead-free hybrid perovskites for multifunctional applications

Seham K. Abdel-Aal[1], A. Ouasri [2], Nicolas Claiser[3], Mohamed Souhassou[3], Claude Lecomte[3],

Physics department, Faculty of Science, Cairo University, Giza 12613, Egypt,[2] Laboratoire (ReSIP), Centre Régional des Métiers de l'Education et de la Formation, Madinat Al Irfane, Souissi, BP 6210 Rabat, Morocco. [3]CNRS, Laboratoire CRM2, UMR CNRS 7036, Université de lorraine,-Nancy, France.

Correspondance email : seham@sci.cu.edu.eg

Keywords: hybrid perovskites, lead free materials, crystal structure

Organic- inorganic hybrid perovskites gain considerable attention recently and more studies have been done as changing the halide, metal ion and the ligand enables to tune the optical, electric, magnetic, ferroelectric properties. Halide perovskites in particular lead halides are interesting semiconductors with a direct band gap (1.5 eV) which enables collecting visible photons. These photoactive crystals have no future for safety and ecological reasons. Diammonium halide perovskite hybrids [NH3(CH2)nNH3]MClxBr4-x ; x= 0, 2, 4; M= Co, Mn, Bi, Cu; n= 3-9 allow mixing of organic and inorganic components in one molecule which possesses a property that may not exist in either of the parent components. The complete structure information as well as lattice parameters for Co series n= 4-9 are provided, and for n = 3-9 for Mn hybrid. Differential thermal analysis DSC shows reversible order - disorder transition for both the Co and Mn hybrids. Permittivity studies confirm the phase transition. The optical properties of Co series show strong absorption in the visible range, the band gap (1.79 eV) which is promising for photovoltaic applications.

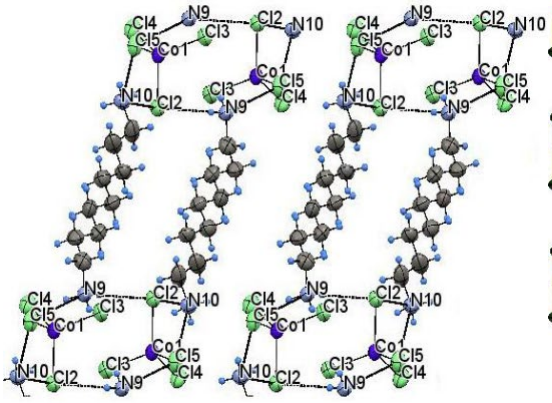

Fig.1 layered structure of [NH3(CH2)9NH3]CoCl4. OIHs

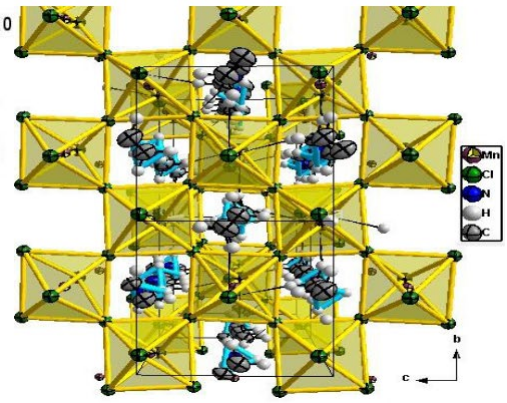

Fig. 2 Associated octahedra of [NH3(CH2)9NH3]MnCl4

[8] Seham K. Abdel-Aal, A. Ouasri,.J. Solid State Chemistry, 2022, 314, 123401
[9] Seham K. Abdel-Aal, A. Ouasri,. J. of Molecular Structure , 2022, 1251, 131997
[10] Seham. K. Abdel-Aal, A. S. Abdel-Rahman, G. Bortel, Á. Pekker, K. Kamarás, G. Faigel J. Physics and Chemistry of Solids, 2022, 161, 110400
[11] Seham K. Abdel-Aal, Ahmed S. Abdel-Rahman, E. Yakimov, Acta Cryst. B75, (2019)

A101-05-260823

Old trick for new dogs – modification of structural and optoelectronic properties in layered methylhydrazinium lead halide perovskites via halide mixing

Drozdowski[1], A. Gągor[1], K. Fedoruk[2], M. Mączka[1], D. Stefańska[1], J. K. Zaręba[2], A. Sieradzki[2]

Institute of Low Temperature and Structure Research Polish Academy of Sciences, Okólna 2 st., 50-422 Wrocław, Poland

Wrocław University of Science and Technology, 27 Wybrzeże Wyspiańskiego st., 50-370 Wrocław, Poland d.drozdowski@intibs.pl

Keywords: hybrid perovskites, phase transitions, crystal engineering

The 3D hybrid perovskites (HOIPs) of ABX3 formula, built of corner-sharing lead halide BX6 octahedra network with voids filled by small organic "A" cations (methylammonium (MA^+) or formamidinium (FA^+)) gained a wide interest of material scientist due to their fascinating properties. With high photoluminescence quantum yield (PLQY), broad tunability of emission colours, power conversion efficiency up to 25% and so on, these materials are strong candidates for revolutionary photovoltaic and light-emitting devices [1-2]. Further improvement of the stability and certain properties of HOIPs (e.g., PLQY) may be achieved via the reduction of structural dimensionality to layered (2D) analogues of formula A2BX4, where the octahedra layers are separated by organic cations. This approach also allowed to expand the variety of organic cations that can be used as *perovskitizers* [3].

The family of *perovskitizers* for both 3D and 2D HOIPs has been enriched by our group with the methylhydrazinium cation (MHy^+). The 3D HOIPs of MHyPbBr3 and MHyPbCl3 formula crystallize in polar structure and reveal Second Harmonic Generation (SHG) effect, thermochromism and switching between two dielectric (MHyPbBr3) or SHG-active (MHyPbCl3) states [4-5]. The layered counterparts (MHy2PbX4, where X = Br, Cl, I) are characterized by record-braking low separation of the perovskite layers. Furthermore, MHy2PbBr4 is ferroelectric at room temperature (RT), MHy2PbCl4 demonstrates sequence of polar, modulated and centrosymmetric phases, whereas in MHy2PbI4 an unique octahedra tilting system is observed [6-8].

The main topic of this presentation is physiochemical characterization of the layered mixed-halide HOIPs of MHy2PbBr4-xIx and MHy2PbBr4-xClx formula. The mixing-halide approach proved its utility for the formerly reported 3D analogues, demonstrating its effect on the stabilization of particular phases in the temperature gradient, as well as tunability of energy bandgap, emission colour and SHG intensity [9]. In the case of MHy2PbBr4-xIx systems, a relatively low contribution of iodine ($x = 0.3$) destroys the polar alignments of MHy2PbBr4 and leads to a sequence of centrosymmetric phases with temperature lowering, i.e., P*mmn* (HT phase, above 370 K), RT *Pnma* and LT monoclinic *P*21/*c* (below 221 K). It is worth noting that symmetry of neither RT nor LT phase was observed in the single-halide analogues. The ferroelectric character of MHy2PbBr4 vanishes and MHy^+ cations are disordered, which might be the consequence of increasing interatomic distances and weakening of hydrogen bonding interactions associated with incorporation of iodine. For greater iodine contribution ($x \geq 1.1$) the RT phase is modulated, with the average structure isostructural to RT phase of MHy2PbBr3.7I0.3 and the modulation vector $q = 0.44$ for $x = 3.1$. It is also worth mentioning that via modifying the synthesis routes we obtained solid-solutions of MHy2PbBr4-xIx and MHy2PbBr4-xClx in the wide range of compositions. Results of this study show that halide-mixing in MHy2PbBr4-xIx and MHy2PbBr4-xClx systems leads to the severe modification of the crystal structure and facile tunability of the optoelectronic properties.

1. Li, W., Wang, Z., Deschler, F., Gao, S., Friend, R. H., Cheetham, A. K. (2017). *Nat. Rev. Mater.*, **2**, 16099.
2. Wang, W., Zhang, Y., Wu, W., Liu, X., Ma, X., Qian, G., Fan, J. (2019). *J. Phys. Chem. C*, **123**, 13110-13121.
3. McNulty, J. A., Lightfoot, P. (2021). *IUCrJ*, **8**, 485-513.
4. Mączka, M., Ptak, M., Gągor, A., Stefańska, Zaręba, J. K., Sieradzki, A. (2020). *Chem. Mater.*, **32**, 4, 1667-1673.
5. Mączka, M., Gągor, A., Zaręba, J. K., Stefańska, D., Drozd, M., Balciunas, S., Šimenas, M., Banys, J., Sieradzki, A. (2020). *Chem. Mater.*,

A115 and A117 Applications of Machine Learning to X-ray Spectroscopy and Scattering and Putting Pressure on Complementary X-ray Spectroscopy and Scattering Method
Room 220
4.00pm - 6.30pm

A115/A117-01-260823

Inelastic X-Ray Study of Elemental 4f Metals under High Pressure

Yang Ding

Center for High-Pressure Science and Technology Advanced Research, Beijing 100094, ChinaEmail of communicating yang.ding@hpstar.ac.cn

Keywords: Inelastic X-Ray, high pressure, 4f metals

The behaviour of 4f electrons plays a crucial role in elucidating various physical phenomena, such as valence fluctuation, insulator-metal, nonmagnetic-magnetic, and superconducting transitions in lanthanide metals and compounds. However, understanding the electrodynamics of 4f electrons remains a significant challenge in many-body quantum physics. Applying external pressure to convert localized 4f states to delocalized ones provides a unique opportunity to explore this phenomenon. In this work, we utilized inelastic x-ray scattering and resonant x-ray emission spectroscopy to investigate changes in 4f states during the volume collapse transition in cerium [1] and the valence transition in europium [2] under high pressure. Our findings shed light on the underlying mechanism of these transitions.

[1] Chen, B., Parschke, E. M., Chen, W. C., Scoggins, B., Li, B., Balasubramanian, M., Heald, S., Zhang, J., Deng, H., Sereika, R., Sorb, Y., Yin, X., Bi, Y., Jin, K., Wu, Q., Chen, C. C., Ding, Y. * & Mao, H. K. Probing Cerium 4f States across the Volume Collapse Transition by X-ray Raman Scattering. J Phys Chem Lett 10, 7890-7897, (2019).

[2] Chen, B., Tian, M., Zhang, J., Li, B., Xiao, Y., Chow, P., Kenney-Benson, C., Deng, H., Zhang, J., Sereika, R., Yin, X., Wang, D., Hong, X., Jin, C., Bi, Y., Liu, H., Liu, H., Li, J., Jin, K., Wu, Q., Chang, J., Ding, Y*. & Mao, H.-k. Novel Valence Transition in Elemental Metal Europium around 80 GPa. Physical Review Letters 129, (2022).

A115/A117-02-260823

A deep neural network for the rapid prediction of L-edge XANES spectra

L. Watson[1], T.J Penfold[1]

Newcastle University, Newcastle Upon Tyne, NE1 7RU

Email of communicating author: l.watson10@newcastle.ac.uk

Keywords: XANES, Deep Neural Network, L-edge

X-ray absorption spectroscopy (XAS) is a powerful technique that can provide element- and site-specific insight into the geometric and electronic structure of matter. At the L2/3-edge of a transition metal, the spectrum is characterised by a sharp rise (called 'edge') in the absorption which encodes the electronic information, followed by several less intense oscillatory resonances which encode geometric structure. The X-ray Absorption Near-edge Structure (XANES) region, typically found at <50 eV above the XAS edge, is challenging to simulate as it requires complex theoretical calculations, hence analysis of this region is far from trivial.

XANESNET[1], a deep neural network (DNN) has been developed to successfully predict the K-edge and, more recently, the L2/3-edge spectra of a given system. At the K-edge, as governed by the dipole selection rules, the bound transitions are disallowed and therefore the spectrum remains relatively simple. We have subsequently extended the DNN to the Pt L-edge (2s/2p n). In contrast to the K-edge, the L-edge usually exhibits two distinct spectral regions, by virtue of the dipole selection rules: i) The 'white line', which is dominated by bound electronic transitions from metal-centres 2p orbitals into unoccupied orbitals with d character. The intensity and shape of this band consequently reflects the d density of states (d-DOS), which is strongly modulated by mixing with ligand orbitals involved in chemical bonding. ii) The post-edge, where oscillations encode the local geometric structure around the X-ray absorption site.

We demonstrate that XANESNET can predict accurately L-edge XANES spectra of second and third row transition metals, including both the parts containing electronic and geometric structural information, with no more information than the local environment around the absorption site. The DNN was trained on thousands of unique molecules harvested from multiple databases, along with their simulated XANES spectrum. The performance of the DNN was assessed by predicting on unseen samples, in which the median percentage difference between target and predicted spectrum was consistently <3%.

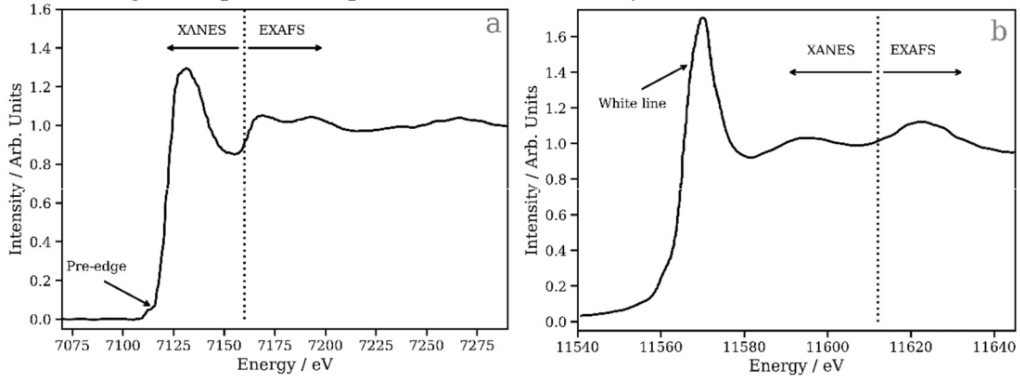

Figure 1. (a) A typical transition metal K-edge X-ray absorption spectrum; weak pre-edge features, arising from dipole forbidden 3d 1s transitions are present. (b) A typical L-edge X-ray absorption spectrum; the "white-line" arising from dipole allowed 5d 2p transitions is shown.

[1] L. Watson, C. D. Rankine and T. J. Penfold, Physical Chemistry Chemical Physics, 2022, 24, 9156–9167.

A115/A117-04-260823

Semi and self supervised approaches to space group and bravais lattice determination

W. Ratcliff1,2, S. Lolla1, Ichiro Takeuchi1,2, Aaron Kusne1,2, Haotong Liang1,2

NIST, Gaithersburg, Maryland, USA, University of Maryland, College Park, Maryland, USA

William.ratcliff@nist.gov

Keywords: Artificial Intelligence, Diffraction, Neural Network

During this talk, I will discuss our work [1] to use neural networks to automatically classify Bravais lattices and space-groups from neutron powder diffraction data. Our work classifies 14 Bravais lattices and 144 space groups. The novelty of our approach is to use semi-supervised and self-supervised learning to allow for training on data sets with unlabelled data as is common at user facilities. We achieve state of the art results with a semi-supervised approach. Our accuracy for our self-supervised training is comparable to that with a supervised approach.

Support for Satvik Lolla was provided by the Center for High Resolution Neutron Scattering, a partnership between the National Institute of Standards and Technology and the National Science Foundation under Agreement No. DMR-2010792.

[1] Satvik Lolla Et al, Journal of Applied Crystallography **55** (2022)

https://doi.org/10.1107/S1600576722006069

A117-05-260823

Direct extraction of Structural Insight from X-ray Absorption Near Edge Spectra using Convolutional Neural Networks

T. W. David, T. Penfold

Chemistry, School of Natural and Environmental Sciences, Newcastle University, Newcastle upon Tyne, NE17RU, UK Tom.Penfold@newcastle.ac.uk

Keywords: X-ray absorption spectroscopy, machine learning, neural networks

X-ray absorption spectroscopy (XAS) is a core technique, widely used across the physical and biological sciences due to its ability to deliver electronic and geometric information about a sample in a huge range of different environments. However, understanding XAS requires high levels of theory, which can be challenging due to resource requirements and complexity of theory [1]. To enhance the accessibility of XAS, a deep neural network has been developed, based on the multilayer perceptron (MLP) model, which can provide instantaneous, qualitative predictions of XAS spectra using nothing more than the local geometry of an arbitrary absorption site [2,3].

In the present work, we present an extension of XANESNET to perform the reverse analysis, *i.e.* spectrum to structure. Using a convolution neural network (CNN) architecture, our new network can translate XAS directly into a radial distribution function describing the arrangement of atoms around the absorbing atom. Furthermore, we present an autoencoder (AE) architecture to complement the CNN model which is able to perform consistent forward and reverse mapping of x-ray spectra within a single model. The CNN and AE are trained on approximately 30,000 calculated x-ray absorption spectra to predict the corresponding structures. The structures are represented in terms of radial distance from the central absorbing atom and an example case is shown in Figure 1 where the actual and predicted absorption intensity is sown as a function of radial distance.

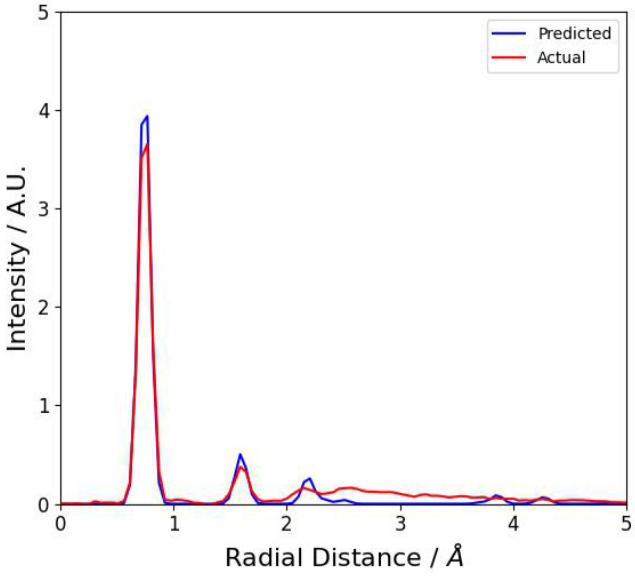

Figure 1. Actual and predicted radial distribution of molecular structure.

[1] Joly, Y.; Grenier, S. Theory of X-Ray Absorption Near-Edge Structure. In X-Ray Absorption and X-Ray Emission Spectroscopy: Theory and Applications; Van Bokhoven, J. A., Lamberti, C., Eds.; Wiley, 2016; Vol. 1, Chapter 4, pp 73−97.

[2] Rankine, C.D., Madkhali, M.M. and Penfold, T.J., 2020. A deep neural network for the rapid prediction of X-ray absorption spectra. *The Journal of Physical Chemistry A*, *124*(21), pp.4263-4270.
[3] Rankine, C.D. and Penfold, T.J., 2022. Accurate, affordable, and generalizable machine learning simulations of transition metal x-ray absorption spectra using the XANESNET deep neural network. *The Journal of Chemical Physics*, *156*(16), p.164102.

A115/A117-06-260823

New Opportunities in Physics, Solid State Theory, Experiment and Synchrotron Science, including Discovery of new satellites using extended range High Energy Resolution Fluorescence Detection

Christopher T Chantler[1]

School of Physics, University of Melbourne, Australia chantler@unimelb.edu.au

Keywords: XR-HERFD, fluorescence, nanostructure, XES

The fundamental process at the heart of X-ray Emission Spectroscopy [XES], after the absorption of a photon which leaves the atom in an excited state, is the subsequent emission of photons of varying energies dependent on the electronic structure of the atom. Recent highlights include Theory and Measurement of plasmon-coupling [1]; XES for fluorescence and self-absorption [2,3]; X-ray Absorption Spectroscopy [XAS] for binary crystals [ZnSe] and Thermal Diffuse Scattering [4]; and XAS for high resolution nanostructure of Zn [5,6,7].

Many-body processes can occur during absorption and relaxation which result in satellite structures, which distort the spectra and limit the detailed insight from X-ray Absorption Spectroscopy. Identification and characterisation of many-body processes can shed light on these spectra and how to interpret them, and hence how to measure the dynamical nanostructure observable with these technologies. Resonant Inelastic X-ray Scattering and High Energy Resolution Fluorescence Detection have recently developed as high-resolution fields of X-ray Spectroscopy and very powerful probes for bonding, nanostructure and oxidation state. Currently unavailable in Australia, we report recent measurements in the UK, and the discovery of a new satellite in manganese using the technique, which we call extended range High Energy Resolution Fluorescence Detection, XR-HERFD. This is foundational for many future studies and for novel X-ray spectroscopy. Identification and characterisation of many-body processes will shed light on analysis approaches and structure observed in XAS, and a new light on Mn.

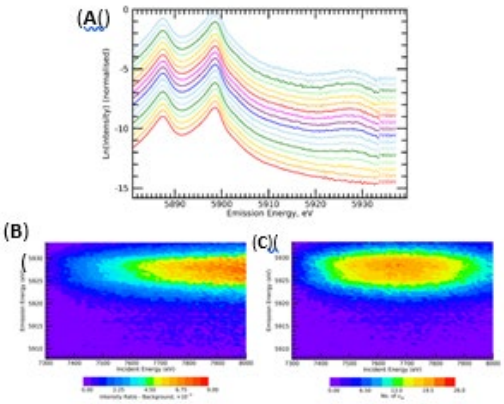

Figure 1. (A) Stack plot of HERFD-XES slices of the manganese metal XR-HERFD data at labelled intervals of 50 eV in incident energy Ω. Evolution of the new satellite with increasing incident energy is observed. The onset of the satellite is below 7300 eV. (B) XR-HERFD map after background subtraction. (C) XR-HERFD Contour plot of the significance of the satellite region. This shows the number of standard errors of the satellite after a background subtraction of the data. At peak regions on this plot, along the peak of the new process, each data point in the two-dimensional area of the new peak has a significance of more than 10 standard errors σse corresponding to a total many 100s of standard errors.

[1] C T Chantler, J D Bourke, Low-energy electron properties: Electron inelastic mean free path, energy loss function and the dielectric function: Recent measurement and the plasmon-coupling theory Ultramicroscopy 201 (2019) 38-48
[2] R M Trevorah, C T Chantler, M J Schalken, Solving Self-Absorption in Fluorescence, IUCr J 6 (2019) 586-602
[3] R M Trevorah, C T Chantler, M J Schalken, New Features Observed in Self-Absorption Corrected X-ray Fluorescence Spectra with Uncertainties, Journal of Physical Chemistry A124 (2019) 1634-1647
[4] D Sier, G P Cousland, R M Trevorah, R S K Ekanayake, C Q Tran, J R Hester, C T Chantler, J Synch Rad 27 (2020) 1262-1277
[5] R S K Ekanayake, C T Chantler, D Sier, M J Schalken, A J Illig, M D de Jonge, B Johannesen, P Kappen, C Q Tran, J Synch Rad 28(5) (2021) 1476-1491
[6] R S K Ekanayake, C T Chantler, D Sier, M J Schalken, A J Illig, M D de Jonge, B Johannesen, P Kappen, C Q Tran, J Synch Rad 28(5) (2021) 1492-1503
[7] D Sier, R S K Ekanayake, C T Chantler, X-Ray Spectrometry 51 (2022) 91-100 doi 10.1002/xrs.3262

DAY 6

Sunday 27 August 2023

Keynote 25
Room 203/204
9.00am - 9.50am

Keynote-025-270823

Structural and functional studies on [NiFe]-hydrogenases

Y. Higuchi[1], T. Hiromoto[1,2], K. Nishikawa[1], H. Ogata[1], Y. Hori[3], Y. Shigeta[2,3], T. Tamada[2]

[1]Graduate School of Science, University of Hyogo, 3-2-1 Koto, Kamigori, Hyogo 678-1297, [2]Institute for Quantum Life Science, National Institutes for Quantum Science and Technology, 2-4 Shirakata, Tokai, Ibaraki 319-1106, Japan, Japan, [3]Center for Computational Sciences, University of Tsukuba, 1-1-1 Tennodai, Tsukuba, Ibaraki 305-8577, Japan

Keywords: [NiFe]-hydrogenase, X-ray crystallography, Neutron crystallography, Fe-S cluster, PCET

[NiFe]-hydrogenases catalyse the reversible conversion of dihydrogen to two protons and electrons [1,2]. The catalytic unit of the enzymes is composed of two subunits (Mr = 28.8 and 62.5 k) that harbours the active site (catalytic center), Fe-S clusters (electron pathway), proton-transfer pathways (hydrogen-bonding networks) and hydrophobic channels (dihydrogen tunnels), which concertedly support the excellent enzymatic catalytic activity (Fig. 1, left).

The active site is a dinuclear Ni-Fe complex with three non- protein ligands (two CN and one CO) to Fe. Ni is coordinated by four thiolate groups of cysteine residues in the large subunit, and two of them bridge Fe and Ni (Fig. 1 in the circle) . The third bridging site between Ni and Fe is vacant (referred as Ni-SIa), occupied by H^- (Ni-R or Ni-C) or OH^- (Ni-B), which are distinguished by the redox states of Ni or spectroscopic properties of non-protein ligands coordinated to Fe. Two inactive oxidized (Ni^{3+}) states are referred as Ni-A and Ni-B, whereas the catalytic reaction comprises mainly Ni-SIa (Ni^{2+}), Ni-R (Ni^{2+}) and Ni-C (Ni^{3+}) . So far, [NiFe]-hydrogenases have been intensively studied by various physicochemical, theoretical and biochemical methods, however, the reaction mechanism of the formation and consumption of H2 at the active site remains to be uncovered.

[NiFe]-Hydrogenases are reversibly inactivated upon exposure to dioxygen (O2) [3]. O2-sensitive enzymes are readily inactivated at ambient O2 concentrations and usually require the prolonged activation time, whereas O2-tolerant enzymes maintain catalytic activity. In O2-tolerant enzymes, a flexible [4Fe-3S]- 6Cys cluster proximal to the active site supplies additional electrons for reduction of invading O 2 with concomitant structural changes [4]. Two protons for this reaction are probably supplied from a nearby backbone amide nitrogen and glutamate which coordinate to a Fe of the deformed [4Fe-3S]-6Cys in the oxidized state. These residues are involved in one of the proton pathways which connects the active site and [4Fe-3S]-6Cys.

Since neutron crystallography is a powerful tool to identify hydrogen species, H^- and H^+, which are the products by H2-decomposition at the active site, could be observed in the neutron scattering length density map in the Ni- C and Ni-R states of the enzyme. The accurate positions of the above hydrogen species at the active site are actually important for theoretical approach to the reaction mechanism of [NiFe]-hydrogenases. In addition, to identify the real proton pathway through the enzymatic reaction is also important for understanding the evolutionally well-tuned molecular system from the view point of not only the catalytic activity, but also O2- tolerance of the enzyme. In the neutron scattering length density map, the negative density of H^+ is distinguishable from the positive density of D^+. Since hydrogenases decompose both H2 and D2, the real proton-pathways for the catalytic reaction could be identifiable by comparing the

scattering length density map of the enzyme activated by D2 with that by H2 as a substrate. We have developed the structural chemistry of [NiFe] - hydrogenase from *Desulfovibrio vulgaris* Miyazaki F by X- ray and neutron crystallography, enzymatic studies by Raman spectroscopy and their theoretical approaches. In this micro-symposium, distinctive catalytic features (possibility of interfacial reactivity) of [NiFe]-hydrogenases, activation mechanism of the Ni-Fe active site and a role of the proton pathways containing structural water molecules for O2-tolerance are discussed on the basis of the precise x-ray and neutron crystal structures of the enzyme.

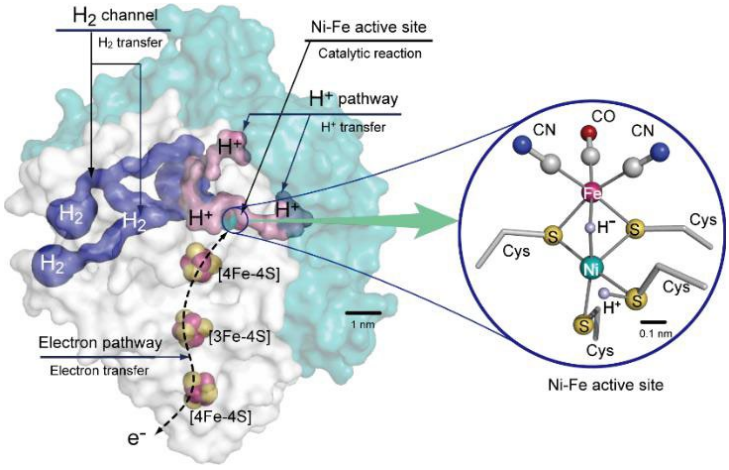

Figure 1. Schematic diagram of the overall structure of DvMF [NiFe]-hydrogenase and the Ni-Fe active site (in the circle)

[1] Vignais, P. M. & Billoud, B. (2007). *Chem Rev.* **107**, 4206−4272.
[2] Nishikawa, K., Ogata, H. & Higuchi, Y. (2020). *Chem. Lett.* **49**, 164−173.
[3] Fernandez, V. M., Hatchikian, E.C., Patil, D.S. & Cammack, R (1986). *Biochim Biophys Acta*, **883**, 145−154.
[4] Shomura, Y., Yoon, K. S., Nishihara, H. & Higuchi, Y. (2011). *Nature*, **479**,253−256.

Keynote 26
Room 210/211
9.00am - 9.50am

Keynote-26-270826

Ptychography Based Resolution-enhanced X-ray Fluorescence Microscopy Using Deep Neural Networks

Longlong Wu[1,2], Seongmin Bak[3], Youngho Shin[4], Yong S Chu[3], Shinjae Yoo[1], Ian K. Robinson[2,5] and Xiaojing Huang[3]

[1]Computational Science Initiative, Brookhaven National Laboratory, Upton, NY 11973, USA
[2]Condensed Matter Physics and Materials Science Department, Brookhaven National Laboratory, Upton, NY 11973, USA
[3]National Synchrotron Light Source II, Brookhaven National Laboratory, Upton, New York 11973, USA
[4]Materials Engineering Research Facility, Applied Materials Division, Argonne National Laboratory, Lemont, IL 60439, USA
[5]London Centre for Nanotechnology, University College London, London, WC1E 6BT, United Kingdom.
lwu@bnl.gov

Keywords: Machine Learning, X-ray Fluorescence, Ptychography

Accurately resolving elemental distributions inside materials at the nanoscale is critical for understanding their physical and chemical properties. Multimodal hard X-ray scanning probe microscopy has been extensively used to study materials providing multiple contrast mechanisms. For instance, combining ptychography with X-ray fluorescence (XRF) microscopy reveals structural and chemical properties simultaneously. While ptychography can achieve diffraction-limited spatial resolution, the resolution of XRF is normally limited by the X-ray probe size. Here, utilizing the multimodal measurement, we develop a machine learning (ML) model to overcome this problem by deconvolving the X-ray probe from the XRF signal [1]. The enhanced spatial resolution was observed for both simulated and experimental XRF data, showing superior performance over the state-of-the-art scanning XRF method with different nano-sized X-ray probes. As one example shown in Figure 1, enhanced spatial resolutions were also observed for the accompanying 3D XRF tomography reconstructions.

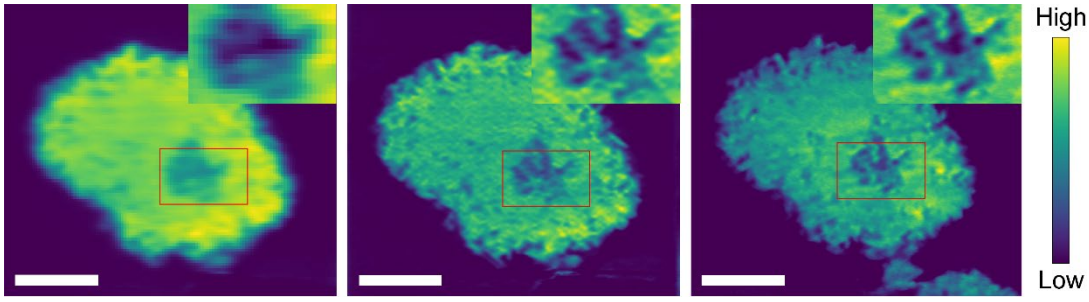

Figure 1. Comparison of experimental 3D low-resolution XRF image and resolution-enhanced XRF image. Here, the central slices of the 3D reconstructed structures of the sample are displayed. The left column shows the central slice of the raw XRF tomography reconstruction. The middle column shows the corresponding central slice of the 3D tomography reconstruction using the spatial resolution-enhanced XRF image from the trained ML model. The right column shows the central slice of the phase-contrast image from the ptychographic tomography reconstruction. Here, all the scale bars are 2 μm.

[1] L. Wu, S. Bak, Y. Shin, Y. Chu, S. Yoo, I. K. Robinson and X. Huang, Resolution-enhanced X-ray Fluorescence Microscopy via Deep Residual Networks, submitted.

Keynote 27
Room 212/213
9.00am - 9.50am

Keynote-27-270823

Towards an “infinite” number of calcium oxalate structures?

C. Bonhomme

Laboratoire de Chimie de la Matière Condensée de Paris, Sorbonne University, Paris, France

christian.bonhomme@upmc.fr

Keywords: NMR crystallography, phase transitions, local dynamics.

Hydrated calcium oxalates are among the most represented mineral structures among human pathological calcifications. Although their presence in kidney stones is crucial, their formation remains largely mysterious. This is primarily due to a confined precipitation environment where the rules of microfluidics fully apply. In addition, organic compounds such as proteins also participate in the crystal growth process. This results in original structures that are not well understood at the moment.

In this presentation, we will show that despite very simple chemical formulas, the detailed study of synthetic and natural calcium oxalates requires the combined approach of advanced NMR (Fig. 1) and DNP experiments [1], DFT calculations of structural models [2] and the GIPAW method [3].

We will show that these structures are extremely dependent on temperature variations leading to phase transitions (reversible and irreversible) which can be monitored inside an NMR rotor rotating at the magic angle. In fact, there is a very large variety of structures that differ only in their ^{13}C CP MAS NMR spectra, on the scale of a few hundredths of ppm. Local dynamics are essential to consider when interpreting the spectra in detail [1, 4]. The study of synthetic compounds has led to a much better understanding of the structure of natural kidney stones and provides a better understanding of their temporal evolution.

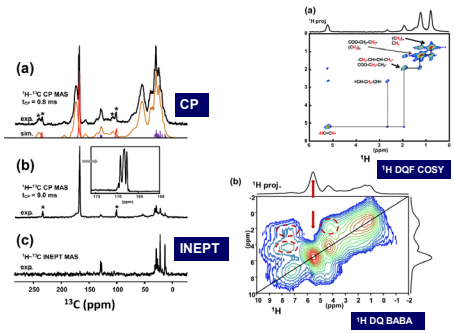

Figure 1. The NMR study of kidney stones: the tool box. Adapted from reference [1].

[1] Leroy, C., Bonhomme-Coury, L., Gervais, C., Tielens, F., Babonneau, F., Daudon, M., Bazin, D., Letavernier, E., Laurencin, D., Iuga, D., Hanna, J.V., Smith, M.E. & Bonhomme, C. (2021). *Magnetic Resonance*, **2**, 653.
[2] Shepelenko, M., Feldman, Y., Leiserowitz, L. & Kronik, L. (2019). *Cryst. Growth Des*., **20**, 858.
[3] Pickard, C.J. & Mauri, F. (2001). *Phys. Rev. B*, **63**, 245101.
[4] Goldberga, I., Patris, C.-H., Thomassot, E., Trebosc, J., Hung, I., Gan, Z., Berthomieu, D., Metro, T.-X., Bonhomme, C., Gervais, C. & Laurencin, D. (2022). *J. Phys. Chem. C*, **126**, 12044.

A005 Sample Preparation
Room 203/204
1.10pm - 3.30pm

A005-01-270823

Advances in Protein Electron Diffraction (3D ED/microED) Sample Preparation

G. Hofer, L. Wang, H. Xu, X. Zou

Department of Materials and Environmental Chemistry, Stockholm University, Stockholm, SE-106 91, Sweden)

gerhard.hofer@mmk.su.se

Keywords: 3D ED, microED, Round Robin, protein

Electron diffraction of proteins has made significant progress in recent years, with many labs around the world now solving proteins using this method [1-3]. However, generating suitable crystals for this new method challenges traditional beliefs in protein crystallography and requires new approaches tailored towards the sub-micrometer crystals required, or simply luck to have suitable crystals come up in classical screening experiments.
Regardless of the source of a suitable protein crystal slurry, the sample needs to be transferred to an electron-transparent carrier and vitrified to allow for data collection at high vacuum. During this procedure, care must be taken to avoid dehydration and physical stress, while excess mother liquor needs to be removed. Classically, this is done with a similar approach to single-particle cryo-EM, by which holey carbon foil-coated copper grids are glow discharged before the sample is applied, dried, and frozen using a plunge freezer.
We have found that alternative methods provide equal or better-quality grids while cutting down on both preparation time and the need for specialized equipment. We developed an optimized preparation protocol (manuscript in preparation) using a detergent to aid in mother liquor removal while eliminating the need for glow discharging. Manual backside blotting gives good visual feedback as to the state of the remaining liquid film and allows reproducible grid preparation without the need for a plunge freezer.

Here our latest advances in sample crystallisation and particularly grid preparation are discussed.

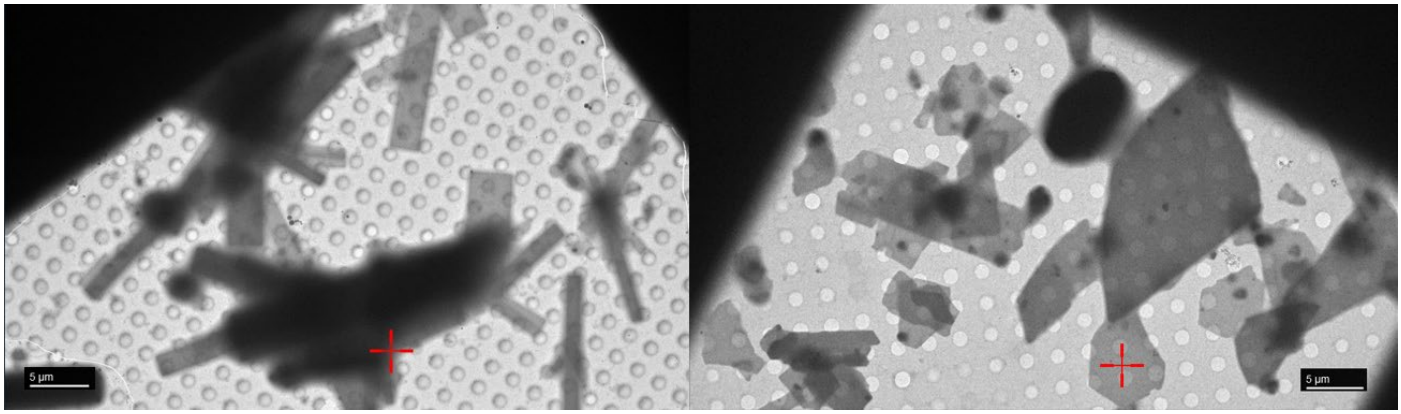

Figure 1. Electron transparent protein crystals on electron microscopy grids, an arginine kinase (left) and a urate oxydase (right).

[1] Taylor, Kenneth A., and Robert M. Glaeser. "Electron diffraction of frozen, hydrated protein crystals." Science 186.4168 (1974): 1036-1037.
[2] Dan Shi, Brent L Nannenga, Matthew G Iadanza, Tamir Gonen (2013) Three-dimensional electron crystallography of protein microcrystals eLife 2:e01345
[3] Martynowycz, Michael W., et al. "Ab initio phasing macromolecular structures using electron-counted MicroED data." Nature Methods (2022): 1-6.

A005-02-270823

Introducing the Bio21-WEHI Crystallisation Facility

R. P. Smith[1], M. A. Gorman[1], J. V. Nguyen[2], C. Lou[2], Y-H. Tan[1], D.W. Keizer[1]

[1]Bio21 Institute, University of Melbourne, 30 Flemington Road, Parkville 3010, Australia [2]WEHI, 1G Royal Parade, Parkville VIC 3052, Australia Communicating author: roxanne.smith@unimelb.edu.au

Keywords: Protein Crystallisation, Structural Biology, Crystallisation Facility, Melbourne Protein Characterisation

Protein crystallisation is a highly specialised and valued technique in the field of structural biology, despite the large expansions into Cryo-Electron Microscopy and its ever-growing popularity. Here in Melbourne, Australia, crystallising proteins to determine their molecular structures is widely used for projects with a structural biology element, especially those with a structure-based drug design focus. Since 2021 access to protein crystallisation equipment and services in the Parkville Biomedical Precinct for researchers has been limited.

To address this shortage of local resources, the Bio21-WEHI Crystallisation Facility has been established. This facility is a joint venture between WEHI and the Bio21 Institute, University of Melbourne, with support from the ACRF Facility for Innovative Cancer Drug Discovery. The facility hosts equipment for drop setting, screen building, plate storage and imaging. Services offered include initial crystallisation screening in a sitting drop, 96 well format with the choice from approximately 30 commercial crystallisation screens, lipidic cubic phase crystallisation of membrane proteins, optimisation of hit conditions, and even a “bring your own screen” option. All services provide regular imaging of your experiments with visible light to allow tracking of crystal growth, plus additional imaging under UV to assist in determining if your crystals consist mainly of protein or salt. The facility will also offer plate compatibility for in-plate data collection at the Australian Synchrotron.

The Bio21-WEHI Crystallisation Facility is a recent addition to the Structural Biology infrastructure located in the Parkville precinct, especially within the Bio21 Institute. This new edition compliments the existing platforms at the Bio21 Institute, including the Ian Holmes Imaging Centre, Melbourne Mass Spectrometry and Proteomics, Metabolomics Australia, and Melbourne Magnetic Resonance which form a comprehensive structural biology and drug discovery pipeline. The Bio21-WEHI Crystallisation Facility is situated in the Melbourne Protein Characterisation, which is a comprehensive technology platform that encompasses other well-known protein techniques including: peptide synthesis, mammalian and insect protein expression, protein interaction techniques such as analytical ultracentrifugation, CD, ITC & mass photometry and X-ray diffraction[#]. This allows users to access a single platform to carry out all experiments from peptide and protein production, protein purification, biochemical characterisation including determining secondary structure, oligomeric state, and binding interactions; through to protein crystallisation and X-ray data collection to solve protein structure at atomic resolution.

Acknowledgements:
Funding for the Bio21-WEHI Crystallisation Facility was provided by WEHI, the Australian Cancer Research Foundation and the University of Melbourne.

[#]For further information see: https://www.bio21.unimelb.edu.au/proteins/

A005-03-270823

Sample preparation of membrane proteins using anti-His tag antibody

Takeshi Murata

Department of Chemistry, Graduate School of Science, Chiba University, Chiba, 265-8522, Japan

t.murata@faculty.chiba-u.jp

Keywords: Expression, Purification, Membrane proteins, Stabilization, Nanodisc

Many membrane proteins play critical roles in biological processes, and it is well established that over 60% of pharmaceuticals exert their effects by interacting with these proteins. However, human membrane proteins often exhibit low thermal stability, making their purification a complex task. The difficulty in producing target molecules has been a bottleneck in drug discovery research. Over the years, we have been conducting fundamental research focused on membrane proteins and have developed a technology to predict heat-resistant mutants of membrane proteins using our unique theoretical calculations [1, 2]. A significant advantage of our calculation method is its very short computational time, as it handles entropy effects originating from the translational movement of hydrocarbon chains in lipid molecules from a statistical mechanics standpoint. To date, we have successfully thermally stabilized 15 membrane proteins. Moreover, we have developed a method for the rapid, simple, and high-purity purification of membrane proteins reconstituted in nanodiscs using our unique anti-His tag antibodies [3] (Fig. 1). In this presentation, I will introduce our developed techniques for the expression and purification of human membrane proteins.

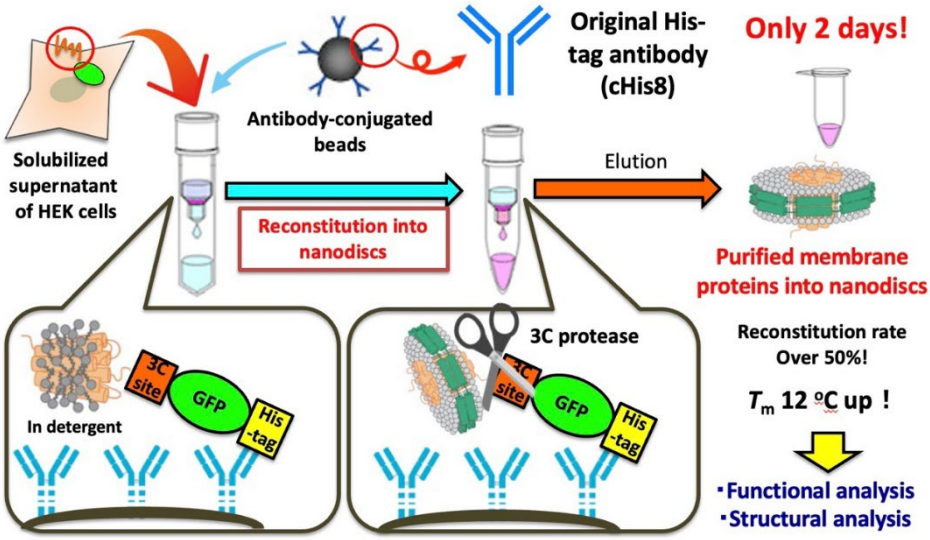

Figure 1. On-column purification technique using anti-His tag antibody.

[1] Satoshi Yasuda, Yuta Kajiwara, Yuuki Takamuku, Nanao Suzuki, Takeshi Murata, and Masahiro Kinoshita (2016) *J. Phys. Chem. B*, **120**, 3833.
[2] Takeshi Murata, Satoshi Yasuda, Tomohiko Hayashi, and Masahiro Kinoshita (2020) *Biophys. Rev.*, **12**, 323.
[3] Tatsuki Asai, Naruhiko Adachi, Toshio Moriya, Hideyuki Oki, Takamitsu Maru, Masato Kawasaki, Kano Suzuki, Sisi Chen, Ryohei Ishii, Kazuko Yonemori, Shigeru Igaki, Satoshi Yasuda, Satoshi Ogasawara, Toshiya Senda and Takeshi Murata (2021) *Structure*, **29**, 203.

A005-04-270823

Development of an efficient pipeline from crystallization to structure determination with the Photon Factory macromolecular crystallography beamline, BL-17A.

Y. Yamada1,2, R. Kato1,2, M. Hiraki2,3, M. Hikita1,2, N. Matsugaki1,2, T. Senda1,2

1Structural Biology Research Center, Institute of Materials Structure Science, High Energy Accelerator Research Organization, 1-1 Oho, Tsukuba, Ibaraki, Japan, 2School of High Energy Accelerator Science, The Graduate University for Advanced studies, 1-1 Oho, Tsukuba, Ibaraki, Japan, 3Mechanical Engineering Center, Applied Research Laboratory, High Energy Accelerator Research Organization, 1-1 Oho, Tsukuba, Ibaraki, Japan,

Email of communicating yusuke.yamada@kek.jp

Keywords: crystallization screening, synchrotron beamline, in-situ data collection

X-ray crystallography is one of the most powerful methods to determine three dimensional structures of macromolecules at the atomic resolution. Structure determination of macromolecules by X-ray crystallography consists of a series of steps including sample production, purification, crystallization, X-ray data collection and data analysis. In the crystallization step, manual screening of crystallization conditions takes a lot of time and effort to set up hundreds of crystallization drops and check them with a microscope periodically. It is also the time-consuming work to fish and freeze crystals obtained in the screening for X-ray diffraction data collection at a synchrotron beamline or a home laboratory. In order to solve these problems, we have developed an efficient pipeline including a crystallization screening and in-situ data collection system, which not only automate these steps individually, but also link them seamlessly.

For crystallization screening, we developed a fully automated crystallization and monitoring system, PXS2[1]. PXS2 consists of a dispenser, incubators, imagers and a transfer robot. Once a purified sample is applied, crystallization plates with selected crystallization screening kits are automatically set up, transferred to incubators and pictures of drops are captured according to a pre-set schedule. The pictures are automatically evaluated and scored based on a deep-learning model.

For X-ray data collection, we developed in-situ data collection system at the beamline, BL-17A, in the Photon Factory (PF), Japan. The diffractometer at BL-17A has two goniometers, the one consists of a horizontal spindle axis for a cryo-pin and the other consists of a vertical spindle axis for a crystallization plate, as shown in Fig.1. By using the vertical goniometer head, X-ray diffraction data is directly collected from a crystal in a drop on the crystallization plate (in-situ data collection), and there are no needs to fish and freeze crystals manually. One of the applications of in-situ data collection is rapid evaluation of diffraction qualities of many crystals obtained from crystallization screening. Another is to collect a data set for structure determination, where small-wedge data sets are collected from many crystals and merge them into a full data set.

In this presentation, we introduce overview of our pipeline, and show some examples in which PXS2 and in-situ data collection system are successfully utilized.

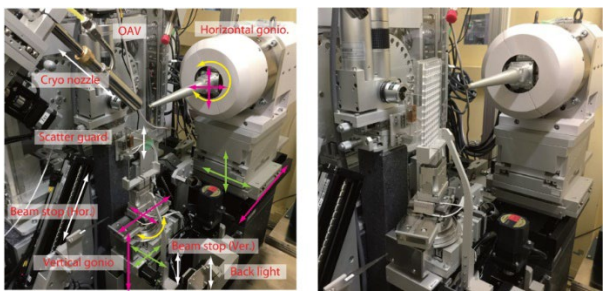

Figure 1. Diffractometer at BL-17A. (left) Overview of the diffractometer at PF BL-17A. (right) Setup for in-situ data collection.

[1] Kato, R., Hiraki, M., Yamada, Y., Tanabe, M. & Senda, T. (2021). *Acta Cryst*. **F77**, 29-36.
[2] Yamada, Y., Hiraki, M., Matsugaki, N., Kato, R. & Senda, T. (2016). *AIP Conf. Proc*. **1741**, 050023.

A005-06-270823

RNA stabilizing modification used in crystallographic research

M. Mateja-Pluta[1], A. Kiliszek[1]

Institute of Bioorganic Chemistry, Polish Academy of Sciences, Z. Noskowskiego St. 12/14, Poznan

mpluta@ibch.poznan.pl

Keywords: RNA crystallization, modification, thermodynamical stabilization

RNA molecules are involved in many important biological processes, especially in regulation of gene expression and pathogenesis of numerous diseases. In order to understand RNA function it is important to investigate its structure using such techniques as X-ray crystallography or NMR. However, these methods require homogeneous samples not only in terms of sequence but also structure[1]. To overcome these difficulties specific modifications can be incorporated into RNA, e.g. replacement of apical loop with the GNRA tetraloop or chemical modifications (ICL – *interstrand crosslink* or disulfide bonds)[2-5].

In these study we will present synthesis of aromatic linkers, introduction of linkers to the RNA sequence, biochemical and physicochemical validation and pre-eliminary results of crystallographic data.

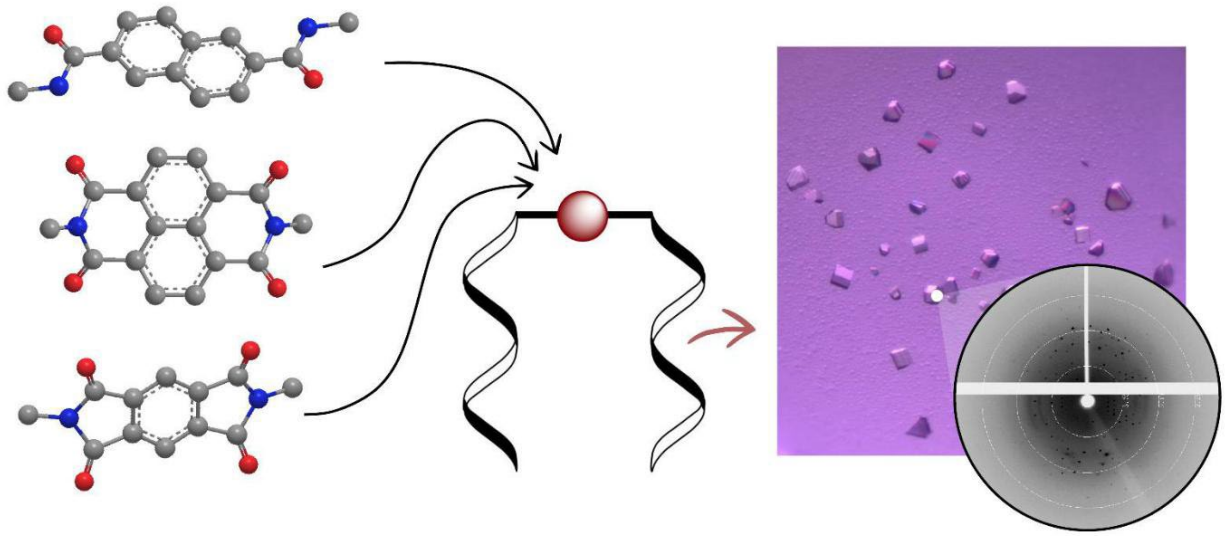

Figure 1. Pathway of crystallographic studies of modified RNA oligonucleotides

.

[1] Kiliszek A., Blaszczyk L., Kierzek R., Rypniewski W. (2017). *Nucleic Acids Research,* 8189-8199.
[2] Lengenagger S.M., Malinovskii V.L., Wenger D., Werder S., Haner R. (2007). *Nucleosides, Nucleotides, and Nucleic Acids*, **26**, 901-903.
[3] Langenegger S.M., Haner R. (2004). *Tetrehedron Letters,* **45**, 9273-9276.
[4] Bianke G., Haner R. (2007). *Nucleosides, Nucleotides, and Nucleic Acids*, **26**, 949-952.
[5] Langenegger S.M., Haner R. (2002), *Helvetica Chimica Acta*, **85**, 3414-3421.

A009 & A010 Use and Comparison of Predicted Models from Primary Sequence in Structural Biology and Deep Learning & Artificial Intelligence in Structural Biology
Room 219
1.10pm - 3.30pm

A009/A010-01-270823

A fully automatic data processing and structure determination pipeline for X-ray biological macromolecule crystallography beamlines

X. Zhang[1], Z. Li[2], W. Ding[2]*, Q. Hao[3]

The University of Hong Kong, Hong Kong, China, The Institute of Physics, Chinese Academy of Sciences, Beijing, China, Institute of High Energy Physics, CAS, Beijing, China

dingwei@iphy.ac.cn

Keywords: Data processing, Structure determination, Pipeline

X-ray crystallography remains the most widely used method for determining the structure of biological macromolecules, with a large proportion of the structures recorded in the Protein Data Bank (PDB) being derived from this technique. With the construction of fourth-generation synchrotron radiation sources, such as the Beijing High Energy Photon Source, experimental data is expected to emerge rapidly. Therefore, there is an urgent need to develop a high-throughput, fully automated X-ray diffraction data processing and structure determination pipeline for biological macromolecular crystallography beamlines.

In this study, we developed a fully automatic pipeline for processing and determining the structure of biological macromolecules. The pipeline is composed of four modules, as shown in Figure 1. The diffraction image processing module processes raw diffraction images of any given format using XDS[1], DIALS[2], XIA2[3] and autoPROC[4] parallelly. The search model derivation module searches for predicted structures in the AlphaFold Database first, and generates a predicted structure using AlphaFold2[5] if no available structure can be found. The best Rmerge result from the diffraction image processing module and predicted structure from the search model derivation module are input to the molecular replacement module. Users can choose from three methods for model building and refinement module: Buccuneer[6] (fast and default method), Phenix.autobuild[7] and IPCAS[8] (a dual-space iterative method, which is relatively slow but gives the best Rwork and Rfree values).

To validate the pipeline, we used diffraction images downloaded from the PDB to test the accuracy of the pipeline. The results showed that the Rwork and Rfree values are comparable to those of the PDB deposit. Our pipeline provides an efficient solution for structural biologists and can significantly reduce the time and effort required for structural determination.

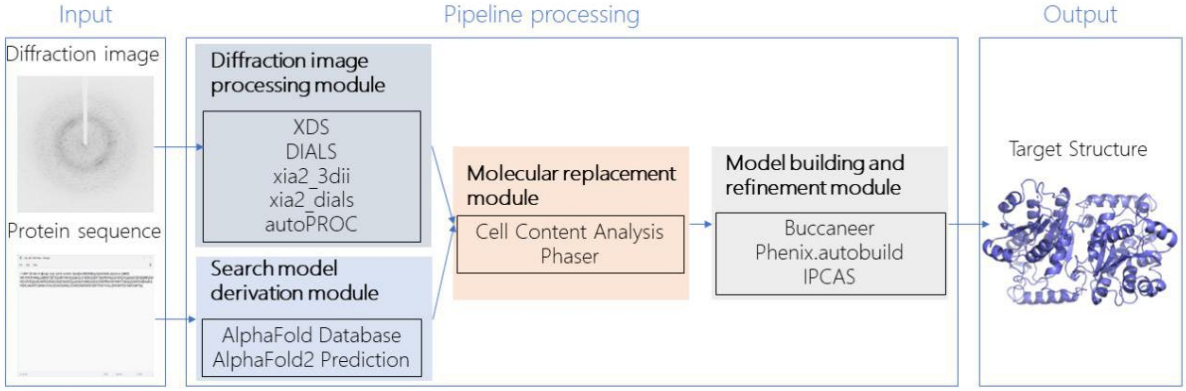

Figure 1. Flow chart of data processing and structure determination pipeline.

[1] Kabsch, Wolfgang. "xds." Acta Crystallographica Section D: Biological Crystallography 66.2 (2010): 125-132.
[2] Winter, Graeme, et al. "DIALS: implementation and evaluation of a new integration package." Acta Crystallographica Section D 74.2 (2018): 85-97.
[3] Winter, G. "xia2: an expert system for macromolecular crystallography data reduction." Journal of applied crystallography 43.1 (2010): 186-190.
[4] Vonrhein, Clemens, et al. "Data processing and analysis with the autoPROC toolbox." Acta Crystallographica Section D: Biological Crystallography 67.4 (2011): 293-302.
[5] Jumper, John, et al. "Highly accurate protein structure prediction with AlphaFold." Nature 596.7873 (2021): 583-589.
[6] Cowtan, Kevin. "The Buccaneer software for automated model building. 1. Tracing protein chains." Acta crystallographica section D: biological crystallography 62.9 (2006): 1002-1011.
[7] Terwilliger, Thomas C., et al. "Iterative model building, structure refinement and density modification with the PHENIX AutoBuild wizard." Acta Crystallographica Section D: Biological Crystallography 64.1 (2008): 61-69.
[8] Ding, Wei, et al. "IPCAS: a direct-method-based pipeline from phasing to model building and refinement for macromolecular structure determination." Journal of Applied Crystallography 53.1 (2020): 253-261.

Exploring experimentally-determined structures and computed structure models from artificial intelligence/machine learning at RCSB Protein Data Bank (RCSB PDB, RCSB.org)

D.W. Piehl[1,2], S.K. Burley[1,2,3,4,5]

[1]RCSB Protein Data Bank, [2]Institute for Quantitative Biomedicine, and [3]Department of Chemistry and Chemical Biology, Rutgers, The State University of New Jersey, Piscataway, NJ 08854, USA [4]Cancer Institute of New Jersey, Rutgers, The State University of New Jersey, New Brunswick, NJ 08903, USA [5]RCSB Protein Data Bank, San Diego Supercomputer Center, University of California San Diego, La Jolla, CA 92093, USA
dennis.piehl@rcsb.org

Keywords: Protein Data Bank, biomolecular structure, database design, database scaling, computation, de novo structure prediction, artificial intelligence/machine learning, computed structure models

The Protein Data Bank (PDB) was established in 1971 as the first open-access digital data resource in biology, and has since grown more than 24,000-fold to become the world's leading repository for atomic-level, experimentally-determined, three-dimensional (3D) structures of biological macromolecules. The PDB archive is jointly managed by the Worldwide PDB (wwPDB) partnership, including RCSB PDB (United States), PDBe (United Kingdom), PDBj (Japan), EMDB (United Kingdom), and BMRB (United States and Japan). Within the wwPDB, the RCSB PDB serves as the Archive Keeper of the PDB.

The RCSB PDB research-focused RCSB.org web portal serves more than six million unique users annually with a rich collection of software tools and features that can be used to search, browse, analyze, and visualize PDB data. These include powerful search and API services as well as interactive analytical and visualization tools such as the Mol* molecular graphics system, 1D-3D protein feature view, and most recently a 1D-3D groups alignment view, all of which have been enabled for the collection of nearly 200,000 experimentally-determined PDB structures stored in the growing PDB archive. Additionally, following from recent significant advances in the accuracy of artificial intelligence/machine learning (AI/ML) based protein structure prediction (*e.g.*, AlphaFold2 and RoseTTAFold [1–3])—enabled by the wealth of experimental biostructure data deposited into the PDB archive by tens of thousands of structural biologists worldwide—we have extended the RCSB.org web portal and its functionalities to support the parallel delivery of more than one million computed structure models (CSMs) from AlphaFold DB (alphafold.ebi.ac.uk) [4] and the ModelArchive (modelarchive.org) alongside the experimental structures in the PDB archive [5]. Interoperation of CSMs with all tools and features at RCSB.org was enabled by the extension of the PDBx/mmCIF data standard with the new ModelCIF data standard developed for CSMs. This expansion of the purview of RCSB.org allows us to continue serving as a one-stop shop for studying the 3D structures of biomolecules by providing PDB data consumers with access to CSMs covering the entire human proteome as well as that of many model organisms, selected pathogens, organisms relevant to bioenergy research, and protein complexes from select studies.

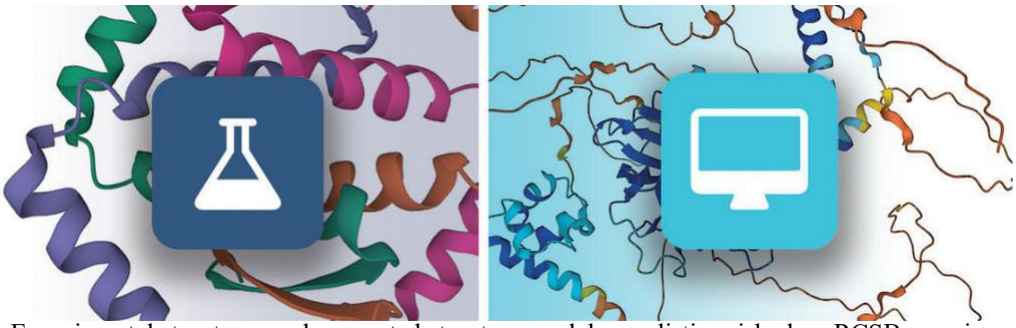

Figure 1. Experimental structures and computed structure models are distinguished on RCSB.org via association of a dark-blue flask icon (left) or cyan computer icon (right), respectively.

[5] Jumper, J., Evans, R., Pritzel, A., Green, T., Figurnov, M., *et al*. (2021). *Nature*, **596**, 583–589.
[6] Baek, M., DiMaio, F., Anishchenko, I., Dauparas, J., Ovchinnikov, S., *et al*. (2021). *Science*, **373**, 871–876.
[7] Humphreys, I.R., Pei, J., Baek, M., Krishnakumar, A., Anischenko, I., Ovchinnikov, S., *et al*. (2021). *Science*, **374**, eabm4805.
[8] Varadi, M., Anyango, S., Deshpande, M., Nair, S., Natassia, C., *et al*. (2022). *Nucleic Acids Research*, **50**, D439–D444.
[9] Burley, S.K., Bhikadiya, C., Bi, C., Bittrich, S., Chen, L., et al. (2023). *Nucleic Acids Research*, in press.

RCSB PDB Core Operations are funded by National Science Foundation (DBI-1832184), US Department of Energy (DE-SC0019749), and National Cancer Institute, National Institute of Allergy and Infectious Diseases, and National Institute of General Medical Sciences of the National Institutes of Health under grant R01GM133198.

A009/A010-03-270823

Validating and Building Biomolecular Structure Models for cryo-EM Maps Using Deep Learning

Prof Daisuke Kihara

Cryo-electron microscopy (cryo-EM) has become one of the main experimental methods for determining biomolecular structures including proteins and nucleic acids. Molecular structure modeling from cryo-EM can be challenging when the resolution of maps is not high enough to specify atom positions. We have been developing a series of computational methods for modeling protein and nucleic acid structures from cryo-EM maps. For maps at medium resolution, deep learning can detect characteristic local density features of amino acids and secondary structures, which can be used to guide structure modeling. Local density features can be also used for validating existing protein structure models in PDB. The protein model quality assessment score, DAQ, we developed recently, compares local density patterns captured by deep learning with amino acid positions in a model and detects potential errors in the model. In a large-scale analysis of protein models from cryo-EM, we found that a substantial small number of models may have some errors. All the tools we developed are available at https://kiharalab.org/emsuites/.

A009/A010-04-270823

SO(3)-equivariant neural networks from cryo-EM particle picking

D. Granberry, A. Nasiri, J. Shou, T. Bepler

Simons Machine Learning Center, New York Structural Biology Center, 89 Convent Avenue, New York, NY 10027
tbepler@nysbc.org

Keywords: equivariance, group convolution, deep learning, object detection, cryoEM

The nature of image formation from physical objects introduces challenges to many computer vision tasks including face and eye tracking, galactic imaging, and single-particle analysis in cryogenic electron microscopy (cryo-EM) [1-4]. In each of these domains, the underlying perceived object is free to rotate and translate in three dimensions before being projected onto a two-dimensional image plane. The specific location and pose of an object does not change its nature, but does present challenges for image processing algorithms designed to perform inference on object properties. In particular, we are interested in algorithms that are *equivariant* or *invariant* to these nuisance transformations Deep learning models incorporating simple equivariance properties, convolutional neural networks, have been common for decades [5], and the translationally equivariant properties of these networks are key to their widespread success in image processing. More recently, new convolutional neural network types have been developed that achieve equivariance to transformations such as 2D rotation and scaling [4,6]. Similarly, a variety of methods have been introduced to incorporate equivariance to rotations in 3D, utilizing point clouds [7], or voxels/regular grids [8]. However, these networks either model 2D transformations of 2D signals or 3D transformations of 3D signals. There are currently no existing deep learning methods that capture 3D equivariances of 2D signals. This is critical for capturing the full space of spatial transformations of objects in imaging domains such as cryoEM.

We propose a new group convolutional layer that operates on 2D images but is SO(3)-equivariant. We accomplish this by learning 3D convolutional filters that are applied to 2D inputs with SO(3)-equivariance via projections of the 3D filters into 2D over a coarse discretization of SO(3). This yields filter outputs that are exactly equivalent to applying the 3D filters to the (unknown) 3D volume and then projecting the resulting filter values along the imaging axis, despite only having access to a 2D projection of the input. This follows from the Fourier slice theorem. The Fourier slice theorem, also known as the projection-slice theorem, states that the 2D Fourier transform of the 2D projection of a volume is equivalent to the central slice of the 3D Fourier transform aligned with the projection axis. In terms of operators, $F_2 \circ P_2 = S_2 \circ F_3$, where F_2 is the 2D Fourier transform, P_2 is the projection operator, S_2 is the slice operator, and F_3 is the 3D Fourier transform. If we introduce W_3, our 3D filter, then we can see that the 2D projection of our filter applied to the 3D volume is equivalent to applying the 2D projection of our filter to the projected input, $S_2 \circ (F_3\, W_3) \circ F_3 = (S_2\, F_3\, W_3) \circ (S_2 \circ F_3) = (F_2 \circ P_2\, W_3) \circ (F_2 \circ P_2) = F_2 \circ P_2\, W_3 \circ P_2$.

In cryoEM, the Fourier slice theorem is widely used to develop algorithms for efficiently solving for 3D volumes given 2D projections from those volumes [3]. To enable efficient computation in our SO(3)-equivariant layer, we make use of the same projection slice trick: we parameterize our 3D filters in the frequency domain, take central slices along a discrete set of viewing angles, and transform these back into the spatial domain before applying them to the 2D input. This results in a group convolutional layer that is SO(3) equivariant but operates on 2D images. By building these layers into deep neural networks, we can produce complex image processing networks. Additionally, we present novel methods for aggregating our model's rotation-specific outputs. We demonstrate excellent performance of this architecture on several tasks, including particle picking, particle pose estimation, and a generic object pose estimation benchmark.

[1] Liu, D. (2022). New *NVIDIA Maxine Cloud-Native Architecture Delivers Breakthrough Audio and Video Quality at Scale.*
[2] Lintott, C. J., Schawinski, K., Slosar, A., Land, K., Bamford, S., Thomas, D., Raddick, M. J., Nichol, R. C., Szalay, A., Andreescu, D., Murray, P., and Vandenberg, J. *Galaxy Zoo: morphologies derived from visual inspection of galaxies from the Sloan Digital Sky Survey*. Monthly Notices of the Royal Astronomical Society, 389 (3):1179–1189, 09 2008.
[3] Lyumkis, D. (2019). *Challenges and opportunities in cryo-EM single-particle analysis.* J Biol Chem, 294(13):5181-5197.
[4] Nasiri, A. and Bepler, T. (2022). *Unsupervised object representation learning using translation and rotation group equivariant VAE.* Advances in Neural Information Processing Systems.
[5] LeCun, Y. and Bengio, Y. (1998) *Convolutional Networks for Images, Speech, and Time Series.* pp. 255–258. MIT Press.
[6] Cohen, T. and Welling, M. (2016). *Group equivariant convolutional networks.* In International conference on machine learning, pp. 2990–2999.
[7] Thomas, N., Smidt, T., Kearnes, S., Yang, L., Li, L., Kohlhoff, K., and Riley, P. (2018). *Tensor field networks: Rotation-and translation-equivariant neural networks for 3d point clouds*. ArXiv:1802.08219.
[8] Weiler, M., Hamprecht, F. A., and Storath, M. (2018). *Learning steerable filters for rotation equivariant cnns.* IEEE/CVF Conference on Computer Vision and Pattern Recognition, pp. 849–858.

We would like to thank the other members of the SMLC and the Flatiron Institute for helpful discussions.

A009/A010-05-270823

Refinement of crystal structures at ultralow resolution with assistance from AlphaFold modeling and Rosetta optimization

Wei Wang[1], Wayne A. Hendrickson[1]

[1]*Department of Biochemistry and Molecular Biophysics, Columbia University, New York, NY 10032 USA*

E-mail: wah2@cumc.columbia.edu

Keywords: AlphaFold, restrained refinement, ryanodine receptor, ultralow resolution

Crystals of large macromolecular complexes often diffract quite poorly, typically having high solvent content, relatively feeble lattice contacts, quite weak subunit associations, and somewhat flexible interdomain linkages. Although resolution may be limited to d_{min} > 7-8 Å, the diffraction amplitudes should suffice, in principle, to specify conformational torsion angles; however, at such ultralow resolution, realizing and maintaining a suitable model within the radius of refinement convergence is a challenge. Important insights into biological processes may be obtained, but only if structural validity can be assured.

Having sucessfully refined a four-copy structure of Hsp70 DnaK in the S-state at 7.7 Å resolution as rigid bodies (Wang *et al.*, *Mol. Cell* **81**, 3919, 2021), we set out to refine a crystal structure of ryanodine receptor RyR1 at 8.0 Å resolution by having multiple quasi-rigid bodies to comprise the 5037 residues in each protomer of the RyR1-tetramer as complexed with calstabin. After molecular replacement from a 65%-complete cryo-EM model at 3.6 Å resolution (des Georges *et al., Cell* **167**, 145, 2016), the structure was refined from a single rigid-body (R_{free} = 0.53), through five linked rigid bodies (R_{free} = 0.47), and finally as 18 linked domains (R_{free} = 0.43) identified in the cryo-EM analysis and then sub-divided as dictated by (F_o-F_c) difference map and the R_{free} analysis. We then turned to AlphaFold, presuming that the process had stalled due to incompleteness and uncertainty in the initial model. Trials showed that AlphaFold-predicted domains reduced R_{free} when fitted into crystal density. We then systematically identified such AlphaFold-modeled domains and obtained substantial improvement (R_{free} = 0.38). Further improvement followed after Rosetta refinement using tight restraints in the *phenix.rosetta_refine* module (R_{free} = 0.35). Finally, after grid-search optimization of the solvent mask, we obtained R/R_{free} = 0.293/0.338 for a model that comprises one protomer (4439 of 5037 RyR1 residues (88% complete), the 107-residue FKBP12.6, and an Au_{102} gold cluster). Its geometry is excellent (97.4% favored Ramachandran angles with only 5/4546 outliers, 0 rotamer outliers, and |Rama-Z| = 0.09). The crystal structure replicates RyR1 as associated into sarcoplasmic-reticulum arrays, which are implicated in cooperative Ca^{2+} release.

We further tested this quasi-rigid-body AlphaFold/Rosetta-aided low-resolution structure (QARLS) refinement procedure in applications to the DNA-dependent protein kinase catalytic subunit (DNA-PKcs) at 6.6 Å resolution (PDB: 3kgv) and to a coat nucleoporin complex (CNC) structure at 7.4 Å resolution (PDB: 4xmn). These tests validate QARLS as a robust procedure for refining ultralow-resolution crystal structures. QARLS-like procedures should be useful in cryo-EM and cryo-ET analyses as well; however, the current lack of an R_{free}-like process complicates the monitoring of effectiveness for molecular microscopy.

A009/A010-06-270823

Zernike3Deep: a semi-classical AI approach for improved heterogeneity analysis

D. Herreros[1], R. R. Lederman[2], J. M. Krieger[1], C. O. S. Sorzano[1], and J. M. Carazo[1]

[1]Centro Nacional de Biotecnologia-CSIC, C/Darwin, 3, 28049 Cantoblanco, Madrid, Spain, [2]The Department of Statistics and Data Science, Yale University, New Haven, CT, USA

carazo@cnb.csic.es

Keywords: Cryo-Electron Microscopy (CryoEM), Zernike polynomials, Spherical harmonics

CryoEM has proven to be a very versatile tool to understand the macromolecule heterogeneity of a specimen. Classically, the extraction of this information was reduced to a discrete number of classes. However, due to the highly dynamic nature of macromolecules, the previous assumption limits our comprehension of the structural landscape explored by the macromolecule and captured at particle level.

The recent developments in the field of conformational heterogeneity are progressively inducing a shift in CryoEM, thanks to the implementation of more powerful algorithms that are no longer limited to the extraction of several stable states. Overall, these algorithms fall into two different types: classical approaches to estimate per-particle conformations and deep learning-based methods able to learn structural embeddings.

In the previous context, we introduced our Zernike3D approach, a completely classical algorithm able to represent molecular motions in terms of the Zernike3D basis [1, 2]. To further improve the Zernike3D algorithm, we decided to mix both the classical and deep learning worlds into our new Zernike3Deep approach. The Zernike3Deep method is settled in a semi-classical deep-learning framework, allowing us to train a neural network to estimate molecular motions without compromising our ability to understand the information learned by the neural network.

The new Zernike3Deep method will be implemented in Scipion, allowing us to connect it to heterogeneity workflows and tools we are developing to explore and understand conformational landscapes easily.
Each **figure** should have a caption placed below the figure. Number the figures and refer to them as Fig. 1 *etc*. The figure layout '*in line with text'* should be used.

[1] Herreros, D., Lederman, R.R., Krieger, J., Jimenez-Moreno, A., Martinez, M., Myska, D., Strelak, D., Filipovic, J., Bahar, I., Carazo, J.M., & Sorzano, C.O.S. (2021). *IUCRJ.*, **6**, 992-1005.
[2] Herreros, D., Lederman, R.R., Krieger, J., Jimenez-Moreno, A., Martinez, M., Myska, D., Strelak, D., Filipovic, J., Sorzano, C.O.S., & Carazo, J.M. (2023). *Nat. Comm.*, **14**, 154.

A022 Computing Intermolecular Interactions
Room 207
1.10pm - 3.30pm

A022-01-270823

A retrospective of the study of noncovalent interactions in highly polymorphic compounds such as ROY, galunisertib, aripiprazole, flufenamic acid, etc.

Anton V. Savchenkov, Viktor N. Serezhkin

Samara National Research University, Samara, Russian Federation

Email: anton.savchenkov@gmail.com

Keywords: noncovalent interactions, conformational polymorphs, Voronoi–Dirichlet polyhedra

Computing interatomic interactions is both beneficial for understanding of general properties of matter as well as challenging at the same time, as we have to describe all types of interactions objectively and desirably automatically for large databases of crystal structures available today. One of the available methods of analysis of interatomic interactions is the method of molecular Voronoi–Dirichlet polyhedra [1], which greatly expands the amount of information that can be obtained from the crystal structure of a compound. Our long-term project is to apply this method to one of the most complicated systems available, which is highly polymorphic compounds with the current record of 12 solved forms. Quantitative description of peculiarities and differences among polymorphs is truly tough with conventional methods. To date we have successfully applied the method of molecular Voronoi–Dirichlet polyhedra to most of the highly polymorphic compounds such as ROY, galunisertib and its solvates, aripiprazole, flufenamic acid, etc. The retrospective of this research together with the new and handy tools developed for the analysis of crystal structures are to be discussed in the respective presentation. Such tools include:

1. the rank of face parameter, which allows one to strictly categorize all types of interactions into covalent and noncovalent intra- and intermolecular;
2. graphs of average partial contributions of *single contacts* (Fig. 1), which help examine roles of various types of contacts and visualize differences among polymorphs;
3. k-Φ criterion – a very sensitive parameter for distinguishing conformational polymorphs, which can easily detect even the subtlest differences in atomic interactions strictly and *quantitatively*;
4. (RF, d) distributions, which can be used as ‘interaction fingerprints’ of individual compounds as well as groups of compounds;
5. and more…

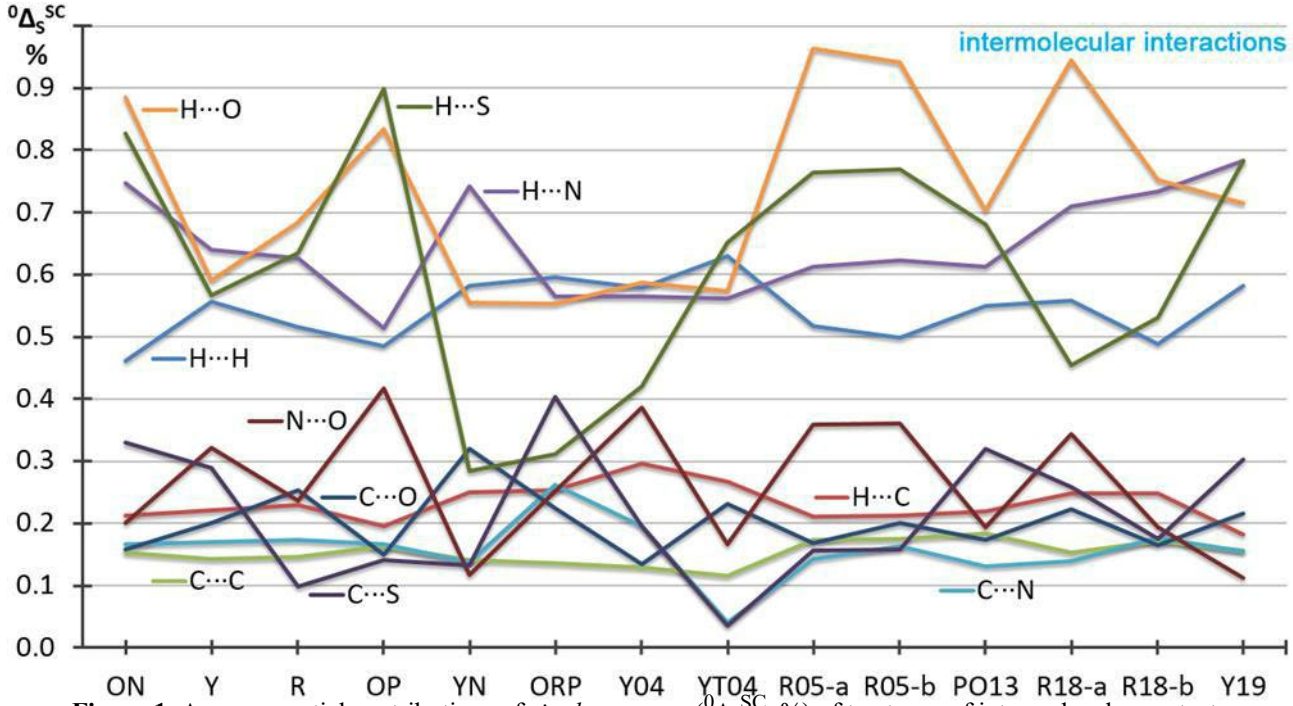

Figure 1. Average partial contributions of *single contacts* ($^0\Delta_S^{SC}$, %) of ten types of intermolecular contacts present in all the known ROY polymorphs (designated by their common names such as ON, Y, R, etc.).

[1] Serezhkin, V. N., Yu, L. & Savchenkov, A. V. (2022). *Cryst. Growth Des*., **22**, 6717.

A022-02-270823

Hydrogen and halogen bonds involving Au(I) complexes

C. Esterhuysen

Department of Chemistry and Polymer Science, Stellenbosch University, Matieland, Stellenbosch, 7602, South Africa
ce@sun.ac.za

Keywords: Hydrogen bonding, Halogen bonding, Calculations

The most challenging aspect in understanding the properties of materials in the solid state is to identify the role that intermolecular interactions play in their behaviour. This has been further complicated in recent years by the realisation that close contacts between two electronegative atoms are not necessarily repulsive. For instance, in halogen bonding formally negatively-charged halogens form attractive interactions with other electronegative species through a positively-charged region on the halogen, known as a σ-hole [1]. These interactions are further strengthened by polarisation and dispersion. Similarly, dispersion interactions lead to aurophilic interactions between formally positively-charged gold centres in complexes [2].

In this work we show that the ligands in a range of Au(I) complexes affect the relative electrophilicity of the gold centre, which in extreme cases enables the gold to behave as a Lewis base by acting as an acceptor for hydrogen and halogen bonds. Depending on the nature of the ligands in the gold complex the resultant hydrogen bonds may be even stronger than those between two water molecules [3], while the halogen bonds are of similar strength to that found within the triiodide ion (Figure 1) [4]. The interactions are, nevertheless, weaker than those involving the auride ion. We show that the effect is very subtle, with the electronegativity and polarisability of the Au(I) centre playing a crucial role in its formation of hydrogen and halogen bonds.

In addition, the computational results show that a second hydrogen-bonding interaction is typically present to support the stabilisation of an Au···H hydrogen bond. Analysis of the Cambridge Structural Database (CSD) shows that some form of additional stabilisation is a common feature: most of the crystal structures containing close intermolecular contacts between Au and H exhibit multiple interactions. Further investigation of the CSD suggests that the additional stabilisation can also be achieved by the the formation of 5-, 6- or 7-membered intramolecular Au···H hydrogen-bonded rings, with graph set notations *S*(5), *S*(6) or *S*(7) [5]. These are less common than 4-membered rings containing short Au···H distances, however, the latter appear to merely be Au···H close contacts and are not structure determining. On the other hand, the additional stabilisation obtained through the formation of hydrogen-bonded rings appears to be lost for larger rings as there are very few examples of these.

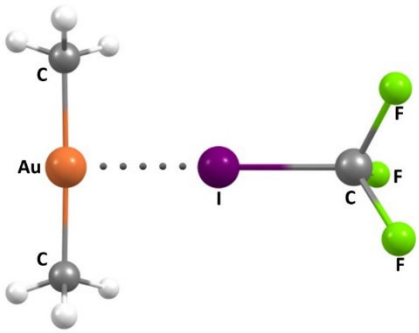

Figure 1. Au···X halogen bond between dimethylaurate ion and trifluoroiodomethane.

[1] (a) Gilday, L. C., Robinson, S. W., Barendt, T. A., Langton, M. J., Mullaney B. R. & Beer, P. D. (2015). *Chem. Rev.* **115**, 7118; (b) Cavallo, G., Metrangolo, P., Milani, R., Pilati, T., Priimagi, A., Resnati, G. & Terraneo, G. (2016). *Chem. Rev.* **116**, 2478.
[2] (a) Schmidbaur, H., Scherbaum, F., Hubert B. & Müller, G. (1988). *Angew. Chem. Int. Ed. Engl.* **27**, 419; (b) Pathaneni S. S. & Desiraju, G. R. (1993). *J. Chem. Soc., Dalton Trans*. 319.
[3] (a) Groenewald, F., Dillen, J., Raubenheimer, H. G. & Esterhuysen, C. (2016). *Angew. Chem. Int. Ed.* **55** 1694; (b) Groenewald, F., Dillen, J., Raubenheimer H. G. & Esterhuysen, C. (2017). *Dalton Trans.* **46**, 4960.
[4] Groenewald, F., Dillen, J. & Esterhuysen, C. (2018). *New J. Chem.* **42**, 10529.
[5] Etter, M. C., MacDonald J. C. & Bernstein, J. (1990). *Acta Crystallogr., Sect. B: Struct. Sci*. **46**, 256.

A022-03-270823

How can we use intermolecular interactions in crystals? Lattice energies, predicting crystal growth and more…

P.R. Spackman[1], M.A. Spackman[2], Dylan Jayatilaka[2], & J.D Gale[1]

[1] Curtin Institute for Computation, School of Molecular and Life Sciences, Curtin University, GPO Box U1987, Perth, WA 6845, Australia,
[2] School of Molecular Sciences, University of Western Australia, 35 Stirling Hwy, Crawley WA 6009
peter.spackman@curtin.edu.au

Keywords: Crystallisation, Quantum Chemistry, CrystalExplorer,

Accurate and fast models for intermolecular interaction energies provide quantitative insight into crystal packing, but their value can extend beyond understanding neighbouring interactions into the prediction of lattice energies [1] and, when combined with solvation models, yield sensible estimates for crystal solubilities in different solvents. We present a new and improved CrystalExplorer interaction energy model [2,3], and its application to predicting lattice energies, solubilities and energies for crystal growth from solution.

We also discuss state-of-the-art Density Functional Tight Binding methods like GFN2-xTB [4], general purpose force-field methods like GFN-FF, [5,6] and machine learning methods to compute intermolecular interaction energies, and how they might be used by theorists and experimentalists alike. In crystals these energies may be visualised through energy frameworks [7], as in Fig. 1, which provide qualitative insight into the underlying energetic structure, and they often correlate with the elastic and mechanical properties of molecular crystals.

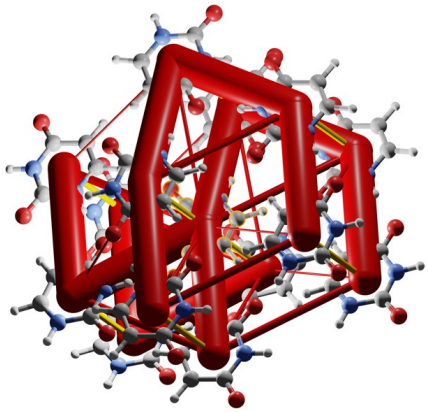

Figure 1. Coulomb energy framework for uracil crystal, CSD ref. code URACIL, showing the strong hydrogen bond interactions (red), along with weakly repulsive non-binding Coulomb interactions (yellow).

[1] Thomas, S. P. et al. *J. Chem. Theory Comput*. **14**, 1614–1623 (2018)
[2] Spackman, P. R. et al. *J. Appl. Crystallogr.* **54**, 1006–1011 (2021)
[3] Mackenzie, C. F. et al. *IUCrJ,* **4**, 575–587 (2017)
[4] Bannwarth, C. et al. *J. Chem. Theory Comput*. **15**, 1652–1671 (2019)
[5] Gale, J. D. et al. *J. Chem. Theory Comput*. **17**, 7827–7849 (2021)
[6] Spicher, S. et al. *Angew. Chem. Int. Ed*. **59**, 15665–15673 (2020)
[7] Turner, M. J. et al. *Chem. Commun*. **51**, 3735–3738 (2015)

A022-04-270823

Mapping the favourable character of crystal and intermolecular contacts by electrostatic fingerprints.

C. Jelsch, B. Guillot, R. Clausse

CNRS CRM2 Lorraine University. Faculty of Sciences & Technologies Laboratoire Cristallographie Résonance Magnétique et Modélisations, Nancy, France christian.jelsch@univ-lorraine.fr

Keywords: Electrostatic complementarity, ligand docking and scoring, crystal structure prediction

Structure-based methods including docking and scoring of ligands aim to select the best potential hits for in vitro assays by ranking them according to predicted binding affinities. Virtual screening is based on docking programs providing several poses of the ligand within a binding site and a score attributed to each pose. Accurate prediction of the correct binding pose remains a major scientific challenge for current scoring functions in order to retrieve the true ligands.

The newly developed descriptor concerns a computer based method for evaluating the stability of a complex formed by two molecular entities. It provides a score and at the same time a fingerprint of the intermolecular interactions. The descriptor can be applied, for example, to a molecule and its environment in a crystal structure. Protein / ligand complexes, either experimental (native) or produced by docking software can also be evaluated. The function is projected on the intermolecular interface, such as the Hirshfeld surface, and is homogenous to an electrostatic energy density. It is obtained by using modified electrostatic potentials.

This electrostatic complementarity descriptor can act as filter to detect most false ligand poses among diverse poses proposed by molecular docking programs. Similarly in the case of small molecules, it can evaluate the quality of crystal packings generated by a crystal structure prediction software. The crystal structure of aceclofenac [1], an anti-inflammatory drug, is analysed in Fig. 1. A good electrostatic complementarity is typically manifested by a correlation coefficient between interior and exterior properties close to -1 and by a fingerprint plot with points located close to the diagonal line. Classical electrostatic maps do not provide such a clear picture of interactions.

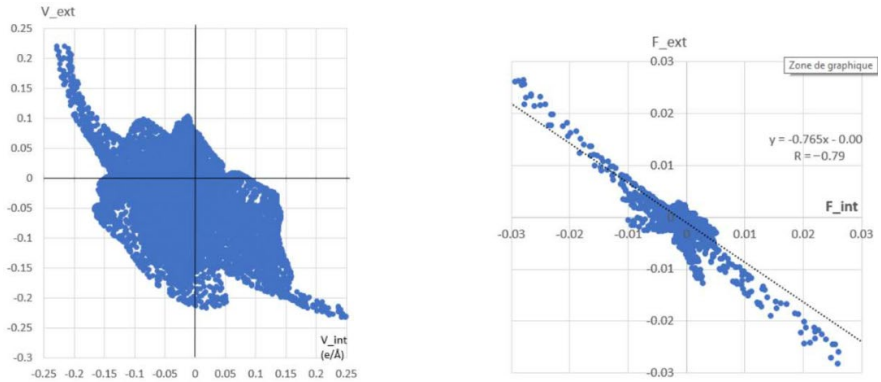

Figure 1. Left: scatterplot (V_int,V_ext) of electrostatic potential generated by the inner molecule of aceclofenac and its immediate surrounding neighbours in the crystal packing. Right: The equivalent scatterplot with our designed electrostatic function shows the good electrostatic complementarity within the crystalline environment. The charge density was transferred from ELMAM2 database [2] of multipolar atoms. Electrostatic and Hirshfeld surface calculations were done with VMoPro [3] and MoProViewer [4] software.

[1] Jelsch, C., Devi, R. N., Noll, B. C., Guillot, B., Samuel, I. & Aubert, E. (2020). J. Mol. Struc. 1205, 127600.
[2] Domagała, S., Fournier, B., Liebschner, D., Guillot, B. & Jelsch, C. (2012). Acta Cryst. A68, 337-351.
[3] Jelsch, C., Guillot, B., Lagoutte, A. & Lecomte, C. (2005). J Applied Crystallogr. 38, 38-54.
[4] Guillot, B., Enrique, E., Huder, L. & Jelsch, C. (2014). Acta Cryst, 70, C279. MS19. O01.

A022-05-270823

Identification of novel Z-DNA binding proteins by computational approaches

K. Kim, S. Kannappan, S. Das

Sungkyunkwan University School of Medicine, Suwon 16419, Republic of Korea

kyengkyu@skku.edu

Keywords: Z-DNA, binding protein, computational approach

Z-DNA has a role in controlling various cellular processes such as chromatin remodeling, gene expression, and genome stability [1]. The structure and function of Z-DNA are tightly regulated by proteins containing Z-DNA binding motifs, but the species of Z-DNA binding proteins are limited. However, considering the role of Z-DNA in key cellular processes, it is expected that many Z-DNA binding proteins must be present in cells. To answer this question, we employed computational methods to predict a novel Z-DNA binding protein present in nature. First, atomic structures or predicted models of proteins were prepared from the Protein Data Bank (PDB) or Alphafold. Their structural similarities to the known Z-DNA were predicted using various available structural comparison programs. The 17 highly-ranked proteins were considered as the first candidates and their Z-DNA binding activity was predicted using the HDOCK server [2]. In addition, their DNA binding properties were also expected using a machine learning process. Finally, the B- and Z-DNA binding activity of the final seven candidates were estimated by molecular dynamic simulation and their binding energies. The experimental validation of this novel Z-DNA binding protein and its biological implications will be further investigated.

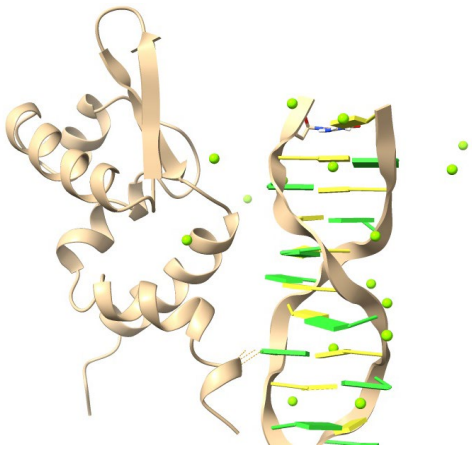

Figure 1. The binding mode of a novel Z-DNA binding protein identified in this study

[1] Ravichandran, S., Subramani, V. & Kim, K. (2019). *Biophys Rev.* **11**, 383.
[2] Yan Y, Zhang D, Zhou P, Li B, & Huang S-Y. (2017) *Nucleic Acids Res*. **45**. W365

A022-06-270823

Deep Learning-based Predictions of Electron Density Maps from Input Patterson Maps

Tom Pan[1], Chen Dun[1], Shikai Jin[2], Ria Stevens[1], Mitchell D. Miller[2*], Anastasios Kyrillidis[1], George N. Phillips[2,3]

Computer Science, Rice University, Houston, TX, 77005, USA. 2. Biosciences, Rice University, Houston, TX, 77005, USA. Chemistry, Rice University, Houston, TX, 77005, USA

mitchm@rice.edu, georgep@rice.edu

Keywords: Deep Learning, Patterson Map, Phasing

We have been testing the ability of deep learning to predict electron density maps given an input Patterson map. Hurwitz [1] reported success in determining the positions of 10 randomly positioned, identical atoms from their Patterson maps via a convolutional neural network(CNN). We have conducted trials using atom arrangements extracted from short peptides. After training U-Net based CNN machine learning models implemented in the Torch Python framework, we found that we can predict a low-resolution electron density estimate from the Patterson maps [2]. The histogram of the phase error of the predicted maps are more accurate than a random distribution. From a recent trial, we estimate that roughly 85% of the output maps were accurate enough for building a startling model to start refinement of the peptide. After these encouraging results, we have tested variations in our training models. Adding prior information from standard amino acid rotamers and incorporating training recycling improved the accuracy of the predicted maps. We found that adding a transformer to our model, inspired by 3D vision transformers [3,4] and implemented using a one-way attention framework to the Patterson map and reference structures, gave more accurate predictions than the UNet only model with lower computational training cost. To see how far various training approaches can take us, we are exploring ways to expand the model to account for symmetry and are continuing to make our training and test model data more like actual crystal data.

[3] Hurwitz, D. (2020). *arXiv:*2003.13767.
[4] Pan, T., Jin, S., Miller, M.D., Kyrillidis, A. & Phillips, Jr, G.N. (2023). *IUCrJ, in press*.
[5] Vaswani, A., Shazeer, N., Parmar, N., Uszkoreit, J., Jones, L., Gomez, A.N., Kaiser, L. & Polosukhin, I. (2017). *Advances in Neural Information Processing Systems*, **30**, 201.
[6] Chen, J., He, Y., Frey, E.C., Li, Y. & Du, Y. (2021) *arXiv*.2104.06468.

This work was supported in part by the NSF (STC 1231306) and the Robert A. Welch Foundation (C-1970). The content is solely the responsibility of the authors and does not necessarily represent the official views of the Funders.

A034 Quantifying the Electrostatic Potential with Accurate Electron Diffraction Studies
Room 220
1.10pm - 3.30pm

A034-01-270823

Beyond IAM refinement for 3D ED data: aspherical scattering factors

Barbara Olech Gruza[1], Petr Brázda[2], Lukáš Palatinus[2], Paulina M. Dominiak[1]

1 Department of Chemistry, University of Warsaw, Poland; 2 Institute of Physics of the Czech Academy of Sciences, Czech Republic
b.gruza@uw.edu.pl

Keywords: electron scattering factors, TAAM, 3D ED

In recent years we observe spectacular development of the methods for 3D electron diffraction (3D ED). Currently, there are available structures from refinements in the dynamical approach [1] with R-factors below 10% and resolution around dmin = 0.5Å. For such data, residual electrostatic potential on bonding paths or lone electron pairs regions can be observed. It gives us an opportunity to use more sophisticated, aspherical models and get closer to obtaining the correct electrostatic potential from the experiment.

We proposed Transferable Aspherical Atom Model (TAAM) refinements against 3D ED data in kinematic approximation [2]. Next, we coupled TAAM with dynamical refinement in Jana2020 [3]. Here, we present refinements of 1-methyluracil crystal structure against dmin = 0.56 Å data with TAAM in the dynamical approach. We use several TAAM versions. TAAM fits to the experimental data better than standard IAM, what is evidenced by a visible clearing of the residual density map (Fig. 1), lowering of the maximum and minimum values and lowering of R-factor. However, after detailed analysis we see the insufficiency of TAAM.

By comparing experimental refinements and theoretical simulations we discuss possibilities of the refinement of the valence populations of multipole model directly against experimental 3D ED data. We show how big impact on electron scattering factors have even small changes in multipole model parameters and how huge impact on the Fourier electrostatic potential maps have incorrect scattering factors. These results help us to understand what we really see on the residual electrostatic potential maps.

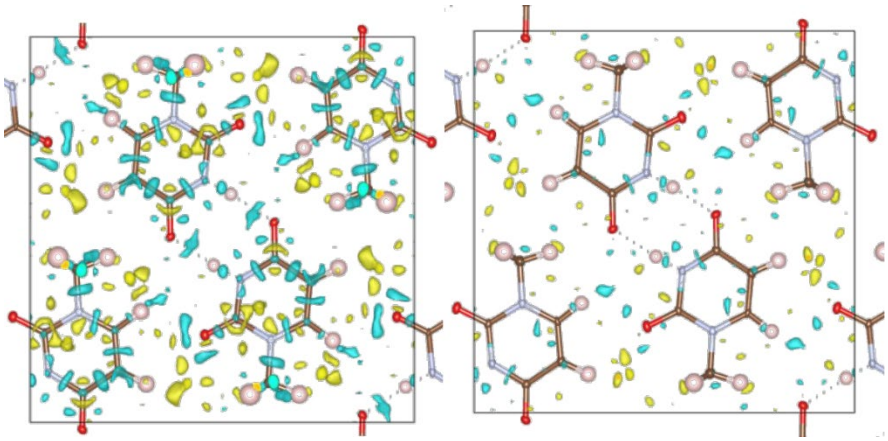

Figure 1. Residual density maps for dynamical IAM refinement (left) and dynamical TAAM refinement (right). Contour level 0.04 eÅ^{-1}, yellow: positive, cyan: negative.

[1] L. Palatinus, V. Petricek, and C. A. Correa, (2015). *Acta Crystallogr. Sect. A Found. Adv.*, **71**, 235–244.
[2] B. Gruza, M. L. Chodkiewicz, J. Krzeszczakowska, and P. M. Dominiak, (2020). *Acta Crystallogr. Sect. A Found. Adv.*, **76**, 92–109.
[3] V. Petrícek, M. Dusek, and L. Palatinus, (2014). *Zeitschrift für Krist. - Cryst. Mater.*, **229**, 345–352.

This research was funded by National Science Centre, Poland 2020/39/I/ST4/02904

A034-02-270823

Toward quantitative analysis of 3D nanostructures using convergent-beam electron diffraction

K. Tsuda[1*] and D. Morikawa[2]

[1] Frontier Research Institute for Interdisciplinary Sciences, Tohoku University, Sendai 980-8578, Japan
[2] Institute of Multidisciplinary Research for Advanced Materials, Tohoku University, Sendai 980-8577, Japan,
**Email: k_tsuda@tohoku.ac.jp*

Keywords: Convergent-beam electron diffraction, 3D nanostructures, Dynamical diffraction calculations

Convergent-beam electron diffraction (CBED), which is the most powerful technique to examine nanometer-scale local crystal symmetries [1,2], has been applied to functional materials with various types of phase transitions, such as a ferroelectric-like transition in metal [3], a ferroaxial transition [4], and ferroelectric transitions [5–10]. Nanoscale local structures of $BaTiO_3$ and $KNbO_3$, which exhibit the same series of structural phase transitions from the paraelectric cubic phase to three ferroelectric phases (tetragonal, orthorhombic, and rhombohedral), were investigated by the combined use of scanning transmission electron microscopy (STEM) and CBED (called STEM-CBED or 4D-STEM) [7–10]. It was revealed that the structures of the cubic, tetragonal, and orthorhombic phases are formed as averages of the polar nanostructures of the lowest temperature phase. This indicates the order-disorder-type behavior of their structural phase transitions [7–10]. Recently, the electric field response of the rhombohedral polar nanostructures was examined by the 4D-STEM technique [11]. By applying an electric field, significant changes in the distributions of the polar nanostructures. 4D-STEM is advantageous for the analysis of such nanoscale local structural variations related to novel physical properties.

CBED was also applied to quantitative refinements of local crystal structures and electrostatic potentials fully based on the dynamical diffraction theory [12–18]. Toward the quantitative analysis of 3D nanostructures using CBED or 4D-STEM, functions to deal with nanostructures in the depth and lateral directions of the electron probe have been implemented into our CBED pattern simulation code MBFIT [12,13], which is based on the Bloch wave formulation. The scattering matrix formulation [19] was used to calculate CBED intensities from the stacking of different structures in the beam direction, together with parallel computation using OpenMPI. The phase of the incident electron wave at the boundary was set to reproduce the size and position of the coherent electron nanoprobe [17]. Quantitative refinement of nanostructures and interfaces using 4D-STEM data is discussed in the talk.

[1] M. Tanaka and K. Tsuda, Microscopy **60**, S245 (2011).
[2] M. Tanaka, in *International Tables for Crystallography*, edited by U. Shmueli, Vol. B (International Union of Crystallography, Chester, England, 2010).
[3] Y. Shi, Y. Guo, X. Wang, A. J. Princep, D. Khalyavin, P. Manuel, Y. Michiue, A. Sato, K. Tsuda, S. Yu, M. Arai, Y. Shirako, M. Akaogi, N. Wang, K. Yamaura, and A. T. Boothroyd, Nat. Mater. **12**, 1024 (2013).
[4] T. Hayashida, Y. Uemura, K. Kimura, S. Matsuoka, D. Morikawa, S. Hirose, K. Tsuda, T. Hasegawa, and T. Kimura, Nat. Commun. **11**, 4582 (2020).
[5] K. Tsuda, R. Sano, and M. Tanaka, Phys. Rev. B **86**, 214106 (2012).
[6] K. Tsuda, R. Sano, and M. Tanaka, Appl. Phys. Lett. **102**, 1 (2013).
[7] K. Tsuda, A. Yasuhara, and M. Tanaka, Appl. Phys. Lett. **103**, 082908 (2013).
[8] K. Tsuda and M. Tanaka, Appl. Phys. Express **8**, 081501 (2015).
[9] K. Tsuda and M. Tanaka, Appl. Phys. Express **9**, 071501 (2016).
[10] K. Tsuda and M. Tanaka, Jpn. J. Appl. Phys. **56**, 10PB09 (2017).
[11] D. Morikawa and K. Tsuda, Appl. Phys. Lett. **119**, 052904 (2021).
[12] K. Tsuda and M. Tanaka, Acta Crystallogr. A **55**, 939 (1999).
[13] Y. Ogata, K. Tsuda, and M. Tanaka, Acta Crystallogr. A **64**, 587 (2008).
[14] K. Tsuda, D. Morikawa, Y. Watanabe, S. Ohtani, and T. Arima, Phys. Rev. B **81**, 180102 (2010).
[15] B. Aryal, D. Morikawa, K. Tsuda, and M. Terauchi, Acta Crystallogr. A **77**, 1 (2021).
[16] P. N. H. Nakashima, A. E. Smith, J. Etheridge, and B. C. Muddle, Science **331**, 1583 (2011).
[17] J. C. H. Spence and J. M. Zuo, *Electron Microdiffraction* (Plenum Press, New York, 1992).
[18] J.-M. Zuo, R. Yuan, Y.-T. Shao, H.-W. Hsiao, S. Pidaparthy, Y. Hu, Q. Yang, and J. Zhang, Microscopy **71**, i116 (2022).
[19] L. Sturkey, Proc. Phys. Soc. **80**, 321 (1962).

The authors would like to thank Emer. Prof. M. Tanaka and Prof. M. Terauchi for their continuous support. The present study was partially supported by JSPS KAKENHI Grant numbers 18H03674, 18K18731 and 22H01150.

A034-03-270823

Measuring vacancy concentrations, chemical bonding and lattice contraction around nanovoids in aluminium by QCBED

P.N.H. Nakashima1, Y.-T. Shao2,3, A.E. Smith4, Z. Zhang5,6,7 T. Liu1, J. Etheridge1,8, L. Bourgeois1,8, J.-M. Zuo9,10, D.R. Clarke11

Dept. of Materials Science and Engineering, Monash Univ., Victoria 3800, Australia, Mork Family Dept. of Chemical Engineering & Materials Science, Univ. Southern California, Los Angeles, CA 90089, USA, Core Center of Excellence in Nano Imaging, Univ. Southern California, Los Angeles, CA 90089, USA, School of Physics and Astronomy, Monash Univ., Victoria 3800, Australia, Electron Microscopy for Materials Research (EMAT), Univ. Antwerp, Groenenborgerlaan 171, 2020 Antwerp, Belgium, NANOlab Center of Excellence, Univ. Antwerp, Groenenborgerlaan 171, 2020 Antwerp, Belgium, Dept. of Materials, Univ. Oxford, 16 Parks Road, Oxford OX1 3PH, United Kingdom, Monash Centre for Electron Microscopy, Monash Univ., Victoria 3800, Australia, Dept. of Materials Science and Engineering, Univ. Illinois Urbana-Champaign, Urbana, IL 61801, USA, Materials Research Laboratory, Univ. Illinois Urbana-Champaign, Urbana, IL 61801, USA. School of Engineering and Applied Sciences, Harvard Univ., Boston, MA 02134, USA.

philip.nakashima@monash.edu

Keywords: Quantitative CBED, Chemical Bonding, Nanostructures, Crystal Defects

A multislice approach [1] to quantitative convergent-beam electron diffraction (QCBED) has been developed to permit the measurement of chemical bonding-sensitive structure factors local to nanostructures embedded within inhomogeneous, multi-phased nano-structured materials.

We apply this method to investigating vacancy concentrations, crystal lattice contraction and chemical bonding around a nanovoid in 99.9999+% pure aluminium (see Fig. 1 for an illustration of CBED through a nanovoid in aluminium). We are not only able to experimentally measure structure factors around these nanovoids with sufficient precision to resolve chemical bonding information, but in the process of doing so, can also measure vacancy concentrations around the nanovoids and the associated degree of contraction by the aluminium host lattice as a function of vacancy concentration. The latter results match DFT modelling of lattice contraction versus vacancy concentration.

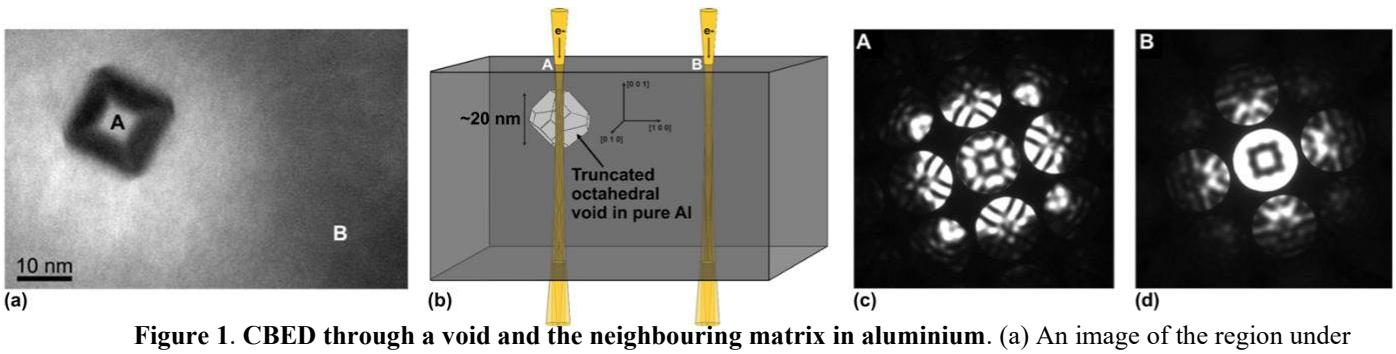

Figure 1. **CBED through a void and the neighbouring matrix in aluminium**. (a) An image of the region under investigation showing the nanovoid at location A and uninterrupted matrix at B. (b) A schematic of the electron beam passing through overlapping parallel facets of the nanovoid at A and through uninterrupted matrix at B. (c) The resulting CBED pattern from A through the nanovoid. (d) The CBED pattern from the uninterrupted volume of matrix at B. Note that both patterns have 4*mm* symmetry but have very different intensity distributions.

[1] Cowley, J. M. & Moodie, A. F. (1957), *Acta Cryst.* ***10***, 609

The authors acknowledge the use of the instruments and scientific and technical assistance at the Monash Centre for Electron Microscopy, a Node of Microscopy Australia, and The Frederick Seitz Materials Research Laboratory at the University of Illinois at Urbana-Champaign. This work was funded by the Australian Research Council (FT110100427 & DP210100308).

A034-04-270823

Charge density refinement on inorganic compounds using electron diffraction

E. Yörük1, A. Suresh1, P. Brázda1, M. K. Cabaj1 L. Palatinus1

[1] *Institute of Physics of the CAS, Na Slovance 2, Prague 8, Czechia*

**yoruk@fzu.cz*

Keywords: kappa refinement, charge density, electron diffraction

Chemical bonding inside crystal structures has an important impact on the charge distribution, due to charge transfer among the bonded atoms. The charge of an atom inside a crystal can therefore be different from its neutral state counterpart. This can lead to accumulation of non-modelled residues in electron density maps post-refinement, both at atomic positions and along the bonds [1]. Furthermore, the knowledge of the charge transfer may be important for understanding the investigated material.

We investigate whether the charge transfer among atoms can be refined for compounds with heavy atoms using 3D electron diffraction (3D ED). 3D ED is an increasingly popular technique for structural analysis of nanocrystals [2], and since electron scattering is more sensitive to fine details in the electron density distribution compared to X-ray scattering [3], it is worthwhile to explore whether 3D ED data can be used for charge density analysis of heavy atoms. This is a challenge due to the small ratio of valence/core electrons contributing to the electron density, requiring an extreme precision in diffraction data to refine the valence electron contributions which are involved in chemical bonding. We use a spherical atom kappa formalism [4] where atomic contributions to the charge density remain spherical, but the population of the valence shell is refined while allowing it to expand or contract as a result of changes in electron-electron repulsion.

We present here results from the application of the kappa formalism to a number of inorganic compounds, including a heavy-metal perovskite CsPbBr3, oxide Lu3Al5O12, quartz SiO2, natrolite Na2Al2Si3O10·2H2O and borane B18H22. All refinements were performed in Jana2020 [5]. Results show reduced noise in potential difference maps and refined valence shell populations are visible on static deformation maps (**Fig. 1**). The experimentally refined charge flows agree with chemical predictions based on electronegativity, and there are improvements in the displacement parameters and R-factors. The results were validated by DFT calculations for comparison.

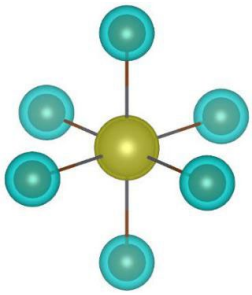

Figure 1: *Static deformation map after kappa refinement on the $PbBr_6$ octahedron. The accumulation of charge on the Br atoms (blue) and the depletion of charge on Pb (yellow) can be seen.*

[1] Grabowsky S. (2021) De Gruyter, *Complementary Bonding Analysis.*
[2] Gemmi M. *et al*. (2019) *ACS Cent. Sci.* **5**, p. 1315.
[3] Zheng J. *et al*. (2004) *J. of Applied Cryst*., **38** (4) p. 648.
[4] Coppens P. (1997) Oxford Univ. Press, *X-Ray Charge Densities and Chemical Bonding.*
[5] Petříček V. *et al.* (2014) *Zeitschrift für Kristallographie*, **229** (5), p. 345

This work was funded by the Czech Science Foundation, Grant No. 21-05926X, and H2020 ITN project NanED, grant agreement No. 956099

A034-05-270823

Quantifying the projected, atomic-resolution electrostatic potential via scanning transmission electron microscopy despite dynamical electron diffraction

A. Sadri, S.D. Findlay

School of Physics and Astronomy, Monash University, Australia

scott.findlay@monash.edu

Keywords: scanning transmission electron microscopy, scattering matrix, phase retrieval

The four-dimensional (4D) data resulting from recording diffraction patterns at each raster scan position of a scanning transmission electron microscopy (STEM) convergent probe is giving rise to new imaging strategies [1]. In thin samples, differential phase contrast [2] and ptychography [3] can quantify the projected electrostatic potential of the sample. However, at atomic resolution, crystalline materials thicker than a few nanometers are no longer simple phase objects [4], and quantifying their electrostatic potential requires accounting for dynamical electron diffraction. Quantitative structure determination in the presence of dynamical electron diffraction can be achieved via the scattering matrix method [5] and via inverse multislice ptychography [6].

The scattering matrix approach breaks the structure determination problem into two steps, as depicted schematically in Fig. 1. The first step is phase retrieval on measured 4D STEM intensities to determine the complex scattering matrix, a matrix operator linearly relating the incident and scattered wavefields. The second step is to determine the projected electrostatic potential from the structure matrix. Elegant formal solutions to the second step when the samples are perfect crystals [7] produce artefacts when applied to resolution-limited STEM data. We show through simulation that this can be largely overcome via a gradient descent approach. We further show that limitations of the phase retrieval in the first step in the presence of shot noise can be mitigated by iterating between the two steps.

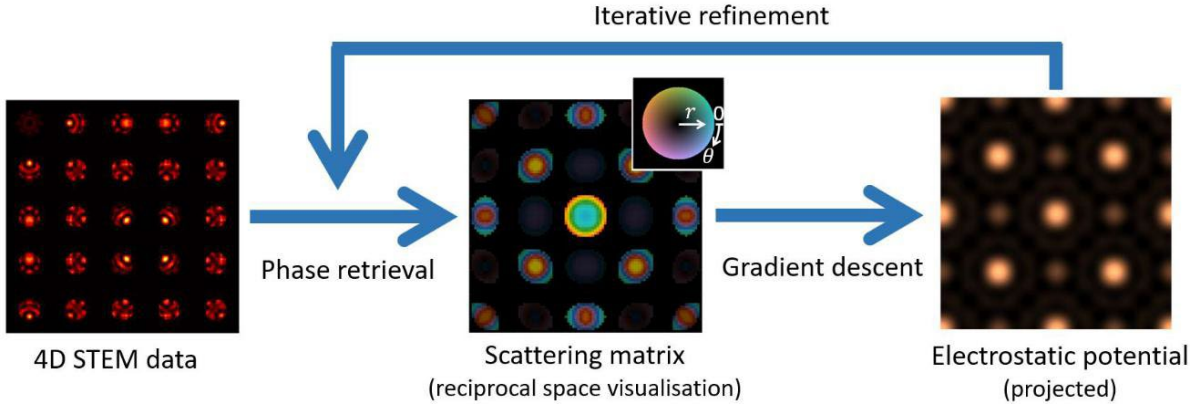

Figure 1. Schematic of structure retrieval algorithm from 4D STEM intensities. The complex scattering matrix is displayed using colour [8] to represent the phase and lightness to represent (the square root, to improve visibility of smaller values) of the modulus, as per the inset colour wheel [9].

[1] Ophus, C. (2019). *Microsc. Microanal.* **25**, 563.
[2] Müller, K., Krause, F. F., Béché, A., et al. (2014). *Nat. Commun.* **5**, 5653.
[3] Yang, H., Rutte, R. N., Jones, L., et al. (2016). *Nat. Commun.* **7**, 12532.
[4] Close, R., Chen, Z., Shibata, N. & Findlay, S. D. (2015). *Ultramicroscopy* **159**, 124.
[5] Brown, H. G., Chen, Z., Weyland, M., et al. et al. (2018). *Phys. Rev. Lett.* **121**, 266102.
[6] Chen, Z., Jiang, Y., Shao, Y. T., et al. (2021). *Science* **372**, 826.
[7] Allen, L. J., Faulkner, H. M. L. & Leeb, H. (2000). *Acta Crystallogr. A* **56**, 119.
[8] Findlay, S. D., Brown, H. G., Pelz, P. M., et al. (2021). *Microsc. Microanal.* **27**, 744.
[9] Waters, M. J., Walker, J. M., Nelson C.T., et al. (2020). *Chem. Mater.* **32**, 5455.

A034-06-270823

Net atomic charges by dynamical kappa refinement against 3D ED data

L. Palatinus1, A. Suresh1, E. Yörük1, P. Brázda1, M. Cabaj1, B. Olech2, P. M. Dominiak2

Institute of Physics of the CAS, Na Slovance 2, Prague 8, Czechia, Department of Chemistry, University of Warsaw ul. Zwirki i Wigury 101, Warsaw, Poland

palat@fzu.cz

Keywords: dynamical diffraction, kappa refinement, nanocrystals

3D electron diffraction has become an increasingly popular tool to obtain structural information from nano- or microcrystalline materials. In just a few years, it evolved into a respected and widely used structure-analysis method, providing all types of structural information from many samples [1].

An important effect affecting the intensities in electron diffraction is dynamical diffraction, i.e., the possibility that an electron scatters more than once in the sample. This effect causes deviations of the diffracted intensities from the kinematical limit. While it is possible to ignore this complication and treat the data as if they were kinematical, such an approach leads to a visibly worse fit to experimental intensities and, correspondingly, to let accurate structure models with lower sensitivity to the details of the electrostatic potential.

An approach that takes the dynamical diffraction into account in the refinement against 3D ED data is called dynamical refinement [2,3]. When the 3D ED data come from a high-quality crystal so that the dynamical effects can be well modelled, such a refinement can provide very good matches with R(obs) values in the range of 2-6%. With such a match, it is possible to extract more information about the electrostatic potential distribution than just the atomic positions, including its deformation due to interatomic interaction.

A so-called kappa refinement is the simplest model that allows a deviation from the basic Independent Atom Model (IAM) [4]. In this refinement, the electron density (and thus also the electrostatic potential) of each atom remains spherical, but the population of its valence electron shell is refined together with an expansion or contraction of the valence shell.

A series of tests on inorganic compounds has shown that this approach is indeed feasible. Kappa refinements on the structures of quartz, natural zeolite natrolite, and even a heavy-atom perovskite $CsPbBr_3$ show that the data contain sufficient information to determine the charge transfer between the atoms. The accuracy of the results is validated by comparison with DFT calculations.

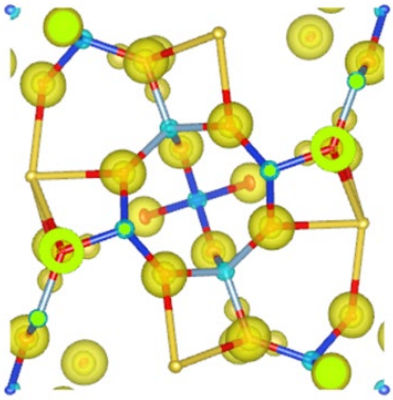

Figure 1. Static deformation maps resulting from kappa refinement of the natural zeolite natrolite showing the accumulation of electron density on the oxygen atoms (yellow isosurfaces) and depletion of electron density on the silicon atoms (blue isosurfaces).

[1] Gemmi, M., Mugnaioli, E., Gorelik, T., Kolb, U., Palatinus, L., Boullay, P., Hovmoller, S., Abrahams, J. P. (2019). *ACS Cent. Sci.* **5**, 1315.
[2] Palatinus, L., Petricek, V., Correa, C. A. (2015). Acta Cryst. A **71**, 235.
[3] Klar, P. B., Krysiak, Y., Xu, H., Steciuk, G., Cho, J., Zou, X., Palatinus, L. (2023). Nat. Chem., in press.
[4] Coppens, P., Guru Row, T. N., Leung, P., Stevens, E. D., Becker, P. J., Yang, Y. W. (1979). Acta Cryst. A **35**, 63.

This work was funded by the Czech Science Foundation, grant No. 21-05926X, National Science Centre, Poland, grant No. 2020/39/I/ST4/02904, and H2020 ITN project NanED, grant agreement No. 956099.

A043 Crystal Growth and Characterization of Biominerals and Biomimetics
Room 208
1.10pm - 3.30pm

A043-01-270823

CRYSTALLIZATION INDUCED BY LITHOBIONT MICROBIAL COMMUNITY

O.V. Frank-Kamenetskaya, D.Yu. Vlasov

Saint Petersburg State University, Universitetskaya nab. 7/9, Saint Petersburg 199034, Russia

Email of communicating o.frank-kamenetskaia@spbu.ru

Keywords: microbial biomineralization, fungi, bacteria

The creative collaboration between crystallographers and biologists of St. Petersburg State University allowed to make a significant breakthrough in research of mechanisms and factors of microbial biomineralization The work was carried out in field and laboratory conditionsıo Syntheses of biofilm mineral analogs with the participation of monocultures of fungi and bacteria, as well as their associations (bioinspired syntheses) were carried out in liquid nutrient media (Chapek-Doksa and others) with different glucose content and under oligotrophic conditions of a humid chamber. In the humid chamber, the biomineralization conditions were close to natural, but the process was very slow. In a liquid medium, crystallization occurred much faster than in nature, but it was possible to reproduce it at later stages. Microorganisms were planted on pieces of rocks and minerals of various compositions and densities (carbonates, silicates, phosphates, oxides, sulfides, etc.). The selection of strains of fungi and bacteria was carried out according to the results of a preliminary study of the products of their metabolism by chromato-mass spectrometry. Preference was given to oxalic acid-producing fungi and EPS-producing bacteria, and their associations. In addition, to identify the effect of organic and inorganic components of biofouling on the formation of biominerals and their morphology, model experiments were carried out in systems with organic and inorganic additives typical of biofilms containing fungi (classical syntheses). The results of these syntheses in many cases made it possible to explain the morphogenetic regularities of biomineralization , revealed on the basis of the study of minerals in biofilms (Fig1a) and products of bioinspired syntheses (Fig.1b). The results obtained allowed significant progress in the study of the mechanisms and factors of oxalate and carbonate crystallization involving fungi and bacteria [1-3], taking a fresh look at a number of the global biogeochemical processes in which microbial biomineralization play an important role and also contributed to the development of effective environmentally, friendly and economical biotechnologies.

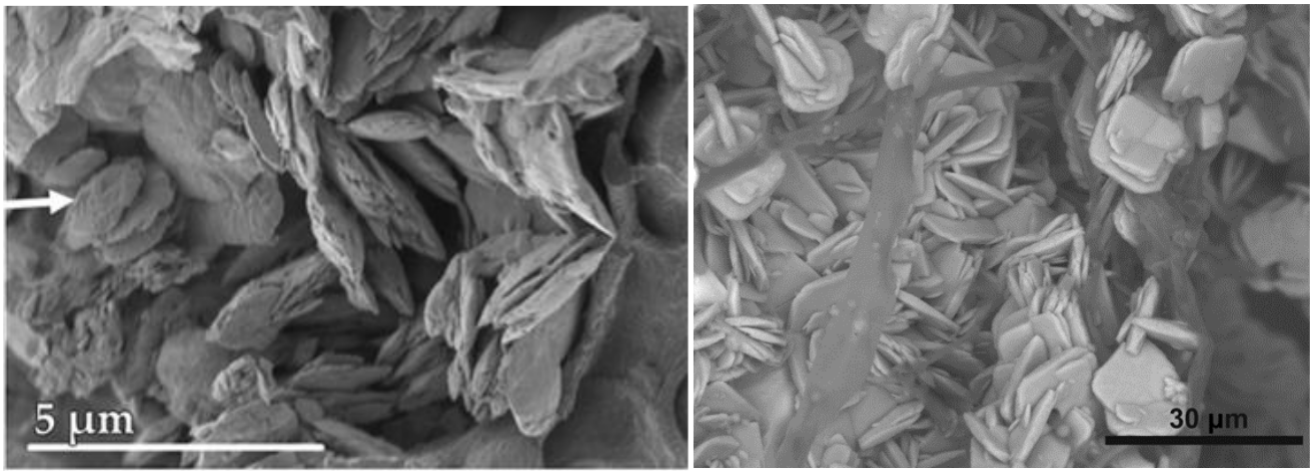

Figure 1. Aggregates of split moolooite crystals on copper ore from the Voronov Bor deposit (Karelia): in the lichen thalli L.inops (a) and on the 5th day of the model experiment with fungus Aspergillus niger (b)

[1] Frank-Kamenetskaya, O.V., Zelenskaya, M.S., Izatulina ,A.R., Gurzhiy, V.V., Rusakov, A.V. & Vlasov, D.Yu. (2022.). *American Mineralogist* 107 (1): 100–109.
[2] Frank-Kamenetskaya, O.V., Zelenskaya, M.S., Izatulina, A.R., Vereshchagin, O.S., Vlasov, D.Yu., Himelbrant., D.E., & Pankin, D.V. (2021) *Scientific Reports* 11:24239.
[3] Vlasov, D.Yu., Frank-Kamenetskaya, O.V., Zelenskaya, M.S., Sazanova, K.V., Rusakov, A.V., Izatulina, A.R. (2020) *Aspergillus niger: Pathogenicity, Cultivation and Uses*, edited by E. Baughan, pp. 1-122. NY: Nova Science Publishers.

The work was supported by the Russian Science Foundation grant 19-17-00141 on the basis of St. Petersburg State University resource centers: RDMI, MIM, Geomodel, RMCT, Nanotechnologies, OLMIV.

A043-02-270823

An in-depth structural and crystallographic analysis of dental enamel: Reconstructing the life history of a medieval population in Lower Saxony (Germany)

Jana Storsberg[1], Kateryna Loza[1], Immo Heske[2], Matthias Epple[1]

[1] Inorganic Chemistry and Center for Nanointegration, Duisburg-Essen (CENIDE), University of Duisburg-Essen, Universitaetsstr. 5-7, 45117 Essen, Germany; [2] Department of Prehistory and Early History, Georg August University Goettingen, Nikolausberger Weg 15, 37073 Goettingen, Germany

jana.storsberg@uni-due.de

Keywords: hard tissue, hydroxyapatite, enamel prisms

Dental enamel is the hardest material in the human body. Enamel consists of prisms which are cylindrical bundles of hydroxyapatite crystals [1]. During the incremental secretion of enamel by ameloblasts, different physiological influences leave an impact on the tooth structure. Daily and weekly patterns can be seen on the enamel prisms. Moreover, systematic disturbances like malnutrition, metabolic diseases, or fever lead to an anomalous arrangement of the enamel prisms [2]. The structural analysis of these crystallite structures and defects can be used to reconstruct the life history of individuals.

We selected 30 teeth sets from 10 individuals buried in a burial ground in Gevensleben (Germany). The Gevensleben burial ground was used as an early Christian cemetery in the 8th-10th century. It represents an important source of information of the social and cultural life of the ordinary population of the early Middle Ages in Lower Saxony, Germany.

Each tooth was embedded in epoxy resin for protection and then cut using a low-speed saw. The tooth surface was examined by optical microscopy and scanning electron microscopy (SEM) as well as energy-dispersive X-ray spectroscopy (EDS) to analyse the chemical composition of the dental enamel. X-ray powder diffraction was used to identify the crystallographic phases present.

With this method, the childhood years of individuals can be reconstructed, based on the crystal arrangement in each individual tooth. This was done to extend the results of previous anthropological examinations. During the age of 3 years, children in Gevensleben were exposed to the greatest stress factors, which are also reflected in the increased mortality during this stage of life. To identify these stressful events, accentuated lines (AL) in tooth enamel structure were quantitatively analysed. It is likely that the children in this population were weaned at around 3 years of age and therefore experienced high physiological stress at that time. Furthermore, the crystallographic composition of the excavated teeth was compared to modern teeth. The surface of the teeth showed clear signs of wear caused by mastication of food containing abrasive stone particles, probably from grain milling.

Teeth are often one of the few human remains found in archaeological excavation sites. Due to the high content of mineral, they are usually well conserved, the in-depth structural analysis of tooth morphology can be used to reconstruct the life history of individuals, supplementing archaeological and anthropological investigations about people buried there more than one thousand years ago.

[1] Maas, M.C. & Dumont, E.R., (1999) Evolutionary Anthropology: Issues, News, and Reviews 8 (4), 133.
[2] Ten Cate's Oral Histology (Eighth Edition) (2013), edited by Antonio Nanci (Mosby, St. Louis (MO)), pp. 122.

A043-03-270823

Casting light on formation of the pearl oyster shell with nanobeam X-ray total scattering

S. Checchia1, T. A. Grünewald2, H. Dicko2, G. Le Moullac3, M. Sham Koua3, J. Vidal-Dupiol4, J. Duboisset2, J. Nouet5, O. Grauby6, M. Di Michiel1, V. Chamard2

[1] ESRF – The European Synchrotron, F-38043 Grenoble Cedex, France, 2 Aix-Marseille Univ., CNRS, Centrale Marseille, Institut Fresnel, Marseille, France, 3 Ifremer, ILM, IRD, Univ. Polynésie Française, F-98719 Taravao, Tahiti, French Polynesia,
[2] IHPE, Univ Montpellier, CNRS, Ifremer, Univ. Perpignan Via Domitia, Montpellier, France, 5 GEOPS, Univ. Paris-Sud, CNRS, Université Paris-Saclay, 91405 Orsay, France, 6 Aix-Marseille Univ., CNRS, CINaM, Campus Luminy, Marseille, France

stefano.checchia@esrf.fr

Keywords: Biomineralization, Total scattering, Amorphous calcium carbonate

The development of bio-inspired mineralization strategies to obtain tough and gossamer materials relies on the quantitative description of biomineralization mechanisms. A unifying feature of the formation of calcareous biominerals is the presence of an amorphous calcium carbonate (ACC) precursor phase, whose purported roles include lowering the energy barrier required for crystallization, pre-moulding shapes of crystallizing units and acting as a reservoir for Ca and $CO3^{2-}$, all the while transforming into crystalline calcite. Crucially, biogenic ACC is often found in the final mineralized state, enabling in principle the analysis of biomineralization precursors. However, the coexistence of multiple crystalline and amorphous compounds in many biominerals is often an obstacle to the selective experimental characterization of the amorphous part. As a result, comparatively little is known about the structure and the spatial organization of amorphous precursors, or even the possible presence of multiple ACC phases.

This work sought to probe deeper into amorphous precursors by focusing on early-stage mineralizing units in the shell of the pearl oyster *Pinctada margaritifera*. In this model organism the growth zone of the shell consists of disc-like units forming a prismatic layer typically containing residual ACC (red regions in Fig. 1a), as opposed to mature prisms rich in crystalline calcite (blue). Using nanobeam X-ray total scattering together with a novel method to separate crystalline and amorphous scattering contributions [1] we obtained the spatially-resolved atomic pair distribution function (PDF) across an early-stage disc (Fig. 1b). Through multivariate analysis and Reverse Monte Carlo modelling of PDF data, we resolved three distinct ACC states, determined their prevalence across the growth zone, and found that their structures differ mostly in the Ca-O pair distances (Fig. 1c-d). Complemented by spectroscopic analysis (Raman spectroscopy, coherent Raman microscopy, SEM-EDX [2,3]) showing the localized presence of Mg in the shell, these results point towards the key role Mg plays in the transition between different amorphous states and ultimately suggest a Mg-mediated crystallization pathway.

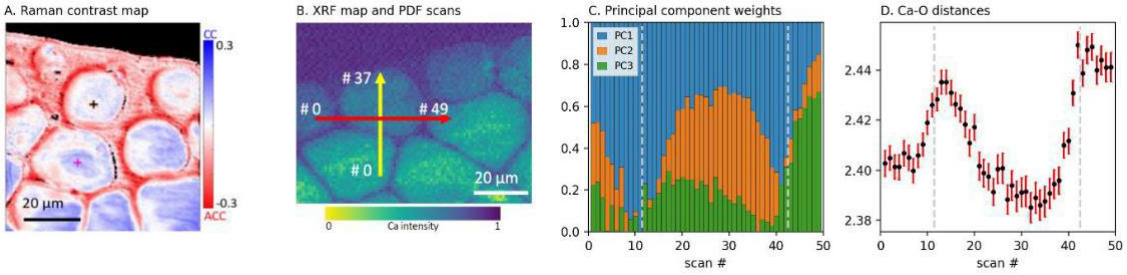

Figure 1. (A) stimulated Raman Scattering map, showing the symmetric contrast between ACC (red), prevalent in young disc-like units and interprismatic space, and calcite (blue). (B) Ca-Kα fluorescence map showing the early-stage disc and neighbouring mature discs; the horizontal (red) and vertical (yellow) arrows indicate the line scans where total scattering/PDF was measured relative prevalence of the principal components of the PDF obtained at each 1 µm step along the horizontal line scan. (D) spatial variation of the average first-neighbour Ca-O distance at each 1 µm step along the horizontal line scan.

[1] Grünewald, T. A., Checchia, S., Dicko, H., et al. (2022). *Proc. Natl. Acad. Sci. U.S.A.* **119 (45)**, e2212616119.
[2] Duboisset, J., Ferrand, P., Baroni, A., et al. (2022). *Acta Biomater.* **142**, 194-207.
[3] Dicko, H., Grünewald, T.A., Ferrand, P., et al. (2022). *J. Struct. Biol.* **214**, 10790

The authors acknowledge funding from the European Research Council (project 3D-Biomat no.724881) and thank Partnership for Soft Condensed Matter (PSCM, Grenoble, France) for support preparing experiments, Ifremer Taravao (Tahiti, French Polynesia) for access to samples, and Dr. Gavin Vaughan (ESRF, Grenoble, France) for discussions on data treatment.

A043-04-270823

Hierarchical structure of the spiralled narwhal tusk studied by X-ray imaging

Rodriguez-Palomo[1,2], J. Palle[2], E. Garde[3], P. A. Vibe[2], T. E. K. Christensen[2,4], N. K. Wittig[2], M. R. V. Jørgensen[2,5], I. Kantor[5,6], M. Burghammer[7], J. Liu[7], K. Jakata[7], P. Cook[7], J. T. Avaro[8], C. Appel[9], L. C. Nielsen[1], M. P. Heide-Jørgensen[3], M. Liebi[1,9,10], H. Birkedal[2]

[1]Chalmers University of Technology, Gothenburg, Sweden. [2]Aarhus University, Aarhus, Denmark. [3]Greenland Institute of Natural Resources, Copenhagen, Denmark. [4]Sino-Danish Center, University of Chinese Academy of Sciences. [5]MAX IV Laboratory, Lund University, Lund, Sweden. [6]Technical University of Denmark, Lyngby, Denmark. [7]European Synchrotron Radiation Facility (ESRF), Grenoble, France. [8]Swiss Federal Laboratories for Materials Science and Technology (EMPA), St. Gallen, Switzerland. [9]Paul Scherrer Institute, Villigen, Switzerland. [10]Federal Polytechnique University of Lausanne (EPFL), Lausanne, Switzerland.

adrian.rodriguez@inano.au.dk

Keywords: X-ray imaging, Mineralised tissue, SAXS/WAXS

Narwhals are fascinating animals whose tusk has caught the attention of humankind for centuries and has been associated with the unicorn myth. Narwhals have a vestigial tooth, a tusk, with a left-handed spiral structure that grows during the animal's life span principally in males. This twisted tusk has highly anisotropic mechanical properties and an extraordinarily high impact resistance [3]

We hypothesize that the orientation of the biological nanostructure reflects the spiral macro-structure, which defines the mechanical properties. Using combined 2D and 3D imaging techniques using X-rays and polarised visible light we studied its hierarchical structure at multiple length scales and with different contrasts. Small-angle X-ray scattering and diffraction imaging [3], X-ray fluorescence, and birefringence microscopy were used to investigate the anisotropy of the tusk building blocks (i.e., mineralised collagen fibrils) from the nano to the macro scale. Narwhal tusks have a central pulp chamber surrounded by primary dentine and a layer of cementum. Unlike human teeth, no enamel is present [2]. The building blocks of the narwhal cementum and dentine are identical to other mineralised tissues; however, their degree of anisotropy and spatial distribution differ from, e.g., bone [3] SAXS tensor tomography revealed a strong anisotropy in the dentine with mineralised collagen aligned in the longitudinal direction. A twist in the orientation of the longitudinal fibres was also found with radially increasing angles, creating a helical pattern from the pulp chamber to the cementum layer. The outer cementum layer that covers the entire tusk had a less anisotropic structure with radially oriented domains embedded in a longitudinally oriented matrix. At the nanoscale, the periodicity of the collagen fibrils was slightly higher in cementum than in dentine. The shape and size of the mineral particles were estimated fitting the SAXS and WAXS patterns, where the particle thickness and length increased from the inner to the outer dentine. These results not only reveal that a strong anisotropy is present in the tusk but also suggest that they follow a three-dimensional spiral structure in the nanoscale. The combination of 2D and 3D imaging techniques achieved an optimal balance between field of view, measurement time, and resolution.

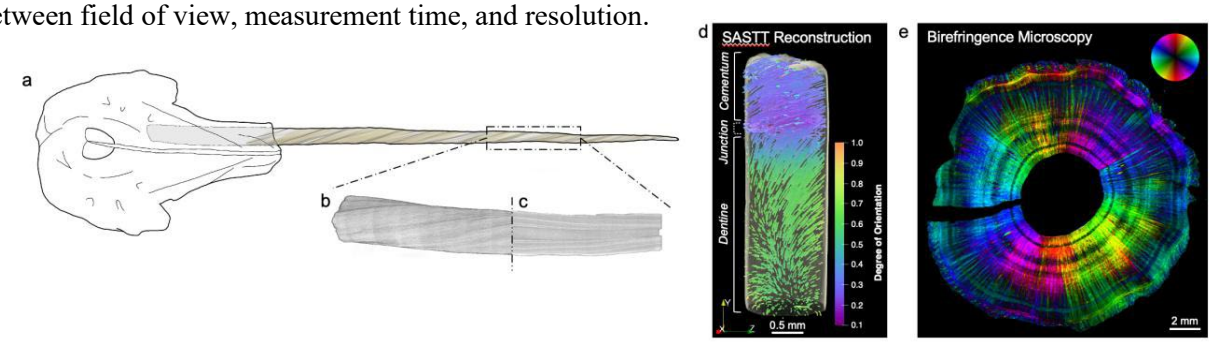

Figure 1. Schematic representation of a narwhal skull with tusk (**a**) and 3D rendered computed-tomography scan of the tusk showing its macroscopic left-handed spiral (**b,c**). 3D representation of the mineralised collagen fibrils' orientation in the narwhal tusk as the streamlines of the orientation of their reconstructed reciprocal space map (SAXS tensor tomography) (**d**). The morphology of the sample was reconstructed using the X-ray transmission signal measured during the experiment. Birefringence microscopy of a transversal slice of the narwhal tusk. The orientation of the mineralised collagen fibres follows the colour wheel where the angle is represented by the hue and the retardance is represented by the value in each pixel (**e**).

[1] Currey, J. D., Brear, K. and Zioupos, P. (1992). *J. Biomech.* **27**, 885-897.
[2] Grandfield, K., Chattah, N.L-T, Djomehri, S. et al. (2014). *Proc. Inst. Mech. Eng. H* **228**, 754-767.
[3] Liebi, M., Georgiadis, M., Menzel, A. et al. (2015). *Nature* **527**, 349-352.
[4] Reznikov, N., Bilton, M., Lari, L. et al. (2018). *Science* **360**, aao2189.

A043-05-270823

Orientation mapping of cholesterol monohydrate in gallstones utilizing X-ray diffraction tensor tomography

Ingvild Uri Hageberg[1], Daniyal Younas[1], Fredrik K. Mürer[2], Katharina Scheidl[1], Marco Di Michiel[3], Yuriy Chushkin[3], Dag W. Breiby[1], Basab Chattopadhyay[1]

[1]Department of Physics, Norwegian University of Science and Technology (NTNU), Høgskoleringen 5, 7491 Trondheim, Norway. [2]SINTEF Helgeland, Halvor Heyerdahls vei 33, 8626 Mo i Rana, Norway [3]ESRF-The European Synchrotron, 71 Avenue des Martyrs, 38000 Grenoble, France.

Ingvild.u.hageberg@ntnu.no

Keywords: Pathological biomineralization, tensor tomography, 3D morphology

Gallstones represents a class of pathological biomineralization affecting people across the world. Hence, they have been a subject of scientific research over several decades[1]. Despite the relatively high prevalence of gallstones, the formation of gallstones, in particular the microstructural nucleation events, remains less understood. As the delicate balance between body fluids and various minerals in the gallbladder becomes unstable either from environmental or genetic factors, uncontrolled nucleation events occur resulting in stone formation. There are two types of gallstones: cholesterol and pigment stones. Pigment stones are made of different mixtures of calcium bilirubinate, calcium, copper, and mucin glycoproteins, while cholesterol stones are mostly made of pure cholesterol crystals [2].

X-ray diffraction tensor tomography (XRD-TT) is a newly developed imaging methodology that facilitates 3-dimensional imaging with chemical as well as orientational contrast [3]. In this presentation we will demonstrate the application of XRD-TT to study the orientational information of cholesterol monohydrate crystallites present within human gallstones and to visualize their preferred orientation. The diffraction data integrated over the entire sample indicated the presence of oriented cholesterol monohydrate within the gallstones; no other minerals were present in the sample. The 001 and 002 diffraction peaks were utilized for the XRDTT analyses. Complementary, attenuation-based μCT experiments have been performed to understand the internal structures of the studied gallstones i.e., morphology, porosity, and density variations. The study demonstrates the unique capability of XRD-TT in studying 3D orientational information which is expected to provide new insights into the process of pathological biomineralization.

[1] Sanders, Grant & Kingsnorth, Andrew. (2007). Gallstones. BMJ (Clinical research ed.). 335. 295-9.
[2] Pramanik, Samiran & Ghosh, Soumen & Roy, Arkaprovo & Mukherjee, Ramanuj & Mukherjee, Alok. (2015). Zeitschrift für Kristallographie - Crystalline Materials.
[3] Mürer, F.K., Chattopadhyay, B., Madathiparambil, A.S. et al. Sci Rep 11, 2144 (2021)

Acknowledgements: We thank the Research Council of Norway for financial funding through FRINATEK (#303252). ESRF—The European Synchrotron is thanked for beamtime at ID15A.

A043-06-270823

Orientation-dependent crystallographic properties in osteocyte -associated bone revealed by nano-scanning X-ray diffraction and fluorescence with a sub-50 nm X-ray beam

J. Palle[1], T. E. K. Christensen[1], N.K. Wittig[1], T. A. Grünewald[2,3], H. Birkedal[1]

[1]Department of Chemistry, iMAT and iNANO, Aarhus University, Aarhus, Denmark, [2] ESRF, Grenoble, France, [3]Aix-Marseille Univ., CNRS, Centrale Marseille, Institut Fresnel, Marseille, France.

hbirkedal@chem.au.dk

Keywords: Bone, Biomineralization, X-ray nanodiffraction

Bone has a complex hierarchical structure built mainly from mineralized collagen fibrils [1]. Bone is traversed by a cellular network of osteocytes that are housed in lacunae interconnected by a few-hundred nm diameter canaliculi [1-2]. It is known that the bone matrix close to osteocyte lacunae has a different protein composition than that further away, yet it has hitherto been assumed that bone biomineral has uniform crystallographic properties on sufficiently small length scales. Herein, we show the existence of orientation-dependent differences in bone biomineral crystallographic properties within a few μm from an osteocyte. Since the osteocyte is about 3-10 μm in diameter and the perilacunar matrix is also in the micron range, ultrahigh spatial resolution is required.

Previously, combined small angle X-ray scattering and wide angle X-ray scattering tensor tomography with a 1 μm voxel size indicated differences in orientation distributions between the biomineral crystallographic c-axis and bone nanostructure in localized areas of human lamellar bone even if most of the sampled material followed the expected co-alignment of the two [3]. X-ray diffraction and fluorescence tomography revealed spatially varying crystallographic properties on the ~10 μm length scale in human bone [4]. These results suggest that indeed, bone biomineralization may locally be more heterogeneous than hitherto believed.

To obtain sufficient spatial resolution, we conducted X-ray diffraction and fluorescence experiments with a sub 50 nm diameter X-ray beam building on previous work [5]. The data were collected at ID13 of the ESRF. We studied a ~4 μm thick human bone specimen that we raster scanned through the beam in two different projective views, i.e. sampling two different orientations of the sample with respect to the beam. Due to the preferred orientation of the bone crystals, each view provides information on different crystal populations from the same bone volume. We analysed each diffraction pattern by Rietveld refinement. Surprisingly, we find systematic differences in lattice constants and apparent crystallite sizes between the two views. Furthermore, we find differences between bone close to and further away from the osteocyte lacuna. This indicates that, on a sub 100 nm length scale, bone mineral crystallographic properties are dependent on the crystal orientation. We expect that this most likely reflect their relation to the collagen network and other non-collagenous proteins.

[2] Wittig, N. K. & Birkedal, H. (2022). *Acta Crystallogr. B* **78**, 305.

[3] Wittig, N. K., Østergaard, M., Palle, J. Christensen, T. E. K., Langdahl, B. Rejnmark, L., Hauge, E.-M., Brüel, A. Thomsen, J. S. & Birkedal, H. (2022). *J. Struct. Biol.* **214**, 107822.

[4] Grünewald, T. A., Liebi, M., Wittig, N. K., Johannes, A., Sikjaer, T., Rejnmark, L., Rosenthal, M., Guizar-Sicairos, Birkedal, H. & Burghammer, M. (2020). *Science Advances*, **6**, eaba4171.

[5] Wittig, N. K., Palle, J., Østergaard, M., Frølich, S., Birkbak, M. E., Spiers, K., Garrevoet, J. & Birkedal, H. (2019). *ACS Nano*, **13**, 12949.

[6] Palle, J., Wittig, N. K., Kubec, A., Niese, S. Rosenthal, M., Burghammer, M. Grünewald, T. & Birkedal, H. (2020). *J. Struct. Biol.*, **212**, 107631.

We acknowledge the European Synchrotron Radiation Facility for provision of synchrotron radiation facilities and we would like to thank Manfred Burghammer for assistance in using beamline ID13. We thank Dr. Maria Francesca Di Filippo for assistance during the experiment at ID13.

A048 Functionality from Broken Inversion Symmetry
Room 216
1.10pm - 3.30pm

A048-01-270823

The structure of a ferroelectric, commensurate low temperature phase of YMn_2O_5

T. Weigel[1], C. Richter[2], M. Nentwich[3], Dirk C. Meyer[1], M. Zschornak[1]

[1]Institute of Experimental Physics, TU Bergakademie Freiberg, 09596 Freiberg, Germany), [2]Leibniz-Institut für Kristallzüchtung, 12489 Berlin, Germany, [3]DESY Photon Science, Deutsches Elektronensynchrotron, 22607 Hamburg, Germany

Tina.weigel@physik.tu-freiberg.de

Keywords: Resonant X-ray Diffraction, ferroelectricity, sub-pm resolution

The material system YMn2O5 has several low temperatures phases, where magnetism and ferroelectricity occur. Especially, the origin of ferroelectricity (see Fig.1) in the commensurate phase is an open question. Literature agrees upon a magnetically driven principal mechanism from changes in the Mn spin configuration, which may be based either on magnetostriction due to symmetric exchange [1], the antisymmetric inverse Dzyaloshinskii-Moriya interaction [2] or a combination of the two [3]. Both mechanisms are accompanied by specific atomic displacements of ions in the structure. The space group *Pbam* (55) of the paraelectric phase does not allow the respective polar displacements and a refinement of the charge structure in a lower symmetric phase has not been successful so far, mostly because conventional structure analysis lacks the sensitivity required to resolve the expected positional displacements [4].

We applied the new *Resonantly Suppressed Diffraction* (RSD) [5] method, which is sensitive to minuscule structural changes in the sub-pm range, in order to resolve potential ionic displacements within a polar space group and shed new light on this controversial discussion. The method is based on the destructive interference of structure factors causing the intensity of a Bragg reflection to approach zero.

We measured the energy dependent RSD spectra of carefully selected reflections above and below the phase transition temperature *T*CM = 39 K. With the data above *T*CM, we refined the static and dynamic displacements (see Fig. 2) of the paraelectric phase to receive an improved starting model for the structural characterization of the ferroelectric phase. With the improved starting model and the data below *T*CM we were able to refine the static displacements of the ferroelectric phase. Therefore, we can present the first structure refinement for the ferroelectric commensurate phase and and gain insight into the structural origin of ferroeletricity in YMn2O5.

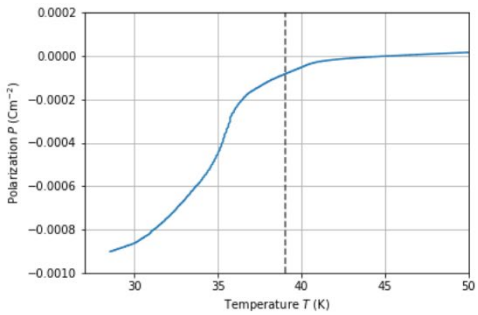

Figure 1. Measured spontaneous polarization of YMn_2O_5 below T_{CM} [1] 39 K along the crystallographic *b* direction. So far the origin of the polarization was not clear and could not be related to structural changes. Now, we can finally present the first structure refinement for the ferroelectric phase.

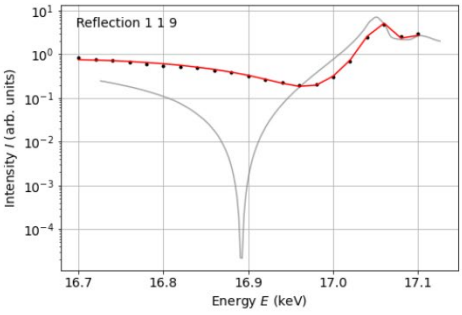

Figure 2. RSD spectra (black) of the 1 1 9 reflection above T_{CM}. Starting with a structure model from database (ICSD 165870) [6] the dynamic and static displacements have been refined, until the simulated curve (red) archived the best match with experimental data (black).

[2] C. Vecchini, L. C. Chapon, P. J. Brown, T. Chatterji, S. Park, S.-W. Cheong, and P. G. Radaelli (2008), *Phys. Rev. B*, **77**, 134434.
[3] L. C. Chapon, P. G. Radaelli, G. R. Blake, S. Park, and S.-W. Cheong (2006), *Phys. Rev. Lett*, **96**, 097601.
[4] A. B. Sushkov, R. Valdés Aguilar, S. Park, S.-W. Cheong, and H. D. Drew (2007), *Phys. Rev. Lett*, **98**, 027202.
[5] Y. Noda, H. Kimura, M. Fukunaga, S. Kobayashi, I. Kagomiya, and K. Kohn (2008), *J. Phys: Condens.Matter,* **20**, 434206.
[6] C. Richter, M. Zschornak, D. V. Novikov, E. Mehner, M. Nentwich, J. Hanzig, S. Gorfman, and D. C. Meyer (2018), *Nat. Commun*., **9**, 178.
[7] I. Kagomiya, K.-I. Kakimoto, and H. Ohsato (2010), *J. Eur. Ceram. Soc*., **30**, 255.

A048-02-270823

Time-resolved nanobeam x-ray diffraction of a relaxor ferroelectric single crystal under an alternating electric field

S. Aoyagi1, A. Aoyagi1, H. Takeda2, H. Osawa3, K. Sumitani3, Y. Imai3, S. Kimura3

Department of Information and Basic Science, Graduate School of Science, Nagoya City University, Nagoya 467-8501, Japan
Department of Applied Chemistry, Faculty of Engineering, Saitama University, Saitama 338-8570, Japan
Center for Synchrotron Radiation Research, Japan Synchrotron Radiation Research Institute, Sayo, Hyogo 679-5198, Japan

aoyagi@nsc.nagoya-cu.ac.jp

Keywords: Relaxor ferroelectrics, Time-resolved x-ray diffraction, Nanobeam x-ray diffraction

Lead-containing composite perovskites, $(1-x)Pb(Mg_{1/3}Nb_{2/3})O_3-xPbTiO_3$ (PMN-PT) and $(1-x)Pb(Zn_{1/3}Nb_{2/3})O_3-xPbTiO_3$ (PZN-PT), are well known as relaxor ferroelectrics and are widely used in many applications due to their excellent piezoelectric properties. Their piezoelectric constants and electromechanical coupling factors strongly depend on the $PbTiO_3$ (PT) fraction x and have a maximum value near the morphotropic phase boundary (MPB) that separates low-PT rhombohedral and high-PT tetragonal phases. It has been suggested that electric field-induced phase transitions involving polarization rotation and electric field responses of polar nano regions (PNRs) aiding the polarization rotation explain the enormous piezoelectric capabilities around MPB. The crystal with PNRs must have a heterogeneous structure in which the lattice is locally strained. The structural responses of the heterogeneous local lattice strain to an electric field are crucial to understanding the giant piezoelectric properties of relaxor ferroelectric perovskites. In this study, we used time-resolved scanning nanobeam x-ray diffraction (XRD) of a single-crystal PMN-PT with $x = 0.30$ (PMN-30PT) under an alternating electric field to show the position and time dependences of the local lattice strain in relaxor ferroelectric perovskites under an alternating electric field [1].

We performed three kinds of XRD experiments on PMN-30PT single crystals: (1) time-resolved XRD for the average structure under an AC field with the frequency of 2.6 kHz, (2) time-resolved nanobeam XRD for the local structure under an AC field with the frequency of 2.0 kHz, and (3) nanobeam XRD for the local structure under a DC field. The time-resolved XRD for the average structure was performed at the beamline BL02B1 of a SPring-8 large synchrotron radiation facility. The x-ray wavelength and beam size were 0.30 Å and 0.2 mm, respectively. The nanobeam XRD for the local structure was performed at the beamline BL13XU of SPring-8. The x-ray wavelength and beam size were 1.55 Å and 430 (horizontal) × 190 (vertical) nm^2, respectively.

The time dependences of the 006 Bragg peak under the AC field along [001] measured for the average structure of PMN-30PT are similar to those of PZN-PT with $x = 0.045$ reported previously [2]. The time dependences of the Bragg intensity distribution, under the AC field, measured for local areas of PMN-30PT are quite different from those measured for the average structure, and show strong position dependences. The results demonstrate that the crystal has a heterogeneous structure consisting of nanodomains with various lattice constants, and orientations exhibiting different electric field responses as the translation symmetry is broken down from nano to microscale pieces. The nano-to-microscale heterogeneous crystal structure, with its widely and continuously distributed local lattice strain, would enable the enormous electric field-induced lattice strain and fatigue-free polarization switching. Dynamic intensity redistributions attributed to reorientations of the nanodomains, which cannot be observed under DC fields [3], were observed in the time-resolved nanobeam XRD under the AC field. The dynamic motion of the nanodomains in the heterogeneous structure relaxes a lattice mismatch of the ferroelectric domains, and should contribute to the enormous electric field induced lattice strain, and the fatigue-free polarization switching.

[1] Aoyagi, S., Aoyagi, A., Takeda, H., Osawa, H., Sumitani, K., Imai, Y. & Kimura, S. (2021). *Crystals* **11**, 1419.
[2] Aoyagi, S., Aoyagi, A., Osawa, H., Sugimoto, K., Nakahira, Y., Moriyoshi, C., Kuroiwa, Y. & Iwata, M. (2020). *Phys. Rev. B* **101**, 064104.
[3] Aoyagi, S., Aoyagi, A., Takeda, H., Osawa, H., Sumitani, K., Imai, Y. & Kimura, S. (2022). *Phys. Rev. B* **105**, 024101.

This work was supported by a Grant-in-Aid for Scientific Research from the Japan Society for the Promotion of Science (JSPS) (Grant Nos. JP16K05017, JP19H02797, and JP20H05879), Tatematsu Foundation, Toyoaki Scholarship Foundation, and Daiko

Foundation. This work was supported by the Research Equipment Sharing Center at the Nagoya City University. The synchrotron radiation experiments were performed at SPring-8 with the approval of the Japan Synchrotron Radiation Research Institute.

A048-03-270823

Large nonreciprocal optical responses in antiferromagnets with broken space-inversion and time-reversal symmetries

K. Kimura

Osaka Metropolitan University, Gakuencho 1-1, Naka-ku, Sakai, Osaka 599-8531, JAPAN
kentakimura@omu.ac.jp

Keywords: Nonreciprocal optical responses, Magnetoelectric materials, Antiferromagnet

Materials with broken space-inversion and time-reversal symmetries, such as magnetoelectric materials and chiral-lattice magnets, can exhibit variety of unconventional phenomena. A prominent example of such phenomena is the so-called nonreciprocal directional dichroism (NDD), that is, the difference in light absorption between two counter-propagating light beams [1,2]. The NDD has attracted considerable attention, for example in view of potential applications for novel nonreciprocal optical devices allowing the control of light propagation. Intensive studies in the past few decades have led to observations of NDD in many materials and broad wavelength regions [1-6]. However, reported NDD signals in the visible to near-infrared light regions are usually small [5] or require high magnetic fields to amplify the magnitude [4,6].

In my talk, after introducing fundamental features of NDD and previous studies, I will show our strategy to explore magnetoelectric materials showing large NDD signals in the visible to near-infrared regions. Then, I will present our recent achievements of the discovery of large visible-light NDD signals in a magnetoelectric antiferromagnet Bi_2CuO_4 [7]. Unlike most of previous observations, the large NDD signals of this material emerge spontaneously without external fields. Moreover, by switching multiple antiferromagnetic domains in this material with an external field, we have succeeded in demonstrating a highly unique magneto-optical functionality, that is, the three-level control of optical transparency. Finally, the results of even larger NDD signals in the near-infrared region in other magnetoelectric antiferromagnets will also be presented.

[1] Rikken, G. L. J. A., Raupach, E. (1997). *Nature*, **390**, 493.
[2] Arima, T. (2008). *J. Phys.: Condens. Matter*, **20**, 434211.
[3] Kézsmárki, I., Szaller, D., Bordács, S., Kocsis, V., Tokunaga, Y., Taguchi, Y., Murakawa, H., Tokura, Y., Engelkamp, H., Rõõm, T. (2014). *Nat. Commun.* **5**, 3203.
[4] Toyoda, S., Abe, N., Kimura, S., Matsuda, Y. H., Nomura, T., Ikeda, A., Takeyama, S., Arima, T. (2015). *Phys. Rev. Lett.* **115**, 267207.
[5] Sato, T., Abe, N., Kimura, S., Tokunaga, Y., Arima, T. (2020). *Phys. Rev. Lett.* **124**, 217402.
[6] Yokosuk, M. O., Kim, H.-S., Hughey, K.D., Kim, J., Stier, A. V., O'Neal, K.R., Yang, J. Crooker, S.A., Haule, K., Cheong, S.-W., Vanderbilt, D., Musfeldt, J. L. (2020). *npj Quantum Mater.* **5**, 20.
[7] Kimura, K., Otake Y., Kimura, T. (2022). Nat. Commun. **13**, 697.

This work was done in collaboration with Mr. Y. Otake, Mr. M. Moromizato, Mr. K. Hattori, and Prof. T. Kimura (The University of Tokyo). This work was supported by JSPS KAKENHI Grant Numbers JP19H01847, JP19H05823, JP21H04436, and JP21H04988, from the MEXT Leading Initiative for Excellent Young Researchers (LEADER), and from The Murata Science Foundation.

A048-04-270823

Ferroelectricty and ferroelasticity in halide perovskites: can one exist without the other?

J. Breternitz 1,2 S. Schorr 2,3

1 Münster University of Applied Sciences, Department Chemical Engineering, Stegerwaldstraße 39, 48565 Steinfurt; 2 Helmholtz-Zentrum Berlin für Materialien und Energie, Structure and Dynamics of Energy Materials, Hahn-Meitner-Platz 1, 14109 Berlin, Germany; 3 Freie Universität Berlin, Departement Geosciences, Malteserstraße 74-100, 12249 Berlin, Germany

Joachim.breternitz@helmholtz-berlin.de

Keywords: Solar cell materials, halide perovskites, non-centrosymmetric structures

Halide perovskite solar cell materials hardly need any introduction anymore. Since their first implementation in solar cells in 2009,[1] their efficiency rocketed to 25.7 % in 2022.[2] While it is possible to produce highly efficient halide perovskite solar cells, the fundamental understanding of the underlying physical processes is still incomplete and sometimes doubtful.

Ferroelectric distortion of the perovskite structure was postulated as one of the reasons for the high efficiency of halide perovskite solar cells and a fierce debate on potential ferroelectricity of $MAPbI_3$ as the prototype halide perovskite is still not fully settled. From a crystallographic point-of-view, a polar crystal structure is a necessary prerequisite for ferroelectricity, but the standard crystal structure of $MAPbI_3$ at room temperature is given in the space group *I*4/*mcm* – which is a centrosymmetric space group not allowing for ferroelectricity. We show that a deviation of the iodide positions caused by attractive interaction with the methylammonium cations can cause a breaking of the centre of symmetry and hence allow ferroelectricity in this material (fig. 1).[3]

Furthermore, many of the studies on ferroelectric effects in $MAPbI_3$ are impacted by their synthesis at temperatures above the tetragonal-to-cubic phase transition, which means that they undergo a ferroelastic phase transition.[4] We aim to provide a guide to the audience as to how ferroelastic and ferroelectric effects may overlay each over and impact the experimental evidences of one another, especially through twinning present for both.[5]

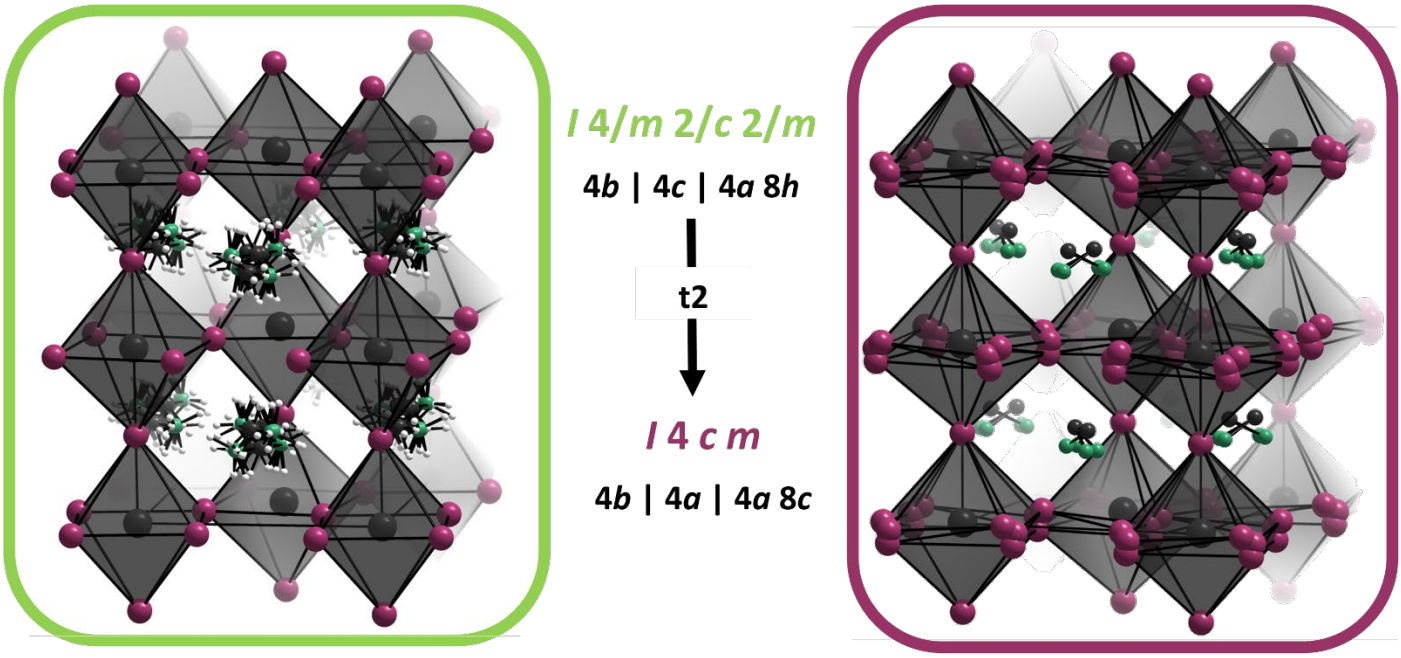

Figure 1: Comparison of the centrosymmetric (left) and non-centrosymmetric models of $MAPbI_3$ at room temperature and their group-subgroup relationship.

[1] Kojima, A., Teshima, K., Shirai, Y. & Miyasaka, T. (2009). *J. Am. Chem. Soc.* **131**, 6050–6051.
[2] Best Research-Cell Efficiency Chart https://www.nrel.gov/pv/cell-efficiency.html.
[3] Breternitz, J., Lehmann, F., Barnett, S. A., Nowell, H. & Schorr, S. (2020). *Angew. Chem. Int. Ed.* **59**, 424–428.
[4] Breternitz, J. (2022). *Z. Kristallogr. – Cryst. Mater.* **237**, 135–140.
[5] Breternitz, J., Tovar, M. & Schorr, S. (2020). *Sci. Rep.* **10**, 16613.

A048-05-270823

Driving forces and phase behaviour in MDABCO-based ferroelectric perovskites

S. D. Gale1, H. J. Lloyd1,2, L. Male1, M. R. Warren2, L. K. Saunders2, P. A. Anderson1, H. H.-M. Yeung1

School of Chemistry, University of Birmingham, UK, Diamond Light Source, Harwell Science and Innovation Campus, UK

H.Yeung@bham.ac.uk

Keywords: perovskite, ferroelectric, MDABCO

Perovskites, such as the canonical ferroelectric BaTiO3, have long been considered state-of-the-art in design of new FE materials owing to desirable properties and tunability of their composition. The recent discovery of a new subset of hybrid organic– inorganic perovskites based on the A-site MDABCO dication (MDABCO = N-methyl-N′-diazabicyclo[2.2.2]octonium) has led to renewed interest in hybrid inorganic–organic ferroelectric materials, owing to their properties that are comparable to BaTiO3. [MDABCO]NH4I3, in particular, has a large spontaneous polarization, high phase transition temperature and facile switching through eight possible polarisation directions.[1]

Until recently, only a handful of compositions of MDABCO-based perovskites had been reported and the driving forces that underpinned the emergence of spontaneous polarisation were poorly understood. In 2021 we showed using coarse-grained and atomistic models that the key factors driving spontaneous polarisation include orientation of the MDABCO dipole moment along the pseudo-cubic 〈111〉 direction, strain coupling and dipolar interactions.[2] Hydrogen bonding was also thought to be important in determining the magnitude of polarisation and coercive field; however, its influence on phase transitions to the high-symmetry centrosymmetric phase remained unclear.

This presentation discusses some of our work on the discovery of new [MDABCO]BX3 compositions (Fig. 1), where B is an alkali metal cation and X is a halide anion, and its implications for the design of new MDABCO-based perovskites.[3] We show that new phases can help to define compositional limits for the pseudo-cubic perovskite structure vs. competing structures, such as hexagonal forms. In addition, access to a wider range of compositions enables us to determine correlations between a variety of structural features and phase transition temperatures, which point towards key design principles for new ferroelectric materials.

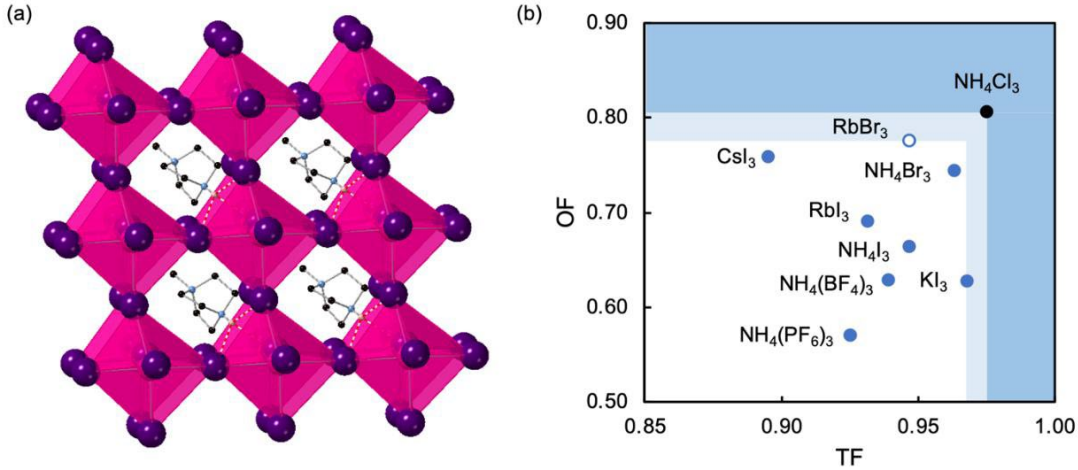

Figure 1. (a) Crystal structure of [MDABCO]CsI_3, showing Cs, C, H, N and I as pink, black, light pink, blue and purple, respectively (H atoms bonded to C are not shown for clarity), and (b) plot of the octahedral factor (OF) vs. Goldschmidt tolerance factor (TF) for structures with compositions [MDABCO]BX_3, showing B- and X-site compositions. Blue circles are pseudo-cubic perovskites and the black circle is the hexagonal-type structure, which defines upper limits of ranges for pseudo-cubic perovskite formation, 0.97 < TF < 0.98 and 0.78 < OF < 0.81, shown in light blue. Darker blue shaded regions lie above these limits.

[1] H.-Y. Ye , Y.-Y. Tang , P.-F. Li , W.-Q. Liao , J.-X. Gao , X.-N. Hua , H. Cai , P.-P. Shi , Y.-M. You and R.-G. Xiong, *Science*, 2018, **361**, 151–155.
[2] D. J. W. Allen , N. C. Bristowe , A. L. Goodwin and H. H.-M. Yeung, *J. Mater. Chem. C*, 2021, **9**, 2706.
[3] S. D. Gale, H. J. Lloyd, L. Male, M. R. Warren, L. K. Saunders, P. A. Anderson and H. H.-M. Yeung, *CrystEngComm* 2022, **24**, 7272–7276.

A057 Crystal and Magnetic Structures of Novel Perovskites
Room 217
1.10pm - 3.30pm

A057-01-270823

Cation ordered doping of ferrite perovskites: influence on redox behaviour, magnetism, and mixed ionic electronic conductivity

A.J. Brown[1], O. Wagstaff[2], A. Manjón-Sanz[3], H. Brand[4], M. Avdeev[1,4], I. Evans[2], C.D. Ling[1]

School of Chemistry, The University of Sydney, NSW 2006, Australia., 2. Neutron Scattering Division, ORNL, Oak Ridge, Tennessee United States, 3. Australian Synchrotron, 800 Blackburn Rd Clayton, VIC Australia, 4. Australian Centre for Neutron Scattering, ANSTO Lucas Heights, NSW Australia., 5. Department of Chemistry, Durham University, Science Site, South Road, Durham, U.K.

The corresponding author e-mail: chris.ling@sydney.edu.au

Keywords: ferrites, magnetism, cation-ordered, phase transitions, redox

The Ba3LnFe2O7.5 family of compounds are oxygen-deficient perovskites the structures of which can be described as ordered arrays of corner-linked LnO6 octahedra and FeO4 tetrahedra on the perovskite B-sites.[1, 2] Reports of magnetic properties of these compounds have been mixed. The initial study of Ba3YFe2O7.5 found no evidence for long-range magnetic order down to 5 K; however, subsequent studies found they do show low-temperature magnetic order.[1, 2] The Ba3LnFe2O7.5 family therefore present a good opportunity to study complex magnetic interactions between magnetic Ln^{3+} 4f and Fe^{3+} 3d cations. We made the Y and Dy compositions with this structure and observed long-range antiferromagnetic order at TN = 6 and 14 K respectively. The magnetic structures for both the Y and Dy compositions were determined using neutron powder diffraction (e.g. figure 1(a)). The Dy composition also shows evidence for metamagnetism with field-dependant hysteresis below TN (figure 1(b)). Ab initio density functional theory (DFT) calculations comparing the energies of different magnetic structures support our experimental data.

Additionally, at high temperatures (above 500 K) we found that these materials undergo multiple redox-associated phase transitions and show high mixed ionic-electronic conductivity. We used variable temperature in situ synchrotron X-ray diffraction to investigate the phase transitions. At approximately 500-600 K (depending on the Ln^{3+} cation), Ba3LnFe2O7.5 compounds undergo first-order phase transitions to an orthorhombic phase. The phase transition is correlated with an uptake of oxide ions into lattice vacancies accompanied by the partial redox of Fe^{3+} to Fe^{4+}. Impedance spectroscopy measurements show that these phases also have high total conductivities (>10^{-2} S.cm^{-1} at 773 K), making them very promising as mixed oxide-ionic and electronic conductors.

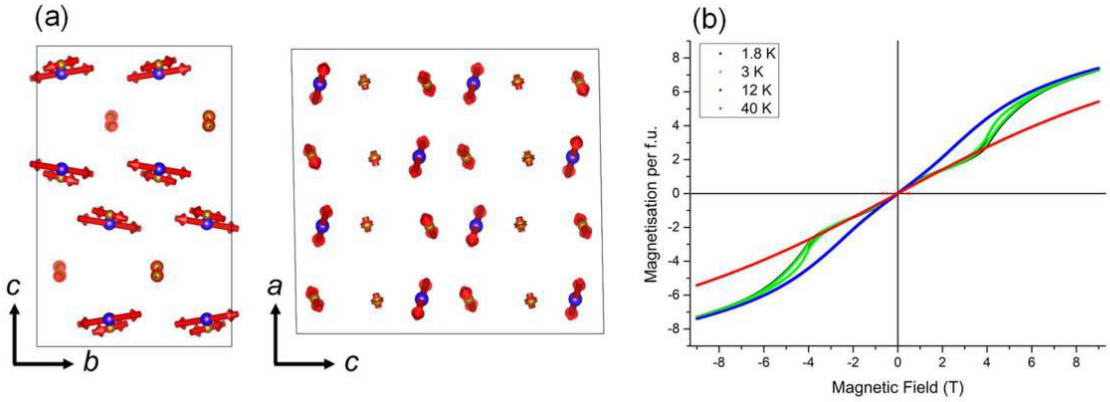

Figure 1. (a) The magnetic structure of $Ba_3DyFe_2O_{7.5}$ at 2 K determined from neutron powder diffraction, Dy atoms blue and Fe atoms brown. (b) Isothermal magnetisation measurements of $Ba_3DyFe_2O_{7.5}$ demonstrating metamagnetic behaviour

[3] K. Luo and M. A. Hayward, Inorganic chemistry 51 (22), 12281-12287 (2012).
[4] A. K. Kundu, et al., Journal of Materials Chemistry C 5 (29), 7236-7242 (2017).

This work was supported by an Australian Government Research Training Stipend. We thank the Australian Nuclear Science and Technology Organisation for providing access to the Australian Synchrotron (PD) and Australian Centre for Neutron Scattering (Echidna) beamlines. We also thank Oak Ridge National Laboratory for beamtime on POWGEN.

A057-02-270823

Nontrivial magnetic structures in cubic quadruple perovskites

Y. Shimakawa, T. Saito, M. Amano Patino, F. Denis Romero

Institute for Chemical Research, Kyoto University, Uji, Kyoto 611-0011, Japan

shimak@scl.kyoto-u.ac.jp

Keywords: A-site magnetism, quadruple perovskites, magnetic interactions

Quadruple perovskite structure oxides with a chemical formula AA' 3B4O12 can accommodate transition -metal ions at both A' and B sites. When the B site is occupied by non-magnetic cations, the magnetic interactions between the spins at the orthogonally-oriented A'-sites provide a variety of nontrivial magnetic structures in the cubic symmetry sublattices. CaCu3Ge4O12 and CaCu3Sn4O12 show ferromagnetism of the A'-site Cu^{2+} ($S = 1/2$) spins due to Cu–Cu direct-exchange interaction, whereas CaCu3Ti4O 12 shows the G-type antiferromagnetim, where the antiferromagnetic Cu–O–Ti–O–Cu superexchange interaction overcomes the Cu–Cu direct-exchange interaction. In the solid solution system of CaCu3(Ge-Ti-Sn)4O12, very unusual ferromagnetic-antiferromagnetic-ferromagnetic spin -structure change was observed [1,2]. In LaMn3V4O12, on the other hands, the nearest neighboring Mn^{2+} high spins ($S = 5/2$) align with each other with an angle of 120 degrees. The electrons of V at the B site are delocalized and do not apparently contribute to the magnetic behavior [3]. In CaFe3Ti4O12 and CaCo3Ti4O12 with respectively the A'-site Fe^{2+} ($S = 2$) and Co^{2+} ($S = 3/2$) spins, the magnetic structures consist of three interpenetrating mutually orthogonal magnetic sublattices. The fourth nearest neighbour spin exchanges as well as spin orbit coupling play an essential role for stabilizing the unusual spin structures [4,5].

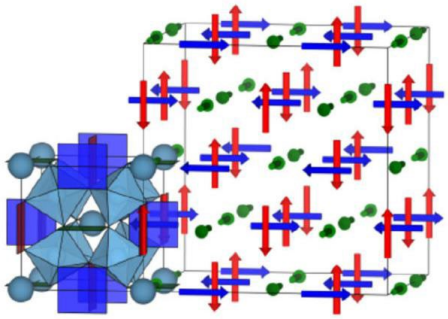

Figure 1. Co^{2+} ($S = 3/2$) spin structure in A-site ordered quadruple perovskite $CaCo_3Ti_4O_{12}$.

[1] Y. Shimakawa, H. Shiraki, and T. Saito, *J. Phys. Soc. Jpn.*, **77**, 113702 (2008).
[2] Y. Shimakawa and T. Saito, *Physica Status Solidi B*, **249**, 423-434 (2012).
[3] T. Saito, M. Toyoda, C. Ritter, S. Zhang, T. Oguchi, J. P. Attfield, and Y. Shimakawa, *Phys. Rev. B*, **90**, 214405/1-6 (2014).
[4] M. Amano Patino, F. D. Romero, M. Goto, T. Saito, F. Orlandi, P. Manuel, A. Szabo, P. Kayser-Gonzalez, K. H. Hong, K. Alharbi, J. P. Attfield, and Y. Shimakawa, *Phys. Rev. Resear.,* **3**, 043208/1-8 (2021).
[5] M. Amano Patino, F. Denis Romero, H. -J. Koo, M. Avdeev, S. D. A. Injac, M. Goto, M. -H. Whangbo, and Y. Shimakawa, *Commun. Mater.*, **3**, 51/1-7 (2022).

A057-03-270823

Studies of magnetism in novel perovskites from double perovskites with 5d ions to hybrid layered perovskites with the Ruddlesden-Popper structure

P. M. Woodward, V. da Cruz Pinha Barbosa, N. P. Holzapfel

Department of Chemistry and Biochemistry, The Ohio State University, Columbus, OH, USA

Woodward.55@osu.edu

Keywords: perovskites, magnetic ordering, halide perovskites, phase transitions

The magnetism of compounds with the perovskite structure has a rich history. Important advances in our understanding of magnetism came from studies of oxide perovskites containing transition metal ions. Interestingly the magnetism of oxides with transition metal ions with partially filled 5d orbitals differ from their 3d counterparts in several fundamental ways: (1) the 5d orbitals extend further from the nucleus which can lead to unexpectedly strong superexchange interactions, (2) for similar electron configurations the spin-orbit coupling of 5d ions is much stronger, and (3) competing magnetic ground states in 5d transition metal oxides are very sensitive to distortions of the lattice. Over the past several years we have studied the magnetism of a family of compounds containing either rhenium or osmium. These studies show how changes in the 5d electron count of double perovskites and relatively subtle crystallographic distortions alter the magnetic exchange interactions and thereby influence the competition between competing magnetic ground states. The balance between ferromagnetic and antiferromagnetic order is particularly sensitive to structural distortions for compounds containing ions with a $5d^1$ configuration. In the second half of the talk I will discuss the magnetism of hybrid layered halide perovskites with stoichiometry A_2MX_4. These compounds consist of layers of corner connected metal halide octahedra separated by A-site cations that are protonated primary amines. While the intralayer magnetic interactions follow the behavior expected from conventional superexchange — antiferromagnetic coupling for M = Mn^{2+} and ferromagnetic for M = Cu^{2+} — the coupling between the layers depends on the nature of layer stacking and octahedral tilting. The structural distortions of these compounds are driven by a combination of hydrogen bonding between organic cations and the inorganic layers as well as packing considerations between organic molecules

A057-04-270823

Low-dimensional magnetism in ordered perovskite and Ruddlesden-Popper variants

Ryan Morrow,[1] Anastasiia Smerechuk,[1] Tamara Holub,[1] Sabine Wurmehl,[1] and Bernd Büchner[1]

Leibniz Institute for Solid-State and Materials Research, IFW-Dresden, 01069 Dresden, Germany

r.c.morrow@ifw-dresden.de

Keywords: Perovskites, magnetism, transition metal oxides

Perovskites and their myriad of structural permutations have long been studied for their intriguing properties and interplay of degrees of freedom, both chemical and physical. While generally three dimensional in nature, perovskites can provide multiple means of access to low dimensional properties as well. In this talk, new results in three different directions pertaining to this concept will be presented. The first, most common approach, is the use of the Ruddlesden-Popper and similar phases, which separate perovskite-like layers with interlaced AO layers, rendering them primarily two dimensional. Several new cation-ordered iridate and rhodate Ruddlesden-Popper phases will be presented. The second approach is that of orbital order using Cu^{2+} in the double perovskite structure to yield in-plane only square lattice like magnetic interactions (e.g. Ba_2CuWO_6). New compounds produced by substitution series and high pressure methods will be shown. The third is that of vacancy ordering. By ordering of vacancies in combination with cation ordering, hexagonal perovskite phases can be reduced to well separated triangular two dimensional magnets with variable spin sizes and frustration. Again, new compounds will be shown. In all three directions, primarily crystallographic and magnetometry data on these new inorganic transition metal oxides will be presented.

A057-06-270823

New perovskites from high pressure synthesis

J. Paul Attfield

Centre for Science at Extreme Conditions and School of Chemistry, University of Edinburgh, Edinburgh EH9 3JZ, UK. j.p.attfield@ed.ac.uk

Keywords: Perovskite, High Pressure, Powder Diffraction

Perovskite is a dense structure so new and unusual examples may be synthesised at high pressure. Among simple ABO_3 types, high pressure can stabilise unusual oxidation states, such as Ru^{3+} in $YRuO_3$ which shows a novel quantised weak ferromagnetism [1], and unusual coordinations such as Mn^{2+} at A-sites of $MnVO_3$ [2] with helimagnetic spin order.

Many cation-ordered superstructures are accessible such as new A-site Mn double perovskites (DPv's). Mn_2FeReO_6 is notable for having a high Curie temperature (~500 K) and a frustation-induced switching of magnetoresistance at low temperatures [2]. A new double double perovskite (DDPv) type with 1:1 order of A and B site cations is found in $MnRMnSbO_6$, $CaMnFeReO_6$ and related materials synthesised at ~10-12 GPa pressure [3,4]. This structure has a robust tetragonal $P4_2/n$ symmetry with columnar order of A/Mn cations and rocksalt-type B/B' ordering. Ferro-, ferri-, and antiferromagnetic orders as well as spin glass ground states are observed across various DDPvs. Some materials exhibit both fully-ordered $AA'BB'O_6$ DDPv and A-disordered $(A_{0.5}A'_{0.5})_2BB'O_6$ DPv polymorphs (Fig. 1), and for $CaMnMnWO_6$ this leads to an interesting switch from ferrimagnetism in the DDPv polymorph to a spin glassy behaviour in the more frustrated DPv form [5]. The first non-Mn based DDPv, ferromagnetic $CaCuFeReO_6$, has recently been synthesised at 15.5 GPa [6], suggesting that the DDPv's reported to date are only the 'tip of the iceberg' of a large high pressure perovskite family.

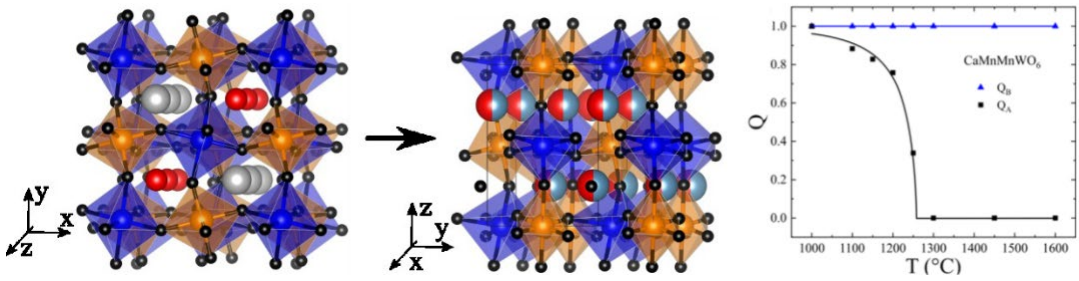

Figure 1. $CaMnMnWO_6$ transforms under 10 GPa pressure from a fully-ordered double double perovskite (DDPv) to a double perovskite (DPv) polymorph with disordered Ca/Mn A-site cations. Cation occupancy order parameters Q from powder X-ray refinements averaged over the DDPv and DPv structures are plotted against synthesis temperature with a modified mean-field fit to the A-site order parameter shown. [5]

High pressure is also good for suppressing loss of volatile elements such as nitrogen, and a method using sodium azide to synthesise nitrides in high oxidation states has recently been developed [7], giving a rare example of a nitride perovskite, LaReN3 [1]. This can be decomposed to give LaReN2.5 and layered LaReN2, the first examples of anion-vacancy ordered nitride perovskites demonstrating topotactic reduction chemistry analogous to that of well-known oxides like LaNiO3 and SrFeO3.

[2] K. Ji, A. Paul, E. Solana-Madruga, A.M.Arevalo-Lopez, U.V.Waghmare & J.P. Attfield (2020). *Phys. Rev. Mat.* **4**, 091402(R).
[3] M. Markkula, A.M. Arevalo-Lopez, A. Kusmartseva, J.A. Rodgers, C. Ritter, H. Wu & J.P. Attfield (2011). *Phys. Rev. B* **84**, 094450.
[4] E. Solana-Madruga, Á. M. Arévalo-López, A. J. Dos Santos-García, E. Urones-Garrote, D. Ávila-Brande, R. Sáez-Puche & J. P. Attfield (2016). *Angew. Chem. Int. Ed.* **55**, 9340.
[5] G. M. McNally, Á. M. Arévalo-López, P. Kearins, F. Orlandi, P. Manuel & J. P. Attfield (2017). *Chem. Mat.* **29**, 8870.
[6] K. Ji, K. N. Alharbi, E. Solana-Madruga, G. T. Moyo, C. Ritter & J. P. Attfield (2021). *Angew. Chem. Int. Ed.*, **60**, 22248.
[7] E. Solana-Madruga, P.S. Kearins, C. Ritter, Á.M. Arévalo-López & J.P. Attfield (2022). *Angew. Chem. Int. Ed.* **61**, e2022094.
[8] S. D. Kloß, A. Haffner, P. Manuel, M. Goto, Y. Shimakawa & J. P. Attfield (2021), *Nat. Commun.*, **12**, 571.
[9] S. D. Kloß, M. L. Weidemann, J. P. Attfield (2021), *Angew. Chem. Int. Ed.*, **60**, 22260.

A069 Structural chemistry at the interface of diffraction, nuclear magnetic resonance and other spectroscopic and computational tools
Room 209
1.10pm - 3.30pm

A069-01-270823

Asymmetric synthesis using chiral-at-metal complexes as catalysts – Underpinning molecular understanding through diffraction & NMR spectroscopy

F.J. Lahoz, P. García-Orduña. R. Rodríguez, A. Tejero, F. Viguri, D. Carmona

Instituto de Síntesis Química y Catálisis Homogénea (ISQCH), CSIC-Universidad de Zaragoza.

Pedro Cerbuna 12, 50009 Zaragoza (Spain)

lahoz@unizar.es

Keywords: Homogeneous catalysis, Metal complexes, Asymmetric synthesis

Chiral metal complexes, an important tool in asymmetric synthesis, are constituted by the assemblies of ligands around a central metal atom, with the stereogenic element(s) located in the ligand and/or, less frequently, in the metal. The asymmetric induction is usually achieved by the coordination of the reagents to the metal atom. Our research group envisages a new approach in asymmetric catalysis, using the metal as the unique source of chirality.

In this context, the challenging control of the absolute configuration of chiral-at metal complexes has been efficiently achieved using tripodal tetradentate ligand LH (Fig. 1a). [1-3]. We have developed a synthetic route for the preparation of octahedral Ru(II) and Ru(III) complexes, bearing LH through a κ^4-*P,N,N',C* coordination model, where the relative configuration of the sp^3 nitrogen atom becomes predetermined by the configuration at the metal. In this communication we present the combined structural characterization of the cationic Ru(III) amido complex $[RuCl_2(\kappa^4$-*P,N,N',C*-LH$)]^+$ and the neutral Ru(II) imido compound $[RuCl_2(\kappa^4$-*P,N,N',C*-L$)]$, depicted in Fig.1b and 1c, respectively, through diffraction and NMR spectroscopies. The differences in catalytic performance of Ru(II) and Ru(III) species in dehydrogenation reactions have been rationalized form the structural information.

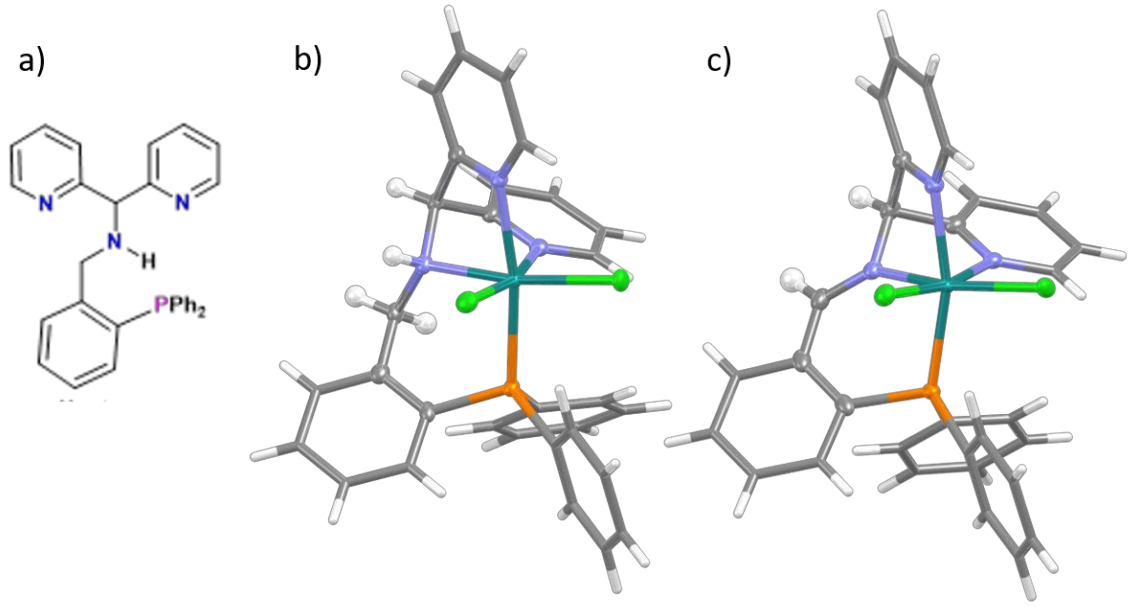

Figure 1. a) Tetradentade ligand LH b) Molecular structure of monocationic Ru(III) amido complex c) molecular structure of neutral Ru(II) imido complex.

[1] Carmona, M., Rodríguez, R., Passarelli, V., Lahoz, F. J., García-Orduña, P, Carmona D. (2018). *J. Am. Chem. Soc.***140**, 912.
[2] Téllez, J., Méndez, I., Viguri, F., Rodríguez, R., Lahoz F.J., García-Orduña, P, Carmona D. (2018). *Organomet.*, **37**, 3450.
[3] Tejero, A. G., Carmona M., Rodríguez R., Viguri F., Lahoz F.J., García-Orduña, P, Carmona D. (2022). *RSC Adv.*., **12**, 34704.

This work was supported by Ministerio de Ciencia, Innovación y Universidades, Agencia Estatal de Investigación de España, Fondo Europeo de Desarrollo Regional (CTQ2018-095561-BI00 and PID2021-122406NB-I00) and Gobierno de Aragón (Grupo de Referencia: Catálisis Homogénea Enantioselectiva). We also thank ALBA for provision of synchrotron radiation facilities (XALOC beamline, proposals 2020094580 and 2021095324).

A069-02-270823

Recent developments in cocrystal engineering via σ-hole interactions. Synergies from X-ray diffraction, solid-state NMR, and computational chemistry

David L. Bryce

Department of Chemistry and Biomolecular Sciences, University of Ottawa, Ottawa, ON K1N6N5, Canada

dbryce@uottawa.ca

Keywords: halogen bond, solid-state NMR, NMR crystallography

Non-covalent □-hole interactions, including e.g., halogen bonds, chalcogen bonds, pnictogen bonds, and tetrel bonds, offer a substantial range of cocrystal engineering opportunities in part owing to their tuneability and directionality. Simultaneously, the diversity of elements capable of acting as □-hole donor and acceptor atoms presents interesting opportunities and challenges for study via solid-state nuclear magnetic resonance, given the broad array of isotopic properties associated with these elements including their natural abundances, nuclear quadrupole moments, and magnetogyric ratios (e.g., ^{13}C, ^{15}N, ^{17}O, ^{19}F, ^{77}Se, ^{125}Te, ^{127}I, $^{121/123}$Sb, etc.). In this talk, I will provide a survey of our recent efforts to engineer, characterize, and understand the structural chemistry of several novel cocrystals featuring halogen bonds (Fig. 1), chalcogen bonds (Fig. 2), pnictogen bonds, and/or tetrel bonds [1-6]. Synthetic methods include slow evaporation, ball milling, gentle mechanochemical grinding, and resonant acoustic mixing. Efforts are made to understand the relationship between experimentally measured NMR and NQR parameters, e.g., quadrupolar coupling and chemical shift tensors, with the aid of advanced density functional theory computations and X-ray diffraction data. Such relationships can be difficult to quantify due to the important role of crystal packing effects and of relativity on the NMR parameters.

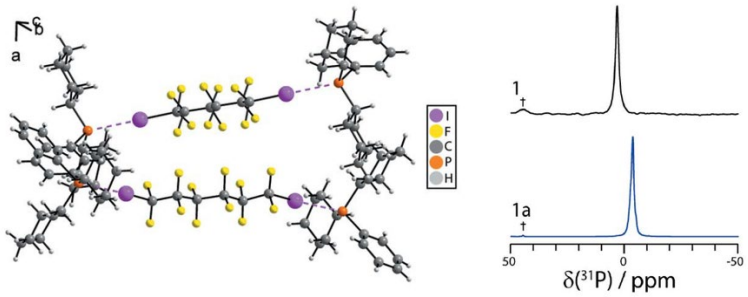

Figure 1. Cocrystal featuring phosphorus as a rare halogen bond acceptor (left) and diagnostic ^{31}P SSNMR shift (right) [4].

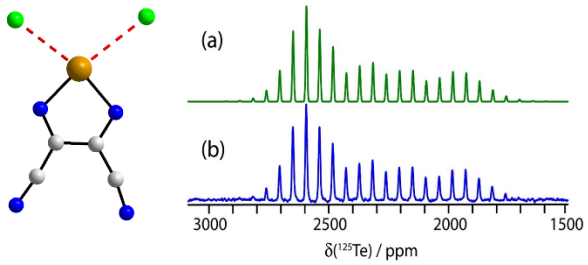

Figure 2. Novel chalcogen-bonded cocrystal structure (left) and diagnostic ^{125}Te magic-angle spinning NMR spectra [1].

[1] Nag, T., Ovens, J. S. & Bryce, D. L. (2022). *Acta Cryst. C.* **78**, 517. https://doi.org/10.1107/S2053229622008518
[2] Côté, M., Ovens, J. S. & Bryce, D. L. (2023). *Chem. Asian J.*, in press. https://doi.org/10.1002/asia.202201221
[3] Hajjar, C., Nag, T., Al Sayed, H., Ovens, J. S. & Bryce, D. L. (2022). *Can. J. Chem.* **100**, 245. https://doi.org/10.1139/cjc-2021-0245
[4] Zheng, D. N., Szell, P. M. J, Khiri, S., Ovens, J. S. & Bryce, D. L. (2022). *Acta Cryst. B* **78**, 557. https://doi.org/10.1107/S2052520622004322
[5] Kumar, V., Triglav, M., Morin, V.M. & Bryce, D. L. (2022). *ACS Org. Inorg. Au* **2**, 252. https://doi.org/10.1021/acsorginorgau.1c00051
[6] Southern, S. A., Nag, T., Kumar, V., Triglav, M., Levin, K. & Bryce, D. L. (2022) *J. Phys. Chem. C* **126**, 851. https://doi.org/10.1021/acs.jpcc.1c10121

A069-04-270823

Hyperpolarization of biomolecules in eutectic crystals at room temperature using photo-excited electron

M. Inukai[1], H. Sato[1], K. Miyanishi[2,3], M. Negoro[3,4], A. Kagawa[2,3], Y. Nishiyama[5,6], K. Nakamura[1]

[1]Graduate School of Technology, Industrial and Social Sciences, Tokushima University, Tokushima 770-8506, Japan, [2]Graduate School of Engineering Science, Osaka University, Toyonaka, Osaka 560-8531, Japan, [3]Center for Quantum Information and Quantum Biology, Osaka University, Toyonaka, Osaka 560-8531, Japan, [4]Institute for Quantum Life Science, National Institutes for Quantum and Radiological Science and Technology, Inage-Ku, Chiba 263-8555, Japan, [5]RIKEN CLST-JEOL Collaboration Center, Yokohama, Kanagawa 230-0045, Japan, [6]JEOL Resonance Inc., 3-1-2 Musashino, Akishima, Tokyo 196-8558, Japan

inukai.munehiro@tokushima-u.ac.jp

Keywords: eutectic crystal, microstructure, dynamic nuclear polarization

NMR spectroscopy is a non- invasive analytical method that provides the structure and dynamics in the materials, drugs, and biomolecules. However, the low sensitivity due to small spin polarization at thermal equilibrium restricts possible applications. Dynamic nuclear polarization (DNP) has been a powerful technique that utilize polarization of electron spins to dramatically increase the NMR signal intensities. DNP using the photo-excited triplet state (Triplet-DNP) have potential to provide highly sensitive NMR spectra at room temperature for various molecules; however, applicable molecules were very limited due to poor solubility of pentacene. Here, we focus on Triplet-DNP of eutectic crystals that are mixtures composed of two types of molecules.

We prepared eutectic crystals composed of pentacene (polarizer) doped benzoic acid (dBA) and biomolecules, including erythritol (ET), succinic acid (SUA), and caffein (CAF), as sugars, metabolites, and drugs, respectively (dBA-ET, dBA-SUA, and dBA-CAF). To confirm crystal structures, we performed powder XRD measurements. The all patterns showed no extra peaks and superposition of the patterns attributed to dBA and the analytes, indicating that the powders were eutectic crystals and the crystal structures of each domain were intact. We performed Triplet-DNP measurements at room temperature for dBA-ET, dBA-SUA, and dBA-CAF. Polarization ratio (P) and enhancement factors (ε) in a triplet-DNP process for 180 s were 0.091% and 6.8×10^2 times for dBA-ET, 0.10% and 7.8×10^2 times for dBA -SUA, and 0.017% and 1.3×10^2 times for dBA-CAF, respectively. Two dimensional ^{1}H -^{1}H exchange NMR experiments were performed at 14.1 T for dBA-ET and dBA-CAF under ultra-fast MAS to clarify the transfer magnetization from BA domain to the analyte domain. The spectra of dBA-CAF at mixing time = 10 s showed the cross peaks between CH3 of CAF and COOH of dBA. The cross peaks indicate magnetization transfer between each domain through spin diffusion. The appearance of cross peaks supports the diffusion of hyperpolarization from dBA domains to the analyte domains.

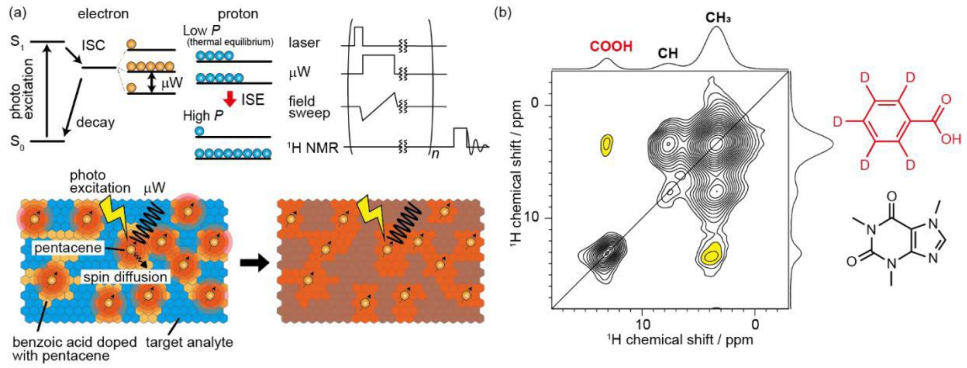

Figure 1. (a) Representation of hyperpolarization in eutectic crystals containing the domains of deuterated benzoic acid doped with pentacene (dBA) and the domains of the analyte. (b) 2D ^{1}H-^{1}H exchange NMR spectra for dBA-CAF. Cross peaks between dBA and CAF were high-lighted by yellow.

[1] Henstra, A.; Lin, T. S.; Schmidt, J.; Wenckebach, W. T. *Chem. Phys. Lett.* 1990, **165**, 6-10.

[2] Kagawa, A.; Negoro, M.; Ohba, R.; Ichijo, N.; Takamine, K.; Nakamura, Y.; Murata, T.; Morita, Y.; Kitagawa, *J. Phys. Chem. A* 2018, **122**, 9670-9675.
[3] Nishimura, K.; Kouno, H.; Kawashima, Y.; Orihashi, K.; Fujiwara, S.; Tateishi, K.; Uesaka, T.; Kimizuka, N.; Yanai, N, *Chem. Commun*. 2020, **56**, 7217-7232.

A069-05-270823

MAS DNP for the detection of crystal formation and polymorph transformations in molecular organics

M. Juramy[1], R. Chèvre[1], S.F. Cousin[1], N. Duong[1], F. Ziarelli[2], S. Viel[1], C.E. Hughes[3], A.C. Pinon,[4] K.D.M. Harris[3], P. Thureau[1], G. Mollica[1]

[1]Aix Marseille Univ, CNRS, ICR UMR 7273, Marseille, France, [2]Aix Marseille Univ, CNRS, Centrale Marseille, FSCM, Marseille, France, [3]School of Chemistry, Cardiff University, Cardiff, Wales, United Kingdom, [4]Swedish NMR Center, University of Gothenburg, Gothenburg, Sweden

giulia.mollica@univ-amu.fr

Keywords: NMR, solid, sensitivity, frozen solution, spin diffusion, polymorphism, crystallization, nucleation

Crystallization plays an important role in many areas of biology, chemistry and materials science, but the underlying mechanisms that govern crystallization are still poorly understood because of experimental limitations in the analysis of such complex, evolving systems. To derive a fundamental understanding of crystallization processes, it is essential to access the sequence of solid phases produced as a function of time, with atomic-level resolution. Rationalization of crystallization processes is particularly relevant for polymorphic functional materials, for which manufacture or storage-induced, unexpected, polymorph transitions can compromise the end-use of the solid product. Interestingly, these transformations often imply the formation of metastable forms. Today, detection and accurate structural analysis of these – generally transient – forms remain challenging, essentially because of the present limitations in temporal and spatial resolution of the analysis, preventing the rationalization – and hence the control – of crystallization processes.

In this contribution, I will show that cryogenic MAS NMR combined with the sensitivity enhancement provided by dynamic nuclear polarization (DNP) can be an efficient way of monitoring the structural evolution of crystallizing solutions with atomic-scale resolution on a time scale of a few minutes. I will discuss current approaches and recent developments allowing to detect, stabilize, and characterize transient, metastable phases formed at the early stages of crystallization as well as to identify and characterize the incipient emergence of new polymorphs in the bulk and under confinement [1-2].

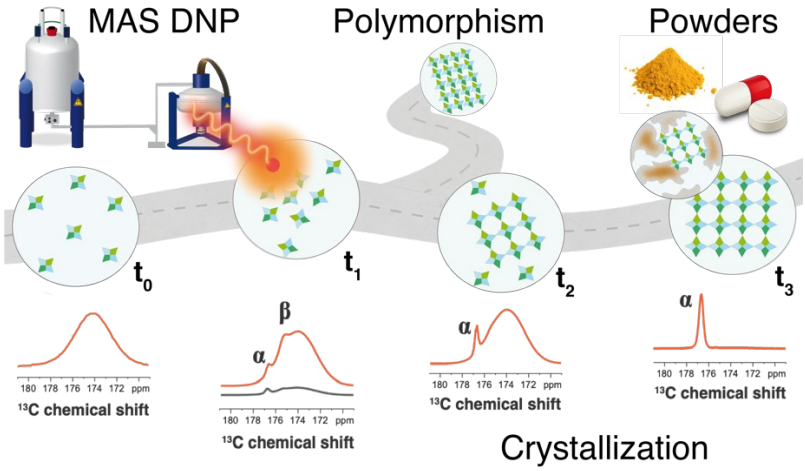

Figure 1. Time-resolved snapshots of crystallization can be detected using MAS DNP in the bulk and under confinement.

[1] Juramy, M., Chèvre, R., Cerreia-Vioglio, P., Ziarelli, F., Besson, E., Gastaldi, S., Viel, S., Thureau, P., Harris, K.D.M. & Mollica, G. (2021). *J. Am. Chem. Soc.***143**, 6095.

[2] Cousin, S.F., Coaux, H., Hughes, C.E., Ziarelli, F., Viel, S., Mollica, G., Harris, K.D.M., Pinon, A.C. & Thureau, P., *submitted.*

This project has received funding from the European Research Council (ERC) under the European Union's Horizon 2020 research and innovation programme (GA 758498).

A069-06-270823

Two-dimensionally geared intermolecular structure in crystal formed by Au(I) complexes bearing triptycene and triadamantylphosphine

Hikaru Yamamoto1, Rempei Ando1, Mingoo Jin2, Hajime Ito1,2

[1]*Division of Applied Chemistry and Frontier Chemistry Center (FCC), Faculty of Engineering, Hokkaido University, Japan*
[2]*WPI-ICReDD, Hokkaido University, Japan*
Yamamoto.hikaru.b2@elms.hokudai.ac.jp

Keywords: Crystalline molecular rotor, Molecular gear, Au(I)complex

Macroscopic gears serve their ability to transmit forces through motion. Over the past decades, there have been numerous studies exploring the development of molecular gears that mimic the macroscale gears [1]. However, most of these studies have been conducted in solution systems, where the high degree of molecular freedom hampers precise control of gear motion and limits the potential for functional developments. In contrast, crystalline molecular gears can exhibit synchronized molecular rotations within a crystalline phase [2]. This class of crystalline materials has integrated significant attention due to their potential in creating functional molecular machines. However, designing molecular structures that can form intermesh intermolecular structure in crystal still remains a challenge, due to the non-predictable molecular packing event in solid state. Here, we describe a gold(I) complex **1** comprising by simple combination of rotators and axis; triptycene and triadamantylphosphine as the rotators that connected by ethyneyl and Au(I) atom as the rotational axis. Interestingly, the gold(I) complex **1** form a two-dimensional geared structure in the crystal. From the single-crystal X-ray analysis, it is evident that the two rotators intermeshed with forming CH-p interaction, creating the two-dimensionally arranged intermolecular geared structure with solvent-included porosity (Fig. 1a). Furthermore, the crystal exhibits dynamic disorder upon heating (Fig. 1b). In the presentation, the molecular motion of the rotators will be discussed which has been elucidated through ^{2}H solid-state NMR and time-resolved XRD analysis, providing comprehensive insights into the correlated motion in the crystalline environment.

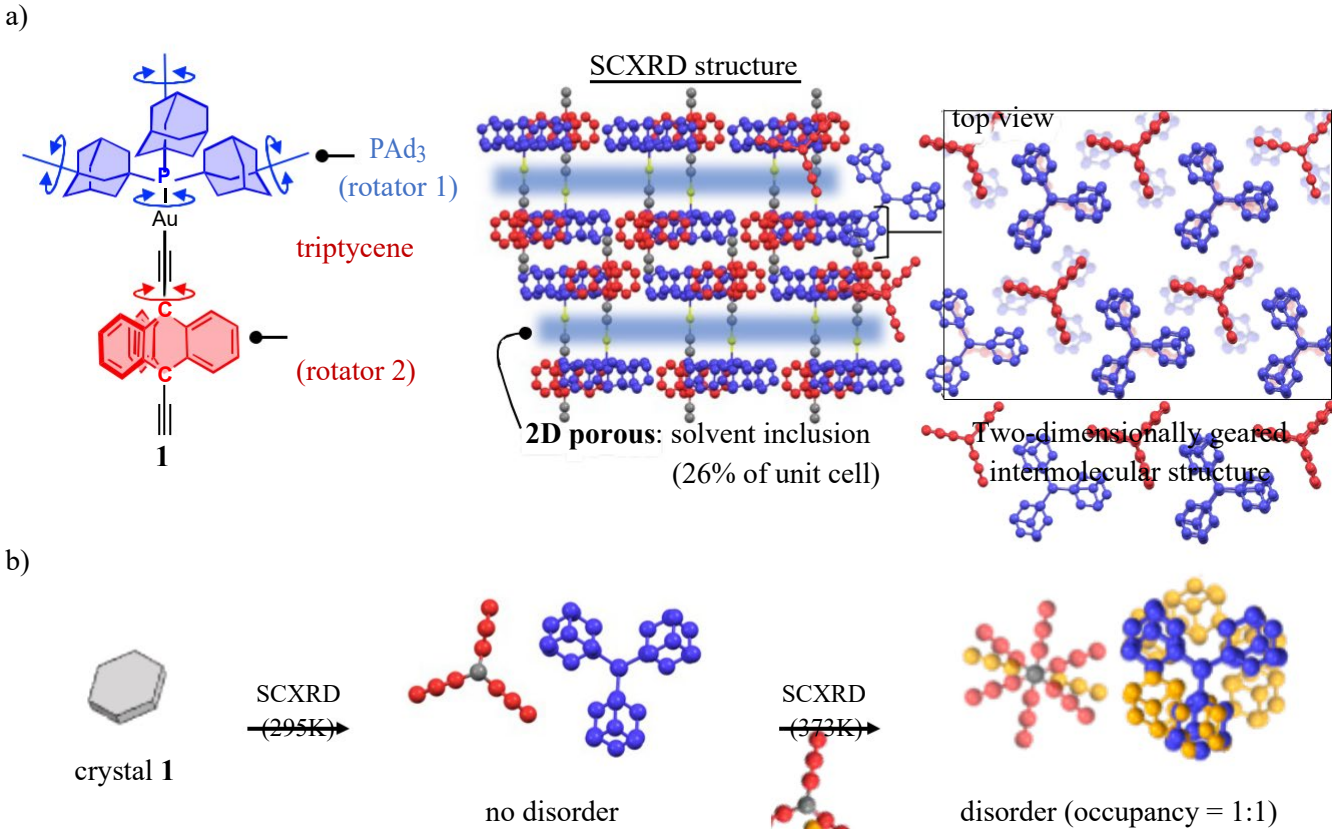

Figure 1. a) Two-dimensionally gear intermolecular structure in crystal **1** formed by triptycene & triadamantylphosphine(PAd_3). b) Confirmation of dynamic disorder by thermal activation in crystal **1**

[1] Gisbert, Y.; Abid, S.; Kammerer, C.; Rapenne, G. (2021) *Chem. Eur. J.* **27**, 12019–12031.

[2] Liepuoniute, I.; Jellen, M. J.; Garcia-Garibay, M. A. (2020) *Chem. Sci.* **11**, 12994–13007.

A078 What Every Crystallographer Should Know About Powder Diffraction
Room 212/213
1.10pm - 3.30pm

A078-01-270823

High-resolution powder diffraction data collection at beamline ID22 at ESRF

A. Fitch, C. Dejoie, G. Confalonieri, O. Grendal, E. Covacci

ESRF, CS40220, 38043 Grenoble Cedex 9, France

fitch@esrf.fr

Keywords: High resolution, Axial divergence, Asymmetry

Following the reconstruction of the ESRF storage ring in 2019 and the restart of user operation in 2020, the high-resolution powder diffraction beamline, ID22, has been upgraded. The source of radiation is now a 2.6 m long in-vacuum u26 undulator which, when combined with the new ring, leads to an approximately two-fold increase in flux and a smaller beam size, typically 0.6 0.8 mm^2 (h v). The powder diffractometer has been equipped with a new detector arm with a Dectris Eiger2 X 2M-W CdTe pixel detector receiving the X-rays transmitted by the thirteen crystals of a new multi-analyser stage, replacing the previous nine-channel version and corresponding array of scintillation counters. A great advantage of the new detector, as well as its intrinsic low background, counting speed, two energy thresholds and overall efficiency, is its spatial resolution, with 512 4148 pixels of size 75 75 m^2. Diffraction signals from the sample are transmitted by the analyser crystals onto 13 regions of interest on the detector [1]. By exploiting the axial resolution this affords, the effect of axial divergence, which causes the low-angle asymmetry in the peak shape of powder diffraction patterns, can be removed. Asymmetry occurs because axially-diverging photons satisfy the Bragg condition at the analyser crystal at lower angles of the detector arm than those scattered closer to the diffraction plane and so appear to be diffracted at lower 2 angles. By recording the axial position at which a photon arrives at the detector, its true 2 angle from the sample can be calculated [2]. The overall effect is that peaks at low angle are more symmetric and narrower when such corrections are applied, Fig. 1. A second advantage is that the axial acceptance of the detector can be increased as 2 increases, up to the 38 mm width of the detector, thus increasing the statistical quality of the high angle data while also improving the angular resolution. ID22 has implemented this approach systematically, as an automatic procedure, into its collection of high-resolution powder diffraction data.

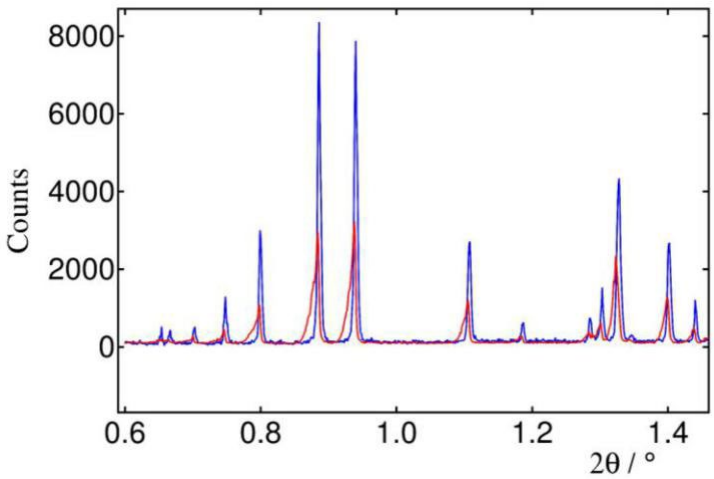

Figure 1. Example of the correction of low-angle asymmetry; red, as measured without correction; blue, with correction

[1] Dejoie, C., Coduri, M., Petitdemange, S., Giacobbe, C., Covacci, E., Grimaldi, O., Autran, P.-O., Mogodi, M. W., Šišak Jung, D. & Fitch, A. N. (2018). *J. Appl. Cryst*. **51**, 1721.

[2] Fitch, A. & Dejoie, C. (2021). *J. Appl. Cryst*. **54**, 1088.

A078-02-270823

Reducing errors and increasing accuracy of small-molecule crystal structures

D. Sisak Jung1, S. Lukin2, I. Halasz2

DECTRIS, Taefernweg 1, Baden, Switzerland, Ruder Boskovic Institute, Bijenicka 54, Zagreb, Croatia

dubravka.sisak@dectris.com

Keywords: crystal structure determination, accuracy, small molecules

Powder X-Ray Diffraction (PXRD) is one of the most powerful tools for structural analysis of micro- and nanocrystalline materials in the bulk. As such, its use and the number of published crystal structures is expected to continuously grow. Populating databases with accurate crystal structures is crucial for two reasons: chemical sensibility of structures and the fact that the PXRD technique heavily relies on chemical (and crystallographic) information stored in databases.

However, the path to an accurate crystal structure determination is paved with sources of errors. While some of them include the usual suspects (e.g. data resolution), the others are sometimes overlooked. To start with, the method requires significant users' input. Furthermore, a lack of *exact* evaluation criteria makes it difficult to monitor the progress of structure determination and Rietveld refinement, and to check the quality of the final structure. Finally, the Rietveld method is not capable of "repairing" a wrong structure. A group of materials that is particularly prone to such errors are small (organic) molecules, due to their limited scattering power, relatively high structural flexibility and a low degree of crystallinity [1,2]. Nonetheless, the power of PXRD for structural analysis of small-molecules is not questionable. But, how to recognize its limits? How to overcome them? How to utilize the power of PXRD the best?

This presentation focuses on increasing accuracy of small-molecule structures by highlighting potential sources of errors and proposing ways to reduce them. Using a series of molecular structures (with different quality of PXRD data), the audience will take a journey through sources of errors and see their effect on crystal structure accuracy. Depending on the source of error and the quality of the associated data, each case will be complemented with appropriate method to improve accuracy (reduce errors). This includes use of difference Fourier maps, complementary analytical techniques, crystal structure databases, as well as an approach to search the parameter space to avoid local minima in testing different sets of geometry restraints [1]. The set of selected examples is suitable for both beginners and advanced PXRD practitioners. The audience is expected to leave with two ideas: importance of obtaining the most accurate structures possible, and some practical advice on how ensure this accuracy.

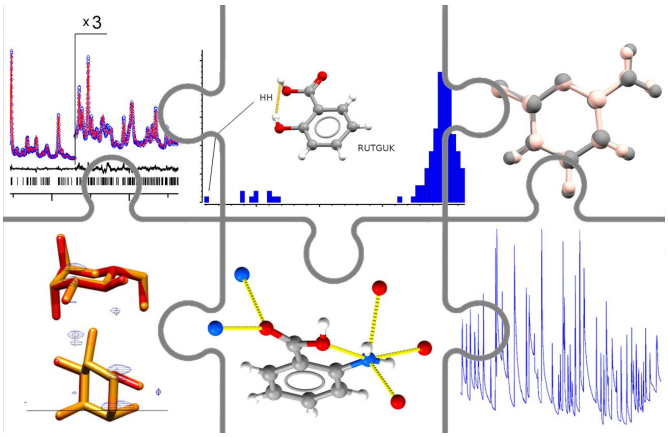

Figure 1. Increasing accuracy of small-molecule structures obtained by PXRD data can be sometimes be achieved by using PXRD data only. However, the use of information and data obtained by different sources are usually needed.

[1] Sisak Jung, D., Lukin, S., Halasz, I. (2023). *Helv. Chim. Acta* **106**, e202200087.
[2] Altomare, A. (2022). *IUCrJ* **9**, 403–405.

A078-03-270823

Quantitative phase analysis in complex (and not so complex) mineralogical systems

M.R. Rowles

Intertek Minerals, Perth, Australia. John de Laeter Centre, Curtin University, Perth, Australia.

Matthew.Rowles@intertek.com, Matthew.Rowles@curtin.edu.au

Keywords: powder diffraction; minerals; quantitative phase analysis

Quantitative phase* analysis (QPA) has its roots in the beginning of powder diffraction itself. While Debye and Scherrer were inventing powder diffraction [1-2], Hull [3-4] and Navias [5] were reporting QPA on various systems. After this, the use of diffraction for QPA was very much overtaken by those solving crystal structures, and it did not come back until the time of Alexander and Klug [6].

Powder diffraction, and by extension, QPA, is used extensively in many industries, such as minerals, pharmaceuticals, and cement, as well as in research in chemical engineering, chemistry, geology, physics, and materials science. The main thrust behind the desire to use diffraction to find out how much of each phase is present, is that the diffraction signal is produced directly by the phase itself, and not inferred by some other measurement.

The mathematical basis of QPA is well understood and its application should be straightforward [7], but the application of the theory quickly runs into reality. The influence of instrument, specimen, and analyst has been studied in many round-robins, looking at the analysis of materials such as Portland cement [8], clays [9], iron ore [10], and pharmaceuticals [11], as well as the previous general QPA round-robin [12-13]. In general, they have found that common issues arise around specimen preparation, data collection, and analyst errors, and state that, amongst other things, ongoing education is key to mitigating these effects.

To this end, several examples of the application of QPA to mineralogical systems will be discussed and methods of results validation will be introduced. Limitations on QPA will be reviewed, and some general "recipes" for QPA will be given.

* "Phase" means a discrete material with a common structure, which may or may not be crystalline. It has nothing to do with "phase" in the sense of the phase problem in X-ray crystallography.

[1] Debye, P. & Scherrer, P. (1916). *Phys. Z.* **17**, 277-283.
[2] Debye, P. & Scherrer, P. (1917). *C. Phys. Z.* **18**, 291-301.
[3] Hull, A. W. (1917). *Phys. Rev.* **10**, 661-696.
[4] Hull, A. W. (1919). *J. Am. Chem. Soc.* **41**, 1168-1175.
[5] Navias, L. (1925). *J. Am. Ceram. Soc.* **8**, 296–302.
[6] Alexander, L. E. & Klug, H. P. (1948). *Anal. Chem.* **20**, 886–889.
[7] Madsen, I.C. et al. (2019). *International Tables for Crystallography Volume H,* edited by C.J. Gilmore, J.A. Kaduk & H. Schenk, pp. 344-373.
[8] Leon-Reina, L. et al. (2009). *J. Appl. Cryst.* **42**, 906-916.
[9] Raven, M.D. & Self, P.G. (2017). *Clay Clay Mineral.* **65**, 122-134.
[10] Raven, M. D. & Birch, S. L.. 2017. "Summary of Results of an Internation X-Ray Diffraction Round Robin for Mineralogical Analysis of Iron Ores" *Iron Ore Conference*, Perth, Autralia.
[11] Fawcett, T. G. et al. (2012). *Powder Diffr.* **25**, 60-67.
[12] Madsen, I. C. et al. (2001). *J. Appl. Cryst.* **34,** 409-426.
[13] Scarlett, N. V. Y. et al. (2002). *J. Appl. Cryst.* **35,** 383-400.

A078-04-270823

Morphological reconstruction from powder diffraction data

A. Corrao[1,2], V. Petrova[3], S. Tan[1,2], T. Kimberly [4], S. Kauzlarich[4], E. Hu[2], P. Liu[3], P. Khalifah[1,2]

[1]Department of Chemistry, Stony Brook University [2]Chemistry Division, Brookhaven National Lab [3]Department of Nanoengineering, University of California San Diego [4]Department of Chemistry, University of California Davis

adam.corrao@stonybrook.edu

Keywords: powder diffraction, morphology, microstructure, nanomaterials

Traditionally, the analysis of powder diffraction data through whole pattern fitting has either focused on structural analysis (through Rietveld refinement) or through peak shape analysis for size/strain studies (through the independent fitting of individual peaks). We have recently pioneered methods that fuse these two approaches [1]. This has advantages both for structural analysis / phase quantification (which can be done more effectively when the particle size and/or strain is complex, as seen in Figure 1) and for peak shape analysis (in which the constraint of intensities based on a structural model allows peak shapes to be more effectively extracted when peak overlap exists). Since this approach enables us to rapidly and robustly quantify the shapes of a hundred or more peaks automatically refined from a powder diffraction pattern (Figure 2), we can use it to effectively reconstruct the morphology (size and shape) of the particles comprising the powder. Some examples of these novel methods applied to the characterization of functional materials (batteries, catalysts, thermoelectrics) will be discussed.

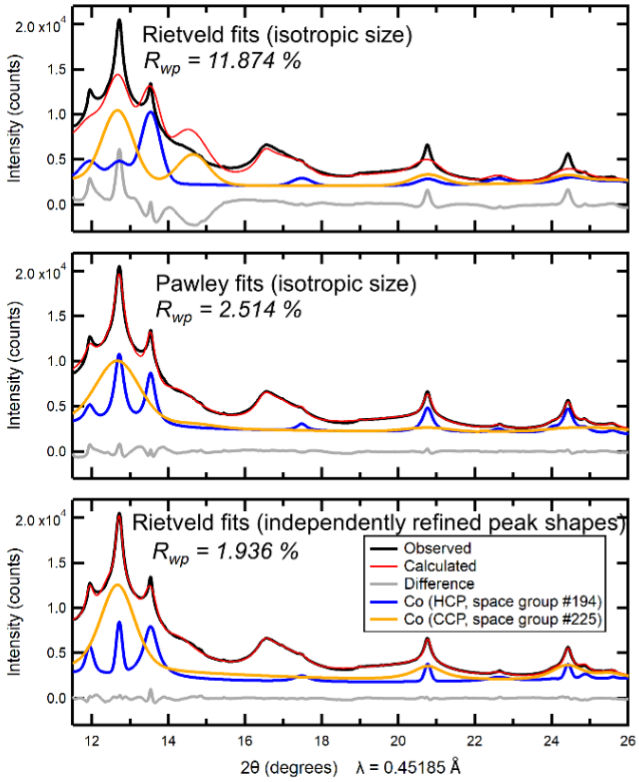

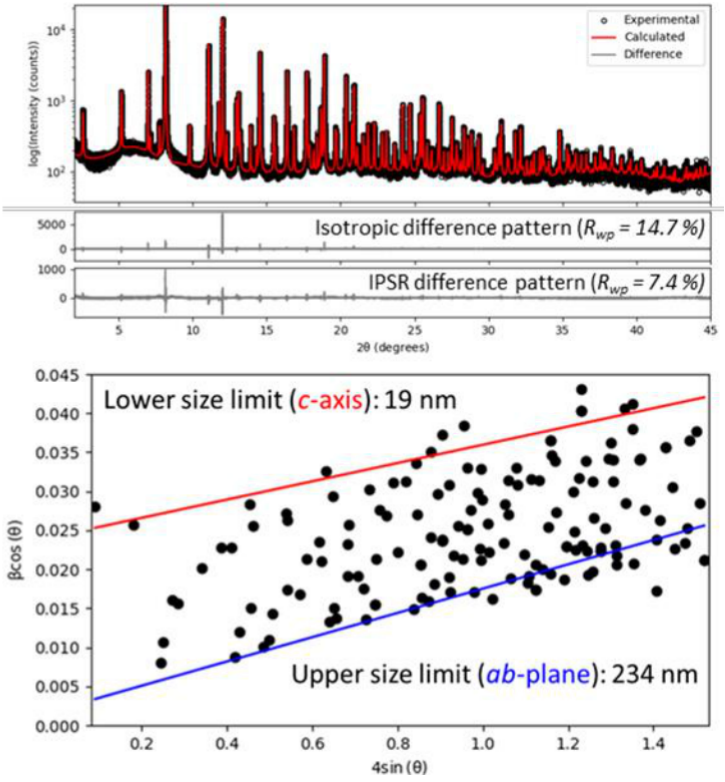

Figure 1. Comparison of different approaches to whole-pattern fitting for synchrotron diffraction data from a sample containing a polymorphic mixture of nanoscale Co: Rietveld refinements with an isotropic size model (top), Pawley fits with an isotropic size model (middle), and our modified Rietveld approach using separately refined peak shapes for each diffraction peak (bottom).

Figure 2. Top: Independent peak shape refinement (IPSR) fit shown on a log scale along with a comparison of the difference plots from IPSR (R_{wp} = 7.4%) and conventional isotropic fits (R_{wp} = 14.7%). Bottom: Morphological information obtained from 100+ automatically extracted peak integral breadths fit while using the constraint of a structural model, shown in a Williamson-Hall type plot.

[1] Petrova, P., Corrao, A. A., Wang, S., Xiao, Y., Chapman, K. W., Fullerton, E. E., Khalifah, P. G., & Liu, P. (2022). *RSC Adv.*, **12**, 21153-21159.

A078-06-270823

What you can, and can't do with *in situ* powder diffraction

H.E. Maynard-Casely[1]

Australian Nuclear Science and Technology Organisation, Locked Bag 2001, Kirrawee DC, 2234, NSW, Australia helenmc@ansto.gov.au

Keywords: powder diffraction, *in situ*, neutron, synchrotron

Powder diffraction is particularly powerful for studying samples *in situ* and within a range of sample environments [1]. This has made it an incredibly powerful tool, in particular for studying samples under extreme conditions. But are there any special considerations that you need to make to these data? Generally, yes, and I will describe some of the potential hiccups when approaching data collected *in situ,* and crucially how to describe these to others. A great advantage to powder diffraction data for *in situ* studies, is the ability to visualise data (for instance with thermodiffractorgrams like Figure 1), enabling you to quickly assess the data and its phase transitions. Additionally seeing the fit can be key [2], as relying only on *R*-factors can result in mis-leading results. Increasingly powerful for this is the powder diffraction CIF format (pd_CIF) [3], which is a useful way to store and deposit your data, and to allow others to easily judge the fit of your data.

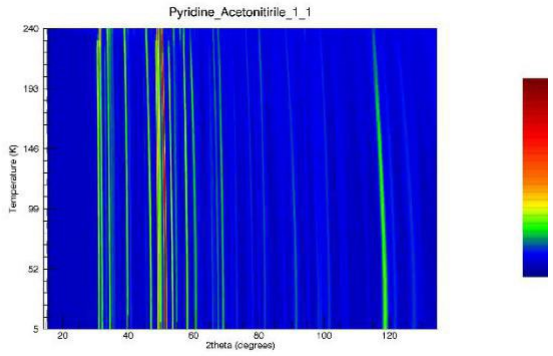

Figure 1. Example of a thermodiffractogram, showing variable temperature powder diffraction collected over a large temperature range. This is a particularly useful tool for *in situ* powder diffraction as phase transitions can easily be seen and tracked.

[1] Dinnebier, R.E. and Billinge, S.J.L (2008) *eds*. Powder diffraction: theory and practice. *RSC*

[2] Rowles, M.R. (2022) *J. App Cryst* **55**.3.

[3] Toby B.H., Von Dreele R.B, and Larson, A.C. (2003) *J. App Cryst* **36**,1290-1294.

The author wishes to acknowledge the Dharawal people, the traditional owners of the land where ANSTO Lucas Heights operates.

A100 The Arsenal of Supramolecular Interactions for Crystal Engineering
Room 210/211
1.10pm - 3.30pm

A100-01-270823

Neutron Laue Diffraction to Probe Hydrogen Bonding Materials

David R. Turner

School of Chemistry, Monash University, Clayton, VIC 3800, Australia
david.turner@monash.edu

Keywords: neutron diffraction, hydrogen bonding, supramolecular

Neutron Laue diffraction allows for rapid data collections of crystalline molecular species using modestly sized samples. As such, the technique allows for systematic studies of hydrogen-bonding supramolecular systems to take advantage of the accurate hydrogen atomic position afforded by neutron scattering. Several systems will be highlighted for which neutron diffraction has provided valuable insight.

- Water squares holding together octahedral coordination complexes provide strong hydrogen bonding that causes axial distortion of the coordination sphere. Determination of the hydrogen positions showed a distortion of the complex and provided the basis model for calculations of the hydrogen bond strengths [1].
- Nitrile groups (R-C≡N) are not typically considered to be strong hydrogen bond acceptors. A systematic study has shown the orientational preferences of donor groups around the nitrile acceptor [2].
- Triazinones are good building blocks for supramolecular systems, acting as both hydrogen bond acceptor/donor species that are analogues of di-substituted urea. The substituent at the nitrogen can play a significant role in affecting the planarity of the ring system and the positions of the NH donor groups [3].
- Oxime/oximate systems have been studied in which the anionic form is isolated alongside the neutral molecule with an apparent shared proton. The hydrogen position can be determined by neutron diffraction and lies close to, but not at, the midpoint between the two oximate sites and therefore represents a highly unusual hydrogen bond.

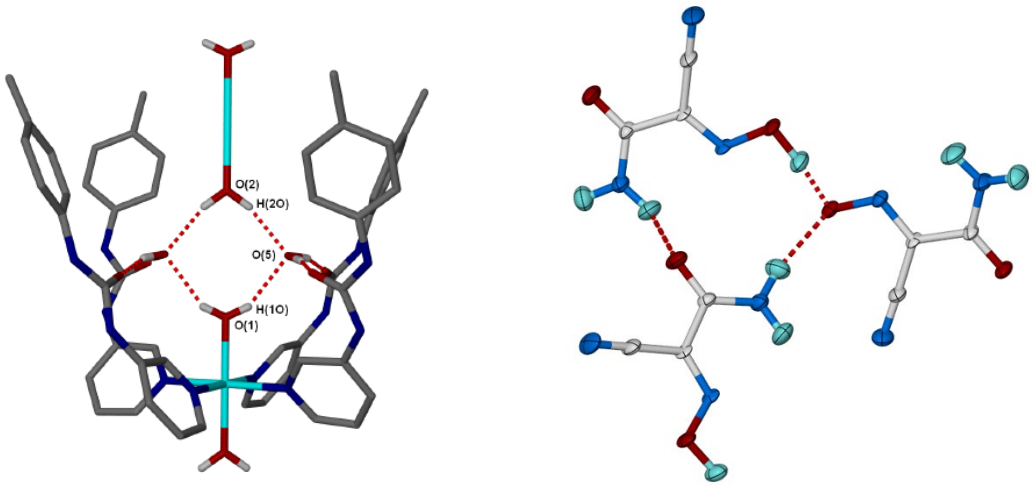

Figure 1. A water square between octahedral complexes (left) and a hydrogen-bonded oxime system (right).

[1] Turner, D.R., Henry, M.C., Wilkinson, C., Mason, S.A., McIntyre, G.J., Goeta, A.E. & Steed, J.W. (2005). *J. Am. Chem. Soc.* **127**, 11063.
[2] Turner, D.R., Edwards, A.J. & Piltz, R.O. (2012). *CrystEngComm*, **14**, 6447.
[3] McCormick, L.J., C.J. McDonnell-Worth, Platts, J.A., Edwards, A.J. & Turner, D.R. (2013). *Chem. Asian J.* **8**, 2642.

A100-02-270823

Full-colour palette from one chromogen – modular design strategy revealed by quantum crystallography

M. Gryl, M. Kozieł, K. Nowakowska, K.Ostrowska

Faculty of Chemistry, Jagiellonian University in Kraków, Gronostajowa 2, 30-387 Kraków, Poland

marlena.gryl@uj.edu.pl

Keywords: chromic materials, crystal engineering, quantum crystallography

Technological applications of *colour chemistry* are enormous. For example, *chromic materials* can be found in photochromic systems or smart self-dimming windows, paints and indicators, thermal papers and visual displays or in biosensors [1].
Many known crystals can change colour selectively. [2] However, not many chromogens can create multi-coloured systems in the presence of a particular colourless coformer. [3] Even fewer show high performance, sufficient flexibility of the chromic response to applied stimuli and reversibility of the process.

It is vital to understand molecular aggregation to obtain materials with enhanced properties. Each structure can be divided into subsections (modules), which can be modified, removed or exchanged with other molecules or between different systems. Understanding how those modules interact with each other and how they change depending on the in-crystal environment is necessary to design smart devices.

In this work, we have used *quantum crystallography tools* [4,5] in conjunction with *H^1 NMR spectroscopy* to formulate a general mechanism of *chromic effects* in violuric acid salts and co-crystals. The obtained results proved that we could influence the light absorption properties of a material using a reformulated reverse crystal engineering concept. The *modular approach* led to distinctly coloured multicomponent crystalline products (Fig. 1) based on colourless starting components (e.g. pyridine, aliphatic and aromatic amine derivatives). Chromic effects were examined using solid-state UV-VIS spectroscopy, XRPD and hot-stage microscopy. Our research will contribute to a more conscious design of *chromic multicomponent materials*.

Figure 1. Full-colour palette from one chromogen – multicomponent chromic materials based on violuric acid.

[1] Vik, M. Periyasamy, A. P. ed. Viková M. (2021) *Chromic Materials. Fundamentals, Measurements and Applications*, CRC Press.
[2] Bamfield, P., Hutchings, M. (2018) *Chromic Phenomena: Technological Applications of Colour Chemistry*, Royal Society of Chemistry.
[3] Gryl, M., Rydz, A., Wojnarska, J., Krawczuk, A., Koziel, M., Seidler, T., Ostrowska, K., Marzec, M. & Stadnicka, K. M. (2019). *IUCrJ* 6, 226-237.
[4] Bader, R. F. W. (2003). *Atoms in Molecules: A Quantum Theory*, International Series of Monographs on Chemistry, Vol. 22. Oxford: Clarendon Press.
[5] AIMAll (Version 19.10.12), Todd A. Keith, TK Gristmill Software, Overland Park KS, USA, 2019 (aim.tkgristmill.com); Dovesi, R.; Erba, A.; Orlando, R.; Zicovich-Wilson, C. M.; Civalleri, B.; Maschio, L.; Rerat, M.; Casassa, S.; Baima, J.; Salustro, S.; Kirtman, B. *WIREs Comput Mol Sci*., 2018, 8, e1360.

National Science Centre Poland supported this research, grant number UMO-2018/30/E/ST5/00638. Furthermore, we gratefully acknowledge Poland's high-performance computing infrastructure PLGrid (HPC Centers: ACK Cyfronet AGH), for providing computer facilities and support within computational grant no. PLG/2023/016132.

A100-03-270823

σ-Hole interactions in tetrahedral compounds and analogous species

M. Calabrese[1], A. Frontera[2], A. Pizzi[1], G. Resnati[1,3]

[1]Dept. Chemistry, Materials, Chem. Engineering "Giulio Natta", Politecnico di Milano, via Mancinelli 7, I-20131 Milano, Italy
[2]Dept. Chemistry, Universitat de les Illes Balears, Crta. de Valldemossa km 7.5, 07122 Palma de Mallorca, Spain
[3]Res. School of Chemistry and Applied Biomedical Sciences, Tomsk Polytechnic University, Tomsk 634034, Russian Federation

E-mail of communicating author: giuseppe.resnati@polimi.it

Keywords: supramolecular chemistry, self-assembly, halogen bond

The anisotropic distribution of the electron density is a common feature in atoms forming covalent bonds. This is the case for elements of both the p- and d-block of the periodic table. As a consequence, regions of depleted electron density are present on the surface of bonded atoms opposite to the single covalent bonds (□-holes) and above and below planar parts of molecules (□-holes). Especially when strong electron withdrawing groups are covalently bonded to the atom, the electrostatic potential is positive at these holes and attractive interactions can be formed with regions of surrounding atoms where the electrostatic potential is negative. In the solid these interactions are strong enough to determine the crystal packing. The behaviour has been extensively studied in mono- and divalent compounds forming halogen and chalcogen bonds. Here we will focus on tetravalent molecular species adopting a tetrahedral geometry. We will show how attractive interactions are formed by positive □-holes present in tetrahedral derivatives of elements of the 7, 8, 14, and 17 groups of the periodic table of elements. For instance, it will be presented how the C(sp^3) atoms of methyl and methylene groups form tetrel bonds [1], the osmium atom of osmium tetroxide forms osme bonds [2], and the rhenium atom of methyl trioxorhenium forms matere bonds [3] (Fig. 1 a,b). Interestingly, positive □-holes can be present also in tetrahedral anions and these holes can drive the formation of anion-anion assemblies. This is the case for permanganate and perrhenate anions [3] as well as for periodate anions [4] (Fig. 1 c,d).

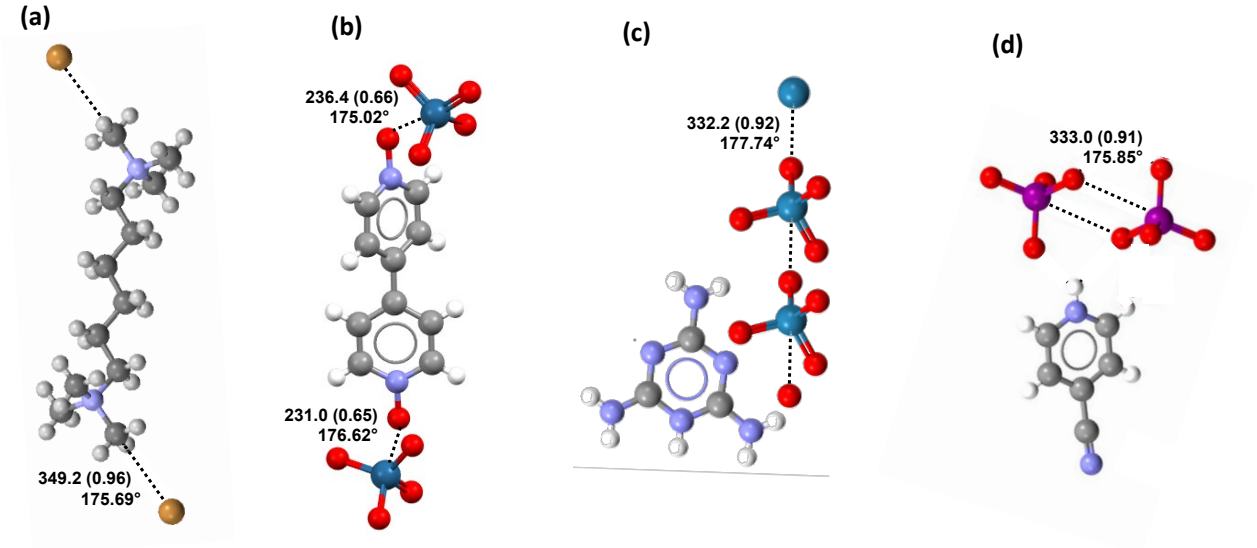

Figure 1. Ball and stick representation of: C···Br tetrel bonds (TtBs) in 1,6-bis(trimethylammonium)hexane dibromide (a), Os···O osme bonds (OsBs) in osmium tetroxide/4,4'-bipyridine *N,N'*-dioxide adduct (b), Re···O matere bonds (MaBs) in melaminium perrhenate (c), and I···O halogen bonds (HaBs) in 4-cyanopyridinium periodate (d). σ-Hole interactions are black dashed lines, respective separations and angles are reported in ppm and degrees.

[1] Daolio, A.; Wieduwilt, E. K.; Pizzi, A.; Genoni, A.; Resnati, G.; Terraneo, G. (2022). *Phys. Chem. Chem. Phys.,* **24**, 24892. [2] Daolio, A.; Pizzi, A.; Calabrese, M.; Terraneo, G.; Bordignon, S.; Frontera, A.; Resnati, G. (2021). *Angew. Chem. Int. Ed.,* **60**, 20723.
[3] Daolio, A.; Pizzi, A.; Terraneo, G.; Frontera, A.; Resnati, G. (2021). *ChemPhysChem*., **22**, 2281.
[4] Calabrese, M.; Pizzi, A.; Daolio, A.; Frontera, A.; Resnati, G. (2022). *Chem. Commun.*, **58**, 9274.

This work was funded by the Italian Ministry of Education, PRIN project NICE, No. 2020Y2CZJ2 and by the Russian Ministry of Science and Higher Education, "Mega-grant" project No. 075-15-2021-585.

A100-04-270823

Intermolecular interactions involving fluorine in small organic molecules: A structural, computational and charge density analysis

Angshuman Roy Choudhury

[a]*Department of Chemical Sciences, Indian Institute of Science Education and Research, Mohali, Knowledge City, S. A. S. Nagar, Manauli PO, Mohali, Punjab, 140306, India.*

Email: angshurc@iisermohali.ac.in

Keywords: weak interactions, organic-fluorine, charge density, deformation density, Crystal17, topological properties

The study of weak interactions and their role in crystal engineering have been a major area of research in the past few decades.[1-4] Interactions involving organic C–X (X = F, Sl, Br and I) groups have attracted significant interest in controlling supramolecular architecture in the solid state.[5-7] The interactions involving "organic fluorine" has always remind controversial due to its uncertain nature. Many simple organic compounds display biological activity when one or more fluorine atom is strategically inserted in the molecule, indicating that fluorinated molecules have biological importance compared to their non-fluorinated and chloro/bromo analogues.[8] Hence, it is believed that the interaction of "organic fluorine" with biological receptors is different from that offered by other C–X (X = Cl, Br, I) groups. We have been involved in the systematic understanding of weak yet significant interactions offered by "organic fluorine" in crystal packing over the last decade.[9-11] Our combined structural, computational and experimental charge density studies[12] on a library of fluorinated small organic compounds will be highlighted in the presentation.

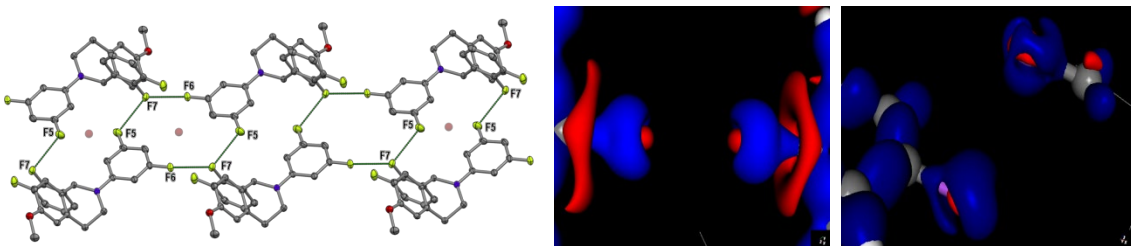

Figure 1. C–F···F–C interactions in small organic molecules, structure to 3D deformation density maps

1. *Thalladi, V. R.; Wiess, H. C.; Bläser, D.; Boese, R.; Nangia, A.; Desiraju, G. R.; J. Am. Chem. Soc., **1998**, 120, 8702-8710.*
2. Choudhury, A. R.; Urs, U. K.; Guru Row, T. N.; Nagarajan, K. *J. Mol. Struct.* **2002**, 605, 71–77.
3. Nayak, S. K.; Kumar, V.; Murray, J. S.; Politzer, P.; Terraneo, G.; Pilati, T.; Metrangolo, P.; Resnati, G. *CrystEngComm*. **2017**, 19, 4955-4959.
4. Chopra, D.; Guru Row, T. N. *CrystEngComm.* **2011**, 13, 2175–2186.
5. Howard, J. A. K.; Hoy, V. J.; O'Hagan, D.; Smith, G. T. *Tetrahedron*, **1996**, *52*, 12613-12622.
6. Choudhury, A. R.; Guru Row, T. N. *Cryst. Growth Des.* **2004**, 4, 47–52.
7. Nayak, S. K.; Reddy, M. K.; Guru Row, T. N.; Chopra, D. *Cryst. Growth Des.* **2011**, 11, 1578–1596.
8. Nagarajan, K., Talwalker, P. K., Kulkarni, C. L. *Ind. J. Chem.* **1985**, *24B*, 83−97.
9. Kaur, G.; Choudhury, A. R. *Cryst. Growth Des.* **2014**, 14, 1600–1616.
10. Kaur, G.; Choudhury, A. R. *CrystEngCom.* **2015**, 17, 2949–2963.
11. Singla, L.; Yadav, H. R.; Choudhury, A. R. *Cryst. Growth Des.* **2022**, *22* (3), 1604–1622.
    Singla, L.; Kumar, A.; Robertson, C. M.; Munshi, P.; Choudhury, A. R. Cryst. Growth Des. **2023**, *23*(2) 853-861.

ARC acknowledges his students, without whom this word would not have been possible, collaborators for their timely contributions and funding agencies for their continuous support. IISER Mohali for the financial, infrastructural and administrative supports.

A304-05-270823

Molecular recognition of amino acids and neurotransmitters by cucurbituril in water

E. Zaorska1, M. Malinska1

Faculty of Chemistry, University of Warsaw, Pasteura 1, 02-093Warsaw, Poland

mmalinska@chem.uw.edu.pl

Keywords: hydrogen bonds, crystal structure, host-guest complex, enthalpy and entropy of binding

Studies of molecular recognition in water using model macrocyclic systems derived key findings on the remarkable properties exhibited by proteins: high binding affinity, superior binding selectivity, and extreme catalytic performance. Importance of the intermolecular forces involved in the reversible binding of the ligands, as well as the hydrophobic and Hofmeister effects operating in aqueous solution between the macrocyclic host molecule cucurbit[7]uril (CB[7]) and amino acids (AAs) or neurotransmitters (NRs), is studied to elucidate the origin of the high selectivity of CB[7]. NRs are generally synthesized in neurons and are made up of, or derived from, precursor molecules that are found abundantly in the cell e.g. amino acids, monoamines, and peptides. Complex formation between CB[7] and each NR or AA was examined in solution by isothermal titration calorimetry, and the results were further combined with computational investigations and X-ray diffraction studies. Generally, the NR show higher binding affinities than the precursor AAs in buffer solutions with various pH values. However, the gas-phase interaction energies between host and guest show a negative correlation to binding affinities, suggesting that the role of non-covalent interactions between the polar side chains is diminished in the presence of water. In contrast, the transfer of the hydrophobic groups from the bulk into the hydrophobic CB[7] cavity suffers less from the desolvation penalty, resulting in higher binding affinities in water. Therefore, initial guest solvation is another key factor which should be considered when designing ligands and hosts.

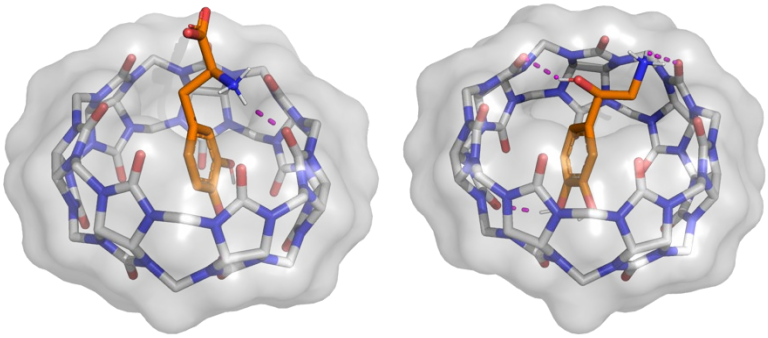

Figure 1. Crystal structures of CB[7] with L-DOPA (left) and CB[7] with L-noradrenaline (right). Dashed magenta lines indicate hydrogen bonds. Only polar hydrogen atoms are shown.

The authors thank the Polish National Science Centre for financial support - Sonata Bis Grant 2021/42/E/ST4/00229.

A100-06-270823

Exploration of primary and secondary sphere coordination by unsymmetric pyrimidine sulfanyl and aminopyrazole ligands

Dawe*[1], S. D. Joekar[1], L. Hiscock[1], K. Anoliefo[1], A. Hankins[1], K. Maly[1], P. Boyle[2]

Department of Chemistry and Biochemistry, Wilfrid Laurier University, Waterloo, ON, Canada, 2. Western University, Department of Chemistry, London, ON, Canada

ldawe@wlu.ca

Keywords: Coordination chemistry, Intermolecular interactions, Structure-property relationships

In our exploration of ligand systems that simultaneously incorporate three types of molecular affinity: (i) coordination of Lewis acids; (ii) intermolecular interactions with anions; and (iii) additional functional modalities, we have recently focused on two classes of unsymmetric molecules based on (a) aminopyrazole and (b) pyrimidine sulfanyl cores (Fig. 1). We have targeted this design strategy because a knowledge gap still exists with respect to controlling the directionality of weak intermolecular forces [1], which may be further complicated in the presence of stronger, competing forces [2].

In the case of the aminopyrazole systems, we have previously observed via polarized optical microscopy that all exhibit supercooling of between 34 and 100 ºC, and upon coordination to ZnCl2 and ZnBr2, we have observed bright, solid-state fluorescence.[3] We have now expanded our coordination chemistry and fluorescence studies to produce adducts with $BF2^{+}$, which are also fluorescent.

We have also expanded on our previously reported results [4] to generate monosubstituted pyrimidine sulfanyl ligands, which we have recently functionalized to produce unsymmetric ligands, for example, with R = morpholine; Fig. 1(b).

Synthesis, characterization, and structural features of primary sphere coordination with Lewis acids will be highlighted, as well as secondary sphere interactions and possible applications for environmental anion sensing.

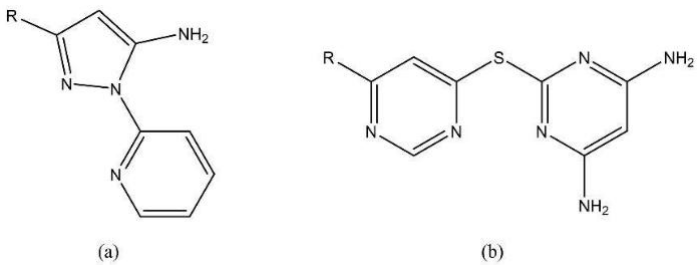

Figure 1. Unsymmetric (a) aminopyrazole and (b) pyrimidine sulfanyl ligand cores explored herein.

[3] Chakrabarty, R., Mukherjee, P. S. & Stang, P. J. (2011) Chem. Rev., 111, 6810.
[4] Robertson, C. C., Wright, J. S., Carrington, E. J., Perutz, R. N., Hunter, C. A. & Brammer, L. (2017) Chem. Sci., 8, 5392.
[5] Hiscock, L. K., Joekar, D., Balonova, B., Tomas Piqueras, M., Schroeder, Z. W., Jarvis, V., Maly, K. E., Blight, B. A. & Dawe, L. N. (2019). Inorg. Chem., 58, 16317.
[6] Moyaert, T. E., Paul, C., Chen, W., Sarjeant, A. A. & Dawe, L. N. (2017). Acta Cryst. E, 73, 1534.

We would like to acknowledge that Wilfrid Laurier University and its campuses are located on the shared traditional territory of the Neutral, Anishnaabe and Haudenosaunee peoples.

A011 Validation of Biological Macromolecular Structure
Room 203/204
4.00pm - 6.30pm

A011-01-270823

CheckMyMetal - an enhanced platform for interactive validation of metal binding sites

M. Gucwa [a,b], J. Lenkiewicz [a], H. Zheng [c], D.R. Cooper [a], K. Murzyn [b], W. Minor [a]

Department of Molecular Physiology and Biological Physics, University of Virginia, 1340 Jefferson Park Avenue, Charlottesville, VA 22908, USA; [b] Department of Computational Biophysics and Bioinformatics, Faculty of Biochemistry, Biophysics and Biotechnology, Jagiellonian University, 30-387 Cracow, Poland; [c] Hunan University

michal_g@iwonka.med.virginia.edu

Keywords: Reproducibility, Metal binding sites validation, Drug discovery, Structure refinement, Metalloprotein

Metal ions bound to macromolecules play an integral role in many cellular processes. They can directly participate in catalytic mechanisms or be essential for the structural integrity of proteins and nucleic acids. CheckMyMetal (CMM) is a validation tool that has gained widespread acceptance as an essential tool for researchers working on metal-macromolecule complexes. An easy-to-use interface allows the evaluation of structures in the PDB or uploaded by the user. The new version incorporates electron density maps, which expands the number of parameters used for validation. One of the most important new features is the ability to conduct a fast refinement of the vicinity around alternate metal candidates. CheckMyMetal guides the metal selection process in two ways. First, it evaluates the substitution of several metals in the current environment, re-scores the binding sites, and displays a ranked list of candidate metals. Second, the researcher is alerted to potential metals from the crystallization conditions when they are available. CheckMyMetal is available at https://cmm.minorlab.org.

A011-02-270823

Cross-reactivity of CD4+ gluten-reactive T cell receptors in celiac disease

Laura Ciacchi[1,2], Carine Farenc[1,2], Jan Petersen[1,2], Shiva Dahal-Koirala[3,4] , Ludvig M. Sollid[3,4], Melinda Y. Hardy[5,6], Jason A. Tye-Din[5,6,7], Hugh H. Reid[1,2] & Jamie Rossjohn[1,2,8]

[1]Infection and Immunity Program and Department of Biochemistry and Molecular Biology, Biomedicine Discovery Institute, Monash University, Clayton, Victoria, Australia [2]ARC Centre of Excellence in Advanced Molecular Imaging, Monash University, Clayton, Victoria, Australia [3]Centre for Immune Regulation, Department of Immunology, University of Oslo and [4]Oslo University Hospital-Rikshospitalet and Department of Gastroenterology, Oslo University Hospital- Rikshospitalet, Oslo, Norway [5]The Walter and Eliza Hall Institute of Medical Research, Parkville, Victoria, Australia [6]Department of Medical Biology, The University of Melbourne, Parkville, Victoria, Australia [7]Department of Gastroenterology, The Royal Melbourne Hospital, Parkville, Victoria, Australia and [8]Institute of Infection and Immunity, Cardiff University School of Medicine, Cardiff, UK.

laura.ciacchi1@monash.edu

Keywords: HLA, TCR, celiac disease, cross-reactivity, gluten, epitope

Celiac disease (CeD) is a chronic inflammatory autoimmune-like condition characterised by disease-relevant HLA-DQ2.5/8 molecules that present gluten epitopes derived from wheat, rye and barley to reactive T cells [1, 2]. We investigated CD4+ T cell responses towards immunodominant gluten epitopes; DQ2.5-glia-α1a (PFPQPEL<u>P</u>Y) and DQ2.5-glia-ω1 (PFPQPE<u>Q</u>P<u>F</u>) by examining patient T cell repertoire [3, 4]. It was found to be composed of highly specific and cross-reactive T cell clones (TCCs) [4].

Next, we determined the ternary complex structures of cross-reactive T cell receptor (TCR) bound to HLA-DQ2.5-glia-α1a and HLA-DQ2.5-glia-ω1 and epitope-specific TCR bound to HLA-DQ2.5-glia-ω1 specific TCR [3, 5]. The interactions at the interface of TCR: peptide-HLA-DQ2.5 required for specificity provide an insight into how the TCRs distinguish between these highly similar peptides [5]. Comparison of the TCR footprint contacts of the ternary complexes for both peptides revealed similar canonical TCR docking with slight shift in docking angle [3, 5, 6]. The hypervariable CDR3 loops were shown to be responsible for differential TCR recognition capacities of the cross-reactive versus discriminatory TCRs [5, 7]. We measured SPR binding affinities of the TCR-pHLA interaction and found that the cross-reactive TCR is selectively promiscuous in binding as this TCR only bound these epitopes with similar affinity [5, 7].

This study highlights that cross-reactive T cells may also contribute to CeD pathogenesis [5, 7]. Furthermore, these cross-reactive and discriminatory T cells may prove to be important therapeutic targets in treatment of CeD [5, 7, 8].

[1] Hardy, M.Y., Tye-Din, J.A., Stewart, J.A., Schmitz, F., Dudek, N.L., Hanchapola, I., Purcell, A.W. & Anderson, R.P., (2015). *J. Autoimmun.*, **56**, 56-65.
[2] Sollid, L.M., Tye-Din, J.A., Qiao, S.W., Anderson, R.P., Gianfrani, C. & Koning, F. (2020). *Immunogenetics*, **72**, 85-88.
[3] Petersen, J., Montserrat, V., Mujico, J.R., Loh, K.L., Beringer, D.X., Van Lummel, M., Thompson, A., Mearin, M.L., Schweizer, J., Kooy-Winkelaar, Y. & Van Bergen, J. (2014). *Nat. Struct. Mol. Biol.* **21**, 480-488.
[4] Dahal-Koirala, S., Ciacchi, L., Petersen, J., Risnes, L.F., Neumann, R.S., Christophersen, A., Lundin, K.E., Reid, H.H., Qiao, S.W., Rossjohn, J. & Sollid, L.M. (2019). *J. Biol. Chem.*, **294**, 941-952.
[5] Ciacchi, L., Farenc, C., Dahal-Koirala, S., Petersen, J., Sollid, L.M., Reid, H.H. & Rossjohn, J. (2022). *JBC*, **298**, 1-11.
[6] Zareie, P., Szeto, C., Farenc, C., Gunasinghe, S.D., Kolawole, E.M., Nguyen, A., Blyth, C., Sng, X.Y., Li, J., Jones, C.M. & Fulcher, A.J. (2021). *Science*, **372**, 1-13.
[7] Petersen, J., Ciacchi, L., Tran, M.T., Loh, K.L., Kooy-Winkelaar, Y., Croft, N.P., Hardy, M.Y., Chen, Z., McCluskey, J., Anderson, R.P. & Purcell, A.W. (2020). *Nat. Struct. Mol. Biol.*, **27**, 49-61.
[6] Frick, R., Høydahl, L.S., Petersen, J., Du Pré, M.F., Kumari, S., Berntsen, G., Dewan, A.E., Jeliazkov, J.R., Gunnarsen, K.S., Frigstad, T. & Vik, E.S. (2021). *Science immunology*, **6**, 1-16.

A011-03-270823

A residue-focused protein crystal structure evaluation method based on electron density

I. Miyaguchi[1], A. Kashima[1], H. Hata[2], T. Kuribayashi[2], S. Matsumoto[3], K. Terayama[4], M. Ohta[5] and M. Ikeguchi[4]

[1]Mitsubishi Tanabe Pharma Co., LTD., 1000, Kamoshida-cho, Aoba-ku, Yokohama, Japan, [2]Mitsui Knowledge Industry Co., LTD., 2-5-1 Atago, Minato-ku, Tokyo, Japan, [3]Graduate School of Medicine, Kyoto University, Kyoto, Japan, [4]Graduate School of Medical Life Science, Yokohama City University, 1-7-29, Suehiro-cho, Tsurumi-ku, Yokohama, Japan, [5]RIKEN Center for Computational Science, 1-7-22, Suehiro-cho

miyaguchi.ikuko@mv.mt-pharma.co.jp

Keywords: electron density, machine learning, structure evaluation

In X-ray crystallography, the determination of coordinates using low-resolution electron density is a major challenge hindering the determination and use of protein structures. To overcome this, we propose a method using machine learning to evaluate the quality of the coordinate structure one residue at a time using electron density and coordinate structure as input data and report output using QAEmap [1].

QAEmap uses an entire box centered on the canter coordinate of each amino acid of interest as a descriptor and predicts its correlation with a putative high-resolution electron density map using a 3D deep convolutional neural network. Since the amino acid of interest and its surrounding environment are both subject to evaluation by this method, it can be applied to evaluating docking poses by evaluating the structure of amino acids in contact with a compound. Thus, it has the potential to be used as a support tool when determining a docking pose using electron density that is unclear owing to low resolution, etc. A preliminary experiment using test data has yielded optimal results (Fig. 1).

In this presentation, we will discuss the applications of this method to bound-compound evaluation and prospects for its future use.

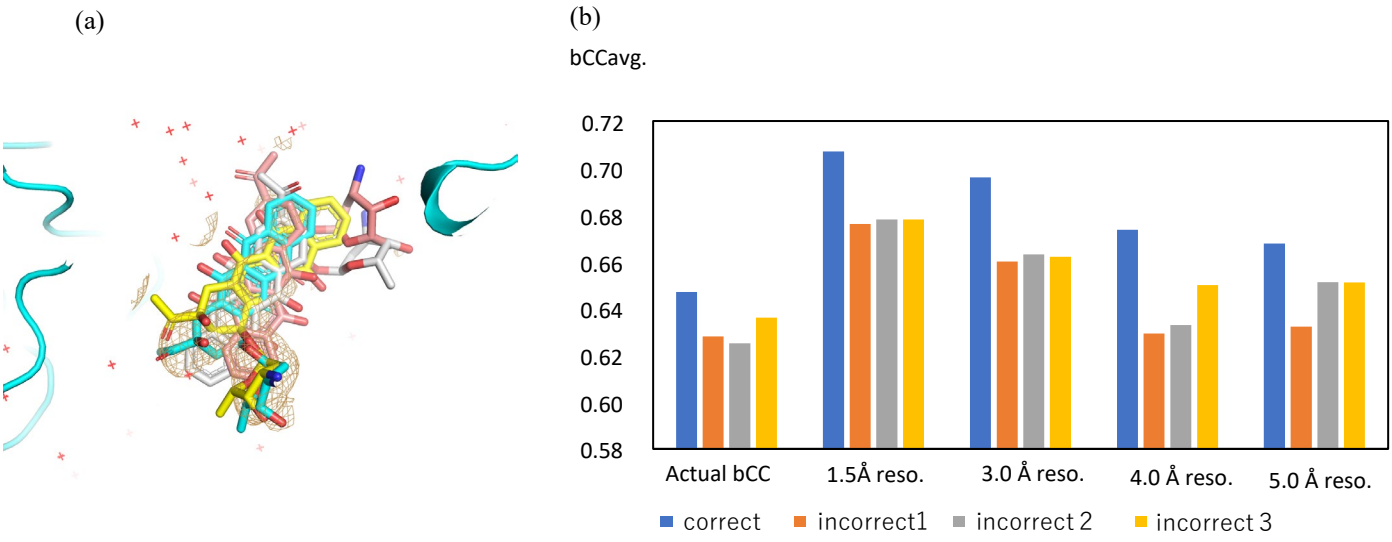

Figure 1. Preliminary experiment evaluating ligand docking pose using QAEmap.
(a) One correct and three incorrect poses and 2mFo-DFc electron density at 4.0Å resolution. Modified from PDB 3ARQ data.
(b) The poses and their corresponding electron densities calculated at various resolutions were input and evaluated with QAEmap. The correct structure yielded the highest score at all resolutions.

[1] Miyaguchi, I., Sato, M., Nakagawa, H., Kokabu, Y., Ma, B., Matsumoto, S., Tokuhisa, A., Ohta, M. & Ikeguchi, M. (2021). *Sci. Rep.* **11**, Article number: 23599.

A011-04-270823

The analysis of protein fine structure is a valuable tool for quality assessment

N. Balasco[1], L. Esposito[2], A.S. Thind[3], M.R. Guarracino[4], L. Vitagliano[2]

[1]Institute of Molecular Biology and Pathology, CNR c/o Sapienza University of Rome, P.le A. Moro 5, 00185 Rome, Italy, [2]Institute of Biostructures and Bioimaging, CNR, Via Pietro Castellino 111, 80131 Naples, Italy, [3]NSW Health Illawarra Shoalhaven - Local health districts (ISLHD), Wollongong, Australia, [4]University of Cassino and Southern Lazio, 0304 3Cassino, Italy.

luigi.vitagliano@cnr.it

Keywords: Protein structure validation, Peptide backbone geometry, Peptide bond planarity

Proteins combine molecular complexity and fine structural regulation. Although protein crystallography provided an enormous contribution to the development of structural biology, crystallographic data are generally not sufficient for effective protein structure refinements. In this framework, the assessment of the validity/quality of three-dimensional models represents a fundamental step in the structure determination process. Although impressive advances have been done [1], there are several unmet needs in this field. We and others have shown that backbone geometry and planarity of individual protein residues strongly depend on their local (φ,ψ) values [2-10]. By analysing the whole structural content of the Protein Data Bank (PDB), we here show that the variability of backbone geometry and planarity can be individually detected in the vast majority of protein structures including those refined at low/moderate resolution (Fig. 1). Our data demonstrate that the detection and the analysis of these fine structural elements are strongly correlated with the overall accuracy of individual structures. These findings clearly indicate that the evaluation of these subtle parameters represents an innovative and valuable tool for structure quality assessment. A web server for the automatic evaluation of the local and global quality of protein structures is under development (QuiProQua – QUIck PROtein structure QUAlity assessment).

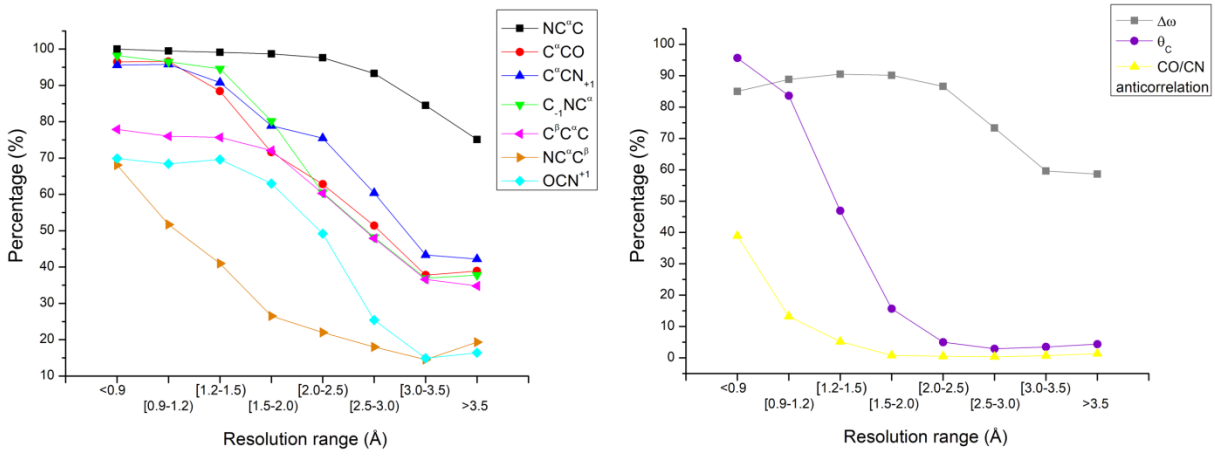

Figure 1. Percentage of PDB structures that show the geometry-conformation interplay for that parameter.

[1] Gore, S. et al. (2017). *Structure,* **25**, 1916-1927.
[2] Esposito, L., De Simone, A., Zagari, A., & Vitagliano, L. (2005). *J. Mol. Biol.*, **347**, 483-487.
[3] Berkholz, D. S., Shapovalov, M. V., Dunbrack, R. L., & Karplus P. A. (2009). *Structure*, **17**, 1316-1325.
[4] Berkholz, D. S., Driggers, C. M., Shapovalov, M. V., Dunbrack, R. L., & Karplus P. A. (2012). *PNAS*, **109**, 449-453.
[5] Esposito, L., Balasco, N., De Simone A., Berisio, R., & Vitagliano, L. (2013). *Biomed. Res. Int.*, 326914.
[6] Improta, R., Vitagliano, L., & Esposito, L. (2011). *PLoS One,* **6**, e24533.
[7] Improta, R., Vitagliano, L., & Esposito, L. (2015). *Proteins*, **83**, 1973-86.
[8] Improta, R., Vitagliano, L., & Esposito, L. (2015). *Acta Crystallogr., Sect. D*, **71**, 1272-83.
[9] Balasco, N., Esposito, L., & Vitagliano, L. (2017). *Acta Crystallogr., Sect. D*, **73**, 618-625.
[10] Balasco, N., Esposito, L., Thind, A. S., Guarracino, M. R., & Vitagliano, L. (2017). *Biomed. Res. Int.*, 2617629.

A011-05-270823

Understanding the molecular basis of retinoid signalling

A. M. Butler[1], E. Pohl[1,2] and A. Whiting[1]

[1]Department of Chemistry, Durham University, South Road, Durham. United Kingdom; [2]Department of Biosciences, Durham University, South Road, Durham. United Kingdom.

abbey.m.butler@durham.ac.uk

Keywords: Nuclear receptors, Vitamin A, Neurodegenerative diseases

Retinoic acid (RA) is one of the active metabolite forms of Vitamin A and functions as a key signalling molecule in the control of many developmental processes including differentiation, proliferation and apoptosis. Intracellular RA interacts with a range of cellular binding proteins and nuclear receptors as part of its key modulatory role in the regulation of transcription [1]. In this role, RA can be bound by Cellular Retinoic Acid Binding Proteins (CRABPs) 1 and 2. CRABP1 is solely localised within the intracellular matrix and functions as part of the non-genomic pathway, controlling a variety of RA-mediated pathways such as RA metabolism and kinase-dependent phosphorylation. CRABP2 functions as part of the genomic pathway and transports RA into the nucleus through interactions with α-importin. Within the nucleus, CRABP2 releases RA where it can be bound by two RA receptor families, Retinoic Acid Receptors (RARs) and Retinoid X Receptors (RXRs). RARs and RXRs can coordinate together through the binding of RA, along with small co-regulatory proteins, to form large heterodimeric complexes. These complexes act as transcriptional modulators to stimulate or repress the transcription of their target retinoid-responsive genes.

Retinoid signalling has been implicated in a wide range of diseases such as Alzheimer's disease, Parkinson's disease, motor neurone disease and cancer. Due to the highly diverse and powerful biological roles of retinoids in humans, studying and understanding the role of retinoids in these complex pathways is challenging as there is no singular structure-function relationship. Using a library of synthetic retinoid analogues, we are adopting an integrative approach by combining standard structural biology techniques with novel biochemical assaying methods to explore the underlying molecular basis for retinoid selectivity by both CRABPs and RAR/RXR heterodimers [2-3].

[1] Pohl, E. & Tomlinson, C. W. E. (2020). *Retinoid Signalling Pathways*, edited by E. Pohl. pp.151-173. London: Academic Press.
[2] Chisholm, D. R., Tomlinson, C. W. E., Zhou G-L., Holden, C., Affleck, V., Lamb R., Newling, K., Ashton, P., Valentine, R., Redfern, C., Erostyák, J., Makkai, G., Ambler, C. A., Whiting, A. & Pohl, E. (2019). *ACS Chem. Biol.,* **14**, 369.
[3] Tomlinson, C. W. E., Chisholm, D. R., Valentine, R., Whiting, A. & Pohl, E. (2018). *ACS Med. Chem. Lett.,* **9**, 1297.

A011-06-270823

Identification and validation of valuable low-pLDDT regions in AlphaFold Predictions

C.J. Williams

Duke University

christopher.sci.williams@gmail.com

Keywords: Structure prediction, low pLDDT, structure validation, molecular replacement

AlphaFold and related techniques are revolutionizing structural biology by providing fast, reliable access to initial models and molecular replacement targets. Many AlphaFold models are produced at high confidence and are ready to use with no intervention. Others are close and can be readily improved [1]. However, structure prediction may also yield models with substantial regions of low confidence. Do low-pLDDT regions contain structural predictions of value?

Here we present MolProbity-style tools for distinguishing between unstructured "barbed wire" [2] regions and structured "near-folded" regions of low-pLDDT AlphaFold predictions. Barbed wire regions may be useful as markers of intrinsic disorder [3], but they carry little other useful information for solving experimental structures. However, we show that near-folded regions can have significant predictive value (Fig. 1).

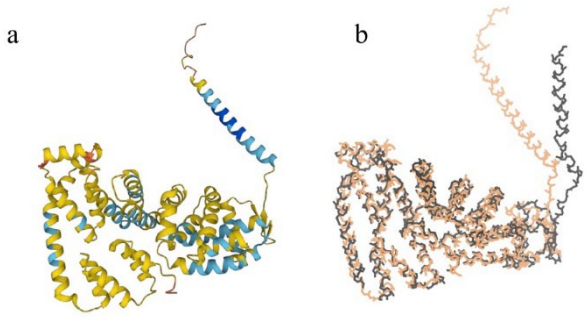

Figure 1. Alignment of a near-folded prediction with experimental structure. (a) AlphaFold prediction for P60228 from EBI database shows well-packed structure but low pLDDT (yellow). (b) AlphaFold prediction (peach) aligns well with experimental structure (black) of eukaryotic translation initiation factor 3 subunit E (from 6zon), despite low pLDDT scores.

Barbed wire regions [3] are distinguishable from near-folded regions by differences in steric contact density. Barbed wire regions also frequently show unusual patterns of backbone geometry, probably derived from the default configuration of AlphaFold's residue gas.

Near-folded regions are varied in their behaviour and useability. In addition to identifying regions of valuable structure prediction that would be lost with a simple pLDDT cutoff, we suggest methods to select, improve, and use the most promising regions.

[1] Twilliger, T. C., Poon, B. K., Afonine, P. V., Schlicksup, C. J., Croll, T. I., Millán, C. Richardson, J. S., Read, R. J., & Adams, P. D. (2022). *Nature Methods.* **19**, 1376-1382.

[2] Williams, C. W., Richardson, D. C., & Richardson, J. S. (2022). *Computational Crystallography Newsletter*. **13**, 7-12.

[3] Ruff, K. M. & Pappu, R. V. (2021). *J. Mol. Bio.*, **433**(20), 167208.

A029 Grain Boundary and Intergranular Phenomena Investigated by Diffraction-based Microstructural Imaging Methods
Room 219
4.00pm - 6.30pm

A029-01-270823

Deep learning for improving grain mapping from Near-field high-energy diffraction microscopy

Xiaoxu Guo, Hemant Sharma

Advanced Photon Source, Argonne National Laboratory, Lemont, IL 60439, USA
hsharma@anl.gov

Keywords: grain mapping, high energy diffraction microscopy, deep learning, denoising

Near-field high-energy diffraction microscopy (NF-HEDM) is an advanced imaging technique for non-destructive 3D characterization of grain structures. An accurate grain reconstruction critically relies on precise segmentation of diffraction spots in the NF-HEDM images. The traditional method utilizing a series of filters generally satisfies segmentation of sharp spots in the images, but it also leads to under segmentation of spots, especially the weaker spots with low signal to noise ratio. A neural network of blind-spot self-supervision deep learning network Noise2Void (N2V) is presented to efficiently and accurately denoise the NF-HEDM data with realistic noise. No need to provide the ground truth or pair of noised data, the N2V could be transferred to other type of images from the lab experiments. First the network is trained with the noised input diffraction images. Then the network is applied to denoise the image. Lower threshold than traditional method can be applied which gives more precise segmentation in general while threshold always a trade-off between saving weak/small spots and removing spots from noise. Comparisons of both processed images and grain reconstructions show that the N2V outperforms the traditional method, demonstrated by the improved confidence map, especially the small grains. Illustrated by the grain orientation map, more small grains have been reconstructed, which can give more accurate information of the grain boundaries.

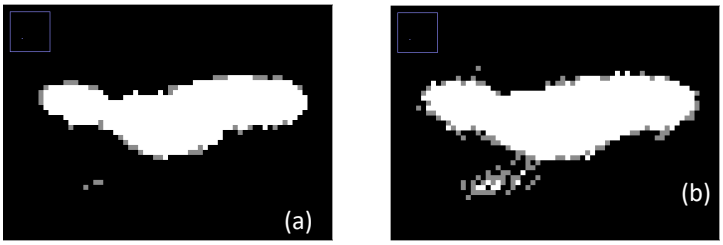

Figure 1. The visualization of the diffraction spots (a) processed with the traditional method, (b) processed with the N2V method.

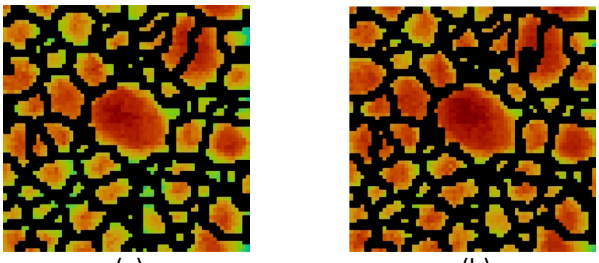

Figure 2. The confidence map and the grain boundaries (black solid line) of part of the sample reconstructed by the (a) traditional method (b) the N2V method.

[1] Joel V. Bernier, Robert M. Suter, Anthony D. Rollett & Jonathan D. Almer, (2020). *Annual Review of Materials Research.* **50**, 395-436.
[2] Alexander Krull, Tim-Oliver Buchholz & Florian Jug, (2019). *arXiv:1811.10980[cs.CV]*

A029-02-270823

Grain structure evolution during heat treatment of a semisolid Al-Cu alloy

J. Sun, J. Oddershede, F. Bachmann, E. Lauridsen

Xnovo Technology ApS, Køge, Denmark

elauridsen@xnovotech.com

Keywords: multimodal X-ray imaging, lab-based diffraction contrast tomography, sintering

3D experimental data of simultaneously high temporal and spatial resolution is key to validation of computational modelling of materials phenomena. In this study, we exploit lab-based X-ray imaging, combining absorption contrast tomography and diffraction contrast tomography [1], to capture the evolution of grain structure over a series of interrupted in-situ heat treatments of a semisolid Al-Cu alloy [2].

Multiple aspects of the microstructure are characterized comprehensively on the mesoscopic scale, including grain coarsening driven by Ostwald ripening, grain rotation driven by grain boundary energy as well as grain boundary wetting. With the time resolved response of the selected Al-Cu model alloy system, the present work provides insights into the rearrangement, densification and coarsening of powder compacts at late-stage sintering, revealing the crucial impact of crystallography upon the microstructural evolution.

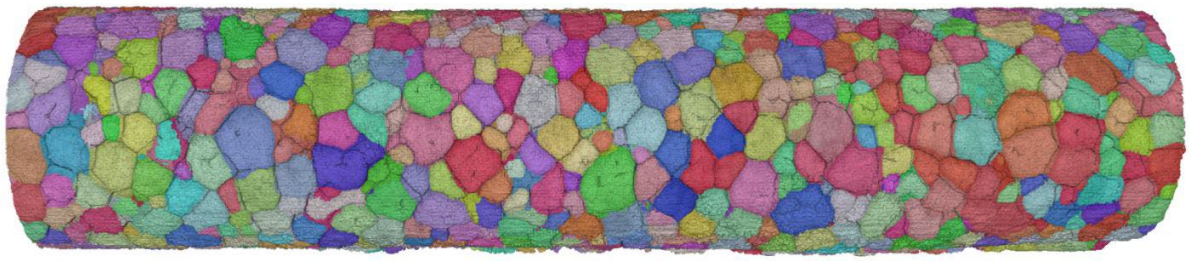

Figure 1. 3D grain map of the Al-Cu alloy sample colored by IPF along the long axis. The sample diameter is 1.6 mm and the length is 6.5 mm. The initial state contains more than 3000 Al grains.

[1] McDonald, S. A., Holzner, C., Lauridsen, E. M., Reischig, P., Merkle, A. P. & Withers, P. J. (2017). *Sci. Rep.*, **7**, 5251.
[2] Dake, J. M., Oddershede, J., Sørensen, H. O., Werz, T., Shatto, C., Uesugi, K., Schmidt, S. & Krill, C. E. (2016). *PNAS*, **113**, E5998.

A029-03-270823

Characterization of 3-D Slip Fields in Deforming Polycrystals

D. Pagan[1], K. Nygren[2], M. Miller[2]

[1]Materials Science and Engineering, Penn State, University Park, PA 16802, [2]Cornell High Energy Synchrotron Source, Cornell University, Ithaca, NY 14853

dcp5303@psu.edu

Keywords: Diffraction Microstructure Imaging, Crystal Plasticity, Titanium

The interconnecting interactions of crystallographic slip systems across ensembles of grains have been posited to be a critical factor in stress localization and subsequent nucleation of damage. To test these hypotheses, quantitative methods are needed to characterize slip activity in-situ in the bulk of deforming polycrystals. Here we present a new methodology that combines measurements of grain average stresses and spatially-resolved lattice orientation fields gathered using high-energy X-ray diffraction microscopy (HEDM) with crystal plasticity kinematics to reconstruct full 3-D slip activity fields at micron-scale resolutions. The utility of the method will be demonstrated through analysis of slip activity in Ti-7Al deformed under uniaxial tension. Focus will be placed on exploring stress dependence, lattice orientation dependence, and connectivity (network relationships) of grains experience elevated amounts of slip.

A029-04-270823

Nanobeam scanning 3D X-ray diffraction microscopy of a CdTe solar cell

Shukla A.[1], Stieglitz H.[2], Wright J.[5], Poulsen H.F.[1], Henningson A.[4], Stuckelberger M.[3], Besley L.[1], Baur C.[1], Krywka C.[2], Davydok A.[2], Andreasen J.W.[1]

Technical University of Denmark, Lyngby[1], Helmholtz-Zentrum Hereon, Geesthacht, Germany[2], Deutsches Elektronen-Synchrotron, Hamburg, Germany[3], Division of Solid Mechanics, Lund University, Ole Römers väg, 221 00 Lund, Sweden [4], European Synchrotron Radiation Facility, 71 avenue des Martyrs, 38000 Grenoble, France[5]

shuk@dtu.dk

Keywords: Diffraction Microscopy, Grain Boundary visualization, Renewable energy

CdTe (Cadmium Telluride) thin film solar cells have reached a device efficiency of 22.1% and are close to challenging silicon technology because of their low manufacturing cost and minimal material and energy use. Understanding the microstructure of grains within these polycrystalline thin film solar cells like CdTe devices is necessary to understand the ***effects of strain distribution within grains and at grain boundaries [1]*** on band fluctuations and overall performance of the device. Our work focuses on using 3D X-ray diffraction microscopy to map the grain structure and strain distribution of the CdTe absorber layer within a complete solar cell.

The CdTe solar cell device used for this experiment was fabricated using the conventional superstrate configuration [1]. The absorber layer was 6 µm thick and 5 µm high. The existing methods of 3DXRD are well-established for mapping the grain structure of polycrystalline systems [2]. In this study, we were able to probe much smaller grains than ever before owing to improvements in beamline hardware and better intragranular strain reconstruction tools [3]. The results in this abstract are from experiment done at ID11 beamline at ESRF with a nano focus beam of 100 nm and at an energy of 42 keV. This helped us visualize grains as small as 500 nm in diameter.

We were successfully able to create grain maps and strain maps [4] of CdTe absorber layer with a 100 nm resolution. We observe that the grains are much bigger in the bulk than near the surfaces.

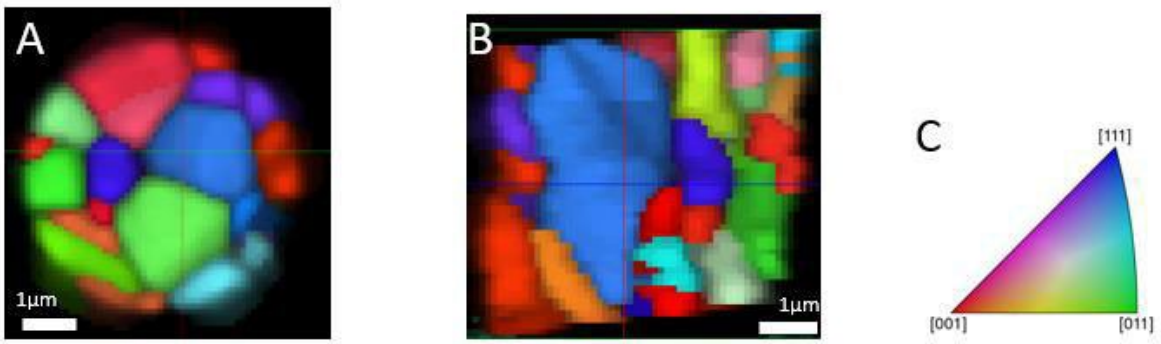

Figure 1. Diffraction grain maps showing individual grains and grain boundaries. A) Top view of a CdTe solar cell horizontal slice. B) Vertical slice across the CdTe solar cell. C) Grains are coloured according to inverse pole figure colouring of their orientations.

[1] I. Calvo-Almazán et al. (2019) *IEEE Journal of Photovoltaics*, vol. 9, no. 6, pp. 1790-1799
[2] H.F Poulsen et al. (2012) *J. Appl. Cryst.* 45, 1084-1097
[3] A. Henningsson et al. (2021) *J. Appl. Cryst*. 54, 1057-1070

These experiments were carried out with the help from scientists and people responsible at ID11 ESRF and P03 nano focus at PETRA III . We are grateful to Tursun Ablekim and Eric Colegrove (National Renewable Energy Laboratory, USA) who provided the solar cell. Special thanks to the DANSCATT instrument centre which is funded by the Danish Ministry for Higher Education and Research.

A029-05-270823

Three dimensional large volume grain mapping and crystallographic orientation by lab-based Diffraction Contrast Tomography

H. Bale[1], N. Gueninchault[1], B. Tordoff[1], J. Sun[2], E. Lauridsen[2]

[1]Carl Zeiss X-ray Microscopy Inc, Dublin, CA, United States
[2]Xnovo Technology ApS, Køge, Denmark
Hrishikesh.bale@zeiss.com

Keywords: laboratory diffraction contrast tomography; large sample characterization; non-destructive analysis

Determining crystallographic microstructure of a given material in 2D can be challenging. Further extending such an investigation to 3D on meaningful volumes (and without sample sectioning) can be even more so. Yet reaching this insight holds tremendous value for 3D materials science since the properties and performance of materials are intricately linked to microstructural morphology including crystal orientation.

Laboratory diffraction contrast tomography (LabDCT) technique implemented on a lab X-ray microscope opens up a whole new range of possibilities for studies of the effect of 3D crystallography on materials performance in the laboratory. Using a polychromatic X-ray source, LabDCT takes advantage of the Laue focusing effect, improving diffraction signal detection and allows handling of many and closely spaced reflections. Grain morphology, orientation and boundaries of metals, alloys or ceramics can be characterized fully in 3D.

The non-destructive nature of LabDCT enables the observation and characterization of microstructural response to stimuli (stress, thermal, radiation) of one and the same sample over time, complementing electron backscatter diffraction (EBSD) for application cases when it is challenging to investigate microstructure evolution when subject to either mechanical, thermal or other environmental conditions.

Recent advances of LabDCT allow to record and reconstruct larger representative sample volumes seamlessly, meeting the demand of statistically relevant characterization of polycrystalline grain microstructure. We will present a study on non-oriented electrical steels using LabDCT covering sample volumes up to 3mm by 3mm by 0.5mm. Additionally, application of LabDCT for geological samples will also be presented and discussed.

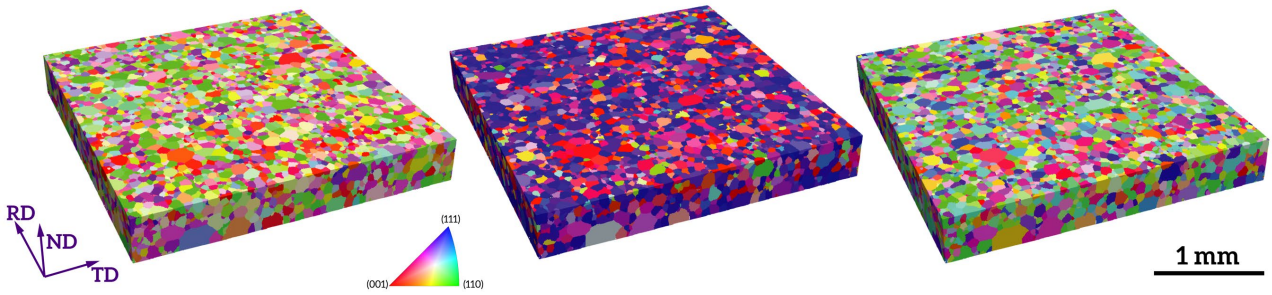

Figure 1. Figure 1: 3D grain map of an electrical steel sample obtained through LabDCT. (Left to right: IPF colored based on RD, ND, TD of the sample)

A029-06-270823

Inclined scanning 3DXRD microscopy for the high-resolution 3D grain orientation mapping

Jaemyung Kim[1], Yujiro Hayashi[1], and Makina Yabashi[1,2]

RIKEN Spring-8 Center, 1-1-1 Kouto, Sayo-cho, Sayo-gun, Hyogo, 689-5148, Japan

Japan Synchrotron Radiation Research Institute, Sayo-cho, Sayo-gun, Hyogo, 679-5148, Japan

jaemyung.kim@riken.jp

Keywords: orientation microscopy, 3DXRD, inclined scanning 3DXRD

Understanding the microstructure of polycrystalline material is essential to accurately predict and optimize the materials' properties. A comprehensive understanding of grain size, grain boundaries, and defect distribution can help predict and optimize the performance, as well as prevent the malfunction of material. Studies have demonstrated that the mechanical strength of polycrystalline metals increases as grain size decreases to a critical value. This is due to the grain boundaries acting as barriers to dislocation propagation and fatigue crack growth, known as the Hall-Petch relation. Other research on the effect of misorientation angle on grain boundary energy has found that under specific angles and axes, the grains form a coincident site. At a low degree of coincidence, grain boundary energy is lower, resulting in improved physical and chemical properties. Those cases give insight into the importance of understanding microstructure in terms of controlling mechanical, and chemical properties.

In recent decades, methods based on x-ray diffraction have proven successful in obtaining spatial maps of the grain orientation within polycrystalline materials. The development of orientation microscopy techniques, including differential aperture x-ray microscopy (DAXM, diffraction contrast tomography (DCT), three-dimensional x-ray diffraction microscopy (3DXRD), and high-energy diffraction microscopy (HEDM), has been accelerated with the help of high-brilliance synchrotron x-rays. Among these methods, scanning 3DXRD microscopy [1, 2] is particularly useful for thick specimens. The scanning 3DXRD uses a point-focused or pencil beam to illuminate a sample, and the diffraction spots are captured through a 3D scan that involves sample rotation. The 3D grain maps are created through voxel-by-voxel multigrain indexing, with each voxel representing a regular grid in three dimensions. The use of a conical slit in the detection of diffracted beams reduces the overlap of diffraction spots by selectively shielding diffracted beams from many grains, except for those from grains in the area of interest. As a result, the scanning 3DXRD is applicable even for thick samples with numerous grains.

A straightforward approach to improve the spatial resolution in scanning 3DXRD is to use brighter x-ray sources, which can increase the intensity of the diffracted x-rays and enhances the signal-to-noise ratio, making it easier to distinguish between different diffraction peaks in the diffraction spots. Furthermore, optimizing the x-ray optics and reducing the detector pixel size can also contribute to the resolution enhancement. Those two approaches enable to enhance the quality of diffraction patterns in the diffraction pattern measurement process, while advanced data analysis techniques achieving high resolution have yet to be explored in the field of scanning 3DXRD microscopy. Here we present a new method, called the inclined scanning 3DXRD, which enhances the spatial resolution by subdividing a voxel into small sub-voxel pieces. This method involves inclining the sample rotation axis similar to x-ray laminography, thereby obtaining geometrical functions for sub-voxel analysis in all sample coordinates. A synchrotron x-ray-based inclined scanning 3DXRD experiment on a polycrystalline α-Fe wire with a sample translation of 10 μm showed a grain microstructure with a sub-voxel resolution of 1.25 μm. The simulation results were in agreement with the experiment, suggesting that the proposed method can significantly improve the spatial resolution of the 3D grain orientation map.

[3] Hayashi, Y., Hirose, Y. & Seno, Y. (2015). *J. Appl. Cryst.* **48**, 1094–1101.
[4] Hayashi, Y., Setoyama, Y., Hirose, Y., Yoshida, T. & Kimura, T. (2019). *Science* **366**, 1492-1496.

A064 New Opto-electronic Functional Materials
Room 217
4.00pm - 6.30pm

A064-01-270823

2D antimony oxide in $K_2(Sb_2O_3)_2Te$ and an unusual optoelectronic behaviour

Huanyu He[1], Ralf Albrecht[1], Kati Finzel[1], Michael Rüsing[1], Michael Ruck[1,2]

[1]Technische Universität Dresden, Dresden, Germany [2]Max-Planck Institute for Chemical Physics of Solids, Dresden, Germany

huanyu.he@tu-dresden.de

Keywords: hydroflux, antimony oxide, layered compounds

We are currently investigating the potential of the novel synthesis approach 'hydroflux', which is intermediate between the alkaline salt flux and the hydrothermal synthesis method as proposed by *zur Loye* et al. in 2013.[1] This method utilizes approximately an equimolar ratio of hydroxide (e.g. KOH) to water, corresponding to concentrations such as 50 M KOH. The high number of new compounds discovered with this method suggest that hydroflux is a unique reaction medium.[2] Acid-base as well as redox chemistry are substantially different from established approaches. This is directly connected to the strong hydrophilicity of the hydroflux. In addition, the use of rather inexpensive Teflon-lined autoclaves, relatively low temperatures (150-250 °C) and short reaction times (within a few hours) make this synthetic method extremely promising. Moreover, crystals with sizes up to centimeters have been grown from hydroflux.

Using this approach, shiny green, air-stable single-crystals of the layered oxide telluride K2(Sb2O3)2Te (Fig.1a, 1b) were synthesized starting from TeO2 and Sb2O3 in a potassium hydroxide hydroflux. The reduction of tellurium(IV) to tellurium(II) in the hydroflux has recently been investigated in detail in our group.[3] The synthesis of K2(Sb2O3)2Te was achieved through the addition of excess Sb2O3 as reducing agent that is oxidized to antimonate(V). Single-crystal X-ray diffraction revealed a rhombohedral layered structure (space group $R\bar{3}m$) with lattice parameters a = 569.31(3) pm and c = 2744.55(13) pm at 100(1) K (Figure.1c, 1d). The unprecedented honeycomb Sb2O3 layer (not known as a polymorph) is uncharged but polar with all antimony cations residing on one side. However, both orientations of the ferroelectric layer exist, connected by inversion symmetry. Potassium cations reside in the gap between two adjacent Sb2O3 layers that face each other with their oxide sides, telluride anions between the layer faces formed by antimony atoms.

The green metallic luster of K2(Sb2O3)2Te is highly unusual. The investigation of the optical and electronic properties in combination with electronic band structure calculations revealed a plethora of exceptional properties, such as compound-intrinsic transistor and varistor behavior, energy up-conversion in steps of 1.3 eV and 2.5 eV, enhancement of electrical conductivity by light of low energy (700 nm), but insulating behavior under light of high energy (300 nm).

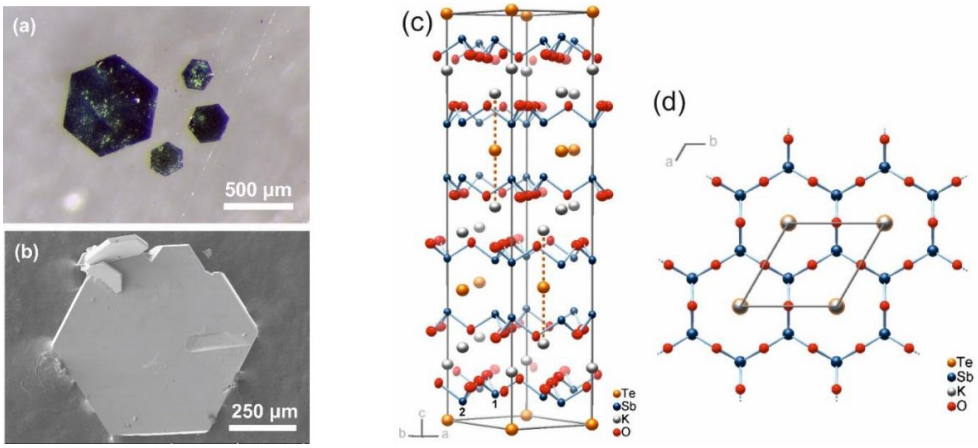

Figure 1. (a): Crystals obtained from hydroflux; (b) scanning electron microscopy (SEM) image of the crystal; (c): Crystal structure of $K_2(Sb_2O_3)_2Te$. (d): Top view of a Sb_2O_3 honeycomb layer and the K···Te···K "dumbbells" that penetrate the layer perpendicularly.

[1] W. M. Chance, D. E. Bugaris, A. S. Sefat, H.-C. zur Loye, *Inorg. Chem.* **2013**, *52*, 11723–11733.

[2] R. Albrecht, *Exploration of the Hydroflux Synthesis*, PhD Thesis, Technische Universität Dresden (Germany), **2022**.

[3] R. Albrecht, M. Ruck, *Angew. Chem., Int. Ed.* **2021**, *60*, 22570–22577.

A064-02-270823

Crystal structure of $Cu_2Zn(Ge_xSi_{1-x})Se_4$ solid solution: the kesterite to wurz-kesterite structural phase transition

Gurieva[1*], S. Niedenzu[1], A. Manjon Sanz[2], M. Kirkham[2], S. Schorr[1,3]

[2] Helmholtz-Zentrum Berlin für Materialien und Energie, 14109 Berlin, Germany, [2]Neutron Scattering Division, Oak Ridge National Laboratory, Oak Ridge, TN 37831, USA, [3]Freie Universität Berlin, Institute of Geological Sciences, 12249 Berlin, Germany

galina.gurieva@helmholtz-berlin.de

Keywords: CZSiGeSe, neutron powder diffraction, phase transition

The quaternary semiconductors Cu2ZnGeSe4 (CZGSe) and Cu2ZnSiSe4 (CZSiSe) belong to the adamantine compound family, contain only earth abundant, non-toxic elements and have drawn wide attention for their potential applications in many fields. Depending on their band gaps these materials are interesting for thin film solar cells [1,2], high-temperature thermoelectric materials [3], and non-linear optics [4]. For instance, CZGSe is a promising candidate for top cell absorber layers in multi junction solar cells due to its band gap of 1.5 eV [1]. The band gap can be tuned by anion substitution applying different anion ratios such as in the solid solution Cu2ZnGe(S1-xSex)4. However due to challenges in controlling the anion ratio, cationic substitution like Ge ↔ Si is considered as an alternative method to perform band gap engineering. Thus CZSiSe, which has a band gap of 2.2 eV [5], is discussed to be of interest as material for nonlinear optics [4].

Experimental and theoretical studies show that CZGSe crystallizes in the kesterite type structure (space group $I\bar{4}$) [6]. It was recently shown by multiple-edge anomalous diffraction method (MEAD) that CZSiSe crystallizes in the monoclinic wurtz-kesterite type structure (space group *P*) [7]. But the difference between wurz-kesterite and previously reported wurz-stannite type structures are very small and are impossible to see in the conventional X-ray diffraction (XRD) patterns. According to our XRD studies, the Si-rich mixed crystals Cu2Zn(GexSi1-x)Se4 with x = 0.1 – 0.37 show the orthorhombic wurtz-stannite type structure (space group P 21) (or undistinguishable monoclinic wurz-kesterite type structure), whereas the Ge-rich mixed crystals Cu2Zn(GexSi1-x)Se4 with x = 0.59 – 0.9 show the tetragonal kesterite (space group $I\bar{4}$) or stannite type structure (space group $I\bar{4}2$), also very unlikely to distinguish by conventional XRD. Cu2Zn(GexSi1-x)Se4 with x = 0.45 – 0.55 show a coexistence of both, the monoclinic and the tetragonal phase [8]. The kesterite and the stannite type structure as well as the wurtz-stannite and wurtz-kesterite type structure distinguish by a different Cu and Zn distribution [9]. A differentiation of Cu^+, Zn^{2+}, and Ge^{4+} is not possible using only XRD since these cations are isoelectronic and have a similar scattering power for X-rays. However, by using neutron diffraction it is possible to distinguish the Cu^+, Zn^{2+}, and Ge^{4+} cations, since they show different neutron scattering lengths. Thus, neutron diffraction data allows a detailed structural characterization, which enables the differentiation between the stannite and the kesterite type structure as well as between the wurtz-stannite and wurtz-kesterite structure. We already applied neutron diffraction to distinguish between kesterite and stannite type structure and found out that CZGSe adopts the kesterite type structure [6]. For CZSiSe MEAD shows wurz-kesterite to be the ground state structure [7]. For the solid solution Cu2Zn(GexSi1-x)Se4 with x = 0.1 – 0.9 only powder XRD data was available by now.

In this study we will present a systematic investigation of the full composition range of Cu2Zn(GexSi1-x)Se4 by powder neutron diffraction, will give insights into the composition dependent structural transition from kesterite to wurtz-kesterite type structure and the variation of structural parameters. The study of the crystal structure, focusing on the effect of the cation distribution, will allow us to determine type and concentration of intrinsic point defects which are crucial since it determines the electronic properties and therefore the functionality of the solid material to a high degree. A better understanding of these materials will lead to an improvement of their characteristics and opens the door to new Photovoltaic devices.

[7] T. Schnabel et al., Energies, 10 (2017) 1813-1822
[8] Q. Guo et al., Sol. Energy Mater. Sol. Cells, 105 (2012) 132
[9] Heinrich et al., J. Am. Chem. Soc. 136 (2014) 442−448
[4 Rosmus et al., Inorg. Chem. 53 (2014) 7809−7811
[4] G.-Q. Yao et., Solid State Ionics, 24 (1987) 249–252
[5] G. Gurieva et al., J. Phys. Chem. Solids, 99 (2016) 100-104

[6] D. Többens et al., Acta Cryst B., (2020). B76, 1-9
[7] S. Niedenzu et al., IEEE (2018), pp. 3290-3293
[8] S. Schorr, Sol. Energy Mater. Sol. Cells, 95 (2011) 1482-1488

This work has received funding from the European Union's Horizon 2020 research and innovation program under grant agreement no.952982. A portion of this research used resources at the Spallation Neutron Source, a DOE Office of Science User Facility operated by the ORNL.

A064-03-270823

Discovery of inorganic functional compounds and their property improvement

Ling Chen,[1,*] Li-Ming Wu[2]

[1]*College of Chemistry, Beijing Normal University, Beijing 100875, People's Republic of China*
[2]*Center for Advanced Materials Research, Beijing Normal University, Zhuhai 519087, People's Republic of China*
E-mail: chenl@bnu.edu.cn

Keywords: nonlinear optical material, thermoelectric compounds, crystal structure-property relationship

I introduce herein our recent research efforts in discovering inorganic solid functional compounds (nonlinear optical doublers, or thermoelectric compounds), revealing the relationship between the crystallographic structures and the macroscopic nonlinear optical properties or thermoelectric properties. The NLO examples include the first SHG monofluorophosphate,[1,2] the new *π conjugation confinement* structure-design-theory of DUV NLO compound [3], and the *band structure engineer bucket effect theory*. [4,5] The examples of thermoelectric compounds include $CsCu_5Te_3$, Bi_8Se_7,[6-8] etc. We reveal that the multiple coordination spheres, component with mixed valence state involved in a complex structure will lead to a low lattice thermal conductivity, in the case of Bi_8Se_7, the interlayer π-bond interactions increase the carrier mobility along the structure stacking direction. [6-10]

[1] Lu, J.; Yue, J. N.; Xiong, L.; Zhang, W. K.; Chen, L.; Wu, L. M. Uniform Alignment of Non-π-Conjugated Species Enhances Deep Ultraviolet Optical Nonlinearity. *J. Am. Chem. Soc.* 2019, *141*, 8093−8097.
[2] Pan, C. Y.; Yang, X. R.; Xiong, L.; Lu, Z. W.; Zhen, B. Y.; Sui, X.; Deng, X. B.; Wu, L. M.; Chen, L. Solid-State Nonlinear Optical Switch with the Widest Switching Temperature Range Owing to Its Continuously Tunable Tc. *J. Am. Chem. Soc.* 2020, *142*, 6423−6431.
[3] Xiong, L.; Wu, L. M.; Chen, L. A General Principle for DUV NLO Materials: π-Conjugated Confinement Enlarges Band Gap. *Angew. Chem. Int. Ed.* 2021, *60,* 25063–25067.
[4] Liu, Q. Q.; Liu X.; Wu, L. M.; Chen, L. $SrZnGeS_4$: A Dual-Waveband Nonlinear Optical Material with A Transparency Spanning UV–Vis and Far-IR Spectral Regions. *Angew. Chem. Int. Ed.* 2022, *61,* e202205587.
[5] Li, R. A.; Liu, Q. Q.; Liu, X.; Liu, Y.; Jiang, X.; Lin, Z.; Jia, F.; Xiong, L.; Chen, L.; Wu, L. M. $Na_2Ba[Na_2Sn_2S_7]$: Structural Tolerance Factor-guided NLO Performance Improvement. *Angew. Chem. Int. Ed.* 2023, 62, e202218048.
[6] Jia, F.; Liu, Y. Y.; Zhang, Y. F.; Shu, X.; Chen, L.; Wu, L. M. Bi_8Se_7: Delocalized Interlayer π Bond Interactions Enhancing Carrier Mobility and Thermoelectric Performance Near Room Temperature. *J. Am. Chem. Soc.* 2020, 142, 12536−12543.
[7] Ma, N.; Li, Y. Y.; Chen, L.;* Wu, L. M.* α-$CsCu_5Se_3$: Discovery of a Low-Cost Bulk Selenide with High Thermoelectric Performance. *J. Am. Chem. Soc.* 2020, 142, 11, 5293-5303.
[8] Ma, N.; Li, F.; Li, J. G.; Liu, X.; Zhang, D. B.; Li, Y. Y.; Chen, L.;* Wu, L. M.* Mixed-Valence $CsCu_4Se_3$: Large Phonon Anharmonicity Driven by the Hierarchy of the Rigid $[(Cu^+)_4(Se^{2-})_2](Se^-)$ Double Anti-CaF_2 Layer and the Soft Cs^+ Sublattice. *J. Am. Chem. Soc*. 2021, **143**, 18490−18501.
[9] Li, F.; Liu, X.; Ma, N.; Chen, L.; Wu, L. M. Thermoelectric Zintl Compound $In_{1-x}Ga_xTe$: Pure Acoustic Phonon Scattering and Dopant-Induced Deformation Potential Reduction and Lattice Shrink. *Angew. Chem. Int. Ed.* 2022, 61, e202208216.
[10] Liu, J. Y.; Chen. L.; Wu, L. M. Ag_9GaSe_6: High-Pressure-Induced Ag Migration Causes Thermoelectric Performance Irreproducibility and Elimination of Such Instability. *Nat. Commun.* 2022, 13, 2966.

A064-04-270823

Linking structure and properties in energy materials: intercalation in hybrid perovskites

Linjie Yang1, Wenye Xuan2,3 David Webster4, Lethy Krishnan Jagadamma4, Teng Li1, David N. Miller,1 David B. Cordes1, Alexandra M. Z. Slawin1, Graham A. Turnbull4, Ifor D. W. Samuel4 , Hsin-Yi Tiffany Chen3, Philip Lightfoot1, Matthew S. Dyer2, Julia L. Payne1*

1. School of Chemistry, University of St Andrews, North Haugh, St Andrews, Fife, KY16 9ST. UK. 2. School of Chemistry, University of Liverpool, Crown St, Liverpool, L69 7ZD. UK and Materials Innovation Factory, University of Liverpool, 51 Oxford St, Liverpool, L7 3NY. UK. 3. Department of Engineering and System Science, National Tsing Hua University, Hsinchu 30013, Taiwan. 4. Organic Semiconductor Centre, School of Physics and Astronomy, University of St Andrews, North Haugh, St Andrews, Fife, KY16 9SS. UK

jlp8@st-andrews.ac.uk

Keywords: Optoelectronic Properties, Intercalation, Hybrid Perovskite

Climate change is one of the most pressing problems of the 21st century and in order to reduce our reliance on fossil fuels, new materials for energy conversion and energy storage are required. One family of materials receiving significant interest in this area are hybrid perovskites, also known as organic-inorganic metal halides, which can be used in photovoltaic devices. The archetypal hybrid perovskite is CH3NH3PbI3 and the key difference with conventional perovskites is the fact that the A site cation is an organic ammonium cation rather than an inorganic cation. Since first being used in a solar cell in 2009, the power conversion efficiencies (PCE) of CH3NH3PbI3 based photovoltaics have increased from 3.8% to 25.7%, whilst tandem solar cells made from silicon and CH3NH3PbI3 have achieved a PCE of 32.5 % [1,2]. These materials have a huge degree of compositional flexibility and as a result, they are highly tuneable, as the band gap of these materials can be adjusted by doping on the cation or anion sites of the perovskite. The most common way of tuning the band gap is by halide substitution, whereby a halide anion can be replaced by a different halide. However, work in our group has recently looked at a new method of tuning the band gap, namely halogen molecule intercalation.

Here we show that we can reversibly intercalate Br2 between the [PbBr4]∞ layers in the two dimensional layered perovskite [H3N(CH2)6NH3]PbBr4 to give [H3N(CH2)6NH3]PbBr4·Br2 [3]. An in-depth study of the crystal structure shows that upon intercalation, there is an expansion of the *a*-axis of the unit cell, the conformation of the organic cation changes to an all-trans configuration and the interlayer shift between the [PbBr4]∞ layers is significantly reduced, changing the structure from a Ruddlesden-Popper-like phase to a Dion-Jacobson-like phase. Together, this results in a decrease in band-gap of 0.85 eV, which is particularly significant as the parent perovskite, [H3N(CH2)6NH3]PbBr4, only contains a single layer of lead bromide octahedra. Our work is backed up by theoretical studies, which shows that Br2 intercalation results in a new band in the electronic structure and a decrease in effective masses by around 2 orders of magnitude. The resistivity also decreases upon intercalation, indicating that [H3N(CH2)6NH3]PbBr4·Br2 has an increased charge carrier mobility/ carrier concentration when compared to [H3N(CH2)6NH3]PbBr4. Further examination of the crystal structure and electron density difference maps show that halogen bonding is a key factor for this change in properties. As a result, the halogen bond is another non-covalent interaction which can be exploited in the design of new hybrid perovskites for optoelectronic applications.

[2] Kojima, A.; Teshima, K.; Shirai, Y.; Miyasaka, T. (2009). *J. Am. Chem. Soc.* 131, 6050−6051.
[3] https://www.nrel.gov/pv/cell-efficiency.html (accessed January 11th 2023)
[4] Yang, L., Xuan, X., Webster, D., Krishnan Jagadamma, L., Li, T., Miller, D. N., Cordes, D. B., Slawin, A. M. Z., Turnbull, G. A., Samuel, I. D. W., Chen, H-Y T., Lightfoot P., Dyer, M. S., Payne, J. L. (2023) *Chem. Mater.* ***in review***.

A064-05-270823

Pas de Deux of a nitrosyl Couple: Synchronous Photoswitching from a Double-Linear to a Double-Bent in a metal dinitrosyl photoinduced linkage isomer

Hasil[1], D. Beck[2], D. Schröder[2], S. Pillet[1], E. Wenger[1], T. Woike[1], P. Klüfers[2], and D. Schaniel[1]

[1]Laboratoire de Cristallographie, Résonance Magnétique et Modélisations, Institut Jean Barriol, Université de Lorraine, CNRS, CRM2, F-54000 Nancy, France [2]Department Chemie der Ludwigs-Maximilians-Universität Butenandtstraße 5–13, 81377 München, Germany Email[1]: asma.hasil@univ-lorraine.fr

Keywords: reversible molecular photoswitches, synchronous dinitrosyl switch, photo-crystallography

Reversible molecular photoswitches are of great interest in the search for fast and sensitive materials that can be used for building photonic devices or molecular machines [1,2]. In this context, photoinduced linkage isomerism (PLI) in transition-metal nitrosyl compounds is of importance since the reversible photoswitching of the NO ligand is accompanied by significant photochromic and photorefractive changes [3]. In order to better understand the PLI mechanism responsible for these exciting properties, the knowledge of the bonding and activation of NO is essential. Here, we present for the very first time $\{Ru(NO)2\}^{10}$ dinitrosylruthenium complex [Ru(NO)2(PPh3)2] showing photo-induced linkage isomerism (PLI) of a special kind (Figure 1): the two NO ligands switch, on photo-excitation, *synchronously* from the ground state (GS) with two almost linear RuNO functions to a metastable state (MS) which persists up to 230 K and can be populated to ≈ 50% [4]. The MS was experimentally characterised by photo-crystallography, IR spectroscopy and DS-calorimetry as a double-bent variant of the double-linear GS. The experimental results are confirmed by computation revealing the GS/MS transition as a disrotatory *synchronous* 50° turn of the two nitrosyl ligands. Only the synchronous disrotatory motion of the pair of nitrosyl ligands, pictorially the *pas de deux* of a nitrosyl couple, allows a smooth transition free of too many bond ruptures. As a result, there is an activation barrier that makes both isomers tangible. This type of motion might find application in molecular motors, since low doses of yellow light can switch it on, inducing a movement in one direction.

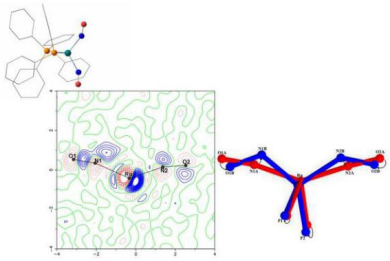

Figure 1. Left: Photodifference map after irradiation with 590 nm laser at 100 K; blue: positive values, red: negative values; contour-lines every 0.5 e $Å^{-3}$. Right: comparison of GS and MS structure illustrating the $(l\text{-}NO\text{-}\kappa N)^2$ GS to the metastable $(a\text{-}NO\text{-}\kappa N)^2$ MS configurational change.

[2] Feringa, B. L. (2017). *Angew. Chem. Int. Edit.,* **56**(37), 11060-11078.
[3] Bléger, D., & Hecht, S. (2015). *Angew. Chem. Int. Edit.,* **54**(39), 11338-11349.
[4] Schaniel, D., Imlau, M., Weisemoeller, T., Woike, T., Krämer, K. W., & Güdel, H. U. (2007). *Adv. mater.*, **19**(5), 723-726.
[5] Hasil, A., Beck, D., Schröder, D., Pillet, S., Wenger, E., Woike, T., ... & Schaniel, D. (2022). *Angew. Chem. Int. Edit.*, **61**(42), e202210671.

A064-06-270823

Mechanically induced energy conversion by polymorphic single crystals of α-[(4-methoxyphenyl)methylene]-4-nitrobenzeneacetonitrile

Durga Prasad Karothu,[1,2] Srujana Polavaram,[1] Ejaz Ahmed,[1] Zainab Alhaddad,[1] Panče Naumov[1,2,3]

[1]*Smart Materials Lab, New York University Abu Dhabi (United Arab Emirates)*
[2]*Center for Smart Engineering Materials, New York University Abu Dhabi (United Arab Emirates)*
[3]*Molecular Design Institute, Department of Chemistry, New York University 100 Washington Square East, New York, NY, USA*

dpk3@nyu.edu

Keywords: phase transition, mechanosalient effect, single-crystal-to single-crystal transformation, polymorphism

Single-crystal-to-single-crystal (SCSC) phase transitions are considered as direct structural transformations between single crystals in the solid state that occur without impairment of the crystal lattice. The SCSC transitions can be induced in organic, inorganic, metal-organic or organometallic crystalline materials by external stimuli such as heat, light, mechanical force, or electricity [1]. The respective crystalline materials have demonstrated potentials for applications in several fields, such as energy harvesting, sensors, actuators and artificial muscles [2–4]. In particular, SCSC transitions triggered by application of mechanical force that result in crystal motion [5,6], known as 'mechanosalient effect', are very rare deformations that occur by sudden release of energy [6,7] originating from the elastic strain accumulated in the crystal lattice. For example, single crystals of the metastable form I of terephthalic acid are known to be mechanosalient, and they move when subjected to localized mechanical stress [6,7]. Inspired by the extraordinary behavior of this material, we have now investigated another material which exhibits the mechanosalient effect. The compound, α-[(4-methoxyphenyl)methylene]-4-nitrobenzeneacetonitrile, is known to display concomitant polymorphism (forms I, II, III, and a *cis* form) and it can also crystallize as solvates [8–11]. The structures of forms II and III are non-centrosymmetric and are thus candidates as non-linear optical (NLO) material. Crystalline samples of form II obtained by crystallization from melt or deposition from vapor phase are mechanically unstable and undergo transformation to form III under mechanical stress [8]. However, this mechanical transformation has not been completely explained, and therefore it warrants further studies with respect to its mechanical, spectroscopic and structural aspects.

Here, we report the results from a detailed study of the mechanosalient effect in this compound. Single crystals of form II are metastable, and upon contact with a metal needle undergo a remarkable reshaping upon transformation to form III. The reversible transition (form III to form II) was performed by heating. Moreover, when they are exposed to mechanical pressure (form II to form III) and heating (form III to form II), the transformations are accompanied by change in color and fluorescence lifetime. The transitions induced by mechanical stimulation and heating were studied by thermal, mechanical, spectroscopic and crystallographic techniques. This material is a rare example of small molecule fluorescent crystal that undergoes a mechanosalient transition, and might be a promising candidate for the development of pressure-responsive materials.

[1] Zheng, Y. S., Jia, X. D., Li, K., Xu, J. L. & Bu, X. H. (2021). *Adv. Energy Mater.* 2100324.
[2] Dong, Y., Wang, J., Guo, X., Yang, S., Ozen, M. O., Chen, P., Liu, X., Du, W., Xiao, F., Demirci, U. & Liu, B. F. (2019). *Nat. Commun.* **10**, 4087.
[3] Dattler, D., Fuks, G., Heiser, J., Moulin, E., Perrot, A., Yao, X. & Giuseppone, N. (2020). *Chem. Rev.* **120**, 310.
[4] Abendroth, J. M., Bushuyev, O. S., Weiss, P. S. & Barrett, C. J. (2015). *ACS Nano* **9**, 7746.
[5] Liu, G., Liu, J., Liu, Y. & Tao, X. (2014). *J. Am. Chem. Soc.* **136**, 590.
[6] Karothu, D. P., Weston, J., Desta, I. T. & Naumov, P. (2016). *J. Am. Chem. Soc.* **138**, 13298.
[7] Ahmed, E., Karothu, D. P., Warren M. & Naumov, P. (2019). *Nat. Commun.* **10**, 3723.
[8] Vrcelj, R. M., Shephered, E. E. A., Yoon, C. S., Sherwood J. N. & Kennedy, A. R. (2002). *Cryst. Growth Des.* **2**, 609.
[9] Jha, K. K., Dutta, S. & Munshi, P. (2018). *Cryst. Growth Des.* **18**, 1126.
[10] Cattoën**, X.,** Kumar, A., Dubois, F., Vaillant, C., Matta-Seclén, M., Leynaud, O., Kodjikian, S., Hediger, S., De Paëpe, G. & Ibanez, A. (2022). *Cryst. Growth Des.* **22**, 2181.
[11] Sanz, N., Baldeck, P. L., Nicoud, J. F., Fur, Y. L. & Ibanez, A. (2001). *Solid State Sci.* **3**, 867.

We thank New York University Abu Dhabi for the financial support of this work. This research was partially carried out using the Core Technology Platform resources at New York University Abu Dhabi. Z. Ah. thanks the Kawader program, NYUAD, for research and travel support. This material is based upon works supported by Tamkeen under NYUAD RRC Grant No. CG011.

A070 Polymorphism, Functional Materials and Structural Transformations: Understanding Properties and Disorder
Room 209
4.00pm - 6.30pm

A070-01-270823

The Influence of Vanadium doped Lanthanum Niobates to Phase Transition of Monoclinic Fergusonite- Tetragonal Scheelite

Ahmadi Jaya Permana, Brendan J. Kennedy

School of Chemistry, The University of Sydney, Sydney, New South Wales 2006,

aper3992@uni.sydney.edu.au)

Keywords: Vanadium doped, Lanthanum Niobates, Monoclinic Fergusonite, Tetragonal Scheelite

Numerous metal oxides like ABO_4 with the scheelite structural type are well-known for being superior oxide ion conductors. Lanthanum niobate is one of the most attractive ABO_4 which is observed in monoclinic fergusonite structure as a distortion of the tetragonal scheelite structure. It is known that lanthanum niobate can change from a low-temperature fergusonite-type structure to high-temperature scheelite-type structure by a reversible ferroelastic phase transition[1]. In order to maintain the tetragonal scheelite structure above room temperature across the entire temperature range, the substitution of niobium with smaller isovalent cations like vanadium is most likely what causes the tetragonal scheelite structure to stabilise at low temperatures. The vanadium dope lanthanum niobates ($LaNb_{1-x}V_xO_4$) were synthesised using solid-state method in various formulation (x = 0.00-0.40). The influence of vanadium dope lanthanum niobates to phase transition especially the distortion of octahedral NbO_6 polyhedra in monoclinic to tetrahedral NbO4 polyhedra in tetragonal studied by powder X-ray Diffraction. The stable low-temperture tetragonal scheelites ($I4_1/a$) structures were obtained in range x = 0.25 – 0.40 while the stable monoclinic fergusonite ($I2/c$) were obtained in range x =0.00 – 0.20.

.

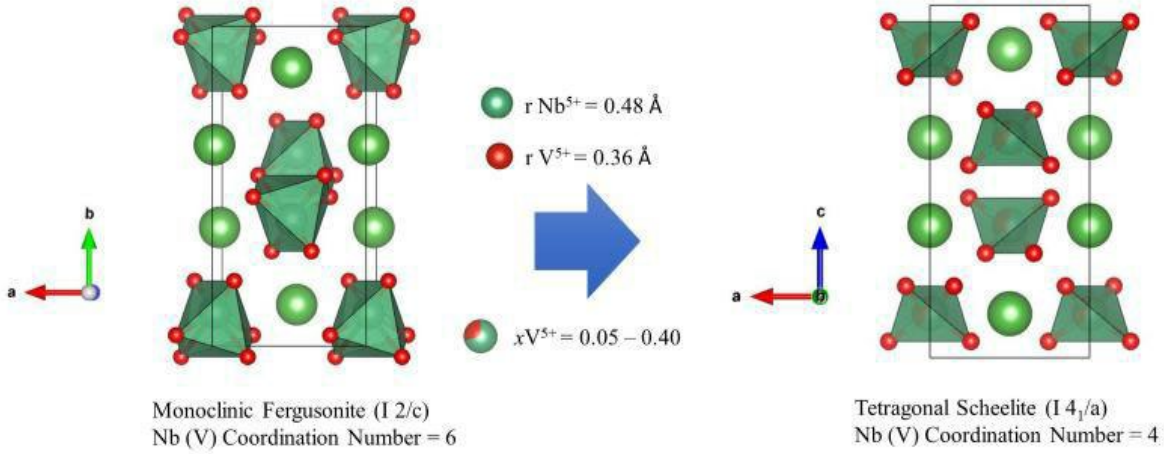

Figure 1. Phase transformation of lanthanum niobates from monoclinic fergusonite to tetragonal scheelite

[2] a) S. W. Arulnesan, P. Kayser, J. A. Kimpton and B. J. Kennedy, *Journal of Solid State Chemistry* **2019**, *277*, 229-239; b) J. E. Auckett, L. Lopez-Odriozola, S. J. Clark and I. R. Evans, *Journal of Materials Chemistry A* **2021**, *9*, 4091-4102; c) S. Wachowski, A. Mielewczyk-Gryn and M. Gazda, *Journal of Solid State Chemistry* **2014**, *219*, 201-209.

A070-02-270823

Investigation of intramolecular charge transfer state geometry in polymorphic crystals of a donor-bridge-acceptor dyad by time-resolved pink Laue X-ray diffraction.

K. Basuroy1, J. Velazquez-Garcia1, D. Storozhuk1, R. Henning2, D. J. Gosztola3, S. Thekku Veedu1, and S. Techert1,4

[1]Photon Science Division, Deutsches Elektronen-Synchrotron DESY, Hamburg, 22607, Germany, [2]Center for Nanoscale Materials, Argonne National Laboratory, Illinois 60439, United States, [3]Center for Nanoscale Materials, Argonne National Laboratory, Lemont, Illinois 60439, United States, [4]Institut für Röntgenphysik, Georg-August-Universität Göttingen, Göttingen, 37077, Germany.

Email of communicating Krishnayan.basuroy@desy.de

Keywords: Time-resolved X-ray diffraction, pump-probe, conformational polymorphism, Intramolecular charge transfer

The photoinduced charge transfer (PCT) process in natural photosynthesis in plants provides an excellent blueprint to create highly responsive, optoelectronic smart materials for the successful conversion of solar energy to electrical currents. Two conformational polymorphs of a donor-bridge-acceptor (D-B-A) dyad, *p*-(CH3)2N-C6H4-(CH2)2-(1-pyrenyl)/ PyCHDMA were studied, where the electron donor (D) moiety p-(CH3)2N-C6H4/DMA is connected through a bridging group (B), -CH2-CH2- to the electron acceptor (A) moiety pyrene. Though molecular dyads like PyCHDMA have the potential to change solar energy into electrical current through the process of photoinduced intramolecular charge transfer (ICT), the major challenge is the real-time investigation of the photoinduced ICT process in crystals, necessary to design solid-state optoelectronic materials. The time-correlated single photon counting (TCSPC) measurements with the single crystals showed that the ICT state lifetime of the thermodynamic form, PyCHDMA1 (pyrene and DMA: axial), is 3ns, whereas, for the kinetic form, PyCHDMA20 (pyrene and DMA: equatorial), it is 7ns, while photoexcited with 375nm radiation (Fig. 1a). The polymorphic crystals were pumped with laser and subsequently probed with a pink Laue X-ray beam in pump-probe photocrystallography/ time-resolved X-ray diffraction (TRXRD) measurements [1]. The TRXRD results suggest that in the ICT state, due to electron transfer from the tertiary N-atom in DMA moiety to the bridging group and pyrene moiety, a decreased repulsion between the lone-pair and the bond-pair at N-atom induces planarity in the C-N-(CH3)2 moiety, in both polymorphs (Fig. 1b,c,d,e). The NBO calculations and partial atomic charge analysis by Hirshfeld partitioning also corroborated the same. Although, the interfragment charge transfer (IFCT) analysis using the TDDFT results showed that for the charge transfer excitation in both conformers, the electrons were transferred from the DMA moiety to mostly pyrene moiety, and the bridging group has little role to play in that.

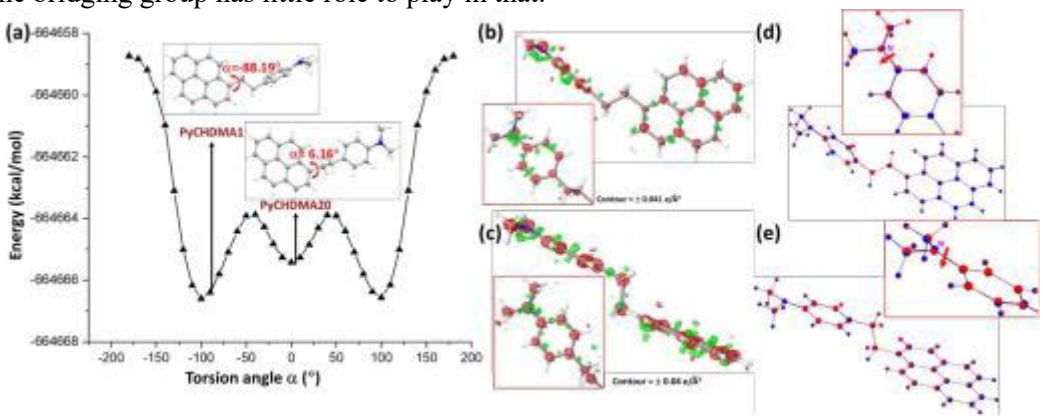

Figure 1. (a) Potential energy scan (PES) plot for energy vs torsion angle. The molecular conformation of the single crystal structures is also shown in the plot. Photodifference maps of (b) PyCHDMA1 and (c) PyCHDMA20. Superposition of ground-state (GS) and excited-state (ES) refined geometries for (d) PyCHDMA1 and (e) PyCHDMA20. Blue is for GS structure and red for ES structure.

[1] Basuroy, K., Velazquez-Garcia, J. D. J., Storozhuk, D., Henning, R., Gosztola, D. J., Thekku Veedu, S. & Techert, S. (2023). *J. Chem. Phys.* **158**, 054304.

A070-03-270823

De-novo approach to elucidate the supramolecular topology of NO_2-PDI derivatives.

Brijith Thomas

Science Division, New York University Abu Dhabi, 129188 Abu Dhabi, UAE

bt2354@nyu.edu

Keywords: NMR Crystallography, solid-state NMR, Perylene

Perylenediimides (**PDI**(s)) are one of the most fascinating classes of dyes in the vast plethora of perylene families. **PDI**s are robust, and have good photochemical and thermal stability, making them suitable candidates for multiple optoelectronic applications. Crystalline packing drives many important physical phenomena like charge transport, electron transfer, electrical conductivity, etc. in molecular solids.[1-2] Recently, Hariharan and co-workers reported a nonparallel stack of donor and acceptor chromophores exhibiting fast charge separation and slow charge recombination.[3-4] The importance of a definitive crystal packing in the solid state for efficient electron transfer and charge separation was unraveled in the above-mentioned work. Among **PDI**s, nitro-perylenediimide(s) (**NO2-PDI**(s)) are previously reported to exhibit light-induced excited-state photorearrangement,[3] strong non-linear optical response,[4] ultrastable radical anion generation,[5] singlet fission in nanocrystal assembly, etc.[6-7] Therefore, understanding the supramolecular assembly and the nature of crystal packing in **NO2-PDI** becomes quintessential for several potential applications. One of the challenges that encountered in the family of **NO2-PDI** with alkyl tail is the difficulty to obtain the single crystal structure through conventional diffraction methods. In this work, we developed a methodology to elucidate the structure of **NO2-PDI** with the disorder in tails. The methodology involves the combination of solid-state NMR, PXRD, three-dimensional electron diffraction, and CSP on a quantum mechanical platform to elucidate the structure.[8-10]

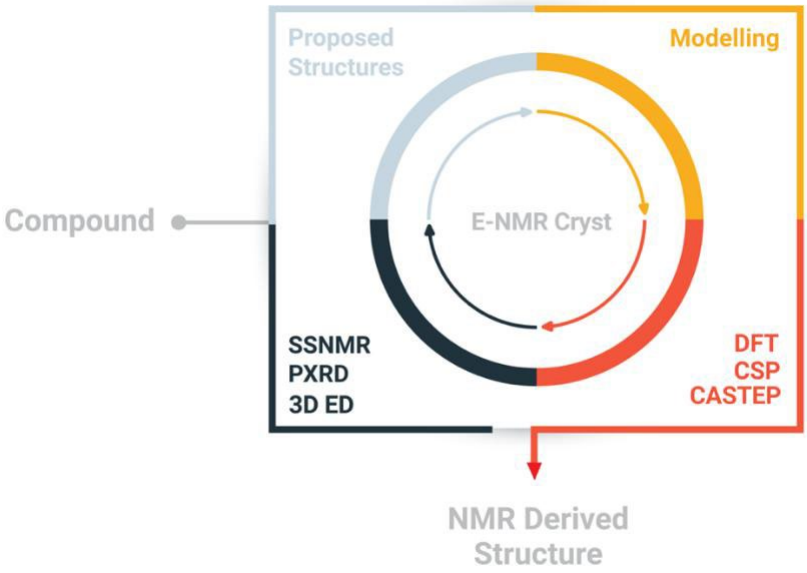

Scheme 1: Schematic diagram of extended NMR crystallographic approach. The approach involves the combination of complementary techniques like X-ray diffraction, and electron diffraction along with solid-state NMR on a quantum mechanical platform to integrate the results.

[1] Li, J.; Qin, Z.; Sun, Y.; Zhen, Y.; Liu, J.; Zou, Y.; Li, C.; Lu, X.; Jiang, L.; Zhang, X.; Ji, D.; Li, L.; Dong, H.; Hu, W., (2022) *Angew. Chem.,* **61**, e202206825.
[2] Huang, L. Y.; Ai, Q.; Risko, C., (2022) *J Chem Phys* 2022., **157**, 084703.
[3] Mallia, A. R.; Salini, P. S.; Hariharan, M., (2015) *J. Am. Chem. Soc.*, **137**, 15604.
[4] Mazumder, A.; Sebastian, E.; Hariharan, M., (2022) *Chem. Sci*., **13**, 8860.
[5] Rosenne, S.; Grinvald, E.; Shirman, E.; Neeman, L.; Dutta, S.; Bar-Elli, O.; Ben-Zvi, R.; Oksenberg, E.; Milko, P.; Kalchenko, V.; Weissman, H.; Oron, D.; Rybtchinski, B., (2015) *Nano Lett.,* **15**, 7232.
[6] Sharma, V.; Puthumana, U.; Karak, P.; Koner, A. L., (2018) J. Org. Chem, **83**, 11458.
[7] Schierl, C.; Niazov-Elkan, A.; Shimon, L. J. W.; Feldman, Y.; Rybtchinski, B.; Guldi, D. M., (2018). Nanoscale 2018, **43**, 20147.

[8] Thomas, B.; Chang, B. S.; Chang, J. J.; Thuo, M.; Rossini, A. J., (2002) Chem. Mater., **34**, 7678.
[9] L. Palatinus, P. Brázda, M. Jelínek, J. Hrdá, G. Steciuk, M. Klementová (2019) *Acta Crystallogr. B*., **75**, 512.
[10] Mohamed, S.; Tocher, D. A.; Vickers, M.; Karamertzanis, P. G.; Price, S. L., (2009) Cryst. Growth Des., **9,** 2881.

A070-04-270823

Guest-induced structural transformation of a coordination cage

Kuntrapakam Hema, Rafal Klajn

Department of Molecular Chemistry and Materials Science, Weizmann Institute of Science, Rehovot, Israel

hema.kuntrapakam@weizmann.ac.il

Keywords: Structural transformation, Stimuli-responsive material, Host-guest complex

Structural transformations of molecules are key to the various biological functions and are essential for the sustenance of life. In other words, 'structure' determines 'function.' Herein, I discuss structural transformations in a coordination cage (Figure 1) induced by encapsulating suitable guest molecules (chemical stimuli).[1]

Inspired by the molecular recognition of enzymes, chemists designed multiple synthetic hosts capable of encapsulating various guest species. The host-guest chemistry finds myriad applications in molecular sensing and separation, drug delivery, or reactivity control. As of now, coordination cages are the most popular synthetic hosts owing to their i) easy synthesis, ii) feasible rational design with precise cavity control (in terms of the size, shape, and polarity), and iii) dynamic nature of the metal-ligand (coordination) bond. The dynamic nature of the coordination bond is fascinating as it enables a cage to undergo adaptation or structural reorganization.[2] We observe the presence of two different isomers of a Pd6L4 cage (L = 1,3,5-trimidazolyl benzene).[3] One of the isomers is predominant (thermodynamically stable isomer - cage 1), with another being present in inconsequential amounts (metastable isomer - cage 2) at ambient conditions. We anticipated that by judicious choice of guests[4] with suitable shapes and symmetries, it would be possible to maximize the population of cage 2. Accordingly, we have chosen various guest molecules and demonstrated the conversion of cage 1 to cage 2 upon guest complexation. Remarkably, we achieved quantitative conversion of cage 1 to cage 2 upon complexation with suitable guests with size and shape complementarity. NMR studies unambiguously confirm the quantitative conversion to cage 2 upon guest encapsulation.

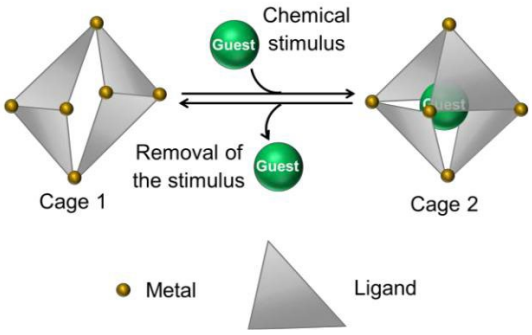

Figure 1. Structural transformation of the coordination cage in the presence of a suitable guest.

Molecular recognition and structural adaptation are fundamental processes in all biological events. In coordination cages, control on structural conversion and the applications are still in the early stage and lately of immense interest. We anticipate that structurally adaptable coordination cages will be valuable candidates for developing smart materials.

[1] Hema, K., Klajn, R. et al. *Manuscript under preparation*

[2] Benchimol, E., Nguyen, B. -N. T., Ronson, T. K. & Nitschke, J. R. (2022). *Chem. Soc. Rev.* **51**, 5101.

[3] Samanta, D., Galaktionova, D., Gemen, J., Shimon, L. J. W., Diskin-Posner, Y., Avram, L., Král, P. & Klajn, R. (2018). *Nat. Comm.* **9**, 641.

[4] Percástegui, E. G. (2021). *Eur. J. Inorg. Chem.* 4425.

A070-05-270823

Understanding the mechanism of polymer- and solvent-mediated mechanochemical synthesis of pharmaceutical polymorphic cocrystals using in-situ CLASSIC NMR spectroscopy

Anna M. Golkowska[1], Yaroslav Z. Khimyak[2], Karol P. Nartowski[1,2]

Wroclaw Medical University, Department of Drug Form Technology, Borowska 211A, 50-556 Wroclaw, Poland
University of East Anglia, School of Pharmacy, Norwich Research Park, NR4 7TJ Norwich, United Kingdom
anna.golkowska@student.umw.edu.pl

Keywords: in-situ, CLASSIC NMR, pharmaceutical polymorphic cocrystals

Pharmaceutical cocrystals are multicomponent solid-state materials of academic and industrial interest due to their ability to modify properties of Active Pharmaceutical Ingredient (API) while its therapeutic activity remains intact. This class of materials, as well as single component crystalline solids, is prone to exhibit polymorphism, i.e. the different packing arrangements.

It was previously reported that polymorphic outcome can be controlled using mechanochemical cocrystallisation techniques via changing the parameters of the process. Especially use of the solvents or polymers differing in polarity can be indicated as one of the most significant factors resulting in cocrystallisation of different polymorphs in liquid- and polymer assisted grinding (LAG, POLAG).[1,] However, the mechanisms that direct the nucleation towards one or another phase are yet to be fully understood.

In situ monitoring methods, such as synchrotron TRIS-PXRD or Raman spectroscopy, are used to gain knowledge of the mechanisms of the abovementioned phase transitions. Nevertheless, those techniques allow to observe changes occurring in solid-state components which can be limiting when solvent or polymer, as in LAG or POLAG, is involved in the mechanism of the reaction. CLASSIC NMR spectroscopy (Combined Liquid- And Solid-State In Situ Crystallisation NMR)[2] was recently proposed as an in situ technique enabling to reveal polymorphic changes, including liquid-state changes of the investigated systems. However, to the best of our knowledge, it has been used to study crystallisation processes of neat pharmaceuticals.

Therefore, in our work we propose the use of CLASSIC NMR as a versatile in situ monitoring technique to gain a molecular level understanding of driving forces, crystallisation pathways and intermediates present during liquid and polymer assisted mechanochemical crystallisation processes of polymorphic pharmaceutical cocrystals. A model pharmaceutical cocrystal of theophylline and benzamide (TP:BZ 1:1) was selected for in situ CLASSIC NMR investigation. TP:BZ cocrystal is known to be polymorphic[1] and has been extensively investigated using synchrotron TRIS-PXRD[3].

During in situ measurements POLAG or LAG process is mimicked via MAS (mechanical force delivered to the system). The selected solvent or polymer were delivered to the system via glass capillary placed in the rotor which broke and released the solvent or polymer under MAS conditions. Amount of powders and liquids corresponds to a ratio used during LAG or POLAG performed in a ball-mill.

The final polymorphic outcome was consistent with the ball-milling results. It stands in agreement with previously collected synchrotron TRIS-PXRD data[3], however, ^{1}H and ^{13}C $\{^{1}H\}$ measurements enabled us to observe the behaviour of the second component – benzamide – which dissolves in water or polymer and then precipitates from liquid-state as a cocrystal. When water is used, theophylline does not dissolve in water but binds with the solvent in a form of monohydrate. Those observations could not be made using synchrotron TRIS-PXRD nor Raman spectroscopy.

CLASSIC NMR spectroscopy can be successfully utilised for in situ monitoring and understanding the mechanism of solvent-mediated mechanochemical cocrystallisation of polymorphic pharmaceutical cocrystals. We proved it to be an effective tool for following the solid-state phase evolution in time, comparable to synchrotron TRIS-PXRD. Therefore, CLASSIC NMR could be an alternative for synchrotron TRIS-PXRD, especially when the accessibility to NMR and synchrotron facilities is considered. Additionally, the possibility of observing changes in liquid-state phase can contribute to a complex understanding of the cocrystallisation mechanism when solvent is involved in the procedure.

[3] Fischer, F.; Heidrich, A.; Greiser, S.; Benemann, S.; Rademann, K. and Emmerling, F. Polymorphism of Mechanochemically Synthesized Cocrystals: A Case Study. Cryst Growth Des., 16, 3, 1701–1707 (2016).
[4] Hughes, C.E.; Williams P.A. and Harris K.D.M. "CLASSIC NMR": An In-Situ NMR Strategy for Mapping the Time-Evolution of Crystallization Processes by Combined Liquid-State and Solid-State Measurements. Angew. Chem. Int. Ed., 53: 8939-8943 (2014).
[5] Lampronti, G.I; Michalchuk A.A.L; Mazzeo, P.P; Belenguer, A.M; Sanders, J.K.M; Bacchi, A. and & Emmerling, F. Changing the game of time resolved X-ray diffraction on the mechanochemistry playground by downsizing. Nat Commun., 12, 6134 (2021)

This project was funded by the National Science Centre in Poland via research grant UMO-2020/01/Y/ST4/00101 (AMG Ph.D. scholarship). The UK 850 MHz solid-state NMR Facility used in this research was funded by EPSRC and BBSRC. The assistance from the 850 MHz Facility Manager (Dinu Iuga, University of Warwick) is acknowledged

A070-06-270823

Design of molecular correlated motions in crystals by utilizing intermolecular cross-stacked packing manner of triaryltriazine derivates

Mingoo Jin

WPI-ICReDD, Hokkaido University

mingoo@icredd.hokudai.ac.jp

Keywords: Organic molecular crystal, Crystalline molecular rotor, Triaryltriazine

Design of correlated mechanical motion of molecules in crystals have been attracting significant interest for the development of molecular machines.[1-3] In particular, gear-like molecular rotation via multiple rotary moieties has been noted as an attractive target because of the ability for transporting mechanical force at molecular-level as well as the alternation of the molecular geometry which can be related to the physical properties of solids.[3] To achieve correlated motions in crystals, the crystal structure should provide (i) a local volume near the dynamic moiety, known as rotator, allowing molecular rotation to occur in the densely packed environment and (ii) a suitable intermolecular geometry between the neighbored rotators to exhibit correlated (geared) motion. However, the number of examples and mode of the correlated motions remains extremely limited due to the inherent difficulty to rationally design molecular crystal structures.

Here, we report the newly developed a crystalline molecular gear by utilizing inter-molecular packing manner of a 2,4,6-triaryl-1,3,5-triazine molecular rotors in crystal. The triazine multi-rotors possessing two different types of bulkiness of tri-alkyl silyl groups in stator as shown in below figure. Single crystal X-ray diffraction analysis revealed that the crystal of the molecular rotor **1** having TBS moiety clearly formed cross-stacked intermolecular packing in two molecules, and the dimer units were packed in separately. On the other hand, the rotor 2 possessing -O-TIPS moiety in stator constructed not only the cross-stacked gear geometry in dimer but also inter-dimer cross stacked packing mode of the gear units (Figure). Interestingly, the phenylene rotation of **1** and **2** occurred in correlated manner, observed by ^{2}H and ^{13}C-CPMAS solid-state NMR studies. Additionally, introduction of 2,3-difluorophenylene as the arylene rotators clearly states that the dipole-dipole interactions induced strong correlation of the geared motion in the solid-state. The precise correlation motions as well as the crystal structures will be described in the presentation.

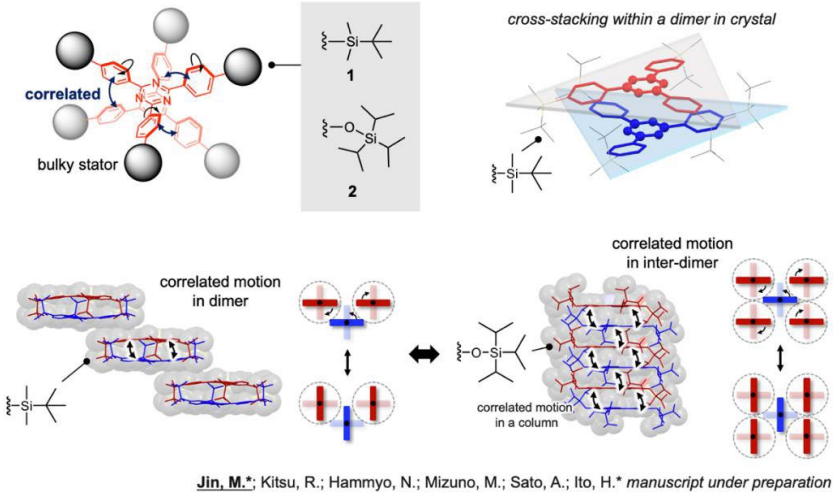

Figure 1. Crystalline molecular gears by triaryltriazine possessing several types of bulky silyl derivates.

[1] Vogelsberg, C. S.; Garcia-Garibay, M. A. *Chem. Soc. Rev.* **2012**, *41*, 1892–1910.

[2] Balzani, V.; Credi, A.; Raymo, F.; Stoddart, J. F. *Angew. Chem., Int. Ed.* **2000**, *39*, 3348–3391.

[3] Liepuoniute, I.; Jellen, M.J.; Garcia-Garibay, M.A. *Chem. Sci.* **2020**, *11*, 12994–13007.

A071 Polarised Neutrons - Future Directions
Room 207
4.00pm - 6.30pm

A071-01-270823

Detection of magneto-electric multipoles

Jian-Rui Soh 1, Andrea Urru 2, Navid Qureshi 3, Anne Stunault 3, Bertrand Roessli 4, Henrik M. Rønnow 1, and Nicola A. Spaldin 2

1 EPFL, Lausanne, Switzerland; 2 ETH Zurich, Zurich, Switzerland; 3 Institut Laue-Langevin, Grenoble, France; 4 Paul Scherrer Institut, Villigen, Switzerland

jian.soh@epfl.ch

Keywords: Spherical neutron polarimetry, magneto-electric multipoles

The fundamental interaction between the neutron dipolar field and the magnetization density surrounding the scattering ion, lies at the heart of magnetic neutron diffraction. However, if the ion resides in an environment which breaks both time and spatial inversion symmetry, the current formalism for magnetic diffraction does not fully account for all the possible scattering mechanisms arising from the asymmetry of the magnetization density cloud of the scatterer [1].

In our work [2,3], we have extended the theory of magnetic neutron diffraction to include these effects. Drawing analogies from the magneto-electric (ME) phenomena and standard magnetic neutron diffraction, developed a framework to calculate the associated ME form factor, size of the ME multipoles and the ME propagation vector from density functional theory (DFT) calculations.

Furthermore, we have identified several material systems, which can not only host these ions but also display an ordered arrangement of these magneto-electric multipoles. Alongside our DFT calculation of the corrections to the scattering amplitudes and form factor of these multipoles, we used spherical neutron polarimetry to provide evidence for the interactions between neutrons and the long-ranged order of these magneto-electric multipoles in CuO.

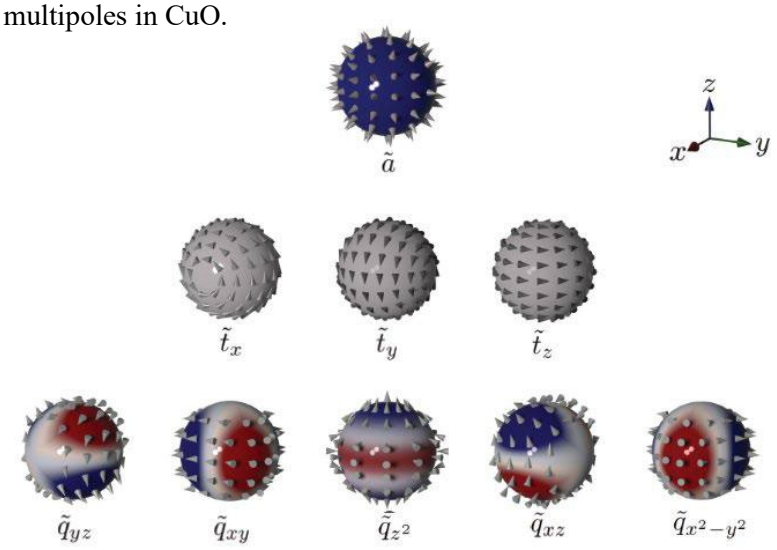

Figure 1. Full family of magneto-electric multipoles.

[1] S. W. Lovesey, J. Phys.: Condens. Matter 26 356001 (2014).

[2] N. A. Spaldin, M. Fechner, E. Bousquet, A. Balatsky, L. Nordström, Phys. Rev. B 88, 094429 (2013).

[3] A. Urru, J.-R. Soh, N. Qureshi, A. Stunault, H. M. Rønnow, N. A. Spaldin, arXiv:2212.06779

A071-02-270823

New experimental and computational developments to enable polarised reflectometry studies of emerging quantum materials

D. L. Cortie 1, A. G. Manning1,

Australian Nuclear Science and Technology Organisation (ANSTO), Lucas Heights, NSW, Australia

Keywords: spintronics, quantum technology, lithography, artificial crystals, surface electronics

The growing demand for new quantum technologies, together with the quest for a fundamental understanding of crystalline matter, has given birth to a new field: the study of quantum materials. Today there is growing interest in combining superconductors, magnets, and topological materials in vertical and lateral junctions for applications in quantum computing and simulation. Polarised neutron reflectometry (PNR) provides unique insights into the nanoscale structure of such junctions [1-2], offering a vertical resolution of 1-500 nm (using specular reflections), and a horizontal spatial resolution of 1 – 100 μm (using off-specular reflections), with the ability to resolve magnetic and superconducting profiles. The combination of the closely-related techniques of grazing incidence diffraction and grazing small-angle scattering can be used to access a wider range of spatial scales if required. In particular, these polarized neutron techniques enable the study of "artificial" 1D and 2D crystals produced with computer-controlled deposition or lithography on surfaces, which are the building blocks of potential quantum technologies.

This presentation provides an overview of the opportunities and challenges for PNR to contribute to studying quantum structures and highlights possible areas for future development including advanced modelling to interpret off-specular reflectometry and in-situ electronic characterization. We highlight the utility of PNR to study various steps of device processing, including ion beam treatments, etching, and heating which are required for constructing lithographic structures [2]. On the experimental front, we discuss the optimization of 3He cells and neutron transport systems, which are used in tandem with supermirror polarizers at the ANSTO to enable sensitive polarization experiments. As an example, we will present recent data on digitally synthesized 1D and 2D crystal samples, which are under development for the Open Reflectometry Standards Organisation (ORSO) [3]. This includes the performance of magnetic surface diffraction gratings recently fabricated at the Melbourne Centre for Nanofabrication. On the theoretical front, new techniques to extract the spin density and magnetic profiles from density functional theory and micromagnetic simulations are under development, and preliminary results will be presented.

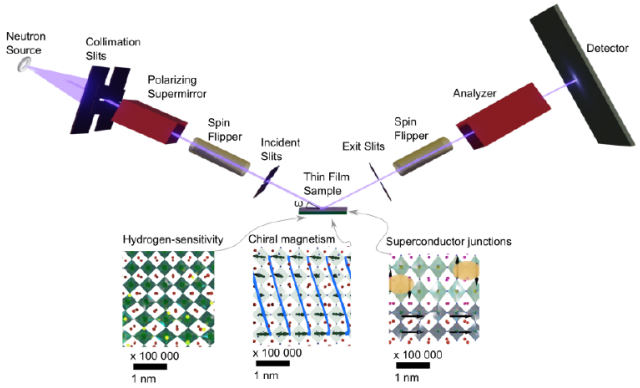

Figure 1. Schematic illustration of the polarised neutron reflectometry technique highlighting some applications in quantum materials. Adapted from Ref [1].

[1] G. Causer, D. L. Cortie et al. (2023), Phys. Status Solidi RRL **2023**, 2200421 .

[2] A. Bake, D. L. Cortie et al, (2023). *Nat. Comms.* (in press)

A071-03-270823

Magnetic anisotropy in Dy garnets

F. Damay[1], I. Kibalin[1], C. Decorse[2], X. Fabrèges[1], A. Gukassov[1], E. Ressouche[3], S. Petit[1]

[1] Laboratoire Léon Brillouin, Université Paris-Saclay, CNRS, CEA, CE-Saclay, 91191 Gif-sur-Yvette, France, [2] ICMMO (UMR CNRS 8182), Université Paris-Saclay, F-91405 Orsay, France, [3] Université Grenoble Alpes, CEA, IRIG, MEM, MDN, 38000 Grenoble, France

francoise.damay@cea.fr

Keywords: Rare-earth garnets, polarized neutron powder diffraction, magnetic anisotropy

Amongst geometrically frustrated architectures candidates is the *hyperkagome* network, which consists in a twisted spatial arrangement of corner-sharing triangles, and which can be found in rare-earth (R) garnets $R_3B_2C_3O_{12}$. $Gd_3Ga_5O_{12}$ (GGG) and $Yb_3Ga_5O_{12}$ (YbGG) are among the most studied members of this family, and it has been proposed that both exhibit an emergent long- or short-range multipolar director state [1, 2], owing to the interplay between anisotropy and near-neighbor exchange. Both also show a modest XY crystal field anisotropy, in contrast with most other rare-earth garnets, which have a strong Ising-like anisotropy. Combined with dipolar interactions, the latter leads to a classical long range (multi-axis) magnetic ordering, thus suggesting a less prominent role of *frustration*, compared with the isotropic case.

Using a comprehensive combination of neutron scattering techniques, including polarized neutron powder diffraction [3] analyzed with the newly developed CrysPy software [4], as well as powder and single-crystal diffraction, and inelastic neutron scattering, we investigated this issue, focusing on the evolution of the magnetic properties between $Dy_3Al_5O_{12}$ (DyAG) and $Dy_3Ga_5O_{12}$ (DyGG). Polarized neutron powder diffraction led to the *first direct measurement* of the Dy^{3+} anisotropy in these two garnets (Fig. 1). Replacing Al for Ga modifies the Dy^{3+} local anisotropy from Ising-like in DyAG to quasi-planar (XZ) in DyGG [5]. This result was confirmed by the Landé factors derived from the crystal electric field scheme determined by inelastic neutron scattering for both compounds. Neutron diffraction was then used to determine the magnetic ground state of both garnets, which was identified as multi-axis in both [5]. These results show that magnetic frustration in garnets can be controlled through the degree of anisotropy of the rare-earth : according to a point charge modeling, anisotropy change is linked with small variations of the oxygen positions surrounding Dy^{3+} ions, calling for further studies on the impact of chemical pressure on the Ising character of the Dy anisotropy. A strong boost in the study of polycrystalline magnetic compounds by polarized neutron diffraction is to be expected in the near future, in parallel with the update of the CrysPy software to treat time-of-flight data from the European Spallation Source instruments for instance.

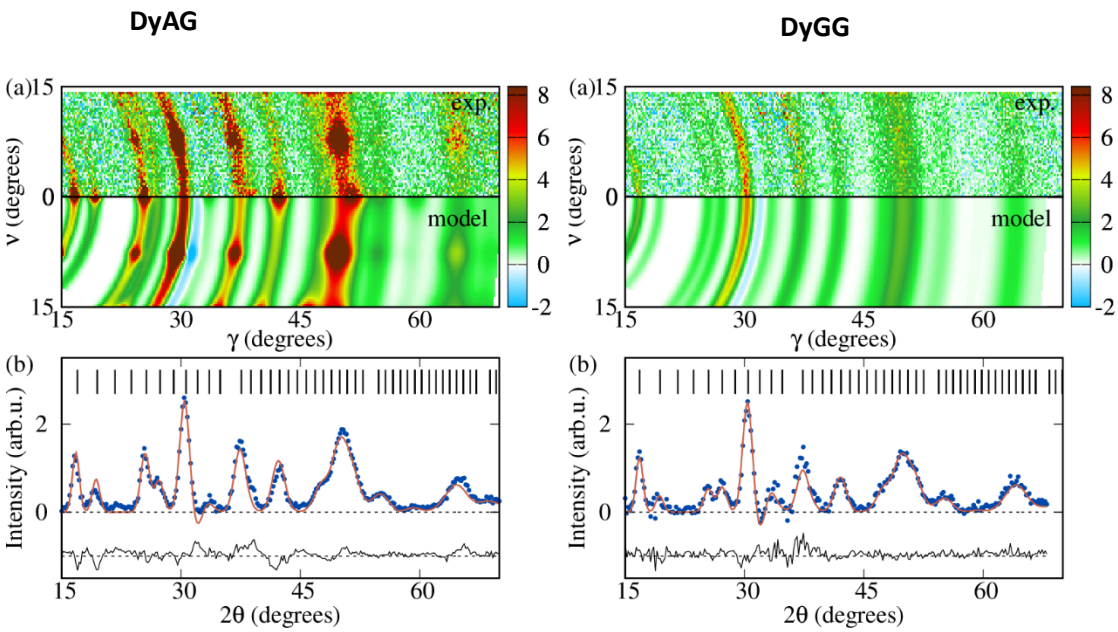

Figure 1. DyAG (left) and DyGG (right) (a) flipping difference ($y_+ - y_-$) diffraction pattern collected at 5 K in 5 T. The measured (calculated with CrysPy) 2D pattern is shown in the top (bottom) panel. (b) Projection on the Bragg angle 2θ. Reflections positions are marked by vertical ticks. The black line shows the difference between the experimental points (blue) and the model (orange line). γ is the azimuthal angle and ν is the elevation angle in the laboratory coordinate system (xyz) [5].

[1] Paddison, J. A. M. et al. (2015). *Science* **350**, 179.
[2] Sandberg, L. O., et al. (2021). *Phys. Rev. B* **104**, 064425.
[3] Kibalin, I. A. et al. (2019). *Phys. Rev. Research* 1, 033100.
[4] CrysPy homepage : https://www.cryspy.fr/
[5] Kibalin, I. A. et al. (2020). *Phys. Rev. Research* **2**, 033509.

A071-04-270823

Polarised neutrons and polarisation analysis at the ESS instrument MAGIC

W. Schweika[1,2], H. Soltner[2], C. Klauser[3], S. Klimko[4], A. Gukasov[4], X. Fabrèges[4]

[1]European Spallation Source, Lund, Sweden, [2]Forschungszentrum Jülich, Germany; [3]Paul-Scherrer Institut,Villigen, Switzerland, [4]Laboratoire Léon Brillouin, Saclay, France
werner.schweika@ess.eu

Keywords: polarised neutrons, polarisation analysis

The instrument MAGIC is a neutron diffractometer currently under construction at the European Spallation Source (ESS) in Lund, Sweden. The instrument is dedicated to studies of magnetic properties in both applied and purely fundamental systems, ranging from magnetic structure refinement to magnetic diffuse scattering from single crystals and powder samples.[1,2]

MAGiC has been designed with polarisation in mind and will deliver a permanently polarised neutron flux on both thermal (0.6-2.3 Å) and cold (2-6 Å) spectra. For the thermal spectrum, reversal of the incident polarised beam in an 8T vertical magnetic field at the sample yields diffraction terms related to nuclear-magnetic interference. For the cold spectrum, longitudinal XYZ-polarisation analysis will allow for separation of all individual scattering terms arising for magnetic diffraction. Examples of simulated experiments are given. In particular, we present the design of a novel concept for the handling of neutron polarisation, which will offer a superior figure of merit P^2T, with very high degree of polarisation P and high transmission and transport T of neutrons through its optical polarising elements and magnetic fields.

The incident thermal beam is polarised in the middle of the neutron guide by FeSi supermirror reflection with a polarisation rate P>0.98; the cold spectrum is polarised by a solid-state bender assembled from Si-wafers, using also an FeSi supermirror coating, with a polarisation rate P>0.96. The RF (radio-frequency) flipper ensures a highly efficient spin-flip for the whole wavelength band. Guide fields >6 mT preserve the incident polarisation along the neutron guide.

For $\lambda > 2$Å, we apply a 120° wide-angle polarisation analyser made of FeSi coated Si-wafer stacks, which are placed in a saturating field of >0.1T. The performance of the analyser is characterised by a figure of merit $P^2T > 0.3$, which gives an improvement of up to a factor 4 (at 2Å) compared to existing polarisation analyser devices.

Near the sample position, the XYZ-magnetic field design allows for a rotation of the magnetic field into an arbitrary direction and subsequently, the rotation of neutron polarisation with high adiabaticity (>60 for 2Å). This was possible to achieve without any blocking of the solid angle of detection in the horizontal scattering plane. One may note further that the XYZ-fields are optimised for minimal field strength at the sample position in a trough-like field shape.

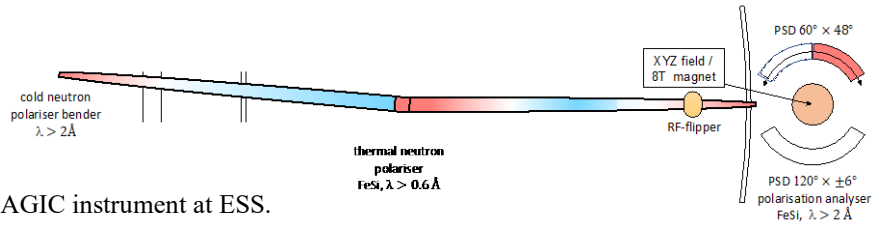

Figure 1. Scheme of the MAGIC instrument at ESS.

[1] https://europeanspallationsource.se/instruments/magic#instrument-description

[2] K.H. Anderson et al. The instrument suite of the European Spallation Source, (2020), *Nuclear Inst. and Methods in Physics Research* A**957**, 163402.

A071-05-270823

Polarised neutrons for magnetic pair distribution function analysis: methods and applications

Benjamin A. Frandsen[1]

Department of Physics and Astronomy, Brigham Young University, Provo, Utah 84602, U.S.A.

benfrandsen@byu.edu

Keywords: magnetic pair distribution function, short-range magnetic correlations, polarized neutrons

Magnetic pair distribution function (mPDF) analysis is a promising method of studying local magnetic correlations. The mPDF approach involves Fourier transforming magnetic scattering data to yield the pairwise magnetic correlation function in real space, which, in some cases, can enable more intuitive interpretation and reliable modelling of the data compared to reciprocal-space approaches. To date, most applications of mPDF analysis have used data obtained from unpolarised neutrons. These efforts have been largely successful, but limitations exist in regard to the real-space resolution of the measured mPDF data and the ability to detect weak signals when unpolarised neutrons are used. Here, we present the first mPDF data obtained from polarised neutrons and introduce a data-processing algorithm that significantly improves upon previous limitations using unpolarised neutrons [1]. We apply this approach to the antiferromagnetic semiconductor MnTe below and above the Neel temperature (see Fig. 1), highlighting the ability to probe both long-range and short-range magnetic correlations with mPDF analysis and revealing nontrivial anisotropic correlations in the paramagnetic state. We conclude with a discussion of the promising outlook of mPDF analysis using polarised neutrons and the potential value of this approach for studying a variety of other magnetic materials, such as geometrically frustrated magnets and multiferroics.

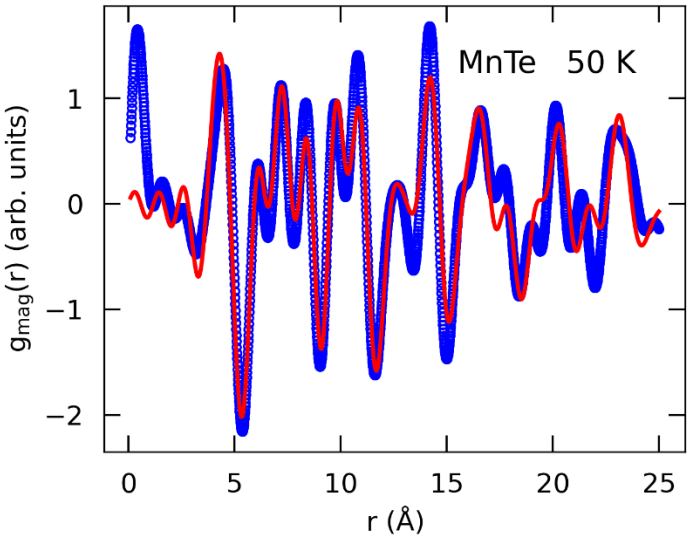

Figure 1. High-resolution magnetic pair distribution function data (blue curve) for MnTe at 50 K obtained from polarised neutron scattering data, together with a fit (red curve) using the known antiferromagnetic structure of MnTe.

[1] Frandsen, B. A., Baral, R.., Winn, B. & Garlea, V. O. (2022). *J. Appl. Phys.*, **132**, 223909.

This work was supported by the U.S. Department of Energy, Office of Science, Office of Basic Energy Sciences through award No. DE-SC0021134.

A071-06-270823

Magnetic ground states of *oxyanion-based compounds* with sawtooth-chain lattices

V. Ovidiu Garlea[1] and Liurukara D. Sanjeewa[2]

[1]Neutron Scattering Division, Oak Ridge National Laboratory, Oak Ridge, TN 37831, USA
[2]University of Missouri Research Reactor (MURR), University of Missouri, Columbia, MO 65211, USA

Email of communicating author: garleao@ornl.gov

Keywords: Frustrated magnetism, neutron diffraction, magnetic structures

The sawtooth spin-chain systems where magnetic ions form chains of corner-sharing triangles have drawn considerable attention from a theoretical standpoint as they can host flat-band magnons [1-3]. The sawtooth spin model is one of the prototype examples of frustrated lattices and can be seen as derived from a kagomé lattice by removing magnetic sites in a regular manner. In practice, such topology implies the presence of magnetic ions in at least two nonequivalent structural positions that creates an interplay between different magnetic order parameters and, consequently, a rich magnetic phase diagram.

To date, experimental realization of a magnetic sawtooth lattice has been limited to a handful of compounds. *We recently undertook* a systematic investigation of the magnetic properties of several sawtooth systems where magnetic chains are linked by nonmagnetic oxyanion groups such as AsO4, MoO4 or SeO3. In this presentation, we will discuss the static and dynamic magnetic properties of three transition-metal sawtooth chain systems: $Rb_2Fe_2O(AsO_4)_2$ [4] $CsCo_2(MoO_4)_2(OH)$ [5] and $NaCo_2(SeO_3)_2(OH)$ [6]. The first two compounds display very similar magnetic behaviour, with the onset of a long-range magnetic order consisting of ferrimagnetic chains that are coupled antiferromagnetically with each other. Within each chain, the magnetic moments located at the tip of the sawtooth are aligned collinearly along the *b*-direction (the chain direction), while the moments on the spine sites are reversely canted by approximately 30º, forming a zigzag pattern in the plane of the triangular chain. The ordering transition occurs at T_N = 25 K for the Fe compound [4] and at 5 K for the Co one [5]. For both compounds, applied magnetic fields induce a transition to a ferrimagnetic state in which the coupling between adjacent sawtooth chains changed from antiferromagnetic to ferromagnetic. Hamiltonian models describing the main magnetic interactions are proposed based on the observed low-energy spin-wave excitations from inelastic neutron scattering data. The third system, $NaCo_2(SeO_3)_2(OH)$, exhibits a more complicated phase diagram consisting of successive magnetic transitions: a ferromagnetic order at 11 K, followed by a reconfiguration of the magnetic structure into an antiferromagnetic state at 3.8 K [6]. Neutron-powder diffraction measurements reveal that at 11 K only one Co site orders to form ferromagnetic zigzag chains along the *b*-axis. Below 3.8 K, both sites order into a complex noncolinear antiferromagnetic structure. A field-induced spin flip transition has been observed at Hc = 1.3 kOe. The analysis of powder inelastic neutron spectrum suggests a complex exchange interaction pattern that goes beyond a Heisenberg Hamiltonian model with nearest neighbour couplings. Our results demonstrate the richness of the magnetic properties of sawtooth-type structures and will motivate further experimental studies of similar sawtooth oxyanions structures.

[1] Nakamura T. and Kubo K., (1996) Phys. Rev. B **53**, 6393
[2] Sen D., Shastry B. S., Walstedt R. E., and Cava R. J., (1996) Phys. Rev. B **53**, 6401
[3] Derzhko, O., Schnack, J., Dmitriev, D.V. *et al.* (2020). Eur. Phys. J. B **93**, 161.
[4] Garlea, O.; Sanjeewa, L. D.; *et. al.* (2014) Phys. Rev. B, **89**, 014426.
[5] Sanjeewa, L. D.; Garlea, V. O.; et al. (2022) Crystals. - *submitted*
[6] Sanjeewa, L. D.; Garlea, V. O.; Taddei, et al. (2022) Inorg. Chem. Front. **9**, 4329

Research conducted at ORNL's Spallation Neutron Source and High Flux Isotope Reactor was sponsored by the Scientific User Facilities Division, Office of Basic Energy Sciences, U. S. Department of Energy. Part of this work was supported by a University of Missouri Research Council Grant (Grant Number: URC-22-021).

A083 Quantum Crystallography Challenges and Opportunities for Magnetic Materials

Room 216
4.00pm - 6.30pm

A083-01-270823

Functionalized borazine derivatives by nitroxide radicals: Synthesis and Magneto-structural Properties

Grenda S [1], Toury B [1], Barbon A [2], Luneau D [1]

Laboratoire des Multimatériaux et Interfaces (UMR 5615) - Université Claude Bernard Lyon 1 - Villeurbanne (France), [2] Electron Paramagnetic Resonance (EPR) Group – University of Padova – Padova PD (Italy)

sabrina.grenda@univ-lyon1.fr

Keywords: Borazine, Nitroxide radicals, Molecular magnetism

Borazine (B3N3H6) are heterocyclic boron-nitrogen compounds, well known as the "Inorganic benzene" due to the B-N bond which is isoelectronic and isostructural to the C=C bond [1- 3]. However, due to the low aromatic character within the molecule compared to benzene, electronic properties are different, with a charge density mainly located on nitrogen atoms [4], and because of this electronical structure, the BN-core is an electron-withdrawing group.

In the frame of an ongoing PhD work, a borazine derivative has been functionalized by free nitroxide radicals, molecule which has never been reported in the literature to our knowledge [5]. The aim of this work is to study the effect of the BN-core on the delocalization of the unpaired electrons carried by the nitroxide functions. Thus, the work carried out during the first year of the thesis allowed the isolation of *N,N',N''*-(tris(4-Bromophenyl))-*B,B',B''*-tris((2,6-dimethyl-4-(N-tert-butyl-N-oxyamino)phenyl) borazine (Borazine-B-Tris-Nitroxide). The crystal structure was determined from X-ray diffraction on single crystal (Table 1) and highlight the evidence of three nitroxide radicals (Figure 1). The study of the magnetic properties in the solid state of this system has been carried out by SQUID magnetometer measurements and in solution by EPR measurements. These studies suggest intermolecular antiferromagnetic (AF) of single state within nitroxide moieties.

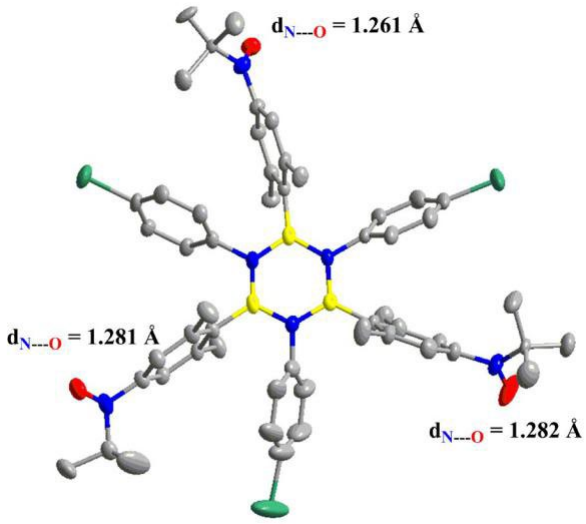

Figure 1 : Crystal structure of Borazine-B-Tris-Nitroxide

Table 1: Crystallographic data for borazine-B-tris-nitroxide

Formula	$C_{54}H_{63}B_3Br_3N_6O_3$
M.W. (g.mol^{-1})	*1116.23*
Crystal system	*Triclinic*
Space Group	*P-1*
a (Å)	*13.0934(11)*
b (Å)	*16.1798(11)*
c (Å)	*16.2429(11)*
α (°)	*104.851(6)*
β (°)	*112.965(7)*
γ (°)	*106.498(7)*
Z	*2*
V (Å^3)	*2762.8(4)*

[2] Lorenzo-Garcia, M.M. & Bonifazi, D., (2017). *CHIMIA*, **71**, 550.

[3] Oubaha, H., Demitri N., Rault-Berthelot, J., Dubois P., Coulembier O., Bonifazi, D. (2019). *J. Org. Chem.,* **84**, 9101.
[4] Fasano, F., Dosso, J., Grazia Bezzu, C., Carta, M., Kerff, F., Demitri, N., Su, B. L., Bonifazi, D. (2021). *Chem. Eur. J.,* **27***,* 4124.
[5] Boese, R., Maulitz, A. H., Stellberg, P. (1994). *Chem. Ber., **127**, 1887.*
[6] Neogi, I. & Szpilman A. M. (2022). *Synthesis., **54**, 1877.*

A083-02-270823

Intermolecular interaction observation of an organic magnet compound by charge density and spin density analysis

Jey-Jau Lee1, Yu Wang2, Garry McIntyre3, J.A.K. Howard4

National Synchrotron Radiation Research Center., Hsinchu , Taiwan R.O.C
Department of Chemistry, National Taiwan University, Taipei, Taiwan R.O.C
Australian Centre for Neutron Scattering, Australian Nuclear Science and Technology Organisation, Australia
Department of Chemistry, Durham University, Durham, United Kingdom

jjlee@nsrrc.org.tw

Keywords: Spin density, Charge density, TEMPO free radical

Intermolecular interaction is important for crystal engineering. Among those that the hydrogen bonding plays an important role in the intermolecular interaction, recognition, and conformations for both small and large molecules. It was well known that weak C-H···O hydrogen bonds play important roles in the formation of molecular solids. Here a case studies on TEMPO- derivative free radical show the importance of C-H···O intermolecular contacts for the transmission of magnetic interactions along a particular direction. Here we combined low-temperature X-ray diffraction charge density, *Polarized Neutron Diffraction (PND) spin density* experiments and also theoretical calculation on the TEMPO- derivative radical compound in order to study such intermolecular interactions through a view of electron density.

In order to get the direct proof of the spin polarization delocalization on C-H···O contacts, we performed the PND experiment to measure the spin density directly on such system. In addition to the PND measurement. The analysis of the total electron density by multipole model and *Atom In Molecule (AIM)* method, also can derive experimental bonding and weak intermolecular interaction characters, which can be compared with those obtained from PND measurements and theoretical calculations. Those can help to recognize the role of intermolecular hydrogen bonding in the organic magnetic system and shows the importance of C-H···O contacts for the transmission of magnetic interactions along one specific axis more clearly.

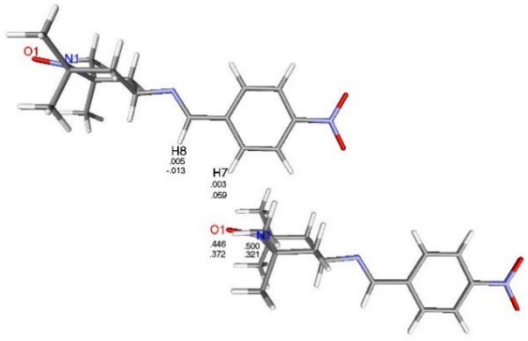

Figure 1. Spin density of selected atom(O1, N2,H7,H8), the first row was from Crystal-98 calculation, the second row was multipole refinement results. (Heading 6 style, Times New Roman 9 pt).

A083-03-270823

Spin/orbital magnetization switching behaviours and electronic states of magnetic thin films

H. Sakurai

Graduate School of Science and Technology, Gunma University, Kiryu, Gunma 376-8515, Japan
sakuraih@gunma-u.ac.jp

Keywords: perpendicular magnetic anisotropy, spintronics, magnetic Compton scattering, spin magnetic moment, orbital magnetic moment

Magnetic Compton profile (MCP) measurements, which probe spin-specific wavefunctions in momentum space, are well suited for electronic structure studies of magnetic thin films with perpendicular anisotropy (PMA), such as Co/Pd and Co/Pt multilayers. We have reported that magnetic quantum number occupancy contributes to the PMA of multilayers [1-5].

Measuring the magnetic field dependence of MCPs yields spin specific magnetic hysteresis (SSMH) curves [6], since MCPs probe spin magnetization [7-9]. Combined with magnetization measurements such as SQUID magnetometers, orbital specific magnetic hysteresis (OSMH) curves can be obtained [10,11]. By analysing the shape of the MCP, magnetic quantum number specific magnetic hysteresis curves [12-15] and element specific magnetic hysteresis curves [16-19] can be obtained.

In CoFeB/MgO multilayers, we found that the magnetization switching behaviour is different between SSMH and OSMH curves [14-15]. Although the total magnetization curve of CoFeB/MgO multilayers does not show PMA, while the OSMH curve shows step function behaviours as if it had perpendicular magnetic anisotropy. The magnetic quantum number specific magnetic hysteresis curves show that the magnetic quantum number state with $|m|=2$ corresponds to the OSMH curve. These facts suggest that the magnetization switching behaviours are governed by the orbital magnetization of the magnetic quantum number state with $|m|=2$.

TbCo amorphous thin film also showed different magnetization switching behaviour between SSMH and OSMH curves [16]. The element specific magnetic hysteresis curves showed that the magnetization of Tb corresponds to the OSMH curve.

These results suggest that magnetic field dependent measurements of MCPs can clarify the magnetic switching behaviour of magnetic thin films from the viewpoints of their electronic states.

These works were supported by the Japan Society for the Promotion of Science (KAKENHI Grant No. 15K05978, 19K04464).

[1] M. Ota et al., J. Phys. Chem. Solids. 65, 2065-2070 (2004)
[2] H. Sakurai et al., Appl. Phys. Lett. 88, 062507 (2006)
[3] M. Ota et al., Appl. Phys. Lett. 96, 152505 (2010)
[4] K. Suzuki et al., Key Eng. Mater. 497, 8-12 (2012).
[5] N. Go et al., Key Eng. Mater. 534, 7-11 (2013)
[6] A. Agui et al., J. Synchrotron Rad. 17, 321-324 (2010).
[7] M. J. Cooper et al., J. Phys. Condens. Matter 4, L399 (1992).
[8] P. Carra et al., Phys. Rev. B 53, R5994 (1996).
[9] N. Sakai, J. Appl. Crystallogr. 29, 81-99 (1996).
[10] M. Itou et al., Appl. Phys. Lett. 102, 082403 (2013)
[11] A. Agui et al., J. Magn. Magn. Mater. 408, 41-24 (2016)
[12] T. Kato et al., Appl. Mech. Mater. 423-426, 271-275 (2013)
[13] K. Suzuki et al., 2014 Appl. Phys. Lett. 105, 072412 (2014)
[14] M. Yamazoe et al., J. Phys. Condens. Matter 28, 436001(2016)
[15] H. Sakurai et al., Mater. Res. Express 6, 96114 (2019)

[16] A. Agui et al., Appl. Phys. Express 4, 083002 (2011)
[17] A. Agui et al., J. Appl. Phys. 114, 183904 (2013)
[18] A. Agui et al., Mater. Res. Express 4 (2017) 106108.
[19] A. Agui et al., J. Magn. Magn. Mater. 484, 207-211 (2019)

A083-04-270823

Understanding Magnetism of Intermediate Valent $CeFe_2Al_8$

Nilofar Kurawle*, Smita Borole, Sudhindra Rayaprol

UGC-DAE Consortium for Scientific Research, Mumbai Centre, CFB-246C, BARC Campus, Trombay, Mumbai – 400085, INDIA

Email of communicating: kurawle31@gmail.com / nilu21@csr.res.in

Keywords: Cerium intermetallic, Intermediate Valence, Magnetism

Cerium intermetallic compounds have largely been studied over the last few decades for their unusual magnetic and electrical properties. Cerium can adopt different electronic states, i.e., diamagnetic Ce^{4+}([Xe] $4f^0$), paramagnetic Ce^{3+} ([Xe] $4f^1$), mixed valence or intermediate valence. The polycrystalline CeFe2Al8 compound was synthesized by arc melting process and detailed investigations of the crystal structures have been performed using x-ray powder diffractogram followed by Rietveld analysis (see Fig. 1). The results confirm single phase formation (orthorhombic structure, space group *Pbam* having lattice parameters, a =12.51167(4) Å, b = 14.43722 (4) Å, c =4.04732 (4) Å, $\alpha = \beta = \gamma = 90^0$, and volume is 731.08 (2) $Å^3$).

There has been some interest in the title compound, and some unresolved issues too. Koterlin et. al., reported intermediate valence (IV) in CeFe2Al8, however they didn't find the low temperature magnetic ordering [1], whereas Mora et al., found low temperature magnetic ordering but no IV state. Interestingly, Ghosh et. al., found both low temperature magnetic ordering as well as intermediate valence [4]. However, it has been observed in previous studies that the IV vanishes under magnetic fields higher than 1 Tesla [1-3].

Low field *dc* magnetization study reveals the antiferromagnetic ordering (TN) = 3.86 K. The broader peak in the M vs. T plot (Fig.1) indicates the intermediate valence state of Ce in the compound, in good agreement with Ghosh et al [4]. However, contrary to their observation we find that the IV state is very robust and was evident even up to very high magnetic fields (> 2 T). Further, the isothermal remanent magnetization (Mirm) as a function of time, t measurement was done to understand the magnetic disorder in the sample, from the actual decay of the magnetic moment. CeFe2Al8 display interesting variations in these correlational behaviours. The sensitive nature of the $4f^1$ state is attributed primarily to variations in the electronic environment of Ce. CeFe2Al8 is a rare example of the valence-fluctuation compounds containing Fe element and also exhibiting magnetic ordering at low temperatures. Further low-temperature measurements including neutron diffraction, with and without applied magnetic field is expected to throw more light in understanding of these interesting properties. These results will be presented and discussed.

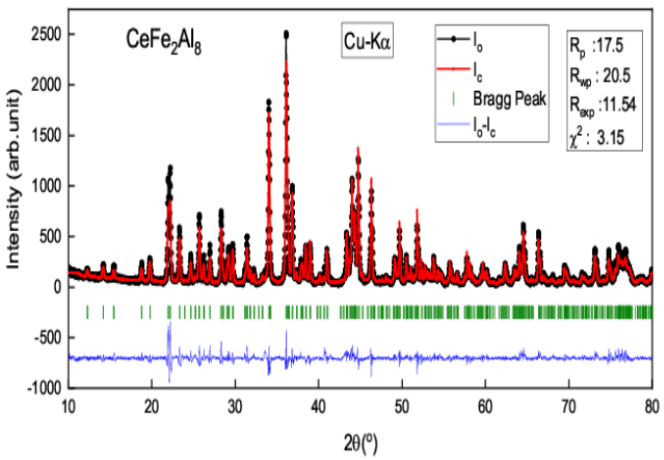

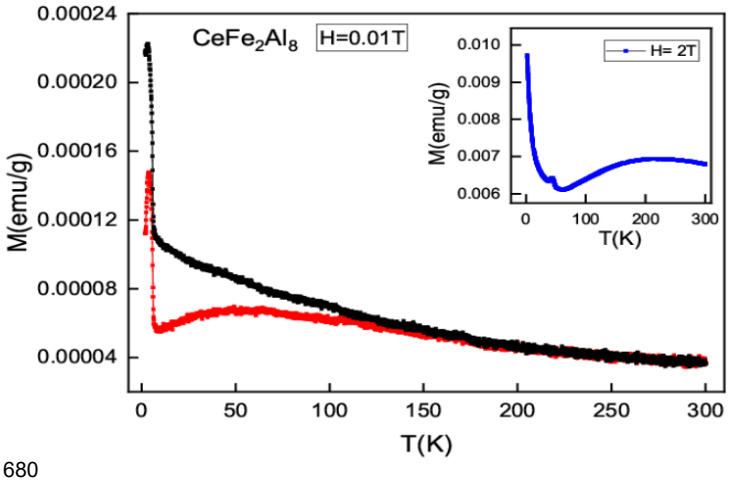

Figure 1. X-ray diffraction patterns of the $CeFe_2Al_8$

Figure 2. Temperature dependence of the magnetic susceptibility (=M/H)

[2] M.D. Koterlin, B.S. Morokhivskii, R.V. Lapunova, O.M. Sichevich, Sov. Phys.-Solid State **31**, 1826 (1989).
[3] Y. Muro, K. Motoya, Y. Saiga, T. Takabatake, J. Phys. Soc. Jpn. **78**, 083707 (2009).
[4] M. Kolenda, M. D. Koterlin, M. Hofmann, B. Penc, A. Szytuła, A. Zygmunt, J. Żukrowski, J. Alloys Compd. **327**, 21 (2001)
[5] S. Ghosh, A. M. Strydom, Acta Phys. Pol., A **121**, 1082– 1084 (2012).

A083-05-270823

Magnetic defect characterization by polarized neutron diffraction

Huibo Cao

Oak Ridge National Laboratory

caoh @ornl.gov

Keywords: Magnetic defects, Polarized neutron diffraction, Local Magnetic Susceptibility

Defects in a material design become an unavoidable topic and can play key roles in certain materials. Magnetic defects originating from frustration can sometimes be easily generated, moved, and suppressed. The method to characterize defects is in urgent need and polarized neutron diffraction (PND) is one of the promising techniques for such a purpose. We have introduced PND for studies in topological insulators, quantum magnets, magnetic texture control, molecular magnets, etc. and here I will introduce our recent progress in this field.

The work at Oak Ridge National Laboratory (ORNL) was supported by the US Department of Energy (DOE), Office of Science, Office of Basic Energy Sciences, Early Career Research Program Award KC0402020, under Contract No. DE-AC05-00OR22725. This research used resources at the High Flux Isotope Reactor, the DOE Office of Science User Facility operated by ORNL. The work at Rutgers University was supported by the DOE under Grant No. DOE: DEFG02-07ER46382.

A083-06-270823

Magneto-Structural relationships in coordination compounds A Polarized Neutron Diffraction vision

Dominique Luneau

Laboratoire des Multimatériaux et Interfaces (UMR 5615), Univ. Claude Bernard Lyon 1, France

Dominique.luneau@univ-lyon1.fr

Keywords: molecular magnetism, coordination compounds, polarized neutron diffraction

PND has proved to be particularly suitable for the study of magnetic molecular compounds and the determination of the spin density. This provides unique information on the paths of magnetic interactions and the nature of magnetic intra-or intermolecular coupling
[10]In this talk, we show on several examples how we can go beyond the spin density reconstruction and use the local susceptibility tensor approach [2] and study the magnetic anisotropy in molecular compounds (Figure 1) [3-6].

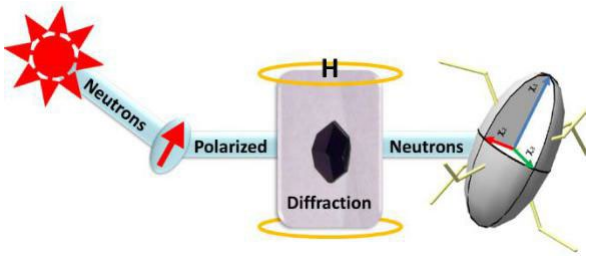

Figure 1. Schematic representation of mapping magnetic anisotropy from polarized neutron diffraction.

This makes PND an excellent tool to help in the design of molecular-based magnets and especially single-molecule magnets for which strong uniaxial magnetic anisotropy is required.

[2] C. Aronica, E. Jeanneau, H. El Moll, D. Luneau, B. Gillon, et al., Chem. Eur. J., 2007, 13, 3666-3674 (link)
[3] A. Gukasov and P. J. Brown, J. Phys-Condens. Mat. 2002, 14, 8831-8839.(link)
[4] K. Ridier, B. Gillon, A. Gukasov, G. Chaboussant, A. Cousson, D. Luneau, A. Borta, J.-F. Jacquot, R. Checa, Y. Chiba, H. Sakiyama, M. Mikuriya *Chem. Eur. J.* ***2016****, 22, 724-735* (link)
[5] O. Iasco, Y. Chumakov, F. Guegan, B. Gillon, M. Lenertz, A. Bataille, J. F. Jacquot, D. Luneau *Magnetochemistry* **2017,** 3 (link)
[6] F. Guégan, J. Jung, B. Le Guennic, F. Riobé, O. Maury, B. Gillon, J-F. Jacquot, Y. Guyot, C. Morell, D. Luneau Inorg. Chem. Front., **2019**, 6, 3152–315 (link)
[7] D. Luneau, B. Gillon *Magnetochemistry* **2021**, 7 (link)

A085 Quantum Approaches in Biocrystallography
Room 208
4.00pm - 6.30pm

A085-01-270823

"Archetype structures" link disorder, polymorphism, and solid solutions via energy

B. Dittrich1,2, L. E. Connor1, P. Piechon1

[1]Novartis Campus, Novartis Pharma AG, Postfach, Basel CH-4002, Switzerland, Mathematisch Naturwiss. Fakultät, Chemie, [2]Universität Zürich, Winterthurer Str. 190, CH-8057 Zürich, Switzerland

birger.dittrich@novartis.com

Keywords: Disorder, Quantum Crystallography, Polymorphism, Solid Solutions

The concept of "archetype structure" links disorder to polymorphism and solid solutions [1], since non-disordered archetypes obtained experimentally in pure form, i.e., without disorder, would be considered polymorphs, or different components of a solid solution. Archetype structures also provide a rationale why disorder occurs based on energy [2] (together with other relevant criteria [3]). Further concept applicability is to crystal structures with solvent disorder on special positions. These systems crystallize as an overlay of archetypes, usually through adding translation symmetry when the solvent itself has higher molecular symmetry. A lower-symmetry subgroup of an experimentally found average structure of higher symmetry (an aristotype [4]) is then observed for the archetype. Several examples from the drug subset [5] of the CSD were evaluated and will be presented.

The concept directly leads to a new practice of modelling disorder in experimental least-squares (LSQ) refinement, where a structural archetype is contributing to an average structure composed of non-disordered components. In this practice, archetypes are initially extracted from a disordered crystal structure –as if each component was not disordered– to provide input for separate quantum mechanical (QM) optimization. When subsequently recombining optimized atomic coordinates of an archetype into a structural model, overlapping atoms would not permit LSQ refinement of their atomic position and displacement parameters due to parameter correlation (depending on experimental resolution and extent of pseudo-symmetry). Therefore, we incorporate structure-specific restraints from QM geometry optimization in refinement, and an entire archetype, rather than only disordered atoms, is assigned a disorder PART. To generate 1,2 (bond distance DFIX) and 1,3 (bond angle DANG) restraints for avoiding hard EXYZ constraints for proximate atoms, we rely on results from molecule-in-cluster (MIC) optimization [6]; proximate atoms however do share their atomic displacement parameters (ADPs) via EADP constraints. We convert computational output to SHELXL input with the program BAERLAUCH [7].

Starting from experimental input (single-crystal X-ray, electron, or powder diffraction) subdivided into archetypes, MIC optimisation of the asymmetric unit content in a cluster of molecules then does not only provide restraints but permits cross-validation of structural model and quantum chemical results.
It was found that the energy of the asymmetric unit of archetypes forming a disordered average structure is within very tight bounds, usually within RT, with T being the temperature and R the ideal gas constant [2]. Another aspect of MIC optimization is that it makes series of structures comparable when different experimental resolution and data quality are encountered.

Overall "archetype structures" are useful from a quantum crystallographic point of view, since archetypes link structure and energy, the essence of quantum crystallography. To accurately quantify energy differences or to support that energetic equality (or similarity) underlies symmetry, we use density functional theory with dispersion correction (DFT-D). Such DFT-D energies of molecules in crystal structures can e.g. be obtained from ONIOM [8] energy partitioning.

Ultimately energy-based analysis using archetypes can be useful in real life application. It can for example guide practical applications in the pharmaceutical industry, as illustrated for predicting cocrystal formation for guiding experimental screening [9].

[1] B. Dittrich, C. Server, J. Lübben (2020). *CrystEngComm*, **22** 7432.
[2] B. Dittrich (2021). *IUCrJ*, **8**, 305.
[3] B. Dittrich, F. P. A. Fabbiani, J. Henn, M. U. Schmidt, P. Macchi, K. Meindl, M. A. Spackman, (2018)**.** *Acta Cryst. B***74**, 416.
[4] U. Müller (2013). *Symmetry Relationships between Crystal Structures: Applications of Crystallographic Group Theory in Crystal Chemistry*, Oxford University Press, Oxford.
[5] M. J. Bryant, S. N. Black, H. Blade, R. Docherty, A. G. P. Maloney, S. C. Taylor (2019). *J Pharm Sci*, **108**, 1655.
[6] B. Dittrich, S. Chan, S. Wiggin, J. S. Stevens, E. Pidcock, (2020). *CrystEngComm* **22**, 7420.
[7] B. Dittrich, S. Pfitzenreuter, C. B. Hübschle (2012). *Acta Crystallogr A***68**, 110.
[8] M. Svensson, S. Humbel, R. D. J. Froese, T. Matsubara, S. Sieber, K. Morokuma, (1996). *J. Phys. Chem.* **100**, 19357.
[9] B. Dittrich, L. E. Connor, D. Werthmueller, N. Sykes, A. Udvarhelyi, (2023). *CrystEngComm*, DOI 10.1039/D2CE00148A.

We would like to acknowledge T. Wager and H. Moebitz for support and P. Müller for discussions.

A085-02-270823

A step forward in accurate modeling of the electrostatic potential maps of macromolecules

M. Kulik, P.M. Dominiak

Biological and Chemical Research Centre, Faculty of Chemistry, University of Warsaw, Poland

m.kulik@uw.edu.pl

Keywords: Transferable aspherical atom model, TAAM, Aspherical atomic scattering factors, Multipolar refinement, MATTS, Quantum crystallography

The quality of image and diffraction data from cryo-electron microscopy and micro-electron diffraction is rapidly increasing. Also, the approaches to model the electrostatic potential maps of macromolecular systems reach beyond the simple point charges or spherical independent atom model (IAM) [1]. We recently applied the multipolar electron scattering factors to calculate the theoretical potential for proteins [2], without using the expensive quantum calculations. We applied the transferable aspherical atom model (TAAM) with the Multipolar Atom Types from Theory and Statistical clustering (MATTS) databank (successor of UBDB2018 [3]). This data bank gathers aspherical atom types, useful for deriving the multipolar electron scattering factors. MATTS is a database universal for proteins, RNA, and other macromolecules as the atom types are transferable between similar chemical environments. Using MATTS it is possible to recreate the electron density distribution of macromolecules via structure factors [4] or to calculate the accurate electrostatic potential maps for small molecules [5]. MATTS is able to reproduce the molecular electrostatic potential of molecules within their entire volume better than the simple point charge models used in molecular mechanics or neutral spherical models used in electron crystallography.

In electron diffraction, the scattering amplitudes may become negative when the negatively charged residues are present. We expect that this effect should be more visible at worse resolution. In the current work, we investigate the differences in the theoretically-obtained potential maps of proteins at various resolutions. In Figure 1, the positive contributions to the 2D Fourier density maps from atomic cores are well visible at 1 Å resolution in both IAM and TAAM approaches. At 2 Å resolution, the positive contribution is diminished by the dominating influence of the valence electrons. By subtracting IAM from TAAM, it is possible to capture the difference between the two oxygen atoms of Asp, where one of them is engaged in a hydrogen bond. The electrostatic potential density maps of helices at 3 Å resolution calculated with IAM and TAAM show differences in the vicinity of charged amino acids. This work contributes to better predictions of the visibility of the molecular features in the cryo-electron microscopy density maps at different resolutions and the rationale behind it. **Figure 1**. Electrostatic potential density maps of lysozyme. a) 2D Fourier density maps at 1 and 2 Å resolutions for Asp66.

The values are given in the absolute scale and the maps take into account the thermal smearing effects. b) 3D Fourier density maps at 3 Å resolution for a helical fragment without thermal smearing.

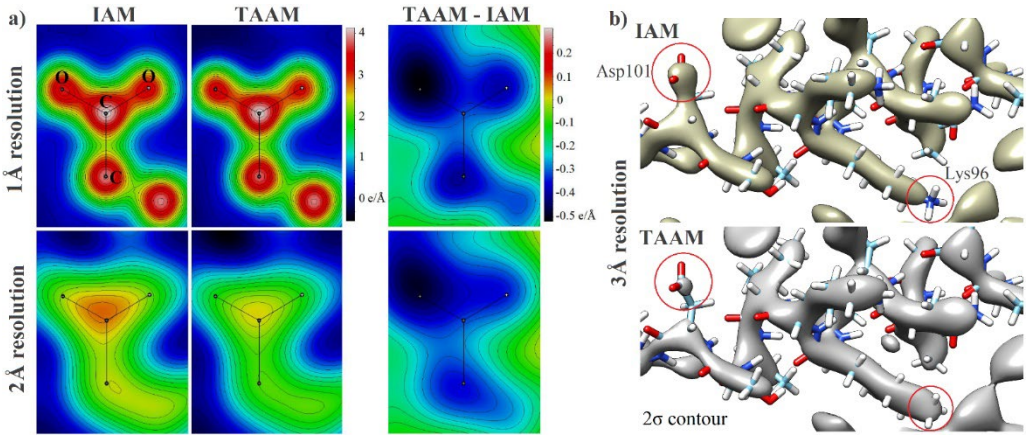

[1] Kulik M., Dominiak P. M. (2022). CSBJ, **20**, 6237-6243
[2] Kulik M., Chodkiewicz M. L., Dominiak P. M. (2022). Acta Cryst. D, **78**, 1010-1020
[3] Kumar P. et al. (2019). Acta Cryst. A, **75**, 398-408
[4] Chodkiewicz M. L. et al. (2018). J. Appl. Cryst. **51**, 193-199
[5] Gruza B. et al. (2020). Acta Cryst. A, **76**, 92-109

The authors acknowledge NCN UMO-2017/27/B/ST4/02721 grant.

A085-03-270823

Recent development in quantum refinement of protein structures

U. Ryde,[a] K. Lundgren,[a] E. Oksanen[b]

[a] Department of Theoretical Chemistry, Lund University, P.O. Box 124, 221 00 Lund, Sweden, [b] European Spallation Source ESS ERIC, P. O. Box 176, SE-221 00 Lund, Sweden

Ulf.Ryde@teokem.lu.se

Keywords: X-ray crystallography, cryo-EM, quantum refinement, protein structures, protonation, nitrogenase, pMMO, MnSOD.

In standard crystallographic refinement of biomacromolecules, the experimental data is normally not enough to unambiguously decide the positions of all atoms. Therefore, the crystallographic data are supplemented by a set of empirical restraints that ensure that bond lengths and angles make chemical sense. In order to obtain more accurate results, we have suggested that this potential is replaced by more accurate quantum-mechanical calculations for a small, but interesting part of the protein, giving the method of quantum refinement [1]. We have shown that quantum refinement can locally improve crystal structures [2], decide protonation state of metal-bound ligands [3–6], oxidation state of metal sites [7,8], detect photoreduction of metal ions [7,9] and solve scientific problems regarding what is really is seen in crystal structures [9–11]. Several other groups have implemented this and similar approaches [12]. In this talk, I will describe the method, show some applications and discuss recent developments, e.g. to cryogenic electron microscopy structures.

[1] Ryde, U., Olsen, L., Nilsson, K., (2002) *J. Comput. Chem.* **23**, 1058.
[2] Ryde, U., Nilsson, K. (2003) *J. Am. Chem. Soc.,* **125**, 14232.
[3] Nilsson, K., Ryde, U. (2004) *J. Inorg. Biochem.*, **98**, 1539
[4] Cao, L., Caldararu, O., Ryde, U. (2017) *J. Phys. Chem B,* **121**, 8242.
[5] Cao, L., Caldararu, O., Ryde, U. (2018) *J. Chem. Theory Comput.,* **14**, 6653.
[6] Caldararu, O., Feldt, M., Cioloboc, D., van Severen, M.-C., Starke, K., Mata, R. A., Nordlander, E., Ryde, U. (2018) *Sci. Rep*. **8**, 4684
[7] Rulíšek, L., Ryde, U. (2006) *J. Phys. Chem. B*, **110**, 11511
[8] Cao, L., Börner, M. C., Bergmann, J., Caldararu, O. & Ryde, U. (2019) *Inorg. Chem.,* **58**, 9672.
[9] Söderhjelm, P., Ryde, U. (2006) *J. Mol. Struct. Theochem,* **770**, 199
[10] Cao, L., Caldararu, O., Rosenzweig, A. C., Ryde, U. (2018) *Angew. Chem. Int. Ed.*, **57**, 162.
[11] Bergmann, J., E. Oksanen & Ryde, U. (2021) *J. Biol. Inorg. Chem.,* **26**, 341-353.
[12] Bergmann, J., E. Oksanen, Ryde, U. (2022) *Curr. Opin. Struct. Biol.,* **72**, 18

A085-04-270823

Hydrogen atom restraints and disorder treatment in Hirshfeld atom refinement of polypeptides

L. A. Malaspina[1], R. Sankolli[1], F. Kleemiss[1,2], E. Wieduwilt[3], A. Genoni[4], S. Grabowsky[1]

[1]Department of Chemistry, Biochemistry and Pharmaceutical Sciences - University of Bern, Freiestrasse 3, 3012 Bern, Switzerland
[2]Universität Regensburg, Universitätsstraße 31, 93053 Regensburg, Germany
[3]Department of Physics, Chemistry and Pharmacy, University of Southern Denmark, Campusvej 55, 5230 Odense M, Denmark
[4]Laboratory of Theoretical Physics and Chemistry, CNRS & University of Lorraine, 1 Boulevard Arago, 57078 Metz, France

lorraine.malaspina@unibe.ch

Keywords: Quantum Crystallography, Software, Method development

Hydrogen atoms play an essential role in protein structures, functions, stabilities as well as protein-ligand interactions. For example, their locations in intermolecular interactions involving peptide groups and water molecules are decisive for the energetics and mechanisms of proton-transfer reactions. More specifically, biologically important proton-transfer and proton-shuttle mechanisms very often involve water molecules as mediators [1-3]. However, in crystals, larger biomolecules are usually disordered which complicates X-ray structure determination especially for hydrogen atom refinement and also lowers the attainable maximum resolution and data quality. Therefore, we will here present new developments in quantum crystallography how to treat disordered (poly-)peptides with a focus on hydrogen atoms.

In general, the use of more advanced models for structure refinement that include a non-spherical description for atoms in molecules, such as Hirshfeld Atom Refinement (HAR) [4,5], significantly improves hydrogen atom localization and the determination of accurate X-H bond lengths. Moreover, it gives access to protonation states and to chemically meaningful electron density overall. However, the computational costs for performing such refinements in large biological systems prevent the widespread use of HAR in protein crystallography. The HAR-ELMO approach [6], as originally implemented in the lamaGOET software [7], uses extremely localized molecular orbitals (ELMOs) [8] in a database-like transfer of fragment-localized orbitals, allowing the reconstruction of molecular wavefunctions for large systems almost instantaneously and therefore expanding the applicability-range of HAR. Although it is easily applicable, in its original implementation this method is limited by the presence of disorder.

Therefore, we expanded the approach and now we offer it via the NoSpherA2 [9] routine implemented in the Olex2 software, where the HAR-ELMO procedure can be performed even with disorder models. In addition, the NoSpherA2-Olex2 implementation allows the use of restraints for hydrogen atoms in HAR, which has not been possible before. In this presentation, we will show the examples of HAR for triaspartic acid which includes dynamic disorder involving water molecules and HAR-ELMO for the following three cases: a co-crystal of L-Asparagine and L-aspartic acid, where, in addition of being monohydrated, the co-crystal is described through a case of substitutional disorder; a tetrapeptide containing disorder about symmetry equivalent positions; and a cyclolinopeptide which presents an extra challenge on the wavefunction transfer due to the cyclic character of the structure.

[1] Garczarek, F. & Gerwert, K. (2006). *Nature*, **439**, 109–112.
[2] Kandori, H., Yamazaki, Y., Sasaki, J., Needleman, R., Lanyi, J. K. & Maeda, A. (1995). *J. Am. Chem. Soc.* **117**, 2118–2119.
[3] Freier, E., Wolf, S. & Gerwert, K. (2011). *Proc. Natl. Acad. Sci. USA*, **108**, 11435–11439.

[4] Jayatilaka, D. & Dittrich, B. (2008). *Acta Cryst. A*, **64**, 383-393.
[5] Capelli, S. C., Bürgi, H., Dittrich, B., Grabowsky, S. & Jayatilaka, D. (2014). *IUCrJ.* **1**, 361–379.
[6] Malaspina, L. A., Wieduwilt, E. K., Bergmann, J., Kleemiss, F., Meyer, B., Ruiz-López, M. F., Pal, R., Hupf, E., Beckmann, J., Piltz, R. O., Edwards, A. J., Grabowsky, S. & Genoni, A. (2019). *J. Phys. Chem. Lett.* **10(22)**, 6973-6982.
[7] Malaspina, L. A., Genoni, A., & Grabowsky, S. (2021). *J. Appl. Cryst.* **54(3)**, 987-995.
[8] Meyer, B., Guillot, B., Ruiz-Lopez, M. F., & Genoni, A. (2016). *J. Chem. Theory Comput.* **12(3)**, 1052-1067.
[9] Kleemiss, F., Dolomanov, O. V., Bodensteiner, M., Peyerimhoff, N., Midgley, L., Bourhis, L. J., Genoni, A., Malaspina, L.A., Jayatilaka, D., Spencer, J. L., White, F., Grundkötter-Stock, B., Steinhauer, S., Lentz, D., Puschmann, H., & Grabowsky, S. (2021) *Chem. Sci.* **12(5)**, 1675-1692.

A085-04-270823

Ultra-high resolution structure of crambin – experimental peculiarities, importance of data processing, influence on multipolar model

M. Kubicki[1], M. Jaskólski[1], M. Gilski[1], A. Joachimiak[2]

[1] Faculty of Chemistry, Adam Mickiewicz University, Poznan, Poland; [2] Structural Biology Center, X-ray Science Division, Argonne National Laboratory, Argonne, IL, 60439, USA

mkubicki@amu.edu.pl

Keywords: crambin, multipolar model, ultra-high resolution

Crambin, small protein (46 residues), present in the seeds of *Crambe abyssinica* is known for giving an opportunity of producing crystals of extraordinary scattering ability, which can produce the measurable diffraction to the ultra-high resolution even in the standards of small molecules. This property was used for the first more or less successful attempt of applying the multipolar model, used for modelling non-spherically symmetric part of the electron density distribution, not only in small molecules (which became quite standard in a sense) but also to macromolecules. This was done by Jelsch et al. [1] in their study of valence electron density distribution in crambin using diffraction data measured to resolution of 0.54 Å. Even better resolution, 0.48 Å, was obtained by Schmidt et al. [2], however, this data was only used for short communication without deeper insight – it was rather an example of the possibilities of PETRA II source. The authors stated, however, that "*We thus presume that in this study we have reached a true resolution limit in terms of electron-density map interpretation and model parameterization: to the level that the currently available software and refinement protocols allow.*"

The chance of challenging this statement was given by the acquiring of data of even better – and much better – resolution of 0.38 Å, which were obtained by quite a special procedure using Argonne synchrotron source. The data were analysed, used for anisotropic refinement and then were subjected to multipolar modelling using MOPRO software [3]. The valence electron density is clearly observed and the results of different refinement procedures, different data processing schemes will be presented together with the analysis of topology of electron density distribution and the weak intra- and intermolecular interactions.

[1] Jelsch, C., Teeter, M. M., Lamzin, V., Pichon-Pesme, V., Blessing, R. H. & Lecomte, C. (2000). *PNAS*, **97**, 3171.
[2] Schmidt, A., Teeter, M., Weckert, E. & Lamzin, V. S. (2011). *Acta Crystallogr. Part F*, **67**, 424.
[3] Guillot, B., Espinosa, E., Huder L. and Jelsch, C. (2014). Acta Crystallogr. Part A, **70**, c279.

Any acknowledgements authors wish to make should be included at the end of the abstract with no heading (use Acknowledgement style, Times New Roman 10 pt, italics).

A085-06-270823

Analysis of non-covalent interactions in proteins

J. Contreras-García1, T. Novoa1

Laboratoire de Chimie Théorique, Sorbonne Université, 75005 Paris

contrera@lct.jussieu.fr

Keywords: non-covalent, proteins, server

NCI [1,2] is a density-based tool that provides a rapid and rich representation of van der Waals interactions (green), hydrogen bonds (blue), and steric clashes (red) as low-gradient-low-density isosurfaces. More generally, a view of non-bonded interactions emerges as continuous surfaces rather than close contacts between atom pairs, providing insight into the multiple small contribution to macromolecular interaction.

We have been working in adapting this tool to biomolecules. Since understanding non-convalent interactions requires an inherent quantification for their comparison, we have introduced the definition of NCI volumes The connexion between integrals and energetics is reviewed for benchmark systems, showing that this simple approach can lead to low cost quality energies while scaling with the number of atoms involved in the interaction (not the total number of atoms). Given the inherent interest of these local approaches to big systems, we have also incorporated an adaptive grid which allows the quantification of NCI properties in big systems where wavefunctions are not available in a fast, parallelizable and efficient manner.

Also, in order to render it more accessible, this latest version of the code [3] has been implemented in the free web server NCIweb [4], which allows the fully **automatized analysis of non-covalent interactions of large PDB files in a matter of minutes**, providing a powerful resource to the biochemistry community. Figure 1 show the steps to launch the NCIWEB calculations of the PET hydrolase with HEMT ligand (PDB ID: 5XH3).

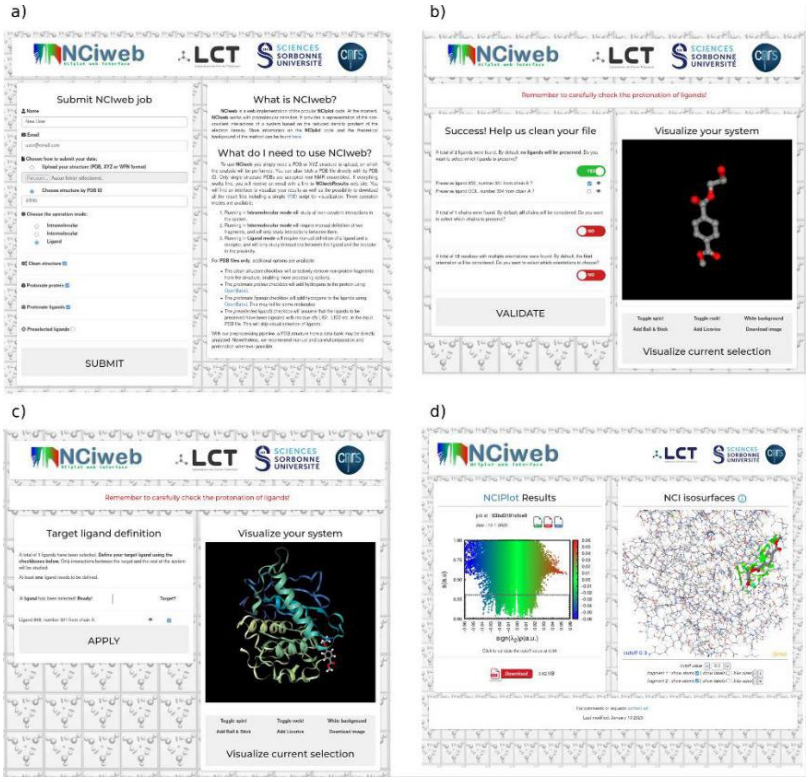

Figure 1. NCIweb overview of the steps for cPDB 5XH3. a) screen 1 personal information is provided, the system is uploaded, the Ligand mode is chosen and the structure is protonated; b) in screen 2 the ligand and chains are chosen, c) in screen 3 the target ligand is determined, and d) the resulting non-covalent interactions are visualized in their 2D representation (left) and as s = 0.3 a.u. isosurfaces (right) on the web server.

[1] E. R. Johnson, S. Keinan, P. Mori-Sanchez, J. Contreras-García, A. J. Cohen, W. Yang, J. Am. Chem. Soc. 2010, 132, 762.
[2] J. Contreras-García, E. R. Johnson, S. Keinan, R. Chaudret, J.-P. Piquemal, D. N. Beratan, W. Yang, J. Chem. Theory. Comput. 2011, 7, 625.
[3] 5. R. A. Boto, C. Quan, R. Laplaza, F. Peccati, A. Carbone, J.-P. Piquemal, Y. Maday, J. Contreras-García, J. Chem. Theory Comput. 16, 7, 4150 (2020)
[4] https://nciweb.dsi.upmc.fr/index.php

A099 Optically and Electronically Active Materials
Room 210/211
4.00pm - 6.30pm

A099-01-270823

Crystallographic mapping of the single gyroid phase in butterfly wings

[1]C.J. Garvey, [2]G.E. Schroeder-Turk, [3]B. D. Wilts

[1]Physik-Department, Technische Universität München, Lichtenbergstraße 1, 85748 Garching, Germany, [2]School of Physics, Chemistry, Mathematics & Statistics, Murdoch University, 6150 Murdoch, WA, Australia, [3]Chemistry and Physics of Materials, University of Salzburg, Jakob-Haringer-Straße 2a, Salzburg 5020, Austria
christopher.garvey@tum.de

Keywords: structural colour, gyroid, SAXS

The phenomenon of structural colour in the wings resulting from the periodic structure in the scales of some insect wings has been described for some time.[1] The periodic structure in wing scales interacts with light, and due to the differential interaction with the incident spectra of ambient light, provides the perception of colour to the observer. While there are different methods for investigating the periodic structure, real space methods such as serial sectioning and electron microscopy [2] and tomography [3] provide an unambiguous real space 3-D reconstruction of the arrangement of chitin and pore space within the wing scales responsible for structural colour. For these methods characterisation of the statistical variations in structure, for example natural variability, is always limited by the practicality of sampling methods. This limitation is serious when investigations of the inherent variability, such as variation in lattice parameters within a single wing, or between individuals of the same species of an insect, are planned.

Small angle X-ray scattering (SAXS) is also suitable for characterisation of the periodic structure in insect wings. In the characterisation the X-ray beam is rastered across a wing surface, the result is an efficient data acquisition over a single wing (Figure 1 left hand side), and simple sample preparation. Data acquired on a 2D detector and provides a representation of the Fourier transform of the density correlation function [4] in 3 dimensions over the volume of the wing sampled by the X-ray beam. Such studies are challenging in view of the large size of unit cells, usually of the order of 200-400 nm, and therefore the very small values and density of points of the scattering vector which are needed to accurately characterise Bragg peak shape due to the periodic structure. Often these patterns are anisotropic and the pinhole geometry measurements are a prerequisite.

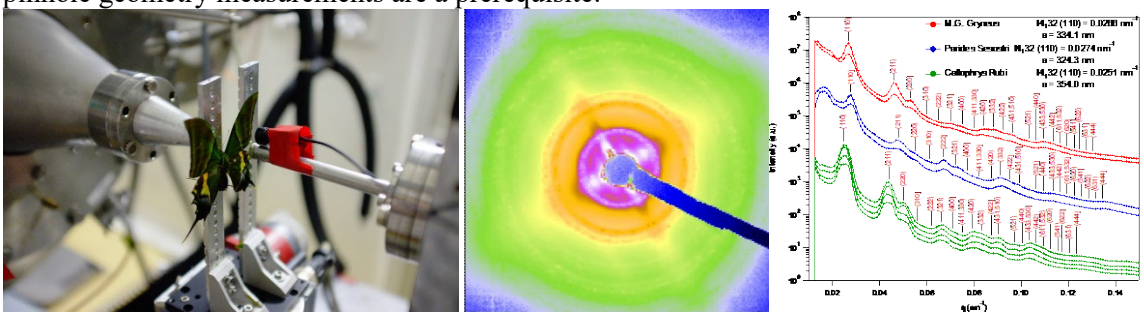

Figure 1. The right hand side shows a typical setup for SAXS measurements at ID02. The centre shows a typical 2D SAXS pattern from a butterfly wing. Typical scattering 1D azimuthally averaged SAXS patterns for 3 different species and peak indexing.

Here we report on pinhole SAXS diffraction measurements made at the ID02 beamline at the European Synchrotron Research Facility (Grenoble, France). Although 2D scattering patterns (Figure 1b) report some degree of anisotropy some important insights can be gained from the automated fitting of lattice parameters to azimuthally averaged 1D patterns (Figure 1c) provided the limitations of such an approach are acknowledged. A particularly important point is the effect of crystallographic orientation on the relative intensities of different peaks. The automated routine assumes that the 1D pattern is a Porod decay with a number of Bragg peaks superimposed (Figure 1c). From the fitting we extract the unit cell size of the single gyroid, and given the assumption of simple size broadening of Bragg peaks according to the

Scherrer equation in a direction normal to that crystallographic axis, some indication of the crystallite size within the wing scale. Previous studies have reported on the variation of lattice parameters between single measurement spots on wings from different species [5]. This work puts those variations in the context of variations within different spots on the same wing and between different members of the same species.

[1] Anderson, T. F. & Richards, A. G. (1942). *J. Appl. Phys.* **13**, 748-758.
[2] Corkery, R. W. & Tyrode, E. C. (2017). *Interface Focus* **7**, 16.
[3] Djeghdi, K., Steiner, U. & Wilts, B. D. (2022). *Advanced Science* **9**, 2202145.
[4] Schmidt-Rohr, K. (2007). *Journal of Applied Crystallography* **40**, 16-25.
[5] Saranathan, V., Osuji, C. O., Mochrie, S. G. J., Noh, H., Narayanan, S., Sandy, A., Dufresne, E. R. & Prum, R. O. (2010). *Proc. Natl. Acad. Sci. U. S. A.* **107**, 11676-11681.

A099-02-270823

Lead-Free Dion–Jacobson halide perovskites $CsMX_2Y_2$ (M = Sb, Bi and X, Y = Cl, Br, I) for optoelectronic applications Via first principle calculations

Izaz Ul Haq, Imad Khan

Center for Computational Materials Science, Department of Physics, University of Malakand, Chakdara, Pakistan
izazuom@gmail.com

Keywords: Two-dimensional layered perovskites; Photovoltaic materials; Electronic

In the present work all-inorganic two-dimensional Dion–Jacobson halide perovskites (DJ-HPs) CsMX2Y2 (M = Sb, Bi; and X/Y= I/I, I/Br, Br/Br, I/Cl, Br/Cl, Cl/Cl) are studied for photovoltaic, photoemission and other potential applications in optoelectronic devices, using first principle calculations within the framework of density functional theory (DFT). The structure symmetry is tetragonal having space group *P4/mmm* (No. 123). In these compounds Cs^+ is a spacer cation, which separates the octahedral layers and balances the charge. The corner sharing M-centered (Sb, Bi) $[MX2Y4]^{3-}$ unit build the 2D $[MX2Y2]n^{n-}$ plane, where X and Y (halogens) atoms occupy the out of plane apical and in-plane bridging site respectively. These DJ-HPs have pseudo-direct band gap semiconducting nature and spin orbit (SO) effect reduces the band gaps as well as splits the Sb/Bi-p orbital in the bottom of conduction band (CB) and X/Y-p orbital in the top of valance band (VB). Among these DJ-HPs, band gap energies of CsSbI2Cl2 (0.87 eV), CsSbBr2Cl2 (1.00 eV), CsSbCl4 (1.40 eV), CsBiI4 (1.10 eV), CsBiI2Br2 (1.40 eV) and CsBiBr4 (1.60 eV) lies in the suitable band gap energy range (0.9-1.6 eV) for photovoltaic applications. M-s (Sb-5s and Bi-6s) and X/Y-p (Cl-3p, Br-4p and I-5p) orbital are responsible for the electrons transition from valance to conduction band, while spacer cation (Cs^+) has limited effect on charge carrier mobility. The effective masses of charge carriers and exciton binding energies of these materials are suitable for solar cell and optoelectronic applications. From the optical coefficients it is clear that in the visible and ultraviolet energy range these DJ-HPs have excellent response to the incident photons.

A099-03-270823

Mechanophotonics: A Roadmap to All-Organic Photonic Integrated Circuits

Rajadurai Chandrasekar

Advanced Organic Photonic Materials and Technology Laboratory
School of Chemistry, University of Hyderabad, Hyderabad – 500046, INDIA

E-mail: *r.chandrasekar@uohyd.ac.in*

Recently, nano/micro organic solids have emerged as promising materials for producing miniaturized organic photonic components, such as optical waveguides (active/passive), lasers, resonators (including chiral ones), filters, and modulators suitable for constructing organic photonic integrated circuits (OPICs).[1-3] Miniature crystal (rigid/flexible) optical waveguides[1-3,5-11,14] are useful for controlling and manipulating light propagation down to microscale. In optical resonators,[4,10,12,13] their mirror-like geometry allows them to trap the photons tightly by repeated total internal reflection at the air-matter interface and produce multimodal optical emissions. Low-optical-loss (high Q) resonators are good optical gain media, therefore potential elements for microlasers. The guided light intensity and- speed can be modulated using light-driven refractive index changes in photochromic optical waveguides.[11(iii)] Selective reabsorbance of broad-band optical emission in microcrystal waveguides lessens the bandwidth of the propagating light signal producing a long-pass filter effect.

Atomic force microscopy (AFM) is an effective technique to mechanically micromanipulate miniature organic photonic components towards OPICs - an approach known as *Mechanophotonics*.[1,2,15-18] I will introduce examples of miniature organic photonic (optically linear and nonlinear[14,15]) components in my talk. I will also discuss the construction of OPICs with active, passive, and energy-transfer attributes using mechanophotonics. The fabricated OPICs switch, split, direct, and filter optical signals for signal enhancement, sensing, information processing and switchable photonic device applications. Recently, we developed a novel molecular-crystal-processing technique via Focused ion beam lithography, namely Crystalphotonics Foundry, the details also will be covered briefly.[19]

1. R. Chandrasekar, *Chem. Commun.* **2022**, *58*, 3415-3428. [Feature Article]
2. R. Chandrasekar, *Small*, **2021,** *17*, 2100277. [Invited Perspective]
3. R. Chandrasekar et al. *Adv. Opt. Mater.* **2020**, *8*, 2000959. [Invited Perspective]
4. R. Chandrasekar, *Phys. Chem. Chem. Phys.* **2014**, *16*, 7173 [Invited Perspective].
5. R. Chandrasekar et al. *Adv. Opt. Mater.* **2018**, *6,* 1800343. [Invited Perspective]
6. D. Venkatakrishna et al. *Adv. Mater.* **2017**, *29*, 1605260.
7. P. Hui et al. *Adv. Mater.* **2013**, *25*, 2963.
8. N. Chandrasekar, et al. *Angew. Chem. Int. Ed.* **2012**, *51*, 3556.
9. S. Basak, et al. *Adv. Funct. Mater.* **2013**, *23,* 5875.
10. YSLV. Narayana et al. *Adv. Funct. Mater.* **2011**, *21*, 667.
11. D. Venkatakrishna et al. (i) *Adv. Opt. Mater.* **2017***, 5*, 1600613; (ii) *Adv. Opt. Mater.* **2016***, 4, 112;* (iii) *Adv. Opt. Mater.* **2015***, 3*, 1035; (iv) *Adv. Opt. Mater.* **2017,** *5*, 1700695; (v) *Adv. Opt. Mater*. **2020**, 8, 1901317.
12. N. Chandrasekar,et al. *Adv. Opt. Mater.* **2013**, *1*, 305.
13. D. Venkatakrishna et al. *J. Mater. Chem. C* **2017**, *5*, 123459.
14. V. Radhika, et al. *Adv. Opt. Mater.* **2020**, *8*, 2000431.
15. V. Nikolai, et al. *Adv. Opt. Mater.* **2019***, 7,* 1801775.
16. M. Annadhasan et al. *Angew. Chem. Int. Ed.* **2020**, *59,* 13852-1385; (ii) *Angew. Chem. Int. Ed.* **2020**, *59*, 13821-13830; (iii) Rohullah et al. *Angew. Chem. Int. Ed*. **2022**, *61*, e202202114.
17. J. Ravi et .al. (i) *Adv. Funct. Mater.* **2021**, in press; (ii) *Adv. Funct. Mater.* **2021**, 31, 2100642.
18. V. V. Pradeep et al. *Small* **2021**, 17, 2006795.
19. V. Vinay Pradeep, R. Chandrasekar, *Indian Patent Application*, Filed, TEMP/E-1/18625/2022-CHE, arXiv:2203.14218v1 [physics.optics], *Adv. Opt. Mater.* **2022**, 10, 2201150.

A099-04-270823

Novel nonlinear optical crystal of L-arginine dichloride

A. Danghyan1, R. Sukiasyan1, A. Ayvazyan2, H. Karapetyan2, A. Atanesyan1

Institute of Applied Problems of Physics, NAS of Armenia, 25 Nersessyan Str., 0014 Yerevan, Armenia, Molecule Structure Research Center NAS of Armenia, 26 Azatutyan Ave., 0014 Yerevan, Armenia

ruzas73@gmail.com

Keywords: L–arginine halides, Chloride, Dichloride, Nonlinear optical crystal

The salts of optically active L–amino acids, particularly L–arginine, crystallize in enantiomorphous space groups $P2_12_12_1$, $P2_1$, P1, and very rarely in others. These space groups being acentric allow displaying nonlinear optical (NLO) and piezoelectric properties, while polar $P2_1$ and P1 groups, also have a pyroelectric effect. Search and investigation of L–arginine (L–Arg) salts is interesting both concerning discovering crystals with above–mentioned properties and to investigating structural features and formation mechanisms. The systematic investigations of L–arginine salts as objects related to proteins began from the study of halides at the beginning of the sixties. We investigated in detail the reaction of L–arginine with hydrochloric acid (HCl) in water solvent at 0–33˚C temperature [1]. In total, five compounds were successfully obtained and identified, of which L–Arg·HCl (P1) [2], L–Arg·HCl ($P2_1$) [3], L–Arg·HCl·H_2O ($P2_1$) [3], L–Arg·2HCl·H_2O ($P2_12_12_1$) [4] were known, and L–Arg·2HCl (new) crystal was a novel finding. The conditions for the formation of all obtained crystals from the L–Arg+HCl+H_2O system were described; the FT–IR ATR spectra were presented and compared in [1].

The subject of the present study is NLO novel crystal of L–Arg·2HCl (3L-Arg^{2+}·$6Cl^-$). The crystal and molecular structure of crystal L–Arg·2HCl was determined by X-ray diffraction method at 295K. This crystallize in the monoclinic ($P2_1$) system. Unit cell parameters: a=7.4907(15)Å, b=20.092(4)Å, c=12.101(2)Å, α=γ=90˚, β=99.35(3)˚, Z=6, Dc=1.370 g/cm^3, V=1797.0(6)Å^3. The asymmetric part of the unit cell of L–Arg·2HCl contains crystallographically independent three L-argininium (2+) cations and six Cl^- anions (Fig. 1a). The guanidyl group of I or III types cations is connected to the carboxyl group of next cations of their type, that is, it forms a chain according to the "head to tail" mechanism, stretching along the *c* axis. And cations of II type are not directly connected to each other, they form hydrogen bonds through the own carboxyl group with the guanidyl group of III type cation, forming layers in the direction of the *b* axis, they are also connected through Cl^- anions. That is, layers of arginine cations are formed in the *bc* plane, and these layers are connected through Cl^- anions, forming strong hydrogen bonds (Fig. 1b). In [5] were divided the interactions of the guanidyl group with carboxylate and phosphate anions into four types, and only one of the 25 studied compounds were encountered a Type D interaction. In the L-Arg·2HCl structure, the interaction between the anion and the guanidyl group is very similar to the rare Type D, but the anion is Cl^-. The crystal can show NLO properties.

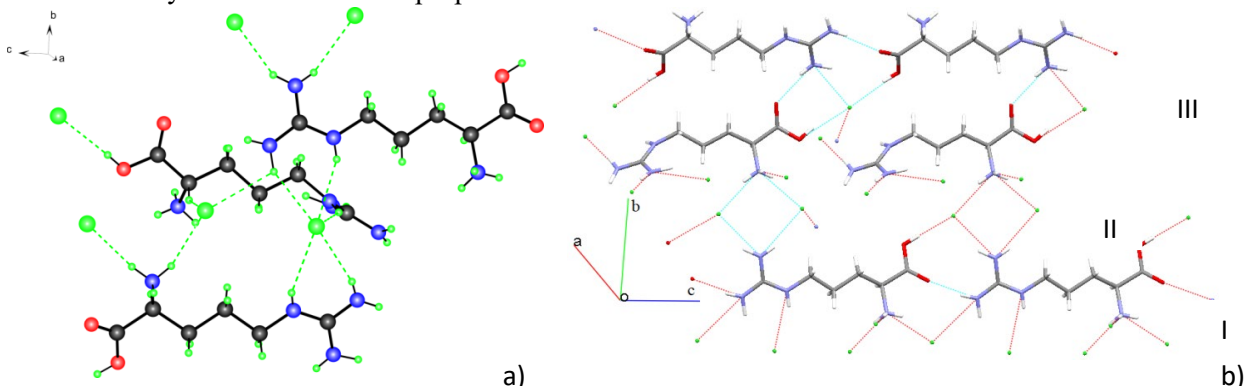

Figure 1. Asymmetric part of the unit cell and hydrogen bonds of (3 L-Arg^{2+}·$6Cl^-$) crystal

[1] Sukiasyan, R. P., Apreyan, R. A., Danghyan, A. A., Bezhanova, L. S., Suponitsky, K. Yu. & Atanesyan, A. K. (2022). *Arm. J. of Physics*, **15**, issue 2-3, 46.
[2] Sridhar, B., Srinivasan, N., Dalhusc, B. & Rajarama, R. K. (2002). *Acta Cryst*. **E58**, o747.
[3] Mazumdar, S. K. & Srinivasan, R. (1964). *Current Science (India),* **33**, 573.
[4] Petrosyan, A. M., Karapetyan, H. A., Bush, A. A. & Sukiasyan R. P. (2004). *Materials Chemistry and Physics*, **84 (1)**, 79.
[5] Salunke, D. M. & Vijayan M. (1981), *Int. J. Peptide Protein Res.* **18**, 348.

This work is supported by the MSE RA, project No.20TTWS-1C026 – 2020.

A099-05-280823

Structural and spectroscopic studies of photo-switchable molecular capsule

M. Choudhari[a], C. Ritchie[a]

a: Monash University, Wellington Rd, Clayton VIC 3800.

manjiri.choudhari@monash.edu

Keywords: Polyoxometalate, Diarylethene, Photochromism

Photochromism is defined as the reversible conversion of two chemical species in response to light, with photochromic compounds being important due to their various real-world applications.[1] Among the different classes of photochromic compounds, diarylethenes (DAEs) offer thermal stability of the photogenerated isomers, fatigue resistance, and high quantum yields, proving them important for various applications.[2] The incorporation of DAEs in metal-organic frameworks, nanomaterials, and polymers has led to substances with novel properties.[3] Polyoxometalates (POMs) are inorganic discrete and nanosized metal-oxygen compounds of early transition metals commonly found in their highest oxidation with a range of structural and compositional diversity, making them suitable for various applications.[4] Functionalization of POMs with organic species results in various organic-inorganic hybrid materials with tunable properties.[5] In 2018, we reported a POM-DAE complex which showed modified photochromic properties compared to the parent DAE.[Based on these earlier findings, we extended our study and have since succeeded in obtaining a photochromic molecular capsule with the generic formula $[(POM)_2(DAE)_3]^{x-}$ **(1)**. The compound has been structurally characterized using single-crystal x-ray diffraction while also being studied extensively in solution using a suite of spectroscopic techniques.

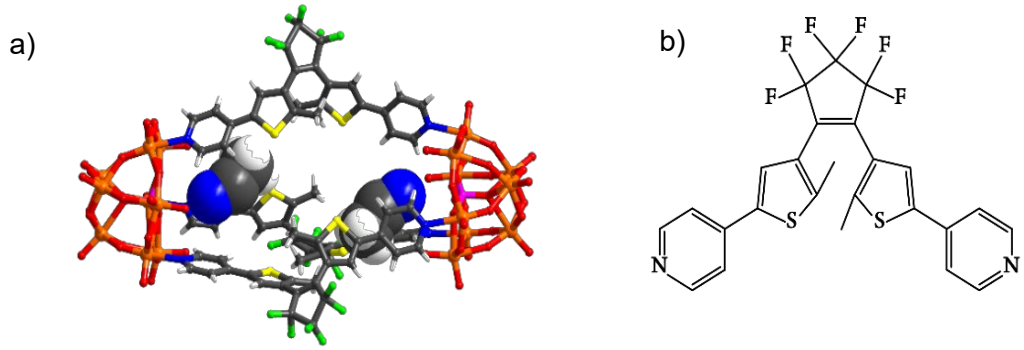

Figure 1: a) Graphical representation of the chiral molecular capsule **(1)** obtained from single-crystal X-ray diffraction structure determination b) Chemdraw representation of **DAE** ($C_{25}H_{16}N_2S_2F_6$).

1. Wang, Y.; Runnerstrom, E. L.; Milliron, D. J., *Annu. Rev. Chem. Biomol. Eng.* **2016**, *7*, 283-304.
2. Irie, M.; Fukaminato, T.; Matsuda, K.; Kobatake, S., *Chem. Rev.* **2014**, *114*, 12174-12277.
3. Han, M.; Luo, Y.; Damaschke, B.; Gómez, L.; Ribas, X.; Jose, A.; Peretzki, P.; Seibt, M.; Clever, G. H., *Angew. Chem., Int. Ed.* **2016**, *55*, 445-449.
4. Juan J. Borrás-Almenar, E. C., Achim Müller,Michael Pope, *Polyoxometalate Molecular Science*. Springer, Dordrecht: Netherlands, 2003.
5. Proust, A.; Thouvenot, R.; Gouzerh, P., *Chem. Commun.* **2008**, 1837-1852.

A099-06-270823

Understanding the mechanisms of bending in flexible crystals

Amy J. Thompson, [a] Anna Worthy, [b] Arnaud Grosjean[a] Jason R. Price,[c] John C. McMurtrie, [b] and Jack K. Clegg*[a]

[a]School of Chemistry and Molecular Biosciences, The University of Queensland, Brisbane St Lucia, QLD, Australia, 4072
[b]School of Chemistry, Physics and Mechanical Engineering, Queensland University of Technology, Brisbane 4001, Australia
[c]ANSTO Melbourne, The Australian Synchrotron, 800 Blackburn Rd, Clayton, Vic 3168, Australia.

E-mail: j.clegg@uq.edu.au

A crystal is normally thought of as *a homogenous solid formed by a periodically repeating, three-dimensional pattern of atoms, ions, or molecules.* Indeed, the regular arrangement of molecules, in a single crystal lead to many useful characteristics (in addition to diffraction!) including unique optical and electrical properties, however, molecular crystals are not typically mechanically robust, particularly compared to crystals of network solids like diamond. Upon the application of stress or strain, these crystals generally irreversibly deform, crack or break resulting in the loss of single crystallinity.

We have recently discovered a class of crystalline compounds that display the intriguing property of elastic flexibility – that is they are capable of reversibly bending without deforming, cracking or losing crystallinity. A number of these crystals are flexible enough to be tied into a knot! (See Figure 1). We have developed a unique approach to determine the atomic-scale mechanism that allows the bending to occur which employs mapping changes in crystal structure using micro-focused synchrotron radiation. We have applied this technique to understand the deformation in both elastically[1] and plastically[2] flexible crystals. Most recently we have used it to show that previous theories regarding the requirement of "interlocked" crystal packing for flexibility is incorrect.

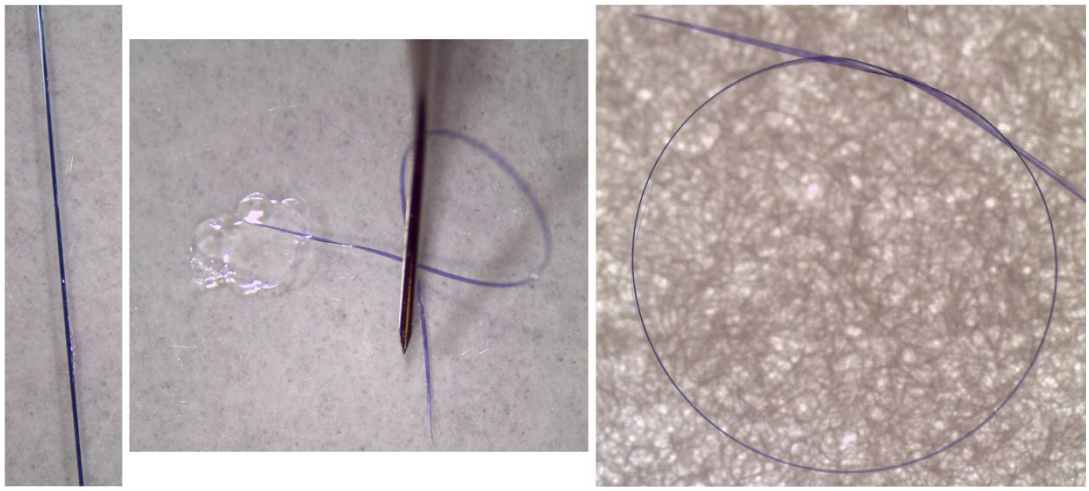

Figure 1: A crystal of $[Cu(acac)_2]$ showing elastic flexibility.

[1] A. Worthy, A. Grosjean, M. Pfrunder, Y. Xu, C. Yan, G. Edwards, J. K. Clegg and J. C. McMurtrie, "Atomic Resolution of Structural Changes in Elastic Crystals of Copper(II) acetylacetonate", *Nature Chemistry*, **2018**, 65-69.
[2] S. Bhandary, A. J. Thompson, J. C. McMurtrie, J. K. Clegg, P. Ghosh, S. R. N. K. Mangalampalli, S. Takamizawa, and D. Chopra, "The mechanism of bending in a plastically flexible crystal." *Chem. Commun.,* **2020**, 12841-12844.

A108 X-ray Ptychography: Recent Developments and Applications
Room 212/213
4.00pm - 6.30pm

A108-01-270823

Ptychography Based Resolution-enhanced X-ray Fluorescence Microscopy Using Deep Neural Networks

Longlong Wu[1,2], Seongmin Bak[3], Youngho Shin[4], Yong S Chu[3], Shinjae Yoo[1], Ian K. Robinson[2,5] and Xiaojing Huang[3]

[1]Computational Science Initiative, Brookhaven National Laboratory, Upton, NY 11973, USA
[2]Condensed Matter Physics and Materials Science Department, Brookhaven National Laboratory, Upton, NY 11973, USA
[3]National Synchrotron Light Source II, Brookhaven National Laboratory, Upton, New York 11973, USA
[4]Materials Engineering Research Facility, Applied Materials Division, Argonne National Laboratory, Lemont, IL 60439, USA
[5]London Centre for Nanotechnology, University College London, London, WC1E 6BT, United Kingdom.

lwu@bnl.gov

Keywords: Machine Learning, X-ray Fluorescence, Ptychography

Accurately resolving elemental distributions inside materials at the nanoscale is critical for understanding their physical and chemical properties. Multimodal hard X-ray scanning probe microscopy has been extensively used to study materials providing multiple contrast mechanisms. For instance, combining ptychography with X-ray fluorescence (XRF) microscopy reveals structural and chemical properties simultaneously. While ptychography can achieve diffraction-limited spatial resolution, the resolution of XRF is normally limited by the X-ray probe size. Here, utilizing the multimodal measurement, we develop a machine learning (ML) model to overcome this problem by deconvolving the X-ray probe from the XRF signal [1]. The enhanced spatial resolution was observed for both simulated and experimental XRF data, showing superior performance over the state-of-the-art scanning XRF method with different nano-sized X-ray probes. As one example shown in Figure 1, enhanced spatial resolutions were also observed for the accompanying 3D XRF tomography reconstructions.

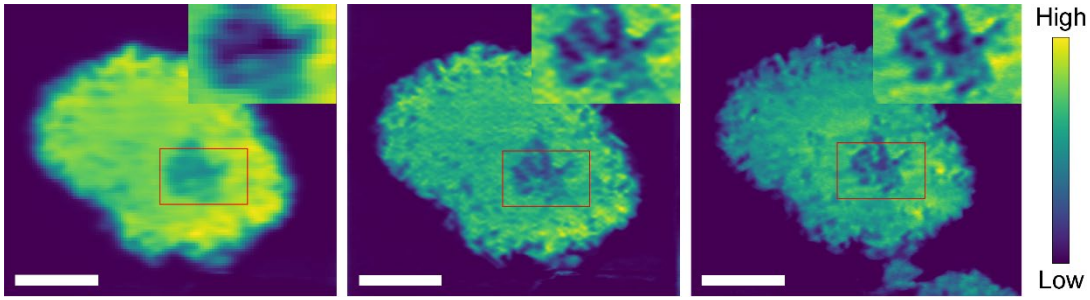

Figure 1. Comparison of experimental 3D low-resolution XRF image and resolution-enhanced XRF image. Here, the central slices of the 3D reconstructed structures of the sample are displayed. The left column shows the central slice of the raw XRF tomography reconstruction. The middle column shows the corresponding central slice of the 3D tomography reconstruction using the spatial resolution-enhanced XRF image from the trained ML model. The right column shows the central slice of the phase-contrast image from the ptychographic tomography reconstruction. Here, all the scale bars are 2 μm.

[1] L. Wu, S. Bak, Y. Shin, Y. Chu, S. Yoo, I. K. Robinson and X. Huang, Resolution-enhanced X-ray Fluorescence Microscopy via Deep Residual Networks, submitted.

A108-02-270823

Multi-beam X-ray ptychography with adjustable beam spacing

M. Kahnt[1]*, M. Åstrand[2], U. Johansson[1] and U. Vogt[2]

1 MAX IV Laboratory, Lund University, 22100 Lund, Sweden

2 KTH Royal Institute of Technology, Department of Applied Physics, Biomedical and X-ray Physics, Albanova University Center, 106 91 Stockholm, Sweden

maik.kahnt@maxiv.lu.se

Keywords: Multi beam, Ptychography, Fresnel Zone Plates

Pushing the limits of ptychography towards imaging more samples and larger areas of samples is the aim of many groups' efforts. One obvious trend in the community is to go faster. Using fly-scanning approaches the higher coherent flux provided by 4th generation sources is spread over a larger sample area which subsequently allows to see more of a sample in the same or even less time.

Multi-beam ptychography (MBP) is a parallel development with the same goal [1]. Instead of necessarily going faster, the speed-up results from the sample being probed simultaneously by multiple spatially separated beams. The mathematical description of motion blur (multiple incoherent modes) in fly-scanned single beam ptychography and multiple beam in MBP is equivalent. Thus, the additional computational efforts required for the reconstruction are comparable in both cases.

In all previous demonstrations of mutli-beam X-ray ptychography the lateral separation of the multiple beams has been fixed [2,3,4]. Hence, the effective speed up of a multi beam measurement, compared to a single beam measurement depended strongly on the sample and the size of the field of view required to be imaged for answering a given scientific question.

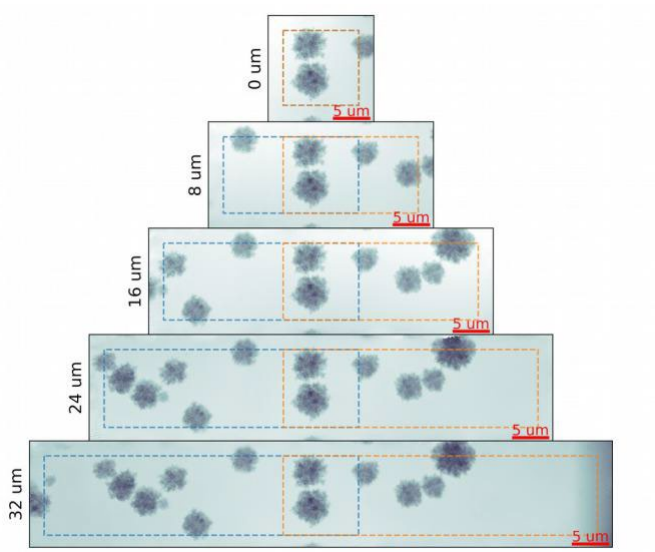

Figure 1. Phase images of multi beam ptychographic reconstructions of the same gold cluster sample recorded with the same setup but varied beam separation distance.

If the field of view is much smaller than the smallest separation of the multiple beams, or much larger than the largest distance between multiple beams, the time gain by performing MBP is strongly diminished.

We present the first implementation of MBP based on Fresnel zone plates [5,6] that allows to actively change the spacing of the multiple beams during the experiment at the press of a button. This allows to choose the optimal spacing, meaning the spacing that allows for the most time efficient scanning, for any sample without having to change the optics (see Figure 1). It is also possible to switch to standard single beam ptychpophy [7]. We show results obtained in two and three spatial dimensions and prove that MBP achieves the same reconstruction quality as comparable conventional single beam ptychography measurements.

[1] C. Bevis, et al. Ultramicroscopy 184, 164 (2018). doi:10.1016/J.ULTRAMIC.2017.08.018.
[2] Y. Yao, et al. Scientific reports 10 (2020). doi:10.1038/s41598-020-76412-8.
[3] M. Lyubomirskiy, et al. Scientific Reports 12, 1 (2022). doi:10.1038/s41598-022-09466-5.
[4] F. Wittwer, et al. Applied Physics Letters 118, 171102 (2021). doi:10.1063/5.0045571.
[5] U. Vogt, et al. Opt. Lett. 30, 2167 (2005). doi:10.1364/OL.30.002167.
[6] H. Ohlin et al, Micromachines 13, 452 (2022). doi.org:10.3390/mi13030452
[7] M. Kahnt, et al. submitted (XRM 2022 proceedings

The authors thank Jens Wenzel Andreasen and Poul Norby (both Department of Energy Conversion and Storage, Technical University of Denmark) for providing the $LaMnO_3$ perovskite microcrystals sample used to demonstrate multi beam ptychograhy in tomography mode.

A108-03-270823

Next frontiers of Bragg Ptychography at 4th generation sources

Dina Carbone 1*, Peng Li 2, Dan Mannix3, Marc Allain 4, Virginie Chamard 4

1 MAX IV Laboratory, Lund, Sweden, [2]Diamond Light Source, Didcot United Kingdoms, [3]ESS, Lund, Sweden, [4]Institut Fresnel, Marseille, France

**gerardina.carbone@maxiv.lu.se*

Keywords: Bragg Ptychography, Crystal microstructure, Strain

X-ray Bragg ptychography [1] is a 3D microscopy technique providing sensitivity to crystal strain with nano-scale resolution that has already demonstrated to be a powerful tool in many fields of science [2-4]. This technique has a high potential for the investigation of functional crystalline nano-scale materials. Here, the understanding of how crystal structure and strain are intertwined with the relevant physical properties (e.g. electrical, magnetic, optical, mechanical ...) is essential for the design of future nanotechnologies.

If compared with forward ptychography, this technique suffers from a lower signal and from severe position instabilities originating from the complex diffraction setup and data acquisition geometry needed. Our experiments performed at MAX IV Laboratory and ESRF-EBS demonstrate that the highly brilliant coherent X-ray beams produced at 4th generation synchrotron sources are hugely beneficial for Bragg Ptychography. The increased coherent flux allows to reduce the overall data acquisition time, helping to reduce the impact of the instabilities intrinsic to the setup. The better signal quality (larger signal-to-noise ratio) of the dataset also allows to utilise "position refinements" in the reconstruction algorithms, that increases the consistency of the iterations improving the quality of its output [5].

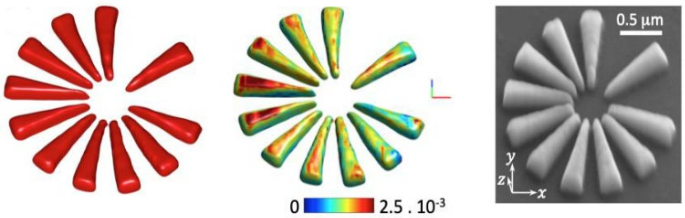

Figure 1. (From left to right): 3D volume rendering of the morphology and strain component along the vertical direction of a crystalline Si test-sample retrieved from Bragg-ptychography, compared with a SEM image of the same sample.

What is the potential of this crystalline microscopy, and what are the next frontiers? Which are the limits that still need to be overcome for this method to respond to pressing questions in material science? New pathways for further developing this already powerful 3D microscopy are currently being explored: following the recent implementation of a magnetic *and* structural microscopy based on scanning X-ray diffraction [6], we exploit the potential of the 4th generation sources to pursue a new 3D magnetic microscopy based on Bragg ptychography to reveal spin texture in prototype crystalline device structures with nanoscale resolution.

[1] P. Godard et al. (2011). *Nat. Commun*. 2**,** 568
[2] S. O. Hruszkewycz et al. (2016). *Nat. Mater*. **16**, 244-251
[3] F. Mastropietro et al. (2017). *Nat. Mater*. **16**, 948-952
[4] M. O. Hill et al. (2018) .*Nano. Lett*. **18**, 811-819
[5] P. Li et al. (2022). *Light: Science and Applications* **11**, 1, 73
[6] Evans et al. (2020). *Sci. Adv.* **6**, eaba935

A108-04-270823

High-resolution resolution X-ray tomography via burst ptychography

T. Aidukas, N. W. Phillips, A. Diaz, E. Müller-Gubler, M. Guizar-Sicairos, M. Holler

Paul Scherrer Institut, Forschungsstrasse 111, Villigen PSI, Aargau 5232, Switzerland

tomas.aidukas@psi.ch

Keywords: ptychography, tomography, X-ray

The resolution attained using X-rays has improved significantly, especially with the introduction of ptychography [1] – a coherent lensless imaging technique. While scanning the sample across the X-ray beam, a diffraction pattern is collected for each scanning position. Once the desired field-of-view is scanned, the recorded diffraction patterns are used to recover the amplitude and phase of the sample transmissivity by iterative phase-retrieval algorithms. Ptychography provides diversity to the measurement [2] via overlapped illumination. Combined with computational optimization routines the missing phase problem can be solved reliably if the forward model, i.e. the mathematical description of interaction of light and matter and its propagation to the detector, is accurate. In the presence of experimental imperfections, the physical measurement will deviate from the assumed forward model and degrade reconstruction quality. A common degradation manifests itself as blurring of the diffraction patterns, caused e.g. by poor spatial coherence of the illumination or by relative motion of the illumination and the sample.

We propose an image acquisition and reconstruction technique called burst ptychography, where for a given scan position and the same photon budget we capture many low-exposure frames, in the order of few milliseconds, for each scanning position. This allows us to resolve the temporal dynamics of the instabilities and decouple them into multiple images, thus we no longer require to infer them from a single image using mixed-state ptychography [3], which reduces algorithmic complexity. Despite the rather trivial image acquisition process, ptychographic reconstruction becomes challenging due to large data quantities and poor signal-to-noise ratio of each low-exposure image. The problem is especially difficult if the underlying instabilities change in nature or amplitude for each scan position. With burst ptychography we can mitigate the aforementioned issues, boost algorithm convergence, and reduce computational load.

To validate burst ptychography we imaged an integrated circuit sample and reconstructed it using burst ptychography, Fig.1(a), and mixed-state ptychography [3], Fig.1(b), which is a common alternative approach to mitigate experimental imperfections. The significantly better image quality of burst ptychography is attributed± to the refined sample scanning positions shown in Fig.1(c). The recovered experimental instabilities had an amplitude of 20 nm, making burst ptychography an ideal candidate to narrow the gap between X-ray and electron microscopy, especially for 4th generation X-ray sources. During the talk, I will introduce the computational and experimental approach of burst ptychography, which will be validated by experimental integrated circuit data reconstructed with a 4 nm voxel size in 3D.

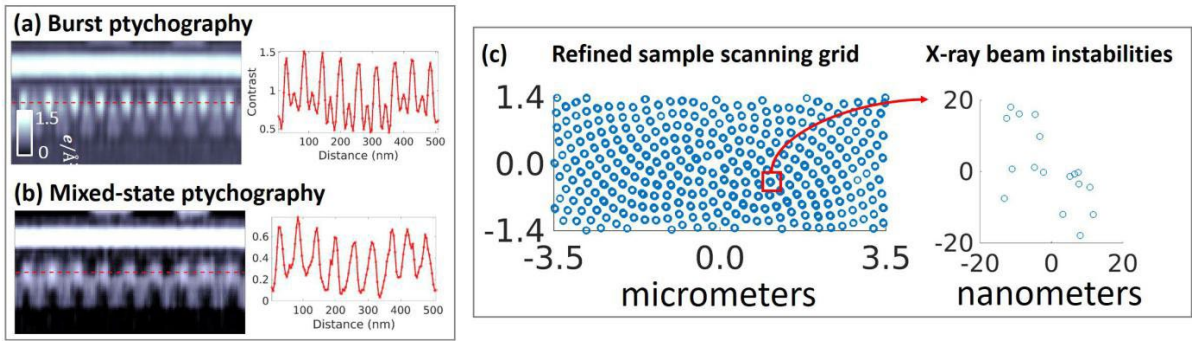

Figure 1. Image quality comparison between (a) burst and (b) mixed-state ptychography using a zoomed-in integrated circuit 3D reconstruction. (c) The improved image quality of burst ptychography is attributed to the X-ray beam instability correction.

[1] Pierre, T., Martin, D., Andreas, M., Oliver, B., Christian, D., & Franz, P. (2008). High-Resolution Scanning X-ray Diffraction Microscopy. Science, 321(5887), 379–382.
[2] Guizar-Sicairos, M., & Fienup, J. R. (2008). Phase retrieval with transverse translation diversity: A nonlinear optimization approach. Optics Express, 16(10), 7264–7278.
[3] Thibault, P., & Menzel, A. (2013). Reconstructing state mixtures from diffraction measurements. Nature, 494(7435), 68–71.

A108-05-270823

Simultaneous x-ray ptychography, x-ray fluorescence, and x-ray excited optical luminescence experiments in metal halide perovskites: correlating morphology, chemical heterogeneity, and optoelectronic properties

Francisco M. C. da Silva[1,2], Maria Gabriella Detone Guaita[2,1], Rodrigo Szostak[1], Verônica C. Teixeira[1], Ana F. Nogueira[2], Hélio C. N. Tolentino[1]

1Brazilian Synchrotron Light Laboratory, Brazilian Centre for Research in Energy and Materials (LNLS/CNPEM), 2Institute of Physics, Campinas State University (IFGW/UNICAMP) 2Institute of Chemistry, Campinas State University (IQ/UNICAMP)

francisco.silva@lnls.br

Keywords: X-ray ptychography, X-ray fluorescence, X-ray excited optical luminescence, correlative imaging, metal halide perovskites, optoelectronics, photovoltaics, synchrotron

The modern lifestyle and the increase in world population have dramatically increased the energy demand, pushing the development of new energy sources. Among new photovoltaic materials, metal halide perovskites (MHP) (ABX_3, where $A=CH_3NH_3^+$, $CH(NH_2)_2^+$ or Cs, $B=Pb^{2+}$, $X= I^-$ or Br^-) are the most promising for solar cells and detectors owing to their low processing cost, easy fabrication, high-power conversion efficiency, and high scintillation yield.[1] Despite that, several aspects of morphology, chemical composition, and optoelectronic properties are to be uncovered from the micro to the nanoscale.[2] X-ray nanoscopy techniques available at the CARNAUBA beamline (SIRIUS/LNLS)[2] are up-and-coming to investigate MHP[3,4], revealing the correlation among morphology (x-ray ptychography), stoichiometric chemical distribution (x-ray fluorescence - XRF), and optoelectronic response (x-ray excited optical luminescence - XEOL) of these materials. We report x-ray nanoscopy experiments, including coherent diffractive imaging (CDI) in flyscan mode.[5] Ptychography in phase contrast (14 nm pixel size @10 keV) reveals morphological aspects not visible in traditional scanning transmission (STXM) maps. In addition, thanks to the XRF maps, we correlate the grain boundary regions to a higher concentration of iodine in the outer regions of the grain and a lower electronic density, as highlighted by the phase advances. (Fig. 1) The possibility of measuring in flyscan mode and N_2 atmosphere was essential to mitigate eventual sample damages that are typically the main limiting factor to applying the CDI in such samples. Our multispectral images of hybrid perovskites are a pivotal step in developing and applying the technique in beam-sensitive samples for high-resolution imaging, especially in the case of heterogeneous and hierarchical functional materials in which the multiscale properties determine final device performances.

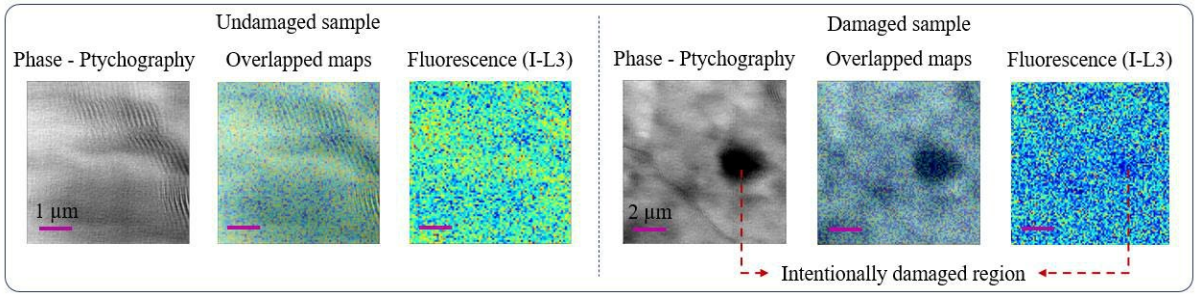

Figure 1. Metal halide perovskite (MHP) multispectral imaging presentation. Reconstruction of the micrometer size grains are shown in phase and respective I-L3 edge fluorescence maps are shown for undamaged and damaged samples.

[1] Li, Wei, et al. "Chemically diverse and multifunctional hybrid organic–inorganic perovskites." Nature Reviews Materials 2.3 (2017): 1-18.

[2] Tolentino, Hélio CN, et al. "X-ray microscopy developments at Sirius-LNLS: first commissioning experiments at the Carnauba beamline." X-Ray Nanoimaging: Instruments and Methods V. Vol. 11839. SPIE, 2021.
[3] Kodur, Moses, et al. "X-Ray microscopy of halide perovskites: techniques, applications, and prospects." Advanced Energy Materials 10.26 (2020): 1903170.
[4] Stuckelberger, Michael E., et al. "Effects of X-rays on perovskite solar cells." The Journal of Physical Chemistry C 124.33 (2020): 17949-17956.
[5] Baraldi, Giovanni L., et al. "Fast reconstruction tools for ptychography at Sirius, the fourth-generation Brazilian synchrotron." Journal of Applied Crystallography 53.6 (2020): 1550-1558.

We want to acknowledge the funding agencies CNPq () and FAPESP (2021/01357-6) along with the Brazilian Synchrotron Light Laboratory, under the funding of the Brazilian Ministry of Science, Technology, and Innovations (MCTI).

A108-06-270823

Correlative imaging with multi-modal scanning probe microscopy

Xiaojing Huang[1], Hanfei Yan[1], Ajith Pattammattel[1], Longlong Wu[2], Ian Robinson[2], Yong Chu[1]

[1]National Synchrotron Light Source II, Brookhaven National Laboratory, Upton NY 11973, USA

[2]Condensed Matter Physics and Materials Science Department, Brookhaven National Laboratory, Upton, NY 11973, USA

xjhuang@bnl.gov

Keywords: X-ray Microscopy, Multi-modality, Ptychography, X-ray Fluorescence

Scanning probe microscopy offers a unique opportunity to detect structural and chemical heterogeneities over the sample volume with high spatial resolution and sensitivity. This approach finds wide applications in functional materials and devices. The multi-modal imaging mode collects fluorescence, transmitted scattering and Bragg diffraction signals simultaneously (as shown in Fig. 1), thus providing a comprehensive characterization of the specimen.

The abundant information embedded in different channels offers a new opportunity to utilize the correlation across various contrast mechanisms and enhance the obtained image quality. We explored the potential to extend the depth of field of the ptychography method using the multi-slice [1] and focus-stacking [2] methods. Adopting the low spatial-frequency information from the fluorescence channel, we can push the depth resolution down to 500 nm [3]. Using the reconstructed beam profile from ptychography, we developed a machine-learning network to decouple the blurry impact from measurement and significantly enhance the fluorescence image quality [4]. Using the multi-model imaging method, we studies the imperfections in self-assembled nanoparticle super-lattices [5], revealed the surface modification and lattice distortion in co-doped cathode particles [6], and observed the healing effect of battery materials in an annealing process [7].

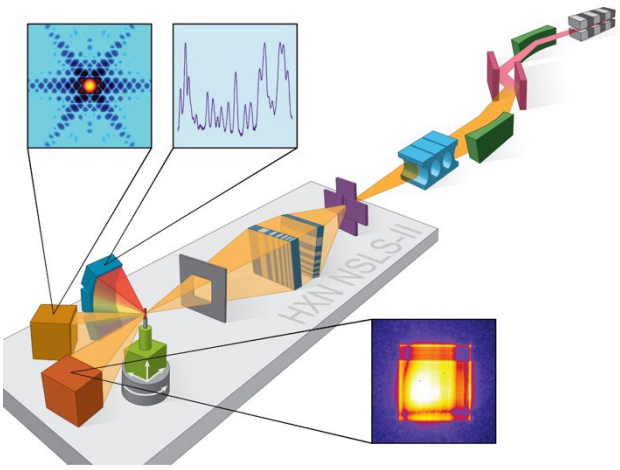

Figure 1. The Hard X-ray Nanoprobe beamline at NSLS-II is operated as a scanning probe microscope collecting fluorescence, transmitted scattering and Bragg diffraction signals simultaneously.

[1] H. Ozturk, H. Yan, Y. He, M. Ge, Z. Dong, M. Lin, E. Nazaretski, I. Robinson, Y. Chu and X. Huang, *Optica*, 5(5), 601-607, (2018).
[2] X. Huang, H. Yan, I. Robinson and Y. Chu, *Opt. Lett.*, 44(3), 503-506, (2019).
[3] X. Huang, H. Yan, Y. He, M. Ge, H. Ozturk, Y. Fang, S. Ha, M. Lin, M. Lu, E. Nazaretski, I. Robinson, and Y. Chu, *Acta. Cryst.*, A75, 336-341, (2019).

[4] L. Wu, S. Bak, Y. Shin, Y. Chu, S. Yoo, I. K. Robinson and X. Huang, submitted.
[5] A. Michelson, B. Minevich, H. Emamy, X. Huang, Y. Chu, H. Yan and O. Gang, *Science*, 376(6589), 203-207, (2022).
[6] Y. Hong, X. Huang, C. Wei, J. Wang, J. Zhang, H. Yan, Y. Chu, P. Pianetta, R. Xiao, X. Yu, Y. Liu, and H. Li, *Chem*, 6(10), 2759-2769, (2020).
[7] J. Li, Y. Hong, H. Yan, Y. Chu, P. Pianetta, H. Li, D. Ratner, X. Huang, X. Yu, Y. Liu, *Energy Storage Materials*, 45, 647-655, (2022).

DAY 7

Monday
28 August 2023

Struchkov Prize
Room 210/211
9.00am - 9.50am

Struchkov Prize-280823

Interatomic interactions in molecules, associates, crystals and transition states in terms of electronic force density fields

Robert R. Fayzullin

Arbuzov Institute of Organic and Physical Chemistry, FRC Kazan Scientific Center, Russian Academy of Sciences
robert.fayzullin@gmail.com

Keywords: Bond theory, Quantum crystallography, Transition states

Within the framework of quantum chemical topology and in terms of electronic force density fields of static and kinetic nature, we have defined the interatomic charge transfer and discovered a previously unknown quantum chemical phenomenon accompanying the electron transfer [1, 2]. This allowed us to describe the directional electronegativity of bonded atoms and the interatomic "through-bond" and "through-space" electronic effects [3, 4]. Furthermore, we proposed to consider the zero-flux surface in the kinetic force field as a topologically defined interatomic turning surface for an electron [2, 3]. The presence of a neighboring nucleus inevitably leads to the appearance of the corresponding zero-flux surfaces between the nuclei in the vector fields of the kinetic and electrostatic forces [3]. Thus, comparing the superpositions of the vector fields in a molecule and its crystal is a direct way to trace the crystal packing effect [3, 4]. All of this forms the basis of the currently developing *orbital-free quantum-topological binding approach* to the mechanical description of chemical bonding, structure, and reactions, which deals with the electrostatic and kinetic force density fields [4]. Fragments of crystal structures, stabilized by the packing effect, have been proposed as experimentally accessible models of initial and transition states of chemical reactions [4]. As an illustration, we refer to the case of the three-center tetrel bonding Cl···C···Cl in the crystal of Appel's salt (Fig. 1a), which resembles the transition state of bimolecular nucleophilic substitution reactions. According to the theoretical calculation, the electroneutral ion pair characterized by the Cl···C interaction is isomerized when isolated from the crystal structure to form the molecule, which leads to the collapse of the respective zero-flux surfaces in the electrostatic and kinetic force fields due to the formation of the Cl–C covalent bond. In this communication, we have for the first time applied the binding approach to describe the structure and bonds in many-electron multinuclear systems corresponding to the transition states of chemical reactions. The trajectory maps in Fig. 1b show that, for the model transition state of the bimolecular nucleophilic substitution reaction, corresponding to the $Cl^{-}\cdots C^{+}\cdots Cl^{-}$ system, the central atom acts as an electron contributor (electropositive atom). The behavior of the force fields and the location of the zero-flux surfaces for the forming and breaking covalent bonds in the transition state are similar to those for the noncovalent interactions. Thus, we emphasize the special role of tetrel interactions in understanding the transition states of organic reactions.

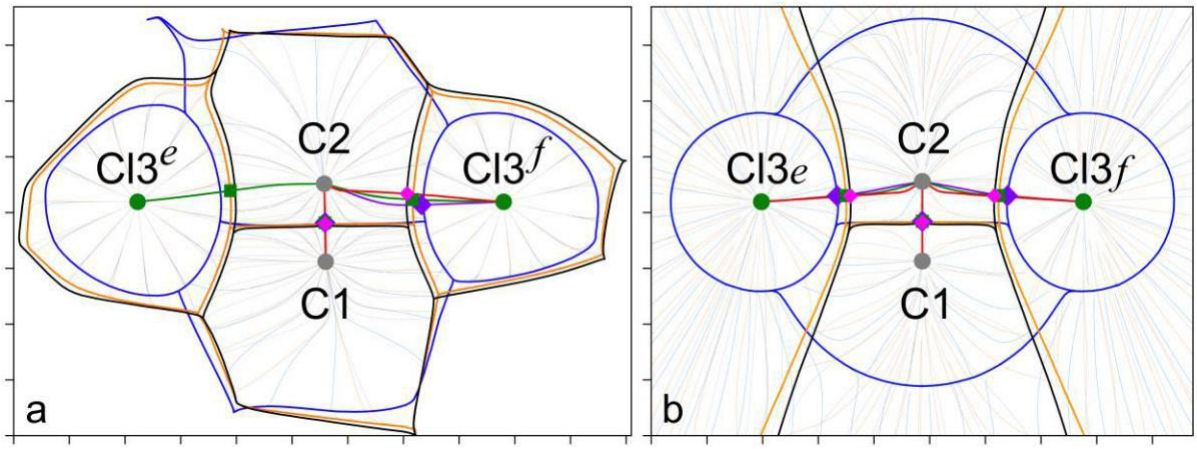

Figure 1. Superpositions of trajectory maps of the vector fields of electron density gradient (black), electrostatic force (blue), and kinetic force (orange) for (a) the three-center tetrel bonding $Cl^{-}\cdots C\cdots Cl^{-}$ in Appel's salt according to the experimental X-ray diffraction data compared to (b) the associated transition state theoretically modeled at the ωB97X-D/aug-cc-pVTZ level (imaginary frequency is –67.4 cm^{-1}). Zero-flux surfaces are highlighted with thicker lines of the corresponding color. Saddle critical points (3, –1) in the electron density, the electrostatic potential, and the kinetic potential are indicated by magenta and violet rhombuses and green squares. Gradient lines starting from these critical points and ending at the nuclei are colored red, violet, and green, respectively. The distance between axis tick marks is 1 Å.

[1] Shteingolts, S. A., Stash, A. I., Tsirelson, V. G. & Fayzullin, R. R. (2021). *Chem. Eur. J.* **27**, 7789.
[2] Shteingolts, S. A., Stash, A. I., Tsirelson, V. G. & Fayzullin, R. R. (2022). *Chem. Eur. J.* **28**, e202200985.
[3] Kartashov, S. V., Shteingolts, S. A., Stash, A. I., Tsirelson, V. G. & Fayzullin, R. R. (2023). *Cryst. Growth Des.* **23**, 1726.
[4] Saifina, A. F., Kartashov, S. V., Stash, A. I., Tsirelson, V. G. & Fayzullin, R. R. (2023). *Cryst. Growth Des.* **23**, 3002.

R. R. F. acknowledges the support of the Russian Science Foundation (Grant No. 21-73-10191) and is also very grateful to Mr. Sergey V. Kartashov for technical assistance.

Keynote 31
Room 212/213
9.00am - 9.50am

Keynote-31-280823

Trekkin' through reciprocal space with Phaser (TNG)

A. McCoy

Cambridge Institute for Medical Research, Keith Peters Building, Biomedical Campus, Hills Road, Cambridge CB2 0XY

ajm201@cam.ac.uk

Keywords: molecular replacement, cryoEM docking, Alphafold.

The use of the method of molecular replacement for phasing macromolecular crystal structures has grown exponentially over the past 50 years. What initially started as a technique to identify the relative orientations of identical subunits within experimentally phased asymmetric units[1] now almost monopolizes macromolecular phasing[2]. One of the contributors to this advancement is our software Phaser, which employs maximum likelihood principles to support robust statistical methods in the quest for extracting a phasing signal, even in the most challenging cases.

Phaser incorporates a diverse range of algorithms designed to enhance the chances of successful phasing, such as ensemble methods, corrections for anisotropy and translational non-crystallographic symmetry, and sophisticated scoring functions. Further algorithms allow accurate prediction of phasing outcomes and reliable analysis of whether or not phasing has succeeded. The widespread adoption of Phaser by the macromolecular crystallographic community has not only expedited the determination of crystal structures but also enabled the investigation of more complex systems and biological processes.

Recently, the arrival of accurate computational models, such as Alphafold2, has had a profound impact on accelerating the molecular replacement workflow. We have adapted our pipelines to exploit these models and associated meta-data[3]. We have also shown that the statistical methods employed for molecular replacement in Phaser can been adapted for docking of these models into cryo-electron microscopy maps, giving fast, robust docking even into poor density[4].

I will reflect on the current state of molecular replacement and explore ongoing research and future prospects for Phaser (TNG)[5] in the ever-evolving field of macromolecular crystallography.

[1] Rossmann, M.G. & Blow, D.M. (1962) *Acta Cryst*. **15**, 24-31.
[2] McCoy, A.J., Sammito, M.D., & Read, R.J. (2022) *Acta Cryst.*. **D78**, 1-13.
[3] Terwilliger, T.C., Afonine, P.V. Liebschner, D. Croll, T.I. McCoy, A.J. Oeffner, R.D. Williams, C.J. Poon, B.K. Richardson, J.S. Read R.J. & Adams P.D. (2023). *Acta Cryst.* D**79**, 234-244.
[4] Millán, C., McCoy, A.J., Terwilliger, T.C. & Read, R.J. (2023). *Acta Cryst*. **D79**, 281–289.
[5] McCoy, A.J., Stockwell, D.H., Sammito, M.D., Oeffner, R.D., Hatti, K.S., Croll, T.I. & Read, R.J. (2021). *Acta Cryst.* **D77**, 1–10.

Gjonnes Medal
Room 203/204
10.20am - 11.10am

Gjonnes Medal-280823

Defects and Thin-films Analysis using Four-Dimensional Scanning Transmission Electron Microscopy

Jian-Min Zuo1, Saran Pidaparthy1, Haoyang Ni1, Hanyu Hou1, Robert Busch1, Kaijun Yin1, Daniel D. P. Abraham2

1. *University of Illinois at Urbana-Champaign, Materials Science and Engineering, Illinois, United States of America*
2. *Argonne National Laboratory, Chemical Sciences and Engineering Division, Lemont, Illinois, United States of America*

jianzuo@illinois.edu

Keywords: Electron crystallography, diffraction imaging, defects and thin-films

The study of order and disorder is a fundamental theme in crystallography and its applications in materials science and condense matter physics. Examples include doping of semiconductors, advanced alloys with complex compositions, nanocrystalline and amorphous materials for energy and environmental technologies. These materials feature minute, significant and strong departures from perfect crystallinity, and their crystallographic analysis is a challenge. Transmission electron microscopy (TEM) has played a predominant role in the discovery of disorder within order or order within disorder, from atomic resolution imaging of crystal defects and fluctuation analysis of short- and medium-range ordering in amorphous solids. However, large gaps remain in our ability for the interrogation of significantly and strongly disordered materials. Here we introduce the concept of cepstral STEM (scanning TEM) for filling these gaps [1-5]. The basic idea is to collect large amounts of nanodiffraction patterns using scanning electron nanodiffraction (SEND) and Fourier transform the logarithmic intensities into cepstral patterns to detect the harmonics captured by diffraction and use the quefrency signals for imaging and structural analysis (Fig. 1). This talk will detail this method and demonstrate its effectiveness through applications to defect analysis in semiconductors, structure determination of high entropy alloys and analysis of silicon anode in lithium batteries.

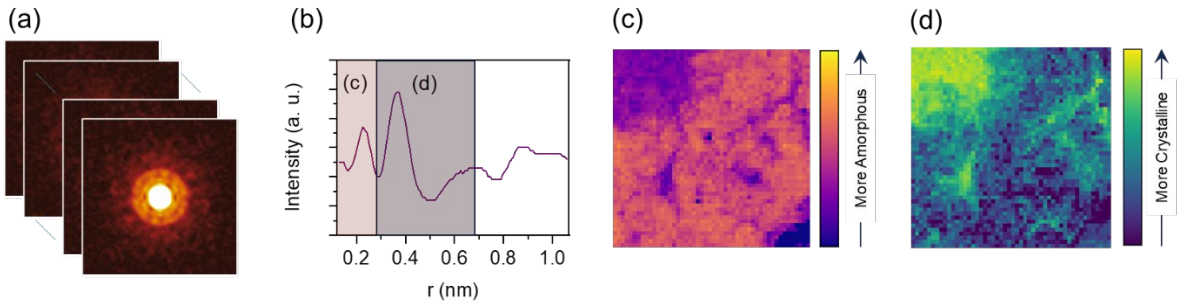

Figure 1. Cepstral STEM for imaging silicon anode. (a) Starting cepstrum stack computed from SEND dataset with (b) corresponding radial cepstrum profile. Image reconstruction of (c) amorphous material and (d) crystalline material.

[1] Shao, Y.-T., Yuan, R., Hsiao, H.-W., Yang, Q., Hu, Y., Zuo, J.-M. (2021), Ultramicroscopy, 113252.
[2] Pidaparthy, S., Ni, H., Hou, H., Abraham, D. P. & Zuo, J.-M. (2022), Microscopy and Microanalysis 28, 450-452, (2022).
[2] Pidaparthy, S., Ni, H., Hou, H., Abraham, D. P., Zuo, J. M. (2022), Ultramicroscopy, Submitted
[3] Hsiao, H.-W., Feng, R., Ni, H., An, K., Poplawsky, J. D., Liaw, P. K. & Zuo, J.-M. (2022), Nature Communications 13, 6651.
[4] Chen, W., Zhan, X., Yuan, R., Pidaparthy, S., Yong, A. X. B., An, H., Tang, Z., Yin, K., Patra, A., Jeong, H., Zhang, C., Ta, K., Riedel, Z. W., Stephens, R. M., Shoemaker, D. P., Yang, H., Gewirth, A. A., Braun, P. V., Ertekin, E., Zuo, J.-M. & Chen, Q. (2022), Nature Materials, doi:10.1038/s41563-022-01381-4.
[5] Zuo, J. M., Yuan, R. L., Shao, Y. T., Hsiao, H. W., Pidaparthy, S., Hu, Y., Yang, Q. & Zhang, J. (2022), Microscopy 71, i116-i131.

Work supported by DMR-2226495 from the Metals and Metallic Nanostructures Program (MMN) within the Division of Materials Research, National Science Foundation.

Keynote 32
Room 210/211
10.20am - 11.10am

Keynote-32-280823

How Crystallography Informs the Design of Functional Materials

Ram Seshadri

Fred and Linda R. Wudl Professor of Materials Science
Distinguished Professor, Materials Department, and Department of Chemistry and Biochemistry
Director, Materials Research Laboratory: An NSF MRSEC,
University of California, Santa Barbara CA 93106-5121

Email: seshadri@mrl.ucsb.edu

Since at least the work of Helen Megaw on the structures of ferroelectric perovskites in the 1940s, it is now received wisdom that delving deep into the property of materials requires a very detailed understating of their structures. I will demonstrate how detailed structural studies in real and reciprocal space using synchrotron X-rays and neutrons have advanced our understanding and helped devise design principles for of a range of functional inorganic and hybrid materials. These include (i) lone pair containing compounds with applications as ferroics and as photovoltaics, (ii) oxide and nitride phosphor hosts for solid-state white lighting, (iii) intermetallic compounds with applications in magnetocaloric refrigeration.

Keynote 33
Room 212/213
10.20am - 11.10am

Keynote-33-280823

Strategic Approaches to Developing MOFs with Novel Characteristics

Hoi Ri Moon

Department of Chemistry and Nanoscience, Ewha Womans University, Seoul, Republic of Korea

Email of communicating hoirimoon@ewha.ac.kr

Keywords: Metal-organic framework, MOF-on-MOF, Sensor, Isotope separation

Over the past two decades, many scientists in various fields have made intensive efforts to develop metal-organic frameworks (MOFs) having novel properties. Recently, MOF-on-MOF architecturing has been actively studied by combining two or more MOFs into a composite. Composite metal-organic frameworks (MOFs) are comprised of one MOF and another material with noticeably different properties. In general, MOFs are viewed as attractive candidates to construct new composite materials given their facile synthesis and a large library of synthesized MOFs (over 100,000) that can be used as building blocks. As such, many researchers have integrated MOFs with other classes of materials (e.g., other MOFs, carbon-based materials, oxides, metal nanoparticles, polymers) to produce new structures with synergetic properties. Unfortunately, in many of these composite MOFs, the precise nature of the interaction and the bonding at the interface between the two materials is unknown and cannot be well-characterized with any of the known methods.

In this talk, we present a joint computational/experimental workflow that screens thousands of metal-organic frameworks (MOFs) and identifies the optimal MOF pairs that can seamlessly "connect" to one another, taking advantage of the fact that the metal nodes of one MOF can form coordination bonds with the linkers of the second MOF.[1, 2] Based on this synthetic strategy, we report the composites of two MOFs with different dimensional (2D and 3D) and functional (conductive and porous) properties in the form of a well-integrated core-shell structure. The hierarchically assembled 2D-MOF@3D-MOF exhibits new interfacial properties that are responsible for synergetically enhanced sensing performances toward toxic H2S gas, with the lowest recorded limit of detection (1.4 ppb), superior sensitivity ($\Delta R/R0 = 3.36$), and outstanding selectivity at room temperature in air.[3] In addition, well-selected pairs of MOFs can construct the MOF-on-MOF architecture having unique pore structures, which can even be fine-tuned using synthetic approaches. These well-designed MOF-on-MOF structures enable to challenging gas separation and purification, especially for D_2 over H_2.

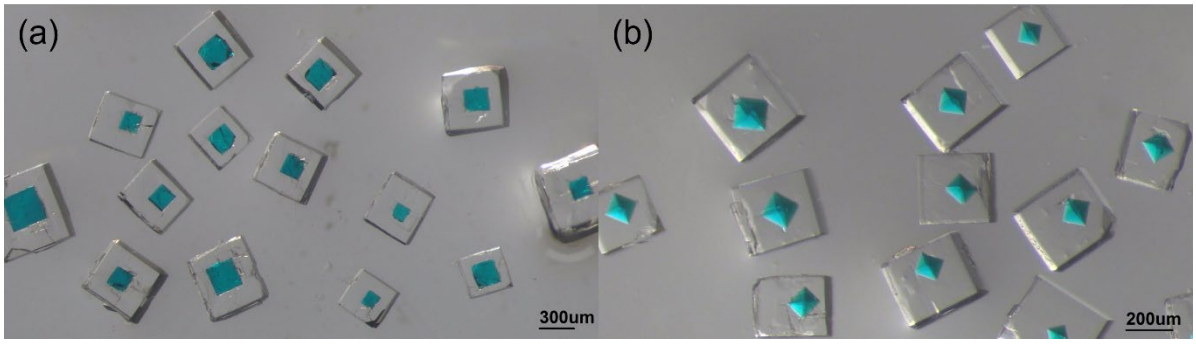

Figure 1. Optical microscope images of HKUST-1@MOF-5 core-shell, synthesized using (a) cubic- and (b) octahedral-shaped HKUST-1.[4]

[1] Kwon, O., Kim, J. Y., Park, S., Lee, J. H., Ha, J., Park, H., Moon, H. R. & Kim, J. (2019). *Nat. Commun.,* **10**, 3620.
[2] Ha, J., Jeon, M., Park, J., Kim, J. & Moon, H. R. (2023), DOI: 10.1039/d2na00790h, *Online published*.
[3] Cho, S., Park, C., Jeon, M., Lee, J. H., Kwon, O., Seong, S., Kim, J., Kim, I.-D. & Moon, H. R. (2022). *Chem. Eng. J.,* **449**, 137780.
[4] Park, J., Ha, J. & Moon, H. R. (2023), *J. Vis. Exp.*, **192**, e64978.

A004 Structure, Modelling and Properties of Quasicrystals
Room 207
1.10pm - 3.30pm

A004-01-280823

Investigating the local structure of icosahedral phases by Atomic Resolution Holography

J. R. Stellhorn1,2, K. Kimura3, K. Hayashi3, N. Happo4, N. Fujita5, F. Labib5, S. Ohhashi5, M. De Boissieu6

1 Nagoya University, Nagoya, Japan, 2 Hiroshima University, Hiroshima, Japan, 3 Nagoya Institute of Technology, Nagoya, Japan, 4 Hiroshima City University, Hiroshima, Japan, 5 Tohoku University, Sendai, Japan, 6 University Grenoble Alpes, Saint-Martin-d'Hères, France

jens.stellhorn@nagoya-u.jp

Keywords: Local structure, Atomic Resolution Holography, Icosahedral quasicrystal

The atomic-resolution holography (ARH) technique [1-3] offers the possibility to experimentally determine the local atomic-scale structure of complex systems. This method can selectively investigate specific elements and their 3-dimensional local atomic environment, without the need of a priori information on the structure. Therefore, it can provide a novel perspective for the visualization of the structure of aperiodic systems, like quasicrystals. Owing to the high complexity of the atomic arrangements in these systems, techniques targeted at the local atomic structure can provide valuable complementary information to understand the crystal chemistry (in addition to e.g. superspace crystallography approaches).

The local perspective of the structure by ARH provides an average view around a specific element in 3-dimensional space. In this presentation, we will show the recent developments for the ARH structure determination for decagonal and for Tsai-type icosahedral systems, in particular the evolution from approximant to quasicrystalline systems. Due to the 3D information available from ARH, it is possible for example to distinguish between intra- and inter-cluster correlations of the icosahedral clusters. Some results from the investigation of a 2/1 approximant (AP) of the Ag-In-Yb system are illustrated in the figure below. The ARH data can also support the understanding of the relationship between magnetic properties and the aperiodic structure, which we investigated for the Cd-Mg-RE system (RE = rare earth). Here, the magnetic characteristics were recently investigated and attributed to the positional (and chemical) disorder of Cd and Mg sites.[4,5] The direct observation of the underlying atomic arrangements is difficult by conventional methods, and the ARH measurements offer a unique new insight into this phenomenon.

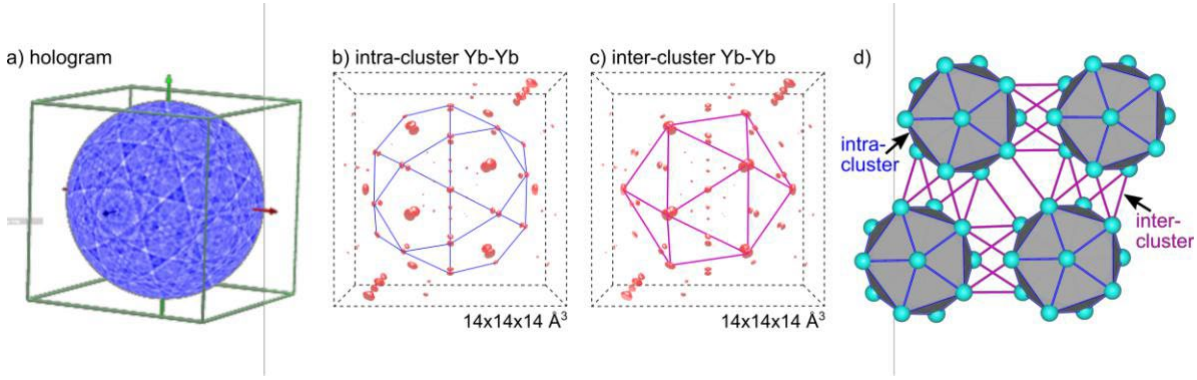

Figure 1: (a) The spherical hologram of a AgInYb 2/1 AP measured at 9.5 keV. (b, c) 3D reconstructions of the ARH data, highlighting the atomic images related to the connections inside (blue) and between (purple) the Yb icosahedra, both having interatomic distances of about 5.7 Å. (d) Structural view in real space along the pseudo-5-fold axis of the approximant.

[1] M. Tegze, G. Feigel, *Nature* **380** (1996) 49
[2] K. Hayashi et al., *J. Phys.: Condens. Matter* **24** (2012) 093201
[3] J. R. Stellhorn et al., *Mater. Trans.* **62** (2021) 342-349
[4] F. Labib et al., *J. Alloys Compd.* **822** (2020) 153541 & *J. Phys. Condens. Matter.* **32** (2020) 415801.
[5] T. Yamada et al., *Acta Cryst.* B **73** (2017) 1125-1141 .

A004-02-280823

Effect of an external potential on the stability of a dodecagonal quasicrystal and its approximants

N. R. Varela-Rosales, M. Engel

Institute for Multiscale Simulation, Friedrich-Alexander-Universität Erlangen-Nürnberg, Cauerstraße 3, 91058 Erlangen, Germany

nydia.varela@fau.de

Keywords: thin-film, quasicrystal, free energy

Quasicrystals are thermodynamic phases that form robustly in particle simulations. Estimating the thermodynamic stability of these phases, in particular relative to their approximant competitor phases, requires calculating free energies to sufficiently high precision. Standard numerical methods, like the Frenkel-Ladd method [1], consider entropic contributions from phonons but struggles with the effect of phason modes at elevated temperatures and other anharmonic effects that are known to be critical in quasicrystals [2]. In this work, we advance free energy calculations of quasicrystals inspired by experiments on thin-film, (Ba/Sr)-Ti-O quasicrystals and their approximants on a Pt substrate [3]. First, we evaluate the effect of a periodic substrate potential on the stability of a dodecagonal quasicrystal in two dimensions [4]. This periodic substrate resembles the Pt substrate from experiments. We found that the periodic substrate enhances the stability of the dodecagonal quasicrystal and its approximants at elevated temperatures. We also find that when the external potential depth has a weak presence and as we increase the temperature in our system, as we increase the temperature in our system, we can see a phase behavior resembling the appearance of modulations in the Ising model with competing interactions. When the external potential depth is increased, the more complex quasicrystal approximants disappear until only the simplest approximants remain.

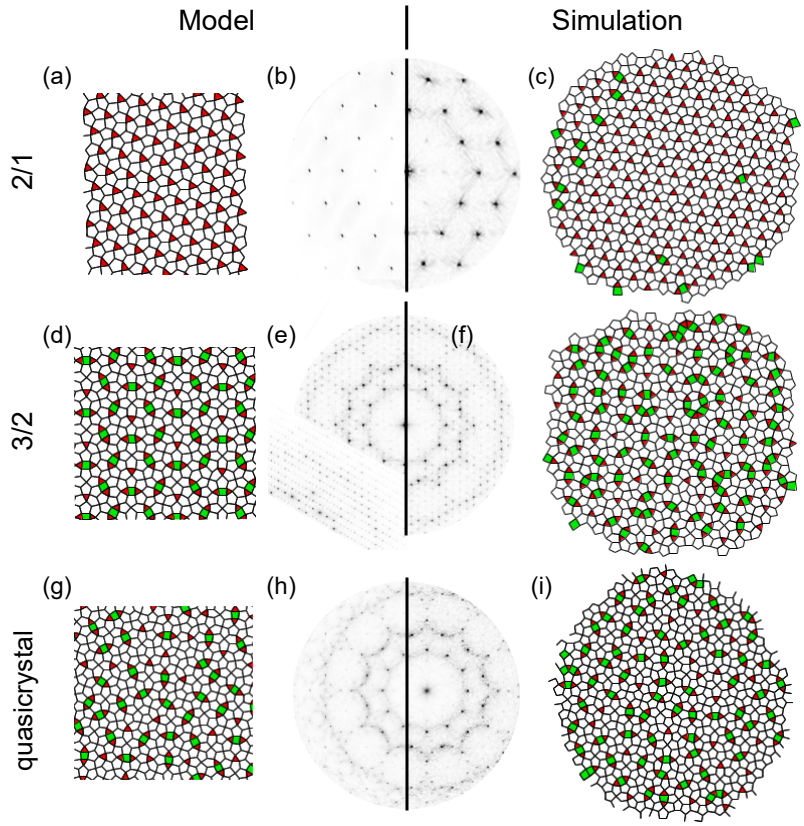

Figure 1. (a, d, g) snapshots from the model structures corresponding to the quasicrystal, and its two simplest approximants; 2/1 and 3/2. (c, f, i) snapshots from molecular dynamics simulations at different external potential depths. (b, e, h) corresponding diffraction patterns from model and simulated structures. The dashed line divides the snapshots from simulations and the approximants used for comparison in this work.

[1] Frenkel, D., Ladd, A. J. C., *J. Chem. Phys*. **81**, 3188-3193 (1984).
[2] Engel, M., Umezaki, M., Trebin, H. R., *Phys. Rev. B,* **82**:134206 (2010).
[3] Förster, S., Widdra, W. et al, *Nature,* **502**(7470):215–218 (2013).
[4] Engel, M., Trebin, H. R., *Phys. Rev. Lett.*, **98**:225505 (2007).

A004-03-280823

Atomic structure of F-type Al-Cu-Ru icosahedral quasicrystal

T. Yamada1, H. Takakura2, A. Yamamoto3

[1]Department of Applied physics, Tokyo University of Science, Tokyo, 125-8585, Japan, [2]Division of Applied Physics, Faculty of Engineering, Hokkadio University, Sapporo, Hokkaido, 060-8628, Japan, [3]National Institute for Materials Science, Tsukuba, Ibaraki, 305-0042, Japan

tsunetomo.yamada@rs.tus.ac.jp

Keywords: quasicrystals, structure analysis, higher-dimensional crystallography

$Al_{65}Cu_{20}M_{15}$ (M = Fe, Ru, Os) and $Al_{70}Pd_{20}TM_{10}$ (TM = transition metals) are stable F-type icosahedral quasicrystals (i-QCs) found more than thirty years ago [1-3]. Their detailed atomic structure is still an open question. Recently, Fujita *et. al.* determined the structure of $Al_{70}Pd_{20}Cr_3Fe_7$ intermetallic, whose atomic structure consists of mini-Bergman and pseudo-Mackay clusters and revealed that the structure can be interpreted as a $2 \times 2 \times 2$ superstructure of the 3/2 cubic approximant (AP) to the above i-QCs [4]. Moreover, they introduced the concept of "site class" to analyze the complex atomic structure and found that specific site classes exhibit occupational and positional disorders. Therefore, it is considered that a six-dimensional (6-d) model which considers these disorders is necessary to analyze the atomic structure of F-type Al-based i-QCs.

More recently, one of the authors (A.Y) proposed a new 6-d model for the F-type Al-based i-QCs [5], based on the atomic structure of the $Al_{70}Pd_{20}Cr_3Fe_7$ AP. In this model, the occupation domains (ODs) which generate the cluster centers have similarity shapes with the overall ODs in the Katz-Gratias model [6, 7], but τ^{-2} times smaller than the latter. The aim of this study is to establish the atomic structure model for the F-type Al-based i-QCs, based on the new 6-d model that is consistent with the $Al_{70}Pd_{20}Cr_3Fe_7$ AP. To this end, the 6-d model has to be built so that we can handle the structural disorders appropriately found in the structure model of $Al_{70}Pd_{20}Cr_3Fe_7$ 2/1 AP. Hence, we subdivided the ODs in terms of site class present in the i-QC. The details of the 6-d model and the results of structure analysis for the Al-Cu-Ru i-QC using single-crystal X-ray diffraction will be presented.

[1] Tsai, A. P., Inoue, A., & Masumoto, T. (1987). *Jpn. J. Appl. Phys.*, **26**(9A), L1505.
[2] Tsai, A. P., Inoue, A., & Masumoto, T. (1988). *Jpn. J. Appl. Phys.*, **27**(9A), L1587.
[3] Tsai, A. P., Yokoyama, Y., Inoue, A., & Masumoto, T. (1990). *Jpn. J. Appl. Phys*., **29**(7A), L1161.
[4] Fujita, N., Takano, H., Yamamoto, A., & Tsai, A. P. (2013). *Acta Crystallogr,* A**69**(3), 322-340.
[5] Yamamoto, A. (2014), Quasicrystal meeting, Miyagi, Japan.
[6] Katz, A. and Gratias, D., (1993). *J. Non-Cryst. Solids* **153-154**, 187
[7] Gratias, D., Puyraimond, F., Quiquandon, M., & Katz, A. (2000). *Phy. Rev. B*, **63**(2), 024202.

The authors acknowledge financial support from JSPS KAKENHI Grant Numbers JP19H05818 and JP19H05819.

A004-05-280823

Determining complex spatial patterns during crystallisation of soft matter

P. Subramanian1 & A. M. Rucklidge2

1*Department of Mathematics, University of Auckland, 38 Princes Street, Auckland 1010, New Zealand,*
2*Department of Applied Mathematics, University of Leeds, Leeds LS2 9JT, United Kingdom*

priya.subramanian@auckland.ac.nz

Keywords: soft matter, phase field crystal modelling, co-existing quasicrystals, symmetry broken quasicrystals

Soft matter such as polymers crystallise when cooled from a melt and can self-assemble into a variety of spatially complex patterns [1]. Phase field crystal (PFC) models that include information about small length scales and operate over diffusive time scales have been employed to model the crystallisation of soft matter [2]. This PFC model is also known as the conserved Swift-Hohenberg equation. When analysing this model beyond linear stability thresholds using a weakly nonlinear analysis, the resulting normal form equations are usually in the form of coupled ordinary differential equations (ODEs) for the amplitudes of the active modes, i.e., modes that are growing or neutrally stable. We use homotopy methods from numerical algebraic geometry to solve for all solutions of the chosen amplitude equations in a non-iterative method [3]. Solutions obtained this way are used as initial guesses for numerical continuation to determine invariant solutions to the full model. Starting with dodecagonal symmetry in 2D, we discover multiple co-existing metastable states at the same parameters with the same symmetry (see Figure 1 (*a*) and (*b*)).

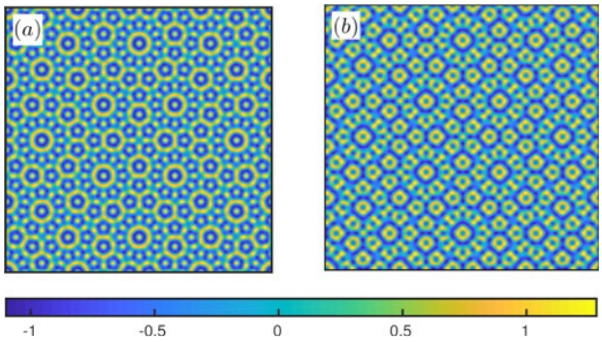

Figure 1. Panels (*a*) and (*b*) both show the variation of scalar density in a 2D soft matter system modelled using a PFC model showing co-existing dynamically stable dodecagonal quasicrystal states

Effects of broken symmetry can also be investigated robustly by solving amplitude equations corresponding to reduced symmetry subgroups. In Figure 2, we show results obtained from starting with full 3D icosahedral symmetry and relaxing constraints to investigate states with different reduced symmetries. We obtain four different metastable states: two different periodic stackings of 2D decagonal QCs, an aperiodic stacking of 2D decagonal QC and the globally stable fully symmetric 3D icosahedral QC at the same parameter combination.

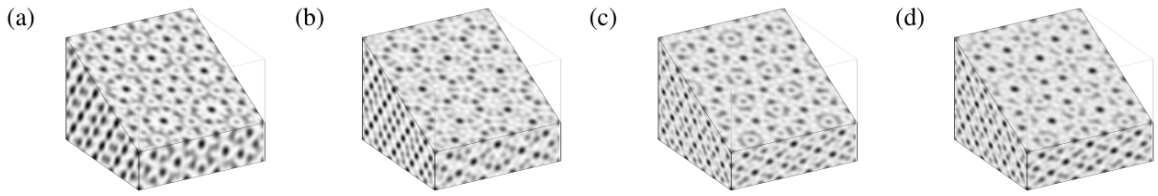

Figure 2. Variation of scalar density in a 3D soft matter system modelled using in a PFC model, sliced along the plane (1.618, 0, 1) for extended dynamically stable states of (*a*) a periodic stacking of 2D decagonal QC with large stacking wavelength, (*b*) a periodic stacking of 2D decagonal QC with small stacking wavelength and (*c*) an aperiodic stacking of 2D decagonal QC and (*d*) a fully symmetric icosahedral QC.

Combining equivariant bifurcation theory along with numerical algebraic geometry allows us to obtain multiple co-existing metastable states with same symmetry properties, obtain solutions for reduced symmetry subgroups and makes it feasible to probe multi-parameter ranges in pattern forming system to identify interesting parameter regimes with multiple invariant solutions.

[1] *Zeng, X.,Ungar, G., Liu, Y., Percec, V., Dulcey, A.E. & Hobbs, J. K. (2004) Nature,* ***428****, 157.*
[2] *Subramanian, P., Archer, A.J., Knobloch, E. & Rucklidge, A.M. (2016) Phys. Rev. Lett.* ***117****, 075501.*
[3] *Bates, D.J., Hauenstein, J.D., Sommese, A.J. & Wampler, C.W. (2013) SIAM, Philadelphia.*

A008 Biomolecules for a Sustainable Future
Room 203/204
1.10pm - 3.30pm

A008-01-280823

Biomineralization of short-chain organosulfonates: charting metabolic pathways by structural enzymology

Mihwa Lee[1], Laura Burchill[1], Spencer J Williams[1]

[1]School of Chemistry, Bio21 Institute, The University of Melbourne, Parkville, Victoria 3010, Australia

mihwa.lee@unimelb.edu.au

Keywords: organosulfonates, sulfite, biomineralization

The element sulfur is essential for life. In the biosphere sulfur is distributed into a wide range of organosulfur species that by definition contain a carbon-sulfur bond. It is estimated that up to half of all organosulfur in the biosphere resides within the organosulfur sulfolipid sulfoquinovosyl diacylglyceride (SQDG), which is produced by all photosynthetic organisms. The annual production of sulfoquinovose (SQ; 6-deoxy-6-sulfo-D-glucose), the sulfosugar headgroup of SQDG, is estimated at 10 billion tonnes per annum. Catabolism of SQ releases ATP, reducing power as NAD(P)H, sulfur- and carbon-based building blocks, and inorganic sulfur (sulfite), contributing to the global biogeochemical sulfur cycle. Biodegradation of SQ occurs in two tiers: sulfoglycolysis involving breakdown of SQ to short-chain (2- and 3-carbon) organosulfonates followed by biomineralization (breakdown of short-chain organosulfonates to sulfite). In contrast to well-characterised sulfoglycolysis pathways, the biomineralization pathways of short-chain organosulfonates are poorly understood.

We present our work on the characterisation of enzymes from *Cupriavidus pinatubonensis* involved in the biomineralization pathway of the 3-carbon organosulfonate, 2,3-dihydroxypropane-1-sulfonate (DHPS). We have dissected the molecular basis of catalysis for activation of DHPS and cleavage of the C–S bond. Enzyme kinetics support a revision of the previously reported substrate specificity and stereospecificity of these enzymes, and 3D structures define substrate binding and implicate catalytic residues involved in catalysis. Knowledge of the key enzymes involved in organosulfur biomineralization will support the development of microbial biostimulants and future efforts at rational engineering of the soil microbiota to unlock unutilized sulfur stores.

A008-02-280823

Crystallographic snapshots of a B12-dependent radical SAM methyltransferase involved in methane biosynthesis

Cameron D. Fyfe[1‡], Noelia Bernardo-García[1‡], Laura Fradale[1‡], Stéphane Grimaldi[2], Alain Guillot[1], Clémence Brewee[1], Leonard M. G. Chavas[3,4], Pierre Legrand[3], Alhosna Benjdia[1*] & Olivier Berteau[1*]

[1]Micalis Institute, ChemSyBio, INRAE, AgroParisTech, Université Paris-Saclay, 78350 Jouy-en-Josas, France
[2]Aix Marseille Univ, CNRS, BIP UMR7281, 13402 Marseille, France
[3]Synchrotron SOLEIL, L'Orme des Merisiers, BP 48 Saint-Aubin, 91190 Gif sur-Yvette CEDEX, France.
[4]Nagoya University, Nagoya 464-8603, Japan

Email of communicating Olivier.Berteau@inrae.fr

Keywords: Methane, Radical SAM enzyme, cobalamin

In the last ten years, radical SAM enzymes have emerged as central catalysts for the biosynthesis of myriad natural products. These enzymes are arguably the most diverse and versatile biocatalysts in living systems and represent novel opportunities to produce clean energy. Among them, one of the largest and least explored group are the "B12-dependent radical SAM enzymes" with more than 200,000 members identified in genomes and metagenomes. These enzymes use the dual catalytic power of S-adenosyl-L-methionine (SAM) and vitamin B_{12} (cobalamin) to notably form carbon-carbon bonds on unactivated atoms. However, despite years of efforts, we have still a poor knowledge of these enzymes which are the only biocatalysts capable to perform such reaction. To gain mechanistic insights into these emerging enzymes, we investigated the methanogenesis marker protein 10 (Mmp10) which catalyzes a key post-translational modification (arginine methylation) in methyl-coenzyme M reductase (MCR). By combining biochemical and biophysical techniques including X-ray crystallography and electron paramagnetic resonance, we discovered an unprecedented enzyme architecture containing four distinct metallic centers and key structural features involved in the control of catalysis [1]. Crystallographic snapshots of the reaction showed that, contrary to current paradigm, major and unprecedented active-site reorganization occurred upon following substrate binding in radical SAM enzymes. Notably, we demonstrated that the unique [4Fe4S] cluster can be transiently coordinated by a tyrosine residue which enables the enzyme to alternate between radical and nucleophilic chemistry. This study not only reveals how B_{12}-dependent radical SAM enzymes catalyze chemically challenging alkylation reactions, but also opens new avenues for clean energy [2].

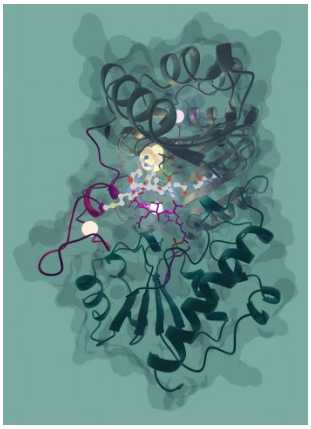

Figure 1. Structure of Mmp10 in complex with its substrate

[1] - Fyfe CD, Bernardo-García N, Fradale L, Grimaldi S, Guillot A, Brewee C, Chavas LMG, Legrand P, Benjdia A*, Berteau O.* - 2022 - Crystallographic snapshots of a B12-dependent radical SAM methyltransferase. Nature (7896):336-342.
[2] - Soualmia F, Guillot A, Sabat N, Brewee C, Kubiak X, Haumann M, Guinchard X, Benjdia A*, Berteau O*. - 2022 - Exploring the Biosynthetic Potential of TsrM, a B12-dependent Radical SAM Methyltransferase Catalyzing Non-radical Reactions. Chemistry. 2022 Jun 1;28(31):e202200627

Acknowledgements: This work was supported by the European Research Council (ERC consolidator grant 617053) and ANR (grant ANR-17-CE11-0014). The authors are grateful to the EPR facilities available at the French EPR network (IR CNRS 3443) and the Aix-Marseille University EPR center

A008-02-280823

Dual-axis aligned artificial water channels formed via water-induced self-assembly

Chien-Lung Wang[1], Yuan Chen[1], and Wei-Tsung Chuang[2]

[1]Department of Applied Chemistry, National Yang Ming Chiao Tung University, 1001 Ta Hsueh Road, Hsinchu 30010, Taiwan,
[2]National Synchrotron Radiation Research Center, 101 Hsin-Ann Road, Hsinchu 30076, Taiwan

kclwang@nycu.edu.tw

Keywords: water-induced self-assembly, artificial water channels, X-ray structural characterization

Water is known as the solvent of life in nature, partly because it can operate the self-assembly structures and functions of living matter.[1] To make water also an active component in the supramolecular chemistry of synthetic molecules, flexible amphiphilic discotic molecules (ADMs) were synthesized, and the active roles of water in the supramolecular chemistry of ADM as illustrated in **Figure 1a** were characterized.[2] Under polarized light optical microscopy, it was found that water induces the self-assembly of the amorphous ADM as shown in **Figure 1b-1c**. Small angle X-ray scattering confirmed that this water-induced self-assembly (WISA) process resulted in the formation of the hexagonal columnar (Col_h) phase of ADM, which contains bulk artificial water channels (AWCs). Moreover, by letting water act as the orientation directing agent, the directional WISA further turned the randomly oriented bulk AWCs into well-oriented AWC array. Grazing Incidence X-ray diffraction (GI XRD) shown in **Figure 1d** indicates that the directional WISA led to the dual-axis alignment of the bulk AWCs.[3] Comparing to the nearly 0 water permeability of the dehydrated ADM, the well-oriented AWC array shown in **Figure 1e** is salt-rejected and delivered a good water permeability, indicating that water not only induces the ordering process, but also turns on the function of the ADM. Water plays important roles in physiological functions of living matters. Through dynamically interacting with biomolecules, water assists them to quickly switch between different physical states in ambient conditions. Combining suitable molecular designs and in-depth structural characterization, the study turns the role of water in the supramolecular chemistry of the synthetic molecule from passive to active. The WISA process allows water to govern the self-assembly and function of the synthetic molecule as it does to the biomolecules. The quick physical transformation resulted from the dynamic interaction with water is highly desirable to the development of condensed-phase soft materials and may inspire more innovation in the development of self-assembled functional materials.

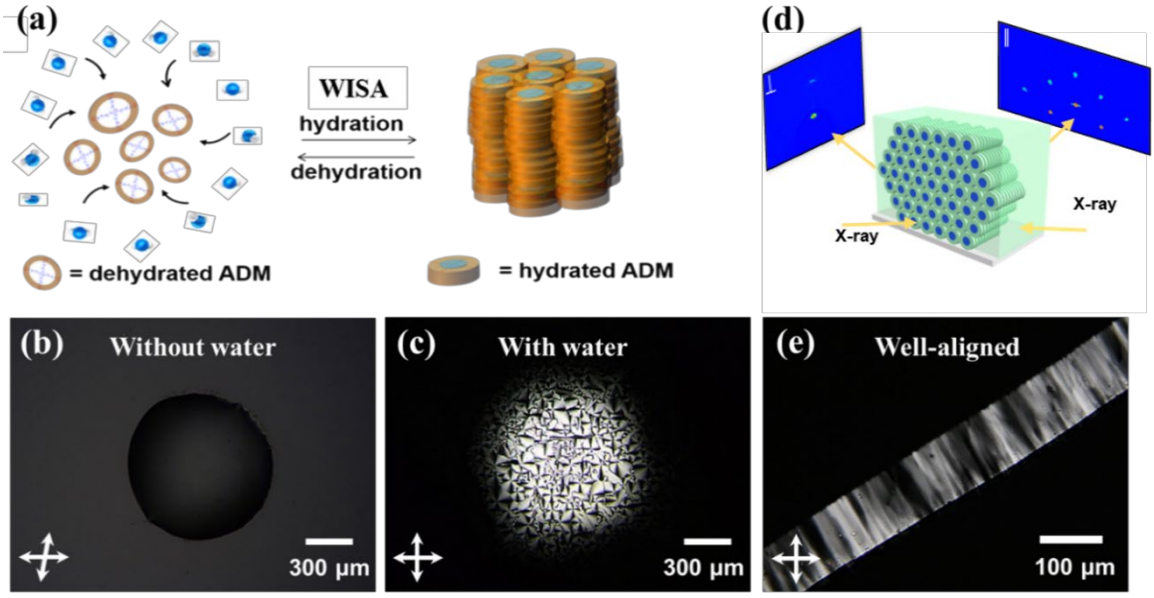

Figure 1. (a) Illustration of the WISA process. The POM images of (b) the dehydrated amorphous ADM and (c) the hydrated ordered phase of ADM. (d) The GI XRD patterns of the oriented AWC array of ADM produced from the directional WISA. (e) The POM image of the well-aligned AWC array.

[1] Beckstein, O.; Tai, K.; Sansom, M. S., *J. Am. Chem. Soc.***2004**, *126*, 14694.
[2] Chang, H. Y.; Wu, K. Y.; Chen, W. C.; Weng, J. T.; Chen, C. Y.; Raj, A.; Hamaguchi, H. O.; Chuang, W. T.; Wang, X.; Wang, C. L., *ACS Nano,* **2021**, *15*, 14885.
[3] Chen, Y.; Chang, H.-Y.; Lee, M.-T.; Yang, Z.-R.; Wang, C.-H.; Wu, K.-Y., Chuang, W.-T, and Wang C.-L. "Dual-Axis Alignment of Bulk Artificial Water Channels by Directional Water-Induced Self-Assembly" *J. Am. Chem. Soc.* **2022**, *144*, 7768.

A008-04-280823

One step forward to understand the biological reduction of CO_2 to formate by Mo/W formate dehydrogenases

Cristiano Mota[1], Ana Rita Oliveira[2], Rita Rebelo Manuel[2], Guilherme Vilela-Alves[1], Inês Cardoso Pereira[2], Maria João Romão[1]

[1]Associate Laboratory i4HB – Institute for Health and Bioeconomy and UCIBIO, Applied Molecular Biosciences Unit, NOVA School of Science and Technology, Universidade NOVA de Lisboa, 2829-516 Caparica, Portugal; [2]Instituto de Tecnologia Química e Biológica António Xavier, Universidade Nova de Lisboa, Av. da República, 2780-157 Oeiras, Portugal

Email of communicating: mjr@fct.unl.pt

Keywords: Mo/W- formate dehydrogenases, CO_2 reduction, enzymatic mechanism

The reversible interconversion of CO_2 into formate by Mo/W-Formate dehydrogenases (Fdhs) placed these enzymes on the spotlight. Probing a promising route not only for green gas sequestration but also a sustainable way to produce fuel.

FdhAB is a periplasmic heterodimer and the main responsible for CO_2 reduction in *D. vulgaris (Dv)* [1]. It comprises a pyranopterin cofactor in the active site (W-bisMGD, selenocysteine and a sulfido ligand) and four [4Fe4S] clusters responsible for electron transfer. Contrary to other Fdhs, this enzyme is oxygen-tolerant and can be purified aerobically [2]. Due to its robustness and high catalytic activity, *Dv*FdhAB is a suitable model for biocatalytic applications for CO_2 reduction. Biochemical and structural studies on *Dv*FdhAB unveiled oxidized and reduced forms of the enzyme and unique features related to its robustness (Fig. 1) [2,3].

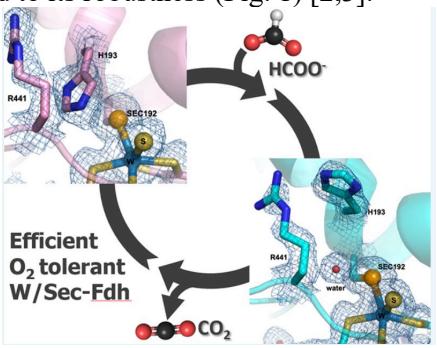

Figure 1. W-FdhAB catalysed reduction of CO_2 to formate

The requirement for its pre-activation with reducing agents led us to consider a disulfide bridge 23 Å away from the active site. C843A and C872A mutants hinder the formation of this disulfide and were shown to be catalytically like the pre-activated wild-type enzyme in the absence of reducing agents, leading to the proposal that this disulfide bridge might work as a redox switch for enzyme activation and O_2 protection [4].

Structural studies disclosed relevant conformational changes promoted by the absence of the disulfide and results and mechanistic implications will be presented.

[1] Silva, S. M. da, Voordouw, J., Leitao, C., Martins, M., Voordouw, G., & Pereira, I. C. (2013). *Microbiology*, ***159***, 1760–1769.
[2] Oliveira, A. R., Mota, C., Mourato, C., Domingos, R. M., Santos, M. F. A., Gesto, D., Guigliarelli, B., Santos-Silva, T., Romão, M. J., & Pereira, I. C. (2020). *ACS Catalysis*, **10,** 3844–3856.
[3] Oliveira, A. R., Mota, C., Klymanska, C.K., Biaso, F., Romão, M.J., Guigliarelli, B. & Pereira, I.C. (2022). *ACS Chemical Biology*, **17**, 1901–1909,
[4] Oliveira, A. R., Mota, C., Klymanska, C.K., Manuel., R.R., Vilela-Alves, G., Biaso F., Fourmond V., Guigliarelli B., Romão, M.J., & Pereira I.C. *under submission*

This work is financed by national funds from FCT - Fundação para a Ciência e a Tecnologia, I.P., project UIDP/04378/2020 and UIDB/04378/2020 and the project LA/P/0140/2020.

A008-05-280823

Crystal structure of Arabidopsis CELLULOSE SYNTHASE3 (CESA3) catalytic domain with its substrate UDP-Glucose provides insight into the molecular mechanism behind cellulose synthesis

Zhu Qiao, Edwin R. Lampugnani, Xin-Fu Yan, Ghazanfar Abbas Khan, Saw Wuan Geok, Patrick Hannah, Feng Qian, Jacob Calabria, Yansong Miao, Gerhard Grüber, Staffan Persson, Yong-Gui Gao

School of Biological Sciences, Nanyang Technological University, Singapore 637551, Singapore)

Email of communicating: zhu.qiao@ntu.edu.sg

Keywords: Cellulose synthase, UDP-Glucose, Plant cell wall, Plant biology

Cellulose is synthesized by cellulose synthases (CESAs) from the Glycosyltransferase GT-2 family. In plants, the CESAs form a six-lobed rosette-shaped CESA complex (CSC). Here we report crystal structures of the catalytic domain of *Arabidopsis thaliana* CESA3 (AtCESA3^{CatD}); both in apo and UDP-Glucose bound forms (*1*) (Figure. 1). The AtCESA3^{CatD} has an overall GT-A fold core domain sandwiched between a plant-conserved region (P-CR) and a class-specific region (C-SR). By superimposing the structure of AtCESA3^{CatD} onto the bacterial cellulose synthase BcsA, we found that the coordination of the UDP-Glc differs, indicating different substrate coordination during cellulose synthesis in plants and bacteria. Moreover, structural analyses revealed that the AtCESA3^{CatD} can form a homodimer mainly via interactions between specific beta strands. We confirmed the importance of specific amino acids on these strands for homo-dimerization through yeast and *in planta* assays using point-mutated full-length AtCESA3. Our work provides molecular insights into how the substrate UDP-Glc is coordinated in the CESAs and how the CESAs might dimerize to eventually assemble into CSCs in plants.

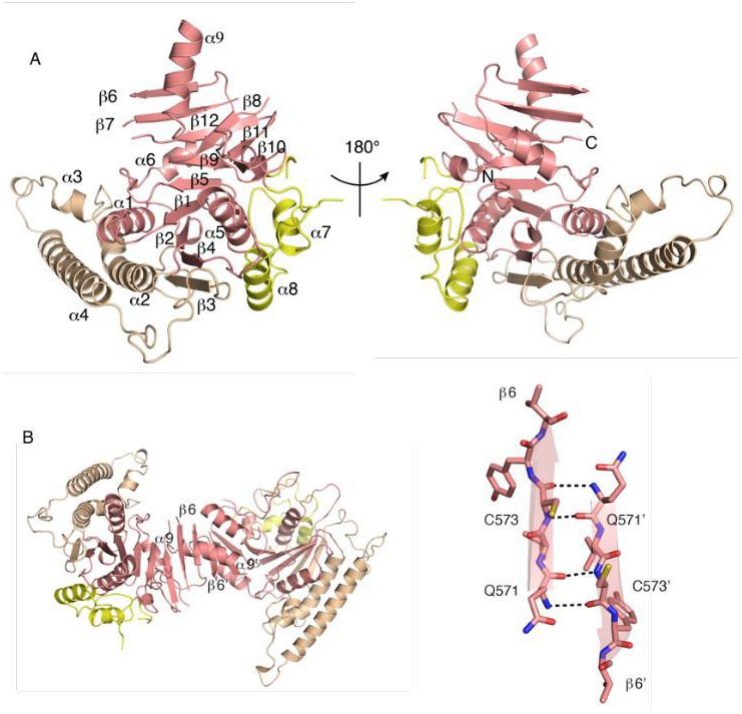

Figure 1. Crystal structural of Arabidopsis CESA3 catalytic domain (AtCESA3^{CatD}).
[6] The crystal structure of AtCESA3CatD is shown as a cartoon. The P-CR domain, C-SR domain, and the core GT domain of AtCESA3CatD are colored wheat, yellow and salmon, respectively. Secondary structure elements are labeled numerically. The unmodeled region is connected by dashed lines. B: Crystal structure of two paired AtCESA3CatD molecules resolved in an asymmetric unit. Details of homo-dimerization mechanism of AtCESA3^{CatD} dimer formation. The b6 of AtCESA3^{CatD} is shown as sticks and cartoon with amino acids labeled, with atoms N, O, and C colored blue, red, and salmon, respectively. Hydrogen bonds are indicated as dashed lines. Note that the prime (¢) indicates the second protomer in the homodimer.

[1] Z. Qiao, E. R. Lampugnani, X. F. Yan, G. A. Khan, W. G. Saw, P. Hannah, F. Qian, J. Calabria, Y. Miao, G. Gruber, S. Persson, Y. G. Gao, Structure of Arabidopsis CESA3 catalytic domain with its substrate UDP-glucose provides insight into the mechanism of cellulose synthesis. *Proc Natl Acad Sci U S A* **118**, (2021).

A008-06-280823

Challenge for Fabrication of Silk-based Sustainable Products Based on Microscopical Biomimetics of Hierarchical Structure in Native Silks

T. Yoshioka[1] and T. Kameda[1]

[1]*National Agriculture and Food Research Organization (NARO), JAPAN*

Emails: yoshiokat@affrc.go.jp, kamedat@affrc.go.jp

Keywords: Silk, Hierarchical structure, Biomimetics

Towards the realization of a sustainable society, silk protein which is the raw-material of native silk fibers have been expected as one of the promising bio-based materials. It is known that more than hundred thousand species of insects produce silk fiber and utilized if for survive. The primary structure (or amino acid sequence) of silk protein differs widely depending on the species. In other words, we have already had a huge number of different silk protein database in this nature. Recent developments of bioinformatics and genetic engineering should enable mass production of any kinds of silk proteins near future. Here the question is how can we process these silk proteins into usable silk-based products? Since the 1990s many attempts have been made to produce various types of silk-based products, such as fibers, films and sponges, from regenerated silk proteins obtained by dissolving native silk fibers. However, those products always show serious brittleness compared to the excellent mechanical property of native silks [1]. The same problem is beginning to known for the products made of recombinant silk proteins [2]. In order to fabricate usable products from the silk proteins, we need to learn and mimic the hierarchical structure microscopically in native silks (we call it microscopical biomimetics) and those structural formation mechanisms, underlying the excellent mechanical properties of native silks. For the purpose of this microscopical biomimetics, we have investigated the hierarchical structure of native silks over wide range of structural scales from primary structure of proteins to microfibrillar assemblies by means of X-ray scattering analysis, combining wide-angle and small-angle measurements (Figure 1) [3-5].

The semi-crystalline native silks are generally divided into "α-silk" forming α-helix crystals including coiled-coil crystals (represented by silks of ants, bees and hornets) and "β-silk" forming β-sheet crystals (represented by silkworms, spiders and bagworms). Based on the quantitative X-ray analysis of hierarchical structures, we have developed the processing schemes of a flexible coiled-cross-β-sheet film (namely, amyloid-β film) from the hornet α-silk (Figure 1a) [6] and a strong β-sheet fiber from the *Bombyx mori* silkworm β-silk (Figure 1b) [7,8].

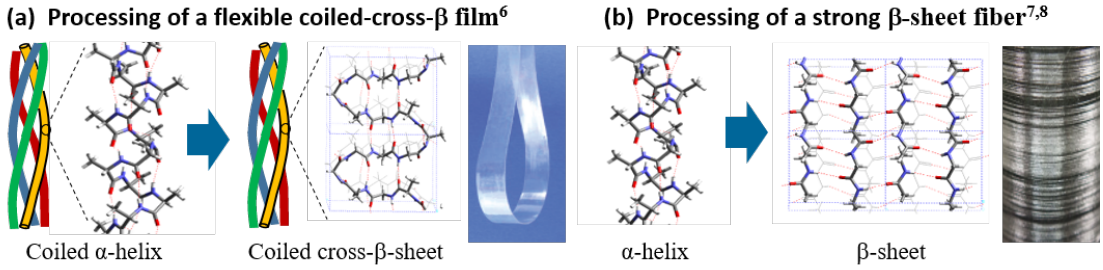

Figure 1 Processing scheme of (a) a flexible coiled-cross-β film from hornet α-silk and (b) a strong β-sheet fiber from silkworm β-silk.

[1] Jin H. J. et al. (2005). *Adv. Funct. Mater.*, **15**, 1241.
[2] Bourzac K. (2015). *Nature*, **519**, s4.
[3] Yoshioka T., Kameda T. et al. (2019). *Nat. Commun.*, **10**, 1469.
[4] Yoshioka T., Kameda T. et al. (2023). *Nano Lett.* (*in Print*)
[5] Yoshioka T. and Kameda T. (2020). *J. Silk Sci. Technol. Jpn.*, **28**, 129-135.
[6] T. Yoshioka, T. Kameda et al. (2017). *Biomacromolecules*, **18**, 3892.
[7] T. Yoshioka et al. (2016). *Biomacromolecules*, **17**, 1437.
[8] T. Yoshioka and T. Kameda et al. (2017). *ACS Biomater. Sci. Eng.*, **3**, 3207.

A023 Comparing Crystal Structures and Data
Room 208
1.10pm - 3.30pm

A023-01-280823

A continuous map of 2.6+ million 2D lattices from the Cambridge Structural Database

M. Bright, A. Cooper, V. Kurlin

Computer Science department and Materials Innovation Factory, University of Liverpool, UK

vitaliy.kurlin@gmail.com

Keywords: periodic lattices, rigid motion, isometry classification, lattice invariants, continuous metrics, chirality distances

The key problem with real data is the lack of an explicitly defined relation saying when given data objects should be considered *equivalent*. Though many equivalence relations between periodic crystals and lattices satisfy the axioms A~A, if A~B then B~A, if A~B~C then A~C, the strongest practical equivalence in crystallography is *rigid motion* composed of translations and rotations.

The slightly weaker but easier relation is an *isometry,* which maintains inter-point distances and hence also includes mirror reflections. Equivalence by symmetry groups is much weaker, producing only five Bravais classes of 2D lattices, see Fig. 1 (left).

Modulo rigid motion, the space of 2D lattices is infinitely continuous and can be bijectively mapped [1-2] to a triangle (modulo isometry and uniform scaling) or a punctured sphere (modulo rigid motion and uniform scaling), where the excluded point represents the limit case of lattices with infinitely long unit cells, see Fig. 1. These continuous maps visualize all Bravais classes as low-dimensional subspaces. For example, the equator on the sphere represents all non-generic (mirror-symmetric) lattices. The coordinates on both maps are *projected invariants* that are defined via a lattice basis but are invariant under a change of basis.

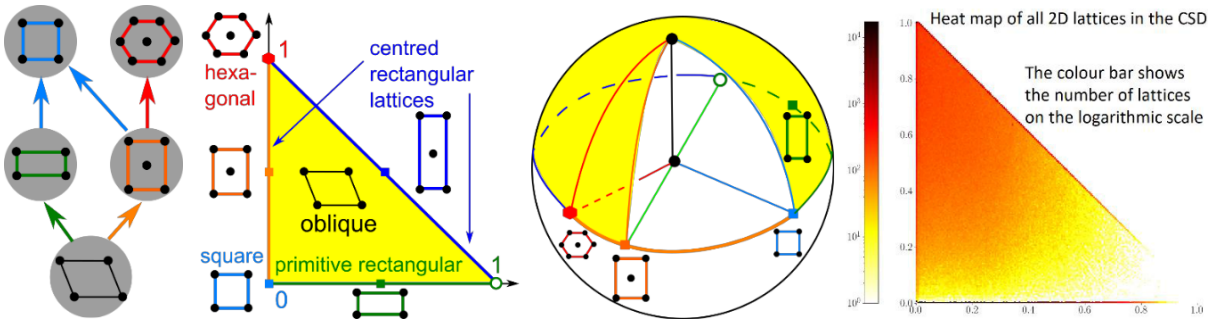

Figure 1. The tree of 5 Bravais classes on the left is extended to the continuous triangle of all 2D lattices up to isometry or the semi-spherical map. The right triangle shows the distribution of all (more than 2.6 million) 2D lattices from real CSD crystals.

The Cambridge Structural Database (CSD) has more than 870 thousand entries with well-defined 3D lattice bases a,b,c. By taking 3 pairs (a,b),(b,c),(a,c) per crystal in the CSD, we extracted more than 2.6 million 2D lattices that naturally appear in real crystals. Fig. 1 (right) shows a heat map where the color of every pixel (x,y) indicates a number of 2D lattices (on the logarithmic scale) whose projected invariant belongs to the square bin at the pixel (x,y). The darkest pixels on the horizontal edge represent tens of thousands of rectangular lattices, see also the dark top vertex of all hexagonal lattices. About 45% of all 2D lattices are oblique and fill the interior of the triangle without any gaps apart from the sparsely populated corner of lattices with long and thin cells.

The excluded point on the spherical map defines the Greenwich meridian and standard geographic coordinates (longitude and latitude). Any geographic location on Earth is now associated with a unique 2D lattice modulo rigid motion and uniform scaling. These maps allow us to find *chiral distances* that continuously measure deviations of a lattice from higher symmetry neighbors.

Similar invariant parameterizations and continuous maps are being developed for 3D lattices [3-4]. The space of arbitrary periodic point sets is also parameterized by complete isometry invariants [5]. Simpler but ultra-fast invariants distinguish all periodic crystals in the CSD and establish the *Crystal Isometry Principle* [6-7] extending Mendeleev's table to a continuous `universe' of all existing and not yet known crystals visualized as `stars', where the diamond and graphite will have different unique locations.

[1] Kurlin, V. Mathematics of 2-dimensional lattices. *Foundations of Computational Mathematics* (2023), http://arxiv.org/abs/2201.05150.
[2] Bright, M., Cooper, A., Kurlin, V. Geographic-style maps for 2-dimensional lattices. *Acta Cryst. A* (2023), http://arxiv.org/abs/2109.10885.
[3] Kurlin, V., A complete isometry classification of 3-dimensional lattices. https://arxiv.org/abs/2201.10543.
[4] Bright, M., Cooper, A., Kurlin, V. Welcome to a continuous world of 3-dimensional lattices, http://arxiv.org/abs/2109.11538.
[5] Anosova, O., Kurlin, V. An isometry classification of periodic point sets. *Proceedings Discrete Geom. Math. Morphology*, 2021, p.229-241.
[6] Widdowson, D., et al. Average Minimum Distances of periodic point sets. *MATCH Comm. Math. Comp. Chem*, v.87(3), p.529-559, 2022.
[7] Widdowson, D., Kurlin, V. Resolving the data ambiguity for periodic crystals. *Adv. Neural Information Processing Systems*, v.35 (2022).

A023-02-280823

Comparing crystallographic data in the Cambridge Structural Database

N. T. Johnson, S. B. Wiggin, S. C. Ward

Cambridge Crystallographic Data Centre, 12 Union Road, Cambridge, CB2 1EZ, UK

njohnson@ccdc.cam.ac.uk

Keywords: Database, Data, Comparison

The Cambridge Crystallographic Data Centre (CCDC) curates around 60,000 small molecule organic and metal-organic crystal structures into the Cambridge Structural Database (CSD) each year. While the vast majority of these structures are novel, approximately 5% of the CSD is made up of repeat determinations of an existing CSD entry or the same experimental data modelled in a different way. The CCDC has developed processes to identify these structures so they can be correctly labelled and linked and to enable cases of misconduct to be more easily spotted. We will present the ways the CCDC compares data to produce the CSD, as well as existing CCDC tools that enable scientists to compare structures.

We will start by exploring what data is available for comparison when crystal structures are deposited for inclusion into the CSD, how this data is utilised and what impact these comparisons have on structures in the CSD. We will highlight the completeness of this data and how this impacts our ability to compare crystal structures.

There are many challenges in correctly identifying similar structures and a key part of this is ensuring data is correctly captured at the outset. The growing popularity of alternative structural refinement techniques and new emerging techniques for data collection can increase those challenges. We will describe the methods we employ to ensure all structures resulting from the same experimental data are labelled and linked appropriately. These new refinement techniques coupled with a number of dedicated, expert crystallographers in our community means that we also need steps to compare, identify and link re-interpretations of crystal structures in the CSD and make these available in a meaningful way to our users.

Finally, we will highlight some of the software available in the wider CSD Portfolio that enables you to compare the wealth of data in the CSD and how you can also use this to compare your own structures against the CSD.

A023-03-280823

A continuous map of the Cambridge Structural Database in meaningful coordinates

Daniel E Widdowson, Vitaliy A Kurlin

Materials Innovation Factory, University of Liverpool, United Kingdom

vitaliy.kurlin@gmail.com

Keywords: Crystal Isometry Principle, periodic crystals, data standard, materials genome, structural invariants, crystal descriptors

Since crystal structures are determined in a rigid form, their most practical equivalence is rigid motion, which is a composition of translations and rotations. If we also allow mirror reflections, we get a general isometry maintaining all inter-point distances.

Crystal structures can be distinguished up to isometry only by invariants that are preserved under all isometric transformations. Since atomic coordinates are not preserved even under translation, there are not isometry invariants. The parameters of Niggli's reduced is invariant but is discontinuous [1] under almost any tiny displacement of atoms, which can make a primitive cell larger.

The physical density is a continuous invariant but is too weak to reliably distinguish many crystals. A strongest invariant is called complete and can be considered a materials genome or a DNA-style code that uniquely identifies any periodic crystal in practice.

The recent AMD (Average Minimum Distances) [2] and PDD (Pointwise Distance Distributions) [3] form an infinite hierarchy of isometry invariants that theoretically distinguish all periodic structures of atomic centers (without any chemical information) up to isometry in all general (non-singular) configurations. These invariants are so fast that more than 200 billion pairwise comparisons of all (more than 660 thousand) periodic crystals in the Cambridge Structural Database (CSD) [1] were completed within two days on a modest desktop and detected five pairs of unexpected duplicates that have all geometric data (even structure factors) identical to the last decimal place, but one atom was replaced with another one, for example, Cd with Mn in the pair HIFCAB vs JEPLIA.

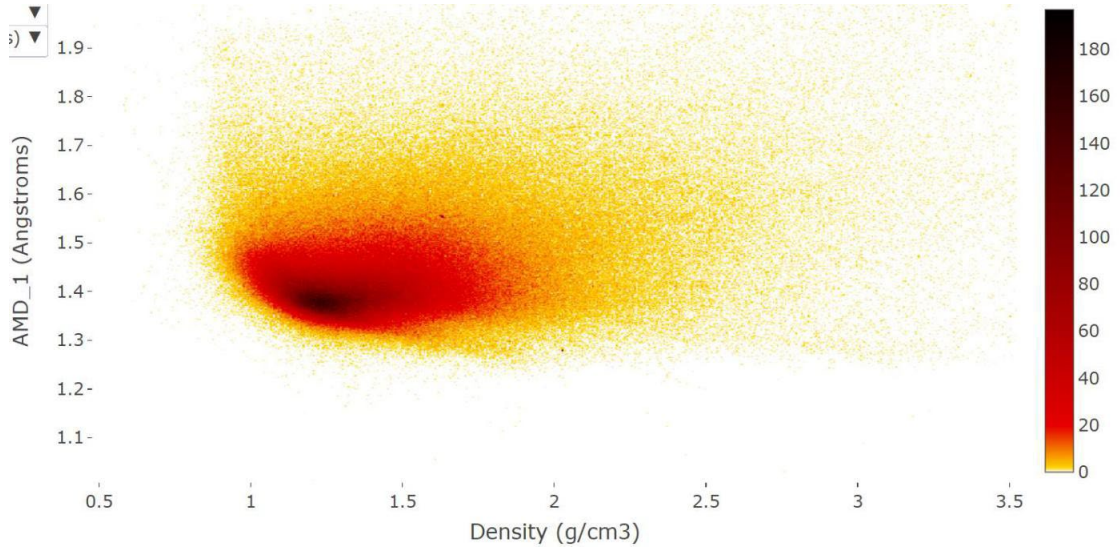

Figure 1. The heat map of all periodic crystals in the Cambridge Structural Database by using density and new invariant AMD1.

The resulting Crystal Isometry Principle (CRISP) says that all periodic structures (irrespective of chemical composition) live in a common Crystal Isometry Space parametrized by complete invariant coordinates. The first maps for 2D lattices [4-5], Figure 1 visualizes the whole CSD in two meaningful coordinates, which can be replaced by more sophisticated ones in an interactive way.

[1] Lawton, S., Jacobson, R. The reduced cell and its crystallographic applications. Tech. Rep., Ames Lab., Iowa State University (1965).
[2] Widdowson, D., et al. Average Minimum Distances of periodic point sets. *MATCH Comm. Math. Comp. Chem*, v.87(3), p.529-559, 2022.
[3] Widdowson, D., Kurlin, V. Resolving the data ambiguity for periodic crystals. *Adv. Neural Information Processing Systems*, v.35 (2022).
[4] Ward. S., Sadiq G. Introduction to the CSD–a wealth of knowledge gained from a million structures. CrystEngComm. 2020;22(43):7143-4.

[5] Kurlin, V. Mathematics of 2-dimensional lattices. *Foundations of Computational Mathematics* (2023), http://arxiv.org/abs/2201.05150.
[6] Bright, M., Cooper, A., Kurlin, V. Geographic-style maps for 2-dimensional lattices. *Acta Cryst. A* (2023), http://arxiv.org/abs/2109.10885.

A023-04-280823

Using data in the PDB and EMDB for testing new algorithms

D. Liebschner[1], P.V. Afonine[1], N.W. Moriarty[1], B.K. Poon[1], P.D. Adams[1]

[1]*Molecular Biophysics & Integrated Bioimaging Division, Lawrence Berkeley National Laboratory, Berkeley, CA, 94720, USA*

dcliebschner@lbl.gov

Keywords: Phenix Software, Reproducibility, Methods development, Algorithms

Data management is an indispensable component of modern scientific research and a key factor that can ensure reproducing experimental results. Two databases widely used in the structural biology community are the Protein Data Bank (PDB) and the Electron Microscopy Data Bank (EMDB). Our team creates tools for *Phenix* [1] – a software package for macromolecular structure determination using crystallographic (X-ray, neutron and electron) and electron cryo-microscopy data – and as part of testing new algorithms we regularly run the tools through models and data deposited in the PDB and the EMDB.

To assess new methods, it is important that we can first reproduce some of the author provided metadata like model-to-data fit, expressed by measures such as R_{work}/R_{free} in crystallography and map-model correlation in cryo-EM. Unfortunately, failure to reproduce metadata with sufficient accuracy is often the major reason for excluding models and data in the assessment of new algorithms. The mismatch can severely impede our efforts in developing new methods. For example, we found that for neutron crystallographic models and data deposited in the PDB, the reported R_{work} and R_{free} values were not reproducible in many cases [2]. Considerable manual effort was necessary to find the issues responsible for the discrepancies, such as limitations to the annotation, deposition and validation of models and data, a lack of community-wide accepted standards for the description of neutron models and data, and deficiencies in current model refinement tools.

The challenges also apply to the widely used technique of cryo-EM, for which the models and the maps are stored in different repositories, namely the PDB and the EMDB. As part of our effort to automatically re-refine many cryo-EM models using current versions of *Phenix* tools [3], we found that many map and model files have inconsistent resolution information. As the resolution parameter is required for refinement, these models could not be processed. Furthermore, some structures have very low map-model-fit, which may occur if the deposited model does not superpose on the map, for example when it is shifted or rotated (or both) with respect to the map (Fig. 1).
Here, we will share our most recent experience with using deposited model and data for testing new computational tools and algorithms in structural biology.

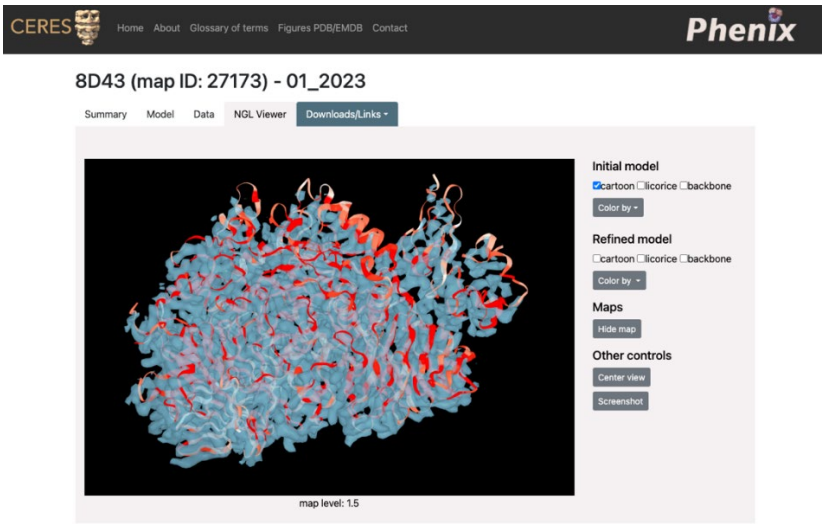

Figure 1. Screenshot from the CERES-website showing results from automated cryo-EM re-refinement efforts: The deposited model is visibly shifted with respect to the corresponding map. The model is coloured by map-model-CC (red: bad, blue: good)

[1] Liebschner, D. et al. (2019). *Acta Cryst. D*, **75**, 861–877.
[2] Liebschner, D. et al. (2018). *Acta Cryst. D*, **74**, 800–813.
[3] Liebschner, D. et al. (2021). Acta Cryst. D, 77, 48–61

A023-05-280823

Continuous maps of molecules and atomic clouds in large databases

D. Widdowson, Y. Elkin, V. Kurlin

Computer Science department, Materials Innovation Factory, University of Liverpool, United Kingdom,

vitaliy.kurlin@gmail.com

Keywords: molecular configurations, atomic clouds, rigid motion, isometry invariants, distance metric, continuous maps

Mendeleev arranged all known chemical elements into a spatial map - the periodic table parametrized by discrete coordinates - the period and group number. The periodic table was initially half-empty but effectively guided the search for new chemical elements.

The modern databases such as QM9 [1] and CSD contain millions of experimental and simulated molecules and solid crystalline materials that are not yet organized into a spatial map with unique and complete coordinates. The first question we should ask about real data is *same or different* [2]? Any answer to this question should provide an equivalence relation satisfying the three axioms: (1) *reflexivity* : any object is equivalent to itself A~A, (2) *symmetry* : if A~B then B~A, (3) *transitivity* : if A~B and B~C, then A~C. The transitivity axiom guarantees a well-defined classification when all data objects (molecules or crystals) are split into disjoint classes of equivalence. For instance, any object A generates its class [A]={B : B~A} of all objects B equivalent to A.
Though one can define many equivalences on molecules by symmetry group or chemical composition, the resulting classifications are weak in the sense that many molecules and materials (graphite and diamond) within the same class have different properties.

The strongest equivalence on molecules and crystals is *rigid motion*, which is a composition of translations and rotations, because any physical object preserves its properties under rigid motion in the same ambient conditions such as temperature and pressure.

Rigid shapes of molecules can be distinguished only by *invariants* that are descriptors preserved under rigid motion. Noisy data motivates as to require continuity under atomic displacements. Considering only atomic centers without chemical elements allows us to continuously quantify differences between close molecules with distinct compositions such as benzene and chlorobenzene.

The recent invariants invariants of periodic crystals [3,4] were adapted to fully complete and continuous invariants of clouds of m unlabeled atoms, which can be computed in a polynomial time in m [5]. These invariants distinguished all molecules in QM9 [1]. Fig. 1 compares a discrete map by chemical composition with a continuous map in the average lengths of bonds and no-bonds.

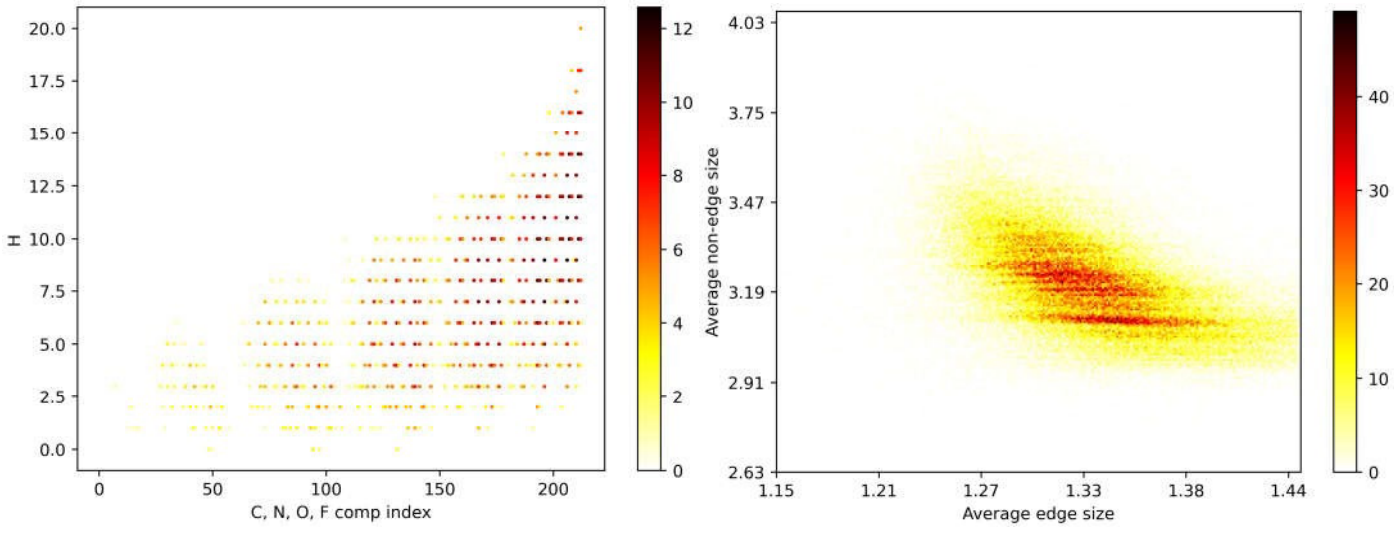

Figure 1. Visualization of 134K molecules in QM9 [1]. **Left**: x is an integer index counting elements C,N,O,F; y is the number of hydrogens; the color reflects the number of molecules with fixed (x,y). **Right**: continuous map of QM9 by (no-)bond lengths.

[1] Ramakrishnan, R., et al. Quantum chemistry structures and properties of 134 kilo molecules. Scientific data, 1(1), 1-7, 2014.
[2] Sacchi et al. Same or different - that is the question: identification of crystal forms. CrystEngComm 22 (43), 7170-7185, 2020.
[3] Anosova, O., Kurlin, V. An isometry classification of periodic point sets. *Proceedings Discrete Geom. Math. Morphology*, 2021, p.229-241.
[4] Widdowson, D., Kurlin, V. Resolving the data ambiguity for periodic crystals. *Adv. Neural Inf. Proc. Systems*, v.35 (2022). [5] Widdowson, D., Kurlin, V. Recognizing rigid patterns of unlabeled point clouds by complete and continuous isometry invariants with *no false negatives* and *no false positives*. Proceedings of Computer Vision and Pattern Recognition 2023.

A023-06-280823

Supramolecular similarity in crystal structures: Use of the similarity indices (I^X)

P. R. S. Salbego[1], T. Orlando[2], M. A. P. Martins[1]

[1]Núcleo de Química de Heterociclos (NUQUIMHE), Departamento de Engenharia e Tecnologia Ambiental, Universidade Federal de Santa Maria (UFSM), Frederico Westphalen Campus, RS, Brazil. [2]Departamento Acadêmico de Química, Universidade Tecnológica Federal do Paraná (UTFPR), Medianeira Campus, PR, Brazil

paulosalbego@gmail.com

Keywords: supramolecular similarity, crystal structure, isostructurality

From the emergence of the concept of isostructurality, various studies have sought to compare supramolecular structures, most of which have been based on geometric data, despite the availability of modern software. This field of study is of great interest to the pharmaceutical industry and for predicting crystal structures. Nonetheless, a method that provides comprehensive quantitative and comparable similarity data between two complete crystalline structures is still required. A need for proper normalization and demarcation related to the size of the system studied is the starting point of the problem in packing similarity research when examining the currently employed methods.

Given these observations, we began working on a model that may fill some gaps. By using supramolecular cluster demarcation,[1] we considered that the similarity of two supramolecular structures of different crystalline phases can be estimated from the similarity of two supramolecular clusters. For the first time, a proposal considered the quantitative data of a geometric parameter (I^D), a contact area parameter (^{IC}), and a stabilization energy parameter (I^G) for proposing indices to assess the understanding of the packing similarity of complete crystal structures. The quantitative indices were shown using a series of nine 5-aryl-1-(1,1-dimethylethyl)-1H-pyrazoles as the model and applied as proof of concept.[1] The proposed indices exhibited a good perspective regarding the similarity data and distinct regions of similarity. A similarity range with distinct regions of similarity was established, in which I^X [5] 0.80, $0.80 > I^X > 0.60$, and $I^X \leq 0.60$ (X = D, C or G) are high, mean, and low values, respectively. These indices can compose a multi-component index of similarity called I^{DCG}, in which values near 1.0 indicate systems with isostructural, isocontact, and isoenergetic behavior. The results showed that supramolecular structures with high similarity must have high values for all three indices.

The similarity indices (I^X) approach was applied to assess the degree of similarity between polymorphs[2] using ten polymorph series with different characteristics. It was possible to situate each comparison in different regions of similarity within the polymorphism phenomenon and determine the boundaries between *quasi*-isostructural polymorphs and polymorphs of low similarity. Additionally, a new descriptor (I^Q) based on the comparison of the energetic contribution of intermolecular interaction types present in each crystal structure is presented. I^Q can be a versatile tool and applicable even for systems that do not share any similarity. The similarity indices have also been successfully used in more complex molecules such as [2]rotaxanes.[3] In the next application step, the I^X indices were successfully used with crystallization mechanism proposals to indicate the origins of the supramolecular similarity between a series of benzimidazole derivative structures.[4] Our results suggest that the origin of the supramolecular similarity was determined after the first crystallization stage.

These findings emphasize that isostructurality must be seen as a broad concept whilst considering a supramolecular perspective using distinct quantitative parameters to perform comparable classifications in regions of similarity. In this sense, when comparing two crystal structures, they must have an isostructural, isocontact, and isoenergetic behavior in order to be considered similar. We hope these indices may be applied to assess future research on comparing crystalline structures and contribute to the ongoing debate regarding the concepts involved in the supramolecular similarity of crystalline structures.

1. Salbego, P., Bender, C., Hoerner, M., Zanatta, N., Frizzo, C., Bonacorso, H. & Martins, M. (2018). *ACS Omega*. **3**, 2569.
2. Salbego, P., Bender, C., Orlando, T., Moraes, G., Copetti, J., Weimer, G., Bonacorso, H. & Martins, M. (2019). *ACS Omega*. **4**, 9697.
3. Orlando, T., Salbego, P., Farias, F., Weimer, G., Copetti, J., Bonacorso, H., Zanatta, N., Hoerner, M., Berná, J. & Martins, M. (2019). *Eur. J. Org. Chem*. **2019**, 3451.
4. Orlando, T., Lopes, L., Neumann, D., Andrade, V., Mittersteiner, M., Rocha, C., Zanatta, N., Bonacorso, H., Martins, M. & Salbego, P. (2022). *CrystEngComm*. **24**, 6600.

The authors acknowledge the Coordenação de Aperfeiçoamento de Pessoal de Nível Superior (CAPES) - CapesPrInt (Project Nanomateriais - Química de Sistemas Supramoleculares (QSS)), and Conselho Nacional de Desenvolvimento Científico e Tecnológico (CNPq).

A026 and A106 Crystallographic Education – Building Community in the 21st Century *and* **Crystallography for the Next Generation: Innovation, Equity, Diversity and Inclusion**
Room 220
1.10pm - 3.30pm

A026/A106-01-280823

Sustaining our community: trust in science and the role of crystallography

John R Helliwell1 and Chiara Massera2

[1] Department of Chemistry, University of Manchester, Manchester M13 9PL, United Kingdom,
[2] Dipartimento di Scienze Chimiche, della Vita e della Sostenibilità Ambientale, Università di Parma, Viale delle Scienze 17/A, Parma 43124, Italy

john.helliwell@manchester.ac.uk

Keywords: trust; reliability; reproducibility; replicability; data reuse

Education has a vital role to play in the scientific process so that it can be trusted. There are efforts by disparate science communities to introduce new terms to ensure trust in science. These new terms have merit for discussion in crystallographic teaching commissions and possible adoption by crystallographers too. We have published a recent Teaching and Education article on this topic [1] where we envisage a students' discussion seminar on `trust in science and the role of crystallography' where the students could explore firstly the domain of crystallography and then, more broadly, history of science examples. Loss of trust reduces the confidence inside a community and, as well, can disparage the way that a community is perceived from outside. Trust in science is built up from different facets. To that end the crystallographic community has for many decades used the word `reliability' as exemplified by its Rfactors as well as other metrics. Other science communities and policy bodies have new terminologies such as FAIR and FACT. These have the following meanings: FAIR data means that the data underpinning a publication are findable, accessible, interoperable, and reusable and is a general term in data science. In fact, crystallography has a long tradition in FAIR data through its databases linked to its publications. FACT, coming from the social sciences, means their data should show fairness, accuracy, confidentiality, and transparency. Whereas FAIR looks at practical issues related to the sharing and distribution of data [2], FACT focuses more on the foundational scientific challenges [3]. These developments connect with efforts to improve reproducibility and replicability in science in general as exemplified by the US National Academies of Sciences, Engineering and Medicine who published in 2019 on the *Reproducibility and Replicability of Science* [4]. Independently the crystallography community has developed, indeed led the way in introducing, a distinct crystallographic information framework (CIF) of clear ontologies within a CIF file [5]. The International Union of Crystallography has a Committee for the Maintenance of the CIF Standard (https://www.iucr.org/resources/cif/comcifs), established in 1993. Central to this approach is a check of the CIF file; *checkCIF* reports on the consistency and integrity of crystal structure determinations reported in CIF format. Similarly, any Protein Data Bank deposition involves an extensive advisory PDB validation report (https://www.wwpdb.org/validation/validation-reports) assessing numerous indicators of correctness against the processed diffraction data and expected molecular geometry values. In conclusion crystallography is a discipline where community-agreed processed diffraction data and model validation checks are routinely made, and now being extended in various ways to the primary experimental data (“the raw data as ground truth”) according to community wishes and standards. These approaches provide the best chance for ensuring reliability and thereby trust in what we do. Most importantly these standards preserve our community. We think though that the terminologies from other areas of the sciences could usefully assist the crystallographic community in its policies such as in journal notes for authors, as well as how we engage with the public and students [1].

[1] Helliwell, J. R. & Massera, C. (2022) J. Appl. Cryst. 55.
[2] Wilkinson, M. D., et al (2016) *Sci. Data*, 3, 160018.
[3] Aalst, W. M. P. van der, Bichler, M. & Heinzl, A. (2017) *Bus. Inf. Syst. Eng.* 59, 311–313.
[4] National Academies of Sciences, Engineering and Medicine (2019) Washington, DC: The National Academies Press.
[5] Hall, S. R. & McMahon, B. (2016) *Data Sci. J.* 15, 3.

A026/A106-02-280823

Infinity and beyond – using virtual reality to teach space group symmetry and periodicity

N. Graw, M. Mücke, A. Krawczuk

Georg-August-Universität, 37077 Göttingen, Germany

ngraw@chemie.uni-goettingen.de

Keywords: virtual reality, space groups, teaching

Unarguably, space groups are among the more complicated symmetry considerations students must tackle during their studies of natural sciences. Yet they are of utmost importance to understand structure property relations and to design new materials with tailored properties. Since space groups are three-dimensional arrangements of symmetry elements, it requires spatial imagination to understand them. Two-dimensional notations, such as those used in the International Tables of Crystallography, Section A[1] are a great tool for trained crystallographers but require a high degree of visuospatial thinking from beginners. To help students develop a better understanding of space groups we designed physical three-dimensional models of whole unit cells, which explicitly depict symmetry elements and allow to comprehend how symmetry determines the arrangement of e.g. molecules inside the cell.[2,3]

However, such physical models have two major drawbacks. First of all, they are usually only available during lectures or seminars. Hence, they are of no use during self-study or for exam preparation. Secondly, for practical reasons physical models are often restricted to one unit cell or only a very limited number of them. This circumstance prevents such models to adequately address periodicity albeit being a core feature of solid-state structures.

To remedy this situation, we prepared digital three-dimensional models of unit cells which can be viewed in *virtual reality* (VR), while the interactability of a classical physical model is retained. The VR models of singular unit cells are 360° accessible and help to grasp the three dimensionality of solid-state structures. Visualisation can be changed between unit cell contents and symmetry elements (or both) depending on what is more appropriate for the topic to be discussed (see **Fig. 1**). Furthermore, this approach allows a model of a single unit cell to be extended to a virtually infinite lattice and generates an immersive teaching experience for students as these can observe the crystal structure from within.

Figure 1. Different visualisations of a unit cell showing only the symmetry elements (left), symmetry elements and molecular content (middle) or only molecular content (right).

[1] Brock, C. P., Hahn, T., Wondratschek, H., Müller, U., Shmueli, U., Prince, E., Authier, A., Kopský, V., Litvin, D. B., Arnold, E., Himmel, D. M., Rossmann, M. G., Hall, S., McMahon, B. & Aroyo, M. I. (2016) *International Tables for Crystallography*, IUCr, Chester, England.
[2] Graw, N. & Stalke, D. (2021). *Acta Cryst.* **77A**, C765.
[3] Graw, N. & Stalke, D. (2022). *J. Appl. Cryst*. **55**, 144-148.

This work was funded by the Niedersächsisches Ministerium für Wissenschaft und Kultur (2022-2023).

A026/A106-03-280823

Teaching a Large Scale Crystallography School with Zoom Webinar

J D. Ferrara, M Del Campo, C Göb, P Le Maguerès, H Puschmann, M Meyer, C Schürmann, P N. Swepston, A Stanley, A Tripathi, F White, J Wojciechowski

In order to address the loss of crystallographic training opportunities resulting from the cancellation of conventional schools around the world due to the COVID-19 pandemic we have begun an online crystallography school with live lectures and live Q&A using Zoom Webinar. Over the course of the first two years of the COVID lockdown we held two beginner schools and two advanced schools. Since we ware trying to reach a large audience in a relatively short period of time we have limited the school to ten 1-1.5 hour lectures covering the basics of small molecule crystallography including data collection, data processing and structure solution. In the schools, we will also cover some advanced topics that students commonly see in their work: absolute structure determination, twinning and disorder. To round out the education, we will provide lectures on macromolecular crystallography and powder diffraction. So that students might practice on their own, we used freely available data reduction and structure solution software, as well as data sets with which to practice. To complete the course we also developed an online examination and certification process.

In this presentation, we will provide some insight into the issues of holding lectures with up to 750 students of very diverse backgrounds and review the efficacy of the school in teaching crystallography for the four cohorts of students.

A026/A106-04-280823

Celebrating the 10th Edition of the Crystal Growing Competition for High School Students of the Argentinian Association of Crystallography

D.G. Lamas[1,2], C.E. Alvarez[1,3], V.G. Franco[1,4], V.C. Fuertes[1,5], M.G. Rodríguez[1,6], S. Klinke[1,7]

Argentinian Association of Crystallography (AACr), Buenos Aires, Argentina; [2] ITECA, UNSAM-CONICET, ECyT, Laboratorio de Cristalografía Aplicada, San Martín, Argentina; [3] Centro de Estudios Fotosintéticos y Bioquímicos-CONICET, FBioyF-UNR, Rosario, Argentina; [4] Instituto de Física del Litoral, UNL-CONICET, Santa Fe, Argentina; [5] INFIQC, UNC-CONICET, Facultad de Ciencias Químicas, Córdoba, Argentina; [6] Instituto de Química Física de los Materiales, Medio Ambiente y Energía, UBA CONICET, Buenos Aires, Argentina; [7] Fundación Instituto Leloir-CONICET, Buenos Aires, Argentina

sklinke@leloir.org.ar

Keywords: Science outreach, Education, Crystallization

The Crystal Growing Competition for High School Students of Argentina is the main outreach activity of the Argentinian Association of Crystallography (AACr), attracting hundreds of groups throughout the country every year in interesting crystallization projects using simple substances. The competition started in 2014 as one of the many AACr activities to celebrate the International Year of Crystallography in our country, and it was so successful that it eventually became a regular contest with the financial support of the Argentinian Research Council, with the major aim to introduce students to the fascinating world of science. Students must carry out a crystallization project by registering all steps of crystal growth and communicating their results in a short video or a written essay that is submitted to a panel of crystallographers from the AACr for evaluation. To conclude the activities, all selected groups are invited to bring their crystals to a Winner´s Day (Fig. 1). In support to the competition, the organizers give short courses on crystallography and crystal growth for teachers from all levels. Overall, more than 4000 high school students have already participated since the first edition, with around 2000 projects submitted and more than 300 courses taught in all 24 provinces of Argentina. Additionally, several projects won medals and honorary mentions at the IUCr International Crystal Growing Competition for Schoolchildren, organized between 2014 and 2019. It is worth to mention that even in the most difficult moments of the pandemic in 2020 and 2021, the competition was adapted to be 100% online, enabling the possibility to participate not only by growing crystals but also with bibliographic research works related to crystallography.

This year we are reaching a major milestone in the contest: its tenth non-stop edition. Special activities are being organized in frame of this occasion, for example a new crystal growth category to pay tribute to successful works submitted to previous editions, and the visit to new cities and towns in our nationwide short courses on crystallography and crystal growth. We hope that these ongoing activities will strengthen the curiosity of more and more high school students, helping them to choose scientific related fields for their future careers.

Figure 1. Winner´s Day of the 2022 Edition held in the city of Córdoba, with students from eight different provinces.

Acknowledgements: The Crystal Growing Competition is supported by the Argentinian Research Council CONICET through its VocAr Initiative (Program for the Promotion of Scientific Vocations), and the José A. Balseiro Foundation. We are grateful to the AACr authorities, regional representatives and members that have been collaborating with us in this activity since 2014

A026/A106-05-280823

A growing crystallographic community: new outreach and education initiatives at the IUCr

M. Zema1

International Union of Crystallography, Chester, UK

Email of communicating author: mz@iucr.org

Keywords: Education, Outreach, Capacity building

At a time when scientific endeavour is critical for societal benefit, the importance of crystallography is greater than ever, yet it remains a science that still has lower visibility than it should. Crystallography underpins all science today, as it enables the inner structure of matter to be accessed and relates it to the properties and functionality of any kind of compound. Understanding the structure of matter has given a new path to scientific research, has transformed industries and created new frontiers, from the design of new medicines and materials to assessing the mineral content of Mars.

In 2014, the International Union of Crystallography partnered with UNESCO to celebrate the success and importance of our science to a broad audience through an International Year of Crystallography (IYCr2014), proclaimed by the UN through Resolution A/RES/66/284 of 12 July 2012. With this resolution, the UN recognized that humankind's understanding of the material nature of our world is grounded, in particular, in our knowledge of crystallography, and stressed that education about and the application of crystallography are critical in addressing fundamental challenges. To build on the success of IYCr2014, the IUCr and partner institutions signed the "Crystallography for the Next Generation" resolution (Morocco, 2015) and committed to enhance the stature of crystallography; build capacity in developing regions of the world; extend further the public understanding of science in general and crystallography in particular.

Nevertheless, fundamental courses on crystallography are disappearing from most academic degree curricula and are almost absent in the developing countries.

The IUCr is actively engaged in a number of outreach and educational initiatives, targeting several regions worldwide and particularly, emerging countries in Africa, Latin America, Middle East and SE Asia, and students of all ages, from schoolchildren to early career researchers and young professors. The IUCr-UNESCO OpenLab has already reached over a thousand students in 25+ countries, and is providing high-level educational opportunities to local students and young professors. The IUCr-IUPAP-ICTP *LAAAMP* programme has initiated several educational programmes targeting from high-school teachers to experts in the field. At the X-TechLab, the crystallography hub established in Benin through the *LAAAMP* project, training sessions, which include hands-on tutorials on top-quality crystallographic instrumentation, are targeting students, researchers and young professors from the whole African continent; in addition, symmetry courses for high-school and university students have already reached a thousand students. Several educational activities are also done in collaboration with initiatives related to the development of new synchrotrons, e.g., the African Light Source or the initiative for the synchrotron in the Caribbean.
Through this journey, this presentation will show how these initiatives contribute to the building of the crystallographic community.

A026/A106-06-280823

CNCC - Concurso Nacional de Crecimiento de Cristales de Uruguay: 10 years of a successful crystal growing competition for schoolchildren and more.

N. Alvarez, I. Aguiar, I. Galain, R. Keuchkerian, N. Méndez, M. Mombrú, I. Núñez, G. Peinado, M. Rodríguez, C. Rojas, S. Valiero, C. Yañez, L. Suescun

Facultad de Química, Universidad de la República, Montevideo, Uruguay

leopoldo@fq.edu.uy

Keywords: Crystal Growing Competition, Inclusion, Outreach

During the International Year of Crystallography, in 2014, Uruguay held the first National Crystal Growing Competition (CNCC, for Concurso Nacional de Crecimiento de Cristales, in Spanish). It was organized by an interdisciplinary group of scientists, students and outreach officers grouped at Facultad de Química and Centro Universitario Regional Este of Universidad de la República. The main goal, aligned with the ones set by the IUCr, was to reach out to the community introducing them to the exciting world of crystals and crystallography by involving young people in growing a single crystal. The competition involved workshops, dictated by the organizers, to enable future tutors of the schoolchildren gain specific knowledge in crystal growth, keeping detailed records of experiments and presentation of results. In order to allow participants to get involved in the Worldwide Crystal Growing Competition organized by the IUCr part of the presentation by participants was a 3 minutes video that was judged together with the crystal. Crystals were judged by the weight and quality of the crystal grown and additional points were awarded for the records of the experiment in terms of creativity and scientific rigor. Throughout the first three editions (2014-2017) more than 800 people, ages 7 to 30, from around 100 schools throughout the country participated in the CNCC. It is worth mentioning, in addition, that participation was not limited to kids, anyone involved with the formal education system, even if receiving adult education in any context (including people in prisons) could participate. [1] Some participants also won prizes in the Worldwide Crystal Growing Competition in 2014, 2015 and 2017. [2]

The competition grew over the years, especially in the period 2014-2019 where a new category of competition was introduced. The creation of "Crystal gardens" allowed kindergarten to 6th grade primary school children participate in large classroom groups with their teachers, instead of the small groups recommended for single crystal work (an activity much harder to organize in a 20-30 children classroom without proper laboratory material and enough teachers). Over 3000 kids and Teachers participated during that period, coming from the 19 departments of the country with creations that overwhelmed the organizers and fellow competitors.

The outbreak of covid-19 pandemic in Uruguay (March/2020) got the organizer in the initial steps of organizing the 7th CNCC, and the group managed to organize a Crystal Growing Competition at Home that got more than 50 schoolchildren involved, growing crystals of sugar, salt and copper sulphate, with the help of their parents or close relatives during lockdown.[3]
In 2021 an abbreviated competition was organized, running from August to October, after nationwide vaccination allowed to restart in-person school activities. The category of crystal garden was extended to secondary school kids to promote participation. Finally, 2022 deserved us great happiness, with a renewed CNCC (9th edition) including the organization of workshops for tutors again, gaining participants by the hundredths. The continued activity of CNCC -even through the pandemic period- was recognized by the producers of a science dissemination TV Program of Uruguay -Sobre Ciencia- and the results of CNCC-9 were announced on public television on November 2nd 2022. [4]

As we are writing this abstract we are organizing the closing of CNCC-9 and are getting ready to launch the activities of the 10th National Crystal Growing Competition of Uruguay that will run from March (competition presentation and opening) till December (closing ceremony). We just received confirmation of financial support from some sources and are getting excited about the presentation of the history of nine editions of CNCC and ongoing activities of CNCC-10 at IUCr26 Congress. A new logo, historical records, dissemination material and news can be found at our web page and social networks: http://www.cncc.fq.edu.uy/, Twitter: @cnccfquy, Instagram: @cnccfquy, Facebook: https://www.facebook.com/cnccfquy/.

[1] Alvarez et al. (2017); "Uruguay´s National Crystal Growing Competition", *Blucher Material Science Proceedings 23a Reunião da Associação Brasileira de Cristalografia* 2(2), 30-33. DOI: 10.5151/23abcr-17
[2] Worldwide Crystal Growing Competition of IUCr. https://www.iycr2014.org/participate/competition-winners/2017-winners
[3] Aguiar et al. (2020); "A crystal growing competition at home: outreach activities during lockdown" IUCr Newsletter Vol 28, Number 3.
[4] https://sobreciencia.uy/ciencia-en-la-escuela-el-liceo-e-incluso-en-la-carcel/ - https://youtu.be/wYMCdc7HgYU

Authors would like to acknowledge the diverse funding agencies that supported the program for the last ten years: Ministerio de Educación y Cultura, Facultad de Química, Centro Universitario Regional Este, Comisión Sectorial de Extensión Universitaria y Actividades en el Medio de la Universidad de la República, Perrin, Droguería Industrial Uruguaya, Agencia Nacional de Investigación e Innovación, Fundación para el progreso de la Química, Programa de Desarrollo de las Ciencias Básicas, among others.

A026/A106-07-280823

University outreach, non-formal education and science literacy in challenging contexts

Fenouli[1], C. Rojas[2], F. Gonzalez[1], S. Valiero[2], C. Yañez[2], I. Núñez[2], I. Galain[2], M. Mombrú[2], R. Keuchkerian[2], I. Aguiar[2], L Suescun[2], N. Alvarez[2]

[1]ECE-DGES Unidad 14 Instituto Nacional de Rehabilitación, Piedra de los Indios, Colonia, Uruguay, [2]Facultad de Química, Universidad de la República, Montevideo, Uruguay

nalvarez@fq.edu.uy

Keywords: outreach, crystal growing competition, national rehabilitation unit

Learning structural chemistry should not be something reserved for secondary and/or higher education, or a certain gender or geographical region. Non formal environments and active learning approaches help in bringing closer these ideas at different levels. 2023 marks the ten-year anniversary of Uruguay's Crystal Growing Competition which has been changing and adapting to the different scenarios we were faced with for the last decade. From personally participating in workshops to a 100 % online edition and nowadays reaching students deprived of liberty. Regardless of the circumstances the competition focuses on giving a platform for teachers countrywide for a project-based learning opportunity to use in class. The main goal of the structural chemists behind the organization of the competition is to encourage the interest in science and research through crystallography, while training the participants in the application of the scientific method and critical thinking, stimulating teamwork as well as knowledge and experience exchanges in nonstructured environments.

Teachers in different educational levels can use the process of growing crystals as a project on itself or applied to different fields of study. For instance, one of the 2022 edition winners were art students exploring science. The project would normally take within 4 to 8 weeks to grow a crystal garden or single crystal, main goals in the contest. During the pandemic the competition turned into a series of virtual proposals from finding crystals at home to some more elaborated like constructing a simple crystal structure (NaCl). The activities were to be carried out at home and had kids and adults equally involved in the process.

During the last decade we had two successful experiences with students from the National Rehabilitation Units that encourage us to follow this path further. During 2022, two groups in lock up environments won prizes in the competition. Results were broadcasted on a science local TV show and participants were able to share their experiences not only with their group but with a wider audience. Since coming to the program was not possible, due to their circumstances, an award ceremony was performed within the Rehabilitation Unit with families and friends of the participants present.

This kind of initiatives are not only rewarding for all people involved but demonstrate that science can reach the most unexpected places and motivate. With this in mind, for the near future, we have decided to focus efforts on reaching rural areas and deprived of liberty students.

Authors would like to acknowledge the diverse funding agencies that supported the program for the last ten years: Ministerio de Educación y Cultura, Facultad de Química, Centro Regional Este, Comisión Sectorial de Extensión Universitaria y Actividades en el Medio de la Universidad de la República, Perrin, Agencia Nacional de Investigación e Innovación, Fundación para el progreso de la Química, Programa de Desarrollo de las Ciencias Básicas, among others.

A026/A106-08-280823

Indigenous Australia's Place in STEM

K. Wruck [1, 2]

(1) Department of Chemical Engineering, Faculty of Engineering and Information Technology, University of Melbourne
(2) School of Chemistry and Physics, Faculty of Science, Queensland University of Technology

katrina.wruck@unimelb.edu.au

Keywords: Indigenous Australia, STEM, Traditional Knowledge systems

For 60,000 years, Indigenous Australian people not only persevered but thrived, displaying an unwavering resilience that continues to inspire generations [1]. From the lush rainforests of the tropical north to the arid plains of the interior, each unique community has a holistic understanding of the environment enabling sustainable practices that have stood the test of time and showcases a profound respect for the delicate balance between human existence and the ecosystems that support it.

Yet, the significance of Indigenous Australia's contribution to STEM (Science, Technology, Engineering, and Mathematics) are seldom recognised within the mainstream academic community in Australia and on the global stage. This may be due to the philosophical differences between Indigenous and Western world views as highlighted in Figure 1 [2].

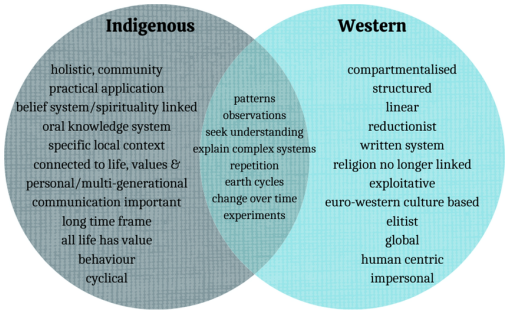

Figure 1. Comparison of Indigenous and Western Worldviews from the perspective of Indigenous and Traditional Peoples [2].

At the same time, there is much evidence of Traditional Knowledges (Indigenous Cultural Intellectual Property) that have been exploited for profit without prior informed consent, acknowledgement, or compensation of the Knowledge Holders [3]. Furthermore, the historic dispossession of land, language and culture has contributed and continues to contribute to the underrepresentation of Indigenous Australians in STEM fields. This reality is reflected in the stark disparities compared to "settler" Australians (per capita) in areas such as educational attainment [4], death from preventable disease [5] and while in custody [6, 7], rates of incarceration (Indigenous Australians are the most incarcerated people in the world) [8] and rates of child removal [9, 10], all which continue today.

In this talk, Katrina will share her journey as an Indigenous Early Career Researcher in Industrial Chemistry drawing from her personal experiences in academia, overcoming educational barriers as well as highlighting the importance of diversity and inclusion in the STEM space. She will also explore the wider implications of Terra Nullius and explain how science was weaponised to justify the dispossession and mistreatment of Aboriginal and Torres Strait Islanders on their own Country. Several examples of Indigenous Innovation in STEM will be discussed which highlight the advanced scientific understanding and sustainable practices developed by the Ancestors over thousands of generations. Katrina believes in the need for truth-telling and hopes to challenge prevailing ideologies regarding Indigenous Australia's place in STEM.

1. Arthur, W. and F. Morphy, *Macquarie Atlas of Indigenous Australia*. 2019: Macquarie Dictionary Publishers.
2. Fischer, M., et al., *Empowering her guardians to nurture our Ocean's future.* Rev Fish Biol Fish, 2022. **32**(1): p. 271-296.
3. Janke, T., *True tracks: Indigenous cultural and intellectual property principles for putting self-determination into practice.* 2019.
4. Coates, S.K., M. Trudgett, and S. Page, *Indigenous higher education sector: The evolution of recognised Indigenous leaders within Australian universities.* The Australian Journal of Indigenous Education, 2021. **50**(2): p. 215-221.
5. Crosland, P., et al., *The health burden of preventable disease in Australia: a systematic review.* Australian and New Zealand journal of public health, 2019. **43**(2): p. 163-170.
6. Gannoni, A. and S. Bricknell, *Indigenous deaths in custody: 25 years since the Royal Commission into Aboriginal Deaths in Custody.* 2019.
7. Whittaker, A., *Despite 432 Indigenous deaths in custody since 1991, no one has ever been convicted. Racist silence and complicity are to blame.* Chain Reaction, 2021(139): p. 14-15.
8. Roettger, M., K. Lockwood, and S. Dennison, *Indigenous people in Australia and New Zealand and the intergenerational effects of incarceration.* Research brief, 2021. **26**.

9. Oates, F., *Barriers and solutions: Australian Indigenous practitioners on addressing disproportionate representation of Indigenous Australian children known to statutory child protection.* AlterNative: An International Journal of Indigenous Peoples, 2020. **16**(3): p. 171-179.
10. Turnbull-Roberts, V., M. Salter, and B. Newton, *Trauma then and now: Implications of adoption reform for First Nations children.* Child & Family Social Work, 2022. **27**(2): p. 163-172.

The author wishes to acknowledge Joe Sambono for his significant contributions in advancing STEM education in the curriculum and academia.

A030 Multigrain Crystallography, Multicrystal Indexings, and Microstructures in High Pressure Experiments
Room 209
1.10pm - 3.30pm

A030-01-280823

Multigrain X-ray Diffraction for the Study of Deformation and Phase Transformation Microstructures at Deep Mantle Pressures and Temperatures

S. Merkel[1], M. Krug[2], E. Ledoux[1*], J. P. Gay[1], J. Chantel[1], S. Speziale[3], C. Sanchez-Valle[2]

Univ. Lille, UMET - CNRS, Lille, France
University of Münster, Institute for Mineralogy, Münster, Germany
Deutsches GeoForschungsZentrum GFZ, Potsdam, Germany

Keywords: Multigrain crystallography, high pressure, microstructure

Understanding how microstructures develop in Earth's materials is critical to constrain mantle processes from geophysical observations, such as seismic anisotropy. In the past, however, high pressure experiments on microtructures could not truly be performed at both mantle pressures and temperatures. Experiments in large volume presses, such as the D-DIA or RDA for instance, can not reach the pressures of the deep mantle. Radial diffraction in the diamond anvil cell have not be performed at sustained lower mantle temperatures. All of these methods also rely on classical sample characterization techniques based on powder X-ray diffraction.

In recent years, multigrain X-ray diffraction emerged as a new technique for experiments in the diamond anvil cell, allowing tracking of the orientation and size of hundreds of individual microstructural elements, in-situ, at a synchrotron beamlines. The method is compatible with other diamond anvil cell procedures, such as double-sided laser-heating and the use of pressure medium to limit the sample deviatoric stresses. Multigrain X-ray diffraction combined with double-sided laser heating is at core the joint ANR-DFG TIMEleSS project, in which we investigated phase transformations and deformation of deep Earth materials.

In the course of the ANR-DFG TIMEleSS project, we streamlined the use of multigrain crystallography in diamond anvil cell experiments, for which we wrote a thourough online manual, which is now available to the community at http://multigrain.texture.rocks/ and a set of dedicated python tools, to help with specifics of diamond anvil cell experiments and post-processing of the experimental results, all available at https://github.com/FABLE-3DXRD/TIMEleSS.

We also addressed several transformation and deformation processes relevant to the Earth mantle, such as the coesite-stishovite phase transition and its potential relation to the X-discontinuity at 300 km depth in the Earth mantle [2], deformation and phase transformation to wadsleyite, for the mantle transition zone [2], and transformation and deformation in a pyrolitic composition past the 660 km discontinuity [3]. With this work, we demonstrate that the method can be used to obtain relevant microstructural results at the pressures and temperatures of a mantle geotherm, and how they are useful for the interpretation of seismic observables.

In this presentation, we will present the main concepts and principles of multigrain X-ray diffraction in the laser-heated diamond anvil cell, how it can be used at the pressures and temperatures of a mantle geotherm, and results relevant for the Earth transition zone and lower mantle. We will also discuss how the technique offers a range of new opportunities for high pressure research, well beyond the field of geosciences.

[1] Krug, M., Saki, M., Ledoux, E., Gay, J.P., Chantel, J., Pakhomova, A., Husband, R., Rohrbach, A., Klemme, S., Thomas, C., Merkel, S. & Sanchez-Valle, C. (2022) *Geochem. Geophys. Geosyst*. **23** doi: 10.1029/2022gc010544
[2] Ledoux, E., Krug, M., Gay, J.P., Chantel, J., Hilairet, N., Bykov, M., Bykova, E., Aprilis, G., Svitlyk, V., Garbarino, G., Guignot, N. Sanchez-Valle, C., Speziale, S. & Merkel, S. (2023) *Amer. Mineral.* In revision.
[3] Gay, J.P., Ledoux, E., Krug, M., Chantel, J., Pakhomova, A., Liermann, H.-P., Sanchez-Valle C. & Merkel, S. (2023) *Earth Planet. Sci. Lett.* **604** 118015 doi: 10.1016/j.epsl.2023.118015

The study was financed by the bilateral ANR-DFG TIMEleSS project (ANR-17-CE31-0025; TH 1530/18-1; SA 2585/3-1; SP1216/8-1) and the bilateral PROCOPE-PPP program (PHC 40555PC; DAAD 57390184).

A030-03-280823

Multigrain crystallography at megabar pressures

Li Zhang

Center for High Pressure Science and Technology Advanced Research (HPSTAR), Shanghai 201203, China

zhangli@hpstar.ac.cn

Keywords: High pressure, Crystal structure, Multigrain, Diamond anvil cell

High pressures produce complicated crystal structures. Single-crystal x-ray diffraction is the idea method for structure determination and refinement. However, the conventional single-crystal methods cannot be applied to a large number of submicron-sized crystals in the studies of phase transitions and chemical reactions at high pressure. Using a multigrain method for high-pressure samples, we have overcome this problem by sorting out crystallographic orientations of individual crystals [1]. In one rotation dataset obtained at megabar pressures, up to one thousand individual grains can be indexed applying the FABLE package [2]. Each grain can be treated as a single crystal [3]. The opening cone of a diamond anvil cell limits the possibility of performing wide omega rotations. We have further overcome this limitation by merging several grains with different orientations into one dataset and obtained high quality crystallographic data for seifertite SiO_2 at 129 GPa [4]. This development provides new opportunities for identification and characterization of unknown phases at megabar pressure and beyond.

Silica is one of the most abundant components on Earth. The phase transitions and structural evolution of SiO_2 with increasing pressure and temperature have been extensively studied over the past several decades. However, not until recently was the alumina-rich NiAs-type silica identified applying the multigrain diffraction method in a H_2O-bearing oceanic crust component under deep lower mantle conditions [5]. The presence of H_2O changes the stability of silica phase that coexist with bridgmanite in oceanic crust component subducted to the deep lower mantle (**Fig. 1**). The stability and chemical composition of mineral phases have to be demonstrated in realistic multicomponent compositions representative of the Earth system.

Multigrain diffraction methods in combination with *ex situ* chemical analysis on samples recovered to ambient conditions have showed great advantages in characterization of unknown phases in a multiphase assemblage at multigrain pressures. The advancement of the analytical techniques further allows us to study the effects of H_2O on the phase assemblages [6]. Knowledge of the mineralogy and chemical composition of lower mantle multicomponent systems, dry or wet, can be used to place constraints on the geochemical and geophysical models of the deep Earth.

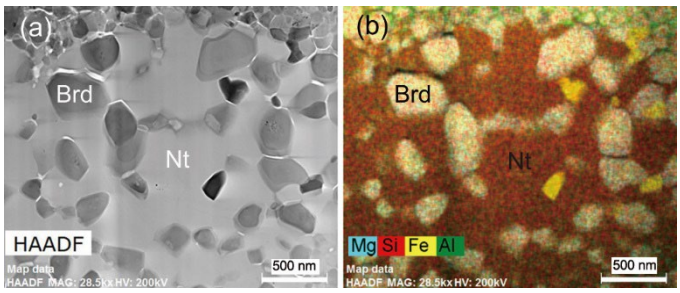

Figure 1. The presence of H_2O determines the stability of silica phase and affects the chemical composition of coexisting bridgmanite. Coexistence of bridgmanite (Brd) and NiAs-type silica (Nt) was observed in experimental simulations of water-rich subduction at conditions corresponding to about 2,000 km depth of the lower mantle [5].

[1] Zhang, L., Yuan, H., Meng, Y., Mao, H.-K. (2019). *Engineering* **5**, 441.
[2] Sørensen, H. O., Schmidt, S., Wright, J. P., Vaughan, G. B. M., Techert, S., Garman, E. F., Oddershede, J., Davaasambu, J., Paithankar, K. S., Gundlach, C. & Poulsen, H. F. (2012). *Z. Kristallogr.* **227**, 63.
[3] Zhang, L., Meng, Y., Dera, P., Yang, W., Mao, W. L., Mao, H. K. (2013). *Proc. Natl. Acad. Sci. U.S.A.* **110**, 6292.
[4] Zhang, L., Popov, D., Meng, Y., et al. (2016). *Am. Mineral.* **101**, 231.
[5] Liu, L. Yuan, H., Yao, Y., Yang, Z., Gorelli, F. A., Giordano, N., He, L., Ohtani, E., & Zhang, L. (2022). *Geophys. Res. Lett.* **49**, e2021GL097178.
[6] Zhang, L. (2022). *Nat. Geosci.* **15**, 964.

The author thanks Dmitry Popov, Yue Meng, Guoyin Shen, Junyue Wang, and Ho-kwang Mao for their helpful discussions and comments. This work was supported by the National Natural Science Foundation of China (42150103).

A030-04-280823

Single-crystal quality data from polycrystalline samples: finding the needle in the haystack

J. K. Cockcroft[1], N. Terzoudis and J. C. Bear[2]

[1]Department of Chemistry, University College London, 20 Gordon Street, London, WC1H 0AJ, United Kingdom; [2]School of Life Sciences, Pharmacy and Chemistry, Kingston University, Penrhyn Road, Kingston-upon-Thames, Surrey, KT1 2EE, United Kingdom

Email of communicating j.k.cockcroft@ucl.ac.uk

Keywords: Multigrain, Polycrystalline, Non-Covalent Interactions

In recent years [1-4], our laboratory has been investigating non-covalent interactions in co-crystals comprising liquid co-formers such as C_6F_6. This type of sample needs to be handled in X-ray capillaries due to the volatile nature of the components and cooled to the solid phase. While it is possible in theory to grow a single-crystal at low temperature in the capillary, it is experimentally demanding to get just one crystal. This led us to the hypothesis: can recent advances in laboratory single-crystal hardware and software be used to determine crystal structures from a polycrystalline sample in much the same way that crystal structures are determined from high-pressure data using a multigrain approach rather than a traditional single-crystal approach? The concept of a multigrain approach is not in itself novel, at least with regard to X-ray data collected at the synchrotron on polycrystalline samples. While the concept of processing and solving structures from data exhibiting twinning due to the presence of two or more crystals goes back decades, the development of "multigrain crystallography" at synchrotron sources, where there is the potential to study multiple crystals under pressure, has been more recent [*e.g.* 5-7].

In this presentation, we will discuss a number of systems studied using the multigrain approach in which we start with a liquid sample in an X-ray capillary, freeze it to the solid state, and determined the structure from what *initially* looks like very poor data (see Fig. 1).

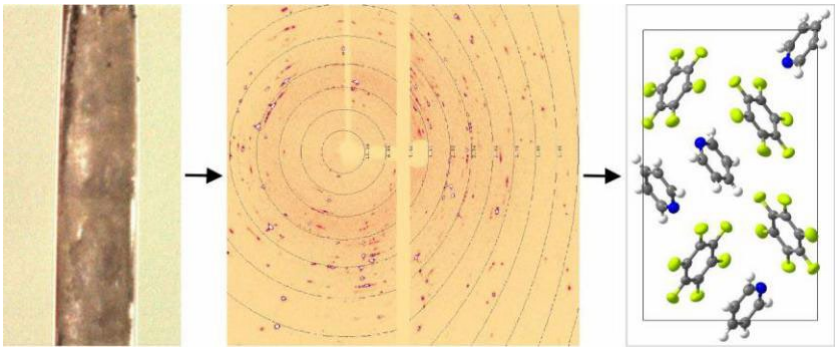

Figure 1. From polycrystalline sample in capillary to multigrain data to a reliable crystal structure.

The reliability of the structures is evident from the fact the geometry of the molecules is as expected. We have used this approach for the last few years and have noted what works and what does not work with modern laboratory hardware and software. One of the crucial steps is identifying the correct unit cell, which is a bit like looking for the "proverbial needle in a haystack" but not knowing the shape of the needle. The second issue is knowing how good the data has to be for the structures to be solved when solid-solid phase transitions occur, something that happens often in the systems we are studying. This presentation will address some of these issues. The methodology of our approach is currently the subject of a paper in preparation (and two further papers on non-covalent interactions in which our approach has been exploited) and may be of interest to those using high pressure.

[1] Cockcroft, J. K.; Ghosh, R. E.; Shephard, J. J.; Singh, A.; & Williams, J. H. (2017) *CrystEngComm* **19**, 1019–1023.
[2] Cockcroft, J. K.; Rosu-Finsen, A.; Fitch, A. N.; & Williams, J. H. (2018) *CrystEngComm* **20**, 6677–6682.
[3] Cockcroft, J. K.; Li, J. G. Y.; & Williams, J. H. (2019). *CrystEngComm*, **21**, 5578–5585.
[4] Bear, J. C., Cockcroft, J. K., & Williams, J. H. (2020) *J. Am. Chem. Soc*. **142**, 1731–1734.
[5] Lauridsen, E. M., Schmidt, S., Suter, R. M. & Poulsen, H. F. (2001). *J. Appl. Cryst.* **34**, 744–750.
[6] Vaughan, G. B. M., Schmidt, S. & Poulsen, H. F. (2004). *Z. Kristallogr*. **219**, 813–825.
[7] Sørensen, H. O., Schmidt, S., Wright, J. P., Vaughan, G. B. M., Techert, S., Garman, E. F., Oddershede, J., Davaasambu, J., Paithankar, K. S., Gundlach, C., & Poulsen, H. F. (2012). *Z. Kristallogr*. **227** 63–78.

A030-05-280823

Negative linear compressibility in Se under pressure

S. Yuan[1,2], L. Wang[2], F. Liu[1], D. Zhang[3], J. Bass[2] and H. Liu[1]*

[1] *Center for High Pressure Science and Technology Advanced Research, Haidian, Beijing 100094, China*
[2] *Department of Geology, University of Illinois at Urbana-Champaign, Urbana, IL 61801, USA*
[3] *Center for Advanced Radiations Sources, University of Chicago, Chicago, IL 60439, USA.*

haozhe.liu@hpstar.ac.cn

Keywords: Pressure-induced phase transition, Negative linear compressibility, Bulk moduli.

Selenium is one of the most classic element materials with rich phase transitions under high pressure. In this work, a series of *in situ* synchrotron X-ray diffraction (XRD) measurements was carried out on Se under pressure, with pressure increased from ambient to 210 GPa, negative linear compressibility (NLC) behavior was first observed from 5.6 GPa to 9.0 GPa with chain structure of Se-I phase, then at pressures between 120 and 148 GPa with *β*-Po structure of Se-V' phase, the latter of which makes Se the NLC material discovered at the highest pressure so far[1]. The schematic of geometrical and atomic interpretation is shown in fig. 1.

Earlier studies by McCann [2] and Keller[3] reported that the NLC behavior along the Se *c*-axis occurred immediately from ambient pressure to about 10 GPa. However, in this work, by using Rietveld fitting method on the XRD data, it was discovered that the NLC behavior along the *c*-axis only existed from 5.1 GPa to 9.0 GPa, before 5.1 GPa there was a continuous compression along both *c*-axis and *a*-axis. The NLC behavior from 5.1 GPa to 9.0 GPa is attributed to the difference in bonding strengths between interchain and intrachain in the trigonal Se.

With pressure increased to 120 GPa, the NLC behavior along the *a*-axis in *β*-Po structure of Se-V' phase was discovered. The appearance of NLC behavior makes the bulk modulus of Se from 120 to 148 GPa the highest (321 ± 2 GPa) compared to the bulk modulus at pressures lower than 120 GPa (83±2 GPa) or higher than 148 GPa (266±7 GPa). The discovery of NLC material in a higher pressure range is always more significant in terms of fundamental mechanism and new materials understanding, yet it has barely been reported at pressures above 100 GPa. The current discovery of NLC in Se will hopefully inspire future studies on other potential NLC materials at ultra-high pressure.

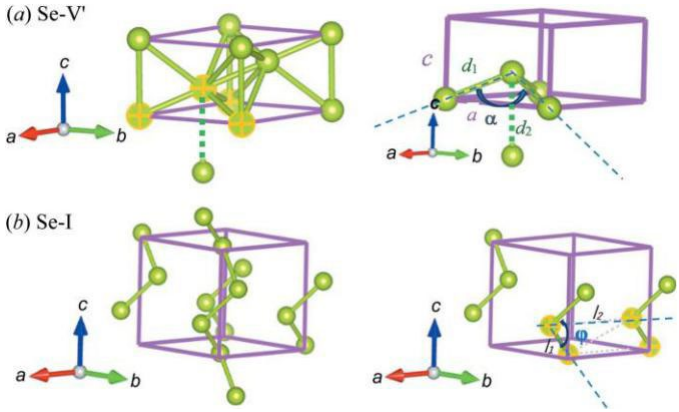

Figure 1. Schematic of the geometrical interpretation of NLC in the structures of (a) Se-V' and (b) Se-I[4].

[1] Cairns, A. B. & Goodwin, A. L. Negative linear compressibility. *Phys. Chem. Chem. Phys.* **17**, 20449–20465 (2015).

[2] McCann, D. R. & Cartz, L. Bond distances and chain angle of hexagonal selenium at high pressure. *Journal of Applied Physics* **43**, 4473–4477 (1972).

[3] Keller, R., Holzapfel, W. B. & Schulz, H. Effect of pressure on the atom positions in Se and Te. *Phys. Rev. B* **16**, 4404–441277).

[4] Yuan, S. *et al.* Negative linear compressibility in Se at ultra-high pressure above 120 GPa. *IUCrJ* **9**, 253–260 (2022).

A030-06-280823

Using synchrotron multigrain X-ray diffraction techniques to determine iron-alloy phase relations at Earth and planetary core conditions.

Claire C. Zurkowski[1], B. Lavina[2.3], E. O'Bannon III[1], S. Chariton[2], V. B. Prakapenka[2], A. J. Campbell[4], Y. Fei[5], Zs. Jenei[1]

[1]Lawrence Livermore National Laboratory 7000 East Ave, Livermore, CA 94550, [2]Center for Advanced Radiation Sources, The University of Chicago, Chicago, IL 60439, USA, [3]Advanced Photon Source, Argonne National Laboratory, Argonne, IL 60439, USA, [4]University of Chicago, Department of the Geophysical Sciences, 5734 S Ellis Ave, Chicago, IL 60637, USA, [5] Earth and Planets Laboratory, Carnegie Institution for Science, 5241 Broad Branch Rd. NW Washington DC 20015

Keywords: multigrain diffraction, iron alloys, diamond anvil cell, laser heating, planetary cores, high pressure

Earth and terrestrial planets are composed of dense iron-alloy cores surrounded by silicate mantles. The composition and crystallization properties of a planet's metallic core influences key characteristics related to its habitability: including, its thermal evolution and the formation of a geodynamo. Experimental explorations into the phase relationships and crystallization sequences of core-like Fe- (Si, Si, O, C, H) compositions at extreme pressures and temperatures provide the only *in-situ* window into the mysterious depths of a planetary core. In this work we utilized synchrotron multigrain X-ray diffraction techniques in the laser-heated diamond-anvil cell to constrain the crystallization thermodynamics of iron-alloys to multi-megabar pressures and high temperatures. We identified and resolved several new stoichiometries and complex structures that will require a reevaluation of planetary core mineralogy. Results from this experimental work will be implemented to update the multi-component core-crystallization regimes for Earth's iron-rich core and Mars' sulfur-rich core.

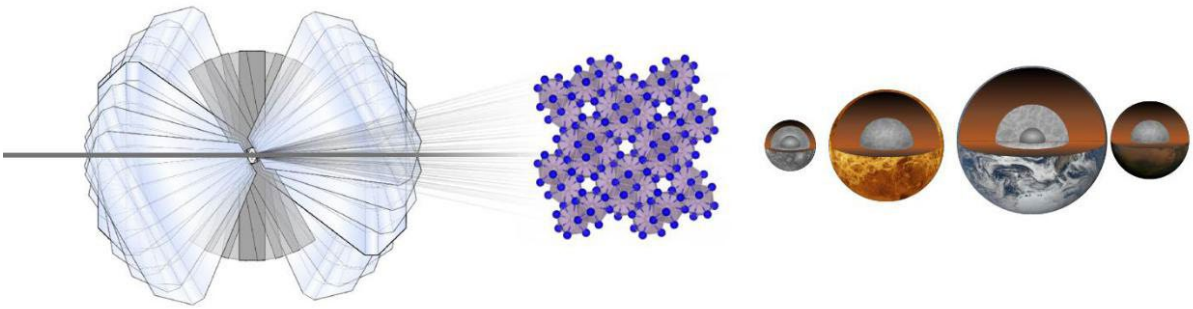

This work was performed under the auspices of the U.S. Department of Energy by Lawrence 957 Livermore National Laboratory under Contract DE-AC52-07NA2.

A051 Applied Mineralogy and Sustainability
Room 216
1.10pm - 3.30pm

A051-01-280823

Evaluation of surrogate-models for the incorporation of tetravalent actinides in monazite- and zircon-type phases for long-term disposal

Lender[1], N. Huittinen[2], K. Kvashnina[2], E. Bazarkina[2], L. Braga Ferreira dos Santos[2], P. Appel[3], L. Peters[1]

[1]*Institute of Crystallography, Rheinisch–Westfälische Technische Hochschule Aachen University, Jägerstr. 17–19, 52066 Aachen,*
[2]*Institute of Resource Ecology, Helmholtz–Zentrum Dresden–Rossendorf, Bautzner Landstr. 400, 01328 Dresden,*
[3]*Institute of Geosciences, Christian-Albrechts-University Kiel, Ludewig-Meyn-Straße 10, 24118 Kiel*

lender@ifk.rwth-aachen.de

Keywords: actinides, radioactive waste, long-term storage

The idea of immobilizing radionuclides in crystalline host materials was put forward 70 years ago [1]. Since then, continuous research has been conducted on a wide variety of crystalline materials that are considered as possible host matrices. However, many challenges remain, owing, *e. g.*, to the complex chemistry of nuclear waste streams and the exceptionally high requirements regarding physical and chemical long-term stability.

Monazite (*Ln*PO4, *Ln* = La-Gd) has long been considered as one of the most promising crystalline host materials for long-term storage of radionuclides, especially actinides. The main reasons for this are its chemical flexibility, its excellent aqueous durability and its low recrystallization temperature, which allows for rapid self-healing of radiation induced damages [2, 3]. It has been shown that monazites can accommodate large amounts of trivalent actinides within its crystal structure [3]. However, the incorporation of tetravalent dopants *via* coupled substitution with divalent cations has proven challenging [4, 5], even though natural monazite is known to contain significant amounts of Th and U (combined up to 27 wt-%) [6]. The incorporation of tetravalent cations into the zircon-type structure (ZrSiO4) was found to be less challenging, probably due to the tetravalent oxidation state of zirconium. A zircon-type structure called Xenotime is also formed by *Ln*PO4 with *Ln* = Tb-Lu. Similar to monazite, this phase exhibits high resistance against leaching, its radiation tolerance, however, is reported to be much lower [7].

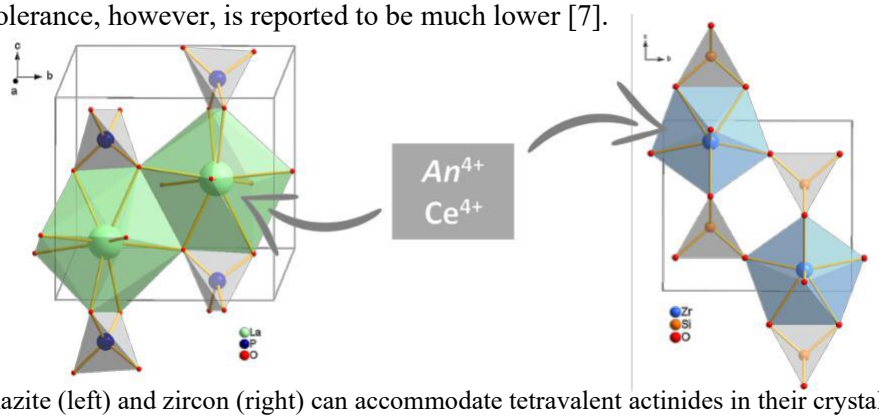

Figure 1. Monazite (left) and zircon (right) can accommodate tetravalent actinides in their crystal structures.

To facilitate assessments with respect to selection criteria such as chemical flexibility, radiation resistance and aqueous durability, efforts are made to identify inactive surrogate-models. The use of cerium as a surrogate for tetravalent actinides will be discussed for monazite- and zircon-type phases based on the solid solutions La1-*x*(Ca,Ce)*x*PO4 and Zr1-*x*Ce*x*SiO4. These were extensively studied using powder and single crystal XRD, electron imaging techniques including EPMA, SEM and TEM, spectroscopic measurements including Raman, TRLFS, EXAFS and in-situ XAS experiments.

1. Hatch, L. (1953). *Am. Sci.* **41**, 410-421.
2. Schlenz, H., Heuser, J., Neumann, A., Schmitz, S., Bosbach, D. (2013). *Z. Kristallogr.* **228**, 113-123.
3. Dacheux, N., Clavier, N., Podor, R. (2013). *Am. Mineral.* **98**, 833-847.
4. Popa, K., Bregiroux, D., Konings, R. J. M., Gouder, T., Popa, A. F., Geisler, T., Raison, P. E. (2007). *J. Solid State Chem.* **180**, 2346-2355.
5. Bregiroux, D., Terra, O., Audubert, F., Dacheux, N., Serin, V., Podor, R., Bernache-Assollant, D. (2007) *Inorg. Chem.* **46**, 10372-10382.
6. Ewing, R. C., Wang, L. (2002) *Rev. Mineral. Geochem*. **48**, 673-699.
7. Lumpkin, G. R. (2006) *Elements* **2** 365-372.

A051-02-280823

Investigation of CO_2 adsorption on a selection of zeolites by combining in-situ high-resolution powder X-ray diffraction, isotherm modeling, and simulation

L. Bénariac-Doumal[1], C. Dejoie[1], L. McCusker[2], C. Baerlocher[2], J-L. Paillaud[3], T. Ors[3], D. Xie[4], A. Fitch[1]

[1]European Synchrotron Radiation Facility, 71 avenue des Martyrs, Grenoble (France),[2]Dept. Materials, ETH Zurich, 8093 Zurich (Switzerland), [3]Université de Haute Alsace, IS2M, 15 rue Jean Starcky, Mulhouse (France), [4]Mater.Innov., 2031 Tamalpais Ave, El Cerrito, 94530, California, (USA)

loic.benariac-doumal@esrf.fr

Keywords: Zeolite, Powder diffraction, CO_2

The adsorption of carbon dioxide (CO_2) by porous materials such as zeolites is of great importance to address current environmental issues, and many zeolites have been used as CO_2 capture agents [1]. Combustion gases, important contributors to the greenhouse effect, are generally composed of a mixture of gases (N_2, CO_2, H_2O, CH_4 …), leading to competition for the most favorable adsorption sites and consequently a decrease in the zeolite's selectivity toward CO_2 adsorption. Determination of the preferred sorption sites for each gas of the mixture is then necessary to gain insights into the host-guest and guest-guest interactions that govern the adsorption capacity of the adsorbent. We propose an approach where high-resolution powder X-ray diffraction, isotherm modeling, and simulations are combined to determine the preferred sorption sites for pure CO_2 and CO_2 in a mixture to unravel the adsorption process of CO_2 in a set of different zeolites.

Selected zeolites were chosen according to their affinity towards each of the constituents of the gas mixtures. We were especially interested in the silica-alumina ratio, to influence the hydrophobicity of the material, and also in the pore size to favor certain types of gas molecules, in order to increase the adsorption capacity towards CO_2. Monte-Carlo sorption simulations were conducted on each of the promising zeolites, in the presence of CO_2 alone and CO_2 in a gas mixture. Si-STT zeolite is an interesting hydrophobic zeolite because it possesses a high adsorption capacity (2.8 $mmol.g^{-1}$ at 1bar) and an advantageous selectivity towards CO_2 in the presence of other gases such as CH_4 (Fig. 1A).

The evolution of the crystallographic structure of each zeolite with applied CO_2 pressure, from 0 to 25 bar, was monitored *in situ* using high-resolution powder X-ray diffraction (ID22, ESRF). The specific positions of the CO_2 molecules were extracted through Rietveld refinement and experimental adsorption isotherms have been retrieved. Furthermore, local information, specific to each adsorption site, was also obtained from parametric Rietveld refinement [2], where structural evolution and adsorption modeling are intrinsically part of the crystallographic model. Using this approach on CO_2@Si-STT, we showed that, over the four sites where CO_2 molecules locate in the Si-STT zeolite (Fig. 1B), the most-favored site (mol4), at the center of the 9 member-ring, follows a Langmuir adsorption model, with the homogeneous adsorption of isolated molecules (Fig. 1C). On the other hand, the less-favored sites (mol2), display a Toth adsorption behavior, under the influence of molecule-molecule interactions.

These experimental results, combined with Monte Carlo simulations, provide a deeper comprehension of the CO_2 adsorption mechanisms, and allow these zeolites to be probed through the host-guest and guest-guest interaction specific to each of them.

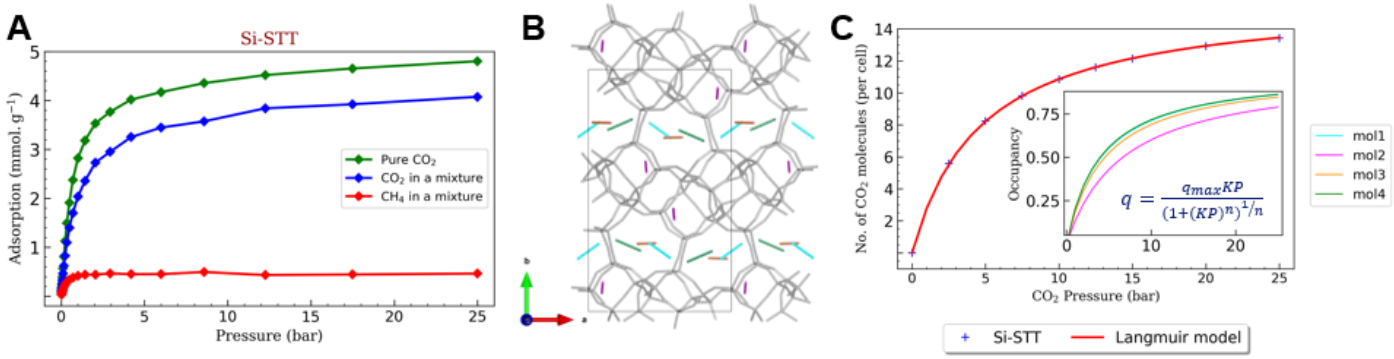

Figure 1. A - Simulated adsorption isotherm of pure CO_2 and a binary mixture of CO_2/CH_4 for Si-STT at 298K. B – Crystallographic model for CO_2@STT at 25 bar. C- Global adsorption isotherm of CO_2 and site-specific isotherms extracted from parametric Rietveld refinement of Si-STT

[1] Fu, D., Davis, M. (2022). ***Chem. Soc. Rev.*, 51**, 9340-9370.
[2] Lill, J., Dejoie, C., Giacobbe, C., Fitch, A.N. (2022). *J. Phys. Chem. C*, **126**, 2214-2225.

A051-03-280823

Mineralogical-crystallographic approach enabling new paths towards a sustainable use of resources

S.C Tarantino[1]

[1]*Department of Chemistry, University of Pavia, viale Taramelli 12, 27100 Pavia, Italy*

Email of communicating author: serenachiara.tarantino@unipv.it

Keywords: Resources, Sustainability, Crystal-chemistry

Awareness of the finite nature of many resources, including the issue of scarcity of many elements, has grown enormously in recent decades. It has become painfully obvious that the linear path of production, in which scarce resources are consumed and their value-added products are degraded to waste, is the cause of many impending global crises such as climate change, declining biodiversity, food and water, and energy shortages.

The international community has begun to explore possible pathways for the transition to a circular economy, which involves closing material cycles as far as possible, reducing the need for raw materials and waste disposal.
The way to a more sustainable future is through the efficient use of resources (energy, water, land, minerals), optimised waste management and value creation. Increasing the use of secondary and renewable resources will probably be the key to achieving a sustainable use of materials.

This talk addresses some examples of transforming biosolids and inorganic sludge into secondary raw materials. A sound mineralogical and crystal-chemical knowledge and the mineralogical-crystallographic methods are key to designing and developing processes for material recovery and recycle, while reducing environmental impact through sustainable practice.

Examples of development of novel materials based on alkali activation of mineral sludge will be illustrated. Alkali activation offers the opportunity not only to divert such aluminosilicates from landfills, but also to reduce reliance on conventional building materials [1,2], which may exhibit large environmental footprints [3]. Finally, a novel approach to tackle the environmental problem linked to sewage sludge will be shown (LIFE19 ENV/IT/000165, https://life-freedom-project.eu/). This approach, based on the hydrothermal process, converts sewage sludge into secondary raw materials, which in turn can be used to manufacture structural ceramics that meet the challenges of sustainability and environmental responsibility.

[1] Clausi, M., Fernandez-Jimenez, A., Palomo, A., Tarantino, S.C., Zema, M. (2018). *Constr. Build. Mater*. **172**, 212-223.
[2] Occhipinti, R., Fernandez-Jimenez, A., Palomo, A., Tarantino, S.C., Zema, M. (2021). *Constr. Build. Mater*. **301**, 124030.
[3] Shi, C., Qu, B., Provis, J.L. (2019) *Cem. Concr. Res*. **122**, 227-250.

A051-04-280823

Investigation of oxidation progress and structural change in hydrous iron phosphates, vivianite and santabarbaraite, by Li-intercalation

R. Yamane, H. Li, T. Ichitsubo, K. Sugiyama

Institute for Materials Research, Tohoku University, Sendai 980-8577, Japan.

ryo.yamane.c2@tohoku.ac.jp

Keywords: Li-intercalation, vivianite, santabarbaraite, oxidation, dehydration, hydrous iron-phosphate

Vivianite is a hydrous iron (II)-phosphate mineral with a chemical composition, $Fe^{2+}{}_3(PO_4)_2 \cdot 8H_2O$. Fe^{2+} in the vivianite structure can be partially oxidized by the deprotonation of water molecules; $Fe^{2+} + H_2O \rightarrow Fe^{3+} + OH^-$ [1]. This oxidation further progresses in heating and parent vivianite turns into a disordered phase of santabarbaraite at around 120 ℃ [1, 2]. Although the structure of santabarbaraite has not yet been elucidated, the overall structural characteristics of santabarbaraite are similar to the crystal structure of vivianite (Fig. 1 (a), [3]). Additionally, the structure of santabarbaraite would have porous nature compared to vivianite, since santabarbaraite is a low-temperature dehydration product [3]. We investigated lithium intercalation ($Fe^{3+} + e^- + Li^+ \rightarrow Fe^{2+}Li^+$) into santabarbaraite, focusing on its oxidation state of Fe and structure.

Santabarbaraite was prepared by heating synthesized vivianite in the air at 120 °C for 2 hours [4]. Li-intercalation into the synthesized vivianite was also investigated to compare the performance of iron phosphates (partially oxidized vivianite and santabarbaraite) as cathode active materials. For the Li-intercalation test, an ordinary two-electrode cell was employed: the active material applied on an Al foil (30 μm) was a mixture of iron phosphate, carbon black, and polyvinylidene fluoride in the ratio of 8:1:1 by weight. The composite electrode was used as the working electrode, the Li metal plate as the pseudo-reference and counter electrode, and a commercial electrolyte solution of 1M $LiPF_6$ in a solution of ethylene carbonate and dimethyl carbonate (1:1 by volume). The electrochemical reaction involved a constant-current-constant-voltage discharge and charge process (cut-off voltage was set to 2.0 V for discharge and 4.0 V for charge).

The results of electrochemical reaction are shown in Fig. 1 (b). Blue and red curves correspond to the results for the synthesized vivianite and santabarbaraite, respectively. The total amount of intercalated Li in the santabarbaraite-electrode was two times larger than that of the vivianite-electrode (in a cathodic capacity, santabarbaraite: 156 $mAhg^{-1}$ and vivianite: 70.9 $mAhg^{-1}$). This is because the total amount of $Fe^{3+}$of santabarbaraite is larger than that of vivianite. Additionally, in the constant-current discharge process, the vivianite-electrode reached the cut-off voltage of 2.0 V immediately compared to the santabarbaraite-electrode. This result is due to a significantly low reaction rate of Li-intercalation in vivianite; the reaction rate is dominated by two factors, electron conductivity and Li^+ diffusivity. The electron conductivity of vivianite is larger than that of santabarbaraite, since santabarbaraite includes structural disorder [4]. On the other hand, santabarbaraite would have more space for Li diffusivity, since the number of water molecules decreases in santabarbaraite due to the dehydration. The higher reaction rate of santabarbaraite was owing to the Li diffusivity. Therefore, santabarbaraite is a suitable active material compared to vivianite in terms of the capacity and reaction rate. In our presentation, structural change of the iron phosphates induced by the Li-intercalation will be also discussed based on powder X-ray diffraction measurements.

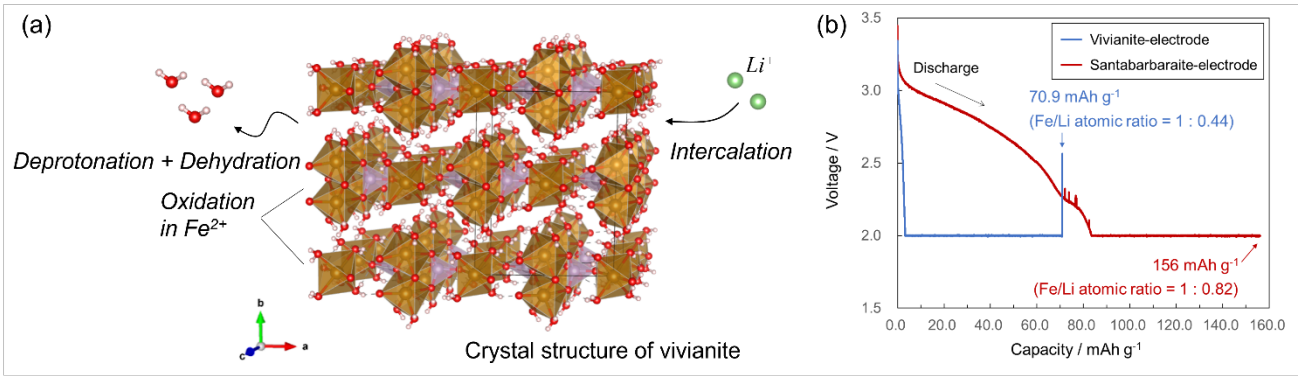

Figure 1. (a) Schematic drawing of Li-intercalation in vivianite (santabarbaraite) (b) Discharge/charge curves of as synthesized vivianite and 120 ℃ heated santabarbaraite.

[1] Pratesi, G., Cipriani, C., Giuli, G. & Birch, W. D. (2003). *Eur. J. Mineral.*, **15**, 185.

[2] Brindusoiu, S., Poienar, M., Marin, C. N., Sfirloaga, P., Vlazan, P. & Malaescu, I. (2019). *J. Mater. Sci. Mater. Electron*., **30**, 15693.
[3] Yamane, R., Kawamata, T., Sugiyama, K. & Oshima, E. (2022). *The 2022 Annual Meeting of Japan Association of Mineralogical Sciences*., R2-08.
[4] Chiba, K., Takahashi, M., Ohshima, E., Kawamata, T. & Sugiyama, K. (2020). *J. Mineral. Petrol. Sci*., **115**, 485.

This research was supported by JSPS KAKENHI Grant Numbers JP18H05456, JP20H00189, and JP22K14750.

A051-05-280823

Structural characterization of pink $CaMg_{0.5}Co_xNi_{0.5-x}SiO_4$ ($0 \leq x \leq 0.5$) solid solutions: towards more sustainable pigments

A. Tena[1], Mohammed S. M. Abdelbaky[2,3], Camino Trobajo[3], José R. García[3], Santiago García-Granda[3]

[1]University of Jaume I - Castellon de la Plana (Spain), [2]University of Salamanca -Salamanca (Spain), [3]University of Oviedo - CINN, Oviedo (Spain)

s.garciagranda@cinn.es

Keywords: Diopside, solid solutions, pigments, sustainable

Diopside finds technological applications in production of ceramic pigments [1]. The colour of materials with diopside structure is due to the presence of metal transition ions in their compositions. Ca(CoxMg1–x)Si2O6 compositions are potential pink-violet pigments [2, 3]. These compositions are used in ceramic industry and synthesized from natural raw minerals to obtained inexpensive materials.

Structural information of CaMg1-xCoxSi2O6 solid solutions indicates than mean M1-O (M1 = Mg, Co) distances are very short, between 2.0807 Å (in CaMgSi2O6) and 2.1013Å (in CaCoSi2O6) [3]. In CaCo1-*x*Ni*x*Si2O6 solid solutions mean M1-O (M1 = Co, Ni) distances ranged between 2.082 Å (in CaCoSi2O6) and 2.031 Å (in CaNiSi2O6) [4]. All of these values are shorter than 2.12 Å, the limit value that explains the yellow, pink or red colour of compound containing octahedral Co(II) ions [5].

In this study, CaMg0.5CoxNi0.5-xSi2O6 solid solutions with diopside structure, Fig. 1, were prepared via the chemical co-precipitation method to minimise the toxic and expensive amounts of cobalt and nickel respect to Ni2SiO4 and Co2SiO4 used in the ceramic industry. The aim of the study was to obtain the structural characterization of these fired materials, to monitor the evolution of their color with composition and temperature and to compare them with the color obtained from MgCoxNi1-xSiO4 ($0.0 \leq x \leq 1.0$) solid solutions with olivine structure [5]. These solid solutions can be used as ceramic dyes when they are dissolved in glazes and the colour in enamelled samples is depending on x. Intense green and blue colorations are developed when these pigments are dissolved in the commercial glaze.

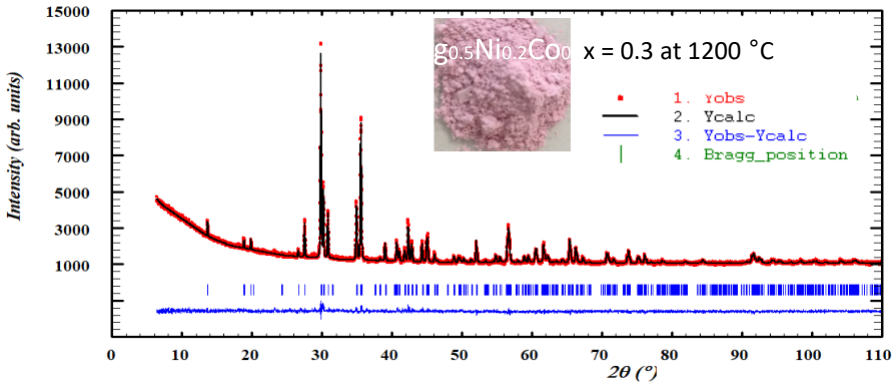

Figure 1. The diffraction profile refinement of $CaMg_{0.5}Co_{0.3}Ni_{0.2}Si_2O_6$ composition with Diopside structure.

1. Pogrebenkov, V.M., Sedel'nikova M.B. and Vereshchagin V.I. (1998). Glass and Ceramics, **55**, 5.
2. Gori C., Tribaudino M., Mantovani L., Gatta G. D., Delmonte D., Gilioli E., Mezzadri F. and Calestani G. (2017). Mineralogical Magazine. **81**, 1129.
3. Gori C., Tribaudino M., Mezzadri F., Skogby H., Hålenius U. (2018) Physics and Chemistry of Minerals. **45**, 443.
4. Durand G., Vilminot S., Rabu P., Derory A., Lambour J.P. and Ressouche E. (1996). Journal of Solid State Chemistry. **124**, 374.
5. Tena M.A., Mendoza R., Trobajo C., García J.R., García-Granda S. (2022). 33rd European Crystallographic Meeting (ECM33) Versailles, France, MS15-01.

We gratefully acknowledge the financial support provided by Spain´s Agencia Estatal de Investigación, Ministerio de Ciencia e Innovación, PID2020-113558RB-C41, Principality of Asturias IDI/2021/50997 and CrysFact Network Red2018-10102574-T (AEI/MCI).

A051-06-280823

Carbonation reactions and performance of cements, minerals, and sustainable materials

A.J. Allen[1], R.P. Murphy[2] , H.E. King[2], S.Z. Jones[3]

[1]NIST Material Measurement Lab. (MML), [2]NIST Center for Neutron Research (NCNR), [3]NIST Engineering Lab. (EL), National Institute of Standards and Technology (NIST), 100 Bureau Drive, Gaithersburg, MD 20899, USA

andrew.allen@nist.gov

Keywords: cement, carbonation, carbon capture

Carbon dioxide reduction (CDR) in the atmosphere, including CO2 direct air capture (DAC), is an increasingly critical international priority. All material processes that can either reduce net carbon emissions or result in the permanent sequestration of CO2 are being considered. For example, the use of efficient additive manufacturing techniques for concrete placement incorporating Portland-limestone-cement (PLC) blends in order to reduce the amount of ordinary Portland cement (OPC) manufacture (reducing associated CO2 emissions) is of interest [1,2]. So is the progressive carbonation of hydrated cement to convert calcium hydroxide (CH) back into CaCO3 (CC), and many other sequestration routes for CO2 are being explored, such as its mineralization in olivine and other ultramafic rocks. We are using a combination of X-ray diffraction (XRD) and small-angle X-ray and neutron scattering (SAXS and SANS), and even imaging, to study both the incorporation of CO2 into cements (OPC and PLCs) and minerals through carbonation reactions, and the microstructural evolution of PLC blends during hydration to determine their suitability for additive manufacturing in the construction industry. In this connection, it is recognized that CDR must be achieved not only with overall net CO2 reduction, but also with acceptable product performance when new processing is involved. We also recognize reliable determination of CO2 sequestration in carbonation and mineralization reactions to need density functional theory (DFT) and other computer simulations already employed for CO2 sorbents [3,4], including in DAC.

In the figure we show the effects of carbonation on cement hydration by comparing cement microstructures (via SAXS) and their XRD patterns after 28 days hydration under either N2 or CO2 atmospheres. SAXS indicates the formation of CC particles at low q for both OPC and PLC in CO2, compared to the N2 case, at the cost of some loss of fine structure at high q. XRD (shown only for OPC for clarity) indicates less CH and more CC for hydration in CO2.

We will review our results and present conclusions both for our findings on carbonation and for the effects on processing.

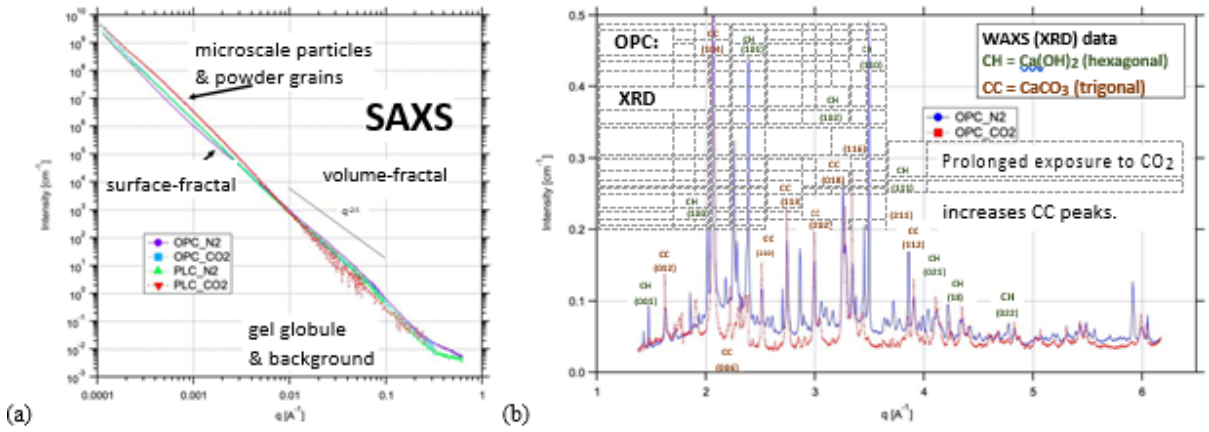

Figure 1. (a) SAXS data versus q, (b) XRD data versus q for non-carbonated (N2) and carbonated (CO2) cements.

[1] Jones, S.Z., Hipp, J.B., Allen, A.J., Gagnon, C.V. (2022). *Cem. Concr. Res.*, **152**, art. no. 106651.
[2] Allen, A.J., Jones, S.Z., Gagnon, C.V. & Hipp, J.B. (2023). *J. Mater. Res.*, submitted.
[3] Allen, A.J., Wong-Ng, W., Cockayne, E., Culp, J.T. & Matranga, C. (2019). *Nanomaterials*, **9**, art. no. 354.
[4] Allen, A.J., Cockayne, E., Wong-Ng, W., Culp, J.T. & Kuzmenko, I. (2023). *J. Appl. Cryst.*, **56**, in press.

Part of this work utilized neutron scattering facilities supported in part by the National Science Foundation under Agreement No. DMR-0944772. Part of this work used resources of the Advanced Photon Source, a U.S. Department of Energy (DOE) Office of Science User Facility operated for the DOE Office of Science by Argonne National Laboratory under Contract No. DE-AC02-06CH11357.

A058 New Phenomena and Applications in Molecular Magnets
Room 217
1.10pm - 3.30pm

A058-01-280823

The impact of non-covalent interactions on magnetic anisotropy

Sofie S. Leiszner[1], Mauro Perfetti[2], Emil Damgaard Møller[1], Jacob Overgaard[1] and Bo B. Iversen[1]

Department of Chemistry, Aarhus University, Langelandsgade 140, 8000 Aarhus C, Denmark.[2] Department of Chemistry "Ugo Schiff", University of Florence, Via della Lastruccia 3, 50019, Sesto Fiorentino (FI), Italy

Email of communicating: bo@chem.au.dk

Keywords: Single Molecule Magnets, Magnetic Anisotropy, non-covalent interactions

Since the discovery of the first Single Molecule Magnet (SMM), a Mn12 cluster that exhibited magnetic hysteresis from a purely molecular origin for temperatures below 4 K [1], a lot of effort has been put towards synthesizing new compounds with improved SMM properties, as the bistability of SMMs makes them ideal for data storage applications. One of the key properties of SMMs is magnetic anisotropy, i.e., the directional dependence of the magnetic response in an external magnetic field. Thus, getting a better understanding of the relationship between structure and magnetic anisotropy is a crucial step towards improving the performance of SMMs.

In this study, the magnetic anisotropy of an axially-compressed octahedral Co(II) complex, CoCl2(S=C(NH2)2)4 (**1**), is examined. In a previous study of **1** [2], the site susceptibility method [3] using Polarized Neutron Diffraction (PND) data was applied, which showed that the direction which was the easiest to magnetize, referred to as *the easy axis*, was not oriented directly along the Co-Cl bond, but tilted by around 31˚ with respect to the Co-Cl bond. To validate this result, we have performed Cantilever Torque Magnetometry (CTM) on a single crystal of **1**, and preliminary fitting of these data yields an easy axis with roughly the same orientation (see Fig. 1a). As seen from Fig. 1a, the easy axes are directed towards H(1B), which is in fact the H-atom closest to Cl in the crystal structure. Moreover, we developed a multipole model of the electron density of **1** which shows bond critical points between Cl and six hydrogen atoms in the crystal structure: two of which are intramolecular and four which are intermolecular interactions.

To evaluate the impact of the non-covalent intramolecular Cl-H interactions on the magnetic anisotropy of **1**, ten computer modifications of its structure has been made by rotating the thiourea ligands around their respective C=S bonds. On all these structures, including the non-modified structure of **1**, a CASSCF-NEVPT2 calculation has been carried out. These calculations reveal that increasing the Cl-H distance, leads to a smaller angle between the easy axis and the Co-Cl bond along with an increased energy barrier for magnetic relaxation, ultimately leading to improved SMM properties. These results show the significant impact of non -covalent interactions on the magnetic anisotropy of **1** and suggests that substituting the thiourea ligands for a more rigid soft-donor ligand like thiophene or ethylene thiourea or a polydentate sulphur-based ligand might greatly improve the SMM properties of such a compound.

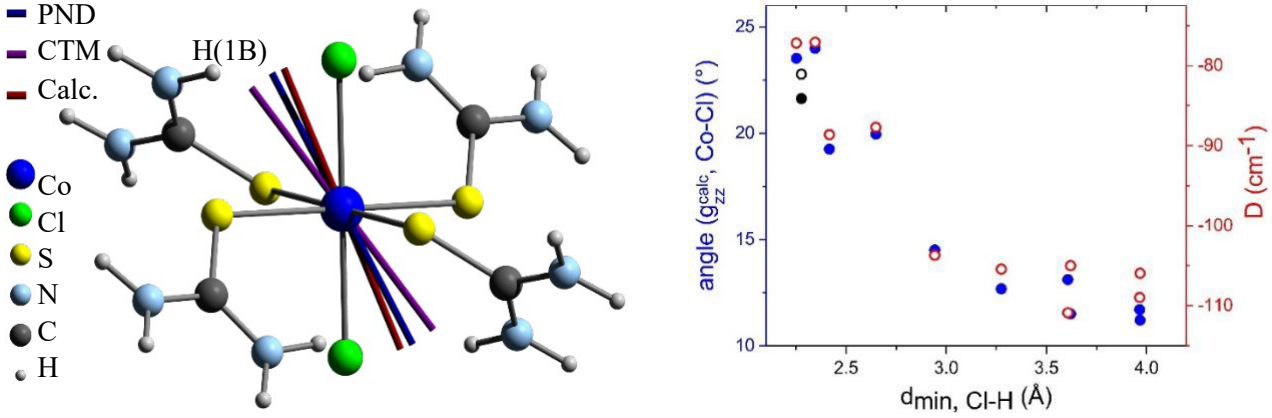

Figure 1. a) The structure of **1** from PND showing the orientation of the easy axis (cylinders) determined by the three different methods. b) The angle between the easy axis and the Co-Cl bond (blue filled circles) and the D-value (red open circles) as a function of the minimum Cl-H distance in the permutated structures of **1**. The calculated values for the non-permutated structure of **1** are given in black. All values in the plot are based on CASSCF-NEVPT2-calculations.

1. R. Sessoli, D. Gatteschi, A. Caneschi, M. A. Novak, *Nature* **1993**, *365*, 141-143.
2. S. Tripathi, S. Vaidya, N. Ahmed, E. Andreasen Klahn, H. Cao, L. Spillecke, C. Koo, S. Spachmann, R. Klingeler, G. Rajaraman, J. Overgaard, M. Shanmugam, *Cell Reports Physical Science* **2021**, *2*, 100404.
3. A. Gukasov, P. Brown, *Journal of Physics: Condensed Matter* **2002**, *14*, 8831.

A058-02-280823

Neutron scattering experiments with high magnetic fields in organic magnets

Javier Campo[1], Yuko Hosokoshi[2]

[1]Aragón Nanoscience and Materials Institute (CSIC-University of Zaragoza) and Physics Condensed Matter department of the University of Zaragoza, [2]Graduate School of Science, Osaka Metropolitan University, Sakai, Japan

Email: javier.campo@csic.es

Keywords: organic magnets, neutron scattering, magnetic fields

Purely organic magnets with -electron spins have essentially negligibly small spin-orbit couplings and are attractive materials because they are archetypical Heisenberg spin systems in which the quantum fluctuations play an important role. The spin size and the connectivity of the network is the key factor of the novel magnetic states arising from quantum fluctuations. Among the representative stable organic radical skeleton, nitroxide radical (-N-O·) has the advantage of making antiferromagnetic spin networks. The positive and negative partial charges on the N and O atoms, respectively, easily gives the intermolecular contact between the NO groups on which the singly occupied molecular orbital (SOMO), that is the molecular orbital with the unpaired electrons, is distributed. The intermolecular overlap between SOMO's always yields the antiferromagnetic interactions [1,2]. The stacking of planar -conjugated molecules gives one-dimensional (1D) network. When two or more NO groups are substituted on a molecule, double spin chain with different spin size is formed [2,3]. After the extensive study on the 1D Heisenberg antiferromagnet, there is growing attention to the effect of the quantum fluctuations in two- or three-dimensional (2D or 3D) Heisenberg antiferromagnets, but the experimental realization is still rare.

Considering the nitroxide radical as magnetic entity we were able to growth and macroscopically study several compounds with different dimensionalities with different magnetic behaviours (frustrated spin ladder, 3D honeycomb with AF LRO [4] or 3D Kagomé layers, etc…). In this presentation several examples will be shown in order to highlight the crucial role of the neutron scattering experiments to understand the basic physics of these interesting materials.

Many times, in organic magnets the first step to understand the magnetic behavior is the study of the overlapping between the magnetic molecular orbitals which is directly related with the experimental spin density determination, and this is often done by using polarized neutrons with applied magnetic fields, what will be also presented.

[1] Y. Hosokoshi, Y. Nakazawa, K. Inoue, K. Takizawa, H. Nakano, M. Takahashi, and T.Goto, Phys. Rev. B, 60, 12924 (1999).
[2] K. Katoh, Y. Hosokoshi, K. Inoue, and T. Goto, J. Phys. Soc. Jpn., 69, 1008 (2000).
[3] Y. Hosokoshi, K. Katoh, Y. Nakazawa, H. Nakano, and K. Inoue, J. Am. Chem. Soc., 123, 7921 (2001).
[4] Naoki Amaya, Toshio Ono, Yuta Oku, Hironori Yamaguchi, Akira Matsuo, Koichi Kindo, Hiroyuki Nojiri, Fernando Palacio, Javier Campo, and Yuko Hosokoshi, Journal of the Physical Society of Japan 86, 074706 (2017)
[5] J. Luzon, J. Campo, F. Palacio, G. J. McIntyre, J. M. Rawson, R. J. Less, C. M. Pask, A. Alberola, R. D. Farley, D. M. Murphy, and A. E. Goeta. Phys. Rev. B 81, 144429 (2010)

A058-03-280823

Multi-technique study of the magnetic anisotropy in two Co(II) based molecular magnets

Hannah H. Nielsen,[a] Sofie S. Leiszner,[a] Andreas M. Thiel,[a] Helene Lassen,[a] Stuart Calder,[b] Jacob Overgaard,[a] Bo B. Iversen[a]

[a]*Department of Chemistry, Aarhus University, Langelandsgade 140, DK-8000Aarhus C, Denmark*
[b]*Neutron Scattering Division, Oak Ridge National Laboratory, Oak Ridge, Tennessee37831, United States*

hannah@chem.au.dk

Keywords: Single molecule magnets, electron density, powder polarized neutron diffraction

Single molecule magnets (SMMs) are molecules that possess magnetic anisotropy and show slow relaxation of their magnetiza-tion. The magnetic anisotropy gives SMMs an energy barrier for reversal of the magnetization and therefore possible candidates as qubits in a quantum computer or as bits in high-density data storage. The size of the energy barrier depends on the spin-orbit coupling (SOC) for 3d-metal molecular magnets, thus, enlargement of this is a primary goal in developing stabile molecules. The size of the SOC in a metal atom can be predicted qualitatively based on the coordination geometry of the atom by looking at the d-orbital splitting. If the coordination geometry gives a d-splitting where the first excited state is dominated by only one transition, and if the two orbitals wherein the electron is excited between are close in energy, it gives a large energy barrier for the molecular magnet. The direction of the magnetic anisotropy can be obtained from theoretical calculations and investigated experimentally using polarized neutron diffraction. From the site-susceptibility method [1] the susceptibility tensor for the metal atom can be derived. This technique provides a unique knowledge on the magnetic anisotropy of a SMM.

In this study, two five- coordinated Co(II) complexes are investigated, [CoX2Cltpy] (X = Cl (**1**), Br (**2**). Cltpy = 4'-chloro-2,2':6',2"-terpyridine). Both **1** and **2** show distorted square-pyramidal geometry, and from *ab initio* calculations both complexes have negative D-values, -78.87 cm^{-1} and -60.61 cm^{-1} respectively, meaning that they have easy-axis magnetic anisotropy and the direction of the easy-axis is expected to be along the Co -X(1) bond (see Figure 1a). From the theoretical calculations the direction of the magnetic easy-axis is found to almost coincide to the Co-X(2) bond for both complexes, and this deviation from the expectations is further investigated in this study.

Multipole models [2] of the experimental charge density of the two molecules is achieved based on data from single crystal X-ray diffraction, obtained from SPring-8 in Japan. From these models, the d-orbital population of the central Co(II) ion in the compounds are determined, together with information on the electron density in the bonds around the Co atom. The experimental d-orbital population does indeed predict easy -axis magnetic anisotropy for both complexes. From the deformation density the interaction between the Co atom and the two Cl/Br atoms is investigated. Figure 1b shows the deformation density in the Co-Cl(1)-Cl(2) plane, and it is clear, that the interaction between these atoms is different, which could be a part of the explanation for the unexpected direction of the magnetic anisotropy. In a previous study,[3] it is shown that powder polarized neutron diffraction (pPND) is sufficient to study the magnetic anisotropy of a complex, and pPND data was measured at Oak Ridge National Laboratory, to study the susceptibility tensor of **1**. The results show that the experimental and theoretical direction of the magnetic anisotropy almost coincide. The experimental susceptibility tensor is shown in Figure 1c and shows that the magnetic anisotropy within **1** indeed can be described as easy-axis.

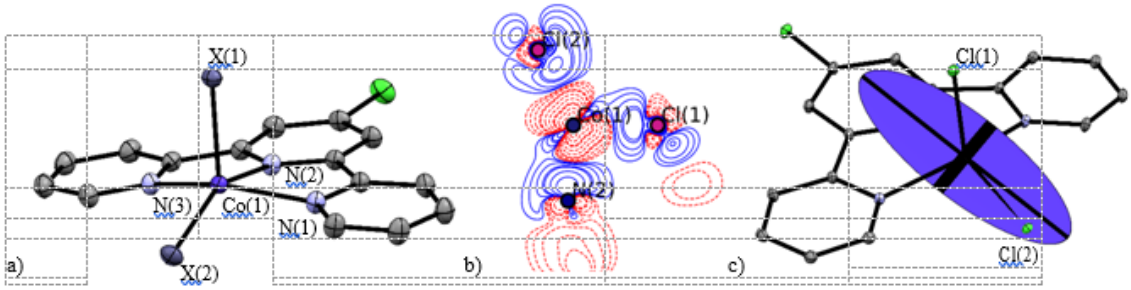

Figure 1. a) Structure of **1** and **2** (90% probability ellipsoids). X = Cl, Br. Co-X(1) and Co-X(2) bonds vary with X. b) Deformation density of **1** in the Co-Cl(1)-Cl(2) plane. c) Experimental susceptibility tensor of **1**.

1. Gukasov, A.; Brown, P., (2002). *Journal of Physics: Condensed Matter* **14**, 8831.
2. P. Coppens, (1997) *X-ray charge densities and chemical bonding*, International Union of Crystallography; England Oxford.
3. Gupta, S. K., Nielsen, H. H., Thiel, A. M., *et al.*, (2023) *JACS Au*

A058-04-280823

Quantum criticality and anomalous magnetization in a purely organic spin ladder

Miguel Pardo-Sainz[1,2], Toshio Ono[2], Ismael F. Diaz-Ortega[3], Takumi Kihara[3], Hiroyuki Nojiri[3], Yohei Kono[4], Toshiro Sakakibara[4], Hironori Yamaguchi[2], Yuko Hosokoshi[2] and Javier Campo[1,*]

1 Instituto de Nanociencia y Materiales de Aragón (INMA), CSIC - Universidad de Zaragoza, Zaragoza, Aragon (Spain), 2 Osaka Metropolitan University, 1-1, Gakuen-cho, Naka-ku, Sakai, Osaka (Japan), 3 Institute for Materials Research, Tohoku University, Sendai, Miyagi (Japan), 4 Institute for Solid State Physics, University of Tokyo, 5-1-5 Kashiwanoha, Kashiwa, Chiba (Japan).

javier.campo@csic.es

Keywords: Spin-ladder, quantum, organic magnetism

The study of quantum spin systems has attracted much attention for several decades [1]. Recently spin-ladder systems, which are in the crossover region between one and two dimensions, have been at the focus of intensive research towards its understanding, since peculiar phenomena, such as the superconductivity in a hole doped S=1/2 two-leg spin ladder, are expected to appear [2, 3]. One limitation to the study of these systems is that this spin gap is usually too large to be accessible by the experiments, and only in the case of organometallic or purely organic magnets can be small enough so as to allow a full investigation of the spectrum by applying a magnetic field [1]. However, only very few of such compounds have been synthesized which can be described by the S=1/2 two-leg Heisenberg antiferromagnetic ladder (THAFL) model.

Here we present the compound 4-F-2-NNBIP [= 4-fluoro-2-(1-oxyl-3-oxide-4,4,5,5-tetramethylimidazolin-2-yl) biphenyl], whose magnetic behaviour comes from a spin 1/2 delocalized between the N and O atoms of the nitronyl nitroxide (NN) group. Both powder and single crystal samples have been characterized by means of X-ray diffraction, electron paramagnetic resonance (EPR), specific heat, magnetization and susceptibility measurements at high magnetic fields and very low temperatures. Quantum Monte Carlo (QMC) calculations have also been performed in order to obtain the relevant magnetic parameters of the systems.

The analysis of the crystal structure and the EPR measurements shows that this system can be well described by a THAFL model. A fit to the susceptibility data using QMC calculations allows to estimate the exchange interactions to be J_L/k_B= 2.7(3) K and J_R/k_B= 7.4(1) K, therefore probing this spin ladder to be in the strong coupling limit $\gamma=J_R/J_L$=2.7(4) > 1. The field and temperature dependence of the specific heat is also in agreement with this model, and we can determine the transition to the gapless Luttinger liquid (LL) phase, identified by a linear behaviour at very low temperature. However, the magnetization data are not well fitted using the coupling parameters obtained from magnetic susceptibility, and a change of slope not characteristic of these systems is also observed at intermediate fields (Fig. 1 (a)). From all these data we propose a magnetic phase diagram (Fig. 1 (b)) in which 3 distinct magnetic phases are present: a quantum disordered (QD) or spin liquid phase, a gapless phase, (LL) or quantum critical (QC) paramagnet, and a fully spin polarized (SP) phase. The anomaly observed in the magnetization is signalled by the region in the phase diagram with question marks (??) and some possible explanations for its origin are discussed.

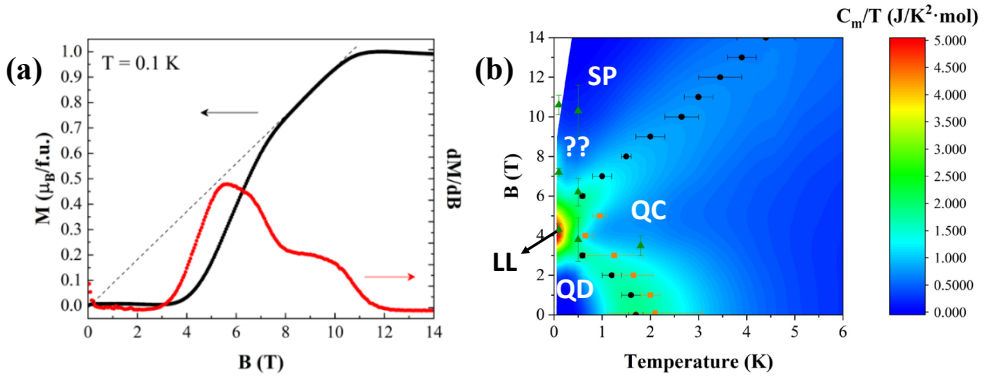

Figure 1. (a) Magnetization curve (black dots) and its field derivative (red dots) of 4-F-2-NNBIP at 0.1 K. The dashed line denotes the change of slope of the data at B_{an} =7.2(2) T. (b) Field-temperature phase diagram of the spin-ladder compound 4-F-2-NNBIP. The contour plot shows the magnetic specific heat as C_m/T. Local maxima are indicated by black circles. Orange squares denote the maximum of dχ/dT, while green triangles mark the critical fields obtained from the magnetization data.

[1] Silva, R. A. L., & Almeida, M. (2021). *Journal of Materials Chemistry C* **9**, 10573.
[2] Dagotto, E. & Rice, T. M. (1996). *Science* **271**, 618.
[3] Sachdev, S. (2017). *Quantum Phase Transitions*. Cambridge: Cambridge University Press.

A058-05-280823

Magnetoelastic coupling and relaxation in lanthanoid single molecule magnets

R.A. Mole

Australian Nuclear Science and Technology Orgainsation, New Illawarra Road, Lucas Heights, NSW, 2234, Australia

richard.mole@ansto.gov.au

Keywords: Inelastic Neutron Scattering, Single ion magnet

Inelastic Neutron Scattering (INS) has been used for many years to probe the magnetic excitations and determine the energy levels of single molecule and single ion magnets.[1] These materials have been shown to have potential uses as qubits for quantum computation or ultra-high density data storage. The functional properties of single ion magnets are inherently dependent on the structure of the complex, however they have also been shown to be dependent on both the localised vibrations[2] and the magnitude of applied magnetic fields.[3] Recently we have demonstrated that inelastic neutron scattering can be used to extract useful information about single ion magnets beyond the simple observation of energy level splitting. In this contribution I will demonstrate that our inelastic neutron scattering data can be used to extract vibrational properties, information about magneto elastic coupling, and determine the behaviour in applied magnetic fields. This experimental information has allowed us to determine the vibrational relaxation method for a model qubit and thus propose possible design strategies for improved functional single ion magnets.

[1] Dunstan, M.A., Mole, R.A., Boskovic, C. (2019). *Eur. J. Inorg. Chem.* 1090.
[2] Goodwin, C.A.P., Ortu, F. Reta, D., Chilton, N.F., Mills, D.P., (2017). *Nature*, **548**, 439.
[3] M. Siddique, Komijani, D., Duan, Y, Gaita-Arinao, A., Coronado, E., Hill, S. (2016) *Nature*. **531**, 348

A058-06-280823

Designing of organic quantum magnets and quantum phenomena in magnetic fields

Y. Hosokoshi

Department of Physics, Graduate School of Science, Osaka Metropolitan University Sakai, Osaka 599-8531

yhoso@omu.ac.jp

Keywords: Quantum spin system, Organic Radicals, Spin density, π-conjugation

Quantum spin system is attractive because quantum fluctuation induces various exotic quantum phenomena. Organic radical system is a good candidate to study quantum phenomena on various spin lattices. The ideally isotropic nature of π-electron spin enables us to observe quantum effect even on the ferromagnetic system [1] and three-dimensional system [2]. Our strategy to tune magnetic interactions to realize various magnetic lattices and the observation of quantum phenomena will be presented.
The spin density of an organic radical is widely distributed on the whole molecule through π-conjugation [3]. When two radical substituents are connected by a π-conjugated linker, the sign of the intramolecular magnetic interaction is well understood by spin polarization [4]. The magnitude of the intramolecular interaction depends on the π-conjugation and tuneable by the dihedral angle between π-conjugated linker and radical units. We have studied the family of nitronyl nitroxide biradicals with tuning the molecular planarity and demonstrated the linear relation between the magnetic interactions and twisted angles. Moreover, the change of the sign of the magnetic interaction in the extreme case of the orthogonality is observed.

We have noticed that biphenyl as an expanded π-conjugation, is useful to tune molecular packing. The π-π stacking between the neighbouring molecules is usually seen in the crystals. In the biradical system, intermolecular interactions occur not only by a direct contact between radical sites but also through the contact between biphenyl groups. As a results, neighbouring two biradical molecules forms a 4-spin cluster model of $S = 1/2$, which sometimes shows frustrated spin structure by the nearest and the next nearest neighbour interactions. The magnetic lattices of ferromagnetic dimer of $S = 1/2$ has been studied. Double-spin chain and two-dimensional lattices with frustration have been realized. In magnetic field, anomalous behaviour was observed near saturation. Such a behaviour has been sometimes reported in the frustrated system with ferromagnetic and antiferromagnetic interactions [5], which is related to spin nematic states.

Biradical system with extremely large ferromagnetic intramolecular interaction, forms $S = 1$ system. A good $S = 1$ species among organic systems is realized by the use of a biradical unit of metaphenylenebis(*N*-*t*-butylnitroxide) [3, 4]. BIP-TENO is the first realization of an $S = 1$ ladder and nontrivial 1/4-magnetization plateau has been observed. Small lattice distortion has been observed depending on the temperature and pressure [6]. Recently, lattice distortion in pulsed high-magnetic field was firstly observed. The origin of the multi-step magnetization curve will be discussed.

[1] (a) Uemoto, N., Kono, Y., Kittaka, S., Sakakibara, T., Yajima, T., Iwasaki, Y., Miyamoto, S., Hosokoshi, Y., & Yamaguchi, H. (2019). *Phys. Rev. B*, **99**, 094418. (b) Kono, Y., Kittaka, S., Yamaguchi, H., Hosokoshi, Y., & Sakakibara, T. (2019). *Phys. Rev. B*, **100**, 054442.
[2] Amaya, N., Ono, T., Oku, Y., Yamaguchi, H., Matsuo, A., Kindo, K., Nojiri, H., Palacio, F., Campo, J., & Hosokoshi, Y. (2017). *J. Phys. Soc. Jpn*., **86**, 074706.
[3] Zheludev, A., Garlea, V. O., Nishihara, S., Hosokoshi, Y., Cousson, A., Gukasov, A., & Inoue, K. (2007). *Phys. Rev. B*, **75**, 104427.
[4] Hosokoshi,Y., Katoh, K., Nakazawa, Y., Nakano, H., & Inoue, K., (2001). *J. Am. Chem. Soc.*, **123**, 7921-7922.
[5] Yamaguchi, H., Okubo, T., Kittaka, S., Sakakibara, T., Araki, K., Iwase, K., Amaya, N., Ono, T., & Hosokoshi, Y. (2015). *Scientific Reports*, **5**, 15327.
[6] (a) Katoh, K., Hosokoshi, Y., Inoue, K, & Goto, T. (2000). *J. Phys. Soc. Jpn.*, **69**, 1008. (b) Goto, T., Bartashevich, M. I., Hosokoshi, Y., Katoh, K., & Inoue, K., (2001). *Physica B*, **294**, 43-46. (c) Hosokoshi, Y., Konishi, Y., Nishihara, S., & Inoue, K. (2007). *J. Mag. Mag. Mater.*, **310**, e420. (d) Nomura, K., Matsuda, Y. H., Ikeda, A., Kohama, Y., Tsuda, H., Amaya, N., Ono, T., & Hosokoshi, Y. (2022). *Phys. Rev. B*, **105**, 214430.

A107 Design and application of porous materials
Room 210/211
1.10pm - 3.30pm

A107-01-280823

A "crystalline sponge" method for metal complexes

C. J. Sumby

Department of Chemistry and Centre for Advanced Nanomaterials, School of Physics, Chemistry and Earth Sciences, The University of Adelaide, Adelaide, Australia

christopher.sumby@adelaide.edu.au

Keywords: Crystalline sponge, metal-organic framework,

The crystalline sponge method is a powerful approach to studying the structures of guest molecules trapped within a porous crystalline framework material.[1] Metal-organic frameworks (MOFs), with a set of features that allow single crystal-to-single crystal transformations and possessing a metal coordinating domain (Figure 1), can be used to structurally characterise mono- and dinuclear metal complexes.[2] This can allow the identification of novel or strained coordination environments,[3] the characterisation of unusual or reactive species,[3,4] and even provide insight into metal centred reactivity that occurs in chemical transformations or catalysis.[5]

This presentation will provide an overview of this chemistry, particularly focussing on the methodology and the approach to providing structural insights into mono- and dinuclear metal complexes “site isolated” in a MOF matrix.

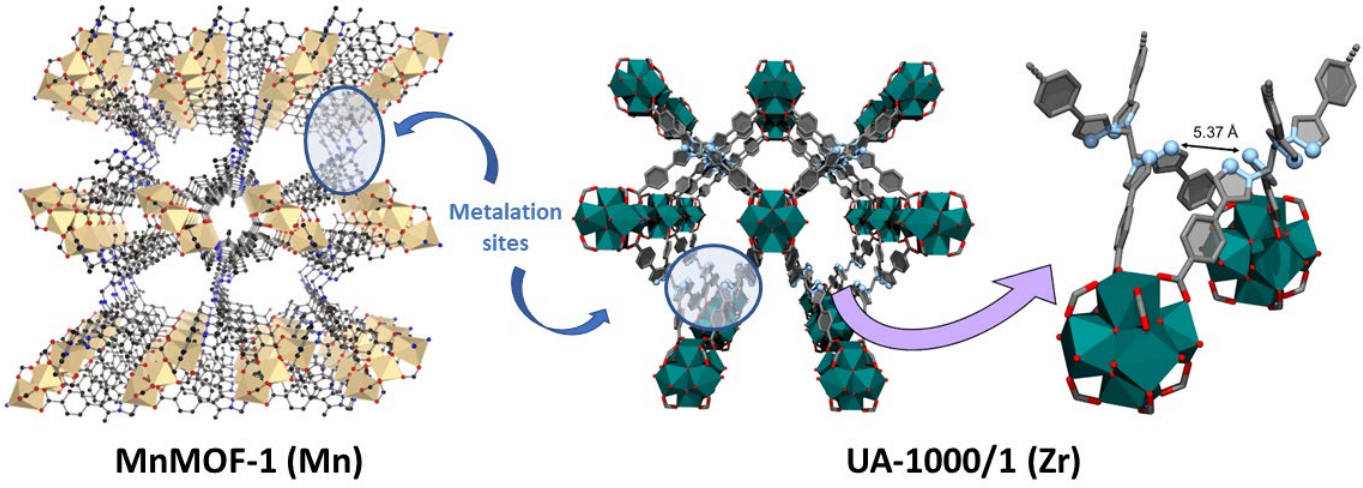

Figure 1. Examples of MOFs that act as crystalline sponges for metal complexes.

[1] Y. Inokuma, S. Yoshioka, J. Ariyoshi, T. Arai, Y. Hitora, K. Takada, S. Matsunaga, K. Rissanen and M. Fujita, *Nature*, 2013, **495**, 461–466.
[2] a) R. J. Young, M. T. Huxley, E. Pardo, N. R. Champness, C. J. Sumby and C. J. Doonan, *Chem. Sci.*, 2020, **11**, 4031–4050. b) J. Albalad, C. J. Sumby, D. Maspoch and C. J. Doonan, *CrystEngComm,* 2021, **23**, 2185-2195.
[3] a) W. M. Bloch, A. Burgun, C. J. Coghlan, R. Lee, M. L. Coote, C. J. Doonan and C. J. Sumby, *Nat. Chem.*, 2014, **6**, 906–912. b) P. Gimeno-Fonquernie, J. Albalad, J. Price, C. J. Doonan, and C. J. Sumby, *unpublished results*, 2022.
[4] Rosemary J. Young, Michael T. Huxley, Lingqiao Wu, Jack Hart, James O'Shea, Michael W. George, Christian J. Doonan, Neil R. Champness and Christopher J. Sumby, *unpublished results*, 2022.
[5] a) A. Burgun, C. J. Coghlan, D. M. Huang, W. Chen, S. Horike, S. Kitagawa, J. F. Alvino, G. F. Metha, C. J. Sumby and C. J. Doonan, *Angew. Chem. Int. Ed.*, 2017, **56**, 8412-8416. b) R. A. Peralta, M. T. Huxley, J. D. Evans, H. Cao, M. He, X. S. Zhao, S. Agnoli, C. J. Sumby and C. J. Doonan, *J. Am. Chem. Soc.*, 2020, **142**, 13533-13543.

A107-02-280823

Robust Neodymium-POM and their composites for efficient electrocatalytic water splitting

Amanpreet Kaur

Chemistry Department, Indian Institute of Technology Delhi, New Delhi-110016, India

amanpreetkaurjassal@gmail.com

Keywords: Polyoxometalate, electrocatalysis, recyclability, agglomerate

Polyoxometalates (POMs) are known as atomically distinct metal-oxide clusters, which exhibited structural versatility due to the presence of oxygen-rich surfaces [1]. Predominantly, the unsaturated coordinating sites in lacunary POMs are perfectly suitable for eternal active metal-atom coordination with restricted leaching and loss of active metal centers [2]. Moreover, POMs offer multifunctionality owing to their attractive properties, including multi-electron redox capability for electrocatalysis, Lewis acidity/basicity, compositional adjustability and structural diversity [3]. The robust all-inorganic ligand system of POMs can encapsulate and protect active water oxidation catalysts (WOCs). The widespread electrochemical activity of POMs may also be exploited if their framework got retained in any reaction media, leads to excellent recyclability due to the presence of active metal sites. Because of insolubility of POMs, they got anticipated to verify the usefulness in efficient electrocatalysis. The solid-state electrochemistry of POMs can be approved out by entrapping them in a carbon paste electrode (CPE), which is a widely used matrix for hybrid electrode materials. The permanent porosity and high specific surface area of POMs may provide advantages towards hydrogen evolution reactions (HER) and oxygen reduction reaction (ORR) [4]. However, POM clusters are usually endowed with low electrical conductivity and tend to easily agglomerate, which would bound the charge transfer in electrocatalytic process and thus, increase the barrier of activation energy. To resolve these issues, efficient and stable nanostructured, oxygen-evolving anode materials can be designed by the assembly of oxygen-evolving POM clusters (e.g., totally inorganic neodymium catalyst) with different conducting materials (e.g., activated carbon, multiwalled carbon nanotubes or Mxenes etc) [5].

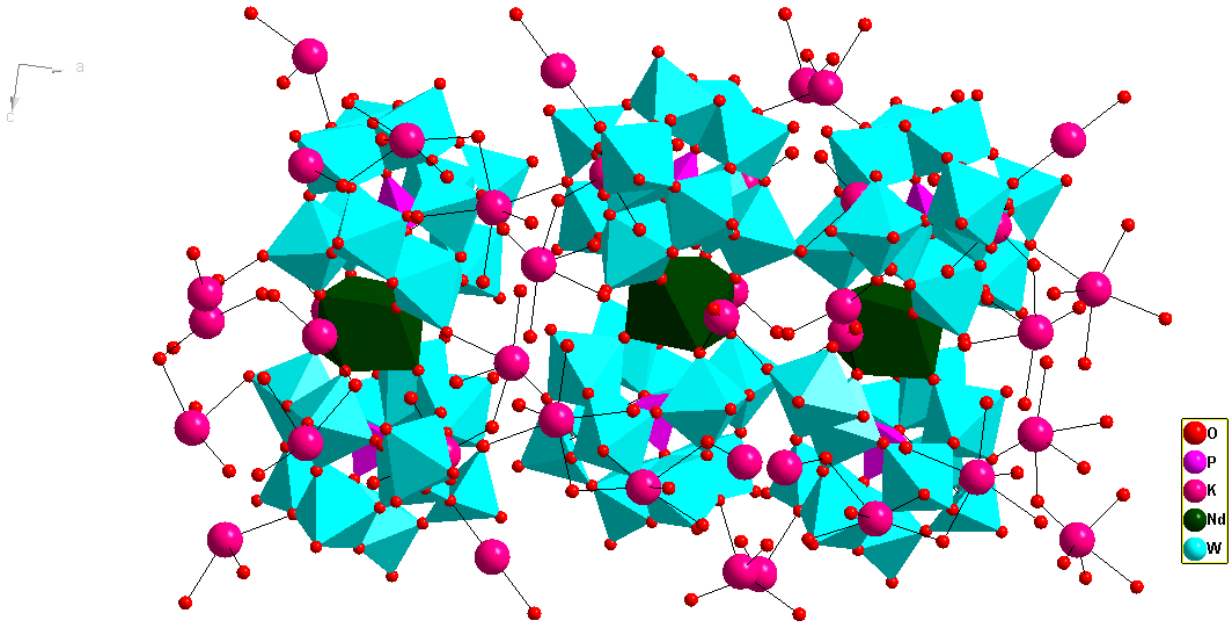

Figure 1. Coordination environment around Nd-POM structure

[1] Lai, R. D., Zhang, J., Li, X. X., Zheng, S. T., Zheng, S. T. (2022) *J. Am Chem. Soc*. **144**, 19603.
[2] Gao, J., Yan, J., Beeg, S., Long, D. L., Cronin, L. (2013) *J. Am Chem. Soc*. **135**, 1796.
[3] Blasco-Ahicart, M., Soriano-López, J., Carbó, J. J., Poblet, J. M., Galan-Mascaros, J. R. (2018) *Nat. Chem.* **10**, 24.
[4] Abdelkader-Fernández, V. K., Fernandes, D. M., Balula, S. S., Cunha-Silva, L., Freire, C. (2020) *ACS Appl. Energy Mater.* 3, 2925.
[5] Lim, K. R. G., Shekhirev, M., Wyatt, B. C., Anasori, B., Gogotsi, Y., Seh, Z. W., (2022) *Nature Synthesis* **1**, 601.

A107-03-280823

Multivariate analysis to understand structure-function relationships in metal-organic frameworks

Zhihengyu Chen, Simon M. Vornholt, Karena W. Chapman'

Department of Chemistry, Stony Brook University

Karena.Chapman@stonybrook.edu

Keywords: Metal-organic framework, *in situ*, pair distribution function analysis

The ordered nature of metal-organic frameworks (MOFs) facilitates crystallographic analysis of their structure and the understanding of their structure-property relationships needed to design function. Increasingly, researchers are recognizing the potential for MOFs to deviate from the ordered structures seen crystallographically. Static and dynamic disordering of the structure, that occurs without disrupting the framework topology and connectivity, underlies important phenomena from catalysis to negative thermal expansion. Intriguingly, widely different properties may be seen for variants of a MOF with a common set of nodes, ligands, connectivity, and topology, but with unrecognized differences in the local structure.

The challenge in recognizing the critical role of local structure variability in MOFs on their function arises because the single-crystal diffraction tools most routinely applied to determine their long-range connectivity and topology cannot resolve critical local structures. Tools such as pair distribution function (PDF) analysis, which can resolve the static and/or dynamic local distortions that can be accommodated by the flexible MOF structures, are need.

This presentation will explore the local- and long-range structure of MOFs related to NU-1000 and UiO-66 using *in situ* synchrotron X -ray scattering, combining both pair distribution function (PDF) and powder diffraction analysis. Through application of multivariate data analysis tools, including non-negative matrix factorization (NMF) and Pearson correlation analysis, to resolve the complex coupling of local structure, long range structure, and functional properties.

This research used resources of the Advanced Photon Source, a U.S. Department of Energy (DOE) Office of Science User Facility operated for the DOE Office of Science by Argonne National Laboratory under contract no. DE-AC02-06CH11357.

A107-04-280823

Hyperfast Rotors, Light-driven Motors and Fast Scintillators in Metal-Organic Frameworks

A. Comotti, S. Bracco, J. Perego, C. X. Bezuidenhout, S. Piva, A. Daolio, P. Sozzani

Department of Materials Science, University of Milano Bicocca, Milan, Italy

Email: angiolina.comotti@unimib.it

Keywords: Metal-Organic Frameworks, motors and rotors, photo-luminescence

Rotors, motors and switches in the solid state find a favorable playground in porous materials, especially in porous frameworks, thanks to their large free volume, which allows for fast dynamics. We have realized a fast molecular rotor in a Zn-MOF whose rotation speed approaches that of unhindered rotations in organic moieties even at 2 K.[1,2] *The three-fold bipyramidal symmetry of the rotator conflicting with the four-fold symmetry of the strut frustrates the formation of stable conformations and allows for the hyperfast rotation of the rotator persistent for several continuous turns, with an energy barrier of 6.2 calmol^{-1} and a high frequency of 10^{10} Hz at 2K (Fig. 1A).* Geared molecular rotors with negligible energy-requirements in MOFs enabled fast yet controllable and correlated rotary motion.[3] The rotors inserted in a MOF exhibited fast motion (10 ^{7} Hz), even at extremely cold temperatures and explored multiple configurations of conrotary/disrotary relationships, switched on and off by thermal energy. Chemical stimuli such as CO2 diffused through the open pores changed dramatically the rotation mechanism and rotor speed.

Furthermore, motors were inserted into porous frameworks and metal-organic frameworks wherein two distinct linkers with complementary light absorption -emission properties were integrated into the same material. Unidirectional motion was achieved by exposure to sunlight of the solid particles, which behave as autonomous nanodevices.[4] Visible light-driven rotation of a molecular switch was proved to be in the solid state at rates similar to those observed in solution.[5] We demonstrated that fluorescent metal–organic framework (MOF) nanocrystals can work as fast scintillators.[6] The MOF comprises high-*Z* linking nodes that interact with the ionizing radiation and are arranged in an orderly fashion at a nanometric distance from 9,10-diphenylanthracene ligand emitters. Their incorporation in the framework enables fast sensitization of the ligand fluorescence, showing an ultrafast scintillation rise time of ~50 ps. Moreover, *two ligands of equal molecular length and connectivity, yet complementary electronic properties, were co-assembled by zirconium oxy-hydroxy clusters, generating crystalline hetero-ligand MOF nanocrystals (Fig. 1B,1C) which result in high efficiency luminescence with significant Stokes shift and benchmark performances.*[7]

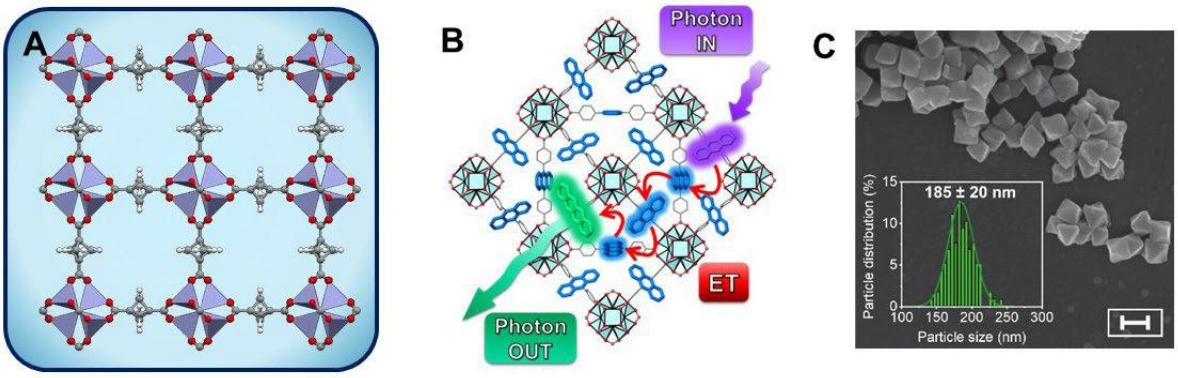

Figure 1. A) Zn-FTR MOF containing ultrafast molecular rotors as ligands. Hetero-ligand zirconium-based metal-organic framework containing antracene- and tetracene-based ligands: crystal structure (B) and SEM images of the nanocrystals (C).

[1] Comotti, A., Sozzani, P. et al (2020) *Nature Chem.* **12**, 845.
[2] Prando, G. et al (2020) *Nanoletters* **20**, 7613.
[3] Comotti, A., Sozzani, P. et al (2021) *J.Am.Chem.Soc*. **143**, 13082.
[4] Comotti, A., Feringa, B. et al (2020) *Nature Chem*. **12**, 595.
[5] Feringa, A., Comotti, A. et al (2020) *J. Am. Chem. Soc*. **142**, 9048.
[6] Comotti, A. et al (2021) *Nature Photonics* **15**, 393.
[7] Comotti, A. et al (2022) *Nature Communications* **13**, 3504.

A107-05-280823

Functional materials design through closed-loop synthesis and characterisation

Thomas Fellowes, Amy Lunt, Louis Longley, Caitlin Shields, Filip Szczypinski, Qiang Zhu, Marc A. Little, Andrew I. Cooper

Materials Innovation Factory, University of Liverpool, Liverpool L7 3NY, United Kingdom

thomas.fellowes@liverpool.ac.uk

Keywords: Automation, porous materials, high-throughput screening

Traditionally, the discovery of new functional materials has been a costly and time-consuming exercise, in part due to the difficulty of designing successful experiments a priori. High-throughput methods are an attractive solution where the low rate of success is mitigated by working on a small scale with robotic assistance. Working on a small scale can improve safety, and the reduced cost of failure allows the researcher to sample a wider cross section of chemical space. This can expose structures and reactivity that would otherwise remain hidden. For these reasons, high-throughput methods have been used routinely in areas such as protein crystallisation and drug screening for some time [1].

Most high-throughput experiments are ultimately controlled and directed by a human researcher, who interprets the data generated and decides on next steps. Humans also often act as the "glue" between various instruments and workflows, performing seemingly trivial tasks such as moving samples and initiating analyses. We have successfully replaced both of these roles with machines with the aim of optimising the activity of a photocatalyst [2, 3].

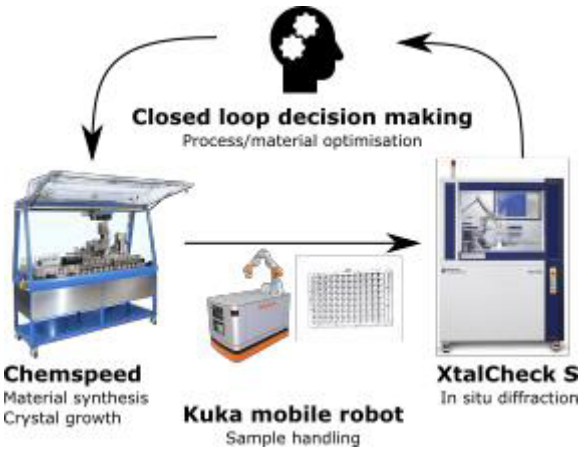

Recently, we have extended this to automated crystallisation, diffraction, and structure solution for low density materials with potential applications in gas separation and storage. Our approach incorporates an initial computer-vision based screening step to decide whether the synthesised material is potentially crystalline, and therefore worth taking to the diffractometer. Both powders and single crystals can be analysed and matched to external and internal databases. The success or failure of a crystallisation is fed back to the synthesis platform via a decision-making program, which chooses suitable conditions for the next steps. The role of the human as an overseer and director of the experiment is thus fulfilled by a machine. As in our previous work, a mobile robot performs the other function of a human; namely, acting as an interface between the various instruments.

Using this process, we were able to obtain a number of extremely low-density structures of organic molecules using solvents and additives that would usually be overlooked by a human researcher guided by their intuition. Several of these experiments have been reproduced by hand on a larger scale, affording quantities suitable for more costly analysis such as gas sorption and NMR.

[1] Blundell, T. L., Jhoti, H. & Abell, C. (2002). *Nat Rev Drug Discov*. **1**, 45–54.
[2] Burger, B., Maffettone, P. M., Gusev, V. V., Aitchison, C. M., Bai, Y., Wang, X., Li, X., Alston, B. M., Li, B., Clowes, R., Rankin, N., Harris, B., Sprick, R. S. & Cooper, A. I. (2020). *Nature*. **583**, 237–241.
[3] Cui, P., P. McMahon, D., R. Spackman, P., M. Alston, B., A. Little, M., M. Day, G. & I. Cooper, A. (2019). *Chemical Science*. **10**, 9988–9997.

We thank the Leverhulme Research Centre for Functional Materials Design and the European Research Council - Autonomous Discovery of Advanced Materials project for funding.

A107-06-280823

Influence of Hydrostatic Pressure on Metal-Organic Frameworks

A. Schneemann1

Department of Inorganic Chemistry, Technische Universität Dresden, 01069 Dresden, Germany

Andreas.Schneemann@tu-dresden.de

Metal-organic frameworks (MOFs) are porous materials build up from organic linker molecules and metal-cluster or ions.[1] One of their unique features that arises from their construction principle is their softness compared to traditional porous materials such as zeolites, activated charcoals or silica. This softness can lead to interesting new applications, since a subclass of MOFs called flexible MOFs can undergo structural changes between distinct defined states upon external stimuli, making them amenable as molecular switches, dampers, pressure absorbers or sensors.[2] However, this softness can also be a curse, since mechanical shaping methods and high pressure conditions in potential industrial applications can destruct their structural integrity and deteriorate their properties.

Within this contribution the influence of hydrostatic pressure on two systems will be discussed. First, the influence of high hydrostatic pressure on the archetypical MOF-5 (Zn4O(bdc)2 with bdc^{2-} = 1,4-benzenedicarboxylate) will be presented.[3] In Diamond Anvil Cell powder X-ray diffraction experiments we show that the intrusion of an alkylated organic guest molecule can fortify the structure of the material to unprecedented high pressures of over 9 GPa. Interestingly, the material retains its structural integrity after pressure release. In the second part the influence of the particle size on the mechanical response of the flexible metal-organic framework DUT-8(Cu) (Cu2(ndc)2(dabco) with ndc^{2-} = 2,6-naphthalenedicarboxylate and dabco = diazabicyclo[2.2.2]octane) is analysed using a hydraulic pressure jump cell for in-situ powder X-ray diffraction experiments.[4] Interestingly, for the material featuring macrosized crystals a phase transition from an open pore state to a much denser, closed pore state can be observed when the pressure is gradually increased, while for submicron sized crystals the material is significantly stiffer and the material remains in the open pore state over the entire applied pressure range. These two studies highlight two methods to fortify MOF structures against hydrostatic pressures, (a) by the inclusion of bulky guest molecules and (b) by engineering the particle size of the crystalline material.

[1] H. Furukawa, K. E. Cordova, M. O'Keeffe and O. M. Yaghi, Science, 2013, 341, 1230444.
[2] A. Schneemann, V. Bon, I. Senkovska, I. Schwedler, S. Kaskel, and R.A Fischer, Chemical Society Reviews, 2014, 43, 6062.
[3] S. J. Baxter, N. C. Burtch, J. D. Evans, A. D. Ready, A. P. Wilkinson and A. Schneemann, Chemistry of Materials, 2022, 34, 768.
[4] M. Maliuta, P. Kolodzeiski, V. Romaka, S. J. Baxter, L. Abylgazina, W. Xue, C. Sternemann, M. Paulus, S. Kaskel. I. Senkovska, S. Henke and A. Schneemann, Unpublished Results, 2023

A110 Room-temperature Serial Snapshot Micro-crystallography: Highlights from XFELs and Synchrotrons
Room 212/213
1.10pm - 3.30pm

A110-01-280823

Developing mix-and-inject serial crystallography at synchrotrons

K. A. Zielinski, L. Pollack

School of Applied and Engineering Physics, Cornell University, Ithaca, New York 14853, United States,

Email of communicating author: lp26@cornell.edu

Keywords: serial crystallography, time-resolved, protein dynamics

The Serial Femtosecond Crystallography (SFX) technique at X-ray Free Electron Lasers (XFELs) has ushered in a new era of room temperature structural enzymology. The opportunity to study biological macromolecules at room temperature allowed for the development of many time-resolved methods. Of great interest is Mix-and-Inject Serial Crystallography (MISC), which utilizes microfluidic mixers to initiate ligand binding reactions inside protein microcrystals. Reaction intermediates have been successfully captured from the single millisecond scale and beyond [1,2], and this information can be used to help elucidate reaction mechanisms by observing the order of events as the reaction progresses. This has many potential impacts, such as clarifying unknown reaction mechanisms or aiding drug design by resolving the action of inhibitors. MISC relies on a robust microfluidic mixer, the flow-focused diffusive mixer, to initiate the reaction rapidly and uniformly [3,4]. This is achieved by utilizing a co-axial flow to create a thin central sample stream that is surrounded by a ligand containing sheath to facilitate the fast diffusion of ligand into the sample stream to trigger the reaction. Different flowrates are used to control the mixing and delay times to reach various timepoints.

MISC is a mature technique and there are exciting opportunities for the method, however, with only five XFELs worldwide, access is extremely limited. Thus, there is a great interest in developing MISC at synchrotrons. Many synchrotron beamlines have been able to support serial synchrotron crystallography (SSX) techniques due to advancements in microfocus beams and fast framerate detectors. There are now many sample delivery systems that are becoming standard, such as various fixed target chip designs, the tape-drive, and high viscosity extruders. These current approaches can provide room temperature structures and can even be combined with pump-probe time-resolved methods, which employ an optical laser as a reaction trigger. The study of ligand binding via fast mixing from microfluidic mixers, however, is not as compatible with the above methods due to limitations of the tape-drive speed and the slow down of diffusion in viscous media required for high viscosity extruders. Here, we will present a new method towards achieving MISC at synchrotrons with a unique sample delivery approach that has been optimized for single crystal hits with long enough exposure times for high quality diffraction patterns with minimal background. We will explain how synchrotron and XFEL studies can be planned synergistically, and which timescales are most appropriate at each source. Lastly, we will discuss the different sample preparation considerations that are needed for SSX and overall best practices.

[1] Olmos, J. L., Pandey, S., Martin-Garcia, J. M., Calvey, G., Katz, A., Knoska, J., Kupitz, C., Hunter, M. S., Liang, M., Oberthuer, D., Yefanov, O., Wiedorn, M., Heyman, M., Holl, M., Pande, K., Barty, A., Miller, M. D., Stern, S., Roy-Chowdhury, S., Coe, J., Nagaratnam, N., Zook, J., Verburgt, J., Norwood, T., Poudyal, I., Xu, D., Koglin, J., Seaberg, M. H., Zhao, Y., Bajt, S., Grant, T., Mariani, V., Nelson, G., Subramanian, G., Bae, E., Fromme, R., Fung, R., Schwander, P., Frank, M., White, T. A., Weierstall, U., Zatsepin, N., Spence, J., Fromme, P., Chapman, H. N., Pollack, L., Tremblay, L., Ourmazd, A., Phillips, G. N. & Schmidt, M. (2018). *BMC Biology*. **16**, 59.
[2] Pandey, S., Calvey, G., Katz, A. M., Malla, T. N., Koua, F. H. M., Martin-Garcia, J. M., Poudyal, I., Yang, J.-H., Vakili, M., Yefanov, O., Zielinski, K. A., Bajt, S., Awel, S., Doerner, K., Frank, M., Gelisio, L., Jernigan, R., Kirkwood, H., Kloos, M. , Koliyadu, J., Mariani, V., Miller, M. D., Mills, G., Nelson, G., Olmos, J. L., Sadri, A., Sato, T., Tolstikova, A., Xu, W., Ourmazd, A., Spence, J. C. H., Schwander, P., Barty, A., Chapman, H. N., Fromme, P., Mancuso, A. P., Phillips, G. N., Bean, R., Pollack, L. & Schmidt, M. (2021). *IUCrJ*. **8**,.
[3] Calvey, G. D., Katz, A. M., Schaffer, C. B. & Pollack, L. (2016). *Struct. Dyn.* **3**, 054301.
[4] Calvey, G. D., Katz, A. M. & Pollack, L. (2019). *Anal. Chem.* **91**, 7139–7144.

This work was supported by the National Science Foundation Science and Technology Center 'BioXFEL' through award STC-1231306

A110-02-280823

Room Temperature Structural Studies of SARS-CoV-2 Protein, NendoU, with an X-ray Free Electron Laser

Botha[1,9], R. Jernigan[1,2], D. Logeswaran[2], D. Doppler[1,2], N. Nagaratnam[1], M. Sonker[2], J.-H. Yang[1], G. Ketawala[1,2], J. M. Martin-Garcia[1,3], M. L. Shelby[4], T. D. Grant[5], V. Mariani[6], A. Tolstikova[7], M. Z. Sheikh[1], M. C. Yung[4], M. A. Coleman[4], S. Zaare[1,8,9], E. K. Kaschner[1,2], M. T. Rabbani[1], R. Nazari[1], M. A. Zacks[1], B. Hayes[6], R. G. Sierra[6], M. S. Hunter[6], S. Lisova[6], A. Batyuk[6], C. Kupitz[6], S. Boutet[6], D. T. Hansen[1], R. A. Kirian[1,9], M. Schmidt[10], R. Fromme[1,2], M. Frank[4], A. Ros[1,2], J. J.-L. Chen[2], P. Fromme[1,2]

[1]Biodesign Center for Applied Structural Discovery, Arizona State University, Tempe, AZ 85287-5001, USA [2]School of Molecular Sciences, Arizona State University, Tempe, AZ 85287-1604, USA [3]Present address: Department of Crystallography and Structural Biology, Institute of Physical Chemistry "Rocasolano", CSIC, Serrano 119, 28006, Madrid, Spain [4]Lawrence Livermore National Laboratory, 7000 East Avenue, Livermore, CA 94550, USA [5]Department of Structural Biology, Jacobs School of Medicine and Biomedical Sciences, SUNY University at Buffalo, 955 Main St., Buffalo, NY 14203, USA [6]Linac Coherent Light Source, SLAC National Accelerator Laboratory, Menlo Park 94025 CA, USA [7]Deutsches Elektronen-Synchrotron, Notkestrasse 85, 22607 Hamburg, Germany [8]Fulton School of Electrical, Computer, and Energy Engineering, Arizona State University, Tempe, AZ 85287, USA [9]Department of Physics, Arizona State University, Tempe, AZ 85287-1504, USA [10]Department of Physics, University of Wisconsin-Milwaukee, 3135 N. Maryland Ave, Milwaukee, WI 53211, USA

sbotha@asu.edu

Keywords: X-ray Free Electron Laser, SFX, SARS-CoV-2

NendoU from SARS-CoV-2 is responsible for the virus's ability to evade the innate immune system by cleaving the poly-uridine leader sequence of antisense viral RNA. Using serial femtosecond crystallography (SFX) at an X-ray free electron laser, the room temperature structure of NendoU was solved to2 .6 Å resolution at the MFX endstation at the Linac Coherent Light Source in California, USA. The protein crystals were injected using the electro-spinning jet produced by the microfluidic electrokinetic sample holder (MESH) injector, as well as through a gas dynamic virtual nozzle (GDVN). The experiments were targeted towards systematically establishing conditions for mix-and inject studies of this protein for time-resolved studies of substrate turnover. With many unforeseen pitfalls presenting themselves during the course of the SFX experiments, this talk is targeted towards presenting a roadmap of considerations for specifically designing such experiments. Furthermore, the room temperature serial femtosecond crystallography structure is compared with previously published cryo-crystallography [1] and cryo-EM 1. structures to reveal and differences and commonalities across the differently determined structures.

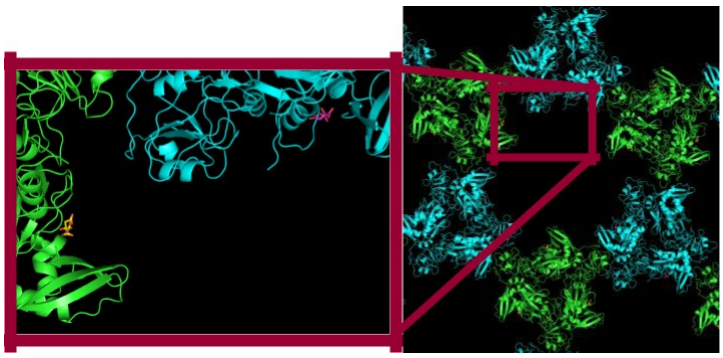

[1] Kim, Y., Jedrzejczak, R., Maltseva, N.I., Wilamowski, M., Endres, M., Godzik, A., Michalska, K., & Joachimiak, A. (2020). *Protein Sci* **29**, 1596-1605.

[2] Frazier, M.N., Dillard, L.B., Krahn, J.M., Perera, L., Williams, J.G., Wilson, I.M., Stewart, Z.D., Pillon, M.C., Deterding, L.J., & Borgnia, M.J. (2021). *Nucleic acids research* **49**, 10136-10149

This work was supported by two RAPID grant awards from the National Science Foundation "IIBR: instrumentation: Time-resolved studies of the SARS-CoV-2 endonuclease NP15" (Award No. 2031343) and "Structure, Function and Dynamics of SARS

Coronavirus-2 Main Protease 3CLpro Determined with Mix-and-Inject Serial XFEL Crystallography" (Award No. 2030466). The work was also supported by the NSF Science and Technology Center award, "Biology with X-ray Lasers (BioXFEL)" (Award No. 1231306). Dhenugen Logeswaran was supported by the NIH grants R01GM094450. Jose Martin-Garcia was funded by the Community of Madrid through the "Atracción y Retención de Talento" Grant (Ref: 2019-T1/BMD-15552). The work was also supported by funds from the National Institute of Health grant R01GM095583 and 5R01GM117342, by the Biodesign Center for Applied Structural Discovery at ASU and the US Department of Energy through Lawrence Livermore National Laboratory under contract DE-AC52-07NA27344. Use of the Linac Coherent Light Source (LCLS), SLAC National Accelerator Laboratory is supported by the US Department of Energy, Office of Science, Office of Basic Energy Sciences under Contract No. DE-AC02-76SF00515

A110-04-280823

Combined X-ray studies on metalloenzymes at room temperature

P. Simon[1], H. Makita[1], A. Bhowmick[1], I. Bogacz[1], R. Hussein[2], M. Ibrahim[2], A. Schmidt[3], M Szczepek[3], V. Srinivas[4], H. Lebrette[4], P. Rabe[5], S. Keable[1], C. Ohmer[6], S. Ragsdale[6], J. Kamps[7], A.M. Orville[7], A. Brewster[1], C. Schofield[5], J. Messinger[8], A. Zouni[2], N.K. Sauter[1], J. Yano[1], V. Yachandra[1], P. Scheerer[3], M. Hoegbom[4], J. Kern[1]

[1]Lawrence Berkeley National Laboratory, MBIB Division, Berkeley, CA 94720, USA, [2]Humboldt University Berlin, Department of Biology, 10099 Berlin, Germany, [3]Charite Berlin, Institute for Medical Physics and Biophysics, 10117 Berlin, Germany, [4]Stockholm University, Department of Biochemistry and Biophysics, SE 10691 Stockholm, Sweden, [5]University of Oxford, Chemistry Research Laboratory, OX1 3TA, Oxford, UK, [6]University of Michigan Medical School, Department of Biological Chemistry, Ann Arbor, MI 48109, USA, [7]DIAMOND Lightsource, OX11 0DE, Didcot, UK, [8]Uppsala University, Department of Chemistry, SE 75120 Uppsala, Sweden

Email of communicating: jfkern@lbl.gov

Keywords: room temperature, x-ray emission spectroscopy, metal centres, reaction mechanism

Obtaining information about changes in the electronic and geometric structure of the active site of a metalloenzyme during catalytic turnover is essential to obtain a detailed understanding of its reaction mechanism. Utilizing femtosecond X-ray pulses of an X-ray free electron laser (XFEL) it is possible to record "undamaged" snapshots of metalloenzymes at room temperature. Given adequate reaction triggering options these can be collated to a "movie" that shows the sequence of events at the catalytic site necessary for the reaction to take place. We developed a drop-on-demand sample delivery system [1] that can be combined with various triggering options and allows for time resolved recording of X-ray diffraction and X-ray spectroscopic data at XFEL sources (Fig. 1). Here we will describe our recent results using this system on a number of metalloenzymes including photosystem II [2,3], ribonucleotide reductases, hydrogenases, methyl coenzyme M reductase [4], and isopenicilin N synthase [5]. We will also highlight the advantages of collecting X-ray emission data concomitantly with the diffraction data, allowing to follow changes of the oxidation state of the metal site over the reaction cycle and correlate these with the structural snap shots obtained from the diffraction measurements. Results for membrane bound O_2 tolerant [Ni/Fe] hydrogenase (MBH) from *R. eutrophia* for example show clear changes in both the Ni and Fe oxidation state (Fig. 1B) at different points in the O_2 induced inactivation as well as the H_2 induced reactivation reaction of the enzyme correlated with different structural changes in the Ni-Fe active site as well as in the proximal FeS cluster (Fig. 1C, D).

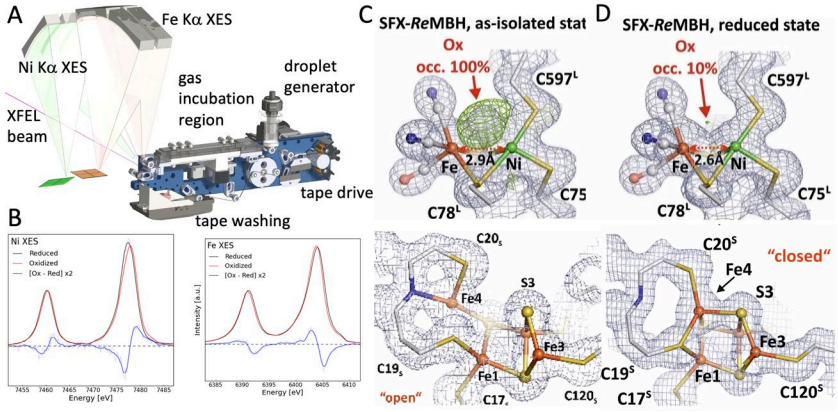

Figure 1. A) Drop-on-Tape setup used for simultaneous X-ray emission (from Fe and Ni) and diffraction data collection at XFELs with light excitation (not shown) or gas-mixing for reaction initiation. B) Ni and Fe Ka XES spectra for oxidized and reduced *Re*MBH. C+D) Electron density map and structural model of the [NiFe] active site and the proximal FeS cluster in as-isolated and reduced state. Clear shift of the proximal cluster between "open" and "closed" state is visible.

[1] F. Fuller, et al. (2017). *Nat. Methods* **14**, 443-449.
[2] M. Ibrahim, et al. (2020). *Proc. Natl. Acad. Sci. USA.* **70**, 3554.
[3] R. Hussein, et al. (2021). *Nat. Comm.***12**, 6531.
[4] C. Ohmer, et al. (2022). *J. Inorg. Biochem.* **230**, 111768.
[5] P. Rabe et al. (2021). *Sci. Adv*. **7**, eabh0250.

A110-04-280823

A route to synchrotron nanocrystallography via fluctuation scattering analysis

A. V. Martin[1], J. Binns[1], P. Adams[1], S. Paporakis[1], M. Hassett[1], C. Darmanin[2], T. L. Greaves[1]

[1]School of Science, RMIT University, Melbourne, Victoria 3000, Australia
[2]La Trobe Institute for Molecular Sciences, La Trobe University, Victoria 3086, Australia

andrew.martin@rmit.edu.au,

Keywords: serial crystallography, fluctuation scattering; disorder

Serial crystallography has opened up possibilities for the study of micron-sized macromolecular crystals at synchrotrons, but there are several instances where even smaller crystal sizes – genuine nanocrystals – are unavoidable[1]. Protein nanocrystals occur in the natural world (e.g. insecticides). They are advantageous for enabling fast timing in diffusion-limited time-resolved experiments. They also arise in studies of the crystallization process itself. Many of these experiments can only be considered at an X-ray free-electron laser. This is because protein nanocrystals can be too small for synchrotron-based crystallography and their unit cells can be too large for powder diffraction, due to peak overlap. There is scope to fill this gap with new analysis techniques that exploit the large datasets of serial crystallography and innovative new approaches to extracting 3D structural information.

Fluctuation x-ray scattering (FXS) [2,3,4] aims to measure the local angular structure in materials using a small x-ray beam to enhance angular scattering fluctuations. Large serial diffraction datasets are analysed statistically via correlation functions. We have developed a method of inverting FXS correlation functions to recover the structure of crystals. This approach is applicable to nanocrystals because it uses dose fractionation, like powder diffraction, while providing 3D structure factors like conventional crystallography. It is also works with multiple crystals in the beam. Hence, it has the potential to give the "best of both worlds" between crystallography and powder diffraction.

We also know how to map FXS correlations into a three- and four-atom distribution call the Pair-Angle Distribution Function (PADF) [5,6,7]. It is a natural generalisation of the widely used 1D PDF to higher dimensions. The PADF contains, for example, a bond angle distribution and greatly increases the amount of structural information beyond that of the PDF. It suitable for both ordered and disordered samples. We will give examples of PADF studies of liquid crystals and proteins.

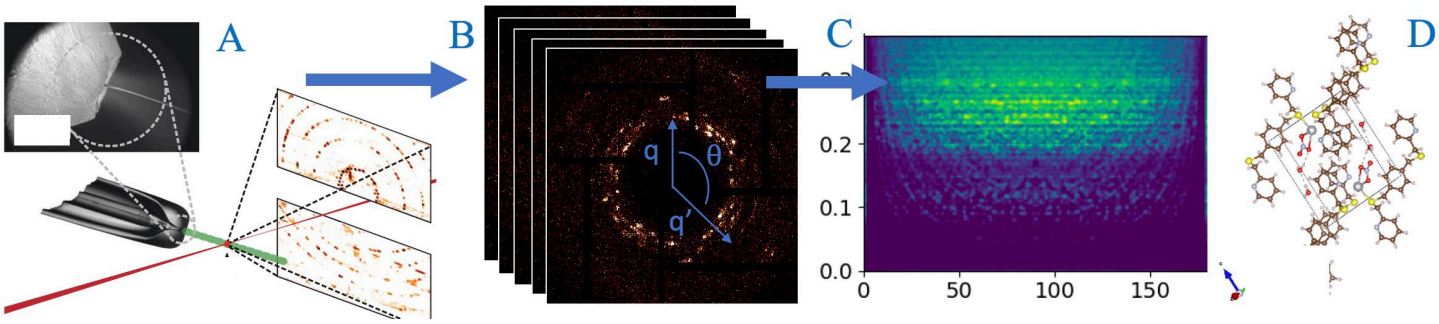

Figure 1. A) Serial crystallography experiment with a liquid injector. Detector pixels are correlated and binned using polar coordinates (B) and then averaged over a large dataset to produce the correlation function shown in (C). The intensity correlations can be used to extract structure factors and solve the structure (D) or converted in to the PADF (not shown).

[1] Shoeman, R.L., E. Hartmann, and I. Schlichting, (2022) Growing and making nano- and microcrystals. *Nature Protocols*, 2022
[2] Kurta, R. P., *et al.*, Structural Analysis by X-ray Intensity Angular Cross-correlations, 1–39 (John Wiley & Sons, Ltd, 2016).
[3] Kam, Z. (1977). *Macromolecules*, 10(5), 927–934.
[4] Wochner, P., *et al.*, (2009). *Proceedings of the National Academy of Sciences of the United States of America*, 106(28), 11511–11514.
[5] Martin, A. V. (2017). IUCrJ, 4, 24–36.
[6] Martin, A. V., *et al.*, (2020). *Communications Materials*, 1(40), 1–8.
[7] Binns, J. et al. (2022) IUCrJ, 9, 231.

A110-05-280823

Structural characterization of the BLUF photoreceptor OaPAC using time-resolved crystallography

Chretien[1], S. Botha[2], P. Mehrabi[3], D. von Stetten[4], A. Mancuso[5], J. Schulz[1], A. Pearson[3], K.Lorenzen[1], R. Schubert[1]

[1]European XFEL, Schenefeld, Germany, [2]Arizona State University, Tempe, Arizona, United States of America, [3]Hamburg University, Hamburg, Germany, [4]EMBL, Hamburg, Germany, [5]Diamond Light Source, Didcot, United Kingdom

Reactions of biological macromolecules can be studied by *time-resolved crystallography* (TRX), as it provides high spatial and temporal resolution. TRX requires the rapid, ideally instantaneous, initiation of the reaction of interest, to ensure that fine structural changes are not "blurred out" by the different molecules in the crystal reacting in a non-synchronized manner. Luckily, naturally light-sensitive signaling proteins such as photoreceptors allow the investigation of biochemical processes in the pico- and nanosecond time range, as these can be efficiently and uniformly activated by a short laser pulse in light-induced pump-probe experiments. Photoreceptors containing a Blue-Light sensor Using Flavin (BLUF sensor domain) have one of the fastest photoreaction cycles of all known photoreceptors and a very short-lived lit state [1, 2]. They are therefore highly attractive for a broad range of applications. Understanding the signal transmission in the complete BLUF sensor–effector system is however required to pave the way for future bioengineering applications [3].

In this project, a multidomain photoactivated adenylate cyclase (PAC) protein from *Oscillatoria acuminata* is studied. OaPAC is a bacterial photoreceptor containing a BLUF sensor domain coupled to an adenylyl cyclase effector domain, involved in the conversion of ATP into cAMP. For this, OaPAC protein was produced, purified and characterized to verify stability and proper functionality of both domains. Complete X-ray crystallography datasets of OaPAC were collected at cryogenic temperature and room-temperature in its dark state with ATP bound in the active site. Pump-probe time-resolved crystallography using XFELs (TR-SFX) (Fig. 1) and synchrotron (TR-SSX) in combination with ultrafast spectroscopy was performed. Structural changes around the FMN chromophore for several time points could already be elucidated and additional experiments are ongoing.

The data shows the rotation of Glu48, which initiates a change in FMN hydrogen bond network and leads to a reduced distance of Glu48 to FMN O4. Notably, the observed kinetics from the TR-SFX experiments differ from spectroscopy data. Onset of the displacement of Met92 initiates signal transmission to the adenylate cyclase domain. Cryo-trapping experiment using the spitrobot is also in progress. The aim is to capture reaction time-points in a light-activated state by flash-freezing it after milliseconds to seconds of illumination at room temperature. By this, we could show that OaPAC also adopts the so called "Tryptophan-in" conformation (Trp90) in the light activated state, which is known from some BLUF proteins, but was not seen for BLUF-PAC so far. The performed experiments will help to visualize and understand the entire signaling process of OaPAC, which can serve as a basis to design novel optogenetic tools.

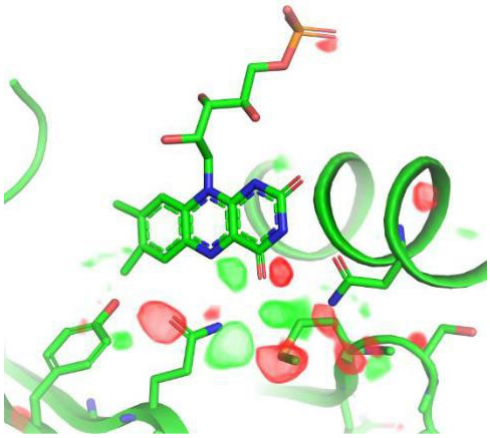

[1] J. Hendriks et al. (2009), Chapter 41 - Photoreceptor Proteins from Purple Bacteria, The Purple Phototrophic Bacteria, Volume 28, pp. 811-837. Berlin: Stringer

[2] R. Brust et al. (2013), Proteins in Action: Femtosecond to Millisecond Structural Dynamics of a Photoactive Flavoprotein, *J. Am. Chem. Soc.*, 135, 43, 16168−16174

[1] K. Moffat (2014), Time-resolved crystallography and protein design: signalling photoreceptors and optogenetics, *Phil. Trans. R. Soc. Lond. B Biol. Sci.*, 369, 1647

[2] P. Mehrabi et al. (2022), Millisecond cryo-trapping by the spitrobot crystal plunger simplifies time-resolved crystallography, *bioRxiv*, doi: 10.1101/2022.09.20.508674

A110-06-280823

Elucidating structural mechanisms of energy transfer in a vertebral- based far-red fluorescent protein

Swagatha Ghosh

Department of Applied Physics, Graduate School of Engineering, Nagoya University, Nagoya 464-8603, Japan

Email: s.ghosh@bmp.ap.pse.nagoya-u.ac.jp

Keywords: Sandercyanin, lipocalin-biliverdin complexes, fluorescent proteins

In the past decades, fluorescent proteins (FPs) have found innumerable and advanced applications in molecular imaging techniques for studying cellular processes. Most FPs known till date have been discovered and isolated from invertebrates, with exception to UnaG (from *Anguilla japonica*) and Sandercyanin (*Stizostedion vitreum*), that have vertebral origin. Sandercyanin is a well-characterized far -red vertebral FP and its structures and properties have been reported previously[1]. It is unique, with its lipocalin fold and non- covalent mode of binding to chromophore (biliverdin) compared all known red and far-red FPs. Native Sandercyanin forms a tetrameric complex with biliverdin and shows far-red fluorescence at 675 nm with a fluorescence life-time ~200 ps on excitation at 375nm and 630nm wavelengths. The far- red fluorescence, large spectral shift between 375 nm (excitation) / 675 nm (emission) wavelengths and uniqueness of vertebral origin of Sandercyanin could be harnessed into multitudes of *in-vivo* applications.

Several crystal structures combined with spectroscopic studies have elucidated that biliverdin can occupy multiple conformations in the protein and these dynamics lead to modulated spectral properties[2,3]. Till date, the molecular basis of exceptionally large spectral shift of ~300 nm remains elusive. Here, we aim to decipher structural mechanisms coupling the large spectral shift to far-red fluorescence in Sandercyanin. Using time- resolved pump- probe crystallography, we will track structural changes from pico-to- nano seconds time- scales and correlate the observed changes to energy transfer in the protein. Overall, this project aims to obtain a molecular movie that could be a representative of lipocalin- based fluorescent proteins.

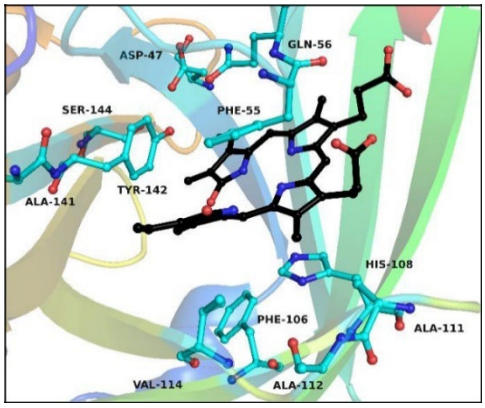

Figure. Chromophore- binding pocket of Sandercyanin shows different modes of interactions with biliverdin

[1] **Ghosh S**, Yu CL, Ferraro DJ, Sudha S, Pal SK, Schaefer WF, Gibson DT, Ramaswamy S; Blue protein with red fluorescence. Proc Natl Acad Sci U S A (2016). 113(41):11513- 11518
[2] Yadav K, **Ghosh S**, Barak A, Schaefer WF, Ramaswamy S; A Phenylalanine Stacking enhances the Red Fluorescence of Biliverdin IXα on UV Excitation in Sandercyanin Fluorescent Protein; FEBS Letters (2022).; 596(6):796-805.
[3] Ghosh S, Mondal S, Yadav K, Aggarwal S, Schaefer WF, Narayana C, Ramaswamy S; Modulation of biliverdin dynamics and spectral properties by Sandercyanin. RSC Adv. (2022).

A114 New Opportunities in X-ray Spectroscopy at Ultra Low Emittance Synchrotron Sources

Room 219

1.10pm - 3.30pm

A114-01-280823

Bent Crystal Laue Analyser Combined with Polarization-dependence Total Reflection Fluorescence X-ray Absorption Fine Structure (BCLA-TRFXAFS) and its Application to Electrode Surface

K. Asakura[1], K.Dong[1], T.Wada[2], D. Kido[1], S. Takakusagi[1]

1 Institute for Catalysis, Hokkaido University, Kita 21-10, Kuta-ku Sapporo 001-21, Japan.
2 Tokyo Medical and Dental University, Yushima, Bunkyo-ku, Tokyo 113-8549,Japan.

askr@cat.hokudaia.c.jp

Keywords: PTRF-XAFS, BCLA, Electrode Surface

Ultra low emittance X-ray source will expand the possibilities for the polarization dependent total reflection fluorescence XAFS (PTRF-XAFS) [1,2] which requires a large flat surface (several cm order) owing to grazing incidence. When the PTRF-XAFS is applied to the electrode surface under the working conditions, the coexisting electrolyte over the electrode surface creates the undesirable scattering to decrease the signal to background ratio. In this work we have investigated the feasibility of the bent crystal Laue analyser (BCLA), for the PTRF-XAFS spectroscopy to separate the fluorescence X-ray emission of a target atom from the elastic scattering X-rays and other fluorescence emission lines [3,4]. The BCLA is an X-ray energy analyser with a medium energy resolution (about 10 eV) and has a focal line parallel to the BCLA surface. We have adjusted BCLA focal line to the X-ray footprint on the substrate surface as shown in Figure 1. We have measured the PTRF-XAFS of the 1 monolayer(1 ML) Pt on the 30 nm thick Au film in the absence and presence of electrolyte. BCLA can successfully remove the elastic X-ray and Au fluorescence as shown in Figure 2. We find the small glitch at the Au L_3 edge which is caused by the sudden change of complex refraction index of the Au substrate at the Au edge. This abnormal spectrum feature can be removed by correction of reflectivity using Au foil absorption data as shown in the green curve of Figure 2 [3]. The BCLA combined with PTRF-XAFS spectroscopy (BCLA + PTRF-XAFS) is a new technique for the in situ surface analysis of highly dispersed systems even in the presence of a liquid overlayer.

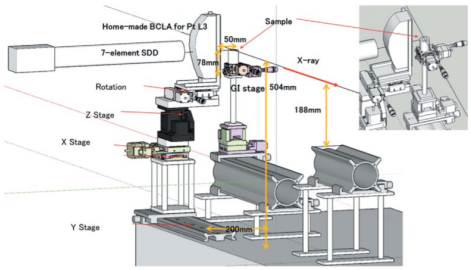

Figure 1 Setup for BCLA+PTRF-XAFS[3]

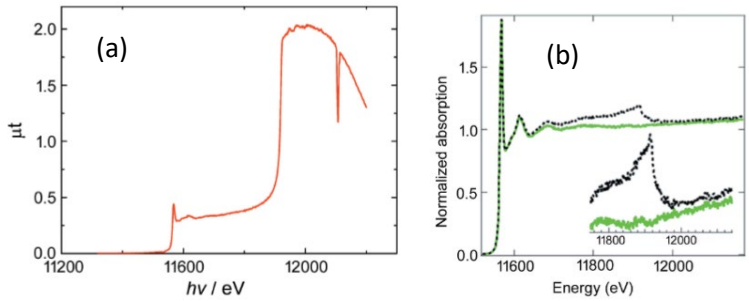

Figure 2. Pt L3 BCLA+PTRF-EXAFS of 1 ML Pt on Au thin film.(a) Without BCLA, (b) with BCLA (Black) and after the correction of the reflectivity (Green). Inset is the magnified image[3].

[1] Asakura, K. (2012). *Catalysis* edited by J. J. Spivey & M. Gupta, pp. 281-322. Cambridge, Royal Society of Chemistry.
[2] Takakusagi, S., Chun, W.-J., Uehara, H., Asakura, K. & Iwasawa, Y. (2013). *Top. Catal.* **56**, 1-11.
[3] Wakisaka, Y., Kido, D., Uehara, H., Yua, Q., Feiten, F. E., Mukai, S., Takakusagi, S., Uemura, Y., Yokoyama, T., Wada, T., Uo, M., Sekizawa, O., Uruga, T., Iwasawa, Y. & Asakura, K. (2019). *The Chemical Record* **19**, 1157-1165.
[4] Wakisaka, Y., Hu, B., Kido, D., Al Rashid, M. H., Chen, W., Dong, K., Wada, T., Bharate, B., Yuan, Q., Mukai, S., Takeichi, Y., Takakusagi, S. & Asakura, K. (2020). *J.Synchron Rad.* **27**, 1618-1625.
[5] Zhong, Z., Chapman, L. D., Bunker, B. A., Bunker, G. B., Fischetti, R. & Segre, C. U. (1999). *J.Synchron Rad.* **6**, 212-214.
[6] Sakayanagi, Y. (1982). *Jpn. J. Appl. Phys.* **21**, L225-L226.

A114-02-280823

Nanoscale spatial mapping of chemical state and bonding variations using XANES and EXAFS: Fast, reduced dose measurements using sparse sampling approaches

P.D. Quinn[1], O. Townsend[2], S. Dolgov[2], S. Gazzola[2]

Diamond Light Source, Harwell Science and Innovation Campus, Didcot, OX11 0DE, UK
University of Bath, Claverton Down, Bath, BA2 7AY, UK

paul.quinn@diamond.ac.uk

Keywords: Nanoprobe, spectromicroscopy, XANES, EXAFS, low-dose, sparse scanning, compressed sensing

Spectromicroscopy is a powerful tool used for studying chemical state distributions at the micro and nano scales. The application of nanoscale spectromicroscopy to EXAFS measurements, in-situ studies and in areas of soft matter or biological materials - is limited by two main factors. First, the total experiment time required to collect the data to a given statistical significance; second, the total radiation dose over the collection and any resulting damage to the object, or changes to the chemical state, that may occur as a result. While new low emittance sources promise increased flux for nano focussing experiments, the issue of damage due to dose still needs to be addressed, particularly for spectromicroscopy measurements where regions of interest are repeatedly scanned across a range of energies.

The Hard X-ray Nanoprobe beamline, I14, at the Diamond Light Source (UK) is a dedicated facility for nanoscale microscopy [1]. The nanoprobe provides a flexible end station, with a beam size of 50 nm, optimised for X-ray spectroscopy with applications across a broad range of areas such as biomaterials, environmental and earth sciences, catalysis, and energy materials. Here, we describe the nanoscale spectromicroscopy capabilities and the implementation of several sparse sampling approaches (Figure 1) on the beamline. These approaches were developed to optimally sub-sample across energy or spatial information [2], to probe the chemical state of beam-sensitive materials, reduce the acquisition times for in-situ studies, and deliver mapping XANES and nanoscale EXAFS capabilities on shorter time scales.

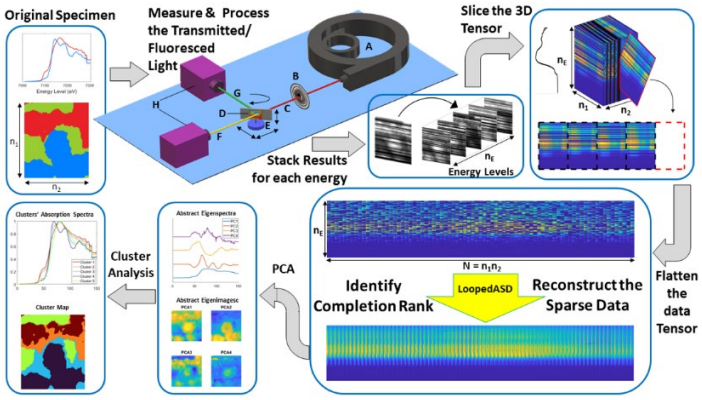

Figure 1. An example of a sparse spatial sampling implemented on the Hard X-ray Nanoprobe.

[1] Quinn, P. D., Alianelli, L., Gomez-Gonzalez, M., Mahoney, D., Cacho-Nerin, F., Peach, A. & Parker, J. E. (2021), J. Synchrotron Rad. **28,** 1006-1013.
[2] O. Townsend, S. Gazzola, S. Dolgov, and P. Quinn, (2022), Opt. Express **30**, 43237-43254.

A114-03-280823

Development and Application of X-ray Spectroscopic Ptychography at SPring-8

Yukio Takahashi

International Center for Synchrotron Radiation Innovation Smart, Tohoku University, Sendai 980-8577, Japan
RIKEN SPring-8 Center, Sayo-gun, Hyogo 679-5148, Japan

ytakahashi@tohoku.ac.jp

Keywords: X-ray ptychography, X-ray absorption spectroscopy

X-ray ptychography is a lensless imaging technique based on the iterative phasing of diffraction amplitudes, which can non-destructively observe thick samples at the nanoscale. So far, we have developed high-resolution hard X-ray ptychography using total-reflection focusing mirrors at SPring-8 in Japan [1, 2]. X-ray ptychography using multiple energies, including the absorption edge of a specific element, which is often referred to as X-ray spectroscopic ptychography, enables us to visualize both the structures and chemical states of bulk materials at the nanoscale. So far, we have demonstrated hard X-ray spectroscopic ptychography using a phase retrieval calculation using the Kramers–Kronig relation [3] and have applied to two-dimensional and three-dimensional visualization of the cerium valence in platinum-supported cerium-zirconium oxide three-way catalyst particles [4, 5]. We have also visualized the chemical state in spinel lithium nickel-manganese oxide particles, which are expected as the next-generation 5 V Li-ion battery cathode material [6]. Recently, we have developed an X-ray ptychography measurement system in the tender X-ray region using Fresnel zone plate as a focusing device at SPring-8 BL27SU, and have succeeded in visualizing the chemical state of sulfur in polymeric sulfur materials [7, 8]. Tender X-ray spectroscopic ptychography is expected to be used in the new 3-GeV synchrotron radiation facility, NanoTerasu, under construction in Japan.

[1] Takahashi, Y. *et al.* (2011). *Phys. Rev. B*, **83**, 214109.
[2] Hirose, M., Ishiguro, N., Takahashi, Y. *et al.*, (2020). *J. Synchrotron Rad.*, **27**, 455.
[3] Hirose, M., Takahashi, Y. *et al.*, (2017). *Opt. Express* **25**, 8593.
[4] Hirose, M., Ishiguro, N., Takahashi, Y. *et al.*, (2018). *Angew. Chem. Int. Ed.*, **130**, 1490.
[5] Hirose, M., Ishiguro, N., Takahashi, Y. *et al.*, (2019). *Communications Chemistry*, **2**, 50.
[6] Uematsu, H., Ishiguro, N., Takahashi, Y. *et al.*, (2021). *J. Phys. Chem. Lett.*, **12**, 5781.
[7] Abe, M., Ishiguro, N., Takahashi, Y. *et al.*, (2021). *J. Synchrotron Rad.*, **28**, 1610.
[8] Abe, M., Ishiguro, N., Takahashi, Y. *et al.*, (2022). *J. Phys. Chem. C*, **126**, 14047

Spectro-Ptychography at the I08-1 instrument at the Diamond Light Source

Benedikt J. Daurer, Majid Kazemian, Tohru Araki, Burkhard Kaulich

Diamond Light Source, Harwell Campus, Chilton, Oxfordshire, OX11 0DE, UK

benedikt.daurer@diamond.ac.uk

Keywords: NEXAFS, Spectromicroscopy, ptychography

The I08-1 soft X-ray ptychography branchline at the Diamond Light Source (UK) is a facility dedicated to the spectromicroscopic and tomographic analysis of the interaction of organic and inorganic matter with unprecedented spatial resolution. It provides capabilities to do NEXAFS spectroscopy for the analysis of transition metals or other elements relevant for biogeochemistry, environmental and earth sciences, medicine and pharmacology, and materials science including magnetism, electrochemistry, catalysis, and battery research.

Here, we present the current capabilities of this new branchline, which is in user operation in optimisation mode since May 2022, as well as give an outline of planned future upgrades. We describe our current instrumentation and software infrastructure, including an automated processing pipeline that provides users with a ptychographic reconstruction in near real time. We show results from early commissioning experiments collecting full spectro-ptychograhic data of Fe nanoparticles across the Fe L3 edge (Figure 1) alongside a few scientific examples of early I08-1 users. Spectro-ptychography offers the unique capability to image organic and inorganic samples at high spatial resolution and with chemical specificity, further enhanced by the upcoming upgrade to Diamond II with an expected increase in coherent flux.

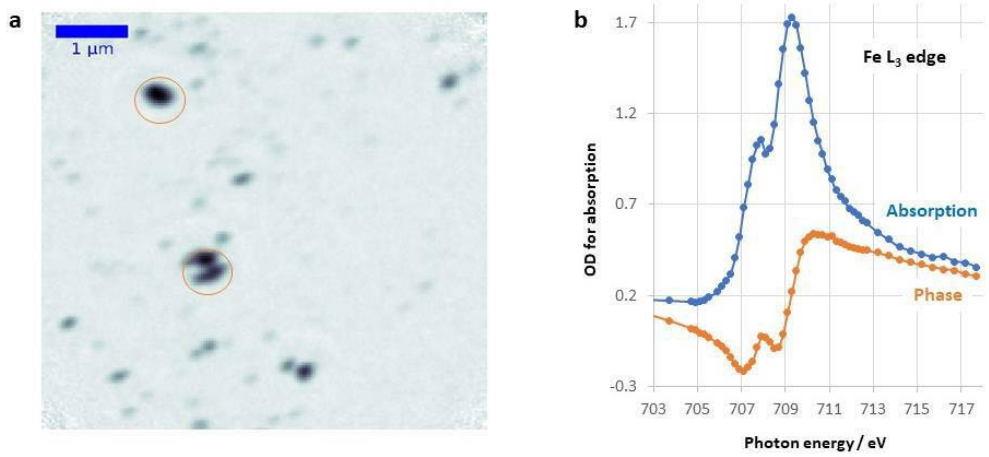

Figure 1. Ptychographic reconstruction (a) of Fe nanoparticles from diffraction data collected at 709 eV alongside absorption and phase spectra (b) extracted from the full energy stack of ptychographic images for the particles highlighted by the red circles.

A114-06-280823

Operando Spectroimaging for Reaction Infography of Heterogeneous Catalysts

Hirosuke Matsui1, Mizuki Tada1

[1]*Department of Chemistry, Graduate School of Science, Nagoya University, Chikusa, Nagoya (Japan)*

matsui.hirosuke.x1@f.mail.nagoya-u.ac.jp

Keywords: XAFS-CT imaging, reaction infography, heterogeneous catalyst, polymer electrolyte fuel cell

Heterogeneous catalysts have crucial roles in various chemical processes and energy conversions, and their heterogeneous structures under reaction conditions are still difficult to understand at multi-scale although they are key factors for catalytic functions. X-ray absorption fine structure (XAFS) is one of the most powerful methods to characterize the local coordination structures of heterogeneous catalysts without crystalline structures. The analysis of local structures in active states of heterogeneous catalysts has been widely developed under *operando* reaction conditions, however, the spatial information of active structures and catalyst performances in heterogeneous solid catalysts is still in a black box. Recently, the development of X-ray imaging is cutting-edge and enables X-ray spectroimaging to visualize the chemical state information of each element in solid materials. We developed spectroimaging called XAFS-CT combining hard X-ray CT imaging and XAFS spectroscopy and achieve reaction infography for the understanding of various reactions proceeding on heterogeneous catalysts.

In this paper, we will introduce our recent research on the *operando* XAFS-CT spectroimaging of several reaction events in polymer electrolyte fuel cells (PEFCs). There are several serious issues in PEFC for practical use and the degradation of electrocatalysts, catalyst poisoning with air contaminants, the treatment of radical species under reaction conditions, the migration of radical scavengers, etc. We applied the XAFS-CT spectroimaging for practical PEFC cells and visualized these crucial events in PEFC cells under working conditions [1-3]. The CT-XAFS data measured at both the Pt L_{III}-edge and Co *K*-edge visualized a heterogeneous degradation manner in the catalyst layer by dealloying of the Pt-Co alloy cathode catalyst and the increase of Pt particle size during accelerated degradation (ADT) tests [1]. Machine learning analysis of huge 3D data sets revealed that the progress of catalyst degradation differs depending on the geometric environment within the catalyst layer. The CT-XAFS analysis extended to EXAFS provided 3D visualizations of not only the heterogeneous distribution and valence state of the Pt cathode catalyst in PEFC but also the spatially heterogeneous variations of the coordination number of Pt-Pt and Pt-O bonds [2]. The spatial distribution of local structures in the cathode catalyst layer changed to a wide variation after the conditioning, while the initial structural variation remained even after the long ADT tests. The CT-XAFS imaging in the X-ray fluorescence yield visualized the function of Ce radical scavengers loaded in trace amounts in the PEFC reaction system [3]. 3D imaging data revealed the distribution of Ce quenched in the cathode catalyst layer and the presence of Ce^{3+} under the operation of PEFC for the first time. Recent examples of our XAFS-CT imaging for reaction infography of fuel cells will be presented and discussed.

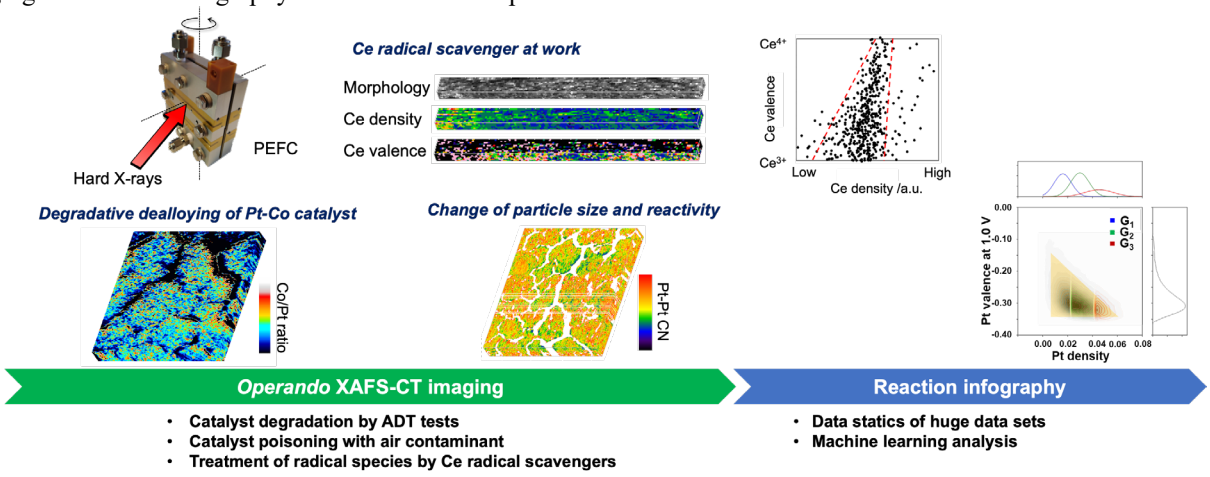

Figure 1. Reaction infography by *operando* XAFS-CT spectroimging for practical PEFC.

[1] Y. Tan, H. Matsui, N. Ishiguro, T. Uruga, D. N. Nguyen, O. Sekizawa, T. Sakata, N. Maejima, K. Higashi, H. C. Dam, M. Tada, *J. Phys. Chem. C* **123**, 18844–18853 (2019).

[2] H. Matsui, N. Ishiguro, Y. Tan, N. Maejima, Y. Muramoto, T. Uruga, K. Higashi, D.-N. Nguyen, H.-C. Dam, G. Samjeske, M. Tada, *ChemNanoMat* **8**, e202200008 (2022).

[3] H. Matsui, S. Takao, K. Higashi, T. Kaneko, G. Samjeske, T. Uruga, M. Tada, and Y. Iwasawa, *ACS Appl. Mater. Interfaces* **14**, 6762-6776 (2022).

A015 Structures of Very Large Assemblies
Room 203/204
4.00pm - 6.30pm

A015-01-280823

Visualizing the nucleoplasmic maturation of human pre-60S ribosomal particles

Yunyang Zhang, Xiaomeng Liang, Ning Gao*

State Key Laboratory of Membrane Biology, Peking-Tsinghua Joint Center for Life Sciences, School of Life Sciences, Peking University, Beijing 100871, China.

Correspondence to: gaon@pku.edu.cn (N.G.)

Keywords: ribosome assembly, cryo-electron microscopy, RNA, chaperone, GTPase

Eukaryotic ribosome assembly is a highly orchestrated process involves over two hundred protein factors. After early assembly events on nascent rRNA in the nucleolus, pre-60S particles undergo continuous maturation steps in the nucleoplasm, and prepare for nuclear export. Here, we report eleven cryo-EM structures of the nuclear pre-60S particles isolated from human cells through epitope-tagged GNL2, at resolutions of 2.8 to 4.3 angstroms. These high-resolution snapshots provide fine details for several major structural remodeling events at a virtual temporal resolution (Fig. 1). Two new human factors, L10K and C11orf98, with no or very low homology to yeast factors, were identified. Comparative structural analyses reveal that many assembly factors act as successive place holders to control the timing of factor association/dissociation events. They display multi-phasic binding properties for different domains and generate complex binding inter-dependencies as a means to guide the rRNA maturation towards the mature conformation. Overall, our data reveal that nuclear assembly of human pre-60S particles is generally hierarchical with short branch pathways, and a few factors also display specific roles as rRNA chaperones by confining rRNA helices locally to facilitate their folding, such as the C-terminal domain of SDAD1.

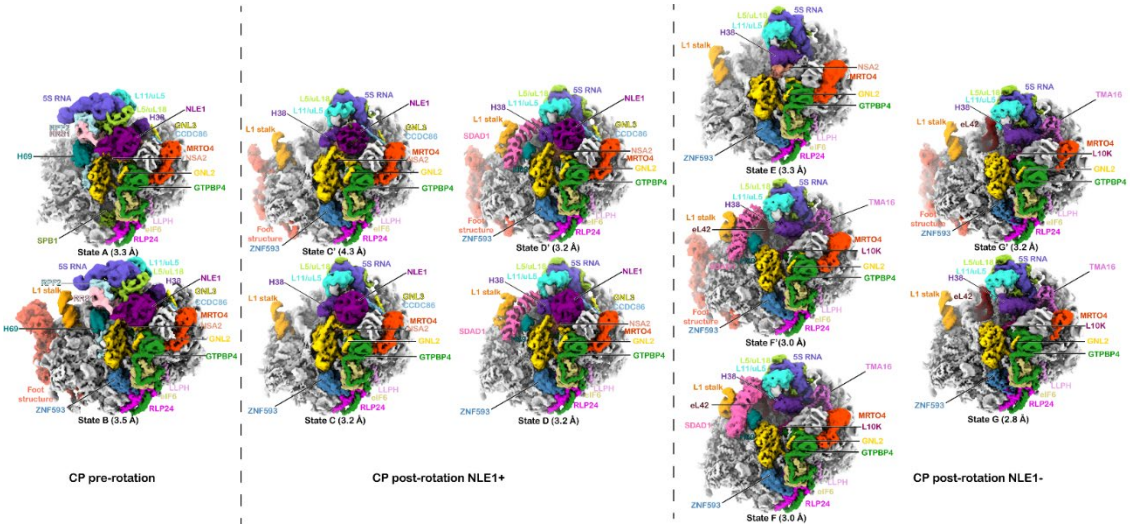

Figure 1 Cryo-EM structures of human pre-60S particles obtained through epitope-tagged GNL2. Cryo-EM density maps of the eleven structures of GNL2-particles were divided into 3 groups according to the conformational difference of the CP and the presence or absence of NLE1. Individual assembly factors, RNA/RNPs (including 5S RNP, L1 stalk, H38, H69, ITS2 and associated factors) and ribosomal protein eL42 are color-coded. Below each map, the overall resolution is shown.

A015-02-280823

BRCA2-HSF2BP oligomeric ring assembly is implicated in the regulation of homologous recombination during meiosis

Rania Ghouil[1], Simona Miron[1], Pierre Legrand[2], Koichi Sato[3], Dejan Ristic[4], Sari E. van Rossum-Fikkert[4], Malika Ouldali[1], Jean-Marie Winter[5], Virginie Ropars [1], Gabriel David[2], Ana-Andreea Arteni[1], Claire Wyman[4,6], Puck Knipscheer[3], Roland Kanaar[4], Alex N. Zelensky[4], Sophie Zinn-Justin[1]

Université Paris-Saclay, CEA, CNRS, Institute for Integrative Biology of the Cell (I2BC), 91198, Gif-sur-Yvette, France. [2] Synchrotron SOLEIL, Gif-sur-Yvette, France. [3] Oncode Institute, Hubrecht Institute–KNAW and University Medical Center Utrecht, Utrecht, The Netherlands. [4] Department of Molecular Genetics, Oncode Institute, Erasmus MC Cancer Institute, Erasmus University Medical Center, 3000 CA, Rotterdam, The Netherlands. [5] Institut Pasteur, Paris, France. [6] Department of Radiation Oncology, Erasmus MC Cancer Institute, Erasmus University Medical Center, 3000 CA, Rotterdam, The Netherlands.

pierre.legrand@synchrotron-soleil.fr

Keywords: Homologous Recombination, Multimeric assembly, IDP, Crystallography + Cryo-EM + NMR + SAXS

BRCA2 is one of the most studied cancer predisposition genes. The protein encoded by this gene, BRCA2, is large (more than 3000 amino acids), and is mutated along its entire length in patients with breast, ovarian and prostate cancers. The absence of BRCA2 also causes a fertility defect in men and women. BRCA2 is essential for homologous recombination, a process central to DNA repair and meiosis. In particular, BRCA2 recruits the RAD51 protein to DNA, in order to search for sequence homologies between two strands and allow their exchange. A team from the ERASMUS Medical Center has recently identified a new BRCA2 partner, HSF2BP, which is widely expressed in meiotic cells. Mutations in HSF2BP are implicated in fertility problems: in particular, loss of HSF2BP prevents homologous recombination during spermatogenesis.

In order to determine whether HSF2BP is involved in the localization of BRCA2 at homologous recombination sites during meiosis, we solved the 3D structure of the interacting domains of BRCA2 and HSF2BP by X-ray crystallography at Synchrotron SOLEIL [1]. From a molecular point of view, BRCA2 is mostly predicted as disordered, as characterized by Nuclear Magnetic Resonance (NMR), which makes its structural analysis particularly complex [2]. By combining NMR and X-ray crystallography, we identified a disordered repeated motif in BRCA2 capable of binding two HSF2BP domains and showed that two BRCA2 fragments bind simultaneously to four HSF2BP domains, leading to a very high affinity between the two partners and to the formation of a tetramer of HSF2BP domains (Figure 1A). Deletion of the first repeat of the motif strongly decreases the affinity between BRCA2 and HFS2BP and prevents tetramerization of the HSF2BP domain. Further in vitro analysis of the complex between the repeated motif of BRCA2 and full-length HSF2BP revealed the assembly of a large (⌀~200Å) ring-shaped 24-mer, consisting of three interlocked octameric rings whose 3D structure has been characterized by cryo-electron microscopy (cryo-EM) up to a resolution of 3.3 Å (Figure 1B). The crystal structure of the interacting domains of BRCA2 and HSF2BP nicely fits into the cryo-EM map of the ring-shaped oligomer. A fragment of BRME1, a HSF2BP partner, inhibits the formation of this oligomer, by preventing interaction between the coiled-coil regions of HSF2BP. The physiological relevance and meiotic function of this oligomer, a 1 MDa complex between 12 * BRCA2-HBD and 24 * HSF2BP, characterized by an unusual and highly symmetric structural organization, will be discussed.

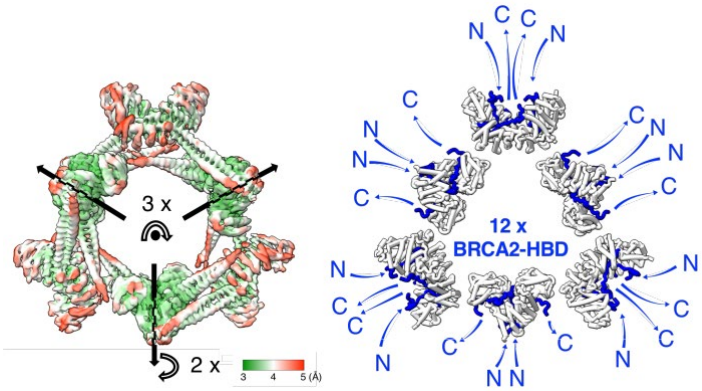

Figure 1. HSF2BP oligomerizes into a ring-shaped complex upon binding to BRCA2-HBD.

Ghouil, R., Miron, S., Koornneef, L., Veerman, J., Paul, M.W., Le Du, M., Sleddens-Linkels, E., van Rossum-Fikkert, S.E., van Loon, Y., Felipe-Medina, N., Pendás, A.M., Maas, A., Essers, J., Legrand, P., Baarends, W.M., Kanaar, R., Zinn-Justin, S., & Zelensky, A.N. (2021). *Nature Communications*, **12**.

Julien, M., Ghouil, R., Petitalot, A., Caputo, S.M., Carreira, A., & Zinn-Justin, S. (2021). *Biomolecules*, **11**.

Ghouil, R., Miron, S., Sato, K. , Ristic, D., van Rossum-Fikkert, S.E., Legrand, P., Ouldali, M., Winter, J.M., Ropars, V., David, G., Arteni, A.A., Wyman, C., Knipscheer, P., Kanaar, R., Zelensky, A., Zinn-Justin S. BRCA2-HSF2BP Oligomeric Ring Disassembly by BRME1 Promotes Homologous Recombination, in revision

A015-03-280823

Structure of the endosomal Commander complex mutated in Ritscher-Schinzel syndrome: combining crystallography, cryoEM and AlphaFold2

Michael D. Healy[1], Kerrie E. McNally[2,3], Rebeka Butkovic[2], Molly Chilton[2], Kohji Kato[2], Joanna Sacharz[4], Calum McConville[4], Edmund R.R. Moody[5], Shrestha Shaw[2], Vicente J. Planelles-Herrero[3], Sathish K.N.

Institute for Molecular Bioscience, The University of Queensland, St. Lucia, Queensland, 4072, Australia. 2.School of Biochemistry, Biomedical Sciences Building, University of Bristol, Bristol BS8 1TD, UK. 3. MRC Laboratory of Molecular Biology, Cambridge, CB2 0QH, UK. 4. Department of Biochemistry and Pharmacology, The Bio21 Molecular Science and Biotechnology Institute, The University of Melbourne, Parkville, Victoria, Australia. 5. School of Biological Sciences, University of Bristol, Bristol BS8 1TD, UK. 6. Cambridge Institute for Medical Research, University of Cambridge, Cambridge CB2 0XY, UK. 7. Institute of Health and Sport (iHeS), Victoria University, Melbourne, Victoria, Australia. 8. Proteomics Facility, School of Biochemistry, Biomedical Sciences Building, University of Bristol, Bristol BS8 1TD, UK. 9. Department of Pediatrics and Neonatology, Nagoya City University Graduate School of Medical Sciences and Medical School, Nagoya, Japan. 10. Max Planck Bristol Centre for Minimal Biology, Department of Chemistry, University of Bristol, BS8 1TS, UK. 11. Murdoch Children's Research Institute, Royal Children's Hospital, Melbourne, Victoria, Australia.

Email of communicating b.collins@imb.uq.edu.au

Keywords: Membrane trafficking, protein complex structure

The Commander complex is required for endosomal recycling of diverse transmembrane cargos and is mutated in Ritscher-Schinzel syndrome. It comprises two subassemblies; Retriever composed of VPS35L, VPS26C and VPS29, and the CCC complex which contains twelve subunits: COMMD1-COMMD10 and the coiled-coil domain-containing (CCDC) proteins CCDC22 and CCDC93. Combining X-ray crystallography, electron cryomicroscopy and in silico predictions we have assembled a complete structural model of Commander [1]. Retriever is distantly related to the endosomal Retromer complex but has unique features preventing the shared VPS29 subunit from interacting with Retromer-associated factors. The COMMD proteins form a distinctive hetero-decameric ring stabilised by extensive interactions with CCDC22 and CCDC93. These adopt a coiled-coil structure that connects the CCC and Retriever assemblies and recruits a sixteenth subunit, DENND10, to form the complete Commander complex. The structure allows mapping of disease-causing mutations and reveals the molecular features required for the function of this evolutionarily conserved trafficking machinery.

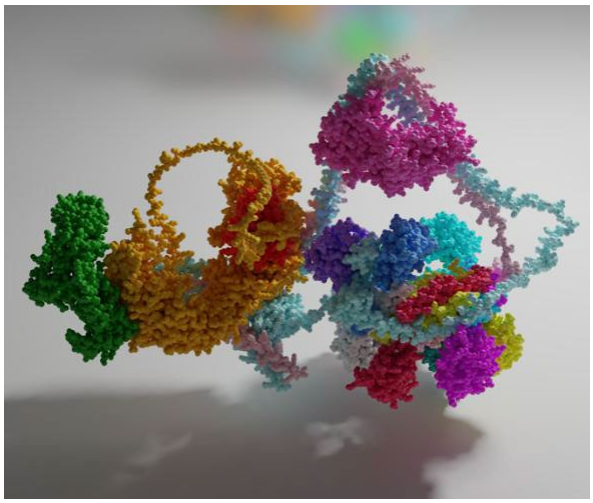

Figure 1. Structure of the sixteen subunit Commander protein complex.

1. Healy MD, McNally KE, Butkovič R, Chilton M, et al.,… Collins BM, Cullen PJ. Structure of the endosomal Commander complex linked to Ritscher-Schinzel syndrome. Cell. 2023 May 11;186(10):2219-2237.e29. doi: 10.1016/j.cell.2023.04.003. PMID: 37172566.

A015-04-280823

Molecular structure of the intact *Salmonella* flagellar basal body

Johnson[1,2*], E. J. Furlong[1,3*], J. C. Deme[1,2,4], A. L. Nord[5,6], J. J. E. Caesar[1,4], F. F. V. Chevance[7], R. M. Berry[5], K. T. Hughes[7], S. M. Lea[1,2,4]

*[1.] Sir William Dunn School of Pathology, University of Oxford, Oxford, United Kingdom, [2]Center for Structural Biology, National Cancer Institute, Frederick, Maryland, United States of America, [3]Research School of Biology, Australian National University, Acton, ACT, Australia, [4]Central Oxford Structural Molecular Imaging Centre, University of Oxford, Oxford, United Kingdom, [5]Department of Physics, University of Oxford, Oxford, United Kingdom, [6]Centre de Biologie Structurale, Universite de Montpellier, Montpellier, France, [7]Department of Biology, University of Utah, Salt Lake City, Utah, United States of America, *Contributed equally*

emily.furlong@uqconnect.edu.au

Keywords: bacteria, cryo-EM, structural biology, bacterial flagellar motor, membrane proteins

Bacterial flagella self-assemble a strong, multi-component drive shaft that couples rotation in the inner membrane to the microns-long flagellar filament that powers bacterial swimming motility. We purified flagellar basal bodies from *Salmonella* and used cryo-electron microscopy to solve structures of the intact multi-megadalton complex, to resolutions between 2.2 and 3.7 Å [1]. The structures reveal molecular details of how 173 protein molecules of 13 different types assemble into a complex spanning two membranes and a cell wall. The helical drive shaft is intricately interwoven with the inner membrane rotor component at one end, and at the other passes through a molecular bearing that is anchored in the outer membrane via interactions with the lipopolysaccharide. Additionally, the *in situ* structure of the hook capping complex at the top of the drive shaft provides insight into the assembly process of this molecular machine.

1. Johnson, S., Furlong, E. J., Deme, J. C., Nord, A. L., Caesar, J. J. E., Chevance, F. F. C., Berry, R. M., Hughes, K. T. & Lea, S. M. (2021) *Nat. Microbiol.* **6**, 712-721.

A015-05-280823

A multifaceted approach: Structural investigation of a filamentous bacterial phage secretion system

E. Mansfield[1], P. G. Young[1], D. C. Goldstone[1], I. D. Hay[1]

[1]School of Biological Sciences, The University of Auckland, Auckland, New Zealand

evie.mansfield@auckland.ac.nz

Keywords: Bacteriophage, Filamentous, Membrane protein, Protein complex, Electron microscopy, Tomography, SEC-MALS, SEC-SAXS, X-ray crystallography

Bacteriophages are the predominant biological entity on Earth [1]. However, despite being among the earliest and best characterised phage family and forming the basis of many tools in molecular biology, we have only recently begun to understand the global diversity and biological impact that the filamentous phage (family *Inoviridae*) have on our biosphere [2]. The filamentous phage are unique in that they can establish a chronic infection, where the phage progeny exit a host cell via a purpose-built phage assembly and secretion system present in the bacterial cell envelope; meaning the host cell is not typically lysed, and the phage evades our detection.

As a result, the structural organisation and complex interaction of this unusual trans-envelope nanomachine is largely uncharacterised. We outline our progress in characterising both the individual components and the interaction interface of this membrane spanning system using a variety of structural technologies, by utilizing traditional crystallography and biophysical techniques, as well as electron microscopy to elucidate this complex system.

[1] Roux, S., Krupovic, M., Daly, R.A. et al. Cryptic inoviruses revealed as pervasive in bacteria and archaea across Earth's biomes. Nat Microbiol 4, 1895–1906 (2019).
[2] Hay, I. D., & Lithgow, T. (2019). Filamentous phages: masters of a microbial sharing economy. EMBO reports, **20**(6), e47427.

A015-06-280823

Tomography studies of the dengue fusion process

J.S.G. Ooi[1,2,8], A.W.K. Tan[1,2,8], S. Wang[3,8], V. Kostyuchenko[1,2], T.S. Ng[1,2], R. Kiewisz[4], E.X.Y. Lim[1,2], X.N. Lim[1,2], G. Fibriansah[1,2], J.K. Marzinek[5], J. Shi[2.6], P.J. Bond[5], M.C. Morais[7], T. Bepler[4], M. Kudryashev[3,*], S.M. Lok[1,2,*]

*[1]Programme in Emerging Infectious Diseases, Duke-National University of Singapore Medical School, 169857 Singapore, [2]Center for BioImaging Sciences, National University of Singapore, 117557 Singapore, [3]Max-Delbrück-Centrum für Molekulare Medizin (MDC), 13092 Berlin, Germany, [4]Simons Machine Learning Center, New York Structural Biology Center, New York, NY 10027, USA, [5]Bioinformatics Institute, A*STAR (Agency for Science, Technology and Research), Singapore, [6]Department of Biological Sciences, National University of Singapore, 138671 Singapore, [7]Department of Molecular and Cellular Biochemistry, Indiana University, Bloomington, IN 47405, USA, [8]These authors contributed equally,*

**Corresponding authors. sheemei.lok@duke-nus.edu.sg, mikhail.kudryashev@mdc-berlin.de*

Keywords: dengue, fusion, tomography

Dengue virus (DENV), a flavivirus, utilizes the endocytic pathway for cell entry. Previous crystal structures of envelope (E) protein ectodomain pre-fusion dimers and the post-fusion trimers reveal only the start- and end-stages of the fusion process, with intermediate remaining uncharacterized. Here, we used a combination of cryoEM tomography and biochemical assays to study the fusion intermediate structures of DENV with liposomes at pH conditions mimicking those of the early (pH6.5) to late endosomal (pH6.0) environment. At pH6.5, virus is attracted to liposomes but no E protein insertion is observed. At pH6.0, segmentation of cryoET tomograms collected with a Volta-phase plate consistently showed that the E protein monomers located at the center of the interaction site have flipped up to interact with the adjacent liposomal membrane, whereas flipped-up monomers located at the periphery of the interaction site have their previously membrane-associated stem regions likely extended. The E protein trimers in the extended form were also observed consistently at the periphery of the interaction site, suggesting trimerization between the extended E monomers. We also collected cryoET data without using a Volta phase plate and manually picked E protein densities at these interaction sites. Subtomogram averaging and classification of these densities yielded three structural classes: (i) short E monomers normal to the liposomal membrane, (ii) longer E protein monomers tilted relative to the liposomal membrane, and (iii) a C3-symmetric density consistent with three E protomers in a looser association than seen in the post-fusion trimer. We then applied a machine learning approach to automatically segment the viral and liposomal membranes in order to measure viral-to-liposomal membrane separation at each of these aligned subtomogram positions, for each class. These results showed that the tilted monomer class likely represents a mixture of tilted E proteins of different lengths, based on whether the stem region is extended. These results are consistent with the conclusions from our segmentation experiments. Our results document important intermediate stages of the virus-liposome fusion process.

A044 High-pressure Quantum Crystallography
Room 209
4.00pm - 6.30pm

A044-01-280823

Determining the structures responsible for the superconducting properties in selected metal and metal hydrides under high pressure conditions

Arthur Haozhe Liu[1], Lisa Luhongwang Liu[2,3]

1. HPSTAR, Beijing, 100094, China
2. University of Illinois at Urbana Champaign, IL, 61801, USA
3. SHARPS, Shanghai, 201203, China

lisaliu@illinois.edu, haozhe.liu@hpstar.ac.cn

Keywords: High pressure, High T_c superconductor, Phase transitions

It was suggested that superhydrides are likely to be a step toward metallic hydrogen since the "chemically pre-compressed" hydrogen in the superhydrides can decrease the critical pressure required for the metallization [1-14]. For example, calcium hydrides, CaH_n (n=2, 4, 6…) were predicted to have stable structures at high pressure and show superconductivities. We just discovered experimentally the superconductivity with critical temperature $T_c \sim 210$ K in Ca-H system which was synthesized at high pressure and high temperature conditions [15]. Based on the *in situ* synchrotron XRD results, we tentatively assigned the superconducting phase as CaH_6, with the possibility that other calcium hydrides with even more hydrogen content, such as CaH_{12} and CaH_{10}, co-exist in the superconducting sample. Among these calcium hydrides, the $Im\bar{3}m$ phase of CaH_6, $C2/m$ phase of CaH_9, $R\bar{3}m$ phase of CaH_{10} and $C2/m$ phase of CaH_{12} have been predicted to host superconductivity with T_c about 235 K @ 150 GPa [4], 266 K @ 300 GPa [9], 175 K @ 400 GPa [9] and 206 K @ 150 GPa [2], respectively. Therefore, the possibility that the high temperature superconductivity found in Ca-H sample arises from the other calcium hydrogen phases above 150 GPa should be carefully investigated. In this presentation, the collaborative effort and recent progress on determining the responsible structures in selected metal and metal hydrides, such as titanium and Hf-H system [16, 17], will be introduced. These researches will enrich our understanding on the relationship of structure and superconductivity in metal hydrides under high pressure conditions, and then find more superconducting materials with high T_c in related metal and metal hydrides.

1. N. W. Ashcroft, *Phys. Rev. Lett*. **92**, 187002 (2004)
2. D. V. Semenok, et al, *Curr Opin Solid St M* **24**, 100808 (2020)
3. P. Drozdov, et al, *Nature* **525**, 73 (2015)
4. H. Wang, et al, *PNAS* **109**, 6463 (2012)
5. F. Peng, et al, *Phys. Rev. Lett*. **119**, 107001 (2017)
6. H. Y. Liu, et al. *PNAS* **114**, 6990 (2017)
7. P. P. Kong, et al, *Nat. Commun*. **12**, 5075 (2021)
8. J. A. Flores-Livas, et al, *Phys. Rep*. **856**, 1 (2020)
9. Z. J. Shao, et al, *Inorg. Chem*. **58**, 2558 (2019)
10. P. Drozdov, et al, *Nature* **569**, 528 (2019)
11. Z. M. Geballe, et al, *Angew. Chem. Int. Edit* **57**, 688 (2018)
12. M. Somayazulu, et al, *Phys. Rev. Lett*. **122**, 027001 (2019)
13. F. Hong, et al, *Chin. Phys. Lett*. **37**, 107401 (2020)
14. E. Snider, et al, *Phys. Rev. Lett*. **126**, 117003 (2021)
15. Z. Li, et al, *Nat. Commun*, **13**, 2863 (2022)
16. C. Zhang, et al, *Nat. Commun*, **13**, 5411 (2022)
17. C. Zhang, et al, *Mater. Today Phys*, **27**, 100826 (2022)

This work was supported by the Natural Science Foundation of China. Portions of this work were performed at GeoSoilEnviroCARS (The University of Chicago, Sector 13), Advanced Photon Source (APS), Argonne National Laboratory. GeoSoilEnviroCARS is supported by the National Science Foundation – Earth Sciences (EAR – 1634415) and Department of Energy- GeoSciences (DE-FG02-94ER14466). This research used resources of APS, a U.S. Department of Energy (DOE) Office of Science User Facility operated for the DOE Office of Science by Argonne National Laboratory under Contract No. DE-AC02-06CH11357.

A044-02-280823

Accurate crystal structures of ices from X-ray and ED with Hirshfeld atom refinement

K. Woźniak[1], M. Chodkiewicz[1], R. Gajda[1], V. B. Prakapenka2, P. Dera[3]

[1]University of Warsaw, Chemistry Department, Pasteura 1, 02093 Warszawa, Poland [2]Advanced Photon Source, Argonne National Laboratory, 9700 South Cass Avenue, Lemont, IL 60439, USA, [3]Hawai'i Institute of Geophysics and Planetology, Université d'hawaï à mānoa, 1680 East-West Road, Honolulu, HI 96822, USA

kwozniak@chem.uw.edu.p

Keywords: Ice, HAR, Quantum Crystallography

Background. Water is an essential chemical compound for living organisms, and twenty of its different crystal solid forms (ices) are known. Still, there are many fundamental problems with these structures such as establishing the correct positions and thermal motions of hydrogen atoms. The list of ice structures is not yet complete as DFT calculations and spectroscopic measurements have suggested existence for additional as of yet unknown phases. In many ice structures, neither neutron diffraction nor DFT calculations nor X-ray diffraction methods can easily solve the problem of hydrogen atom disorder or accurately determine their atomic displacement parameters.

Methods. We applied a new way of refinement of single crystal high pressure X-ray synchrotron and laboratory X-ray and electron diffraction data called Hirshfeld Atom Refinement. This method utilizes aspherical atomic scattering factors (X-rays), and aspherical atomic electrostatic potentials (ED), based on so called stockholder (Hirshfeld) partition and is especially effective in the case of refinement of crystals of H-rich compounds.

Results. Here we present accurate crystal structures of H_2O, D_2O and mixed (50%H_2O/50%D_2O) ice VI and ice VII obtained by Hirshfeld Atom Refinement (HAR) against high pressure single crystal synchrotron and laboratory X-ray diffraction data as well as results of refinement of hexagonal ice obtained by HAR against electron diffraction data. It was possible to obtain O-H bond lengths and anisotropic atomic displacement parameters for disordered hydrogen atoms which are in good agreement with the corresponding results of single crystal neutron diffraction data.[1]

Conclusions. Our results show that Hirshfeld atom refinement against X-ray diffraction and electron diffraction data is a tool which can compete with neutron diffraction in detailed studies of polymorphic forms of ice and crystals of other hydrogen rich compounds. As neutron diffraction is relatively expensive, requires larger crystals which might be difficult to obtain, and access to neutron facilities is restricted, cheaper and more accessible X-ray measurements combined with HAR can facilitate the verification of the existing ice polymorphs and the quest for the new ones.[1]

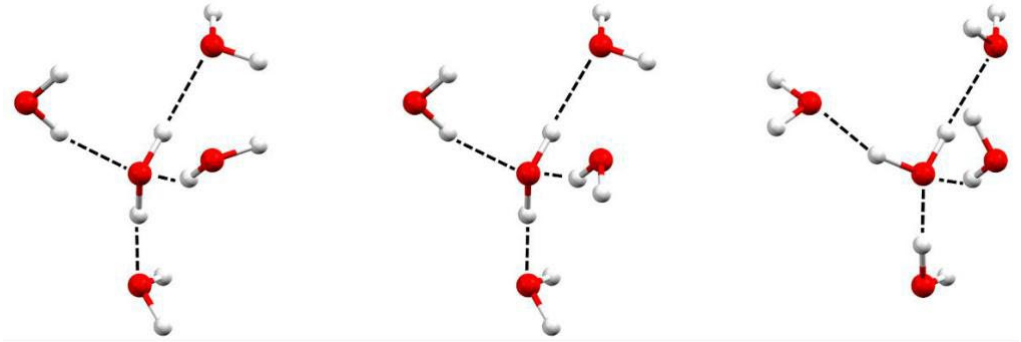

Figure 1. Examples of water clusters (259 in total) considered for ice VI.

Financial support of this work by the National Science Centre, Poland, through OPUS 21 grant number DEC-2021/41/B/ST4/03010 is gratefully acknowledged. The work was accomplished at the TEAM TECH Core Facility for crystallographic and biophysical research to support the development of medicinal products sponsored by the Foundation for Polish Science (FNP) and at the Cryoelectron Microscopy and Electron DIffraction Core Facility at CENT (Univercity of Warsaw, Poland). The synchrotron radiation experiments were performed at the APS (Proposal No. GUP-71134) and DESY (Proposal I-20200083 EC).

[1] Chodkiewicz, M. L., Gajda, R., Lavina, B., Tkachev, S., Prakapenka, V. B., Dera, P. & Woźniak, K. (2022). Accurate crystal structure of ice VI from X-ray diffraction with Hirshfeld Atom Refinement, *IUCRJ*, **9**, 573-579.

A044-03-280823

Luminescent Materials at High-Pressure: Why Crystal Orientation Matters

A. Makal[1]

[1] *University of Warsaw, Chemistry Department, ul. Zwirki i Wigury 101, 02-089 Warsaw, Poland*

am.makal@uw.edu.pl

Keywords: high-pressure, X-ray diffraction, diffraction data completeness, diffraction data quality

Solid state luminophores make inviting targets for high-pressure structural studies owing to their sensitivity to molecular and crystalline environment. Application of quasi-hydrostatic pressure can serve as a means to modify crystalline environment in a controllable manner or induce phase transitions. As a result, applied pressure can modify and regulate chemical bonding, intermolecular interactions and derived physicochemical properties, such colour [1], luminescence emission wavelength and quantum efficiency [2]. Modern quantum crystallography tools, such as TAAM or HAR approaches, allow studying such properties and their evolution with pressure in more detail [3].

Unfortunately, experiments performed at high pressure in a diamond anvil cells (DAC) yield inherently biased intensities and incomplete datasets. The lack of completeness alone may impede space group determination, render solution of a crystal structure or determination of absolute configuration impossible, and conceal or misrepresent fine details such as disorder or unusual charge density distribution (Fig. 1). While data completeness is less of an issue in a regular crystal system, where abundance of symmetry elements allows for the retrieval of almost all unique reflections, the majority of interesting organic and metalorganic materials tend to crystallize in lower-symmetry systems (like monoclinic) or transform to low-symmetry phases as the pressure is increased. The fact that sample orientation in a DAC can improve reciprocal space coverage is generally acknowledged throughout the high-pressure crystallographic community [4, 5]. However, the extent to which data completeness can be improved by proper sample placement and how much can actually be gained by it has not been systematically investigated until recently.

In this presentation, I will present examples where carefully planned *in-house* experiments and controlled sample orientation allowed to study pressure-induced, symmetry-lowering phase transitions in luminescent organic [6] and organometallic materials. Effective sample orientation and careful data processing has ensured over 90% coverage even for the monoclinic system and enabled unrestrained structure refinements in TAAM formalism and access to complete systematic extinction patterns. I will also shortly comment on what artefacts would have arisen had the datasets been less complete.

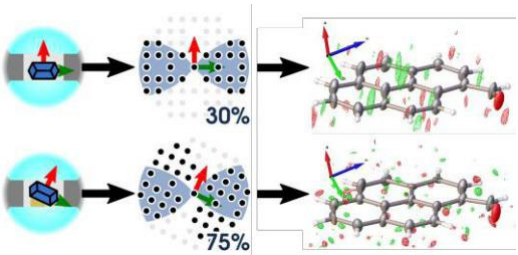

Figure 1. The crystal orientation in a DAC affects attainable data completeness and features in the residual density map.

[1] Nogueira, B. A., Castiglioni, C.; Fausto, R., (2020). *Communications Chemistry*, **3**, 2399-3669.
[2] Tchoń, D., Trzybiński, D., Wrona-Piotrowicz, A., Makal, A., (2019). *CrystEngComm*, **21**, 5845-5852.
[3] Casati, N., Genoni, A., Meyer, B., Krawczuk, A., Macchi, P., (2017). *Acta Cryst.*, **B73**, 584-597.
[4] Dziubek, K., Katrusiak, A., (2002). *Defect Diffus. Forum*, 208-209, 319-322.
[5] Dawson, A., Allan, D.R., Parsons, S., Ruf, M., (2004). *J. Appl. Cryst.*, **37**, 410-416.
[6] Tchoń, D., Makal, A., (2021). *IUCrJ,* **8**, 1006-1017

A044-04-280823

High-pressure x-ray crystallographic investigation of chalcogen bonding

Robinson[1,*], G. Turner[1], A. Summers[1], I. Jones[1], S. Moggach[1], S. Boer[2], J. White[3]

The University of Western Australia, 35 Stirling Highway Crawley WA 6009 Australia
Australian Synchrotron, 800 Blackburn Road Clayton VIC 3168 Australia
The University of Melbourne, Grattan Street Parkville VIC 3010 Australia

hayden.robinson@research.uwa.edu.au

Keywords: High-pressure, Chalcogen Bonding, Organoselenium Molecules

Non-covalent interactions play a central role across a broad range of fields including drug design, molecular biology, and crystal engineering. Chalcogen bonding, a close relative of hydrogen and halogen bonding, is one such non-covalent interaction that is known to occur in crystalline solids.[1]

Ebselen is an organoselenium molecule that is known to exhibit anti-inflammatory and anti-viral properties,[2] and as a crystalline solid it has previously been shown to form chalcogen bonds in part due to its Se-N covalent bond.[3,4] Many derivatives of ebselen exist, and are also likely to form chalcogen bonding interactions, however not a lot is known about what would happen to these interactions under high-pressure conditions. Is there a shortening of the intermolecular chalcogen bond length, does the chalcogen bonding interaction become more stable, or is there a phase transition that alters the binding motif under high-pressure conditions?

To answer these questions, derivatives of ebselen have been investigated utilising high-pressure x-ray crystallography to better understand what happens to chalcogen bonding interactions when subjected to high-pressure conditions. Recently, the ebselen derivative 2-(3-pyridyl)-1,2-benzisoselenazol-3(2H)-one was investigated at the Australian Synchrotron, where structural information was determined at various pressures that range from ambient conditions up to 5.5 GPa, with a phase transition occurring at approximately 3 GPa. The chalcogen bond interaction was shown to occur between the pyridyl nitrogen and the selenium, with the intermolecular bond length decreasing under high pressure conditions.

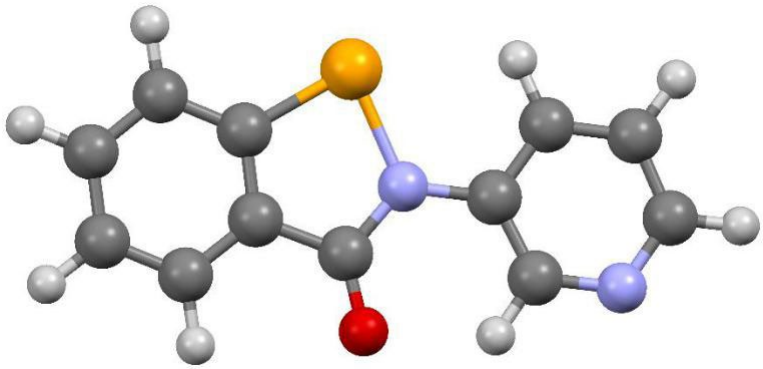

Figure 1. Structure of 2-(3-pyridyl)-1,2-benzisoselenazol-3(2H)-one, a derivative of ebselen, under ambient conditions.

1. P. Scilabra, G. Terraneo, G. Resnati, *Acc. Chem. Res*. **2019**, *52*, 1313-1324.
2. H. Sies, M. J. Parnham, *Free Radic. Biol. Med*. **2020**, *156*, 107-112.
3. T. Fellowes, J. M. White, *CrystEngComm* **2019**, *21*, 1539-1542.
4. S. P. Thomas, K. Satheeshkumar, G. Mugesh, T. N. Guru Row, *Chem. Eur. J*. **2015**, *21*, 6793-6800.

A044-06-280823

Near Ambient Superconductivity in a N-doped Lutetium Hydride

N. Dasenbrock-Gammon[1], E. Snider[2], R. McBride[2], H. Pasan[1], Dy. Durkee[1], N. Khalvashi-Sutter[2], S. Munasinghe[2], S. E. Dissanayake[2], K. V. Lawler[3], A. Salamat[3], R. P. Dias[1,2*]

[1]Department of Physics and Astronomy, University of Rochester, Rochester, NY 14627, USA.[2]Department of Mechanical Engineering, School of Engineering and Applied Sciences, University of Rochester, Rochester, NY 14627, USA. [3]Unearthly Materials Inc., Rochester, NY 14627, USA.

Email of communicating rdias@rochester.edu

Keywords: Superconductivity, Quantum Materials, High pressures physics

The absence of electrical resistance exhibited by superconducting materials would have enormous potential for applications if it existed at ambient temperature and pressure conditions. Despite decades of intense research efforts, such a state has yet to be realized. At ambient pressures, cuprates are the material class exhibiting superconductivity to the highest critical superconducting transition temperatures (T_c) – up to ~133K [1]. Over the last decade, high pressure 'chemical precompression' [2] of hydrogen-dominant alloys has led the search for high temperature superconductivity, with demonstrated T_c approaching the freezing point of water in binary hydrides at megabar pressures [3]. Ternary hydrogen-rich compounds, such as carbonaceous sulfur hydride, offer an even larger chemical space to potentially improve the properties of superconducting hydrides. Here, we report evidence of superconductivity on a nitrogen-doped lutetium hydride with a maximum T_c of 294 kelvin at 10 kilobar, that is, superconductivity at room temperature and near-ambient pressures. The compound was synthesized under high pressure-temperature conditions, and then, after full recoverability, its material and superconducting properties were examined along compression pathways. These include temperature dependent resistance with and without an applied magnetic field, the magnetization M-H curve, a.c. and d.c. magnetic susceptibility, as well as heat capacity measurements. X-ray diffraction, EDX, and theoretical simulations provide insight into the stoichiometry of the synthesized material.

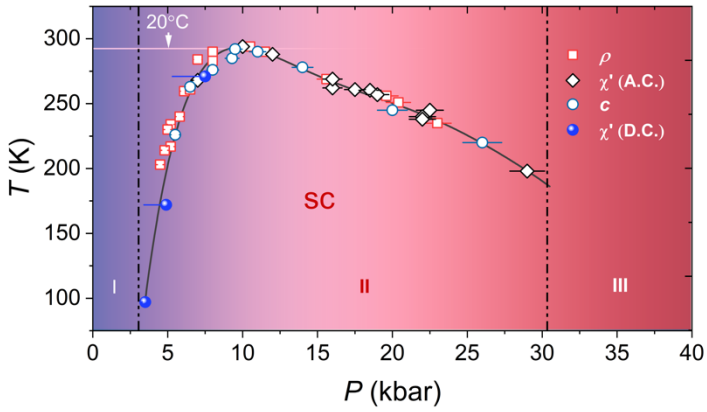

Figure 1. Evolution of the superconducting transition temperature of nitrogen doped lutetium hydride as a function of pressure.

[1] Bednorz, J. G. & Müller, K. A. Possible highTc superconductivity in the Ba−La−Cu−O system. *Zeitschrift für Phys. B Condens. Matter* **64**, 189-193 (1986).
[2] Ashcroft, N. W. Hydrogen dominant metallic alloys: High temperature superconductors? *Phys. Rev. Lett.* **92**, 187002 (2004).
[3] Liu, H., Naumov, I. I., Hoffmann, R., Ashcroft, N. W. & Hemley, R. J. Potential high- T c superconducting lanthanum and yttrium hydrides at high pressure. *Proc. Natl. Acad. Sci.* **114**, 6990–6995 (2017).

This research was supported by NSF, Grant No. DMR-2046796, Unearthly Materials Inc., and US Department of Energy, Office of Science, Fusion Energy Sciences under award number DE-SC0020340.

A061 Magnetism in Topological Materials
Room 217
4.00pm - 6.30pm

A061-01-280823

Interplay between magnetism and electronic band topology

Jian-Rui Soh 1, A. T. Boothroyd 2

1 EPFL, Lausanne, Switzerland; 2 Clarendon Laboratory, Department of Physics, Oxford University

jian.soh@epfl.ch

Keywords: Non-trivial topology, magnetic structure, polarised and unpolarised neutrons

The exploration of magnetic materials with topologically non-trivial electronic band structure has become a key topic of quantum materials physics. The goal of our research is to find novel materials where the electronic states can be controlled by their magnetic order.

We have studied a wide range of materials where the non-trivial topological properties in the electronic band structure are endowed by the corresponding ground state magnetic order. These include $Co_3Sn_2S_2$, Mn_3Ge, $YbMnBi_2$, $YbMnSb_2$, $EuMnSb_2$, EuCuAs, $EuIn_2P_2$ [1-7]. Our careful magnetic structure determination of the topological materials with polarised and unpolarised neutron diffraction indicate that *ab- initio* calculations usually predict the wrong type of magnetic structure. Instead, neutron diffraction remains the most **decisive** tool to determine the topology of the electronic band structure in these magnetic topological materials.

In my talk, I will give an overview of material systems which display a strong coupling between magnetism and the topology of the electronic bands. I will highlight systems where the magnetic configuration is key to their non-trivial topological properties, from a symmetry perspective. Next, I will outline several of our studies where neutron diffraction has been decisive in the determination of the topology of the electronic bands by the careful study of the magnetic order. Finally, I will discuss some future directions for the field of magnetic topological materials.

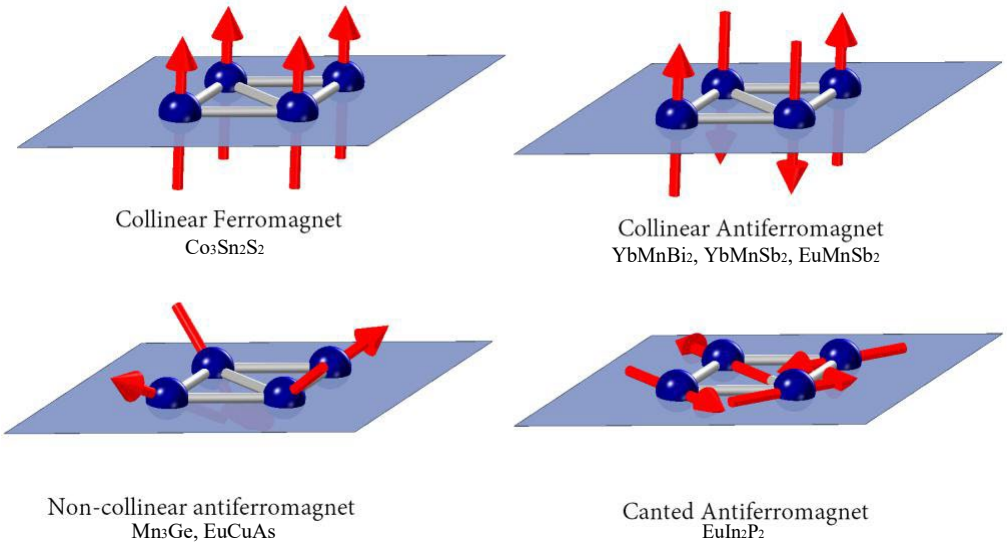

Figure 1. Various magnetic configurations of topological materials.

[1] J.-R. Soh, C. Yi, I. Zivkovic, N. Qureshi, A. Stunault, B. Ouladdiaf, J. A. Rodriguez-Velamazan, Y. Shi, H. Ronnow and A. T. Boothroyd Phys. Rev. B 105, 094435 (2022)
[2] J.-R. Soh, F. de Juan, N. Qureshi, H. Jacobsen, H.-Y. Wang, Y.-F. Guo, and A. T. Boothroyd Phys. Rev. B 101, 140411R (2020)
[3] J.-R. Soh, H. Jacobsen, B. Ouladdiaf, A. Ivanov, A. Piovano, T. Tejsner, Z. Feng, H. Wang, H. Su, Y. Guo, Y. Shi, and A. T. Boothroyd Phys. Rev. B 100, 144431 (2019)
[4] J.-R. Soh, S. M. Tobin, H. Su, I. Zivkovic, B. Ouladdiaf, A. Stunault, J. A. Rodriguez-Velamazan, K. Beauvois, Y. Guo, and A. T. Boothroyd Phys. Rev. B 104, L161103 (2021)
[5] J.-R. Soh, P. Manuel, N. M. B. Schröter, C. J. Yi, F. Orlandi, Y. G. Shi, D. Prabhakaran, and A. T. Boothroyd
[6] J.-R. Soh, A. Stunault, J. A. Rodriguez-Velamazan, D. Prabhakaran and A. T. Boothroyd (in preparation)
[7] J.-R. Soh, X. Yang, A. Urru, W. R. Pudelko, S. Francoual, S. A. Ekahana, O. Zaharko, D. Yevtushynsky, D. Tolj, I. Zivkovic, A. Stunault, J. A. Rodriguez-Velamazan, Y. Shi, N. A. Spaldin, J. Hugo Dil, H. M. Ronnow (in preparation)

A061-02-280823

Magnetic soliton layers in epitaxial MnSi

G. L. Causer[1], M. Azhar[2], T. Hesjedal[3], M. Garst[2], C. Pfleiderer[1]

[1]Physics Department, Technical University of Munich, 85748 Garching, Germany, [2]Institute of Theoretical Solid State Physics, Karlsruhe Institute of Technology, 76131 Karlsruhe, Germany, [3]Clarendon Laboratory, Department of Physics, University of Oxford, Oxford OX1 3PU, United Kingdom

grace.causer@tum.de

Keywords: thin films, magnetism, small-angle neutron scattering, mumax

We have charted the phase diagram of epitaxial MnSi films grown on Si(111) by magnetometry, differential susceptibility, extended X-ray absorption fine structure, planar Hall, polarised neutron reflectometry and small-angle neutron scattering [1-3]. Our experimental results are supported by micromagnetic simulations, which jointly reveal a magnetic phase diagram dominated by a field-induced cascade of single-Q soliton layers. The soliton layers are stabilized through the applied field which modifies a zero-field, out-of-plane propagating helix with $\lambda = 11.5$ nm. Field and temperature history provide specific routes for the nucleation of the distinct soliton phases, comprising of four-, three-, two-, and single-soliton layers depending on the field strength. At low temperatures ($T < 10$ K) a discrete phase regime can be discerned unambiguously in the susceptibility, which may be attributed to the irreversibility of the two-soliton and single-soliton regimes. These observations provide insights into the integral role of magnetic anisotropy and dimensionality on the low-temperature phase diagram of thin film MnSi.

[1] Wiedemann, B., Chacon, A., Zhang, S. L., Khaydukov, Y., Hesjedal, T., Sotlwedel, O., Keller, T., Mühlbauer, S., Adams, T., Halder, M., Pfleiderer, C. & Böni, P. (2017). arXiv:1710:00544 [cond-mat.str-el]
[2] Figueroa, A. I., Zhang, S. L., Baker, A. A., Chalasani, R., Kohn, A., Speller, S. C., Gianolio, D., Pfleiderer, C., van der Laan, G., & Hesjedal. T. (2016). Phys. Rev. B **94**, 174107
[3] Causer, G. L., Chacon, A., Heinemann, A. & Pfleiderer, C. (2022). *J. Appl. Cryst.* **55**, https://doi.org/10.1107/S1600576722010755.

This work has been funded by the Deutsche Forschungsgemeinschaft (DFG, German Research Foundation) under TRR80 (From Electronic Correlations to Functionality, project No. 107745057, Project F7), the priority program SPP 2137 (Skyrmionics) under grant PF393/19 (project-id 403191981) and the excellence cluster MCQST under Germany's Excellence Strategy EXC-2111 (project No. 390814868). Financial support by the European Research Council (ERC) through Advanced Grants No. 291079 (TOPFIT) and No. 788031 (ExQuiSid) is gratefully acknowledged.

A061-03-280823

Phase Transformations In Chiral Magnets

C. Pappas[1], M. Crisanti[1], L. J. Bannenberg[1], R. Cubitt[2], E. Lelièvre-Berna[2], A. Lahb[1], D. Alba Venero[3], J. White[4], H. Wilhelm[5,6], Marcus P. Schmidt[7], M. Mostovoy[8]. A.O. Leonov[9,10.11]

[1]Faculty of Applied Sciences, Delft University of Technology, Mekelweg 15, 2629 JB Delft, The Netherlands.
[2]Institut Laue-Langevin, 71 Avenue des Martyrs, CS 20156, 38042 Grenoble, France.
[3]ISIS Neutron Source Didcot OX11 0QX, Didcot, UK.
Laboratory for Neutron Scattering and Imaging, CH-5232 Villigen PSI , Switzerland.
[5]Diamond Light Source Ltd., OX11 0DE Didcot, UK.
[6]Helmholtz-Institute Ulm, Helmholtz-Stra.e 11, 89081 Ulm, Germany.
[7]Max Planck Institute for Chemical Physics of Solids, 01187 Dresden, Germany.
[8]University of Groningen, The Netherlands.
[9]Department of Chemistry, Faculty of Science, Hiroshima University, Japan.
[10]IFW Dresden, Postfach 270016, D-01171 Dresden, Germany.
[11]International Institute for Sustainability with Knotted Chiral Meta Matter, Higashi Hiroshima, Hiroshima Japan.

Email of communicating c.pappas@tudelft.nl

Keywords: Chiral Magnetism, Phase Transitions, Skyrmions.

The lack of inversion symmetry in the crystal lattice of magnetic materials gives rise to complex noncollinear spin orders through the Dzyaloshinskii-Moriya interaction, resulting in new physical phenomena, such as emergent electromagnetism. In the archetype cubic chiral magnets a universal magnetic phase diagram has been found composed of helical spiral, conical spiral, and the skyrmion lattice phase. The latter appears in a narrow region of the phase diagram, the so-called A-phase, just below the magnetic ordering temperature.

Recent SANS and magnetization measurements on the Mott insulator Cu_2OSeO_3, however, indicate remarkable deviations from this universal behavior [1-5]. Just below the critical field at which the conical spiral state disappears, the spiral wave vector rotates away from the magnetic field direction and a new multidomain state sets-in. This new phase occurs where it is least expected, at low temperatures, where thermal spin fluctuations are suppressed, and at magnetic fields strong enough to align all spirals along their direction [1]. This instability of the conical spiral state, which can be considered as a re-entrance into the helical state, is sensitive to the direction of the magnetic field and occurs only when the field is applied along the [001] easy crystallographic axis. This tilted spiral state originates from the interplay of competing anisotropies, which are generic to chiral magnets, and may stabilize novel skyrmionics states in a wide range of magnetic fields and temperatures, beyond the A-phase [2,3].
Indeed, SANS experiments show that, depending on the magnetic history, extremely robust skyrmionic states can be produced in large areas of the magnetic phase diagram, from the lowest temperatures up to the A-phase [4, 5]. Nascent and disappearing spiral states near critical lines catalyze topological charge changing processes, leading to the formation and destruction of skyrmionic states at low temperatures, which are thermodynamically stable or metastable depending on the orientation and strength of the magnetic field. The metastable low temperature skyrmions are surprisingly resilient to high magnetic fields: the memory of skyrmion states persists in the field polarized state, even when the skyrmion lattice signal has disappeared [5].

In an attempt to reach quantitative agreement between the experiment and theory, we find that the temperature dependent anisotropy constants are the drivers behind the observed behaviour [6,7]. This quantitative comparison between experiment and theory provides an in-depth understanding of chiral magnets in view of tailoring their properties for future applications.

[1] F. Qian, L. J. Bannenberg, H. Wilhelm, G. Chaboussant, L. M. DeBeer-Schmitt, M. P. Schmidt, A. Aqeel, T. T. M. Palstra, E. H. Bruck, A. J. E. Lefering, C. Pappas, M. Mostovoy, and A. O. Leonov; Sci. Adv. **4**, eaat7323 (2018).
[2] A. Leonov, arXiv:1406.2177; [3] A.O. Leonov, C. Pappas; Phys.Rev.B. **99**, 144410 (2019)
[4] A. Chacon, L. Heinen, M. Halder, A. Bauer, W. Simeth, S. Mühlbauer, H. Berger, M. Garst, A. Rosch, and C. Pfleiderer, Nat. Phys. **14**, 936 (2018).
[5] L. J. Bannenberg, H. Wilhelm, R. Cubitt, A. Labh, M. Schmidt, E. Lelievre-Berna, C. Pappas, M. Mostovoy, and A. O. Leonov, NPJ Quantum Mater. **4**, 11 (2019).
[6] A.O. Leonov and C. Pappas, Phys. Rev. Research **4**, 043137 (2022).
[7] M. Crisanti, A. O. Leonov, R. Cubitt, A. Labh, H. Wilhelm, Marcus P. Schmidt, and C. Pappas submitted to Phys. Rev. Research.

A061-04-280823

SANS and μSR studies on the new state at low temperatures, "B-Phase", in MnSi

Ohkuma[1], M. Pardo-Sainz[2,3], M. Mito[1], K. Ohishi[4], Y. Kousaka[3], K. Kojima[5], K. Inoue[6], V. Laliena[2], J. Campo[2,*]

[1]Graduate School of Engineering, Kyushu Institute of Technology, Kitakyushu 804-8550, Japan; [2]Aragón Nanoscience and Materials Institute (CSIC - University of Zaragoza), 50009 Zaragoza, Spain; [3] Osaka Metropolitan University, Sakai, Osaka 599-8531, Japan; [4]Neutron Science and Technology Center, Comprehensive Research Organization for Science and Society (CROSS), Tokai, Ibaraki 319-1106, Japan; [5]TRIUMF, University of British Columbia; [6]Chirality Research Center, Hiroshima University, Higashihiroshima 739-8526, Japan

Javier.Campo@csic.es

Keywords: MnSi, DM interaction, chirality

Recently, we suggested theoretically, that at low *T* the conical (CH) and forced-ferromagnetic (FFM) phases in cubic helimagnets, are not connected but are separated by another Skyrmion Lattice phase (SkL), which could be metastable, and a new phase of unknown nature just below the critical field *H*c at low *T* [1]. The theoretical prediction of the new SkL phase at low *T* is in good agreement with the experiments reported in ref [2,3]. On the other hand, by using careful ac susceptibility at low temperature, we determined the magnetic phase diagrams of oriented crystals of MnSi [4] in which a new phase (*B-phase)* emerges which could be consistent with the theoretical prediction for the new unknown low temperature phase.

In order to clarify the nature of this *B-phase* at low *T* near critical field, we performed SANS measurements at TAIKAN in J-PARC and muon spin rotation (μSR) measurements at M15 in TRIUMF. Figure 1 shows the magnetic field dependence of the SANS patterns at 2 K. At both 0.3 T and 0.5 T the SANS patterns show two peaks along the horizontal axis in Fig. 1(a) and (b) for $H \perp$ in coming neutron beam wave vector $\boldsymbol{ki}$. These are the magnetic Bragg peaks of the conical state. On the other hand, as shown in Fig. 1(c) and (d), no diffraction peaks were observed for H // $\boldsymbol{ki}$, in which, for example, a six-fold-symmetric diffraction pattern due to a formation of SkL is observed in SkL. These results suggest the CH phase exists in *B-phase* being different from the *A*-phase near *T*c. According to the μSR results, we found the internal magnetic field distribution in *B-phase* is apparently different from that in CH at low fields and FFM phases, consistent with the SANS results.

In the presentation, we will talk about the results of both SANS and μSR in detail, and discuss a spin texture in *B-phase*.

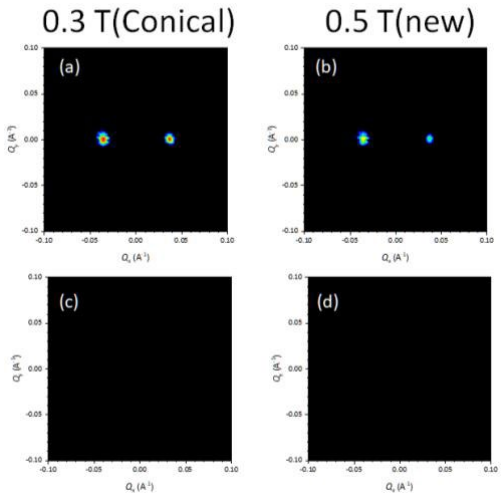

Figure 1. *H* dependence of the SANS patterns at 2 K (a,b) with the condition of H // [111] $\perp \boldsymbol{k}_i$, and (c,d) that of H // [111] // $\boldsymbol{k}_i$.

1. V. Laliena and J. Campo, Phys. Rev. B 96, 134420 (2017).
2. H. Oike et al., Nat. Phys. 10, 62 (2016).
3. T. Nakajima et al., Phys. Rev. B 98, 014424 (2018).
4. M. Ohkuma et al., APL Mater. 10, 041104 (2022);

A061-05-280823

The double-Q ground state with topological charge stripes in the skyrmion candidate $GdRu_2Si_2$

D. A. Wood[1], D. D. Khalyavin[2], D. A. Mayoh[1], J. Bouaziz[3], A. E. Hall[1], S. J. R. Holt[4,5], F. Orlandi[2], P. Manuel[2], S. Blügel[3], J. B. Staunton[1], O. A. Petrenko[1], M. R. Lees[1], and G. Balakrishnan[1]

[1]Department of Physics, University of Warwick, Coventry, CV4 7AL, United Kingdom. [2]ISIS Facility, STFC Rutherford Appleton Laboratory, Harwell Science and Innovation Campus, Oxfordshire OX11 0QX, United Kingdom. [3]Peter Grünberg Institut and Institute for Advanced Simulation, Forschungszentrum Jülich & JARA, D-52425 Jülich, Germany. [4]University of Southampton, Southampton SO17 1BJ, United Kingdom. [5]Max Planck Institutes for the Structure and Dynamics of Matter, Luruper Chaussee 149, 22761 Hamburg, Germany

George.wood@warwick.ac.uk

Keywords: skyrmions, multi-Q, centrosymmetric

GdRu2Si2 is a centrosymmetric magnet in which skyrmion and meron lattices have recently been discovered [1,2]. The stabilisation of these extraordinary spin-textures in centrosymmetric materials is of great interest, since it is possible to realise these topologically non-trivial spin textures without a magnetic field, which is not possible in non-centrosymmetric materials which rely on the Dzyaloshinskii-Moriya interaction. The absence of magnetic field to stabilise these spin configurations significantly increases the likelihood of developing a widespread spintronic device which uses the range of emergent phenomena in these systems.

Here, we present a time-of-flight neutron experiment on single crystal and polycrystalline ^{160}GdRu2Si2 in which we have discovered a new double-Q incommensurate magnetic ground state [3]. In addition to observing the $\mathbf{q}1$ and $\mathbf{q}2$ propagation vectors, we have found magnetic satellites of the form $\mathbf{q}1+2\mathbf{q}2$. The appearance of these satellites are explained within the framework of a constant moment solution. Using powder diffraction we have implemented the first quantitative refinement of this model. The structure, which contains vortex-like motifs, is shown to have a novel one-dimensional topological charge density. More generally, this work establishes that GdRu2Si2 has a wealth of topologically non-trivial spin textures and is therefore an ideal setting in which phase transitions between distinct topological structures can be experimentally probed.

1. N. D. Khanh *et al.* Nanometric square skyrmion lattice in a centrosymmetric tetragonal magnet, Nat. Nanotechnol. 15, 444 (2020).
2. N. D. Khanh *et al.* Zoology of multiple-Q spin textures in a centrosymmetric tetragonal magnet with itinerant electrons, Adv. Sci. 9, 2105452 (2022).
[3] G. D. A. Wood *et al.* The double-Q ground state with topological charge stripes in the skyrmion candidate $GdRu_2Si_2$, (submitted) Phys. Rev. B. Letter (2023).

A061-06-280823

Topological States Protected by Magnetic Space Groups and Spin Space Groups

Zhida Song[1+], Benjamin J. Wieder[2,3,4], Luis Elcoro[5], Zhen-Yu Xiao[1], Jian-Zhou Zhao[6], Yuanfeng Xu[2,], Barry Bradlyn[7], B. Andrei Bernevig[2]

[1] International Center for Quantum Materials, School of Physics, Peking University, Beijing 100871, China
[2] Department of Physics, Princeton University, Princeton, NJ, USA
[2] Department of Physics, Massachusetts Institute of Technology, Cambridge, MA, USA
[3] Department of Physics, Northeastern University, Boston, MA, USA
[5] Department of Condensed Matter Physics, University of the Basque Country UPV/EHU, Bilbao, Spain
[6] Co-Innovation Center for New Energetic Materials, Southwest University of Science and Technology, Mianyang 621010, China.
[7] Department of Physics and Institute for Condensed Matter Theory, University of Illinois at Urbana-Champaign, Urbana, IL, USA

songzd@pku.edu.cn

Keywords: Topological States, Magnetic Materials, Magnetic Space Group, Spin Space Group

The group-theoretic characterization of crystalline solids has provided the foundational language for diverse problems in physics and chemistry. However, the group theory of crystals with commensurate magnetic order has remained incomplete for the past 70 years, due to the complicated symmetries of magnetic crystals. In this work, we (i) complete the the representation theory of the magnetic space group by deriving the small corepresentations, momentum stars, compatibility relations, and magnetic elementary band corepresentations of the 1,421 magnetic space groups (MSGs). We also (ii) extend Topological Quantum Chemistry to the MSGs to form a complete, real-space theory of band topology in magnetic and nonmagnetic crystalline solids – Magnetic Topological Quantum Chemistry (MTQC). Using a combination of real space layer construction and the MTQC method, we derive the complete set of symmetry-based indicators of electronic band topology, for which we identify symmetry-respecting bulk and anomalous surface and hinge states. In the end, we (iii) fully classify the spin space groups (SSGs) (more than 50 thousands) that characterize magnetic materials with negligible spin-orbit coupling and discuss exotic topological states protected by SSGs.

[1] L. Elcoro, B. J. Wieder, Z. Song, Y. Xu, B. Bradlyn, and B. A. Bernevig, Magnetic Topological Quantum Chemistry, Nature Communications 12, 5965 (2021).
[2] Z. Song, T. Zhang, Z. Fang, and C. Fang, Quantitative Mappings between Symmetry and Topology in Solids, Nature Communications 9, 3530 (2018).
[3] Zhen-Yu Xiao, Jian-Zhou Zhao, and Zhida Song, Full Classification of Spin Space Groups, to appear

A072 Understanding Energy System Processes and Function
Room 207
4.00pm - 6.30pm

A072-01-280823

Neutron scattering studies of bio-oil on NiMo-pillared clay catalysts for energy applications

I. B. Adilina[1,2], M. A. Fitriady[1], F. Oemry[2,3], G. B. G. Stenning[4], S. F. Parker[4]

[1]Research Center for Chemistry, National Research and Innovation Agency, Kawasan Puspiptek Serpong, Tangerang Selatan, Banten, Indonesia 15314, [2]Australian Centre for Neutron Scattering, Australian Nuclear Science and Technology Organization, Lucas Heights, NSW 2234, Australia, [3]Research Center for Quantum Physics, National Research and Innovation Agency, Kawasan Puspiptek Serpong, Tangerang Selatan, Banten, Indonesia 15314, [4]ISIS Facility, STFC Rutherford Appleton Laboratory, Chilton, Didcot, Oxfordshire, OX11 0QX, United Kingdom

Email: indr030@brin.go.id

Keywords: inelastic neutron scattering, catalyst, hydrodeoxygenation, bio-oi, energy

A NiMo catalyst supported on pillared bentonite clay was developed as a new HDO catalyst for the upgrading of bio-oil, a promising source of biomass energy, which is readily obtained from the pyrolysis of lignocellulosic biomass waste making the environment cleaner. The sulfided NiMo/PILC catalyst showed high activity 65% DOD, a 15% improvement on the commercial $NiMoS_2/Al_2O_3$ catalyst. Neutron scattering techniques were carried out to understand the details of the interaction between the catalyst and bio-oil compounds in the HDO reaction.

Figure 1 (left) shows the INS spectra of bio-oil dosed catalyst samples before and after the HDO reaction obtained with the ISIS TOSCA spectrometer in the 600–2000 cm^{-1} region. The clean catalyst was also measured as a reference. The vibrational modes of bio-oil compounds were seen in the dosed sample with the CH and OH bending modes observed at 1452 and 1155 cm^{-1}. An intense band at 935 cm^{-1} was observed on the clean PILC assigning to the SiOH groups on the clay surface, whereas the band at 694 cm^{-1} is assigned to the MoSH groups. In the reacted catalyst samples, the CH and OH bands were not significantly observed suggesting a high conversion of bio-oil. Figure 1 (right) shows the INS spectra of bio-oil dosed catalyst samples before and after the HDO reaction obtained with the ISIS MAPS spectrometer in the 2000-4000 cm^{-1} region. In the dosed catalyst samples, the splitting of the CH stretch peak of the bio-oil compounds were observed in the 2800 and 3050 cm^{-1} regions, indicating the modes of the sp^3 and sp^2 carbon, respectively. Meanwhile in the reacted samples, these modes show lower intensity with a slightly higher composition of the sp^2 carbon compared to the sp^3. Catalytic test using the NiMo/PILC catalyst demonstrates that the catalyst was active for the HDO of bio-oil reaction giving 65% degree of deoxygenation (DOD), a 15% improvement on the commercial $NiMoS_2/Al_2O_3$ catalyst.

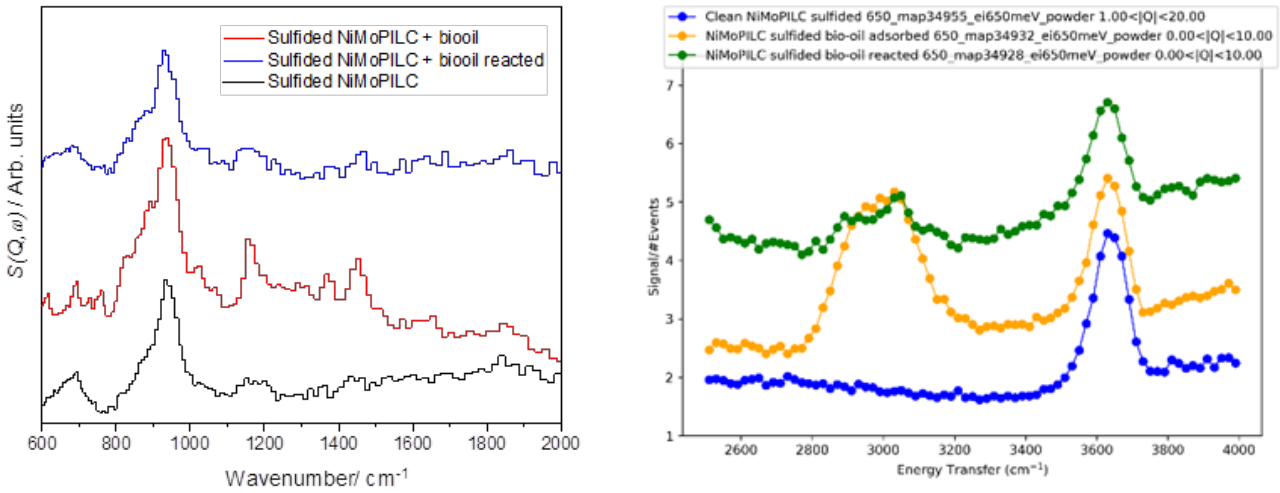

Figure 1. INS spectra of bio-oil dosed catalyst samples obtained on TOSCA in the 600–2000 cm^{-1} region (left) and on MAPS in the 2500–4000 cm^{-1} region (right). S(Q,w)= scattering law value.

[1] Adilina, I. B., Rinaldi, N., Simanungkalit, S. P., Aulia, F., Oemry, Stenning, G. B. G., Silverwood, I. P. & Parker, S. F. (2019). *J. Phys. Chem. C*, **123**, 21429.
[2] Oemry, F., Adilina, I. B., Cahyanto, W. T., Rinaldi, N., Aulia, F., Jackson, A., Parker, S. F., Kroner, A. B. & Shotton, E. J. (2023) *Phys. Chem. Chem. Phys*., **25**, 2978.
[3] Parker, S. F. & Lennon, D. (2021). *Physchem*, **1**, 95.
[4] Centi, G, Lanzafame, P. & Perathoner,. *Catal. Today* (2011), **167**.
[5] Mitchell, P. C. H., Green, D. A., Payen, E., Tomkinson, J. & Parker, S. F. (2000), *Stud. Surf. Sci. Catal.*, **130**, 2789.

A072-02-280823

Phase transitions and ion transport dynamics driven by water in Prussian White cathode materials

I. Nielsen[1], M. S. Andersson[1], M. Karlsson[2], W. R. Brant[1]

[1]*Department of Chemistry – Ångström Laboratory, Uppsala University, SE-751 21 Uppsala, Sweden,* [2]*Department of Chemistry and Chemical Engineering, Chalmers University of Technology, SE-412 96 Göteborg, Sweden*

ida.nielsen@kemi.uu.se

Keywords: Prussian blue analogues, sodium-ion batteries, octahedral tilting, neutron diffraction, quasi-elastic neutron scattering

A promising cathode material for Na-ion batteries is the Fe-based vacancy-free Na-rich Prussian Blue Analogue (PBA) known as Prussian White (PW) Na2Fe[Fe(CN)6]·zH2O. Na-based PBAs adopt different structures depending on the Na and H2O content (Fig. 1). For example, dehydration of PW results in a phase transition from $2_1/$ to $\bar{3}$ symmetry and an 18% volume contraction. Desodiation of the dehydrated PW subsequently results in a transformation to $\bar{3}$ symmetry and a 17% volume expansion. This large change in volume is not observed during the desodiation of the hydrated structure. It is clear that H2O plays a vital role in structural stability [1] and yet its presence is highly damaging in non-aqueous battery systems. Despite the large volume of work done on PBAs, the dominant use of X-ray diffraction to study the structure [2, 3] has resulted in a limited understanding of the mechanism behind the observed phase transitions [4].

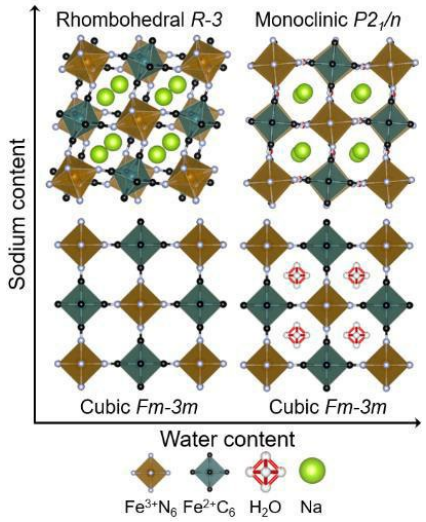

Figure 1. Phase diagram for low-vacancy iron-based PW (Na2Fe[Fe(CN)6]) as a function of the sodium and water content.

Here, we show neutron diffraction (ND) and quasi-elastic neutron scattering (QENS) experiments on a series of PW compounds with varying Na contents. For the first time, a phase transition is observed at 35 ˚C from $2_1/$ to $\bar{3}$ for PW with 2 Na-ions per formula unit (f.u.) due to an octahedral tilt transition from $^{---+}$ to $^{---}$ without any changes in volume or water content. This implies that the tilt system does not necessarily depend on the composition. The structural model fitted to the $2_1/$ phase contained a split-site for one of the oxygen atoms located between two Na-ions suggesting that in reality water must lie slightly closer to one of the two Na-ions [5]. These displacements are not long-range ordered indicating different water orientations and surroundings within PW with a Na content of 2. Furthermore, dehydration results in a severe tilting of the Fe octahedra along with displacements of Na, while retaining the $\bar{3}$ symmetry and $^{---}$ tilt pattern indicating that water does not induce phase transitions but rather modulates the magnitude of pre-existing distortions. PW with lower Na contents (0 and 1 per f.u.) have a cubic $\bar{3}$ symmetry that is maintained during heating. Combining ND with QENS gives insight into the interaction between water and the structure of PW and how this relates to the Na content. Specifically, whether there are multiple unique structural water sites in terms of mobility and how the dynamics of water change with less or no Na present in the structure. Understanding how neutral guest species, such as water, interact with mobile *A*-site cations lay the groundwork for designing chemically modified PW compounds containing alternative molecules to water that stabilize the structure. These results are vital for understanding and eliminating the origin of capacity fade in PW when used as a positive electrode in batteries.

[1] X. Guo *et al.* (2019). *Chem. Mater.* **31**, 5933–5942.

[2] V. D. Ivanov (2020). *Ionics (Kiel).* **26**, 531–547.
[3] H. L. B. Boström *et al*. (2019). *Chem. Commun*. **55**, 10230–10233.
[4] H. L. B. Boström *et al*. (2022). *J. Mater. Chem. C*, **10**, 13690–13699.
[5] I. Nielsen *et al.* (2022). *J. Phys. Energy*, **4**, 044012.

A072-03-280823

Aging-driven Composition- and Distribution- Changes of Electrolyte and Graphite Anode in 18650-type Li-ion Batteries

D. Petz[1,2], M. Mühlbauer[1], V. Baran[1,3], S. Nowak[4], M. Hofmann[1], R. Kostecki[5], A. Senyshyn[1]

[1]Forschungs-Neutronenquelle Heinz Maier-Leibnitz FRM II, Technische Universität München, Lichtenbergstr. 1, 85748 Garching b. München, Germany, [2]Lehrstuhl für Funktionelle Materialien, Technische Universität München, James-Franck-Straße 1/I, 85748 Garching b. München, Germany, [3]Deutsches Elektronen Synchrotron (DESY), Notkestr. 85, 22607 Hamburg, Germany,[4]Münster Electrochemical Energy Technology (MEET), Westfälische Wilhelms-Universität Münster, Corrensstr. 47, 48149 Münster, Germany,[5]Energy Storage and Distributed Resources Division, Lawrence Berkeley National Laboratory, Berkeley, California 94720, USA

anatoliy.senyshyn@gmail.com

Keywords: Li-ion batteries, *in operando* characterisation, aging

Carbonate-based esters used as solvents in real-life Li-ion battery electrolytes exhibit a long range order in a frozen state, which enables their accurate and non-destructive quantification and localisation by diffraction methods. In the current study lithium concentration inside the graphite anode and distribution of electrolyte were determined simultaneously for series of differently cycled (variously aged) Li-ion cells using neutron diffraction at low temperatures. Differently stabilized aging states was supplemented by the pronounced and systematic losses of lithium inventory, increase of internal resistance (also reflected in the increase Joule heating of the cells) as well as drying out of cells (loss of electrolyte inventory). An independent electrolyte characterization is performed via quasi adiabatic calorimetry on variously aged 18650-type lithium-ion batteries, where the shape of the thermodynamic signal has been found strongly evolving with the state of fatigue of the cells. A clear correlation of lithium losses and remaining electrolyte amount was observed, where two regimes of their consumption can be identified and attributed to a characteristic cell capacity fade. Analyzing the liquid electrolyte extracted/harvested from the studied cells reveals the decomposition of conducting salt to be the main driving factor for fatigue in the electrolyte degradation.

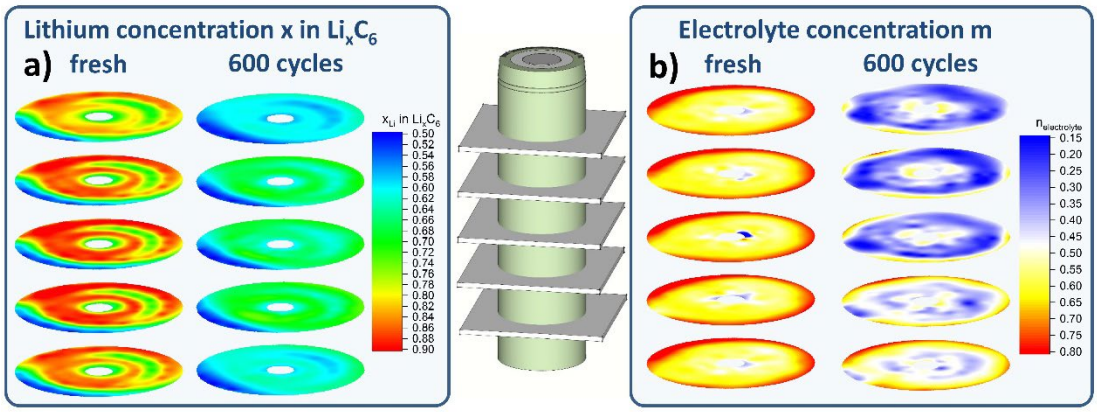

Figure 1. *Lithium and electrolyte concentrations at different planes of fresh and aged (600 cycles) studied cylinder cells.*

[1] Mühlbauer M.J., Petz D., Baran V., Dolotko O., Hofmann M., Kostecki R., Senyshyn A. (2020) *J. Power Sources* **475,** 228690.
[2] Petz D., Baran V., Peschel C., Winter M., Nowak S., Hofmann M., Kostecki R., Niewa R., Bauer M., Müller-Buschbaum P., Senyshyn A. (2022) *Adv. Energy Mat.* **12**, 2201652

The authors gratefully acknowledge the financial support provided by the Heinz Maier-Leibnitz Zentrum (Technische Universität München), German Federal Ministry of Education and Research (BMBF project 05K16VK2 and 05K19VK3) and Bavaria California Technology Center (BaCaTeC, project 14[2014-02]). Authors thank the Heinz Maier-Leibnitz Zentrum for the provision of beamtime and access to their infrastructure.

A072-04-280823

Neutron scattering to probe nanostructure-property relationships in composite proton exchange membranes for fuel cells

Smith[1], D. J. L. Brett[2], T. S. Miller[2] and F. Foglia[1]

Department of Chemistry, University College London, Christopher Ingold Building, 20 Gordon Street, London, WC1H 0AJ, UK
Electrochemical Innovation Lab, Department of Chemical Engineering, University College London, London, WC1E 7JE, UK

keenan.smith.18@ucl.ac.uk

Keywords: Ion exchange membrane, Quasi-elastic neutron scattering, Neutron reflectivity

Proton exchange membranes (PEMs) that conduct protons between electrodes, whilst minimizing the transport of reactant molecules are vital components of energy storage and conversion devices, such as fuel cells (FC), electrolysers and redox flow batteries. Despite over half a century of synthetic development, perfluorosulfonic acid membranes (PFSA), such as Nafion, remain the industry standard. Performance improvements have thus relied on use of additives to improve water retention and proton conductivity. 2D nanomaterials, such as graphene oxide (GO) and carbon nitrides with non-size consistent properties have been found to tune the microstructure of PFSA membranes, resulting in favourable properties.[1, 2] Whilst enhancements have been attributed to hygroscopic proton hopping sites, understanding the way in which these additives arrange favourably into the phase separated morphology and positively influence water uptake and proton conductivity has eluded researchers.

Herein, we fabricated high-performance composite PEMs by incorporating polytriazine imide structured carbon nitride (PTI),[3] and GO into a Nafion matrix. This provided two composite systems containing graphitic additives of variable size and functional groups which allowed an in-depth study of the structural tuning of PFSAs. Dynamic processes of ions and water within the ionic domains were probed with quasi-elastic neutron scattering at a range of instrument resolutions to reveal mechanisms occurring at ps to ns timescales that collectively contribute to superior overall transport process.[4] Thin film composite samples, that experience confinement induced crystallisation, were used to gain a greater understanding of the way in which PTI and GO, tune the phase separation of Nafion and alter the response due to operational humidities and temperatures. Quartz crystal microbalance, variable angle spectroscopic ellipsometry and neutron reflectivity revealed domain morphology in unprecedented resolution.

This work highlights PTI as an effective 2D material for structural tuning of phase separated polymers for contiguous proton and water transport, as well as highlighting an experimental approach to reveal nanoscale structure-property relationships. Most importantly, correlation of structural tuning and performance has provided key parameters of importance when selecting nanomaterial additives from a vast parameter space, which will help guide the design of future composite PEMs.

[1] Kumar, R., Xu, C., and Scott, K., (2012). *RSC Adv., 2012,* 2, 8777–8782
[2] Velayutham, P., and Sahu, A.K., (2018). *J. Phys. Chem. C,* 122, 21735–21744
[3] Foglia, F., Clancy, A.J., Berry-Gair, J., Lisowska, K., Wilding, M.C., Suter, T.M., Miller, T.S., Smith, K., Demmel, F., Appel, M., García Sakai, V., Howard, C.A., Tyagi, M., Corà, F., and McMillan, P.F., (2020). Sci. Adv., 6, eabb6011
[4] Foglia. F., Berrod, Q., Clancy, A.J, Smith, K., Gebel, G., García Sakai, V., Appel, M., Zanotti, J., Tyagi, M., Mahmoudi, N., Miller, T.S., Varcoe, J.R., Periasamy, A.P., Brett, D.J.L., Shearing, P.R., Lyonnard, S., McMillan, P.F., (2022). *Nat. Mater.* 21, 555–563

A079 Dealing with the Data Deluge
Room 208
4.00pm - 6.30pm

A079-01-280823

CrystalMELA: A machine learning-based web platform for crystal system classification

R. Rizzi1, N. Corriero1, N. Del Buono2, G. Settembre2, D. Diacono3

1 Institute of Crystallography (CNR), Bari, Italy, 2 Department of Mathematics, University of Bari, Bari, Italy, 3 National Institute for Nuclear Physics, Bari, Italy.

Email of communicating: rosanna.rizzi@ic.cnr.it

Keywords: Machine Learning; Powder X-ray Diffraction; Crystal Systems

A powder diffraction pattern is mainly affected by peak overlaps, difficulty in the correct background estimation, presence of preferred orientation effects, and limited experimental resolution. All this makes the structure solution process non-trivial. Most importantly, it is difficult to establish the critical initial steps such as pattern indexation and space group determination, especially if more than one chemical phase is present in the compound. On the other hand, an incorrectly defined unit cell does not lead to the structural solution. It happens despite the progress, availability, and variety (in terms of strategies and methods implemented) of automatic indexing software such as DICVOL [1], N-TREOR09 [2] and ITO [3].

In the past few years, extraordinary advances in data-driven models and the availability of large amounts of experimental data from many different sources have enabled the development and application of Artificial Intelligence in materials science [4], especially machine learning (ML) algorithms for diffraction data analysis.

A new machine learning (ML) based web platform, named *CrystalMELA* (Crystallographic MachinE LeArning) [5], for crystal system classification has been developed. The aim is to try to overcome the difficulties posed by the structure solution process from powder diffraction data, and to complement traditional indexing approaches. The tool is currently designed for the classification of the seven crystal classes. In the current version, the platform can run three different and complementary ML models: a Convolutional Neural Network (CNN), a Random Forest (RF) and an Extremely randomized trees (ExRT). The models have been trained on theoretical powder diffraction patterns of more than 280,000 crystal structures of inorganic, organic, organo-metallic compounds and minerals as collected in the POW_COD database [6]. A 70% of classification accuracy was achieved, improved to 90% if the top-2 accuracy is considered.

CrystalMELA is free available for the scientific community and its home web page is shown in Fig. 1. All the classification options in *CrystalMEL*A platform are designed to be powerful and easy to use, supported by a user-friendly graphic interface. Their main aspects and some examples of applications to real cases will be presented.

Figure 1. The Home web page of CrystalMELA platform

[1] Boultif, A., Louer, D. (2004). *J. Appl. Cryst*., **37(5)**, 724.
[2] Altomare, A., Campi, G., Cuocci, C., Eriksson, L., Giacovazzo, C., Moliterni, A., Rizzi, R., Werner, P.-E. (2009). *J. Appl. Cryst*., **42(5)**, 768.
[3] Visser, J. W. (1969). *J. Appl. Cryst*., **2(3)**, 89.
[4] Mueller, T., Kusne, A. G., Ramprasad, R. (2016). *Machine Learning in Materials Science*, John Wiley and Sons, Ltd., chap. 4, pp. 186–273.
[5] Corriero, N., Rizzi, R., Settembre, G., Del Buono, N., Diacono, D. (2022). *J. Appl. Cryst*., Submitted.
[6[Altomare, A., Corriero, N., Cuocci, C., Falcicchio, A., Moliterni, A., Rizzi, R. (2015). *J. Appl. Cryst*., **48**, 598.

A079-02-280823

Game-theoretic crystal structure determination by combining diffraction experiments and ab-initio calculations

T. Hawai1, M. Matsumoto2, K. Ono1,2

1Osaka University, 1-1 Yamadaoka, Suita city, Osaka 565-0871, Japan, 2High Energy Accelerator Research Organization, 1-1 Oho, Tsukuba, Ibaraki, Japan

hawai@ap.eng.osaka-u.ac.jp

Keywords: Rietveld analysis, ab-initio calculation, crystal structure determination, game theory

Due to errors caused by overfittings such as uncertainties, approximations, and setting conditions, the smallest cost function, such as Rwp or total energy, does not always mean a "scientifically valid result" in Rietveld analysis or KKR calculations. Therefore, "reasonable" results from previous studies are often introduced as prior knowledge as a constraint condition so that physically meaningful solutions can be obtained. However, it is up to each expert to determine which results are "valid."

Therefore, we propose an approach to obtain "scientifically valid results" without relying on experts by combining different analyses and calculations, based on game theory. Data analysis [1] and theoretical calculations [2] are alternated, and the results of each are fed back to each other until the convergence of solutions is achieved. This procedure could be considered a procedure for finding Nash equilibrium solutions in non-cooperative strategic game theory [3]. Although the solution obtained by our approach does not minimize the cost function of each analysis and calculation, it could be a "scientifically valid result" because it can explain all the analyses and calculations without contradiction. The results of the proposed game-theoretic analysis will be presented using diffraction experiments and first-principles calculations on actual materials.

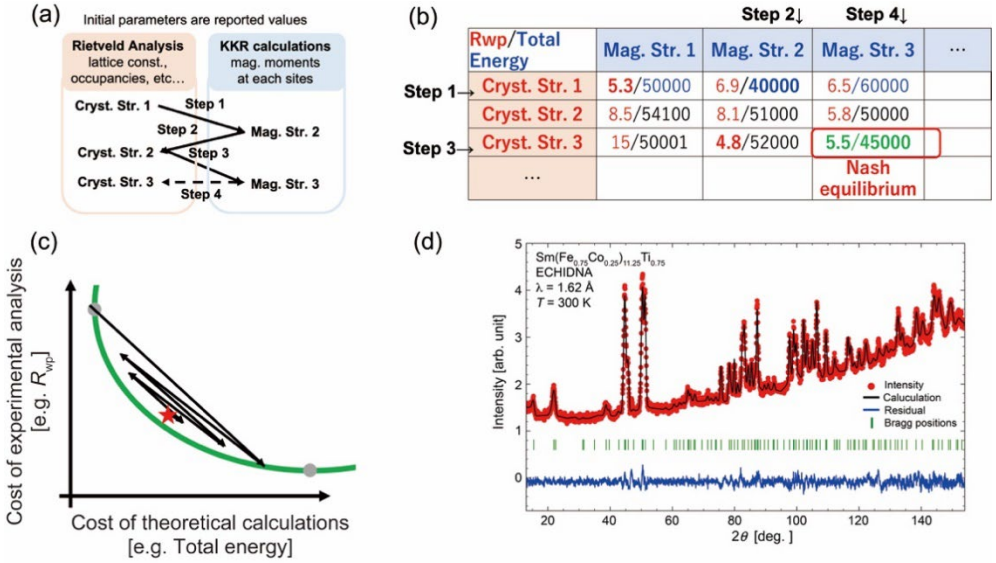

Figure 1. (a) Schematic figure for our game-theoretic procedure to determine crystal structures. Rietveld analysis is performed, and the obtained Cryst. Str. 1 is passed to the KKR calculations as the initial crystal structure in Step 1. Then KKR calculation feedbacks the results Mag. Str. 2 to Rietveld analysis in Step 2. Finally, there is no change in both structures obtained by Rietveld analysis and KKR calculations in Step 4. The converged structure is the final result of our procedure. (b) A payoff table of the schematic procedure shown in (a). The converged structure is Nash equilibrium and does not achieve the lowest Rwp or Total energy. (c) Schematic figure of our procedure in cost function space. The gray circles indicate the lowest Rwp/Total energy. Our result corresponds to the red star. (d) The result of Rietveld analysis for powder neutron diffraction data using the structure obtained by our game-theoretic procedure.

[1] Ozaki, Y., Suzuki, Y., Hawai, T., Saito, K., Onishi, M. & Ono, K. (2020). npj Computational Materials, 6, 1−7.
[2] Munehisa Matsumoto, Takafumi Hawai, and Kanta Ono. (2020). Phys. Rev. Applied 13, 064028.
[3] Akira Okada. (1992) [*Game theory*] *Ge-mu riron* (in Japanese) 3rd edition, Yuhikaku, pp. 24-25; D. Fudenberg and J. Tirole: *Game Theory*, MIT Press, 1991

This work was partly supported by JST-Mirai Program Grant Number JPMJMI21G2.

A079-03-280823

Integration of X-ray measurement and analysis and data science

K. Ono

Department of Applied Physics, Osaka University, 2-1, Yamadaoka, Suita, Osaka 565-0871, Japan.

ono@ap.eng.osaka-u.ac.jp

Advanced characterization using quantum beams is used in many natural science fields, from condensed matter physics to life sciences, and has become an indispensable tool in scientific research. However, there are problems in measurement and analysis using quantum beams, such as the effective use of limited beamtime in synchrotron and neutron facilities. Solving these problems is necessary for further progress in scientific research. We are promoting efficient, automated, and autonomous X-ray measurement and analysis using data science to solve these problems.

These research fields are called measurement informatics and are being developed through advances in data science, as well as recent advances in computational resources, and are expected to:

1. enable measurements that previously required synchrotron radiation and neutron facilities to be made with the laboratory source.
2. enable the optimization and improvement of the efficiency of X-ray measurement and analysis.
3. enable observation of previously unobservable phenomena through data sciences.

The research and development of measurement informatics related to quantum beams will make it possible to realize advanced measurements by data science without significant hardware upgrades. The key to the next generation of quantum beam measurement will be using data science to achieve advanced measurements. Autonomous measurement and data analysis will be essential for the next generation of quantum beam measurement.

We will introduce the following topics by integrating x-ray measurement, analysis, and data science.

1) Automatic design of an optimal x-ray experiment [1].
2) When should x-ray experiments stop [2]?
3) Speed up x-ray measurements with data science [3]?
4) Automating x-ray data analysis: crystallography and spectroscopy [4,5,6].
5) Decision-making in x-ray data analysis [7].
6) Cartography of inorganic materials using crystal structure [8].

[1] Ueno, T., Hino, H., Hashimoto, A., Takeichi, Y., Sawada, M. & Ono, K. (2018). *npj Computational Materials* **4**, 4.
[2] Ueno, T., Ishibashi, H., Hino, H. & Ono, K. (2021). *npj Computational Materials* **7**, 139.
[3] Saito, K., Yano, M., Hino, H., Shoji, T., Asahara, A., Morita, H., Mitsumata, C., Kohlbrecher, J. & Ono, K. (2019). *Sci. Rep.* **9**, 1526.
[4] Suzuki, Y., Hino, H., Kotsugi, M. & Ono, K. (2019). *npj Computational Materials* **5**, 39.
[5] Ozaki, Y., Suzuki, Y., Hawai, T., Saito, K., Onishi, M. & Ono, K. (2020). *npj Computational Materials* **6**, 75.
[6] Suzuki, Y., Hino, H., Hawai, T., Saito, K., Kotsugi, M. & Ono, K. (2020). *Sci. Rep.* **10**, 21790.
[7] Matsumoto, M., Hawai, T. & Ono, K. (2020). *Phys. Rev. Applied* **13**, 064028.
[8] Suzuki, Y., Taniai, T., Saito, K., Ushiku, Y. & Ono, K. (2022). *Mach. Learn.: Sci. Technol.* **3,** 045034.

A079-04-280823

High-throughput scattering data processing on field-programmable gate arrays

Z. Matěj[1], K. Skovhede[1,2], C.P. Johnsen[2], A. Barczyk[1], C. Weninger1, A. Salnikov[1], B. Vinter[2]

MAX IV Laboratory, Lund University (Sweden), Niels Bohr Institute, University of Copenhagen (Denmark)

zdenek.matej@maxiv.lu.se

Keywords: scattering, azimuthal integration, FPGA

Increasing brightness of new generation light sources and developments in X-ray detectors allow faster diffraction experiments and higher data rates. Reducing data first before storing them is one of the most effective strategies of dealing with expanding data volumes. The effective and real time data reduction is also imperative to near-real time experiment feedback, dynamical events selection and data filtering. Field-programmable gate arrays (FPGAs) are very common hardware used for data acquisition, in particular detector readout, but they perform usually rather simple compute operations. With recent developments in computer science (synchronous message exchange, high level synthesis) these computer chips are also available for scientific programmers and the number of applications is increasing, including applications related to crystallography: spot-finding, tomographic reconstructions, simulations of small angle scattering patterns or azimuthal integration (AZINT). This contribution deals mainly with the last application of AZINT on FPGAs. Modern “compute” FPGAs can be equipped with large memory and hosted in a computer the same way as graphical processing units (GPUs). They are excellent candidates for processing high throughput detector data. All the tasks of receiving, decompressing the detector image stream and the final AZINT computation can be handled on a single device providing fixed and extremely short latencies of data processing. Optimized software allows beside others power costs reductions. Even space application can profit from the latter and from a good radiation tolerance of FPGAs. The computer software performing AZINT on FPGAs is available in the Intel DevCloud and compute infrastructure of MAX IV synchrotron laboratory. It is demonstrated the FPGA implementation can process several (>6) Giga-pixels per second on the mid-range cost and energy-effective FPGAs. That matches well the maximum frame-rates of detectors in labs and at synchrotron facilities nowadays and scales to needs of future detectors. The solution [1] allows seamless integration with standard software, in particular Python, including examples using Jupyter notebooks.

[1] Matěj Z. et al., https://gitlab.com/MAXIV-SCISW/compute-fpgas/bincount (last visited on the November 22nd, 2022)

A079-05-280823

Using on-the-fly Rietveld analysis to follow in situ synchrotron X-ray powder diffraction experiments in real time

Monty R. Cosby[1,2], Adam A. Corrao[2], Gerard S. Mattei[2], Kevin H. Stone[1], Peter G. Khalifah[2]

[1]*Stanford Synchrotron Radiation Lightsource, Menlo Park, CA USA 94025,* [2]*Stony Brook University, Stony Brook, NY USA 11794*

mcosby@slac.stanford.edu

Keywords: On-the-fly, Powder diffraction, In situ

For most compounds, high resolution powder diffraction patterns of samples at modern synchrotron beamlines are collected within seconds. These acquisition times will further decrease by more than an order of magnitude as synchrotrons undergo upgrades to increase beam flux. For *in situ* or *operando* studies tens of thousands of patterns can be collected on a single reaction within a single day. For these *in situ* reactions the only way of evaluating experimental progress is by following structural changes from resulting 1D patterns via visual inspection. Without distinct structural changes to the reactants within the system to indicate a reaction's completion it is on the user to make their best estimate on when they have collected enough data. These worries often lead to overcollection on the sample to ensure desired outcomes are met.

To combat these issues plaguing *in situ* and *operando* experiments, we created a Python code to run Rietveld refinements on collected patterns *on-the-fly*. The typical Rietveld analysis is finished within days to years after the experiment completion while the software does not replace this process it provides a first look at the structure changes *in real time*. Existing refinement (TOPAS [1]) and integration (pyFAI [2]) software enabled the rapid analysis leading to a full structural determination within seconds of a pattern's acquisition collection. This allows the user to make informed decisions on the experiment at hand. An example is given below where ion exchange [3] was impossible to follow by the 1D patterns, yet had clear kinetic rates were determined from the on-the-fly refinements. This software has been tested at the Advanced Photon Source, National Synchrotron Light Source II, and Stanford Synchrotron Radiation Lightsource powder diffraction beamlines. On-the-fly Rietveld analysis is an important step in creating structure informed autonomous beamline experiments.

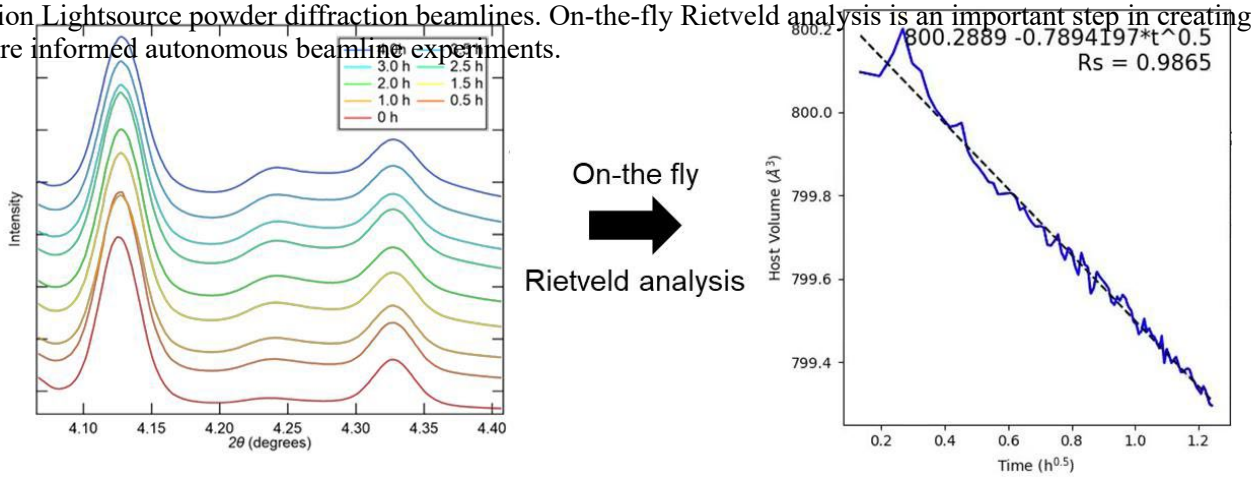

Figure 1. 1D diffraction patterns taken by synchrotron diffraction of the intermediate $Na_{2-x}Li_xMg_2P_3O_9N$ phase 301 and 311 peaks during ion exchange (left). The reaction progression is indicated by a peak shift for a lattice parameter change <0.1%, impossible to see by eye. Using on-the-fly Rietveld analysis (right) not only was the reaction followed, but a kinetic rate with an $R^2 > 0.985$ was determined for the ion exchange reaction based on the peak shifts within the first two hours.

[1] Coelho, A. A. (2018). *J. Appl. Crystallogr*. 51, 210-218.
[2] Ashiotis, G., Deschildre, A., Nawaz, Z., Wright, J. P., Karkoulis, D., Picca, F. E. & Kieffer, J. (2015) *J. Appl. Crystallogr.* **48**, 510-519.
[3] Cosby, M. R., Mattei, G. S., Wang, Y., Li, Z., Bechtold, N., Chapman, K. W. & Khalifah, P. G. (2020). *J. Phys. Chem. C.* **124**, 6522-6527.

We acknowledge the Stanford Synchrotron Radiation Lightsource (2-1, 11-3), The Advanced Photon Source (11-ID-B, 11-ID-C, 17-BM), and National Synchrotron Light Source (28-ID-1, 28-ID-2) for the use of their beamlines for this work.

A079-06-280823

Data Analytics at the Linac Coherent Light Source

J. Thayer, R. Claus, D. Damiani, M. Dubrovin, C. Ford, W. Kroeger, S. Marchesini, V. Mariani, R. Melchiorri, C. O'Grady, A. Perazzo, H. Schwander, M. Shankar, M. Uervirojnangkoorn, C. Wang, M. Weaver, C. Yoon

SLAC National Accelerator Laboratory, 2575 Sand Hill Road, Menlo Park, CA 94025

jana@slac.stanford.edu

Keywords: LCLS, Computing, Big Data

The increase in velocity, volume, and complexity of the data generated by the Linac Coherent Light Source upgrade (LCLS-II), present a considerable challenge for data acquisition, data processing, data management, and workflow orchestration. These systems face formidable challenges due to high data throughput and intensive computational demand for scientific interpretation. Increasingly large data sets at high velocity open new areas of science but make it more difficult to extract desired physical information. Raw data collected cannot all be saved to disk. Handling the throughput between the front-end electronics and the storage layers and between the storage and processing is a critical element of the system. Conventional human-in-the-loop workflows are too slow to process data on useful timescales. Likewise, current analysis pipelines rely on human-in-the loop decision-making and fine tuning of algorithm parameters that do not scale with increased data rates. Compute-intensive analyses require access to compute resources of the appropriate scale which may be local or remote to the facility generating the data and may include ASCR Leadership Class Facilities.

A further challenge, once the data have been recorded, is the useability of the overall system to access the data and analyze it at scale. Providing fast feedback to experimenters on the timescale of seconds and for complex analyses, minutes, reduces the time to complete the experiment, improves the quality of the data, and increases experiment success rate. Speed and flexibility of the development cycle are critical due to the wide variety of experiments, rapid turnaround required, and the need to modify data analysis during experiments even for complex scientific workflows. Integration of simulations, real-time data analysis, computation-assisted experiment design at large scales, and Machine Learning techniques drive the computation and networking needs of the data system.

The LCLS-II Data System architecture addresses these challenges [1]. To reduce data volume and handle the high throughput, we provide an adaptable, heterogeneous data reduction pipeline (DRP), a compute layer composed of edge accelerators (FGPA, GPU, etc) and CPU that can run experiment-specific algorithms in real time to reduce data volumes by an order of magnitude while preserving the science content of the data. The Fast Feedback layer offers dedicated processing resources to running experiments for the purpose of data quality feedback within minutes. LCLS-II's data management system handles automated data movement through various storage layers such as offline storage and long-term data archiving as well as providing transparent data transfer between local and external compute facilities such as National Energy Research Scientific Computing Center (NERSC). A web-based portal allows users to manage their experiments. The data management system integrates with HPC workload managers and SLAC, NERSC and other facilities to automatically trigger analysis jobs providing easy access to local and remote offline processing capabilities. A real-time analysis framework provides visualization and graphically-configurable analysis of data on the timescale of seconds. The LCLS-II Data System mitigates bottlenecks in computing, storage, and network resources and enables tighter integration between data collection and analysis. An overview of the LCLS-II Data System architecture will be presented. New innovations to accommodate AI/ML at the edge will be described [2].

[1] Thayer, J., Damiani, D., Dubrovin, M., Ford, C., Kroeger, W., O'Grady, C., Perazzo, A., Shankar, M., Weaver, M., Wennger, C., Yamajala, S., and Zohar, S *Data Processing at the Linac Coherent Light Source.* IEEE/ACM 1st Annual Workshop on Large-scale Experiment-in-the-Loop Computing (XLOOP), Denver, CO, 18 Nov 2019.
[2] Z. Liu et al., *Bridging Data Center AI Systems with Edge Computing for Actionable Information Retrieval*, **2021** 3rd Annual Workshop on Extreme-scale Experiment-in-the-Loop Computing (XLOOP), St. Louis, MO, USA. 2021, pp 15-23.

This material is based upon work supported by the U.S. Department of Energy, Office of Science, Office of Basic Energy Sciences under Award Number FWP-100643. Use of the Linac Coherent Light Source (LCLS), SLAC National Accelerator Laboratory, is supported by the U.S. Department of Energy, Office of Science, Office of Basic Energy Sciences under Contract No. DE-AC02-76SF00515. This material is based upon work supported by the U.S. Department of Energy, Office of Science, Office of Basic Energy Sciences under Award Number FWP-100643.

A087 Simultaneous Small-angle Scattering of Soft Materials During Deformation: Recent Developments in rheoSAS and in Operando Deformation
Room 210/211
4.00pm - 6.30pm

A087-01-280823

Conductive Pluronic F127 blended PEDOT:PSS hydrogel for electric-response drug delivery

Vo Thuy Thien Ngan[1], Yi-Wei Chang[2], Wei-Tsung Chuang[3], Chih-Chia Cheng[4]

Graduate Institute of Applied Science and Technology, National Taiwan University of Science and Technology, Taipei 10607, Taiwan
National Synchrotron Radiation Research Center, Hsinchu 30076, Taiwan
National Synchrotron Radiation Research Center, Hsinchu 30076, Taiwan
Graduate Institute of Applied Science and Technology, National Taiwan University of Science and Technology, Taipei 10607, Taiwan

thiennganvothuy@gmail.com

Keywords: Pluronic F127, PEDOT:PSS, conductive hydrogel, drug delivery, electrical responsive hydrogel

Recently, stimulus-responsive hydrogels have been developing due to its biocompatible and adjustable physiochemical properties for bio-applications such as tissue engineering, wearable devices and drug delivery.[1] The promise of stimulus-responsive hydrogels as drug delivery systems for precisely controlled release of drugs toward stimuli such as pH, temperature, magnetic or electric benefits for designing hydrogel structures.[2] Electrically responsive hydrogels allow the hydrogels to disrupt its structure for releasing loaded drugs by electric trigger.[3, 4] Here in, this study reports a novel design of electric-response hydrogel made of Pluronic F127 and PEDOT:PSS polymer. Pluronic F127 was firstly terminal modified by benzene sulfonic acid to obtain negative charge F127 (SF127) which was further blended with PEDOT:PSS for constructing the conductive hydrogel (SFP). After terminal modification, the hydrogel remains the sol-gel transition ability at body temperature confirming by DSC test. Remarkably, the physical properties of the system investigated by Rheology-SAXS experiment reveals the structure transition from face-centred cubic (FCC) to hexagonal cubic packing (HCP) under applied strain. Furthermore, Piroxicam (PX) used as a model hydrophobic drug was encapsulated by SF127 for the drug release evaluation. The electric drug delivery test was designed by using two preparation methods of coating and immersion of the hydrogel on the substrate to imitate the strain effect on hydrogel microstructure toward release behaviour. The results interestingly show an improvement of drug release amount against applied electric and higher release in the coating compared to immersion method. These findings clearly proved the effectively response of the conductive hydrogel against electric stimulus and subsequently implied the strongly effect of hydrogel microstructure on the drug release efficacy in which HCP structure with higher order showing higher drug release behaviour. Moreover, by turning neutral to negative charge, the grain size of hydrogel crystal packing becomes smaller which benefits for structure disruption for increasing drug release amount. Therefore, this conductive hydrogel makes a promise as electric-responsive hydrogel for drug delivery in local treatment with safety and highly electric-control drug release.

A. P. Singh, A. Biswas, A. Shukla, and P. Maiti, Signal Transduct Target Ther, vol. 4, p. 33, 2019.
Z. Xie, J. Shen, H. Sun, J. Li, and X. Wang, vol. 137, p. 111333, May 2021.
A. Naharros-Molinero, M. Á. Caballo-González, F. J. de la Mata, and S. García-Gallego, Pharmaceutics, vol. 14, no. 12, p. 2628, 2022.
C. Boehler and M. Asplund, J Biomed Mater Res A, vol. 103, no. 3, pp. 1200-7, Mar 2015.

A087-02-280823

Evolution of elliptical SAXS patterns from aligned objects and lamellar arrays during deformation

N. Sanjeeva Murthy[1] and David T. Grubb[2]

[1]Rutgers University, Piscataway, New Jersey U.S.A. [2]Cornell University, Ithaca, New York U.S.A.

murthy@chem.rutgers.edu

Keywords: SAXS, Lamellar arrays, Elliptical trace

Two distinct features of small-angle X-ray scattering (SAXS) patterns are the central diffuse scattering (CDS) from uncorrelated structures and the discrete reflections from long-range order. Upon deformation, the CDS from voids, particles and interfaces present in polymers becomes an equatorial streak. Polymers with lamellar structures aligned by stretching or by a magnetic field produce four distinct SAXS patterns: 2-point 'banana', 4-point pattern, 4- point 'eyebrow', and 4-point 'butterfly' (Fig. 1) [1, 2]. Simulations show that when stack orientation (interlamellar shear), angle α, and chain slip, angle φ, act to rotate the lamellae in the same sense, the result is an eye brow pattern; opposite sense give a 'butterfly pattern [3]. When the lamellae are not tilted, then the result is a 2-point pattern. Changes in these two features in semicrystalline polymers during deformation were monitored to understand the changes in the structure at microstructural length scales and their implications on polymer properties.

In semicrystalline polymers, structures that gives rise to 4-point patterns reversibly transform under strain into structures that gives rise to 2-point patterns [1]; these patterns arise from lamellae with oblique and normal lamellar surfaces, respectively. These two structures represent bistable states of the lamellae that coexist until fiber breakage. The structures that give rise to the 2-point pattern is probably the load carrying lamellar entity in these fibers, and determine the ultimate strength of the fiber.

In magnetically aligned liquid crystalline (LC) phases of bent-core mesogens (BCMs), evolution from smectic C (SmC) to cybotactic nematic (Ncyb) and finally to isotropic phase can be understood by following the changes in their 4-point pattern [2]. As the temperature is increased, the increase in the orientational disorder is accompanied by a decrease in the tilt angle of the lamellae and in the ellipticity of the lamellar intensity distributions.

Detailed analyses show that the peak intensities of the reflections lie not on a layer line, or on the arc of a circle but are distributed in an elliptical trajectory (Figure 1). A moderate amount of disorder can make the peak positions trace out the ellipse.

Elliptical shape of the scattering pattern is a natural consequence of the scattering objects being elongated along the flow or the draw direction. Thus, in addition to the 2 - and 4-point reflections, even equatorial streaks (CDS) with shapes of an oval, diamond or 2-bladed propeller also have elliptical characteristics [4]. These equatorial streaks are commonly present in Poiseuille and extension flows [4], and in fibrous materials embedded with elongated voids or solid particles [5].

Elliptical features of the SAXS patterns, including the equatorial streak, suggests that the entire SAXS pattern can be optimally fitted in elliptical coordinates with least number of parameters. In contrast to this functional fitting, structural models generated using known principles of lamellar assembly and evolution can be validated by simulating scattering to agree with the observed diffraction patterns. Currently available computational tools allow these microstructures to be rapidly refined [3].

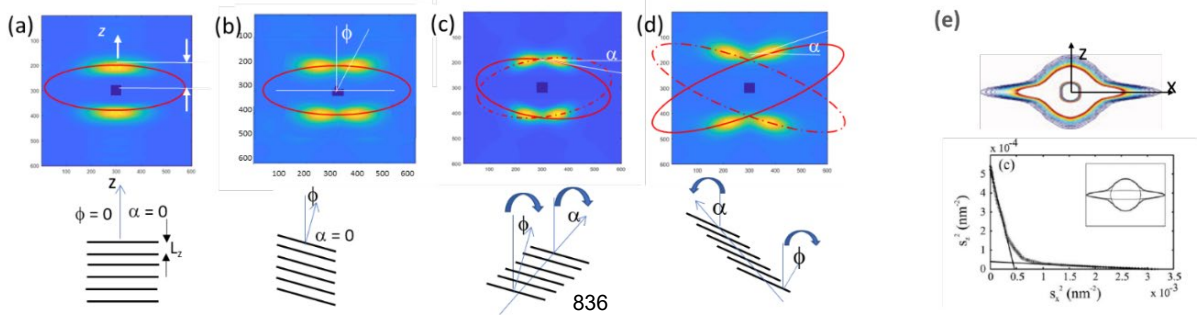

FIGURE 1. (a-d) Four classes of SAXS patterns and corresponding lamellar arrangements. Overlaid are the proposed elliptical tracks. (a) two-point banana pattern; (b) four-point pattern; (c) four-point eyebrow; (d) four-point butterfly. (e) Central diffuse scattering interpreted as composite of isotropic and an elliptical shaped equatorial streak.

[1] Murthy, N.S, and Grubb, D.T. (2002). *J. Polym. Sci. Part B Polym. Phys,* **40**, 691.
[2] Francescangeli, O., Vita, F., Ferrero, C., Dingemans, T., and Samulski, E.T. Soft Matter. 2011, **7**, 895.
[3] Grubb, D.T., Kennedy, W.J., Koerner, H., and Murthy, N.S. (2021). *Polymer* **220**, 123566.
[4] Bharati, A., Hudson, S. D. and 3 and Katie M. Weigandt, K. M. (2019). *Curr. Opin. Colloid Interface Sci.* **42**, 137
[5] Wang, W., Murthy, N.S. and David T. Grubb, D.T. (2012) *J. Polym. Sci. Polym. Phys.* **50**, 797.

A087-03-280823

Flow-induced structural transitions and instability formation in self-assembled micelles revealed by flow-small angle neutron scattering

Patrick J. McCauley 1, Satish Kumar 1, Michelle A. Calabrese 1

Department of Chemical Engineering and Materials Science, University of Minnesota Twin Cities, 421 Washington Avenue SE, Minneapolis, Minnesota, 55455 USA

mcalab@umn.edu

Keywords: rheo-SANS 1, micelle 2, self-assembly 3

Spatially-resolved flow-small angle neutron scattering (flow-SANS) methods paired with time-resolved data processing algorithms are employed to link flow-induced structural transitions and instability formation to measured rheology in surfactant and polymeric wormlike micelles (WLMs) [1-3]. The shear-induced alignment of the micelles is spatially and temporally characterized under shear startup flows by flow-SANS in the flow-gradient planes; results are verified by rheo-particle tracking velocimetry (rheo-PTV). Newly developed, advanced methods of time-resolved data analysis improve the temporal resolution of the SANS experiments by orders of magnitude [1]. By employing SANS during flow startup, we gain insight into how flow-induced structures and WLM flow instabilities like shear banding form and evolve, which differs for surfactant vs. polymeric WLMs (Fig. 1) [2, 3]. Local segmental orientation and alignment in the flow-gradient plane is found to be a complex function of the amphiphile type (surfactant vs. polymer), radial position, and deformation rate. Advances in time-resolved measurements upon shear startup allow both previously observed and new mechanisms of shear band formation to be identified in these solutions. This research quantitatively links micellar flow-induced microstructure and instability formation to the measured nonlinear shear rheology of WLM solutions, aiding in the formulation of WLMs for specific applications, as well as providing data necessary for critically testing modern, microstructure-based constitutive equations.

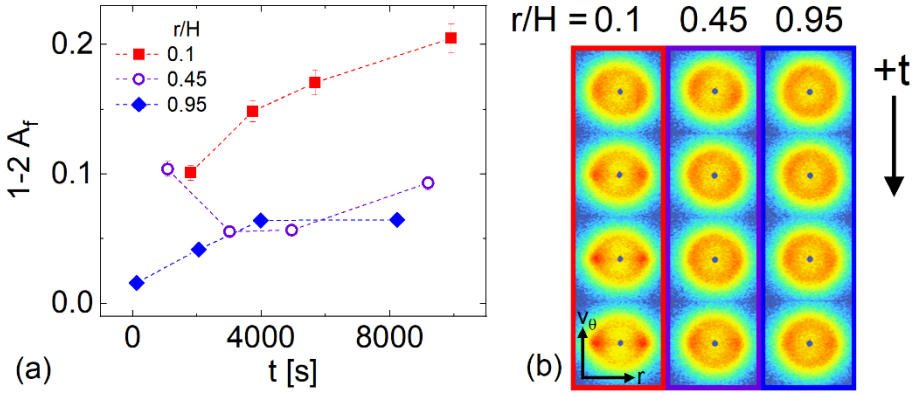

Figure 1. Time- and spatially-dependent alignment factor (a) and corresponding 2D scattering patterns (b) for a polymeric wormlike micelle (WLM) solution during shear startup. Unlike in surfactant WLMs which exhibit a decrease in alignment and scattering anisotropy in time following shear startup, for polymer WLMs, the alignment (a) and degree of anisotropy in the 2D patterns (b) increase in time.

[1] Calabrese, M. A., Wagner, N. J. & Rogers, S. A. (2016). *Soft Matter,* **12**, 2301.
[2] Calabrese, M. A. (2017). *Developing structure-property relationships in branched wormlike micelles via advanced rheological and neutron scattering techniques.* University of Delaware.
[3] McCauley, P. J., Huang, C., Porcar, L., Kumar, S. & Calabrese, M. A. (2023). *J. Rheol.*, **67**, 661.

A087-04-280823

Laboratory RheoSAXS studies of non-ionic surfactants

Andreas Keilbach1, Andrew Jones1, Barbara Puhr1, Yoshifumi Yamagata2, Yuichi Takasaki2

1Anton Paar GmbH, Anton-Paar-Strasse 20, 8052 Graz, Austria, 2Anton Paar Japan K.K., 1st Fl, Riverside Sumida, Tokyo, Japan

andreas.keilbach@anton-paar.com

Keywords: RheoSAXS, Surfactants

Non-ionic surfactants are widely used in the form of cleaning agents, detergents, wetting agents, emulsifiers and solubilizers in cosmetics, to name just a few. Here, we demonstrate the results of a combined rheological and X-ray scattering (RheoSAXS) study of a non-ionic ethoxylate surfactant in water system. The experiments where done using the unique RheoSAXS module for SAXSpoint 5.0 by Anton Paar. The RheoSAXS module is based on the DSR 502 rheometer head, which is fully integrated into the SAXSpoint sample chamber. This setup allows for full rheological measurements during a small-angle experiment. Combined RheoSAXS studies of surfactant systems such as non-ionic surfactants reveal material properties that are not accessible with other techniques or simple shear-cell add-ons.

Using this setup, we were able to characterize not only the macroscopic properties such as the sample's flow behaviour but also simultaneously changes to the nanostructure of the non-ionic surfactant polyoxyethylene alkyl ether (CmEn)-water two-component system. These systems are known to form planar lamellae at no shear or low shear rates, however, at higher shear rates and in dependence of the temperature onion-like structures can evolve [1]. For analyzing the present surfactant system the sample was measured at varying shear rates and temperatures. An in-depth evaluation of the nanostructure was done using the generalized indirect Fourier transformation (GIFT) approach [2].

Summa summarum, in this study the formation of an onion-like structure of the non-ionic polyoxyethylene alkyl ether surfactant at higher shear rates was studied. Furthermore, a detailed data evaluation revealed valuable information on the structure of bilayers as well as their flexibility in dependence of the shear rate [3].

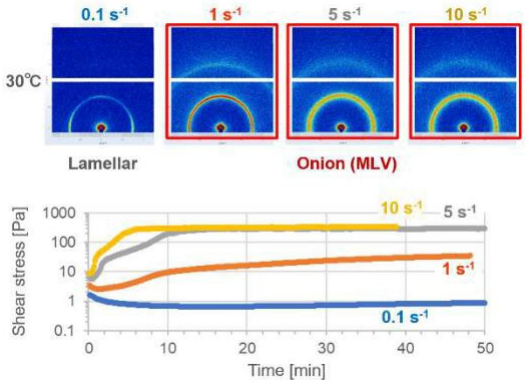

Figure 1. 2D scattering patterns of C12En in water at 30 °C. SAXS data was measured at various shear rates.

[1] Oliviero C., et al., Dynamic phase diagram and onion formation in the system C10E3/D2O. Colloids Surf. A: *Physicochem. Eng. Asp.* **228** (2003) 85.
[2] Fritz G., Glatter O., Structure and interaction in dense colloidal systems: evaluation of scattering data by the generalized indirect Fourier transformation method. *J. Phys.: Condens. Matter* **18** (2006) S2403.
[3] Takasaki Y., Yamagata Y., in preparation.

A087-05-280823

RheoSAXS study of aiyu gellation

Jing-Ting Zhu, Jung-Ren Huang

Institute of Physics, Academia Sinica, Taipei, Taiwan

ajrhuang@gate.sinica.edu.tw

Keywords: RheoSAXS, aiyu, gelation, rheology, small-angle X-ray scattering

The fig plant Ficus Pumila var. Awkeotsong, commonly known as aiyu, is a native plant of Taiwan. The mucilage obtained by rubbing the aiyu fruit seeds in water becomes edible jelly via calcium-pectin binding. We studied the aiyu gelling process and the corresponding structural change using RheoSAXS. Initially, the mucilage is practically a viscous liquid having a microstructure of fractal dimension slightly less than one in the q range of 0.02/A – 0.4/A. After roughly 30-60 minutes of experiment, the storage modulus starts to rise quickly whereas the loss modulus increases only gently. The accompanying SAXS measurement indicates a gradual increase (decrease) in the fractal dimension toward two (zero) in the low (high) q regime as gelation progresses. The results may provide useful information for understanding the gelation mechanism of aiyu and other similar biomaterials at nanoscales.

A087-06-280823

Nanostructured fluids in simple and not so simple flows examined by small-angle X-ray scattering

Kádár[1,2], A. Terry[2], K. Nygård[2]

[1]Chalmers University of Technology, 412 96 Göteborg, Sweden; [2]Wallenberg Wood Science Centre (WWSC), Chalmers, 412 96 Göteborg, Sweden; [3]MAX IV Laboratory, Lund University, 224 84 Lund, Sweden

Roland.Kadar@chalmers.se

Keywords: Rheo-SAXS, cellulose nanocrystals, PLI, CoSAXS, ForMAX

Elucidating the rheological behavior of hierarchical nanostructured fluids is an ideal study case for combined rheological methods as they have the potential to relate bulk-averaged rheological properties to their hierarchical microstructural dynamics [1]. Here, we report for the first time on simultaneous rheology combined with polarized light imaging (PLI) and small-angle X-Ray scattering (SAXS) experiments performed at the CoSAXS beamline, MAX IV Laboratory. We use as case study primarily aqueous dispersions of cellulose nanocrystals (CNCs), 1D nanoparticles that are a part of the family of lyotropic materials, but also graphene oxide dispersions. CNCs self-assemble into nematic / chiral nematic liquid crystalline orders in a water suspension, that can be observed as rich birefringence patterns in PLI. The setup is based on a standard parallel-plate glass measuring geometry, Fig. 1(a). PLI was performed in the (1)-(3) plane (transmission; linear, cross-polarized). PLI can capture qualitatively the change in shear induced microstructure through color developments with increasing shear rate while the appearance of a Maltese-cross pattern signals a general orientation in the flow direction, Fig. 1(b). To complement the qualitative PLI data, SAXS tests were simultaneously performed in the (1)-(2) plane, with the incident X-rays in the (A) and (B) configurations, see the azimuthal integration example in Fig. 1(c). The SAXS data was recorded at rheological steady state, Fig. 1(d). Thus, we study the influence of CNC concentration, counterions and surface grafting with symmetric and asymmetric dialkylamine groups from the perspective of structural and orientation dynamics in steady shear with the aim of correlating the three combined methods. In addition to the simple, viscometric flows described above, we will also highlight of self-assembling CNC and GO aqueous in flows beyond the laminar flow limit and their complex flow patterns as studied by SAXS.

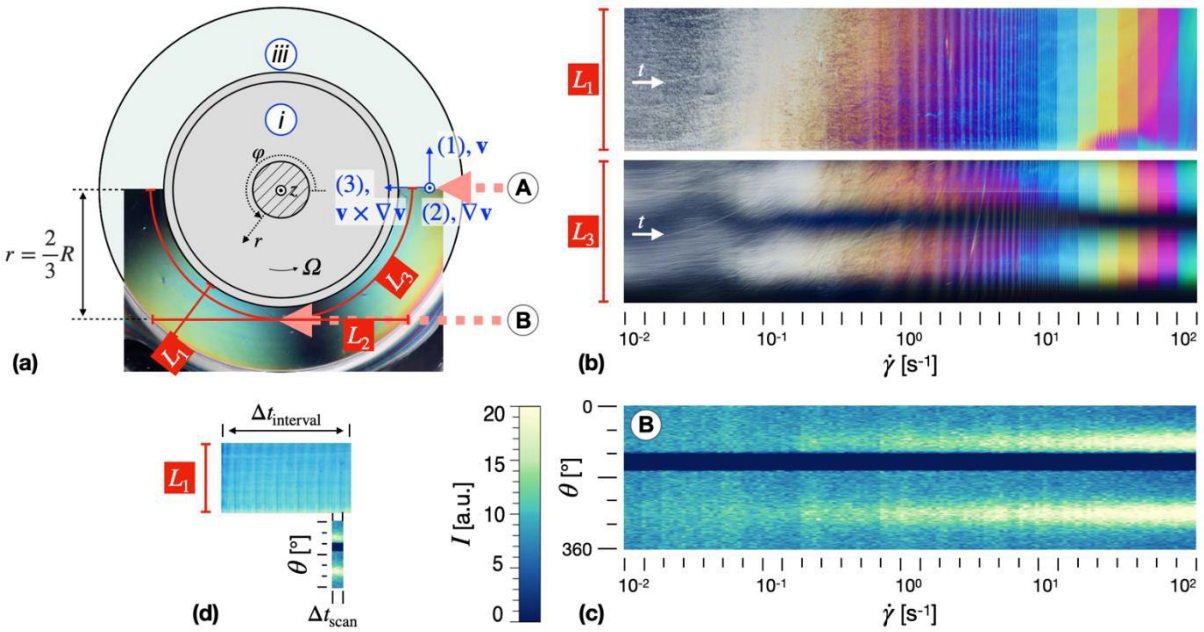

Figure 1. (a) The experimental transparent plate-plate geometry used in the study (view from the top); (A) and (B) are incident light configurations used in the experiments. (b) Space -time visualizations from (cross) PLI during steady shear, (1)-(3) plane. (c) Corresponding intensity from azimuthal integration for $0.15 < q < 0.19$ from SAXS at steady state for each shear rate interval, (1)-plane. (d) Correspondence between the PLI and SAXS scans.

[1] Kádár, R., Spirk, S., Nypelö, T. (2021) *ACS Nano* 15, 7931

A113 Materials for Advanced Energy Technologies
Room 219
4.00pm - 6.30pm

A113-01-280823

Bimetallic MOF-808 Nanozymes with Enhanced Biological Reactivity

A. Mullaliu[1], C. Simms[1], F. de Azambuja[1], G. Aquilanti[2], T.N. Parac-Vogt[1]

Department of Chemistry, KU Leuven, Celestijnenlaan 200F, 3001 Leuven, Belgium, Elettra Sincrotrone, Basovizza, Trieste, 34149, Italy

angelo.mullaliu@kuleuven.be

Keywords: MOF, nanozyme, XAFS

Bimetallic metal-organic frameworks (MOFs) are highly promising nanozymes, i.e., nanomaterials with remarkable enzymatic capabilities.[1] Although MOFs have attracted increasing attention in bio-inspired catalytic reactions,[2-4] atomic-level characterization of the interactions with substrates remains challenging, and the exact determination of a structure/activity relationship represents an open challenge. Here, we correlate the atomic-level structural effects of introducing cerium into Zr-MOF-808 on the reactivity and stability by means of an in-depth structural analysis comprising X-ray Absorption Fine Structure (XAFS) spectroscopy and X-ray Diffraction (XRD). Zr/Ce-MOFs with increasing Ce content were synthesized using a previously reported DMF/formic acid synthesis[5] and compared to our novel, green, and safer synthesis in water and acetic acid. While the former gave high levels of impurities, low structural stability, and poor reactivity, our new synthetic route produced stable MOFs with enhanced reactivity (cf. **Fig 1**). Extensive materials characterization using X-ray Absorption Near Edge Structure (XANES) coupled with ab-initio spectra calculation reveals Ce is in its (+4) oxidation state before and after reaction. Moreover, Extended X-ray Absorption Fine Structure (EXAFS) analysis corroborated that the new synthesis protocol forms Zr/Ce bimetallic oxo clusters (cf. **Fig 1**), where Zr and Ce are part of the same secondary building unit (SBU). Our results show that acetate ligands enhanced the MOF stability in water, promoting the usability of these materials in aqueous environments for biological reactions, paving the path for future applications in water involving, for instance, the incorporated metals' redox properties.

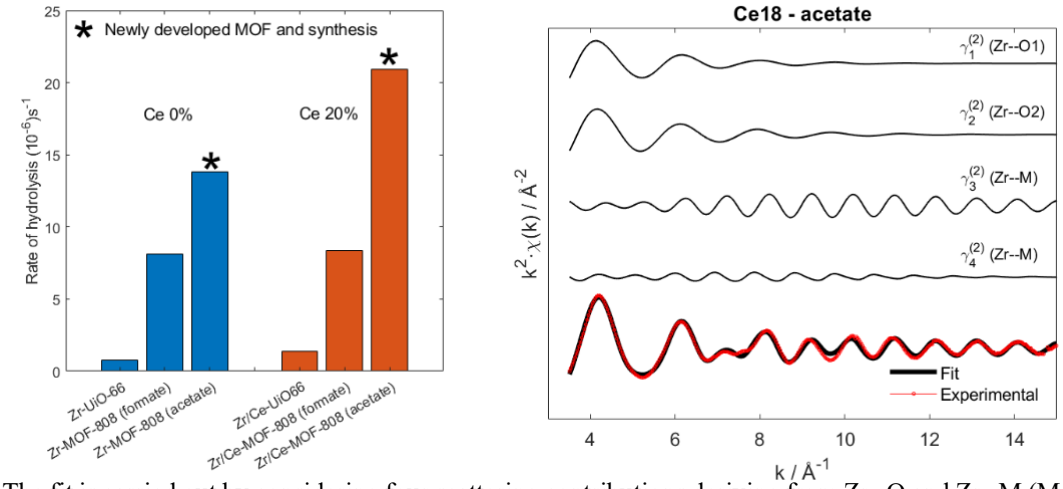

Figure 1. (Left) The fit is carried out by considering four scattering contributions deriving from Zr--O and Zr--M (M = Zr/Ce) pairs, corroborating the bimetallic nature of the oxo cluster. (Right) The rate of peptide hydrolysis is compared for two sets of data corresponding to 0% and 20% Ce content: the catalyst activity increases from UiO-66 to MOF-808, and it is further enhanced in our newly developed material using an acetate precursor.

1. C. Simms, A. Mullaliu, S. Swinnen, F. de Azambuja, T. Parac-Vogt (2023) *Molecular Systems Design & Engineering*
2. Z. Fang, B. Bueken, D. E. De Vos, R. A. Fischer (2015) *Angewandte Chemie International Edition*, **54**, 7234
3. S. Dai, C. Simms, I. Dovgaliuk, G. Patriarche, A. Tissot, T. N. Parac-Vogt, C. Serre (2021) Chemistry of Materials, **33**, 7057
4. C. Simms, F. de Azambuja, T. N. Parac-Vogt (2021) *Chemistry - A European Journal*, **27**, 17230
5. M. Lammert, C. Glissmann, N. Stock (2017) *Dalton Transactions*, **46**, 2425

We thank KU Leuven and Research Foundation – Flanders (FWO) for funding. C. S. (68090/11C9320N), A. M. (1228622N), F.d.A (195931/1281921N) thank the FWO for fellowships. We acknowledge Elettra Sincrotrone Trieste for providing access to its synchrotron radiation facilities (Project no. 20220131, A.M. as PI) and for financial support under the IUS internal project. Moreover, A.M. acknowledges FWO for an extended research stay grant at the Elettra synchrotron facility (Grant no. V439222N). We thank Prof. Marco Giorgetti from the University of Bologna, Italy, for the helpful discussion on EXAFS analysis.

A113-02-280823

New X-ray spectroscopy techniques for energy materials research

S. Diaz-Moreno1, O. Blackman1,2, A. Ibraliu1,3,4, A. Russell2, D. Bowron3, C. Hardacre4

1. *Diamond Light Source, Harwell Science and Innovation Campus, Didcot OX11 0DE, UK.*
2. *School of Chemistry, University of Southampton, Southampton SO17 1BJ, UK.*
3. *ISIS Neutron and Muon Source, Rutherford Appleton Laboratory, Didcot OX11 0QX, UK.*
4. *Department of Chemical Engineering and Analytical Science, The University of Manchester, Manchester M13 9PL, UK.*

Sofia.diaz-moreno@diamond.ac.uk

Keywords: spin-selective XAS, modulation-excitation, XES

X-ray Absorption Spectroscopy (XAS) is an established experimental technique that is used for the study of the electronic and local atomic structure of materials. The high sensitivity of the method together with its element selectivity make it very suitable for the study of energy materials. The technique is also frequently used for the study of processes in situ and under operando conditions.

In recent years, advanced spectroscopy techniques and analysis methods have been used to circumvent some of the shortcomings of traditional XAS. For example, X-ray Emission Spectroscopy at the Kβ emission line can be used to perform spin-selective spectroscopy. In addition, the use of Modulation Excitation assisted by phase-sensitive detection (ME-PSD) analysis methods can significantly enhance the sensitivity of XAS by filtering out contributions of spectator species that are unaltered by the external stimulation.

In this contribution I will present two recent examples illustrating the application of these new methodologies to the study of electrochemical systems and energy materials. The changes in the structure of the iron metal centre in Prussian blue and Prussian blue analogues have been studied as a function of the applied potential, and the changes have been assigned to the iron in low and high spin. ME-PSD analysis has been applied to the study of the reversible ferrocyanide/ferricyanide couple using XAS.

A113-03-280823

Core-shell Spectroscopy Studies of Energy Storage Materials

Mahalingam Balasubramanian

Electrification and Energy Infrastructures Division, Oak Ridge National Laboratory, Oak Ridge, Tennessee, USA

balasubramam@ornl.gov

Keywords: XAFS, batteries, operando

Battery based energy storage is expected to play a vital, enabling role in future energy supply and demand. It is likely that storage of electricity generated from renewable energy sources (such as solar, wind, or wave power) will be an important component of future energy portfolios worldwide. In the realm of transportation, rechargeable batteries are already being successfully used for light-duty all-electric vehicles. However, for mass adaptation of battery technology, either for grid-storage or transportation applications, transformative changes in battery technology are still required. It is now also generally accepted that a variety of battery chemistries will be required for a multitude of applications. Critical to the advancement of batteries (Li-ion or other beyond Li-ion solutions) is a fundamental and in depth understanding of the electronic and structural changes of the battery materials during battery operation. Our research using hard x-ray spectroscopy (energy in the range 2.5-55 KeV) focuses on x-ray absorption fine structure spectroscopy (XAFS), x-ray emission spectroscopy, x-ray Raman scattering, and micro beam (mapping, micro-XAFS) applications of hard x-rays. Using operando core-shell spectroscopic methods, we seek to capture the intricate details of the redox behavior (electronic structure) as well as the element specific local structure of battery materials. In this talk, we will highlight the application of core-shell spectroscopy methods to understand fundamental structure-function relationships of materials and systems relevant to electrochemical energy storage. The first part of the talk will focus on the solvation structure of multivalent cations in organic, aprotic solvents and will explore the relationship between solvation structure and metal plating/stripping behavior. In the second part, we will discuss the evolution of the local electronic and atomic structure of transition metals in conventional and lithium-rich oxide materials during electrochemical cycling. Our studies provide unique insights that are important to predict battery performance, shed light on degradation mechanisms, and help tailor novel materials for emerging battery technologies.

A113-04-280823

Quick-EXAFS Hyperspectral Full Field X-ray Imaging: Tracking Dynamic Electrode Heterogeneity During Batteries Cycling

S. Belin1, C. La Fontaine1, L. Perez Ramirez1, A. Beauvois1, O. Roudenko1, V. Briois1

Synchrotron SOLEIL, L'Orme des Merisiers, Départementale 128, 91190 Saint-Aubin, France

briois@synchrotron-soleil.fr

Keywords: Quick-EXAFS, Imaging, Positive Electrodes

The high time-resolution provided by Quick-EXAFS beamlines operating on third generation synchrotron radiation facilities makes the technique powerful for monitoring redox change occurring during battery cycling. However, due to intrinsic complexity in the composite electrode or cell characteristics affecting the close contact between active particles, it is not rare to observe discrepancy between the targeted voltage composition and speciation measured by Quick-EXAFS or XRD [1]. In this work, we discuss how *Quick-EXAFS hyperspectral Full Field (FF) Imaging can be used for mapping speciation heterogeneity at the µm scale with second time resolution and overcoming beam-induced damage to battery operation during operando characterizations*.
Hyperspectral FF X-ray imaging operates at the ROCK-SOLEIL beamline [2] in transmission by collecting the visible light emitted by a scintillator imaging the sample absorption by a pixelated CMOS camera (ORCA Flash 4.0 V3, Hamamatsu). The pixel size and Field of View (FoV) can range from 0.65 µm to 1.625 µm and 1.3 mm to 3.3 mm, respectively, with intrinsic beamline spatial resolution of ca. 5 µm. Around 600 images at different energies of the XAS spectrum are collected during the Quick-EXAFS monochromator energy scan yielding to one complete hyperspectral cube every 10-13 s. Post-processing for spectra normalization, spatial pixel binning or cube binning is based on Jupyter notebooks. Speciation in each cube is determined by Multivariate Curve Resolution with Alternating Least Square (MCR-ALS) analysis [3].

Charge and discharge of $LiFePO_4$ and $LiNiO_2$ electrodes have been imaged using the electrochemical cell developed at SOLEIL [1] with 2.6 x 0.5 and 1.8 x 1.2 mm^2 FoV, representative of beam sizes used for conventional Quick-EXAFS acquisitions. Figure 1 displays the spatial distribution of $Li_{1-x}FePO_4$ measured for two electrodes at voltage corresponding to 0.5 Li^+ extracted. Local over-charge and over-discharge clearly coexist in the imaged area. FF imaging displays clear advantage compared to conventional Quick EXAFS since the Region of Interest (ROI) matching the expected rate of Li deintercalation, herein the green color in the speciation map for $Li_{0.5}FePO_4$ composition, can be isolated later by post-processing to facilitate electrochemistry interpretation and draw correct conclusions from *operando* experiments (Fig. 1c). This is illustrated for Electrode 2 in Figure 1 (c) and (d).
In addition to ROIs selection in the 2D-maps for matching the intercalation-deintercalation rate with speciation, hyperspectral FF imaging allows to mitigate radiation damage of the electrode materials or electrolyte [4]. Indeed, the beam size for FF imaging can be much larger to the one used for conventional measurements, leading to an effective decrease of photon density and thus to a radiation dose bearable by the sample. Despite a significant S/N decrease of hyperspectral images recorded with so low photon density, we will show how the MCR-ALS is powerful to extract from noisy spectra accurate redox evolution.

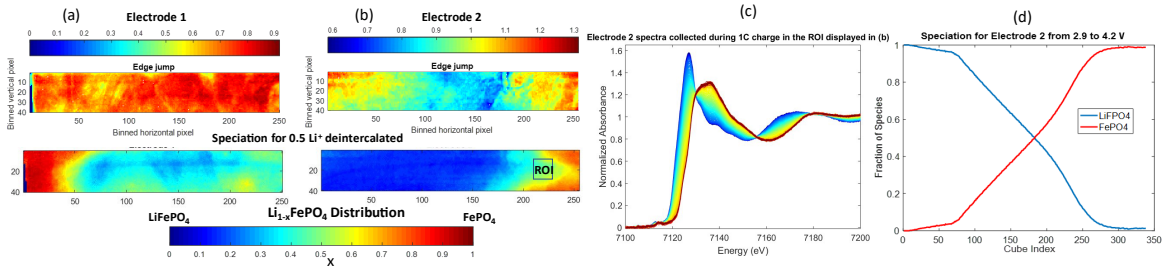

Figure 1. (a) and (b) Fe distribution deduced from the edge jump map (top) and $Li_{1-x}FePO4$ distribution (bottom) for two electrodes at 0.5 Li deintercalated (size of binned pixels: 10.4 x 10.4 μm^2). (c) Spectra and (d) speciation recorded upon electrode charge (1C) at the 65 x 65 μm^2 ROI displayed in (b).

[1] Leriche, J. B., Hamelet, S., Shu, J., Morcrette, M., Masquelier, C., Ouvrard, G, Zerrouki, M., Soudan, P., Belin, S., Elkaïm, E. & Baudelet, F. (2010). *J. Electrochemical Society,* **157**, A606.

[2] La Fontaine, C., Belin, S., Barthe, L, Roudenko, O. & Briois, V. (2020). *Synchrotron Radiation News*, **33**, 20.
[3] de Juan, A., Jaumot, J.& Tauler, R. A. (2014). *Anal. Methods*, **6**, 4964.
[4] Blondeau L., Surblé, S., Foy, E., Khodja, H., Belin, S. & Gauthier, M (2022). *Anal. Chem.*, **94**, 9683.
This project has received funding from the "Investissements d'Avenir" program (reference: ANR-10-EQPX-45) and from the European Union's Horizon 2020 research and innovation program under grant agreement No 957189.

A113-05-280823

Unravelling the structural changes of Bi-Mo-Co-Fe-O catalysts during selective olefin oxidation by complementary *operando* synchrotron-based techniques

L. Klag[1], A. Gaur[1], T. L. Sheppard[1,2], J.-D. Grunwaldt[1,2]

[1]*Institute for Chemical Technology and Polymer Chemistry (ITCP), Karlsruhe Institute of Technology, 76131 Karlsruhe, Germany* [2]*Institute of Catalysis Research and Technology (IKFT), Karlsruhe Institute of Technology, 76344 Eggenstein Leopoldshafen, Germany*

grunwaldt@kit.edu, abhijeet.gaur@kit.edu

Keywords: *operando* characterization, XAS, XRD, mixed metal oxides, selective oxidation

The selective oxidation of propylene and isobutene are key reactions in chemical industry for large-scale production of various intermediates (*e.g.*, Acrolein).[1] Typically, these are catalysed by bismuth molybdate based multicomponent systems (*e.g.,* Bi-Mo-Fe-Co-W-K-Si-O), which exhibit a high structural complexity, forming composites of active, selective, inert and promoter phases.[2] However, the roles and interactions of individual (mixed) metal oxide phases during selective olefin oxidation are still under strong discussion.[3] In the past, academic research commonly focused on simplified model systems (*e.g.*, 2-component Bi-Mo-O) to get a fundamental understanding of catalytic function.[4] Based on this knowledge, the next step towards the 4-component system, Bi-Mo-Co-Fe-O, is very promising, as it provides a suitable representation of complex metal oxide phases mixtures and superior catalytic performance.[5] To study structure-activity relationships in such complex, dynamic systems, various complementary and advanced characterization methods are needed that probe the catalyst under operating conditions.[6]

We investigated the structural evolution of Bi-Mo-Co-Fe-O catalysts by the means of *synchrotron-based operando* X-ray absorption spectroscopy (XAS), X-ray diffraction (XRD) and *laboratory-based* Raman spectroscopy under different gas atmospheres. While *operando* XAS allowed to monitor structural changes of each metal individually at Mo K-, Bi L3-, Co K- and Fe K-edges (Fig. 1), *synchrotron-based* XRD with Rietveld refinement (Fig. 2) gave qualitative and quantitative insights into crystalline catalyst phases (e.g., Bi3FeMo2O12 formation). Complementary *operando* Raman spectroscopy completed the understanding of the catalyst workings by probing contribution and stability of non-crystalline species during selective propylene and isobutene oxidation.

Determining the structural transformations within these systems under different gas atmospheres by an *operando* approach was crucial to reveal the role of individual catalyst phases, their dynamic behaviour, and interaction with other phases. Comparing characterization data obtained for selective propylene and isobutene oxidation allowed us to define the catalyst working principles more accurately in terms of active or selective metal oxide phases. Finally, studying 4-component systems is essential for closing knowledge gaps between the functionality of model systems, and complex industrially-applied catalysts, and thus contributes to a knowledge-based catalyst design and improvement.

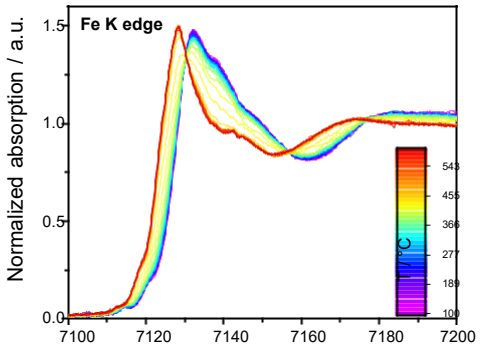

Figure 1 Structural evolution of $Bi_1Mo_{12}Fe_3Co_8O_x$ derived from XAS at the Fe K edge during selective isobutene oxidation.

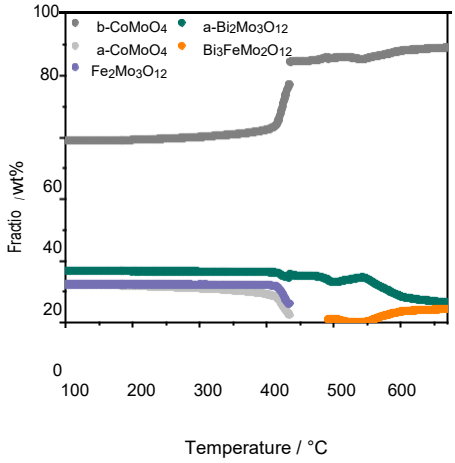

Figure 2 Structural evolution of $Bi_1Mo_{12}Fe_3Co_8O_x$ derived from synchrotron-XRD during selective isobutene

[1] J. Haber, *Handbook of Heterogeneous Catalysis*, Wiley-VCH, Germany, **2008**, 3350-3384.
[2] Y. Moro-Oka, W. Ueda, *Adv. Catal.* **1994**, *40*, 233-273.
[3] P. Sprenger, W. Kleist, J.-D. Grunwaldt, *ACS Catal.* **2017**, *7*, 5628-5642.
[4] P. Sprenger, M. Stehle, A. Gaur, A. Gänzler, D. Gashnikova, W. Kleist, J.-D. Grunwaldt, *ACS Catal*. **2018**, *8*, 6462-6475.
[5] M. Stehle, A. Gaur, S. Weber, T. L. Sheppard, M. Thomann, A. Fischer, J.-D. Grunwaldt, *J. Catal.* **2022**, *408*, 339-355.
[6] L. Klag, T. L. Sheppard, J.-D. Grunwaldt, *ChemCatChem* **2023**, *15*, e202201276.

A113-06-280823

Charge compensation mechanism and structural evolution in metal-ion battery cathodes studied by XAS and XRD

P. A. Morozova, S. D. Shraer, A. D. Dembitskiy, N. D. Luchinin, S. S. Fedotov

Skolkovo Institute of Science and Technology (Skoltech), 121205, Moscow, Russian Federation

s.fedotov@skoltech.ru

Keywords: metal-ion battery, cathode, charge compensation, structural evolution, $KTiOPO_4$, Prussian blue analogs

The skyrocketing demand for Li-ion batteries placed a focus of science and industry at post-lithium technologies like Na- and K-ion batteries (NIBs and KIBs) intended to alleviate risks of insufficient supply or lagging production of critical components used in Li-ion technology. To realize wide commercialization of both NIB/KIBs advances in electrode materials are vital. On a fundamental level, the processes occurring in the bulk of the electrode material hugely affect the resulting electrochemical properties. For instance, structural transformations in the course of electrochemical de/intercalation determine the long-term cycling stability, ionic diffusivity and rate capability, volume variation; charge compensation mechanisms define achievable specific capacities and electrode potentials, as well as electronic conductivity, and indirectly influences the ionic conductivity and local structure. Understanding these mechanisms opens up ample opportunities in designing and fine-tuning new and existing electrode materials to endow with specific properties or mitigate some adverse effects of intrinsic processes [1].

Using modern *operando* techniques based on X-ray diffraction and absorption, we studied structural evolution and charge compensation mechanisms in two contemporarily popular families of electrode materials for NIBs and KIBs, namely $KTiOPO_4$-(KTP)-type polyanion materials of the $AMPO_4X$ general formula (A = Na, K; M = Ti, V; X = O, F) [2,3] and $K_{2-\delta}M^I[M^{II}(CN)_6]_{1-\gamma}$($M^I$ = Fe, Mn, Co; M^{II} = Fe, Mn, Cr) hexacyanometallates also known as Prussian blue analogs (PBA) [4] showing great promise as electrodes for NIB/KIBs. In this talk, a short overview of the recent research activities of our group on novel electrode materials for NIBs and KIBs will be presented with a special focus on the interrelation between chemical composition, synthesis conditions, crystal structure peculiarities, de/intercalation and charge compensation mechanisms and electrochemical properties. A particular attention will be given to the leading role of *operando* XRD and XAS analyses (Figure 1).

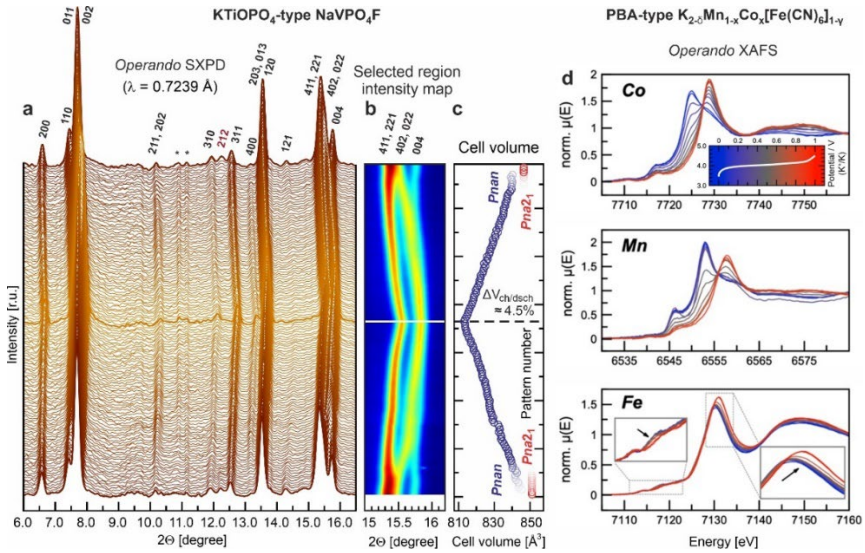

Figure 1. Waterfall *operando* diffraction pattern, intensity map and volume variation of $NaVPO_4F$ (**a**, **b**, **c**) [3] and Co/Mn/Fe K-edge evolution of $K_{2-\delta}Mn_{1-x}Co_x[Fe(CN)_6]_{1-\gamma}$ by *operando* XANES (**d**) [4].

[1] Abakumov, A. M., Fedotov, S. S., Antipov, E. V., & Tarascon, J. M. (2020). *Nat. Commun*. **11**, 4976.
[2] Fedotov, S. S., Luchinin, N. D. et al (2020). *Nat. Commun.* **11**, 1484.
[3] Shraer, S. D., Luchinin, N. D. et al (2022). *Nat. Commun.* **13**, 4097.
[4] Morozova, P. A., Ryazantsev S. V., Dembitskiy, A. D. et al (2023). *Chem. Mater*. Under revision.

Russian Science Foundation (#20-73-10248) and Russian Foundation for Basic Research (#21-53-12039) are acknowledged.

A119 Interoperability of Crystallographic Data and Databases
Room 212/213
4.00pm - 6.30pm

A119-01-280823

Applications of metadata collection and analysis to parallel crystallisation and the ENaCt technique

T. Smith, M. Probert, M. Hall

School of Natural and Environmental Sciences, Bedson Building, Newcastle University, NE1 7RU, Newcastle Upon Tyne

t.smith7@newcastle.ac.uk

Keywords: Crystallisation, Automation, Software

The analysis of large datasets forms the backbone of many aspects of today's scientific literature. Modern modes of data interrogation, such as machine learning techniques, have become ever more popular alongside the explosion of experimental data size. These methods can enable the unbiased extraction of information that may be overlooked or simply ignored by the human eye. This trend towards large data use and its analysis is a trend that is expected to grow and flourish to become a dominant aspect of modern research. Behind the glamor of the headline results and algorithms lies an ugly truth: large datasets are hard to manage, and the associated difficulties only increase with the size and scope of the intended interrogation. Proper data management techniques and tools are often an afterthought, and only considered in earnest when datasets begin to become unruly – the FlexTape™ patch for an already sinking vessel. We aim to show that by considering data management early, and investing time in quality tooling, it is possible to achieve a more harmonious existence that alleviates the need for patches and disentanglement problems during analysis.

High-throughput crystallisation experiments using the ENaCt technique[1] have the potential to generate significant amounts direct data (images, success/failure, etc.). However, collecting these data can be tedious and error-prone when left in the hands of humans. Herein is described an automated optical microscope coupled to a desktop application which significantly increases the reliability of collected data. In combination with an industrial machine vision camera containing a built-in grid of polarising filters, a real-time image processing system has been developed to automatically extract information about crystal quality from captured images and save that alongside relevant experimental metadata in a consistent and structured way.

Using a combination of a central relational database; python-powered JSON API; and custom-designed and implemented Query Language; we were able to provide team members with varying levels of programming ability a mechanism to efficiently access this dataset. As a result, they can make more informed decisions about which experiments to perform to enhance the likelihood of overall success.

[1] Tyler *et al.*, (2020). *Cell Chem.* **6**, 1755

Thanks to Newcastle University for funding this project.

A119-02-280823

DIMAS: A web-based service crystallography submission and data management system

Toby Blundell[1*] and Oleg Dolomanov[2]

[1]Department of Chemistry, Durham University, South Road, Durham, DH1 3LE [2]OlexSys Ltd., Durham University, South Road, Durham, DH1 3LE

Toby.j.blundell@durham.ac.uk

Keywords: Service Crystallography, Database, User Management

The Department of Chemistry at the University of Durham, UK has a long and prestigious reputation in the field of single crystal x-ray crystallography. As the premier technique allowing full structural identification of crystalline materials, crystallographers at Durham University work with researchers in numerous fields including materials science, chemistry, physics, biology, and engineering.[1]

In collaboration with OlexSys Ltd. [2] And Labsafe [3] we have developed a web-based platform to allow researchers to submit crystalline samples for x-ray diffraction analysis to the in-house crystallography service. DIMAS guides users through the process of submitting samples allowing them to include details about the synthesis and crystallisation conditions. There is an imbedded chemical drawing module to input the expected compound and users can keep track of all their submissions in one convenient location.

Following collection, a full set of crystallographic files, including data reduction outputs, structure solution and refinement files, as well as rendered images of the structures can be uploaded. DIMAS automatically extracts the relevant unit cell parameters, symmetry and data statistics as well as allowing the user to download the archived files and giving research group leaders oversight over their research group data.

Figure 1. DIMAS, a collaboration between Durham University, OlexSys Ltd. And Labsafe.

[1] https://crystallographygroup.webspace.durham.ac.uk/
[2] https://www.olexsys.org/
[3] https://www.olexsys.org/labsafe/

We acknowledge Dr Dmitry Yufit and OlexSys Ltd, particularly Prof. Horst Puschmann and Prof. Judith Howard.

A119-03-280823

Protein-Ligand Binding Database (PLBD) of Crystal Structures and Intrinsic Thermodynamic Parameters

D. Lingė[1], M. Gedgaudas[1], A. Merkys[2], V. Petrauskas[1], A. Vaitkus[2], A. Grybauskas[2], V. Paketurytė[1], A. Zubrienė[1], A. Zakšauskas[1], A. Mickevičiūtė[1], J. Smirnovienė[1], L. Baranauskienė[1], E. Čapkauskaitė[1], V. Dudutienė[1], E. Urniežius[1], A. Konovalovas[3], E. Kazlauskas[1], K. Shubin[4], H. B. Schiöth[5], W.-Y. Chen[6], J. E. Ladbury[7], S. Gražulis[2], D. Matulis[1]

1Department of Biothermodynamics and Drug Design, Institute of Biotechnology, Life Sciences Center, Vilnius University, Saulėtekio 7, Vilnius, LT-10257, Lithuania, 2Sector of Crystallography and Cheminformatics, Institute of Biotechnology, Life Sciences Center, Vilnius University, Saulėtekio 7, Vilnius, LT-10257, Lithuania, 3Department of Biochemistry and Molecular Biology,, Institute of Biosciences, Life Sciences Center, Vilnius University, Saulėtekio 7, Vilnius, LT-10257, Lithuani, 4Latvian Institute of Organic Synthesis, Riga LV-1006, Latvia, 5Functional Pharmacology and Neuroscience, Department of Surgical Sciences, Uppsala University, Uppsala, Sweden, 6Department of Chemical and Materials Engineering, National Central University Jhong-Li 320, Taiwan, 7School of Molecular and Cellular Biology, University of Leeds LC Miall Building, Leeds, LS2 9JT, United Kingdom

daumantas.matulis@bti.vu.lt

Keywords: Protein-ligand binding, X-ray crystallography, Thermal shift assay, Differential scanning fluorimetry, Isothermal titration calorimetry, Carbonic anhydrase, Sulfonamide

Here we introduce a Protein-Ligand Binding Database (PLBD) of thermodynamic and kinetic data of protein interaction with small molecule compounds, available at https://plbd.org. The binding data are linked to the same protein-ligand co-crystal structures, enabling the structure-thermodynamics correlations both in terms of protein structure and compound chemical formula. Currently, the database contains over 5500 binding datasets of 556 sulfonamide compound interactions with the 12 catalytically active human carbonic anhydrase (CA) isozymes determined by the fluorescent thermal shift assay, isothermal titration calorimetry, inhibition of enzymatic activity, and surface plasmon resonance [1,2]. In the PLBD, we emphasize the intrinsic thermodynamic parameters that account for the binding-linked protonation reactions. In addition to the protein-ligand binding affinities, the database provides calorimetrically measured binding enthalpies, enhancing the understanding of reaction mechanisms. The database also contains 127 X-ray crystal structures of six CA isozyme complexes with ligands [1,2]. The database has been built using the FAIR data principles and the model was originally developed for exchanging crystallographic data in the CIF framework. The database schema and deposited data have revision and versioning systems providing historical traces of database evolution. The PLBD is useful for the investigations of protein-ligand recognition principles and could be applied for small molecule drug design.

Acknowledgement. This research was funded by a grant S-LLT-20-2 from the Research Council of Lithuania, Lithuanian-Latvian-Taiwan Cooperation Programme.

[1]. Matulis (Ed.), D. Carbonic Anhydrase as Drug Target: Thermodynamics and Structure of Inhibitor Binding; Springer Nature, 2019.
[2]. Linkuvienė, V.; Zubrienė, A.; Manakova, E.; Petrauskas, V.; Baranauskienė, L.; Zakšauskas, A.; Smirnov, A.; Gražulis, S.; Ladbury, J. E.; Matulis, D. Thermodynamic, Kinetic, and Structural Parameterization of Human Carbonic Anhydrase Interactions toward Enhanced Inhibitor Design. *Q. Rev. Biophys*. 2018, 51, 1–48.

A119-04-280823

Database interoperability: A powder diffraction perspective

S. Kabekkodu and T. Blanton

International Centre for Diffraction Data 12 Campus Blvd, Newtown Square, PA19073, USA

Kabekkodu@icdd.com

Keywords: Crystallographic database, Interoperability, Powder Diffraction, Raw Data Archival, Phase Identification,

Crystallographic database interoperability is essential to support growing data driven innovation in materials research. ICDD's Powder Diffraction File™ (PDF®) is the database that has been used by all of the major powder diffractometer manufactures for phase identification for several decades. Maintaining database interoperability to work with all of the public and proprietary phase identification software is crucial. The ICDD PDF database was first published in 1941 and since 1967 (first digital crystallographic database) The PDF has been configured keeping in mind the software developers in terms of data interoperability. ICDD adopted RDBMS (Relational Database Management System) in the year 2000. RDBMS provides flexible access to the database for programming and a relational database construct allows ICDD to adhere to FAIR (Findable Accessible Interoperable Reusable) principles. Software developers are able to maintain database interoperability even as there are continuous and dynamic changes to the PDF database. Metadata also plays a very important role in adhering to FAIR principles. In powder diffraction there is a challenge as there is no common raw data format among the diffractometer manufactures. The PDF is accessible independent of these varying formats.

The ICDD PDF is a curated database with every entry evaluated using a combination of computer and human editorial review and presented using a quality mark nomenclature that provides the user with a systematic process for understanding data entry quality and a consistent approach in assessing the goodness-of-match for phase identification. These quality marks are also important from the interoperability perspective, given the existence of multiple automated software routines used for phase identification. An additional feature of the Powder Diffraction File it the inclusion of 18,000+ entries with raw data powder diffraction patterns that can be used to direct comparison to user data.

ICDD PDF database interoperability in terms of structure and semantics will be discussed in this presentation.

A119-05-280823

Interoperability of Databases as viewed by the Publisher

B. McMahon

International Union of Crystallography, 5 Abbey Square, Chester CH1 2HU, UK

bm@iucr.org

Keywords: Databases, Interoperability, Scientific publishing

The emergence of interoperable protocols that allow curated databases and publishers to exchange research data sets and associated metadata brings great benefits for the way that databases and journals can complement each other. The International Union of Crystallography (IUCr) is a publisher of several data-rich journals, and has taken full advantage of these protocols. Indeed, it has sponsored the Crystallographic Information Framework (CIF) project, which provides crystallography with greater interoperability than most other scientific domains.

Structural databases began by manually harvesting tabulated data from printed journals, in arbitrary formats and needing much effort to re-keyboard the data, an error-prone exercise. The introduction of the CIF format in 1991 [1] provided a standard machine-readable presentation that could be easily harvested over the network and ingested error-free into the databases' own internal formats. While practice has evolved so that many data sets are now deposited directly with databases before publication, the availability of these data sets, still mandated by IUCr journals, from the publisher's own website allow future harvesting by new and diverse databases.

IUCr journals routinely provide links to the structure representation views of published structures in the relevant databases. They now also import data sets from external databases, allowing readers of published structural articles to manipulate value-added visual representations of the structures within the online article environment itself (Fig. 1).

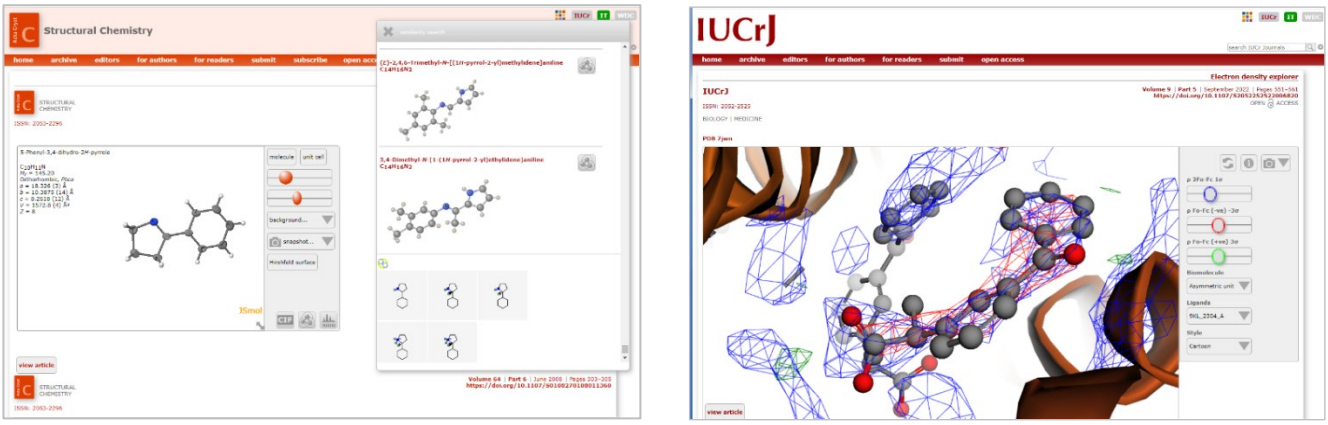

(*a*) (*b*)

Figure 1. Value-added structure exploration within IUCr journals. (*a*) Interactive electron density maps. (*b*) Three-dimensional ellipsoid visualization and similarity searches against both other articles published in IUCr journals and the PubChem database.

As IUCr journals become rich repositories of deposited structural data sets, so they have the potential to host novel data discovery systems that do not use the formal relational schemas of the conventional databases [2]. New approaches using artificial intelligence techniques open the possibility of even

greater synergy between traditional publishing and database platforms. These may, further, help to address the challenge of making scientific connections across different disciplines, where there are not as yet widely available tools to make semantic links between different domain-specific metadata standards such as those catalogued by the Research Data Alliance [3].

[1] Hall, S. R., Allen, F. H. & Brown, I. D. (1991). *The Crystallographic Information File (CIF): a new standard archive file for crystallography. Acta Cryst.* A**47**, 655–685.
[2] Özer, B., Karlsen, M. A., Thatcher, Z. *et al*. (2022). *Towards a machine-readable literature: finding relevant papers based on an uploaded powder diffraction pattern. Acta Cryst.* A**78**, 386–394.
[3] Research Data Alliance (2023). Metadata Standards Catalog. https://rdamsc.bath.ac.uk/

A119-06-280823

The Cambridge Structural Database: A multidisciplinary resource

S. C. Ward1, M. P. Lightfoot1

The Cambridge Crystallographic Data Centre, Cambridge (United Kingdom)

ward@ccdc.cam.ac.uk

Keywords: CSD, FAIR, Interoperability

The Cambridge Structural Database (CSD) was founded on a vision that collective use of data would lead to the discovery of new knowledge which transcends the results of individual experiments. The existence of a common crystallographic language, an ability to understand crystallographic information, and an awareness of the importance of data interoperability have enabled that vision to come to true. The database is now a valued multidisciplinary resource used extensively in academia as well as in industry particularly as part of drug development and materials design.

In crystallography we are extremely fortunate that a standard file format has been adopted by researchers, software creators and publishers alike providing a strong foundation for data sharing. As a proponent of the FAIR data principles, the Cambridge Crystallographic Data Centre (CCDC) has supported the community by developing a workflow from structure deposition to data sharing. This workflow seeks to promote these guiding principles by enabling depositors to provide information which renders the datasets more Findable, Accessible, Interoperable and Reusable. As the curators of a domain specific repository, we also work to ensure this crystallographic data can be utilised across disciplines to enable the advancement of science as well as crystallography.

This talk will explore the part we can play in helping the reliable sharing of data between disciplines and how we are supporting efforts to adhere to new best practices for data management that will enable researchers to get the most from crystal structure data. It will focus on the steps the CCDC has made to increase interoperability, as well as some of the opportunities and challenges we face as we work to ensure the wealth of information contained in 1.2 million structures in the CSD can exploited by machines as well as people from across disciplines.

A120 IUCr 75th Anniversary
Room 219
4.00pm - 6.30pm

A120-01-280823

The IUCr and International Science

Brian McMahon

International Union of Crystallography, 5 Abbey Square, Chester CH1 2HU, UK)

bm@iucr.org

Keywords: History of IUCr, International Scientific Unions, International Science

Individual scientists have always collaborated enthusiastically with colleagues from other nations, but the seeds of organized international scientific cooperation were sown with the International Polar Year project of 1882-3. The first attempt to impose a framework on international science was a cartel of national academies in 1899. International Scientific Unions began to form around 1919, and the International Council of Scientific Unions (ICSU) was established in 1931 to coordinate national adhering organisations and the growing number of Unions. The IUCr was accepted into ICSU in 1947. UNESCO, founded in 1947, provided a global umbrella for cultural, scientific and educational developments under the aegis of the United Nations. The IUCr publishing programme has benefited from its association with both UNESCO and ICSU. UNESCO provided financial support for many of the IUCr's early publishing activities, and was a Partner in the International Year of Crystallography 2014. ICSU has provided guidance in the development of electronic publishing and data management through its associated organizations ICSTI and CODATA, and established the scientific freedom policy that the IUCr upholds. It is significant that the major inflection points in the development of international science organizations have coincided with periods of global conflict. ICSU merged with the International Social Science Council in 2018 to become the International Science Council.

A120-02-280823

The International Importance of the IUCr

E. N. Baker

School of Biological Sciences, University of Auckland, New Zealand

Ted.baker@auckland.ac.nz

Keywords: International role, scientific advances, quality

My personal involvement with the IUCr began with the 14th Congress, held in Perth, Australia in 1987. Before then, the costs of attendance of international meetings had been too great, coming from a small country with limited funding. This meeting opened my eyes to the world of crystallography, and I have attended every Congress since then (except Prague). After every one of these I came away inspired. In my remarks, I would like to focus on three aspects: the role of the IUCr as a truly international organisation; its ability to bring the latest advances to people round the world, and to inspire; and its importance in leading the way in standing for both quality and equality – rigorous scientific standards, and leadership in supporting inclusion and diversity.

A120-03-280823

75th Anniversary of our union

S Lidin

Department of Chemistry, Lund university, POB 188, Lund, Sweden

Sven.lidin@Chem.lu.se

Keywords: Presidency, Traditions, Change

75 years is a long time for a scientific union and much has changed since the first IUCr congress in 1948. New sources, detectors and methods have transformed crystallography and the subject keeps reinventing itself, morphing to meet ever-new challenges and the union must change accordingly to stay relevant to the subject.

Concurrently, the scientific community changes; it expands and grows in new geographical areas and the scientific culture changes everywhere. This poses a challenge to our union to maintain and improve the service we provide to the scientific community.

We see the constant emergence of entirely new sub-fields in crystallography that complement but also challenge existing methods. We are in the middle of a transition to new financial models for publishing and the way we communicate with each other changes continuously with the emergence of new platforms for exchange of opinions and data.

Structural science has come a long way since the Braggs taught us to see a world in a grain of salt, but the changes in our community are even greater. The union has weathered these changes and will continue to do so, as long as we stay in tune with the young crystallographers who constitute our future.

A120-04-280823

The IUCr's Finance Committee – what is it and what does it do?

Malcolm J Cooper,

Department of Physics, University of Warwick, Coventry CV47AL, UK

Keywords: Journals, Investments, People

The IUCr first created a Finance Committee in 1981, thirty-three years after the Union was created. Michael Wolfson as its Convenor and its role was to advise the Executive Committee on the running of the Union's finances. Prior to that the first Executive Secretary, Jim King, who was appointed in 1969 and the first General Secretary and Treasurer, Durward Cruickshank, who was appointed in 1970 were the only ones with overall oversight of the IUCr's *business*. The Finance Committee was established under the tenure of Professor Kaarle Kurki-Suonio, as General Secretary and Treasurer, to advise him on the Union's finances. It is the profitability or otherwise of the journals which dictates the extent to which the organisation can sponsor its *good works* in the crystallographic community; subscriptions from adhering body countries and sales of volumes of International Tables constitute a very minor part of the Union's turnover. It was during the period of office of the second Convenor, Bob Diamond, that the idea of maintaining a healthy excess of journal income over expenditure not only to sponsor its good works but also to build up investment reserves for times when journals were not profitable gained currency, Over the years problems occurred, for example, due to rises in printing costs, adverse changes in currency exchange rate movements or because expensive investment was needed to transform the publishing process to become electronic. The members of the Finance Committee tend to serve a longer term than members of the Executive in order to develop long term oversight of the business and there have been relatively few Convenors over the years. The role and composition of the Finance Committee and some of the challenges that it currently faces will be discussed in this presentation.

A120-05-280823

Scientific publishing at the IUCr

Peter R. Strickland

International Union of Crystallography, Editorial Office, 5 Abbey Square , Chester CH1 2HU, United Kigdom

ps@iucr.org

Keywords: crystallography, structural science, scientific publishing, IUCr

This short presentation provides a personal view of over 35 years of working for the IUCr in its Editorial Office. The presentation will focus on the changes that have occurred in the publishing operations during this time. One of main challenges has been staying abreast of the rapidly evolving landscape of scientific publishing. The rise of digital publishing and open access has led to significant changes in the way that research is disseminated, and the IUCr has worked hard to adapt to these changes while maintaining our commitment to high-quality content and rigorous peer review. The most rewarding aspect of the work has been meeting and collaborating with the many editors and other members of the IUCr family who volunteer their time to make our operation a success.

A120-06-280823

The outreach and education programme of the IUCr

M. Zema1

1 International Union of Crystallography, Chester, UK

mz@iucr.org

Keywords: outreach, education, infrastructure

At a time when scientific endeavour is critical for societal benefit, the importance of crystallography is greater than ever, yet it remains a science that still has lower visibility than it should. Crystallography underpins all science today, has given a new path to scientific research, has transformed industries, and created new frontiers, from the design of new medicines and materials to assessing the mineral content of Mars. Despite this, access to crystallographic knowledge, technology and infrastructure is very limited or almost absent in several regions of the world.

Since its foundation, the IUCr has stimulated and supported the growth of the crystallographic community. With the resolution A/RES/66/284 of 12 July 2012 proclaiming the *International Year of Crystallography* (IYCr2014), the UN recognized that *humankind's understanding of the material nature of our world is grounded, in particular, in our knowledge of crystallography, and stressed that education about and the application of crystallography are critical in addressing fundamental challenges*. The IUCr, in a close collaboration with UNESCO, has built up an ambitious programme for IYCr2014 aimed at disseminating the crystallographic culture in those parts of the globe where it is still latent, and at fostering new collaborations. The conference "*Crystallography for the next generation*" (Morocco, 2015) reviewed the accomplishments of IYCr2014, and the potential for building on those successes to maintain the momentum of the IYCr2014. As an outcome of that event, the IUCr and partner institutions signed a resolution and committed to enhance the stature of crystallography; build capacity in developing regions of the world; extend further the public understanding of science in general and crystallography in particular.

For the last ten years, the IUCr has been actively engaged in a number of outreach and education initiatives, targeting emerging countries worldwide and students of all ages, from schoolchildren to early career researchers and established crystallographers.

The geographical scope of the crystallographic community has expanded significantly, and with a strong sense of inclusiveness. The admission of two new Regional Associates (Latin American Crystallographic Association, LACA in 2014 and African Crystallographic Association, AfCA in 2023) and few new national members is a clear indication of such a transformation.

The IUCr has been partnering with several other societies and organizations and has reinforced its high reputation in the contexts of the global science diplomacy and advocacy debate, as demonstrated by the constant participation in strategic science-policy meetings, like the World Science Forums and the CiLAC Forums, and of science capacity building assessment through the implementation of actions towards developing scientific research, education and infrastructure worldwide. Initiatives like the IUCr-UNESCO OpenLab, implemented in over 25 countries, or the IUCr-IUPAP-ICTP *LAAAMP* have acquired enormous visibility and high recognition, so that now they represent a reference point for many researchers and organisations. Around a thousand students have been trained in crystallography and synchrotron-based techniques through these initiatives, and some crystallography labs launched by an OpenLab are now reference centres in their countries or regions.

The experience gained through the OpenLab and *LAAAMP* initiatives have brought to the foundation of the *X-TechLab*, a top-quality crystallography hub for Central and Western Africa, located in Benin,

and representing one of the flagship laboratories of Sèmè City, the International City of Innovation and Knowledge. A similar facility, named *crXstal*, is being implemented in Jamaica to act as a crystallography hub for the Greater Caribbean region. Interestingly, *X-TechLab* and *crXstal* are seen by the international scientific community as 'feeders' for the African Light Source and the Synchrotron for the Greater Caribbean initiatives, respectively.

Most recently, new actions have been initiated in the Pacific islands and Central Asia, and for the Portuguese-speaking scientific community. The IUCr outreach and education programme is getting richer and richer almost every day, and new initiatives are being implemented to continue sustaining the growing community of crystallographers and to target more and more regions of the world.

A120-07-280823

Crystallography in Africa

Delia A. Haynes

Department of Chemistry & Polymer Science, Stellenbosch University, P. Bag X1, Matieland, Stellenbosch, 7602, Republic of South Africa

dhaynes@sun.ac.za

Keywords: crystallography, Africa

This short presentation will briefly discuss the development of crystallography in Africa, as well as presenting ideas for the future of crystallography on the continent.

A120-08-280823

How do we make sure everyone feels welcome in Crystallography?

H.E. Maynard-Casely[1]

Australian Nuclear Science and Technology Organisation, Locked Bag 2001, Kirrawee DC, 2234, NSW, Australia

helenmc@ansto.gov.au

Keywords: Equity, Diversity, Role Models, Disability, Representation

Reflections and projections are regular tools of any crystallographer's trade. However, they are also essential tools when thinking about the 75th anniversary of the IUCr and in exploring how welcoming and inclusive our union is. When beginning a crystallographic career, like any field, it can be incredibly influential to see those you identify with, both historic and current, actively succeeding. Crystallography has a reputation for being more inclusive than other science areas, but the reality is and the data show that we still have a long way to go. So rather than question the problem, we must move on and seek solutions, ask ourselves *'What concrete actions should the IUCr take to ensure our union truly reflects our world?* We can all reflect on how to make crystallography a science that everyone feels they can participate in, and use this as a projection for the future.

The author wishes to acknowledge the Dharawal people, the traditional owners of the land where ANSTO Lucas Heights operates.

A120-09-280823

Education never ends

A. Guerri1

Department. of Chemistry U. Schiff – University of Florence (IT)

annalisa.guerri@unifi.it

Keywords: Education, outreach, tradition

IUCr has always worked for education in crystallography with different projects which started with the help of profits from the publishing activities. All the initiatives have been developed ever since and flourished with the International Year of Crystallography (IYCr) in 2014. A lot has been done during the IYCr, especially in the developing counties to work also for the equity and diversity balance.

The IUCr commission on Crystallographic Teaching is very devoted to help all the educational events, especially those who reaches the more remote countries.

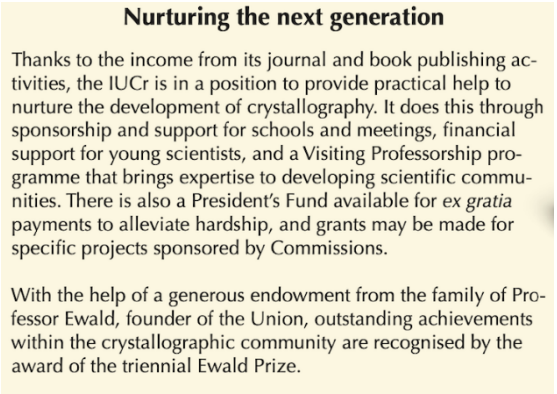

Nurturing the next generation

Thanks to the income from its journal and book publishing activities, the IUCr is in a position to provide practical help to nurture the development of crystallography. It does this through sponsorship and support for schools and meetings, financial support for young scientists, and a Visiting Professorship programme that brings expertise to developing scientific communities. There is also a President's Fund available for *ex gratia* payments to alleviate hardship, and grants may be made for specific projects sponsored by Commissions.

With the help of a generous endowment from the family of Professor Ewald, founder of the Union, outstanding achievements within the crystallographic community are recognised by the award of the triennial Ewald Prize.

Figure 1. From a poster in https://www.iucr.org/iucr

One of the supporting activities of the Union is the one in favour of the International School of Crystallography which was born in 1974 thanks to the idea of Prof. Lodovico Riva di Sanseverino and Prof. Michael Woolfson (and some other supporting friends, like Prof. Mario Nardelli, President of the IUCr from 1987 to 1990 and Prof. Davide Viterbo, member of the executive committee from 2002 to 2008) who envisioned a tradition of courses with renowned lecturers and students from every corner of the world. The school is still working and will celebrate the 50th anniversary next year.

As a final remark, it must not be forgetting the difficult years of the pandemic which impacted in the education of the younger generation: the experience of the senior crystallographers and new approaches for teaching will help to continue building the road of education with the support of the Union, acting as a connection and support for the crystallographers.

A120-10-280823

Exploration of primary and secondary sphere coordination by unsymmetric pyrimidine sulfanyl and aminopyrazole ligands

Dawe*[1], S. D. Joekar[1], L. Hiscock[1], K. Anoliefo[1], A. Hankins[1], K. Maly[1], P. Boyle[2]

Department of Chemistry and Biochemistry, Wilfrid Laurier University, Waterloo, ON, Canada, 2. Western University, Department of Chemistry, London, ON, Canada

Keywords: Coordination chemistry, Intermolecular interactions, Structure-property relationships

In our exploration of ligand systems that simultaneously incorporate three types of molecular affinity: (i) coordination of Lewis acids; (ii) intermolecular interactions with anions; and (iii) additional functional modalities, we have recently focused on two classes of unsymmetric molecules based on (a) aminopyrazole and (b) pyrimidine sulfanyl cores (Fig. 1). We have targeted this design strategy because a knowledge gap still exists with respect to controlling the directionality of weak intermolecular forces [1], which may be further complicated in the presence of stronger, competing forces [2].

In the case of the aminopyrazole systems, we have previously observed via polarized optical microscopy that all exhibit supercooling of between 34 and 100 ^{o}C, and upon coordination to ZnCl2 and ZnBr2, we have observed bright, solid-state fluorescence.[3] We have now expanded our coordination chemistry and fluorescence studies to produce adducts with $BF2^{+}$, which are also fluorescent.

We have also expanded on our previously reported results [4] to generate monosubstituted pyrimidine sulfanyl ligands, which we have recently functionalized to produce unsymmetric ligands, for example, with R = morpholine; Fig. 1(b).

Synthesis, characterization, and structural features of primary sphere coordination with Lewis acids will be highlighted, as well as secondary sphere interactions and possible applications for environmental anion sensing.

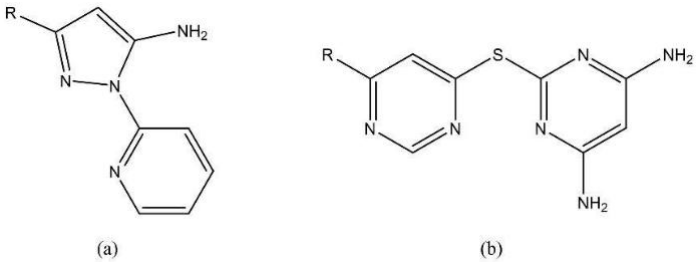

Figure 1. Unsymmetric (a) aminopyrazole and (b) pyrimidine sulfanyl ligand cores explored herein.

[1] Chakrabarty, R., Mukherjee, P. S. & Stang, P. J. (2011) Chem. Rev., 111, 6810.
[2] Robertson, C. C., Wright, J. S., Carrington, E. J., Perutz, R. N., Hunter, C. A. & Brammer, L. (2017) Chem. Sci., 8, 5392.
[3] Hiscock, L. K., Joekar, D., Balonova, B., Tomas Piqueras, M., Schroeder, Z. W., Jarvis, V., Maly, K. E., Blight, B. A. & Dawe, L. N. (2019). Inorg. Chem., 58, 16317.
[4] Moyaert, T. E., Paul, C., Chen, W., Sarjeant, A. A. & Dawe, L. N. (2017). Acta Cryst. E, 73, 1534.

We would like to acknowledge that Wilfrid Laurier University and its campuses are located on the shared traditional territory of the Neutral, Anishnaabe and Haudenosaunee peoples.

A120-11-280823

The four stacking modes of experimental and predicted Lapachol polymorphs.

N. Di Benedetto1, Brad C. Ayers2, Mario A. Macías3, Grame P. Day2, Miguel A. Martínez-Cabrera4, L. Suescun1

Cryssmat-Lab/DETEMA, Facultad de Química, Universidad de la República, Casilla 1157, Montevideo, Uruguay, School of Chemistry, University of Southampton, Southampton, SO17 1BJ, United Kingdom, Departamento de Química, Facultad de Ciencias, Universidad de los Andes, Carrera 1 # 18A – 12, Bogotá, Colombia, Facultad de Ciencias Exactas y Naturales, Universidad de Asunción, Asunción, Paraguay.

leopoldo@fq.edu.uy

Keywords: Lapachol, Polymporphism, Structure prediction

Lapachol (2-hydroxy-3-(3-methyl-2-butenyl)-1,4-naphthoquinone) is a pigment extracted from the bark of *Handroanthus heptaphyllus* (Vell.) Mattos commonly known as pink trumpet tree or lapacho. The group of 1,4-naphthoquinones and its derivatives has always attracted a lot of attention since these compounds exhibit a wide range of biological and pharmacological effects. In particular, lapachol has demonstrated properties as an antitumor, anticarcinoma, antiviral, bactericidal, fungicidal and antimalarial agent, among others. Two lapachol polymorphs were described by Larsen et al. (1992) [1] with triclinic $P\bar{1}$ (LAPA I: a=5.960(1), b=9.569(2), c=10.679(2) Å, α=96.82(2), β=98.32(2) and γ=90.32(2) ˚) and monoclinic $P2_1/c$ (LAPA II: a=6.035(1), b=9.427(2), c=20.918(5) Å and β=98.27(2) ˚) crystal structures at 105K.

During the course of an investigation of lapachol complexes we accidentally found a new polymorph, also monoclinic $P2_1/c$ (LAPA III: a= 9.5943(19), b= 6.0173(10), c= 21.566(2) Å, α= 90, β=96.815(2), γ= 90 ˚) with the unit cell closely related to that of LAPA I and LAPA II. The three structures show identical lapachol dimeric layers (formed by centrosymmetric lapachol dimers) that define the constant a~6.0, b~9.6 Å and g≈90 ˚ unit cell parameters, with exact overlap of lapachol conformations among crystal structures. These layers stack through van der Waals interactions in three different ways defining the three observed crystal structures. In LAPA I consecutive layers are just related by translation along c. In LAPA II and LAPA III consecutive layers are related by a 2_1 screw axis along a and b axes respectively.

The rigid behaviour of lapachol molecule in the three experimental crystal structures led us to examine the energy landscape of lapachol crystals, in order to test if the new lapachol polymorph could have been predicted and whether other molecular conformations are able to produce low energy crystal structures. The structure prediction algorithm [2] found the three observed crystal structures among the four lowest energy predicted structure, and additionally a fourth crystal structure with similar energy to that of LAPA III showing the same dimeric layers of lapachol with consecutive layers related by a 2_1 axis along the normal to the invariant a-b plane (LAPA IV, monoclinic $P2_1/n$: a=9.078, b=21.611, c=6.350 Å, α= 90, β=89.7, γ= 90˚).

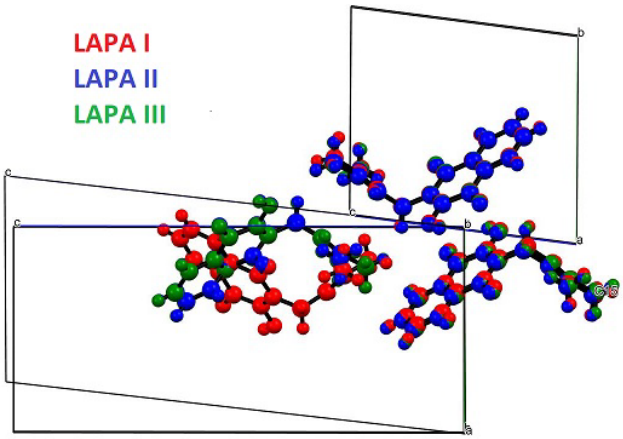

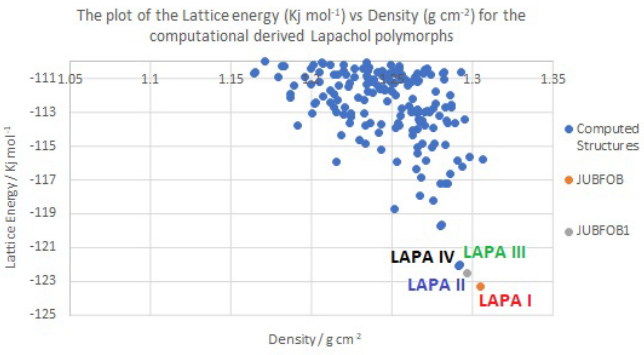

Figure 1. Left: Overlay of experimental lapachol crystal structures & unit cells. Molecules of one layer fit perfectly while the next layer shows a change in orientation in II and III. Right: Plot of lattice energy vs density for predicted crystal structures.

We will present the structural analysis of the four lapachol polymorphs emphasizing on the similarities and difference and inform of the results of the on-going search of the missing polymorph in the lab.

[1] Larsen, I.K., Andersen, L.A. & Pedersen, B.F. (1992). *Acta Cryst.* C**48**, 2009-2013.
[2] Case, D. H., Campbell, J. E., Bygrave, P. J. & Day, G.P. (2016) *J. Chem. Theory Comput.* 12(2), 910-924.

A120-12-280823

Multi-step crystallization processes of cosmic dust analogues founding in microgravity experiments

Yuki Kimura1, Kyoko K. Tanaka2, Yuko Inatomi3

1Institute of Low Temperature Science, Hokkaido University; Kita-19, Nishi-8, Kita-ku, Sapporo, 060-0819, 2 Astronomical Institute, Tohoku University; 6-3 Aoba, Aoba-ku, 985-8578, Sendai, Japan, 3Japan, Institute of Space and Astronautical Science, Japan Aerospace Exploration Agency; 3-1-1 Yoshinodai, Chuo-ku, Sagamihara, Kanagawa 252-5210, Japan, and School of Physical Sciences, SOKENDAI (Graduate University for Advanced Studies); 3-1-1 Yoshinodai, Chuo-ku, Sagamihara, Kanagawa 252-5210, Japan

ykimura@lowtem.hokudai.ac.jp

Keywords: Dust, Sounding rocket, Crystal growth

We aim to understand the formation processes and characteristics of cosmic dust, which is ubiquitous in space. Generally, cosmic dust has been discussed based on findings from experiments conducted in Earth's gravitational environment, despite the fact that cosmic dust is formed in microgravity environment. In addition, the characteristics of dust have been discussed based on the physical properties of bulk particles, even though the size of dust is less than 100 nm, where nanoparticles have unique physical properties and peculiar phenomena that are different from those of bulk particles. Therefore, we have conducted an experiment of dust analogues formation under the microgravity environment obtained by using sounding rockets. With optical methods such as interferometry and infrared spectroscopy, we determined the sticking probability and surface free energy of the nanoparticles, and investigated the crystallization pathway.

We performed sounding rocket experiments in five times in a past decade and produced metal [1], oxide [2, 3] and carbide [4] nanoparticles as dust analogues via homogeneous nucleation from supersaturated vapor. Based on nucleation temperature, timescale for gas cooling and size of produced particles, sticking probabilities and surface free energies have been successfully determined by means of nucleation theory. Sticking probabilities are usually assumed to be close to 100% because it is convenient to explain the abundance of dust in the universe and bulk experiment supported the assumption [5]. In contrast, the sticking probabilities obtained from our formation experiments of nanoparticles are two to five orders of magnitude smaller, 0.002% for Fe [1] and 0.5-1.6% for SiO [3], for instance. These values were also 1-2 orders of magnitude smaller than those obtained in the ground experiments. Nanoparticles are produced by heating an evaporation source to generate high-temperature vapor in argon gas, which works to decrease mean free path of evaporated vapor. On the ground, the high-temperature evaporation source generates density-difference convection, resulting in gas flow, whereas in a microgravity environment, the isotropically evaporated high-temperature gas cools slowly in a calm environment with no flow, forming nanoparticles. Just as shaking a plastic bottle filled with supercooled water induces the formation of ice, a flow of supercooled vapor promotes the formation of nanoparticles. Therefore, microgravity experiments are essential to determine the precise physical quantity.

In-situ observation of the formation of aluminum oxide nanoparticles from supersaturated vapor by infrared spectroscopy revealed that the nanoparticles undergo a crystallization process via a droplet [2]. At the beginning for nucleation, since the size of nuclei is very small, couple of nanometres or even smaller, melting point of the nuclei is lower than corresponding bulk material. Namely, when nucleation temperature is higher than the melting point of nucleating nanoparticle, the two-step nucleation process, a droplet is first nucleated from the supersaturated vapor and then crystals are nucleated from the supercooled droplet, becomes common. Furthermore, the formation process of carbonaceous particle with a titanium carbide core, which is well-known pre-solar particle, was found

to proceed by three processes: formation of initial particles, development of core-mantle structure, and fusion growth of nanoparticles [4]. Our series of experiments have revealed that such non-classical nucleation processes are universally observed in a variety of materials. In the presentation, we discuss new findings on the formation of nanoparticles from the gas phase and on the formation process of cosmic dust.

[1] Kimura, Y., Tanaka, K. K., Nozawa, T., Takeuchi, S. & Inatomi, Y. (2017). *Sci. Adv.* **3**, e1601992.
[2] Ishizuka, S., Kimura, Y., Sakon, I., Kimura, H., Yamazaki, Y., Takeuchi, S. & Inatomi Y. (2018). *Nat. Commun.* **9**, 3820.
[3] Kimura, Y., Tanaka, K. K., Inatomi, Y., Ferguson, F. T. & Nuth III, J. A. (2022). *Astrophys. J. Lett.* **934**, L10.
[4] Kimura, Y., Tanaka, K. K., Inatomi, Y., Aktas, C. & Blum J. (2023). *Sci. Adv.* **9**, eadd8295.
[5] Tachibana, S., Nagahara, H., Ozawa, K., Ikeda, Y., Nomura, R., Tatsumi, K. & Joh Y. (2011). *Astrophys. J.* **736**, 16.

Microgravity experiments using sounding rockets were conducted and/or supported with ISAS/JAXA. NASA, SSC and DLR. Development of the experimental system was supported by the Technical Division of the Institute of Low Temperature Science, Hokkaido University, and the Advanced Machining Technology Group of JAXA. We thank Grant-in-Aids for Scientific Research (S) from KAKENHI 20H05657.

A120-13-280823

Experiences with the IUCr over nearly 60 years

A.M. Glazer

Physics Department, University of Oxford, Parks Road, Oxford OX1 3PU, UK & Department of Physics, University of Warwick, Coventry, CV4 7AL, UK

Mike.glazer@physics.ox.ac.uk

Keywords: IUCr

My first encounter with the International Union of Crystallography was when I was able to attend the 1966 Congress in Moscow. Since then I have attended every Congress, apart from the one in Prague, because of the Covid epidemic. In this brief talk, I will describe some of my experiences with the IUCr over this period.

A120-15-280823

IUCr, the glue of the crystallographic community

S. Larsen

Department of Chemistry, University of Copenhagen, Denmark

sine@chem.ku.dk

Keywords: IUCr-journals, Regional Associates, Large Facilities

At a 75th anniversary, it is appropriate to look back. Knowing that the history of the Union up to 1998 is covered by the two excellent papers by Hamminga [1] and Cruickshank [2]. I use this opportunity to report on my time as a member of the IUCr Executive Committee (EC) from 1995 to 2005 as a General Secretary and Treasurer (GST) and as President and past President from 2008 to 2014 in a short video presentation.
The journals published by IUCr had grown from one (Acta Crystallographica) in 1948 to seven (Acta A, Acta B, Acta C, Acta D, JAC and JSR) in 1995, all in printed version. The IUCr publications had since 1952 been handled by the Danish publisher Munksgaard. The IUCr could use my base in Copenhagen to strengthen personal contacts to Munksgaard in the challenging necessary development of the journals towards on-line access and digitization. The IUCr was certainly at the forefront as a learned society publisher. So one could launch Acta E (2001), Acta F (2005) and IUCrJ (2014).

The IUCr plays an important role in the internationalization of crystallography. The Regional Associates the European (ECA) and the American (ACA) was followed by the Asian/Australian (AsCA) in 1987. When the IUCr could celebrate its 50th anniversary in 1998 it was an important component of the celebrations that the Executive Committee participated in three successful meetings of the Regional Associates, in Prague, Washington DC and Bangi, Malaysia, and it was a pleasure to welcome LACA (Latin American Crystallographic Association) as Regional Association of the IUCr in 2013. These close international interactions were important to get the approval of UNESCO for the International Year of Crystallography in 2014.

The research, which takes place on the large X-ray (synchrotron) and neutron facilities is richly facetted and could appear very diverse. But I realized. when I worked at the European Synchrotron Radiation Facility, that all the research at the large X-ray and neutron research facilities have their scientific base in one or two of the IUCr Commissions. The IUCr serves also like an important host for the research at the large facilities.

Figure 1. The IUCr Chester staff in 2005, photograph taken at Abbey Square, Chester, UK

[1] Kamminga, H. (1989). *Acta Cryst.* **A45**, 581.
[2] Cruickshank, D.W. J. (1998) *Acta Cryst.* **A54**, 696.

DAY 8

Tuesday 29 August 2023

Plenary Speaker
Prof Mark Spackman
Plenary
9.00am – 10.00am

Plenary-01-290823

Molecules in crystals

Mark A. Spackman

School of Molecular Sciences, University of Western Australia, Perth WA, Australia

mark.spackman@uwa.edu.au

Keywords: molecular crystals, charge density analysis, intermolecular interactions

The design and synthesis of crystalline materials with desired chemical or physical properties is the ambitious goal of crystal engineering and, when successful, it will facilitate many technological advances. Achieving this goal with molecular crystals requires a hierarchy of knowledge and understanding: the structure and properties of the constituent molecules; how the interactions between these molecules lead to observed crystal structures; and the relationship between the properties of isolated molecules, the changes experienced on crystal formation, and the properties of the bulk.

Our research has touched on all aspects of this hierarchy, and the common thread in our studies has been a detailed appreciation of the nature of the electron distribution. We have been particularly interested in how and where that distribution differs from that due to a simple sum of spherical atoms (the common 'independent atom model' of crystal structure analysis - the 'promolecule'), and devising ways in which the two can be used together to facilitate understanding of how molecules pack in crystals, why it makes sense that a particular crystal packing occurs, and what can be learned about the bulk in this manner.

In this lecture I will touch on the important role of the promolecule and several of its properties that can be exploited to advantage (e.g., electrostatic energies between spherical atoms, electron density and its isosurfaces, mapping of voids in crystals, and the Hirshfeld surface). Insights obtained from *CrystalExplorer* [1] will be briefly discussed, especially electrostatic complementarity, models for intermolecular interaction energies, lattice energies and energy frameworks. I will also discuss key results from our forays into charge density analysis and X-ray constrained wavefunctions: electric moments and polarizabilities of molecules in crystals; electric fields in molecular crystals and their relevance to research on oriented electric fields for chemical catalysis, enzyme catalysis, and the vibrational Stark effect. The discussion will also cover bulk properties (e.g., refractive indices derived from in-crystal polarizabilities), and the relationships between nanoindentation measurements, elastic tensors and energy frameworks.

[1] Spackman, P. R., Turner, M. J., McKinnon, J. J., Wolff, S. K., Grimwood, D. J., Jayatilaka, D. & Spackman, M. A. (2021). *J. Appl. Cryst.* **54**, 1006.

Keynote 34
Room 203/204
10.20am – 11.10am

Keynote-34-290823

Visualizing macromolecular structures *in situ* by cryoEM and cryoET

Peijun Zhang

Division of Structural Biology, Wellcome Trust Centre for Human Genetics, University of Oxford, Oxford, OX3 7BN, UK

peijun.zhang@strubi.ox.ac.uk

Keywords: cryoEM, cryoET, in situ, viruses

Cryo-electron microscopy (cryoEM) is a powerful method for the high-resolution three-dimensional structural characterization of a wide range of biological samples in a close-to-native, frozen-hydrated state. Such biological samples, preserved in vitrified ice, are extremely radiation sensitive, therefore images of these have low signal-to-noise ratios and low contrast [1]. Recent development in microscope instrumentation, direct electron detector, microscope automation and high throughput imaging, and advanced software for data processing and image reconstruction, has revolutionized the field of structural biology, allowing protein structures to be determined at the atomic resolution, especially using cryoEM SPA method (Fig. 1). For studying macromolecular complexes that are intrinsically flexible and dynamic, and often function in higher-order assemblies that are difficult to purify, cryoET and subtomogram averaging (cryoET STA) has emerged as a potent tool to obtain structures of these at near-atomic resolution (Fig. 1). The study of such complexes and assemblies in situ using cryoET STA, coupled with cryoFIB/SEM and correlative and integrative imaging, opens a new frontier in structural cell biology [2]. I will present our recent studies on human viruses, including HIV-1, SARS-CoV-2, and reovirus [3-5], to demonstrate the power of high-resolution cryoEM and *in situ* structural biology using cell lamellae-based cryoET STA.

Figure 1. Schematic workflow of cryoEM using three imaging modalities, cryoEM single particle analysis (cryoEM SPA), cryo-electron tomography and subtomogram averaging (cryoET STA) and cryo-electron diffraction (cryoED). The workflow involves

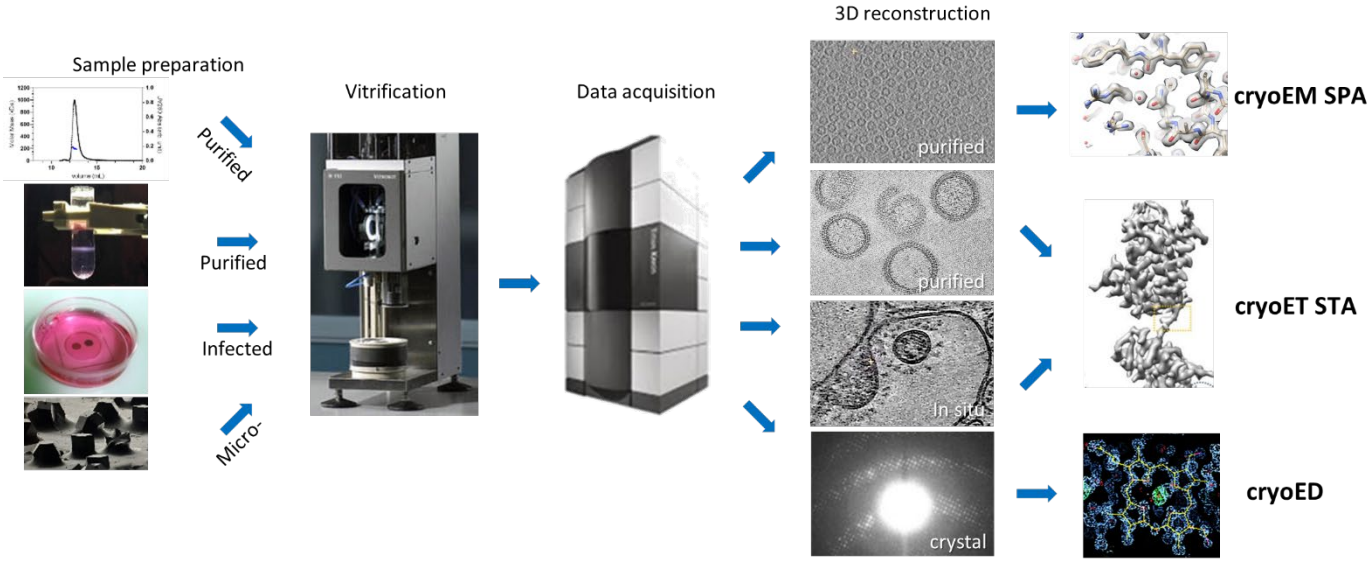

1) sample preparation, 2) sample vitrification, 3) data acquisition, and 4) 3D reconstruction. A representative structure from each modality is shown.

References:

[1] Henderson, R. (2009). *Quarterly Reviews of Biophysics* **28**, 171.

[2] Zhang, P. (2019) *Curr Opin Struct Biol* **58**, 249-258

[3] Sutton, G. (2020). *Nat Commun* **11**(1):4445

[4] Mendonça, L. et al. (2021). *Nat Commun* **12**(1):4629

[5] Ni, T. *et al*. (2022). *Sci Adv* **7**(47):eabj5715

Keynote 35
Prof T.N. Guru Row
Room 210/211
10.20am – 11.10am

Keynote-35-290823

Unravelling non-covalent interactions in molecular crystals via experimental charge density analysis

T. N. Guru Row

Solid State and Structural Chemistry Unit, Indian Institute of Science, Bangalore 560012,India

gururow@iisc.ac.in

Keywords: Non-covalent interactions; electron density; multipole modelling; crystal engineering

A review of the work carried out by our research group over the last couple of decades involving the analysis of intermolecular interactions such as carbon (tetrel) bonding, pnicogen bonding, chalcogen bonding, and halogen bonding using experimental charge density methodology to obtain insights into quantitative crystal engineering will be presented. Primarily, the aim is to evaluate the strength and directionality of interactions in intermolecular space in terms of the distribution of electron density leading to the design of molecular crystals with desired properties. Among the various approaches suggested both from theory and experiment, Experimental X-ray charge density analysis [1,2] has proved to be a powerful tool in unravelling the strength and electronic origin of intra- and intermolecular interactions, providing insights beyond the theoretical estimates from gas-phase molecular dimer calculations. Several "sigma-hole" interaction types with similar electrostatic origins have been explored in recent times for their strength, origin, and structural consequences. These include interactions such as carbon (tetrel) bonding, pnicogen bonding, chalcogen bonding and halogen bonding **(Figure 1**). In fact, these studies in general cover the intermolecular expanse involving elements of groups 14-17 of the periodic table. . Examples of weak interactions will be presented in terms of their experimental charge density features to represent elements in each group. Quantitative insights obtained from the experimental electron density distribution and the subsequent topological analysis based on the quantum theory of atoms in molecules (QTAIM) [3] provides specific inputs towards molecular design. These examples reveal not only the strength and beauty of X-ray charge density multipole modelling as an advanced structural chemistry tool but also the utility in providing experimental benchmarks for the theoretical studies of weak interactions in crystals.

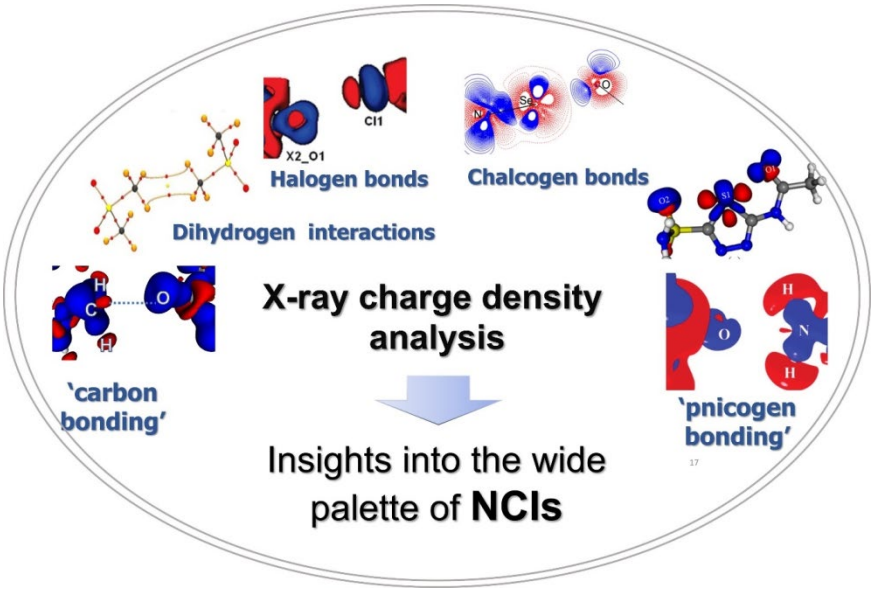

Figure 1. The spread of non-covalent interactions explored using X-ray charge density analysis.

References:

[1] Hansen, N.K.; Coppens, P.(1978). *Acta Crystallogr. Sect. A* **, 34,** 909.

[2] Koritsanszky, T.; Macchi, P.; Gatti, C.; Farrugia, L.; Mallinson, P.; Volkov, A.; Richter, T. XD2016 (2016) -a Computer Program Package for Multipole Refinement, Topological Analysis of Charge Densities and Evaluation of Intermolecular Energies from Experimental and Theoretical Structure Factors. (2016).

[3] Bader, R. (1990). *Atoms in Molecules—A Quantum Theory*; Oxford University Press: Oxford, UK..

A003 Composite and Incommensurate Modulated Crystals: Structural and Physical Properties
Room 204
1.30pm – 3.50pm

A003-01-290823

Commensurate and incommensurate superstructures in rare earth metal chalcogenides *REX*$_{2-\delta}$

Th. Doert, H. Poddig

Faculty of Chemistry and Food Chemistry, Technische Universität Dresden, 01062 Dresden, Germany

thomas.doert@tu-dresden.de

Keywords: superstructures, aperiodic structures, chalcogenides

The structures of the chalcogenides *REX*$_{2-\delta}$ (*RE* = La-Nd, Sm; Gd-Lu; *X* = S, Se, Te) of trivalent rare earth metals attracted some attention as different commensurate and incommensurate superstructures are found in a quite narrow composition range $0 \leq \delta \leq 0.2$. All structures share a common structural motif of an alternating stacking of puckered [*REX*] and planar [*X*] layers and are closely related to the ZrSSi structure (space group *P*4/*nmm*), which is regarded as their common aristotype, Figure 1 (left) [1]. For electronic reasons, the planar [*X*] layer shows distortions from a perfect square net, as dianions X_2^{2-} are found for the non-deficient *REX*$_2$. By reducing the chalcogenide content, ordered vacancy patterns are observed within the planar layers. The different amounts of vacancies, i.e. the value of δ, drives the structures towards the formation of different commensurate and incommensurate superstructures for the *REX*$_{2-\delta}$ compounds. For each single vacancy in the chalcogen layer of the sulfides and selenides, one X^{2-} anion is found to maintain a charge balanced composition. In a chemical sense, this can be rationalised as a disproportionation reaction upon elimination of X_2. The tellurides show different ordering patterns in the planar [Te] layer for the non-deficient *RE*Te$_2$ compounds, but also a tendency to form larger anionic fragments for the deficient *RE*Te$_{2-\delta}$ compounds, as seen for the commensurate structure of GdTe$_{1.8}$, e.g. [2].

LaTe$_{1.94}$ and LaTe$_{1.82}$ are two examples of different incommensurate crystal structures for *RE*Te$_{2-\delta}$ compounds, e.g., driven by a different amount of vacancies in the planar [Te] layer [3, 4]. Both compounds share an average tetragonal unit cell with $a \approx 4.50$ Å and $c \approx 9.17$ Å, reflecting the structure of their aristotype. The major difference of these compounds are their respective *q* vectors, which are compatible with tetragonal symmetry for LaTe$_{1.94}$, but indicate a loss of the fourfold rotational axis for LaTe$_{1.82}$, ending up in an orthorhombic superspace group. The [Te] layer of LaTe$_{1.94}$ is mainly composed of single vacancies, isolated Te^{2-} anions and Te_2^{2-} anions. LaTe$_{1.82}$ is more Te deficient and features adjacent vacancies in addition to Te_3^{4-} anions to guarantee charge balance. The chemical bonding within different chalcogen layers is compared by the DFT-based ELI-D descriptor.

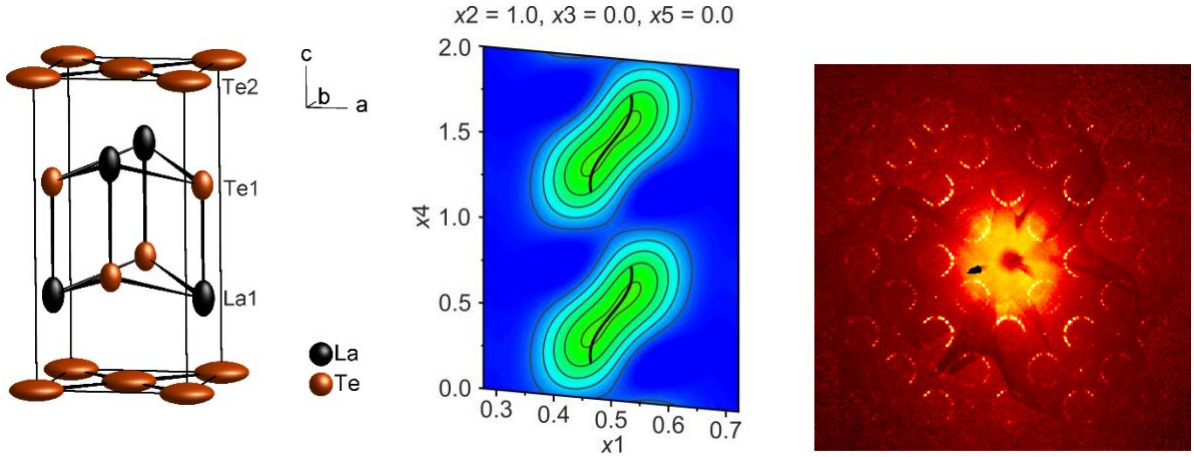

Figure 1. Average structure of LaTe$_{1.82}$ (left), Fourier section around Te2 atoms in the modulated structure of LaTe$_{1.82}$ (centre), and section of the diffraction image of GdTe$_{1.8}$ (right).

[2] Doert, T. & Müller, C. J. (2016). *Binary Polysulfides and Polyselenides of Trivalent Rare-Earth Metals*, in: *Reference Modules in Chemistry, Molecular Sciences and Chemical Engineering*, Elsevier.

[3] Poddig, H., Donath, T., Gebauer, P., Finzel, K., Kohout, M., Wu, Y., Schmidt, P. & Doert, T. (2018). *Z. Anorg. Allg. Chem*. **644**, 1886–1896.

[4] Poddig, H., Finzel, K., Doert, T. (2020) *Acta Crystallogr. Sect.* **C 76**, 530–540.

[5] Poddig, H., Doert, T. (2020), *Acta Crystallogr. Sect.* B, **76**, 1092–1099.

A003-02-290823

Dynamics of the incommensurately modulated Rb2ZnCl4 phase

G. de Laitre1, S. R. Kotla2, S. van Smaalen2, Y. Sidis3, Q. Berrod3,4, J-M. Zanotti3, 4, J. Ollivier4, S. Raymond4,5, F. Bourdarot4,5, A. Piovano4, G. Beutier1, M. de Boissieu1

1 Univ. Grenoble Alpes, CNRS, Grenoble-INP, SIMaP, F-38000 Grenoble, France
2 Laboratory .of Crystallography, University of Bayreuth, Bayreuth, Germany
3 LLB, CNRS, CEA Gif-sur-Yvette, France
4 ILL, Grenoble, France
5 Univ. Grenoble Alpes, IRIG, CEA, Grenoble, France

Email marc.de-boissieu@simap.grenpble-inp.fr

Keywords: aperiodic crystals, phason, inelastic neutron scattering

The Rb_2ZnCl_4 phase displays a crystal structure where the orientations of its $ZnCl_4$ tetrahedrons plays a crucial role. Whereas in the high temperature phase the tetrahedra occupies randomly to equivalent positions, they order incommensurately along the c* axis from T_i=303 K, down to T_C=195K where the modulation get locked-in with a 1/3 ratio of the periodicitiy at lower temperature.

In the incommensurately modulated region, phason modes are expected to be observed [1]. Moreover the modulation function goes from an harmonic to a strongly anharmonic shape as T decreases and approaches the lock-in transition. Finally, the transition is of the order/disorder type related to the tetrahedron orientation, with thus expected overdamped phason modes, as predicted by the theory [2,3]. This phase offers thus a variety of phases to probe the dynamics of phason modes and its relation with acoustic phonon modes.

We have tackled this problem using inelastic and quasielastic neutron scattering measurement on a large single crystal, to investigated the dynamics of this phase as a function of temperature between 140 and 350 K.

The picture that emerges from this study is more complex than the one predicted by long wavelength theories. Nevertheless, we confirm that phason modes are most likely overdamped harmonic oscillators, leading to a diffusive like excitation in the long wavelength limits, whereas there are broad and dispersive excitations in a very small energy range for higher wave-vectors. On the other hand in the lock-in phase at least at temperature of the order 150K the picture is much simpler, as expected from theory.

[1] T. Janssen, G. Chapuis, and M. de Boissieu, *Aperiodic Crystals. From modulated phases to quasicrystals (second edition)* (Oxford University Press, Oxford, 2018), Vol. 20, IUCr Monographs on Crystallography.
[2] R. Currat and T. Janssen, Sol. Stat. Phys. **41**, 201 (1988).
[3] M. de Boissieu, R. Currat, and S. Francoual, in *Handbook of Metal Physics: Quasicrystals*, edited by T. Fujiwara, and Y. Ishii (Elsevier Science, Amsterdam, 2008), pp. 107.

A003-03-290823

Solving the incommensurate modulation in tetragonal tungsten bronze structures from neutron total scattering and single-crystal X-ray diffuse scattering data

I. Levin[1], V. Krayzman[1], A. Bosak[2], H. Y. Playford[3], B. Ravel[1]

[1]Materials Measurement Science Division, National Institute of Standards and Technology Gaithersburg MD 20899, [2]European Synchrotron Radiation Facility, 38043 Grenoble, Cedex, France, [3]ISIS Neutron and Muon Source, Rutherford Appleton Laboratory Oxfordshire, OX11 0QX, Didcot, UK

igor.levin@nist.gov

Keywords: incommensurate modulation, total scattering, diffuse scattering

Many oxides crystallizing with tetragonal tungsten bronze structures (TTB) exhibit the same type of incommensurate modulation [1 -2]. Despite decades of studies in TTBs, which exhibit dielectric and polar properties of interest to applications, the exact nature of this modulation has remained elusive [1-4]. Here, we identified the types and patterns of displacements that give rise to the incommensurate periodicity using $Sr_{0.61}Ba_{0.39}Nb_2O_6$, a classic uniaxial relaxor ferroelectric, as a representative system. We solved this problem using atomistic structural refinements while simultaneously fitting neutron total-scattering, extended X-ray absorption fine structure, and single-crystal X-ray diffuse scattering data. We used results from transmission electron microscopy to guide the refinement procedure. The modulation appeared to arise from the intergrowth of structural slabs featuring distinct types of octahedral rotations directed to minimize octahedral deformations (Figure 1). This modulation involves displacements of the Sr and Ba but exerts no significant effect on the displacements of Nb. The refinements also highlighted the impact of the chemical disorder on the displacements contributing to the modulation.

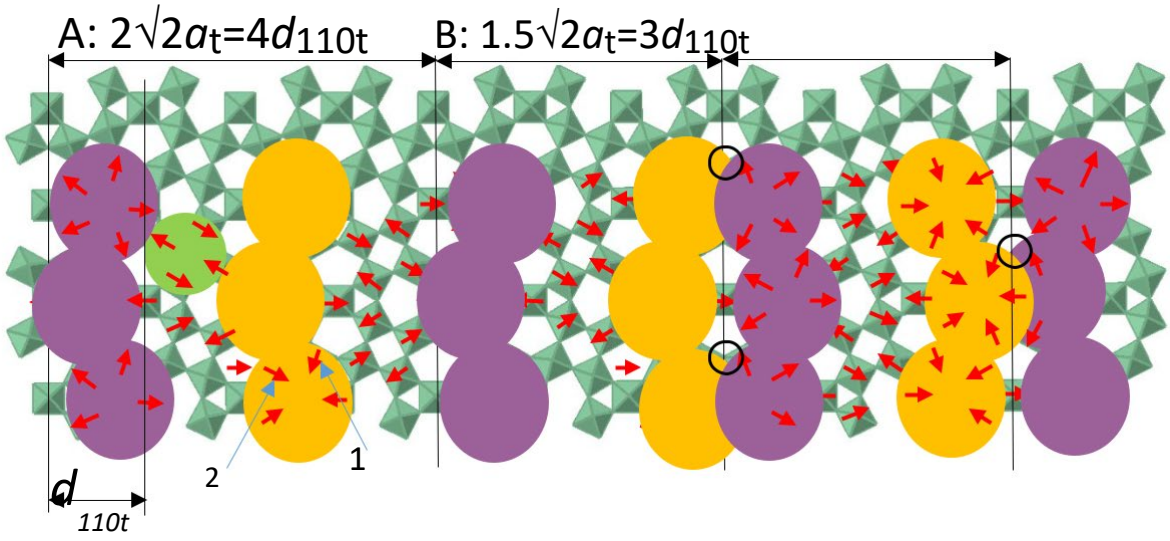

Figure 1. Schematic rendering of a (001) octahedral layer illustrating patterns of octahedral tilts in a single modulation variant in the refined configurations

[6] Shcneck, J; Toledano, J. C.; Whatmore, R.; Ainger, F. W. (1981) *Ferroelectrics*, 36, 327-330
[7] Bursill, L. A.; Lin, P. J. (1987) *Acta Cryst.* B43, 49-56
[8] Woike, T., Petricek, V.; Dusek, M.; Hansen, N. K.; Fertey P.; Lecomte, C.; Arakcheeva, A.; Chapuis, G.; Imlau, M., Pankrath, R. (2003) *Acta Cryst. B* 59, 28-35
[9] Bosak, A. A.; Vakhrushev, S. B.; Naberezhnov, A. A.; Vanina, P. Yu. (2015) *St- Petersburg Polytech. Univ. J.-Phys. Math*., 1(3), 235-238

A003-04-290823

Modulated crystallographic shear structure in titanium-chromium oxides: their structure and phonon transport properties

S. Harada*†, T. Hattori†, M. Inden†, S. Sugimoto†, M. Itoh†, M. Tagawa*†, T. Ujihara*†

*Institute of Materials and Systems for Sustainability (IMaSS), Furo-cho, Chikusa-ku, Nagoya, Japan 464-8601

†Department of Materials Science and Engineering, Furo-cho, Chikusa-ku, Nagoya, Japan 464-8603

shunta.harada@nagoya-u.jp

Keywords: Crystallographic shear structure, coherent phonon transport, titanium oxide

Control of heat conduction through the manipulation of phonons as coherent waves have been attracted great interest for the advanced thermal management [1]. Although smooth interfaces were reported to be obtained in artificial superlattices, preparation of coherent interfaces for terahertz phonons having nanoscale periodicity with atomic-scale perfection are still challenging since metal organic chemical vapor deposition (MOCVD) and molecular beam epitaxy (MBE) were nonequilibrium growth process. Therefore, we focus on crystallographic shear (CS) structures, in which planar faults are periodically introduced to a mother structure with their spacing depending on their composition [2]. Homologous series of titanium-based oxides with CS structure have been long investigated by various researchers since Magneli and co-workers first reported in 1957 [3, 4]. Recently, we have revealed that the titanium oxides with CS structure possess nearly pristine interfaces and behave as coherent interface for thermal phonons [5-8]. In the present study, we have aimed to produce aperiodic arrangements of CS planes with nearly pristine interfaces toward experimental demonstration of phonon Anderson localization evoked by aperiodic arrangements of interfaces [9].

Figure 1 shows the transmission electron microscopy observation of titanium-chromium oxide crystals grown by floating-zone melting method before and after annealing at 1673 K for 24 h. Lines of satellite spots due to the arrangements of the CS planes are directed along the $(121)_{rutile}$ for both specimens. However, the interval of the satellite spots seems to be randomly arranged for the specimen before annealing while those for the specimens after annealing are homogeneous. HAADF-STEM observation (Fig. 1(c)) clearly show that the modulation of the interval of the CS planes for the specimen before annealing. Note that any anomaly in the atomic structure is noticed although the interval of CS planes are modulated. Current results implies that phonon Anderson localization, which was theoretically predicted in the materials having disordered interfaces, is expected to emerge in thermal conduction in titanium-chromium oxides with the modulated CS structures.

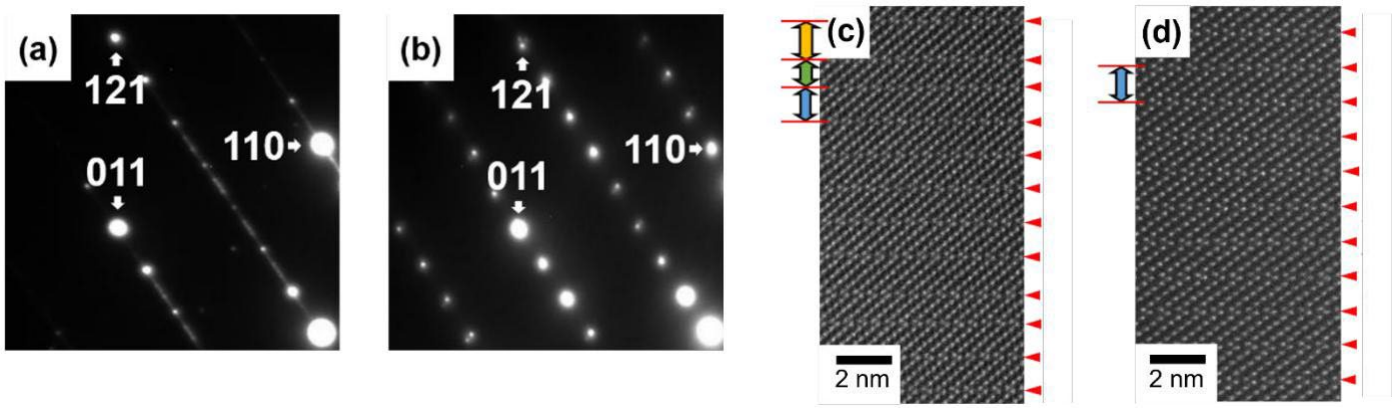

Figure 1. Selected area diffraction patterns of titanium-chromium oxide with $(121)_{rutile}$ CS structure (a) before and (b) after annealing. HAADF-STEM images of titanium-chromium oxide with $(121)_{rutile}$ CS structure (c) before and (d) after annealing.

[10] Maldovan, M. (2013) *Nature* **503,** 209.

[11] Bursil, L. A. (1969). *Proc. R. Soc. London Ser. A* **311**, 267.

[12] Andersson, J. S., Collen, B., Kuylenstierna, U. & Magneli (1957). *Acta Chem.* **14**, 1641.

[13] Harada, S., Tanaka, K. & Inui, H. (2010). *J. Appl. Phys.* **108**, 083704.

[14] Harada, S., Kosaka, N., Tagawa, M. & Ujihara, T. (2021). *J. Phys. Chem. C* **125**, 11175.

[15] Harada, S., Sugimoto, S., Kosaka, N., Tagawa, M. & Ujihara, T. (2021). *J. Phys. Chem. C* **125**, 15730.

[16] Harada, S., Kosaka, N., Yagi, T., Sugimoto, S., Tagawa, M. & Ujihara, T. (2022). *Scr. Mater.* **208**, 114326.

[17] Sugimoto, S., Kim, G., Takeuchi, Tagawa, M. & Ujihara, T. (2023). *J. Alloys Comppd.* **934**, 167915.

[18] Hu, R. & Tian, Z. (2021) *Phys. Rev. B* **103**, 045304.

A003-05-290823

Anharmonic modulation and its interplay with twinned microstructure in Ni-Mn-Ga-(Fe) 10M martensite

Veřtát[1], L. Straka[1], H. Seiner[2], M. Klicpera[3], M. Poupon[1], O. Heczko[1]

[1]FZU – Institute of Physics of the Czech Academy of Sciences, Na Slovance 1999/2, 18221 Prague 8, Czech Republic, [2]Institute of Thermomechanics of the Czech Academy of Sciences, Dolejškova 1402/8, 18200 Prague 8, Czech Republic, [3]Faculty of Mathematics and Physics, Charles University, Ke Karlovu 5, 12116 Prague 2, Czech Republic. vertat@fzu.cz

Keywords: Magnetic Shape Memory, Phase Transformations, Ni-Mn-Ga, Twinned Microstructure, Incommensurate Modulation

Ni-Mn-Ga-based Heusler alloys exhibit magnetic shape memory (MSM) functionality originating from coupling between ferroelastic and ferromagnetic orders. The ferroelastic order is established by diffusionless, displacive transformation from cubic austenite to modulated martensite of lower symmetry. Spontaneously formed ferroelastic (twin) domains with different lattice orientation are separated by twin boundaries. In modulated martensite phases, these boundaries can be extremely mobile and thus they can be manipulated by very small mechanical stress or even by magnetic field resulting in ferroelastic domain redistribution and large deformation [1], e.g., the single crystals of five-layered "10M" modulated martensite exhibit up to 7 % magnetic field induced strain in a moderate field of the order of 0.1 T [2] at room temperature [3] and down to 2 K [4]. The effect is called magnetically induced reorientation (MIR). Such unique behaviour makes the 10M martensite perfect candidate for sustainable applications in actuators, sensors, and energy harvesters in broad temperature range.

Complete understanding of the modulated martensite structure is prerequisite for understanding the MIR effect and extremely high mobility of twin boundaries. It has been previously shown that the modulation of the 10M martensite changes with temperature. Using X-ray and neutron diffractions we found that the commensurate modulated structure in the vicinity of the austenite phase evolved with decreasing temperature into incommensurate, and the modulation vector continuously grew until the structure attained yet another commensurate metastable state followed by the intermartensitic transformation to the "14M" modulated martensite. Moreover, the changes in structural modulation exhibited thermal hysteresis.[5] However, the character of the modulation remained puzzling.

In this work we present new findings on the structural modulation in Ni-Mn-Ga-derived 10M martensite and how evolving modulation affect the martensite twinned microstructure, particularly resulting in refinement of *a*/*b* twins upon cooling. Our measurements indicate highly anharmonic modulation. By refinement of the structural model and following physical theory of martensite we determine the function waveform significantly more precisely in comparison with any previous approach. Furthermore, we correlate the temperature-induced hysteretic changes in modulation with the changes of other physical properties, such as electrical resistivity and elastic moduli and, most importantly, the twin boundary mobility essential for the material functionality.

[1] Ullakko, K., Huang, J. K., Kantner, C. & Handley, R. C. O. (1996) *Appl. Phys. Lett.* **69**, 1966–8.

[2] Straka L., Lanska, N., Ullakko, K. & Sozinov, A. (2010) *Appl. Phys. Lett.* **96**, 131903.

[3] Pagounis, E., Chulist, R., Szczerba, M. J. & Laufenberg, M. (2014) *Appl. Phys. Lett.* **105**, 052405.

[4] Heczko, O., Kopecký, V., Sozinov, A. & Straka, L. (2014) *Appl. Phys. Lett.* **103**, 198–211.

[5] Veřtát, P., et al. (2021) *J. Phys.: Condens. Matter* **33**, 265404

This work was supported by the Czech Science Foundation (Czech Republic) [Grant Number 21-06613S]. We acknowledge the Institut Laue-Langevin for the provision of neutron radiation facilities and thank O. Fabelo for assistance with the ND measurements. We kindly thank V. Petříček for fruitful discussions and M. Dušek for assistance with the XRD data collection

A003-06-290823

Modulated sulfosalt thermoelectrics

B. Stöger

TU Wien, Getreidemarkt 9, 1060 Vienna, Austria

bstoeger@mail.tuwien.ac.at

Keywords: incommensurate modulation, oriented intergrowths, twinning, sulfosalts

Thermoelectric materials convert temperature differences into electric potential. Owing to numerous potential applications, such as conversion of waste heat into electrical energy, they may play an important role in the energy revolution. A high-performance thermoelectric is characterized by a high electrical conductivity paired with a low thermal conductivity. Unfortunately, these two properties are often in conflict.

Sulfosalts are a class of sulfide (sometimes also selenide or telluride) minerals, which often form modular structures, whereby PbS-like (NaCl structure type) modules are connected in different ways. Despite this simple building principle, they typically feature a complex crystal chemistry, forming commensurately or incommensurately modulated crystal structures. Moreover, the metal sites are usually disordered. These features lead to a strongly reduced thermal conductivity. Numerous members of the family would therefore be prime candidates as thermoelectrics, if it weren't for their poor electrical conductivity.

To improve electrical conductivity, we synthesized the Se analogues of natural sulfosalts by reacting PbSe, Sb_2Se_3 and Cu_2Se in silica ampoules. In particular, we investigated the crystal chemistry of analogues of the andorite family (approximate composition $CuPbSb_3Se_6$). The crystal structures can be derived from a basic structure with *Cmcm* space group symmetry (Fig. 1).

Incommensurately modulated phases (*Cmcm*(α00)00*s*, **q** = 0.684**a***), twofold ($P2_1/c$, **q** = **a***/2 − **b***/2) and threefold ($Cmc2_1$, **q** = **a***/2) superstructures were observed. Practically all metal sites are disordered and additional Cu atoms are located at interstitial positions. The preference of Cu for tetrahedral coordination plays a crucial role in the modulation (Fig 2).

For certain compositions, oriented intergrowths of both superstructures were obtained. Using high-temperature single-crystal diffraction up to 400°C, we could show that the modulation of the structures and the existence of twinning not only depend on the elemental composition, but also on the formation conditions.

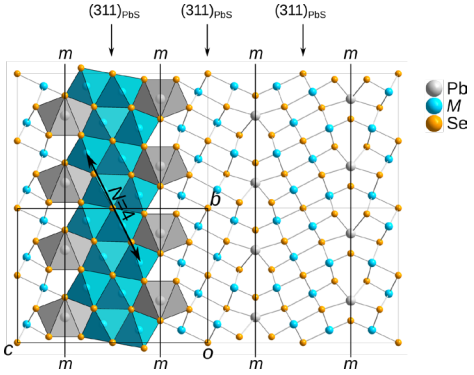

Figure 1. *Cmcm* basic structure of the investigated andorite-type sulfosalts. Four octahedra wide slabs of $(311)_{PbS}$ sheets are connected by capped prismatic Pb/Sb positions.

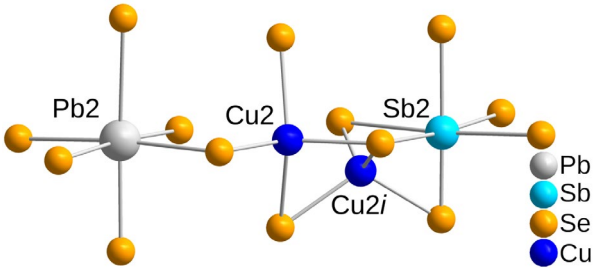

Figure 2. Tetrahedrally coordinated Cu atoms in octahedral (Cu2) and interstitial (Cu2i) positions.

A014 Databases and Data Management
Room 207
1.30pm – 3.50pm

A014-01-290823

Macromolecular Crystallography Laboratory Information Virtual Environment (MxLIVE): A full-featured web platform for data management

K. Janzen, J. Gorin, D. Lang, S. Colville, D. Spasyuk, M. Fodje

Canadian Light Source, 44 Innovation Blvd, Saskatoon, SK, Canada, S7N 2V3

kathryn.janzen@lightsource.ca

Keywords: mxlive, mxdc, shipping, sample management, data transfer

MxLIVE (Macromolecular Crystallography Laboratory Virtual Environment) is a development platform and web application for managing synchrotron visits at all stages - from experiment planning and organisation to shipment tracking to data and analysis access.

MxLIVE relies on MxDC (Macromolecular Crystallography Data Collector) as a source of meta-data from data collection sessions on the beamline, and acts as a resource from which MxDC can fetch sample information. This close-coupling provides researchers with a cohesive experience from the sample shipping to data transfer. Since all connections are handled through the use of APIs (Application Programming Interfaces), other data collection applications could also be modified to complement MxLIVE.

The beginnings of MxLIVE were at CMCF (Canadian Macromolecular Crystallography Facility), a suite of beamlines at the Canadian Light Source dedicated to MX (Macromolecular Crystallography). For that reason, many features have been developed in an MX context, but can easily be extended to new sample container layouts and new data types or techniques at any beamline.

A014-02-290823

RCSB Protein Data Bank: Sustaining a living digital data resource that enables breakthroughs in scientific research and biomedical education

Christine Zardecki[1,2], S.K. Burley[1,2,3,4,5]

[1]RCSB Protein Data Bank, [2]Institute for Quantitative Biomedicine, and [3]Department of Chemistry and Chemical Biology, Rutgers, The State University of New Jersey, Piscataway, NJ 08854, USA

[4]Cancer Institute of New Jersey, Rutgers, The State University of New Jersey, New Brunswick, NJ 08903, USA

[5]RCSB Protein Data Bank, San Diego Supercomputer Center, University of California San Diego, La Jolla, CA 92093, USA

Christine.zardecki@rcsb.org

Keywords: Protein Data Bank, biomolecular structure, database design,

The Protein Data Bank (PDB) was established as the 1st open-access digital data resource in biology and medicine in 1971 with seven X-ray crystal structures of proteins. Today, the PDB houses ~200,000 experimentally-determined, atomic-level, three-dimensional (3D) structures of proteins and nucleic acids and their complexes with one another and small molecules (*e.g.*, approved drugs, enzyme cofactors). The US-funded Research Collaboratory for Structural Bioinformatics Protein Data Bank (RCSB PDB) and other members of the Worldwide Protein Data Bank (wwPDB) partnership jointly manage the PDB archive and support >55,000 data depositors worldwide, ensuring quality for the ever-growing body of experimentally-determined 3D biostructure information. Within the wwPDB, data processing responsibilities are distributed geographically. As the US wwPDB Data Center, RCSB PDB rigorously-validates and expertly biocurates new structures coming into the archive from the Americas and Oceania. RCSB PDB also serves as the wwPDB-designated PDB Archive Keeper, responsible for safeguarding ~1 Tb of data (amassed during five decades of continuous operations) and updating the PDB on a weekly basis.

The RCSB PDB research-focused web portal (RCSB.org) supports many millions of users worldwide, representing a broad range of expertise and interests. In addition to retrieving 3D structure data at no charge and with no usage limitations, PDB data consumers access comparative data, and external annotations, such as information about point mutations and genetic variations. Alongside ~200,000 PDB structures, RCSB.org now provides access to >1,000,000 Computed Structure Models (CSMs) generated using artificial intelligence/machine learning methods. For the avoidance of doubt, experimentally-determined PDB structures and CSMs are clearly identified as to provenance and reliability.

Specialized RCSB.org data delivery tools include:

- Structure Motif Search: Finds structures with a small number of specific amino acids in specific 3D configurations.
- Pairwise Structure Alignment calculates alignments using different trusted methods and displays sequence alignments and superposed 3D visualization. Comparisons can be made for any protein in the PDB archive and/or uploaded data files including computed structure models.
- For result sets containing multiple structures representing highly similar proteins, a new Grouping Option generates a non-redundant search result set based on sequence identity, UniProt ID, or Group depositions.
- Ligand structure quality assessment metrics are available for PDB structures determined by X-ray crystallography. Quality indicators (*e.g.*, RSR, RSCC) have been aggregated into a ranking score that can be used for comparison across the archive and allow any user to quickly review ligand structure quality.

Additionally, Training and outreach materials are hosted at PDB101.rcsb.org to help users learn how to utilize PDB data and tell structural biology stories. *Guide to Understanding PDB Data* covers topics such as PDBx/mmCIF format; exploring carbohydrates in the PDB; and Computed Structure Models. The *Molecule of the Month* series introduces the structure and function of interesting and notable PDB structures, such as Respiratory Supercomplexes and SARS-CoV-2 structures.

RCSB PDB Core Operations are funded by National Science Foundation (DBI-1832184), US Department of Energy (DE-SC0019749), and National Cancer Institute, National Institute of Allergy and Infectious Diseases, and National Institute of General Medical Sciences of the National Institutes of Health under grant R01GM133198.

A014-03-290823

The Cambridge Structural Database: A multidisciplinary resource

S. C. Ward, M. P. Lightfoot

The Cambridge Crystallographic Data Centre, Cambridge (United Kingdom)

ward@ccdc.cam.ac.uk

Keywords: CSD, FAIR, Interoperability

The Cambridge Structural Database (CSD) was founded on a vision that collective use of data would lead to the discovery of new knowledge which transcends the results of individual experiments. The existence of a common crystallographic language, an ability to understand crystallographic information, and an awareness of the importance of data interoperability have enabled that vision to come to true. The database is now a valued multidisciplinary resource used extensively in academia as well as in industry particularly as part of drug development and materials design.

In crystallography we are extremely fortunate that a standard file format has been adopted by researchers, software creators and publishers alike providing a strong foundation for data sharing. As a proponent of the FAIR data principles, the Cambridge Crystallographic Data Centre (CCDC) has supported the community by developing a workflow from structure deposition to data sharing. This workflow seeks to promote these guiding principles by enabling depositors to provide information which renders the datasets more Findable, Accessible, Interoperable and Reusable. As the curators of a domain specific repository, we also work to ensure this crystallographic data can be utilised across disciplines to enable the advancement of science as well as crystallography.

This talk will explore the part we can play in helping the reliable sharing of data between disciplines and how we are supporting efforts to adhere to new best practices for data management that will enable researchers to get the most from crystal structure data. It will focus on the steps the CCDC has made to increase interoperability, as well as some of the opportunities and challenges we face as we work to ensure the wealth of information contained in 1.2 million structures in the CSD can exploited by machines as well as people from across disciplines.

A014-04-290823

SBGrid: Optimizing your software and compute environment to accelerate structural biology/cryoEM research.

Thomas Nicholson[2], Jason Key[1], Peter A Meyer[1], Shaun Rawson[1], Alex Ho[1], Kurt L Krause[2], and Piotr Sliz[1]

[1]Department of Biological Chemistry and Molecular Pharmacology, Harvard Medical School, Boston, MA, USA
[2]Department of Biochemistry, University of Otago, Dunedin, New Zealand
piotr_sliz@hms.harvard.edu, http://sbgrid.org

Keywords: cryoEM, software database, high-performance computing

The Structural Biology Grid (SBGrid) [1,2] is an open consortium of research and development (R&D) laboratories that cooperate to create and maintain a homogeneous structural biology research software infrastructure. Established in 1999, SBGrid initially focused on providing access to macromolecular X-ray crystallography applications. Over the years, SBGrid, which is located at Harvard Medical School, has expanded to encompass macromolecular structure determination by cryogenic electron microscopy (cryoEM), microcrystal electron diffraction (MicroED), cryogenic electron tomography (cryoET) and nuclear magnetic resonance (NMR). SBGrid has a growing number of consortium members, and all 456 partners are involved in the structural biology R&D community at large. They include academic research laboratories, and extend to a growing number of pharmaceutical companies. To support the increasing use of SBGrid in Australasia, SBGrid recently established a satellite site at University of Otago in New Zealand, which coordinates regional software installations.

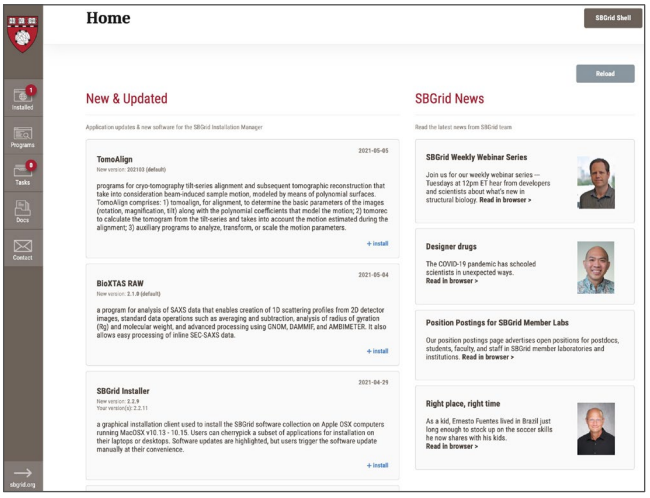

Figure 1. The SBGrid installation manager is available in graphical and command-line flavors for macOS and Linux and supports installation of any of ~1000 SBGrid supported applications. It also provides an extensive software database, with software citations, ~200 training videos, and software metadata.

SBGrid supports structural biology laboratories and biomedical researchers with a tested and refined software infrastructure that includes a large library of scientific applications. The SBGrid team configures, compiles, tests, and continuously upgrades a comprehensive and growing collection of about 500 built-to-run structural biology applications, which is augmented by an additional 600+ computational biology applications. SBGrid members utilize the SBGrid installation manager (Figure 1) to locally install the SBGrid supported applications on Mac and Linux workstations, High Performance Computing (HPC) clusters and in various cloud environments. Once the SBGrid software is installed no further configuration is needed. All applications are packaged by SBGrid with required libraries and supporting software.

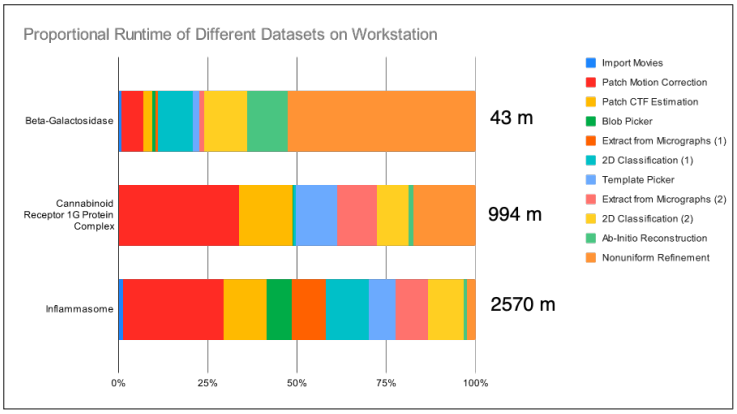

Figure 2. Benchmarking of Harvard's On-The-Fly CryoEM pressing pipeline was completed with three datasets, with the number of images ranging from 24 to 6594, and corresponding storage space ranging from 3.0 gigabyte to 1.6 terabyte. More recently our tests were also expanded to Amazon Web Services (AWS) cloud environment.

SBGrid facilitates rapid access to the newest versions of software and routinely disseminates applications within days of the initial release by developers. Compute-intensive applications are optimized, and instructions for effective execution are provided in the SBGrid web-based software directory (sbgrid.org/software). To advise on the most cost-effective hardware configurations, SBGrid benchmarks CryoEM software with a widely ranging types of datasets. In Figure 2 we present a standard CryoEM structure determination workflow, which consist of 11 steps that need to be completed in sequence. The workflow was tested on dozens of various hardware configurations. Depending on the dataset size, the computational runtimes for a single iteration of structure determination on a single workstation varied from 43 minutes to over 42 hours. In general, the total runtime was proportional to the number of images and storage space of the dataset. Patch Motion Correction (PMC) and Non-Uniform Refinement were the most time-consuming steps and as the number of GPUs increased, the runtime for PMC drastically decreased.

[1] Morin A, Eisenbraun B, Key J, Sanschagrin PC, Timony MA, Ottaviano M, Sliz P. Collaboration gets the most out of software. *Elife* 2013; 2: e01456–e01456.

[2] Meyer PA, Socias S, Key J, et al, Sliz P. Data publication with the structural biology data grid supports live analysis. *Nature Communications* 2016; 7: 10882.

A014-05-290823

Protein Data Bank Japan: the Asian hub of 3D macromolecular structural data

G-J. Bekker. M. Yokochi, R. Yamashita, K. Tsunezumi, T. Iwata, T. Kudo, J. Yu1, T. Nakane1, Y. Miyanoiri, G. Kurisu

1Institute for Protein Research, Osaka University, Suita, Osaka 565-0871, Japan, 2Protein Research Foundation, Minoh, Osaka 565-8686, Japan

gkurisu@protein.osaka-u.ac.jp

Keywords: PDB, BMRB, EMDB, EMPIAR, Xtal Raw Data

Protein Data Bank Japan (PDBj), a founding member of the worldwide Protein Data Bank (wwPDB) has accepted, processed and distributed experimentally determined biological macromolecular structures from Asia and middle east for more than 20 years [1, 2]. Initially, PDBj also covered Oceania but later has focused on Asia because the number of Asian depositions is increasing. Last year, wwPDB welcomed Protein Data Bank China (PDBc) as an Associate member of wwPDB and PDBc has started remote processing of the structures from main land China deposited to PDBj, which was about 10% of Chinese depositions in 2022.

In addition to archiving the PDB data in collaboration with other wwPDB core members (RCSB PDB, PDBe, BMRB and EMDB), PDBj also provides a wide range of original and unique services and tools, which are continuously improved and updated [3]. We outline the updated web user interfaces together with RESTful web services and the backend relational database that support the new PDBj Mine 2 service. To enhance the interoperability of the PDB data, wwPDB/RDF, PDB data in the Resource Description Framework (RDF) format, have been developed. We have enhanced the connectivity of the wwPDB/RDF data by incorporating various external data resources. We also developed the WebGL molecular viewer Molmil 2, the ProMode-Elastic server for normal mode analysis, the eF-site of the pre-calculated molecular electrostatic potentials, and the integration searches of PDB, EMDB (Electron Microscopy Data Bank) and BMRB (Biological Magnetic Ressonance data Bank) that is a repository for data from NMR spectroscopy on Proteins, Peptides, Nucleic Acids, and other Biomolecules.

Recently we have started several unique activities as shown in Fig. 1, EMPIAR-PDBj (empiar.pdbj.org) as a regional brokering site of EMPIAR at EMBLE-EBI with our original web page, BSM-Arc (Biological Structure Model Archive: bsma.pdbj.org) for computational structure models [4], and XRDa (Xtal Raw Data Archive: xrda,pdbj.org) for raw Xtal diffraction images, all of which promote open science in the structural science community. PDBj has also provided the translated versions for molecule of the month in Japanese, Chinase, and Korean as a collaboration with RCSB PDB (numon.pdbj.org/mom/). During the COVID-19 pandemic, PDBj has started feature pages for COVID-19 related entries across all available archives at PDBj from raw experimental data and PDB structural data to computationally predicted models, while also providing COVID-19 outreach content for high school students and teachers.

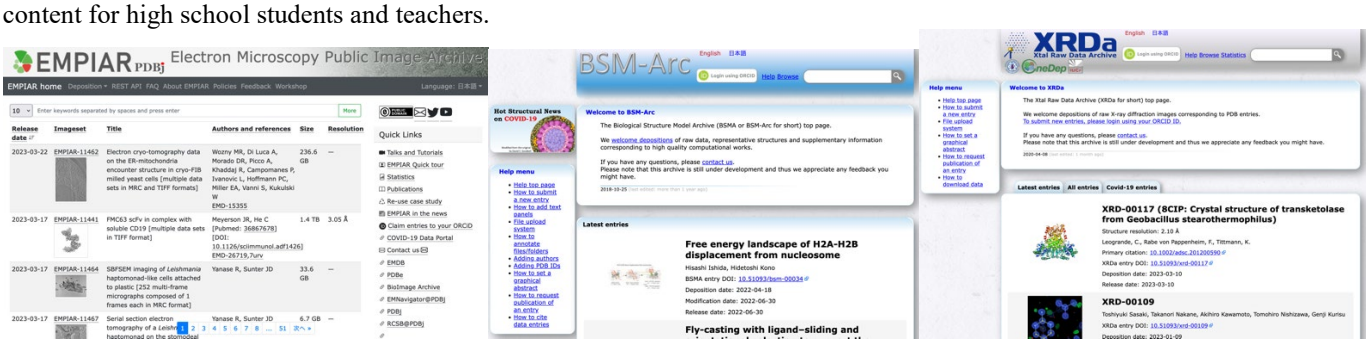

Figure 1. New PDBj services: EMPIAR-PDBj (left), BSM-Arc (middle), and XRDa (right).

[1] Kinjo, A., Yamashita, R. & Nakamura, A. (2010). *Database.* **2010**, baq021.

[2] wwPDB consortium. (2019). *Nucleic Acids Research*, **47**, D520-D528.

[3] Bekker, G. J., Yokochi, M., Suzuki, H., Ikegawa, Y., Iwata, T., Kudou, T., Yura, K., Fujiwara, T., Kawabata, T. & Kurisu, G. (2022). *Protein Science*.**31**, 173-186.

[4] Bekker, G. J., Kawabata, T. & Kurisu, G. (2020). *Biophysical Reviews*, **12**, 371-375.

PDBj was supported by grants from the Database Integration Coordination Program from NBDC-JST under Grant Number JPMJND2205, and partially supported by Platform Project for Supporting Drug Discovery and Life Science Research (BINDS) from AMED under Grant Number JP21am0101066..

A018 Viruses
Room 203
1.30pm – 3.50pm

A018-01-290823

Structural characterization of light-gated ion channels from giant viruses.

Dmitrii Zabelskii[1,*], Kirill Kovalev[2], Sergey Bukhdruker[3], Adam Round[1] and Valentin Gordeliy[6]

[19] European X-Ray Free-Electron Laser Facility GmbH, Schenefeld, Germany 2 European Molecular Biology Laboratory, Hamburg, Germany

3 European Synchrotron Radiation Facility, Grenoble, France

4 Institut de Biologie Structurale, Grenoble, France

Email: dmitrii.zabelskii@xfel.eu

Keywords: Giant viruses, Ion channels, Rhodopsins, Membrane proteins.

Viral channelrhodopsins VirChRs are one of the new members of ion channeling rhodopsins in the microbial rhodopsins superfamily VirChRs are Na+/K+ selective ion channels that can be reversibly inhibited by Ca 2 ions We solved a 1 4 Å of OLPVR1 rhodopsin that allowed us to observe the compact fold of VirChRs and multiple constriction sites inside the protein Understanding the molecular mechanisms of ion channeling could be beneficial for the improvement of existing channelrhodopsin based optogenetic tools, and also for the search for ion channeling rhodopsins with new functions As such Viral channelrhodopsins might be of significant value for calcium related methods in the fields of optogenetics and neuroscience research [1]

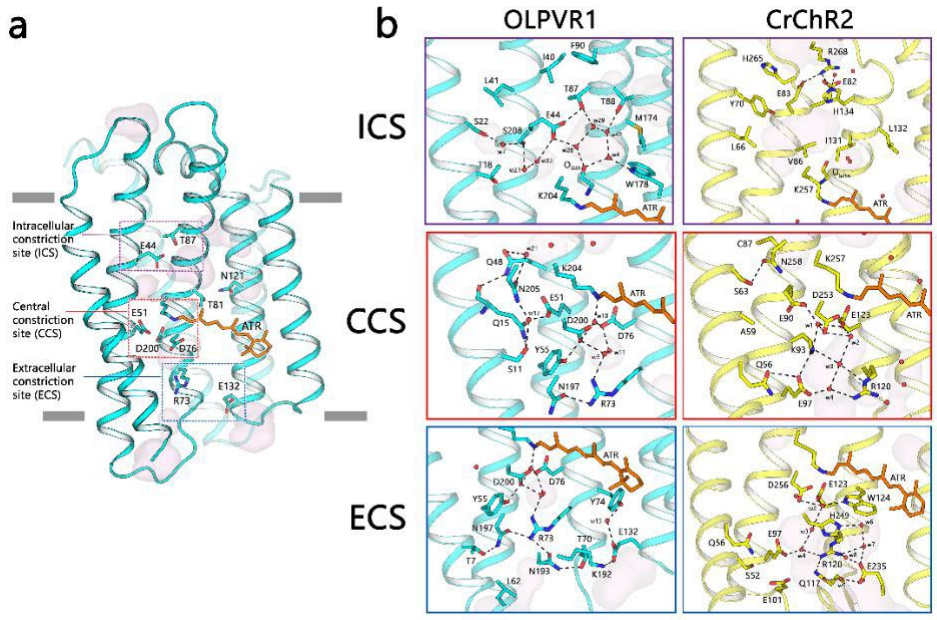

Figure 1. (a) Three constriction sites (CS) and cavities are forming the putative ion-conductive pathway in viral channelrhodopsins and highly conservative residues of OLPVR1. TM6 and TM7 helices are omitted for clarity. Membrane core boundaries are shown with gray lines. (b) Magnified view of the CSs in OLPVR1 (left, present work) and CrChR2 [2] (middle, PDB ID: 6EID8) structures, colored cyan and yellow respectively. Water-accessible cavities are shown in pink.

We expressed, purified, and crystallized one of the light-gated ion channels from giant viruses, OLPVR 1 rhodopsin from the Organic Lake Phycodna Virus. The protein was crystallized using *in meso* crystallization method that yielded rhombic-like crystals up to 200 µm. The best crystals were tested at beamline ID30b (ESRF, Grenoble), where they diffracted up to 1 4 Å resolution which is currently the highest resolution achieved for a channelrhodopsin. Similar to ChR2 channelrhodopsin, OLPVR1 has three consecutive constriction sites that facilitate ion transport upon photon absorption. The OLPVR1 protomer has short extracellular loops, which sharply differentiates it from other channelrhodopsins that typically have large N- and C-terminal domains. Unlike in other microbial rhodopsins, helices TM3 and TM4 of OLPVR1 are connected by the loop containing the membrane-associated helix (ICL2 helix), which is composed of hydrophilic residues[3]. Understanding of molecular composition of light-gated ion channels opens new perspectives for time-resolved crystallography and cryo-trapping of protein intermediate states. The next goal of the project is to determine the structure of the open state of OLPVR 1 rhodopsin via the time resolved crystallography method at modern synchrotron and XFEL light sources In addition, we are looking for ways to improve plasma membrane localization of viral rhodopsins that can help VirChRs to find their niche in optogenetics applications

References:

[5] D. Zabelskii *et al.*, 'Viral rhodopsins 1 are an unique family of light-gated cation channels', *Nat. Commun.*, vol. 11, no. 1, p. 5707, Dec. 2020, doi: 10.1038/s41467-020-19457-7.

[6] O. Volkov *et al.*, 'Structural insights into ion conduction by channelrhodopsin 2', *Science*, vol. 358, no. 6366, p. eaan8862, Nov. 2017, doi: 10.1126/science.aan8862.

[7] O. P. Ernst, D. T. Lodowski, M. Elstner, P. Hegemann, L. S. Brown, and H. Kandori, ‘Microbial and Animal Rhodopsins: Structures, Functions, and Molecular Mechanisms’, *Chem. Rev.*, vol. 114, no. 1, pp. 126–163, Jan. 2014, doi: 10.1021/cr4003769.

A018-02-290823

Structural landscape of SARS-CoV-2 entry and activation of spike glycoprotein by engaging unique host factors & potential interventions

[20] Vankadari [1], M. Sasikala[2], X. Fang[3], L. Tian[4], S.S. Latha[5], K. Wang[6] , P. Peng[7], J.A. Wilce[8], D.N. Reddy [2] and D. Ghosal[1]

Bio21 Institute, Dept. Biochemistry and Pharmacology, University of Melbourne, Parkville, VIC, Australia, Institute of Translational Research, AIG Hospital, Hyderabad, Telengana, India. (3) Graduate School of Health Innovation, Kanagawa University, Japan. (4) Department of Biomedical Data Science, Stanford University, California, CA, USA. (5) Center for Innovation in Molecular and Pharmaceutical Sciences, Dr. Reddy's Institute, Hyderabad, Telengana, India. (6). Department of Pulmonary and Critical Care Medicine, Tongji Hospital, Wuhan City, Hubei Province, China. (7). Wuhan Institute, Wuhan Pulmonary Hospital, Wuhan City, Hubei Province, China, (8) Monash Biomedicine Discovery Institute, Monash University, Clayton, Victoria 3800, Australia.

Email of communicating author naveen.vankadari@unimelb.edu.au

Keywords: Host factors, viral entry, antivirals, structure, molecular dynamics, genetic variants

The ongoing COVID19 pandemic caused by SARS-CoV-2 with lower respiratory tract infections, is an enduring public health concern [1]. Emergence of new immune evading variants are challenging the current effective vaccines and several antiviral treatments are being clinically evaluated to fill the "therapeutic gap" in treating infected people
[8] Understanding the entire repertoire of diverse host factors engaged by SARS-CoV-2 for entry and pathogenicity is required for long-lasting potential therapeutics or vaccines. Here, using a structural and molecular approach, we show multistage processing of SARS-CoV-2 spike-protein for virion activation, infection, and how mutations influence it. We solved the structures of spike protein in complex with different host cell factors (TMPRSS2, Furin, CD26, and NRP1) with functional activity, and these insights into uncovering how viral spike-protein engages and primed with these multiple host factors, in addition to ACE2, to hijack host cell entry [3-6]. Furthermore, our COVID19 patient genome sequencing reveals that allele in TMPRSS2 (V160M) [7], and Furin provided protection from COVID19 infection, and its structural mechanism is further addressed and potential drug clinical trials. Additionally, our large-scale retrospective cohort studies proved Arbidol and derivatives as potential therapies for COVID19, using structural studies, we demonstrated the mechanism of action of Arbidol in disrupting spike function [8,9]. These findings cognize the complete mechanism of viral spike-glycoprotein processing/priming that leads to cascading entry into the host cell, paving the door for future vaccine development and identifying key targets. Our comprehensive, multifaceted research reveals the complexity of the SARS-CoV-2 spike-protein and clinical studies aid in therapies.

[1] R Verity et al., (2020), Lancet Infectious diseases
[2] M Young et al., (2022), BMJ Medicine
[3] N Vankadari *et al.,* (2022), ACS. J. Phys. Chem Lett
[4] N Vankadari & JA Wilce. (2020), Emerging Microbes & Infections
[5] Jun Lan *et al.,* (2020) Nature
[6] N Vankadari, (2020), ACS. J. Phys. Chem Lett
[7] Ravikanth V, Minta S & N Vankadari * et al., (2021), NEJM and GENE
[8] Qibin L*, Xuemin F*, Lu T*, N Vankadari*.*et al.,* (2021), MedRxiv
[9] N Vankadari. (2020), Int. J. Antimicrobial Agents

A018-03-290823

Enter and Hide: Molecular mechanisms at the host-viral interface

Gaya K. Amarasinghe, Ph.D.

Department of Pathology and Immunology, Washington University School of Medicine in St Louis, MO 63105

gamarasinghe@wustl.edu

Keywords: viral interactions, molecular mechanisms

We use a multidisciplinary research program that spans length and time scales to address this question by characterizing the molecular mechanisms of initial interactions at the host-pathogen interface. Using this information, we expect to develop a framework to manipulate viruses by modulating virulence (less virulent) in order to gain insight into immune mechanisms that are at play during these critical time points. Our current efforts are aimed toward defining the molecular basis for viral hemorrhagic fever (VHF) at the host-viral interface. VHF is a complex multivariable challenge with contributions from the virus and from the host dictating the outcome. We have begun a series of studies to understand the viral components, host factors and their interactions between each other. Recent studies of Ebola viruses and their interactions, including X-ray crystallographic and cryoelectron microscopy studies reveal how viral proteins VP35, VP24, and nucleoprotein (NP) promote viral replication and immune suppression. Structural insights will be discussed in the context of viral immune evasion and replication.

A018-04-290823

Structures of honeybee-infecting Lake Sinai virus reveal domain functions and capsid assembly with dynamic motions

N.-C. Chen1, C.-H. Wang2, M. Yoshimura1, Y.-Q. Yeh1, H.-H. Guan1, C.-C. Lin1, Y.-C. Huang1, S. Wakatsuki3, M.-C. Ho2, C.-J. Chen1

Scientific Research Division, National Synchrotron Radiation Research, 101 Hsin-Ann Road, Hsinchu 30076, Taiwan, Institute of Biological Chemistry, Academia Sinica, 128 Academia Road, Sec. 2, Taipei 115, Taiwan, SLAC National Accelerator Laboratory, Structural Molecular Biology, 2575 Sand Hill Road, Menlo Park, CA 94305, USA. cjchen@nsrrc.org.tw

Keywords: Lake Sinai virus, cryo-EM structures, Colony Collapse Disorder

Understanding the structural insight and diversity of honeybee-infecting viruses is critical to maintain pollinator health and manage the spread of diseases in ecology and agriculture. We determine cryo-EM structures of *T*=4 and *T*=3 capsids of virus-like particles (VLPs) of Lake Sinai virus (LSV) 2 and delta-N48 LSV1, belonging to tetraviruses, at resolutions of 2.3–2.6 Å in various pH environments [1]. Structural analysis shows that the LSV2 capsid protein (CP) structural features, particularly the protruding domain and C-arm, differ from those of other tetraviruses. The anchor loop on the central β-barrel domain interacts with the neighboring subunit to stabilize homo-trimeric capsomeres during assembly. For a comparison, we also determine the cryo-EM structure of the *T*=3 delta-N48 LSV1 VLP at 2.6 Å. Delta-N48 LSV1 CP interacts with ssRNA via the positively charged domains of the rigid helix α1', α1' –α1 loop, β-barrel domain, and C-arm. Cryo-EM reconstructions, combined with X-ray crystallographic and small-angle X-ray scattering analyses, indicate that pH affects capsid conformations by regulating reversible dynamic particle motions and sizes of LSV2 VLPs. C-arms with continuous densities exist in all LSV2 and delta-N48 LSV1 VLPs across varied pH conditions, indicating that autoproteolysis cleavage for g peptide release, which was generally observed in other known *T*=4 and *T*=3 viruses, is not required for LSV maturation. Interestingly, an introduction of a double mutation of M83E/D461F on the LSV2 CP, mimicking the key residues at the autoproteolysis sites from other tetraviruses Providence virus (PrV) and *Nudaurelia* capensis ω virus (NωV), potentially triggers a self-cleavage process on the specific scissile bond of LSV2 CP. Moreover, the observed linear domino-scaffold structures of various lengths, made up of trapezoid-shape capsomeres, provide a basis for icosahedral *T*=4 and *T*=3 architecture assemblies. These findings advance understanding of honeybee-infecting viruses that can cause Colony Collapse Disorder [2, 3, 4].

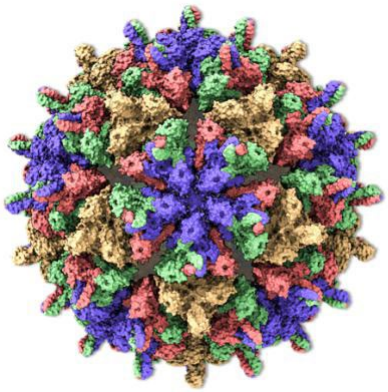

Figure 1. The structure of *T*=4 LSV2 VLP.

[21] Chen, N.-C., Wang, C.-H., Yoshimura, M., Yeh, Y.-Q., Guan, H.-H., Chuankhayan, P., Lin, C.-C., Lin, P.-J., Huang, Y.-C., Wakatsuki, S., Ho, M.-C. & Chen, C.-J. (2023). *Nat. Commun*. **14**, 545.

[22] Cox-Foster, D. *et al.* (2007). *Science* **318**, 283–287.

[23] Daughenbaugh, K., Martin, M., Brutscher, L. M., Cavigli, I., Garcia, E., Lavin, M. & Flenniken, M. L. (2015) *Viruses,* **7**, 3285–3309.

[24] Simenc, L., Kuhar, U., Jamnikar-Ciglenecki, U. & Toplak, I. (2020). *J. Econ. Entomol.* **113**, 1055–1061.

A018-06-290823

Structure of the Human T cell Leukaemia Virus capsid protein – a new drug target

Ruijie Yu1, Nan Li1, David A. Jacques1

1 Single Molecule Science, School of Biomedical Sciences, UNSW Sydney, Sydney, New South Wales 2052, Australia

d.jacques@unsw.edu.au

Keywords: indigenous health, HTLV-1, capsid protein

Human T cell leukaemia virus 1 (HTLV-1) is a retrovirus belonging to the family of Retroviridae and causes adult T cell leukaemia (ATL) and HTLV-1-associated myelopathy (HAM). HTLV-1 subtype C is highly prevalent in the indigenous peoples of central Australia with over 40% adults were testing seropositive in 2018[1]. The viral capsid is essential for the maturation of virions and protects the RNA genome from hydrolysis by cytosolic enzymes. Here, we report novel structural information of HTLV-1 capsid protein (CA) by crystallising the N-terminal domain (NTD), C-terminal domain (CTD) and full-length, respectively. Intriguingly, three crystal forms with different space groups of NTD were obtained: 1) triclinic P 1 with an ultra-high resolution of 0.87 Å that offers unambiguous atomic information of each residue, including the N-terminus β-hairpin which is important in HIV-1 CA for nucleotides transport[2]; 2) hexagonal P 6 2 2 which diffracted to 2.05 Å showing that crystallographic six-fold symmetry appears in the hexagonal capsid lattice, indicating HTLV-1 CA could potentially assemble to a hexameric conformation that is canonical in HIV-1 CA hexamer; 3) orthorhombic P $2_12_12_1$ diffracted to 1.47 Å displaying that a sulfate occupies the positively charged pocket, enclosed by H71/72, R98 and W117, implying HTLV-1 CA might interplay with new cellular factors that are different from the cofactors interacting with the HIV-1 capsid. The HTLV-1 CA-CTD was also solved to 1.47 Å and reveals the dimerisation packing of the capsid lattice. The crystal of HTLV-1 CA-full-length diffracted to 2.25 Å belonging to the F 2 2 2 space group, which also contains a six-fold crystallographic symmetry to generate a hexameric lattice. With the insight these structures have given us, we can predict how the HTLV-1 CA protein self-assembles and begin exploring how to disrupt the capsid pharmaceutically.

[25] Karl Gruber. Australia tackles HTLV-1. *The Lancet Infectious Diseases* 2018, 18 (10), 1073-1074.

[26] Jacques, D. A.; McEwan, W. A.; Hilditch, L.; Price, A. J.; Towers, G. J.; James, L. C. HIV-1 uses dynamic capsid pores to import nucleotides and fuel encapsidated DNA synthesis. *Nature* 2016, *536* (7616), 349-353.

A047 Crystallography in Space Research
Room 210
1.30pm – 3.50pm

A047-01-290823

A Decade of Quantitative Mineralogy on Mars: Results from the CheMin X-ray Diffractometer on the Mars Science Laboratory rover *Curiosity*

D. Blake1, T. Bristow1, E. Rampe2 and the CheMin Team

[1]NASA Ames Research Center, Moffett Field, CA USA; [2]NASA Johnson Space Center, Houston, TX USA. Email of communicating author: david.blake@nasa.gov

Keywords: Mars, mineralogy, X-ray Diffraction

For more than a decade, the CheMin X-ray diffraction instrument on the Mars Science Laboratory rover Curiosity has been returning definitive and quantitative mineralogical and mineral-chemistry data from ~3.5-billion-year-old (Ga) sediments in Gale crater, Mars. To date, 36 drilled rock samples and 3 scooped soil samples have been analyzed over the course of a 29+ km transit. These samples document the mineralogy of more than 600 vertical meters of flat-lying fluvial, lacustrine and aeolian sediments that comprise the lower strata of the central mound of Gale crater (Aeolis Mons; informally known as Mt. Sharp) and the surrounding plains (Aeolis Palus). The principal mineralogy of the sediments is basaltic, with evidence of early and late-stage diagenetic overprinting. The rocks in many cases preserve much of their primary mineralogy and sedimentary features, suggesting that they were never strongly heated or deformed. Using aeolian soil composition as a proxy for the composition of the deposited and lithified sediment, it appears that in many cases diagenetic changes observed are principally isochemical. Exceptions to this trend include secondary nodules, calcium sulfate veining, and rare Si-rich alteration halos. A striking hematite-rich feature in lower Mt. Sharp called Vera Rubin ridge is interpreted to be lake sediment diagenetically altered by dense, silica-poor brines. A surprising and yet poorly understood observation is that nearly all of the ~3.5 Ga old sedimentary rocks analyzed to date contain 15-70 wt.% X-ray amorphous material. Overall, this 600+ meter vertical section of sedimentary rock explored on lower Mt. Sharp documents a perennial shallow lake environment grading upward into alternating lacustrine/fluvial and aeolian environments.

Highlights of CheMin's results from Mars include: The first quantitative mineralogical analysis of the global Mars soil [1-2]; Discovery and characterization of the first habitable environment on another planet [3-5]; Evidence of low Hesperian PCO2, calling into question the role of CO2-based greenhouse warming [6]; Evidence for a highly diverse basalt mineralogy on early Mars [7]; and Changes in clay mineral and Fe-oxide chemistry, documenting the drying out and oxidation of the Martian hydrosphere [8]. All data and open access publications can be downloaded from the CheMin ODR website: http://odr.io/chemin.

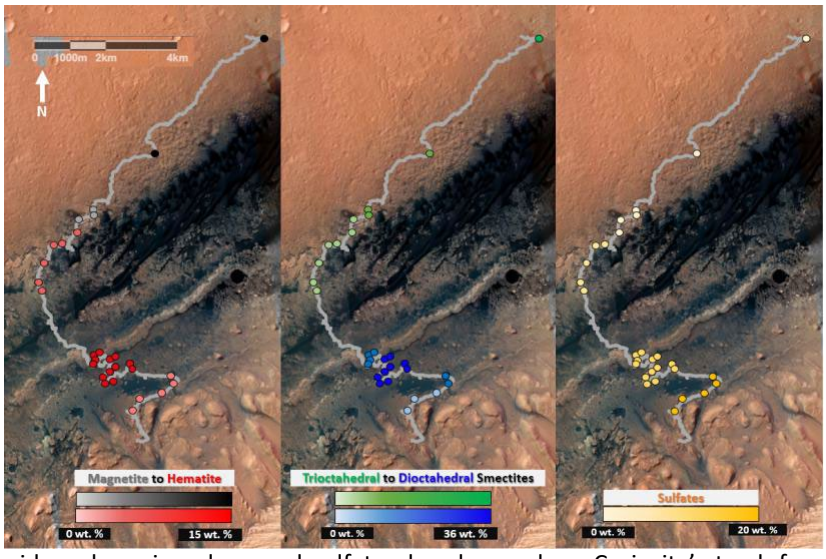

Figure 1. Changes in Fe-oxides, clay mineralogy and sulfate abundance along Curiosity's track from Yellowknife Bay to the Clay-Sulfate transition.

[27] Bish, et al., (2013) *Science,* 10.1126/science.1238932
[28] Blake et al., (2013) *Science*, 10.1126/science.1239505
[29] Vaniman et al., (2013) *Science*, 10.1126/science.1243480
[30] Bristow et al., (2015) *Am. Min*., 10.2138/am-2015-5077CCBYNCND
[31] Grotzinger et al., (2013) *Science*, 10.1126/science.1242777
[32] Bristow et al., (2015) *PNAS*, 10.1073/pnas.1616649114
[33] Treiman et al., (2015) *JGR Planets*, 10.1002/2015JE004932
[34] Bristow et al., (2018) *Sci. Adv*. 10.1126/sciadv.aar3330

A047-02-290823

Determining suitable periodic DFT methods for modelling Titan-relevant molecular minerals

N.D Stapleton[1], H.E. Maynard-Casely[2], S.A Moggach[1], D. Spagnoli[1]

[1]School of Molecular Sciences, the University of Western Australia, Perth, WA, Australia [2]Australian Nuclear Science and Technology Organisation, Sydney, NSW, Australia nicholas.staplteon@research.uwa.edu.au

Keywords: Titan-relevant, Molecular co-crystals, Periodic DFT

Saturn's largest moon, Titan, has geological features similar to those found on Earth, with seas, lakes and sweeping dunes. Unlike the Earth, however, the temperature hardly varies from around 92 K and the surface composition is dominated by molecular materials composed of H, C and N. The presence of liquid hydrocarbon seas and an active weather system on Titan could allow for deposited 'pure' compounds from the atmosphere to mix and form molecular co-crystals. No comprehensive computational chemical methods have been applied to all currently known Titan co-crystals. Determination of co-crystal structures could lead to more complete understandings of how geological processes affect and interact with minerals on the surface of Titan, as currently little is known of such phenomena [1].

A thorough periodic density functional theory (DFT) study of the set of structurally determined Titan-relevant molecular co-crystals and the single-component crystals of their respective co-formers was completed. A range of different exchange-correlation functionals were tested along with various dispersion correction methods. This included a combination of post-hoc corrected and inherent van der Waals dispersion functionals, including the cutting edge D4 correction, which has been shown to accurately reproduce unit cell volumes and lattice energies of a generic benchmark set [2]. To ensure structures converged as accurately as possible, a multi-step geometry optimisation was performed on all systems. This method has been previously used by Taylor and Day [3] on a large set of molecular crystals whose structures were obtained from diffraction data. The more accurate DFT dispersion corrected methods calculate lattice parameters and cell volumes closer to experimental data. Many of the functionals consistently underestimated cell volumes, which has been observed in previous work by Moellmann and Grimme [4]. Overall, we found the RPBE-D4 functional performed the best on average for recreating experimental cell volumes. Co-crystallisation was generally seen to be a thermodynamically unfavourable process, however, the magnitude of decrease in stability was usually relatively small.

[35] Cable, M. L., Runčevski, T., Maynard-Casely, H. E., Vu, T. H. & Hodyss, R. (2021). Acc Chem Res., 54, 3050.
[36] Caldeweyher, E., Mewes, J–M., Ehlert, S. & Grimme, S. (2020). Phys. Chem. Chem. Phys., 22, 8499.
[37] Taylor, C. R. & Day, G. M. (2018). Crst. Growth Des. 18, 892.
[38] Moellmann, J. & Grimme, S. (2014). J. Phys. Chem. C., 118, 7615.

This work was supported by resources provided by the Pawsey Supercomputing Centre with funding from the Australian Government and the Government of Western Australia.
This work was also supported by the AINSE Postgraduate Research Award (PGRA), and the Australian Government Research Training Program (RTP) fees offset scholarship and stipend.

A047-03-290823

Multi-step crystallization processes of cosmic dust analogues founding in microgravity experiments

Yuki Kimura1, Kyoko K. Tanaka2, Yuko Inatomi3

1Institute of Low Temperature Science, Hokkaido University; Kita-19, Nishi-8, Kita-ku, Sapporo, 060-0819, 2 Astronomical Institute, Tohoku University; 6-3 Aoba, Aoba-ku, 985-8578, Sendai, Japan, 3Japan, Institute of Space and Astronautical Science, Japan Aerospace Exploration Agency; 3-1-1 Yoshinodai, Chuo-ku, Sagamihara, Kanagawa 252-5210, Japan, and School of Physical Sciences, SOKENDAI (Graduate University for Advanced Studies); 3-1-1 Yoshinodai, Chuo-ku, Sagamihara, Kanagawa 252-5210, Japan
ykimura@lowtem.hokudai.ac.jp

Keywords: Dust, Sounding rocket, Crystal growth

We aim to understand the formation processes and characteristics of cosmic dust, which is ubiquitous in space. Generally, cosmic dust has been discussed based on findings from experiments conducted in Earth's gravitational environment, despite the fact that cosmic dust is formed in microgravity environment. In addition, the characteristics of dust have been discussed based on the physical properties of bulk particles, even though the size of dust is less than 100 nm, where nanoparticles have unique physical properties and peculiar phenomena that are different from those of bulk particles. Therefore, we have conducted an experiment of dust analogues formation under the microgravity environment obtained by using sounding rockets. With optical methods such as interferometry and infrared spectroscopy, we determined the sticking probability and surface free energy of the nanoparticles, and investigated the crystallization pathway.

We performed sounding rocket experiments in five times in a past decade and produced metal [1], oxide [2, 3] and carbide [4] nanoparticles as dust analogues via homogeneous nucleation from supersaturated vapor. Based on nucleation temperature, timescale for gas cooling and size of produced particles, sticking probabilities and surface free energies have been successfully determined by means of nucleation theory. Sticking probabilities are usually assumed to be close to 100% because it is convenient to explain the abundance of dust in the universe and bulk experiment supported the assumption [5]. In contrast, the sticking probabilities obtained from our formation experiments of nanoparticles are two to five orders of magnitude smaller, 0.002% for Fe [1] and 0.5-1.6% for SiO [3], for instance. These values were also 1-2 orders of magnitude smaller than those obtained in the ground experiments. Nanoparticles are produced by heating an evaporation source to generate high-temperature vapor in argon gas, which works to decrease mean free path of evaporated vapor. On the ground, the high-temperature evaporation source generates density-difference convection, resulting in gas flow, whereas in a microgravity environment, the isotropically evaporated high-temperature gas cools slowly in a calm environment with no flow, forming nanoparticles. Just as shaking a plastic bottle filled with supercooled water induces the formation of ice, a flow of supercooled vapor promotes the formation of nanoparticles. Therefore, microgravity experiments are essential to determine the precise physical quantity.

In-situ observation of the formation of aluminum oxide nanoparticles from supersaturated vapor by infrared spectroscopy revealed that the nanoparticles undergo a crystallization process via a droplet [2]. At the beginning for nucleation, since the size of nuclei is very small, couple of nanometres or even smaller, melting point of the nuclei is lower than corresponding bulk material. Namely, when nucleation temperature is higher than the melting point of nucleating nanoparticle, the two-step nucleation process, a droplet is first nucleated from the supersaturated vapor and then crystals are nucleated from the supercooled droplet, becomes common. Furthermore, the formation process of carbonaceous particle with a titanium carbide core, which is well-known pre-solar particle, was found to proceed by three processes: formation of initial particles, development of core-mantle structure, and fusion growth of nanoparticles [4]. Our series of experiments have revealed that such non-classical nucleation processes are universally observed in a variety of materials. In the presentation, we discuss new findings on the formation of nanoparticles from the gas phase and on the formation process of cosmic dust.

[1] Kimura, Y., Tanaka, K. K., Nozawa, T., Takeuchi, S. & Inatomi, Y. (2017). *Sci. Adv.* **3**, e1601992.

[2] Ishizuka, S., Kimura, Y., Sakon, I., Kimura, H., Yamazaki, Y., Takeuchi, S. & Inatomi Y. (2018). *Nat. Commun.* **9**, 3820.

[3] Kimura, Y., Tanaka, K. K., Inatomi, Y., Ferguson, F. T. & Nuth III, J. A. (2022). *Astrophys. J. Lett.* **934**, L10.

[4] Kimura, Y., Tanaka, K. K., Inatomi, Y., Aktas, C. & Blum J. (2023). *Sci. Adv.* **9**, eadd8295.

[5] Tachibana, S., Nagahara, H., Ozawa, K., Ikeda, Y., Nomura, R., Tatsumi, K. & Joh Y. (2011). *Astrophys. J.* **736**, 16.

Microgravity experiments using sounding rockets were conducted and/or supported with ISAS/JAXA. NASA, SSC and DLR. Development of the experimental system was supported by the Technical Division of the Institute of Low Temperature Science, Hokkaido University, and the Advanced Machining Technology Group of JAXA. We thank Grant-in-Aids for Scientific Research (S) from KAKENHI 20H05657.

A047-04-290823

Diffraction studies of meteorites at the Australian Synchrotron

H. E. A. Brand[1], N. R. Stephen[2], A. D. Langendam[1], E. C. Campbell[1] and A. G. Tomkins[3]

1. ANSTO, Australian Synchrotron, 800 Blackburn Rd., Clayton, VIC 3168, Australia, 2. Plymouth Electron Microscopy Centre, University of Plymouth, Drake Circus, Plymouth, PL4 8AA, United Kingdom, 3. School of Earth, Atmosphere and Environment, Monash University, Melbourne, VIC 3800, Australia;

helenb@ansto.gov.au

Keywords: Mineralogy, Meteorites, powder diffraction

Meteorites are windows on the solar system. They provide invaluable insights into the composition and geological processes which formed and continue to shape the solar system. Most of the investigations into these planetary materials typically use microscopic and spectroscopic techniques. However, there is much to be learned using scattering techniques to investigate the bulk properties and mineralogy of these materials.

In this contribution we will summarise projects undertaken across beamlines at the Australian synchrotron. Topics discussed will include:

Thermal properties of meteorites and terrestrial analogues with a view to ISRU
Planetary analogue simulants are materials, terrestrial in origin and usually mixtures of minerals, which are designed to be spectrally and compositionally identical to the materials we observe on other planets. Both ESA and NASA produce and curate simulant materials for various planetary bodies. In coming years, there are a number of sample return missions scheduled and interest in benchmarking simulant materials and their properties relative to "real" extra-terrestrial samples is growing. This is especially timely in relation to In Situ Resource Utilisation (ISRU) requirements as human space flight programs such as Artemis begin in earnest. Most analogues are made of pristine materials and although they may be chemically similar to the rocks they emulate, mineralogically they can be very different. In this study, we compare the thermal properties of a range of meteorites to their curated analogue materials.

Using powder diffraction to classify micrometeorites
Micrometeorites are samples of extraterrestrial dust that continually fall to the surface of the Earth. They hold records of the early solar system as well as the state of the Earth's atmosphere when they passed through it. Handling these tiny samples, sometimes as small as 10 micron, can be difficult. Sectioning means that you can only see a 2-dimentional section that is unlikely to be fully representative of the mineralogy. Powder diffraction offers a pathway to obtain a bulk mineralogy analysis of individual micrometeorites, which is not possible by other approaches. Here we will discuss the best way to screen and classify micrometeorites using lessons learnt from other crystallographic disciplines and develop a sample holder that allows entire populations to be screened using powder diffraction before being easily transferred for other studies such as microscopy.

Development of simultaneous microdiffraction and fluorescence mapping of meteorite mineral phases on the X-ray Fluorescence microscopy beamline
Being able to spatially determine mineralogical changes across a sample are key to understanding the process that shaped the rock. At the Australian synchrotron we are developing a new technique to conduct simultaneous microdiffraction analysis and fluorescence mapping. The meteorites chosen for this exploratory experiment demonstrate how we can use the XFM beamline to map mineralogy and to investigate texture in texturally complex but mineralogically simple natural samples.

A047-05-290823

In-situ energy dispersive X-ray diffraction microscopy with the Planetary Instrument for X-ray Lithochemistry (PIXL) on Mars

W. M. Jones[1,2], D. T. Flannery[2,3], A. C. Allwood[4], M. M. Tice[5], J. A. Hurowitz[6], Y. Liu[4], B. J. Orenstein[2,3], S. Davidoff[4], N. J. Tosca[7], K. R. Moore[8], B. C. Clark[9] S. J. Van Bommel[10], M. E. Schmidt[11], T. V. Kizovski[11], A. H. Treiman[12], L O'Neil[13]

[1]School of Chemistry & Physics and Central Analytical Research Facility, Queensland University of Technology, Australia, [2]Centre for Planetary Surface Exploration, Queensland University of Technology, Australia, [3]School of Earth & Atmospheric Sciences, Queensland University of Technology, Australia, [4]Jet Propulsion Laboratory, California Institute of Technology, USA, [5]Department of Geology & Geophysics, Texas A&M University, USA, [6]Department of Geosciences, Stony Brook University, USA, [7]Department of Earth Sciences, University of Cambridge, United Kingdom, [8]Division of Geological and Planetary Sciences, California Institute of Technology, USA, [9]Space Science Institute, USA, [10]McDonnell Center for the Space Sciences, Department of Earth and Planetary Sciences, Washington University of St. Louis, USA, [11]Department of Earth Sciences, Brock University, Canada, [12]Lunar and Planetary Institute (USRA), USA, [13]Department of Earth and Space Sciences, University of Washington, USA

mw.jones@qut.edu.au

Keywords: Perseverance rover, Mars2020, *In-situ* crystallography, ED-XRD

The Planetary Instrument for X-ray Lithochemistry (PIXL) contains an X-ray fluorescence (XRF) spectrometer mounted on the arm of the *Perseverance* rover which landed in Jezero Crater, Mars in 2021 and is capable of creating maps at centimetre scale. PIXL features a micro focused X-ray beam with an approximate 120 um spot from a tube mounted polycapillary optic, with a pair of KETEK VITUS H50 silicon drift detectors mounted either side of the incident beam with an internal angle of 22.5 degrees between the beam and each detector [1]. While primarily designed as an X-ray fluorescence instrument, PIXL also collects a significant amount of backscattered X-ray diffraction, which can be interpreted to allow scientific outcomes that would not be possible using fluorescence alone [2, 3].

Here we show how *in-situ* energy-dispersive X-ray diffraction (ED-XRD) data is collected by PIXL and separated from the fluorescence signal, and highlight recent results from *Perseverance*'s Crater Floor Campaign. In addition, we describe a method that combines ED-XRD, XRF, and macroscopic images with a forward simulated ED-XRD look up table [4] to decipher *in-situ* crystallographic orientation from a limited dataset to map *in-situ* crystallographic information on the surface of Mars.

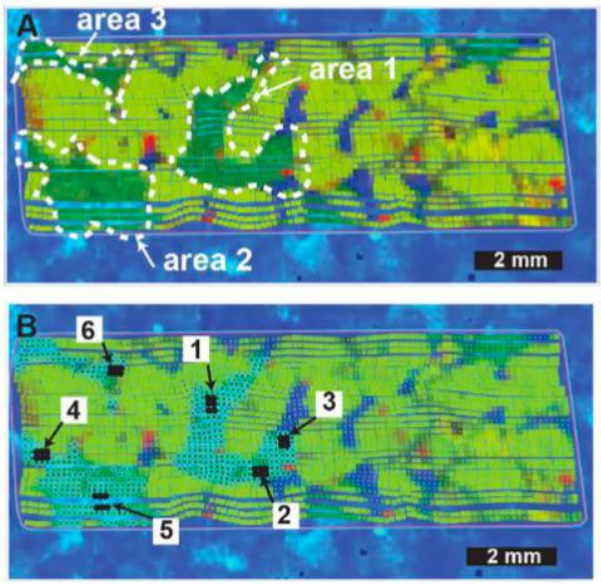

Figure 1. PIXL *in-situ* ED-XRD identifies a single contiguous pyroxene grain (A: areas 1, 2, and 3) on the Dourbes abrasion patch, Jezero Crater, Mars, revealing that the Séítah formation on the crater floor is igneous olivine cumulates. Figure from [2], used with permission.

[9] Allwood, A. C., Wade, L. A., Foote, M. C. et al., (2020) *Space Science Reviews* **216** 134

[10] Liu, Y., Tice, M. M., Schmidt, M. E., et al. (2022) *Science* **337** 1513-1519

[11] Tice, M. M., Hurowitz, J. A., Allwood, A. C. et al., (2022) *Science* Advances accepted

[12] Gupta, V. K. & Agnew, S. R. (2009) *Journal of Applied Crystallography* **42** 116-124

A054 Methods for the Determination and Analysis of Magnetic Structures for Powders and Single Crystals
Room 211
1.30pm – 3.50pm

A054-01-290823

Structural, morphological and magnetic properties of Fe_xCo_{1-x} nanoparticles. A multi-method approach.

C. Mondelli[1], V. Vadillo[2], P. Lazpita[2-3], Ines Puente-Orench[4,5] and M. Insausti[2-3]

[1]CNR-IOM, Institut Laue Langevin , Grenoble 38042, France [2]BCMaterials, UPV/EHU Science Park, Leioa 48940, Spain

[3]University of Basque Country (UPV/EHU) Leioa 48940, Spain, [4]CSIC- Universidad de Zaragoza, Zaragoza, 50009, Spain

[5]Institut Laue Langevin, Grenoble 38042, France

Email of communicating mondelli@ill.fr

Keywords: Magnetic nanoparticles of Iron Cobalt alloy, Neutron diffraction, EXAFS and XANES techniques

Magnetic nanoparticles (MNPs) are nowadays a key class of materials that has contributed very quickly to the improvement and development of applications in the nanotechnology field [1-2]. It is already well stablished that magnetic properties shown by nanostructured magnetic materials are different if compared with the same parent composition at the bulk state and that reducing material dimensions to the nanoscale magnetic properties (saturation, permeability and remanence) becomes size-dependent. Recently, the authors performed the synthesis of FexCo1 -x (0<x<1) alloy nanoparticles (NPs) with different compositions, as well as pure Fe and Co NPs for comparison, by the chemical reduction technique. The subsequent first characterization made at room temperature by X-ray diffraction (XRD) and vibrating sample magnetometry (VSM) demonstrated an excellent quality NPs with the expected bcc cubic (for Fe and FeCo alloys) and hcp hexagonal structures showing a soft magnetic character at room temperature with a magnetization as high as 235 emu/g for the Fe66Co34 composition alloy [3].

Nevertheless, this soft magnetic character is accompanied by an unexpected high value of effective anisotropy (2 MJ/m^3) [3]. To make shade on the origin of this high magnetic anisotropy we needed a multi-methods approach using several techniques: Neutron Powder Diffraction (NPD) to obtain long range nuclear and magnetic structure; synchrotron X-ray Absorption Spectroscopies (XAS) sensitive to a local-structure in two different regions: the near edge structure (XANES) and the extended fine structure (EXAFS); Atomic Force Microscopy (AFM) and Magnetic Force Microscopy (MFM) to study the morphology of the nanoparticles and their magnetic clustering. A plethora of other magnetic techniques complete the magnetic characterization of the systems. We present here this extensive study of the synthesized Fe, Co and FexCo1 -x alloy nanoparticles at the nanoscale. NPD and EXAFS and XANES spectroscopy combined with AFM/MFM images (see Fig. 1), have revealed that, despite the cubic bcc structure observed for all FeCo alloys (in excellent concordance with the pure Fe one) the NPs show a "flaky" shape of 20-60 nm size but only 2-3 nm thickness, giving rise to a strong shape anisotropy contribution to the observed total effective anisotropy.

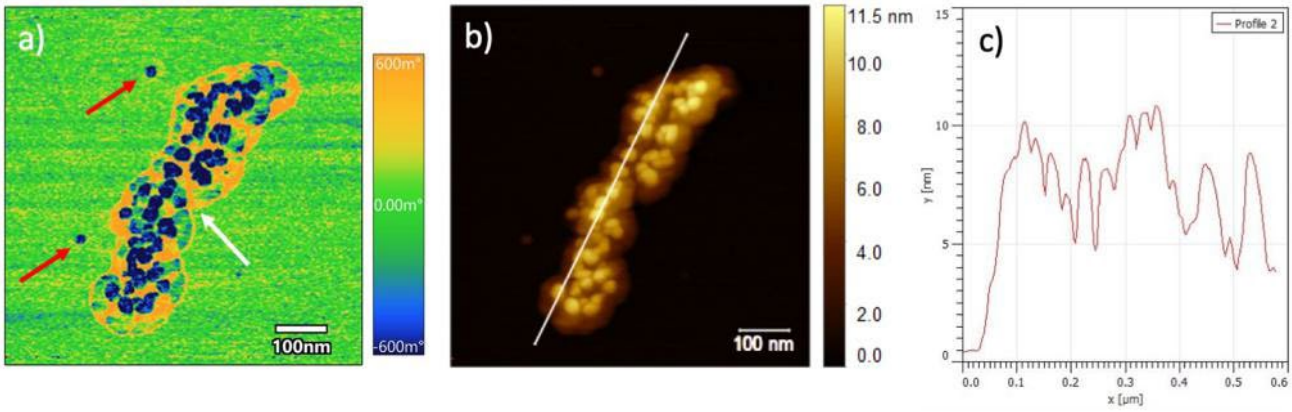

Figure 1. a) MFM phase shift image for the Fe51Co49 composition nanoparticles showing both single nanoparticles (red arrows) and one agglomerate of them (white arrow); b) topology of the same cluster. Note the two single nanoparticles are not visible with this choice of range because too flat. The max height of the cluster is 11.5 nm and the single particles are only 3 nm. c) Profile along the white line in b).

[39] Ali, A., Shah, T., Ullah, R., Zhou, P., Guo, M., Ovais, M., Tan, Z., Rui, Y. (2021) *Frontiers in Chemistry* **9**, Article 629054.

[40] Ma, Z., Kecheng Wei, J.M., Liu, J.P., Sun, S. (2021) *Chemical Reviews,* DOI: 10.1021/acs.chemrev.1c00860

[41] Vadillo, V., Insausti, M., Gutiérrez, J. (2022) *J. Magnetism and Magnetic Materials* ***563****, 169975.*

A054-02-290823

Magnetism of low dimensional quasi-1D spin-one chain $PbM_2Ni_6Te_3O_{18}$

S.Uthayakumar1,3, D. T. Adroja1, Dmitry Khalyavin1, D.Prabhakaran2,J P Goff3 and A. Ewings1

[1]ISIS Pulsed Neutron and Muon Source, STFC Rutherford Appleton Laboratory, Didcot, Oxfordshire OX11 0QX, U.K.
[2] Department of Physics, University of Oxford, Clarendon Laboratory, Oxford OX1 3PU, U.K.
[3] Department of Physics, Royal Holloway University of London Egham, TW20 0EX, U.K.

Keywords: Quasi-1D chain, powder neutron, magnetic structure

The search for realizations of spin systems where magnetic exchange between localized spins is restricted to one (1D) or two (2D) spatial dimensions is important for the verification of modern theories of quantum magnetism and for the exploration of novel magnetic phenomena and topological behaviour [1-4]. Therefore, the low-dimensional (LD) magnetic materials have attracted a great deal of interest recently, because of their anomalous magnetic properties at low temperatures [5,6]. Among the LD systems, the subject of one-dimensional (1D) spin-chain systems has attracted considerable attention due to the well-known fact that an ideal 1D S=1/2 system does not undergo long-range order (LRO) at finite temperatures due to strong quantum spin fluctuations [1,4]. Quantum spin fluctuations in a 1D or frustrated magnet destabilize the magnetic ground state, while keeping sizable strength of spin correlations and hence results in a new ground state called a quantum spin liquid (QSL).

One of the important classes of spin chains is the Haldane chain, which is a one-dimensional (1D) Heisenberg chain with integer spins and antiferromagnetic (AFM) nearest neighbour coupling. Haldane predicted that the ground state of such a system would be a nonmagnetic singlet state which would be separated in energy from the excited triplet state by a gap (Δ) [7]. Another incredibly special feature of the Haldane gap state is the existence of long-range correlations that lead to edge modes, which have been observed in experiments [8]. On the other hand, the ground state of a half-integer valued spin chain is gapless. In a 1D spin-1/2 chain, a particle-like excitation called a spinon is known to be responsible for spin fluctuation in a paramagnetic state.
Such 1D spin-chain systems have attracted considerable attention due to the possibility of Haldane gap formation for an integer spin system.

The compounds $PbM_2Ni_6Te_3O_{18}$ (M=Cd and Mn) having quasi-1D chains of Ni^{2+} (S=1) and Mn^{2+} (S=5/2) in their crystal structure exhibit remarkably interesting magnetic properties. To fully understand the nature and origin of the magnetic structure, we investigated the magnetic behaviour of a polycrystalline sample of $PbCd_2Ni_6Te_3O_{18}$ (with Cd-114) using the WISH beam line at the ISIS facility and we find an AFM ordering with propagation vector (1/3 1/3 0) with the Ni-moments along the c-axis. We also investigated magnetic excitations in a powder sample of $PbMn_2Ni_6Te_3O_{18}$ using the MARI spectrometer at the ISIS facility, which shows two bands of magnetic excitations near 8 and 17 meV. At 100 K the magnetic excitations transformed into very broad diffuse scattering indicating the presence of magnetic frustration. The obtained results will be discussed in detail.

[1] I. Affleck, J. Phys.: Condens. Matter 1, 3047 (1989).
[2] H.-J. Mikeska and A. K. Kolezhuk, in Quantum Magnetism, edited by U. Schollwöck, J. Richter, D. J. J. Farnell, and R. F. Bishop (Springer, Berlin, 2004), pp. 1–83. [3]
A.N. Vasil'ev et al, Low temp. Physics. 31, 203 (2005)
[4] H. A. Bethe, Z. Phys. 71, 205 (1931).
[5] S. Ma et al, Phys. Rev. Lett. 69, 3571 (1992).
[6] Y. Zhou et al, Rev. Mod. Phys., 89, 025003 (2017)
[7] F. D. M. Haldane, Phys. Rev. Lett. 50, 1153 (1983)
[8] M. Hagiwara et al, Phys. Rev. Lett. 65 (25) (1990)

A054-03-290823

Magnetic ground state of NdB4: Interplay between anisotropic exchange interactions and hidden order on a Shastry-Sutherland lattice.

R. D. Johnson1, D. D. Khalyavin2, D. Brunt3, N. Qureshi4, G. Balakrishnan3, A. R. Wildes4, B. Ouladdiaf3, and O. A. Petrenko4

1) Department of Physics and Astronomy, University College London, Gower Street, London WC1E 6BT, United Kingdom. 2) ISIS facility, Rutherford Appleton Laboratory-STFC, Chilton, Didcot OX11 0QX, United Kingdom. 3) Department of Physics, University of Warwick, Coventry CV4 7AL, United Kingdom. 4) Institut Laue-Langevin, 6 Rue Jules Horowitz, BP 156, 28042 Grenoble Cedex 9, France

roger.johnson@ucl.ac.uk

Keywords: Frustrated magnetism, Hidden order, Shastry-Sutherland

The Shastry-Sutherland lattice, introduced as a theoretical model of a frustrated antiferromagnet [1], has been at the forefront of condensed matter research over several decades. The model has been experimentally realized for both quantum and classical spins, and one of the well-known representatives of the latter case is neodymium tetraboride NdB_4, crystallising into a tetragonal crystal structure [2]. The compound exhibits several magnetic phases and a complex multi-k ground state that has been elusive for a long time [2,3]. Here we report the solution and quantitative refinement of the magnetic ground state of NdB_4 based on neutron diffraction data. The obtained magnetic structure consists of two components; one of them is confined within the ab-plane and makes an orthogonal all-in all-out configuration maintaining translation symmetry of the crystal. Another is along the c-axis, and this component forms an anharmonic spin density wave consisting of three-up-two-down sequences with fivefold periodicity. The in-plane and out-of-plane spin structures represent distinct magnetic instabilities which normally would not coexist. Their simultaneous presence in the same phase is an interesting phenomenon associated with anisotropic exchange interactions and coupling to a symmetry breaking non-magnetic order parameter undetectable by the available diffraction data.

[1] B. S. Shastry and B. Sutherland, Physica B+C **108**, 1069 (1981), https://doi.org/10.1016/0378-4363(81)90838-X
[2] 6. H. Yamauchi, N.Metoki, R.Watanuki, K. Suzuki, H. Fukazawa, S. Chi, and J. A. Fernandez-Baca, J. Phys. Soc. Jpn. **86**, 044705, (2017), https://doi.org/10.7566/JPSJ.86.044705
[3]. N. Metoki, H. Yamauchi, M. Matsuda, J. A. Fernandez-Baca, R. Watanuki, and M. Hagihala, Phys. Rev. B **97**, 174416 (2018), https://doi.org/10.1103/PhysRevB.97.174416

A054-06-290823

Solving the magnetic structures in the complex in-field phase diagram of YMn6Sn6−xGex using single crystal neutron diffraction

Rebecca L. Dally[1], Hari Bhandari[2,3], Peter E. Siegfried[2,3], Resham Regmi[2,3], Kirrily C. Rule[4], Songxue Chi[5], Igor I. Mazin[2,3], Jeffrey W. Lynn[1], Nirmal J. Ghimire[2,3]

[1]NIST Center for Neutron Research, National Institute of Standards and Technology, Gaithersburg, MD 20899, USA, [2]Department of Physics and Astronomy, George Mason University, Fairfax, VA 22030, USA, [3]Quantum Science and Engineering Center, George Mason University, Fairfax, VA 22030, USA, [4]Australian Nuclear Science and Technology Organisation, New Illawarra Road, Lucas Heights, NSW, 2234, Australia, [5]Neutron Scattering Division, Oak Ridge National Laboratory, Oak Ridge, TN 37831, USA

Email of communicating rebecca.dally@nist.gov

Keywords: neutron diffraction, incommensurate magnetic structure, kagome lattice magnet, topological Hall effect

The $\mathbf{B} \parallel ab$-plane in-field magnetic phase diagram of YMn_6Sn_6 has recently garnered attention due to the coexistence of a large topological Hall effect with one of the phases namely, a transverse conical spiral magnetic phase [1]. This spin texture can be directly related to the observation of the real-space Berry curvature arising from a fluctuation-driven mechanism. Generally, the crystal structure of magnetic compounds forming the $HfFe_6Ge_6$-type structure (*P6/mmm* and shown in Fig. 1(a)) lays much of the foundation for the interesting physics observed. For example, the topological Hall effect in YMn_6Sn_6 originates from parametrically frustrated interplanar exchange interactions that arise due to the particular stacking sequence of the Mn kagome planes. It is also this frustrated interplanar exchange and delicate balance of energy scales with the inclusion of an in-plane applied magnetic field that leads to the complex magnetic phase diagram shown in Fig. 1(b).

Recently, we have explored what happens when the stacking of the Mn planes is tuned via Ge doping [2]. For $YMn_6Sn_4Ge_2$, Ge preferentially replaces the Sn at the 2*c* Wyckoff position, which is in the same layer as the Y atoms. This results in the J_1 and J_p exchange interactions (Fig. 1(a)) essentially staying constant, whereas J_2 and J_3 switch signs and change in magnitude, leading to a quite different in-field phase diagram. Additionally, even a subtle change to the zero-field ground state magnetic structure influences the Fermi surface making $YMn_6Sn_4Ge_2$ more conductive along the *c*-axis.

Crucially, single crystal neutron diffraction was required to solve the magnetic structures of $YMn_6Sn_{6-x}Ge_x$ (x = 0, 2) in the **B**-*T* magnetic structure phase diagram. The intimate relationship between the electronic structure and magnetic structure in $YMn_6Sn_{6-x}Ge_x$ required knowledge of the spin textures which could only be gained from neutron diffraction. This talk will discuss the practical details of experiment planning, magnetic neutron diffraction, and interpreting the $YMn_6Sn_{6-x}Ge_x$ results via Rietveld refinement.

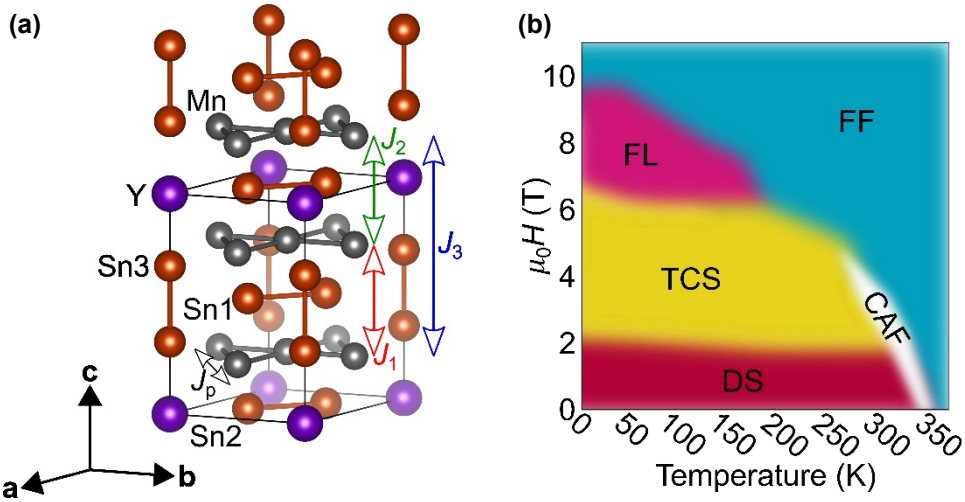

Figure 1. (a) The crystal structure and exchange interaction pathways (J_p, J_1, J_2, and J_3) for YMn_6Sn_6. (b) Magnetic structure phase diagram for an applied field within the ab-plane of YMn_6Sn_6. The phases shown are distorted spiral (DS), transverse conical spiral (TCS), fan-like (FL), forced ferromagnetic (FF), and canted antiferromagnet (CAF).

[1] Ghimire et al., Sci. Adv. 6, eabe2680 (2020).

[2] Bhandari et al. (2023) (in preparation).

A065 Different Approaches to Comparing Crystal Structures in Massive Datasets
Room 209
1.30pm – 3.50pm

A065-01-290823

Automatic comparison of crystal structures by CrystalCMP

J. Rohlíček

Institute of Physics of the Czech Academy of Sciences, Na Slovance 2, Prague 8, 182 21, Czech Republic

rohlicek@fzu.cz

Keywords: crystal structure comparison, program, molecular packing

Numerous approaches for determining and quantifying similarity between crystal structures have been published. These methods include comparing the so-called "fingerprints" of crystal structures [1–3], comparing the positions of atoms, entire fragments, and molecular packing within structures [4–10], simplifying the arrangement of crystal structures to connective rods to create structural motifs [11], and comparing based on several geometrical criteria including the contact area and energy of neighboring molecules [12].

The CrystalCMP [9] method is based on the comparison of a representative molecular cluster that includes one type of molecule, typically the largest. During the comparison, the molecular clusters of the individual crystal structures are superimposed, and the similarity is calculated as the sum of the average deviation of the centers of the overlapping molecules with a parameter representing the angle between them. The program offers a semi-automatic mode, where the user defines a small fragment of the central molecule to find the transformation between molecular clusters, or an automatic mode, where the program itself finds this fragment and performs a fully automatic calculation.

After the calculation, the program outputs a similarity matrix and sorts the results into similarity groups using a dendrogram. The program reads the command line and can be run with or without a graphical user interface. Thus, the program can be used to compare both small and large datasets, where in one case the user tends to choose the advantages of the GUI and in the other, the user appreciates the possibility of passing parameters via the command line. The program was tested on a large dataset containing over 100 x 10^3 cif files of molecular structures extracted from the CSD database using CSD python API [13] and sorted to the 28 x 10^3 series of individual compounds containing from two to 647 entries [9]. For such a diverse dataset, approximately 2 x 10^6 comparisons had to be performed, which took approximately 8 days on a common PC using a single core. The result is an HTML list of similarity matrices and dendrograms sorting the CSD entries into the similarity groups.

[42] M. Valle, A. R. Oganov, *Acta Crystallogr. A* **2010**, *66*, 507–517.
[43] H. R. Karfunkel, B. Rohde, F. J. J. Leusen, R. J. Gdanitz, G. Rihs, *J. Comput. Chem.* **1993**, *14*, 1125–1135.
[44] E. L. Willighagen, R. Wehrens, P. Verwer, R. de Gelder, L. M. C. Buydens, *Acta Crystallogr. B* **2005**, *61*, 29–36.
[45] A. V. Dzyabchenko, *Acta Crystallogr. B* **1994**, *50*, 414–425.
[46] R. Hundt, J. C. Schön, M. Jansen, *J. Appl. Crystallogr.* **2006**, *39*, 6–16.
[47] G. de la Flor, D. Orobengoa, E. Tasci, J. M. Perez-Mato, M. I. Aroyo, *J. Appl. Crystallogr.* **2016**, *49*, 653–664.
[48] J. A. Chisholm, S. Motherwell, *J. Appl. Crystallogr.* **2005**, *38*, 228–231.
[49] A. J. Nessler, O. Okada, M. J. Hermon, H. Nagata, M. J. Schnieders, *J. Appl. Crystallogr.* **2022**, *55*, 1528–1537.
[50] J. Rohlíček, E. Skořepová, *J. Appl. Crystallogr.* **2020**, *53*, 841–847.
[51] T. Gelbrich, T. L. Threlfall, M. B. Hursthouse, *CrystEngComm* **2012**, *14*, 5454.
[52] V. A. Blatov, A. P. Shevchenko, D. M. Proserpio, *Cryst. Growth Des.* **2014**, *14*, 3576–3586.
[53] P. R. S. Salbego, C. R. Bender, M. Hörner, N. Zanatta, C. P. Frizzo, H. G. Bonacorso, M. A. P. Martins, *ACS Omega* **2018**, *3*, 2569–2578.
[54] C. R. Groom, I. J. Bruno, M. P. Lightfoot, S. C. Ward, *Acta Crystallogr. Sect. B Struct. Sci. Cryst. Eng. Mater.* **2016**, *72*, 171–179.

A065-02-290823

Efficient crystal packing similarity algorithms for large sets of theoretically predicted structures

Nicholas Francia1, Isaac Sugden1, Lily M. Hunnisett1, Jonas Nyman1, Ghazala Sadiq1, Susan Reutzel-Edens1, Jason Cole1

The Cambridge Crystallographic Data Centre, 12 Union Road, Cambridge, CB2 1EZ, UK

nfrancia@ccdc.cam.ac.uk

Keywords: Crystal Structure Prediction, Crystal Packing Similarity

Computational Crystal Structure Prediction (CSP) methods have evolved over the past few decades from studying small rigid molecules to being able to predict polymorphs of molecules of increasing molecular size and conformational complexity, attracting the interests of pharmaceutical and functional materials companies [1]. This is reflected in the targets for the recent 7th CSP Blind Test, organised by the Cambridge Crystallographic Data Centre (CCDC), featuring highly flexible molecules, multi-component systems and challenging molecular sizes [2]. CSP methods typically consist of a first generation step that produces 10^3-10^6 structures, followed by a series of increasingly more accurate energy evaluations, with the highest-energy structures rejected at each stage [3].

Crystal structure similarity algorithms are used in CSP workflows to remove duplicates that can arise at different steps and detect matches between predicted and experimental structures. Moreover, they are employed in the analysis of the final set of plausible crystals to identify common structural trends, such as the presence of dimers as the building block of multiple structures, chains, or layers of hydrogen bonded molecules. Given the substantial number of structures (even the final output of CSP searches usually consists of thousands of structures), fast and reliable packing similarity methods are essential in this analysis.

In this work, we take advantage of the >100 000 computationally generated structures divided over 6 systems and produced by 28 research groups, in the recent 7th CSP Blind Test. Traditionally used analysis tools, such as the Crystal Packing and PXRD Similarity programs, have been employed together with the more computationally efficient Pointwise Distance Distributions method [4, 5], which allowed full comparison of the sets in a reasonable time. Apart from the identification of theoretical-experimental structure matches, this analysis explores the agreement between different structure generation and ranking methods and identifies low-energy geometries common to many group sets.

A065-03-290823

Continuous maps of molecules and atomic clouds in large databases

D. Widdowson, Y. Elkin, V. Kurlin

Computer Science department, Materials Innovation Factory, University of Liverpool, United Kingdom
vitaliy.kurlin@gmail.com

Keywords: molecular configurations, atomic clouds, rigid motion, isometry invariants, distance metric, continuous maps

Mendeleev arranged all known chemical elements into a spatial map - the periodic table parametrized by discrete coordinates - the period and group number. The periodic table was initially half-empty but effectively guided the search for new chemical elements.

The modern databases such as QM9 [1] and CSD contain millions of experimental and simulated molecules and solid crystalline materials that are not yet organized into a spatial map with unique and complete coordinates. The first question we should ask about real data is same or different [2]? Any answer to this question should provide an equivalence relation satisfying the three axioms: (1) reflexivity : any object is equivalent to itself A~A, (2) symmetry : if A~B then B~A, (3) transitivity : if A~B and B~C, then A~C. The transitivity axiom guarantees a well-defined classification when all data objects (molecules or crystals) are split into disjoint classes of equivalence. For instance, any object A generates its class [A]={B : B~A} of all objects B equivalent to A.

Though one can define many equivalences on molecules by symmetry group or chemical composition, the resulting classifications are weak in the sense that many molecules and materials (graphite and diamond) within the same class have different properties.

The strongest equivalence on molecules and crystals is rigid motion, which is a composition of translations and rotations, because any physical object preserves its properties under rigid motion in the same ambient conditions such as temperature and pressure.

Rigid shapes of molecules can be distinguished only by invariants that are descriptors preserved under rigid motion. Noisy data motivates as to require continuity under atomic displacements. Considering only atomic centers without chemical elements allows us to continuously quantify differences between close molecules with distinct compositions such as benzene and chlorobenzene.

The recent invariants invariants of periodic crystals [3,4] were adapted to fully complete and continuous invariants of clouds of m unlabeled atoms, which can be computed in a polynomial time in m [5]. These invariants distinguished all molecules in QM9 [1]. Fig. 1 compares a discrete map by chemical composition with a continuous map in the average lengths of bonds and no-bonds.

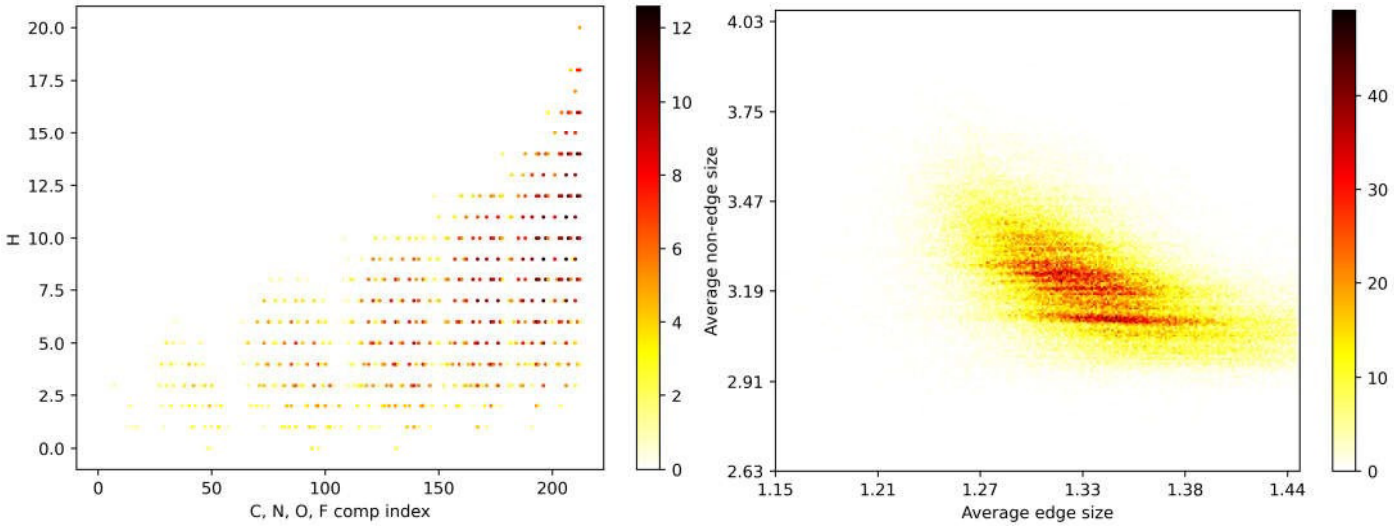

Figure 1. Visualization of 134K molecules in QM9 [1]. **Left**: x is an integer index counting elements C,N,O,F; y is the number of hydrogens; the color reflects the number of molecules with fixed (x,y). **Right**: continuous map of QM9 by (no-)bond lengths.

[55] Ramakrishnan, R., et al. Quantum chemistry structures and properties of 134 kilo molecules. Scientific data, 1(1), 1-7, 2014.
[56] Sacchi et al. Same or different - that is the question: identification of crystal forms. CrystEngComm 22 (43), 7170-7185, 2020.
[57] Anosova, O., Kurlin, V. An isometry classification of periodic point sets. Proceedings Discrete Geom. Math. Morphology, 2021, p.229-241.

[58] Widdowson, D., Kurlin, V. Resolving the data ambiguity for periodic crystals. Adv. Neural Inf. Proc. Systems, v.35 (2022). [5] Widdowson, D., Kurlin, V. Recognizing rigid patterns of unlabeled point clouds by complete and continuous isometry invariants with no false negatives and no false positives. Proceedings of Computer Vision and Pattern Recognition 2023.

A065-04-290823

Comparison of isopointal structures with the same or different composition in the Bilbao Crystallographic Server

G. de la Flor[1], E. S. Tasci[2], J. M. Perez-Mato[3], and M. I. Aroyo[4]

[1]Institute of Applied Geosciences, Karlsruhe Institute of Technology, Karlsruhe (Germany), [2]Department of Physics Engineering, Hacettepe University, Ankara (Turkey), [3]Facultad de Ciencia y Tecnología, Universidad del País Vasco UPV/EHU, Leioa, (Spain), [4]Departamento de Física, Universidad del País Vasco UPV/EHU, Leioa, (Spain), Email: gemma.delaflor@kit.edu

Keywords: isopointal structures, the program COMPSTRU, Bilbao Crystallographic Server

A quantitative comparison of similar crystal structures is often convenient to cross-check different experimental and/or theoretical structural models of the same phase coming from different sources. It is also important for the identification of different phases with the same symmetry, and it is fundamental for the still open problem of the classification of structures into (isoconfigurational) structure types.

In general, structures are described through their space-group symmetry and unit-cell parameters, along with the atomic positions in the asymmetric unit. This description depends on the coordinate system, *i.e.* on the chosen setting of the space group. However, even after fixing the setting of the space group, in most cases there are several equivalent but different descriptions of the same structure [1]. The existence of various equivalent structure descriptions makes the comparison of different structural models a non-trivial task in general. This means that the process cannot be reduced to a direct comparison of the unit cells and atomic positions of the two structures, but for one of the structures all the alternative descriptions compatible with the space-group setting have to be explored. Based on this, a procedure was developed and implemented in the program COMPSTRU [2], available in the *Bilbao Crystallographic Server* (http://www.cryst.ehu.es) [3-4]. The aim of this contribution is to present the procedure of the program COMPSTRU in detail and demonstrate by illustrative examples its applications.

This method was developed to compare two isopointal crystal structures belonging to the same space-group type (or space groups that form an enantiomorphic pair) with the same or different composition. Preliminary standardization of the structures is not necessary; the only requirement is that the structures are described with respect to the standard setting of the space group. This procedure for comparing crystal structures also supports the comparison of enantiomorphic structures with different space groups and composition. Applying the affine and Euclidean (or enhanced Euclidean) normalizers of space groups the best match of the lattice parameters and the atomic coordinates of the two structures is found. Several different quantities to evaluate the similarity between the two structures are also calculated. For example, the degree of lattice distortion (S) is quantified by the spontaneous strain while the difference between the atomic positions of the paired atoms are represented either by the maximal (d_{max}) or the averaged (d_{av}) distances of the paired atoms. As a global quantitative measure of similarity of two structures the so-called measure of similarity (Δ) [5] is also calculated.

A065-05-290823

Tilings from Square and Hexagonal Lattices

M. L. A. N. De Las Peñas* and M. Tomenes

Department of Mathematics, Ateneo de Manila University, Philippines

mdelaspenas@ateneo.edu

Keywords: (, ,) tilings, vertex-edge-tile transitive tilings, square lattice, hexagonal lattice

A 2-dimensional tiling is called an (, ,) tiling if it forms orbits of vertices, orbit of edges and orbit of tiles under the action of its symmetry group. Studies on the enumeration of (, ,) tilings for certain values of , and , include the following: (2,2,2) tilings [2]; (3,2,) tilings [1]; (, 2,) tilings and (, 3,) tilings [3]. In crystallography, families of (, ,) tilings are studied in the context of reticular chemistry as targets for design synthesis (see for instance [1])

There are currently no known results on (, ,) tilings characterized by symmetry group types and this paper aims to fill that gap in the literature. In this work, we discuss the construction of (, ,) tilings derived from tilings corresponding to square or hexagonal lattices using an approach involving subgroup relations and orbit-stabilizer conditions. Given a tiling with symmetry group we investigate how fundamental regions of subgroups of varying indices grow, and observe how symmetries on these regions affect the vertex, edge and tile transitivity properties of the tilings that may arise.

To illustrate the idea, consider the tiling ≔ [3!] with symmetry group = ⟨ , , ⟩ ≅ 6 (Figure 1(a)). To derive (, ,) tilings with symmetry group type 6 , we consider the subgroups " = 9 , , ( )"# $ ( )#("#$); ≅ 6 of of index ' (Figure 1(b)). By analyzing the number of vertices, edges and tiles in the fundamental regions, a conjecture on the types of (, ,) tilings can be drawn. For example, Figures 1(c) to 1(g) show respectively the tilings (1,1,1), (2,2,2), (3,4,3), (4,6,5) and (5,9,7) from the respective subgroups $ to (.

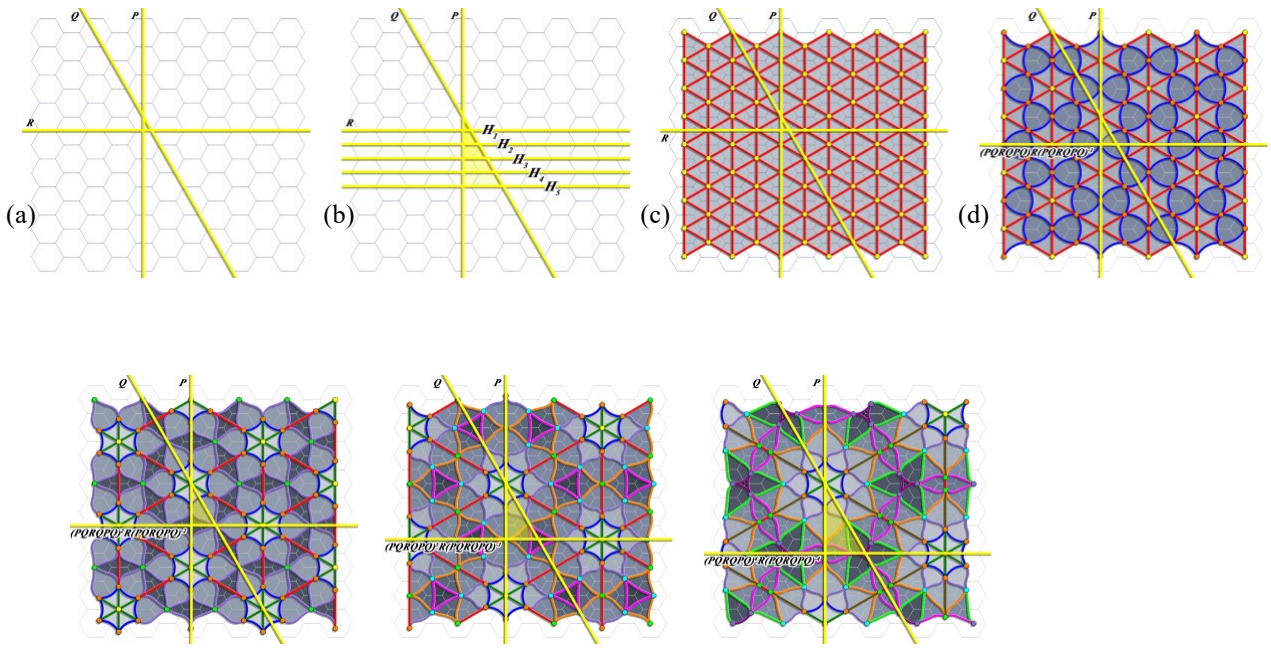

[59] Figure 1. (a) ≔ [3!] with axes of reflections , , ; (b) subgroups " with corresponding axes of reflections and fundamental regions; (c)-(g) (, ,) tilings obtained from ", = 1, … ,5.

[60]

[61] O. Delgado-Friedrichs and M. O'Keeffe, Edge-2-transitive Trinodal Polyhedra and 2-periodic Tilings, Acta Cryst. A, 73, 227-230, 2017.

[62]

[63] A. W. M. Dress and R. Scharlau, The 37 Combinatorial Types of Minimal, Non-transitive, Equivariant Tilings of the Euclidean Plane, Discrete Math., 60, 121-138, 1986.

[64]

[65] M. Tomenes, M.L.A.N. De Las Peñas, Construction of tilings of the Euclidean Plane, Hyperbolic Plane and the Sphere, (submitted to Contrib. Discrete Math.)

A065-06-290823

A continuous map of 2.6+ million 2D lattices from the Cambridge Structural Database

M. Bright, A. Cooper, V. Kurlin

Computer Science department and Materials Innovation Factory, University of Liverpool, UK, vitaliy.kurlin@gmail.com

Keywords: periodic lattices, rigid motion, isometry classification, lattice invariants, continuous metrics, chirality distances

The key problem with real data is the lack of an explicitly defined relation saying when given data objects should be considered *equivalent*. Though many equivalence relations between periodic crystals and lattices satisfy the axioms A~A, if A~B then B~A, if A~B~C then A~C, the strongest practical equivalence in crystallography is *rigid motion* composed of translations and rotations.

The slightly weaker but easier relation is an *isometry,* which maintains inter-point distances and hence also includes mirror reflections. Equivalence by symmetry groups is much weaker, producing only five Bravais classes of 2D lattices, see Fig. 1 (left).

Modulo rigid motion, the space of 2D lattices is infinitely continuous and can be bijectively mapped [1-2] to a triangle (modulo isometry and uniform scaling) or a punctured sphere (modulo rigid motion and uniform scaling), where the excluded point represents the limit case of lattices with infinitely long unit cells, see Fig. 1. These continuous maps visualize all Bravais classes as low-dimensional subspaces. For example, the equator on the sphere represents all non-generic (mirror-symmetric) lattices. The coordinates on both maps are *projected invariants* that are defined via a lattice basis but are invariant under a change of basis.

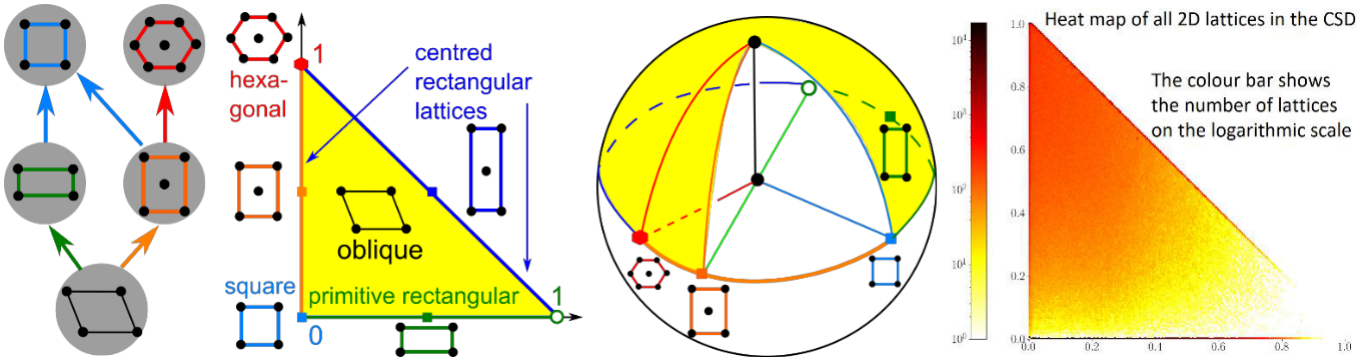

Figure 1. The tree of 5 Bravais classes on the left is extended to the continuous triangle of all 2D lattices up to isometry or the semi-spherical map. The right triangle shows the distribution of all (more than 2.6 million) 2D lattices from real CSD crystals.

The Cambridge Structural Database (CSD) has more than 870 thousand entries with well-defined 3D lattice bases a,b,c. By taking 3 pairs (a,b),(b,c),(a,c) per crystal in the CSD, we extracted more than 2.6 million 2D lattices that naturally appear in real crystals. Fig. 1 (right) shows a heat map where the color of every pixel (x,y) indicates a number of 2D lattices (on the logarithmic scale) whose projected invariant belongs to the square bin at the pixel (x,y). The darkest pixels on the horizontal edge represent tens of thousands of rectangular lattices, see also the dark top vertex of all hexagonal lattices. About 45% of all 2D lattices are oblique and fill the interior of the triangle without any gaps apart from the sparsely populated corner of lattices with long and thin cells.

The excluded point on the spherical map defines the Greenwich meridian and standard geographic coordinates (longitude and latitude). Any geographic location on Earth is now associated with a unique 2D lattice modulo rigid motion and uniform scaling. These maps allow us to find *chiral distances* that continuously measure deviations of a lattice from higher symmetry neighbors.

Similar invariant parameterizations and continuous maps are being developed for 3D lattices [3-4]. The space of arbitrary periodic point sets is also parameterized by complete isometry invariants [5]. Simpler but ultra-fast invariants distinguish all periodic crystals in the CSD and establish the *Crystal Isometry Principle* [6-7] extending Mendeleev's table to a continuous `universe' of all existing and not yet known crystals visualized as `stars', where the diamond and graphite will have different unique locations.

[1] Kurlin, V. Mathematics of 2-dimensional lattices. *Foundations of Computational Mathematics* (2023), http://arxiv.org/abs/2201.05150.
[2] Bright, M., Cooper, A., Kurlin, V. Geographic-style maps for 2-dimensional lattices. *Acta Cryst. A* (2023), http://arxiv.org/abs/2109.10885.
[3] Kurlin, V., A complete isometry classification of 3-dimensional lattices. https://arxiv.org/abs/2201.10543.
[4] Bright, M., Cooper, A., Kurlin, V. Welcome to a continuous world of 3-dimensional lattices, http://arxiv.org/abs/2109.11538.
[5] Anosova, O., Kurlin, V. An isometry classification of periodic point sets. *Proceedings Discrete Geom. Math. Morphology*, 2021, p.229-241.
[6] Widdowson, D., et al. Average Minimum Distances of periodic point sets. *MATCH Comm. Math. Comp. Chem.*, v.87(3), p.529-559, 2022.
[7] Widdowson, D., Kurlin, V. Resolving the data ambiguity for periodic crystals. *Adv. Neural Information Processing Systems*, v.35 (2022).

A086 SANS for Biomolecular Function and Cellular Organization
Room 219
1.30pm – 3.50pm

A086-01-290823

The NADase:SLO complex from Group A Streptococcus: SANS with contrast variation investigates dynamics in the new crystal structure

Wei-Jiun Tsai[1], Yi-Hsin Lai[1,18], Yong-An Shi[2,18], Michal Hammel[3], Anthony P. Duff[4], Andrew E. Whitten[4], Karyn L. Wilde[4], Chun-Ming Wu[5], Robert Knott[4], U. Ser Jeng[5,6], Chia-Yu Kang[7], Chih-Yu Hsu[8], Jian-Li Wu[9], Pei-Jane Tsai[1,8,10], Chuan Chiang-Ni[2,11,12,13], Jiunn-Jong Wu[14,15], Yee-Shin Lin[7,10], Ching-Chuan Liu[7], Toshiya Senda[16], Shuying Wang[1,7,10,17]

[1]Institute of Basic Medical Sciences, College of Medicine, National Cheng Kung University, Tainan, Taiwan. [2]Graduate Institute of Biomedical Sciences, College of Medicine, Chang Gung University, Taoyuan, Taiwan. [3]Molecular Biophysics and Integrated Bioimaging, Lawrence Berkeley National Laboratory, Berkeley, CA, USA. [4]Australian Nuclear Science and Technology Organisation, Lucas Heights, NSW, Australia. [5]National Synchrotron Radiation Research Center, Hsinchu Science Park, Hsinchu, Taiwan. [6]Department of Chemical Engineering, National Tsing Hua University, Hsinchu, Taiwan. [7]Department of Microbiology and Immunology, College of Medicine, National Cheng Kung University, Tainan, Taiwan. [8]Department of Medical Laboratory Science and Biotechnology, National Cheng Kung University, Medical College, Tainan, Taiwan. [9]Institute of Biological Chemistry, Academia Sinica, Taipei, Taiwan. [10]Center of Infectious Disease and Signaling Research, National Cheng Kung University, Tainan, Taiwan. [11]Department of Microbiology and Immunology, College of Medicine, Chang Gung University, Taoyuan, Taiwan. [12]Molecular Infectious Disease Research Center, Chang Gung Memorial Hospital, Linkou, Taiwan. [13]Department of Orthopedic Surgery, Chang Gung Memorial Hospital, Linkou, Taiwan. [14]Department of Medical Laboratory Science and Biotechnology, Asia University, Taichung, Taiwan. [15]Department of Medical Research, China Medical University Hospital, China Medical University, Taichung, Taiwan. [16]Structural Biology Research Center, Institute of Materials Structure Science, High Energy Accelerator Research Organization (KEK), Tsukuba, Ibaraki, Japan. [17]Department of Biotechnology and Bioindustry Sciences, College of Bioscience and Biotechnology, National Cheng Kung University, Tainan, Taiwan.

Anthony.Duff@ansto.gov.au

Keywords: Group A Streptococcus, X-ray crystallography, Small-angle scattering

We recently characterised the structure of the complex of NAD^+-glycohydrolase (NADase) and Streptolysin O (SLO) from Group

[66] Streptococcus (GAS), using X-ray crystallography to determine atomic coordinates, small-angle scattering to investigate solution dynamics in the complex, and mutagenesis, cell-culture and animal studies to validate key structural observations [1].

GAS is a clinically significant human pathogen renowned for its highly aggressive destruction of host tissues [2]. It exploits the cooperative activity of NADase and SLO to enhance its virulence and achieve infection [3]. However, the details of the synergistic interaction that promotes the cytotoxicity and intracellular survival of GAS have been elusive. The modelled results of the crystallography and small angle scattering, shown in Figure 1, indicate multiple modes of interaction, and low resolution characterisation of the flexible regions not present in the crystallised constructs. Structure-guided studies show an electrostatic interaction between NADase and SLO is crucial for cytotoxicity and resistance to phagocytic killing during GAS infection.

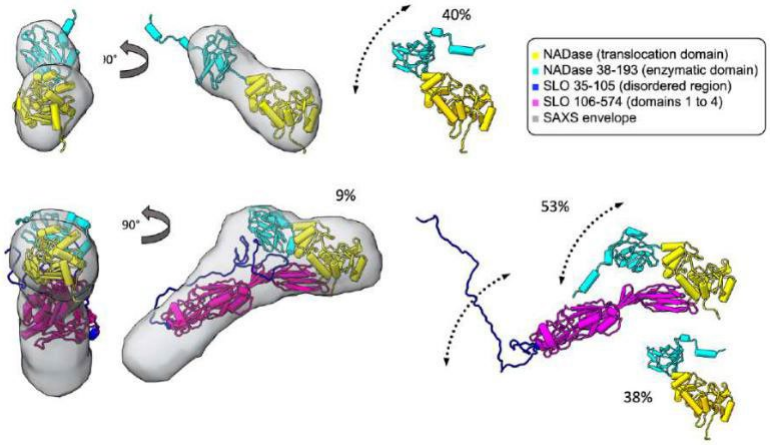

We demonstrate that the complex formation between NADase and SLO is critical for GAS virulence by a murine infection model. Our work deciphers the atomic details of the NADase-SLO interaction and pinpoints the key residues that are crucial for the coordinated actions of NADase and SLO in the pathogenesis of GAS infection. The structural information we presented may open up a prospect for the design of alternative agents aiming to disturb the NADase-SLO interaction to suppress GAS virulence.

Figure 1. Multistate models of NADase and the NADase/SLO complex

[13] Tsai, W-J. et al "Structural basis underlying the synergism of NADase and SLO during group A Streptococcus Infection" Communications Biology (2023) Jan 31;6(1):124. doi.org/10.1038/s42003-023-04502-0

[14] Walker, M. J. et al. "Disease manifestations and pathogenic mechanisms of Group A Streptococcus". Clin Microbiol Rev (2014) 27, 264-301, doi:10.1128/CMR.00101-13.

[15] Sharma, O., O'Seaghdha, M., Velarde, J. J. & Wessels, M. R. "NAD+-Glycohydrolase Promotes Intracellular Survival of Group A Streptococcus". PLoS Pathog (2016) 12, e1005468, doi:10.1371/journal.ppat.1005468

A086-02-290823

SARS CoV-2 Vaccine Particle Structure via Contrast Variation SANS, SAXS, and Cryo-EM

A. Grishaev[1], S. Krueger[1], T. Cleveland[1], A. Portnoff[2]

[1]National Institute of Standards and Technology, 9600 Gudelsky Drive Rockville MD 20850 USA

[2]Novavax Inc, 21 Firstfield Rd Gaithersburg MD 20878 USA

Email of communicating author: grishaev@umd.edu

Keywords: SARS CoV-2, Contrast variation SANS, SAXS, vaccine structure

Understanding of the action of the anti-viral vaccines is hindered by the near-complete lack of information on their structure as most of the mainstream techniques of structural biology such as X-ray crystallography, cryo-electron microscopy, or NMR face difficulties in application to these complex multi-component formulations. In addition, the rapid rate of mutation of the single-strand RNA containing viruses such as SARS CoV-2 requires use of techniques capable of fast data collection and analysis. In this study we overcome these challenges by studying the spike protein-based vaccine developed against the SARS CoV-2 virus via joint application of contrast variation SANS, SAXS, and electron microscopy. In collaboration with Novavax Inc., we have determined the structure of the vaccine material containing the ~1200 a.a. trimeric spike proteins solubilized via their transmembrane cores with the polysorbate 80 (PS80). We found that the vaccine material exhibits concentration- and formulation-dependent size differences while the overall structure of the spike protein is maintained. Our contrast variation neutron scattering results showed that the micellar cores form long (~90nm) elongated particles (Figure 1) associated with multiple copies of spike protein.

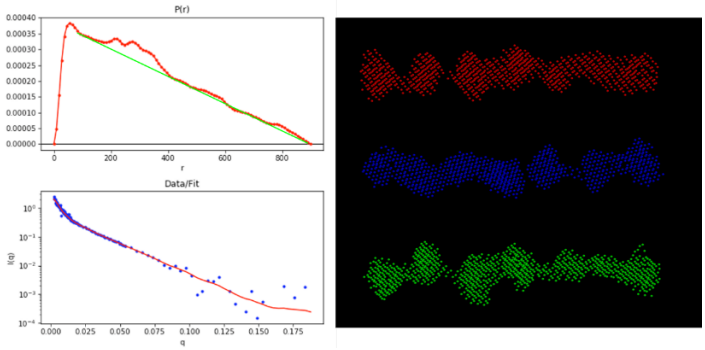

Figure 1. SANS data at 45% D_2O: P(r) distribution and data fit (left), and low-resolution reconstructions of the PS80 cores (right)

While electron microscopy data were consistent with formation of close contacts between the trimeric spike protein cores and overall compact particle dimensions not exceeding ca. 40nm, our contrast variation SANS and SAXS data disagreed, indicating that these effects were brought by the cryogenic conditions at which electron microscopy data were collected.

Multi-parametric optimization of the protein/PS80 structural models for the best fit against the scattering data was carried out. Obtaining satisfactory data fit required introduction of irregularities in the cross-section parameters and the persistence length of the PS80, as well as accounting for the kinks in the helical stems connecting the cores of the spike protein trimers to the PS80, as well as the presence of multiple conformations of the spike protein with partially open receptor binding domains (Figure 2). Our study provides a detailed view of the native-state vaccine particles at an unprecedented level of detail, furthering better and more timely understanding of the mechanism of the vaccine's action.

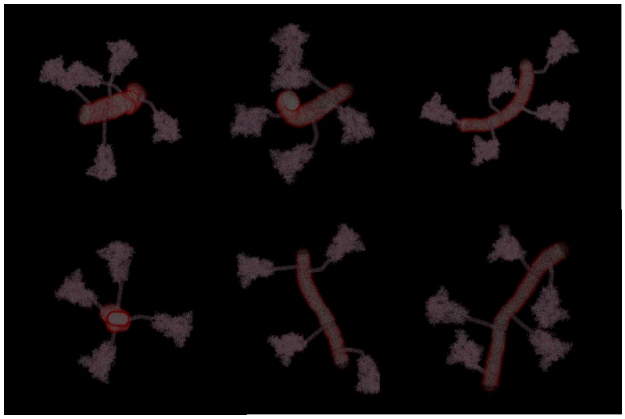

Figure 2. Examples of the SARS CoV-2 spike protein/PS80 assemblies best-fitted to the scattering data

A086-03-290823

p14^{Arf} Disrupts Ribosome Biogenesis and Function to Inhibit Cell Proliferation

Gibbs. E[1], Miao. Q[1], Ferrolino. M[1], Stanley. C[2], Heller. W[3], Hassan. A[4], Kümmerle. R[4], Perrone. B[4], Kriwacki. R[1]

1) Structural Biology Department, St Jude Children's Research Hospital, Memphis, TN, USA, 2) Computational Sciences and Engineering Division, Oak Ridge National Laboratory, Oak Ridge, TN, USA, 3) Neutron Scattering Division, Oak Ridge National Laboratory, Oak Ridge, TN, USA, 4) Bruker Switzerland AG, Industriestrasse 26, Fällanden, Switzerland
Richard.Kriwacki@stjude.org

Keywords: p14^{Arf}, NPM1, biomolecular condensates, structural biology, cancer biology

ARF (Alternative Reading Frame; p14^{Arf} in human, p19^{Arf} in mouse) is an essential tumor suppressor whose gene is commonly deleted or silenced in human cancers [1]. Both human and mouse ARF are localized to the nucleolus through interactions with nucleophosmin (NPM1), where they regulate ribosome biogenesis. p14^{Arf} and NPM1 associate with nucleolar 60S pre-ribosomal particles [2]. Furthermore, deletion of p19^{Arf} aberrantly increases ribosome biogenesis, protein synthesis and nucleolar size, which are three phenotypic hallmarks of cancer cells [3]. Expression of p14^{Arf} is upregulated by oncogenes (e.g., MYC), which results in cell cycle arrest through p53-dependent and p53-independent pathways [1]. However, the molecular mechanisms underlying p14^{Arf}'s p53-independent nucleolar tumor suppressor function is poorly understood.

To understand the molecular basis of p14^{Arf}'s tumor suppressor function in the nucleolus, we extensively characterized the p14^{Arf} -NPM1 interaction *in vitro* and in live cells. We found that NPM1 and p14^{Arf} undergo phase transitions *in vitro*, forming arrested condensates that immobilize both proteins [4]. To understand the molecular basis of the p14^{Arf}-dependent immobilization of NPM1 within condensates, we characterized the phase separated p14^{Arf}/NPM1 complex using an integrated structural biology approach encompassing contrast variation small-angle neutron scattering (CV-SANS) and nuclear magnetic resonance (NMR) spectroscopy. CV-SANS showed that the p14^{Arf} /NPM1 condensate is perforated with meso-scale (10-100 nm length scale) pores. Strikingly, this structural organization is enforced by p14^{Arf}. NMR showed that p14^{Arf} assembles a rigid scaffold within condensates (on the 1-10 nm length scale) through self-association, mediated by hydrophobic motifs within an N-terminal α-helix and β-sheets, thus restricting NPM1 mobility and causing liquid-like condensates to become semi-solid.

Using live cell imaging we found that p14^{Arf} can restrain NPM1 diffusion within nucleoli in a hydrophobic motif and concentration dependent manner, causing nucleolar amyloidogenesis and rRNA processing defects at high p14^{Arf} levels. Strikingly, p14^{Arf} expression resulted in the cytoplasmic accumulation of 80S ribosomes and a concomitant reduction in the abundance of polysomes, thus inhibiting protein synthesis and cell proliferation. Collectively, our results demonstrate that p14^{Arf} acts as a modulator of ribosome biogenesis and function, thus inhibiting cell proliferation.

Our findings have broad relevance as they demonstrate that p14^{Arf} exerts its tumor suppressive effects in part by altering the fluid properties of nucleoli, ribosome biogenesis, and protein synthesis. Further, our studies of biomolecular condensates highlight the power of SANS to probe long-range ordering of biomacromolecules within condensates, which represents a new and exciting frontier for the field.

[1] Sherr, C.J. (2006). Nature Reviews Cancer **6**, 663–673.

[2] Rizos, H., McKenzie, H.A., Ayub, A.L., Woodruff, S., Becker, T.M., Scurr, L.L., Stahl, J., and Kefford, R.F. (2006). Journal of Biological Chemistry **281**, 38080–38088.

[3] Apicelli, A.J., Maggi, L.B., Hirbe, A.C., Miceli, A.P., Olanich, M.E., Schulte-Winkeler, C.L., Saporita, A.J., Kuchenreuther, M., Sanchez, J., Weilbaecher, K., et al. (2008). Molecular and Cellular Biology **28**, 1068–1080.

[4] Gibbs, E., Perrone, B., Hassan, A., Kümmerle, R., and Kriwacki, R. (2020). Journal of Magnetic Resonance **310**.

A086-06-290823

Small-angle neutron scattering of a pentameric ligand-gated ion channel reveals a dynamic regulatory domain

M. Lycksell[1], U. Rovšnik[1], A. Hanke[1,2], A. Martel[3], R.J. Howard[1], E. Lindahl[1,4]

[1]*Biochemistry and Biophysics, Stockholm University, Stockholm, Sweden,*

[2]*Pharmacy and Molecular Biotechnology, Heidelberg University, Heidelberg, Germany,*

[3]*Institut Laue-Langevin, Grenoble, France,*

[4]*Applied Physics, KTH Royal Institute of Technology, Stockholm, Sweden*

marie.lycksell@gmail.com

Keywords: small-angle neutron scattering, membrane proteins, molecular dynamics simulations

Pentameric ligand-gated ion channels (pLGICs) perform electrochemical signal transduction in organisms ranging from bacteria to humans [1]. Among the prokaryotic pLGICs there is an architectural diversity involving N-terminal domains (NTDs) not found for the eukaryotic relatives, exemplified by the calcium-sensitive channel DeCLIC [2]. Here [3], we characterized DeCLIC structure using cryogenic electron microscopy (cryo-EM), small-angle neutron scattering (SANS), and molecular dynamics (MD) simulations. In both the presence and absence of calcium, cryo-EM reconstructions were similar to a previously reported calcium-bound X-ray structure. The NTD exhibited lower local resolution than the canonical unit, consistent with this domain being relatively mobile. The small-angle scattering profile revealed a feature not explained by the available structures, indicating that further conformational diversity is available to DeCLIC. MD simulations indicated that this profile is largely attributable to rigid-body motions of the NTD relative to the protein core, including conformations similar to those in experimental structures, as well as more expanded and asymmetric conformations. Using these expanded conformations, it was possible to fit the previously unexplained SANS feature, indicating the presence of such conformations under solution conditions. This work reveals the range of motion available to the DeCLIC NTD, expanding the conformational landscape of the pLGIC family; and demonstrates the power of combining low-resolution, high-resolution, and simulations data in the study of protein structure.

A095 Dynamic Aspects of Crystals
Room 213
1.30pm – 3.50pm

A095-01-290823

On the accuracy of DFT methods for supporting the discovery of mechanically compliant molecular crystals using predicted face-dependent Young's moduli

S. Mohamed, M. Almehairbi, A. Irfan, Z. Saeed, A. M. Abdelhaq, T. Alkhidir

Green Chemistry & Materials Modelling Laboratory, Department of Chemistry, Khalifa University of Science and Technology, Abu Dhabi, United Arab Emirates

sharmarke.mohamed@ku.ac.ae

Keywords: Young's Modulus, DFT, Mechanical Properties

The mechanical properties of molecular crystals influence a range of bulk properties. For example, the tabletting behaviour of drugs are affected by the mechanical properties of the active ingredient. The traditional view of molecular crystals as brittle objects is challenged by recent observations of exceptional elastic bending, plastic deformation, shape memory effects, thermosalience and mechanosalience. The mechanism by which each of these effects takes place is a topic of ongoing debate, although recent microfocus X-ray diffraction work has shed some light on the mechanism of bending in crystals of $Cu(acac)_2$ [1].

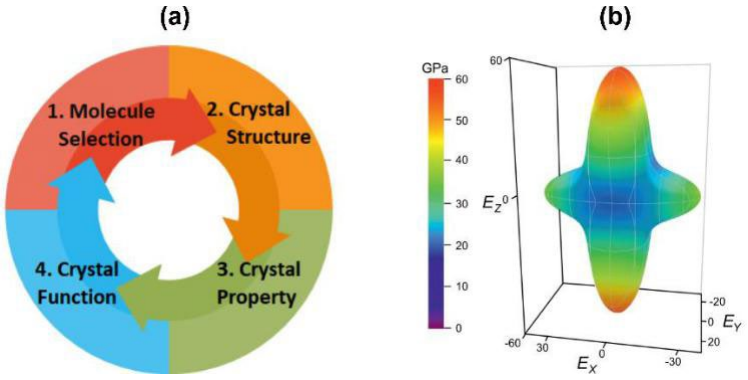

Figure 1. (a) Flowchart for the structure-property-function framework for the discovery of mechanically compliant molecular crystals. (b) Computed Young's Modulus surface projected on the *xz* plane for the amino acid L-threonine [2].

Despite the increasing community-wide interest in the mechanical effects of molecular crystals, most of the interesting examples of elastic/plastic deformation and other phenomena reported in the literature are based on empirical observations, often as a result of serendipity. There is therefore a paucity of data on whether any of these mechanical effects can actually be discovered *a priori* using rigorous theoretical methods. In this work, we disclose the results from the largest benchmarking study focussed on assessing whether periodic density functional theory (DFT) methods can be used to predict the observed second-order elastic constants and by extension the Young's moduli of molecular crystals. We do this by using a structure-property-function framework that is both automated and entirely *ab initio* (Fig. 1). To do this, we have developed a new code that directly interfaces with VASP and translates the DFT strain-energy data into face-dependent Young's moduli for candidate structures. We compare the results from our code with a range of face-dependent Young's moduli of molecular crystals reported in the literature, all derived from nanoindentation measurements. Our results indicate that in general static dispersion-corrected DFT methods are accurate to within ± 3 GPa for crystals such as amino acids that comprise very strong electrostatic intermolecular interactions, suggesting promise for the *ab initio* discovery of stiff and ultra-stiff molecular crystals. For crystals comprising weak dispersive intermolecular interactions, the accuracy of the predictions is generally poorer. Our work suggests that for strongly bound crystals, DFT methods can be a reliable complement to experimental screens and can support experimental efforts for the discovery of crystals that may be used in applications (e.g., waveguiding) where the high stiffness is an important asset [2]. The calculated average Young's moduli of crystals show significant variations to the experimental face-dependent stiffness from nanoindentation in some cases. As a consequence, caution must be exercised in using computationally-derived average stiffness constants to infer the nanoindentation face-dependent stiffness of molecular crystals.

[67] Worthy, A., Grosjean, A., Pfrunder, M. C., Xu, Y., Yan, C., Edwards, G., Clegg, J. K. & McMurtrie, J. C. (2018). *Nature Chemistry* **10**, 65-69.

[68] Karothu, D. P., Dushaq, G., Ahmed, E., Catalano, L., Polavaram, S., Ferreira, R., Li, L., Mohamed, S., Rasras, M. & Naumov, P. (2021). *Nature Communications* **12**, 1326.

A095-02-290823

Nanomechanics in barocaloric plastic crystals: repurposing for SHG application

A. Mondal[1], S. Ahmad[1], S. Roy[2], B. Pal[2], C. M. Reddy[1]

[1]Department of Chemical Sciences, Indian Institute of Science Education and Research Kolkata, 741246, India, [2]Department of Physical Sciences, Indian Institute of Science Education and Research Kolkata, 741246, India sa19rs024@iiserkol.ac.in; cmreddy@iiserkol.ac.in

Keywords: Plastic crystals, Second harmonic generation, Barocalorics.

Plastic crystals (PCs) [1, 2] or orientationally disordered crystals show large isothermal entropy changes during phase order-disorder transitions through single or multiple phases, hence have attracted great attention for applications as solid state coolants. Recently, some excellent PCs, namely, NPG (neopentylglycol), PE (pentaerythritol), PG (pentaglycerin), TRIS ((tris(hydroxymethyl)amino-methane), NMP (2-nitro-2-methyl-1,3-propanediol), etc, have been reported to show colossal baroclaoric effects [3, 4]. In this systematic study, we provide deep insights for the design of efficient barocalorics, by examining their barocaloric performances, qualitative and quantitative mechanical properties, energetics obtained by energy frameworks calculations, from crystal engineering point of view. This not only allowed us to establish a structure-property relationship, but also to repurpose them for non-linear optical property or SHG switching [5]. Our study will certainly provide new insights into the ongoing research in understanding the PCs especially in terms of their barocaloric and nonlinear optical applications, and allow designing of novel PCs with new properties with greater promise, beyond their original scope.

We explain how the mechanical properties of the aforementioned crystals correlate well with their phase transition temperatures and interaction energies. These crystals could mechanically be thinned upon the transition from rigid to a plastic crystalline state (thinning of TRIS and NMP, at 140 °C and 85 °C, respectively, are shown in the Fig. 1c). PE, TRIS, NMP and PG crystalize in non-centrosymmetric space groups, and all of them show significant SHG intensity. TRIS with *Pna*2$_1$ space group shows the attenuation in the SHG intensity upon phase transition nearly at 130 °C to the plastic crystalline phase, which recovers upon cooling to 60 °C for the thin film (Fig. 1d).

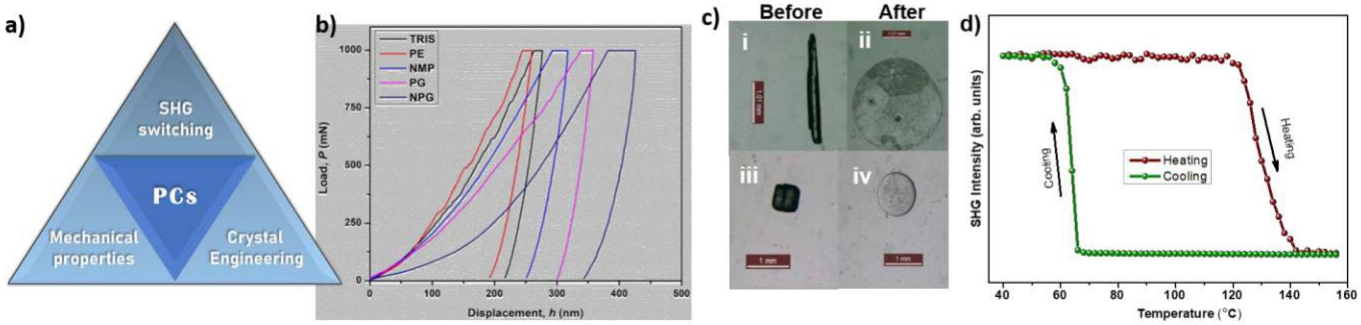

Figure 1. a) Schematic representation of the scope of the work, b) *P-h* curves at 1mN load, c) before (i & iii) and after (ii & iv) mechanical thinning of TRIS and NMP above transition temperatures, d) SHG switching upon phase transition in TRIS.

[69] Das, S., Reddy. C. M. et. al. (2022). *Angew. Chem. Int. Ed*., **61**, 1.

[70] Mondal. A., Reddy. C. M. et. al. (2022). *Angew. Chem. Int. Ed*., **59**, 10971

[71] Li, B. et. al. (2019). *Nature*, **567**, 506.

[72] Tamarit, J. L. et. al. (2019). *Nat. Commun.*, **10**, 1803.

[73] Luo, J. et. al. (2015). *J. Am. Chem. Soc*., **137**, 15660.

We thank DST for Swarnajayanti fellowship (DST/SJF/CSA-02/2014-15) to Prof. Chilla Malla Reddy. Fellowship for SA (CSIR-SRF, File No. 09/921(0264)/2019-EMR-I) and AM (IISER-KOLKATA) are acknowledged.

A095-04-290823

Interplay of short-range orientational order and lattice dynamics in negative thermal expansion material $Cd(CN)_2$

Johnathan Bulled1, Ross Stewart2, Helen Walker2, Ben Slater3, Andrew Goodwin1

[1]Inorganic Chemistry Laboratory, University of Oxford, South Parks Road, Oxford, U.K, OX1 3QR, [2]ISIS Neutron and Muon Source, STFC Rutherford Appleton Laboratory, Chilton, Didcot, U.K., [3]Department of Chemistry, University College London, London, U.K., OX11 0QX,

johnathan.bulled@balliol.ox.ac.uk

Keywords: negative thermal expansion, inelastic neutron scattering, lattice dynamics, short-range order, mode softening

Cubic cadmium(II) cyanide is amongst the most important isotropic negative thermal expansion (NTE) materials [1, 2], with behaviour more than twice as extreme as that of better known systems such as ZrW_2O_8 [3]. The NTE of isostructural $Zn(CN)_2$ is understood to stem from low-energy phonon modes [4]. Recent work shows $Cd(CN)_2$ to be interesting for another reason: the cyanide dipole acts as an orientational pseudospins on the frustrated pyrochlore lattice [Fig 1(a)], with short range order evolving over a range of temperatures above the eventual antiferroelectric phase transition at 130 K [5]. The reorientation dynamics are slow but thermally accessible above the phase transition [5]. We aim to understand the interplay between these slow (ms) dynamics which govern orientational short-range order and fast (fs) lattice dynamics which seemingly lead to NTE.

A combination of inelastic neutron scattering (INS), molecular dynamics (MD) and density functional theory (DFT) simulations, are used to probe the sensitivity of a low energy phonon to this correlated orientational order. INS–measured on a polycrystalline sample of isotopically enriched $^{114}Cd(CN)_2$–shows a complex evolution as a function of pressure and temperature, seemingly dependant on the short-range order of cyanide orientations. We use DFT-parameterised MD simulations to test this theory and understand its implications role in NTE.

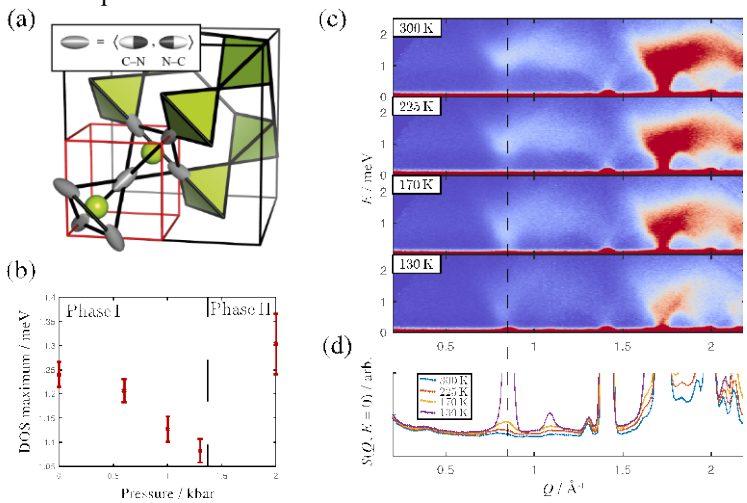

Figure 1. One of two interpenetrating sublattices in the cubic $Cd(CN)_2$ structure: Cd tetrahedra are bridged by cyanide dipoles, which are disordered over two orientations at high temperature. (b) The pressure dependence of the maximum in the neutron-DOS shows mode softening with increasing pressure up to a phase transition. (c) *S(Q,E)* measured by INS at four temperatures on polycrystalline $^{114}Cd(CN)_2$. Complex mode softening occurs in the high temperature phase on cooling, particularly at ~0.8 $Å^{-1}$. (d) The corresponding elastic scattering shows a diffuse maximum at this momentum transfer in the high temperature phase, which evolves as a function of temperature, condensing into a Bragg peak at 130 K.

[1] Goodwin, A. L. & Kepert, C. J., (2005). *Phys. Rev. B* **71**, 140301.

[2] Coates, C. S. and Goodwin, A. L., (2019). *Mater. Horiz.* **6**, 21.

[3] Mary, T. A., Evans, J. S. O., Vogt, T., & Sleight, A. W., (1996). *Science* **272**, 90.

[4] Zwanziger, J. W., (2007). *Phys. Rev. B* **76**, 052102.

[5] Coates, C. S., Baise, M., Schmutzler, A., Simonov, A., Makepeace, J. W., Seel, A. G., Smith, R. I., Playford, H. Y., Keen, D. A., Siegel, R., Senker, J., Slater, B. & Goodwin, A. L., (2021). *Nat. Commun.* **12**, 2272.

A095-05-290823

High-speed and high-efficient actuation of molecular crystals by photothermally induced natural vibration

S. Hasebe1, Y. Hagiwara1, T. Asahi1,2, H. Koshima2

[1]*Graduate School of Advanced Science and Engineering, Waseda University, 3-4-1 Okubo, Shinjuku-ku, Tokyo 169-8555, Japan*

[2]*Research Organization for Nano and Life Innovation, Waseda University, 513 Wasedatsurumaki-cho, Shinjuku-ku, Tokyo 162-0041, Japan*

jenepaletemps@suou.waseda.jp

Crystal actuators, Photothermal effect, Natural vibration, Salicylideneaniline

Recent discovery of molecular crystals that deform flexibly without deterioration upon light irradiation shake the common perception of molecular crystals as brittle, inflexible, and unresponsive to external stimuli. These light-driven mechanical crystals (*photomechanical crystals*) have attracted much attention in both basic research and applications to light-fueled actuators and soft robotics [1]. We have developed many light-driven mechanical crystals over the past decade, mainly based on photoisomerization [2,3]. Recently, we reported high-speed (~25 Hz) bending induced by the photothermal effect [4]. The photothermal effect is a phenomenon by which thermal energy (heat) is produced by nonradiative deactivation of the photoexcited state during a photophysical process We then elucidated the bending mechanism that a nonsteady temperature gradient in the thickness direction triggers photothermally driven crystal actuation, ultimately achieving 500 Hz high-speed bending [5]. Very recently, we discovered high-speed bending of an enol-**1** crystal (Figure 1a) by natural vibration induced by the photothermal effect.

When the enol-**1** crystal was irradiated with ultraviolet (UV) light irradiation for 0.1 s (Figure 1b), the crystal underwent fast and small bending due to natural vibration of 773 Hz, which was accompanied by the large photothermal bending (Figure 1c). The crystal was then exposed to a pulsed UV light of the same frequency as its natural frequency; the bend angle was greatly amplified to 7.2° by resonance, achieving high-speed (773 Hz) as well as the high energy conversion efficiency of 0.22% (Figure 1d). Any light-absorbing crystal can be actuated by photothermally induced and resonated natural vibration, which gives a versatile actuation methodology.

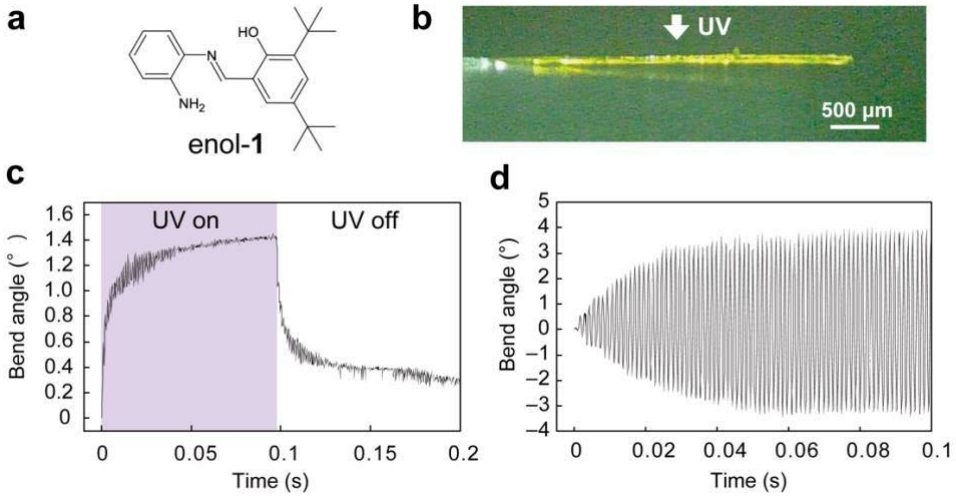

Figure 1. (a) Molecular structure of enol-**1**. (b) Photograph of a plate-like enol-**1** crystal viewed from the side face. (c) Large photothermally driven bending and small, repetitive natural vibration upon UV irradiation for 0.1 s. (d) Amplification of 773-Hz natural vibration by resonance upon pulsed UV irradiation.

[1] *Mechanically Responsive Materials for Soft Robotics*, edited by H. Koshima (2020), Wiley-VCH, Weinheim.

[2] Koshima, H., Ojima, N. & Uchimoto, H. (2009). *J. Am. Chem. Soc.,* **131**, 6890–6891.

[3] Koshima, H., Takechi, K., Uchimoto, H., Shiro, M. & Hashizume, D. (2011). *Chem. Commun.,* **47**, 11423–11425.

[4] Hagiwara, Y., Taniguchi, T., Asahi, T. & Koshima, H. (2020). *J. Mater. Chem. C,* **8**, 4874–4884.

[5] Hasebe, S., Hagiwara, Y., Komiya, J., Ryu, M., Fujisawa, H., Morikawa, J., Katayama, T., Yamanaka, D., Furube, A., Sato, H., Asahi, T. & Koshima, H. (2021). *J. Am. Chem. Soc.,* **143**, 8866–8877.

A105 Stimuli-responsive Crystals
Room 212
1.30pm – 3.50pm

A105-01-290823

Effect of substrate on vapor phase crystal growth of diarylethene and photomechanical behaviors of rod crystals

M. Isobe1, D. Kitagawa1,2, S. Kobatake1,2

Graduate School of Engineering, Osaka Metropolitan University, 3-3-138 Sugimoto, Sumiyoshi-ku, Osaka 558-8585, Japan, Graduate School of Engineering, Osaka City University, 3-3-138 Sugimoto, Sumiyoshi-ku, Osaka 558-8585, Japan so22063c@st.omu.ac.jp

Keywords: Diarylethene, Photomechanical effect, Vapor phase crystal growth

Diarylethene is the photochromic compound, which undergoes reversible photoisomerization upon alternating irradiation with UV and Vis. lights, showing absorption spectral change. Photomechanical effects are obtained from photo-induced shape change on solid-state materials and the photochromic crystals are the attractive candidate for photoactuators because of the reversible response without any direct contact. It has been reported that the crystals of some diarylethene derivatives can exhibit diverse photomechanical behaviors such as bending[1] and twisting[2], due to geometric changes in molecular structure in their crystalline phases. These photomechanical properties require controlling by preparing separately crystals having the different morphology, shape, and size. Therefore, we focused on the effect of substrates on their morphology, shape, size of diarylethene rodlike crystals in the vapor phase crystal growth process[3].

When sublimating **1a** (Fig. 1) to the ice-cooled glass substrates with the different surface wettability by heating its powder crystals at 100°C, rodlike crystals having the different crystal morphology, classified into the hollow and feather-like crystals, are generated densely on the substrates with the hydrophilic and hydrophobic surfaces, respectively (Fig. 2a,b,c). According to miller indices of the rodlike crystals determined from XRD measurements, they have the same molecular arrangement and the different crystal growth direction (Fig. 2d,e). The XRD measurements for generated crystals on each of the substrate surface in the sublimation process indicate that on the hydrophilic surface, crystal faces of the (011) plane are attached on it in the early stage of sublimation and those of the $(01\bar{1})$ plane increase while crystal faces of the $(01\bar{1})$ plane are firstly deposited on the hydrophobic surface and then those of the (011) plane spreads on it (Fig. 3). In addition, the microscopic observation for each of the substrate surface after 2h of sublimation shows that the polycrystalline thin film and dendrite crystals are formed on the hydrophilic and hydrophobic surface, respectively. As the results, it is considered that rodlike crystals having each crystal morphology are produced on surfaces of these thin films through heterojunction between $(01\bar{7}4)$ and (011) planes. Finally, under irradiation with UV light to the side of the hollow crystals, they bend toward the light source. In case of the feather-like crystals, however, they bend against the light source (Fig. 4).

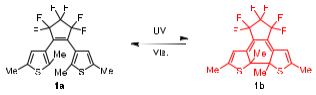

Figure 1. Photochromic reaction of **1a**.

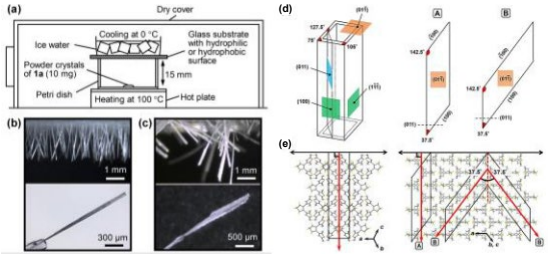

Figure 2. (a) Setup of the sublimation method, (b,c) crystal morphologies of rodlike crystals grown on glass substrates with (b) hydrophilic and (c) hydrophobic surfaces, respectively, (d) crystal shapes identified with miller indices for each rodlike crystal of **1a** (triclinic, $P\bar{1}$, a = 8.833 Å, b = 11.178 Å, c = 11.431 Å, α = 100.588°, β = 112.708°, γ = 113.218°)[4] and (e) packing diagrams of **1a**. The black and red arrows in (e) indicate glass surface and crystal growth directions from the glass surface, respectively.

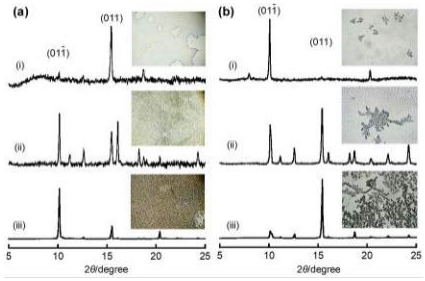

Figure 3. XRD patterns and photographs for sublimation (a) on the hydrophilic substrate surface by heating for (i) 3 min at 80 °C, (ii) 10 min at 100 °C, and (iii) 120 min at 100 °C and (b) on the hydrophobic substrate surface by heating for (i) 2 min heating at 65 °C, (ii) 5 min heating at 95 °C, and (iii) 120 min heating at 100 °C.

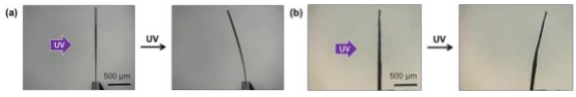

Figure 4. Photoinduced bending behaviors of (a) the hollow crystal and (b) the feather-like crystal under irradiation with UV light to the left side of each rodlike crystal.

[10] Kitagawa, D., Kawasaki, K., Tanaka, R., Kobatake, S. (2017). *Chem. Mater.* **29**, 7524.
[11] Kitagawa, D., Tsujioka, H., Tong, F., Dong, X., Bardeen, C. J., Kobatake, S. (2018). *J. Am. Chem. Soc.* **140**, 4208.
[12] Isobe, M., Kitagawa, D., Kobatake, S. (2022). *Cryst. Growth Des.* **22**, 5489.
[13] Kobatake, S., Yamada, T., Uchida, K., Kato, N., Irie, M. (1999). *J. Am. Chem. Soc.* **121**, 2380.

A105-02-290823

Guest disorder as a way to achieve multistep spin crossover in metal–organic frameworks

H. J. Windsor[a*] and C. J. Kepert[a]

School of Chemistry, The University of Sydney, New South Wales 2006, Australia
hunter.windsor@sydney.edu.au

Keywords: spin crossover, disorder, supramolecular chemistry

Designing new materials is challenging from both a crystal engineering and functional properties perspective. The principles of crystal engineering which enable the *a priori* design of new crystal structures can equally be applied to metal–organic frameworks (MOFs) which, due to their modular construction, are excellent candidates for producing crystalline architectures that exist over a wide topological space. Thus, these principles can be exploited to achieve MOF topologies that are predisposed towards exhibiting desired properties.

We have been interested in MOFs that exhibit spin crossover (SCO), which is an electronic switching phenomenon associated with the thermally-induced intraionic shift between the paramagnetic high spin and diamagnetic low spin states of iron(II). The SCO response in these systems can thus be tuned by incorporation of supramolecular interactions that lead to cooperative or anti-cooperative communication pathways between the iron(II) nodes. Through this switching modality, the physicochemical differences between the iron(II) high spin and low spin states can be exploited to achieve sensing and data storage applications [1].

Incorporating guest molecules within a porous host lattice offers another way to modulate the resulting SCO behaviours. Accordingly, we synthesised and characterised the 3D Hofmann-like MOF $[Fe^{II}(dpbtz)(Au^{I}(CN)_2)_2]\cdot 0.5$chrysene (**1**) (dpbtz = 4,7-di(4-pyridyl)-2,1,3-benzothiadiazole) by an array of structural and physical techniques. Encapsulation of the polycyclic aromatic hydrocarbon (PAH) chrysene within **1** results in a host–guest arrangement where the host lattice itself is periodic yet the arrangement of chrysene guest molecules is aperiodic. Framework **1** displays an unusual example of two-step SCO which we ascribe to a guest disorder effect in the chrysenes causing local site inequivalencies of the iron(II) nodes in the host lattice [2]. The principle of exploiting aperiodic moieties in an underlying periodic lattice is known to occur for example in DNA when comparing the structure of the double helix to the base-pair sequence itself. Such structures offer higher density information storage capacities due to the absence of a domain-size constraint that limits the amount of information that is accessible within each crystalline domain. Extending these ideas into the realm of materials chemistry is a challenging yet rewarding task for producing complex materials, one that we hope has been advanced by our work.

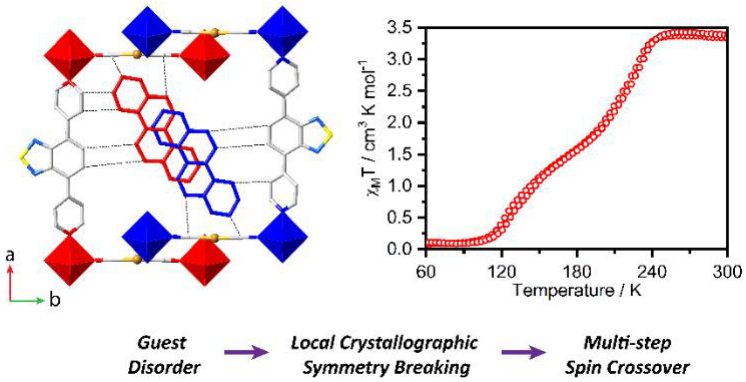

Figure 1. A chrysene-loaded spin crossover material exhibits a two-step thermally-activated spin transition driven by guest-induced local symmetry breaking.

[17] Gütlich, P., Garcia, Y. & Goodwin, H. A. (2000). *Chem. Soc. Rev.*, **29**, 419.
[18] **Windsor, H. J.**, Lewis, W., Neville, S. M., Duyker, S. G., D'Alessandro, D. M. & Kepert, C. J. (2022). *Chem. Commun.*, **58**, 1312

This work was supported by the Fellowship and Discovery Project funding from the Australian Research Council (D. M. D. – FT170100283 and S. M. N. and C. J. K. – DP200100305/DP170102980). The authors acknowledge the facilities and the scientific and technical assistance of Sydney Analytical, a core research facility at The University of Sydney.

A105-03-290823

Mechanically Induced Structural Transformations in Luminescent Gold Complexes

Hajime Ito

1Division of Applied Chemistry, Faculty of Engineering, Hokkaido University, Sapporo, Hokkaido 060-8628, Japan;

[2]Institute for Chemical Reaction Design and Discovery (WPI-ICReDD), Hokkaido University, Sapporo, Hokkaido 001-0021, Japan.

hajito@eng.hokudai.ac.jp

Keywords: Keyword 1, Keyword 2, Keyword 3

In recent years, the mechanical properties of organic and organometallic compounds and their associated optical property changes have become an important topic among researchers. In particular, since 2008, our research group has focused on the mechanical behavior of Au(I)–isocyanide complexes and the associated changes in their luminescent properties. As a result, we have discovered several gold isocyanide complex crystals with multiple polymorphs and luminescent mechanochromism. We have reported phenomena such as single-crystal-to-single-crystal phase transitions due to mechanical stimuli or crystal contacts, reversible single-crystal-to-single-crystal phase transitions induced by mechanical stimuli and solvents, and mechanochromism with near-infrared emission. In addition, these gold complexes have found ferroelasticity with thermal phase transition. Such a variety of crystal structures and accompanying changes in luminescence color are due to the switching of aurophilic interactions, CH-π interactions, and other interactions in the crystal structure. This presentation will discuss their semi-rational design attempts.

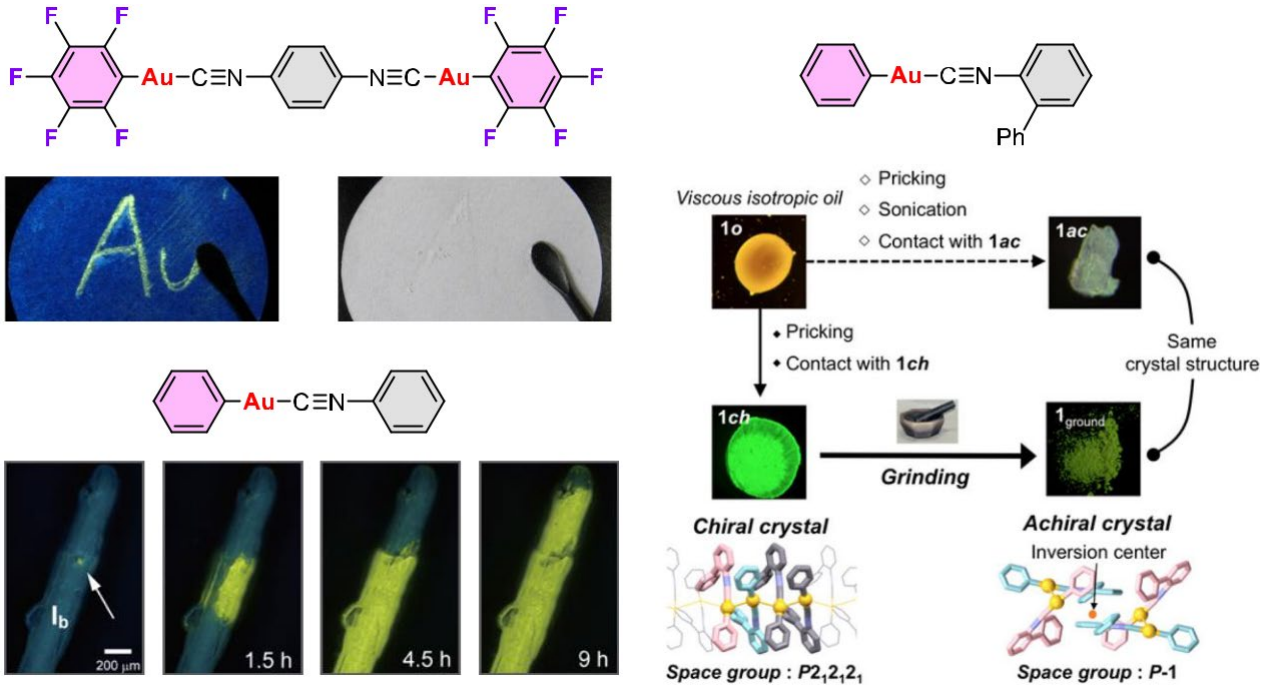

Figure 1. Mechanically Induced Structural and Optical Property Changes of Au(I) Complexes

[75] Ito, H.; Saito, T.; Oshima, N.; Kitamura, N.; Ishizaka, S.; Hinatsu, Y.; Wakeshima, M.; Kato, M.; Tsuge, K.; Sawamura, M. *J. Am. Chem. Soc.* **2008**, *130*, 10044–10045.
[76] Ito, H.; Muromoto, M.; Kurenuma, S.; Ishizaka, S.; Kitamura, N.; Sato, H.; Seki, T. *Nature Commun.* **2013**, *4,* 2009.
[77] Seki, T.; Takamatsu, Y; Ito, H. *J. Am. Chem. Soc.* **2016**, *138*, 6252–6260.
[78] Seki, T.; Tokodai, N.; Omagari, S.; Nakanishi, T. ; Hasegawa, Y.; Iwasa, T.; Taketsugu, T.; Ito, H. *J. Am. Chem. Soc.* **2017**, *139*, 6514–6517.
[79] Jin, M.; Sumitani, T.; Sato, H.; Seki, T.; Ito, H. *J. Am. Chem. Soc.* **2018**, *140*, 2875–2879.
[80] Jin, M.; Chung, T. J.; Seki, T.; Ito, H.; Garcia-Garibay, M. A. *J. Am. Chem. Soc.* **2017**, *139*, 18115–18121.
[81] Jin, M.; Yamamoto, S.; Seki, T.; Ito, H.; Garcia-Garibay, M. A. *Angew. Chem. Int. Ed.* **2019**, *58*, 18003–18121.

A105-04-290823

Metal-like ductility and malleability in organic plastic crystals

A. Mondal, B. Bhattacharya, S. Das, S. Bhunia, R. Chowdhury, S. Dey, C. M. Reddy*

Department of Chemical Sciences, Indian Institute of Science Education and Research (IISER) Kolkata, Mohanpur Campus, Mohanpur, Nadia-741246, West Bengal, India.

Email: cmreddy@iiserkol.ac.in (CMR)

Keywords: Organic Plastic Crystals, Ductility & Malleability, Adaptable Electronics

Ductility, which is a common phenomenon in many metals, is difficult to achieve in molecular crystals. Organic crystals have been recently shown to bend plastically on one or two face specific directions, but they fracture when stressed in any other arbitrary directions.[1] Here, we present an exceptional *metal-like ductility and malleability* in the isomorphous crystals of two globular molecules, BH_3NMe_3 and BF_3NMe_3, with characteristic *tensile stretching*, *compression*, *twisting*, *thinning (increase of width over 500%)* and so on.[2] Surprisingly, the mechanically deformed samples not only retain good long range order, but also allow structure determination by single crystal X-ray diffraction. Molecules in these high symmetry crystals interact predominantly via electrostatic forces (B^{-}-N^{+}) and form columnar structures, thus forming multiple slip planes with weak dispersive forces among columns due to the presence of shape synthon forming methyl groups. While the former interactions hold molecules together, the latter facilitate exceptional ductility. On the other hand, the limited number of facile slip planes and strong *dihydrogen bonding* in BH_3NHMe_2 negates ductility. The structure property correlation established in these aminoborane plastic crystals with exceptional ductility and ability to retain crystalline order may enable designing highly modular, easy-to-cast crystalline functional organics, for applications in *solid-state electrolytes*, *adaptable electronics*[3] (soft *ferro/piezo/pyro-electrics*), *barocalorimetry* (*solid coolants*) [4], *soft-robotics* etc.[5]

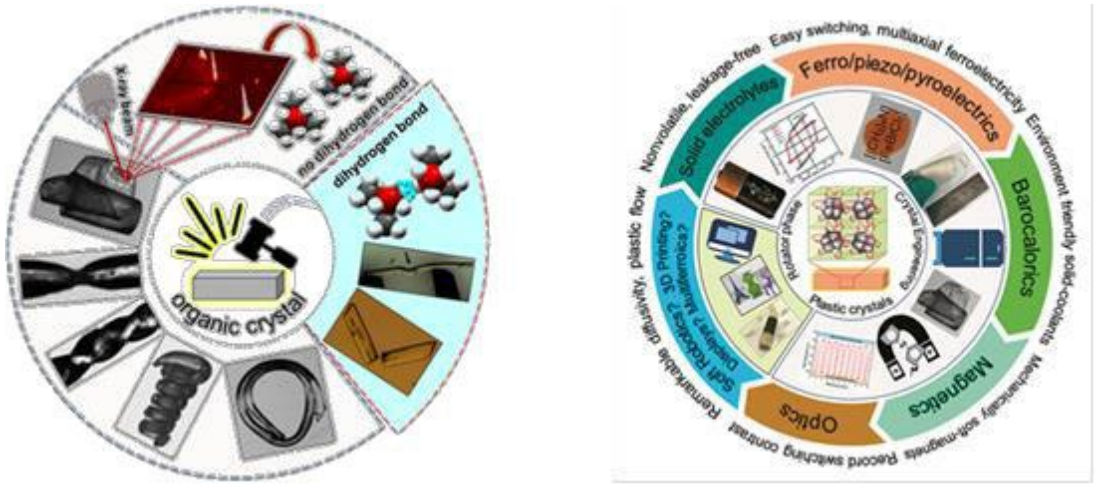

Figure 1. [Left] Peculiar mechanical properties of BR_3NMe_3 (R = H, F) which show metal like ductility & malleability along with X-ray diffraction from mechanically yielded thin film and 1D plasticity in BH_3NMe_3 due to presence of dihydrogen bonding.[2] [Right] Emerging applications of plastic crystals in diverse fields like solid-state electrolytes, barocalorimetry, adaptable electronics etc.[5]

[82] Saha, S., Mishra, M. K., Reddy, C. M. & Desiraju, G. R. (2018). *Acc. Chem. Res*. **51**, 2957-2967.

[83] Mondal, A., Bhattacharya, B., Das, S., Bhunia, S., Chowdhury, R., Dey, S., & Reddy, C. M. (2020). *Angew. Chem. Int. Ed.* **59**, 2-12.

[84] Harada, J., Shimojo, T., Oyamaguchi, H., Hasegawa, H., Takahashi, Y., Satomi, K., Suzuki, Y., Kawamata, J. & Inabe, T. (2015). *Nat. Chem* **8**, 946-952.

[85] Li, B., Kawakita, Y., Kawamura, S. O., Sugahara, T., Wang, H., Wang, J., Chen, Y., Kawaguchi, S. I., Kawaguchi, S., Ohara, K., Li, K., Yu, D., Mole, R., Hattori, T., Kikuchi, T., Yano, S. I., Zhang, Z., Zhang, Z., Ren, W., Lin, S., Sakata, O., Nakajima, K. & Zhang, Z. (2019). *Nature*, **567**, 506-510.

[86] Das, S., Mondal, A. & Reddy, C. M. (2020). *Chem. Soc. Rev*. **49**. 8878-8896.

AM acknowledges IISER Kolkata for PhD fellowship & instrumentation facility, also IUCr 2023 organizers.

A105-05-290823

Photochemical motions in organoboron-based phosphorescent molecular crystals driven by a crystal-state [2+2] cycloaddition reaction

S. Bhandary,[1] M. Beliš,[1] A. M. Kaczmarek,[2] K. Van Hecke[1]

[1]XStruct and [2]NanoSensing Group, Department of Chemistry, Krijgslaan 281-S3, Ghent University, B-9000 Ghent, Belgium
Kristof.VanHecke@UGent.be

Keywords: Photodynamic molecular crystals, [2+2] Cycloaddition, Room temperature phosphorescence

Photoluminescent molecular crystals, integrated with the ability to transform light energy into macroscopic mechanical motions, are a promising choice of materials for both actuating and photonic devices [1]. However, such *dynamic photomechanical effects*, based on *molecular organoboron compounds* as well as phosphorescent crystalline materials, are not yet known. Here we present an intriguing example of *photomechanical molecular single crystals* of a newly synthesized organoboron containing Lewis acid-base molecular adduct (BN1, substituted triphenylboroxine and 1,2-di(4-pyridyl)ethylene) having a capsule shape molecular geometry [2]. The single crystals of BN1 under UV light exhibit controllable rapid bending-shape recovery, delamination, violent splitting/fragmenting-jumping, and expanding features (Fig. 1). The detailed structural investigation by single-crystal X-ray diffraction and ^{1}H NMR spectroscopy reveals that the photosalient behavior of the BN1 single crystals is driven by a *crystal-to-crystal [2+2] cycloaddition* reaction, supported by four donor-acceptor type B←N bonds. The instant photomechanical reaction in the BN1 crystals occurs under UV on the account of sudden release of stress associated with the strained molecular geometry, significant solid-state molecular movements (major supramolecular change), and cleavage of half intermolecular B←N linkages to result in a complete photodimerized single-crystalline product *via* the existence of two other intermediate photoproducts. In addition, a solid-state photoluminescence study indicates that single crystals of BN1 display short-lived *room temperature phosphorescence*, while the light-induced topochemical reaction is accompanied by the enhancement of their phosphorescence intensity to yield the [2+2] photocyclized crystals. Interestingly, the molecular crystals of the final photoproduct polymerize at ambient conditions when recrystallized from the solution forming a 2D supramolecular crystalline polymer stabilized by the retention of all B←N coordination modes.

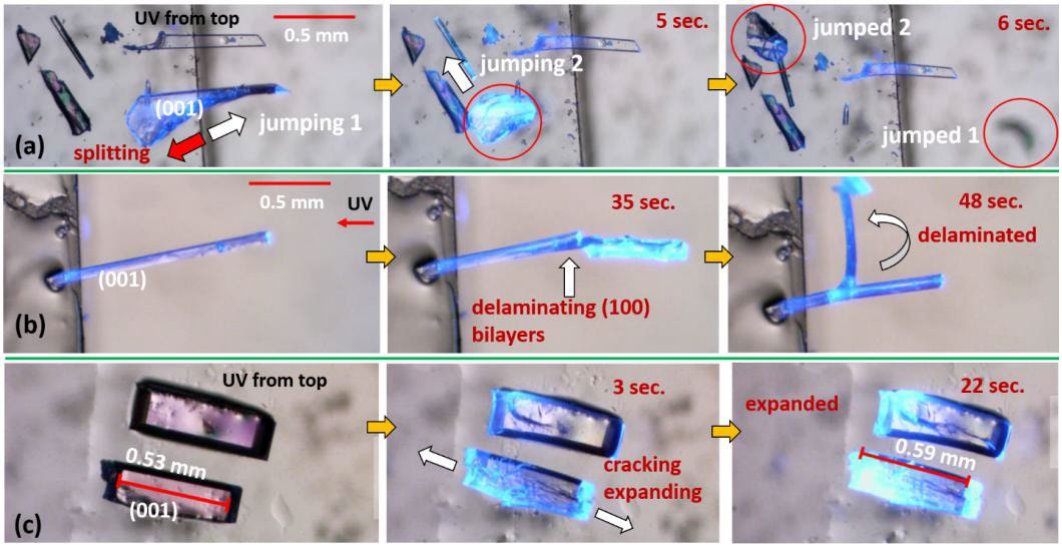

Figure 1. Different morphologies of BN1 single crystals showing (a) violent splitting (explosion into pieces) followed by popping/ jumping of small thick plates, (b) delamination of a rod-shaped crystal, and (c) cracking-expansion features of block-like crystals, under irradiation with a 375 nm CW laser.

[87] Mahmoud Halabi, J., Ahmed, E., Sofela, S., Naumov, P. (2021), *Proc. Natl. Acad. Sci. U.S.A.*, **118**, e2020604118.

[88] Bhandary, S., Beliš, M., Kaczmarek, A.M., Van Hecke, K. (2022), *J. Am. Chem. Soc.*, in press, DOI: https://doi.org/10.1021/jacs.2c09285.

A105-06-290823

Ultrafast, light, soft martensitic materials

E. Ahmed*[1], D. P. Karothu[1], A. Slimani[2], J. M. Halabi[1], I. Tahir[1], P. Naumov[1]

[1]Smart Materials Lab, New York University Abu Dhabi, UAE, [2]Sciences and Engineering Department, Sorbonne University Abu Dhabi, UAE

Email: ea79@nyu.edu

Keywords: Crystal structure, Martensitic transformations, Thermosalient crystals

Martensitic transformations are well documented in metals and alloys where the atoms connected via metallic bonds rearrange concertedly and rapidly; however, due to the metal atoms, these materials are inherently very dense and add significant weight and bulkiness to actuating devices. Here, remarkably rapid lattice switching of molecular martensitic materials is reported in crystals of (phenylazophenyl)palladium hexafluoroacetylacetonate (PHA) and L-pyroglutamic acid (L-PGA) where the rate of structural transformation exceeds other phase transitions several orders of magnitude [1,2]. With a determined speed in the range of 0.3–0.6 m s^{-1}, the new phase advances throughout the crystal about ten thousand times faster relative to spin-crossover transitions, and about hundred to hundred thousand times faster than other common structural phase transitions. Macroscopic crystals of these materials respond by rapid expansion or contraction of about 0.02 m s^{-1} for unrestrained crystals and 0.02–0.03 m s^{-1} for clamped crystals. Monte–Carlo simulation of the spatiotemporal profile of the transition and of the local distribution of elastic and kinetic energies induced by domain growth reveals the critical role of the dynamic phase boundary and the lattice edges in the structure switching. Within a broader context, this study indicates that the martensitic organic crystals are prospective lightweight substitutes of metals for ultrafast and clean energy transduction.

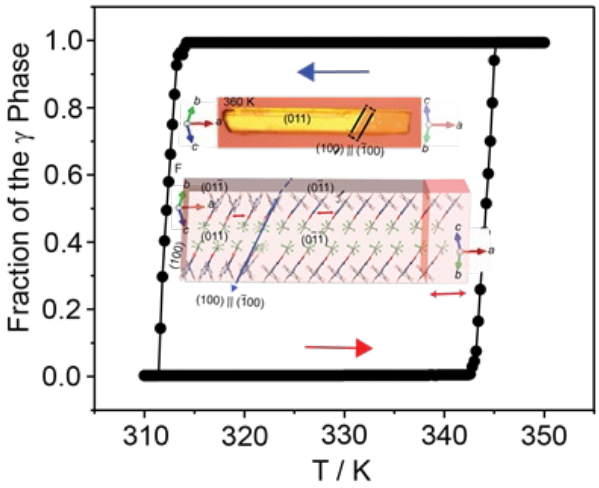

Figure 1. Thermosalient transition in PHA crystals simulated by the Monte-Carlo method (n_γ denotes the fraction of the cells that are in the γPHA phase.

References:

[1] Ahmed, E., Karothu, D. P., Slimani, A., Halabi, J. M., Tahir, I., Canales, K. Q. & Naumov, P. (2022). *Adv. Funct. Mater.*, **32**, 2112117.

[2] Park, S. K. & Diao. Y. (2020). *Chem. Soc. Rev.*, **49**, 8287.

22-29 August 2023
Melbourne Convention and Exhibition Centre
www.iucr2023.org

Congress Management by

ICMS AUSTRALASIA PTY LTD
CELEBRATING 55 YEARS 1966-2021
www.icmsaust.com.au